FACULTY OF MECHANICAL ENGINEERING KRALJEVO
UNIVERSITY OF KRAGUJEVAC
KRALJEVO – SERBIA

THE SEVENTH INTERNATIONAL TRIENNIAL CONFERENCE

HEAVY MACHINERY
HM 2011

PROCEEDINGS

Vrnjačka Banja, June 29th – July 2nd 2011.

FACULTY OF MECHANICAL ENGINEERING KRALJEVO
UNIVERSITY OF KRAGUJEVAC
KRALJEVO – SERBIA

THE SEVENTH INTERNATIONAL TRIENNIAL CONFERENCE

HEAVY MACHINERY
HM 2011

PROCEEDINGS

ORGANIZATION SUPPORTED BY:

Ministry of Education and Science, Republic of Serbia

Vrnjačka Banja, June 29th – July 2nd 2011.

FACULTY OF MECHANICAL ENGINEERING KRALJEVO
UNIVERSITY OF KRAGUJEVAC
KRALJEVO – SERBIA

PUBLISHER:
Faculty of Mechanical Engineering, Kraljevo

EDITORS:
Prof. dr Novak Nedić, mech. eng.

PRINTOUT:
SaTCIP d.o.o. Vrnjačka Banja

No. of copies: 200

REVIEWS:
All papers have been reviewed by members of scientific committee

FACULTY OF MECHANICAL ENGINEERING KRALJEVO
UNIVERSITY OF KRAGUJEVAC
KRALJEVO – SERBIA

CONFERENCE CHAIRMAN

Prof. dr Novak Nedić, FME Kraljevo

INTERNATIONAL SCIENTIFIC PROGRAM COMMITTEE

CHAIRMAN

Prof. Dr Milomir Gašić, FME Kraljevo

VICE-CHAIRMAN

Prof. Dr Mile Savković, FME Kraljevo, Serbia

MEMBERS

1. Prof. Dr M. Alamoreanu, TU Bucharest, Romania
2. Prof. Dr S. Arsovski, FME Kragujevac, Serbia
3. Prof. Dr D. Atmadzhova, VTU “Todor Kableshkov”, Sofia, Bulgaria
4. Prof. Dr A. Babić, FME Kraljevo, Serbia
5. Prof. Dr M. Berg, Royal Institut of Tecnology-KTH, Sweden
6. Prof. Dr H. Bogdevicius, Technical University, Vilnus, Lithuania
7. Prof. Dr A. Bruja, TU Bucharest, Romanija
8. Prof. Dr Z. Bučevac, FME Belgrade, Serbia
9. Doc. Dr R.Bulatović, FME Kraljevo, Serbia
10. Prof. Dr A. Bukvić, FME East Sarajevo, Bosnia and Herzegovina
11. Prof. Dr V. Čović, FME Belgrade, Serbia
12. Prof. Dr M. Dedić, FME Kraljevo, Serbia
13. Prof. Dr R. Durković, FME Podgorica, Montenegro
14. Prof. Dr Z. Đinović, Integrated MicroSystem, Vienna, Austria
15. Prof. Dr K. Ehmann, Northwestern University, Chicago, USA
16. Prof. Dr A. Emeljanova, HGTUSA Harkov, Ukraine
17. Doc. Dr V. Filipović, FME Kraljevo, Serbia
18. Prof. Dr C. Fragassa, University of Bologna, Italy
19. Prof. Dr M. Gagl, Integrated MicroSystem, Vienna, Austria
20. Prof. Dr D. Golubović, FME East Sarajevo, Bosnia and Herzegovina
21. Prof. Dr V. Jovišević, FME Banja Luka, Bosnia and Herzegovina
22. Prof. Dr B. Jerman, FME Ljubljana, Slovenia
23. Prof. Dr Z. Jugović, Tehnical Faculty Čačak, Serbia
24. Prof. Dr V. Karamarković, FME Kraljevo, Serbia
25. Prof. Dr M. Karasahin, Demirel Univerity, Istanbul, Turkey
26. Prof. Dr I. Kiričenko, HNADU Kiev, Ukraine
27. Prof. Dr M. Kolarević, FME Kraljevo, Serbia
28. Prof. Dr K. Kocman, Tecnical University of Brno, Czech Republic
29. Prof. Dr M. Kostic, Northern Illinois University, DeKalb, USA
30. Prof. Dr M. Králik, Faculty of Mechanical Engineering Bratislava, Slovakia
31. Prof. Dr E. Kudrjavcev, MGSU, Moskow, Russia
32. Prof. Dr LJ. Lukić, FME Kraljevo, Serbia

33. Prof. Dr Z. Marinković, FME Niš, Serbia
34. Prof. Dr N. Mešćerin, MGSU, Moskow, Russia
35. Prof. Dr N. Nenov, VTU “Todor Kableshkov”, Sofia, Bulgaria
36. Prof. Dr V. Nikolić, FME Niš, Serbia
37. Prof. Dr E. Nikolov, Technical University, Sofia, Bulgaria
38. Prof. Dr P. I. Nikulin, VGASU, Voronezh, Russia
39. Prof. Dr M. Ognjanović, FME Belgrade, Serbia
40. Prof. Dr J. Peterka, FMS&T, Trnava, Slovakia
41. Prof. Dr Z. Petković, FME Belgrade, Serbia
42. Prof. Dr D. Petrović, FME Kraljevo, Serbia
43. Prof. Dr Z. Petrović, FME Kraljevo, Serbia
44. Prof. Dr J. Polajnar, BC University, Prince George, Canada
45. Prof. Dr S. Radović, FME Kraljevo, Serbia
46. Prof. Dr V. Raičević, FME Kosovska Mitrovica, Serbia
47. Prof. Dr M. Rajović, FME Kraljevo, Serbia
48. Prof. Dr R. Rakanović, FME Kraljevo, Serbia
49. Prof. Dr M. Stefanovć, FME Kragujevac, Serbia
50. Prof. Dr D. Sever, Maribor, Civil Engineering, Slovenia
51. Prof. Dr M. A. Stepanov, MGSU, Moskow, Russia
52. Prof. Dr I. S. Surovcev, VGSU, Voronezh, Russia
53. Doc. Dr Z. Šoškić, FME Kraljevo, Serbia
54. Prof. Dr LJ. Tanović, FME Belgrade, Serbia
55. Prof. Dr S. Trifunović, FME Kraljevo, Serbia
56. Prof. Dr M. Vesković, FME Kraljevo, Serbia
57. Prof. Dr J. Vladić, Faculty of Tehnical Sciences, Novi Sad, Serbia
58. Prof. Dr M. Vukićević, FME Kraljevo, Serbia
59. Prof. Dr K. Weinert, University of Dortmund, Germany

ORGANIZING COMMITTEE

CHAIRMAN:

Prof. Dr Ljubomir Lukić, FME Kraljevo

VICE-CHAIRMAN:

Prof. Dr Milan Kolarević, FME Kraljevo, Serbia

MEMBERS:

Doc. Dr M. Đapić, FME Kraljevo, Serbia
Doc. Dr O. Erić, FME Kraljevo, Serbia
Doc. Dr D. Pršić, FME Kraljevo, Serbia
Doc. Dr S. Šalinić, FME Kraljevo, Serbia
Doc. Dr S. Ćirić-Kostić, FME Kraljevo, Serbia
M.Sc. M. Bjelić, FME Kraljevo, Serbia
M.Sc. N. Bogojević, FME Kraljevo, Serbia
M.Sc. Lj. Dubonjić, FME Kraljevo, Serbia
M.Sc. Z. Glavčić, FME Kraljevo, Serbia
M.Sc. N. Zdravković, FME Kraljevo, Serbia
M.Sc. R. Karamarković, FME Kraljevo, Serbia
M.Sc. Lj. Lalović, FME Kraljevo, Serbia
M.Sc. M. Marašević, FME Kraljevo, Serbia
M.Sc. G. Marković, FME Kraljevo, Serbia
M.A. N. Pavlović, FME Kraljevo, Serbia
M.Sc. B. Radičević, FME Kraljevo, Serbia
M. Bižić, FME Kraljevo, Serbia
Z. Bogićević, FME Kraljevo, Serbia
M. Veljović, FME Kraljevo, Serbia
A. Petrović, FME Kraljevo, Serbia

PREFACE

The Faculty of Mechanical Engineering Kraljevo has been traditionally organizing the international scientific conference devoted to heavy machinery every three years. The VII International Scientific Conference HM 2011 is considering modern methods and new technologies in the fields of transport design in machinery, control energy, production technologies, urban engineering and civili engineering through thematic sessions for the purpose of sustainable competitiveness of economic systems. Modern technologies are exposed to fast changes at the global world level so that their timely application both in large industrial systems and in medium and small enterprises is of considerable importance for the entire development and technological progress of economy as a whole.

The VII International Scientific Conference Heavy Machinery HM 2011 is a place for exchange of experiences and results accomplished in domestic and foreign science and practice, with the goal to indicate directions of further development of our industry on its way toward integration in european and world economic trends. Exchange of experiences between our and foreign scientific workers should contribute to extension of international scientific-technical collaboration, initiation of new international scientific-research projects and broader international collaboration among universities.

The papers which will be presented at this Conference have been classified into seven thematic fields:

A. Railway Engineering
B. Earth-Moving and Transportation Mechanization
C. Automatic control and fluid technique
E. Mechanical Design and Mechanics
F. Production Technologies
G. Urban Engineering
H. Structures And Materials In Civil Engineering

Within this Conference, the First International Students Symposium will be held. The aim is to open a scientific discussion on this actual problem in industry among young students.

The sponsorship by the Ministry of Science of the Republic of Serbia is the proper way to promote science and technology in the area of mechanical engineering in Serbia.

On behalf of the organizer, I would like to express our thanks to all organizations and institutions that have supported this Conference. I would also like to extend our thanks to all authors and participants from abroad and from our country for their contribution to the Conference. And last but not the least, dear guests and participants in the Conference, I wish you a good time in Kraljevo – Vrnjačka Banja and see you again at the Eight Conference, in three years.

Kraljevo – Vrnjačka Banja, June 2011

Conference Chairman,

Prof. Dr Novak Nedić, mech eng.

CONTENTS

PLENARY SESSION

A SESSION: RAILWAY ENGINEERING

B SESSION: EARTH-MOVING AND TRANSPORTATION MACHINERY

C SESSION: AUTOMATIC CONTROL AND FLUID TECHNIQUE

D SESSION: DESIGN AND MECHANICS

E SESSION: PRODUCTION TECHNOLOGIES

F SESSION: URBAN ENGINEERING

G SESSION: STRUCTURES AND MATERIALS IN CIVIL ENGINEERING

PLENARY SESSION

HEAVY MACHINERY - HM 2011, 1-12
ISBN 978-86-82631-58-3
Paper accepted: 30.05.2011

Finite element analysis of sandwich panels with openings

Boris Jerman[1,*] - Metod Čuk[1] - Franc Resman[1] - Tomaž Popit[2] - Silvo Štih[2]
[1] University of Ljubljana, Faculty of Mechanical Engineering, Slovenia
[2] Trimo d.d., Trebnje, Slovenia

Lightweight structural sandwich panels made of two thin steel facings, which are bonded to relatively thick and light insulating rock wool core, are often used for wall claddings. The sandwich panel clad structures are frequently weakened by cut-outs and openings for doors, windows, and in other cases. The paper concerns effects of these large openings on load-bearing capacity and structural stiffness of sandwich panel claddings. Since it is not possible to give generally acceptable rules to evaluate their complex structural behaviour at the present time this research project was conducted using a series of numerical analyses and laboratory experiments to study the local and global behaviour for a certain sandwich panel product and certain design case. A few typical design examples of claddings with a large opening were studied. Finite element analyses (FEA) of the simply supported interconnection systems with three sandwich panels and a large rectangular opening placed symmetrically to the mid-line of middle panel were undertaken. Detailed investigation for a case of a large opening in panel interconnecting system with a middle sandwich panel completely cut is presented. In this case, the load transfer from a sandwich panel with a large opening through the longitudinal joints to the adjacent panels is of the main importance. For this reason, the longitudinal joints were modelled very carefully. The numerical computations provided the stress and strain distributions in the steel faces and mineral wool core and further failure mechanism estimation was made based on the results. The laboratory experiment of the studied design case was also conducted. The results obtained from the experiment were reasonably agreeable to support the FEA results. In addition, the further local finite element model was built to study the structural behaviour of the longitudinal joints between the panels and the shear load-bearing capacity of these joint was determined.

Keywords: sandwich structures, buildings, structural wall panels, window openings, mineral wool, finite element method, structural analysis, testing, load-bearing capacity, panel interconnection

0 INTRODUCTION

The use of sandwich panels in the construction of industrial and commercial buildings has become widespread. The panel clad structures offer protection against rain, snow and wind, thermal and sound insulating capacity and fire resistance while beeing lightweight, durable and cost effective.

Structural sandwich panels used for wall claddings consist of two flat or lightly profiled thin facings, which are bonded to relatively thick and light core. Structural behaviour of sandwich panels is complex: the lightly profiled steel faces takes compressive and tensile loads whilst flexible core made of mineral wool transfers shear loads between the faces. The resulting composite has relatively high load-bearing capacity and high bending stiffness [1].

The panel clad structures also need to have construction cut-outs and openings for doors, windows, pipe penetrations and other devices. Openings in sandwich panel claddings may vary in size, location and by span direction (horizontal, vertical) [2]. They may cut only a part of a panel or parts of two adjacent panels symmetrically or asymmetrically relative to the mid-line of the panel or the mid-span of the panel. The decrease of the area of face and core because of the openings reduces the flexural, shear and tensional rigidity and bending and shear resistance of sandwich panels [1].

The existing European standard EN 14509 does not provide design and testing procedures for sandwich panels with openings [3]. The accepted common technical solution for the openings within sandwich panels is to use a “replacement” in the form of an additional supporting structure. Such reinforcement has to replace the load-bearing capacity, which has been removed from the self-supporting sandwich panels by the openings, and transfer applied loads

*Corr. Author's Address: University of Ljubljana, Faculty of Mechanical Engineering, Aškerčeva 6, 1000 Ljubljana, Slovenija, boris.jerman@fs.uni-lj.si

on the openings to the spaced structure. The results of research show that sandwich wall panels with openings can be designed without the additional supporting structure.

The first design rules for sandwich panel walls with window openings were proposed by Höglund [4]. It was suggested that properly designed unstrengthen panels with window openings may be used. The design formulae to evaluate the transfer of the load from a panel with openings to the adjacent panels were based on the compatibility of deflections at the midspan of the longitudinal joints of simply supported sandwich panels due to bending moments, shear forces and torsional moments caused by uniformly distributed pressure load and the temperature difference between the inside and outside of the sandwich elements.

Toma and Courage [5] proposed a design procedure to determine the strength and stiffness of sandwich panels with openings without additional stiffeners. Correction factors taking into account the stress concentrations in the core and the faces around the opening determined by a numerical study and the strength capacity of the panel without opening determined experimentally were introduced to the calculation rules based on the design rules for sandwich panels without openings.

Berner and Pfaff [2] suggested common solutions and introduced a supporting reinforcement within the range of openings with particularly conceived framework. Firstly, the sufficient load-bearing capacity of the panels with openings can be achieved by the resistance of the remaining cross section. Rough computations under approach of the remaining cross section and the stress peaks for panels with realistic spans and realistic loads showed that this solution could only be applied for small openings. Secondly, because of smaller flexural rigidity, the panel with an opening (without reinforcing) supports itself onto the panels without openings through the longitudinal joints. In this case, two substantial conditions must be present: adjacent panels that are additionally stressed must not have any openings and the transmission of loads into the carrying not weakened panels must be ensured through the longitudinal joints. The activation of load-bearing support of adjacent panels can only be achieved to the extent permitted by shear force capacity of the longitudinal joints. Thirdly, a supporting frame from special thermally separated aluminium profiles with plastic webs as longitudinal beams to reinforce the openings is introduced. All openings, independently of size and location are reinforced by structural measures within the window and door frame. In this case useful allowable spans may be achieved (even with large openings up to entire panel width) similar to those of not weakened panels without participation of adjacent panels and therefore without additional stress of the longitudinal joints between the panels. However, it has been suggested, that for a final practical application further investigations were necessary.

Böttcher and Lange [6] presented a calculation model of wall sandwich panels with openings, which considers the load transfer over the longitudinal joints into neighbouring elements. The global load model is based on the beam theory and is used to calculate loads and displacements, while a further local finite element model is used to determine stress distribution in the cross section of the opening.

Warmuth and Lange [7] presented some test results of sandwich elements with large windows openings. A comparison clearly shows the increase of load-bearing capacity for panels with reinforcing window frame in comparison to frameless openings. In some cases the results varied within a wide range, so further testing is necessary to get more exact knowledge that may bring better correlations between the tests and the calculations. A comparison of experimental and calculated results for openings without frames according to calculation proposals is also presented.

In “Recent European Recommendations on Design and Testing” [8] the latest ECCS/CIB Joint Committee work was presented. The Committee publication “State of the art report for Design of Sandwich Panels with Openings” [9] (will be probably published in 2011) will introduce the possibility of designing panels with openings without the need for any additional strengthening. The report gives basic design formulas to calculate the remaining resistance of a panel with “small” openings. The basic principles of activation of the load-bearing resistance of neighbouring panels is also presented with a test set-up and design formulas for the determination of the stiffness and resistance of the longitudinal joints and the required torsional and bending stiffness of the panels. For panels with large-sized openings an additional frame has to be designed to carry the whole load of the sandwich panel with openings.

The objective of this paper is to present details of finite element analyses of structural behaviour of wall sandwich panels with large openings. Two different studies have been performed. Firstly, the interconnection system with three simply supported sandwich panels and a large window opening (width of the opening equates to the width of the panel) at midspan in the middle panel was studied to determine load-bearing capacity at maximum span used for panels without openings. Secondly, a further model for studying the structural behaviour of the longitudinal joint between the panels was built. In addition, a laboratory experiment was carried out for the studied case of the interconnection system with three sandwich panels and a large opening and the comparison of the results is presented.

1 FINITE ELEMENT ANALYSIS

Structural behaviour of wall structural sandwich panel cladding with large openings was investigated using the ANSYS® simulation software package. A series of finite element models of the panel interconnection systems with openings that cut a part of the panel (up to the entire width of the panel) were built. The models incorporated a detailed longitudinal joint between the panels to simulate load transfer from the weakened panel to the neighbouring panels. Even more details were included in the further local model that was built to study load transfer through the longitudinal joints.

A great emphasis was also given to the application of appropriate finite elements, material models and material properties that conformed to the material test results provided by the sandwich panel manufacturer. The steel face was modelled using shell elements (SHELL181) and orthotropic linear elastic – ideal plastic (value of tangent modulus is effectively zero) material model was specified. Mechanical properties of the steel sheet are shown in table 1a).

Mineral wool core was modelled using solid elements (SOLID45) and anisotropic bilinear plastic material model (uniaxial bilinear tension and compression stress-strain curves in three orthogonal directions and shear stress-engineering shear strain curves in the corresponding directions [9]) was determined. Table 1b) shows mechanical properties of mineral wool core. Orthogonal directions (as specified in table 1b) coincide with axial directions of global coordinate system that was used in all models: X axis is parallel to the width of the panel, Y axis is parallel to the panel thickness and Z axis lays parallel to the length of the sandwich panel.

The results of finite element analyses performed during this study showed that some of the material properties of the mineral wool have impact on the structural behaviour of the sandwich panel that is more significant if compared to the impact of some other properties. Among the first are shear yield strength and shear modulus in the longitudinal vertical plane of the panel (YZ) and the compressive strength and compression elastic modulus in the direction of the panel thickness (Y).

All mechanical properties of mineral wool core, which is made of lamellas cut from mineral wool plates, may vary depending on manufacturing process and thickness of the plates of mineral wool plates. The values of some mechanical properties may even vary in a wide range from batch to batch by the same manufacturer.

Table 1. *Mechanical properties of steel faces and mineral wool core*

a) Mechanical properties of steel sheet

Elastic modulus [GPa]	Yield strength [MPa]	Poisson ratio	Tangent modulus [GPa]
210	320	0,3	0,1

b) Mechanical properties of mineral wool

Elastic modulus [MPa]			Poisson ratio			Shear modulus [MPa]		
X	Y	Z	XY	YZ	XZ	XY	YZ	XZ
≈0*	≈10*	≈50*	0	0	0	–*	–*	–*

	Yield strength [MPa]			Tangent modulus [MPa]		
	X	Y	Z	X	Y	Z
Tension and Compression	–*	–*	–*	–*	–*	–*
	XY	YZ	XZ	XY	YZ	XZ
Shear	–*	–*	–*	–*	–*	–*

* - (exact) values are made unavailable at the request of the panel manufacturer

1.1 Panel interconnection system with a large opening

As previously stated, for the effective use of the sandwich panels in the wall claddings with openings it is necessary to consider the load transfer from the cut-out panels to the unleavened neighbouring panels. In case of large openings, a single sandwich panel may be cut out to the extent that almost the whole load of the weakened panel is supported by the two adjacent panels. Further enlarging of the opening leads to the case when the openings occupy the whole width of one panel.

A numerical study of the activation of the load-bearing resistance of the neighbouring panels in the panel interconnection systems was carried out. A series of finite element models of interconnection systems with three panels and centrally placed large opening in the middle panel was built.

In this paper, a study of specific design case of the interconnecting system with three panels and a large opening in the middle panel is presented where a centrally placed large opening extends to the entire width of the panel as show in figure 1. The modelled panels have a thickness of 120 mm, nominal width of 1000 mm and total length of 3800 mm. Due to the symmetry of the analysed system, only one half-model (one and a half panel) has been built and symmetry boundary conditions were applied (although, considering the double-symmetry of the structure, a model of one-fourth of the system could have been used).

In addition to the bricks and shells, as it has beeen mentioned above, linear compression-only elements (LINK10) were used to simulate simple supports at both ends of the interconnection system. Surface-to-surface contact elements (CONTA174 and TARGE170) were used to describe an interaction between male and female means of the longitudinal joint along the panels.

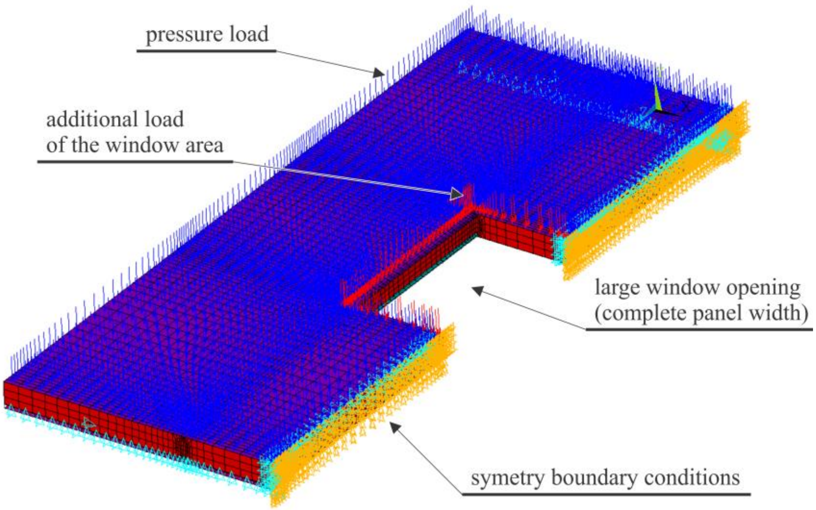

Fig. 1. *FE model of interconnection system with three sandwich panels and large window opening of a size* 1 × 1 m *(the width equates to entire width of the middle panel) in the middle panel with applied loads and boundary conditions (the simple supports (light blue triangles) are situated on the both ends of the panel system; on the right side of the model symmetry boundary conditions (orange) are applied; on the upper face of the panels (wind) pressure is applied (blue arrows); at the edges of the opening additional loading is applied (red arrows) to compensate the pressure, which is in real world applied on the window mounted in the opening)*

The wind action simulation was performed by applied pressure load on upper face of the panels. The loading of the window opening was uniformly distributed on the 40 mm wide marginal area of both middle and adjacent panels around the opening, which corresponds to the

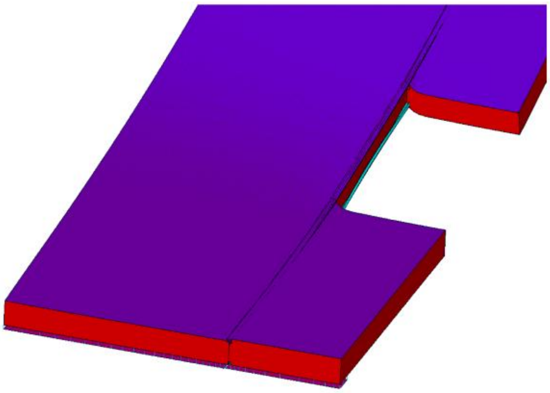

Fig. 2. *Deformed shape of calculation model at pressure load* 2,3 kN/m^2. *The global bending deflection and big local deformations of the longitudinal joints near the opening are noticeable*

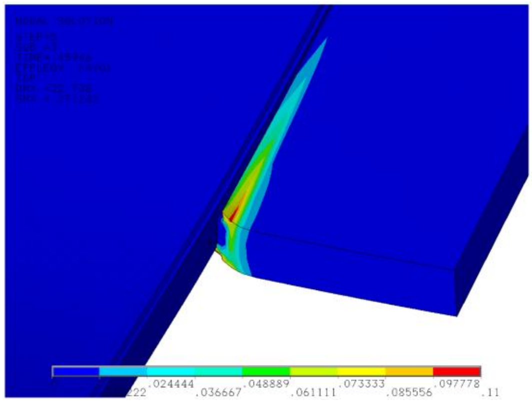

Fig. 3. *Equivalent plastic strain (von Mises) in mineral wool core near longitudinal joint at the edge of window opening (pressure load* 2,3 kN/m^2*). In this picture, only the core is shown whereas the steel plates are hidden.*

load application used in the comparative laboratory experiment.

The numerical simulation results at applied pressure load of 2.3 kN/m^2, which matches the maximum load pressure applied before failure in the laboratory experiment are shown in figures 2–4. In figure 2 the deformed shape of the interconnecting system is shown. The global bending deflection is noticeable and big local deformations of the longitudinal joints near the opening can be seen. Von Mises equivalent plastic strain of the mineral wool core is shown on figure 3. Plastic (permanent) deformation of the core through the whole thickness is discovered in the region of the longitudinal joints near the cut-out where big local deflections are located. From figure 4 where the upper steel sheet is shown similar conclusions can be settled. The stresses σ_x are significantly higher in the area where high local deflection and important plastic deformation were discovered.

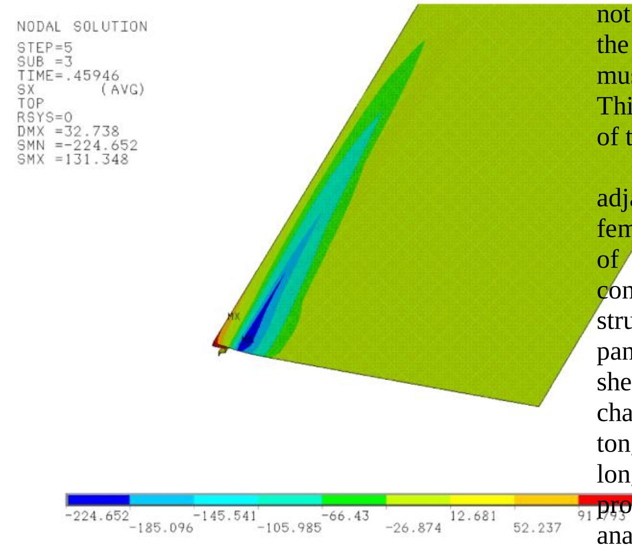

Fig. 4. *Stress distribution* σ_x [MPa] *in upper steel face (pressure load* 2,3 kN/m^2*). High stress due to the local bending of the metal face is noticed in the area of the longitudinal joint near the edge of window opening*

It is obvious that because of the greatly reduced load bearing capacity of the middle panel, a major part of the load is transferred to the adjacent panels through the longitudinal joint. Because the majority of this loading tends to be transferred in the vicinity of the cut-out where the load-bearing capacity of the middle panel is compromised the concentrations of loading arise. Therefore, the distribution of the transferred force along the joint is not uniform but rather rises highly near the opening. The transferred forces at these places clearly exceed the load-bearing capacity of the longitudinal joints as indicated by the excessive yielding of mineral wool core (figure 3.) and almost up to yield strength high local bending stresses in steel face (figure 4.).

These results clearly suggest that the longitudinal joint is the weakest link of the analysed interconnection system (when the cut middle panel is not considered) and that failure mode is joint failure. For this reason, a more detail investigation of the load-bearing capacity of the longitudinal joint is conducted and presented in the next section.

1.2 Longitudinal joint load-bearing capacity

To activate the load-bearing capacity of not weakened adjacent panels the transmission of the loads from the middle panel with the opening must be ensured through the longitudinal joints. This means that a sufficient shear force capacity of the longitudinal joints must be available.

A joint along longitudinal edges of adjacent sandwich panels comprises male and female means between both inner and outer faces of adjacent panels. The male and female connecting means are interlocked providing a structural connection between the sandwich panels in the wall claddings. A calculation of shear force capacity is (because of nonlinear characteristics and complicated geometry of tongue and groove inner and outer joint of longitudinal edges) not a simple procedure and is probably feasible only with finite element analysis. In addition, such finite element analysis can also be used to further study local phenomena that cannot be accomplished by any other research tool.

To determine load-bearing capacity of longitudinal joint a tenth-width finite element model was used. A sandwich panel brick by effective dimensions (effective width × length × height) of 100 ×100 ×120 mm was modelled with the male and female connecting end on the each side as shown in fig. 5. Adjacent sandwich panel bricks with the opposite connecting ends were added on the each side of the main brick for support. These adjacent bricks are modelled only half in their width as they would be cut. Symmetry boundary conditions are applied on the both cut side surfaces of the adjacent half width bricks providing corresponding boundary conditions. Zero vertical displacement boundary conditions were additionally applied on the both lower edges of cut side surfaces. The pressure applied on the outer steel face (effective area $100 \times 100\ mm^2$) of the middle brick is increased for the factor of ten thus effectively simulating surface load (such as wind load) of the real sandwich panel within its full width of 1000 mm.

The analysis of the model was performed in two steps. Firstly, a load pressure of $1,4\ kN/m^2$ (which is a design resistance of modelled panel at maximum allowable spans) was applied. Secondly, a load-bearing capacity was determined by gradual increasing of applied load through the simulation until the expected failure mode - the joint failure occurs.

The criterion for determination of the ultimate strength of the joint (the point of the joint failure) was set at the value of 3 % of von Mises equivalent plastic strain in mineral wool core under the steel faces in the area of observed longitudinal joints.

Von Mises equivalent plastic strain in the mineral wool core is shown in figures 8a and 8b. The first figure shows the conditions at the load pressure of $1.4\ kN/m^2$. Almost no plastic strain is encountered there. The second figure shows the conditions at the load pressure of $2.1\ kN/m^2$. In the area of the longitudinal joint, the plastic strain up to 3.9 % is encountered. The maximum values are present only in small portion of the area of interest whereas the value of 3 % (or higher) is present in almost complete volume of the upper left corner of the brick. For this reason, the ultimate strength of the longitudinal joint is determined as $2.1\ kN/m^2$.

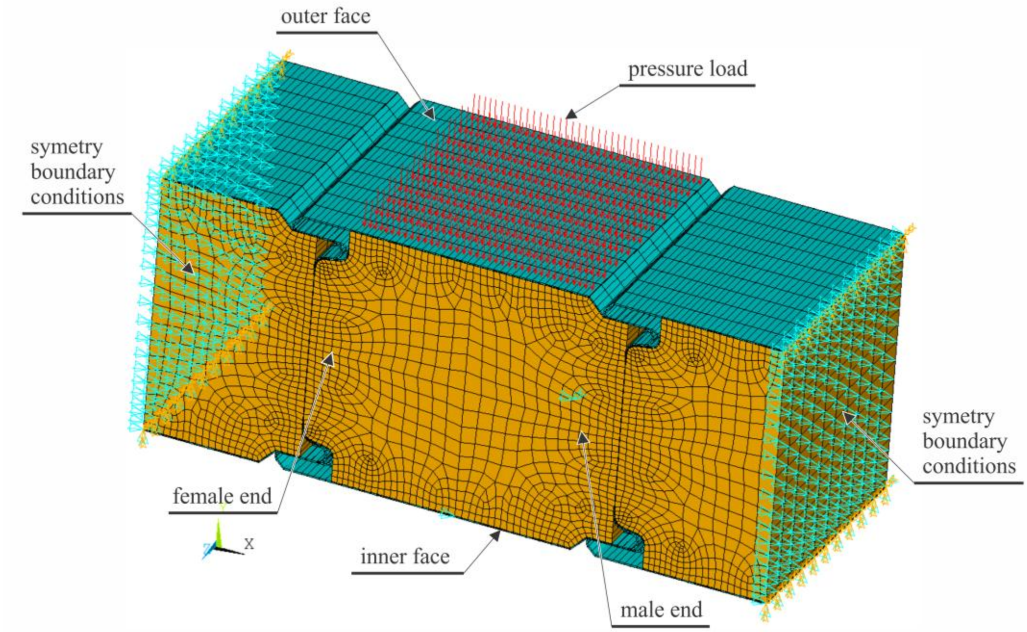

Fig. 5. *Load-bearing capacity of a longitudinal joints is investigated using the FE calculation model with applied corresponding boundary conditions (on both sides of the panel system the vertical supports are positioned; on both sides also the symmetry boundary conditions are applied; on the upper face of the middle panel the pressure is applied (this pressure is 10-times the normal pressure, ensuring the normal loading is provided in spite of the small width of the panel)*

Table 2. *Load-bearing capacity and transmitted forces in longitudinal joints*

a) Load-bearing capacity of longitudinal joints

Pressure load [kN/m^2]	Transmitted vertical load [N/m]		Transmitted load ratio [%]	
	female end	male end	female end	male end
1,40	723	677	51,6	48,4
2,10	1095	1005	52,1	47,9

b) Transmitted forces between outer and inner longitudinal joints

Pressure load [kN/m^2]	Vertical (shear) force [N/m]				Transverse force [N/m]	
	Outer face		Inner face			
	female end	male end	female end	male end	female end	male end
1,40	453	283	278	406	168	97
2,10	629	480	476	544	331	173

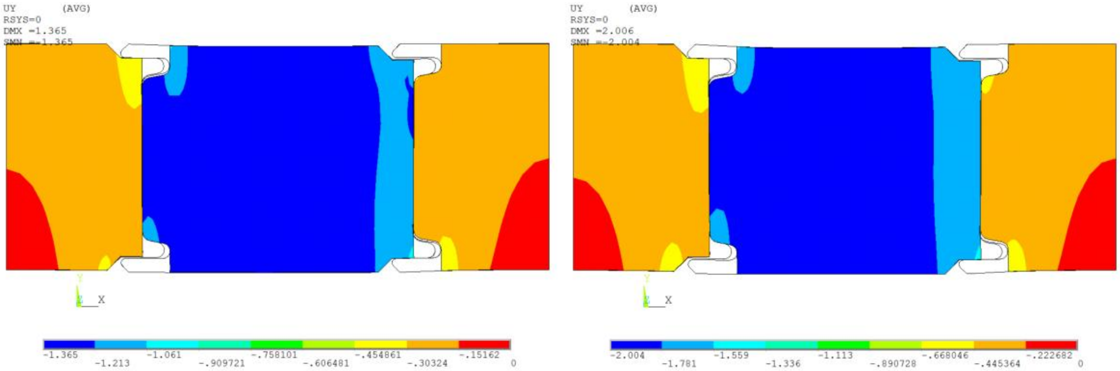

a) *Pressure load* 1,4 kN/m^2 b) *Pressure load* 2,1 kN/m^2

Fig. 6. *Vertical (out-of-plane) deflections* u_y [mm]

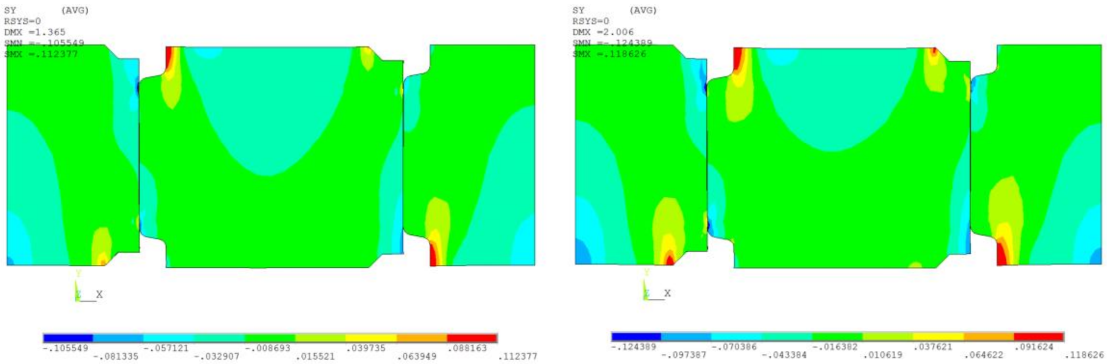

a) *Pressure load* 1,4 kN/m^2 b) *Pressure load* 2,1 kN/m^2

Fig. 7. S*tress distribution* σ_y [MPa] *in mineral wool core*

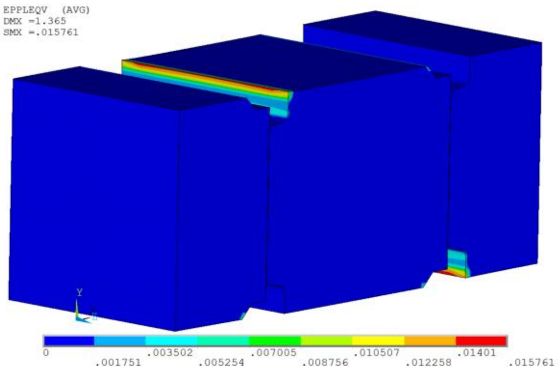

a) *Pressure load* 1,4 kN/m^2

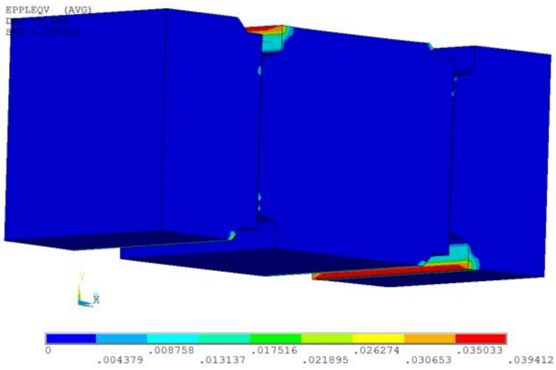

b) *Pressure load* 2,1 kN/m^2

Fig. 8. *Equivalent plastic strain (von Mises) in mineral wool core*

In the figure 6 the deflection in the direction of the thickness of the sandwich panel plate (y-axes) is shown. Under the pressure of 1.4 kN/mm^2, the maximal deflections are +0,151 mm, and -1.365 mm. Under the pressure of 2.1 kN/mm^2, the maximal deflections are +0,223 mm, and -2,004 mm. The negative values are caused by external pressure load in –y direction.

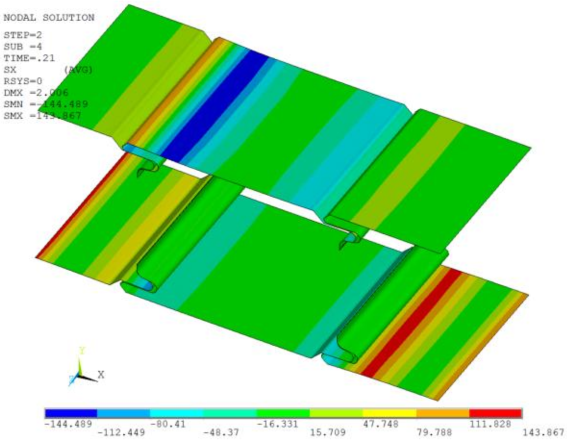

Fig. 9. *Bending stresses* [MPa] *in steel faces at pressure load* 2.1 kN/m^2

Figure 7 shows the stresses in the mineral wool core in the direction of the thickness of the sandwich panel plate (y-axes). The maximum positive and negative values for the loading of 1.4 kN/mm^2 and 2.1 kN/mm^2 correspondingly are +0.112 N/mm^2 and -0.106 N/mm^2, and +0.119 N/mm^2 and -0.124 N/mm^2. The yield strength of the mineral wool in y-direction is clearly exceeded.

Bending stresses in steel faces of the sandwich panels in the direction of the width of the panels (x-direction) are shown in figure 9. The values are in the span from -144.5 N/mm^2 to +111.8 N/mm^2.

2 EXPERIMENTAL INVESTIGATIONS

To verify the numerical investigations, laboratory experiment was conducted using the same configuration of three sandwich panels for the test system as it was used in the case of the finite element analyses.

The experimental setup is shown in figure 10. The panel interconnection made of three panels connected into a single span system can be recognized. In the centre of the span, the entire width of the middle panel was replaced with an opening. A centrally placed opening of size 1 × 1 m was covered with an oversized wooden board (thickness: 22 mm, 40 mm overlap on all sides) to substitute the effect of real world window by transferring applied loads on the window opening to the uncut parts of the middle panel and directly to the border region of both outer panels. The system was simply supported by using 50 mm wide vertical support on both ends.

The pressure load on the entire upper face of all three panels (including then opening) was spread by gradually placing 25 kg sandbags layer by layer.

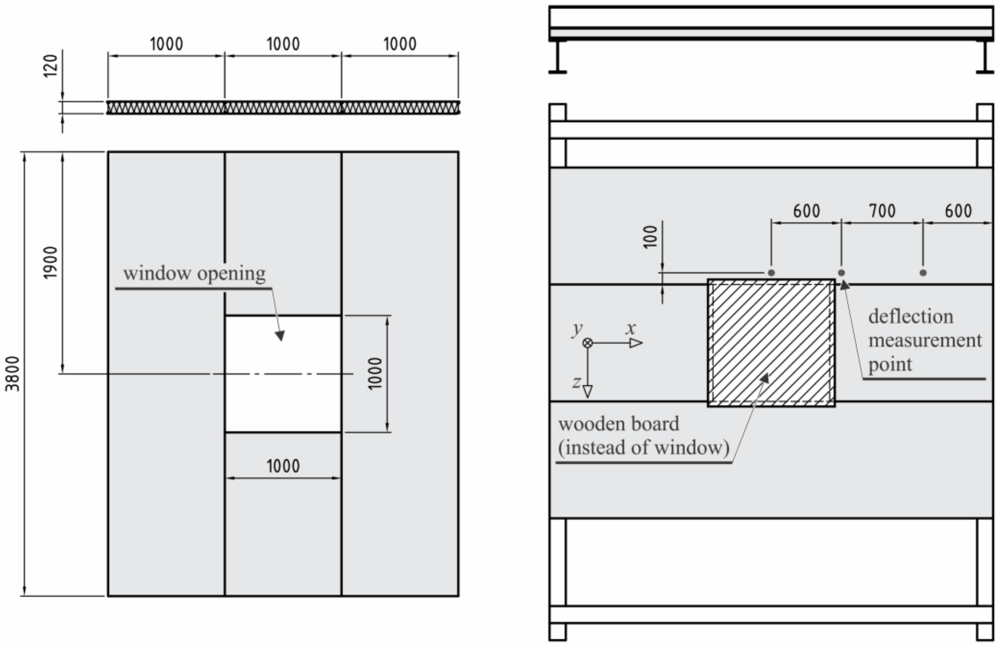

Fig. 10. *Test setup for interconnection system with three sandwich panels and large window opening of size* 1 × 1 m *(width equates to entire width of the panel) in the middle panel. The dimensions of the panels are shown on the left figure where the position of the supports, the wooden board and the deflection sensors are presented on the right figure*

Table 3. *Load bearing capacity of interconnection system with three sandwich panels and large window opening in the middle panel*

Test	Max. load (before failure) [kN]	Pressure load [kN/m^2]	Failure mode
1	25,5	2,24	complete collapse
2	25,6	2,25	complete collapse

During the laboratory experiment two types of measurement were conducted: at each loading step the mass of added sandbags was weighted and a total load was calculated, while at the end of the stages a measurement of vertical displacements at three measurement points was performed manually using a measure.

In both of two tests that were carried out the maximum applied total load before the failure was approximately 2,30 kN/m^2 as shown in table 3. In both cases, the spreading of the next layer of sandbags caused a complete collapse of entire panel interconnection system.

Figures 11a) and b) show the comparison of the deflections obtained from finite element analysis and laboratory experiment. The comparison is made for two applied pressure loads: maximum load of 2,30 kN (results for two tests are available) and approximately half of the maximum load of 1,22 kN (only one set of test results is available). The error in the FEA simulation of the vertical displacement is in range 6% - 12% for half of maximum pressure load and in range 7% - 12% for full maximum pressure load when compared to experimental results.

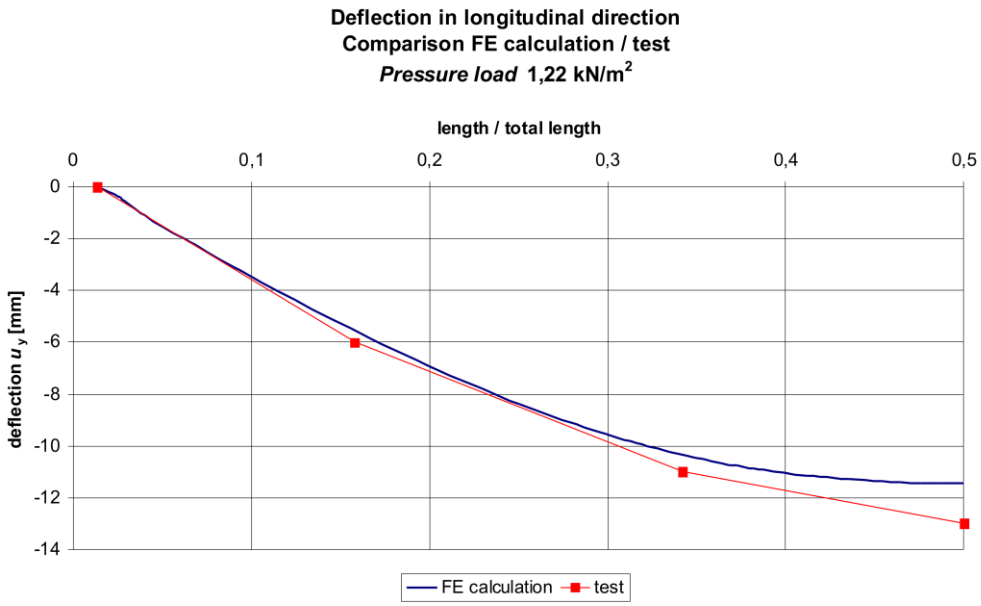

a) *Pressure load* 1,22 kN/m^2

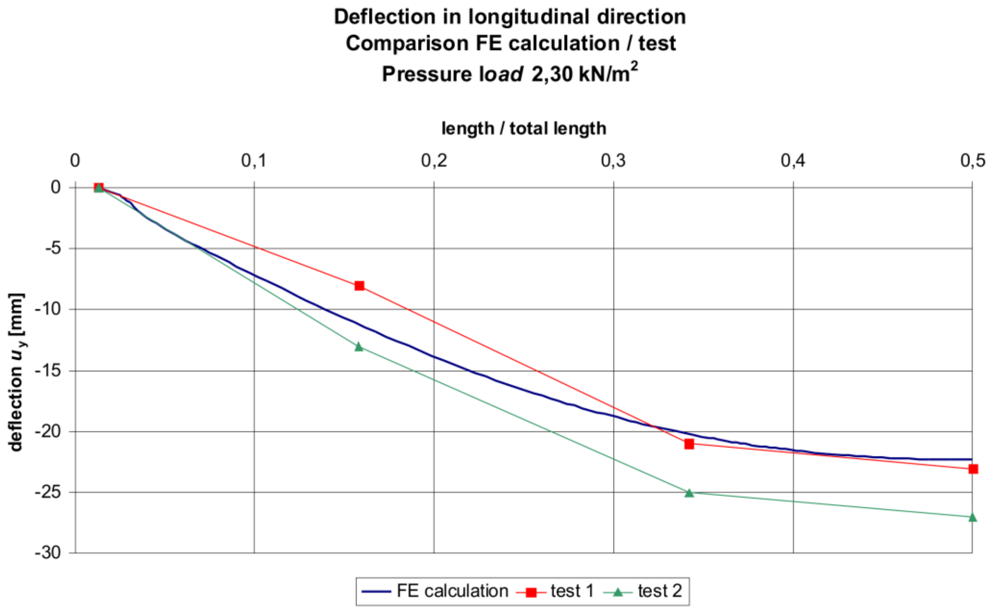

b) *Pressure load* 2,3 kN/m^2

Fig. 11. *Comparison of deflections of interconnection system with three sandwich panels and large window opening in the middle panel*

3 CONCLUSIONS

The results of numerical studies of wall sandwich panels with large openings have been presented in this paper. The investigations were focused on the interconnection system of three simply supported panels with a large window opening in the middle panel and appropriate models were built using finite elements. The pressure load was applied simulating wind actions. A detailed analysis for the specific case where the width of the centrally placed opening equates to the panel width is presented.

Because of the opening that cut out the width of a complete panel, almost entire load from the middle panel is transferred to the adjacent panels. The forces that are transferred through longitudinal joints at maximum pressure loads are clearly beyond their load-bearing capacity, which is indicated by excessive yielding of the mineral wool core.

Besides numerical analysis, a laboratory experiment of the studied interconnection system of three panels with a large opening in the middle panel was also carried out. The satisfactory correlation can be observed by comparing the computed displacement to the measured displacement from the experiment. The failure mode of the tested panel interconnection system was complete collapse while the numerical simulation suggested that the detected failure mode should be the longitudinal joint failure in the corner region of the opening.

The results from both the experimental and numerical investigations showed that a large opening (width of the opening equates to the width of the panel) has a significant negative effect on load-bearing capacity of the interconnection system. The value of maximum load that was applied in the experiment before the failure is vastly reduced (more than half) compared to the values of the characteristic resistance for the same interconnection system without any openings.

Additionally, a numerical study of structural behaviour of the longitudinal joint between the panels was also undertaken using further local finite element model. The detailed model of longitudinal joint was implemented. The results of analyses showed that the shear load-bearing capacity of longitudinal joint is small and probably sufficient for the wall panels with small openings. However, in the case of the large openings the use of additional supporting structure or reinforcing frame may be necessary.

4 REFERENCES

[1] Davies, J. M., Lightweight Sandwich Construction, Blackwell Science, Oxford, 2001

[2] Berner, K., Pfaff, U., Openings in sandwich panels, Institute for Sandwich technology, Mainz, 2005

[3] EN 14509:2006 (E), Self-supporting double skin metal faced insulating panels – Factory made products – Specification, CEN – Comité Européen de Normalisation, Brussels, 2006

[4] Höglund, T., Load Bearing Strength of Sandwich Panel Walls with Window Openings, Proceedings of IABSE Colloquium, IABSE Reports Vol. 49, pp. 349-356, Stockholm, 1986

[5] Toma, T., Courage, W., Structural detailing of openings in sandwich panels, Proceeding of Thirteenth International Specialty Conference on Cold-Formed Steel Structures: Recent Research and Developments in Cold-Formed Steel Design and Construction, pp. 309-320, St. Louis, Missouri U.S.A., 1996

[6] Bottcher, M., Lange, J., Sandwich Panels with Openings, Proceedings of the 5th International Conference, pp. 722, Kruger National Park, Berg-en-Dal, Mpumalanga, South Africa, 2004

[7] Warmuth, F., Lange J., Openings in Sandwich Elements, International Conference on Steel & Composite Structures, Sydney, 2010

[8] Davis, J. M., Hassinen, P., Heselius, L., Misiek, T., ECCS/CIB Joint Committee on Sandwich Constructions: Recent European Recommendations on Design and Testing, Proceedings: W056 – Special Track 18th CIB World Building Congress, Salford, UK, 2010

[9] ECCS/CIB State of the art report for Design of Sandwich Panels with Openings, ECCS, TWG 7.9 Sandwich panels and related structures & CIB, W056 Lightweight Constructions, Brussels/Rotterdam, (will be published in 2011?)

[10] Release 11.0 Documentation for ANSYS, Wickens, SAS IP, Inc., 2007

HEAVY MACHINERY - HM 2011, 13-24
ISBN 978-86-82631-58-3
Paper accepted: 30.05.2011

Fiber Optic Sensing Technology for Health Monitoring of Heavy Structures

Zoran Djinovic[1*], M. Tomic[2]

Structural Health Monitoring (SHM) is an emerging technology in the modern society due to of paramount benefits that come out from such an approach; higher safety and security of human life, better insight into the material behaviour, safe money. This paper is dealing with the SHM subject performed with Fiber Optic Sensing (FOS) technology, also a relatively new technique in family of Non-destructive Testing (NDT) of materials and structures. We highlighted some basic requirements of SHM and introduced the reader with basic data about optical fibers and advantages of FOS technology. We briefly explained basic principle of operations of several most frequently used FOS techniques. Then, we presented some laboratory and industrial examples of application of FOS technology that partially reflect state of the art of R&D activities and capability of already commercialized SHM systems.

Keywords: Fiber-optic sensors, structural health monitoring, heavy structures

1 INTRODUCTION

Structural Health Monitoring (SHM) is an interdisciplinary engineering field aimed to inform about the working conditions of a structure so that the engineers and management are acquired in the real time and be able to make a decision. SHM know-how in recent decades dramatically increased safety and security level in different industries and help a lot in better insight into the material and structure behaviour such as endurance versus fatigue problems, aging, wear, corrosion, cyclic loading, harsh environmental applications, natural disasters etc. [1]. Generally, all of that makes SHM a powerful means to safe money both by direct avoidance of catastrophic scenarios or by substantial decrease of maintenance time of a structure.

Practically, every structure in use should be under some kind of monitoring: continuous, short- or long-term, local or global, etc. The most important are those “heavy” structures carrying the high potential risk such as nuclear power plants, dams, offshore platforms, ocean structures, pipelines, bridges, buildings, airplanes, railways, but also wind farms, turbine blades, museums and monuments, etc. [2].

There is a number of terrible examples that show how dramatic are consequences of collapsing of a construction. The newest and may be the most difficult is catastrophe in the Fukushima nuclear power plant in Japan caused by earthquake and tsunami with more than 25000 casualties. The World Bank estimated the cost of the nuclear crisis of about US$ 235bn, making it one of the world's most expensive disasters [3]. A second example is the sudden collapse of the Minneapolis Bridge caused loss of 13 lives, while 145 people were injured and accompanied economic losses of about US$ 400.000 per day for road users [2].

Some serious collapses have taken place in railway transportation too [4]. In Germany only in the last several years happened several catastrophic derailments causing in 2006, 23 killed people and 101 people died in 1998, when a high-speed train derailed near Eschede (see Fig. 1) [5]. Beside of direct causalities very often derailment of freight trains causes poisoning of soil or river by leakage of dangerous chemicals and goods. Lastly, in May 2011 near Freiburg in southern Germany occurred such an event [6].

The above several examples well illustrate that different structures are prone to deteriorating and eventually collapsing either new or old one. In order to mitigate risk, prevent catastrophe and schedule maintenance plan it is worth to deal with some kind of SHM. Today it is more feasible thanks to the remarkable progress in technical development of sensors, data acquisition, signal processing and analysis and communication.

There is a few major questions that SHM dealing with: a) if a damage exist in a structure at all? b) where the damage is? c) how severe the damage is? d) how long the service life is?

*Corr. Authorćs Adress: Integrated Microsystems Austria, Viktor Kaplan str. 2, 2700 Wr. Neustadt, Austria, djinovic@ima-mst.at

e) could we use the SHM data to design a more lightweight, more reliable and more cost efficient structure?

Fig. 1. *The WCR ICE 884 train derailed in Eschede 1998, Germany*

The goal of this paper is to try to offer possible answers by presentation of a (still) novel sensing technology based on optical fiber waveguides. This approach seems to be very close to an ideal copy of human being nervous system [7]. Primarily because optical fibers are tiny dielectric conductors, similar to nervous, that can be easily applied all around or embedded in the structure creating so called "smart" structure.

2 STRUCTURAL HEALTH MONITORING

Basically, SHM system consists of sensing network applied over or embedded into the structure. Ideally, the system should work in a closed loop configuration capable to detect, evaluate and alert the second part of the system, actuators to respond on the threat. The reaction could be immediately done or postponed through the repair, maintenance, and reconstruction depending on the degree of the malfunctions.

One of the main tasks of SHM is to detect the "hidden" structural failure in the early stage. Usually such failures are invisible for common nondestructive testing (NDT) of structures performed in the frame of regular maintaining schedule. Very often, damages such as cracks, caused by material fatigue, delamination in composite reinforced plastics (CRFP), displacement, etc. are the first origin of a malfunction. Fig. 2 depicts very well how a "hidden" crack of the wheel web (see arrow), caused breaking of the wheel and finally induced derailment of the entire freight train with dangerous chemicals [8].

Aforementioned structural disturbances belong to the mechanical phenomena that we can quantify as a change in time of strain, deformation, stress and load. However, structural health is affected with chemical and physical influence as well. Therefore a complete SHM has to be able to monitor data about pH, corrosion, temperature, humidity, etc.

There is a huge number of different structural health monitoring (SHM) techniques that are in use today: acoustic emission, ultrasound systems, Eddy currents, phased array, fiber-optics, etc. [9]. Various fiber-optic sensing techniques have found application in SHM systems, because of well-known features of optical fibers: EMI resistance, small size and weight, corrosion immunity, etc. [10,11].

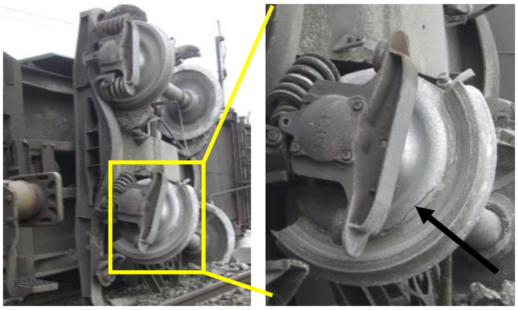

Fig. 2. *Derailment of the freight train in Neufchateau 2010, France caused by the wheel braking due to initial crack in the rim (detail)*

3 FIBER OPTIC SENSORS (FOSs)

3.1 Basic data

Optical fibers are tiny dielectric devices usually made of glass of specific structure composed of core, cladding and plastic coating. Typical telecommunication optical fibers, working at 1310nm of light wavelength, have core/cladding/coating diameter ratio of 9/125/250µm. This is a single-mode fiber characterized with step index geometry of refractive index of the core and mostly used for interferometric sensing configurations. For intensity modulation sensors are more convenient multi-mode fibers of 50/125µm, 62.5/125µm and 100/140µm, core/cladding ratio [12].

Nowadays, fiber optic technology is mature and finds a broad application in telecommunication industry causing tremendous decrease in price of fiber of about 0,1 US$ per meter. Telecommunication at all pushed a strong development of another optoelectronic devices especially light sources (laser diodes, superluminescent diodes, LEDs, etc.) as well as photodiodes and a list of different passive and/or active fiber optic devices. Under these circumstances starts developing of a niche field of fiber optic sensors (FOS).

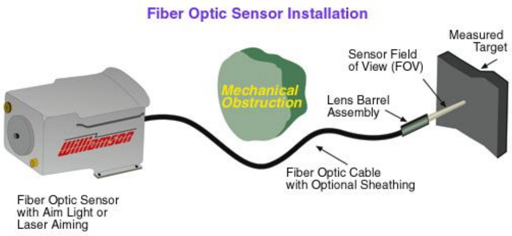

Fig. 3. *Typical configuration of a FOS composed of a light source, fiber optic cable and target.*

Basically, FOSs are composed of light source, fiber optic waveguide and transducer (Fig. 3). There is a huge number of different light sources but which one will be used depends on the concrete application of FOS. The most frequently used are high-coherence pig-tailed laser diodes emitting different wavelengths of lights from visible to near infrared. The most popular are those at about 1300nm and 1550nm since can be easy lunched into the single mode fibers for different sensing configurations. Superluminescent diode (SLD) is a light source that makes a compromise between powerful coherent laser and week low-coherence LED. Typical coherence length of a SLD diode is about 20-30µm. SLDs are available in all wavelength of interest (850, 1310, 1550nm). It is possible to couple it with single-mode fiber where can be introduced more than 1mW of the optical power.

There is a list of various photodiodes on the market. Two main groups are in use for FOS application; silicon photodiodes working at about 850nm and InGaAs photodiodes for spectral range at 1310 and 1550nm. Just behind the photodiode is a transimpendance amplificatory that prepare the raw signal for data processing and demodulation. Afterwards, we obtain the output signal in function of measurand affecting the fiber or transducer.

3.2 Adventages of FOSs in SHM

The main advantages of FOSs steam from the intrinsic properties of silica glass that is absolutely passive, dielectric, and with low attenuation of optical power at working optical frequency. Therefore FOSs are intrinsically immune to any electromagnetic interference (EMI). In comparison with classical electrical sensors, FOSs are obviously an ideal solution for usage in presence of strong EMI, radio frequency (RF), microwave (MW) or high-voltage (HV) radiation. These unique features naturally determine the field of application of FOSs. A good example of harsh environment application is for hot spots monitoring in high-power electric transformers by FO temperature sensor. Another illustration of great advantage of FOSs is they application for SHM of risky structures such as gas pipelines, mines, chemical plants etc. [13].

Silica glass is well known chemically inert and thermally stable material even at elevated temperatures till to 400-500°C. That brings additional advantages to FOSs to be applied in chemically harsh environment such as oil and gas wells, sparkplug engines, etc. [14,15]. Glass fibers are very resistant against corrosive effects of weathering that makes FOSs to be reliable part of the whole SHM system.

FOSs are relatively small and lightweight that is important for some applications in confined rooms or to be attached or embedded into the domicile matrix such as CFRP without disturbance of its initial characteristic.

Optical fibers provide a remote operation of FOSs since the distance between the reading and measuring points can be of many kilometers. This benefit comes due to extreme small attenuation of single-mode optical fibers.

Finally, equally important advantage of FOSs for SHM is an ability to be multiplexed providing in this way many measuring points along the sensing configuration and distributed measuring [16].

However, there is also some concerns about the FOSs too. At first it is still a new technology without standardization. Optical fibers are fragile and require a careful handling and manipulation. Usually, they need a special protection. The output signal is often nonlinear and "hidden" in raw noise signal and requires a complex demodulation technique. It can in some cases corrupt the reliability of FOS as a whole. Finally, despite of substantial decrease of price of several key fiber optic and optoelectronic components the whole system still have high cost, mainly induced by demodulation software/hardware subsystem, e.g. Optical Spectrum Analyzer (OSA)..

3.3 Clasification

There is several clasifications of FOSs in the art. At first we can devide them in terms of what parameter they measure. Generally, they can measure all *physical* and/or *chemical* parameters that can interact with the fiber optic waveguide itself or with an appropriate transducer inducing alternation of some of the light properties. Therefore, FOSs can measure: temperature, pressure, dispalacement/position, force/weight, strain/deformation, velocity, aceleration, amplitude of vibrations, pH, index of refraction, concentration, etc.

The aforementioned parameters tipically induce alternation of one or more characteristics of propagating light. According to this the FOSs can be considered as *intensity based, interferometric and spectrally encoded*.

Depending on the means of interaction between the external measurand and light properties, the FOSs can be devided as *extrinsic* or hybrid and *intrisic* or »all-in-fiber«. The first group requires a transducer along the fiber link or at the end of the sensing fiber to convert a measurand (e.g. pressure) into a more suitable parameter for measurement (e.g. position). In the second group a fiber optic waveguide directly overtakes an external disturbances causing light properties alternation (e.h. phase). The FOSs of this kind are more simple, the optical powe leak is smaller and rliability is higher.

In terms of means of application and sensing design the FOSs can be clasified as point, integrated, quasi-distributed and distributed [17]. The last group provides »spatial maping« of the monitored structure by means of simultaneous measurement of parameters of interest along the fiber link.

4 BASIC PRINCIPLES OF SOME FOS TECHNOLOGIES USED FOR SHM

4.1 Low-coherence interferometry

Measurement of main structural properties such as strain and deformation as well as damage detection in CFRP is based on low-coherence interferometry (LCI) [18], performed by an "all-in-fiber" interferometric configuration [19, 20]. The basic sensing configuration is shown in Fig.4. The central part of the interferometer is a 3×3 fiber-optic coupler, made of single-mode optical fiber. Such a configuration provides a passive stabilization of the signal, using a combination of the two low-coherence interferograms mutually shifted by $2\pi/3$.

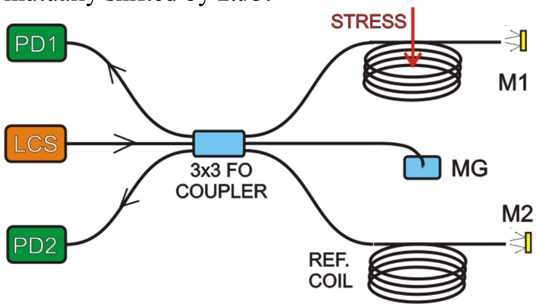

Fig. 4. *Low-coherence sensing set up; PD_1, PD_2-photodiodes, LCS-low-coherence source, MG-index matching gel, M_1, M_2–mirrors*

The low coherence light source (LCS) is coupled into an input arm of the 3×3 coupler; two receiving photodiodes (PD1 and PD2) are connected to the two other input arms. A sensing fiber optic coil is attached to one of the output arms. The other coil, having the same size and number of turns, is attached to the other output arm, making the reference path. Fiber tips of both arms face Al mirrors at a very close distance. The middle output arm is an unused fiber, immersed into the index matching gel (IMG), in order to avoid the back reflection from the fiber tip. The light back-reflected from the Al mirrors recombine in backward path within the 3×3 coupler, making two quasi-quadrature interferometric signals. These signals are captured by two photodiodes. Signal processing has been made of line in order to demodulate the raw photodiode signals.

When an external force acts on the fiber coil that carries optical signal, it induces the change of the optical path length in the sensing arm. Hence, the expression for the phase change induced directly from the stain applied is given by [14]:

$$d\phi = k \cdot d(n \cdot L) = k \cdot L \cdot \left(n \frac{dL}{L} + dn \right) \quad (1)$$

where: n is the refractive index of glass in the core region and L is the overall sensing length of the fiber. L is equal to $2\pi RN$, where R is the coil radius an N is the number of the turns. The term ndL reflects the physical change of the fiber length while the term Ldn reflects the change of the refraction index of glass.

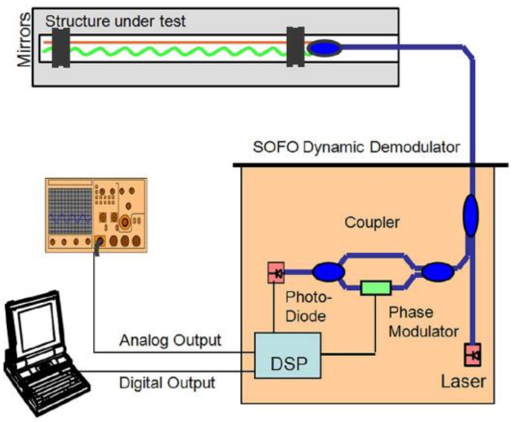

Fig. 5. *Conceptual illustration of SOFO Dynamic.[23]*

Basically, the same principle uses the SOFO system, (Fig. 5), composed of a low-coherence double Michelson interferometer. The first interferometer is sensing one, made of the sensing and reference arms, while the second, i.e. the reading one is packed in the portable unit. The SOFO precision and stability obtained by one year of laboratory and field tests is 2 μm, regardless of the total length of the fiber optic arms. The system is developed at the IMAC laboratory of the Swiss Federal Institute of Technology in Lausanne (EPFL) and fabricated and commercialized by Smartec SA as a part of the Roctest Group [21-23].

The main characteristic of this system is ability to measure elongation of a structure, primary in civil engineering, by embedding the *long-gage transducers* into concrete.

Another FOS type having *short-gage transducers* is also very popular as a point sensor. It operates on Fabry-Perot interference principle. The sensor design is consisting of two parallel mirrors forming an interference cavity along the optical fiber. The measurand changes the length of the cavity or the index of refraction of the medium between the mirrors, causing changes in the interference between the beams. By using high- or low-coherence light in the sensing fiber it is possible to get a characteristic interference pattern and measure very precisely the cavity length in dependence on the measurand magnitude. FISO technology patented a low-coherence, i.e. white-light interferometer and fabricated a whole family of different point FOSs for strain, temperature and pressure measurement [23].

4.2 Fiber Bragg Grating (FBG) technology

Common FBG structure (Fig. 6) is characterized with a periodic alternation of index of refraction of glass core of single-mode fiber-optic waveguide over a sensing length. Lunching a broadband light into the single-mode fiber with already written FBG therein a portion of light will be back-reflected as a narrow spectral peak with distinctive wavelength. This is so called Bragg-wavelength, λ_B and it is given by eq. (2) [25]:

$$\lambda_B(T, \varepsilon_i) = 2 \cdot n_{eff}(T, \varepsilon_i) \cdot \Lambda(T, \varepsilon_i) \quad (2)$$

where n_{eff} and Λ are the average refractive index and grating period, respectively. We can see that temperature, T and strain ε_i, could simultaneously alternate the Bragg-wavelength if a FBG suffers an external thermal or mechanical load. It is described by eq. (3) [25]:

$$d\lambda_B(T,\varepsilon_i)=\frac{\partial\lambda_B}{\partial T}dT+\frac{\partial\lambda_B}{\partial\varepsilon_i}d\varepsilon_i \quad (3)$$

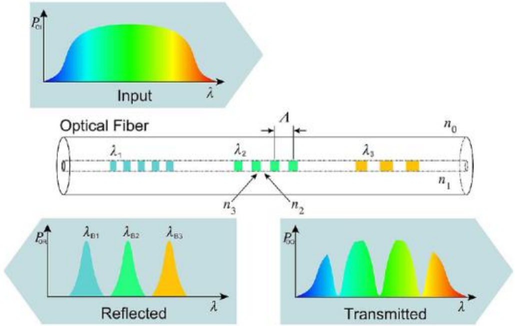

Fig. 6. *Illustration of the fiber Bragg grating concept and its optical function. It should be noted that* $\lambda_B=2n_{eff}\Lambda$

Fig. 7a shows a shift of Bragg wavelength Δλ caused by uniform tensile and thermal stress along the axial direction of the subjected FBG sensor. In this case the FBG sensor behaves as an array of Fabry-Perot (F-P) interferometers undergoing a uniform increase of separation between the F-P mirrors. However, the main feature of FBG, to be a sort of interference filter, is saved so the shifted peak (dashed line in Fig 7a) has the same intensity and width, w_0 as original one. The peak shift Δλ of a FBG sensor, exposed to different mechanical and thermal loads, is modeled by Scheerer et al. [26].

The main problem of standard FBG sensors is how to separate the useful signal, caused by strain, from a parasitic one, like temperature effects, which is for an order of magnitude higher. One approach [27] is to use two FBGs in close proximity to one another. The strain sensitive FBG has to be firmly fixed to the subjected structure while the second FBG should loosely float nearby. By another technique the strain sensitive FBG should be used together with some kind of temperature sensor [27]. In both cases it is necessary to have independent data about the temperature and strain and to normalize the useful strain signals for the spectrum peak sift caused by the temperature effect.

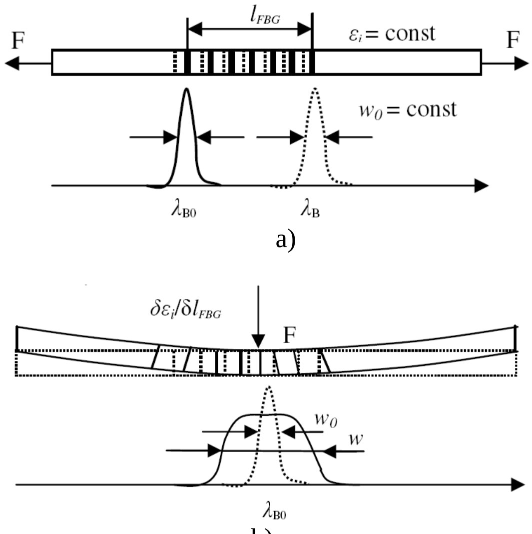

Fig. 7. *a) FBG sensor under uniform strain and b) FBG sensor under gradient strain*

In Fig. 7b we present another solution for avoiding the parasitic temperature effect [29]. That is the case when a FBG sensor is exposed to an external force F in the transversal direction that induces bending of the fiber and strain gradient δεi/δl in it. It is the main reason for the alternation of uniform periodical structure of refractive index in the FBG sensing area. The FBG loses now the Fabry-Perot structure and reflective mirrors are not any more planparallel. Contrary, they make an array of wedges becoming, in this way, a characteristic configuration of a Fizeau interferometer. The back-reflected spectrum keeps the central value of the Bragg-wavelength λ_{B0} but bandwidth of the spectrum increases due to taking part in the interference of light beams of different wavelengths. It is proven in the work [26] that thermal load had no effect on the broadening of the spectrum peak.

The spectrum width *w* directly depends on the averaged strain gradient in the fiber, i.e. on the average strain ε_i and this is defined by eq. (4) [26]. Therefore, if we measure a relative change $\Delta w/w_0$ of the back-reflected spectrum by an OSA we are able to evaluate the strain magnitude in the fiber, i.e. in the monitoring structure caused by some sort of damage.

$$\frac{\Delta w}{w_0}=k\cdot\frac{\partial\varepsilon_i}{\partial l} \quad (4)$$

where: Δw is spectrum width difference between the load and unload FBG, k is a proportional constant that depends on the real sensor parameters and has to be determined by the experimental measurements.

4.3 FOS technology based on light scattering phenomena

There are three main scattering phenomena in optical fibers that can be exploited in distributed sensing. They are Rayleigh, Raman and Brillouin scattering. Brillouin scattering occurs when traveling light inelastically scattered backward by interaction with acoustic phonons [30]. Brillouin scattering causes a frequency shift with of the incident light proportional to the acoustic velocity within a fiber. The frequency shift magnitude is called Brillouin frequency shift ν_B and it is given by [31]:

$$\nu_B = \frac{2n \cdot V_a}{\lambda} \qquad (5)$$

where n is the fiber-core refractive index, V_a is the acoustic velocity and λ is the light wavelength. The shift is about 11GHz at a wavelength of 1550 nm. It was reported that the Brillouin frequency shift in silica fibers varies greatly with strain and temperature [32,33]. The strain and temperature coefficients of the ν_B change are given by [34]:

$$\frac{d\nu_B}{d\varepsilon} = 49{,}3GHz \quad \frac{d\nu_B}{dT} = 1{,}00MHz/^{\circ}C \qquad (6)$$

This fact was used for design and fabrication of distributed FOS for simultaneous measurement and monitoring of strain and temperature over subjected structure. Stimulated Brillouin Scattering (SBS) can increase sensitivity of the system. It can be achieved by using two optical light waves; optical pulse or pump in addition with a continuous wave (CW), e.e. the probe signal. Such a technique, known as Brillouin optical time domain analysis (BOTDA), Fig. 8, are already in use for measurement of local changes in the Brillouin shift along the sensing fiber. As with conventional OTDR, the spatial resolution, δz, of BOTDR is determined by:

$$\partial z = \frac{\nu \cdot W}{2} \qquad (7)$$

where ν is the light velocity in the fiber and W is the incident width of the pulsed light. The spatial resolution of BOTDR is generally more than 1m and the accuracy for strain measurement is about ±30με along the fiber length of about 10km to 30km.

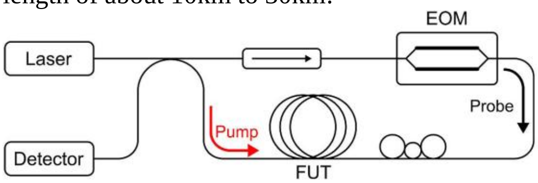

Fig. 8. *Schematic presentation of basic setup of BOTDA.*

The Rayleigh-scattered light is used to measure the attenuation profiles of long-haul fiber-optic links using Optical Time Domain Reflectometry (OTDR). These profiles are very useful to localize breaks, to evaluate splices and connectors and, in general, to assess the overall quality of a fiber link [35].

The Raman-scattered light is used for temperature distributed sensors, recording the ratio between the anti Stokes and Stokes side-lobes ratio of the Raman scattering spectrum.

5 SOME LABORATORY EXAMPLES OF FOS TECHNOLOGIES FOR SHM

5.1 Strain and deformation measurement by FO low-coherence interferometry

Experiments have been performed using set up shown in Fig.4. Both coils, the sensing and the reference, are terminated with bare fiber tips, directed towards Al mirrors. The mirror at the reference arm was firmly fixed on the motorized DC stage. The stage was used to scan the optical path difference, in order to find the position of the first and second interferometric pattern. Then, the reference mirror is placed in the central zone of the second interferometric pattern.

The tested beam of overall size 250x25x1.3 mm was made of carbon reinforced thermoplastic composite. The sensing coil was bonded underneath of the beam, in direction of acting the compression nose. The composite beam and the sensing coil in the middle of the sample are shown in Fig. 9. The three-point loading test was performed against the composite beam using a compression nose and two supporting lines in a tensile test mashine

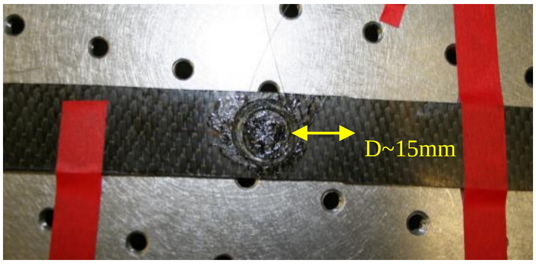

Fig. 9. *Photo of a fiber-optic coil 15mm in diameter glued in the middle of the CFRP beam*

We simultaneously acquired the two photodiode signals during the three-point loading test. After signal processing using the algorithm given in depth in [18], the two resulted photodiode signals are presented in Fig.10, in a Lissajous form. We can see a characteristic spiral shape of the interferometric signal , illustrating the pass of the phase change through several interferometric fringes, during the three-point loading test.

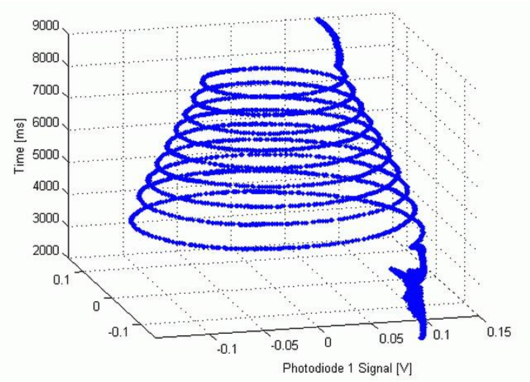

Fig. 10. *Time change of processed photodiode signals in Lissajous presentation [19]*

The calculated optical path change during the loading test, is shown in Fig. 11. The abscissa of the graph in Fig. 11 is obtained from the stress/strain diagram recorded during the test, the strain is calculated using deflection data of the beam.

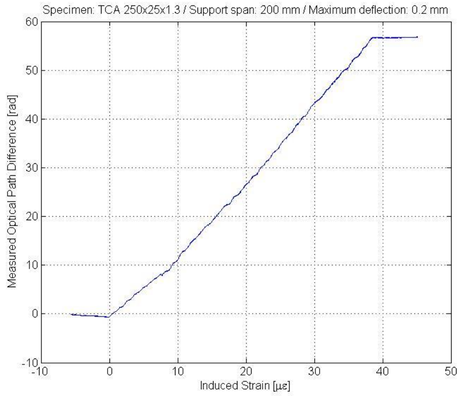

Fig.11. *Interferometer optical path change vs. strain in composite/coil, induced by 0.2 mm specimen deflection [19]*

.

5.2 Failure detection by a FO low-coherence interferometry

Experiments have been done using a sensing set up shown in Fig. 4.

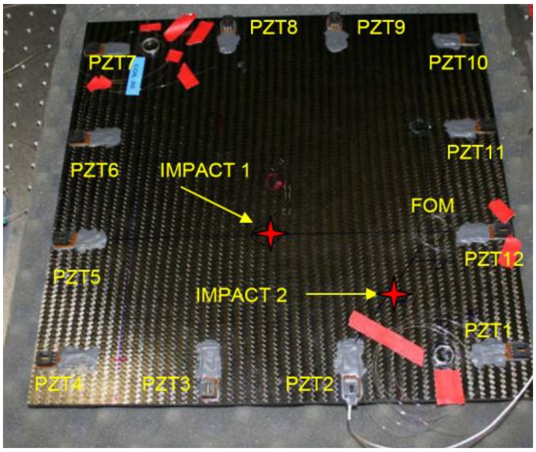

Fig. 12. *Photo of the subjected CFRP plate with FO sensing coil denoted as FOM [20]*

The CFRP plate (Fig.12) of overall size of 350x350x5mm made of 16plys was equiped by the sensing coil (FOM) and piezo ceramic transducers (PZT) actuators. In experiments we exposed the sensing fiber coil to an external vibrations caused by PZT actuators in frequency range from 40 to 200kHz at 50Vpp. We measured the interferometric signals before and after the impact of about 10J of applied energy.

Using the raw photodiode signals and »arc-tan« algorithm we performed data processing in order to demodulate the optical phase signal. In Fig. 13 we present the demodulated and normalized signals before (blue) and after (green) the impact of 10J applied between the PZT No.2 and fiber-optic coil (see Fig. 12). We can note a frequency change of phase response curve that proves the existence of the failure on the plate.

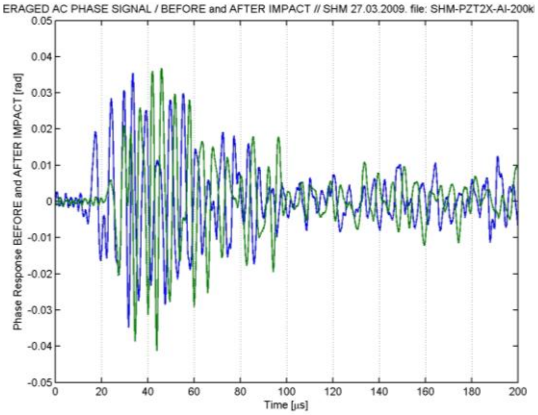

Fig. 13. *Demodulated FOS signals before (blue) and after (green) impact [20]*

5.3 Impact damage detection of composite materials by FBGs

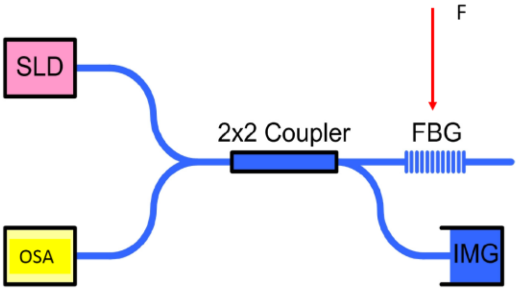

Fig. 15. S*etup for impact damage detection by measuring of spectrum width of FBG [29]*

In this investigation we used a sensing configuration schematically presented in Fig. 15. A 2x2 coupler made of single-mode fiber 4/125/250µm was connected to a pig-tailed superluminescent (SLD) diode of 830nm of emitting light. The second input arm was interrogated with an Optical Spectrum Analyzer (OSA) of about 1nm resolution. One output arm was connected to the subjected FBG sensor. The second output arm was inactive and was immersed into the index matching gel (IMG). The arrow depicts the transversal direction of mechanical load denoted by F.

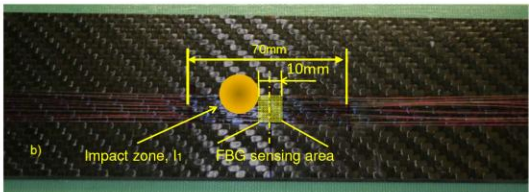

Fig. 16. *CRFP plate used for the impact damage test by FBGs [29]*

In Fig. 16 we present a rectangular composite plate with overall dimensions of 400x80x4mm with 8 plies that we used for the impact test. The used impact energy was 10J and 20J. The later impact was marked as circle nearby the sensing area of 10 FBSs.

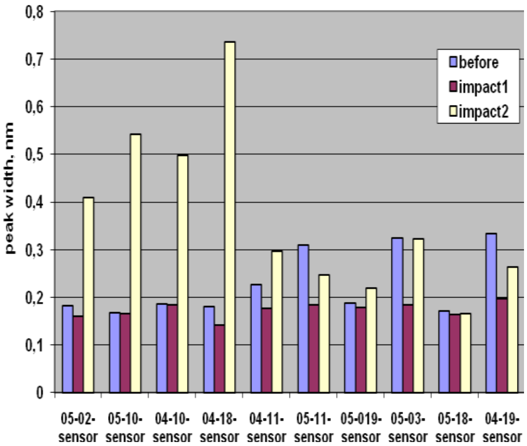

Fig. 17. Spectral p*eak width of FBGs before, after the first and second impact of 20J*

Before impact campaigns we measured the back-reflected spectrum of FBGs in the virgin state. Center wavelength λ_{B0} was determined by calculating the center of gravity of the spectrum, while the width *w* of the spectrum was calculated as the width of a rectangular with equal area [26].

Analysing the acquired FBG spectrum we observed an increase of width as a result of strain gradient induced in the plate, i.e. in the by impact affected FBG sensors. We didn't note such effect in the virgin plate. The final results are graphically presented in Fig. 17 after signal processing of raw data.

6 SOME INDUSTRIAL EXAMPLES OF FOS TECHNOLOGIES FOR SHM

There is a long list of examples of application of some kind of SHM system in industry. FOS technologies have found a broad application in monitoring of civile engineering structures (bridges, buildings, dams, hystorical monuments, etc.) as well as for continuous monitoring of gas and oil pumplines [17]. We will focus here more on FOSs for SHM in wind turbines and transportation structures such as railway and aircrafts.

6.1 FOSs for SHM of wind turbines

Nowadays there is a lot of wind farms all around the world (Fig. 18). They are exposed to severe weathering and loading conditions that sometimes induces failing of the system. Practically, every mechanical part could decline but mostly failed the rotor blades. They are produced of CFRP so FOS, such as FBGs or Brillouin technology [17] can be used for on line monitoring as embedded or attached sensing network.

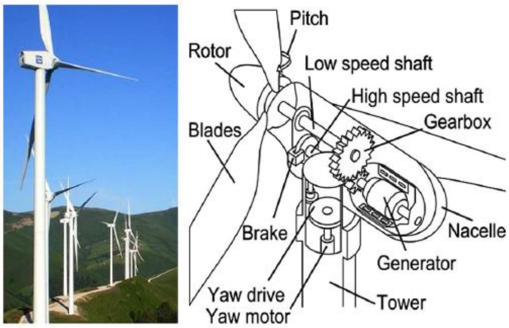

Fig. 18. *Wind turbine and details of key subsystems to be monitored [17].*

6.2 FOSs for SHM of transportation structures

High speed trains and freight wagons needs some kind of SHM because of extreme working conditions and overloading. It is well known that wheels and axels due to hidden fatigue cracks can suddnly colapse even if they passed regular masintaining test (see Fig. 1).

In order to suppres such events it is necessatry to equip these structural elements with FOSs for on-line monitoring and evaluation abouut the cracks, obverheating, or another irrehularities. A lot of can be known based on vibrational spectra acquired by FOS demonstrated in Ch. 5.2

BOTDR or FBGs can be used for distributed measurement of railway parameters like rail imbalance, train speed or weight. Fig. 19 shows response of FBG sensor installed on rail track in order to follow up the “weight in motion” of freight wagons [36].

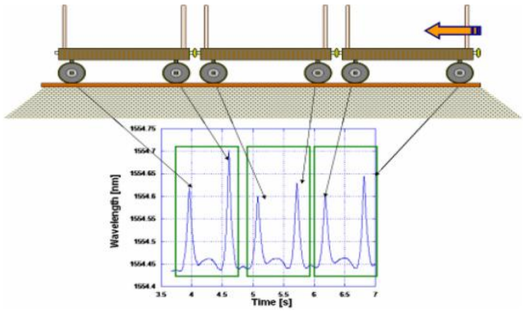

Fig. 19. *Response of a single FBG sensor subject to running trains [36]*

Aircraft transportation is very dimanding field from technical pointr of view due to very sharf working conditioons. Beside of regular on ground check through the maintenance procedure there is a need for »on board« monitoring of crucial structural parts. Fig. 20 shows some of them. Some metal parts are going to be substituted by CFRP composite materials where another challenges occure. For example, cracks of fabrics, delamination, etc.

It seems that FOSs are the best solution to be used for »on board« monitoring of structural composite parts . This may be done either by emmbeding or attaching the FBG [17] or another sensors such as those described in Ch. 5.1, 5.2. and 5.3.

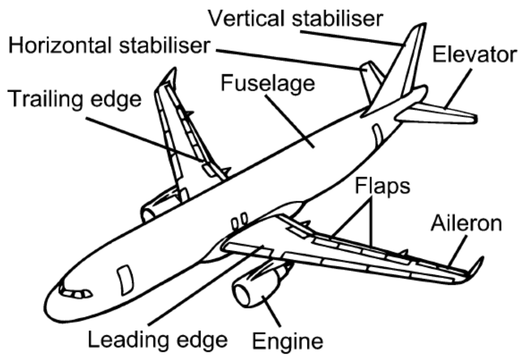

Fig. 17. Schematic presentation of several *aircraft parts that need a SHM [17].*

7 CONCLUSION

We presented several advantages fiber-optic sensing technology that can be used for SHM of different "heavy" structures in civil engineering, transportation, wind power farms, etc. We particularly highlighted the low-coherence interferometry (LCI) as a common platform for different sensor solutions. Using this technique have been already realized reliable average strain and temperature sensors. We also presented several laboratory examples of specific sensors aimed for damage and deformation detection of CFRP by LCI. Further, through several industrial applications we have illustrated the capability for quasi-distributed and fully distributed measurement of strain and temperature by FBG and Brillouin scattering based sensors.

ACKNOWLEDGMENT

The authors would like to thank the Integrated Microsystems Austria for the partial support of this paper.

8 REFERENCES

[1] B. Glisic, D. Inaudi, N. Casanova, "SHM process as perceived through 350 projects," in Smart Struct Mater./NDE Symp., San Diego, CA, 2010, p. 76480P.

[2] M. Enckell, "Structural Health Monitoring using Modern Sensor Technology- Long-term Monitoring of the New Årsta Railway Bridge", PhD, KTH, September 2006

[3] USDOT, FHWA, and FTA, 2006 Status of the Nation's Highways, Bridges and Transit: Conditions and Perfomance 2007.

[4] www.derailments.com

[5] http://pbma.nasa.gov/docs/public/pbma/general/derailed.pdf

[6] http://www.china-daily.org/China-News/Train-derailment-in-southern-Germany-caused-by-leakage-of-dangerous-goods/

[7] É. Pinet, C. Hamela, B.Glišić, D. Inaudi, N. Miron, "Health monitoring with optical fiber sensors: from human body to civil structures", SPIE Smart Structures and Materials & Nondestructive Evaluation and Health Monitoring, 14th International Symposium, 18-22 March 2007, San Diego, California USA

[8] www.oebb.at/infrastruktur/__resources/llShowDoc.jsp?nodeId.

[9] S.Mancini, G. Tumino, P. Gaudenzi, "Structural Health Monitoring for Future Space Vehicles", Journal of Intelligent Material Systems and Structures 17(7), 577-585 (2006)

[10] G. Zhou1, L.M Sim, "Damage detection and assessment in fibre-reinforced composite structures with embedded fibre optic sensors", Smart Mater. Struct., 11(6), 925-939 (2002)

[11] C.K. Kirkendall, C.K. A. Dandridge, "Overview of high performance fiber-optic sensing", J. Phys. D: Appl. Phys., 37(18), 197-216 (2004).

[12] http://www.corning.com/opticalfiber/

[13] D. Inaudi, B. Glišić "Long-range pipeline monitoring by distributed fiber optic sensing", Proc. IPC2006, 6th Int. Pipeline Conf. (Calgary, Al, Canada), Sept. 25th-29th (2006).

[14] D. Inaudi, B. Glišić "Integration of distributed strain and temperature sensors in composite coiled tubing", SPIE Smart Struct. and Mat. Conf. (San Diego, Ca, USA), Feb. 27th-March 2nd (2006).

[15] 7. T. Bae et al. "Interferometric fiber-optic sensor embedded in spark plug for in-cylinder pressure measurement in engines", Appl. Opt., Vol. 42 (6), pp. 1003-1007 (2003).

[16] J. M. Lopez-Higuera, "Introduction to optical fiber sensor technology," in

Handbook of Optical Fibre Sensing Technology, J. M. Lopez-Higuera, Ed. New York: Wiley, 2002, pp. 1–21.
[17] J. M. Lopez-Higuera, L. R. Cobo, A. Q. Incera, A. Cobo, “Fiber Optic Sensors in Structural Health Monitoring”, Journal of Lightwave Technology, 29 (4) 587-608 (2011)
[18] M. Tomic, J. Elazar, Z. Djinovic, “Low-coherence interferometric method for measurement of displacement based on a 3x3 fibre-optic directional coupler”, J. Opt. A: Pure Appl. Opt., 4, 381 (2002)
[19] M. Tomic, Z. Djinovic, “Strain and Deformation Measurement Using Intrinsic Fiber Optic Low Coherence Interferometric Sensor”, Proc. of the 32nd MIPRO 09, Opatija, Croatia, 25.-29. May 2009
[20] Z. Djinovic, M. Tomic, M. Stojkovic, G. Schmid,” Failure Detection by a Fiber Optic Low Coherence Interferometric Sensor”,The Fifth European Workshop on SHM, Sorrento, Italy, 29. 06 -0 2. 07.2010
[21] D. Inaudi, “Photonic sensing technology in civil engineering,” in Handbook of Optical Fibre Sensing Technology, J.M. Lopez-Higuera, Ed. New York: Wiley, 2002, pp. 517–542.
[22] S. Casciati, M. Domaneschi, D. Inaudi, “Damage assessment from SOFO dynamic measurements,” in 17th Int. Conf. Opt. Fibre Sens.,Parts 1 and 2, , vol. 5855, pp. 1048–1051, 2005
[23] www.smartec.ch
[24] US 5,202,939 & 5,392,117
[25] V.G. Schlüter, „Entwicklung eines experimentell gestützten Bewertungsverfahrens zur Optimierung und Charakterisierung der Dehnungsübertragung oberflächenapplizierter Faser-Bragg-Gitter-Sensoren“, BAM-Dissertationsreihe - Band 56, Berlin 2010
[26] M. Scheerer, P. A. Hahn, , A. Pönninger, T. Goss, A. Reutlinger,“Simultaneous Monitoring of Strain and Temperature in Composite Materials by one single FBG Sensor” Proc. of the 6th International Workshop on SHM, Sept 11th – 13th 2007, Stanford, US
[27] W.W. Morey,"Fiber Optic Grating Technology", Proc. SPIE 2574, 22-31 (1995).
[28] H. K. .Kang, C. Y. Ryu, C. S.Hong, C. G. Kim, “Simultaneous Measurement of Strain and Temperature of Structures Using Fiber Optic Sensor”, Journal of Intelligent Material Systems and Structures 12, 277-281 (2001).
[29] Z. Djinovic, M. Scheerer, M. Tomic, “Impact Damage Detection of Composite Materials by Fiber Bragg Gratings”, SPIE Conference 8066, Smart Sensors, Actuators and MEMS, Prag, Czech Republik, 18-20 April 2011
[30] J. Dakin, B. Culshaw, “Optical Fiber Sensors”, Vol. 4, ArtechHouse, Inc., Norwood, MA. (1997)
[31] D. Cotter, “Stimulated Brillouin Scattering in Monomode Optical fiber”, J. Opt. Commun., 4(1),10–19 (1983)
[32] D. Culverhouse, F. Farahi, C.N.Pannel, D. A. Jackson, “Potential of Stimulated Brillouin Scattering as Sensing Mechanism for Distributed Temperature Sensors”, Electronics Lett., 25(14), 913–915 (1989)
[33] T. Horiguchi, T. Kurashima, M. Tateda, “Tensile Strain Dependence of Brillouin Frequency Shiftin Silica Optical Fiber”, IEEE Photonics Tech. Lett., 1(5), 107–108 (1989)
[34] T. Kurashima, T. Hogari, S. Matsuhashi, T. Horiguchiand, Y. Kyamoda, H. Hirano, “Measurement of Distributed Strain in Frozen Cable and Its Potential for Use in Predicting Cable Failure” , in: International Wire and Cable Symposium Proceedings, pp. 593–600 (1994).
[35] X. Y. Bao, C. Huang, X. D. Zeng, A. Arcand, P. Sullivan, “Simultaneous strain and temperature monitoring of the composite cure with a Brillouin-scattering-based distributed sensor,” Opt. Eng., 1(7)1496–1501 (2002)
[36] A. Cutolo, A. Cusano, F. A. Bruno, A. Iele, A. Laudati, G. Parente, M. Giordano, G. Breglio, N. Mazzino, A. Bocchetti” Weight in Motion using Fiber Bragg Grating Sensors: An Industrial Case in Italy”,The Fifth European Workshop on SHM, Sorrento, Italy, 29.06- 02.07. 2010

HEAVY MACHINERY - HM 2011, 25-29
ISBN 978-86-82631-58-3
Paper accepted: 30.05.2011

Logical Aggregation and Real-Valued Realization of Finite Boolean Algebra

D. Radojevic[1,*]
[1]Mihajlo Pupin Institute, University of Belgrade, Volgina 15, 11060 Belgrade, Serbia

Abstract: *The aggregation of many features into one representative is relevant for quite different research areas such as: social science, engineering (control engineering), computer science, psychology, etc. In this paper, aggregation is treated as a logical and/or pseudo-logical operation . Aggregation function in a general case is the weighting sum of partial demands. Partial demands for pseudo-logical operation can be adequately described only by logical functions of analyzed attributes. Any logical function can be uniquely transformed into a corresponding generalized Boolean polynomial, using real-valued realization of finite Boolean algebra, known as Interpolative Boolean algebra . It is interesting that most of conventional aggregation operators (for example Choquet integral and fuzzy measure) are only the special cases of logical aggregation operators. In this paper is given technical realization of real-valued Boolean algebra and its application in logical aggregation as a transparent way of aggregation.*

Keywords: *Aggregation, pseudo-logical operation, Boolean polynomial, Choquet integral, fuzzy measure*

1 INTRODUCTION

The aggregation of many features into one representative is relevant for quite different research areas such as: *social science, engineering, computer science, psychology*, etc. In this paper, aggregation is treated as a logical and/or pseudo-logical operation (LA). Aggregation function in a general case is the weighting sum of partial demands. Partial demands for LA can be adequately described only by logical functions of analyzed attributes. Any logical function can be uniquely transformed into a corresponding generalized Boolean polynomial, using real-valued realization of finite Boolean algebra, known as Interpolative Boolean algebra (IBA) [1]. It is interesting that most of conventional aggregation operators (for example Choquet integral and fuzzy measure [2], [3], [4]) are only the special cases of logical aggregation operators.

The motives that gradation should be treated in the Boolean frame and/or way real-valued realization of Boolean algebra is necessary for consistent realization of fuzzy logic are [5], [6], [7]:

- According to G. Boole, the laws of cognition are defined by Boolean algebra. From our point of view, Boolean algebra defined laws of cognition as a fundament for thought as a roof. It means that cognition laws are independent (indifferent) from application domain. Classical realization of Boolean algebra: two-valued Boolean arithmetic is fundament for black and white view, which is adequate for classical mathematic, physics (except quantum physics).

- The main reason for introducing the gradation, as a fundament of fuzzy logic in wider sense, is reducing of (cognition) complexity and/or possibility to do more with less information. The gradation is inherent for some problems and black-white approach is inadequate (known paradoxes, quantum physics, etc.). We suppose that laws of cognition and/or thought would not be changed in the case of introducing gradation and as a consequence real-valued realization of Boolean algebra is necessary.

Real-valued realization of finite (atomic) Boolean algebra (RVR-BA) [1] , [2] preservation of all algebraic properties – all axioms and theorems of Boolean algebra in general [0, 1] case. As a consequence all theories based on classical realization {0, 1} of finite Boolean algebra, using RVR-BA, can be generalized straight away. Fuzzy logic in wider sense: theory of fuzzy sets, fuzzy logic and fuzzy relations

[*] Corr. Author's Address: Mihajlo Pupin Institute, University of Belgrade, Volgina 15, 11060 Belgrade, Serbia, dragan.radojevic@pupin.rs

based on RVR-BA are Boolean consistent generalization of classical theory of sets, classical logic and classical relations retrospectively (contrary to conventional fuzzy logics based on truth functional principle).

In this paper is given technical realization of real-valued Boolean algebra and its application in logical aggregation as a transparent way of aggregation.

2 GENERALIZED BOOLEAN POLYNOMIALS

Primary Boolean elements (attributes, properties, relations) define a finite set $\Omega=\{a_1,...,a_n\}$. Boolean algebra generated by primary set of attributes is $BA(\Omega)=\mathrm{P}(\mathrm{P}(\Omega))$. Any element of Boolean algebra $\varphi\in BA(\mathbf{\Omega})$ can be represented by the canonical disjunctive normal form:

$$\begin{aligned}\varphi &= \bigcup_{S\in\mathrm{P}(\Omega)|\sigma_\varphi(S)=1}\alpha(S),\\ &=\bigcup_{S\in\mathrm{P}(\Omega)}\sigma_\varphi(S)\bigcap_{a_i\in S}a_i\bigcap_{a_j\in\Omega\setminus S}Ca_j.\end{aligned}\tag{1}$$

where:

$$\alpha(S)=\bigcap_{a_i\in S}a_i\bigcap_{a_j\in\Omega\setminus S}Ca_j,\quad S\in\mathrm{P}(\Omega);$$

$\alpha(S),\ \ S\in\mathrm{P}(\Omega)$ *are atomic Boolean elements* [1], which are the simplest elements of $BA(\mathbf{\Omega})$ in the sense that they do not include in themselves anything except for a trivial Boolean constant 0;

$\sigma_\varphi:\mathrm{P}(\Omega)\to\{0,1\}$ is a *structural function* [1] of analyzed element $\varphi\in BA(\Omega)$ that determines which atomic elements are included in it and/or which are not.

Any element of Boolean algebra on a value level can be represented by a *generalized Boolean polynomial* [1]:

$$\varphi^{\otimes}(x)=\sum_{S\in\mathrm{P}(\Omega)}\sigma_\varphi(S)\alpha^{\otimes}(S)(x)\tag{2}$$

A generalized Boolean polynomial $\varphi^{\otimes}(x)$ enables calculating the value of a corresponding Boolean element (analyzed property and/or relation) $\varphi\in BA(\Omega)$ for an analyzed object $x\in X$.

Boolean polynomial of atomic elements $\alpha^{\otimes}(S)(x)$, is defined by the following expression [1]:

$$\alpha^{\otimes}(S)(x)=\sum_{K\in\mathrm{P}(\Omega\setminus S)}(-1)^{|K|}\bigotimes_{a_i\in K\cup S}a_i(x)\tag{3}$$

where: $S\in\mathrm{P}(\Omega)$, $x\in X$, and operator $\otimes$ is a generalized product [1].

Example: *Generalized discrete Choquet integral is defined by the following expression [8]:*

$$GC_\mu\left(a_1^v,...,a_n^v\right)=\sum_{k=1}^{n+1}\left(a_{(k)}^v-a_{(k-1)}^v\right)\mu\left(A_{(k)}\right),$$

where:

$$a_{(1)}^v\le...\le a_{(n)}^v\le a_{(n+1)}^v=1;\quad A_{(k)}=\left\{a_{(k)},...,a_{(n)}\right\};$$
$$A_{(n+1)}=\varnothing;\quad \mu(\varnothing)\in[0,1].$$

In the case of 0-1 mesure $\mu_\varphi(S)=\sigma_\varphi(S)\in\{0,1\}$ *Generalized discrete Choquet is a special case of GBP with a generalized product* $\otimes:=min$ *:*

$$\begin{aligned}GC_\mu\left(a_1^v,...,a_n^v\right)&=\varphi^{min}\left(a_1^v,...,a_n^v\right)\\ &=\sum_{S\in\mathrm{P}(\Omega)}\sigma_\varphi(S)\sum_{C\in\mathrm{P}(\Omega\setminus S)}(-1)^{|C|}\min_{a_i\in S\cup C}a_i^v\end{aligned}$$

To the generalized discrete Choquet integral for 0-1 measure corresponds a consistent real-valued logical function. In the case of discrete Choquet integral for monotone 0-1 measure there corresponds only a monotone real-valued function.

A generalized Boolean polynomial (GBP) can be represented as a scalar product

$$(\varphi)^{\otimes}(x)=\vec{\sigma}_\varphi\vec{\alpha}^{\otimes}(x)$$

of the following two vectors: (a) *structural vector* of analyzed Boolean function (element of Boolean algebra) [3]:

$$\vec{\sigma}_{\varphi}=\left[\sigma_{\varphi}\left(S\right)\middle|S\in\mathrm{P}\left(\Omega\right)\right]\ ,\tag{4}$$

and (b) *vector of atomic Boolean polynomials*

$$\vec{\alpha}^{\otimes}\left(x\right)=\left[\alpha^{\otimes}\left(S\right)\left(x\right)\middle|S\in\mathrm{P}\left(\Omega\right)\right]^{T}\ .\tag{5}$$

For structural functions of Boolean algebra elements all Boolean axioms and theorems are valid [1].Actually, a Boolean polynomial maps a corresponding element of Boolean algebra into its value from the real unit interval [0, 1] on the value level so that a partial order on the value level is preserved contrary to other MV and/or fuzzy approaches.

Direct transformation of any Boolean function (element of finite Boolean algebra) into a corresponding GBP is given by the following procedure:

$$\begin{aligned}
&F\left(a_1,...,a_n\right),G\left(a_1,...,a_n\right)\in BA\left(\Omega\right)\\
&\left(F,G\in BA\left(\Omega\right)\right)\\
&\left(F\wedge G\right)^{\otimes}=_{def}F^{\otimes}\otimes G^{\otimes},\\
&\left(F\vee G\right)^{\otimes}=_{def}F^{\otimes}+G^{\otimes}-\left(F\wedge G\right)^{\otimes},\\
&\left(\neg F\right)^{\otimes}=_{def}1-F^{\otimes}.
\end{aligned}\tag{6.1}$$

$\vdots$

$$\begin{aligned}
&\left(a_i\wedge a_j\right)^{\otimes}=_{def}\begin{cases}a_i\otimes a_j,\ i\neq j, & \left(\otimes\in\left[Luk,min\right]\right)\\ a_i, \qquad i=j, & \left(\otimes=_{def}min\right)\end{cases}\\
&\left(a_i\vee a_j\right)^{\otimes}=_{def}a_i+a_j-\left(a_i\wedge a_j\right)^{\otimes};\\
&\left(\neg a_i\right)^{\otimes}=_{def}1-a_i;\\
&\left(a_i,a_j\in\Omega\right).
\end{aligned}\tag{6.2}$$

3 GENERALIZED PSEUDO BOOLEAN POLYNOMIAL

To every element of IBA corresponds a generalized Boolean polynomial with the ability to process all values of primary variables from a real unit interval [0, 1]. A *pseudo-Interpolative Boolean polynomial* is a *linear convex combination of analyzed elements of IBA – generalized Boolean polynomials:*

$$\begin{aligned}
&\pi\varphi^{\otimes}\left(a_1^v,...,a_n^v\right)=\sum_{i=1}^{m}w_i\varphi_i^{\otimes}\left(a_1^v,...,a_n^v\right),\\
&\sum_{i=1}^{m}w_i=1,\ w_i\geq 0,\ i=1,...,m.
\end{aligned}\tag{7}$$

From the definition of generalized Boolean polynomials, *an interpolative pseudo-Boolean polynomial* is given by the following expression:

$$\begin{aligned}
\pi\varphi_{\mu}^{\otimes}\left(a_1^v,...,a_n^v\right)=&\sum_{S\in\mathrm{P}(\Omega)}\mu\left(S\right)\cdot\\
&\cdot\sum_{C\in\mathrm{P}(\Omega\backslash S)}\left(-1\right)^{|C|}\bigotimes_{a_i\in S\cup C}a_i^v.
\end{aligned}\tag{7.1}$$

Structure function μ of pseudo-Boolean polynomial $\pi\varphi_{\mu}^{\otimes}$ is a set function $\mu:\mathrm{P}(\Omega)\to[0,1]$, $\Omega=\{a_1,...,a_n\}$ defined by the following expression, [9]:

$$\mu\left(S\right)=\sum_{i=1}^{m}w_i\sigma_{\varphi_i}\left(S\right)\tag{8}$$

where:

$$\sum_{i=1}^{m}w_i=1,\quad w_i\geq 0,\quad i=1,...,m.,\quad S\in\mathrm{P}\left(\Omega\right).$$

The characteristics of pseudo-Boolean polynomial depend on the generalized product, and its structure function. Structure functions can be classified into: (a) additive, (b) monotone and (c) generalized ($\left(a\right)\subset\left(b\right)\subset\left(c\right)$).

4 LOGICAL AGGREGATION

A starting point is a finite set of primary quality attributes $\Omega=\left\{a_1,...,a_n\right\}$. The task of logical aggregation (LA) [9] is the fusion of primary quality attribute values into one resulting globally representative value using logical tools. In a general case LA has two steps:

(1) Normalization of primary attributes values:

$$^{v}:\Omega\rightarrow\left[0,\ 1\right].$$

The result of normalization is a generalized logical and/or [0, 1] value of analyzed primary quality attribute, and

(2) Aggregation of normalized values of primary quality attributes into one resulting value by a pseudo-logical function as a logical aggregation operator:

$$Aggr : [0,1]^n \to [0,1].$$

A Boolean logical function φ is transformed into a corresponding generalized Boolean polynomial (GBP), $\varphi^{\otimes} : [0, 1]^n \to [0, 1]$. Actually, to any element of Boolean algebra of quality attributes $\varphi_i \in BA(\Omega)$ there corresponds uniquely GBP $\varphi_i^{\otimes}\left(a_1^v,...,a_n^v\right)$. GBP is defined by expression (2) and/or (2.1).

Pseudo-logical function is a linear convex combination of generalized Boolean polynomials [5], defined by expression (7) and/or (7.1).

Operator of logical aggregation in a general case is a pseudo-logical function:

$$Aggr_{\mu}^{\otimes}\left(a_1^v,...,a_n^v\right) = \pi\varphi_{\mu}^{\otimes}\left(a_1^v,...,a_n^v\right) \quad (9)$$

Aggregation measure is a structural function of pseudo-logical function – a logical aggregation operator [9]. So, *Aggregation measure* is a set function $\mu : \mathrm{P}(\Omega) \to [0,1]$, which in a general case is not a monotone function (generalized capacity), defined by the following expression:

$$\mu(S) = \sum_{i=1}^{m} w_i \sigma_{\varphi_i}(S), \quad S \in \mathrm{P}(\Omega), \quad \varphi_i \in BA(\Omega). \quad (10)$$

As a consequence, logical aggregation operator depends on the chosen: (a) measure of aggregation and (b) operator of generalized product. By a corresponding choice of the measure of aggregation μ and generalized product $\otimes$ the known aggregation operators can be obtained as special cases [9]: Weighted sum, Arithmetic mean, K-th attribute only, Discrete Choquet integral, Minimal value of attributes, Maximal value of attributes, OWA-ordered weight aggregation, k-th order statistics.

5 CONCLUSION

The aggregation of partial goals - attributes, into one representative global goal is a very important task. Conventional aggregation tools are very often inadequate. Partial demands for aggregation can be and usually are logical demand which can be adequately described only by logical expressions. In this paper logical aggregation as a tool for aggregation is analyzed. Logical aggregation has multiple advantages among others from the stand- point of its possibility and interpretability. The new approach treats logical functions – partial aggregation demand, as a generalized Boolean polynomial which can process values from the whole real unit interval [0, 1]. Logical aggregation in a general case is a weighted sum of partial demands. Therefore, aggregation in a general case is a generalized pseudo-logic function. It is interesting that conventional aggregation operators are only a special case of logical aggregation operators and, as a consequence of using LA, one can do much more in an adequate manner direction than before.

6 REFERENCES

[1] D. Radojević, New [0,1]-valued logic: A natural generalization of Boolean logic, *Yugoslav Journal of Operational Research – YUJOR*, Belgrade, Vol 10, No 2, 185-216, 2000.

[2] G. Choquet, Theory of capacities, *Annals de l'Institute Fourier*, 5:131-295, 1953.

[3] M. Sugeno, *Theory of fuzzy integrals and its applications*. Doctoral Thesis, Tokyo Institute of Technology, Tokyo, Japan

[4] M. Grabisch, The application of fuzzy integrals in multicriteria decision making. *European Journal of Operational Research*, 89(3):445-456, 1996.

[5] D. Radojević, Interpolative realization of Boolean algebra as a consistent frame for

gradation and/or fuzziness, *Forging New* Frontiers*: Fuzzy Pioneers II*, Ed. M. Nikravesh, J. Kacprzyk L. A. Zadeh, Studies in Fuzziness and Soft Computing, pp. 326-351, Springer, 2007.

[6] D. Radojević, Interpolative realization of Boolean algebra, NEUREL 2006, Eight IEEE Seminar on Neural Network Applications in Electrical Engineering, 201-206, 2006.

[7] D. Radojević, Logical aggregation based on Interpolative realization of Boolean algebra, Mathware & Soft Computing, Vol. XV, n. 1, 125-141, 2008.

[8] D. Radojević, Logical interpretation of discrete Choquet integral defined by general measure, International Journal of Uncertainity Fuzziness and Knowledge-Based Systems, 7(6): 577-588 (1999).

[9] D. Radojevic: Logical Aggregation Based on Interpolative Realization of Boolean Algebra. EUSFLAT Conf. (1) 2007: 119-126

HEAVY MACHINERY - HM 2011, 31-40
ISBN 978-86-82631-58-3

Paper accepted: 30.05.2011

International Science and Technical Cooperation of the Faculty of Mechanical Engineering in Kraljevo

Novak Nedić[1,*], Dragan Petrović[1], Dragan Pršić[1], Mirko Djapić[1], Snežana Ćirić-Kostić[1], Ljubomir Lukić[1]
[1] University of Kragujevac, Faculty of Mechanical Engineering Kraljevo, Serbia

The Faculty of Mechanical Engineering of Kraljevo is the bearer of regional, commercial and technological development and is also a significant bearer of an international science and technical collaboration of the Republic of Serbia. By participating in the realization of science and research projects was achieved collaboration with the recognized universities and science institutions in the world, which brought an international affirmation of the science and research programs of the Faculty of Mechanical Engineering in Kraljevo. With the realization of two projects from the FP 7 program and two from the regional programs over the past three years were achieved vital results in terms of integration of research activities of the Faculty of Mechanical Engineering in Kraljevo into European flows, the burst of science and research staff and laboratory furnishing.

The paper shows the realized goals and results from the four current projects realized by and in which participates the Faculty of Machine Engineering in Kraljevo: SeRViCe - Center for Strengthening Railway Vehicles of the Faculty of Mechanical Engineering Kraljevo, TransBonus - Western Balkan Network for Training, Support and Promotion of Cooperation in FP7 research activities, ATC Serbia – Automotive Training Centre for Central Serbia and IMPuls - Innovation Management for new Products.

Keywords: International projects, research, development, education

0 INTRODUCTION

The Faculty of Mechanical Engineering in Kraljevo first began its international science and technical cooperation in the field of railway mechanical engineering, through the development of its own research center, only to later broaden this collaboration by building one of the most modern experimental facilities in Europe for testing railway vehicles. After this project, the collaboration extended to the TransBonus project through which activities took place in several countries in the Balkans.

The competence of the Faculty of Mechanical Engineering in Kraljevo in the education of engineers was confirmed by its participation in the project – ATC Serbia. Furthermore, through the IMPuls project, valued at around EUR 1mn, realized over the following two years, the Faculty of Mechanical Engineering became one of the most significant bearers of science and technical cooperation from the University in Kragujevac. With the realization of a couple of project from the FP 7 program over the past three years were achieved vital results in terms of integration of research activities of the Faculty of Mechanical Engineering in Kraljevo into European flows, the burst of science and research staff and laboratory furnishing.

1 SeRViCe PROJECT

The project Center for Strengthening Railway Vehicles of the Faculty of Mechanical Engineering Kraljevo (SeRViCe) is the first big international project coordinated and realized by the Faculty of Mechanical Engineering of Kraljevo. Dragan Petrovic took over the duty of project manager after Ranko Rakanovic.

The basic goal of the project is the development of the Center for Railway Vehicles of the Faculty of Machine Engineering in Kraljevo, and is focused on:

- Higher quality and more efficient teaching process and education of students of all study levels from the field of railway mechanical engineering and testing of machine constructions,
- The growth of staff in line with leading global trends from the field of railway mechanical engineering and procurement of lab equipment and
- Participation in science and research and development projects with commerce,

*Corr. Authorćs Adress: University of Kragujevac, Faculty of Mecahnical Engineering Kraljevo, nedic.n@mfkv.kg.ac.rs

participation in science conferences, publishing the achieved results.

Project SeRViCe for the Faculty of Mechanical Engineering in Kraljevo has great significance because the faculty, as an institution-coordinator, is thus included in the FP program of projects, thereby making it a relevant partner for European research projects. The significance of the project is reflected in the improvement of collaboration between MFK and renowned global and domestic institutions and scientists from this field. Particular importance within a European framework plays the development of the railway as a mass transport system, safe, economical and with the least harmful effects on the environment.

The content of the project is the improvement of collaboration with domestic and foreign commerce, science and research centers, local government and Republic institutions, particularly the Ministries of Education, Science and Technological Progress. A qualitative improvement of collaboration, teaching and science and research work leads to raising the reputation of the Center for Railway Vehicles and the Faculty of Mechanical Engineering, and was attained through seven work packages, including:
WP-1 Knowledge – exchange of employees and study visits,
WP-2 Newly employed and researchers,
WP-3 Workshop,
WP-4 Measuring equipment and S-shape tracks,
WP-5 Partnerships,
WP-6 Advertising and promotion,
WP-7 Management.

A significant result of the project is an overall increase in the level of knowledge of researchers of the Center for Railway Vehicles that was realized through an exchange of employees and expert training at renowned research institutions like KTH Royal Institute of Technology from Stockholm and the DIEM Department of the University in Bologna. Also, several study visits took place at leading European institutes and companies from railway mechanical engineering of which the most important are ALSTOM – France (figure 1), VUKV – the Czech Republic and IMA – Austria. These activities resulted in signing an agreement on strategic collaboration with KTH, the Royal Institute of Technology from Stockholm and the DIEM Department of the University in Bologna.

Fig. 1. *Study visit to company Alstom – France*

This was realized primarily through the direct organization of several workshops under the auspices of the Faculty of Mechanical Engineering of Kraljevo (figure 2) at which had participated, apart from domestic, the leading worldwide experts from the field of railway vehicle dynamics, mechanical construction fatigue, sensory analysis and other areas. Through these activities was realized the connecting and transfer of knowledge between domestic and foreign researchers and introduction to leading global trends from the field of railway mechanical engineering.

Fig. 2. *Work group "Workshop on Railway Vehicle Dynamics" – Kraljevo*

Among the more important realized results of the project is the employment of several younger researchers – students of postgraduate, PhD programs, that through the realization of the project had gained significant experience in research and know-how that will be of use to them in their further work and for the writing of their Doctor’s Dissertation. Also, it should be highlighted that through the realization of the project was achieved a significant affirmation of the Faculty of Mechanical Engineering in Kraljevo, both in domestic and international frameworks.

The most significant output of the project is reflected in the development and procurement of modern measuring equipment for dynamic and quasistatic testing of railway vehicles according to the international UIC standards in force. This is a measuring equipment that is one of the most contemporary achievements from this area. The following measuring systems were developed and procured:

- Measuring system for measuring the lateral (Y) and vertical (Q) components of the force that occurs in the contact between the wheel and rail,
- Measuring system for measuring the lateral force (H) and lateral acceleration of the axial structure, as well as the height of raising the wheels,
- A measuring system for measuring the pressure force on an automatic clutch,
- A measuring system for measuring the acceleration of the railway car,
- Test stand for calibration and testing of measuring axial structures (figure 3).

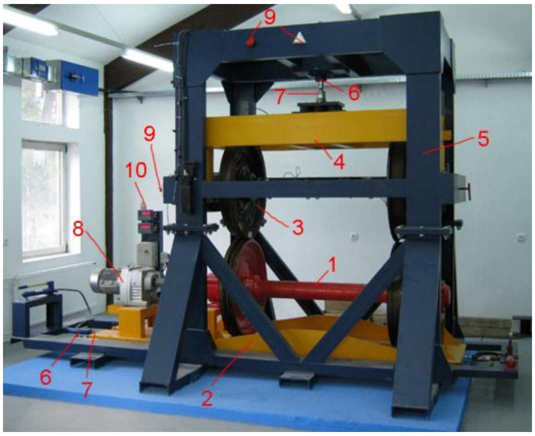

Fig. 3. *Device for calibrating and testing measuring axial structures of the cars*

This measuring equipment enables a further planning and participation in very current research in the field of security and safety of axial structures of railway vehicles, optimization shapes and dimensions.

The project should result in the building of a test polygon with an S-shaped track for testing railway vehicles in line with international standard UIC 530-2. It should be mentioned that no such polygon existed in Serbia or the neighboring countries, up till now, and that the domestic railway car factories were forced to perform such research in countries of Western Europe, at very high prices. The project results directly cause a growth in competitiveness of domestic railway car factories on foreign markets. Also, conditions are created for increasing export through the possibility of car factories from neighboring states testing their cars on the polygon in Kraljevo.

2 TransBonus PROJECT

The TransBonus project (Transport EU-Western Balkan Network for Training, Support and Promotion of Cooperation in FP7 research activities) is co-managed by Novak Nedic, Mirko Djapic and Dragan Petrovic, while the project coordinator is the institution Applied Research and Communications (ARC) Fund – Sofia from Bulgaria. The project participants/institutions are:

- SenterNovem, Den Hague, Nederland,
- Foundation for Research and Technology Hellas (HELP-FORWARD), Thessaloniki, Greece,
- Integrated Resources Management (IRM) Company, Valeta, Malta,
- Higher school of Transport “Todor Kableshkov”, Bulgaria,
- University of Kragujevac, Faculty of Mechanical Engineering Kraljevo, Serbia,
- Automotive center - Centar for Vehicles, Sarajevo, Sarajevo, Bosnia and Herzegovina,
- University of Skopje, Faculties of Mechanical Engineering Skopje, Macedonia and
- Polytechnic University of Tirana, Mechanical Engineering Faculty, Albania

The overall objective of TransBonus is to improve and promote closer scientific and technological (S&T) cooperation opportunities between European Member States (Greece, the Netherlands, Malta and Bulgaria) and the Western Balkan Countries (WBCs: Albania, Bosnia and Herzegovina, Former Yugoslav Republic of Macedonia and Serbia). It further seeks to establish a *Balkan Transport Network of Researchers, Universities and Experts* among these countries in order to improve and enlarge the research capacity of Western Balkan centers, competence in terms of research programs and human resources through trans-national placements of research staff and knowledge.

During the life span of the project, the partners carried out the following activities and contributions:

- Creation of a freely accessible database providing Collaboration and technology profiles for WBCs and Bulgarian transport research.
- Promotion of Research and Technological Development funding opportunities available at European level that can support international cooperation with WBCs transport researchers.
- Training and support in FP7 knowledge and best practices for academic personnel. Enhance the readiness of the Balkan transport research community to prepare cooperative activities and joint RTD proposals in European RTD programs.
- Setting up a matching tool – "Project Lab", supporting the creation and preparation of efficient and innovative project proposals. Stimulate partnering schemes and facilitated knowledge transfer at National and European level.
- Implementing expert study visits between WBC partners and EU partners in order to expand the specific relationships and networking between the two regions.
- Stimulate partnering schemes and national collaboration between researchers and the industry in the surface transport sector in the Balkan region.

The project was realized through six subprojects:

WP1 Identifying the existing capacities and specific researcher needs in the Western Balkan countries in terms of FP7 funding opportunities,

WP2 Partner training and support to WBC transport researchers of FP7 knowledge and practices for dissemination and effective support,

WP3 Setting up of a partnering tool – "Project Lab",

WP4 "Research Bonus" services,

WP5 Dissemination and awareness-raising,

WP6 Project Management.

In regard to the targets of the TransBonus project the Serbian partner collected 42 collaboration organization profiles which are a part of some research in the field of surface transport.

The structure of the Serbian research systems in surface transport consist of:

- Knowledge suppliers,
- Knowledge users,
- Research infrastructure and intermediaries and
- Organizations engaged on the national level.

Main results are: Training in 'Six hat' methodologies for new idea generation (figure 4) and translation of Manuals for researchers in the field of transport – 50 pages (figure 5).

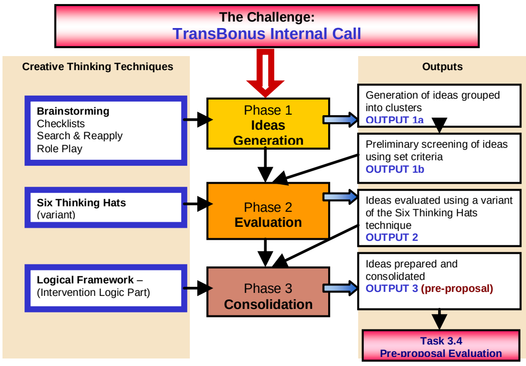

Fig.4. *Training in the 'Six hat' methodology*

Fig.5. *Manual for transport researchers*

The Faculty of Mechanical Engineering Kraljevo, organized in Serbia two "Idea Generation Events" (IGE) on September 10th

2009 and April 15th 2010. More than 40 new ideas were generated for the FP7 project. The direct results from this meeting are two new project proposals for the FP7 call from June 2010. On figures 6 and 7 are presented some of the parts of the SmartAxles project proposal.

List of participants:

Participant no. *	Participant organisation name	Country
1 (Coordinator)	University of Kragujevac, Faculty of Mechanical Engineering Kraljevo, (**FME**)	Serbia
2	University of Bologna, Department of Mechanical Engineering, (**DIEM**)	Italy
3	Higher School of Transport – Todor Kableshkov, (**FMCTT**)	Bulgaria
4	University of Belgrade, Faculty of Electrical Engineering, (**FEEB**)	Serbia
5	Integrated Microsystems Austria GmbH, (**IMA**)	Austria
6	The Laboratory for ICT Technologic Transfer, (**T3LAB**)	Italy
7	Optical Sensor Systems d.o.o., (**OSS**)	Serbia
8	Thermal Power Plants "Nikola Tesla" Ltd, (**TENT**)	Serbia
9	Rail Authority, (**RA**)	Czech Republic

Fig.6. *Part of the SmartAxles project proposal*

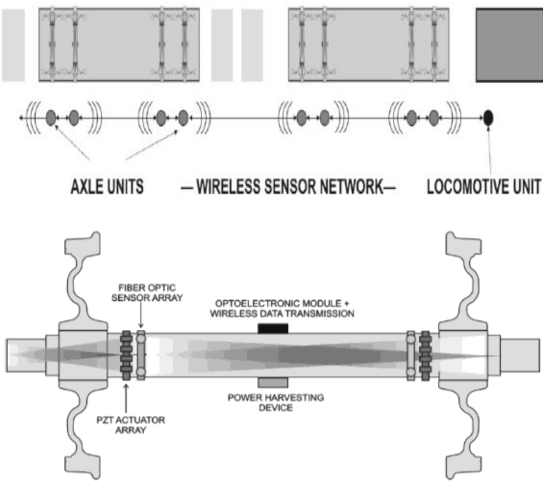

Fig.7. *Technical part of the SmartAxles project proposal*

Main results of WP4 are study visits (figure 8):

- Thessaloniki, October 1-2 2009,
- Sofia , November 5-8 2009,
- Sofia, January 27-29, 2010,
- Sarajevo, July 7-9, 2010,
- Netherlands (Den Hague, TU Delft and TU Eindhoven) September 15-18, 2010,
- Sofia, December 06-08, 2010.

Fig.8. *TransBonus study visits*

The TranBonus project was completed on December 31st, 2010. The researchers who were involved in its realization have a duty to disseminate the knowledge and experience they gained by working on this project.

Regarding this, the researchers from the Faculty of Mechanical Engineering in Kraljevo had actively participated at the conference SEETRANS 2011 (Transport Research Opportunities for South East Europe In the EU) held in Ljubljana, Slovenia from April 12-13th, 2011. At this conference a possibility was given to researchers from Eastern Europe to present their ideas for new research projects and to attempt to find partners that would participate in this research. All this is linked to the upcoming publishing of the competition of the European Commission for projects that will be financed starting from 2012 by the framework programs of the FP7 program.

3 ATC SERBIA PROJECT

The project ATC - Automotive Training Centre for Central Serbia coordinated by the Polytechnic School in Kragujevac refers to enabling the technical staff in working in Fiat's factories that will be working with the new car industry technology in Serbia. The project managers on this project are Novak Nedic and Dragan Prsic. The project will last for two years and the following will participate:

- UNIBO – University in Bologna, Italy
- MFKG – Faculty of Mechanical Engineering in Kragujevac, Serbia
- MFKV – Faculty of Mechanical Engineering in Kraljevo, Serbia
- TFCK – Faculty of Technics, Chachak, Serbia
- IAL – Friuli – Venezia Giulia region, Italy
- RCCK– Regional Chamber of Commerce of Kragujevac, Serbia.

For the past two decades, the Serbian automotive industry, mainly located in the Central Serbian region, has gone through a very difficult period in its development. There was a drastic reduction of the market, reduction of production capacities, worker layoffs, losing step with technological development. At Kragujevac-based Zastava in 1989 worked 35,000 mainly involved in car production. This number had by 2000 gone down to 13,000 with only 3,500 workers working in Zastava in 2010. The negative trends in Zastava reflected on the supplier network that accompanied their production. Based on official reports of the Agency for Business Registers in Serbia around 160 companies from the field of the automotive industry are registered with a total of 25,000 employees. However, according to SIEPA standards, for the realization of current products and services demand in the field of the automobile industry, some 70 companies are sufficient.

This situation is a serious economic problem, with unwanted effects in other areas of the social life, especially in Central Serbia. The Serbian tradition in technics and knowledge, for years among the strongest in Europe, has faced the risk of a complete and speedy disappearance.

On the other hand, one of the leading global car manufacturers, Italian FIAT had officially expressed its intention in broadening its investments in Serbia, raising the level from the current 20,000 to 200,000 vehicles per annum since 2011. Accordingly, a significant demand for workers, technicians and engineers is to be expected, with somewhere around 3,000 employed in 2012. Furthermore, an increase in the number of employees in the ancillary industry is expected (Magneti Marelli has already signed a contract for significant investments in Sumadija region).

There are several problems that make the integration of FIAT into our environment harder and in general don't facilitate the development of the car industry:

- Outdated technology and production equipment;
- Poor connection between education institutions (high schools and faculties) and companies;
- The lack of specialized educational programs;
- The lack of courses for retraining and additional training of workers.
- Lack of experts for project management;
- Lack of entrepreneurial initiative;

This project has as a goal to advance the level of training in faculties and technical schools in Central Serbia so as to prepare the people in line with the needs of the labor market. The project aims to reduce the existing gap between industrial requirements, and the offer of the educational system by bringing the syllabus and labs up to date. The automobile sector is exposed to intensive technological innovation, and the high schools and faculties can't keep up with this. Therefore this proposal is aimed at testing a new training model for high school students and workers that would use new teaching resources (labs, education at work).

The Faculty of Mechanical Engineering of Kraljevo is one of the partners on the realization of development projects of the automobile training center of Central Serbia. The goal is to promote the skills and knowledge from the field of hydraulics and pneumatics, as parts of a broader specter of knowledge that characterize the modern car industry. Activities unfold in two directions:

- The modernization of syllabuses and their adapting to the needs of the car industry. Training for different levels is envisaged (figure 9).
- Equipping the didactical lab for hydraulics and pneumatics as support to practical teaching.

Fig.9. *The experimental device for training of specialists for work in the automotive industry*

It is planned that training in the training center for hydraulics and pneumatics is realized through five thematic wholes (figure 10):

- Hydraulics and pneumatics.
- Measuring and acquisition of data in fluid techniques.
- Management systems in fluid techniques.
- Software tools in fluid techniques.
- Use of hydro-pneumatic systems in the car industry.

Fig.10. *Laboratory equipment for the project ATC Serbia*

The classes will go through 15 themed courses of modular type, suited to different levels of enrollee knowledge (figure 11).

1. Basic principles in hydraulics and pneumatics
2. Hydraulic and electro-hydraulic components
3. Hydraulic and electro-hydraulic systems
4. Pneumatic and electro- pneumatic components
5. Pneumatic and electro-pneumatic systems
6. Measure transducer and data acquisitions in hydraulic and pneumatic systems
7. Control of hydraulic and pneumatic systems
8. Hydraulic brake systems - basic course
9. Hydraulic brake systems - advanced course
10. Pneumatic brake systems - basic course
11. Pneumatic brake systems - advanced course
12. Hydraulic suspension systems
13. Pneumatic suspension systems
14. Software tools for engineering calculations in hydraulic and pneumatic systems
15. Software tools for modeling and simulation hydraulic and pneumatic systems

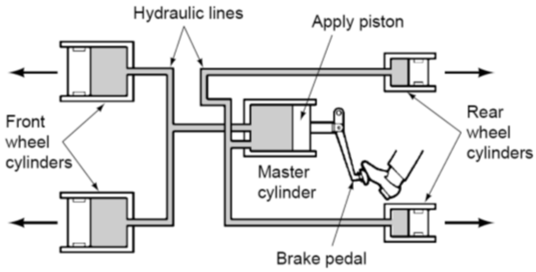

Fig.11. *Scheme of the hydraulic brake system for cars*

For practical teaching are planned 4 training desks: for hydraulics, pneumatics, braking and leaning.

4 IMPuls PROJECT

IMPuls - Innovation Management for new Products is a project backed by IPA funds, and was gotten by the invitation of the Regional Socio-Economic Development Program II (RSEDP2). The project manager is Snezhana Chirich Kostich, PhD and is realized by the Faculty for Mechanical Engineering of Kraljevo, while the participants are:

- Regional Chamber of Commerce of Kraljevo,
- City of Kraljevo,
- DIEM Department of the University in Bologna and
- Regional Center for the Development of Small and Medium-sized companies – Kruševac.

The basic goal of the project is to raise the competitiveness of small and medium-sized companies in the Morava, Rasina and Raska districts. The expected project results are:

- Regular on-line informing about new technologies for a faster development of products for 500 companies,
- Monitoring and continued systematic valuating of competitiveness of 200 companies,
- Increasing capacities for innovations in 100 companies,
- The development of the 300 CAD model of products and the appropriate technical documents for the needs of 100 companies
- The development of 100 prototypes of new products for the requirements of 50 companies.

The project idea is governed by results and experiences of previous projects performed by partners in the past. The recent projects “Strategy for Competitive and Innovative Small and Medium-sized Enterprises 2008 - 2012” and “Assessment of the Level of Innovativeness and Competitiveness in the SME Sector in the Raska and Morava Districts” showed that the key for improvement of competitiveness of companies from the Morava, Raska and Rasina Districts is the development of new and improved products which would be more attractive to customers.

The conclusion leads to an idea to achieve the overall objective of the campaign, improvement of competitiveness of the manufacturing industry of companies in the Morava, Raska and Rasina Districts, through enhancing innovation activities in the companies by modern design technologies, as a specific objective. The project addresses not only the technical aspect of innovation, but also considers support to product implementation and marketing, considering the product from the marketing aspect, tending to measure competitiveness through the capacity to generate revenue.

The expected result is support to the development of 300 models of new and improved products in 100 companies and 100 prototypes of new and improved products in 50 companies from all three considered districts over a period of 24 months. A fast development of such a large number of products will be facilitated by application of modern fast design methods, reverse engineering and rapid prototyping. Therefore, the first activity of the project activities will be the establishment of a technological basis for rapid product development.

The technology basis for the project will be established at the Faculty of Mechanical Engineering Kraljevo, located in the geographical centre of the considered region. The present knowledge, equipment and software will be complemented by a 3D scanner and a 3D printer which will be provided for the purposes of the project and training of personnel for application of the new equipment. The faculty will be in this activity supported by the DIEM department of University of Bologna that already has experience in rapid development technologies.

The second project scope of activities comprises the development of models for new and improved products. The faculty of Mechanical Engineering in Kraljevo will provide initial information on rapid development technologies on the project website and organize on-line support to at least 500 companies from the considered region. The faculty will also organize suitable quick courses for 100 targeted companies in order to facilitate efficient communication between the Faculty of Mechanical Engineering

Kraljevo and the companies during the process of rapid product development.

The companies that will be supported will be selected by the Regional Center for SME Development Kruševac, center for the Rasina District and Regional Chamber of Commerce Kraljevo, which is gathering companies from the territory of the Morava and Rashka district. The criteria for selection will be results obtained in the project "Assessment of the level of Innovativeness and Competitiveness in the SME Sector in the Raska and Morava District", while also taking into consideration the regional distribution and issues of gender equality and vulnerable groups (figure 12). In this process, the companies will provide the technical documentation for the proposed new products, and in cases where such documentation does not exist, the Faculty of Mechanical Engineering Kraljevo will apply a reverse engineering methodology for a fast development of models of present products which are going to be the basis for development of new and improved products, and more competitive compared to existing ones.

In the third project activity, the development of prototypes of new products, the Faculty of Mechanical Engineering Kraljevo will apply rapid prototyping techniques to produce a very large number of prototypes in a short period of time. Prototypes will be examined by the relevant criteria, and companies will afterwards submit documentation for the revised prototypes, which will also be made in a short period of time. In cases where it is needed, the Faculty of Mechanical Engineering Kraljevo will also support the production of tools and moulds by rapid prototype technologies.

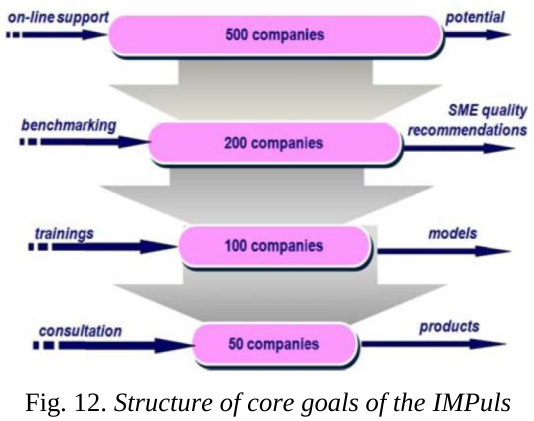

Fig. 12. *Structure of core goals of the IMPuls project*

After the technical phase of development of new products, targeted companies will receive consulting services regarding the implementation and marketing of each individual product as the fourth project activity, in order to provide for maximal market effect of new products. Consulting will be provided by the Regional Center for SME Development in Krushevac, the Center of the Rasina District, which will engage consultants to develop plans on how to make improvements or adapt specific best practices with the aim of increasing business performance and market positions of companies who will utilize new products created in this project.

The Regional Center for SME Development Kruševac will also provide analysis of project results as the fifth project activity, by benchmarking a change of competitiveness and innovation capacity of supported companies against companies that have not received the support during the project. Competitiveness benchmarking will enable comparison of business processes and performance metrics and also enable further improvements from learning – which means doing things better, faster, and cheaper. Benchmarking in enterprises will include measuring and benchmarking of 5 dimensions of competitiveness (speed, dependability, flexibility, quality, price) and 11 dimensions (innovative activities, innovative politics, innovative goals, innovation sources, innovation expenses, innovation strategy, innovative practice, obstacles or innovation, market orientation, factors of innovation, innovation motivation) of innovation capacity for each of the 200 enterprises included in the project. The goal of the benchmarking would be measuring the relation between competitiveness of the companies before and after the implementation of new product development and their market utilization.

5 CONCLUSION

Project SeRViCe is a foundation for the further development of science and research potential of the Faculty of Mechanical Engineering in Kraljevo in the area of promoting security, safety and comfort of riding railway vehicles. In that regard, great importance will have diversified measuring equipment and realized contacts with institutions in member countries of the EU, Russia and Turkey.

The TransBonus project has fullfilled its basic goals in relation to requests and expectations of the Faculty of Mechanical Engineering in Kraljevo and the broader regional community in the field of surface transport. Over 40 ideas have been generated for new projects in the field of surface transport, two of which were entered at the invitation of the European Commission from June 2010. Researchers from Serbia had a chance to visit the leading universities in the Netherlands (Delft and Eindenhoven) and to become familiar with the latest research there and which are related to the field of surface transport.

Project ATC Serbia will enable for our engineers, technicians and highly qualified workers to overcome new technologies that are today applied in the automobile industry and to provide employment in the Fiat factories in Kragujeac, which will further affirm the Faculty of Mechanical Engineering in Kraljevo as a scientific institution that develops its own program for domestic industry needs.

Project IMPuls will provide for the development of small and medium-sized companies in the Republic of Serbia on the basis of introducing modern technologies of product design and technologies and the transfer of knowledge and experiences from the Universities of developed European countries.

Through the realization of international research projects will be conducted the education of a large number of researchers according to the methodology of the Universities of countries of the EU, which will contribute to the integration of the Faculty of Mechanical Engineering in Kraljevo into European flows and the raising of the overall scientific and technical-technological level of our country as a whole.

6 REFERENCES

[1] Šoškić Z., Petrović D., Bogojević N., Rakanović R. FP7 project SeRViCe – Support to Reinforcement of Railway Research Potential of Serbia, Proceedings of the second international Railway Symposium IRS Turkey, Istanbul, pp 1147, 2008.

[2] Petrović D., Babić A., Bižić M., Đelošević M. Measuring equipment for dynamic and quasistatic testing of railway vehicles, Proceedings of the XIV Scientific-Expert Conference on Railways RAILCON, Nis, pp 177-181, 2010.

[3] Bižić M., Tomić M., Đinović Z., Petrović D. Test stand for calibration of measurement railway wheelsets, Proceedings of the 7th international scientific conference Research and development of mechanical elements and systems IRMES 2011, 27-28.04.2011, Zlatibor, Serbia, pp 419–424, 2011.

[4] Nedic,N., Djapić,M., Petrović,D., Brasić, V., TransBonus, Transport EU-Western Balkan Network for Training, Support and Promotion of Cooperation in FP7 research activities, project Documentation, Faculty of Mechanical Engineering Kraljevo, 2009-2010.

[5] Ciric Kostic,S., and colleagues, IMPuls Innovation Management for new Products, Project Documentation, Faculty of Mechanical Engineering Kraljevo, 2010.

[6] Nedić,N., Pršić,N., and colleagues, ATC - Automotive Training Centre for Central Serbia, Project Documentation, Faculty of Mechanical Engineering Kraljevo, 2010.

A SESSION

RAILWAY ENGINEERING

HEAVY MACHINERY - HM 2011, 1-8
ISBN 978-86-82631-58-3
Paper accepted: 18.05.2011

The Wheel Flat – Rail Interactions

Dobrinka Atmadzhova[1]
[1] Todor Kableshkov University of Transport

The increased load and speed, the issue of wheel flats and a strategy for in-time maintenance and replacement of defective wheels has become an important concern for railway. In this study, an analytical model of the coupled vehicle-track system is developed by integrating a pitch plane model of the vehicle with a two-dimensional model of the flexible track together with a nonlinear rolling contact model. The validated model is utilized to investigate the characteristics of impact forces due to wheel flats and its effect on motions and forces transmitted to vehicle and track components. The influence of the flat on various components of the vehicle and track is analyzed. This study illustrated the significant influence of wheel flat on the components of vehicle and track system. The current study also shows that flat present in one wheel has strong influence not only in wheel-rail impact forces but also on bearing, pad and ballast forces at the defective as well as adjacent wheelset.

Keywords: Wheel flat, wheel-rail impact, defective wheels, component force.

1 INTRODUCTION

Wheel flat is the most common type of wheel defect encountered by railway industry, which develops due to sliding of the wheel on the rail under braking, when the braking force is larger than the available wheel/rail friction or when the brake system poorly adjusted or defective [12].

During sliding, part of the wheel tread could be removed causing a flat surface to form on the wheel profile. This surface irregularity causes impact loads on the rail and track structure as the wheel rolls. This impact load induces high frequency vibration of the track and the vehicle components.

It has been suggested that excessive magnitude of the impact load may even shear the rail [10].

A number of studies have attributed the wheel sliding to poorly adjusted, frozen, or locked wheels or excessive braking forces in relation to the wheel/rail adhesion [3].

Contaminations on the rail surface, such as leaves, grease, frost, and snow could also aggravate the sliding at the wheelrail contact. Jergeus et al. reported in [3] that the area of actual wheel/rail contact changes during the formation of a flat and thus the shape of the railhead also have great influence on the growth of the wheel flat.

With continuing increases in the axle loads and operating speed, the wheel flats are becoming increasingly common.

The high magnitude of impacts due to wheel flats, whether single or multiple, not only induce high magnitude impact force and stress on vehicle components but also to the rails and the sleepers [5]. Wheel flats thus affect track maintenance and the reliability of the vehicle’s rolling elements. In addition to safety and economic considerations, these defects affect passenger comfort and significantly increase the intensity of noise. A damaged bearing that seizes can also cause skidding.

The high impact forces from a flat wheel cause stress in the rail, and in extreme cases can break the track or cause the wheel to jump off the track, resulting in a derailment. The contact forces are quite high; therefore, damage and wear are consistently relevant, mainly due to the great weights involved in the rail traffic and to the hardness of rail and wheel materials. It is clear that the continuous repetitions of impacts on rail, together with the high forces involved, cause rapid deterioration of, both, rolling and fixed railway equipments. If ignored or underestimated, the fault will wear out materials up to the breakdown. Various methods have been proposed for detecting flat wheels. One method is to employ inspectors to listen to the trains as they move through a particular location.

Some flat wheels are found through routine inspections when the cars are being serviced. A wide range of sensors has been proposed for detecting flat wheels. These employ a range of technologies from optical systems that gauge the

[*]Corr. Author's Address: Todor Kableshkov University of Transport, Sofia, Bulgaria, atmadzhova@abv.bg

wheels in real time to sensors that look for vibrations and stress.

The dynamic interaction between the vehicle, the wheel, and the rail track systems has been the subject of extensive research in recent years. Many studies [3, 10, 12] have focused on the vibrations of a railway track under moving vehicles with wheel defects, and different theories and models have been presented on this issue. A detailed review in the area of railway vehicle dynamics featuring the historical survey of the dynamic models to study the vehicles-track interactions due to wheel defects at high frequency range have been presented by Knothe and Grassie [5]. In analysis of the coupled vehicle-track system, some of these studies [3, 5] have employed finite element method and some [4, 15, 16] have used modal analysis method. Two types of track models are generally employed in the study of vehicle-track interactions. Early track system studies considering rail as a discretely supported beam [7, 12] is now widely used for modelling of wheel-rail interactions [4, 10, 11, 15, 16,]. Vehicle-track interaction studies in general consider track as a continuous system as Euler-Bernoulli [4, 15, 16] or Timoshenko beam [7, 10, 11, 12]. Most of these studies, however, represent vehicle by a rolling wheel to investigate the wheel-rail contact forces. The impact force response such as the bearing force, rail pad force, and the ballast force as well as the wheel-rail contact force in the presence of wheel flat utilizing comprehensive vehicle model is not available in literature.

2 MATHEMATICAL MODELING

2.1. Vehicle and track model

The vehicle system model used in this study consists of a quarter car supported on a bogie, while the side frame is supported on two wheelsets. The primary suspension connecting the wheels and the bogie frame is modeled as a parallel combination of a linear spring and a viscous damping element. The secondary suspension modeled by parallel spring and damping elements. The mass of the car body $\mathbf{M_c}$, bogie mass $\mathbf{M_t}$, wheel mass $\mathbf{M_w}$ are coupled through the suspension elements, as shown in Fig. 1.

The vehicle is thus represented by a 5-DOF dynamic system that includes the car body vertical motion, $\mathbf{z_c(t)}$; the bogie vertical and pitch motions, $\mathbf{z_t(t)}$ and $\mathbf{\psi_t(t)}$; and vertical motions of the wheels, $\mathbf{z_{w1}(t)}$ and $\mathbf{z_{w2}(t)}$. The primary suspension stiffness and damping elements are represented by $\mathbf{C_{s1}}$ and $\mathbf{\beta_{s1}}$, respectively, while $\mathbf{C_{s2}}$ and $\mathbf{\beta_{s2}}$ represent the stiffness and viscous damping coefficient due to secondary suspension. The contact force at the leading wheel-rail and trailing wheel-rail are denoted by $\mathbf{P_1(t)}$ and $\mathbf{P_2(t)}$, respectively. $\mathbf{J_t}$ and $\mathbf{r(t)}$ are mass moment of inertia of the bogie and wheel defect profile, respectively. $\mathbf{l_f}$ and $\mathbf{l_r}$ are the distance from the mass center of the bogie to the front and rear wheel centers, respectively.

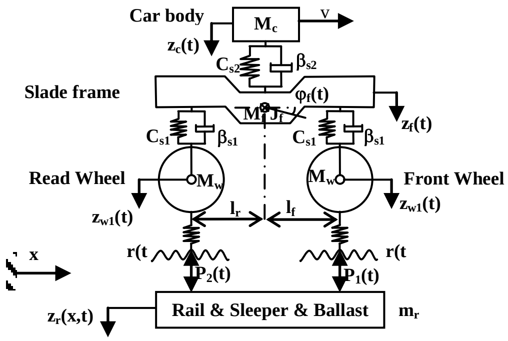

Fig. 1. Vehicle system model

The motion of the rail beam coupled with the sleeper and ballast is expressed as $\mathbf{z_r(x,\ t)}$, while $\mathbf{z_{si}(t)}$ and $\mathbf{z_{bi}(t)}$ describe the motions of the sleeper and ballast masses. $\mathbf{C_p}$, $\mathbf{\beta_p}$, $\mathbf{C_b}$ and $\mathbf{\beta_b}$ are the railpad and ballast stiffness and damping coefficients, respectively. $\mathbf{C_w}$ and $\mathbf{\beta_w}$ are the shear stiffness and damping coefficients of the ballast, respectively, as shown in Fig. 2. The subgrade stiffness and damping are denoted as $\mathbf{C_f}$ and $\mathbf{\beta_f}$, respectively. The rail mass per unit length is represented by $\mathbf{m_r}$, $\mathbf{M_s}$ is mass of half of the sleeper and $\mathbf{M_b}$ is mass of each ballast block. In this study, **100** sleepers/ballasts are considered in order to ensure that there is no influence of rail end conditions. In general, **50** to **60** sleepers/ballast are considered sufficient for such study [16].

The detailed descriptions of the mathematical model combined with the equations of motion for the vehicle and track system can be obtained in reference [8].

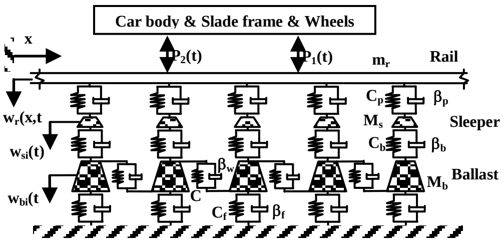

Fig. 2. Track system model

The final forms of the equations for vehicle and track subsystem are as follows:

Vehicle subsystem:

$$\mathbf{M_V \ddot{d}_V + \beta_V \dot{d}_V + C_V d_V = F_{VT}} \tag{1}$$

Track subsystem:

$$\mathbf{M_T \ddot{d}_T + \beta_T \dot{d}_T + C_T d_T = F_{VT}} \tag{2}$$

Wheel-rail interface subsystem:

$$\mathbf{F_{VT} = \beta_H (\Delta z)^{3/2}} \tag{3}$$

Where $\mathbf{M_V}$, $\boldsymbol{\beta_V}$ and $\mathbf{C_V}$ are mass, damping and stiffness matrices of the vehicle subsystem respectively. $\mathbf{d_V}$, $\mathbf{\dot{d}_V}$ and $\mathbf{\ddot{d}_V}$ are displacement, velocity and acceleration vectors of the vehicle subsystem respectively. $\mathbf{F_{VT}}$ is the interface force vector between the vehicle and track subsystem. $\mathbf{T_M}$, $\boldsymbol{\beta_T}$ and $\mathbf{C_T}$ are mass, damping and stiffness matrices of the track subsystem respectively. $\mathbf{d_T}$, $\mathbf{\dot{d}_T}$ and $\mathbf{\ddot{d}_T}$ are displacement, velocity and acceleration vectors of the track subsystem respectively. $\mathbf{\Delta Z}$ is the wheel-rail overlap in the vertical direction and $\boldsymbol{\beta_H}$ is the Hertzian constant.

2.2. Wheel flat model

A wide range of mathematical descriptions has been evolved to characterize the geometry of wheel flats in order to investigate the impact loads [1, 2, 16]. The wheel flats have been classified as chord type flat, cosine type flat and combined flat. On the basis of the reported flat geometries, the wheel flat can be divided into two categories: (i) chord type flat; and (ii) haversine type flat. The former one represents a freshly formed flat, while the latter is used to describe the geometry of the flat on the wheel in service that yields rounded edges [8].

After formation of a wheel flat, the sharp edges at the end of the profile of a fresh profile become rounded, while continued in service. This type of flat is commonly known as haversine flat, which is shown in Fig. 3.

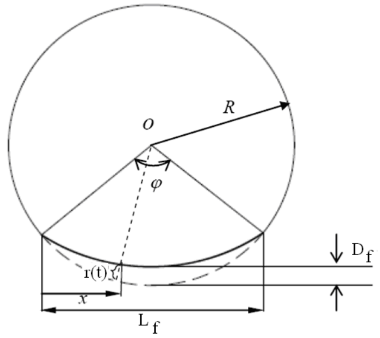

Fig. 3 A haversine type wheel flat [11]

The variation in the radii of a contact point **r(t)** within a haversine flat is expressed as:

$$\mathbf{r(t) = \frac{1}{2} D_f \left[1 - \cos(2\pi x / L_f)\right]} \tag{4}$$

Where $\mathbf{D_f}$ is the flat depth that has been related to wheel radius R, in the following manner [1]:

$$\mathbf{D_f = L_f^{\,2} / (16R)} \tag{5}$$

Equations (1-3) coupled with Equation (4) are simultaneously solved together in order to obtained the acceleration level of the wheel in the presence of a flat.

3. SYSTEM EQUATIONS OF MOTION

3.1 Equations of Vehicle

The equations of motion of the vehicle model are derived upon neglecting the contribution due to track roughness, while the contact forces developed at the wheel-rail interface are represented by $\mathbf{P_1(t)}$ and $\mathbf{P_2(t)}$. It is further assumed that the resultant secondary suspension force acts at the bogie mass center. The equations of motion of the vehicle system are summarized as:

Car body bounce motion:

$$\mathbf{M_c \ddot{z}_c + \beta_{s2} \dot{z}_c + C_{s2} z_c - \beta_{s2} \dot{z}_t - C_{s2} z_t = 0} \tag{6}$$

Bogie bounce motion:

$$\begin{aligned}\mathbf{M_t \ddot{z}_t} &+ \mathbf{C_{s1}(z_t + \ell_f \varphi_t - z_{w1})} + \\ &+ \mathbf{C_{s1}(z_t - \ell_r \varphi_t - z_{w2}) + C_{s2}(z_t - z_c)} + \\ &+ \mathbf{\beta_{s1}(\dot{z}_t + \ell_f \dot{\varphi}_t - \dot{z}_{w1})} + \\ &+ \mathbf{\beta_{s1}(\dot{z}_t - \ell_r \dot{\varphi}_t - \dot{z}_{w2}) + \beta_{s2}(\dot{z}_t - \dot{z}_c) = 0}\end{aligned} \tag{7}$$

Bogie pitch motion:

$$
\begin{aligned}
&\mathbf{J_t\ddot{\varphi}_t + C_{s1}\ell_f\left(z_t + \ell_f\varphi_t - z_{w1}\right) -}\\
&\mathbf{- C_{s1}\ell_r\left(z_t - \ell_r\varphi_t - z_{w3}\right) +}\\
&\mathbf{+ \beta_{s1}.\ell_f\left(\dot{z}_t + \ell_f\dot{\varphi}_t - \dot{z}_{w1}\right) +}\\
&\mathbf{+ \beta_{s1}.\ell_f\left(\dot{z}_t - \ell_r\dot{\varphi}_t - \dot{z}_{w2}\right) = 0}
\end{aligned} \tag{8}
$$

Front wheel vertical motion:

$$
\begin{aligned}
&\mathbf{M_w\ddot{z}_{w1} + \beta_{s1}\left(\dot{z}_{w1} - \dot{z}_t\right) + C_{s1}\left(z_{w2} - z_t\right) -}\\
&\mathbf{- \beta_{s1}\ell_f\dot{\varphi}_t - C_{s1}\ell_f\varphi_t + P_1(t) = 0}
\end{aligned} \tag{9}
$$

Rear wheel vertical motion:

$$
\begin{aligned}
&\mathbf{M_w\ddot{z}_{w2} + \beta_{s1}\left(\dot{z}_{w2} - \dot{z}_t\right) + C_{s1}\left(z_{w2} - z_t\right) +}\\
&\mathbf{+ \beta_{s1}\ell_r\dot{\varphi}_t + C_{s1}\ell_f\varphi_t + P_2(t) = 0}
\end{aligned} \tag{10}
$$

3.2 Equations of Rail Track

The equations of motion of the entire track system are derived upon integrating the equation of motion for the rail as an Euler beam with the differential equations of motions for the discrete sleeper and ballast supports. The deflection of the continuous rail can be derived from the partial differential equation for the Euler beam as [15]:

$$
\begin{aligned}
&\mathbf{EI\frac{\partial^4 z_r(x,t)}{\partial x^4} + m_r\frac{\partial^2 z_r(x,t)}{\partial t^2} =}\\
&\mathbf{= -\sum_{i=1}^{N} F_{rsi}(t)\delta(x - x_i) + \sum_{j=1}^{2} P'_j(t)\delta\left(x - x_j\right)}
\end{aligned} \tag{11}
$$

Where **N** is total number of sleepers considered in the model, **k** is the number of deflection modes considered for the rail beam and **j** is the number of wheelsets. **E** is the elastic modulus of rail beam materials and **I** is the second moment of area. The coordinate **x** represents the longitudinal position of the beam with respect to the left end support of the rail beam. $\mathbf{x_i}$ defines the position of the **i** th sleeper and $\mathbf{\delta(x)}$ is the Dirac delta function. $\mathbf{F_{rsi}(t)}$ is the force developed at the **i** th rail/sleeper interface and given by:

$$
\begin{aligned}
&\mathbf{F_{rsi}(t) = C_{pi}\left[z_r(x_i,t) - z_{si}(t)\right] +}\\
&\mathbf{+ \beta_{pi}\left[\dot{z}_r(x_i,t) - \dot{z}_{si}(t)\right]}
\end{aligned} \tag{12}
$$

The term $\mathbf{P'_j(t)}$ in Eq. (11) defines the total vertical force acting at the **j** th wheel and rail interface. It comprises both the static vehicle load and the contact force $\mathbf{P_j(t)}$, **j =1, 2**, such that:

$$\mathbf{P'_j(t) = P_j(t) + \left[0.5\left(M_c + M_t\right) + M_w\right]g};\ \boldsymbol{j} \mathbf{=1, 2}$$

The contact force $\boldsymbol{P_j(t)}$ is derived using the Hertzian contact model described in section 3.3.

The equation of motion for the discrete sleeper and ballast masses are derived as follows:

$$
\begin{aligned}
&\mathbf{M_{si}\ddot{z}_{si} + \left(\beta_p + \beta_b\right)\dot{z}_{si}(t) + \left(C_p + C_b\right)z_{si}(t) -}\\
&\mathbf{- \beta_b\dot{z}_{bi}(t) - C_b z_{si}(t) -}\\
&\mathbf{- \beta_p\sum_{k=1}^{K} Y_k(x_i)\dot{q}_k(t) - C_p\sum_{k=1}^{K} Y_k(x_i)q_k(t) = 0}
\end{aligned} \tag{13}
$$

i = 1, 2, … N

$$
\begin{aligned}
&\mathbf{M_{bi}\ddot{z}_{bi} + \left(\beta_b + \beta_f + 2\beta_w\right)\dot{z}_{bi}(t) +}\\
&\mathbf{+ \left(C_b + C_f + 2C_w\right)z_{bi}(t) -}\\
&\mathbf{- \beta_b\dot{z}_{si}(t) - C_b z_{si}(t) - \beta_w\dot{z}_{b(i+1)}(t) -}\\
&\mathbf{- C_w z_{b(i+1)}(t) - \beta_w\dot{z}_{b(i-1)}(t) -}\\
&\mathbf{- C_w z_{b(i-1)}(t) = 0}
\end{aligned} \tag{14}
$$

i = 1, 2, … N

3.3 Wheel-Rail Interaction

The wheel-rail contact has been widely described by the nonlinear Hertzian contact theory is commonly used for the wheel/rail interaction problems [12, 15, 16], which is also used in the present study. According to the Hertzian contact theory, the wheel-rail contact force is related to the rail deflection in a nonlinear manner, such that:

$$\mathbf{P(t) = \beta_H\Delta z(t)^{3/2}} \tag{15}$$

Where $\mathbf{\Delta z(t)}$ is the wheel-rail overlap in the vertical direction. In the presence of a wheel defect, the overlap is defined by the relative motion of the wheel with respect to the rail as:

$$\mathbf{\left[z_{wj}(t) - z_r\left(x_j,t\right) - r_j(t)\right]};\ \boldsymbol{j} \mathbf{=1, 2} \tag{16}$$

Where $\mathbf{r(t)}$ is the wheel flat function. $\mathbf{z_w(t)}$ and $\mathbf{z_r(x,\ t)}$ are the wheel and rail deflections in vertical direction, respectively.

For a haversine flat, **r** is expressed as:

$$\mathbf{r = \frac{1}{2}D_f\left[1 - \cos\left(2\pi x / L_f\right)\right]} \tag{17}$$

Where $\mathbf{D_f}$ is the flat depth, $\mathbf{L_f}$ is the length of the flat, **x** is the longitudinal coordinate of the contact point within the flat.

The contact force diminishes when a loss of contact of the wheel with the rail is encountered, when $\mathbf{\left[z_{wj}(t) - z_r\left(x_j,t\right) - r_j(t)\right] \le 0}$; $\boldsymbol{j}$ **=1, 2**

4. ANALYSIS METHOD

The track system model formulated in this study comprises both ODEs and PDE describing the deflection of the lumped sleeper and ballast masses, and the continuous rail, respectively. The PDE is expressed as ODEs by assuming a mode shape function. The Rayleigh-Ritz method is used to express the fourth order PDE describing the motion of the continuous rail by a series of second order ordinary differential equations in terms of the time coordinates.

The resulting ODEs of the track and vehicle systems are than solved in time domain to obtained responses of individual components of the vehicle-track system model. The relative responses between the components are used to derive the dynamic interaction forces.

The deflection modes and the natural frequencies of an Euler beam in the absence of sleeper supports and external loads have been well documented and can be expressed as [15]:

$$\mathbf{Y_k(x) = \sin\left(\frac{k\pi x}{\ell}\right)} \text{ and}$$
$$\boldsymbol{\omega_k} = \left(\frac{\mathbf{k\pi}}{\ell}\right)^{\mathbf{2}}\sqrt{\frac{\mathbf{EI}}{\mathbf{m_r}}}\ \mathbf{,\ k = 1, 2, 3, \ldots\ K} \tag{18}$$

Where is the deflection mode, ω_k is the corresponding natural frequency and ℓ is the beam length.

The deflection response of the rail is then derived from :

$$\mathbf{z_r(x,t) = \sum_{k=1}^{K} Y_k(x) q_k(t)} \tag{19}$$

Where **K** is the number of modes considered.

The substitution of the rail deflection response from Eq. (19) together with the mode shape $\mathbf{Y_k}$ in the PDE, Eq. (6) yields a set of ODEs in **q(t)** , expressed as:

$$\begin{aligned}
&\mathbf{\ddot{q}_k(t) + \alpha\sum_{i=1}^{N}\beta_{pi}Y_k(x_i)\sum_{k=1}^{K}Y_k(x_i)\dot{q}_k(t) +} \\
&\mathbf{+\frac{EI}{m_r}\left(\frac{k\pi}{\ell}\right)^4 q_k(t) +} \\
&\mathbf{+\alpha\sum_{i=1}^{N}C_{pi}Y_k(x_i)\sum_{k=1}^{K}Y_k(x_i)q_k(t) -} \\
&\mathbf{-\alpha\sum_{i=1}^{N}\beta_{pi}Y_k(x_i)\dot{z}_{si}(t) -} \\
&\mathbf{-\alpha\sum_{i=1}^{N}C_{pi}Y_k(x_i)z_{si}(t) =} \\
&\mathbf{=\alpha\sum_{j=1}^{2}P'_j(t)Y_k(x_{Gj})}
\end{aligned} \tag{20}$$

Where $\alpha = (2/m_r\ell)$ and $k = 1, 2, 3\ldots\ldots K$

The equations of motion of the vehicle system described by Eqs. (6) to (10), and of the track system derived in Eqs. (11) to (14) together with the Hertzian nonlinear contact model in Eq. (15) describe the dynamics of the coupled vehicle-track system. Detail derivation of the vehicle-track model and method of analysis can be found in [8].

5. RESPONSE ANALYSES OF THE VEHICLE TRACK SYSTEM

The dynamic response of the entire vehicle-track system is evaluated under a constant speed of **27 km/h** in the presence of a **50 mm** long and **1 mm** deep flat in the leading wheel. The time history of the dynamic contact force at the defective wheel-rail interface is compared with that reported in [15], as shown in Fig. 4. The results presented in Fig. 4 clearly show the effectiveness of the proposed quarter car vehicle model in predicting the contact force with the accuracy of a full vehicle model. This suggests negligible contributions due to the vehicle pitch, and a reduced model would be sufficient for accurately predicting the dynamic contact force due to a wheel flat.

The results in Fig.4 further show the sequence of events in terms of contact force and their frequency of oscillation, which can be explained in the following manner. As the wheel flat enters the contact area, there is a sudden drop in the contact force followed by a large peak due to the wheel-rail impact. This referred to as $\mathbf{P_1}$ force in literature [15], lasts for a short duration, which correspond to the duration of the flat in contact with the rail. The frequency of $\mathbf{P_1}$ can therefore be referred to as the excitation frequency due to the flat, and is a function of flat size and forward speed. The following sequence of peak force known as $\mathbf{P_2}$ force oscillates at a frequency of **125 Hz**. This is primarily due to oscillation of the rail on the support pads. From various simulation runs, it is noticed that this frequency is unaffected by the flat size and speed, and is a function of pad properties. As shown in

Fig. 4, the final sets of oscillation in wheel rail contact force takes place at a frequency of **56 Hz**, which is attributed to the coupled vehicle-track natural frequency.

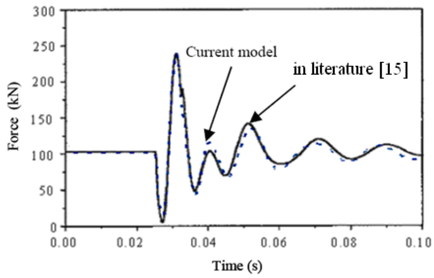

Fig. 4. Comparison of wheel-rail impact force response of the present model with that reported in literature [6].

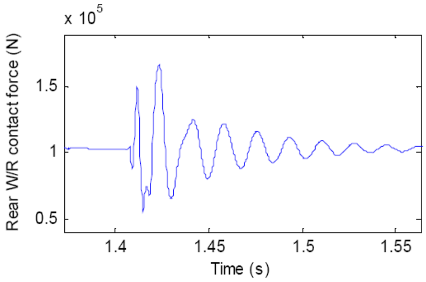

Fig. 5. Time-history of impact force response at flat-free rear wheel-rail contact

The results clearly show significantly high contact force at the rear wheel-rail interface, even though the rear wheel is considered to be free of defects. For the flat size and speed considered, the peak contact force at the rear wheel reaches **1.62 times** the static load while the peak impact force at the wheel with flat (Fig. 4) can reach **2.5 times** the static load. The sequence of events at the rear wheel (Fig. 5) is somewhat different than that of the front wheel with flat (Fig. 4). This is attributed to the pitch motion of the bogie and phase difference between the motions of the wheel and rail at the front and rear axles.

These force time histories can be easily related to the wheel-rail displacement time histories presented in Fig. 6 (a) and 6 (b) for the defective and defect free wheels respectively.

The validated vehicle-track system model is utilized to investigate the dynamic contact force at a constant forward speed of **70 km/h**. The simulations are performed for a haversine wheel flat using the parameters presented in Table 1. The type of flat considered closely meets the wheel removal criterion recommended by a number of European railroad organizations [6, 9, 10, 13].

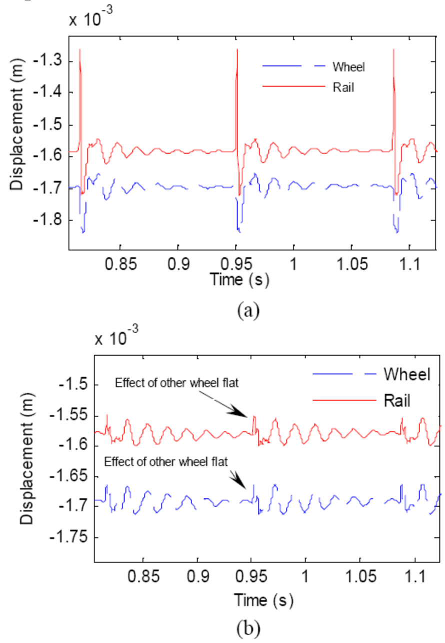

Fig. 6. Wheel-rail displacement time history: (a) Defective wheel; (b) Defect-free wheel.

Table 1: Simulation parameters

Sym-bol	Parameter	Value
$\mathbf{M_c}$	Car body mass (quarter car)	19400 kg
$\mathbf{M_t}$	Bogie mass	500 kg
$\mathbf{M_w}$	Wheel mass	500 kg
$\mathbf{J_t}$	Bogie mass moment inertia	176 kg.m^2
$\boldsymbol{\beta_{s1}}$	Primary suspension damping	3.5 kN.s/m
$\mathbf{C_{s2}}$	Secondary suspension stiffness	6.11 MN/m
$\boldsymbol{\beta_{s2}}$	Secondary suspension damping	158 kN.s/m
$\boldsymbol{\ell_t}$	Wheelset distance	1.25 m
R	Wheel radius	0.42 m
$\mathbf{L_f}$	Flat length	52 mm
$\mathbf{D_f}$	Flat depth	0.4 mm
$\boldsymbol{\beta_H}$	Hertzian spring constant	87 GN/m$^{3/2}$
$\mathbf{m_r}$	Rail mass per unit length	60.64 kg/m
EI	Rail bending stiffness	6.62 MN.m^2
$\mathbf{M_s}$	Sleeper mass	118.5 kg
$\mathbf{M_b}$	Ballast mass	739 kg
$\mathbf{C_p}$	Railpad stiffness	120 MN/m

C_b	Ballast stiffness	182 MN/m
C_w	Ballast shear stiffness	147 MN/m
C_f	Subgrade stiffness	78.4 MN/m
β_p	Railpad damping	75 kN.s/m
β_b	Ballast damping	58.8 kN.s/m
β_w	Ballast shear damping	80 kN.s/m
β_f	Subgrade damping	31.15kN.s/m
ℓ_s	Sleeper distance	0.6 m
N	No. of sleepers	100

The variations in bearing force are investigated using the baseline model for three different loading as shown in Fig. 7. The figure shows that the bearing forces at the defective wheel follow the same trend as the impact force at the wheel-rail contact. The results further show that the peak bearing force at the bearing reaches **1.5**, **1.73** and **1.93 times** the static force for a **102**, **82**, **63 kN** wheel loads, respectively. Corresponding to the above wheel loads, the wheel rail contact force was found to be **1.77**, **1.96** and **2.45 times** the static force.

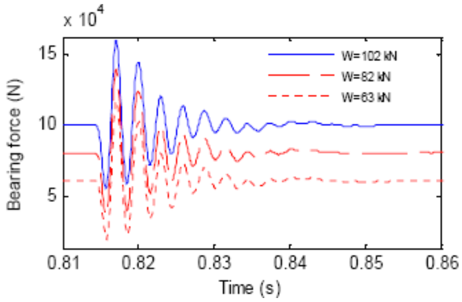

Fig. 7. Variations in the bearing force response due to a rear-wheel flat as a function of static wheel load.

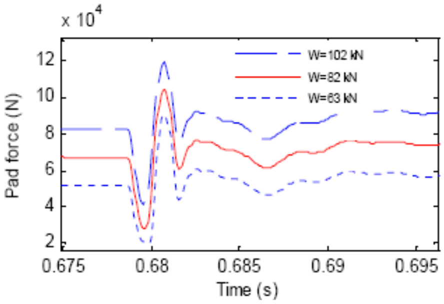

Fig. 8. Variations in railpad force due to a rear wheel flat as a function of static wheel load.

The dynamic rail pad force is computed from relative deflection of the rail and sleeper, using Eq. (12). As an example, the variations in the rail pad force developed at sleeper no. 22, due to a flat within the rear wheel, are illustrated in Fig. 8.

Figure 8 shows that as the wheel flat enters the wheel-rail contact region, the pad force first decreases from its static level. Similar to contact and bearing forces, the ratios of the peak pad force to static pad force are obtained as **1.46**, **1.57**, and **1.77** for static wheel load of **102**, **82** and **63 kN**, respectively. The results also show that the magnitudes of pad forces are significantly smaller than those of the contact forces, which can be attributed to inertia force of the rail.

The impact force developed at wheel-rail interface due to a wheel flat is also transmitted to the ballast blocks, which is ultimately transmitted to the ground. The force developed at the sleeper-ballast interface is known as ballast force. The ballast force is computed by summing up the reaction forces obtained from a particular sleeper and the shear forces arising from couplings with the adjacent ballast blocks in the presence of a single flat in the rear wheel. The time histories of the ballast forces for ballast no. 22 under three different load conditions are shown in Fig. 9. The results suggest that variations in ballast forces are similar to those observed for the pad forces shown in Fig. 8. The peak magnitudes of the ballast forces, however, are considerably smaller than those of the pad forces. The ratios of peak to static ballast forces for wheel loads of **102, 82**, and **63 kN** are obtained as **1.32**, **1.38**, and **1.46**, respectively. The normalized ballast forces are found to be relatively less sensitive to variations in the static wheel load in the range of variations considered.

Comparison of ballast force results (Fig. 9) with pad force results (Fig. 8) clearly shows that the frequency of oscillation of the ballast force is significantly less than that of the pad force, while their trend is very similar.

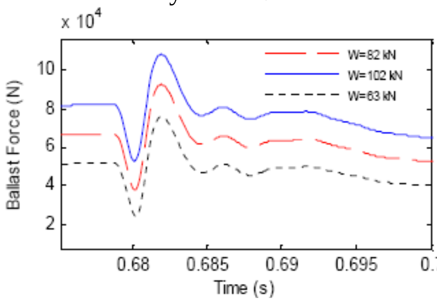

Fig 9: Variations in ballast force due to a rear wheel flat as a function of static wheel load.

6. CONCLUSION

This paper presents the responses of the railway vehicle and track components in terms of contact forces and displacements. The considered vehicle model is a five-DOF pitch-plane lumped parameter quarter car model supported on two-dimensional track systems comprising three layers. The car body is linked with the vehicle bogie through secondary suspension springs and damper elements, which is further linked to the wheels through primary suspension springs and damper elements. In modeling of the track, the rail is considered as an infinitely long beam discretely supported by a series of springs, dampers and masses representing the elasticity and damping effects of the rail pads, ballasts, and subgrades respectively. The non-linear Hertzian contact theory is employed to accomplish the dynamic interactions between the lumped mass vehicle and the continuous rail. The drastic effect of one wheel flat to the other perfect wheel-rail contact point is also taken into account.

This study illustrated the significant influence of wheel flat on the components of vehicle and track system. The current study also shows that flat present in one wheel has strong influence not only in wheel-rail impact forces but also on bearing, pad and ballast forces at the defective as well as adjacent wheelset. The investigations further show that the magnitudes of these transmitted forces as a ratio of static load could be significant and in general is lower for the lightly loaded wheel.

7 REFERENCES

[1] Dong, R.G., “Vertical dynamics of railway vehicle-track system,” Ph.D. Thesis, Dept. of Mechanical and Industrial Engineering, Concordia University, Montreal, Canada, 1994.

[2] Ishida, M., and Ban, T., “Modelling of the wheel flats for track dynamics” XXX Convegno Nazionale AIAS- Alghero (SS), 12-15 September 2001.

[3] Hou, K., Kalousek, J., Dong, R., “A dynamic model for an asymmetrical vehicle/track system” Journal of Sound and Vibration 267 (2003) 591–604.

[4] Jin, X., Wen, Z., Wang, K., and Xiao, X., “Effect of passenger car curving on rail corrugation at a curved track” Volume 260, Issue 6, 10 March 2006, p619-633.

[5] Knothe, K., and Grassie, S.L., “Modeling of railway track and vehicle/track interaction at high frequencies”, Vehicle System Dynamics 22 1993, pp. 209 – 262.

[6] Lonsdale, C., Dedmon, S., and Pilch, J., “Effects of increased gross rail load on 36-inch diameter freight car wheels” available at www.standardsteel.com/rdpapers/2001

[7] Nielsen, J.C.O., and Oscarsson, J., “Simulation of dynamic train–track interaction with state-dependent track properties” Journal of Sound and Vibration, vol. 275 (2004) 515–532

[8] Rajib Ul Alam Uzzal, “Role of Railway Vehicle-Track System and Design Parameters on Flat-Induced Impact Load” M. A. Sc thesis, Dept. of Mechanical & Industrial Engineering, Concordia University, Montreal, Quebec, Canada 2007.

[9] Reilly, K., “Railway Wheelsets”, Rail Safety and Standards Board, London, UK, June 2003.

[10] Sun, Y. Q., Dhanasekar, M., and Roach, D., “A three-dimensional model for the lateral and Vertical Dynamics of wagon-track system.” Proceedings of the institution of Mechanical Engineers, Part F: Rail and Rapid Transit. Vol. 217 (1), 2003, p 31-45.

[11] Sun, Y. Q., and Dhanasekar, M., “Importance of the track modeling on the determination of the critical speed of wagons” Vehicle system Dynamics Supplement 41 (2004), p232-241.

[12] Thompson, D., and Wu, T.X., “The effect of non-linearity on wheel/rail impact” Journal of Rail and Rapid transit, volume 218, part F, 2003, p1-15.

[13] Transport Canada “Railway Freight Car Inspection and Safety Rules” available at http://www.tc.gc.ca/railway/Rules/TC_0-06-1.htm

[14] Wen, Z., Jin, X., and Zhang, W., “Contact-impact stress analysis of rail joint region using the dynamic finite element method” Wear 258 (2005) p1301–1309.

[15] Zhai, W. M., Cai, C. B., Wang, Q. C., Lu, Z.W., and Wu., X. S., “Dynamic Effects of Vehicles on Tracks in the Case of Raising Train Speed” Proceedings of the Institution of Mechanical Engineers, Part F, v 215, 2001, p125-135

[16] Zhai, W., and Cai, Z., “Dynamic interaction between a lumped mass vehicle and a discretely supported continuous rail track” Computers and Structures Vol. 63, No. 5, pp. 987-997, 1997.

[17] Zhai, W. M., Cai, C. B., Wang, Q. C., Lu, Z.W., and Wu., X. S., “Dynamic effects of Vehicles on Tracks in the case of raising train speed” Proceedings of the Institution of Mechanical Engineers, Part F, v 215, 2001, p125-135

HEAVY MACHINERY - HM 2011, 9-12
ISBN 978-86-82631-58-3
Paper accepted: 25.05.2011

Identification of wave phenomena at wagons impact

Dragan Petrović[1,*] – Milan Bižić[1] – Mirko Đelošević[1] – Ranko Rakanović[1]
[1] University of Kragujevac, Faculty of Mechanical Engineering Kraljevo

At longitudinal impacts, when the structure members are very quickly deformed, complex physical phenomena occur, such as: changes of rheological properties of the material, temperature and chemical changes, etc. During these phenomena, the behaviour of the structure can be completely different from its behaviour at static loading. The structure fails in getting displacements which correspond to fast changes of loads. Such delay can cause abrupt deformation of the structure. This paper presents theoretical and experimental analysis of wave phenomena at impact of railway wagons. Theoretical considerations have been realized on an idealized beam model, and experimental results refer to test of wagon type Zagkks for transport of liquid petroleum gas.

Keywords: Railway vehicle, wagon, wave, identification, impact

0 INTRODUCTION

Theoretical and experimental analysis of behaviour of body at wagon impact cannot be precisely determined without considering wave processes. In railway vehicles, where the geometry of the carrying structure is complex, and speeds of impact are not so great, a model of elastic body neglecting some phenomena can be formed. In that way, local effects which refer to the three-axis stress state is avoided. This postulation defines impact by a certain speed of a cross-section of the member or the shell and the ratio between masses of the observed elements and load. Consideration of impact phenomena is, in this way, different from the case where the change of several physical factors is present and where changes of the structure of the material are dominant. Most real structures subjected to impact action can be treated in this way. In that case, equations of motion [1, 2] have the form:

$$
\begin{aligned}
&(\lambda+G)\frac{\partial \varepsilon_v}{\partial x}+G\nabla^2 u+F_x-\rho\frac{\partial^2 u}{\partial t^2}=0\\
&(\lambda+G)\frac{\partial \varepsilon_v}{\partial y}+G\nabla^2 v+F_y-\rho\frac{\partial^2 v}{\partial t^2}=0 \qquad (1)\\
&(\lambda+G)\frac{\partial \varepsilon_v}{\partial z}+G\nabla^2 w+F_z-\rho\frac{\partial^2 w}{\partial t^2}=0
\end{aligned}
$$

Where:
λ, G, ρ – constants of material
ε_v – volume deformation
u, v, w – displacements in x, y, z directions
F_x, F_y, F_z – external volume forces,
t – time, and ∇^2 – Laplace operator

1 BEHAVIOUR OF ELASTIC BODIES AT IMPULS LOADS

Behavior of an elastic body loaded with forces which do not change in time belongs to the field of statics. These problems can include the case where the change of load in time is slow, i.e. quasi-static. If changes of load in time are faster, as in the case of impact loads, then the problems are transferred to the field of dynamics. In this case, action of dynamic (impact) load is not immediately transmitted to all points of the body. Waves of stresses and strains start to propagate from the loaded surface and they have finite speed of propagation.

1.1 Longitudinal and transversal waves in isotropic elastic continuum

If a certain point of the elastic continuum is incited, waves will start to propagate from that point to all sides. At a distance from the centre of incitation, all particles will move in parallel with the direction of propagation of waves (longitudinal waves) or normally to that direction (transversal waves) (Fig. 1).

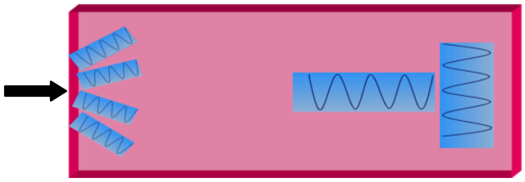

Fig. 1. *Distribution of waves in elastic continum*

Under the assumption that, in the existence of waves, the volume deformation is equal to zero, i.e. that deformation consists of sliding and rotating only, equations (1) obtain the form [1, 2]:

*Corr. Author's Address: Faculty of Mechanical Engineering Kraljevo, Dositejeva 19, 36000 Kraljevo, Serbia, petrovic.d@mfkv.kg.ac.rs

$$\frac{\partial^2 u}{\partial t^2} = c_i^2 \frac{\partial^2 u}{\partial x^2}$$
$$\frac{\partial^2 v}{\partial t^2} = c_i^2 \frac{\partial^2 v}{\partial y^2} \qquad (2)$$
$$\frac{\partial^2 w}{\partial t^2} = c_i^2 \frac{\partial^2 w}{\partial z^2},$$

Where i=1, 2

Previously obtained equations have shown that the waves in elastic environment can be distributed in two different speeds. When *i=1* these are longitudinal waves, and when *i=2* these are transversal waves.

If the axis x is in the direction of propagation of waves (Fig. 2), then $v=w=0$, so that the displacement u is a function of the coordinate x. Every function $f(x+c_1t)$ can be a solution to the previous equation. Also, every function $f_1(x-c_1t)$ is a solution to that equation, so that it is possible to write the general solution in the form [3]:

$$u = f\left(x + c_1 t\right) + f_1\left(x - c_1 t\right) \qquad (3)$$

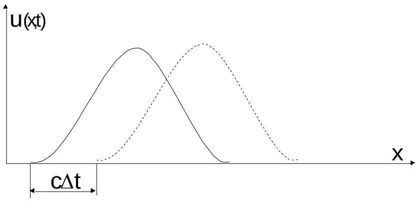

Fig. 2. *Propagation of waves in the elastic continuum*

The general solution to the equation (3) can be represented by two waves moving along the axis x in two opposite directions at the constant speed c_1 (Fig. 3).

Fig 3. *Moving of waves over the elastic body*

1.2 Beam at longitudinal impact

At the beginning of impact (Fig. 4), the beam is compressed, so that the initial speed v_1 of the mass m_1 is momentary changed until the speed of displacement of the beam end which undergoes the impact $\dot{u} = \partial u / \partial t$. This leads to fast occurrence of deformations $\varepsilon = \partial u / \partial x$, that is the stresses:

$$\sigma_x = E \cdot \varepsilon \qquad (4)$$

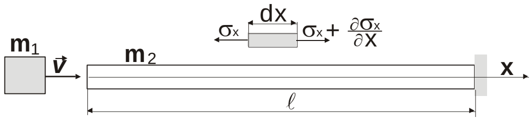

Fig. 4. *Beam at longitudinal impact*

On the basis of the expression (2), the differential equation of displacement of the beam along the axis x has the form:

$$\frac{\partial^2 u}{\partial x^2} = \frac{1}{c^2} \frac{\partial^2 u}{\partial t^2} \qquad (5)$$

Where the speed of propagation of waves in the beam is [4]:

$$c = \sqrt{\frac{E \cdot g}{\gamma}} = \sqrt{\frac{E}{\rho}} \qquad (6)$$

At the moment of reaching the maximum displacement in the beam u_{max}, the mass m_1 will be in the state of rest. If the kinetic energy before the impact is $E_{k,o}$ and the maximum potential energy of the system is $E_{p,max}$, then, on the basis of the law of conservation of energy, it can be written:

$$E_{k,o} = E_{p,max} = \frac{1}{2} m_1 v_1^2 = \frac{1}{2} EA\ell \left(\frac{u_{max}}{\ell} \right)^2 \qquad (7)$$

$$\varepsilon_{max} = -\frac{u_{max}}{\ell} = -v_1 \sqrt{\frac{m_1}{EA\ell}} = -\frac{v_1}{c} \sqrt{\frac{m_1}{m_2}} = -\frac{v_1}{c} \sqrt{\kappa} \qquad (8)$$

Where κ is the ratio between the mass of load and the mass of the beam.

In the case of propagation of waves in the beam whose end $x = \ell$ is stationary, the solution must satisfy the following boundary conditions:

$$u(x,0) = 0; \quad \frac{\partial u}{\partial t}(x,0) = v_1; \text{ when } x=0$$

$$\frac{\partial u}{\partial t}(x,0) = 0; \text{ when } x>0 \qquad (9)$$

$$\frac{\partial^2 u}{\partial t^2}(0,t) = \frac{c^2}{\kappa \ell} \frac{\partial u}{\partial x}(0,t); \quad u(\ell,t) = 0$$

The local speed of the beam particles $\dot{u}$ and deformations ε is determined by appropriate derivations:

$$\left.\begin{aligned}\dot{u} &= \frac{\partial u}{\partial t} = cf_1'(ct-x)+cf'(ct+x)\\ \varepsilon &= \frac{\partial u}{\partial x} = -f_1'(ct-x)+f'(ct+x)\end{aligned}\right\} \qquad (10)$$

Let us consider the initial period of deformations $0 \le t \le \ell/c$. If $f=0$ and $x=0$, the equation for determination of displacement of the loaded end is obtained:

$$f_1''(t^*)+\frac{1}{\kappa\ell}f_1'(t^*)=0 \qquad (11)$$

Where $t^*=ct$

By using the limiting conditions, the following expressions for the speed of displacement of the movable end of the beam and for the corresponding deformation are obtained:

$$\left.\begin{aligned}\dot{u}(0,t) &= \frac{\partial u(0,t)}{\partial t} = v_1 \cdot e^{-\frac{t^*}{\kappa\ell}}\\ \varepsilon(0,t) &= -\frac{v_1}{c}\cdot e^{-\frac{t^*}{\kappa\ell}}\end{aligned}\right\} \qquad (12)$$

Hence, it follows that at the moment of impact the members of the beginning of the beam, which are subjected to impact, obtain the deformation equal to the ratio of the local speed of the initial point of the beam and the speed of sound in the beam. The displacement of the end point of the beam is determined by the expression:

$$u(0,t)=v_1\frac{\kappa\ell}{c}\left(1-e^{-\frac{t^*}{\kappa\ell}}\right) \qquad (13)$$

If the mass of the body which performs impact is considerably greater than the mass of the beam, it can be considered that $\kappa=\infty$, and at the speed $v_1=const.$ from the equation (12), it follows $u(0,t)=v_1 t$.

For the analysis of the time period $\ell \le ct \le 2\ell$, it is necessary to determine the function *f* and limiting conditions at the stationary end. In that way, direct integration of the equation (5) results in functions whose form is changed upon running out of the period which is equal to the period of passing of the elastic wave along the beam. In the time period $t=2\ell/c$, the pressure wave returns to the beam beginning, which is in contact with the body. The speed of the body cannot be abruptly changed, so that the wave will reflect as if from the fixed end, and thus be doubled.

The characteristic curve of the beam deformation at longitudinal impact has the exponential form which decreases in time and after the period $2\ell/c$ has a rise. The value of the exponent is determined by the ratio between the masses of the body and the beam κ. The length of duration of the contact depends on the speed of members at impact v_1 and the ratio of masses κ. The contact stops at the moment when deformation of the beam beginning is equal to zero, which corresponds to passing through the equilibrium state.

2 SPEEDS OF WAGONS AT IMPACT

The impact of two wagons can be observed as the impact of two beams (Fig. 5) moving at the speeds v_1 and v_2 ($v_1 > v_2$).

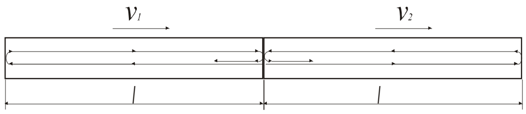

Fig. 5. *Impact of two beams*

At the moment of impact, two identical pressure waves start moving along both beams. In order to obtain equal absolute speeds of particles of both beams over the continuous surface, the values of those speeds must be equal to $(v_1 - v_2)/2$. After the time interval ℓ/c, pressure waves reach free ends of the beams. At this moment, both beams are in the state of uniform pressure and the absolute speeds of all particles of the beams are:

$$v_1-\frac{v_1-v_2}{2}=v_2+\frac{v_1-v_2}{2}=\frac{v_1+v_2}{2} \qquad (14)$$

Pressure waves will then reflect from the free end, and at the moment $2\ell/c$, when these waves reach the contiguous surface of both beams, their speeds become:

$$\frac{v_1+v_2}{2}-\frac{v_1-v_2}{2}=v_2 \qquad (15)$$

$$\frac{v_1+v_2}{2}+\frac{v_1-v_2}{2}=v_1 \qquad (16)$$

The previously exposed theory of impact is based on several assumptions, such as, it is the impact of two homogeneous beams, the contact occurs over the whole surface of the beam, at the same moment, etc. In practice, such a case is rare and that is why the results of theoretical and experimental research do not agree. However, the knowledge of principles of occurrence and propagation of waves can help us in the analysis of experimentally obtained results of tests of real structures.

3 EXPERIMENTAL RESULTS OF IMPACT OF WAGONS

Experimentally obtained results (Fig. 6.) show effects of wavy motion, i.e. the time necessary for the wave to pass from the buffer to the end of the wagon and back. The experimentally determined time for this is between *21* and *24 ms* and it is somewhat longer than in the case when two homogeneous members of the same length would be at impact. The cause of this "delay" of wave is explained by the non-homogeneous structure which is interweaved with elements of different characteristics, then by the shape of the contiguous surfaces participating in the impact, etc. It can be indirectly concluded that the transducers, which record the impact force, have a satisfactory dynamic characteristic because they are able to record a phenomena which lasts more than ten times less than the time of impact duration. In the transducers which do not have a satisfactory dynamic characteristic, the curve would have a continual increase (without rises), and in that case there would appear an error in recording the maximum impact force.

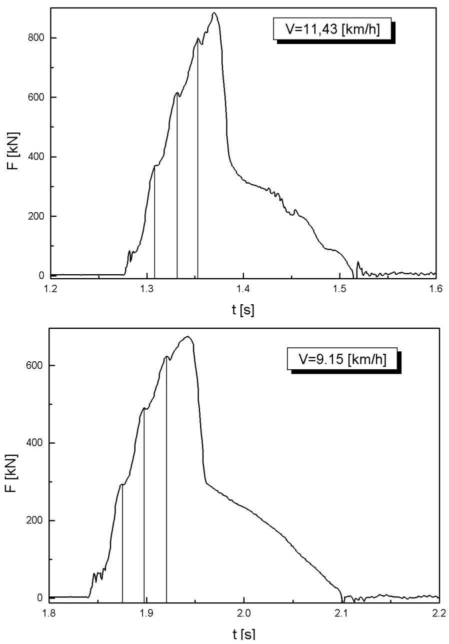

Fig. 6. *Change of force on the buffers at impact of wagons*

4 CONCLUSION

The aim of this paper is to draw attention to the phenomena that occur in impulse loading. This is particularly important for experimental investigation of wagons impact when it is necessary to determine the data acquisition frequency. As shown in Fig. 7, if the speed of acquisition is insufficient it is possible that the measurement does not register the maximum value of force at a collision.

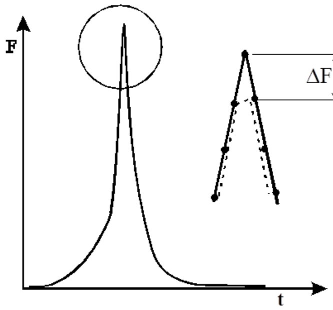

Fig. 7. *Measurement of force in a collision with insufficient a frequency of acquisition*

For this reason it is necessary to carry out the more theoretical study of impulse phenomena, and based on that performing the preparation for experimental investigation.

5 REFERENCES

[1] Petrović D., Stability of wagon carrying structure at impact, Ph. D. thesis, Faculty of Mechanical engineering Kraljevo, 2000.

[2] Petrović D., Dynamic of impact of wagons, Zadu`bina Andrejević, 2001g., Beograd.

[3] Goldsmith W., Impact, The theory and Physical behavior of colliding solids, London1965.

[4] Petrović D, Rakanović R, Šoškić Z, Stress and strain waves at impacts of Waggons, XIII International Conference Transport 2003, 13-14 novembar, Sofija, Bugarska, str. 143-148.

[5] Petrović D, Rakanović R, Šoškić Z, Waggon impact coefficient of restitution, XII International Conference Transport 2002, 14-15 novembar, Sofija, Bugarska, str. 181-184

HEAVY MACHINERY - HM 2011, 13-15
ISBN 978-86-82631-58-3
Paper accepted: 25.05.2011

Application of Regression Analysis in Studying the Interaction of Terrestrial Vehicles with Road

Borislav Benchev[1,*] - Veselin Stoyanov[1]
[1] VTU "Todor Kableshkov"

The technical performance of vehicles is in direct relationship with their design and influence of the environment. Energy loss during the movement of vehicles reflects chassis and road interaction. This report outlines methods for mathematical modelling based on data from active-passive experiment. Presence of significant input factors shows the impact of regression equations coefficient. Advantages of using regression analysis in examining vehicles and road interaction are presented.

Keywords: Vehicle, regression analysis, input factors, ellipsoid, coefficient.

INTRODUCTION

Technical performance of the vehicles is in direct relation to their design and influence of the movement environment. Energy losses in vehicles movement reflect chassis and road interaction. Performed scientific and experimental research has shown that such losses are determined by a significant number of input factors. Functional relationship between input factors and target function (output parameter) is in compliance with the law that underlies rolling process and manages the interaction of the running gear with the road.

The disclosure of this law allows more profound penetration into the nature of studied process, running gear improvement and thereby improvement of technical and economic performance of vehicles.

Regression analysis is one of the most common statistical methods for modeling and optimization of multi-factor objects. This method advantage over many others (variance, correlation, factor, etc.) lies in the fact that under certain conditions it allows the construction of a mathematical model of studied process, while its statistical evaluation is being carried out simultaneously.

The main prerequisite for conducting qualitative regression analysis is the fact that the measurement of objective function (output parameter) "$\boldsymbol{y}$" is carried out in a predefined experimental plan that allows the formation of an output matrix with orthogonal columns.

Implementation of such an experiment related to testing interaction of vehicles with road freedoms principle is impossible due to the following:

- the experiment does not allow the factors to be maintained at a constant level
- the object does not work in some experimental plan points

Mathematical Modeling of the Use of Regression Analysis

Current work objective is to develop methodologies for mathematical modeling of process of using regression analysis on data from active-passive experiment.

To attain this purpose it is necessary to define the coefficients of the full quadratic form, including in itself all possible functions.

$$\boldsymbol{b} = \left| \boldsymbol{X}^{\boldsymbol{T}} . \boldsymbol{X} \right|^{-1} . \boldsymbol{X}^{\boldsymbol{T}} . \boldsymbol{Y} , \qquad (1)$$

Disturbance is a random variable, with varying force and direction as a function of time "$\boldsymbol{t}$" [2]. It has normal distribution and, number of attempts being sufficiently large, it has zero mathematical expectation, so coefficients of insignificant functions are obtained with zero meaning. Limited number of tests carried out in practical experiments leads to real coefficients of random functions, but at the cost of resulting errors.

The requested value of coefficients is in the trust area, defined by equation of ellipsoid [2]:

$$(\boldsymbol{\beta} - \boldsymbol{b})^{\boldsymbol{T}} . \boldsymbol{X}^{\boldsymbol{T}} . \boldsymbol{X} (\boldsymbol{\beta} - \boldsymbol{b}) = \boldsymbol{k} . \boldsymbol{S}_{\boldsymbol{\varepsilon}}^{2} . \boldsymbol{F} , \qquad (2)$$

where the indications are:

$\boldsymbol{\beta}$ - confidence interval of the coefficients;
$\boldsymbol{X}$ - output matrix;
$\boldsymbol{k}$ - number of coefficients;

*Corr. Author's Address: VTU "Todor Kableshkov", 158 Geo Milev Str., Sofia, Bulgaria, ves@vtu.bg

$\boldsymbol{F}\left|\begin{matrix}\boldsymbol{\alpha}\\ \boldsymbol{n-k}\\ \boldsymbol{k}\end{matrix}\right|$ - coefficient of Fischer

$\boldsymbol{\alpha}$ - significance level.

$\boldsymbol{S}_{\boldsymbol{\varepsilon}}^{2}$ - dispersion of disturbance

The relative error of the models can be expressed by the relation:

$$\Delta = \frac{\boldsymbol{\beta} - \boldsymbol{b}}{\boldsymbol{b}} \tag{3}$$

$$\text{or } \Delta.\boldsymbol{b} = \boldsymbol{\beta} - \boldsymbol{b} \tag{4}$$

When substituting in (1) we obtain the relative error:

$$\Delta^2 = \boldsymbol{k}.\boldsymbol{S}_{\boldsymbol{\varepsilon}}^{2}.\boldsymbol{F}\left[\boldsymbol{b}^{\boldsymbol{T}}\left(\boldsymbol{X}^{\boldsymbol{T}}.\boldsymbol{X}\right)\boldsymbol{b}\right]^{-1} \tag{5}$$

Quadratic form in brackets is always positive down, thus resulting functional is always a real number, the value of which is a criterion for the accuracy and reliability of experimental material. Likelihood by which accuracy is guaranteed coincides with the probability at which criterion of Fisher was selected. Confidence ellipsoid equation does not allow to assess confidence intervals of each coefficient separately, but it contains the information necessary for their significance.

Confidence ellipsoid dimensions depend on the value of $\boldsymbol{F}$ - criterion and increase with increasing probability $\boldsymbol{p = 1\text{-}\alpha}$.

Therefore, there exist values of Fisher criterion - $\boldsymbol{F}\left|\begin{matrix}\boldsymbol{\alpha}\\ \boldsymbol{n-k}\\ \boldsymbol{k}\end{matrix}\right|$ where the boundary of the trust region has common points $\boldsymbol{p}$ ($\boldsymbol{p = 1\text{-}\alpha}$) with one of central planes, and border coefficient, whose axis is normal to this plane, acquires zero importance.

The graphical interpretation is shown in Fig. 1.

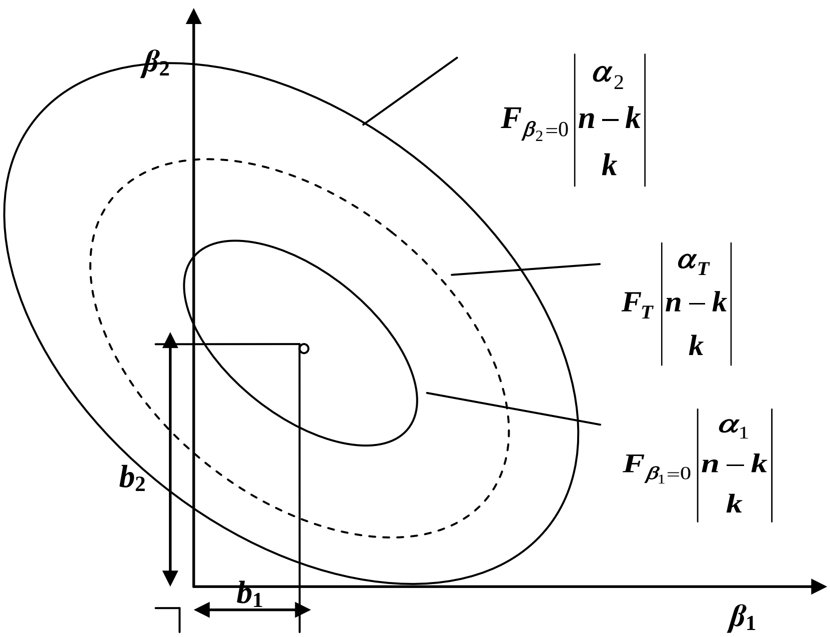

Fig. 1. *Confidence ellipsoid for k = 2*

When $F_{\beta_1=0}\begin{vmatrix}\alpha_1\\ n\\ n-k\end{vmatrix}$ coefficient b_1 is with a probability of $P_1=1-\alpha_1$, whereas if $F_{\beta_2=0}\begin{vmatrix}\alpha_2\\ n\\ n-k\end{vmatrix}$, b_2 is with a probability of $P_2=1-\alpha_2$, and acquires zero meaning.

Confidence probability $P_T=1-\alpha_T$ has Fisher criterion. $F_T\begin{vmatrix}\alpha_T\\ n-k\\ n\end{vmatrix}$. In this case, at probability $P_1=1-\alpha_1$, coefficient b_1 limit value is greater than the theoretical one; it (b_1) is considered insignificant and should be discarded from the model.

Determination of Fisher criterion F of any of regression coefficients (b) can be done by finding the minimum of function (1) at zero importance of limit value. After this task leads to the formula:

$$F_{\beta_{i=0}}=\frac{b_i^2}{k.S_\varepsilon^2.c_{ii}}, \qquad (6)$$

where:

c_{ii} - corresponding diagonal element of the coefficient b_i, belonging to the matrix $\left|X^T.X\right|^{-1}$

Assessment of factors (1) and their meaning determination (6) for a number of factors "k" requires considerable computing operations and relevant programs development.

Conclusions:

1. The developed methodology allows a significant expansion of regression analysis capabilities for the study of consequential events accompanying movement of vehicles.
2. As a result of data processing of multi-experiment matrix of planning and carried out statistical analysis of regression coefficients regression equations are obtained.
3. The resulting coefficients of regression equation show selected input factors influence to the process described in mathematical models

REFERENCES

[1] Adler YU.P., Introduction to the planning of the experiment "Metallurgy", M. 1969

[2] Bojanov K. Vuchkov I., Statistical methods for modeling and optimization of multi-objects. S., "Technique" 1979.

[3] Benchev B., Dimitrov E., Engineering experiment VTU, 2009

[4] Vedenyapin D. C. General methodology of experimental research and treatment of experimental data. "Colossus", M., 1978

HEAVY MACHINERY - HM 2011, 17-20
ISBN 978-86-82631-58-3
Paper accepted: 27.05.2011

Study Of Noise Characteristics Of The Brake Blocks Related With Roughness Of The Wheel Tread

Vasko Nikolov[1,*]
[1]Todor Kableshkov University of Transport - Sofia

Abstract: *The correlation between noise and roughness on the wheel tread caused by braking is studied. Eighteen prototypes of brake blocks are investigated. Wheel tread temperatures are measured during braking. The wheel roughness is measured after each brake cycle when the wheel has cooled down. Some conclusions about the rate of dependence of the roughness generation on the brake blocks material.*

Keywords: noise, hot spots, roughness, braking, railways.

1. INTRODUCTION

The focus of present work is on noise which arises in the rolling caused by circumferential roughness of the wheel tread. When loaded wheel rolls along the rail, vibrations are induced in wheels, bogies and superstructure of the vehicle and also in rails, sleepers and subgrade. Vibrations transform these components as noise to the surroundings. Roughness levels and the resulting noise depend on the brake system, i.e. from the brake blocks. This article consider the rising and development of the roughness caused by brake blocks acting on the wheel tread [1]. The most effective way to reduce the noise of rolling elements is to reduce the roughness of wheels and rails. It is assumed that the main reason for the occurrence of roughness is thermomechanical interaction between brake blocks and wheel tread. The creation of hot spots, i.e. sites with significantly higher temperature than the surrounding surface of the wheel tread is probably the key to this phenomenon. There is a certain critical speed when dragging the wheel towards brake blocks above which termoelastical instability causes formation of hot spots.

2. PREPARE AND PERFORM EXPERIMENTS

Several tests on the inertia dynamometer were conducted [3]. Tests were performed using the standard wheels of wagons, which corresponds to UIC-R7. The wheel is a whole, rim has been chilled. The typical hardness near the tread surface of the new wheel is 275 HB. The brake blocks used were the same shape and length 250 mm except in one case in which the block is a 500 mm long, so called multiblock. Three types of material blocks were examined (table 1). During the braking the temperature on wheel tread was recorded with its speed, normal and tangential forces on the blocks. The average friction coefficient at the contact surface was calculated by the force measuring.

2.1. Temperature measurement

For the temperature measurement infrared camera is used. The camera scans transversely over the wheel tread along the line, located a few centimeters from the brake block (Fig. 1). In this figure the coordinate y_t, indicating different circumferential tracks on the he wheel tread is introduced. By assuming a value of the coefficient of radiation of the wheel tread the temperature can be calculated.

3. ROUGHNESS MEASUREMENT

The roughness measurements were performed after the wheel had cooled down so that any influence from thermal expansion due to the braking was avoided. Roughness was measured along a number of circumferential tracks on the wheel tread, centered around the places where it appears that the surface is most damaged.

*Corr. Author's Address: Todor Kableshkov University of Transport – 158 Geo Milev Str., Sofia, Bulgaria, e-mail: va_r_nikolov@abv.bg

The same test program for all tests is used. Each tested block was worn to a certain degree before the actual testing and each block has been tested on a new wheel with a low initial roughness. This means that each wheel is tested with one specific block only.

Test program for each test blocks and the wheel is as follows:

- Three consecutive drag brakings with a braking force of 4 kN, from a train speed of 80 km/h (wheel circumference speed) and a braking time of 5 min. The wheels are cooled down and the roughness was measured 5 min after each drag braking.
- Three consecutive stop braking with braking force of 8 kN, from train speed 100 km/h and axle load of 10,4t. The wheels are cooled down after each brake cycle. Roughness was measured after the last braking cycle.

Cast iron blocks

Four different designs of cast iron blocks have been tested. The series of roughness data were compared with those for temperature and in many cases it was found that the peak of roughness after braking coincides with the hot spots during braking. This shows that the transfer of material is a process that generates roughness for cast iron blocks. Peaks of roughness launch hot spots during the subsequent braking cycles, leading to a stable spatial pattern during all braking.

Roughness levels are relatively high after drag braking, except for block 3 and higher after stop braking except for blocks 4. The friction coefficients is around $\mu = 0{,}20$ for all blocks with both drag and stop braking and they may increase to $\mu = 0{,}45$ at the end of stop braking. The maximum temperatures during the drag braking are about 450 and 500 ºC during the stop braking for blocks 1 and 2. For blocks 3 and 4, the maximum temperatures are about 225 ºC during the drag braking and about 425 ºC during the stop braking.

Composition blocks

Composite blocks often have a satisfactory behavior in terms of the generation of roughness. The amount of heat transmitted through a friction

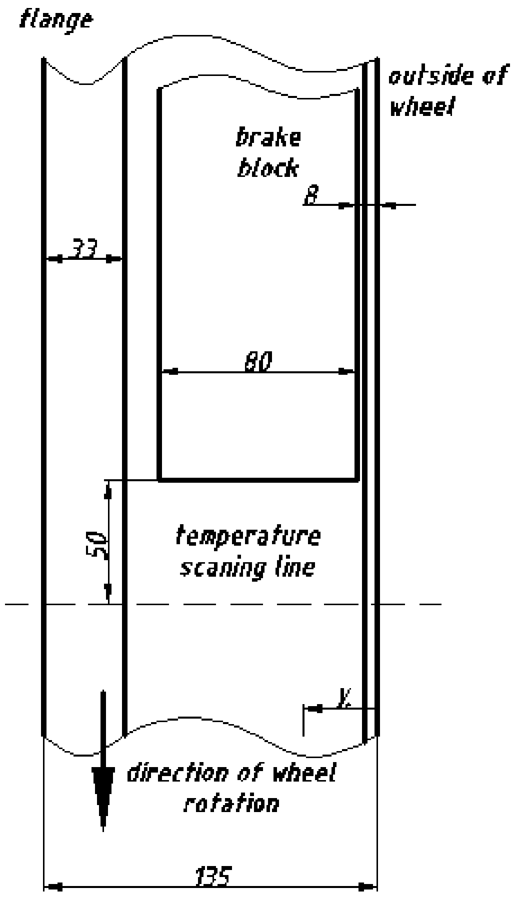

Fig. 1

between the wheel and brake blocks have to be low, since the braking with composition blocks 95% of the total generated heat enters the wheel. This high percentage is at least partly due to the fact that the composition blocks typically have thermal conductivity about 50 times lower than that of cast iron blocks, a fact which prevents the passage of heat from the contact zones in blocks. In other words, composition blocks normally acts as an insulator. To increase their thermal conductivity the main method has been to add metallic inclusions to the blocks, and to add a damping shelter and reduce the elastic modulus *E*. These measures should suppress termoelastical instability and decrease the temperature in the hot spots.

The maximum temperature is about 150°C. Such behavior is found in blocks 7, 9, 10, 13 and 14. All these blocks are modified with metallic inclusions to become better conductors of heat than are normally or its friction coefficient is reduced, which influences the reduction of total friction heat. For them, the registered maximum wheel temperature is below 160 °C during all drag braking and below 300 °C during all stop braking.

The roughness levels are generally very low for these blocks. The roughness of the unbraked wheel is similar to the braking with composition blocks. This indicates that the braking with a composition block decreases rather than increases the roughness.

For the other blocks (5, 6, 8, 12) a periodic hot spots pattern is observed. Hot spots typically extend over the whole block width.

Sinter blocks

Sinter blocks are often satisfactory in terms of roughness generation. It is desirable to decrease wear of the wheel tread and to reduce the friction coefficient. For this purpose, sinter blocks with abrasive properties were constructed (Blocks 16 and 18).

By studying the temperature pattern at different time of the braking cycle it is found that the hot spots are not spatially fixed. Obviously, protrusions are worn down and moved to other locations. In the case of the drag braking, there is one set of hot spots only, thus giving a correlation between temperature and roughness. Further brakings will destroy this correlation, since wear will move the hot spots to other locations.

It was found that the friction coefficient is about μ = 0.3-0.4 for all blocks for both drag and stop braking. The maximum temperature (at hot spots) during the drag braking is about 600ºC for blocks 15, 17 and 18, and 400ºC for block 16. During the stop braking maximum temperatures are 400ºC for blocks 15 and 18 and about 650ºC for block 16 (no data for block 17).

Sinter blocks generate a regular pattern with hot spots, but the correlation between temperature and roughness varies. This is attributed to wear of the hot spots. и 15 и 18. Roughness levels after drag braking were low for blocks 16 and 17 and medium for blocks 15 and 18. After stop braking roughness levels were low for blocks 15 and 17 and medium blocks 18. It should be noted that three of the four test blocks of roughness levels are reduced by applying the stop braking.

Table 1

Block	Description
1	Cast iron block modified for low friction coefficient
2	Cast iron block with abrasive ends (tungsten carbide, WC)
3	Cast iron block with sinter ends
4	Cast iron multiblock with damping
5	Composition block with cast iron inclusions
6	Composition block with metallic inclusions
7	Composition block with metallic inclusions and damping underlayer
8	Composition block with metallic inclusions
9	Composition block with metallic inclusions
10	Composition block from non-European producer
11	Composition block with metallic inclusions and damping underlayer
12	Composition block with metallic inclusions
13	Composition block with metallic inclusions and damping underlayer
14	Composition block proposed for European railway traffic
15	Sinter block with low density
16	Sinter block with reduced abrasion
17	Sinter block with low abrasion
18	Sinter block with low abrasion

4. CONCLUSION

In *cast iron blocks* normally result in fairly high roughness levels on the wheel tread, which to a high degree due to the material transfer from block to wheel. The fact that hot spots are fixed (for all braking) so the same locations, fixed to the wheel tread are always affected, accelerates the roughness generation. Abrasive inserts do not have the desired effect on the wearing of transferred material at least not to a sufficient degree. In general, cast iron blocks generate extremely high roughness levels. The multiblock solution shows promising properties and it would be interesting to test a more developed multiblock, where multiple contacts with the wheel is ensured.

Composition blocks normally show a strong correlation between temperature and roughness, provided that there was a pattern of hot spots. The reason could be the that wear rate is so low that the 5-minute braking is not enough to wear a hot spot protrusion, thereby forcing a new one somewhere else. Since there is no transfer of material, roughness levels are too low. Thus composition blocks generally result to lower roughness levels than do cast iron. The adding of metal inserts and friction modifiers to reduce the input of frictional heat to the wheel shows promising results in terms of wheel tread temperature.

Sinter blocks result the weakest correlation between temperature and roughness, probably depending on the high wear caused by these blocks. The protruding hot spots are thus worn and are newly hot spots are created elsewhere, which means even wear on the surface. If the wear rate is not high enough, a temperature stable pattern is develops and a correlation between temperature and roughness can be found. The sinter blocks result the lowest roughness levels and fairly even distribution of the wavelength. It was found that the stop braking can reduce the initial roughness levels, which is interpreted as an effect of the abrasive properties of the sinter blocks.

The friction coefficients are found to be lowest for cast iron blocks (about μ = 0,2), and vary for composition blocks (μ = 0,2-0,5) and sinter blocks (μ = 0,3-0,4). Very large increases in the friction coefficients are found for cast iron blocks at the end of stop braking. The maximum local temperature on the wheel tread observed in the hot spots (where present) are high for cast iron blocks, low for sinter blocks and lowest for the composition blocks.

The correlation between temperature and roughness is often found but not always observed. However, we can say that the existence of hot spots is related to the development of roughness pattern.

Cast iron blocks result relatively high levels of roughness on the wheel tread, partly depending on the material transfer from the blocks to wheel. Composition blocks generally result in lower roughness levels (5-10 μm) than do cast iron and dominant wavelengths are often longer (13 cm) than cast iron (3-6 cm). Sinter metal blocks result the lowest roughness levels (3-5 μm) and fairly even distribution of the wavelength.

5. REFERENCES

[1]. **Burton, R. A., Kilaparti, S.R. and Nerlikar, V.,** Thermoelastic instability in a seal-like configuration. *Wear*, 1973, 24, 177-188.

[2]. **Dings P., Dittrich M**., Roughness on Dutch railway wheels and rails. *J. Sound Vibr*, 1996.

[3]. **Petersson, M.**, Noise-related roughness of railway wheel treads – full-scale testing of brake blocks, IMechE, 2000.

[4]. **Thompson D. J.**, Wheel-rail noise generation: Parts I-V. *J. Sound Vibr*, 1993.

[5]. **Vernersson, T. V.** Thermally induced roughness of tread braked railway wheels – a noise-related problem. Thesis for the degree of licentiate of engineering, Chalmers Solid Mechanics, Göteborg, 1997, 77 pp.

[6]. **Vernersson, T. V., Petersson, M. and Hiensch, E. J. M.**, Thermally induced roughness of tread braked railway wheels. In proceedings of 12th international wheelset congress, Qingdao, China, 1998, pp. 68-75.

HEAVY MACHINERY - HM 2011, 21-24
ISBN 978-86-82631-58-3 Paper accepted: 30.05.2011

Wagon Manufacturing and Maintenance in the Balkans. Part 2: Romania, Turkey and Other Countries

dr Anna Dzhaleva-Chonkova[1, *]
[1]VTU "Todor Kableshkov", 158 Geo Milev Street, Sofia, Bulgaria

The paper presents the second part of a study on the wagon maintenance and manufacturing in the Balkan region. After the examination of the railway industry development in Serbia and Bulgaria, the focus is set on the problems of repairs and production of rolling stock in Romania, Turkey and other countries. The first two countries are considerable manufactures of wagons both for domestic needs and export. The final conclusion is that under the new conditions of integration in Europe both industry and researchers should cooperate to exchange knowledge and experience in modernization of wagon fleet in the Balkans.

Keywords: wagon maintenance and manufacturing, Balkan countries, cooperation.

INTRODUCTION

The first part of the historical examination on wagon manufacturing and maintenance in the Balkan countries presents a comparative examination on the historical development of railway industry in Bulgaria and Serbia. As the second part concerns more than two states, the narrative follows the historical facts and current activities by countries.

In the first years of railway operation rolling stock serving the traffic in the Balkan region (mostly ruled by the Ottoman Empire) was not only delivered but also maintained by the manufacturers from West-European countries. It was not as early as at end the 19th century when national railways opened their own shops for vehicle repairing, some of which began to produce locomotives and wagons.

I ROLLING STOCK MAINTENANCE AND MANUFACTURING IN ROMANIA

Romania was the first country in the Balkan region to open a workshop to maintain railway vehicles. It was established in 1882 and the place was intentionally chosen to be in Turnu Severin. The town not only provided well trained workforce but also was of particular geographical location bordering the Austrian-Hungarian Empire. The union of the railways of both countries on the Vârciorova - Orsova line required inspection of locomotives and wagons, which created conditions for prospective development of the establishment.

The workshop was an independent entity within the railways structure until 1960 when together with the local Shipyard formed the Mechanical Works. In 1968-1991 the workshop existed independently as Railcar Plant and then it was transformed into a joint-stock company under the name of S.C. MEVA S.A. Drobeta Turnu Severin.

Nowadays MEVA S.A is one of the largest wagon manufacturers in Romania with a production capacity of seven to eight wagons per day. Its current portfolio includes wagons for general use, covered and open box cars, container platforms, vessels and flat cars. The company produces wagons for the Serbian Railways, AAE, DB, European Rail Rent, CB Rail.

The second railway shop in Romania, founded in Arad in 1891 by Johan Weitzer also became a factory that has produced more than a quarter million of wagons, exported in 35 countries in the world. In 1998 it split into a new company ASTRA Passenger Coaches was registered. In 2000 the company was completely privatized integrally with Romanian capital. In 2006 it was acquired by International Railway Systems.

The modernization of technical lines has made possible for the company to manufacture any type of covered or uncovered flat wagons, tank wagons for petroleum products and special wagons (for overgauge transport, vertically and horizontally adjustable wagons, uncovered

*Corr. Author's Address: VTU"Todor Kableshkov", 158 Geo Milev Street, Sofia, Bulgaria, adzhaleva@abv.bg

gondola wagons for ore, coal, ballast stone transportation, hopper wagons for transport of ballast using special unloading devices, port container and low liner wagons. The company has also a special line for manufacturing bogies. Its production is known in many railway companies, among them being: AAE, DB, Ermewa-Geneva S.A., EWS, ERR, Freightliner, GATX Germany, GB Railfreight, Hupac, HHPI, Nacco S.A., Network Rail, SNCB, SBB, Touax, Trenitalia, VTG, Wascosa, GB Railfreight.

The latest establishment in the railway industry Romvag, existing in Caracal since 1973, was one of the largest worldwide exporters of freight wagons, focused mainly on the former East Europe market. In 2003 the company was privatized, the majority package being acquired by KEG Germany, and in 2004 it was taken over by International Railway Systems.

With a capacity of over 1,800 wagons per year, Romvag manufactures a wide range of freight wagons in different gauges, starting with general use cars for transport of bulk goods like coal, sand, gravel, wood, up to specialized cars like containers, self discharging wagons for bulk cereals, grain, wagons for transport of coils of laminated steel, tank wagons, wagons for the transport of saw dust, special wagons for transport of hot agglomerate up to 700 degree Celsius. Romvag also produces parts and underframes for other wagon producing companies.

It is important to trace how the companies mentioned above turned to operate in one and the same establishment based in Luxembourg and called International Railway Systems SA (“IRS”) – the European leader in the railcar industry. In 2002 IRS acquired the control on Meva, in 2004 on Romvag and in 2006 on Astra Vagoane railcar manufacturing facility. Thus IRS became the European leader of Railcar manufacturing with three railcar factories producing the largest number of railcars and bogies in the European market.

The International Railway Systems is a Romanian rail company. In its structure it includes the Czech establishment MSV Metal Studenka, which is famous for being the leading producer of forgings for the railcar and automotive industry. The IRS acquired also 49 % of the Serbian rail holding MIN-Mašinska Industrija Niš (Mechanical Industry Niš), the largest manufacturer of wagons and locomotives in Serbia.

III FROM REPAIRS IN THE OTTOMAN EMPIRE TO MANUFACTURING IN TURKEY

The railway construction in the Ottoman Empire began with a line in the Asian territory of the country in 1856 but later the government focused its infrastructure policy in Europe. Having finished two lines of minor importance (Constanza - Danube, 64 km,1860 and Rousse-Varna, 224 km,1866), it started its main railway project of connecting Istanbul and Vienna. In 1873 the Company of Eastern Railways known as Baron Hirsch’s company, opened for operation only part of it: to the station of Belovo (Bulgaria). The Baron Hirsch’s company built also a section going out of this line to Yambol (1875) and a line from Thessaloniki to Mitrovitsa. The railway operation of these lines was entirely implemented by imported vehicles and maintenance by the manufacturers. The lack of a repair shop in the country led to problems such as interruptions of railway traffic and consequently to increasing the repair costs.

The situation changed when a number of new lines were opened in Anatolia at the end of the 19^{th} century: Haydarpaşa-İzmit section of the Anatolia-Baghdad Railway line (1886), İzmit-Ankara (1888) Alayunt-Kütahya (1893), Eskişehir-Konya (1896). It was during the construction works of the latter one, in 1894, when a small repair workshop was established in Eskişehir by the Germans in order to perform maintenance of steam locomotives and wagons used in the Anatolia-Baghdad Railway Line. The workshop did small-scale repairs of locomotives, coaches and freight cars as all spare parts were imported from other countries.

The Anatolian-Ottoman Rail Company experienced dramatic events during the British occupation of Anatolia in 1919, was taken back by the Nationalist Forces, captured by the Greeks and taken back in 1922. However, it managed to preserve its capacity and played an important role in development of the newly-formed country. Aiming at creating technology-based economy, in 1925-1928 the government of Kemal Ataturk opened new units for producing steam locomotive boilers, gears, a carpenter’s shop, other units producing materials for railway bridges, switches and tracks were established to reduce the dependency to other countries.

The Railway Repair Workshop was strongly affected by the draft of experienced workers during the mobilization period in the World War II. It was when the problem of training new people appeared and, as a result of it, Boarding Apprentice Training Schools were opened to ensure a continuous training opportunity for many students.

In the post-war period, the workshop widened with an Engine Division (1956). In 1957 it produced two small steam locomotives "Mehmetçik" and "Efe" for Ankara Youth Park. Next year the Traction Workshop in Eskişehir was reorganized into Eskişehir Railway Factory. The aim was to manufacture steam locomotives and in 1961 the first Turkish steam locomotive "KARAKURT" was set in operation.

Another workshop for reparing steam locomotives and freight wagons was established in 1939 under the name of Sivas Cer Atelyesi. It started to produce freight wagons in 1953. Renamed to SİDEMAS in 1972, the factory became famous as TÜDEMSAŞ after the change of 1986. The company's portfolio includes both repairs of freight and passenger wagons and production of freight wagons and spare parts of any type.

The newgest establishment in the Turkish railway industry is the Coach Repair Workshop opened in Adapazarı in 1951, which 10 years later was called Adapazarı Railroad Factory (ADF). The first coach was manufactured in 1962 and soon its production became part of the country's export to Pakistan and Bangladesh.

The factory under the name Adapazarı Coach Industrial Establishment (ADVAS) is an important manufacturer of electric powered suburban series with Alstom firm license for the needs of Turkish State Railways. In 1985 it was renamed to Turkish Coach Industry Incorporation (TÜVASAŞ) and focused on new projects by research and development. The industrial process was interrupted for a short period due to damages caused by the Marmara earthquake (1999). Since the company restored its facilities in 2001, it has cooperated with SIEMENS assembling 38 vehicles for Bursa Metropolitan Municipality light rail vehicle fleet. Besides for the Turkish Railways (including the suburban lines), wagons produced are intended for İstanbul underground and exported to Asian countries. For Marmaray project, in 2010 TÜVASAŞ was assigned to manufacture 275 vehicles within the framework of joint production with Hyundai-Rotem Company.

Last year the company was included in a consortium with Sakarya University and Uludağ University to jointly develop an important research project: construction of Climatic Test Tunnel where the air conditioning systems of rail vehicles will be tested.

IV RAILWAY INDUSTRY IN OTHER BALKAN COUNTRIES

Although Romania and Turkey have proved to be the most important players in the international rolling stock market, it should be mentioned that some of the other Balkan countries also have achievements in rolling stock repairs and manufacturing.

Croatia is famous not only for the Koncar traction vehicles but also for its wagon production. TŽV Gredelj was founded in 1894 as a main workshop of the Hungarian state railways for repair of steam locomotives. Soon after its establishment the rolling stock factory Gredelj began to produce parts and tools for maintenance of rolling stock widening its activities to repairs and production of wagons. At present the manufacturing portfolio of TŽV Gredelj offers coaches (1st and 2nd class, dining, sleeping, restaurant, etc.), trams, diesel-electric locomotives, diesel and electric multiple units for regional and suburban transport, container wagons, car transportation wagons, etc. as well as modernization, rehabilitation and maintenance of rolling stock.

The factory complex, which represents a valuable part of Croatia's technical and industrial history, is registered in the List of protected cultural heritage of the Republic of Croatia. After the production moves from that area, the old industrial workshops will be preserved and adapted to accommodate the Croatian Railway Museum "in situ".

Unlike the Yugoslavian period when all republics and autonomous regions relied on the railway industry located mostly in Serbia and Croatia, nowadays the independent countries from the West Balkan region perform at least maintenance activities of their own. Slovenia has established a place at the Koper tovorna station (tracks No 15 and 16) where the staff of CD Divača carries out small wagon repairs. Similar situation exists in FYROM, Bosnia and Herzegovina, Montenegro.

Comparing the facts concerning the manufacturing of wagons in the Balkans, it is worth saying that Greece was the first who produced a very special wagon as early as in 1888. The royal wagon built for a present to King George I became known as the "crown jewel" of the Piraeus Works. The luxurious vehicle was transported to Zappeion and shown at the "Olympia Fair" held in the 1888. At present the wagon can be seen exhibited in the Railway Museum of Athens.

The development of railway transport in Greece in the 19th century involved a number of different companies, which created their own workshops for maintenance and constructions. As mentioned, the most important ones were Railway Works in Piraeus, operated by Athens-Piraeus Railways (later transformed into Hellenic Electric Railways, EIS) and Piraeus, Athens and Peloponnese Railways (SPAP, forerunner of OSE). The factory not only performed maintenance, repairs and rebuilding but also constructed a significant number of railroad cars, mostly between 1880 and 1960. The production included also a small number of electric trams (clearly copies of a Dick Kerr model) built by EIS in 1939, and Greece's first Diesel locomotive, designed and built by SPAP in 1961.

VI CONCLUSIONS

The history of railway industry in the Balkans was different in each country. All of them began with foundation of repair shops but only some managed to develop modern manufacturing capacities competitive and sustainable on the international rolling stock market.

The contacts and cooperation between rolling stock repair and manufacturing companies in the region have been increasing for the last years. It is due not only to the establishment of the IRS as a leading player in the sector but also because of the positive tendencies that have appeared in bilateral and multilateral relations of wagon manufactures.

Moreover, the necessity of implementing innovation products and technologies has resulted in networking of scientists and research organizations. The new types of communication and interaction are an indicator not only for creating powerful economic establishments, but also for the new climate of integration aimed to create modern, competitive and environment-friendly railway transport in the region.

VII REFERENCES

[1] http://www.irsgroup.eu/about_irs/History/ind
[2] ex.1.html. Accessed on 15 May 2011.
[3] http://www.railwaymarket.eu/rm2008/pdf/IRS_Challenges_the_Global_Railcar_Production_Market.pdf. Accessed on 15 May 2011.
[4] http://www.tuvasas.com.tr/yeni/index.php?sayfa=about&sayfa_no=6. Accessed on 15 May 2011
[5] http://www.tulomsas.com.tr/en/main.php?kid=67. Accessed on 15 May 2011.
[6] http://www.tudemsas.gov.tr/tudemsas/en/en_
[7] HTML/20100121_110019_1_2_1.html
[8] Accessed on 15 May 2011.
[9] http://tzv-gredelj.biz.hr/eng/index.php?option=com_content&task=view&id=132&Itemid=1. Accessed on 15 May 2011.
[10] http://www.slo-zeleznice.si/en/freight/services/port_koper/wagon_repairsAccessed on 15 May 2011.

HEAVY MACHINERY - HM 2011, 25-32
ISBN 978-86-82631-58-3
Paper accepted: 30.05.2011

Transportation and Manipulation Processes in the Overhaul of Energy Transformers

Ljubomir Lukić[1,*] - Mirko Djapić[1]
[1] University of Kragujevac, Faculty of Mechanical Engineering Kraljevo, Sebia

Energy transformers fall under the category of capital electric energy equipment that have an exploitation period of over 30 years on hydro energy and thermal energy plants or high-voltage substations. Depending on the power and voltage level, the mass of an energy transformer can be up to 400t, while the price can reach as much as a million Euros. There are currently around 140 energy transformers on electric energy plants in our country, that have been in exploitation for over 30 years. The overhaul of energy transformers of great power is a very specific technological process that is carried out in specially equipped factories.The transportation and manipulation process of energy transformers during the overhaul is particularly complex, since it is specified as the railway freight of oversized capital product cargo.

The paper displays the realization of the railway transportation of the biggest step-up transformer, not only in Serbia but in the southern part of Europe, rated 725 MVA, from thermal power plant TENT B in Obrenovac to the ABS Minel Transformatori factory in Ripanj, where the general overhaul of this energy transformer is under way.

Keywords: Energy transformers, railway transportation, manipulation processes

0 INTRODUCTION

Energy transformers fall under the category of capital electric energy equipment that has an exploitation period of over 30 years in hydro energy and thermal energy plants or high-voltage substations. Energy transformers can be classified into several groups, according to the function they perform, or technical solution, on which their construction is based.

Step-up transformers are directly connected with generators via disconnecting gear, and have a function of raising the voltage, where the input on the primary coil is 6 kV to 22 kV, and the output on the secondary coil is 35 kV, 110 kV, 220 kV or 400 kV. Step-up transformers fall under the category of primary electric energy equipment.

Auxiliary transformers in hydro power plants and thermal power plants are of lesser strength, but have an important role in providing the power supply with an adequate voltage of all feeders on the power plant and to provide the power supply of the energized coil on the generator when the generator is let into operation.

Interconnecting transformers are used to connect two electrical grids of different voltage levels, e.g. connecting a 400 kV grid with 220 kV or 110 kV grids which are placed in transformer substations. Interconnecting transformers can in construction be created as auto transformers or transformers. Transformers have one primary and one secondary coil while autotransformers have a functional primary and secondary coil within one coil. That is why they are cheaper but with the same power as transformers, all up to the transformation of ratio 1:4.

Since the exploitation period of energy transformers is very long, and as there are over 140 energy transformers in operation for over 30 years at the facilities of the Serbian Electric Power Industry and the Serbian Transmissions System and Market Operator, this diminishes the reliability of operation of the facilities in the production of electric energy, which destabilizes the electric power system of the country. A breakage on an energy transformer is fatal because the operation of the entire energy unit must be stopped on the thermal power plant or hydro power plant until the broken down transformer is taken off the grid and a spare one is put in its place. However, during the replacement of a transformer that is out of commission, costs are incurred because the power unit stops working, that are multiply greater than the price of the transformer. That is why it has been put into practice that there are spare transformers in all energy units which would be placed on the

[*]Corr. Author's Address: Faculty of Mechanical Engineering Kraljevo, 36000 Kraljevo, Serbia, lukic.lj@mfkv.kg.ac.rs

grid in case of accidents. Spare transformers should be in the power plants because of quick replacement, since its transport is quite specific and can take a while to ship it from another location. Each energy transformer has designed technical characteristics that comply with the characteristics of the generator and high-voltage grid, making it almost impossible to move them from one energy unit to another.

In March 2010 on thermal power plant TENT B in Obrenovac, there occurred a heavy accident occurred on the step-up transformer of French producer CEM, type TR – 9208, No. H26602, 410/21 kV, 1020/19930 A, 725 MVA, connection group Yn, d5 and 490 tons in total weight. The weight of the transformer oil is 90 tons, and the transport weight is around 360 tons. This step-up transformer has been in exploitation since 1983 (figure 1), when thermal power plant TENT B with two 620 MW power units was let into operation. This is one of the biggest energy transformers in the Balkans, transforming an eighth of the total electric energy produced in the Republic of Serbia.

Fig. 1. *725 MVA step-up transformer CEM, in thermal power plant TENT B in Obrenovac*

When this transformer broke down, an entire thermal power plant unit of 620 MW stopped working. The accident happened as a consequence of break downs and short-circuits on the high voltage substation in Obrenovac. There was a breach in the insulation on the HV coil of phase A, but the entire damage of the transformer can be seen after a breakage diagnosis and expert analysis of the structure. The 725 MVA step-up transformer CEM was in the shortest possible timeframe, during snow, rain and great cold, by working day and night, removed from the generator and the HV grid, in order to replace it and put into operation the spare transformer produced by Končar-Siemens of Zagreb. The spare transformer that was let into operation is also not in a good condition, because it has characteristic gasses that arise as a product of a chemical reaction in the transformer oil caused on places of poor insulation. This complex job was realized by the team from the ABS Minel Transformatori energy transformer factory in Belgrade, immediately after the accident in March 2010 in thermal power plant TENT B in Obrenovac.

1 TRANSFORMER BOX ON THE ENERGY UNIT

There is a special transformer box on energy units in which are placed step-up transformers and in that place they are connected to the generating power unit and high-voltage electrical grid. Because of transportation and manipulation processes, the transformer box is equipped with a dual-gauge railway of the appropriate bearing, - an appropriate, permitted axial pressure, for dragging the transformer in both directions from the place of unloading on the facility to the place of installation (figure 2). The railway track from the transformer box intersects with the transportation gauge where the places of loading and unloading are projected, as is the position of the energy transformer. The transportation gauge is connected to the railways system of Serbia, so the transformer can be transported to a factory for repairs.

Given its large mass, the step-up transformer is moved along transportation gauges with the tensioner pulley, driver train or is compressed with hydraulic compressors to the place where the transportation gauges intersect the gauge of the transformer box. In that place the transformer is with hydraulic cranes lifted, the wheel carts turn by 90° and the transformer is lowered and moved sideways to the place of functional operation. Depending on whether the front or back carts turn at the junction, transport can be carried out so that the HV insulation side is on the left or right against the direction of movement. It’s very important to have in mind the position of the HV insulator against the direction of movement during transportation, because of the placement of the transformer box towards the power unit and the correct position of the transformer at the place of unloading.

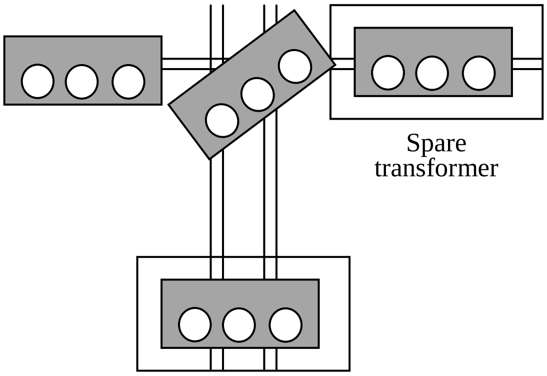

Fig. 2. *Transportation system of the energy transformer in the electric energy facility*

2 RAILWAY TRANSPORT OF A 725 MVA STEP-UP TRANSFORMER FROM THERMAL POWER PLANT TENT B TO THE ABS MINEL TRANSFORMATORI FACTORY IN RIPANJ

The value of a 725 MVA step-up transformer is around EUR 5 mn and its rail transport from the transformer box in thermal power plant TENT B in Obrenovac to the ABS Minel Transformatori factory in Ripanj (where the overhaul is being performed) costs around EUR 300.000. All the energy transformer factories in the world are built on locations with good possibilities for rail or water transport, so lower transportation costs would enable competitive prices for the clients. Transformers of lower rates are transported via road on trucks with trailers for oversized cargo, on distances where there are no possibilities for railway transport. Given that the 725 MVA step-up transformer from Obrenovac could be transported via rail to the factory in Ripanj, this was executed.

The project analysis for this transport was done, with defined manipulation processes for freighting the transformer from the transformer box to the place of loading, the manner of loading and all questions related to the railway transport to the factory in Ripanj, the unloading and placement at the position of disassembly in the assembly hall of the ABS Minel Transformatori factory. Transport was organized according to all the standing railway transportation regulations with all the necessary permits and special examination of the railway gauges by an authorized institution, which also prescribed the repairs that need to be performed on individual sections of the railway track, as well as all other security measures that need to be taken.

Since this is a transport of oversized cargo of great value, it’s important to know the permitted transport profiles on the railways that are defined by the regulations of all national railways through which the transport is taking place. The railway transport of energy transformers is performed by using special wagons of great carrying capacity, depending on the power and transport weight of the energy transformer (figure 3).

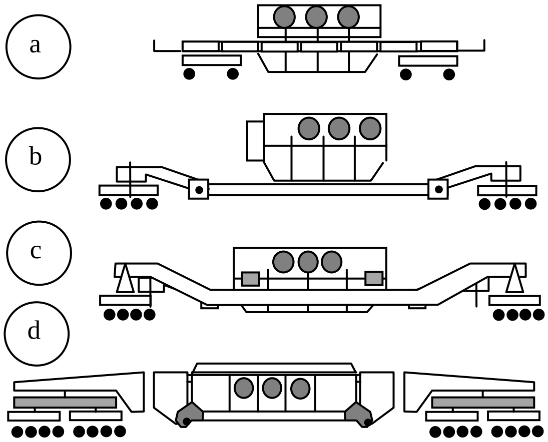

Fig. 3. *Types of railway wagons for the transport of energy transformers*
a) flat wagon b) tank wagon c) wagon with carrying construction d) “Schnabel” wagon

Flat wagons are placed on two rotary traps which are used for loads of up to 50 tons, tank wagons, used for loads of up to 100 tons, wagons with carrying constructions, used for weights of 200 – 250 tons and a special multiaxial Schnabel wagon – a wagon with a beak that is used for the transportation of energy transformers of the biggest loads.

An energy transformer of great power and load must be specially constructed for railway transportation, with elements for tying it to the wagon, which must withstand horizontal or vertical tension in places of hydraulic supports. The special, Schnabel wagons are constructed with 24 and 32 axles depending on the carrying capacity, fluctuating from 300 to 500 tons. The wagons themselves, without the cargo, are over 50 m long, so hydraulic devices are necessary for moving the load sidewise against the axial movement, in order to return it to the axle of the transport profile.

For the transport of the 725 MVA step-up transformer was provided the special "Schnabel" wagon with 32 axles, which no transporter on the territory of the former Yugoslavia possesses. The only authorized transporter for oversized cargo transport in Serbia is company "Bora Kečić" of Belgrade, which reserved the wagon for the first week of February 2011 and rented it in Austria with its own crew of 6 wagon operators (figure 4). The annual timetable of the use of these wagons is prearranged, so that a timely planning of transport is a very important activity in the dynamic plan of the transformer's overhaul.

Fig. 4. *725 MVA transformer on the loading position for the "Schnabel" wagon at thermal power plant TENT B in Obrenovac*

The transformer is specially prepared for transport, by disassembling all the parts that exceed the permitted loads, which are technologically finally assembled at the very facility, and which reduce the transport weight (insulators, conservator, cooling system, domes, joining pipes, control cabinet, motor drive of the voltage regulator). The disassembled parts are packed into closed containers and transported separately. To reduce the transport weight the insulation oil is transported separately. When transporting a new energy transformer, nitrogen is placed into the case and a device for maintaining the overpressure in the container, to prevent the penetration of external air into the transformer container and disable the moisture from penetrating into the cellulose insulation.

The transport was finally realized on February 6th, 2011 by loading the step-up transformer onto the Schnabel car and shipping it via the TENT railway from Obrenovac to Divci. From Divci to Belgrade the transport was realized via the Belgrade-Bar railway, to finally ship it from Belgrade to Ripanj via the Belgrade-Nis railway (figure 5).

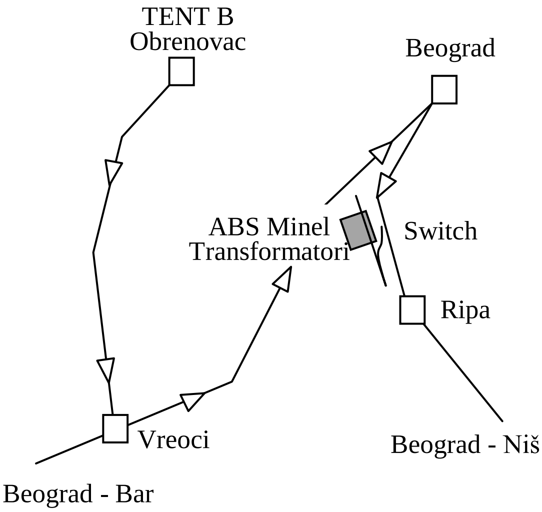

Fig. 5. *Transportation route of the 725 MVA step-up transformer from Obrenovac to Ripanj*

During transport, the entire railway traffic was stopped, while on the Belgrade-Nis track, traffic was halted for an entire 6 hours because of an intervention on the railway switch to the ABS Minel Transformatori factory. The factory tracks are not connected to the railway track by a standard switch but the intersected railway track was moved to the right and the railway tracks welded to the factory's tracks. Such a prepared switch (figure 6) was in function for only a couple of hours, to get the transformer into the factory, unload it from the wagon and return the wagon onto the Belgrade-Nis railway track. All this was done in less than 6 hours, in order to maintain regular railway transport on the Belgrade-Nis line (figure 7). The transport of energy transformers is carried out by the

Schnabel wagon being drawn by a diesel engine, because due to electromagnetic phenomenological occurrences that can arise between the contact grid and the active part of the transformer, the electric contact grid for charging the electric locomotive must be shut down.

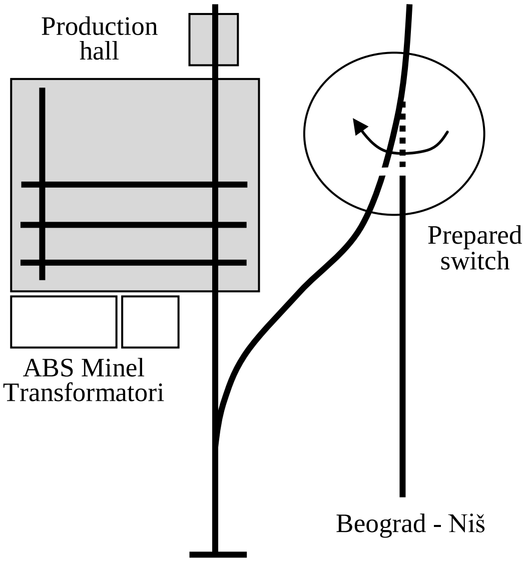

Fig. 6. *Switch from the Belgrade-Nis track to the ABS Minel Transformatori factory in Ripanj*

By shipping the step-up transformer onto the ingoing/outgoing factory track of ABS Minel Transformatori in Ripanj (figure 8), the entry of the transformer into the assembly/disassembly hall of the factory was enabled. Here, the unloading took place and the unit was placed on a special cart wheel to transport it inside the hall. Upon unloading the transformer, the Schnabel wagon was prepared for no-load stroke and returned via rail to Austria.

Disassembly was performed upon completed transport, to establish the detailed damages because of the accident, test the functional characteristics and damages of the step-up transformer, so as to make the final decision on its revitalization and general overhaul.

Fig. 7. *Connected factory tracks with the Belgrade-Nis railway track*

Fig. 8. *Entrance of the Schnabel wagon into the ABS Minel Transformatori factory in Ripanj*

It was decided for new LV and HV coils to be made, to install new insulation arrangements and to fit in a new magnetic circuit because of damages that were identified on the magnetic circuit's insulation. The costs of overhauling this step-up transformer of capital worth for the TENT B thermal power plant in Obrenovac and the Serbian Electric Power Industry are around EUR 3.5 mn.

3 MANIPULATION PROCESSES DURING THE OVERHAUL OF ENERGY TRANSFORMERS

Manipulation processes are technologically very significant and when constructing a transformer must be anticipated the places of bearing and special elements like: hooks for steel slings, reclining elements, suspension elements, suspension lugs, transportation platform supports, wheel supports and so on, which must be correctly placed on the housing of the transformer and reliably dimensioned. The safety fuses that connect the transformer housing to the wagon must be tested and certified by an accredited lab. The places of support must be visibly marked and during transport and manipulation must be correctly used (for example, the transformer can be lifted only with the simultaneous use of an anticipated number of hydraulic cranes, because otherwise, its own weight could deform the housing of the transformer). Bearing in mind the value of energy transformers and significance of their reliability in work and the possible damages during transport and manipulation, special attention is given to finding the optimal construction solutions for preventing a potential moving of active parts in the housing or displacement of individual elements (regulator, trappers, conducting lines and other). During transport, the inertia forces due to acceleration/deceleration or shakes must be limited and their values monitored from the moment of loading to the placement into the transformer box. That is why special measuring devices are placed on the transformer during transport – impact metering devices that mark the accelerations in three directions (direction of movement, diagonal movement, up/down movement) over time.

Furthermore, to perform the disassembly of a step-up transformer weighing over 350tons, we need to design the technological process for disassembly from the aspect of large masses and the aspect of security from damaging the vital parts of the transformer. Also, special tools are designed and manipulation tools for taking down the "bell" of the transformer housing. The height of the hall in the disassembly area is some 18m, and for all the process to unfold without interruptions, first the transformer housing is opened (figure 9) to access the active part of the transformer–the magnetic circuit and coils (figure 10).

After opening the transformer housing, the disassembly of the upper part of the magnetic circuit was performed (figure 11), in to disassemble the coils. The disassembly of the coils is performed by first disassembling the outer coil of the LV phase A, and then taking off the internal coil of LV phase A from the magnetic circuit column (figure 12).

Fig. 9. *Raised "bell" of the transformer housing*

Fig. 10. *Active part of the 725 MVA step-up transformer – HV side*

Fig. 11. *Disassembling the upper part of the magnetic circuit*

By the same procedure the coils are disassembled and the other two phases from the magnetic circuit columns, as well as the tertiary coil on the fourth column of the magnetic circuit.

Plus, every coil for one phase has a weight of around 30tons. Special auxiliary tools and equipment were constructed for the disassembly of the coils that would be used in the assembly process too, after the new low voltage and high voltage coils are made.

Fig. 12. *Disassembly of the external and internal coil of LV phase A from the magnetic circuit column*

The disassembled coils are moved onto the coil line where the complete disassembly of the coils and subassemblies of the active part of the transformer is performed. The lower part and columns of the magnetic circuit remain tightened in the lower part – basin of the transformer housing (figure 13), where insulation quality is checked and based on it a decision made whether to replace the insulation by refolding the magnetic circuit or to make a new magnetic circuit from high quality sheets that will provide significantly lower losses during exploitation.

Because of the great power of this transformer and possibility of cutting losses by making a new magnetic circuit, a complete revitalization of this transformer will be performed by the end of 2011, when it will again be placed in thermal power plant TENT B and where it will operate for the next 30 years with significantly lesser losses than before.

5 CONCLUSION

The transport of the 725 MVA step-up transformer, from Obrenovac to Ripanj, is a great technological and transportation venture, primarily because for the first time, the 32 axle Schnabel wagon moved across Serbian railways, transporting a 360ton load. The overhaul of the biggest energy transformer in the Balkans is an extreme technical and technological venture not just for the ABS Minel Transformatori in Ripanj but any factory in the world. The company that realized the transport, "Bora Kečić" of Belgrade is the only company in Serbia that has the equipment and capacity to safely realize such a responsible and complex transportation project. The Schnabel wagon doesn't exist in Serbia and Bora Kečić, thanks to the requirements of the ABS Minel Transformatori factory in Ripanj, has arranged for the production of a 32- axle "Schnabel" wagon with the Wagon Production Factory in Kraljevo, for the requirements of their business in the area of oversized transport of energy transformers in Europe. It's safe to say that the design and production of the Schnabel wagon will significantly affect the development of wagon-building in Serbia.

Fig.13. *Disassembled active part of a 725 MVA transformer*

The transport of energy transformers sometimes takes very long (e.g. the transport of a 300 MVA transformer from Subotica to Ripanj lasted over 2 months) due to the combination of road-railway transportation, providing the necessary permits and other approvals for oversized transport. The transport of the 725 MVA step-up transformer in 2 days, Saturday-Sunday, is an extreme venture carried out jointly by the workers of thermal power plant TENT B, the workers of factory ABS Minel Transformatori and "Bora Kečić" company.

6 REFERENCES

[1] Lukić, Lj., Božić, M., "Project report for the transport of an 725 MVA CEM energy

transformer from thermal power plant TENT B to the ABS Minel Transformatori factory in Ripanj", ABS Minel, Beograd, 2010.

[2] Lukić, Lj., Petrović, Lj., „Ремонт энергетических автотрансформаторов 300 MVA", Доклады VII Международной научно технической конференции "Силовые трансформаторы и системы диагностики", Москва, 2010.

[3] Lukić, Lj., Djapić, M.: "Revitalization of 725 MVA Power Transformer for TENT B in Obrenovac", Proc. 34th International Conference on Production Engineering, September 28–30, 2011, Niš (in preparation).

ACKNOWLEDGMENT

The results presented in this work are a result of project TR 37020, realized by the Faculty of Mechanical Engineering in Kraljevo, University in Kragujevac and funded by the Ministry of Education and Science of the Republic of Serbia.

HEAVY MACHINERY - HM 2011, 33-38
ISBN 978-86-82631-58-3
Paper accepted: 30.05.2011

Iron Ore Transportation Wagon with Three-Piece Bogies – Simulation Model and Validation

Nebojša Bogojević[1,*] - Per-Anders Jönsson[2] - Sebastian Stichel[3]
[1] University of Kragujevac, Faculty of Mechanical Engineering Kraljevo, Dositejeva 19, Kraljevo, Serbia
[2] Tikab Strukturmekanik AB, Stockholm, Sweden
[3] Royal Institute of Technology, Stockholm, Sweden

Model verification and validation are essential parts of the model development process. This paper presents validation of a model of an iron ore wagon with three-piece bogies. The validation of the model has been made by comparison of the lateral and vertical accelerations of the car body obtained by simulation and by measurements. A good agreement between the compared variables has been achieved, but the model validation process needs also to be made by comparison between the vertical and lateral forces in the wheel/rail contact.

Keywords: railway vehicle, modelling, validation, three-piece bogie.

1 INTRODUCTION

Wagons with three-piece bogies have been in use for more than 150 years, mainly in USA, Australia, Russia, China and South Africa [1], [2] but they are not common in Western Europe. The three-piece bogie has a simple robust design and have therefore, low initial cost and are easy to maintain.

Conventional types of three-piece bogies may have low warping stiffness, low critical speed on tangent tracks, high wear of wheels and track and strongly nonlinear dynamic behaviour [3].

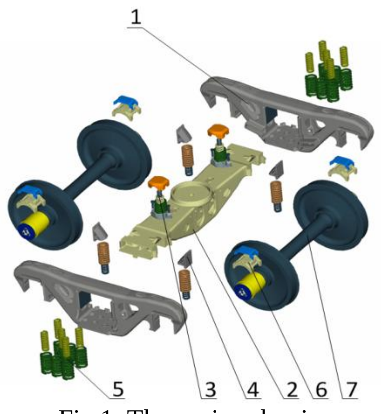

Fig 1. Three-piece bogie
1-side frame, 2-bolster, 3-side bearers,
4-wedge, 5-coil spring in suspension system,
6-adapter, 7-wheelset.

The main parts of three-piece bogies are bolster, two side frames and wheelsets as it is shown in Fig 1. The side frame is connected to the wheelset via adapters. The bolster and the side frames are connected via groups of coil spring and friction wedges. Friction wedges are the coupling elements between bolster and side frame that provide most of the damping in the suspension system.

Two different types of damping principles are used on three-piece bogies using wedges with constant or variable damping as shown in Fig 2.

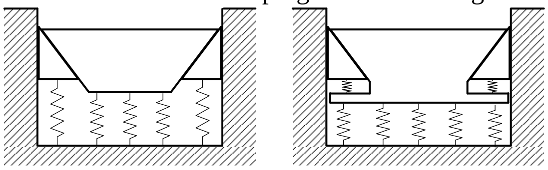

Fig 2. Friction wedge
a) variable damping; b) constant damping

The friction wedges with constant damping have a constant friction force on the surfaces between the bolster and the side frame. The friction force on the wedge with the variable damping depends on the movement of the bolster and the side frame, which is realized with a coil spring positioned between wedge and side frame [4], see Fig 2a.

The wheelset it is connected to the side frames via adapters. In order to achieve better curving performance, the adapters may be connected to the side frame via friction plates or via elastic pads [4]. In both cases, due to the gaps between the side frame and the adapters, the wheelset can move in three directions in order to take a proper position in curves and on tangent track.

[*]Corr. Author's Address: Fac. of Mec. Eng. Kraljevo, Dositejeva 19, Kraljevo, Serbia, bogojevic.n@mfkv.rs

2 THE MODEL OF THE WAGON

The wagons used for transportation of iron ore are about 10 meters long and approved for axle load of 30 tones. The ratio of the weights of empty and loaded wagon is between 5 and 6. The car body consists of a basket for carrying the iron ore and a frame, that connects the car body with the bogies. The wagon has ASF-Keystone "Motion Control M976 Truck System" three-piece bogies with load dependent - variable friction damping [4].

A nonlinear model of the three-piece bogie has been developed using various coupling elements to represent the suspension system. The main source of the nonlinearity in the model is dry friction contacts between the bolster, the wedge and the side frame, which leads to stick-slip motion of the wedge. The nonlinear behaviour of the model arises also from contacts between elements of the bogie, from the gaps and from nonlinear characteristics of elastic elements.

The friction contact in the suspension system of the wagon can be described with several models. In the model of the wagon presented here, the friction contacts between the bolster, the wedge and the side frame are modelled as Saint Venant elements [4], as is shown in Fig 3.

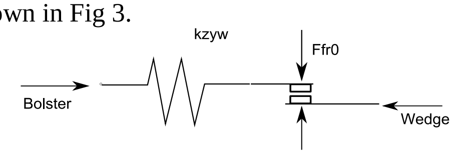

Fig 3. Saint Venant element – model of the Columb friction

2.1 THE MODEL OF THE WAGON

The model assumptions can be summarised as follows:

- Car body, bolster, side frames and wheels are modelled as rigid bodies,
- Side bearers have always contact with car body,
- Wedges are massless elements,
- Contact between the bolster and the wedge is a one-dimensional friction block,
- Contact between wedge and side frame is a two-dimensional friction block – in lateral and vertical direction,
- Adapter is modelled as rubber element with high stiffness in vertical direction,
- Clearances between elements are implemented in the model (bolster-side frame, axle-side frame, etc).

In order to investigate the dynamic behaviour of the wagon for iron ore transportation the model of the vehicle has been implemented in multibody dynamic software "Gensys". Schematic representation of the model of the wagon is given in the Fig. 4.

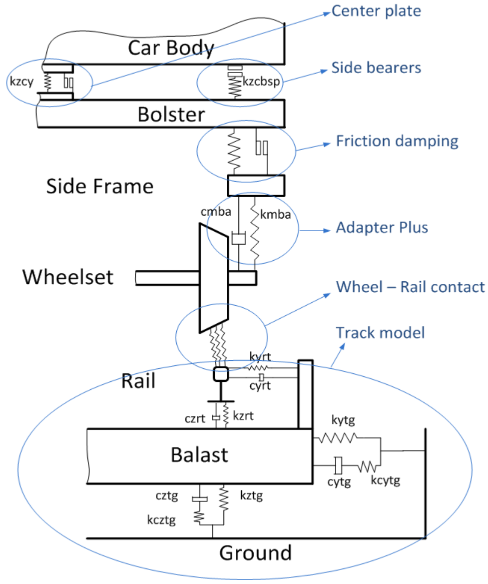

Fig 4. Connection between masses in vertical direction

The connection between car body and bolster is provided by a central plate and side bearers, as shown in Fig. 4. The side bearers have always contact with the car body, which causes a friction force in longitudinal direction. This friction force is important for stability of the vehicle on tangent track because it is providing damping of the yaw motion of the bogie. In the case of the empty wagon, the side bearers are loaded with 80% of the carbody weight, and the rest of the weight is carried by the central plate. In the case of the loaded wagon, the central plate is loaded with 90% of the vertical load, while 10% is carried by the side bearers.

The outer part of the central plate has chamfers, as shown in Fig. 5, which allow the bolster to roll. The proposed model also takes into consideration the fact that the bogie travels longitudinally under the car-body when the body swings.

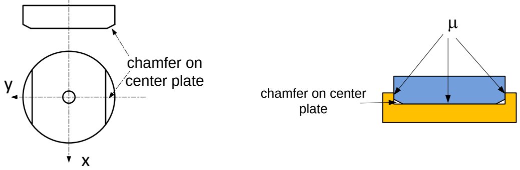

Fig 5. Central plate

The wedges are modelled as massless bodies, and the position of the wedge is calculated by solving the local equilibrium matrix [4]. The friction in the contact surface between the bolster and the wedge is modelled as one-dimensional friction block, as it is shown in Fig. 6. As a friction surface between wedge and side frame, two-dimensional friction blocks are introduced, as it is shown in Fig 6. Normal contact forces acting on the surfaces of the wedge are used to calculate the friction forces, Ffr0, in the friction block.

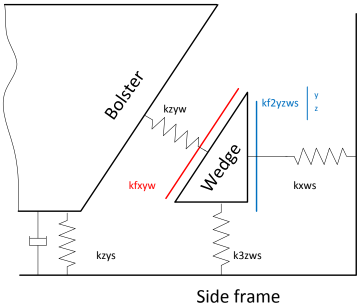

Fig 6. Wedge element in the suspension system of the wagon

Values of the coefficient of friction in the friction blocks, which are exposed to vibrations, are hard to be determined exactly. This parameter can be roughly assumed on the basis of materials from which the bodies in the contact are made, surface contamination, surface roughness, etc.

In this model, the values of the coefficient of friction have been selected to be μ=0.25 for the contact between the bolster and the wedge, and μ=0.35 for the contact between the wedge and the side frame.

As it can be seen from Fig. 7, damping in the suspension system depends on the coefficient of friction μ, the contact stiffness between two bodies *kzyw* and the sliding stiffness between two bodies *kfxyw*.

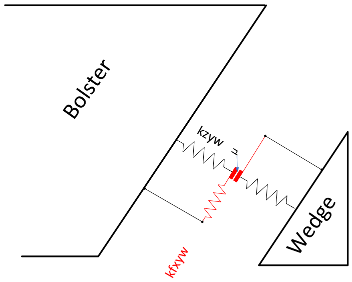

Fig 7. One-dimensional friction block between bolster and wedge

Side frame and axle box are connected via Adapter Plus, which is represented as a rubber element that provides elastic coupling between two bodies in three directions.

The wagons for iron ore transportation on Malmbanan use worn profiles with designation Malmbanan UNO-WP-4 MTAB. In the curves, usually, the outer rail has the profile MB1 and the inner rail has the profile BV50. In the model of the wagon, wheel and rail contact has been modelled using kpfr function. The output (equivalent conicity for the case of measured WP4 wheel and BV50 rail profiles) from the KPF program, a part of Gensys, is shown in Fig 8. The model allows for contact between wheel and rail at 3 points simultaneously.

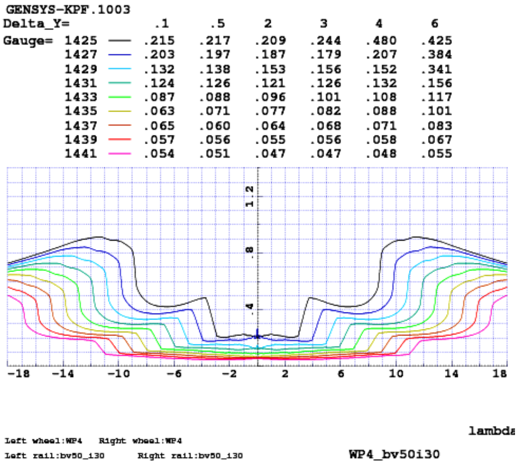

Fig 8. Equivalent conicity for the WP4BV50 wheel/rail combination

On the tangent track, at Malmbanan, the rail profile is BV50I30. In the curves, the outer rail has the profile MB1I30, and the inner rail has the profile BV50I30.

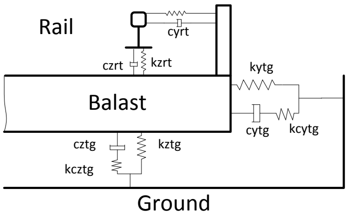

Fig 9. Model of the track

The model of the track takes into account ground, ballast, rails and the stiffness between these bodies as it is shown in Fig 10. By variation of the characteristics of the springs and the dampers in the model, tracks with wooden and concrete sleepers may be modelled, as well as different track stiffness, for example track stiffness during summer and winter ambient conditions.

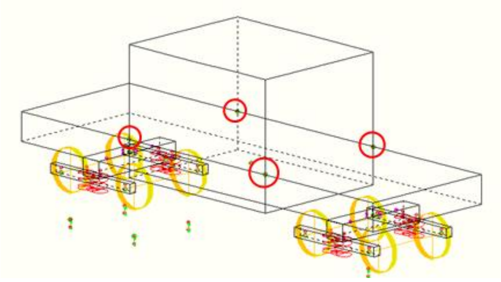

Fig. 10. Model of the vehicle with suspended load

For the freight vehicles, the differences in weight between loaded and empty vehicle are significant. Therefore, the dynamic behaviour of the load has also to be taken into account in models. In this model, the load of the freight vehicle is connected to the car body with 4 springs with high stiffness, marked with circles in Fig 10.

3 SIMULATION AND MEASUREMENT RESULTS

The verification of the model has been made by comparison between vertical and lateral accelerations in the car body obtained in simulations and measurements, on tangent track and in the curve, for empty and loaded wagon.

On-track tests with empty and loaded wagon have been performed between Kiruna and Riksgränsen, in the north of Sweden.

Good agreement between the simulated and the measured accelerations has been achieved for the case of the empty vehicle on tangent track and in the curve, as it is shown in the figures 11-18.

The diagrams present acceleration signals filtered so that quasi-static component of acceleration is removed.

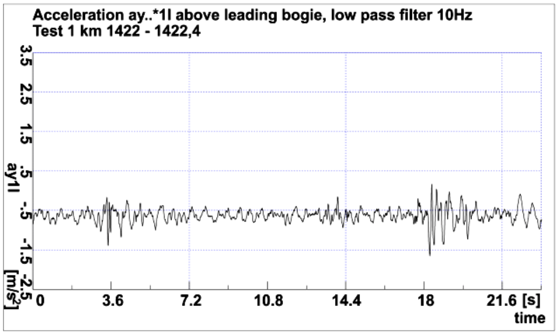

Fig 11. Measured lateral acceleration of the car body of the empty vehicle on the tangent track

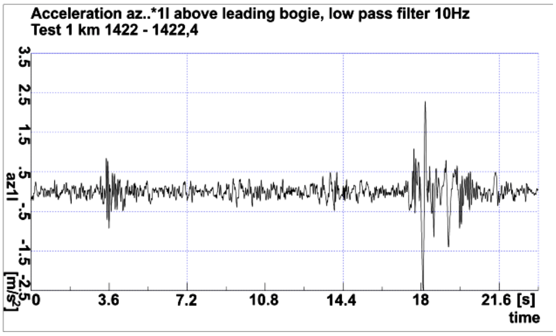

Fig 12.Measured vertical acceleration of the car body of the empty vehicle on the tangent track

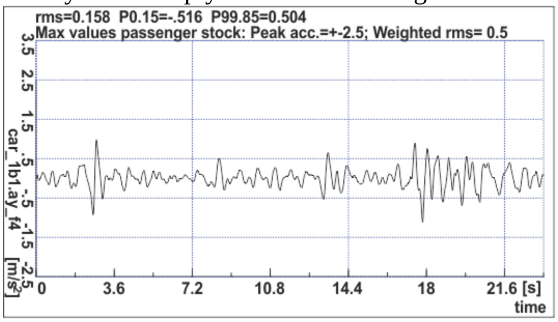

Fig 13.Simulated lateral acceleration of the car body of the empty vehicle on the tangent track

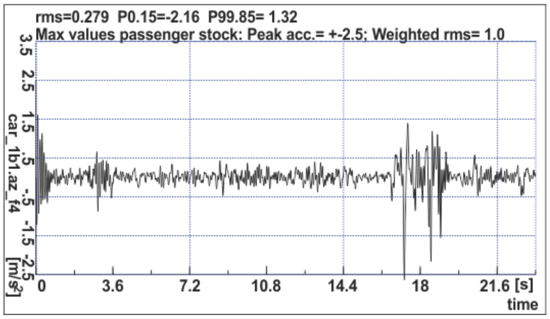

Fig 14. Simulated vertical acceleration of the car body of the empty vehicle on the tangent track

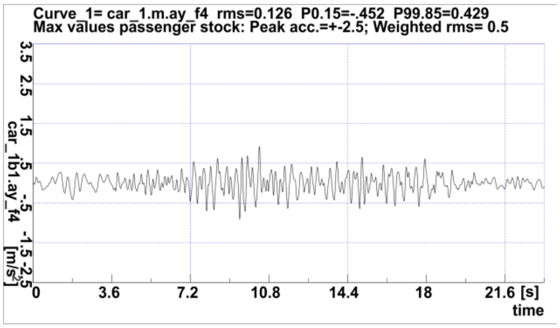

Fig 15.Simulated lateral acceleration of the car body of the empty vehicle in the curve

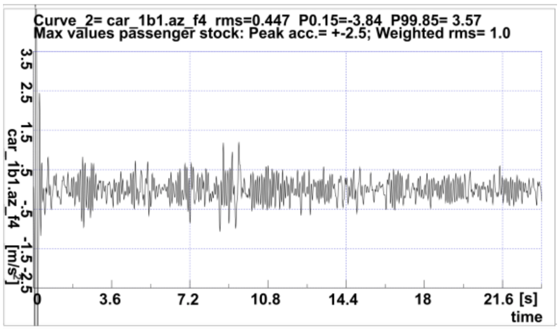

Fig 16.Simulated vertical acceleration of the car body of the empty vehicle in the curve

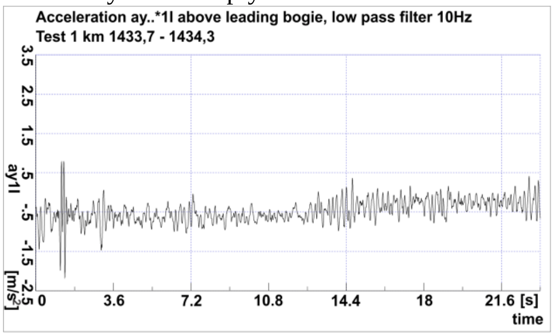

Fig 17. Measured lateral acceleration of the car body of the empty vehicle in the curve

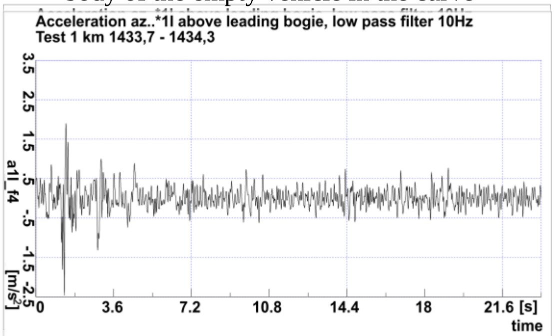

Fig 18. Measured vertical acceleration of the car body of the empty vehicle in the curve

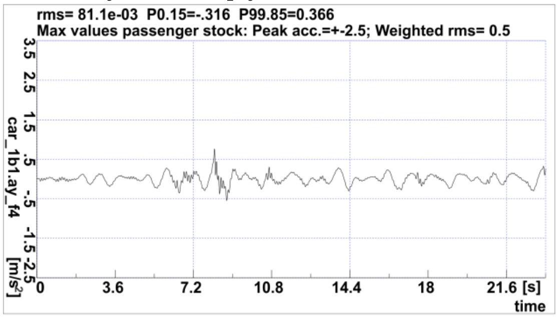

Fig 19.Simulated lateral acceleration of the car body of the loaded vehicle on the tangent track

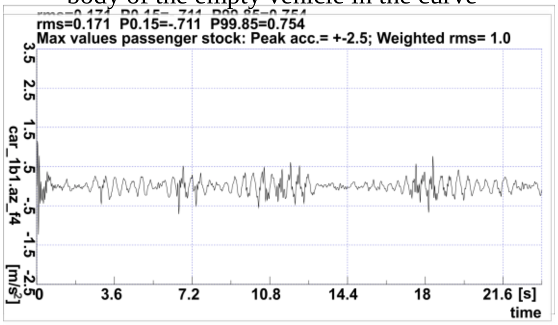

Fig 20.Simulated vertical acceleration of the car body of the loaded vehicle on the tangent track

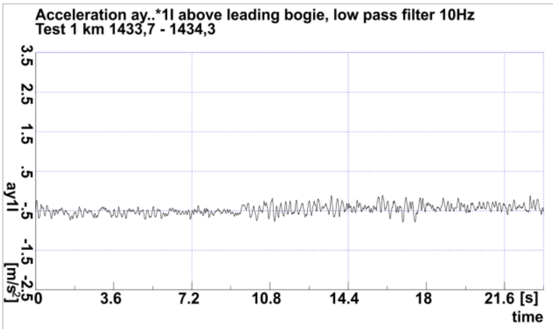

Fig 21.Measured lateral acceleration of the car body of the loaded vehicle on the tangent track

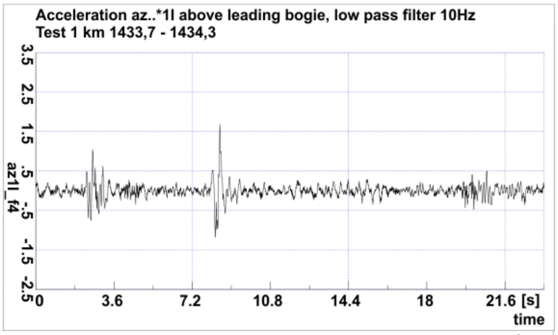

Fig 22.Measured vertical acceleration of the car body of the loaded vehicle on the tangent track

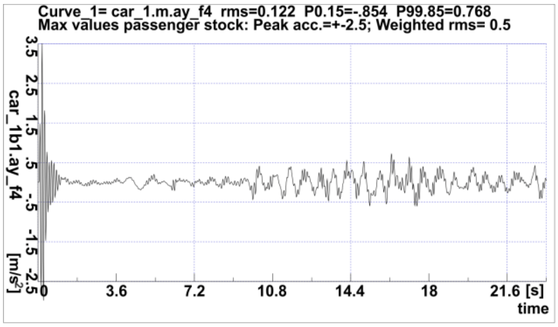

Fig 23.Simulated lateral acceleration of the car body of the loaded vehicle in the curve

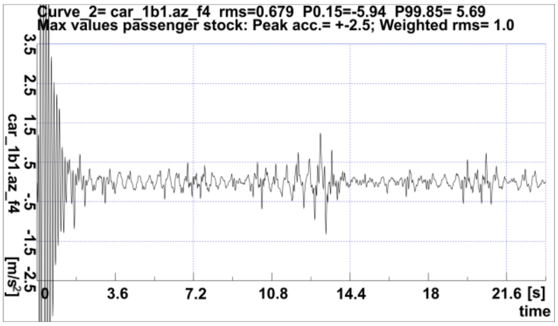

Fig 24. Simulated vertical acceleration of the car body of the loaded vehicle in the curve

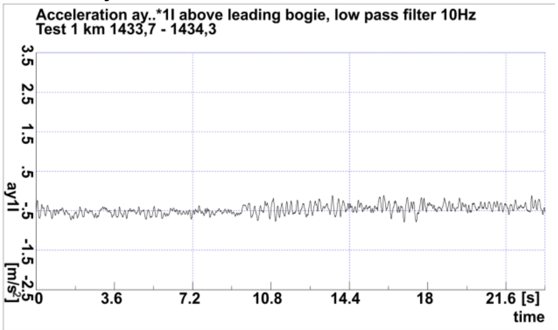

Fig 25. Measured lateral acceleration of the car body of the loaded vehicle in the curve

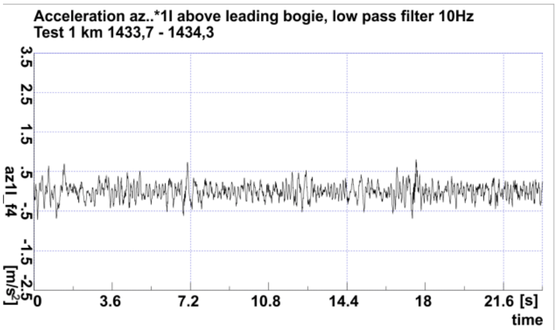

Fig 26.Measured vertical acceleration of the car body of the loaded vehicle in the curve

From results of the simulations, shown in figures 19, 20, 23 and 24, it can be concluded that car body of the loaded wagon may have periodical motion in lateral direction, both on tangent track and in the curve. The observed behaviour of the car body can be explained by low values of the equivalent conicity of the wheel/rail combination taken in the model, see Fig. 9.

3 CONCLUSION

Model validation, shown in this paper, has been made by comparison of the results obtained in simulations and measurements, for loaded and empty vehicle, on tangent track and in the curve. The validation has been performed by comparison of the accelerations of the car body in the time domain. A good agreement between the results of the simulations and the measurements has been observed in the case of the empty vehicle. In the case of the loaded vehicle, significant differences between measured and simulated accelerations of the car body are observed.

Considering that stiffness of the springs and the coefficient of friction on the wedges are adopted, the future research should be focused on better determination of those parameters.

Further validation of the model also should be made by comparison of the lateral and the vertical wheel-rail contact forces.

X REFERENCES

[1] Fuji Xia, “The dynamics of three-piece freight track”, PhD thesis, Lyngby, July, 2002

[2] Robert F. Harder, “Dynamic Modeling and Simulation of Three-Piece North American Freight Vehicle Suspension with Non-Linear Frictional Behavior Using ADAMS/Rail”, 5th ADAMS/Rail User’s Conference, Haarlem 10-12 may 2000

[3] Berghuvud, Ansel and Stensson Anika (1998) ’Dynamic Behaviour of Ore Wagons in Curves at Malmbanan’, Vehicle System Dynamics, 30: 3, 271 - 284

[4] Y. Q.Sun, C. Cole.(2008) 'Vertical dynamic behaviour of thre-piece bogie suspension with two types of friction wedge', Multibody Sys Dyn, 19: 365 — 382

Acknowledgment: Nebojša Bogojević wishes to acknowledge his gratitude to <Ministry of Education and Science of Republic of Serbia> for the support to the research through project grant TR37020

HEAVY MACHINERY - HM 2011, 39-42
ISBN 978-86-82631-58-3
Paper accepted: 20.05.2011

Measuring Railway Vehicle Wheel Load in Motion

Emil Dimitrov[1], Nencho Nenov[2,*]
[1] Department of Electronic Engineering and Technologies, TU of Sofia, Bulgaria
[2] Vice-Rector, VTU T. Kableshkov, Sofia, Bulgaria, nnenov_58@abv.bg

The paper presented is dedicated to developing a simulation model of an electronic system for measuring the load of railway vehicle wheels at an operational speed. The aim is to define the possibility to develop an electronic system for determining the value of force applied to the rail by the wheel on the base of the under-rail fundament reaction. The metrological qualities of the system defined through the model as well as good technical possibilities of its implementation have shown that the principle assumed is appropriate. The simulation model developed makes possible to determine the main parameters of the system with the particular requirements to it given and on this base to design the system.
Keywords: Railway vehicle, Wheel Load in Motion

0 INTRODUCTION

The railway transport features of reliability depends on the load of vehicle wheels both by absolute value and in respect to the difference between the values for individual wheels of a given vehicle. The influence of load is expressed in the following main trends: change of the intensity of wheel wear-out; increase of derailing risk.

The above mentioned evidently results in traffic safety deterioration thus influencing not only on the economic efficiency but also causing problems of humanitarian nature. To determine the wheel load, it is necessary to develop measuring devices. The equipment required for locomotives and passenger carriages has already been created [2].

As for freight wagons, it is expedient to develop a system of measuring the load of their wheels that will be able to perform that with running at an operational speed (of more than 60km/h). The results of similar measurements are of certain significance to exactly determine the weight of transported cargo.

The data of railway vehicle wheels measuring in motion published presented in international publications is scarce and of advertising nature [1]. It is the reason for the authors of this paper to investigate possible developing of a system for measuring the load of locomotive and wagon wheels in motion, at operational speeds, and further implement the system in practice.

1 THE STRUCTURE AND MAIN FEATURES OF THE SYSTEM

The development of the mechanical part of the measuring system model is performed assuming that the rail line is a continuous beam laid on an elastic fundament. This approximation gives a possibility to define the value of the railway vehicle wheel loads acting onto the rail from the determined sum of continuous reaction forces to the elastic fundament. Assuming the linear connection between the beam deflection and the distributed reaction forces of elastic fundament density q ($q=-Uy$) and the dependency of distributed reaction forces q of the fourth derivative of elastic line y^{IV} ($q=EJy^{IV}$), for the case examined (a beam of constant cross section loaded only by concentrated forces) the following homogeneous linear differential equation of the fourth order is valid: $y^{IV}+4k^4y=0$. The following valid boundary conditions have also been used as a base to determine constant values in the solution of differential equation:

$$x=\infty, y=0; x=0, y'=0; x=0, Q=-\frac{P}{2};$$

To determine the rail deflection $y(x)$ under the conditions described, the following expression is obtained: $y(x)=-\frac{P}{8EJk^3}e^{-kx}(\cos kx+\sin kx)$.

To determine the normalization value of rail fundament reaction $R_n(s)$ ($P=1$) in a section of length s (s -distance from the beginning of the

*Corr. Author's Address: VTU"Todor Kableshkov", 158 Geo Milev Street, Sofia, Bulgaria, nnenov_58@abv.bg coordinate system), it is obtained that $R_n(s) = \frac{k}{2}\int_0^s e^{-kx}(\cos kx + \sin kx)\,dx$. In this case the value of distance s corresponds to half of the section length (its whole length is 3,2m) foreseen to measure the wheel load on the rail. There are five force sensors mounted on this section.

With a relatively short distance between neighboring wheel-axles (e.g. the wheel-axles in the freight wagon bogies with a distance between wheel-axles of $L = 1,8\text{m}$), the sensor reacts to the wheel load of the wheel-axle $R2_n$, which is conditionally accepted as the second one in number (Fig. 1). This should be considered with the structure of the sensor and the time when it is activated.

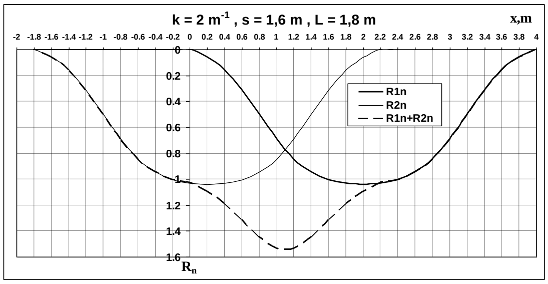

Fig. 1: Normative reaction to wheel loads of the 1st and 2nd wheel-axles $R1_n$ and $R2_n$.

The electronic system for load measuring consists of five smart strength sensors from S_1 to S_5 (Fig. 1). The output signals of the sensors are transmitted to tensometric amplifiers A_1 – A_5. The signals are introduced in a computer (PC) using a data acquisition system (DAS). The analysis and processing of information for determining the loads of individual wheels are performed by the computer.

The electronic system for load measuring consists of five smart strength sensors from S1 to S5 (Fig. 2). The output signals of the sensors are transmitted to tensometric amplifiers A1 – A5. The signals are introduced in a computer (PC) using a data acquisition system (DAS). The analysis and processing of information for determining the loads of individual wheels is performed by the computer.

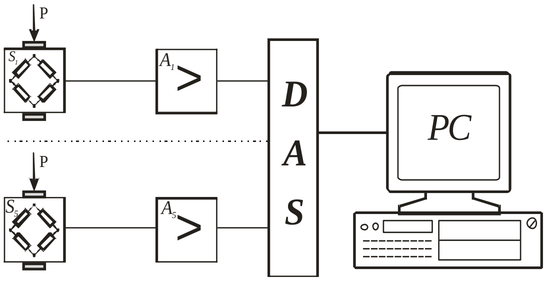

Fig. 2: Electronic system for measuring the load of wheels in motion.

The results obtained from the system examined have shown that it is capable of ensuring reliable data of the railway vehicle wheels loads while the train is running at operational speeds in a certain section.

The rail itself is used as a sensitive element of the sensor. The tensoresistor bridges are mounted on the rail. The tensometric amplifier is near the bridge to reduce the level of noises. A standard module USB-6009 of National Instruments Company is used as a Data Acquisition system. The DAS is a multifunctional one with eight analogue inputs and 12 digital inputs/outputs. The distance between the individual tensometric amplifiers and DAS is different: from 1m to 10 m.

In general, industrial electronics rely on current signaling because of its better noise immunity. The 4-20mA current interface has a wide application in industrial electronics because of high signal/noise ratio, especially in high noise environment. The concept behind the 4÷20 mA interfaces is to power the sensor using current of less than 4mA along the two-wire interface line. While using bridges, higher current or voltage should be applied in order to achieve better sensitivity. To avoid the 4mA constraint, a separate power line can be used increasing the number of wires to three. The integral scheme AD694 of the Analog Devices Company is used as a voltage-current transformer. It contains a stabilized power supply source (2V/10V), a buffer amplifier stage, a V-I converter, recalibrated for 0-2V and 0-10V input ranges, and an output stage, featuring output current adjustment and open loop alarm. The IC allows 4.5V to 36V for single or dual supply operations. The internal reference source can only supply as much as 5mA.

We aim to achieve the following goals:

- higher supply current;
- provide the means to supply the bridge sensor by constant current;
- simple preamplifier circuit that will allow proper input signal amplification;
- extend the input to accept “bipolar” signals.

Fig. 3 shows the proposed schematic. It requires external power supply for the bridge and transmits only positive input signals.

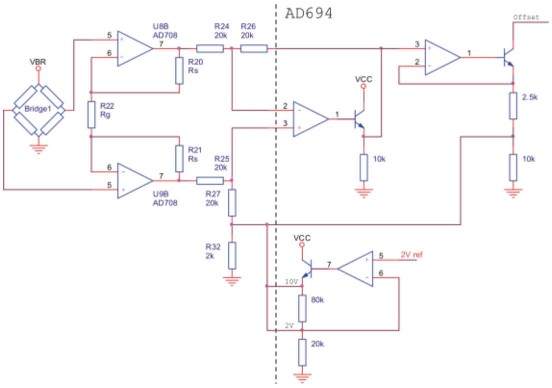

Fig. 3. Recommended wiring diagram of AD694.

To use the internal voltage reference for powering the sensing bridge, the schematic shown in Fig. 4 has been proposed. It is capable to feed bigger currents into the bridge, through the external transistor. The external feedback circuit allows to manually choose the supply voltage (R2/R3) or current (R4) applied to the bridge.

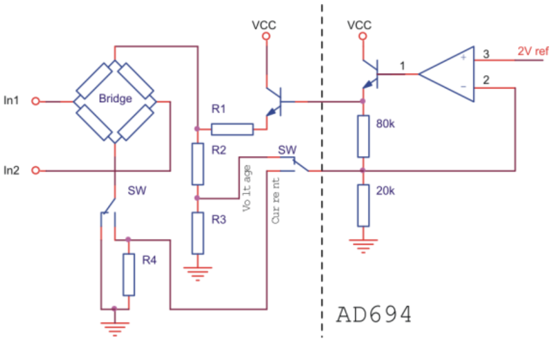

Fig. 4. Diagram of tensometric bridge powering.

In order to amplify and transmit “bipolar” signals, the “zero” output signal has to be lifted up to half the output scale. The offset voltage is applied at the V0 point (Fig. 5).

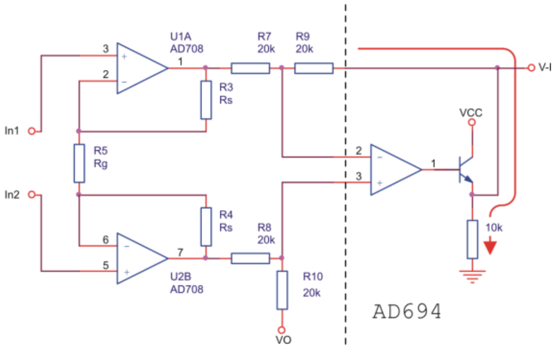

Fig. 5. Tensometric amplifier of bipolar signals.

Although the circuit operates particularly well with high input signals, it has problems with low signal processing. Because of the current flowing through R9 and the internal pull-down resistor the amplifier is unable to pull the V-I input down to 0V.

An alternative circuit is proposed and tested as shown in Fig. 6.

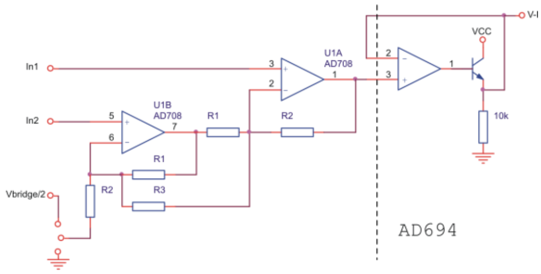

Fig. 6. Alternative circuit of the tensometric amplifier.

It has the extra capability to shift the zero line up to the value of Vbridge/2. Nevertheless, it uses fewer components than the circuit in **Fig. 5** and does not introduce voltage dependant error on the output value. Its transfer function is calculated as follows:

$$K = 1 + \frac{R2}{R1} + 2\frac{R2}{R3} \qquad (1)$$

The entire electronic system to measure the load of railway vehicle wheels in motion has not been implemented as no experimental section has been available. Experimental results have been obtained from the developed tensometric amplifier. A weight sensor with a full-bridge strain gauge is switched on at the input. The sensor is with a nominal value of force Po=50 kN. The dependency of output current in the scheme on the standardized value of force (P/Po) is shown in Fig.7.

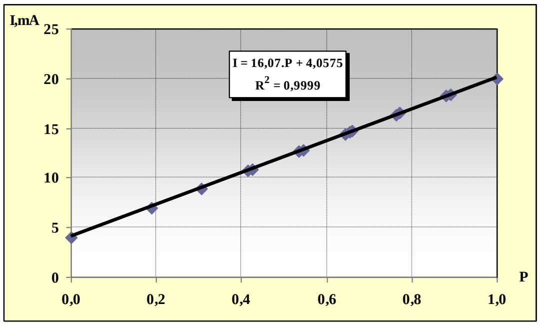

Fig. 7. Transmitting characteristics of the tensometric amplifier.

The percentage error of individual measurements with the assumed linear dependency between output current I and the applied value of force P is given in Fig. 8.

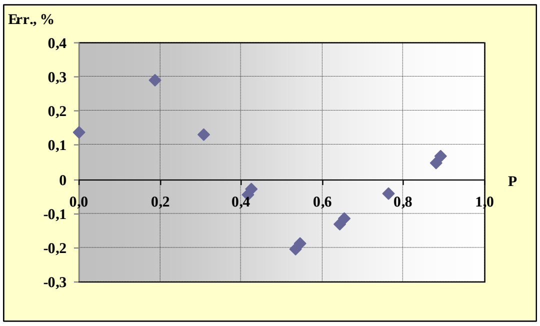

Fig. 8. Percentage error.

2. CONCLUSION

The experimental results obtained from the tensometric amplifier developed and analytical results from train traffic modeling have shown that the system proposed can ensure reliable information about the load of railway vehicle wheels with motion at an operational speed.

3 REFERENCES

[1] Buurman, G. den, A. Zoeteman, “A vital instrument in asset management”, European Railway Review, 2005, №11, pp. 80-85.

[2] Nenov N., E. Dimitrov, G. Mihov, T. Ruzhekov, P. Piskulev, A Study on Sensors for Measuring Load of Railway Vehicle Wheels in Motion, 31st International Spring Seminar on Electronics Technology, pp.558-563, May 7÷11, 2008, Budapest, Hungary

HEAVY MACHINERY - HM 2011, 43-47
ISBN 978-86-82631-58-3
Paper accepted: 20.05.2011

Networking as a Tool For Supporting Research in the Balkan Region (The Case of Surface Transport)

Zoya Damianova[1], Anna Dzhaleva-Chonkova[2, *], Nencho Nenov[2], Novak Nedic[3]
[1]ARC Fund, 5 Alexander Zhendov Street, Sofia, Bulgaria
[2] VTU "Todor Kableshkov", 158 Geo Milev Street, Sofia, Bulgaria
[3] University of Kragujevac, Faculty of Mechanical Engineering, Kraljevo, Kraljevo, Serbia

The opening of the European Research Area (ERA) to third countries is a strategic objective of the European Union. As the integration of the Western Balkan countries (WBCs) is a key priority, the EC supports many initiatives which aim at unlocking and developing the existing research potential in the region. However, little has been done in the field of transport research. Only the FP6 project RRTC (Regional railway transport research and training centre foundation) and the ASO project CONSTANT (CONcepts for life long learning to further increase SafeTy on rail based trANsporT systems) were focused to networking of scientists in the Balkan region.

The further contribution to cooperation of transport researchers in West Balkans was made by the FP7 project TransBonus. Applying an effective methodology, the team with the ARC Fund as Coordinator managed to improve contacts and promote closer Scientific and Technological (S&T) opportunities of collaboration in surface transport between Europe and the WBCs. The project established an EU-Balkan Transport network of researchers (more than 200) from different universities in order to enlarge the research capacity in the region.

Keywords: networking, transport research, FP7, West Balkan countries, TransBonus project.

INTRODUCTION

Networking is a common synonym for developing and maintaining contacts and personal connections. The aim is to create a group of professional acquaintances and associates and keep it active through regular communication for mutual benefit.

Research networking is the provision of data communications for the use of research and academic communities. The involvement of organizations from different countries in pan-European research networking is a good example of European cooperation, which is fundamental to the objectives of the EU itself. The European research networking provides possibilities for all researchers, wherever in Europe they work, to participate in collaborative research projects contributing to the best of their abilities.

Of the TransBonus partners, the coordinator ARC Fund, the Higher School of Transport (VTU) and the Faculty of Mechanical Engineering in Kraljevo (MFK) have had experience in networking activities in the Balkans. The VTU organized the first meeting of Balkan higher education institutions in the field of transport as early as in June 2002. Three years later with the MFK as a partner it coordinated the FP6 project RRTC, which full name "Regional railway transport research and training centre foundation" clearly reveals the networking nature of the project aims. The successful partnership of the two institutions continued in the ASO project CONSTANT (CONcepts for life long learning to further increase SafeTy on rail based trANsporT systems). In fact TransBonus was the third research project where the two institutions cooperated.

I TRANSBONUS: SCIENTIFIC AREA AND CONSORTIUM

The project aimed at research networking in the field of surface transport (road, rail and water-borne), which is considered critical to driving Europe's employment, prosperity and global exports and with positive impact on economic and social integration as a whole. The EU has targeted a number of objectives in surface transport research to meet the existing challenges, namely to:

[*]Corr. Author's Address: VTU "Todor Kableshkov", 158 Geo Milev Street, Sofia, Bulgaria, adzhaleva@abv.bg

- Improve the competitiveness of surface transport manufacturers, operators and infrastructure managers;
- Improve the safety and security of transport operations and services;
- Reduce the environmental effect of transport, including emissions and noise;
- Increase the mobility of people and goods by a better balance between all three surface transport modes.

An opportunity to achieve these goals is to take advantage of participation in the European RTD and innovation instruments to pursue excellence through research, innovation, technology transfer and collaboration with experienced EU partners. The opening of the European Research Area (ERA) to third countries and especially to the Western Balkan Countries (WBCs, incl. Albania, Bosnia and Herzegovina, Serbia, Montenegro and the Former Yugoslav Republic of Macedonia) has been seen as a key priority. The EC supports many initiatives which aim to stimulate the realization of the full research potential in the Balkans by unlocking and developing research potential and helping to successfully participate in research activities at EU level.

Several Specific Support and Coordination Actions have been undertaken so far to help co-operation with WBCs. Some of the most important actions include ERA WESTBALKAN that aims at creating and supporting a network of National Contact Points in the countries of the region, SEEREN connectiong the Research and Education Networks with the European high-speed electronic network GEANT, as well as SEE 5 ERA.NET working to create synergy among bilateral S&T agreements of the EU member states with the WBCs.

However, little has been done in the area of transport research. It was where the overall objectives of the project TransBonus had been set.

The project focused on four countries of the Western Balkans region, namely: Albania, Bosnia and Herzegovina, Serbia and the Former Yugoslav Republic of Macedonia and one convergence-region country to EU, also from the Balkan region, Bulgaria. The consortium was coordinated by the Applied Research and Communications Fund (Bulgaria) and included representatives from Greece, Malta and the Netherlands [Appendix 1].

Thought the project lifetime, the partners collaborated with other EU-funded projects: WBC-INCO.NET, ETNA, SEE IFA Network.

II ACTIVITIES FOR INCREASING KNOWLEDGE, SKILLS AND INTERACTION

The surveys made in stage of preparing the project proposal and within the project lifetime had shown that, despite difficulties and rapid political change in the region, the WBCs had skilled individuals and high potential organizations in the field of transport. However, that was not accordingly reflected in the participation in the EU framework programs. That is why the project aimed at building sustainable capacity and know-how transfer in all aspects of the FP7. It further sought to establish an EU Balkan Transport network of researchers, universities and experts to improve and enlarge the research capacity of Western Balkan centres in terms of their research programmes and human resources.

Following the project work program, during the first project year (2009) ARC Fund designed a methodology for mapping the research potential of the WBC in the surface transport domain, which was implemented in the participating WBCs and Bulgaria. All target beneficiary groups (universities, researchers, research companies, research NGOs, government bodies in the surface transport domain) were approached in order to record their research profiles and technology expertise: 91 collaboration profiles and 91 profiles of exploitable research results and technologies have been collected and used as a database for next events in the project program. Parallel to that, the consortium partners from Bulgaria, Greece and Malta mapped (additional to FP7) the funding opportunities (available locally or on a bi-lateral basis) for international research projects with WBC partners, in order to better understand the environment in which researchers in the WBCs operate.

In methodological terms the EU partners from Greece and the Netherlands developed a guide on the FP7 for transport researchers in English, which was then translated in the national languages of the participating WBCs 7 and Bulgarian. The Malta's partner developed the concept of the "Ideas Generation Events" and elaborated the guide on how to organise such training sessions applying it in practice during the three-day training on the FP7 organised in Malta.

The Ideas Generation Events (IGEs) intended to increase the experience in research project development and were organised by the participating WBCs and Bulgaria in September-November 2009 and in March-April 2010. Their purpose was to stimulate and collect innovative RTD ideas in the field of surface transport, to strengthen the research capacity of transport experts in the Western Balkans area through training on FP7 and create favourable conditions for networking among the participants.

An innovative project feature of great impact was the internal call for pre-proposals launched by the ARC Fund in August of 2009 and May 2010. The aim was to gather promising research ideas, evaluate them and assist the proposers to submit projects to the Transport theme of FP7 (Cooperation).

During the first round of the Open Call there were 30 research ideas submitted (against the target of 50 research ideas as per the Work Program). By the end of May 2010 another 33 pre-proposals were developed (the 3 research ideas from Bulgaria were not evaluated, since by the time they were already submitted as full proposals to FP7 call in transport).

After evaluating the pre-proposals (done according to the FP7 criteria), in order to maximise the opportunities provided by the TransBonus project itself, the partners organised a workshop for project proposals development in Sarajevo, Bosnia and Herzegovina on 7-9 July 2010. The four pre-proposals, which received the highest scores during the evaluation process, were extended as a base for further preparation of full FP7 applications.

Furthermore, to overcome the gap existing between researchers and industry, the TransBonus team organized 5 national research promotional meetings in Albania, Bulgaria, Bosnia and Herzegovina, FYR of Macedonia and Serbia. The goal was to present specific research ideas to the local transport sectors as well as to encourage joint industry-research actions.

At the same time the consortium undertook a number of activities aimed to raise awareness of skilled potential partners from WBCs who could be involved in projects, industry developments and relevant technology platforms in the transport sector. The project contributed to promoting closer Scientific and Technological (S&T) cooperation opportunities between EU („old member states – Greece, The Netherlands, Malta, the EU' s convergence region – Bulgaria) and the Western Balkan Countries (Albania, Bosnia and Herzegovina, Former Yugoslav Republic of Macedonia and Serbia).

The most important outcomes intended to promote the research potential were the PR research profiles (26) of organizations operating in the field of transport in the participating WBCs plus Bulgaria. The PR profiles were disseminated not only at the TransBonus website, but also through the EEN and ETNA networks.

In addition, all partners had a possibility to participate in the FP7 Information Day in Thessaloniki, Greece and visit the Netherlands in September 2010. The team members from the WBCs and Bulgaria had meetings at the technical universities of Delft and Eindhoven and two transport research centers. Besides that, the partners from the MFK made an expert study visit to Bulgaria prior to 19th International Scientific Conference TRANSPORT 2009 and the representatives of the Higher School of Transport (VTU) visited the facilities of the University of Skopje in FYR of Macedonia (a project partner) and the Aristotle University in Greece in October 2010 to discuss possibilities of joint research and projects. The last expert study visit was organized as an accompanying event to the final project meeting in Bulgaria in December 2010.

Finally, the progress in transport research networking in the Balkans was clearly demonstrated during the last event implemented under the TransBonus project. The Regional Workshop "Transport Research and Business Cooperation in SEE" hosted by the Higher School of Transport (VTU) in Sofia on 6 December 2010 was attended by more than 40 representatives of 10 countries from the region: the partners from Albania, Bosnia and Herzegovina, Bulgaria, Greece, Macedonia, Serbia and guests from academic and business organizations from Bulgaria, Croatia, Romania, Slovenia, Turkey. The scientists made presentations on their research priorities and results while three leading Bulgarian companies, DISSY Ltd. – Sofia, VRZ 99 – Septemvri and TRANSWAGON Plc – Bourgas, showed new technologies and innovations. The discussions focussed on the possibilities of wider cooperation between research and business in the field of surface transport.

The TransBonus project not only covered its planned objectives, but succeeded in over-performing in comparison to the indicators, presented in the work programme, and even executed some additional activities. The organized “Idea Generation Events” became 11 thanks to the additional session organized by the VTU. It also produced 6 PR research profiles, thus exceeding by one the common planned number of 25.

As a result of the TransBonus activities, 7 projects were submitted under the FP7 Transport calls in 2009 and 2010 by the consortium partners, which had not been targeted in the work programme of the project.

III DISSEMINATION OF RESULTS, INNOVATION ELEMENTS AND PROJECT IMPACT

The promotional activities during the first project year encompassed the project public web-site, information on the project on the partners’ institutional web-sites, publication of articles and presentations, especially at the Plenary Session of the 19th International Scientific Conference TRANSPORT 2009 in Sofia. A promotional leaflet was published, available in English and the national languages of the partners.

In 2010, besides the publications in mass media, the team presentated TransBonus during the Info Day of the ETNA network in August in Bulgaria and the First Innovation Dialogue Forum (1st IDF) in November 2010 as an activity of the WBC-INCO.NET project in Montenegro.

The VTU prepared a leaflet on Applied Research in Transport promoting the most recent university achievement.

To a great extent, TransBonus achieved excellent results thanks to its efficient methodology. The two most interesting elements of the methodology were internal open calls for pre-proposals and the workshop for project proposals development. This additional activity made TransBonus more beneficial to its target group. It was a step further to present the FP7 rules in details and assist applicants to develop their pre-proposal ideas into real FP7 project proposals. Another aim of the workshop in Sarajevo was to bring together potential applicants and provide them with consultations by four facilitators from the organizations that were experienced in project development and implementation. 46 researchers and experts from different Balkan countries sat on one table to work on common proposal ideas, thus networking by exchange of experience and know-how and forming consortia for project submission under FP7.

The TransBonus impact is wide enough to be assessed by different objectives and levels. Concerning the ERA strengthening, the project has contributed much to involving the researchers from the WBCs closer to the most urgent transport problems in the region as well as to ERA aims and strategy.

The project was directly connected with the societal needs of the region since the Surface transport sector plays a major role in Western Balkan economies, both in terms of GDP share and employment and research could, in a long term, lead to stability, prosperity and a higher pace of integration. The project directly stimulated the participation of local research and industrial actors in the European research programme in the Transport sector.

The TransBonus project contributed also to the support of the S&T cooperation aspect of the Stabilisation and Association Process, which is the cornerstone of the EU policy for the WBC region.

In compliance with the project idea of networking, the Faculty of Transport and Traffic Sciences with the University of Zagreb (Croatia) and the VTU, Sofia (Bulgaria) initiated the establishment of Cluster for Science and Research in Transport. In July 2010 in Sarajevo, parallel to the workshop on project proposals development, four academic institutions from South East Europe formally signed an Agreement on Cluster. Its main objective is to enhance the research collaboration and develop joint research projects for improving the transport system in the SEE area. It is envisaged that the cluster will expand including other members: universities and research institutes, SMEs, public administrations and NGOs from SEE and other European countries. The other two founding members, are the Faculty of Traffic and Communications with the University of Sarajevo (Bosnia and

Herzegovina) and Faculty of Civil Engineering with the University of Maribor (Slovenia)

There is no doubt that the cluster formation was inspired by the TransBonus project and this fact proved the tangible impact of the project on international cooperation and networking.

IV CONCLUSIONS

It should be emphasized that all partners involved in the TransBonus project brought their respective expertise, worked together as a team and effectively applied the "knowledge and skills" acquired to local target audiences across the Balkan countries. They all used various means to disseminate the results of the project. All publicly available materials were uploaded: the FP7 handbooks, the map document "Roadmap to excellence," the PR profiles, the collaboration profiles from each WBC and Bulgaria, since the actual objective of this joint effort was to assist researchers from WBCs to participate in the FP7.

Summarizing the project outcomes, it should be emphasized that TransBonus successfully achieved its most important goal: to establish an EU-Balkan Transport network of scientists and universities in order to improve and enlarge the research capacity of the Balkan countries. However, networking should be further developed following the TransBonus methodology that can be strengthened by:

• More workshops with diversified participation on proposal development with hands-on support by moderators;

• More national events for capacity building on FP7;

• More researchers from different fields of surface transport involved in future projects like TransBonus.

• Further support for setting up real consortia and getting involved as consortium members.

V REFERENCES

[1] http://www.transbonus.net. Accessed on 15 May 2011.

APPENDIX1: TRANSBONUS CONSORTIUM

Bulgaria

- Applied Research and Communications (ARC) Fund – *Coordinator* (www.arcfund.net)
- Todor Kableshkov Higher school of Transport (www.vtu.bg)

Albania

- Polytechnic University of Tirana, Mechanical Engineering Faculty (www.upt.al)

Bosnia and Herzegovina

- Automotive center - Centar za vozila, Sarajevo (www.automotivecenter.ba)

Former Yugoslav Republic of Macedonia

- Ss. Cyril and Methodius University – Skopje (www.ukim.edu.mk)

Serbia

- University of Kragujevac, Mechanical Engineering Faculty – Kraljevo (www.mfkv.kg.ac.rs)

The Netherlands

- SenterNovem (www.senternovem.nl)

Greece

- Foundation for Research and Technology Hellas /HELP-FORWARD (www.help-forward.gr)

Malta

- Integrated Resources Management (IRM) Company (www.environmentalmalta.com)

HEAVY MACHINERY - HM 2011, 49-54
ISBN 978-86-82631-58-3
Paper accepted: 30.05.2011

Study On Wheel Profile of Tram In Operation

Emil Mihaylov[1] - Dobrinka Atmadzhova[1,*]
[1] Todor Kableshkov University of Transport

The article examines the profile of tram wheels in the process of operation. The received function of distribution of horizontal deterioration (undercut) of a flange on a wheel structure allows simulating the shaping process of wheel structures on certain dynamic models of vehicle movement. The methods for modelling the process of change for each parameter of deterioration as a structure model of the surface of a driving wheel during operation. The method of geometrical shape modelling of the worn-out structures of wheels and rails is based on an assumption that the deterioration of cooperating wheels and rails is proportional to a degree of mutual penetration of contours of the structures examined and the factor of relative wheel and rail deterioration. The method allows receiving a ratio of wear and undercutting in the modelling process of a structure on certain dynamic models of vehicle movement.
Keywords: Tram, wheel profile,wear.

I INTRODUCTION

Huge progress has been made in design of running gears and railway vehicles. Tilting trains, high speed trains, active steering wheelset and many other brilliant solutions had been implemented in recent years on the railways. But beyond this progress the mechanics of railway wheelset remains the same and an inappropriate combination of wheel and rail profiles can vanish all this technological advances. And also a lot of old fashion vehicles are still in good condition to be replaced but they especially need appropriate combination of wheel/rail profiles, because they do not have high-tech devices which improving performance.
Problem of wheel/rail profiles design exists for many years and different approaches have been developed to obtain satisfactory wheel/rail profile combinations. It is possible to find an optimal combination of wheel and rail profile when dealing with closed railway system, i.e. when the same type of rolling stock is running on the same track and no influence of other type railway vehicles presents. Example of such systems includes heavy haul and tramlines.
Due to the fact that a rail costs much more than a wheel and wheels are more often re-profiled, it looks attractive to design a new wheel profile, which matches an existing rail profile.
Using geometrical characteristics of a contact between wheel and rail it is possible to judge about dynamic parameters of wheelset and ultimately parameters of vehicle since a wheelset represents a source of disturbances from track to vehicle. The wheel-rail geometry plays a dominant role in vehicle lateral dynamics. When a wheelset travels along a track the centre of axle makes the sinusoidal movement. The rolling radii, contact angles and the wheelset roll angle vary as the wheelset moves laterally relative to the rails. The nature of the functional dependence between these geometrically constrained variables and the wheelset lateral position depends on the wheel and rail cross-sectional shape.
The rolling radii enter the wheelset equations of motion due to the difference between the rolling radii of the two wheels of the wheelset. A rolling radii difference is one of the main characteristics that describe a contact between wheelset and railway track, which in turn defines the dynamic behaviour of a wheelset [4, 5, 6].
Determination of geometric contact characteristics for given wheel and rail profiles, wheel and rail gauge, and railhead cant angles is a well-known and solved problem for many years. These nonlinearities have been investigated by Wickens [8], Cooperrider [2], and De Pater [3]. The linear conical wheel profile widely used before has burst linear characteristics of rolling radii difference that results in shocks during a contact between wheel flange and rail at a motion of wheelset. The worn wheel usually has the smooth continuous characteristics of a contact. However high conicity of a worn wheel reduces critical speed of a wheelset and results in high oscillations of vehicle. Naturally, there is a desire to find a compromise between these two extremes. A traditional way to achieve the compromise is by trying different wheel profiles,

*Corr. Author's Address: Todor Kableshkov University of Transport, Sofia, Bulgaria, atmadzhova@abv.bg

with the purpose to find one of it with the characteristics satisfied to given conditions (usually curving, hunting, and contact stresses are taken into account).

II STATEMENT OF A PROBLEM

"Tram–train" systems carry out the integration of an urban tramway with the surrounding railway network, by means of light rail vehicles often provided with special wheel profiles in order to fit both grooved and flat-bottomed rails.

The numerous researches of the reasons of increased deterioration of flanges have allowed to define its reasons and to develop some ways of its reduction.

The joint operation of ways by trams has resulted to inconsistent and even to the mutually exclusive requirements in parameters of a way.

The reason of increase of lateral deterioration of rails and undercuts of flanges is not the level of lateral forces, but the dynamic factors. These factors are determined by a condition of running parts of the rolling-stock, on which, in particular, the angles of attack of wheels on rails depend.

For reduction of lateral pressure by a rail:

- The eminence of an external rail in a curve is accepted;
- In a design of carriages use elements facilitating negotiation in curves;
- Radius of curves is reduced.

For reduction of speeds of relative sliding of wheel flanges and rails:

- A structure of a wheel is carried out cone-shaped;
- Special polishing of rails for increase of a difference of circles of driving wheels in a curve is made.

Hardening of a wheel surface with application of steels by hardness up to **240 HB** is rather effective. The most effective way to increase the service life of wheel flanges and rails considers application of a flange.

The problem of intensive flanges undercut of wheels has remained and is the reason of significant material losses.

Fig.3a show contact hummock by wheel and rail in straight of the way when moving wheel pair on 20 mm with steppe 0,5 mm, before full loss directing ability. The Beginning on coordinate systems was geometric centre wheel pair.

Table 1. Basic parameters of the curved track.

Radius, m	Elevation of high rail, mm	Enlargement of track gauge, mm	Velocity, km/h	Length of spiral track, m	Length of circular track, m	Note
19	20	10	10	20	210	One site
50	20	5	25	30	125	One site
100	60	10	40	60	360	Two site

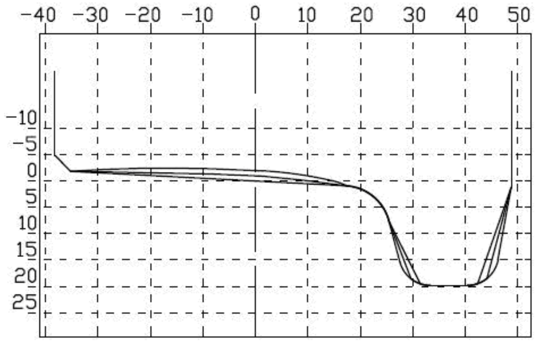

Figure 1. The measured wheel profiles of a bogie.

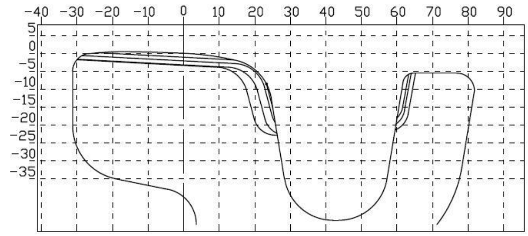

Figure 2. The measured rail profiles.

Fig.3b show contact hummock by the left wheel and rail in straight of the way when moving wheel pair on ±14,29 mm with steppe 0,5 mm, before full loss directing ability. The Beginning on coordinate systems was geometric centre wheel pair.

The most widespread method of an estimation of deterioration of surfaces of the wheels driving - relative method under the factor of deterioration:

$$\mathbf{I = N.f.V_{ck}}, \tag{1}$$

where: **N** – regular loading in the contact, **f** – friction factor, $\mathbf{V_{ск}}$ – slippage speed.

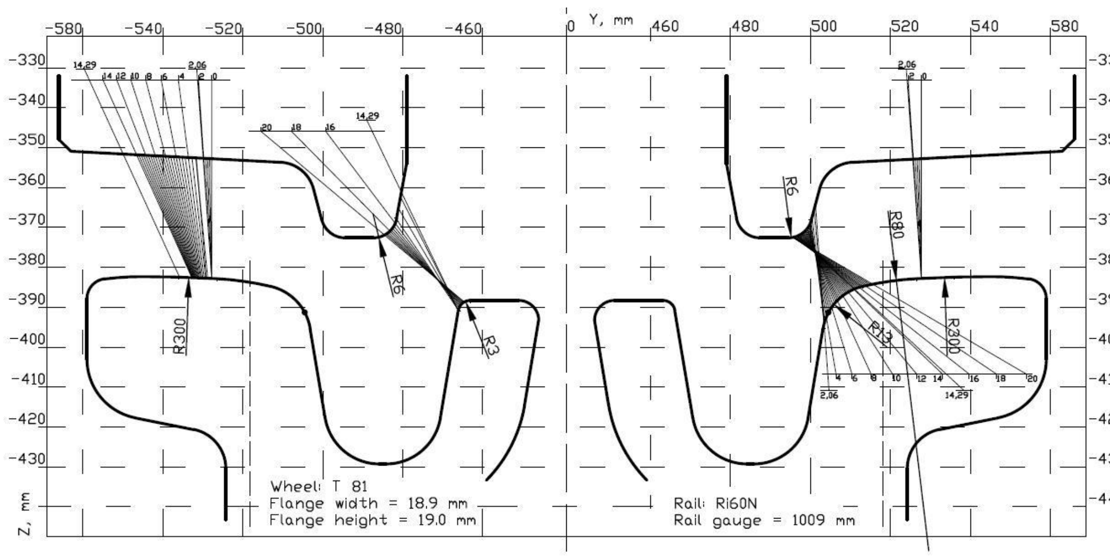

Figure 3a. The contact distribution.

In (1) the factor of deterioration has the dimension of capacity and is equal to work spent on galling of surfaces in a contact zone in unit of time. Such technique, however, does not allow estimating two major characteristics of deterioration: absolute size of deterioration and its distribution on a surface of a flange.

The absolute size of deterioration can be submitted as weight of the galling metal of a rim (mass deterioration), or as thickness of a galling layer (hire or undercut). The modern line of increase of hardness of a material of wheels is based on ability of firmer steels to transform work of friction to a thermal energy, instead of spending it for removal of a layer of metal.

Concerning the proportionality of deterioration of forces of friction, the formula allowing calculating size of volumetric deterioration, similar to the formula offered by Masliev [7], could look as follows:

$$\mathbf{V = \varsigma.N.f.V_{ck}.t,} \qquad (2)$$

where: ς − deterioration factor, that has dimension of [m^3/J] with the dimension of **V** [m^3]; **t** – time of deterioration process.

However, because of the difficulties of determination of deterioration factor ς we should content us with the comparing analysis of deterioration in the regular contact on the surface of the rim rolling in the flange contact.

2. METHODS OF THE MODELING PROCESS OF THE CHANGES IN THE DETERIORATION CHARACTERISTICS

The deterioration of a surface of driving tires is estimated in three parameters: by hire thickness of a flange and parameter of a steepness of a flange.

The technique of modelling of process of change of each parameter of deterioration as a model of a structure of a surface of driving of a wheel during operation.

The value of speeds of slippage $\mathbf{V_{скI}}$ и $\mathbf{V_{скII}}$ within the limits of the first and the second spots of contacts, factor of coupling f and factor - ς are accepted by constant sizes. The distributions of volumetric deterioration within the limits of areas of the first and second contacts will submit to the following laws:

$$\mathbf{dv_I = \varsigma.f.V_{ckI}(t).n_I(x_I, y_I, t).dx_I.dy_I.dt;} \qquad (3)$$

$$\mathbf{dv_{II} = \varsigma.f.V_{ckII}(t).n_{II}(x_{II}, y_{II}, t).dx_{II}.dy_{II}.dt;}$$

where: $\mathbf{n_I}$ $\mathbf{(x_I, y_I, t)}$, $\mathbf{n_{II}}$ $\mathbf{(x_{II}, y_{II}, t)}$ − functions of distribution of specific pressure on areas of the first and second contacts.

According to the theory of Herz, with an assumption about elasticity of deformations within the limits of a stain of contact, the function **n(x, y)** looks like this:

$$\mathbf{n(x,y) = n_o\sqrt{1-\left(\frac{x}{a}\right)^2-\left(\frac{y}{b}\right)^2},} \qquad (4)$$

where: **a**, **b** − half-axes of a contact ellipse; $\mathbf{n_o}$ − the maximal specific pressure at centre of a stain of contact; **x**, **y** – coordinates of a point within the limits of a stain of contact.

Half-axes **a** и **b**, в according to the theory of Herz equal:

$$\mathbf{a = n_a \sqrt[3]{\frac{2}{3}\left(\frac{1-\nu_k{}^2}{E_k}+\frac{1-\nu_p{}^2}{E_p}\right)\frac{N}{k_s}}} \tag{5}$$

$$\mathbf{b = n_b \sqrt[3]{\frac{2}{3}\left(\frac{1-\nu_k{}^2}{E_k}+\frac{1-\nu_p{}^2}{E_p}\right)\frac{N}{k_s}}}$$

where: ν_k, ν_p, E_k, E_p − factors of Poisson and modules of elasticity of materials of a wheel and rail.

With $\nu_k = \nu_p = \nu$ и $E_k = E_p = E$:

$$\mathbf{a = n_a \sqrt[3]{\frac{4}{3}\cdot\frac{1-\nu^2}{E}\cdot\frac{N}{k_s}}} \tag{6}$$

$$\mathbf{b = n_b \sqrt[3]{\frac{4}{3}\cdot\frac{1-\nu^2}{E}\cdot\frac{N}{k_s}}}$$

where: $\mathbf{n_a}$, $\mathbf{n_b}$ − factors dependent on the geometrical form of surfaces of contacting. The form of surfaces is characterized in factors **A** and **B** [1].

Factors **A** and **B**:

$$\mathbf{A = \frac{1}{4}\left[k_s - K\right];\ B = \frac{1}{4}\left[k_s + K\right]} \tag{7}$$

where: **K** − relative curvature of contacting surfaces of a wheel and rail:

$$\mathbf{K = \left(k_{kx} + k_{px}\right) - \left(k_{ky} - k_{py}\right)} \tag{8}$$

where: $\mathbf{k_s}$ – the given curvature of contacting surfaces of a wheel and rail:

$$\mathbf{k_s = k_{kx} + k_{ky} + k_{px} + k_{py}} \tag{9}$$

where: $\mathbf{k_{kx}}$, $\mathbf{k_{ky}}$, $\mathbf{k_{px}}$, $\mathbf{k_{py}}$ − curvature of contacting surfaces, accordingly, wheel both rail in longitudinal and cross planes of symmetry, return appropriate radiuses of curvature in all sections (fig. 4):

$$\mathbf{k_{kxI} = \frac{1}{R_I^x};\quad k_{kyI} = \frac{1}{R_I^y};\quad k_{kyI} = \frac{1}{R_I^y};} \tag{10}$$

$$\mathbf{k_{pyI} = \frac{1}{R_{pI}^y};\ k_{kxII} = \frac{1}{R_{II}^x};\ k_{kxII} = \frac{1}{R_{II}^x};}$$

$$\mathbf{k_{kyII} = \frac{1}{R_{II}^y};\ k_{pyII} = \frac{1}{R_{pII}^y}}$$

Curvature of a rail in sections $\mathbf{K_{II}}$ on fig. 1: $\mathbf{k_{pxI} = 0}$ and $\mathbf{k_{pxII} = 0}$, as $\mathbf{R_{pxI} = \infty}$ and $\mathbf{R_{pxII} = \infty}$.

The maximal pressure at centre of a stain of contact according to the theory of Herz-Belyaev depends on a normal loading in contact and sizes of contact:

$$\mathbf{n_o = \frac{3}{2}\cdot\frac{N}{\pi.a.b}} \tag{11}$$

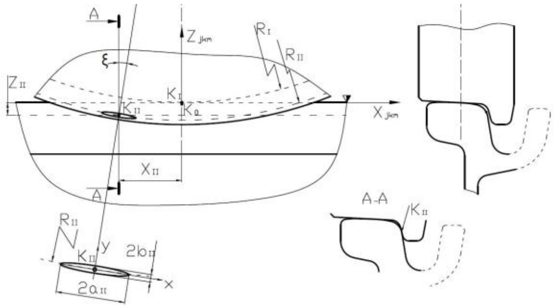

Figure 4. The circuit of contacting of a tire surface with a surface of a rail

The volumetric deterioration of a tire surface in a contact zone can be defined by integration:

$$\mathbf{V = \varsigma.f.\int_t \iint_S V_{ck}(t).n(x,y,t).dx.dy.dt =} \tag{12}$$

$$\mathbf{= \varsigma.f.\int_t V_{ck}(t).\int_{-b}^{b}\left(\int_{\varphi_1(y)}^{\varphi_2(y)} n(x,y,t).dx\right).dy.dt}$$

where: **S** − area of an ellipse of contacting of a flange with a rail (area of integration); $\boldsymbol{\varphi_1(x)}$, $\boldsymbol{\varphi_2(x)}$ − functions, describing borders of a stain of contact:

$$\mathbf{\varphi_1(y) = \frac{a}{b}.\sqrt{b^2 - y^2}\ ;} \tag{13}$$

$$\mathbf{\varphi_2(y) = -\frac{a}{b}.\sqrt{b^2 - y^2}}$$

Distribution of volume of a material worn in unit of time, on a surface of a flange in radial section ***A-A*** (fig. 4) is defined by integration:

$$\mathbf{V(y) = \varsigma.f.V_{ck}.\left(\int_{\varphi_1(y)}^{\varphi_2(y)} n(x,y).dx\right)} \tag{14}$$

or, counting on (4):

$$\mathbf{V(y) = \varsigma.f.V_{ck}.\left[\int_{\varphi_1(y)}^{\varphi_2(y)}\left(n_o\sqrt{1-\left(\frac{x}{a}\right)^2-\left(\frac{y}{b}\right)^2}.dx\right)\right]} \tag{15}$$

$$\int_{\varphi_1(y)}^{\varphi_2(y)}\left(\mathbf{n_o}\cdot\sqrt{1-\left(\frac{x}{a}\right)^2-\left(\frac{y}{b}\right)^2}.dx\right)= \tag{16}$$

$$=\mathbf{n_o}\cdot\int_{\varphi_1(y)}^{\varphi_2(y)}\sqrt{1-\left(\frac{x}{a}\right)^2-\left(\frac{y}{b}\right)^2}.dx$$

Let's calculate uncertain integral, previously by simplifying its kind:

$$\int\sqrt{1-\left(\frac{x}{a}\right)^2-\left(\frac{y}{b}\right)^2}.dx=\int\sqrt{A-B.x^2}.dx \tag{17}$$

where:

$$A=1-\left(\frac{y}{b}\right)^2;\quad B=\frac{1}{a^2} \tag{18}$$

Then:

$$I=\int\sqrt{A-B.x^2}.dx= \tag{19}$$

$$=\sqrt{A}.\int\frac{\sqrt{1-\left(\sqrt{\frac{B}{A}}\right)^2}.d\left(\sqrt{\frac{B}{A}}.x\right)}{\sqrt{\frac{B}{A}}}$$

Changing $\sqrt{\frac{B}{A}}.x=y$, we get:

$$\boxed{I=\frac{A}{\sqrt{B}}.\int\sqrt{1-y^2}.dy} \tag{20}$$

After changing **y = □sin t**; **dy = cost.dt**, we get:

$$I=\frac{A}{\sqrt{B}}.\int\sqrt{1-\sin^2 t}.\cos t.dt= \tag{21}$$

$$=\frac{A}{\sqrt{B}}.\int\cos^2 t.dt=$$

$$=\frac{A}{2.\sqrt{B}}.\left(t+\frac{1}{2}.\sin 2t\right)$$

Counting that

$$t=\arcsin y=\arcsin\left(\sqrt{\frac{B}{A}}.x\right); \tag{22}$$

$$\sin 2t=\frac{2.\sqrt{B}}{A}.x.\sqrt{A-B.x^2}$$

we get:

$$I=\frac{A}{2.\sqrt{B}}\left[\arcsin\left(\sqrt{\frac{B}{A}}.x\right)+\right. \tag{23}$$

$$\left.+\frac{\sqrt{B}}{A}.x.\sqrt{A-B.x^2}\right]$$

Definite integral

$$I=\int_{\varphi_1(y)}^{\varphi_2(y)}\sqrt{1-\left(\frac{x}{a}\right)^2-\left(\frac{y}{b}\right)^2}.dx= \tag{24}$$

$$=\frac{A}{2.\sqrt{B}}\left[\arcsin\left(\sqrt{\frac{B}{A}}.x\right)+\right.$$

$$\left.+\frac{\sqrt{B}}{A}.x.\sqrt{A-B.x^2}\right]_{\varphi_1(y)}^{\varphi_2(y)}$$

Inserting into (24) limits of integration (13) and counting the changes (18), we get the equation:

$$I=\frac{a.\sqrt{b^2-y^2}.\left(1+1{,}57.b.\sqrt{b^2-y^2}\right)}{b^3}.t \tag{25}$$

Based on the equation (12), we can write down the function of distribution of undercut of a flange along an axis **Y** of the contact area (fig. 4):

$$\lambda(y)=\varsigma.f.V_{ck}.n_0.\frac{a.\sqrt{b^2-y^2}.\left(1+1{,}57.b.\sqrt{b^2-y^2}\right)}{b^3}.t \tag{26}$$

or, counting (11):

$$\lambda(y)=\frac{3}{2.\pi}.\varsigma.f.V_{ck}.N.\left[\frac{\sqrt{b^2-y^2}.\left(1+1{,}57.b.\sqrt{b^2-y^2}\right)}{b^4}\right].t \tag{27}$$

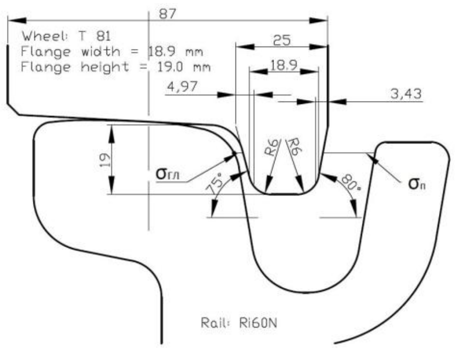

Figure 5. The flange shape with groove rail.

To get the distribution of deterioration of a flange, given in radical distance **r** (fig. 5) we need to be sure that:

$$\mathbf{r = z_{II} - y.sin\gamma_{II}},$$

where:

$$\mathbf{y = \frac{z_{II} - r}{sin\gamma_{II}}} \qquad (28)$$

The received function of distribution of horizontal deterioration (undercut) of a flange on a wheel structure, allows simulating the shaping process of wheel structures on the determined dynamic models of a movement of vehicle.

3. CONCLUSIONS

1. The method of geometrical shaping modelling of the worn-out structures of wheels and rails is based on an assumption that the deterioration of cooperating wheels and rails is proportional to a degree of mutual penetration of contours of researched structures and factor of relative deterioration of a wheel and rail.
2. Modelling of relative intensity of the undercut of flanges is based on a power method of an estimation of mass deterioration. The method allows receiving a ratio of hire and undercutting in the modelling process of a structure on the determined dynamic models of a movement of vehicle.

REFERENCES

[1] Belyaev N.M.: Using to theories of the Hertz to count of the local voltages in point соприкасания travell about and rail. Moscow, Herald of the engineer, T.3, 12, 1917, c.281-288.

[2] Cooperrider, N.K., E. H. Law, et al., Analytical and Experimental Determination of Nonlinear Wheel/Rail Constraints, Proceedings ASME Symposium on Railroad Equipment Dynamics, 1976

[3] De Pater A.D., The Geometrical Contact Between Track and Wheelset, Vehicle System Dynamics, vol. 17, pp 127-140, 1988

[4] Dukkipati, R.V., Vehicle Dynamics, Boca Raton, CRC Press, ISBN 0-8493-0976-X, 2000

[5] Esveld, C., Modern Railway Track, (Second Edition), MRT-Productions, Zaltbommel, ISBN 90-8004-324-3-3, 2001

[6] Kalker, J.J., Three-Dimensional Elastic Bodies in Rolling Contact, Kluwer Academic Publishers, Dordrecht, ISBN 0-7923-0712-7, 1990

[7] Masliev V.G.: Scientific bases of the choice design-technological parameter device for reduction of the wear-out of the paddling tires travell about locomotive: Diss. dokt. tehn. sciences. Harkov, HPI, 2004, c. 464.

[8] Wickens, A.H., The Dynamic Stability of Railway Vehicle Wheelsets and Bogies Having Profiled Wheels, International Journal of Solids Structures, vol. 1, pp 319-341, 1965

HEAVY MACHINERY - HM 2011, 55-61
ISBN 978-86-82631-58-3
Paper accepted: 30.05.2011

Development of the Methods of the Analysis Behavior of the Hopper Cars And Determination of the Period to Operation Exploitation For Transportation Corrosion -Active Materials

Milen Mihalev[1] - Dobrinka Atmadzhova[1,*]
[1] Todor Kableshkov University of Transport

The methods of research of static and dynamic behaviours of the granular materials are developed in the paper. Represented procedure allows raising survivability of the hopper cars on phases of their designing and perfection. Offered methods of simulation modeling at determination of the period to exploitation hopper cars for transportation corrosion-active materials, is considered realization to mathematical model to coach of the hopper type with reference to, used for transportation of the mineral fertilizers

Keywords: Railway vehicle, hopper cars, reliability, life cycle.

0 INTRODUCTION

One of the main tasks of rolling stock of railways is the development and introduction of methods of predicting the service life of cars, searching for ways to improve their operational reliability. Meeting this challenge requires the implementation of the complex issues associated with the analysis of the technical condition of car design, their diagnosis, as well as theoretical studies on the prediction of their life. When transporting corrosive cargo (acids, fertilizers, etc.) due to corrosion of structural components of cars change their state of stress. In turn, the increase in stress increases the corrosion of metal, which significantly reduces the carrier spossobnosti, reduce reliability and shorten the life of cars [9].

Issue of increasing the survivability of hoppers is associated with the decision very difficult research problem loading their supporting structures from the effect of bulk cargo. Existing methods of describing the behaviour of bulk cargo in the bodies of cars include the use of wedge or a ball of solid models that can not effectively analyze the behaviour of the fine media, such as sand, grain and fertilizer.

Objective of this paper:

- Development computational procedure for proximate analysis in static and dynamic productions of the objects of this type with the introduction of the continuum model for granular material, which interacts with the supporting structure;

- Study of car design, interacting with a corrosion-active media, showed that the basic approach for studying the effect of corrosion damage on the stress-strain state (SSS) of structures is to reduce the car body cross-sectional area of elements is proportional to the corrosion wear.

The regulations, methods of calculation for strength and durability of the car design [3] does not take into account the type and level of stress state, temperature, concentration and aggressiveness of cargo, operating conditions of rolling stock, structural features of car bodies and many other factors affecting the corrosion rate.

Such problems are nonlinear and multivariate, require the construction of computational models that take into account the peculiarities of interaction with the corrosive medium, the nonlinear deformation of structural elements, the condition for occurrence of the limit state, especially the constructive execution [7].

One of the ways to improve the reliability of cars is the organization of monitoring of the strength of car designs. Key provisions of the concept of the strength of monitoring were considered in [9]. By analogy with [3,9,10] by monitoring the strength we mean the control and management of construction of a wagon (in terms of strength) to ensure its reliability for a specified period of service. Consider the general scheme of simulation of complex dynamic system, which is a wagon

To determine the safe life of the car used in the approach to implement a scaling in the

[*]Corr. Author's Address: Todor Kableshkov University of Transport, Sofia, Bulgaria, atmadzhova@abv.bg

description of the system with the union through the numerical data that show the input and output parameters of particular models. Appropriateness of the partition of a complex system into blocks due to the fact that the partial model of the system described is often heterogeneous mathematical dependencies and do not merge into a single system of functional relationships that describe the various physical phenomena.

I THE COMPUTATIONAL PROCEDURE FOR PROXIMATE ANALYSIS IN STATIC AND DYNAMIC PERFORMANCES OF OBJECTS

Deformation of the cargo described on the basis proposed by Grigoryan [8] theory of elastic-plastic deformation of the material that was used by several authors to study the behaviour of sandy soils. The main provision of this theory is that when the shear strain can not proceed purely elastic, part of the infinitesimal deformation is plastically and irreversibly in proportion to the corresponding elements of the stress deviator. As a condition of stress is taken dependence:

$$\mathbf{J_2 = F(p)}, \qquad (1)$$

where $\mathbf{J_2}$ – second invariant of stress deviator; **F(p)** – a non-decreasing function of pressure

$$\mathbf{p = (\sigma_x + \sigma_y + \sigma_z)/3}, \qquad (2)$$

σ_x, σ_y , σ_z – normal stresses in the directions of the axes Ox, Oy and Oz of the Cartesian coordinate system 0xyz.

Based on the equation of Grigoryan [8] represent the increment vector {s} of deviator stress at the condition stress in the form:

$$d\{s\} = [T(\{s\})]d\{f\} - \lambda\{s\}, \qquad (3)$$

where **d** – symbol differential;
{f} – vector is written as follows:

$$\{f\} = [A]\begin{Bmatrix} u \\ v \\ w \end{Bmatrix} \qquad (4)$$

[A] – matrix-differential operator is written as follows:
[A] =

$$\begin{bmatrix} \frac{\partial}{\partial x} & 0 & 0 & \frac{\partial}{\partial y} & \frac{\partial}{\partial z} & 0 & 0 & 0 & 0 \\ 0 & \frac{\partial}{\partial y} & 0 & 0 & 0 & \frac{\partial}{\partial x} & \frac{\partial}{\partial z} & 0 & 0 \\ 0 & 0 & \frac{\partial}{\partial z} & 0 & 0 & 0 & 0 & \frac{\partial}{\partial x} & \frac{\partial}{\partial y} \end{bmatrix}^T \qquad (5)$$

u, v, w – projection of the displacement vector on the axis **Ox, Oy** и **Oz**;
[T{s}] - matrix is written as follows:
[T{s}] =

$$\begin{bmatrix} \frac{4}{3}G & -\frac{2}{3}G & -\frac{2}{3}G & 0 & 0 & 0 & 0 & 0 & 0 \\ -\frac{2}{3}G & \frac{4}{3}G & -\frac{2}{3}G & 0 & 0 & 0 & 0 & 0 & 0 \\ -\frac{2}{3}G & -\frac{2}{3}G & \frac{4}{3}G & 0 & 0 & 0 & 0 & 0 & 0 \\ 0 & 0 & 0 & G & \frac{s_{yz}}{2} & G & \frac{s_{xz}}{2} & -\frac{s_{xz}}{2} & -\frac{s_{yz}}{2} \\ 0 & 0 & 0 & \frac{s_{yz}}{2} & G & -\frac{s_{yz}}{2} & -\frac{s_{xy}}{2} & G & \frac{s_{xy}}{2} \\ 0 & 0 & 0 & -\frac{s_{xz}}{2} & -\frac{s_{xy}}{2} & \frac{s_{xz}}{2} & G & \frac{s_{xy}}{2} & G \end{bmatrix} \qquad (6)$$

G – shear modulus of the material before the plastic deformation;

s_{xy} , s_{xz} , s_{yz} – deviator stress;

λ - parameter:

$$\lambda = \beta H(\beta);$$

$$\beta = \left(\frac{G}{F(p)}\{s\}^T d\{e\} - \frac{F'(p)}{2 \cdot F(p)}dp \right) \qquad (7)$$

$\mathbf{H(\beta)}$ – Heavisid's function; $\mathbf{F'(p)}$ – derivative of $\mathbf{F(p)}$ the pressure **p**; $\{e\}$ – vector of deviator strain, which can be expressed through the vector **{f}** using the dependence:

$$\{e\} = [Q][\Lambda]\{f\} \qquad (8)$$

matrixs $[Q]$ and $[\Lambda]$ equal:

$$[Q] = \begin{bmatrix} \begin{matrix} 2/3 & -1/3 & -1/3 \\ -1/3 & 2/3 & -1/3 \\ -1/3 & -1/3 & 2/3 \end{matrix} & 0 \\ 0 & [E]_3 \end{bmatrix};$$

$$[\Lambda] = \begin{bmatrix} [E]_3 & 0 \\ 0 & \begin{matrix} 1 & 0 & 1 & 0 & 0 & 0 \\ 0 & 0 & 0 & 1 & 0 & 1 \\ 0 & 1 & 0 & 0 & 1 & 0 \end{matrix} \end{bmatrix}^T \qquad (9)$$

$\mathbf{[E]_3}$ – identity matrix of third order.

When you work the material in the λ = 0, and it actually becomes aλelastic stage in equation (1) should be taken record of the generalized Hook's law.

Note that the vector {s} can be expressed in terms usually considered the stress vector {σ} relation:

$$\{s\} = [Q]\{\sigma\} \qquad 10)$$

Reduce (3) to a form suitable for use in the procedure of the finite element method. Based on matrix transformation, we have:

$$d\{s\} = [D_\tau] d\{e\}, \tag{11}$$

where $[D_\tau]$ – "Regarding" the matrix of elasticity, determined by the following formula:

$$[D_\tau] = [\Omega]^{-1}\left([T(\{s\})][\Lambda]^{-1}[Q]^{-1} - \frac{G}{F(p)}\{s\}\{s\}^T\right)[\Lambda] \tag{12}$$

matrix

$$[\Omega] = [E] - \frac{F'(p)}{2 \cdot F(p)}\{s\}\left\{\tfrac{1}{3} \quad \tfrac{1}{3} \quad \tfrac{1}{3} \quad 0 \quad 0 \quad 0\right\}[Q]^{-1} \tag{13}$$

$[E]$ – identity matrix of order 6.

Using relations (11) - (13) was built incremental scheme for solving the problem, taking into account physical and geometric nonlinearity. For the case of dynamic loading design introduced a combination of the incremental approach with the Newark's method for differential equations. At every new step of the integration is considered a linear problem on the basis of displacements, velocities, accelerations, strains and stresses obtained in the previous step. In this case, translated, taking into account the increments of the displacement coordinates of the nodal points. Accumulated in the finite element strains and stresses are determined in accordance with those found their increments and rotation effect.

II MODEL THE BEHAVIOR OF STRUCTURES DURING THE INTERACTION WITH A CORROSION-ACTIVE MEDIA

The theoretical basis of simulation - a mathematical model of the behavior of structures in contact with corrosion-active media [7], based on the technology of finite element analysis and the phenomenological approach, describing the kinetics of destruction of materials:

$$\begin{cases} [K(x,y)].\{u(x,y)\} = \{Q(x,y)\} \\ \dfrac{dY_i}{dt} = y_i(t,x) \\ S = H(A(t,p),B(t)) \end{cases} \tag{14}$$

where **x = {C, T, P, σ, p, S,...}** — vector, which reflects the conditions of interaction design elements from the goods being carried;

p — function that determines the type of cargo;

Y = {L, Φ_k, R,...} — vector, which reflects the composition of the generalized model, including the factors;

C, T, P — parameters of the cargo, respectively, concentration, temperature and pressure of an aggressive load;

σ — stresses in structural elements of the car, arising from operational loads;

Φ_k — function that determines the nature of the interaction of structural elements with the cargo. Depending on the nature of interaction design with corrosion-active medium can be used to model corrosion deterioration model or the accumulation of rust. As the structural parameters of Φ_k may be taken: the depth of corrosion wear, damage parameter;

L — function to reduce the protective properties of coatings with time;

R — function that determines the condition of occurrence of the limit state;

S — function (profile) life cycle, reflecting the operating modes of the car and modifications to the car due to operational loads and carrying out planned and ongoing repairs;

A(t, p) — vector modes of operation of the car. Due to natural variations of properties of different cars and their operating conditions are indicators of strength in a wide range. Therefore, for coping with the operation of cars and their intensity in the general mathematical model we introduce the function of life cycle. Analysis of processes operating car shows that these processes are time-ordered sequence of typical modes of operation. In some modes, this change is purposeful, the other depends on the conditions;

B(t) — vector, which reflects changes in the structure caused by the action of service loads and carrying out planned and ongoing repairs.

Consider the implementation of the proposed model with regard to the cars of the bunker type used for transportation of fertilizers.

General mathematical model for this case in the operator form can be represented by a set of resolving equations of the finite element method (FEM) (15), the equations of corrosive wear (16), the equations describing the kinetics of changes in the instantaneous strength (17), the equation to reduce the protective properties of coatings (18):

$$\left[\mathbf{K}\right]_{|\Delta t}\left\{\mathbf{u}\right\}=\left\{\mathbf{Q}\right\}_{|\Delta q'} \qquad (15)$$

$$\left\{\frac{\mathbf{d\delta}}{\mathbf{dt}|_{\Delta t}}=\mathbf{f(C,T,\sigma,t)};\quad \delta|_{t=0}=\mathbf{0}\right. \qquad (16)$$

$$\left\{\frac{\mathbf{dR}}{\mathbf{dt}|_{\Delta t}}=\mathbf{f(C,T,\sigma,t)};\quad \sigma_{eq}\le \mathbf{R}|_{\Delta t}\right. \qquad (17)$$

$$\begin{cases}\dfrac{\mathbf{dD}}{\mathbf{dt}|_{\Delta t}}=\mathbf{f(A_{pr}(C,\sigma,T),t)}\\ \mathbf{D}|_{t=0}=\mathbf{0};\ \mathbf{D}|_{t=t_u}=\mathbf{D_k}\end{cases} \qquad (18)$$

where **[K]** - stiffness matrix; **{u}** - a vector of virtual displacements; **{Q}** - a vector attached to the system load; **R** - instantaneous strength; Δt - time step; Δq - step load; δ - the quantity of corrosive wear; σ_{eq} - equivalent stress, defined by the theory of specific potential energy of deformation (hypothesis Huber - Mises - Genk); $A_{pr}(C, \sigma, T)$ - indicators of quality of protective coatings; **D** - indicator of anti-resistance coatings, varying from **1** at time t_0 to D_k at $t = t_u$, where t_u, - a period during which the protective coating properties.

In general, the kinetic equation (17), (18), (19) depend on the concentration of corrosive environment **C**, the temperature **T**, the stress state of the element and the life of the car **t**. The explicit form of these equations is determined separately for each specific task, depending on the design of the car and cargo.

In solving problems of structural strength elements are represented as physically nonlinear systems. The solution is constructed in a nonlinear elastic formulation based on the Newton - Raphson method, based on the steps of the procedure, using a multilinear approximation of the deformation diagrams of the material.

The problem of determining the stress-strain state of elements in corrosive wear is reduced to successive solution of FEM equations (16). Method of calculation involves two steps.

The first stage - the solution of nonlinear problems instantaneous strain with an incremental loading design value Δq of After achieving a given level of loading the transition to the second phase - the integration of corrosive wear.

In the second stage given the time step Δt. According to equation (17) for each structural element is determined by the quantity of corrosive wear δ during the timeΔt. The current value of the residual thickness is reduced by the corrosion wear, and then repeats the solution of nonlinear problems instantaneous strain (step 1) for the stiffness parameters of the new design. Settlement cycle is repeated until as long as the strength condition.

In assessing the durability of structural elements operating under the influence of corrosive media, in general, it is believed that the state of any point of construction is estimated instantaneous strength (18), equal to the voltage required for its destruction in a given time.

Durability of structural elements t define equivalent stresses in$\Delta$is determined as follows: at each time step all the characteristic points of the finite-element design (finite element nodes). Time, after which at least one of the characteristic points of the finite-element model construction of the condition (18), is taken as the durability of the structural element.

The general methodology described by operator equations (17), (18), (19), extends to the design of the surfaces of which have direct contact with the corrosive environment. In assessing the durability of structures with anticorrosive protective coatings in the general method of calculation is additionally introduced a mathematical model of durability of protective coatings in the form of (18). In our model, it is believed that under the protective layer does not arise corrosive wear of the metal to the time during which the protective coating properties. During the period of cover is not going penetration of aggressive media in the layer of protective material.

Method of calculating the durability of structural elements with anticorrosion protective coating consists of two phases:

First step: the equation (18) is determined by the degree of reduction of the protective properties over time. Settlement cycle is repeated until, until the protective properties of the coating. Longevity of Anticorrosive coating assumed to be time saving protective properties.

The second step - the solution to the problem of stress state of elements in corrosive wear of elements of a design by successive sequential decision authorizing the FEM equations (2) and (16) (17).

To assess the durability of protective coatings can be used procedure taking into account the reduction of the protective properties of coatings through the indicators of quality of protective coatings [7]. The value of indicators of quality of protective coatings is the expression.

$$\mathbf{A_{pr} = \sum_{i=1}^{n_\phi} k_i a_i}, \qquad (19)$$

where $\mathbf{n_\phi}$ — number of factors affecting the durability of coatings;

$\mathbf{a_i}$ — a relative assessment of the degree of destruction as a result of the i-th factor;

$\mathbf{k_i}$ — weighting factor accounted for i-th factor.

Assessing the adequacy and accuracy of the proposed method by comparing the results of numerical solutions to the FEM results of bench experiments and data of the known numerical solutions showed that the discrepancy between the results of theoretical and experimental research is not more than **13%** [1].

Based on its review procedure, the estimate life time of the wagon-minerals type Tals (fig.1) (with technical parameters given in Table 1), without corrosion protection of internal and external surfaces.

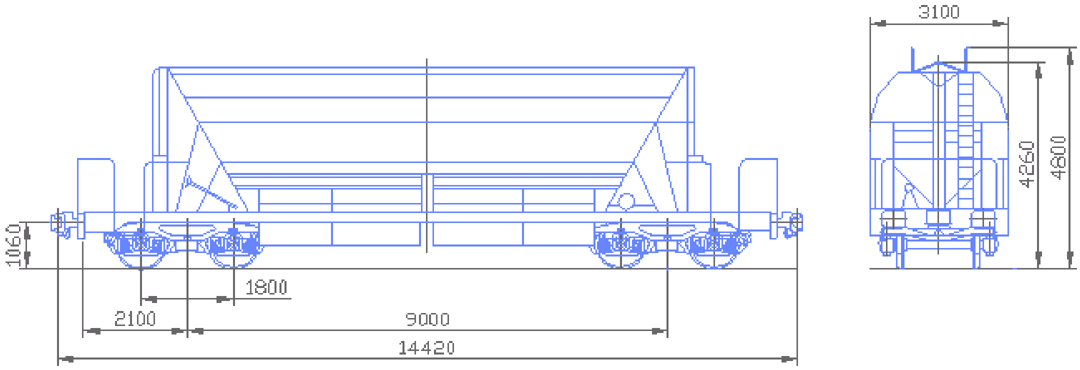

Fig.1. Tals, a wagon with a saddle bottom, designed for the transportation of phosphates, sulfates and other cargo with a particle size of the granules from 0 to 150 mm and specific weight of 1 to 1,6 t/m^3, requiring protection from the weather

To solve the finite element method is used separate problem of mesh on the surface of a geometric model using eight-a finite element type of serendipity - the intermediate nodes on the sides of the finite element (FE). This has increased the size of TBE in the approximation of supporting body elements having small dimensions of the walls.

Table 2 - Technical data of wagon type Tals

Parameters	Values
Gauge UIC 505-1	-
Gauge (mm)	1435
Bogie	Y25Cs (Rsa)
Number of axles	4
Maximum load (tons)	53
Axle load (tons)	20
Tara (tons)	27
Maximum speed (km/h) - Empty - Loaded	 120 100
Distance between bogie pivots (mm)	9000
Cargo volume (m^3)	45

Function of corrosion deterioration of structural elements wagon for transport of mineral fertilizers was presented as a set of dependency types $\mathbf{f = \delta(t)}$.

For each item identified special values $\mathbf{\delta_i(t_0), \delta_i(t_1), \delta_i(t_2), \ldots, \delta_i(t_{eq})}$ at time $\mathbf{t_0, t_1, t_2, \ldots, t_{eq}}$ (where **i** - index denoting the current number of elements in the body structure; $\mathbf{t_{eq}}$ - life coach). As special features of corrosive wear taken a unique dependence of wear elements from time to time, obtained by processing results of field surveys wagons for minerals [2].

Such a representation of the corrosive wear due to the fact that during the operation wagons mineral fertilizer used for the transportation of various fertilizers (phosphate, potash, nitrogen, combined, etc.), different chemical activity with respect to the metal bodywork. In addition, the various elements of the design of the body have different intensity corrosive wear caused by the interaction with the aggressive environment and the impact of operational factors.

In developing the finite element model body a base of leaf idealized structural elements of the wagon for minerals. Using the plate model of the body allowed to take into account structural features of the car Bunker type, the mutual influence of the body and frame design eccentricities in the zones adjacent elements, bizarre skin adherence to the bearing elements of construction. In this case, enter the following idealizations:

- Do not consider rounding in the transition zone from the end wall to the side walls;
- Ignored the effect of loading hatches on the overall stress-strain state;
- Cover discharge gate replaced by a continuous sheet with a stiffness equivalent to the rigidity of the real cover design;
- The pressure load on the covers of unloading the cargo bins transmitted by the body in their places of hinging to the waist;
- The construction of the roof were excluded fillet welding in the area of medium-sheet with the extreme roof sheets.

The introduction of these idealizations, greatly improving the efficiency of the model without prejudice to its adequacy and accuracy of the calculations.

For practical implementation of algorithm for calculating the strength and durability of the car-based Mineral corrosive wear of the vehicle were developed by batch files, data, implementing a step by step solution to the problem of time FEM.

For qualitative assessment of the impact of corrosive wear on the change of stress state of structural elements wagon analyzed the distribution of stress fields at times **t = 0, 4, 8, 12 years**.

The analysis of numerical data strength thin-walled elements showed that the maximum stress level in the cladding sheets observed in the field of welding to the supporting elements of the body shell. The value of equivalent stresses in these zones is **29 - 37%** more than in the middle of the sheet. Growth stresses in sheets of skin in the reinforcements (in the zone of welding of the elements of the frame), caused by corrosive wear, more than in the middle of the sheet. Over **12** years of operation the level of stress at the rack side walls increased by **41%,** while in the mid-span cladding - **28%.**

Calculations show that the lifetime of thin-walled elements of the car body is in the range **8** - **12** years. The biggest impact corrosive wear has on loading skin side walls in the area of welding to the posts and bottom trim. In these cells after **8** years of operation, equivalent stresses exceed the yield stress of the material. The results obtained are confirmed by operational tests [1,2]. So, after a **7 - 9** years of operation, there are irreversible deformation of sheet cladding, and after **11** - **12** years at the planned types of repairs the car make it a full or partial replacement.

The dependences obtained were used to assess the limits of thickness of the vehicle car in operation, which were determined from the kinetic dependence of growth stresses to achieve the strength condition. Limit values of thickness are shown in Table 2.

Table 2 - Maximum allowable values of the thickness and durability of the vehicle

Name of element	Gauge, mm	Life cycle, years
Plating the side walls in the area of welding to the posts and bottom trim	2,4	8
Plating the side walls in the middle of the span	2,3	12
Sheathing end walls	3,2	16
Sheet roofs in the area of welding to the upper trim	1,2	8
The walls of the discharge hopper	3,3	10
Sheets of longitudinal and transverse ridge	3,3	10

Tabular analysis indicates that the appointment of planned repairs should be made on the basis of the technical condition of the car, with the replacement and repair of thin-walled elements.

Evaluation of strength properties of the bearing elements of the frame body showed that the maximum stresses occur at the pivot node frame. This distribution of stress due to the design concept of the cap beams, due to the creation of longitudinal ridge.

The numerical data indicate that an increase in corrosive wear by **20%** leads to an increase in equivalent stresses at **18,5%.** With decreasing cross-sectional area of the cap beam maximum stress in the zone of welding pivot beams are local in nature and form: the design mode III - **274 MPa**; on I design mode - **309 MPa**.

III CONCLUSION

The bearing system is described plate and rod finite elements, an array of granular material - tetrahedral finite elements. To account for the peculiarities of the interaction of cargo from the walls of the car entered the contact finite elements that enable the transmission of normal and tangential forces.

The considered method of proximate analysis of deformations of hopper cars, which is currently being implemented, provides the ability to manage the process of providing high survivability of these facilities in their development and improvement.

The studies found that the carrying capacity of car body-mineral fertilizer on the state of thin-walled elements. According to numerical simulations developed recommendations for the improvement of car bodies, Mineral: increasing the thickness of a last sheet roofs, arches and strengthen cross-ties, as well as interchangeable (operating) items.

X REFERENCES

[1] Atmadzhova D. Specifications for the calculation of rolling bearing with a cage liner. Sofia, XVII NC with international participation of the Higher School Transport, 2007 No: 0151 s.VI-1

[2] Atmadzhova D. Optimization as elements of structures in transport engineering. Sofia, El. journal Mechanics Transportation Communications,1, 2010, № 0469 BG-1.1 - BG-1.12

[3] Atmadzhova D., Some data for calculation of fatigue in probabilistic aspect of railway vehicles. XIV Conference RAILCON‘10 takes place in Niš, Serbia, at the Faculty of Mechanical Engineering on 07 – 08 October, 2010

[4] Bachurin N., Butkin M., VF Lapshin, Smolyaninov, AV. A mathematical model to evaluate strength - T and durability of cars during transport corrosive cargo/rolling stock XXI Century: Ideas, requests, projects: Abstracts of the III International Scientific Conference.2003. — s. 136–138.

[5] Ivanova M., N. Georgiev, Atmadzhova D. Some peculiarities in calculating the basket of wagons for transportation of bulk cargoes. XII NC with international participation "TEMP 2002 of the Higher School of Transport, Sofia, 2002

[6] Georgiev, N. Fundamentals of the theory of reliability, Higher School of Transport 2009

[7] Lapshin V. A mathematical model for calculating carriage structures with corrosion damage/improvement of design, technology and organization of repairs and maintenance of wagons: Intercollegiate. Thematic. Sat Scient. tr./Omsk State. Univ. of communications. - Omsk, 2000 - s. 104-108.

[8] Nowacki, VK Wave problem in the theory of plasticity. - Moscow: Mir, 1978 – 312 s.

[9] Penchev Ts., Atmadzhova D. Strength and durability of automobile and railway equipment, Higher School of Transport, S. 2007

[10] Penchev Ts., Atmadzhova D. For some initial remarks, principles and criteria for determining the safety coefficient of fatigue strength of the transport structures XIX NC with international participation of the Higher School Transport, 2009 No: 0421 s. VI-44

HEAVY MACHINERY - HM 2011, 63-66
ISBN 978-86-82631-58-3
Paper accepted: 30.05.2011

Simulation Modeling of Train Service With Locomotives

Tosho Kachaunov[1,*], Zlatin Trendafilov[1]
[1]Todor Kableshkov, University of Transport, Bulgaria, Sofia

The paper presents the data collected in practice and the probability of train movement by days of the week has been defined. The simulation model has been developed in the Excel medium. Based on the application of the model, the paper shows how to determine the number of locomotives necessary for train traffic to examine and guarantee the robustness of the closed loop.

Keywords: *Simulation, locomotives, trains, adjustment.*

1. INTRODUCTION

To provide trains with locomotives is a main task of railway operation. In the departments of Bulgarian railways this task is implemented in the following sequence:

- Determining the sections and corresponding railway operation, which the particular locomotive shed is responsible for;
- Adoption of determined train traffic schedule, i.e. departure and arrival times exactly determined;
- Biding trains graphically and using it to determine the minimal number of locomotives in working condition;
- The problem whether it is necessary to take into account also the time of planned repairs (routine and capital) is disputable. We consider that with the existing seasonal irregularity of transportation it is possible to make repairs in the periods in decreased intensity without it results in worsening the quality of service.

With applying the way of binding mentioned above, there are substantial problems reported. First, train traffic is not determinable as a great part of trains are not running at certain random moments.

Second, the time of trouble-free operation of locomotives is random, so the number of locomotives in working condition that can participate in biding is also random.

The consideration of those two random factors is a complex problem that cannot be solved with the help of the known and comfortable dependencies of the theory of mass service. That imposes the necessity to use more complex methods such as the simulation modelling.

The principles of solving the problem of serving the train traffic with locomotives are developed in [1].

This paper presents the specific implementation of the simulation model of serving train traffic and its application under the conditions of a locomotive shed and its adjacent sections.

2. MODEL DESCRIPTION

To solve the problem of serving train traffic with locomotives, it is suggested to develop a simplified simulation model connected with the operation of a particular locomotive shed. This model creates a possibility to simulate the train traffic and adjustment of trains with traction rolling stock considering the random factors influencing on the operation of locomotives.

For solving the problem of train traffic service, it is proposed to develop simplified Simulation models related to the work of a particular locomotive depot. This model enables simulation of train movements and train with adjustment with the traction rolling stock, taking into account random factors affecting the performance of locomotives. Thus we can determine the impact of variability of train movements and reliability of traction rolling stock taking into account the number of locomotives actually used in the shed. Performance indicators for locomotives can be defined: the number of used locomotives, burden in work, downtimes, tonne/km work, etc. The discussed approach gives a possibility to forecast/predict the number of locomotives necessary for operation.

The implementation of the model is with the help of a PC using both standard applications (Microsoft Excel) and applications developed additionally at the Department of Technology, Organization and Management of Transport. The simulation model developed has two basic modules. The first one is connected with creation of an input data array. The second one is connected with the interpretation of the input information in an appropriate kind aiming at

*Corr. Author’s Adress: Todor Kableshkov University of Transport, Bulgaria, Sofia, f_tm@vtu.bg

algorithmic realization of adjustment and obtaining the number of locomotives necessary for operation. The input data for the model implementation are entered in a medium of Microsoft Excel using its in-built functions to generate random quantities with preliminarily specified parameters. Part of the information entered is static and refers to the stations in the railway network. This information serves as indicators with the model development and expressing the output data. The bigger information array is connected with the trains and their traffic and can be conditionally divided into two: "general features of trains" and "probability features of trains". The general characteristic of trains - $\mathbf{V^o}$ contains information, which is preliminarily defined and relatively determined:

$$V^0 = f(N_в, D_{дв}, T_{бр}, T_н, S_{\%}, L_{вл}) \qquad (1)$$

where: $N_в$ – the train number, $D_{дв}$ – days of train movement during the week, Тбр/Тн – gross/net tonnage, $S_{\%}$, - the percentage of stopping, $L_{вл}$ –the train length.

The information in the array: "time features of trains" - $V^в$ has a probability nature according to us and can be presented in the following way:

$$V^в = f(N_в, G, t_{пр}, t_з, t_{вп}, t_п, W_T, L_K, t_{Lk}, t_{пз}) \qquad (2)$$

where: G-station, $t_{пр}$-time of arrival, $t_з$-time of departure, $t_{вп}$- travel time, $t_п$-downtimes, W_T-type of traction, L_K-number of locomotives with departure from each station, t_{Lk}-time of arrival of locomotive, $t_{пз}$-time before departure.

With determination of most quantities examined: journey time, time of departure/arrival of trains from/to stations, etc., methods from Probability Theory are applied. For precise determination of downtimes of locomotives at stations: being available, technical inspections, waiting, etc., they are examined separately with their probability features. Some of the parameters used are composite. Using the functions of Microsoft Excel built-in to generate random quantities with preliminarily specified parameters of their distribution and functions for conditions, an array of information is created to determine the "time features of trains" - $V_в$. The general kind for obtaining the main parameters can be presented in the following way:

$$t_к = f(Z_j, PAR_1, .. PAR_i) \qquad (3)$$

where: $t_к$ – monitored time interval of the array $V^в$, Z_j – the kind of the determined law of quantity monitoring, $PARi$ – determined parameters of the law.

It is necessary to note that the parameters used in the model refer to the whole week as in this way the density of train appearance is considered in compliance with the Train Traffic Schedule and due to the irregularities in train traffic. Thus the different load of machines during the days of the week is considered. On that purpose it is suggested to use records in the model – indicators for appearance of trains running during the days of the week that serve to prepare algorithmic interpretation of the model. The results obtained together with the determed input information are interpreted in an appropriate kind to use further in the simulation model [1].

The aim is to present a graph structure expressed by a matrix of links (arrays). The nodes parameters are obtained using the arrays of input information already created and the contingent functions embedded in Microsoft Excel. The graph presents the known problem of scheduling from the Graph Theory as defined. Thus the multitude of apexes is defined by the moments of arrival and departure of each train at and from each station where a locomotive can be transferred (including the intermediate stations) as the apexes/nodes are recorded consequently for all days of the week with availability of a departing train.

The formation of the arcs from the apexes formed of all arriving trains to the apexes formed of all departing trains is based on the weekly train traffic. Here, with the determination of the values $C_{i,j}$, it is proposed to use original conditions taking into account the 7-day 24-hour's operation of locomotives, transfer of the locomotive to the following day during the operation. The results obtained together with the determined input information are interpreted in an appropriate kind for further using.

The second basic module in the model suggested is connected with solving the problem of binding the locomotives with weekly operation. For the solution of this problem it is suggested to use the known algorithm of the Defects of Graph Theory [2, 3].

The solution of the problem is done with the help of software especially developed to solve a problem with employment through the algorithm of defect using the imported interpretation of the graph structure. Thus the downtimes between the operations of locomotives are minimized that is a criterion to determine an optimal variant for binding locomotives.

3. STARTING PREREQUISITES FOR MODEL SIMULATION

The locomotive shed in Plovdiv have been used to implement the simulation model. The shed serves a considerable number of trains using traction RAMENA different in length. The locomotives used for trunk traffic are mainly electric locomotives of series 44, 45 and 46. They are locomotives of one and the same type with comparatively similar features. To simplify the model, a number of admissions connected with the parity of trains served have been assumed as well as omitting (not taking into consideration) of some trains – 6 in number. Their movement is not regular due to the track rehabilitation in the sections and it is not characteristic for the whole operation in the locomotive shed. According to the Train Traffic Schedule for 2010 examined with the assumed simplifications, the number of trains served with electric locomotives is 38 daily as some of the trains are running during different days of the week in compliance with the plan for train formation. To determine the model parameters monitored: times of traveling, times of departures, etc. considerable statistical surveys on train irregularity and changes in the hours of departure and arrival have been made. Special attention has been paid to the determination of reliability of locomotives and its influence on the model. The information about the delayed and left trains dated from 2005-2010 has been collected and processed. Analyzing the train traffic in the locomotive shed in Plovdiv in the period 01.06-31.012.2010, it has been established that about 18% of freight trains included in the Train Traffic Schedule run every day. The trains forming the “basic kernel” of serving, moving at minimum 20 days a month, are about 40% of the total number of scheduled trains. It is noticed that there is a considerable discrepancy between the scheduled and actual times of the departures of freight trains. From the investigations made it has been established that the time of departure has a mean quadratic deviation of 34 minutes. The passenger traffic is considerably regular. Their movement is irregular because of track rehabilitation in the sections of movement and is not typical of the entire work in the shed. According to TTS (Train Traffic Schedule) for 2010 with the simplifications adopted the trains served with electric locomotives are 38 a day, as some trains at different days of the week. To determine the observed parameters in the model – time of journey, departure time and others have made significant statistical studies on train inequality and changes in the times of departure of trains. Particular attention was paid to determining the reliability of the traction rolling stock and its influence in the model. The processed information was about the trains delayed and left from 2005-2010. In analyzing the movement of trains in depot Plovdiv for the period 01.06-31.12.2010 is found that about 18% of freight trains included in the Train Traffic Schedule run daily. Trains, which form the "core" of services - moving at least 20 days of the month are about 40% of the total number of scheduled trains. There is considerable discrepancy between planned and actual departure time of freight trains. From research done it is found that the time of departure is mean square deviation of 34 minutes. Passenger traffic has substantially regularly.

The trains removed and included in the schedule are about 1% related to the passenger traffic and to make it easier; it can be assumed that the flow of passenger trains is determined. With the analysis of train traffic it is noticed that the percentage of trains delayed and left due to reasons in locomotive fleet is increasing. For the locomotive shed in Plovdiv, in 2010 1% of the total number of trains is of such a type. The number of trains left is also increasing; they form 60% of faults during the time of running as for the last five years the increase has been by about 10% a year. The study on the reliability of the traction rolling stock is considerably detailed as failures have been determined in the main units of electric locomotives. A summarized index is presented: the coefficient of availability ***Kг***. The tendency noticed is that its value has been decreasing for the past years as in 2010 it is about 0,76 for the three types of electric locomotives. Similar studies have been done also in other locomotive sheds and the results are similar for electric locomotives. The data for ***Kг*** as well as the analysis of the period of electric locomotives operation have shown that about 1/3 of the time when the locomotives are operated passes in non-operation state. The decrease of ***Kг*** in the last yeas could be due both to significant aging and wear-out of the locomotive fleet and the quality of repairs.

The obtained results related to the laws of distribution of quantities examined with locomotives do not give us a reason to state that the values can be approximated with known theoretical distributions. For the needs of the simulation model the probability of trouble-free operation of electric locomotives has been assumed as exponential that is usually suggested in references. [3]

4. RESUCTS AND CONCLUSIONS FROM THE MODEL IMPLEMENTATION

The multiple implementation of the locomotive adjustment task with considering the frequency of train appearance during the days of the week for a period of 8 weeks with constant and variable parameters under monitoring has lead to results near to the real operation conditions. The mean number of locomotives for operation (by the turnover during the whole period of the model) in the locomotive shed examined is 12 electric locomotives.

According to the simulation model it is most frequent to use 9 locomotives during the 17-day period examined. The minimal and maximal numbers of locomotives necessary is 7 and 18 respectively being necessary for a day in this period. These boundary values are determined by the prolonged journey time of some trains and dropping of some freight trains from the daily operation schedule. Comparing the indicators of operation in the model variant with determined parameters, the necessary the necessary number of electric locomotives number of electric locomotives is 14. The increased number of locomotives in this variant is due to the fact that the planned Train Traffic Schedule is used.

It is supposed that all scheduled trains will run. Due to the different number of trains in the variants for assessment, relative loading of trains with running has been used. With using 12 locomotives, their load while running is 11 hours a day. With 14 locomotives they are employed with running average about 10 hours a day. Even with the minimal number of locomotives – 18, the load is about 9 hours of running. It can be supposed that the number of locomotives depends mainly on the probability of a train available in Train Traffic Schedule but not as much as on the irregularities connecter with the journey times and failure during the time of running. The recommendation is to make the times of departure more precise, especially of freight trains on the purpose to provide a better inscription of the locomotive adjustment with dropping of scheduled trains.

Analyzing the downtimes for waiting the adjustment of trains, it is observed that the difference between the variant using 13 locomotives and the variant with determined parameters is minimal: 10.8 hours. It is interesting to note that with using a bigger number of locomotives (with the variant with the maximum number), the difference in the hours of downtime while waiting for adjustment increases to about 60 hours. Due to the limitation of the paper length, the details in results and their analysis will not be examined.

We consider that the approach examined above gives a possibility to estimate/forcast the number of locomotives necessary for operation and take into account train traffic irregularities. The model is suitable for implementation by computers and, besides for planning of the locomotive fleet, could be appropriate for operational management of train traffic and locomotive dispetching.

REFERENCES

[1] Kachaunov T., Trendafilov Z., “A New Approach with Adjustment of Trains with Locomotives”, 12 International Scientific Conference TRANSPORT 2002.

[2] Philips D., A. Garcia-Dias A., ”Methods of Network Analysis”, MIR, Moscow, 1984.

[3] Dimitrov Zh., “Reliability of Railway Equipment”, TU-Sofia, 1989.

B SESSION

EARTH-MOVING AND TRANSPORTATION MACHINERY

HEAVY MACHINERY - HM 2011, 1-4 Paper accepted: 20.05.2011
ISBN 978-86-82631-58-3

Design of New Structures of Vibro-Shocking Building Machines by Internal Characteristics of Oscillating System

Nazarenko I.I.[1,*], Sviderski A.T.[1], Dedov O.P[1]
[1] National University of Civil Engineering and Architecture, Kiev

One of the methods to increase the efficiency and to decrease the energy consumption and the quantity of installed vibro-machine material is to apply a systematic approach when introducing new structural design based on analyzing common motion of the machine and machining surroundings. The approach involves internal characteristics of the subsystem along with sub resonant, super resonant and resonant operating regimes.

The paper shows theoretical basis for production of vibrator of volumetric action with high performances of energy and material efficiency for various conditions for making the concrete and products made of concrete, by means of creation and control of the changes into internal properties (elastic, inertial and dissipative) of the system ''machine-surroundings'' in the regime which is similar to the regime of free oscillations.

The theory of interaction between operating members of vibrator and machining surroundings is suggested. The interaction is based on the estimation of stress state in the contacting zone. Thus the influence of machining surroundings on dynamics of operating machine elements can be determined.

The methods suggested to manufacture the vibrator of volumetric action have high efficiency indicators related to energy and material consumption.

Keywords: vibration systems, vibro-bending, discrete continuum model, contacting force, higher harmonics, efficiency of vibrating machines

Vibrating building machines are applied for different technological processes. The most prominent machines are the ones used for compression of building mixtures when making concrete and reinforced concrete, and for tamping the ground when building the roads. The main purpose of vibrating machines is to precisely provide defined technological parameters influencing the amplitude and frequency of oscillation. Therefore, process engineers' efforts are directed to establishing the change of boundaries of these parameters while design engineers' efforts are directed to developing the calculation method.

The authors of the paper suggest that efficiency of machines should be increased by means of new ideas, such as developing and producing the machines which oscillate along with the centre of gravity according to previously defined regime. This regime efficiently enables the application of internal oscillating characteristics of machines and operating surroundings as a unique vibrating system.

In order to realize the idea the chief result involves the application of the mathematical models for machines and operating surroundings which reflect the real process and also contain exactly the properties which can be controlled.

Such a model is discrete continuum model (analysed in [1,2]) in which the machine is presented as discrete, while the operating material is presented as continuous quantity. According to the theory oscillations [3] the motion of dynamic systems consists of free and forced oscillations with estimated proportion of influence of elastic inertial characteristics and dissipative characteristics. If this phenomenon is regarded as the most crucial one, it is necessary to make the interaction between the machine and operating surroundings. The interaction reflects the above mentioned properties, which enables the proper control.

Thus the surroundings included in the equation of motion of operating element of vibrator involve the contacting forces (fig. 1) which are called the reactions of the surroundings [1]. The equation of motion is:

$$\frac{\partial^2 u\ (z,\ t)}{\partial\ z^2} = \frac{\rho^*(z,\ t)}{E^*\ (z,\ t)} \cdot \frac{\partial^2 u\ (z,\ t)}{\partial t^2} \tag{1}$$

*Corr. Author's Address: Nazarenko I.I.National University of Civil Engineering and Architecture, Kiev, i_nazar@i.ua

where *u (z, t)* is longitudinal motion of surface of the column of the surroundings being machined during oscillations. The motion depends on the position of section (coordinate Z) and on the time t ;

$\rho^*(z,\ t)$ - density of the surroundings;

$E^*(z,t)$ - complex elastic modulus

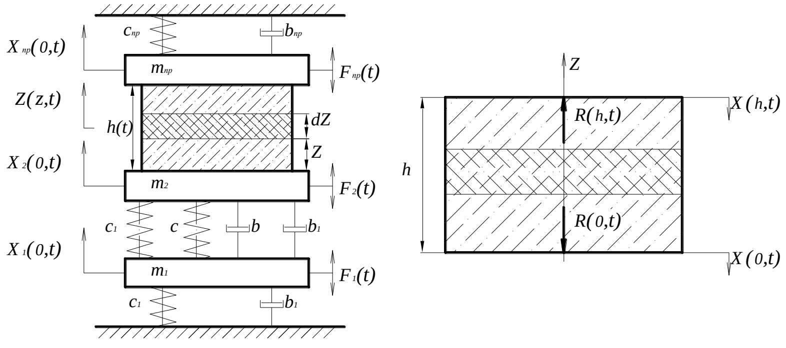

a) б)

Fig. 1. Calculation model: a) general model; b) reduced model

The law of surroundings deformation when loaded is:

$$\sigma = E^*\varepsilon = \left(E' + iE''\right)\varepsilon \tag{2}$$

where E', E'' are the elements of complex modulus of elasticity;

i - imaginary unit, which implies the motion $\pi/2$ between E' and E'';

ε - deformation of a part of surroundings.

If the general law of force action is adopted:

$$F(t) = \sum_{n=-\infty}^{+\infty} F_n e^{in\omega t} \tag{3}$$

where

$\omega = 2\pi/T;\ n = \pm 1;\ \pm 2;\ F_n = F_n^* = \int_{-\tau/2}^{\tau/2} F(\tau) e^{-in\omega t} d\tau$,

then the solution of the equation, in compliance with Fourier's method, can be represented as the following function:

$$U(z,t) = \sum_{n=-\infty}^{+\infty}\left(U_{1n}e^{k_n z} + U_{2n}e^{-k_n z}\right)e^{in\omega t} \tag{4}$$

The motion U is obtained by multiplying two functions; one of them depends on the argument $z(z) = U_1 e^{nk_n z} - U_2 e^{-nk_n z}$, whereas the other one depends only on the argument $T_n(t) = e^{in\omega t}$. U_{1n} and constants included in the function (4) are determined from boundary conditions, k_n - complex number, $k_n = \left(\alpha_n + i\beta_n\right)$, where α_n, β_n - coefficients, obtained when function (4) is put into equation (1):

$$\alpha_n = \frac{\omega_n}{c_в}\sqrt{\frac{\sqrt{1+\gamma^2}-1}{2\left(1+\gamma^2\right)}};\ \beta_n = \frac{\omega_n}{c_в}\sqrt{\frac{\sqrt{1+\gamma^2}+1}{2\left(1+\gamma^2\right)}}; \tag{5}$$

When transformation (5) is done, the complex modulus of elasticity is regarded as:

$$E^* = E\left(1 + i\gamma\right) \tag{6}$$

where E - expression for modulus;

γ - coefficient of losses.

To obtain the relation (6) the following equation is used:

$$\left(\alpha_n + i\beta_n\right)^2 = -n^2\omega^2 \Big/ \left[c_в^2\left(1 + i\gamma\right)\right] \tag{7}$$

where $c_в$ (5, 7) represents the speed of wave propagation in the column of the surroundings being machined.

In the case of indefinite surroundings in z direction, U_{2n} tends to zero, so the function (4) transforms into the following form:

$$U(z;t) = \sum_{n=-\infty}^{+\infty} U_{1n} e^{k_n z} e^{in\omega t} \tag{8}$$

Reactions of the surroundings to oscillations of operating element are obtained by solving the problem according to boundary conditions (fig. 1):

$$R(0,t) = \frac{m\omega^2}{h}\left[\sum_{n=-\infty}^{+\infty} \frac{x_n th\left[h(\alpha_n + i\beta_n)\right]}{(\alpha_n + i\beta_n)} n^2 e^{in\omega t}\right] \quad (9)$$

where:

$$a_{1n} = \frac{\alpha_n sh2\alpha_n h + \beta_n \sin 2\beta_n h}{h\left(\alpha_n^2 + \beta_n^2\right)\cdot\left[ch2\alpha_n h + \cos 2\beta_n h\right]} \quad (10)$$

$$d_{1n} = \frac{\alpha_n \sin 2\beta_n h - \beta_n sh2\alpha_n h}{h\left(\alpha_n^2 + \beta_n^2\right)\cdot\left[ch2\alpha_n h + \cos 2\beta_n h\right]} \quad (11)$$

Expression (9) transforms into the form:

$$R(0,t) = m_c x_1 \omega^2 \sqrt{a_1^2 + d_1^2} \quad (12)$$

i.e. if compared to the vibrations of vibro-machine having the amplitude x_0, the reaction of the surroundings is the oscillation having the following amplitude: $R \to m_c \omega^2 x_1 \sqrt{a_1^2 + d_1^2}$

For $n = \pm 1; \pm 2; \ldots$;the modulus of reaction is:

$$\left|R(0,t)\right| = \left|\sum_{n=-\infty}^{+\infty} x_n e^{in\omega t} n^2 \omega^2 m_c \left(a_n + i d_n\right)\right|. \quad (13)$$

Each spectral component of the vibration of vibro-machine gets its own ''supplement'' $x_n \to x_n n^2 m_c \omega^3 \left(a_n + i d_n\right)$.

Generally speaking, the reaction considering the phase change is:

$$R(0,t) = \sum_{n=-\infty}^{+\infty} x_n m_c \omega^2 n^2 \sqrt{a_n^2 + d_n^2} \cdot e^{iarctg\frac{d_n}{a_n}} \cdot e^{in\omega t} \quad (14)$$

Dependence (14) is represented within common motion with operating elements through two wave coefficients; one coefficient (a) identifies elastic and inertial characteristics of operating surroundings, while the other characteristics (d) identifies the dissipative characteristics.

Hence, if the machine parameters are chosen in such a manner that reactive and active components of machine resistance are compatible with active and reactive components of operating surroundings, then a new generation of machines may be developed. The essence of this perspective can be formulated in terms of suggested principles which result in:

1. Characteristics and parameters presenting the machine and operating surroundings are modelled by equations of motion of one oscillating system having the dynamic properties. This principle ensures the motion of the machines for vibro-compression in previously defined operating regime.
2. Maximum energy concentration of operating element for calculating higher harmonics. Technological energy efficiency of higher harmonics is obtained by defined application of shocks and vibrations (fig. 2), which is done by additional oscillation boundaries and appropriate rigidities, and by selection of rational dependence between shock time and oscillation period.
3. Realization of technological feasibility of acceleration asymmetry. This principle provides the acceleration which is important for asymmetry of operating element of vibro-shocking system.
4. Synchronous formation of polyphase auto oscillatory regimes. These regimes are realized by applied shocks in phases or by applied dynamic systems with independent blockade of oscillating shocker.
5. Implementation of dynamic control of the system, based on the application of internal characteristics of the system, is provided by hydraulic actuator for vibro-shocking frog (fig. 3).

Conlusions

The analytical model suggested to identify the influences of operating surroundings on dynamics of operating elements of vibro-shocking machines is based on the analysis of stress state in the contacting zone of surroundings.

The principles are formed to produce the new vibrator with highly efficient performances of operating process.

The theory analysed in the paper enables creation of the machines which operate under sub resonant, super resonant and resonant operating regimes. These machines contribute to the evaluation of higher harmonics thus intensifying the operating process itself.

These machines have low energy consumption, low material consumption and improved performances.

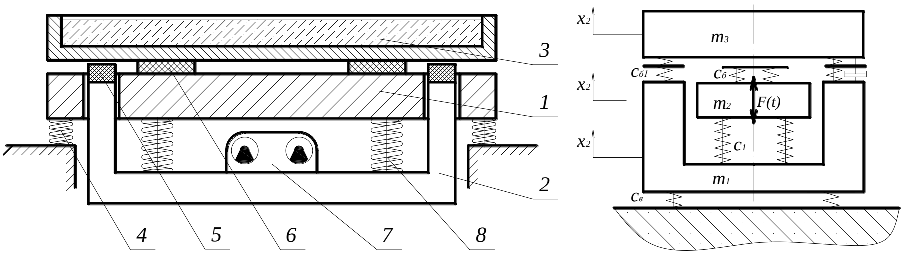

а) б)

Fig. 2. Vibro-shocking plate: a) constructive scheme; b) calculating scheme
1 – frame, 2 – shocker, 3 – mixture, 4 – vibro-isolating absorbers, 5 – buffer, 6 – extra buffer, 7 – vibrator.

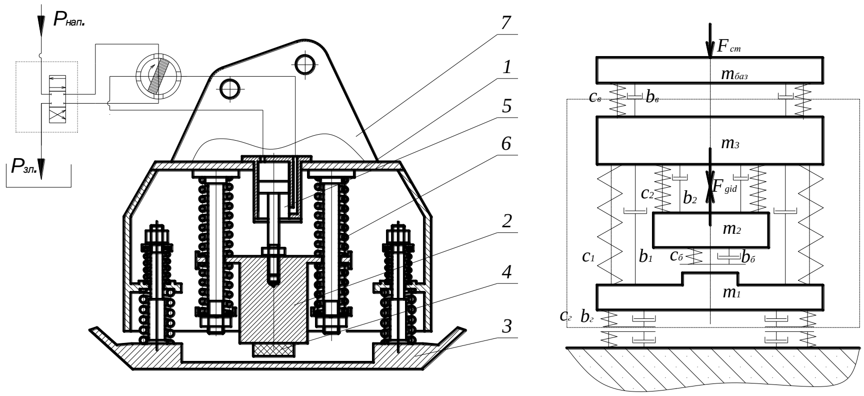

а) б)

Fig. 3. Hydraulic vibro-shocking frog: a) constructive scheme; b) calculating scheme
1 – housing, 2 – shocker, 3 – contacting plate, 4 – buffer, 5 – hydraulic vibrator, 6 – elastic elements, 7 – mounting device.

Литература:

1. Назаренко І.І. Прикладні задачі теорії вібраційних систем (2-е видання) / Назаренко І.І. – К.: Видавничий Дім “Слово”. 2010. – 440 с.

2. Назаренко І.І. Вібраційні машини і процеси будівельної індустрії / Назаренко І.І. – К.:КНУБА, 2007. – 203 с.

3. Дж.П Ден-Гартог. Механические колебания. Пер. с IV амер.изд./ Дж.П Ден-Гартог. – М.: Физматгиз, 1960. – 193с.

4. Свідерський А.Т. Вивчення та впровадження сучасних гідравлічних вібраційних систем у виробничий процес – шлях до створення універсальних самоадаптованих високопродуктивних віброущільнювачів // Техніка будівництва, – 2004. – № 13 – С. 66-70.

Дєдов О.П. Математична модель та визначення параметрів руху вібротрамбовки для ущільнення ґрунтів // Гірничі, будівельні, дорожні та меліоративні машини, – 2006. – Вип.66,–С.41-46.

HEAVY MACHINERY - HM 2011, 5-10
ISBN 978-86-82631-58-3
Paper accepted: 20.05.2011

Efficiency of Double-Piston Pumps For Concrete Applied To Bulky Concrete Mixtures At The Building Sites

Емельянова И.А.[1], Задорожный А.А.[1], Непорожнев А.С.[1], Гузенко С.А.[1]
[1]Харьковский государственный технический университет строительства и архитектуры, Харьков, Украина

The paper considers the characteristics of existing double-piston concrete pumps. The pumps are used in technological schemes for bulky concrete mixtures at the building sites. The costs of energy expenditure was analysed for the process of transportation of bulky concrete mixture by means of pneumatic installation. Also the relation for identification of efficiency coefficient of the plant was determined.

Keywords: concrete pump, bulky concrete, pneumatic transportation, coefficient of efficiency.

Double-piston concrete pumps, whose basic scheme is shown in figure 1, were presented at the fifth international conference Heavy Machinery HM 2005 in Kraljevo [1].

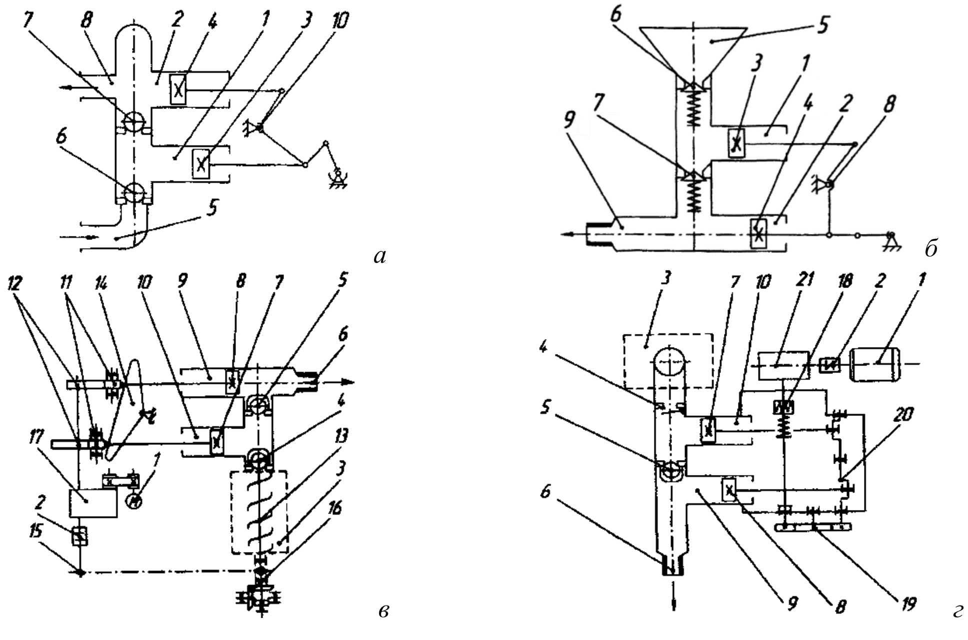

Fig. 1. Double-piston concrete pumps
a - counterflow and ball switch, b - rectilinear flow and elastic ball switch, c - rectilinear flow and horizontal arrangement of cylinders and forced load, d - rectilinear flow and horizontal arrangement of cylinders and switches with lock washers

All these concrete pumps were tested at the building sites when fine concrete mixtures were used. The concrete pumps presented in figs 1c and 1d have special significance.

*Corr. Author's Address: Харьковский государственный технический университет строительства и архитектуры, ул. Сумская 40, Харьков, 61002 Украина, office@kstuca.kharkov.ua

There is no crank bar mechanism and appropriate cam profiles (fig. 1c), so this type of double-piston pumps provide small impulsive slow mixture (P=4…5 cm).

Technical characteristics of double-piston concrete pump with forced loading

Capacity, m^3/h	3.6
Operating pressure, MPa	4
Horizontal transportation distance, m	100
Vertical transportation distance, m	20
Maximum size of concrete particles, mm	10
Diameter of operating piston, mm	110
Diameter of compensating piston, mm	110
Stroke of operating piston, mm	140
Stroke of compensating piston, mm	70
Length, mm	1650
Width, mm	1530
Height, mm	1250
Electromotor power, kW	5.5
Diameter of rubber rings, mm	50
Mass, kg	340
Pressure, MPa	1.3
Minimum mobility of the mixture, cm	4

The exploitation of concrete pumps with elastic ball and cone switches showed that, when there was no forced loading, the switches were not always reliable when concrete mixture came from receiving box. Therefore, double-piston concrete pump having the switch with discs (fig. 1d) was designed, manufactured and tested. Installation of suction spring switch with disc is enabled during the suction of the operating piston when it transmits a huge amount of concrete mixture due to increased area of cross section formed by the clearance between the basic valve and the port in the pump casing. Apart from that, during the process of emptying the concrete mixture into the compensating chamber, the pressure acts on the switch disc which results in its fast closing and decrease of the flow of concrete mixture into the receiving box. The second characteristic of this type of concrete pump is the presence of axial joint disc of operating and compensating pistons, which provides decrease of sealing wear and journal when the pistons go through the cylinder.

Technical characteristics of concrete pump with horizontal rectilinear motion of cylinders and switches with lock washers.

Capacity, m^3/h	4 – 4.5
Operating pressure, MPa	3.8 – 4.0
Frequency of piston motion, min^{-1}	58
Horizontal transportation distance, m	200
Vertical transportation distance, m	70
Electromotor power, kW	5.5
Length, m	1480
Width, m	810
Height, m	930
Mass (without pipes), kg	500

The transportation of bulky concrete mixture at the building sites is very important if, for these purposes, small-sized equipment is used instead of massive concrete auto pumps.

During building, repairing work and reconstruction work it is often necessary to transport and store the bulky concrete mixture (maximum size of concrete particles is d_{max}=20mm) of small volumes to the heavily accessible places. It can be successfully done by small-sized equipment is simply improved. Apart from transportation of concrete mixture, such equipment can be applied to concreting by jet or by jerking by using ring nozzle [2].

In addition to small-sized equipment for bulky concrete mixture with double-piston concrete pump it was suggested to apply pneumatic installations equipped with cellular doser (technological scheme is presented in fig. 2). Such a scheme enables a series of operations: transportation of various mixtures, jet-concreting and jerk-concreting.

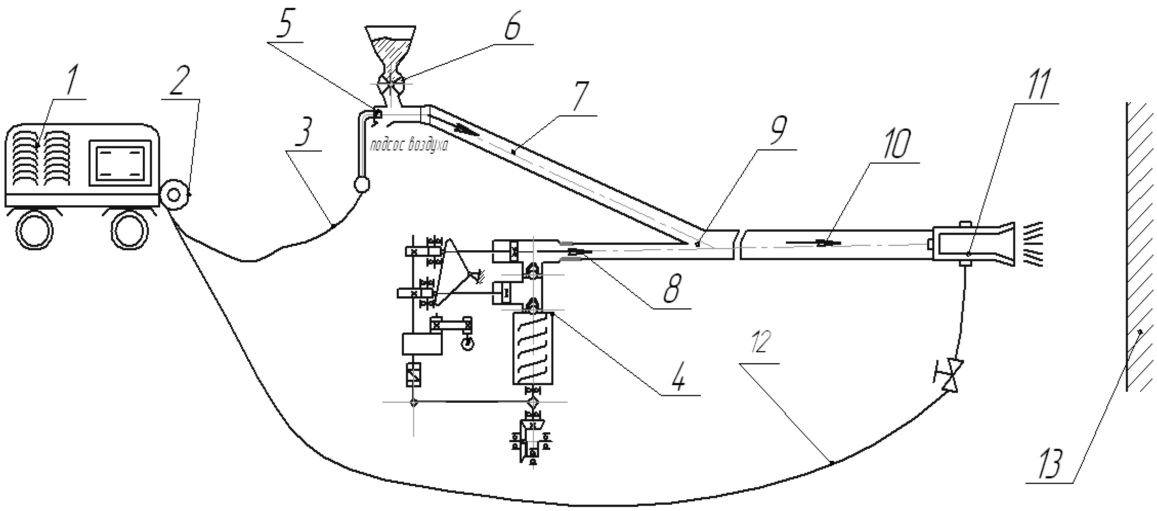

Fig. 2. Technological scheme of jet-*concreting (jerk-concreting) when fine (bulky) concrete mixtures are applied*

1 – mobile compression installation, 2 – compressor receiver, 3 – pipe transporting compressed air, 4 – double-piston concrete pump with forced filling of concrete mixture, 5 – pneumatic installation, 6 – cellular doser, 7 – pipeline transporting bulky mixture, 8 – pipeline transporting fine mixture, 9 – mixing chamber, 10 - main pipeline for transmission of bulky concrete mixture (air-concrete) towards the nozzle, 11 – jerking nozzle, 12 – pipeline for transportation of compressed air, 13 –area being jerked

The simplified technological scheme can include any double-piston concrete pump presented in fig. 1. In this case, the concrete pump with cam drive and forced loading is shown (1c).

Technical characteristics of small-sized equipment with bulky mixture

Capacity, m^3/h	4
Operating pressure of compressor installation, MPa	0.8
Diameter of operating piston, mm:	90
Diameter of compensation piston, mm:	90
Pressure obtained by spiral transmission	1.3
Maximum size of concrete particles, mm	20
Maximum operating pressure, MPa	2…3
Minimum mobility of the lifting mixture, cm	4
Electromotor power, kW	5.5
Diameter of journal, mm	50
Mass, kg	400

Technological scheme (figure 2) functions like is: fine concrete mixture is transported by concrete pump 4 into the mixing chamber 9. Bulky concrete particles are added by compressed air 5 and cellular doser 6. Concrete mixture is transported through the main pipeline 10.

Small-sized equipment may be applied thanks to pneumatic transportation installation in the technological scheme presented in fig. 3.

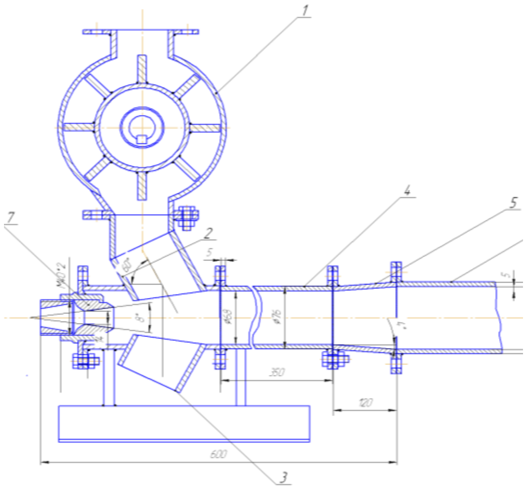

Fig. 3. Pneumatic installation with cellular doser 1 – cellular doser, 2 – output, 3 – pipes sucking the surrounding air, 4 – mixing chamber, 5 – diffuser, 6 – transportation pipeline, 7 – ejector (De Laval nozzle)

The pneumatic installation operates like this: compressed air is transmitted to De Laval nozzle 7 from mobile compression installation. Larger particles of pebbles (10 …20mm) come from cellular doser 1 to the output 2. Mixing of air and concrete particles is done in the chamber 4. The sucking effect enables the decrease of air flow from compression installation which is necessary to transport the mixture of air and concrete.

The coefficient of efficiency of pneumatic installation can be identified by analyzing the energy expenditure in some phases of mixture loading towards the nozzle [3]. Therefore the structural scheme of jet concreting (jerk concreting) (figure 3) should be analysed.

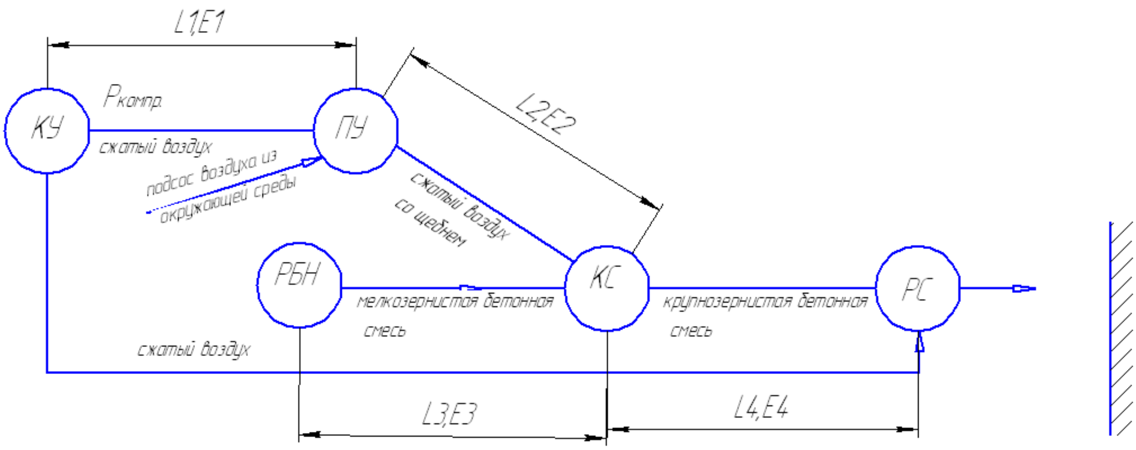

Fig. 3. Structural scheme of jet concreting (jerk concreting) applied to small-sized equipment

КУ – mobile compression installation, ПУ – pneumatic installation, РБН – concrete pump, КС – mixing chamber, РС – nozzle, L1 – distance between compression installation and ejector, L2 – distance between doser and mixing chamber, L3 – distance between concrete pump and mixing chamber, L4 – distance between mixing chamber and nozzle

The coefficient of efficiency of pneumatic installation is:

$$\eta_{пневм.уст.} \quad \frac{E_{пол.}}{E_{затр.}} = \frac{{}^{1}/_{L}(E_1 L_1 + E_2 L_2 + E_3 L_3)}{{}^{1}/_{L}\left(\sum \frac{E_i L_i}{\eta_{прив.}} - E_{подс.} L_{намр.}\right)}$$

, (1)

Where $E_{пол.}$ is energy expended for transport of bulky mixture of air and concrete; $E_{затр.}$ –energy expended in the process of transport of bulky concrete mixture at the length L; E_1- energy expended for supplying the pneumatic installation by compressed air (ПУ) from compression unit (КУ); E_2- energy expended for transportation of pebble to the mixing chamber (ПУ); E_3- energy expended for transport of fine concrete mixture from the concrete pump (РБН) to the mixing chamber; L_1, L_2, L_3 –segments of distance travelled; L –

total length of main transportation pipeline, $\sum E_i L_i$ – total energy expended in transportation of bulky mixture of air and concrete;

$$Å_{çàòð.} = \sum Å_з L_з = \begin{bmatrix} Å_1 L_1 + Å_2 L_2 + Å_3 L_3 + \\ + (Å_4 + Å_5 + Å_6) L_4 \end{bmatrix} + \\ + Å_{ÏÈÒ.} \qquad (2)$$

Where E_4- energy expended for transportation of bulky mixture of air and concrete; E_5- energy expended for overcome the forces of internal friction of the mixture; E_6- energy expended for mixing the components of bulky concrete mixture from the mixing chamber to the nozzle; $E_{пит.}$ – energy expended for the work of cellular doser; L_4 – distance travelled by bulky concrete mixture from mixing chamber to the nozzle;

$E_{подс.}$ – energy of sucking the surrounding air into the main transportation pipeline; $L_{намр}$ - length of pipes through which the air goes out;

$\eta_{прив.}$ – efficiency coefficient of drive of elements of small-sized equipment;

$$\eta_{прив.} = \eta_{ку} \cdot \eta_{рбн} \cdot \eta_{пит.} \qquad (3)$$

Where $\eta_{ку}$ - efficiency coefficient of compression installation;;

$\eta_{рбн}$ - efficiency coefficient of concrete mixer;

$\eta_{пит.}$ - efficiency coefficient of doser;

The components of energy expenditure, which are presented in the numerator of expression (1), are determined according to the formulas below.

In each real case, the energy loss is analysed and it is reduced to the unit of transportation length.

$$E_1 = \left[\left(P_в + \frac{\rho v_b^2}{2}\right) v_в \left(S_в - \frac{\pi d^2}{2}\right)\right], \qquad (4)$$

Where $P_в$- air pressure in the pipeline (L_1) before entering the mixing chamber; ρ - air density for the pressure $P_в$; $v_в$- air velocity in the pipeline (L_1); $S_в$- area of the inlet port of the mixing chamber; d - diameter of the concrete particles;

$$E_2 = \frac{M_щ^* v_щ^2}{2} = \frac{M_щ^*}{2}\left[\frac{M_{щ(3-2)}^*}{\pi d^2 \rho_щ} \kappa_1\right]^2, \qquad (5)$$

where, $M_щ^*$ - mass of pebble entering the mixing chamber in 1 second; $M_{щ(3-2)}^*$ - mass of two or three concrete particles entering the mixing chamber in 1 second ; $v_щ$ - velocity of pebble in pneumatic transportation pipeline; $\rho_щ$ - average density of pebble; κ_1 - coefficient for correction of pebble volume if it is not ball-shaped (к<1);

$$E_3 = \frac{M_{мбс}^* v_{мбс}^2}{2}, \qquad (6)$$

where, $M_{мбс}^*$ - mass of fine concrete mixture entering the mixing chamber in 1 second; $v_{мбс}$-velocity of fine concrete mixture entering the mixing chamber;

$$E_4 = \frac{M_{вбс}^* v_{ср}^2}{2} = \left[v_в\left(S_в - \frac{\pi d^2}{2}\right) + \frac{M_{бс}^*}{\rho_{бс}}\right] \cdot \Bigg| \cdot$$

$$\cdot \left[v_в\left(S_{1mp} - \frac{\pi d^2}{2}\right) + \frac{M_щ^*}{\rho_щ} + \frac{M_{мбс}^*}{\rho_{мбс}}\right]^2 /2 \qquad (7)$$

where, $M_{вбс}^*$ - mass of the mixture of air and concrete being transported in 1 second;

- mass of bulky concrete mixture being transported into cellular doser in 1 second; $\rho_{бс}$ - average density of bulky concrete mixture; $\rho_{мбс}$ - average density of fine concrete mixture; S_{1mp}- area of cross section of pipeline elements; L_4 - distance travelled by bulky concrete mixture; $v_{ср}$ - average velocity of mixture moving through the pipeline;

$$E_5 = \frac{2.133 \cdot \mu \cdot v_{ср}}{Д_{1mp}} \cdot Q, \qquad (8)$$

where μ - dynamic viscosity of bulky concrete mixture; $Д_{1\,тр.}$ – diameter of pipeline at the section

$$E_6 = \kappa_2 \frac{(M_щ^* + M_{бс}^*) \cdot v_{ср}^2}{2}, \qquad (9)$$

где је: κ_2 – коефициент, који обухвата губитак енергије у процесу транспорта ситнозрнасте бетонске смеше са крупним пуњењем (шљунком); $E_{пит.}$- енергија, утрошена за рад ћелијског додавача.

$$E_{пит.} = \frac{M_{щ} \upsilon_{щ}^2}{2}, \qquad (10)$$

where: κ_2 – coefficient which includes the energy loss in the process of transporting fine concrete mixture with bulky load (pebble); $E_{пит.}$ - energy expended for work of cellular doser.

where: $M_{щ}$ – mass of pebble loaded through cellular doser; $\upsilon_{щ}$ – velocity of pebble entering the doser.

The experimental tests confirmed that the presence of air sucked from surroundings may decrease the need for consumption of compressed air to 20%, which has a positive influence on the coefficient of efficiency of pneumatic installation. This equipment was used for rebuilding the Harkov airport (fig. 4).

Fig. 4. Small-sized equipment with pneumatic installation

Conclusions

It has been proved that small-sized double-piston concrete pumps may be applied to bulky mixture s

Coefficient of efficiency of pneumatic installation was identified on the basis of analysis of energy expenditure

References

1. Емельянова И.А., Баранов А.Н., Задорожный А.А., Грачев Ф.А. пути совершенствования малогабаритного оборудования для условий строительной площадки.// Материалы V – ой международной конференции «Heavy Machinery HM 05» Кральево, 2005 – С. 1А13 – 1А16.

2. І.А. Ємельянова. Малогабаритне обладнання для умов виконання торкрет робіт і транспортування будівельних сумішей в умовах будівельного майданчика – ФО – Рибалко Д.Л., 2009 – 84 с.

3. Емельянова И.А., Гузенко С.А., Непорожнев А.С. определение коэффициента поленого действия пневмотранспортной установки при работе малогабаритного оборудования на крупнозернистой бетонной смеси в условиях строительной площадки // Науковий вісник будівництва. Харків: ХДТУБА, Вип. 57 – С. 448 – 452.

HEAVY MACHINERY - HM 2011, 11-14 20.05.2011
ISBN 978-86-82631-58-3

Analysis of the Operation of Concrete Mixer With Gravitational And Forced Action

Емельянова Инга Анатольевна[1], Блажко Владимир Владимирович[1],
Анищенко Анна Игоревна[1,*], Доброходова Ольга Валериевна[1]
[1]Харьковский государственный технический университет строительства и архитектуры

The paper gives general information on the concrete mixer which has gravitational and forced action. Physical and mathematical model of particles of concrete mixture moving along the mixer vanes has been set with regard to friction coefficient. Optimal angles of vane inclination have been defined in terms of horizontal axis.
There is a table containing proposed angles of vane inclination depending on the friction coefficients and values which depend on mobility of concrete mixture. The mixture particles move over the mixer vanes in the mixing process..
Keywords: concrete mixer, vanes, friction coefficient, concrete mixture, particle

In the building industry it is always tempting to produce the equipment for concrete manufacture which at the same time provides high level of homogeneity.

As already presented in various tests this function is successfully done by the mixers operating at cascade regime. Triaxled mixer used for producing slow concrete mixture [1,2] was presented at the Sixth International Triennial Conference "Heavy Machinery HM 2008". As already mentioned, the advantage of these machines is their operation in cascade regime, i.e. the components of the mixture which are thrown into the machine drum have tricontour motion, which significantly intensifies the mixing process thus creating the conditions for obtaining homogenous mixture. After that, some machine structures were simplified by means of advantages of mixer cascade regime, and a new mixer was made which combined gravitational and forced mixing methods (fig. 1) [3].

Technical characteristics of concrete mixer with gravitational and forced mixing

Technical capacity, m^3/h	10
Coefficient of volumetric loading	0,6…0,65
Maximum diameter of mixture particles, mm	20
Number of revolutions of concrete drum, rev/min	16…18
Number of revolutions of shaft with vanes, rev/min	60
Electromotor power, kW	18

The drum of new mixer and horizontal vane of the shaft rotate in different directions during the mixing of mixture components. Unloading of finished concrete mixture is done by shaft vanes which are spirally arranged.

The paths of mixture particles, when falling from the edges of rotating drum, define the position of vanes at the rotating shaft. Therefore the effect of cascade regime must be kept because the operation of triaxled concrete mixer enables the quality concrete mixtures.

Харьковский государственный технический университет строительства и архитектуры, , ул. Сумская 40, Харьков, 61002 Украина, aanishenko87@mail.ru

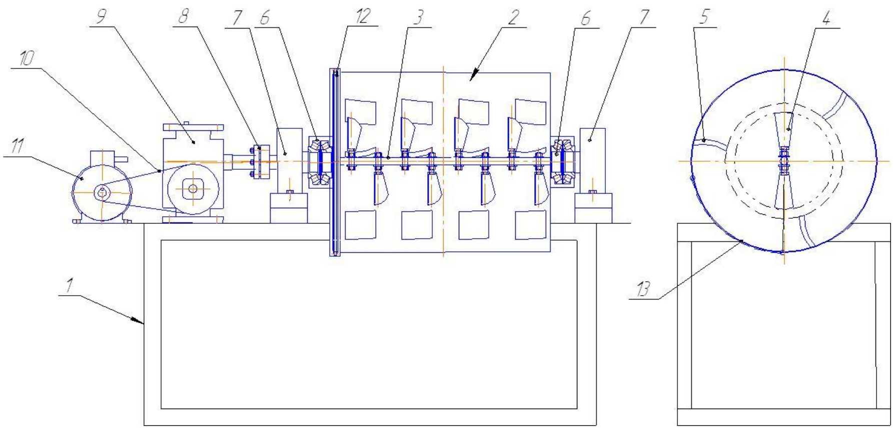

а)

Fig. 1a. *Concrete mixer with gravitational and forced action**:***
1 – mixer frame; 2 – drum; 3 – shaft; 4 – shaft vane; 5 – corpus vane; 6 – bearing; 7 – bearing supports; 8 – coupling; 9 – worm reductor; 10 – belt drive; 11 – electromotor; 12 – chain wheel gear; 13 – port for loading and unloading

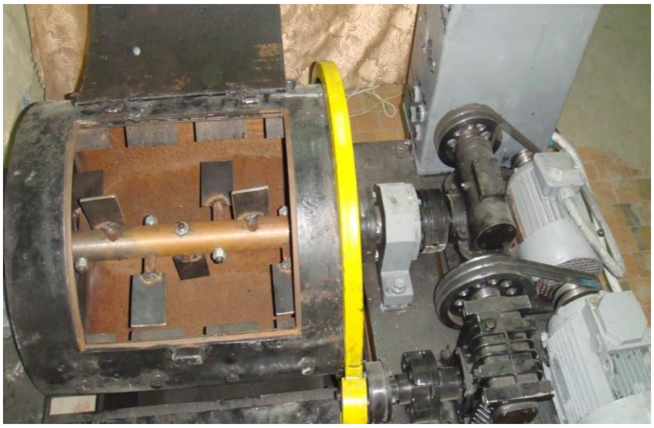

б)

Fig. 1b. *Concrete mixer having gravitational and forced action*

The mixer having gravitational and forced action can provide quality mixing if optimum arrangement of vanes is achieved. Therefore the motion of mixture particles moving along the shaft and drum must be analysed.

The mixer is analysed as the tridimensional model (fig.2). The rotation of vanes around the horizontal axis in coordinate system OXYZ is analysed.

If radial vane (cos $90^0 = 0$; sin $180^0 = 0$) is taken into consideration, the system of equations for motion of mixture particles is as follows:.

$$\begin{cases} x'' = g \cdot \sin \omega t + \omega^2 \cdot x - 2\omega \cdot z'; \\ z'' = -g \cdot \cos \omega t + \omega^2 \cdot z + 2\omega \cdot x'. \end{cases} \quad (1)$$

The second equation of the system (1) for initial conditions $y|_{t=0} = y'|_{t=0} = 0$ shows that there is no rotation of mixture partcles along the axis OY. The system of differential equations for axes OX and OZ can be presented like this:

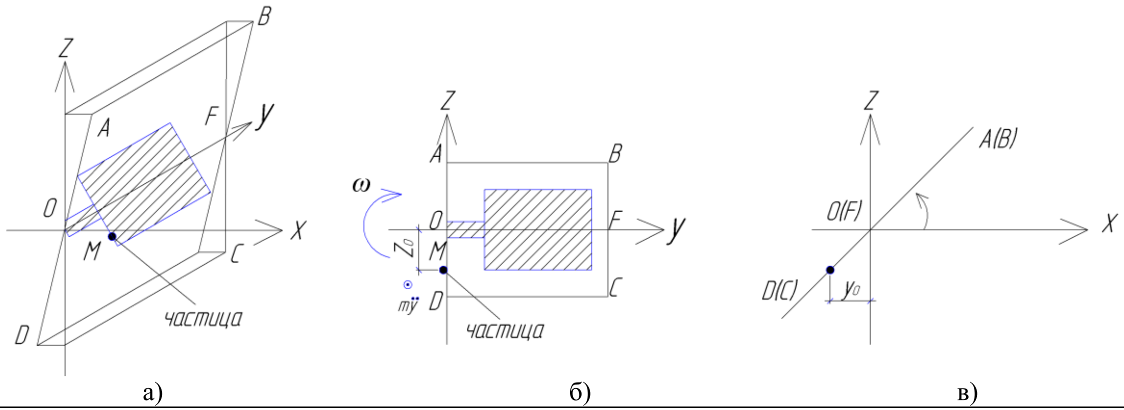

***Fig. 2**. Calculation scheme for making mathematical model of relative motion of mixture particles along the rough surface of mixer vane:*

a) general form ; b) in the plane ZOX; c) in the plane ZOY; ($m\ddot{y}$ - vector $m\ddot{y}$ is perpendicular to axis OY.

$$\begin{cases} x'' - \omega^2 \cdot x + 2\omega \cdot z' = g \cdot \sin \omega t; \\ z'' - \omega^2 \cdot z + 2\omega \cdot x' = -g \cdot \cos \omega t, \end{cases} \quad (2)$$

where ω - angular velocity of vane with shaft or drum;
g - acceleration of gravity;
t - time of moving the mixture particles along the vanes.

Solution of equation system (2) shows that if vane is radially arranged (angle of vane inclination towards horizontal axis $\alpha = 90^o$) along the axes OX and OZ, perpendicular to the axis of drum/shaft rotation, the mixture particles move along the vanes in oscillation manner, which can cause improper mixing of mixture components.

In case of $\alpha = 0^o$ (vanes are longitudinally arranged along the axis of rotation), taking into consideration the coefficient of sliding friction of particles moving over the vanes, the equation has the following form:

$$\begin{cases} x'' + 2\omega \cdot z' - \omega^2 \cdot x = g \cdot \sin \omega t - f \cdot g \cdot \cos \omega t \cdot \dfrac{x'}{\sqrt{(x')^2 + (y')^2 + (z')^2}}; \\ z'' - 2\omega \cdot x' - \omega^2 \cdot z = -f \cdot g \cdot \cos \omega t \cdot \dfrac{z'}{\sqrt{(x')^2 + (y')^2 + (z')^2}}; \\ y'' = -f \cdot g \cdot \cos \omega t \cdot \cos \alpha \cdot \dfrac{y'}{\sqrt{(x')^2 + (y')^2 + (z')^2}}. \end{cases} \quad (3)$$

The analysis of this system shows that the process related to $\alpha = 90^o$ repeats itself. Hence the angles $\alpha = 0^o$ and $\alpha = 90^o$ are not efficient angles of vane arrangement. Therefore, to provide proper mixing of concrete mixture components it is necessary to have $0^0 < \alpha < 90^0$.

In case when $x' = y' = 0$ virtually there is no motion along these axes, and in the case when $(y') \neq 0$ research is done for $\sin \alpha = f$.

Under these conditions it is possible to stabilise the motion of mixture particles along the mixer vanes, i.e. their motion along the axes *x* and *z* is eliminated.

When mixture particles of different mobility move along the mixer vanes, and if friction coefficient *f* is taken into consideration, the angles presented in table 1 are suggested.

The mixer with gravitational and forced action on dry concrete mixture was tested.

If the inclination angle of drum vane is $\alpha_1 = 30^0$ and if the inclination angle of horizontal shaft vane is $\alpha_2 = 45^0$, the best measuring results of mixing the dry concrete mixture particles are obtained when drum vanes and shaft vanes are arranged as presented in figs. 3a and 3b.

Such arrangement of vanes enables high level of mixing the dry concrete particles, as shown in fig. 4.

Table 1. Values of angle α for different values of *f*

f	α, ⁰	*f*	α, ⁰	*f*	α, ⁰
0,01	0,57	0,30	17,46	0,60	36,87
0,05	2,87	0,35	20,49	0,65	40,54
0,10	5,74	0,40	23,58	**0,70**	**44,43**
0,15	8,63	0,45	26,74	0,75	48,59
0,20	11,50	**0,50**	**30**	0,80	53,13
0,25	14,48	0,55	33,37	0,866	60

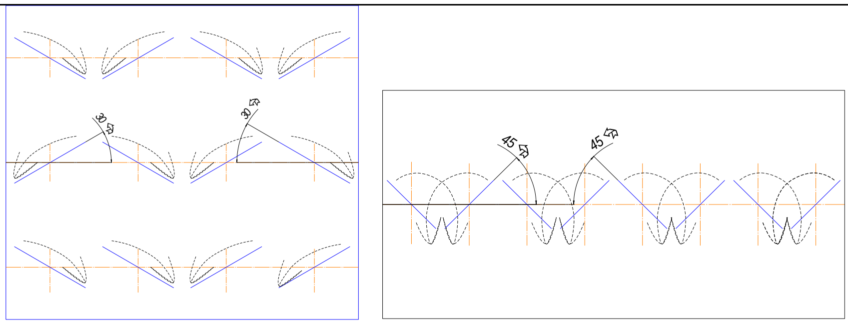

а) б)

Fig. 3. *Arrangement of drum blades (a) and shaft blades (b)*

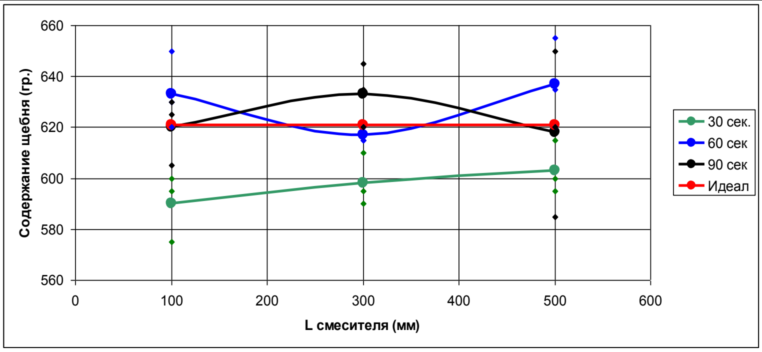

Fig. 4. *Arrangement of mixture particles for different mixing time (30, 60 and 90 seconds.)*

Conclusions

General scheme of mixer having gravitational and forced action in cascade regime was presented is the paper.
Physical and mathematical model of mixture particles moving along the mixer vanes is formed.
Arrangement of mixer vanes in terms of horizontal shaft is suggested.

References

[1] Ємельянова І. А., Баранов А. М., Блажко В.В. Змішувач для приготування будівельної суміші. Патент на винахід №74444. Бюл. №12, 2005.

[2] Инга Анатольевна Емельянова, Владимир Владимирович Блажко, Ольга Валерьевна Доброходова. Использование трехвального бетоносмесителя для приготовления малоподвижных бетонных смесей. // Труды VI-ой международной конференции «Heavy Machinery HM 2008» – Сербия: Кральево, 2008 – С. B23 – B27.

[3] Емельянова И. А., Блажко В. В., Анищенко А. И. Особенности работы бетоносмесителей в каскадном режиме. // Материалы международной научно-технической конференции – Бишкек, 2009 – С. 90 – 9

HEAVY MACHINERY - HM 2011, 15-18
ISBN 978-86-82631-58-3 Paper accepted: 22.05.2011

Wear fatigue defects of vibration equipment in industry of reinforced concrete

А.И. Доценко [1,*]
Moscow State Academy of Municipal Economy and Construction (MSAMEC)

The influence of vibration, abrasive dust, fretting-corrosion and other factors on deep-groove bearing and parallel bearing were studied. On foundation achievements of tribology is presented a supplement and made precise well-known model of friction contact employmently to the vibratory loading. The completely model and calculationly work out on its base apparatus, will allow to solve series of problems under prognostic of resource and reliability of technological equipment in industry of reinforced concrete

Keywords: tribology,vibration, bearings, resources prognosis

0 INTRODUCTION

Equipment quality improvement is one of the main conditions for production growth and efficiency in production in companies of prefabricated steel-concrete products. Of special significance is the quality improvement of prefabricated steel-concrete equipment regarding the economy growth and market relations, as well as the increase of demands for quality of products. The basic equipment, which is the crucial factor in technological production process of concrete accessories and is used in various groups and lines, include vibratory plates, cassette installations, machines for making roadsides, concrete making machines. Quality of the above mentioned equipment influences the reliability of technologic line works which include this equipment.

1. FACTORS THAT PROVOKE THE WEAR FATIGUE

About 80% of equipment defects occur due to wear-fatigue and abrasive damages in moving joints and parts, which puts this problem among the most current. At the moment, the quality of vibro-booster in the above mentioned equipment that uses supports with bearings, where the research results show the following negative characteristics: [1] fatigue of subsurface and support surface, abrasive wearing of support surface, fretting corrosion and sealing surfaces brineling, plastic deformation and rollers path dents, ring and cage damages; overheating.

Fatigue of subsurface and support surface in vibrator rolling bearings features the high frequency of voltage change, structural change in material, appearance of subsurface cracks and their growth, spreading and joining, which results in pealing and braking (pitting).

Surface fatigue features the damage increase in surface layer in unfavorable lubrication conditions, by micro-cracks forming and irregular micro-breaks and bulges.

Abrasive wearing represents gradual material removing, worsened by inadequate lubricating and penetrating in contact zone of interaction between worn particles and other polluters. This is accompanied with occurrence of matt deposit on chrome surfaces, as well as with the speedup of contact destruction process.

Fretting corrosion is a kind of friction corrosion. It usually occurs on sealing surface, on surfaces over which the load is conveyed, at pressence of micro-movements between neighbouring surfaces. This mechanism is followed by micro-surfaces oxydation and forming of powder rust and material wearing. Another type of corrosion is brineling. If bearing unit is in the state of inaction, e.g. non-working state of technological equipment, in the zone of interaction between the elements for rollers support and path: there is no lubricating filling. Contact of metals, in combination with vibrations from the appropriate surrounding equipment, leads to micro-movements and elastic deformations in contact zone. The result is forming of small wearing particles that damage

[*]Corr. Author's Address: Moscow State Academy of Municipal Economy and Construction, Russian Federation
dotsenko_ant@mail.ru

the rollers paths. Joints get spherical cavities, and beads get notches „washing board" type.

Plastic deformations can cause damages and bearings destruction at extremely high static and vibro-striking loads. At the same time, on bead and roller path the dents form.

Dents from various wearing particles of steel or hard minerals formed during the particle's hardening as a result of local overloads. In this case, the dents, as a rule, are of small dimensions and are distributed over the whole surface of rollers path.

Bearing rings damage under load occurs when voltage concentration is bigger than default hardness. This stands for machines that work in vibro-striking regime. Separate damages occur at breaking the limit of fatigue hardness of material while bending.

Bearings overheating occurs at high sliding speeds, or at insufficient lubrication, which provokes great frictional heating of rubbing bodies.

2. SPECIFICITIES OF SLIDING BEARINGS WORK AT VIBRATING LOADS AND ESTIMATION OF THEIR PERFORMANCE

As the studies have shown, after replacing the rolling bearings with sliding ones, carried out in Moscow State Academy of utility economy and construction (МГАКХиС), together with the Institute for Engineering Sciences А.А.Благонравова (РАН), opposed to rolling bearings, the work of sliding bearings features less determining conditions, which allows the dynamic load influence compensation. Подшипники скольжения позволяют уменьшить изнашивание опор, в которых перемещается вал путем обеспечения хорошей прилегаемости вкладыша подшипника к валу. Sliding bearings allow the reduction of support wearing where the shaft spins in the way that it provides good adaptability of embedded bearings to the shaft. Positive aspect regarding the use of sliding bearings in vibrating construction machines and equipment is the convenience of their elements, especially for inserting different anti-friction materials that have damper properties.

Most of sliding bearings now in use in exploitation of construction machines and equipment are made of anti-friction alloys from non-ferrous metals. Evolution of these materials went through creation of more sound alloys which, compared to others, have increased soundness to material fatigue, but worsened anti-friction characteristics. When the alloys of greater soundness are used, the problem of increase of durability on encroachment is faced. This has especially shown for bronzes (BrC30, Br0C22 and others). For that reason, a special attention has been paid to possibility of using the alloys with additions of soft phases of metal and cadmium, that feature high anti-friction characteristics at satisfactory fatigue soundness. Especially wide use have the bimetallic bearings, made from valid bimetallic tape with an alloy layer A020-1(20%Sn, 1%Cu, the rest Al).

Together with aluminum-tin alloys, there are also in use the alloys that contain tin and lead. Carried out researches and technological development for creating the mixture with solid and liquid alloy composition, that contain lead, are in prospect, which contributes to interest for them in the country and abroad.

Parallel with work on improving the anti-friction features, there has not been lost the significance of researches and developments dedicated to the increase of fatigue soundness of alloys. In Russia, the increase of fatigue soundness of alloys has been achieved at the expense of com- bining the anti-friction aluminum alloy type A020-1 with steel by destroying energy. In such variant, the static soundness and the life of joined layers have been almost doubled.

The task of creating anti-friction materials resistant to wearing is also current, on the base of fireproof compounds of boride titan, zirconium and hafnium with coating by metals of the same group.

Together with metal materials in sliding bearings, the composite materials on polymer base are used. The use of such materials in supports of vibrating machines that work in conditions unfavorable for lubrication depends on their self-lubricating capability. In these days, various technologies are used for self-lubricating sliding bearings, for example on the base of hard-plastic materials.

Presently, great attention is paid to creation of new thermo-resistant polymers and anti-friction composites which can provide a stable work of sets with friction in wide range of temperatures, loads and sliding speeds. Application in construction machines and equipment for work in vibratory regime and solution to this problem is in the first place connected to studying of tribological characteristics in contact zones of bearing vibro-booster, for which reason there has been developed a mathematical-physical model for vibratory load of tribo-technical pair. [2].

Contact interaction of friction pair elements while sliding at stationary effect of outer load normally to the surface is significantly different from analog effect at vibratory effect. Vibratory load makes change in interaction on micro-contacts, and also leads to accumulation of damage which leads to damage due to fatigue.

In order to estimate the performance, in the first approximation, of friction work pair at vibratory load, we should consider the chemical composition of friction pair elements, macro and micro-geometrical parameters, energetic load and interaction time, which determine the outer friction conditions.

In calculation of friction force work at vibro-dynamic loads, friction force cannot reach the nominal value and there comes the estimation of rheological characteristics of the contact, as well as the time necessary and sufficient for converting the unsaturated contact into saturated.

In the first approximation [3], the friction quotient fnk for saturated contact is slightly bigger than at unsaturated fnnk:

$$f_{нк}=f_{адг}+f_{деф}=F/P_c^{1/3}+P_c^{1/3}$$

$$f_{ннк}=1/P_c^{2V/(2V+1)}+P_c^{2V/(2V+1)}$$, where

$f_{адг}$, $f_{деф}$ – adhesion and deformation components

F- friction force;

P- contour load;

$_V$- degree parameter for curved bearing surfaces.

So, there are difficulties in determining the real value (quotient) of friction force for material contact pair.

In that case, we suggest to use the method of friction on heat resistance [4], which enables to take into consideration the maximal and minimal values of friction quotient.

Cyclic loads lead to fatigue damages, both on surface and in the deep. During the incubation period from 10 to 10 , the cycle makes surface and subsurface cracks that provoke the wear fatigue and damages due to reduced material capability for hardening. Further effect of vibratory load leads to formation of wearing particles and their separation.

To check the results of theoretical research of the Institute for Engineering and A.A. Blagonravov, together with МГАКХиС, a special tribological system has been prepared for experimental researches.

Base of tribologic complex is the machine ИМ-58 M, on which the cinematic effect vibrator has been installed, which provides the vibratory effects on the examined tribo-technic pair with frequencies from 0 to 30 Hz. In the contact zone between the examined pairs, there is used the consistent or sloppy grease for lubricating that is obtained by the method “drop by drop”. Temperature in friction zone is fixed by thermo-steam, crossed which are submerged into the test sample at depth of 1mm from surface. Tribo-technic pair research is done until the moment when temperature in friction zone reaches the given level. Experimental researches helped, for the examined tribologic pair, at various vibratory effects, determine the relative wearing value and friction quotient that, at certain conditions, can be less than in the case of rolling bearings. At these results, the fault of sliding bearings in contact zone of tribo-technic pair does not observe such fatigue damages such as brineling and holes, that can occur as one of the factors, that confirm the prospect of sliding bearings use in vibratory machines supports that currently figure at concrete producing companies.

3. CONCLUSION

As opposed to rolling bearings, the work of sliding bearings is featured by smaller determining conditions. The results show the fault of rollers bodies sliding in tribo-technic pair contact zone disregarding such fatigue damages like brineling and holes, which makes the ground for recommending the sliding bearings for use in machines that work in vibro-dynamic loads regime.

4. References:

1. Доценко А.И., Добронравов СС., Тяпкин A.F. О надежности виброплощадок на заводах железобетонных изделий. Ж-Л "Строительные и дорожные машины №9, 1991.
2. Доценко А.И., Браун Э.Д. Модель фрикционного контакта при вибрационном нагружении. Известия вузов. Северокавказский регион. Спецвыпуск, 2001.
3. Крагельский И.В., Михин ИМ. Узлы трения машин. Справочник, М., 1984.
4. Браун Э.д. и др. Основы трибологии (трение, износ, смазка). Под ред. А.В Чичинадзе, М., 1995.

HEAVY MACHINERY - HM 2011, 19-22
ISBN 978-86-82631-58-3
Paper accepted: 20.05.2011

The Analysis of Significance of Design And Operational Parameters That Affect the Productivity of Earthmoving Machines

I.Kirichenko[1,*]
[1]Kharkiv National Automobile and Highway University, Kharkiv, Ukraine

The method of stochastic analysis has been considered in application to bulldozer productivity as a non-linear function of nine independent factors that describe design and operational features of machines of various standard sizes with preset indeterminate variations in the factors.
A mathematic model of productivity functional decomposition into multidimensional Taylor's series with a subsequent significance coefficient determined and parameters arranged according to reduction in significance has been obtained.

Keywords: productivity, bulldozer, Taylor's series, parameter ranking, stochastic analysis, weight coefficients.

0 INTRODUCTION

A method of stochastic analysis has been considered for variations in productivity of earthmoving machines, with bulldozers as an example. The productivity is given as a non-linear function of affecting design and operational parameters when indeterminate variations in the latter are preset. A mathematic model of this function decomposition into multidimensional, by number of parameters, Taylor's series with a subsequent impact significance coefficient calculated and parameters arranged according to reduction in significance has been offered.

1 PROBLEM-SETTING

Productivity of earthmoving machines is a complex index of operational efficiency, which is a function of standard technical parameters as well as of operational conditions and process flowsheets with stochastic variations not determined by standards. Indeterminacy of such parameters causes a problem of planning multi-factor research into productivity, especially when dealing with large (more than 3-4) sizes of factor spaces. Evaluation of significance of impact made by varying technical and operational parameters on probable variations in productivity, especially for groups of machines that differ in type and purpose becomes problematic as well.

2 ANALYSIS OF WRITINGS

To analyse the significance of impact made by operational parameters on machine productivity is a goal for planning and improving while building mathematic models of engineering systems [1]. Methods of solving such tasks are well-developed, especially for regression analysis in planning active experiments [2, 3]. However, these experiments require large arrays of sampled data, in particular when factor spaces feature large sizes. To ensure representative multivariate data for these experiments is an independent problem, which is quite often unsolvable.
The aim of this article is to reveal the potential of probabilistic analysis of mathematic models for productivity of earthmoving machines as non-linear functions of finite aggregate of operational parameters and to describe a method to evaluate the significance of impact made by these parameters on variations in machine productivity.

3 FUNCTIONAL MODEL OF PRODUCTIVITY

Irrespective of the earthmoving machine type (bulldozer, scraper, motor grader, loader), the productivity is a one-valued function of at least four variables

$$P = \frac{3600 \cdot F_f \cdot V}{F_{rp} \cdot T_c} (\frac{m^3}{h}), \qquad (1)$$

[*]Corr. Author's Address: Kharkiv National Automobile and Highway University, Kharkiv, Ukraine, igor.kyrychenko@mail.ru

where V - geometric volume of earth moved within one cycle; F_f - bucket fill factor; F_{rp} - soil loosening factor; T_c - cycle time (*sec*.)

In its turn, cycle time depends on arguments (travel length, velocity) describing stages of the production cycle (cutting, travel, and reverse motion) and is described, e.g. for bulldozers,

$$T_c = \frac{l_{ct}}{V_{ct}} + \frac{l_t}{V_t} + \frac{l_{ct} + l_t}{l_{rv}} + t_{ad}, \qquad (2)$$

where (l_{ct}, l_t) - cutting length and travel length; (V_{ct}, V_t) - cutting velocity and travel velocity; (l_{rv}) – reverse speed; (t_{ad}) additional time related to transition processes when stages change.

Combining equations (1) and (2) we obtain a mathematic functional model of bulldozer productivity, which properties are singly valued with nine variables $V, F_f, \ldots, V_{rv}, t_g$:

$$P = \frac{3600 \cdot F_f \cdot V}{F_{rp} \cdot \left(\frac{l_{ct}}{V_{ct}} + \frac{l_t}{V_t} + \frac{l_{ct}}{V_{rv}} + \frac{l_t}{V_{rv}} + t_{ad} \right)}. \qquad (3)$$

3 STOCHASTIC MODEL OF PRODUCTION

Any variations in values of the variables lead to fluctuations in function P. We shall assume variations in values of the variables to be fixed and constant deviations from preset (rated) values within one bulldozer cycle.

Let us consider the sequence of bulldozer cycles. In this case, parameter deviations are random values as neither their signs nor absolute values recur from one cycle to another. Function (3) can now be considered a random value determined by non-linear transformation of independent initial random values $V, F_f, \ldots, V_{rv}, t_{ad}$, that have constant mathematic expectations. Deviations (increments) of original random values can also be considered constant or preset as dispersions of these values are constant.

The degree of impact made by argument increments on increment of function Y = P is found

$x_1 = V$, $x_2 = F_f$, $x_3 = F_{rp}$, $x_4 = l_{ct}$, $x_5 = l_t$, $x_6 = V_{ct}$, $x_7 = V_t$, $x_8 = V_{rv}$,, $x_9 = t_{ad}$.

In accordance to new symbols, the equation (3) takes the form

$$Y = \frac{3600 \cdot x_1 \cdot x_2}{x_3 \cdot \left(\frac{x_4}{x_6} + \frac{x_5}{x_7} + \frac{x_4}{x_8} + \frac{x_5}{x_8} + x_9 \right)}. \qquad (4)$$

Let $\overline{Y}$ и $\overline{x_i}$ be mean values of function Y and arguments x_i, i = 1.9. Non-linear function Y is decomposed into m-dimensional Taylor's series [4], m = 9, by increment degrees of arguments $x_1, \ldots, x_{ad}$ of the function (4).

$$\Delta x_i = x_i - \overline{x_i} \qquad (5)$$

If the mean value of function Y is

$$\overline{Y} = \overline{f}\left(\overline{x_1}, \ldots, \overline{x_m}\right) \qquad (6)$$

then this decomposition

$$Y = \overline{f}\left(\overline{x_1}, \ldots, \overline{x_m}\right) - \\ -\sum_1^m \left(\frac{d\overline{Y}}{d\overline{x_1}} \cdot \Delta x_i \right) + A_т, \qquad (7)$$

where $A_т$ – remainder of Taylor series:

$$A_т = \frac{1}{2}\left(\sum_{i=1}^m \frac{d\Delta x_i}{d\overline{x_i}} \right)^2 \cdot \overline{f} \cdot \\ \cdot \left[\left(\overline{x_1} + \Delta x_1\right), \ldots, \left(\overline{x_m} + \Delta x_m\right) \right]. \qquad (8)$$

Functional dependence $\overline{f}$ (.) expression (6) corresponds to the dependence of general expression (2) with corresponding argument symbols $V = x_1, \ldots, t_{ad} = x_9$.

Assuming that

$$Y = \overline{Y} - \Delta Y,$$

expressions for ΔY of Y function are obtained from (7)

$$\Delta Y = \sum_{i=1}^m \left(\frac{d\overline{Y}}{d\overline{x_i}} \cdot \Delta x_i \right) - A_т \qquad (9)$$

If the remainder $A_т$ meets the requirement [5]

$$A_т \le 0,8 \cdot \sqrt{\sum_{i=1}^{m}\left(\frac{d\overline{Y}}{d\overline{x}_i}\cdot\Delta x_i\right)^2 \cdot \sigma_i^2} \qquad (10)$$

where σ_i^2 - dispersion of deviations Δx_i, then the confidence interval for deviation ΔY can be calculated as

$$\Delta y = \sqrt{\sum_{i=1}^{m}\left(\frac{d\overline{Y}}{d\overline{x}_i}\cdot\Delta x_i\right)^2}, \qquad (11)$$

with dispersion σ_y^2 being constant.

In this case, confidence probability P is the same both for Δy interval and for confidence intervals Δx_i i = 1, m, within which the requirement is met (10).

4 EVALUATION OF IMPACT SIGNIFICANCE

Let us use expression (11) for evaluating the significance of impact made by deviations Δx_i of arguments x_1, …, x_m on deviation of function Y (bulldozer productivity).

Let us introduce the notion *coefficient of impact* and designate it as

$$F_i = \frac{\partial\overline{Y}}{\partial\overline{X}_i} \qquad (12)$$

Then expression (11) is

$$\Delta y = \sqrt{\sum_{i=1}^{m}(F_i\cdot\Delta x_i)^2} \qquad (13)$$

Table 1 gives initial data, functional transformations and calculated results of function Y components (in absolute values and percentage in relation to deviation $(\Delta y)^2$).

Table 1. *Initial data and calculated results for components of functional impact*

Argument X_i	Variation boundary $X_{iH}-X_{iB}$	Mean value $\overline{X}_i$	Coefficient of impact on Y F_i	Functional impact made on productivity	
				absolute	relative (%)
$X_1=V$ (cu m)	(0.9V−1.1V) cu m	rated	$F_1=\overline{Y}\cdot V^{-1}$	$1\cdot10^{-2}$	20. 205
$X_2=F_f$	0.9 K_f−1.1 K_f	rated	$F_2=\overline{Y}\cdot F_f^{-1}$	$1\cdot10^{-2}$	20. 205
$X_3=F_{rp}$	0.9 K_{rp}−1.1 K_{rp}	rated	$F_3=\overline{Y}\cdot F_{rp}^{-1}$	$1\cdot10^{-2}$	20. 205
$X_4=l_{ct}$ (m)	(6−10) m	8 (m)	$F_4=-\overline{Y}\cdot(\frac{1}{V_{ct}}+\frac{1}{V_{rv}})\cdot S^{-1}$	$2.142\cdot10^{-4}$	0.433
$X_5=l_t$ (m)	(50−100) m	75 (m)	$F_5=-\overline{Y}\cdot(\frac{1}{V_t}+\frac{1}{V_{rv}})\cdot S^{-1}$	$72.69\cdot10^{-4}$	14.687
$X_6=V_{ct}$ (m/sec)	(0.4−0.5) m/sec	0.45 (m/sec)	$F_6=\overline{Y}\cdot\frac{l_{ct}}{V_{ct}^2}\cdot S^{-1}$	$1.107\cdot10^{-4}$	0.224
$X_7=V_t$ (m/sec)	(0.9−1.0) m/sec	0.95 (m/sec)	$F_7=\overline{Y}\cdot\frac{l_t}{V_t^2}\cdot S^{-1}$	$21.848\cdot10^{-4}$	4.414
$X_8=V_{rv}$ (m/sec)	(1.1−1.2) m/sec	1.15 (m/sec)	$F_8=\overline{Y}\cdot(\frac{l_{ct}+l_t}{V_{rv}^2})\cdot S^{-1}$	$18.259\cdot10^{-4}$	3.689
$X_5=t_{ad}$ (sec)	(10−20) sec	15 (sec)	$F_9=-\overline{Y}\cdot S^{-1}$	$78.87\cdot10^{-4}$	15.936

In Table 1 multiplicands $\overline{Y}$ and S are determined by expressions

$$\overline{Y} = \frac{3600 \cdot \overline{X}_1 \cdot \overline{X}_2}{\overline{X}_3 \cdot (\frac{\overline{X}_4}{\overline{X}_6} + \frac{\overline{X}_5}{\overline{X}_7} + \frac{\overline{X}_4}{\overline{X}_8} + \frac{\overline{X}_5}{\overline{X}_8} + \overline{X}_9)},$$

$$S = \frac{\overline{X}_4}{\overline{X}_6} + \frac{\overline{X}_5}{\overline{X}_7} + \frac{\overline{X}_4}{\overline{X}_8} + \frac{\overline{X}_5}{\overline{X}_8} + \overline{X}_9 .$$

All results have been obtained for 10%-variations in initial arguments X_1, …, X_9 of function Y, which ensures meeting the condition (10).

As follows from Table 1, arguments can be arranged according to reduction in significant impact on bulldozer productivity (Table 2).

Table 2. *A series of arguments (operational parameters) arranged according to reduction in significant impact on bulldozer productivity*

Rank according to significant impact on productivity	1. 2. 3	4	5	6	7	8	9
Weight (%)	20.205	15.936	14.687	4.414	3.689	0.433	0.224
Operational parameter	$V.\ F_f.\ F_{rp}$	t_{ad}	l_t	V_t	V_{rv}	l_{ct}	V_{ct}

5 PRACTICAL IMPORTANCE

The proposed method of transforming non-linear functions of multiple variables with subsequent stochastic analysis of deviations from these functions allows evaluating components of these deviations according to types of affecting initial parameters. The method could be used for preliminary minimization of a number of such parameters when planning further factor experiments in order to identify productivity models for earthmoving machines.

6 CONCLUSIONS

1. The developed method of stochastic analysis of non-linear multi-parametric dependencies allows quantitative eval·uations of any operational parameters according to their significant impact on productivity of earthmoving machines.
2. Ranking the parameters according to their significant impact on productivity allows forming sub-multitudes of parameters that ensure maximum impact thus planning multi-factor machine tests at minimum test volumes.

7 REFERENCES

[1] Барабащук В.И. и др. Планирование эксперимента в технике / В.И. Барабащук, Б.П. Креденцер, В.И. Мирошниченко; под ред. Б.П. Креденценра. – К.: Техніка. 1984. − 200с.

[2] Джонсон Н., Лион Ф. Статистика и планирование эксперимента в технике и науке: Методы планирования эксперимента / Н. Джонсон, Ф. Лион; пер. с англ. под ред. Э.К. Лецкого.− М.: Мир, 1981. − 520 с.

[3] И.Г. Кириченко. Модульная концепция проектирования … Х. ХНАДУ, 2002. −119с.

[4] Корн Г., Корн Т. Справочник по математике для научных работников и инженеров. – М.: Наука, 1978. − 832с.

[5] Вентцель Е.С., Овчаров Л.А. Теория вероятностей и ее инженерные приложения: Учеб. пособие для вузов. – М.: Высш. шк., 2000.−480 с.:ил.

HEAVY MACHINERY - HM 2011, 23-26
ISBN 978-86-82631-58-3
Paper accepted: 30.05.2011

The Analysis of Vibratory Roller Motion

Polidor Bratu[1], Carmen Debeleac[1,*]
[1]"Dunarea de Jos" University of Galati, Engineering Faculty of Braila

In road building, the compaction equipments like rollers with single or tandem vibratory drum are used both for soil or mixture. A numerical and dynamical model of the drum-soil system is described in this paper. The model takes into account the most important parameters specifically for vibratory roller and, respectively for road pavement material. The soil is considered by an elastic medium.

A programme in Matlab/Simulink 7 was developed to solve the system of differential equations, which describe the vibratory roller movement. In paper the authors make a study of the roller's stabile motion during the compaction process through correlation of the machine's technological parameters with soil parameters. The simulation results are presented as diagrams of displacement and velocity of the vibratory drum.

Keywords: vibratory roller, soil, interaction, dynamic analysis.

1 INTRODUCTION

The soil compaction is a complex process influenced by the technological parameters of compaction equipment and the properties of road system layer's. The correlation of all these factors leads to obtaining an optimal compaction degree after a minimum roller's passes.

The analysis of compaction process and implicit of the contact between drum and ground [1] supposes

- knowing of mathematical models, which describe the behaviour of machine-ground system [2], [4];
- writing and solving of differential equation of motion for the main subassemblies (drum, chassis);
- validation of results obtained by numerical simulation process based on experimental tests.

In addition, the compaction efficiency it is appreciated if we know the values of chassis and drum vertical accelerations during on compaction process.

2 MATEMATICAL MODEL OF ROLLER-GROUND INTERACTION

The vibratory roller can be describing, in simplified way, by a system with two degree of freedom (figure 1).

The roller's motion is defining by the vibratory drum displacement (x_2) and chassis's displacement (x_1). The main parameters of roller-ground system are show in table 1.

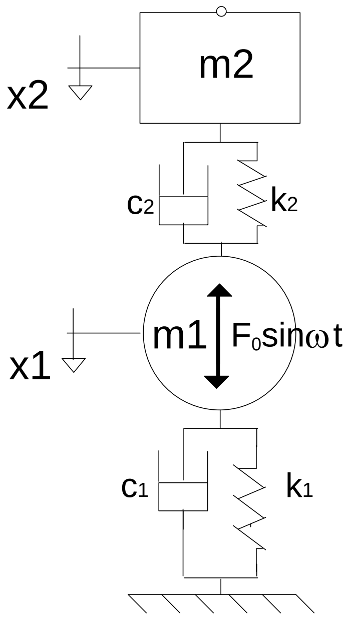

Fig. 1. *Dynamic model of roller-ground interaction*

The vibration system maintained into roller drum produces oscillatory force with amplitude

$$F_0 = m_0 e \omega^2 \tag{1}$$

where $\omega = 2\pi f$ represents the force pulsation.

*Corr. Author's Address: "Dunarea de Jos" University of Galati, Calea Domneasca, no.47, Galati, Romania, cbordea@ugal.ro

Table 1. *Parameter's identification*

Systems	Parameters	Notations
roller-ground system	chassis mass drum mass eccentrically pieces mass	m_1 m_2 m_0
vibration system	eccentricity frequency	e f
ground system	stiffness coefficient damping coefficient	k_1 c_1
suspension system	stiffness coefficient damping coefficient	k_2 c_2

The differential equations of motion for the two mass (m_1 and m_2) under dynamic force action are the next forms [2]

$$\begin{cases} m_1\ddot{x}_1 + c_1\dot{x}_1 + k_1x_1 - c_1\dot{x}_2 - k_1x_2 = 0 \\ m_2\ddot{x}_2 + (c_1 + c_2)\dot{x}_2 + (k_1 + k_2)x_2 - \\ \qquad - c_1\dot{x}_1 - k_1x_1 = m_0e\omega^2 \sin\omega t \end{cases} \tag{2}$$

or in matrix writing

$$\begin{bmatrix} m_1 & 0 \\ 0 & m_2 \end{bmatrix}\begin{Bmatrix} \ddot{x}_1 \\ \ddot{x}_2 \end{Bmatrix} + \begin{bmatrix} c_1 & -c_1 \\ -c_1 & c_1 + c_2 \end{bmatrix}\begin{Bmatrix} \dot{x}_1 \\ \dot{x}_2 \end{Bmatrix} + \\ + \begin{bmatrix} k_1 & -k_1 \\ -k_1 & k_1 + k_2 \end{bmatrix}\begin{Bmatrix} x_1 \\ x_2 \end{Bmatrix} = \begin{Bmatrix} 0 \\ 1 \end{Bmatrix} m_0e\omega^2 \sin\omega t \tag{3}$$

Applying Laplace transformation to the eq.(3) in zero conditions it's obtained:

$$[A]\begin{Bmatrix} X_1(s) \\ X_2(s) \end{Bmatrix} = \begin{Bmatrix} 0 \\ 1 \end{Bmatrix} F(s) \tag{4}$$

where

$$[A] = \begin{bmatrix} m_1s^2 + c_1s + k_1 & -c_1s - k_1 \\ -c_1s - k_1 & m_2s^2 + (c_1 + c_2)s + k_1 + k_2 \end{bmatrix} \tag{5}$$

Relation will be given by the displacements of the two masses of dynamical system is

$$\begin{Bmatrix} X_1(s) \\ X_2(s) \end{Bmatrix} = [A]^{-1}\begin{Bmatrix} 0 \\ 1 \end{Bmatrix} F(s). \tag{6}$$

where determinant of matrix A useful for evaluation of $[A]^{-1}$ is:

$$det(A) = \\ = (m_1s^2 + c_1s + k_1)[m_2s^2 + (c_1 + c_2)s + k_1 + k_2] - \\ - (c_1s + k_1)^2 \tag{7}$$

If we suppose that det(A) must be null, it is possible the polls evaluation of the characteristic equation (7).

In absence of external force and amortisation, motion equation of m_1 and m_2 becomes:

$$\begin{bmatrix} m_1 & 0 \\ 0 & m_2 \end{bmatrix}\begin{Bmatrix} \ddot{x}_1 \\ \ddot{x}_2 \end{Bmatrix} + \\ + \begin{bmatrix} k_1 & -k_1 \\ -k_1 & k_1 + k_2 \end{bmatrix}\begin{Bmatrix} x_1 \\ x_2 \end{Bmatrix} = \begin{bmatrix} 0 \\ 0 \end{bmatrix}. \tag{8}$$

The solution for the eq.(8) are

$$x_1 = A_1 \sin(\omega t + \varphi_1) \\ x_2 = A_2 \sin(\omega t + \varphi_2) \tag{9}$$

and eq.(8) becomes

$$[A^*]\begin{Bmatrix} A_1 \\ A_2 \end{Bmatrix} = \begin{bmatrix} 0 \\ 0 \end{bmatrix} \tag{10}$$

where

$$[A^*] = \begin{bmatrix} m_1\omega^2 + k_1 & -k_1 \\ -k_1 & m_2\omega^2 + k_1 + k_2 \end{bmatrix} \tag{11}$$

If we suppose that $det(A^*)$ must be null, then we obtained the expressions for eigenvalues of roller-ground system

$$m_1m_2\omega^4 - \omega^2(m_1k_1 + m_2k_1 + m_1k_2) + \\ + k_1k_2 = 0 \tag{12}$$

with solutions

$$\omega_{1,2} = \sqrt{\frac{a \pm \sqrt{a^2 - b^2}}{2m_1m_2}}. \tag{13}$$

In eq.(13) we make the next notations:

$$a = m_1k_1 + m_2k_1 + m_1k_2 \\ b = (4k_1k_2m_1m_2)^{0.5}. \tag{14}$$

Evaluation on analytical way of eigenvalues of dynamical system depicted into figure 1 leads to finding of pulsations resonance [5]. The knowing of these values, in completion with a set of experimental data offers the possibility of damping coefficient evaluation for the analysed system [6], [3].

3 NUMERICAL SIMULATION

An important aspect of compaction process study consists on stability analysis of roller-ground system motion function by main parameters of two subsystems in contact [7],[8]. For example, in the next are presented the results of numerical simulation for some cases supposed to be representative.

For simulation roller-ground interaction, following data are used: $m_1=2000$ kg; $m_2=2800$ kg; $f=30$ Hz; $c_1=10^6$ Ns/m; $k_1=3.5x10^8$ N/m; $c_2=5$ Ns/m; $k_1=4.5x10^6$ N/m. We supposed that the ground material is sand.

Firstly, it has been used sine exciter dynamic force (F_0) with frequency of *30* Hz and variable amplitude function by static torque of eccentric mass m_0. Simulation time was *400* ms.

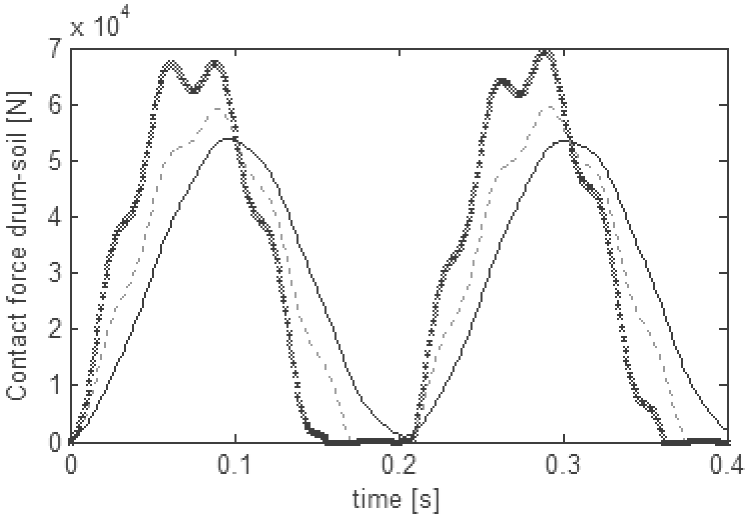

Fig. 2. *Contact force vs time*

—— $M_{st}=0.5$ kgm^2;---------$M_{st}=2.5$ kgm^2; ---x---$M_{st}=5$ kgm^2;

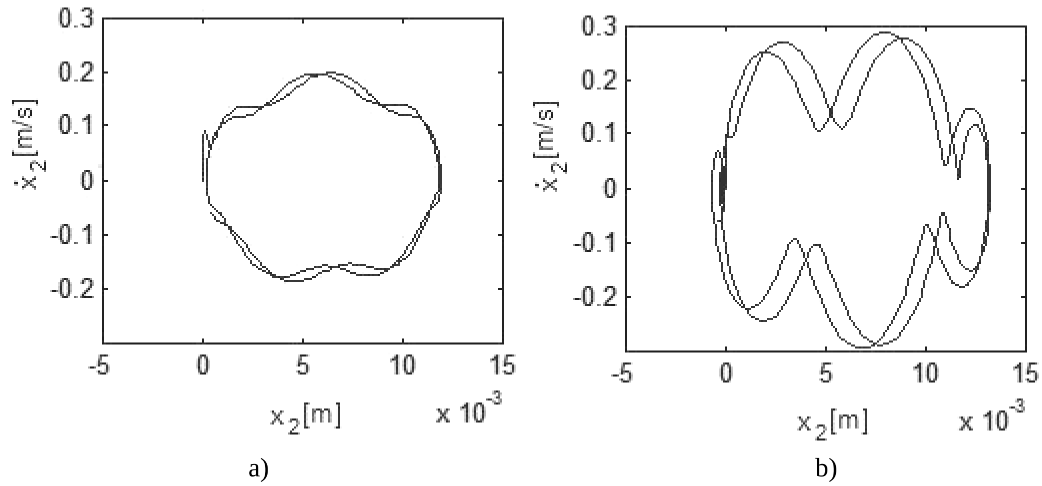

Fig. 3. *Phases plane*

a) $M_{st}=0.5$ kgm^2; *b)* $M_{st}=2.5$ kgm^2.

In figure 2 was show the diagram of contact force variation between roller-sand and I figure 3 the motion into phases plane for the system.

4 CONCLUSIONS

Based on diagrams from figure 2, we can observe some aspects which appear because the roller technological parameters are not correlated with terrain characteristics:

- the contact force between drum and soil have only positive values that means the contact is permanently (linear), as can be seen in figure 2 and figure 3a);
- the contact force have short duration time when his value is null that means the contact is temporary (nonlinear), such as figure 2 and Figure 3b).

In the last case, the no uniformity of contact deals to the instable motion of roller under dynamical forces.

In conclusion, knowing the soil properties, the computer simulation enables to establish the stabile and optimal regimes for working process.

5 REFERENCES

[1] Anderegg, R., Von Felten, D., “Nonlinear Dynamic of Compaction Equipment – an Overview (in German)’’, Österreichische Ingenieur-und Architekten-Zeitschrift (ÖIAZ), 150. Jg., Heft 4-5/2005, p. 145-149, 2005.

[2] Bratu, P., "Mecanica teoretica’’, Impuls Publishing House, Bucharest, Romania, 2008.

[3] Brandl, H., ,,Compaction of Soil and Other Granular Materials Used in Construction Work’’, Građevinar 54 (2002) 9, Zagreb, Hrvatska, 2002, pp. 513-527.

[4] Debeleac, C., "On the efficiency of compacting equipment", The Annals of “Dunarea de Jos” University of Galati, Vol.2, Issue XVI, Fascicle XIV Mechanical Engineering, ISSN 1224-5615, 2010, pp.51-54.

[5] Debeleac, C., "Cap. 4 On computational dynamics of tool - soil interaction", Research Trends in Mechanics, vol. 4, Romanian Academy Publishing House, Bucharest, Romania, 2010, pp. 83-108.

[6] Gorman, P.B., "Exploring the Relationship Between Roller Vibration and Soil Compaction", M.S. Thesis, University of Oklahoma, 2003.

[7] Nicoara, E.T.,"Influence of Moisture Content on Dynamic Behavior of Sand Under Vibratory Roller Compaction", M. Sc. Thesis, IHE Delft, 2001.

[8] Popa, G., Nicoara, S.V., ,,Study of Soil – Vibratory Roller Response’’, Ovidius University Press, 3,4(2002)1, Timisoara, Romania, 2003, pp. 151-156.

HEAVY MACHINERY - HM 2011, 27-32
ISBN 978-86-82631-58-3
Paper accepted: 20.05.2011

Self-Erecting Crane Simulation While Raising And Lowering Stages

Catalin Francu[1,*], Adrian Bruja[1], Marian Dima[1]
[1] Technical University of Civil Engineering Bucharest

In this paper the authors present a comparative study for simulation of a self erection mechanism which is a component of a self erecting crane. The study was done, using several methods, all using the computer.
The first is an analytical method, in which the computer is used to calculate the formulas resulted from applying the method.
The second method involves using dedicated software for the simulation study of plane mechanisms.

Keywords: self-erecting cranes, kinematic analysis, analytical methods

0 INTRODUCTION

The folding-unfolding mechanism of a self-erecting tower crane is presented in unfolded state in figure 1.

Unfolding mechanism is done by using a tackle placed between D and E joints and is done in 2 stages, figure 3. In the first stage (the backstay fixed between A and H is loosened), by shorting the length of the tackle, the lower tower BCE rotates counter clockwise around the B joint and the rocker bar 1, through 3 and 4 bars, are pushing up the superior tower EFG along with the HGK boom and are rotating clockwise around the E joint. In stage 2, when the AH distance becomes equal with the backstay length, the HGK boom is rotating around G joint until GK becomes horizontal.

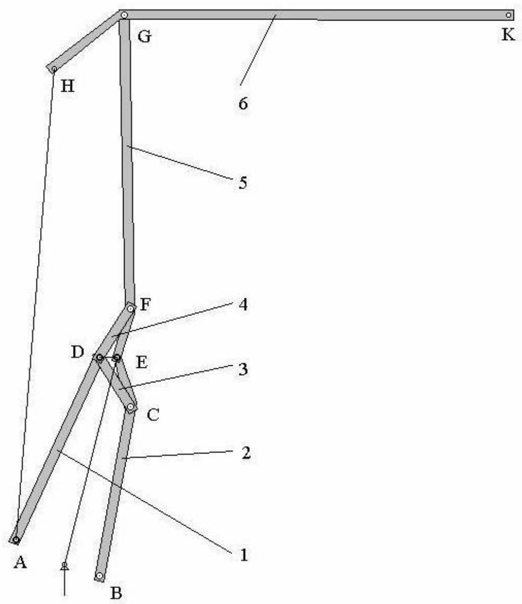

Fig. 1 Self-erecting tower crane in unfolded state

2. ANALYTICAL SIMULATION OF THE MECHANISM

2.1. Method overview Positions study

For this study was used the matrix method (geometric places method). This method is applied on dyads starting with the dyad linked to the end-effector. The coordinate system to which the mechanism relates has the origin in the fixed hinge A.

Considering a RRR dyad related to a reference coordinate system and for which are known the positions of the external joints and the lengths of the bars, figure 2, can be written the following system:

$$\begin{cases} (x_3 - x_1)^2 + (y_3 - y_1)^2 = l_1^2 \\ (x_3 - x_2)^2 + (y_3 - y_2)^2 = l_2^2 \end{cases} \qquad (1)$$

By solving the system 1 solutions are given (x_3, y_3),

$$x_3 = \frac{-B \pm \sqrt{B^2 - 4AC}}{2A} \qquad (2)$$

*Corr. Author's Address: Technical University of Civil Engineering Bucharest, Romania, francu@utcb.ro

$$y_3 = \frac{D-(x_2-x_1)x_3}{y_2-y_1}$$

where:

$$\left.\begin{aligned} D &= \frac{x_2^2+y_2^2-x_1^2-y_1^2+l_1^2-l_2^2}{2} \\ A &= (y_2-y_1)^2+(x_2-x_1)^2 \\ B &= 2y_1(x_2-x_1)(y_2-y_1)- \\ &-2x_1(y_2-y_1)^2-2D(x_2-x_1) \\ C &= (y_2-y_1)^2(x_1^2+y_1^2-l_1^2)+ \\ &+D^2-2y_1(y_2-y_1)D \end{aligned}\right| \quad \textbf{(3)}$$

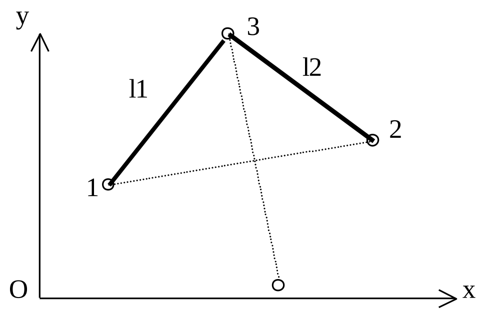

Fig. 2 Geometric places method for a dyad

The real position of the interior joint is chosen according to the principle of position succession.

The angles that the bars have with the OX axis measured counter clockwise are determined with the equation

$$\alpha_i = arctg\,\frac{y_2-y_1}{x_2-x_1} \qquad (4)$$

where x1, y1, x2, y2 represents the coordinates of the bar i.

2.2. Applying the method

The algorithm for applying the method follows:

a) knowing the positions of the D_3 and B joints and D_3C and BC lengths the position of the joint C is determined;
b) the position of joint E_2 is determined by knowing the positions of B and C joints and BE and CE lengths;
c) the position of joint F is determined by knowing the positions of D_4 and E_5 joints and DF and EF lengths;
d) the position of joint G is determined by knowing the positions of E and F joints and EG and FG lengths;
e) For the first stage of unfolding the position of joint H is determined according to the positions of F and G joints and FH and GH lengths and in the 2nd stage of the unfolding the AHG dyad is considered (backstay AH is stretched) and the position of the joint H is determined according to the positions of the A and G joints and AH and GH lengths;
f) The position of the joint K is determined according to the positions of G and H joints and GK and HK lengths.

2.3. Obtained results

By following the algorithm paragraph 2.2 and using the formulas in paragraph 2.1 a computer program was written using a high level programming software.

In figure3 is presented the crane in initial position, and in final working position respectively.

In figure 4 is presented the entire workplace of the crane from the initial position to the final position.

In figure 5 the crane also presents the trajectories of the characteristic points (joints are represented in pink and centres of gravity in red).

3. SIMULATION OF THE MECHANISM USING DEDICATED SOFTWARE FOR PLANE MECHANISMS

There are companies in the software market that have created dedicated software for kinematic and dynamic studies for plane mechanisms.

Such software involves creating a scale 2D model of the studied mechanism and specifying the constraints between the kinematic elements (Fig.6)

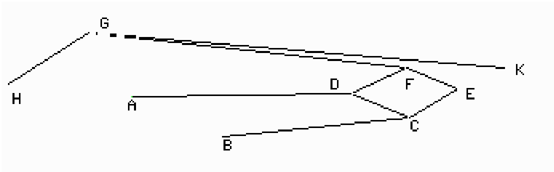

a)

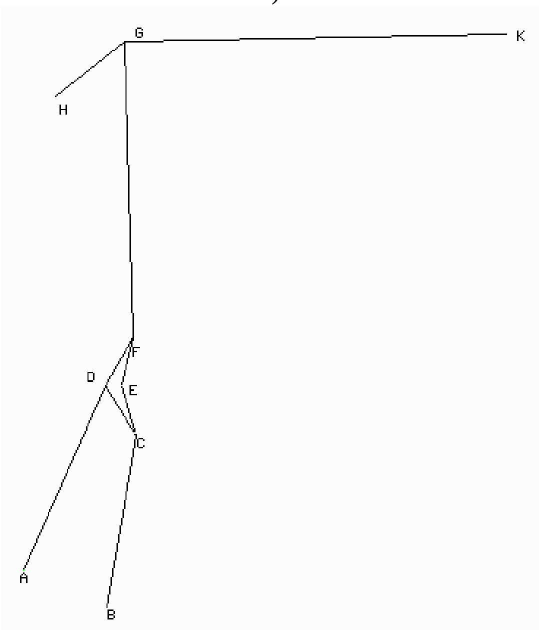

b)

Fig. 3 The self erecting crane: a) initial position b) final position (in working state)

The software writes automatically the equations system, and solves it using numerical methods. The obtained results are presented in graphics and tables.

The self erection mechanism of the self erecting tower crane was studies with such software.

3.1. Using the software

For the self erecting mechanism kinematic elements were built on 1:1 scale in bar shape (figure 1) and then the constraints between the kinematic elements were specified and the mechanism was brought to the initial position. By specifying the motion to the driving element, the software calculates the kinematic and dynamic parameters and the working simulation of the studied mechanisms

3.2. Obtained results

Using this software the **results** are obtained easily by specifying to the software the studied kinematic element.

In figure 7 is presented the workspace of the self-erecting crane while erecting

In figure 8 is presented the same self erecting crane studied with another software called SAM , in which the paths of the joints are highlighted.

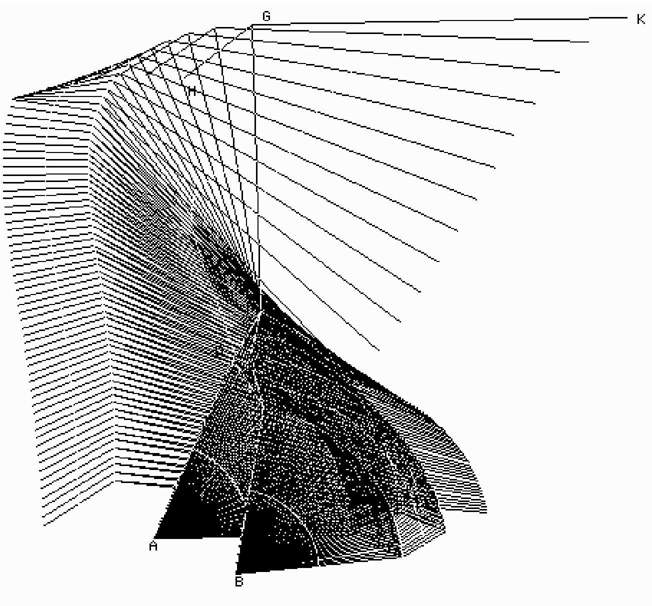

Fig. 4 The workspace of the self erecting crane while erecting using a computer program

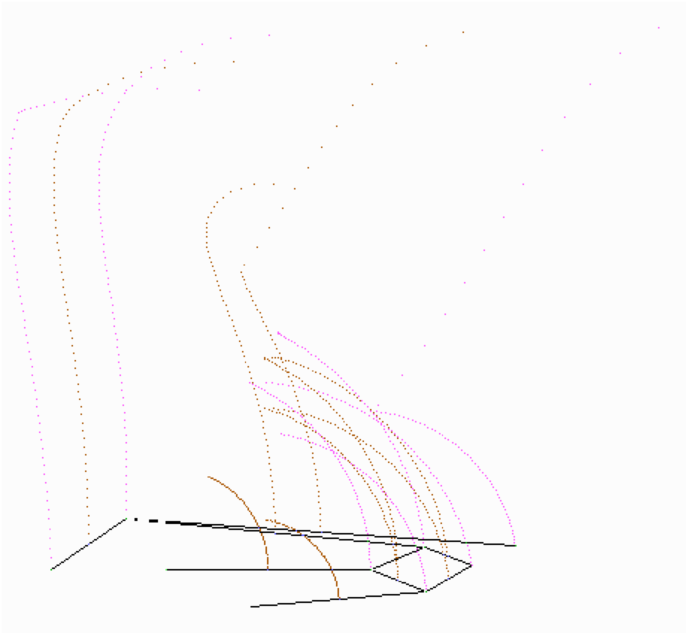

a)

b)

Fig 5. Trajectories of the characteristic points (joints are represented in pink and centres of gravity in red)

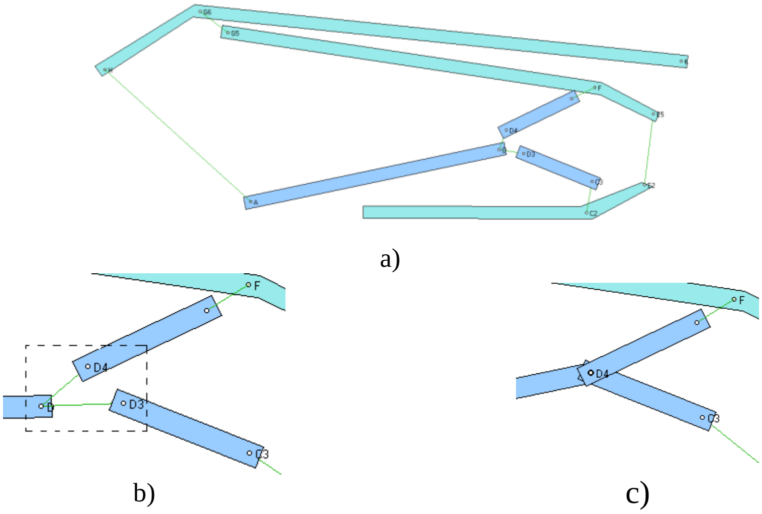

Figure 6 a) Built kinematic elements with connecting points, placed in position to apply the geometric constraints; b) applying constraints between kinematic elements (selection of the points); c) the created constraint between the kinematic elements

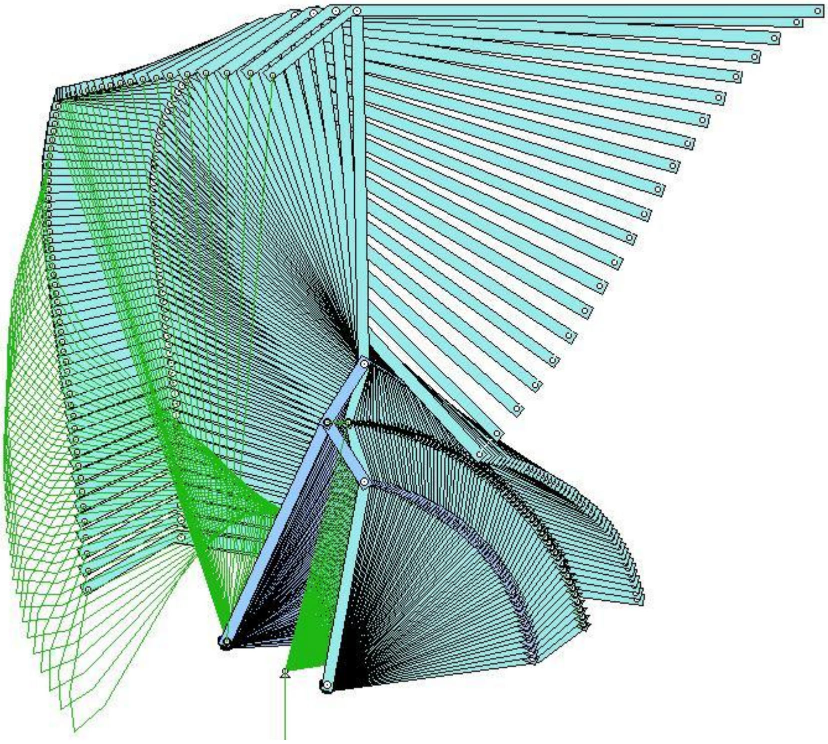

Fig.7 The workspace of the self erecting crane while erecting

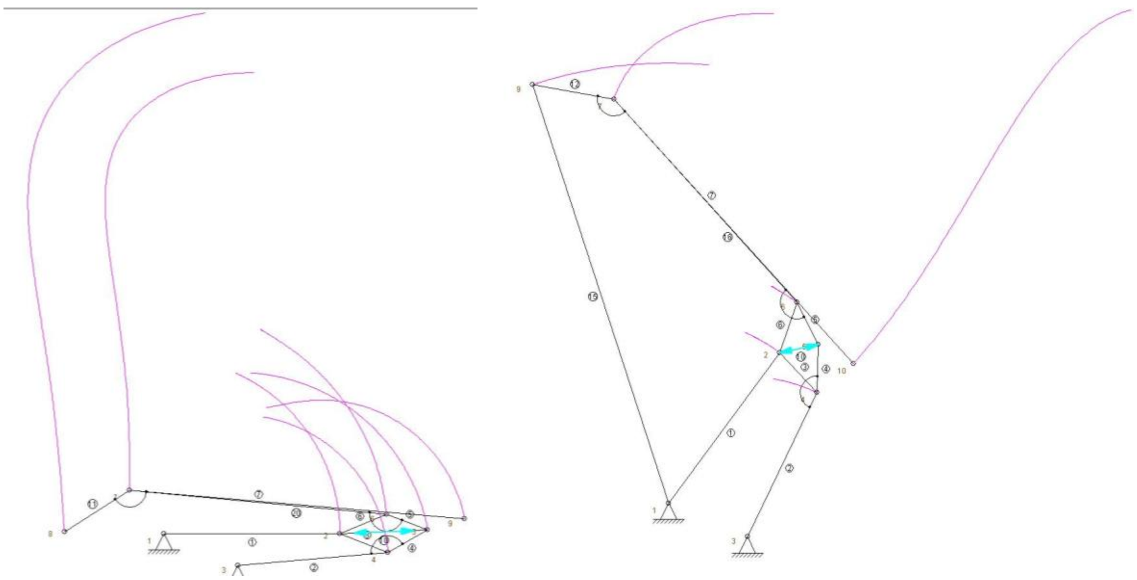

a) b)

Fig.8 Paths of the characteristic points a) first stage of erection while the boom remains aligned with the tower; b) second stage of erection when the backstay is fully stretched and the boom is detaching from the tower

4. CONCLUSION

Regarding the first method, a program written in a high level programming language using analytical equations deducted by the authors, the following conclusions arise:

- This method allows configuring any type of plane mechanism since it can be separated in fundamental structures like (dyads)

- Is very precise because of the analytical equations; eventual errors may exist solely by the CPU precision (negligible).

- Assumes a laborious work in order to determine the analytical equations before the program is written;

- For any mechanism the transfer function can be determined in analytical way.

In case of the dedicated software for 2D mechanisms some conclusions arise:

- The 2D model is built fairly easy;

- The equations system which describes the motion of the mechanism is solved numerically, and the precision of the results is influenced by the precision of the numerical method to solve the system;

- Not any plane mechanism can be studied but only those for which the software has defined the types of kinematic elements and constraints; For example in the figure 7 the software allows adding wires (ropes), which is a very important feature in studying this type of mechanisms (self erecting cranes) while the second doesn't allow the use of wires, thus the study must be completed in stages, which can be a serious problem for more complicated mechanisms with a higher number of wires (in this case is only one wire).

- The results are obtained easy;

5. REFERENCES

[1] Raicu , A - Mecanisme I.C.B. 1980

[2] *** - Flyer self erecting tower crane ELBA Germany

[3] *** - " Optimizarea parametrilor cineto-statici ai mecanismului de pliere depliere a macaralei turn de 7,5 tm ", Grant 59/1991

HEAVY MACHINERY - HM 2011, 33-36
ISBN 978-86-82631-58-3

Paper accepted: 20.05.2011

Improving The Information Accuracy In Building And Road Machines

A. Poliarus[1], E. Poliakov[1, *]
[1] Mechanical Faculty, Kharkov National Automobile and Highway University, Kharkov, Ukraine

This article presents a new method for improving the reliability of data measurements while testing building and road machines.

Keywords: sensor, inverse problems, genetic algorithm.

0 INTRODUCTION

Various important parameters of building and road machines are measured in testing with using different sensors. Many sensors are inertial, therefore their output characteristics of signals can differ greatly from the input ones. Consequently, there are conditions for making wrong decisions on test results and doubts on the accuracy of information obtained. Thus, we might estimate both output and input signal characteristics of the sensor.

1 PROBLEM SOLVING

Similar problems relate to inverse problems [1,2]. We assume that a signal is exactly known at the output of the sensor and the impulse response or transfer characteristic of this sensor is unknown. In this formulation, the problem of input signal estimation is unsolvable. Therefore, we shall use a priori information about some characteristics of a sensor. In particular, we believe that the form of sensor impulse response could be written as function of the general form, for example,

$$h(t) = \begin{cases} \dfrac{k}{\lambda}\left(\dfrac{t}{\lambda}\right)^{k-1} e^{-\left(\frac{t}{\lambda}\right)^k}, & t \geq 0, \\ 0, & t < 0, \end{cases} \tag{1}$$

where λ, k - the unknown parameters that characterize the shape of the impulse response.

Random input signal can be expanded into a Karhunen - Loeve series [3]. An individual realization of the input signal with n-dimensional representation

$$x(t) = \sum_{i=1}^{n} a_i \psi_i(t). \tag{2}$$

In expression (2) random coefficients a_i of this series are unknown, functions $\psi_i(t)$ create an orthonormal basis and are selected by the researcher.

The realization of the output signal of linear transducer

$$y(t) = \int_{-\infty}^{\infty} h(\tau)x(t-\tau)d\tau + n(t), \tag{3}$$

where $h(t)$ - the impulse response of the sensor, and $n(t)$ - an additive random process (noise), which we assume as white Gaussian noise.

Taking into account (1) and (2) the expression (3) can be written as

$$y(t) = \int_{-\infty}^{\infty} h(\tau)\sum_{i=1}^{n} a_i \psi_i(t-\tau)d\tau + \\ +n(t). \tag{4}$$

In expression (4) we know the output signal $y(t)$ and functions $\psi_k(t)$. This expression includes n +2 unknown parameters, and among them n coefficients are random. Their number is possible to reduce in case when the form of an input signal $x(t)$ is simple.

In the mathematical formulation the problem of the unknown coefficients evaluation comes to the problem of minimization of the functional

*Corr. Author's Address: Mechanical Faculty, Kharkov National Automobile and Highway University, Kharkov, Ukraine, Eug_P@mail.ru

$$J(a_1,...,a_n,...)=\int_{-\infty}^{\infty}[y(t)-$$
$$-\int_{-\infty}^{\infty}h(\tau)\sum_{i=1}^{n}a_i\psi_i(t-\tau)d\tau-n(t)]^2dt \qquad (5)$$

for each realization of the output signal and noise. Realization of noise is computer simulated. The expression (5) contains difference between the known output signal and its approximation represented by the sum.

The problem of the functional (5) minimization with a large number of unknown coefficients a_i can be solved by using of global random search methods, e. g. a genetic algorithm. By means of this algorithm we obtained all necessary coefficients and actually solved the problem of sensor identification (evaluation of sensor impulse response), as well as the problem of "blind" signal processing, i. e. evaluation of signal at transducer input.

Let's show the validity of the proposed method. For this purpose, we shall use the mathematical model of the sensor (1) and the example of input signal realization (Figure1), that we can consider as a standard one for this problem.

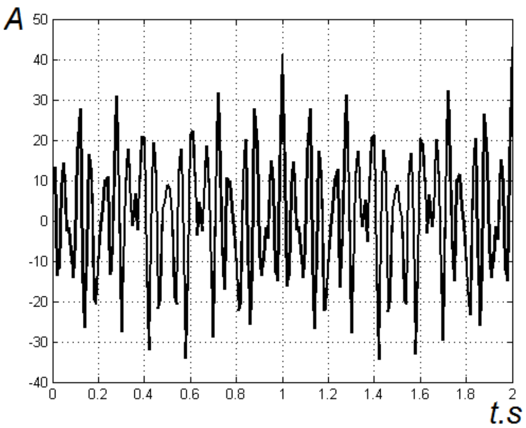

Fig. 1. *The example of input signal*

As an orthonormal functions, we choose the trigonometric functions by analogy with a generalized Fourier series. In this case, it is easy to determine the coefficients of series (2). An output signal $y(t)$ is computed by using the convolution equation, and then the inverse problem of the coefficients evaluation is solved. These coefficients, as we have shown, are known because they describe the standard input signal.

As the integral characteristic of the receiving results validity we used the angle in a functional space between a given function $x(t)$ and recalculated signal $x_r(t)$ [5].

$$\varphi=\arccos\frac{\int_{-\infty}^{\infty}x(t)x_r(t)dt}{\sqrt{\int_{-\infty}^{\infty}x^2(t)dt}\sqrt{\int_{-\infty}^{\infty}x_r^{\,2}(t)dt}}. \qquad (6)$$

Minimizing of the functional (5) was carried out by using a genetic algorithm. After finding the global minimum of (5) we determined the coefficients in the Karhunen-Loeve expansion and parameters of the impulse response (1) and then defined the realization of the input signal. Consequently, it was possible to determine the angle between the signal obtained and the given one. Depending on the signal-noise ratio, this angle is changed as shown in Figure 2.

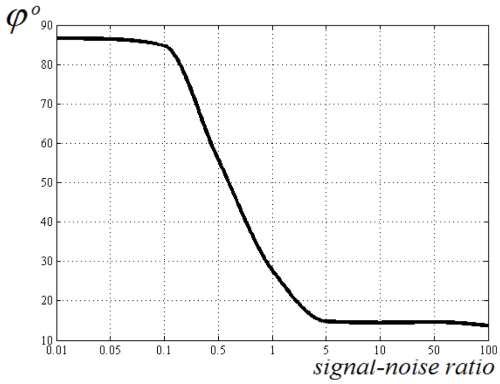

Fig. 2. *Dependence of the angle between the input signal realization and the recalculated signal on signal-noise ratio*

Similarly, the angle between the known and the recalculated sensor impulse response is represented in Figure 3.

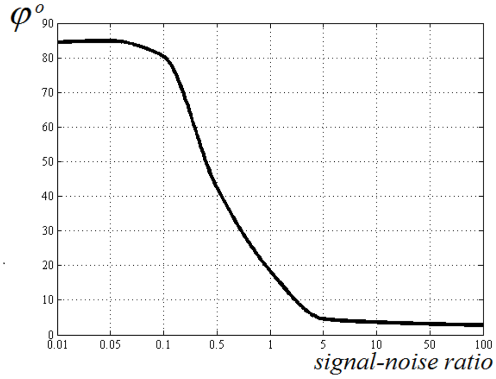

Fig. 3. *Dependence of the angle between the known and the recalculated sensor impulse response on signal-noise ratio*

Thus, for sufficiently accurate reconstruction of the signal at the input of sensor signal to noise ratio should exceed the value of about five.

Calculation accuracy is also largely depended on the correct choice of the coefficient number to describe the unknown input signal and sensor impulse response as shown in Figures 4, 5.

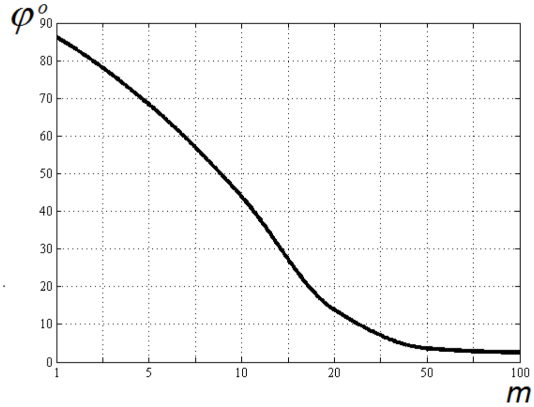

Fig. 4. *Dependence of the angle between the input signal realization and recalculated signal on the number of random coefficients*

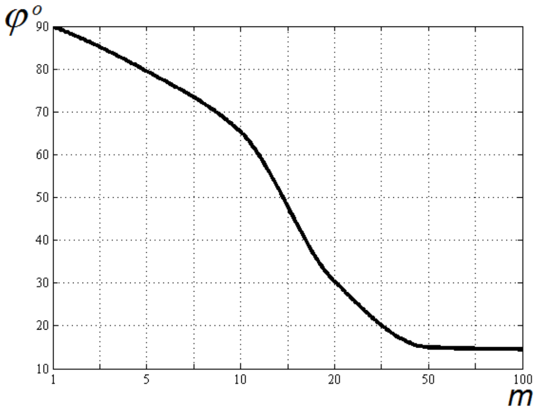

Fig. 5. *Dependence of the angle between the known and recalculated impulse response of the sensor on the number of random coefficients*

Computation time of sensor impulse response and realization of the input signal depends on many factors. They include the complexity of the input signal and the impulse response form as well as a priori information about them. The increasing number of coefficients leads to longer computation time (Figure 6).

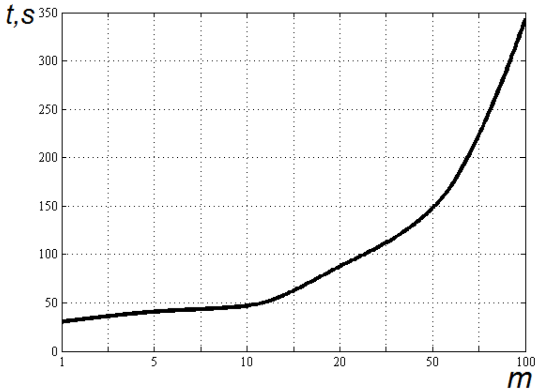

Fig. 6. *Dependence of the calculation time on the number of random* coefficients

Thus, the simulation results show a high level of accuracy of the input signal reconstruction and the sensor impulse response. However, it takes some time because of the features of stochastic search of the extremum in genetic algorithms. It complicates the application of the method in real work of building and road machines. To improve the accuracy of calculations we must have a priori information about the form of the impulse response of the sensor.

2 REFERENCES

[1] Горячкин, О. В. Методы слепой обработки сигналов и их применение в системах электросвязи [Текст] / О. В. Горячкин. - // Электросвязь. - 2006. - N 7. - С. 22-24.

[2] Abed-Meraim, K. Blind System Identification [Текст] / K. Abed-Meraim, W. Hua, Y. Liu // IEEE Proceeding. - 1997. - vol.85. – P.1308-1322

[3] Френкс Л. Теория сигналов. М.: Сов. радио, 1974. – 344с.

[4] Mitsuo Gen, Runwei Cheng. Genetic algorithms and engineering optimization- New York: A Wiley-Interscience Publication, 2000. – 495 p.

[5] И. И. Гихман, А. В. Скороход, Введение в теорию случайных процессов.- М.: Наука, 1965.

HEAVY MACHINERY - HM 2011, 37-42
ISBN 978-86-82631-58-3
Paper accepted: 31.05.2011

Fuzzy-Neural Approach to Modeling a Tower Crane

Elizabeta Lazarevska[1,*] - Jovan Trpovski[2]
[1] Faculty of Electrical Engineering and Information Technologies – Skopje, Karpos II b.b., 1000 Skopje, Macedonia
[2] "Makpetrol" A.D. – Skopje, Mito Hadzivasilev - Jasmin 4, 1000 Skopje, Macedonia

The paper presents a method for modelling a tower crane based both on fuzzy logic and artificial neural network techniques. In the adopted approach the tower crane is treated as multi-degree-of-freedom robot and modelled as such. While the direct kinematics of the mechanism can be modelled with ease by the same approach, the paper focuses on the much more interesting inverse kinematics task and presents a fuzzy model of the inverse kinematics of the tower crane as a 4 DOF robotic mechanism. The fuzzy model employs a neural network learning algorithm based on M. E. Tipping's relevance vector machines. The model can be successfully used for simulation of tower crane movements and for effective control design of its operations. Although the operator-less robotic cranes are not yet a reality, the conducted research is another step towards this ultimate goal of creating fully automated robotic cranes that can operate without human intervention.

Keywords: Tower crane, robotic crane mechanism, inverse kinematics model, fuzzy-neural modelling, relevance vector machine.

1 INTRODUCTION

Tower cranes are a common sight at any major construction site. They often rise hundreds of feet into the air, and can reach out just as far. K-10000 tower crane by KROLL GIANT TOWER CRANES with 100 tons lifting capacity at 100 meters radius is at the present by far the largest tower crane in the world [1]. Being fixed to the ground on a concrete slab, tower cranes posses the ability to carry greater loads and reach greater heights due to increased stability in comparison to the mobile cranes and are used in construction of tall buildings for lifting steel, concrete, large tools like acetylene torches and generators and a wide variety of other building materials. Some estimation is that currently more than hundred thousand tower and other type cranes are engaged in the construction industry worldwide, being responsible for a large portion of construction activities. Hence, the use of the tower crane may have a direct impact on the overall productivity of the building project.

There are several major motivations for studying the behaviour and motion of a tower crane in operation, such as: lowering the construction costs, improving the safety issues in the construction processes, improving significantly the efficiency of crane utilisation by optimizing its movements and operation etc. For example, safety is a very critical issue in every construction process. Each crane accident not only means human and/or material losses, but also increases the construction budget due to project delays, cost of insurance, lawsuits, and could be easily prevented or greatly reduced by careful planning of cranes operation. Equally important is the efficiency of crane utilization, which can be considerably improved by carefully planning and optimizing the moving path, thus eliminating the wasted time due to inefficient operation. All this can be supported by successful modelling of the crane movement and operation.

Fig.1. A tower crane [2]

*Corr. Author's Address: FEIT–Skopje, P Box 574, 1000 Skopje, MK, elizabeta.lazarevska@feit.ukim.edu.mk

Some of the previous research work in the field of modelling, simulation and control of tower cranes includes [3] and [4], where mathematical models of construction cranes have been developed for estimating total building times. Others, such as [5] and [6], deal with visualisation of crane operations, giving 3D crane models in virtual environment. More recent papers introduce the more advanced modelling and simulation methods such as fuzzy modelling, neural networks and genetic algorithms, [7] and [8].

The model of a tower crane motion presented in this paper is based on [9]. The paper is organized as follows. Section 2 introduces the fuzzy inference system with a relevance vector learning mechanism used for modelling the tower crane inverse kinematics. Section 3 gives the simulation results which demonstrate the effectiveness of the model. The conclusion is given in Section 4.

2 FUZZY MODELING THE INVERSE KINEMATICS OF A TOWER CRANE

The modelling process employs the idea that a tower crane can be treated as 4 degrees-of-freedom (4 DOF) robotic arm [10]. In this way, the tower crane can be presented as in Fig.2, where each degree of freedom of the arm corresponds to one movable part of the crane. The robotic arm joint variables are: θ_1 - representing the rotation of the crane's jib, d_2 - representing the crane's trolley radial movement, d_3 - representing the lowering or rising of the crane's hook and θ_4 - representing the rotation of the hook. According to Denavit-Hartenberg convention, the direct kinematics of the robotic arm in Fig.2 is given by the following transformation matrix:

$$\mathbf{T} = \begin{bmatrix} C_1C_4 + S_1S_4 & S_1C_4 - C_1S_4 & 0 & -d_2S_1 \\ S_1C_4 - C_1S_4 & -C_1C_4 - S_1S_4 & 0 & d_2C_1 \\ 0 & 0 & -1 & d_3 \\ 0 & 0 & 0 & 1 \end{bmatrix} \quad (1)$$

where:

$$\begin{aligned} C_1 &= \cos(\theta_1), S_1 = \sin(\theta_1) \\ C_4 &= \cos(\theta_4), S_4 = \sin(\theta_4) \end{aligned} \quad (2)$$

Knowing the values of the joint variables θ_1, d_2, d_3 and θ_4, one can always determine the position and orientation of the crane's hook according to (1), which is the direct kinematics task. In other words, the direct kinematic model of a robotic arm describes the relationship between the joint positions and the position of the robot's hand. On the other hand, the inverse kinematics of the robotic arm allows one to determine the values of the arm joint variables that secure given position and orientation of the robot's hand, that is – the crane's hook. This is much more interesting problem, because it allows the robotic arm i.e. the crane to fulfil given operational task. Namely, in order to place the robotic arm in a certain position, or to force it to follow a certain trajectory, the robotic arm control system must always know the exact values of the arm joint movements that will provide the desired position and orientation of the crane's hook. On the basis of these values, it then determines the forces and torques that are to be applied to the arm joints to secure the necessary joint movements.

Although lengthily, computation of the direct kinematic model is methodical and always leads to a single solution. In contrast to the direct kinematics model, computation of the inverse kinematic model may be highly complex and may yield multiple solutions.

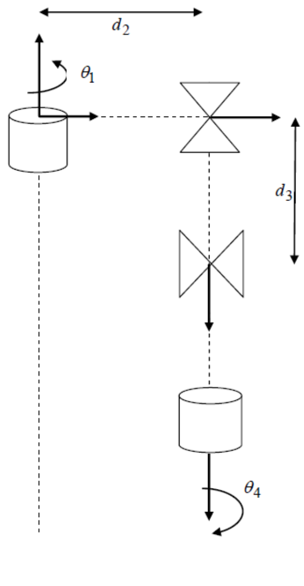

Fig.2 – 4 DOF Robotic arm

In order to surpass the mentioned difficulties accompanying computation of the inverse kinematic model of the robotic arm in Fig.2, a fuzzy inference system for modeling of nonlinear dynamic systems based on input and output data measurements with noise is applied, as proposed in [9]. The structure of this fuzzy system is the same as that of the Takagi-Sugeno (TS) fuzzy model. However, its fuzzy rules and parameter values of membership functions are automatically generated using the extended relevance vector machine (RVM).

The fuzzy inference systems (FIS) alone are very effective for modeling of nonlinear dynamic systems. However, FIS based only on human expertise does not always posses sufficient accuracy in the case of complex and uncertain systems. Therefore, neuro-fuzzy modeling acquiring knowledge from a given input-output data has been actively investigated and applied. Neural Networks (NN) have also proven to be a powerful tool in the field of system modeling. Thanks to interdisciplinary studies, reliable training methods have been developed. Despite many of these advances, there still remain a number of weak points such as difficulty of choosing the number of hidden units, over-fitting problem, existence of local-minima solutions etc. In order to overcome those difficult problems, further research has been conducted in order to determine the appropriate structure of a neuro-fuzzy model that can perform good generalization. This has been attempted by introducing additive noise to the training samples and applying statistical approach methods [11]. Particularly, major breakthrough is achieved with a class of NN called support vector machine (SVM), developed within the area of statistical learning theory [12]. SVM has many advantages, such as nonexistence of local minima solutions, automatically choosing model complexity (e.g. number of hidden units), possessing good generalization performance and so on. SVM expresses predictions in terms of a linear combination of kernel functions centered on a subset of the training data, known as support vectors (SV). The SVM has been used in various applications and has delivered good performance such as obtaining the neural network nodes or fuzzy rules based on given error bound. Therefore the SVM has become widely established as one of the leading approaches to machine learning. However, despite its widespread success, the SVM suffers from some important limitations, one of the most significant being that it makes point predictions rather than generating predictive distributions. Therefore Tipping [14] has formulated the relevance vector machine (RVM), a probabilistic model whose functional form is equivalent to SVM. It provides a full predictive distribution requiring substantially fewer kernel functions. The RVM not only does not suffer from the SVM disadvantages, but above all, it has shown a comparable generalization performance and accuracy to the SVM, with a fewer kernel functions than the SVM.

The RVM has a probabilistic Bayesian learning framework based on a kernel- estimation method. It acquires relevance vectors and weights by maximizing a marginal likelihood. The structure of the RVM is described by the sum of products of weights and kernel functions. Given an input-output data set $\{\mathbf{x}_n, y_n\}$ $(n=1,2,\ldots,N)$, where $\mathbf{x}_i=[x_1^i, x_2^i, \ldots, x_m^i]$ is an input variable of dimension *m*, and assuming that the outputs $y_i(i=1,2,\ldots,n)$ are independent and contaminated with mean-zero Gaussian noise ε_n with variance σ^2:

$$y_n=\varphi(\mathbf{x}_n;\mathbf{w})+\varepsilon_n \tag{3}$$

the RVM without a bias term can be represented as follows:

$$\varphi(\mathbf{x};\mathbf{w})=\sum_{i=1}^{N} w_i K(\mathbf{x},\mathbf{x}_i) \tag{4}$$

N being the length of the data set, $\mathbf{w}=[w_1 \quad w_2 \quad \ldots \quad w_N]^T$ being the weight factor, and $K(\mathbf{x},\mathbf{x}_i)$ being a kernel function. The adopted TS fuzzy model with fuzzy if-then rules can be represented as:

$$\begin{aligned}
&R1: If\ x_1\ is\ K(x_1, x_{11}^*) and \cdots and\ x_D\ is\ K(x_m, x_{1m}^*)\\
&then\ f_1 = a_{10}+a_{11}x_1+\cdots+a_{1m}x_m\\
&R2: If\ x_1\ is\ K(x_1, x_{21}^*) and \cdots and\ x_m\ is\ K(x_m, x_{2m}^*)\\
&then\ f_2 = a_{20}+a_{21}x_1+\cdots+a_{2m}x_m\\
&\qquad\vdots\\
&Rn: If\ x_1\ is\ K(x_1, x_{n1}^*) and \cdots and\ x_m\ is\ K(x_m, x_{nm}^*)
\end{aligned} \tag{5}$$

where n is the number of fuzzy rules, m is the dimension of input variables, $x_j\,(j=1,2,\ldots,m)$ is an input variable, f_i is the i-th local output variable, $K\left(x_j, x_{ij}^*\right)\,(i=1,2,\ldots,n;\ j=1,2,\ldots,m)$ is a fuzzy set and a_{ij} is a consequent parameter.

The structure of the adopted FIS using RVM is shown in Fig.3 and it consists of five layers. From the first layer input variables are distributed to the next layer. In the second layer the distributed input space is nonlinearly projected into feature space using kernel functions. Each kernel function corresponds to one fuzzy set. Although different types of kernel functions can be used, such as polynomial, triangular, bell, trapezoidal etc., Gaussian kernel function is adopted since it allows the exact computation of the center and variance of predictive distribution:

$$K\left(x_j, x_{ij}^*\right) = \exp\left[-\frac{\left(x_j - x_{ij}^*\right)^2}{2\theta_{ij}^2}\right] \tag{6}$$

where x_{ij}^* is the relevance vector (RV), θ_{ij} is called a kernel parameter, n is the number of RVs and $i=1,2,\ldots,n;\ j=1,2,\ldots,m$. After all, this kernel function becomes a Gaussian membership function in the proposed FIS, $K\left(x_j, x_{ij}^*\right)$ is the grade of membership of x_j and x_{ij}^* and θ_{ij} are, respectively, the center and variance of the Gaussian membership function of the j-th dimensional term of i-th input variable x_i. The relevance vector learning algorithm plays a role of a fuzzy inference engine finding the number of fuzzy rules in the FIS. The Layer 1 and 2 are related to the antecedent part of the FIS. In Layer 3 the normalized weight β_i of each fuzzy rule (node) is computed as follows:

$$\beta_i = \frac{K\left(\mathbf{x}, \mathbf{x}_i^*\right)}{\sum_{k=1}^{n} K\left(\mathbf{x}, \mathbf{x}_k^*\right)};\ K\left(\mathbf{x}, \mathbf{x}_i^*\right) \geq 0;\ \sum_{k=1}^{n} K\left(\mathbf{x}, \mathbf{x}_k^*\right) > 0 \tag{7}$$

while in Layer 4 it is multiplied by i-th local output variable f_i of the TS fuzzy model. In Layer 5 defuzzification using the center of gravity method is performed for the overall output of the fuzzy model and each node corresponds to one output variable $f(\mathbf{x})$. Through the generalization strategy of the RVM, the built neuro-fuzzy model estimates the noise of the system and determines fuzzy rules and parameters of membership functions automatically.

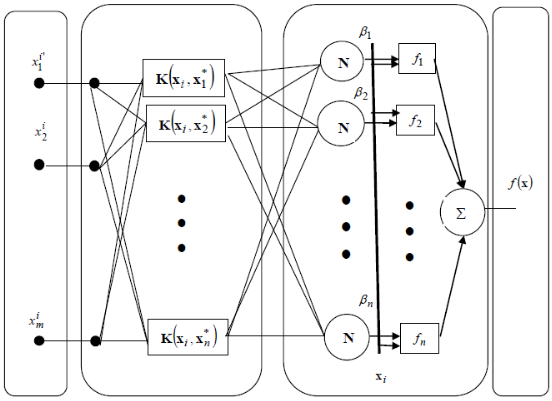

Fig.3. Structure of the FIS using RVM

3 MODELING AND SIMULATION RESULTS

The training input output data are obtained from the relationship between the input variables $(\theta_1, d_2, d_3, \theta_4)$ of joint angles and the output variables (p_x, p_y, p_z) defining position of the modeled system:

$$\begin{aligned} p_x &= -d_2 \sin(\theta_1) + \varepsilon \\ p_y &= d_2 \cos(\theta_1) + \varepsilon \\ p_z &= d_3 + \varepsilon \end{aligned} \tag{8}$$

where ε is a Gaussian noise with zero mean and variance $\sigma^2 = 0.05^2$. Total of 400 input output pairs were used, divided in two data subsets. The first subset of 200 input output data were used for training the FIS and the rest were used as test data. The built FIS model has the following fuzzy IF-THEN rules:

$$\begin{aligned} &R_i : \mathit{If}\ x_1\ \mathit{is}\ K\left(x_1, x_{i1}^*\right) \mathit{and} \cdots \text{and}\ x_m\ \mathit{is}\ K\left(x_m, x_{im}^*\right) \\ &\quad \mathit{then}\ f_i = a_{i0} + a_{i1}x_1 + \cdots + a_{im}x_m \\ &\qquad\qquad i = 1,2,\ldots n \end{aligned} \tag{9}$$

After the simulation from the training input data, the built FIS generates 10, 5 and 14 RVs $\left(\mathbf{x}_i^*\right)$ for the three outputs defining θ_1, d_2 and d_3, so that it has 10, 5 and 14 rules. To analyze the performance of the FIS, the model error is defined as average square of the difference between original system and fuzzy model output:

$$e = \frac{\sum_{n=1}^{N} \left[y_n - f(x_n) \right]^2}{N} \tag{10}$$

Two steps of the learning process – at the beginning and at the end are presented in Fig.4 and Fig.5.

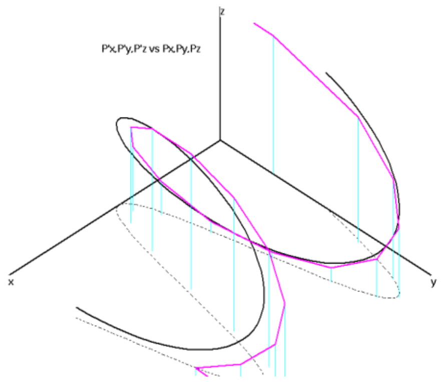

Fig.4. Comparison between the actual system and its model at the beginning of the learning process

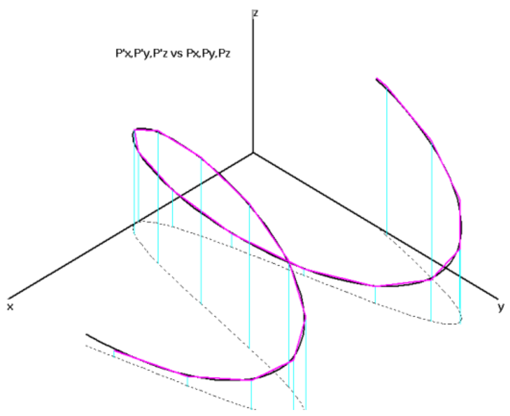

Fig.5. Comparison between the actual system and its model at the end of the learning proces

4. CONCLUSION

The simulation results showed the following errors: $e_1 = 0.000033$ for θ_1, $e_2 = 0.00001$ for d_2 and $e_3 = 0.004337$ for d_3, thus proving the built FIS effective in modeling the chosen system. The main advantages of the RVM learning algorithm are: the ability to provide accurate prediction model with fewer basis functions, automatic estimation of "nuisance" parameters, and the facility to utilize arbitrary basis functions. Further simulations are in progress in order to apply the model on different actual systems.

REFERENCES

[1] http://www.towercrane.com
[2] http://www.arthursclipart.org/machines/
[3] Gray, C. "*Buildability - The Construction Contribution: Occasional Paper No29*", Chartered Institute of Building, 1983
[4] Furusaka S. and Gray C., "A model for the Selection of the Optimum Crane for Construction Sites", *Construction Management and Economics*, Vol.2, No. 1, 1984, pp.157-176
[5] Lipman R.R. and Reed K.A., "Using VRLM in Construction Industry Applications, *Web3D: VRLM 2000 Symposium Proceedings*, Monterey, California, 2000, pp.1-7
[6] Chui, M. L. "A Virtual Reality Environment for Construction Simulation", *Proceedings of the 17th IAARC International Symposium on Automation and Robotics*, Taipei, Taiwan, 2000, pp.1147-1152
[7] Li X. H., Zhou J., Zhang Y. and Day L., "Fuzzy Optimal Design of Tower Crane Jib", *Advanced Material Research*, Vol.199-200, 2011, pp.530-533
[8] Tam C. M. And Tong T.K.L., "GA-ANN Model for Optimizing the Location of Tower Crane and Supply Points for High-rise Public Housing Construction", *Construction Management and Economics*, Vol. 21, No. 3, 2003, pp. 257-266
[9] Jongcheol K., Yasuo S. and Sangchul W., "A New Approach to Fuzzy Modelling of Nonlinear Dynamic Systems With Noise: Relevance Vector Learning Mechanism", *IEEE Transactions on Fuzzy Systems*, Vol. 14, No. 2, 2006

[10] Kang S. C. and Miranda E., " Planning and Visualisation for Automated Robotic Crane Erection Processes in Construction", *Automation in Construction*, Vol. 15, No. 4, 2006, pp. 398-414

[11] Vapnik, V. "*The Nature of Statistical Learning Theory*", Springer Verlag, 1995

[12] Vapnik V., Golowich S. E. and Smola A., "Support Vector Method for Function Approximation, Regression Estimation and Signal Processing", Neural Information Processing Systems, Vol.9, MIT Press, Cambridge, MA,1997

[13] Zhang H. R., Wang X. D., Zhang C. J. and Xu X. L., "Modeling Nonlinear Dynamical Systems Using Support Vector Machine", *Proceedings of the 4. International Conference on Machine Learning and Cybernetics*, Guangzhou,2005, pp.3204-3209

[14] Tipping, M. E. "The Relevance Vector Machine", *Advances in Neural Information Processing Systems 12*, Cambridge, Mass. MIT Press, 2000.

[15] Tipping, M. E. "Sparse Bayesian learning and the relevance vector machine", *Journal of Machine Learning Research*, Vol.1, 2001, pp.211-244

[16] Baudat G. and Anouar F., "Kernel-Based Methods and Function Approximation", International Joint Conference in Neural Networks, Washington D.C.

HEAVY MACHINERY - HM 2011, 43-48
ISBN 978-86-82631-58-3

Paper accepted: 20.05.2011

Modal Analysis of an Aerial Mono-cable Chair-ropeway

Radostina Petrova[1*], Silvia Dechkova[1]
[1] Faculty of Engineering and Education, Technical University of Sofia, Bulgaria

The study performs modal analysis of a span of an aerial mono-cable chair-ropeway. It investigates frequency and vibration forms of an elastic multi-body system consisting of two ending pillars, a transport rope and moving chairs inside the span. The chairs (with or without passengers) are modelled as rigid body spatial pendulums. The elastic deformation of the rope is taken into account when deriving the laws of motion. All external forces such as wind loads, motor drives, etc. are neglected. It is assumed that the rope and the chairs move with a constant velocity. The pulling force is introduced as a tensile force in the rope. The solution is based on the methods of Lagrangian mechanics, precisely Lagrange equations of the second kind. The method is represented by a numerical example of an elastic multi-body system with 15 degrees of freedom (DoFs), modelling a span of an existing double-seated chair-ropeway and simulating its motion.

The obtained results are going to be used in studying the vibrations inside the span caused by cross wind impact or vortex excitation, as well as in simulating the process of accidental stop of the ropeway. Thus, consequently, the safety and comfort of passengers could be increased.

Keywords: Aerial mono-cable ropeway, Elastic multi-body system, Lagrangian mechanics

1. INTRODUCTION

Improvements of the aerial passenger ropeways in recent years are evident in the use of new materials and technologies in the manufacturing of cabins and ropes, in automating of the operating processes at stations, in increasing security and the comfort of passengers. Moreover, taking into account environmental effectiveness and the fact that in some high-mountain regions this is the only tourist and business transport, it is easy to explain the construction of new and the annual renovation of existing ropeways.

Up to now, for the conceptual design of aerial ropeways the fundamental equations given in [1] and [2] are used. The next step is to check the dynamic behaviour of the ropeway. There are many attempts at developing mathematical models, reflecting and analysing the dynamic effects of the elastic ropeway system ([4], [5], [6], [7], etc.). The results of any numerical modelling stage are regularly compared to experimental data, collected by measuring systems similar to the ones described in [3], etc.

The goal of the presented work is to analyse the vibrations that occur in a span of a mono-cable double-chair circulating ropeway, due to the motion of the rope and the chairs, considering the deformation of the rope. The equations are obtained under the basic assumptions of the non-linear theory of cables in a dynamic scenario.

2. DESCRIPTION OF THE MECHANICAL AND MATHEMATICAL MODELS

The object of this study is a mono-cable double-chair ropeway. A scheme of a span of the described type of ropeway is shown in fig. 1. The horizontal distance between the pillars is labelled as L, the altitude between the saddles is denoted h and the horizontal distance between every two chairs is a. An elastic mechanical system comprising of two pillars, transport rope and fixed chairs is considered.

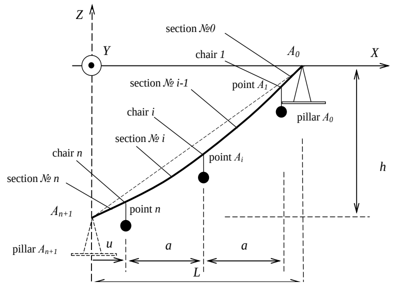

Fig. 1. *Scheme of the studied span of the aerial ropeway*

*Corr. Author's Address: Technical University of Sofia, Faculty of Engineering and Education, Bourgasko Shossee N59, Sliven 8800, Bulgaria, rpetrova123@abv.bg

The laws of motion of mechanical system are derived using Lagrange equations of II kind:

$$\frac{d}{dt}\left(\frac{\partial E_K}{\partial \dot{q}_j}\right) - \frac{\partial E_K}{\partial q_j} + \frac{\partial U}{\partial q_j} = 0 \qquad (1)$$

wherein q_j denotes the generalized coordinates, E_K denotes the kinetic energy and U is the potential energy of the whole mechanical system.

The impacts of external loads such as cross wind, vortex effect, inertia loading at starting or at braking the ropeway are ignored at this point. Motion of the system is a result of the tension force in the transport rope, which is assumed to be constant at the top of the span.

2.1. Model of a chair.

2.1.1. Geometry.

Fig. 2a shows a mechanical model of a chair in the fixed coordinate system $OXYZ$. The chair is modelled as a mathematical pendulum, whose mass is concentrated in the centre of gravity of the chair $K_i(X_{Ki}, Y_{Ki}, Z_{Ki})$. The suspending point of the chair is denoted $A_i(X_i, Y_i, Z_i)$. Point A_i labels the origin of the mobile coordinate system $A_i x_i y_i z_i$, whose axes are parallel to the corresponding immovable ones.

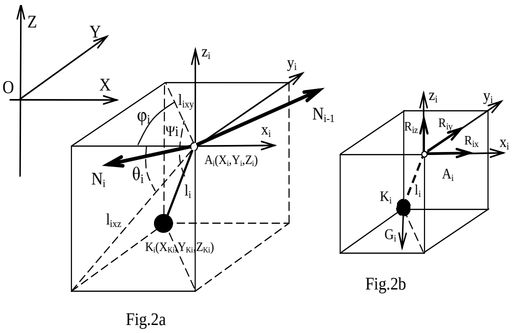

Fig. 2. *Model of chair № i*

For each chair (fig. 2a) the following symbols are introduced:

m_i - mass of the chair. This is a lump mass with three degrees of freedom. Its value is equal to the mass of the chair, including the mass of the passengers (if there are any).

l_i - distance from suspending point A_i to the centre of gravity of the chair K_i;

φ_i - angle, determining the cross oscillation of the chair. It is measured as the angle between axis x_i and projection l_{ixy} of the pendulum in horizontal plane $A_i x_i y_i$;

θ_i - angle, determining the longitudinal oscillation of the chair. It is measured as the angle between axis x_i and projection l_{ixz} of the pendulum in vertical plane $A_i x_i z_i$;

$\vec{R}_i(R_{ix}, R_{iy}, R_{iz})$- dynamic reaction and its projections in suspending point A_i of the chair (fig. 2b).

The chair is modeled as a rigid body with five degrees of freedom: three translations, that characterize the position of the chair in space - these are the coordinates of suspending point A_i in the fixed coordinate system - X_{Ai}, Y_{Ai}, Z_{Ai} and two rotations, which characterize the swing of the chair: cross oscillation (φ_i) and longitudinal oscillation (θ_i). The coordinates of the center of gravity K_i, denoted x_{Ki}, y_{Ki}, z_{Ki} in moving coordinate system $A_i x_i y_i z_i$ (fig. 2a) are:

$$\begin{aligned} x_{Ki} &= l_i \cos\psi_i \cos\varphi_i \\ y_{Ki} &= l_i \cos\psi_i \sin\varphi_i \\ z_{Ki} &= l_i \sin\psi_i \end{aligned} \qquad (2)$$

As $tg\psi_i = {|z_{Ki}|}\big/{|l_{ixy}|}$, wherein z_{ki} is the vertical coordinate of point K_i in moving coordinate system $A_i x_i y_i z_i$. Fig. 2a shows that $l_{ixy} = \frac{x_{Ki}}{\cos\varphi_i}$, wherein x_{ki} is the projection of the pendulum, modeling the chair, along axis x_i. It is assumed that φ_i is a small angle. Therefore $\cos\varphi_i \approx 1$, i.e. $tg\psi_i = \frac{|z_{Ki}|}{|x_{Ki}|}$. But as it is obvious in fig. 2a, $tg\theta_i = \frac{|z_{Ki}|}{|x_{Ki}|}$. Consequently, the angles ψ_i and θ_i are almost equal. Hence:

$$\begin{aligned} x_{Ki} &= l_i \cos\theta_i \cos\varphi_i \\ y_{Ki} &= l_i \cos\theta_i \sin\varphi_i \\ z_{Ki} &= l_i \sin\theta_i \end{aligned} \qquad (3)$$

Therefore the coordinates of the center of gravity K_i of chair №i in the fixed coordinate system are:

$$\begin{aligned} X_{Ki} &= X_{Ai} + l_i \cos\theta_i \cos\varphi_i \\ Y_{Ki} &= Y_{Ai} + l_i \cos\theta_i \sin\varphi_i \\ Z_{Ki} &= Z_{Ai} + l_i \sin\theta_i \end{aligned} \qquad (4)$$

Thus the motion of the i -th chair in space can be defined by five generalized coordinates $X_{Ai}, Y_{Ai}, Z_{Ai}, \theta_i$ and φ_i . Below, for convenience, the three translating coordinates will be denoted X_i, Y_i, Z_i .

2.1.2. Kinetic energy of a moving chair.

Kinetic energy of the i -th moving chair is:

$$E_{ki} = \frac{m_i V_{Ki}^2}{2} \qquad (5)$$

wherein m_i is the mass of the i -th chair with or without passengers and V_{K_i} is the velocity at its center of gravity, i.e. the kinetic energy of the modeled chair is:

$$E_{Ki} = \frac{m_i}{2}\begin{bmatrix} \left(\dot{X}_i - l_i\dot{\varphi}_i \sin\varphi_i \cos\theta_i - l_i\dot{\theta}_i \cos\varphi_i \sin\theta_i\right)^2 \\ + \left(\dot{Y}_i - l_i\dot{\varphi}_i \sin\varphi_i \sin\theta_i + l_i\dot{\theta}_i \cos\varphi_i \sin\theta_i\right)^2 \\ + \left(\dot{Z}_i + l_i\dot{\varphi}_i \cos\theta_i\right)^2 \end{bmatrix} \qquad (6)$$

2.2. Model of the rope

2.2.1. Tensile forces, deformation and strain in section № i of the rope

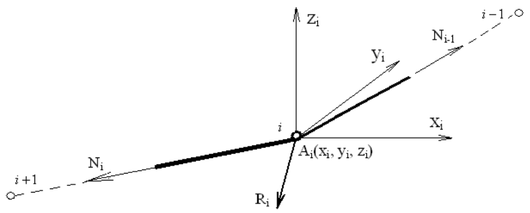

Fig. 3. *The vicinity of suspending point A_i of i - chair № i*

The potential energy of the system is calculated as only the strain energy of the rope is considered. The tensile force in the rope at the top of the span is denoted N, while its horizontal projection along axis X is T. The equilibrium of the rope in the vicinity of the suspending point A_i of the i -th chair is studied (fig. 3). N_i is the tensile force in the section between chairs №i and №$(i+1)$, and N_{i-1} is the tensile force is in the section between chairs №$(i-1)$and №i .

Projections of the tensile force N_i inside section №i are (see fig. 4a):

$$\begin{aligned} N_{ix} &= N_i \cos\beta_i \cos\alpha_i \\ N_{iy} &= N_i \sin\beta_i \\ N_{iz} &= N_i \cos\beta_i \sin\alpha_i \end{aligned} \qquad (7)$$

wherein α_i denotes the inclination angle of the projection of the deformed rope in section i in a vertical plane and β_i denotes its angle in an inclined plane shown in fig. 4a.

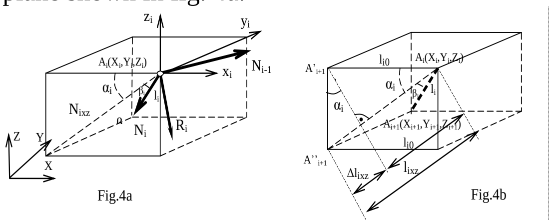

Fig. 4. *Projections of tensile force N_i in section № i*

After studying the equilibrium of the rope in the section №i between chairs №i and №$(i+1)$ (fig. 4b) and denoting the lengths of the rope before the deformation l_{i0} and after the deformation l_i, the following relation is obtained:

$$\cos\alpha_i = \frac{l_{i0}}{l_{ixz}} \qquad (8)$$

Considering the deformation of the rope in section i in vertical plane XZ , it can be written that

$$l_{ixz} = l_{i0} + \Delta l_{ixz} = l_{i0} + \left(Z_{i+1} - Z_i\right)\sin\alpha_i .$$

But as α_i is a small angle, it is accepted that $\sin\alpha_i \approx tg\alpha_i = \frac{Z_{i+1} - Z_i}{l_{0i}}$. Therefore

$$l_{ixz} = l_{i0} + \frac{\left(Z_{i+1} - Z_i\right)^2}{l_{i0}} = \frac{l_{i0}{}^2 + \left(Z_{i+1} - Z_i\right)^2}{l_{i0}} \qquad (9)$$

Thus

$$\cos\alpha_i = \frac{l_{oi}{}^2}{l_{oi}{}^2 + \left(Z_{i+1} - Z_i\right)^2} \qquad (10)$$

Similarly:

$$cos\,\beta_i = \frac{\left[{l_{oi}}^2 + (Z_{i+1} - Z_i)^2\right]^2}{{l_{oi}}^2\left[{l_{oi}}^2 + (Y_{i+1} - Y_i)^2 + (Z_{i+1} - Z_i)^2\right]} \quad (11)$$

wherein $l_i = \sqrt{{l_{oi}}^2 + (Y_{i+1} - Y_i)^2 + (Z_{i+1} - Z_i)^2}$ is the length of rope section after considering its full deflection.

We substitute (10) and (11) into (7) and obtain:

$$\begin{aligned} N_{ix} &= N_i\,\frac{{l_{i0}}^2 + (Z_{i+1} - Z_i)^2}{{l_{i0}}^2 + (Y_{i+1} - Y_i)^2 + (Z_{i+1} - Z_i)^2} \\ N_{ix} &= N_i\,\frac{(X_{i+1} - X_i)^2 + (Z_{i+1} - Z_i)^2}{(X_{i+1} - X_i)^2 + (Y_{i+1} - Y_i)^2 + (Z_{i+1} - Z_i)^2} \end{aligned} \quad (12)$$

Consequently, from (12) and from the equilibrium of point A_i (fig. 3) along axis X, i.e. $N_{ix} + R_{ix} + N_{i-1,x} = 0$ follows:

$$N_i = \frac{(X_i - X_{i-1})^2 + (Y_i - Y_{i-1})^2 + (Z_i - Z_{i-1})^2}{(X_i - X_{i-1})^2 + (Z_i - Z_{i-1})^2}\left[\left(\sum_{j=1}^{i-1} R_j\,cos\,\varphi_j\,cos\,\theta_j\right) + T\right] \quad (13)$$

for section № i .

2.2.2. Determination of the potential energy of the rope

As known, the potential energy of the rope is:

$$U = \sum_{i=0}^{n}\int_0^{l_i}\frac{{N_i}^2(x)}{2EA}dx \quad (14)$$

wherein the number of rope sections is denoted n, N_i is the tensile force in section № i, l_i is the length of the same section and EA is the tensile stiffness of the rope. Since N_i has a constant value in each section, it can be rewritten:

$$U = \sum_{i=1}^{n}\frac{N_i \Delta l_i}{2} \quad (15)$$

wherein Δl_i denotes the deformation of the section i of the rope. Then the potential energy of the entire system is:

$$U = T\sum_{i=1}^{n+1}\overline{G}_i + \sum_{i=1}^{n} R_i\,sin\theta_i\,cos\,\varphi_i \sum_{j=i+1}^{n+1}\overline{G}_j \quad (16)$$

where

$$\overline{G}_i = (Y_{i-1} - Y_i)^2 (X_{i-1} - X_i)^2\,\frac{\left[(X_{i-1} - X_i)^2 + (Z_{i-1} - Z_i)^2 + (Y_{i-1} - Y_i)^2\right]}{2\left[(X_{i-1} - X_i)^2 + (Z_{i-1} - Z_i)^2\right]^2}$$

for $i = 0 \div n$. Here n denotes the total number of the chairs inside the span and i is the consequent number of the chair. As shown in fig. 1 the coordinates of the pillars at the both sides of the span are: $A_0(X_0 = L, Y_0 = 0, Z_0 = 0)$ and $A_{n+1}(X_{n+1} = 0, Y_{n+1} = 0, Z_{n+1} = -h)$.

2.3. Model of the studied mechanical system

The motion of the rope and the chairs in the system is derived using Lagrange equations of second kind (1). The laws of motion of the mechanical system are presented by a system of differential equations of the following type:

$$[M]\{\ddot{Q}\} = \{B\} \quad (17)$$

wherein $[M]$ is the assembled mass matrix of the system. It is a striped block matrix of the type:

$$[M] = \begin{bmatrix} \overline{m}_1 & 0 & 0 \\ \cdots & \cdots & \cdots \\ 0 & \overline{m}_i & 0 \\ \cdots & \cdots & \cdots \\ 0 & 0 & \overline{m}_n \end{bmatrix}$$

The block $\overline{m}_i$ is the matrix of chair № i and is also a striped symmetric matrix of the type:

$$[\overline{m}_i] = \begin{bmatrix} m_i & 0 & 0 & -m_i l_i\,sin\varphi_i\,cos\,\theta_i & -m_i l_i\,cos\,\varphi_i\,sin\theta_i \\ 0 & m_i & 0 & -m_i l_i\,sin\varphi_i\,sin\theta_i & m_i l_i\,cos\,\varphi_i\,cos\,\theta_i \\ 0 & 0 & m_i & m_i l_i\,cos\,\varphi_i & 0 \\ -m_i l_i\,sin\varphi_i\,cos\,\theta_i & -m_i l_i\,sin\varphi_i\,sin\theta_i & m_i l_i\,cos\,\varphi_i & m_i {l_i}^2 & 0 \\ -m_i l_i\,cos\,\varphi_i\,sin\theta_i & m_i l_i\,cos\,\varphi_i\,cos\,\theta_i & 0 & 0 & m_i l^2{}_i\,cos^2\,\varphi_i \end{bmatrix}$$

The vector of all generalized accelerations for the system is a block-array of the type:

$\{\ddot{Q}_i\}^T = \left[\ddot{q}_1{}^T, \ldots\ldots \ddot{q}_i{}^T, \ldots\ldots \ddot{q}_n{}^T\right]$, wherein

$\{\ddot{q}_i\}^T = \left[\ddot{X}_i, \ddot{Y}_i, \ddot{Z}_i, \ddot{\varphi}_i, \ddot{\theta}_i\right]$

The right side of the differential system is the block-array $\{B\}^T = \left[\overline{b}_1{}^T, \ldots\ldots \overline{b}_i{}^T, \ldots\ldots \overline{b}_n{}^T\right]$, which considers the impact of the gravity and inertia forces due to the motion of the chairs. $\{\overline{b}_i\}$ is a block, related to chair № i, whose elements b_{ij}, $j = 1 \div 5$ correspond to the chosen generalized coordinates $\{q_i\}$:

$$\begin{aligned} b_{i1} &= m_i l_i \dot{\varphi}_i{}^2\,cos\,\varphi_i\,cos\,\theta_i - 2m_i l_i \dot{\varphi}_i \dot{\theta}_i\,sin\varphi_i\,sin\theta_i + m_i l_i \dot{\theta}_i^2\,cos\,\varphi_i\,cos\,\theta_i + \\ &+ TA_i - TB_i + \sum_{j=1}^{i-1} A_j R_{j-1}\,cos\,\varphi_{j-1}\,sin\theta_{j-1} - \sum_{j=1}^{i-1} B_j R_j\,cos\,\varphi_j\,sin\theta_j \end{aligned}$$

$$\begin{aligned} b_{i2} &= m_i l_i \dot{\varphi}_i{}^2\,cos\,\varphi_i\,sin\theta_i + 2m_i l_i \dot{\varphi}_i \dot{\theta}_i\,sin\varphi_i\,cos\,\theta_i + m_i l_i \dot{\theta}_i^2\,cos\,\varphi_i\,cos\,\theta_i - \\ &- TC_i - TD_i + \sum_{j=1}^{i-1} C_j R_{j-1}\,cos\,\varphi_{j-1}\,sin\theta_{j-1} - \sum_{j=1}^{i-1} D_j R_j\,cos\,\varphi_j\,sin\theta_j \end{aligned}$$

$$b_{i3} = m_i l_i \dot{\varphi}_i^2 \sin\varphi_i - TE_i + TF_i + \\ + \sum_{j=1}^{i-1} E_j R_{j-1} \cos\varphi_{j-1} \sin\theta_{j-1} + \sum_{j=1}^{i} F_j R_j \cos\varphi_j \sin\theta_j$$

$$b_{i4} = \frac{1}{2} m_i l_i^2 \dot{\varphi}_i \dot{\theta}_i \sin 2\theta_i \cos 2\varphi_i - m_i l_i^2 \dot{\theta}_i^2 \sin^2\theta_i \sin 2\varphi_i - \\ - m_i l_i^2 \dot{\varphi}_i \dot{\theta}_i \sin^2\theta_i \cos 2\varphi_i + R_i \sin\theta_i \sin\varphi_i \sum_{j=i}^{n} G_j$$

$$b_{i5} = m_i l_i^2 \dot{\varphi}_i \dot{\theta}_i \sin 2\varphi_i + m_i l_i^2 \dot{\theta}_i^2 \cos^2\varphi_i \sin 2\theta_i - R_i \cos\varphi_i \cos\theta_i \sum_{j=i}^{n} H_j$$

Here $A_i, B_i, C_i, D_i, E_i, F_i, G_i$ and H_i $i = 0 \div (n+1)$ (fig. 2) denote the following relations:

$$A_i = (Y_{i-1} - Y_i)^2 \left\{ \frac{\left[3(X_{i-1} - X_i)^2 + (Y_{i-1} - Y_i)^2 + (Z_{i-1} - Z_i)^2\right]\left[(X_{i-1} - X_i)^2 + (Z_{i-1} - Z_i)^2\right]}{2\left[(X_{i-1} - X_i)^2 + (Z_{i-1} - Z_i)^2\right]^3} - \\ - \frac{4(X_{i-1} - X_i)^2\left[(X_{i-1} - X_i)^2 + (Y_{i-1} - Y_i)^2 + (Z_{i-1} - Z_i)^2\right]}{2\left[(X_{i-1} - X_i)^2 + (Z_{i-1} - Z_i)^2\right]^3} \right\}$$

$$B_i = (Y_i - Y_{i+1})^2 \left\{ \frac{\left[3(X_i - X_{i+1})^2 + (Y_i - Y_{i+1})^2 + (Z_i - Z_{i+1})^2\right]\left[(X_i - X_{i+1})^2 + (Z_i - Z_{i+1})^2\right]}{2\left[(X_i - X_{i+1})^2 + (Z_i - Z_{i+1})^2\right]^3} - \\ - \frac{4(X_i - X_{i+1})^2\left[(X_i - X_{i+1})^2 + (Y_i - Y_{i+1})^2 + (Z_i - Z_{i+1})^2\right]}{2\left[(X_i - X_{i+1})^2 + (Z_i - Z_{i+1})^2\right]^3} \right\}$$

$$C_i = (X_{i-1} - X_i)(Y_{i-1} - Y_i)\frac{(X_{i-1} - X_i)^2 + 2(Y_{i-1} - Y_i)^2 + (Z_{i-1} - Z_i)^2}{\left[(X_{i-1} - X_i)^2 + (Z_{i-1} - Z_i)^2\right]^2}$$

$$D_i = (X_i - X_{i+1})(Y_i - Y_{i+1})\frac{(X_i - X_{i+1})^2 + 2(Y_i - Y_{i+1})^2 + (Z_i - Z_{i+1})^2}{\left[(X_i - X_{i+1})^2 + (Z_i - Z_{i+1})^2\right]^2}$$

$$E_i = (X_{i-1} - X_i)(Y_{i-1} - Y_i)^2(Z_{i-1} - Z_i)\frac{(X_{i-1} - X_i)^2 + 2(Y_{i-1} - Y_i)^2 + (Z_{i-1} - Z_i)^2}{\left[(X_{i-1} - X_i)^2 + (Z_{i-1} - Z_i)^2\right]^3}$$

$$F_i = (X_i - X_{i+1})(Y_i - Y_{i+1})^2(Z_i - Z_{i+1})\frac{(X_i - X_{i+1})^2 + 2(Y_i - Y_{i+1})^2 + (Z_i - Z_{i+1})^2}{\left[(X_i - X_{i+1})^2 + (Z_i - Z_{i+1})^2\right]^3}$$

$$G_i = (Y_{i-1} - Y_i)^2(X_{i-1} - X_i)\frac{\left[(X_{i-1} - X_i)^2 + (Y_{i-1} - Y_1)^2 + (Z_{i-1} - Z_i)^2\right]}{2\left[(X_{i-1} - X_i)^2 + (Z_{i-1} - Z_i)^2\right]^2}$$

$$H_i = (Y_i - Y_{i+1})^2(X_i - X_{i+1})\frac{\left[(X_i - X_{i+1})^2 + (Y_i - Y_{i+1})^2 + (Z_i - Z_{i+1})^2\right]}{2\left[(X_i - X_{i+1})^2 + (Z_i - Z_{i+1})^2\right]^2}$$

3. NUMERICAL EXAMPLE

The analyzed model is represented by a numerical example of a span of the chair ropeway "Sliven–Karandila". This is a mono-cable circulating aerial ropeway with fixed double-seated chairs. The number of the circulating chairs along the rope depends on seasonally-expected passenger flow.

The modeled span has a horizontal distance between the pillars $L = 160m$ and altitude between them $h = 15m$ (fig. 1). The distance between the chairs is denoted with *a* and is equal to *50m*. The speed of the rope is constant $V = 2m/s$. The data for the chairs is obtained through finite element model of a chair with or without passengers ([6]). The numerical example illustrates the oscillation of the rope in points A_i as well as transverse and longitudinal swing of the chairs. The number of chairs inside the span is equal to 3 ($i = 1 \div 3$) during the analyzed 5 seconds of the motion of the ropeway. The issued differential system is with 15 degrees of freedom.

The calculation and systematizing of the obtained numerical results and graphs has been carried out by MatLab software, special toolbox for solving dynamic problems Simulink ([8]).

Below are given the graphs of the projections of the velocities and the accelerations of the suspending points of the chairs A_i ($i = 1 \div 3$) and the angular velocities and accelerations of the chairs as functions of time.

Legend of the given graphs

chair № 1 – with no passengers

chair № 2 – with 1 passenger

chair № 3 – with 2 passengers

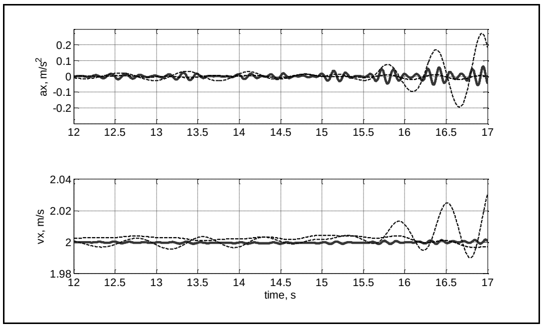

Fig. 5. *Velocity and accelaration of points* A_i *(* $i = 1 \div 3$ *) along axis X*

4. CONCLUSIONS

The presented dynamic model determines the oscillation, occurring in an aerial ropeway, as result of the motion of the rope and the chairs, when taking into account the deformation of the rope. The non-linear theory of cables is used to derive the above equations. This model is a step

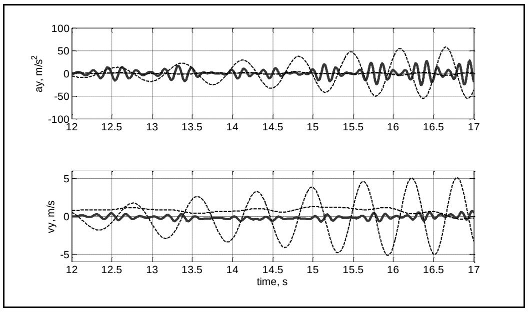

Fig. 6. *Velocity and accelaration of points* A_i *(* $i = 1 \div 3$ *) along axis Y*

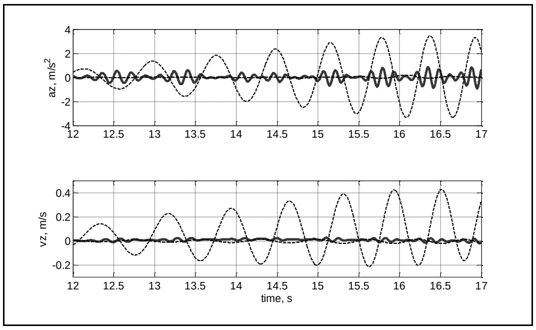

Fig. 7. *Velocity and accelaration of points* A_i *(* $i = 1 \div 3$ *) along axis Z*

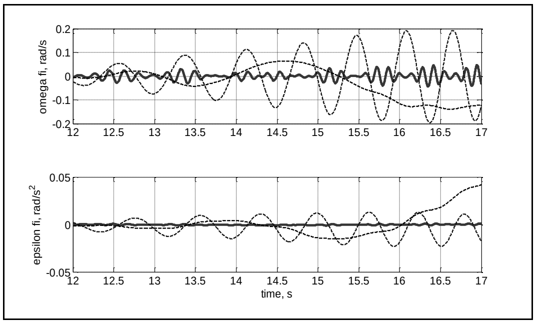

Fig. 8. *Lateral angular velocity and acceleration of chair* i *(* $i = 1 \div 3$ *) (along axis Y)*

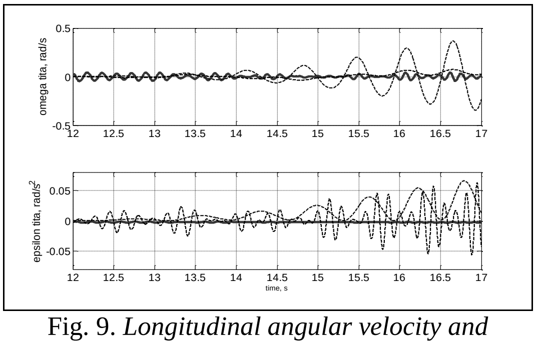

Fig. 9. *Longitudinal angular velocity and acceleration of chair* i *(* $i = 1 \div 3$ *) (along axis X)*

towards creating a dynamic model, simulating the operation of a mono-cable circulating ropeway impacted by crosswind, air turbulence behind the chairs (cabins), inertia forces at star or sudden stop, etc. This will allow the engineers when calculating similar ropeways to make numerical simulations of the dynamics of the system under different input data and to seek an optimal design solution under various criteria.

The authors believe that this study will support the efforts of designers and producers aiming to enhance the safety and comfort of the passengers and to facilitate the development of this environmental transport in tourist mountainous regions.

5. ACKNOWLEDGEMENTS

The studies are supported by project 102PD091-16/2010 of Technical University-Sofia, Bulgaria.

6. REFERENCES

[1] Czitary E., “Seilschwebebahnen”, Wien, Springer-Verlag, 1962

[2] Diviziev V., “Ropeways and cable cranes”, “Technica” Publishing House, Sofia, 1975

[3] Hoffmann Kl.,Liehl R.,“Measuring system for characterisation of the interaction between crosswind and gondola inclination of ropeways”, XVII IMEKO World Congress, Croatia, 2003

[4] Hoffmann Kl., Oscillation Effects of Ropeways Caused by Cross-Wind and Other Influences, FME Transactions Vol. 37, 2009

[5] Knawa M., Danuta Bryja, Vibrations of carrying cable of ropeway system loaded by passengers carriers modelled by series of moving pendulums, 7-th European Conference of Structural Dynamics, EURODYN 2008

[6] Petrova R., St. Karapetkov, S. Dechkova, J. Slavcheva, Modal analysis of a chair of an aerial ropeway “Sliven – Karandila”, Mechanics of Machines, №90, (in Bulgarian)

[7] Petrova R., St. Karapetkov, S. Dechkova and Pl. Petrov, ”Mathematical Simulation of Cross-Wind Vibrations in a Mono-Cable Chair Ropeway”,EASEC12–Hong Kong,2011

[8] User’s Guide for Simulink 7.6, MatLab Release 2010b, Sept. 2010

HEAVY MACHINERY - HM 2011, 49-54
ISBN 978-86-82631-58-3
Paper accepted: 30.05.2011

Construction performances of building and transport mechanization revolving support

Milomir Gašić - Mile Savković - Goran Marković - Nebojša Zdravković - Marko Nikolić[1,*]
[1]University of Kragujevac, Faculty of Mechanical Engineering Kraljevo

Different working and construction demands have conditioned the development of bonds between revolving and non-revolving constructions of building and transport mechanization machines. Solutions that have been used so far, basically represent the revolvin and non-revolving construction, carried out in the shape of ''H'' and ''X'' type. Such construction solutions do not contribute the reliable and long-term work of indirect components embedded between the revolving and non-revolving parts in the following machines:excavators, construction pole cranes, truck-cranes and portal cranes. Problem occurs due toinsufficient torsion stiffness of carrying construction, which manifests further on through unfavourable load distribution within the indirect components (big diameter bearings).

Tha paper shows the use of the above mentioned two construction types (''H'' and ''X'') as well as the other characteristic construction types in use. Besides the mentioned ones there is also a display of support surface construction to the radial-axial bearing bond, as well as the summary from the comparative analysis of ''H'' and ''X'' construction types, carried out in the paper [6].

Keywords: supporting frame, conceptions, stiffness

1 INTRODUCTION

Through development evolution of transport and building mechanization machines constructions, there have occured different construction types conditioned by their purpose. So, two basic types were extracted that have been in use so far. Namely, ’’H“ and ’’X’’ construction types, that are applied with the machines: excavators, construction pole cranes, truck-cranes and portal cranes.

According to the analysis of carried out solutions, we can see that their development happened influenced by various working and construction demands, such as:

- construction dimensions must be within certai limits in order to enable the efficient transport of machines or their segments
- construction stiffness is to be satisfactory so that the deplanation of surface on which radial-axial bearing lays should be the least possible
- maintenance and corrosion protection should cost the least possible
- construction should be simple and light and to demand small material consumption at making, etc.

We can see that the above mentioned restrictions characterize an ideal construction, and that all this is difficult to achieve. Nevertheless, such construction solution should be amed, which would be the best possible compromise between all the demands.

Due to support surface bumps, while the excavator works, it is not possible to make a full contact between caterpillar runnung gear machine and support surface, so the support structure torsion occurs, which causes the support surface deplanation of structure for radial-axial bearing bond. Long life and functionality of these bearings largely depends on support surface stifness to bearing bond.

2 DISPLAY OF EXISTING CONCEPTION SOLUTIONS AND THEIR USE

Need for carrying out different work demands regarding the use of construction mechanization conditioned great presence of revolving movement at many machine segments. Of special significance is the bond of revolving

*Corr. Author's Address: Faculty of Mechanical Engineering Kraljevo, Dositejeva br. 19, Kraljevo, Serbia, markmfkv@gmail.com.

and non-revolving parts of top and bottom building of characteristic construction machines.

Bottom building is spatial, thin-walled cast or welded steel construction which leans on moving mechanism with wheels or caterpillars. Older constructions end on their top side with a cylinder which has a toothed wheel and with a column (vertical tube) in the middle. Modern constructions end with a ring horizontal surface. Shape of upper part of bottom building depends on the shape of radial-axial bearing with toothed wheel, which is mounted on it.

Constructive shape of bottom building carrier is adapted to moving mechanism and to top building revolving mechanism.

Bottom building function is:

- to carry the load of radial-axial bearing to the base (ground),
- to provide the change of work position machine moving,
- to provide stable work position of the machine, etc.

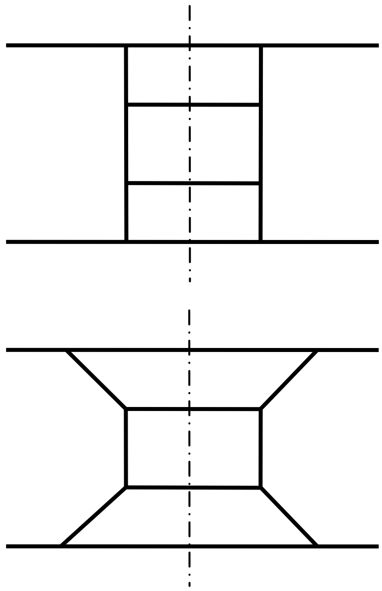

Fig. 1. *Schematic display of bottom building ''H'' and ''X'' types*

Fig. 2. *Examples of top and bottom building revolving bond use with various machines*

The biggest rise in development of constructive performances of ’’H’’ and ’’X’’ bottom building types is achieved with excavators due to its wide usage, where these conception solutions were carried out exactly for the reason of unfavorable terrain conditions. All these improvements were also applied to other machines, such as: construction pole cranes, truck-cranes and portal cranes, because support problems are of crucial significance for their proper functioning.

Some of ’’H’’ conception type performances are illustrated in Figure 3, while ’’X’’ conception type performances are illustrated in Figure 4.

Fig. 3. *Bottom building type ’’H’’*

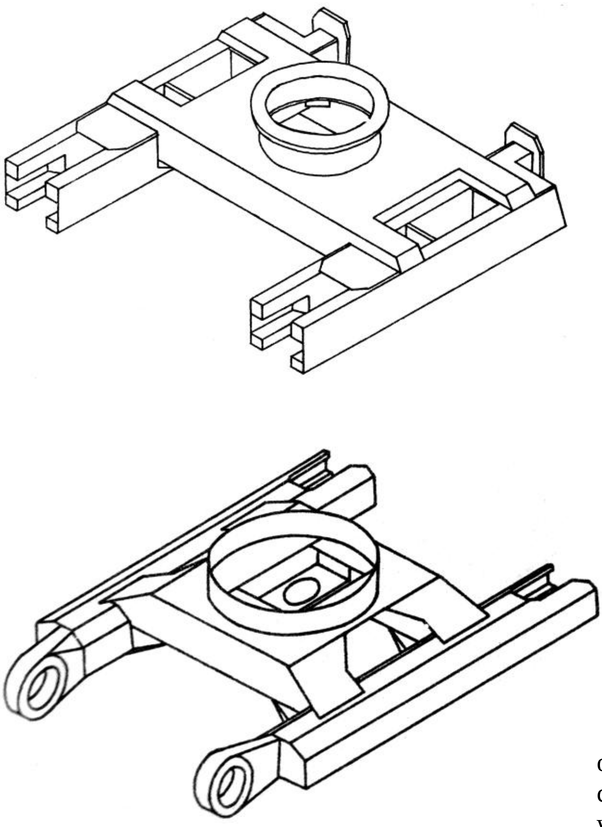

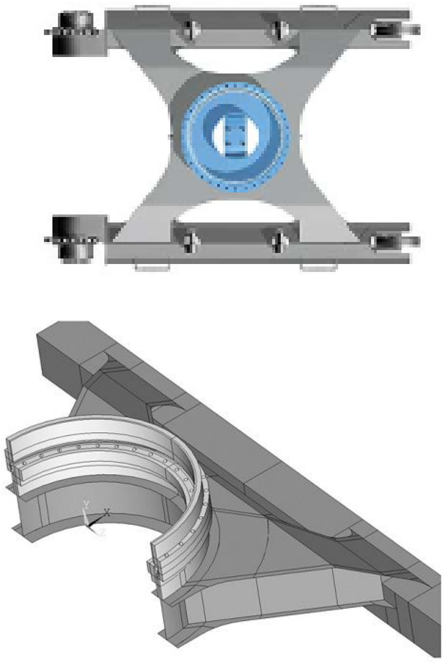

Fig. 4. *Bottom building type ’’X’’*

Besides ’’H’’ and ’’X’’ types, there are others which are most often used with truck-cranes, portal cranes and rotating excavators and whose construction is conditioned by different application demands.

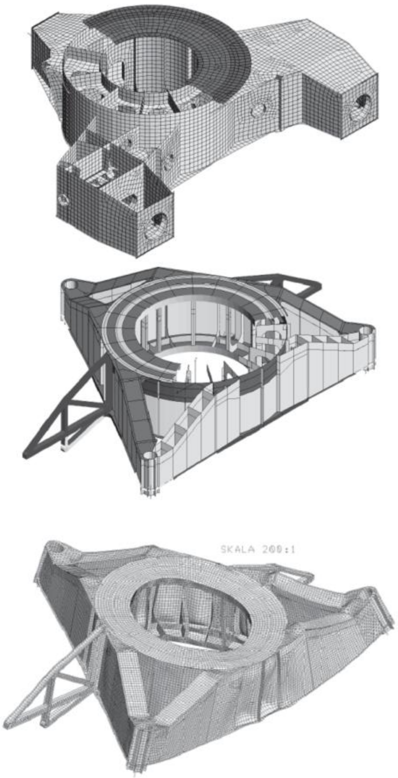

Fig. 5. *Other characteristic construction types*

Torsion stiffness of radial-axial bearing is very small. Thus, it is necessary to design a structure that will fulfill the following:

- provide the base for bearing installation
- protect from over deformation to provide the proper bearing geometry
- provide the installation of additional mechanisms (top building revolving drive mechanism, etc.).

What is common for all types of bottom building is the shape of stand where radial-axial bearing leans and it is the integral part of this construction. This stand can be made of plates by welding or casting, depending on its dimensions, complexity and economic use adaptability of all the named production procedures.

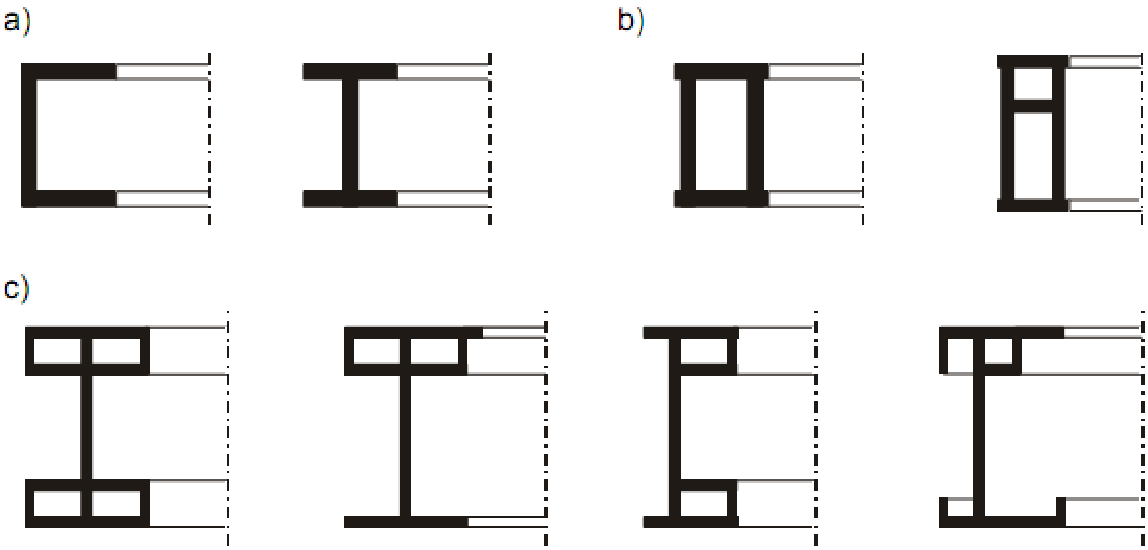

Fig. 6. Schematic display of support surfaces for radial-axial bearings bond:
a)open; b)closed; c)open– closed;

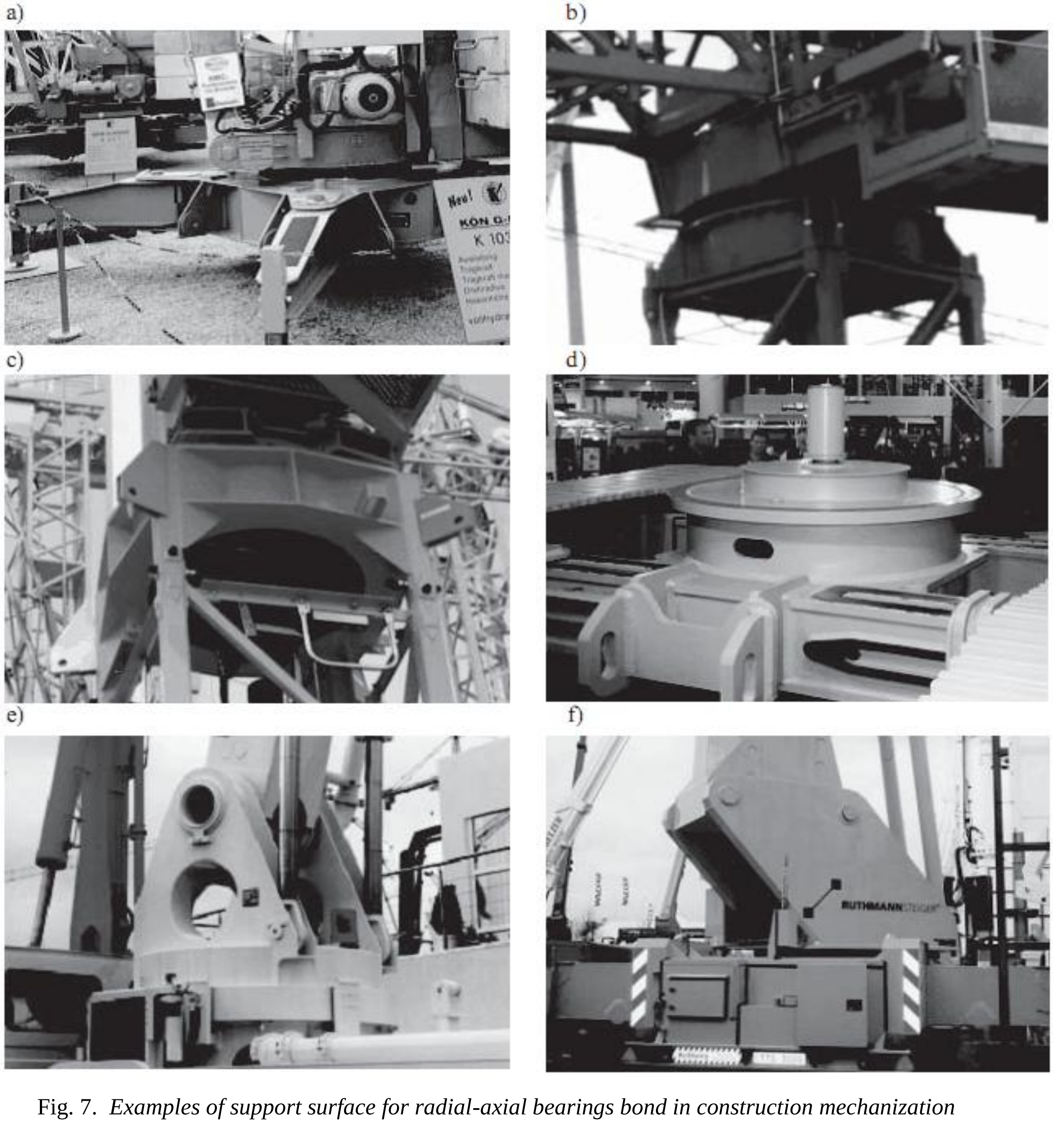

Fig. 7. *Examples of support surface for radial-axial bearings bond in construction mechanization*

3 COMPARATIVE ANALYSIS OF BOTTOM BUILDING ''H''& ''X'' STRUCTURE TYPES

The paper [6] shows comparative analysis of bottom building ''H'' & ''X'' structure types. On the ground of obtained results, the conclusion is that support structure ''H'' type is more elastic than ''X'' type, i.e. it is more adaptable to track conditions for about 15%. In practice, the percentage is even bigger.

Figure 8 shows the diagrams of load and stiffness relations in ''H'' and ''X'' types.

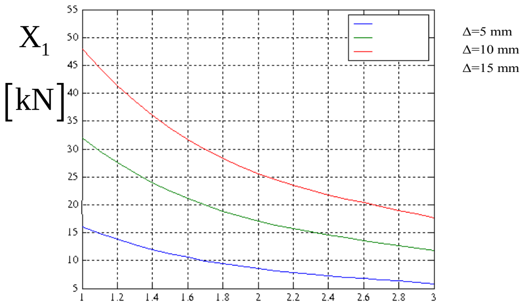

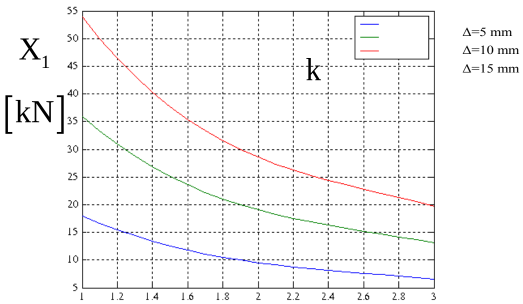

Fig. 8. *Comparative diagram of relation X_1 from quotient k for 'H'&'X'construction types*

The aim of this analysis was to show the influence of support structure shape and geometry on proper function of revolving and non-revolving machine parts bond.

4 CONCLUSION

The paper is a survey of existing bottom building structure types, as well as the support structures for radial-axial bearing bond. Also, the summary from comparative analysis of ''H'' and ''X'' structure types carried out in the paper [6] is shown.

It is clear that for proper function of revolving and non-revolving machine parts, the crucial role has the stiffness of whole bottom building structure, as well as, separately viewed, suppor surface stiffnes to radial-axial bearing bond. The whole structure stiffness and also the support surface stiffness to radial-axial bearing bond can be realized by suitable choice of geometric values and support structure shape.

5 REFERENCES

[1] Jevtić, D., Gašić, M. "The influence of relation between elements geometric dimensions of a dredger supporting structure and the connection with the rotating platform," International conference on engineering design, IECD, Dubrovnik, 1990
[2] Gašić, M., Marković, G., Savković, M. "Supplement to development of new solution of bond between revolving and nonrevolving parts of construction and transport mechanization machines," IMK 14 Research and development, 2009
[3] Gašić, M., Petrović, D. "Geometric identification of cylindric carriers of radial-axial bearings with big diameters," International conference on transport in industry, Belgrade, 1992
[4] Gašić, M., Karamarković, V., Savković, M., Marković, G. "Research and development of new solution to the connection of excavator carrying construction," International Conference -Heavy Machinery HM 2002, Kraljevo, 2002
[5] Smolnicki, T. "Fizykalne aspekty koherencji wielkogabarytowych łożysk tocznych i odkształcalnych konstrukcji wsporczych," Oficyna Wydawnicza Politechniki Wrocławskiej, Wrocław, 2002
[6] Marković, G. "Influential parameters to revolving and non-revolving parts bond in construction and transport mechanization machines",
Faculty of Mechanical Engineering Kraljevo, 2004
[7] Jovanović, M., Radoičić, G., Milić P: "Dynamic Sensitivity Research Of Portal-Rotating Cranes", XIX International Conference on "MATERIAL HANDLING, CONSTRUCTIONS AND LOGISTICS", MHCL'09, Belgrade, 2009., pp. 61- 66. ISBN 978-86-7083-672-3
[8] Jovanović, M., Milić, P., Janošević, D., Petrović, G.: Accuracy of FEM analysis in function of finite element type selection, Facta Universitatis series Mechanical Engineering 2010, Vol. 8, No. 1, Niš 2010. pp.1-10, ISSN 0354-2025

ACKNOWLEDGMENT

A part of this work is a contribution to the Ministry of Science and Technological Development of Serbia funded Project TR35038

HEAVY MACHINERY - HM 2011, 55-60
ISBN 978-86-82631-58-3
Paper accepted: 30.05.2011

The Design – in Faults as a Causes of the High Performance Machines Failures

Srđan M. Bošnjak[1,*] - Zoran D. Petković[1] - Milojević Z. Goran[1] - Vaso M. Mihajlović[1]
[1]University in Belgrade - Faculty of Mechanical Engineering

High capacities and key roles in the technological processes cause the extremely high financial losses in the case of high performance machines failures. This paper presents case studies of bucket wheel excavators, stackers and bucket chain reclaimers failures caused by design – in faults. Besides that, paper gives a redesign solutions which are developed by University of Belgrade – Faculty of Mechanical Engineering.

Keywords: High performance machines, design-in faults, redesign

0 INTRODUCTION

The high performance machines (HPM), such as bucket wheel excavators (BWE), Fig. 1, bucket chain excavators (BCE), Fig. 2, and bucket chain reclaimers (BCR), Fig. 3, are the backbones of the open pit coal mining and thermal plant mechanization systems. Their exploitation in harsh working conditions provides fertile ground for the occurrence of various types of failures [1-10]. In reference [11] it was stated that there are four main reasons for the collapse of high-capacity earthmoving and lifting/conveying machines:

- design faults, so-called ‘designing-in’ defects;
- manufacture faults causing the so-called ‘manufacturing-in’ defects;
- exploitation faults (by analogy, these causes can be named ‘operating-in’ defects);
- extreme environmental impacts – unusual occurrences (extreme storm, earthquake, fire); by analogy, these causes can be named ‘environment-in’ defects.

Common denominators to all failure of machines, particularly the HPM, are very high financial losses and serious risks to the worker’s safety and life [12]. When it comes to BWE, BCE and BCR, financial losses caused by production delays due to the principal machine failure in a surface mining system, i.e. coal storage and shipment, often significantly exceed the financial losses caused by direct material damage. The size of the negative economic effects caused by failures is remarkably revealed in the fact that the total cost of failure in USA and Europe is of order of 4% of GNP [13].

Researches presented in this paper are focused on HPM vital parts damages caused by design – in folts and their redesign.

Fig. 1. *Bucket wheel excavator SRs 1201*

Fig. 2. *Bucket chain excavator ERs 1000*

Fig. 3. *Bucket chain reclaimer Metalna 300*

*Corr. Author's Address: Faculty of Mechanical Engineering, Kraljice Marije 16, Belgrade, Serbia, sbosnjak@mas.bg.ac.rs

1 FAILURE AND REDESIGN OF THE BWE BUCKET AND BUCKET WHEEL

BWE SRs 1201.24/4, Fig. 4, was put in exploitation in 2003. During exploitation some drawbacks in buckets' leaning zones were observed, as follows:

- Damages of the pins and bushing of the bucket eyes, Fig. 4;
- Damages and plastic deformations of the bucket wheel front supporting eyes, Fig. 5;
- Plastic deformations of the bucket wheel rear supporting eyes, Fig. 6;
- Bucket "opening" in the rear support zone, Fig. 6.

In order to eliminate the presented drawbacks, it was necessary to redesign the bucket supporting zones, Figs. 7-10.

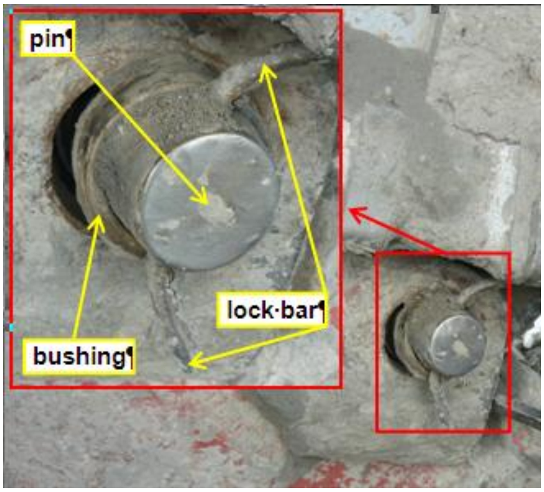

Fig. 4. *Pushed out bushing of the front bucket eye*

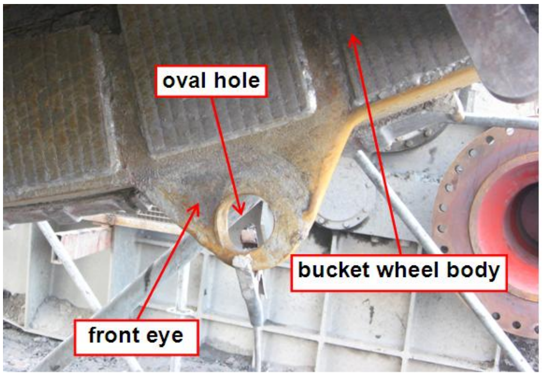

Fig. 5. *Plastic deformations of the front bucket wheel eye*

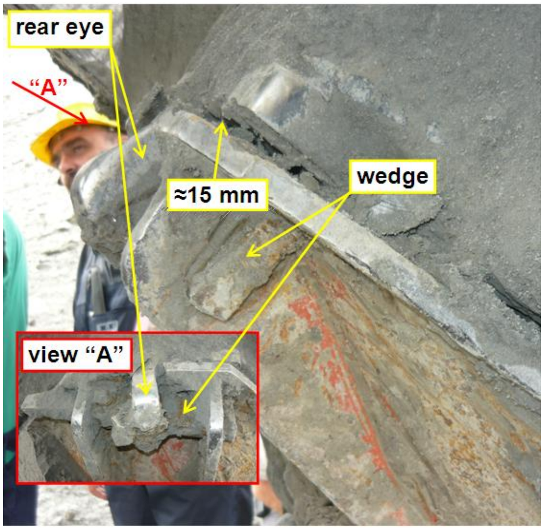

Fig. 6. *Plastic deformations of the rear support eye and bucket "opening" in the rear support zone*

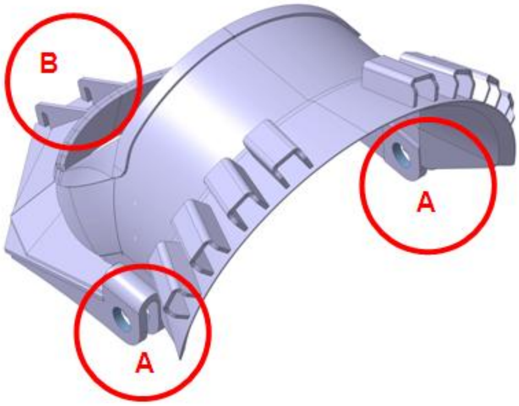

Fig. 7. *3D model of the original bucket: zones of redesign*

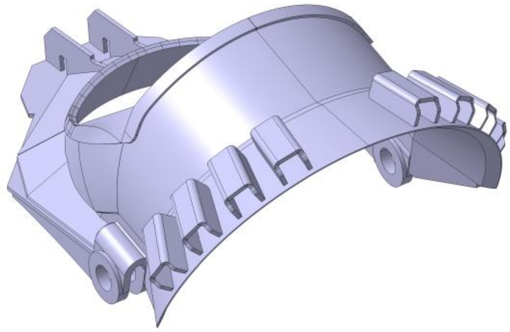

Fig. 8. *Redesigned bucket*

Fig. 9. *Welding of the redesigned front support eye*

Fig. 10. *Welding of the redesigned rear support eye*

Obviously, redesign of the bucket cause the change of its weight. In considered case, reconstruction of one bucket with its supports on bucket wheell incerease weigth for $\Delta G_B = 43.2$ daN. Having in mind that total number of bucket is $n_B = 14$, total weight increase can be calculated as

$$\Delta G = n_B \Delta G_B = 14 \times 43.2 = 604.8 \text{ daN} \qquad (1)$$

Fig. 11.

Center of gravity location, Fig. 11, is calculated by using Varignon's theorem

$$x_{GN}^{*} = \frac{G_N x_{GN} + \Delta G_{PU} x_{\Delta GPU} + \Delta G x_{\Delta G}}{G_N + \Delta G_{PU} + \Delta G} = \\ = \frac{7705.3 \times 0.011 + 450 \times 7.95 - 6.1 \times 33.083}{7705.3 + 450 + 6.1} = \qquad (2) \\ = 0.424 m$$

So, the increase of the redesigned buckets' weight cause the change of the center of gravity location. For horizontal position of the bucket wheel boom shifting of the center of gravity is

$$x_{GN} - x_{GN}^{*} = 0.449 - 0.424 = 0.025 \text{ m} \qquad (1)$$

which is allowable.

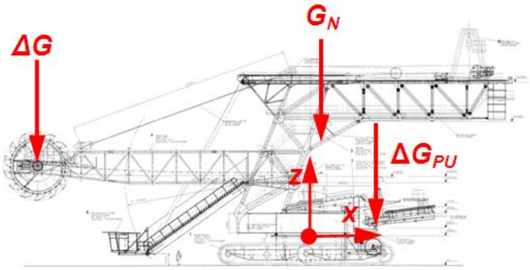

Fig. 11. *Scheme for calculation of the center of gravity location after buckets redesign*
(superstructure weight G_S=7705.3 kN, *x_{GN}=0.449* m; *part of conveyor weight ΔG_C=450* kN, *$x_{\Delta GC}$=7.95* m*; total weight increase ΔG=6.1 kN, $x_{\Delta G}$* = *- 33.083* m*)*

Buckets and bucket wheel were redesigned in october 2009. Validation of the applied solution is done by expert's evaluation of the machine behaviour during exploitation as well as by visual inspection of the critical zones.

2 FAILURE AND REDESIGN OF THE BCE STRUCTURE

BCE ERs 1000, Fig. 2, is in use in open pit mine ''Kolubara''. During perennial exploitation cracks were observed on the column heads of supporting truss of the counterweight boom (CWB) Fig. 12. These cracks have been weld repaired, but after some time they appear again, being longer and longer.

The cracks propagation could lead to catarstrophic consequences – collapse of the machine, such as described in [1,6]. The goals of the study presented in the paper were to:

- Diagnose the cause of cracks occurrence;
- Define the reconstruction design of the truss columns, Fig. 13;
- Verify the reconstructed structure by numerical-experimental analysis, Figs. 14 and 15.

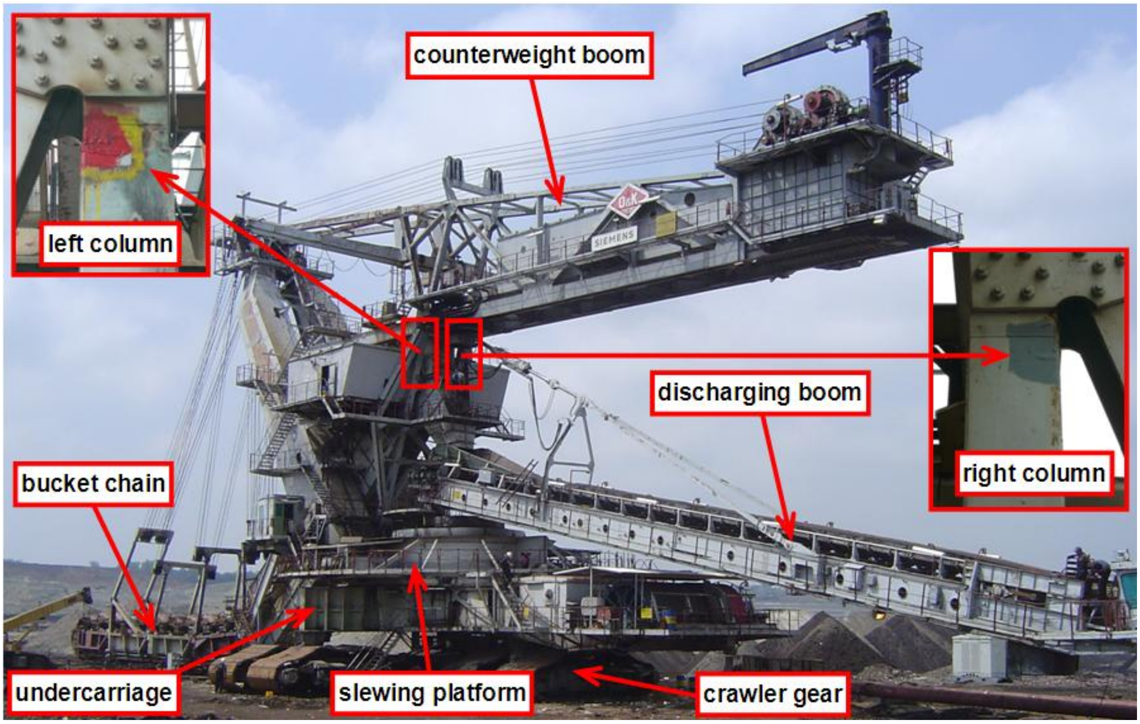

Fig. 12. *Cracks on the CWB supporting truss columns*

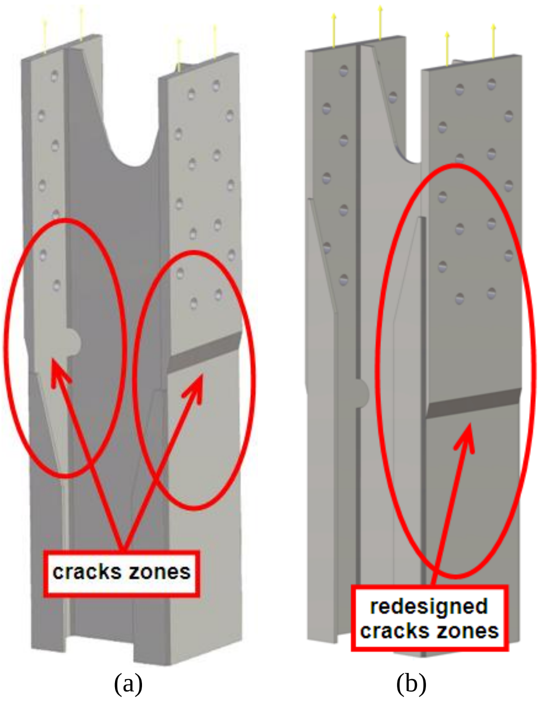

Fig. 13. *3D models of the original (a) and redesigned (b) column head*

Fig. 14. *Set up and connection of strain gauges*

Based on the results of a comparative numerical analysis of the original and redesigned structure of the column head, the authors conceived a reconstruction solution that meets the following requirements:

- a significantly lower stress state (≈ 3 times) in crtitical zones, where peaks do not exceed allowable values;
- a very short time for manufacturing of the redesigned columns' parts;
- the possibility of performing reconstruction in field conditions, without dismantling the BCE superstructure components.

Experimental analysis of the stress state of the redesigned column heads was carried out in June 2010, during BCE testing immediately after the finished reconstruction.

Visual inspection performed in April 2011 proved that there are no defects in the structure of the redesigned column heads. The validity of the presented reconstruction, besides experimental investigations, unquestionably confirms failureless exploitation, where BWE excavated more than $1.4x10^6$ t of coal after the reconstruction.

3 FAILURE AND REDESIGN OF THE BCR STRUCTURE

Design-in faults led to buckling of the rigid portal bracing, Fig. 15, and collapse of the machine structure.

Fig. 15. *Detail of rigid leg*

After the reconstruction of the truss substructure in critical zone, stress levels became considerably lower. Besides that, increasing of bracing and horizontal truss stiffness, Figs. 16 and 17, as well as increasing of torsional stiffness of portal legs, Fig. 18, led to displacements decreasing [14-17].

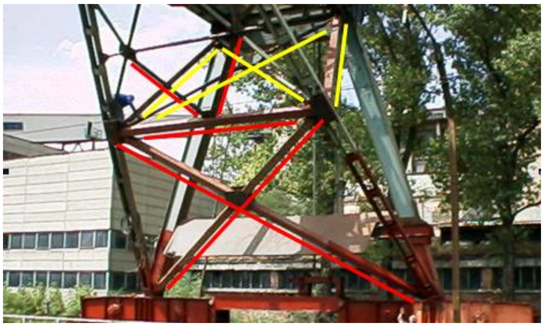

Fig. 16. *Redesigned bracing truss*

Exploitation expirience after the structure reconstruction confirmed the validity of applied redesign solutions as well as calculation procedure.

Fig. 16. *Redesigned bracing truss*

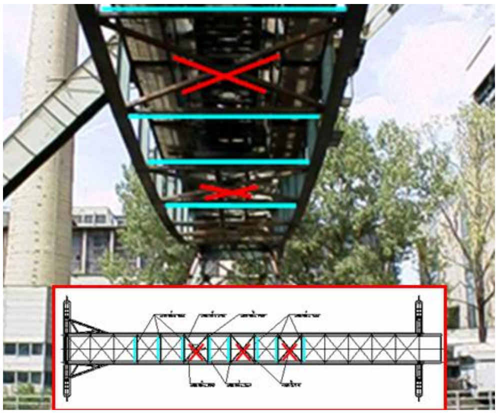

Fig. 17. *Redesigned horizontal truss*

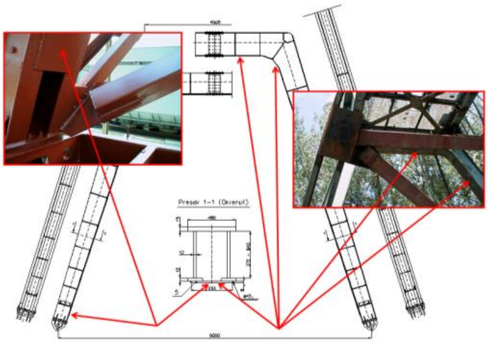

Fig. 18. *Closing of the portal cross-section*

4 CONCLUSION

The fundamental problems of any machine subsystem's redesign, therefore the BWE, BCE and BCR substructures as well, are caused by the restriction ensuing from installation conditions and functionality. Special difficulties result from the relative complexity of the considered structures, as well as the nature of external operational loads. The mentioned loads are of an outsandingly dynamic and stochastic nature, so that calculated loads are assumptions, in the full sense of the word. And exactly because of that, comparative stress analysis presents an indispensable and inevitable part of the redesign process.

Finally, the validity of the presented reconstructions, besides expert evaluations and experimental investigations, unquestionably confirms failureless exploitation.

Acknowledgement

This work is a contribution to the Ministry of Science and Technological Development of Serbia funded project TR 35006.

4 REFERENCES

[1] Rusiński E, Czmochowski J, Iluk A, Kowalczyk M. An analysis of the causes of a BWE counterweight boom support fracture. Eng Fail Anal 2010;17:179–91.

[2] Rusiński E, Czmochowski J, Moczko P. Half-shaft undercarriage systems – designing and operating problems. JAMME 2009;33:62–9.

[3] Rusiński E, Czmochowski J, Smolnicki T. Failure reasons investigations of dumping conveyor breakdown. JAMME 2007;23: 75–8.

[4] Rusiński E, Harnatkiewicz P, Kowalczyk M, Moczko P. Examination of the causes of a bucket wheel fracture in a bucket wheel excavator. Eng Fail Anal 2010;17:1300–12.

[5] Savković M, Gašić M, Arsić M, Petrović R. Analysis of the axle fracture of the bucket wheel excavator. Eng Fail Anal 2011;18:433–41.

[6] Bošnjak S, Zrnić N, Simonović A, Momčilović D. Failure analysis of the end eye connection of the bucket wheel excavator portal tie-rod support. Eng Fail Anal 2009;16:740–50.

[7] Bošnjak S, Petković Z, Zrnić N, Simić G., Simonović A. Cracks, repair and reconstruction of bucket wheel excavator slewing platform. Eng Fail Anal 2009;16:1631–42.

[8] Bošnjak S, Petković Z, Zrnić N, Pantelić M, Obradović A. Failure analysis and redesign of the bucket wheel excavator two-wheel bogie. Eng Fail Anal 2010;17:473–485.

[9] Bošnjak S, Pantelić M, Zrnić N, Gnjatović N, Đorđević M. Failure analysis and reconstruction design of the slewing platform mantle of the bucket wheel excavator O&K SchRs 630. Eng Fail Anal 2011;18:658–69.

[10] Arsić M, Bošnjak S, Zrnić N, Sedmak S, Gnjatović N. Bucket wheel failure caused by residual stresses in welded joints. Eng Fail Anal 2011;18:700–12.

[11] Bošnjak S, Arsić M, Zrnić N, Rakin M, Pantelić M. Bucket wheel excavator: integrity assessment of the bucket wheel boom tie – rod welded joint. Eng Fail Anal 2011;18:212–222.

[12] Wintle JB, Pargeter RJ. Technical failure investigation of welded structures (or how to get the most out of failures). Eng Fail Anal 2005;12:1027–37.

[13] de Castro PMST, Fernandes AA. Methodologies for failure analysis: a critical survey. Mater Design 2005;25:117–23.

[14] Bošnjak S, Gašić V, Petković Z. Determination of resistances to coal reclaiming at bridge - type stacker – reclaimer with bucket chain booms. FME Transactions 2005; 33:79 – 88.

[15] Bošnjak S, Petković Z, Gašić V, Zrnić N. Pretovarni mostovi sa elevatorima – Deo I: Identifikacija opterećenja, proračun strukture i zakošavanje. Tehnika – Mašinstvo 2006; 55:1–6. (in Serbian)

[16] Bošnjak S, Petković Z, Gašić V, Zrnić N. Pretovarni mostovi sa elevatorima – Deo II: Konstrukciono rešenje, tehnologija i proračun rekonstruisane strukture. Tehnika – Mašinstvo 2007;56:7–13. (in Serbian)

[17] Bošnjak S. Some of the problems on dynamics and strength of the high - performance machines. iipp 2010;8:1–12. (in Serbian)

HEAVY MACHINERY - HM 2011, 61-66
ISBN 978-86-82631-58-3
Paper accepted: 20.05.2011

Eco Issues in Belt Conveying Technologies

Nenad Đ. Zrnić[1] – Miloš D. Đorđević[1,*] – Zoran D. Petković[1] - Srđan M. Bošnjak[1]
[1]University of Belgrade – Faculty of Mechanical Engineering

Bulk materials handing technology is the most difficult of the engineering sciences as it incorporates all the features of liquids, gasses and mass solids. This paper deals particularly with eco issues in bulk material handling in belt conveying technologies and also points to possible solutions of those problems.

Keywords: Belt conveying technologies, bulk materials, eco issues, energy efficiency.

0 INTRODUCTION

Solids handling technology is the most difficult of the engineering sciences as it incorporates all the features of liquids, gasses and mass solids. Solid, free-flowing materials are said to be in bulk.

This paper deals particularly with eco issues in bulk material handling in belt conveying technologies such as dust, noise, energy efficiency and costs saving, protection of environment and handled material, and spillage.

Conveyor system output requirements are increasingly greater and configurations more complex resulting in development in belt design, solutions that use conventional components in non conventional applications, development in distributed power and torque control etc.

1 OPERATING COSTS

1.1 Truck vs conveyor consideration

Main contribution to typical open pit operating costs based on conventional shovel-truck methods goes to haulage costs [1].

There is a need to reduce haulage costs, carbon emissions and maintain flexibility.

Because of their operating flexibility, relatively low capital cost, resale value and mobility from operation to operation, trucks have historically been the favored method of moving both ore and waste from open pit mines [2]. Nowadays, conveyors are the lowest cost method of handling bulk materials.

Conveying advantages over conventional shovel-truck methods are [1]: operating costs per tone-kilometer is low, electric power, environmentally friendly (reduced carbon emissions), labour requirements are reduced, operational safety is better, lower maintenance cost. Disadvantages: high initial investment costs, poor flexibility, impact on blasting operation, loading efficiency of shovel affected by down-stream units.

For truck haulage, 60% of the fuel energy goes to moving the truck weight and only 40% to moving the payload [2]. For belt haulage, the corresponding relationship is 20% to belt weight and 80% to payload. Useful conveyor life of more than 25 years. In contrast, off-highway trucks have life spans of six to eight year. The larger and deeper open-pit mines are, the more profitable is the technology of continuous haulage mining systems.

When it comes to overland and long distances conveying, Scotland - ATH Resources Glenmuckloch Open Cast Coal Site is a clear example of how employing modern machinery and mining methods can reduce costs and be less harmfull to the environment [3]. Continental Conveyor's 12.2 km overland conveyor transports some 2.8 million tonnes of coal a year, removing the need for 54 000 lorry journeys from Scotland's roads - around two million miles a year!

1.2 Transfer points

Issues during mass flow at transfer points:

- Plugging
- Belt and chute damage and abrasion
- Material degradation
- Dust
- Off center loading/spillage [5]

A major problem with transfer systems, especially when moving large, blocky types of stone or ore, is excessive wear on the belt

*Corr. Author's Address: Faculty of Mechanical Engineering, Kraljice Marije 16, Belgrade, Serbia, mddjordjevic@mas.bg.ac.rs

surfaces and idlers directly below the loading area caused by the impact of the material [2].

In surface mining applications transfer systems must be installed to facilitate the change in direction of the conveyors at each switch point, Fig. 1, or a greater amount of waste material must be removed from the pit to create a lower slope angle, Fig. 2.

Fig. 1. *Conveyor flights leaving a pit via swichbacks*

Fig. 2. *Open pit conveyor trench*

2 ENERGY EFFICIENCY

Most of our energy resources are based upon fossil energy sources [4]. That means that responsible and efficient energy consumption is the most important contribute to climate protection. Climatic change means the continuing increase of the average earth temperature.The bulk materials handling industry still has an enormous potential to save energy and costs as well. The ecological necessity is now also economically reasonable.

In bulk materials handling most of the energy is consumed by electric motors. The drives can be energetically optimised.

Because of the high fuel prices and the long delivery times of the dumpers, which are highly demanded, belt conveyor systems become more and more attractive. Compared to dumpers with regard to personal, operating costs and environmental issues, belt conveyor systems have enormous advantages. Belt conveyors are considered as very energy efficient for transporting big quantities over long distance. Main resistances in long distance conveyors and distributed power are shown in Fig. 3, 4 [5].

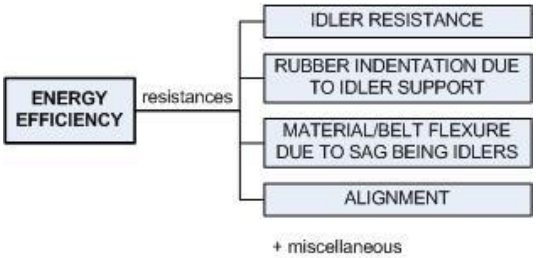

Fig. 3. *Main resistances in long distances belt conveying technologies*

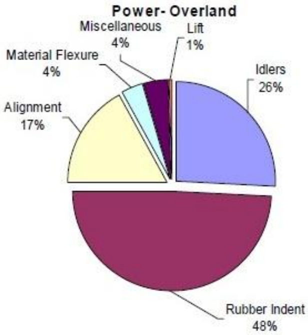

Fig. 4. *Distributed power in overland conveyance*

Since there is no way to reduce gravity forces, there are no means to significantly reduce power on high incline belts, Fig. 5. In addition there is a problem with the large size of high power drives not to mention being able to handle and move them around [6]. Intermediate drive technology is therefore very well accepted and widely used in underground mining.

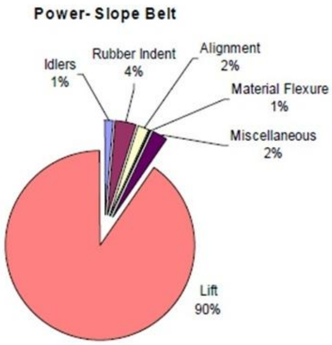

Fig. 5. *Distributed power in underground mining*

3 ANALYSIS AND SIMULATION

3.1 Starting and stopping

Traditional static analysis techniques were inadequate for analyzing starting and stopping. Conveyors must be analyzed as flexible systems and therefore dynamic analysis has to be applied. Failure to include transient response to elasticity can result in inaccurate prediction of [5]: maximum belt stresses, maximum forces on pulleys, minimum belt stresses and material spillage, take-up force requirements, take-up travel and speed requirements, drive slip, breakaway torque, holdback torque, load sharing between multiple drives, material stability on an incline.

3.2 Mass flow at transfer points

Many of the most difficult problems associated with belt conveyors center around loading and unloading (transfer points) [5]. Today, numerical simulation methods exist which allow designers to "test" their design prior to fabrication.

The Discrete Element Method (DEM) is a family of numerical modeling techniques and equations specifically designed to solve problems in engineering and applied science that exhibit gross discontinuous mechanical behavior such as bulk material flow. It should be noted that problems dominated by discontinuum behavior cannot be simulated with conventional continuum based computer modeling methods such as finite element analysis, finite difference procedures and/or even computational fluid dynamics (CFD). This modeling technique provides a quantitative description of the bulk solids movement through the transfer point, Fig. 7.

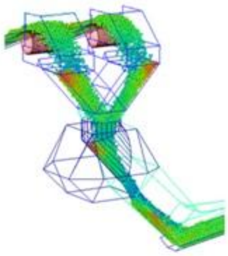

Fig. 7. *Simulation of mass flow through a transfer chute*

4 ROUTE OPTIMISATION

Route optimization refers to the overcoming obstacles, long distances and tight radius horizontal and vertical curves with preservation of natural environment. In tunneling application conveyors are relatively narrow and low strength belts must be used to accommodate the narrow widths. Horizontal curves are often required in tunnels as small as 250m [6].

5 DUST

In belt conveying technologies dust can cause seizure of idlers bearings. Also, a large number of dust explosions occur in industry each year: these take place in all industries and locations, in which flammable powders are being handled or processed [3]. Dust extraction filters, cyclones and silos and their associated ducting are probably the plant locations, where most dust explosions occur.

Three conditions need to exist simultaneously for a dust explosion:

- A flammable dust cloud
- An ignition source which contains enough energy to trigger combustion
- An atmosphere which supports combustion

Possible ignition sources include friction or mechanical failure, an overheated surface (e.g. a faulty bearing), a glowing ember (e.g. a burning wood shaving, paper fragment or small dust ball), tramp metal or stone causing a spark, welding or cutting, static electrical discharge, electrical failure...

6 PROTECTION OF ENVIRONMENT AND CONVEYED MATERIAL

Sometimes there is a need to protect conveyed material (e.g. food) from external influences like rain and wind and protect the environment by avoiding spillage of the conveyed material (toxic or otherwise hazardous material). In more severe northern climates may occur snow and ice problems. Ocasionaly there is a need for overcoming obstacles without violating the natural environment.

7 POSSIBLE SOLUTIONS

An advanced solution for overcoming single flight long distances and route optimization is Metso Rope Conveyor or RopeCon, Fig. 9 [5, 7]. By use of this new conveyor system very large distances (above 20km) can be overcome while placing supports in distances of above 2km.

Fig. 9. *RopeCon*

The driving tensions (ropes) and the carrying medium (belt) of RopeCon are separated which allow very small radius horizontal curves, Fig. 10.

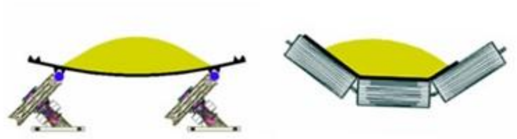

Fig. 10. *Advantage of RopeCon over conventional belt conveyor in overcoming horizontal curves*

Cross sectional area of the RopeCon is only 30% of a conventional belt conveyor, 3-times lower sound emissions and the saving of drive power is around 50%.

Enclosed conveyor belts (pipe, tube or hose conveyor belts) are primarily used where bulk materials must be conveyed along horizontal and vertical curves in confined spaces, and/or where the environment has to be protected and where spillage must be avoided [5, 8]. Tube conveyor, Fig. 11, is a rubber conveyor belt rolled into a pipe shape with idler rolls which constrain the belt on all sides allowing much tighter curves to be negotiated in any direction. The only area where the belt is open is at the head, take-up and tail end areas.

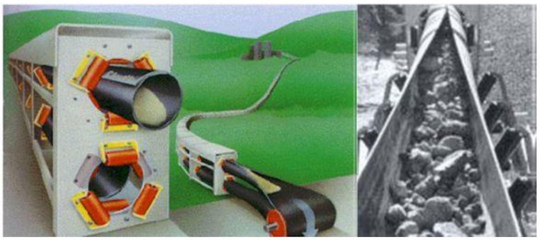

Fig. 11. *Tube (pipe) conveyor*

Such problems as transfer points at conveyor flight swichbacks and open pit conveyor trenches have led to the development of new solutions for vertical adaptation. Some of them are high angle conveyor (HAC) and Pocketlift [5]. The Continental Conveyor HAC, Fig. 12, can transport almost any type of material at any angle up to and beyond vertical (from -35° to +90°) and carry out lifts of +180 m. The concept is known as a sandwich conveyor as the material is carried between two belts.

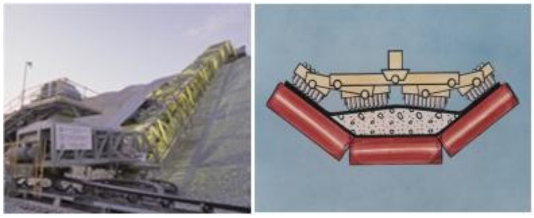

Fig. 12. *High angle conveyor*

Another variant of high angle conveyor is a Flexowell's POCKETLIFT, Fig. 13, a non-traditional belt construction which can be used to convey vertically.

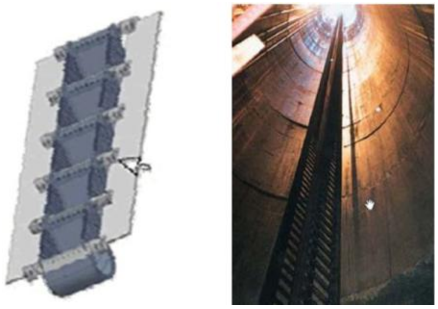

Fig. 13. *Pocketlift*

JOY Flexible Conveyor Train is a unique solution for tunneling [9]. It is the only simultaneous tram-and-convey, single-operator, underground continuous haulage system available in the world today, Fig. 14.

Fig. 14. *The JOY Flexible Conveyor Train*

Use of booster drives installed at strategic calculated points along conveyor can [5, 6]:

- Reduce the overall tension in the system
- Introduce an increase in power

Although the average belt tension during each cycle is only about 40% of the peak value, all the belting must be sized for the maximum. By splitting the power in two locations (red line), the maximum belt tension is reduced by almost 40% while the total power requirements remains virtually the same, Fig. 15. A much smaller belt can be used and smaller individual power units too.

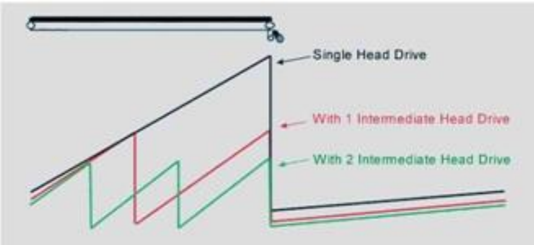

Fig. 15. *Belt tension diagram*

Today commonly used intermediate drive technology is tripper drive configuration, Fig. 16. Trouble with intermediate drives is that if too much power is applied at the wrong location, belt tensions can drop too low and drive slip or belt sag and material spillage can occur. If too little power is applied at one drive location, other drive locations may become overloaded and stall. Thus tripper drive is usually combined with frequency inverter resulting in variable frequency drive (VFD) which provides power and tension control.

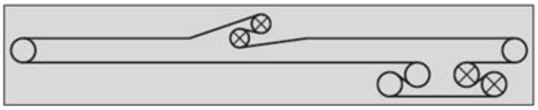

Fig. 16. *Tripper drive configuration*

Along with intermediate drives technology come torque control and constant tension systems. There are several types of constant tension winches: gravity towers, hydraulic type, variable frequency drive (VFD) type and vectored flux drive system, Fig.17 – new type of constant tension winch which provides full torque and full braking capability in both directions.

Fig. 17. *Vector Flux winch system*

Constant tension winch system significantly contribute to the life and reliability of system, automatically adjusts tension for start-up, running and stopping, eliminates the need for weights and towers where space and height are not readily available and provide safer and easier belt maintenance.

Torque control and controlled acceleration and braking can be achieved by using of such devices as hydroviscous clutch, DC and VFD, variable fill fluid couplings, Fig. 18, centrifugal clutch couplings, eddy-current couplings, wound-rotor motors with step starting, squirrel-cage induction motor with autotransformer…

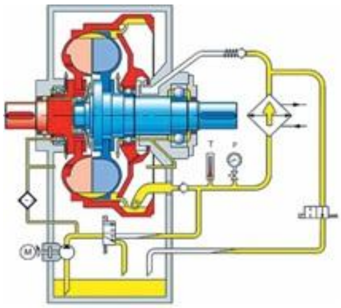

Fig. 18. *Voith TPKL variable fill fluid coupling*

Inpro/Seal Company offers a solution for dust protection of conveyor's bearings. That is a zero maintenance powder seal. The Inpro/Seal

Air Mizer - PS is non-contacting compound labyrinth seal made from bearing bronze that uses a positive air purge to create a barrier for powders, liquids and bulk solids [3].

Dust control at transfer points is usually achieved by applying dust controlled chutes and hoppers.

When it comes to the dust explosions issue, there is readily available reliable equipment for the prevention of dust explosions and fires which includes ignition source detectors and extinguishing devices.

When transporting materials using conveyors protecting of conveyed material and environment can be accomplished by using of enclosed conveyors. Enclosing conveyors can be achieved by using of conveyor hoods, Fig. 23, and wind guards or special types of conveyors like tube conveyors [10]. In more severe northern climates , the hoods greatly reduce the snow and ice problems. Hoods also retain dust at the approach and take-away areas of a transfer station.

Fig. 23. *Conveyor cover*

Vacuum conveyors are preferred choice for toxic or otherwise hazardous materials because air is sucked-in in the event of accidental damage to the conveying tubes thus minimizing the escape of the product to atmosphere.

8 CONCLUSION

There is still a great potential in energy saving by using energy saving belts, reducing bearing resistances of the idlers, better sealings for the idler rols bearings, etc. As belt lengths increase and as horizontal curves and distributed power becomes more common, the importance of dynamic analysis taking belt elasticity into account is vital to properly develop control algorithms during both stopping and starting. Intermediate drives are often used as a method of maintaining low and more consistent belt tensions allowing conveyors to negotiate tight horizontal curves. One of the reasons for using intermediate drives and running single flight conveyors longer and longer is to eliminate transfer points.

9 ACKNOWLEDGEMENTS

A part of this work is a contribution to the Ministry of Science and Technological Development of Serbia funded project TR 35006.

10 REFERENCES

[1] D. Tutton, W. Streck, “The application of in-pit crushing and conveying in large, hard rock open pit mines,” in Mining Magazine Congress, Niagara-on-the-Lake, Canada, 2009.

[2] E. M. Frizzell, T. W. Martin, “In-pit crushing and conveying”, SME MINING ENGINEERING HANDBOOK, 2nd edition, Vol. 1, Society for Mining, Metallurgy, and Exploration, Inc., Littleton, Colorado,1992.

[3] Solids & Bulk Handling, August 2007, www.solidsandbulk.co.uk

[4] W. A. Günthner, Ch. Tilke, S. Rakitsch, “Energy efficiency in bulk materials handling”, Bulk Solids Handling, Vol. 30, 2010, No. 3, Pages 138-142

[5] M. A. Alspaugh, Overland Conveyor Co., Inc, “Latest developments in belt conveyor technology”, MINExpo 2004, Las Vegas, NV, USA

[6] M. A. Alspaugh, “The evolution of intermediate driven belt conveyor technology”, Bulk Solids Handling, Vol. 23, 2003, No. 3

[7] F.Kessler, “Recent developments in the field of bulk conveying”, FME Transactions, edition 34, 2006, pages 213-220

[8] F. J. Loeffler, USA, “Pipe/tube conveyors – a modern method of bulk materials transport”, www.ckit.co.za/secure/tech-focus/loeffler/loeffler.htm

[9] www.joy.com

[10] www.continentalconveyor.ca

HEAVY MACHINERY - HM 2011, 67-72
ISBN 978-86-82631-58-3
Paper accepted: 30.05.2011

In-plane vibrations of the gantry crane structure due to a load moving with constant speed

Vlada Gašić[1,*], Nenad Zrnić[1], Milorad Milovančević[1]
[1] University of Belgrade, Faculty of Mechanical Engineering Belgrade

The dynamics of gantry crane structure subjected to a trolley with payload is considered in this paper. The model of crane structure is done with finite element method with frame elements discretization. The model represents type of gantry crane which is often used. The trolley is modelled as a force moving with constant speed. The overall mass and stiffness matrices are calculated. There is shown formulation of equivalent force vector due to a moving force. Equation of motion of MDOF system is given and used for obtaining the horizontal and vertical displacement of the characteristic points of the structure. The algorithm is first validated with comparison of vibration frequencies with known ones. It is studied trolley moving speed influence on structural dynamic responses and shown correspondence with increase of vibration amplitude.

Keywords: Gantry crane, moving force, FEM, dynamic response

0 INTRODUCTION

The moving load problem is considered as special topic in structural dynamics. Interest for it is originated in civil engineering for the design of rail-road bridges and highway structures. Typical structures under a moving load in mechanical engineering are bridge cranes, gantry cranes, unloading bridges, tower cranes, cableways, guideways, shipunloaders and container cranes.

Application of the moving load problem has been presented in mechanical engineering studies for the past 30 years. However, crane dynamics under moving load has little literature available, especially in Serbian studies. The attention is first paid in [1], with study of dynamic behaviour of the boom of container crane. The technique for consideration of moving load at cranes is given in [2], performed on finite element model of bridge crane.

Generally, dynamics of crane include structure-trolley interaction. The basic approaches in trolley modelling are: the moving force model, moving mass model and the trolley suspension model-moving oscillator as existing in some special structures of gantry cranes and unloading bridges. The simplest dynamic model is moving force model. The consequences of neglecting the structure-trolley interaction in these models may sometimes be minor. In most moving force models the magnitude of the contact force are constant in time. A constant force magnitude implies that the inertia forces of the trolley are much smaller than the dead weight of the structure. Thus the structure is affected dynamically through the moving character of the trolley only. Even they don't provide structure-trolley interaction the moving force models are simple to use and yield reasonable structural results in some cases [3].

This paper studies the in-plane vibrations of the structure of the gantry crane under trolley moving with constant speed.

1 DYNAMICS OF GANTRY CRANE

Gantry cranes are widely used in ports and rail-head freight yards all over the world. They are equipped with wheels and may run along a parallel pair of rails. Typical gantry crane structure is consisted of top girder(s), pier leg and sheer leg. Also, top girder can have cantilever parts over the legs, usually over the pier leg, Figure 1. It is very rare that legs are not of equal height, i.e. don't stand on same level, but present at some stockyards. The trolley with payload is moving on the top girder(s).

Modern gantry cranes have outstanding performances. One may found cranes with span over 150 m which handle loads up to 1650 t and can lift up to 90 m high, e.g. Goliath shipyard cranes which are designed for handling ship sections in shipyards (Konecranes, 2010).

Permanent demand for quick and precise manipulation of the payload calls for analysis of dynamic behaviour of such cranes.

*Corr. Author's Address: Faculty of Mechanical Engineering, Belgrade, Serbia, vgasic@mas.bg.ac.rs

Fig. 1. *Gantry crane*

In open scientific literature are given natural frequencies of vibrating frames that are symmetric, i.e. two legs are identical. Such formulas for 1st symmetric and 2nd anti-symmetric mode are presented in [4] with trigonometric-hyperbolic functions (Fillipov, 1970). But, even that process of gaining frequency equation was defined, solutions were difficult to find because of its transcendental nature. Free in-plane vibrations are studied in [5] with mathematical model of portal frame with universal character of structure described with non-dimensional parameters. The elements of structure are uniform and governed by Euler-Bernoulli transverse vibration theory.

Application of moving load problem at gantry crane structures by using and developing FEM, are presented in last 10 years. First, calculation of the effects of two-dimensional motion of the trolley on the response of the base structure of a mobile gantry crane model is given in [6]. Later on, Wu [7] gave responses of a three-dimensional framework due to a moving carriage hoisting a swinging object. Moreover, Wu [8] introduced moving finite element as a technique to replace the moving load in calculation of dynamic responses of a frame structure.

Following current trends in structural dynamics, this paper presents the comprehensive model of the structure of a gantry crane subjected to a force moving at constant speed. Because the moving speed of the entire structure is usually low and constant, the vibration components due to the movement of the entire structure are assumed negligible here. The finite element method (FEM) is used for obtaining the structural matrices. The technique for gaining the equivalent nodal forces and moments due to moving force is shown. Finally, the results for dynamic responses of main structural parts are obtained numerically, with direct integration.

2 MODEL FORMULATION

Schematic presentation of the finite element model of the crane is shown in Fig. 2.

The relation between the top beam and the moving substructure is simplified into one moving force due to assumption that a loading is symmetrically distributed on the rail(s). The global position of the moving substructure is measured form the left end and defined by coordinate $x_m(t)$. The force acting upon the structure include masses of payload, hoist and trolley.

The whole system is consisted of n=14 elements connected with 15 nodes. The top beam of span L is composed of 8 elements, the cantilever of span L_c (=L/4), pier leg of height H and sheer leg of height h are composed of 2 elements. The elements properties are Young's modulus E, volume density ρ, cross-sectional area A_n, length l_n (obtained from L, L_c, H, h) and sectional moment of inertia I_n.

Every node has longitudinal, transversal and rotational DOF, except the nodes at supports which have only rotational DOF's. Thus, whole system has 41 DOF's (3x11=33 from the top beam and cantilever, plus 8 from the legs).

3 OVERALL PROPERTY MATRICES

The governing equation of motion of multi-degree-of-freedom (MDOF) structural system is written as:

$$[M]\{\ddot{q}\}+[C]\{\dot{q}\}+[K]\{q\}=\{F(t)\} \tag{1}$$

where $[M],[C],[K]$ are the mass, damping and stiffness matrices of system, respectively; $\{\ddot{q}\},\{\dot{q}\},\{q\}$ are the acceleration, velocity and displacement vectors for the whole system, respectively, while $\{F(t)\}$ is the external force vector. When a beam is subjected to a concentrated force P, the forces and moments on all the nodes of the beam are equal to zero except the nodes of elements s (as shown in Fig. 3) which is subjected to the force.

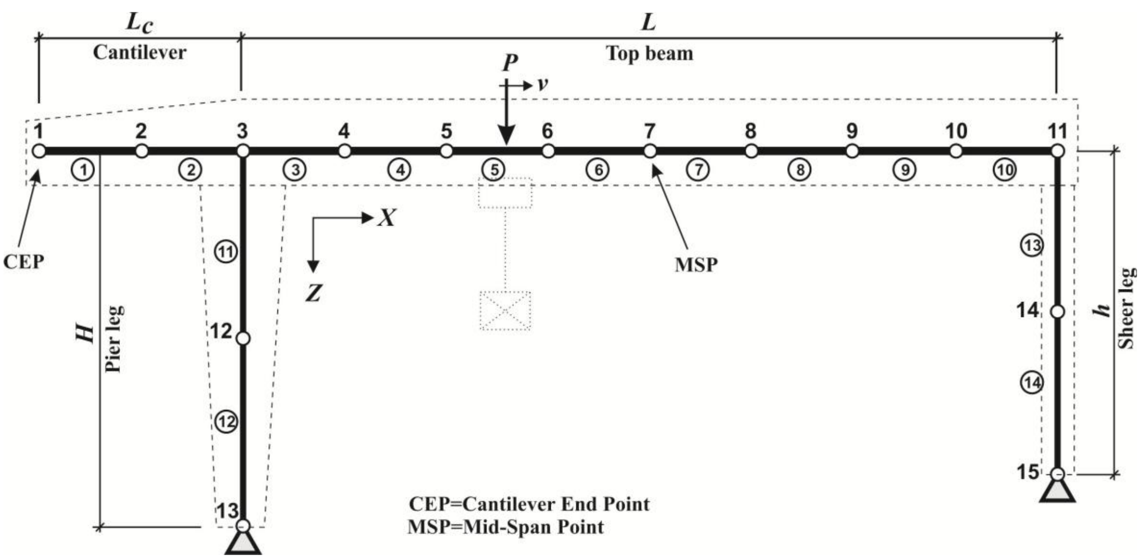

Fig. 2. FE model of the gantry crane structure

According to the Clough and Penzien [9], the external force vector in Eq. (1) takes the following form:

$$\{F(t)\} = \{0\,0\,..f_1^s\;f_2^s\;f_3^s\;f_4^s\;f_5^s\;f_6^s\,..0\,0\}^T \tag{2}$$

where f_i^S (i=1-6) represent the equivalent nodal forces.

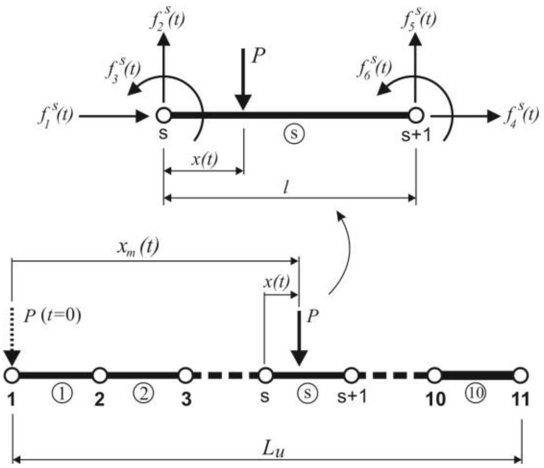

Fig. 3. *Nodal forces of the element s for a beam subjected to a concentrated vertical force*

As assumed no axial forces on the top beam, structure nodal forces are determined as

$$[\,f_1^s\;f_2^s\;f_3^s\;f_4^s\;f_5^s\;f_6^s\,] = P[0 N_1\,N_2 0 N_3 N_4] \tag{3}$$

such that these represent shape functions, Hermitian polynomials, given by

$$N_1 = 1 - 3\xi^2 + 2\xi^3 \tag{4}$$

$$N_2 = l(\xi - 2\xi^2 + \xi^3) \tag{5}$$

$$N_3 = 3\xi^2 - 2\xi^3 \tag{6}$$

$$N_4 = l(-\xi^2 + \xi^3) \tag{7}$$

$$\text{where } \xi = x / l \tag{8}$$

noting that l is the element length and x is distance along the element to the point of application of P, Figure 3.

Considering m time steps and choosing a time interval Δt, the total time is then given by

$$\tau = m \cdot \Delta t \tag{9}$$

At any time $t = r\,\Delta t$ (r = 1 to m), the position of the force moving with constant speed v, relative to the left end of the beam, is given by

$$x_m(t) = v \cdot r \cdot \Delta t \tag{10}$$

One can find the element number s, which the moving mass is applied to at any time t, as

$$s = \mathrm{Int}[\frac{x_m(t)}{l}] + 1. \tag{11}$$

Equation (8) can be rewritten in terms of the global $x_m(t)$ instead of the local $x(t)$:

$$\xi = \frac{x_m(t) - (s-1)l}{l} \tag{12}$$

Hence, the instantaneous force and moments vectors for each node on the beam are determined when the beam is subjected to a moving force.

3.1 Stiffness and mass matrices

Here, the damping matrix of the system is neglected because it is usually unobtainable. The frame element stiffness $[k]_n$ and $[m]_n$ (n = 1-14) matrices are postulated as in [10]. The matrices are assembled directly to find overall [K] and [M]. Eventually, for n=11-14 the transformed stiffness and mass matrices are obtained with $[K]_n = T^T [k]_n T$ and $[M]_n = T^T [m]_n T$. Here, the angle of these frame elements is 270°, which determines the transformation matrix T, [10].

4 NUMERICAL RESULTS

4.1 Model verification

As usual in similar research studies, given model is first verified. Validation is done upon the model of gantry crane with 1 top beam, single column pier leg and 2 column sheer leg. The crane properties are outlined in [5].

The given algorithm is adjusted (L_c<<L) to solve the frequency equation of the system

$$\left\| K - \omega^2 M \right\| = 0 \tag{13}$$

Following Table gives first 4. frequencies obtained by this algorithm along with comparison of results from mentioned reference, obtained with FEM software SAP 2000. The FEM model is presented on Figure 4.

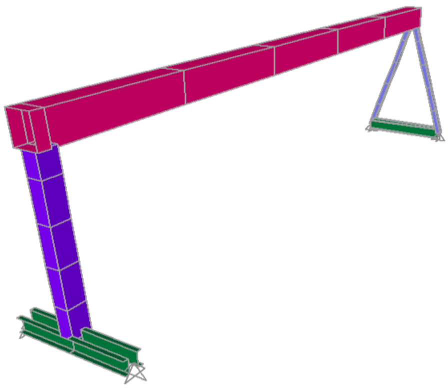

Fig. 4. *FE model of gantry crane*

Table 1.

Mode No	Frequency		
	Refer. [5] Hz	This paper Hz	Error %
1.	1.44	1.46	1.3
2.	6.14	6.25	1.7
3.	14.30	15.2	6.2
4.	21.56	22.8	5.7

One may see from Table 1. that differences are negligible which ensure validation of postulated system. The first 2 mode shapes are depicted in [5].

4.2 Results

The equations (1-12) are used for studying the dynamic response of a crane structure due to a force moving with constant speed, and solved by means of the direct step-by-step-integration method based on Newmark algorithm [11]. The maximum interval for direct integration is $\Delta t = 0{,}05\,\mathrm{s}$.

The characteristics of the S235J2G3 steel-made structure of gantry crane are: Young's modulus E = 2,1 10^{11} N/m^2 and mass density ρ = 7850 kg/m^3.

Overall dimensions are: L = 40 m, L_C = 10 m, H = 10 m and h = 10 m. The box tube section properties of elements are: A_n= 0,0784 m^2, I_n= 0,01254 m^4 (n=1-10), A_n= 0,062 m^2, I_n= 0,008 m^4 (n=11), A_n= 0,0512 m^2, I_n= 0,0047 m^4 (n=12) and A_n= 0,0432 m^2, I_n= 0,0024 m^4 (n=13-14). The load is 20 t (~200 kN). There are investigated influences for two speeds: 2 m/s, which is a real parameter and 5 m/s, which is now maximum speed for trolleys at gantry cranes.

The dynamic responses are calculated for cantilever end point (CEP) and mid-span point (MSP) as main spots for design check.

First, the periods of vibrations are obtained and in this case are: T=1.40549 s, 2.81432 s , 6.95342 s, 10.6883 s, 19.9331s ..

Figure 5. shows horizontal displacement for CEP and MSP, where load is moving with speed of 2 m/s. For both the points the displacements are very much the same which comes from the fact that axial rigidity of beam elements (box tubes) is very high.

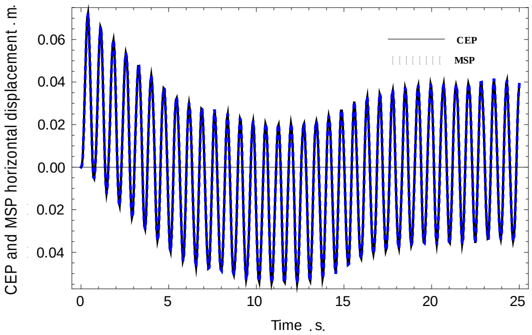

Fig. 5. *CEP horizontal displacement*

The CEP vertical displacements for two speeds are given in Figure 6. One can see that vibration amplitude increases with the increase of speed. The maximum values (0,12 m) occurs at starting of load movement, i.e. when the structure is subjected to a force at cantilever free end.

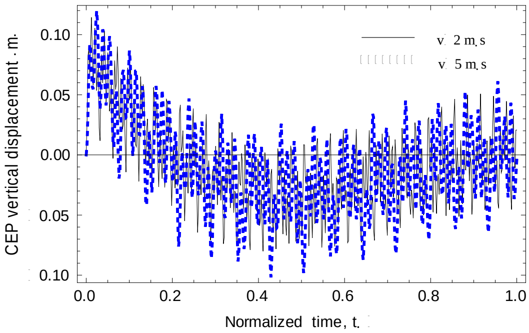

Fig. 6. *CEP vertical displacements*

The MSP vertical displacements for two speeds are given in Figure 7. Vibration amplitude also increases with the increase of speed. The maximum values (0,092 m) occurs when load is near the mid-span, which is expected from practical intuition.

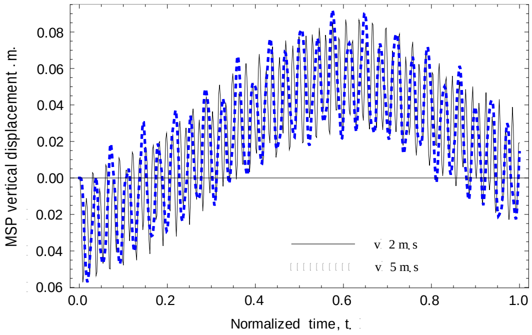

Fig. 7. *MSP vertical displacements*

Figures 6.,7. show the logical lines of deflections for cantilever end point and mid-span point when load is moving over, considering these lines as made of points in the middle of amplitudes. One can use these values to compare with permissible deflections of these points to validate the design of the structure.

5 CONCLUSION

The in-plane vibrations of gantry crane structure due to moving force are studied in this paper. In addition to the conventional vertical (or transverse) responses the horizontal displacements are also obtained.

The technique is first validated by comparison with earlier work.

The FEM model of gantry crane structure with universal character is created and subjected to force moving with constant speed. The full method is used for definition of equivalent nodal forces. It is shown that increase of trolley speed increase the vibration amplitude of the structural system displacements. As expected for top beam, the vertical displacements are higher then horizontal. The maximum values, for this example of gantry crane, are at cantilever part when force starts the movement. Since gantry crane structure comprises many parameters, one can't give general rule for crane design, but this paper and design experience show that all the parts of the structure have important part in design process. Thus, design of gantry cranes should rely, at least, on standard software finite elements models. Moving load problems calls for more complex models, as shown here, using combined finite element and analytical methods.

ACKNOWLEDGEMENT

This paper is a part of the research project no 35006 supported by Serbian Ministry of Science and Technological Development.

X REFERENCES

[1] Zrnić, N., "Uticaj kretanja kolica na dinamičko ponašanje obalskih kontejnerskih dizalica", Doktorska disertacija, Beograd, 2005.

[2] Gašić, V., Zrnić, N., Obradović, A., Milovančević, M., „Revisiting the use of finite element packages for moving load problem at bridge cranes", *Proc. XIX International Conference MHCL 09*, Belgrade, Serbia, 2009., pp.71-74

[3] Zrnić, N., Bošnjak, S., Hoffmann, K., „Application of non-dimensional models in dynamic structural analysis of cranes under moving concentrated load", *Proc. of the 6th Mathmod*, Vienna, Austria, 2009., pp. 327-336

[4] Karnovsky, I., Lebed, O.: *Formulas for structural dynamics*, McGraw-Hill, 2004.

[5] Gašić, V., Obradović, A., Petković, Z., „Mathematical modelling of the in-plane vibrations of portal cranes with FEM verification", Machine Design 2009, Novi Sad, Serbia, 2009., pp. 121-126

[6] Wu, J. J., Cartmell, M. P., Whittaker, A. R., "Dynamic Response of Structures to Moving Bodies Using Combined Finite Element and Analytical Methods", International Journal of Mechanical sciences, 43, pp. 2555-2579, 2001.

[7] Wu, J. J., "Dynamic response of a three-dimensional framework due to a moving carriage hoisting a swinging object", International Journal for Numerical Methods in Engineering, 59, pp. 1679-1702, 2004.

[8] Wu, J.J: "Transverse and longitudinal vibrations of a frame structure due to a moving trolley and the hoisted object using moving finite element", International Journal of Mechanical Science, 50, 2008, pp. 613-625

[9] Clough, RW., Penzien, J.: Dynamics of structures, McGraw-Hill, New York, 1993.

[10] Liu, G.R., Quek, S.S.: The finite element method, a practical course, Butterworth-Heinemann, 2003.

[11] Bath, KJ: Finite element procedures in engineering analysis, Prentice-Hall, 1982.

HEAVY MACHINERY - HM 2011, 73-78
ISBN 978-86-82631-58-3
Paper accepted: 30.05.2011

Dynamical Eigenvalue Identification of Heavy Structures Machine

Miomir Jovanović[1,*] - Goran Radoičić[2] - Taško Maneski[3]
[1] University of Niš, Faculty of Mechanical Engineering
[2] Public Utility Company "Mediana" Niš
[3] University of Beograd, Faculty of Mechanical Engineering

Abstract: *The dynamic behavior of large supporting structures machine has a special importance for assessing the quality of their design. Especially actual are the structures of large range. One such support structure of the processing plant in opencast mining systems (slewable boom conveyor - stacker) is observed numerically and experimentally. The eigenvalue dynamic properties of free-oscillation are observed. The aim of this research is to qualitatively assess trends, determine the dynamic coefficients, find the natural frequencies, determine the structural damping, ambient impact assessment of the structure. This paper reviews the theoretical modeling of structures, numerical solution of frequency equation, the characteristic modal forms. The paper presents an extract from the experimental researches that points to the important structure dynamic parameters. To check the model a real support structure is used for the slewable boom conveyor (stacker) at the open mining RBB. The experiment was seeking dominant eigenfrequencies. The strain energy of members and the continuous dynamics shadow image of grid structure members determine the developed numerical models. Such an identification of dynamic properties allows a good knowledge of their own properties, the area of stable operation and areas of risk. Finally, we show an overview of research design model and of FEM Computer Design technology.*
Keywords: Stacker, boom conveyor, modal analysis, eigenfrequencies, experimental values

0. INTRODUCTION

The largest opencast mining transport machines are Stacker and Bucket-wheel excavators on surface mining. Stacker have constructions whose masses often exceed 500 t [5]. Characteristic of their geometry is to have a slewable platform which carries the mechanical plant and boom with bridging conveyor. The connection between the tracked undercarriage and slewable platform was made through axial-bearing (*RotheErde -ThyssenKrupp*). Connection between the two large masses of the main sub-structures with main axial-bearing, gives soft areas and increases oscillations of the upper mass of slewable platform and bridging boom. Quality design of Stackers is not based on the static checks, but on the group of dynamic analysis. Dynamic analysis determine the amplitude of the oscillation structure parts at the forced harmonic action, incidental resistance at impact, random and seismic actions.

Analysis are are a way to check the dynamic stability of structural parts, to search for locations of the biggest stress, locations with accumulation of mechanical energy. Experiments are made with the basis of potential action caused by extreme aero impact. Opencast mining machinery - Excavators and Stacker can move in unconsolidated - soft ground. Their inclination additionaly increases the complexity of situations in which they are located. Therefore, the basis of dynamic design is primarily the analysis of its own structure parts. This is the basic dynamic analysis known as - modal analysis. Modal analysis of support structure of Stackers is the subject of numerical and experimental research in this paper. Modal analysis is performed as the basis of transient analysis for damping modeling. Modal analysis is performed before the harmonic analysis to determine its own values in the particular solutions of differential equations.

1. DYNAMIC MODELING OF STRUCTURES

Dynamic modeling of Stackers was made by forming of a discrete system mass of support structure members and equipment involved. The masses are mutually coupled with elastic connections structure members. The modeling was done using the pre / post processor FEMAP [6] for the finite element method. The supporting structure of slewing platform and bridging boom of Stacker is a lattice type and was modeled by

*Corr. Author's Address: Faculty of Mechanical Engineering, A.Medvedeva 14, Niš, Serbia, miomir@masfak.ni.ac.rs

finite element type beam. The Accessories, belts, rollers and material are modeled with grid point-mass finite element in the lattice structure parts. Counter-weight mass is represented by an element of mass concentrated in two rear nodes of the model. Previous studies [2] have considered similar structure parts modeled for FEM analysis or analytical forming of differential equations of simpler models. Consequently, geometry of dynamic model has Stacker 55x16x5.4 m and slewing mass of 175 t. The model has a total of 2012 finite elements (mass) and 934 nodes (Fig.1). This large number of masses makes the modeling more real and leads to better results. The model enables easy dynamic checking of incidental situations with failures of structure parts. This is a special purpose of modeling. The model is supported with elastic rotating bearing to underframe Stacker with the system tracked the movement. The elasticity of rotating bearing is placed in the domain of rigid links. The influence of the incoming conveyor (at the top stacker bunkers), is modeled with elastic link using spring elements.

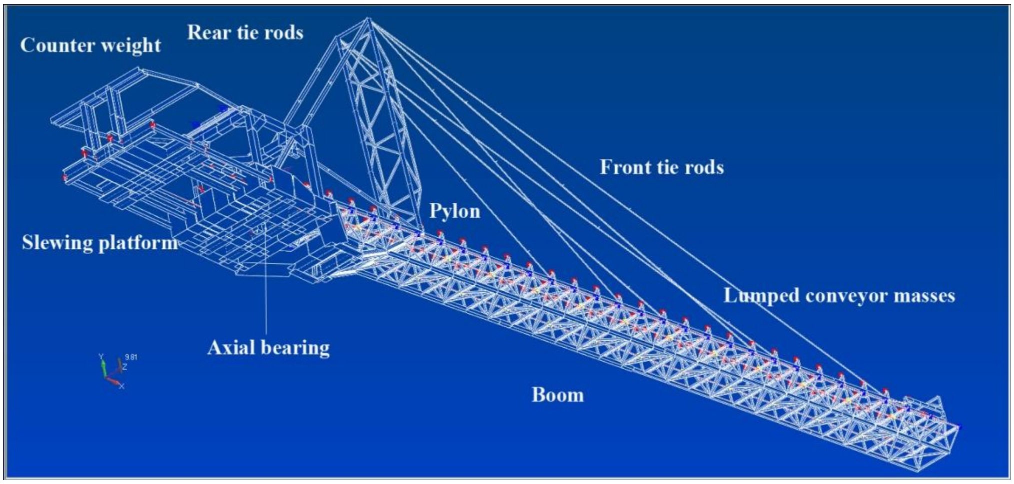

Fig. 1. *View of the ground: Dynamic model sleving supporting structure of the Stacker*

2. NORMAL MODES ANALYSIS

The equation of motion for an undamped system, expressed in matrix notation using the above assumptions is (1) and for a linear system, free vibrations will be harmonic of the form [1] (2):

$$[M]\cdot\left\{\ddot{q}\right\}+[K]\cdot\left\{q\right\}=\left\{0\right\}, \tag{1}$$

$$\left\{q\right\}=\left\{\Phi\right\}_i\cdot\cos\omega_i\cdot t, \tag{2}$$

In normal modes analysis we determine the eigenvalues and eigenvectors of the model. For each eigenvalue, which is proportional to a natural frequency, there is a corresponding eigenvector, or mode shape. Normal modes analysis solves for the undamped free vibrations as follows (1):

$$\left|[K]-\omega^2\cdot[M]\right|\cdot\left\{\Phi\right\}=\left\{0\right\}, \tag{3}$$

In equation (3) there are mass matrix [M], stiffness structure matrix [K], $\boldsymbol{\omega_i}$ - i[th] natural circular frequency (radians per unit time) and $\{\Phi\}_i$ eigenvector representing the mode shape of the i[th] natural frequency.

Normal modes analysis computes the natural frequencies and mode shapes of a structure. The natural frequencies are the frequencies at which a structure will tend to vibrate if subjected to a disturbance. The deformed shape at a specific natural frequency is called the mode shape. Normal modes analysis is also called real eigenvalue analysis.

Normal modes analysis forms the foundation for a thorough understanding of the dynamic characteristics of the structure. Normal modes analysis is performed for many reasons, among them assessing the degree of correlation between modal test data and analytical results. Also, normal modes analysis is a base for selecting the proper time or frequency step for transient and frequency response analyses.

The eigenvalues are related to the natural frequencies as follows: The first option-unit modal mass-is generally preferred, though the scaling of a maximum displacement to 1.0 is useful for comparison to modal test data.

This examples take *Lanczos* method, Modified *Givens* method and *Sturm* modified inverse power method for eigenvalue extraction [1]. The *Lanczos* method is the best overall method due to its robustness, but the other methods (particularly the modified *Givens* method and the *Sturm* modified inverse power method) have applicability for particular cases.

3. RESULTS OF MODAL **FEM** ANALYSIS

The following tables I, II summarize the results of the oscillation frequency of boom structure, frames, stands and the pylon without details of the rod frequencies. Rod frequencies are actually between tabular frequencies of oscillation of the main structure parts. By using the modal analysis [3], the first 100 eigenvalues and eigen vectors (modes) were identified. Those first 100 natural frequencies should be placed (distributed) between the values of Ω = 0.02 Hz and 20 Hz. Very low basic frequency is a consequence of suspension of massive structure parts over a small axial-bearing and large boom overhang forward and stand back. Various models of suspension rotating pedestal, the model tested, have the biggest influence (as compared to other structure parts) on the eigenvalues of the modal analysis. Fig.2 shows the basic form of oscillation rotating of Stacker body. It is actually a lateral body rocking Stacker with pylon rotation around the longitudinal boom axis. Fig.3 shows the mod-87 with two successive vertical sine wave at 15.9539 Hz. The overal structural damping coefficient G=0.1 and coefficient of material damping ζ=0.02 were used in modal analysis [1].

Tabela I	**Mod-1**	Mod-28	Mod-31	Mod-47	Mod-56	Mod-57	Mod-58	Mod-68
Ω [Hz]	0.0199211	0.921305	0.986803	2.687841	3.997874	4.569916	5.079411	8.762432

Tabela II	Mod-71	Mod-74	Mod-78	Mod-87	Mod-89	Mod-92	Mod-100	Mod-00
Ω [Hz]	9.31258	10.27829	12.48331	15.95396	16.24567	17.43946	19.39693	

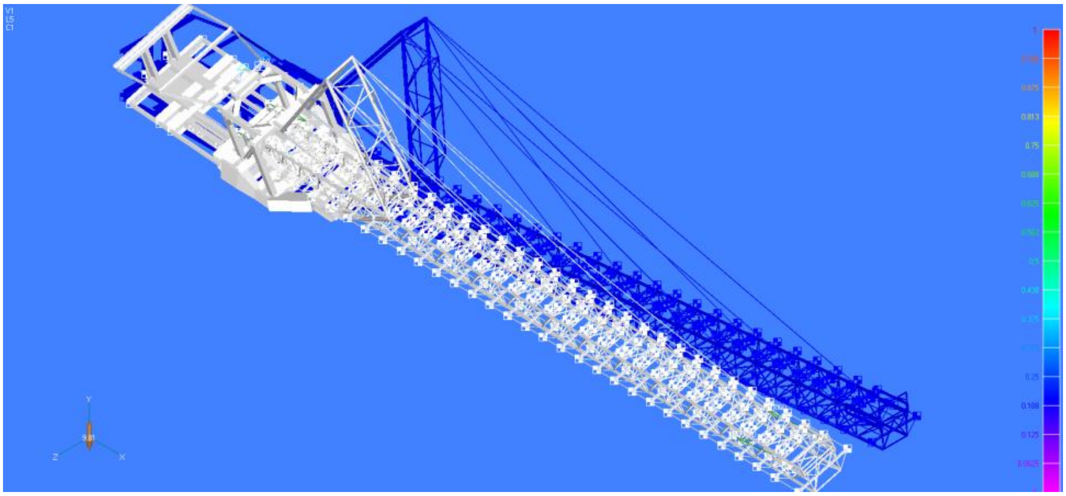

Fig. 2. *Mode 1: First (basical) eigenfrequence of rotated assembly Stacker structure Frequency 0.0199211 Hz (lateral oscillation of the body around the longitudinal boom axis)*

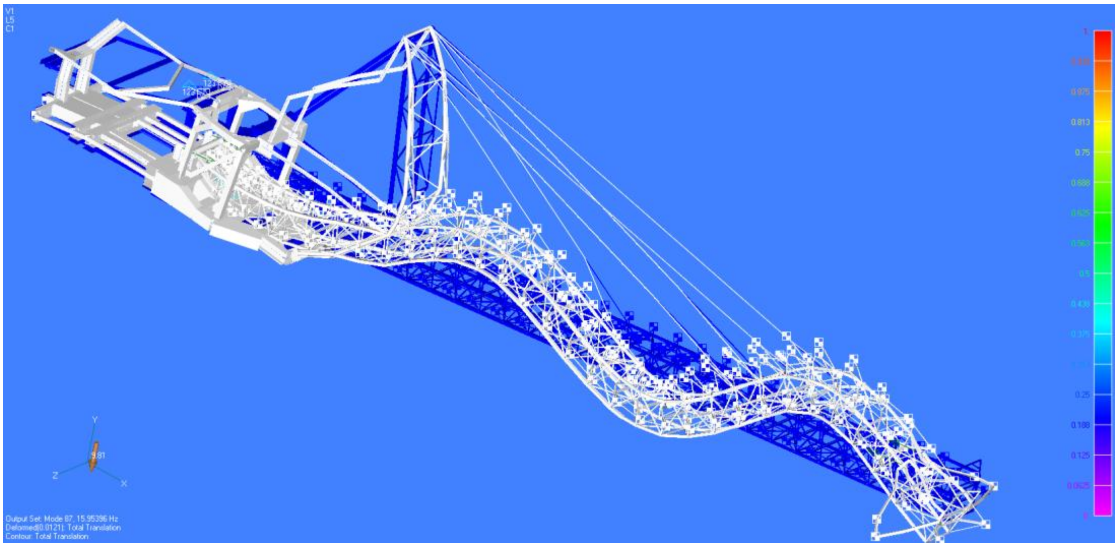

Fig. 3. Mode 87: Hight eigenfrequence (n=87) with charakteristic modal shape
Frequency 15.9539 Hz (double vertical sine wave)

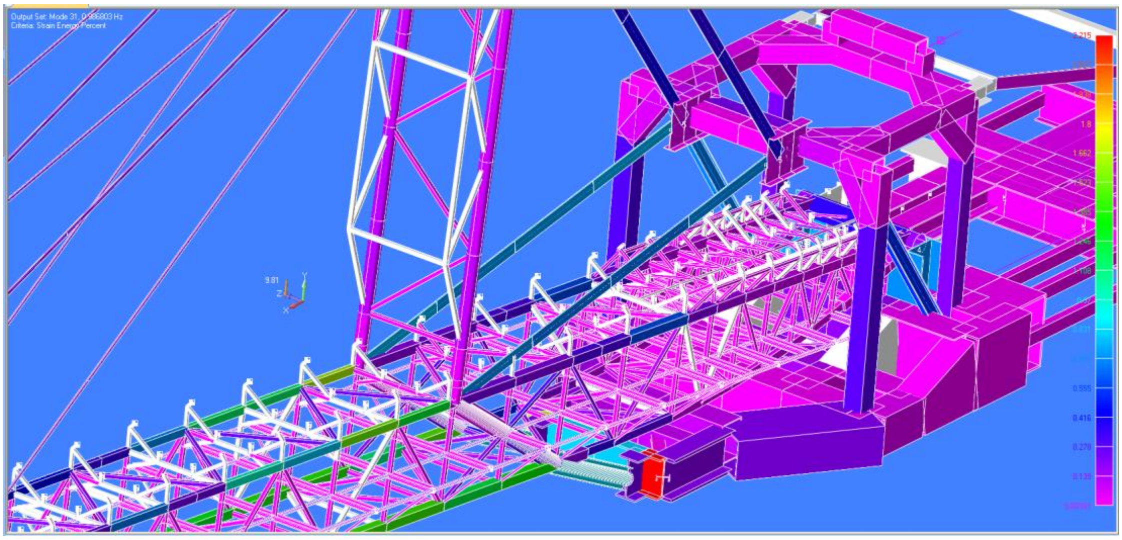

Fig. 4. *Strain Energy Persent (Density) – Mode 31,* f_{31}*=0,9868 Hz,*
Red color is the higest Strain Energy Density – under boom on the frontal beam of sleewing platform.

With modern software it is possible to see the percentage distribution of strain energy for each model value. This can be seen in the defect of geometric elements design of the structure (fig. 4, red colored structure parts). The occurrence of high strain energy in several modes demonstrates overloading parts of the structure and a necessary change of geometry. Thus, based on dynamic analysis, it is possible to improve the initial solution structure and provide a good behavior in exploitation.

4. EXPERIMENTAL TESTING

Reality of investigated eigenvalue was checked experimentally by measuring the acceleration of the characteristic points of structure [4]. The three component acceleration with excitation caused by the driving motor of the belt conveyor were measured on the basis of the pylon (vertical column on the boom, fig 1.). A three-component piezo sensor ADXL-312 brand MEMS with integrated amplifier Analog Device AD-320 and SD memory of 4 GB were used as the sensor. Record of measurements in binary format were analyzed by HBM Catman software. On the basis of measured accelerations in time domain, the acceleration and speed in the frequency domain were identified using FFT transformations. Thus are clearly defined all the present dominant frequencies - enforced and their own. Figure 5-a shows an experimental record acceleration in the three component directions of the pylon base. Red curve (**A**y) is the acceleration in the vertical direction, the blue curve (**A**x) is the acceleration in the lateral direction, black curve (**A**z) are boom accelerations in the longitudinal direction. Component accelerations are up to 0.2 m/s^2. Figure 5-b shows the FFT transformation in the frequency domain. In the domain of 0-20 Hz dominated the accumulation of natural frequencies. In all three directions there are about 125 peaks corresponding to scale number of selected solutions. The drive motor excitation appears at 25 Hz (Figure 5-b, blue curve).

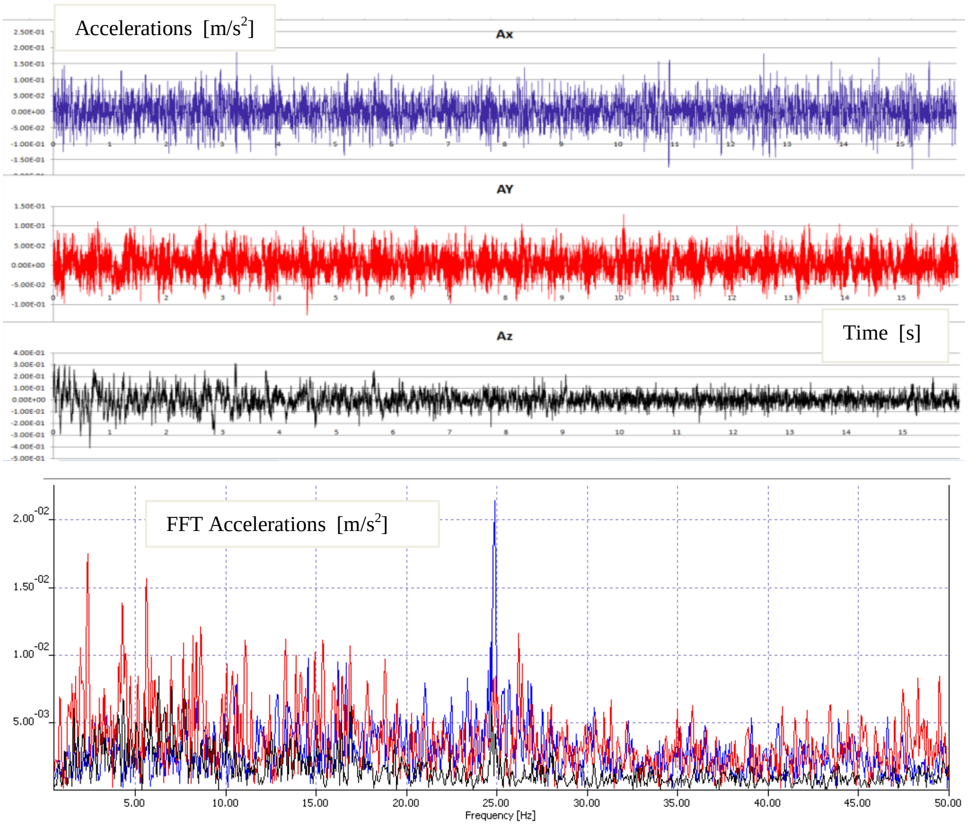

Fig. 5-a,b *Experimentally measured acceleration xyz and FFT frequency signals as a function of time. Measuring location: The basis of the pylon.*

The maximum acceleration experimentally determined (measured) on the pylon was in the time domain of 0.15 m/s^2 while its acceleration in the frequency domain was 0.02 m/s^2. The measured velocity in the time domain is 2 mm/s while in the frequency domain it is 1.3 mm/s.

5. CONCLUSION

Commenting on the dynamic properties of Stackers, for its importance and great working capacity, it can be concluded:

1. Experimental finding of single frequencies is much more efficient using actuators working with adjustable excitation.
2. Vibro-excitation must have sufficient force to cause the frequency response with the corresponding elastic forms - modes. This way a verified dynamic system is obtained.
3. The quality of the developed models is in small approximations (high detail of structure), which were introduced to all supporting structural elements of the real object.
4. The disadvantage of developed model is an inexperience of the true summary stiffness of the main support (axial bearing, tracked undercarriage and soil stiffness).
5. Additional quality of the model can be set easily for incident check situation with ties, wind and structures inclination in unconsolidated soft ground.
6. The experimental vibration-analysis showed a steady dynamic behavior of boom with small amplitude acceleration.
7. Modal analysis and experimental analysis introduce us to real frequency range of structure and show the presence of a large number of frequencies in the model. This fact suggests future studies using transient dynamic analysis of the range of applied frequencies.
8. The accuracy of some numerically obtained and experimentally established frequencies can be improved by carefully adjusting the suspension stiffness of the whole structure through main axial bearing.
9. Developed model allows the identification of locations where vibration sensors, stress sensors and deviation sensors in order to reliably follow the dynamic properties of structures in different situations. This hold transportation capacity on the maximum.
10. The developed software, which can include various of material properties of the structure [1,6], the type of dynamic actions and which can solve different types of dynamic analysis, are good tools for industrial design of lattice supporting structure of opencast mining heavy machines.

6. REFERENCES

[1] Basic Dynamic Analysis, MSC Nastran, Version 68, Santa Ana, CA, USA, 2004

[2] Ostrić D., Gašić M., Simonović M., Savković M.: "Dynamic models of Portal rotating Cranes", *XIV ECPD International conference on material handling and warehousing*, p.p. 4.93÷4.98, Beograd, 1996.

[3] Jovanović M., Milić P.: "Statical Stacker-boom Inspection on Opencast mining system Veliki Krivelj RBB-Bor", Project no. 612-22-70/11, Mechanical faculty University of Niš, 2011.

[4] Maneski, T.: "Vibration measuring on Stacker supporting structure OU-1 in Opencast mining system Veliki Krivelj RBB-Bor", IC Mechanical faculty University of Belgrade, Dec. 2010.

[5] http://www.fam.de/Stacker-reclaimers.html,

[6] MSC NASTRAN (2004), MSC. Software Corporation, Santa Ana, CA 92707, USA, www.mscsoftware.com

ACKNOWLEDGEMENTS

The dynamic research is realized with the Ministry of Science and Education of Republic Serbia funds within the project **35049** in 2011. The authors would like to thank the sponsor.

HEAVY MACHINERY - HM 2011, 79-84
ISBN 978-86-82631-58-3
Paper accepted: 23.05.2011

Incidental Behavior of the Structure with Reduced Technical Correctness

Miomir Jovanović[1,*] - Goran Radoičić[2]
[1] University of Niš, Faculty of Mechanical Engineering
[2] Public Utility Company "Mediana" Niš

The paper studies the behavior of lattice structure of tower crane elastically supported on the ground in the case of incidental event. A random event, caused by sudden fall of load due to disruption of link, has consequences such as the occurrence of large amplitudes of oscillation, the reduction or even loss of stability. Changed oscillation forms are expected in the dynamic response to the incident and at the tower crane with damaged structure. Damage is the result of the previous incident and it is reflected in the failure of several major elements (angled rods) of lattice structure in the suspension area. Modeling of crane, in this paper, was performed using finite element method. FEM model is a discrete form of tower crane and it is enhanced by introducing spring element in the suspension area. The research was based on finding the critical value of load which leads to loss of local stability of structure in the damaged area. The paper describes the differences between the two indicators of the dynamic behavior of structures (correct and damaged). On the basis of the obtained solutions of analysis, the general conclusions with the graphics that indicate on the degree of risk of accidental event are derived.
Keywords: Tower crane, incident, dynamic response, stability, oscillation forms, large amplitudes.

0 INTRODUCTION

Tower cranes are in fourth place in the number of incidents with more than 2.5% of the total number of incidental events with cranes and behind of mobile (most incidents), bridge and portal cranes [4]. Random events, such as: fall of load due to sudden disruption of the link between hook and load, attack of strong wind, seismic activity, etc., are causes of the incidental states with cranes. Dynamic forces, due to incidents, can lead to decrease or loss of stability, as well as the damage to structure. Due to using, damages of elements of tower cranes and other lattice structures occur in practice. Technical correctness can be conditioned by the previous incident, such as the failure of one or more elements (angled rods) in the suspension zone of crane, which is a real practical problem. Dynamic response of the structure with reduced technical correctness is different in relation to the correct structure at incidental event.

Research in this paper relates to tower crane TOPKIT FO/23 B POTAIN-MIN, as represent of lattice structures, with basic characteristics: capacity of m_n=2.3 tons, maximal range of 50 meters. Material of supported structure is constructive steel EN 10025 (S 355).

1 DYNAMIC MODELING OF CRANE

Modeling was performed using finite element method in software FEMAP [5]. Tower crane is presented with a discrete model based on the elements of the typical geometric forms. Members of the lattice structure are presented with BEAM finite elements and different cross sections. The model contains four equal concentrated forces in four nodes at the end of the boom. The mass of load for stabilizing on the pedestal of crane is divided on eight concentrated masses and mass of the counter-weight is divided on four concentrated masses in four nodes at the opposite end of the boom. All concentrated masses are presented with MASS finite element. Own weight (LOAD BODY) is taken into account, too. Previous research [3] has considered the model of tower crane, which contains a rigid connection between structure and base with constraints of translation in tree directions, in each of the supports. Improvement of the model would imply the introduction of the elastic supporting elements, which would lead to more realistic conditions of exploitation while keeping the existing conditions of movement constraints. Because of that, each of the supports has installed one SPRING finite element which includes elasticity. Spring finite element better defines the

*Corr. Author's Address: University of Niš, Faculty of Mechanical Engineering, A.Medvedeva 14, Niš, Serbia, miomir@masfak.ni.ac.rs

stiffness of the link “ground - supporting rod”. The expansion with new elements made the improvement of a discrete FEM model, which now contains in total 807 finite elements and 297 nodes (Fig. 1).

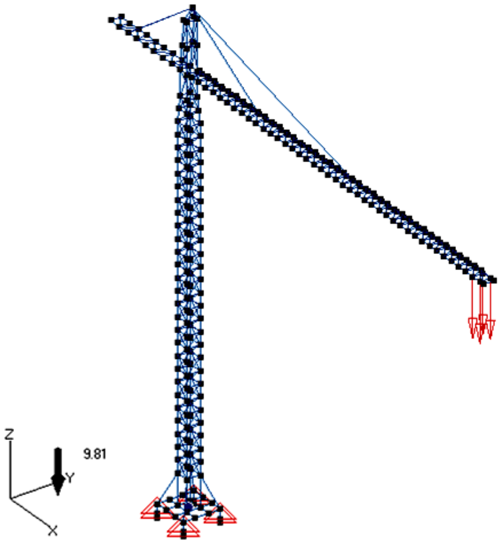

Fig. 1. *Dynamic model of tower crane with concentrated masses and load forces*

After making the dynamic model, task is solved by finite element method using the principle of functional variation [1] in software MSC NASTRAN [6]. Law of motion of the system is requested on the basis: matrix of mass **M**, damping matrix **B**, stiffness matrix **K** and external forces **Q** (t). Transient response of structure q(t) is defined with eq. (1):

$$[M]\cdot\left\{\ddot{q}(t)\right\}+[B]\cdot\left\{\dot{q}(t)\right\}+[K]\cdot\left\{q(t)\right\}=\left\{Q(t)\right\}, \qquad (1)$$

which is a modified form (2):

$$[M]\cdot\left\{\ddot{q}(t)\right\}+(1+i\cdot G)\cdot[K]\cdot\left\{q(t)\right\}=\left\{Q(t)\right\} \qquad (2)$$

where are:
G – Overall structural damping coefficient and
K – Stiffness matrix of considered system.

The structural damping force is function of a damping coefficient G and a complex component of the structural stiffness matrix, eq. (2). Two parameters are used to convert the structural damping in the equivalent viscous damping – parameter $\omega_{3,r}$ and $\omega_{4,r}$. Both parameters are calculated from previous modal analysis (b=G·k/ω).

Previous incidents, in the form of failures, first in one of the structural element in suspension area (E33), and then another in the same zone (E34), caused reduction of the overall technical correctness of structure of the crane. Elements in failure are shown dashed in Fig. 2. Partially correct structure should then be tested dynamically (transient dynamic analysis) on the following incident in the form of sudden fall of load. After the analysis, it should be estimated if the disturbance of dynamic stability of the structure and its values occurred.

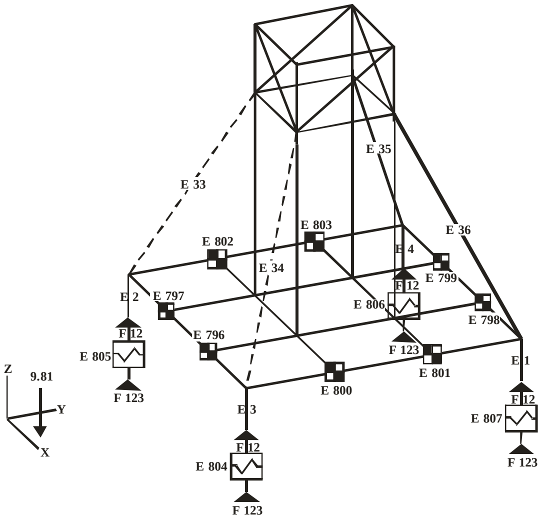

Fig. 2. *FEM model of the pedestal of crane with spring and mass elements*

2 SCENARIO TESTING

Testing of the model on the incident, in order to obtain the dynamic response of the structure, is based on the scenario which has three parts: 1) stabilization of the position of the lifted load (calming of oscillation) in period of 500 sec; 2) disruption of link between load and hook in period of 1 sec; 3) calming of structure after sudden fall of load and discharging of the crane in period of 399 sec. The change of perturbation force *y* in function of time testing *t* is shown in Fig. 3. Time step of integration is 0.1 sec and total number of steps is 9000. Coefficient of structural damping is G=0.05. After a certain number of tests on the model with different values of load and simulation of the incident, the value of critical load is found for which the disorder of the structural stability occurs.

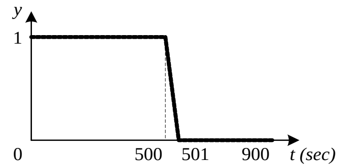

Fig. 3. *Form of the perturbation load force*

3 CHARACTERISTICS OF DYNAMIC BEHAVIOR OF STRUCTURE

Dynamic analysis of the model included three states of correctness of the crane: correct structure (state 1), structure with one faulty element (state 2) and with two faulty elements (state 3) in the suspension area. In the first and the second case of tests (cases 1 and 2), stresses in elements of the structure during the testing didn't overstep the allowed values:

$$\sigma_i < \sigma_{\max}^{III} = 30\frac{kN}{cm^2}. \tag{3}$$

Dynamic tests of the structure in the state of correctness No. 3 showed the existence of the limit value of stress (bending) and the risk of occurrence of plastic deformation on a small number of elements which indicates the need for remodeling of the structure from the aspect of increasing cross-section of the critical elements, and strengthening the structure in the reliance zone.

Further analysis will refer to the cases of correctness of the structure No. 1 and No. 2.

Assessment of static stability of the model was made previously. The problem requested nonlinear static analysis. Both models have reserve of static stability, which indicates the possibility of accepting something greater static load than the nominal ($m_{S(1)}$=3.8 tons, $m_{S(2)}$=3.475 tons). The coefficients of static stability are:

$$K_{S(1)} = \frac{m_{S(1),kr}}{m_n} = \frac{3.8}{2.3} = 1.65 \tag{4}$$

$$K_{S(2)} = \frac{m_{S(2),kr}}{m_n} = \frac{3.475}{2.3} = 1.51 \tag{5}$$

Incidental dynamic strain is caused in each of the tests with disruption of the link "hook-load", which leads to fall of the load. By performing dynamic tests, with changing the nominal load, a change of sign of axial force is required in some of support rods. Then the axial force from the press goes into tensile (leading to the separation of wheels from base), which directly undermines the stability of the crane. A test load which causes disturbance of stability is the critical dynamic load and it is m=3.3 tons (case 1), and m=1.64 tons (case 2).

Element E1 is located on the front side of pedestal crane in the position of testing (load side) and it has first change of the sign of axial force after incident of the fall load in both states of correctness of the structure and after certain number of dynamical tests (Fig. 4). For that time the element E4 on the opposite side (counter-weight side) remained pressed and didn't have influence on the reduction of stability. Pressure force in this rod of reliance is in the interval of 130 ÷ 560 kN.

The dynamic coefficients for both cases of examination are:

$$K_{D(1)} = \frac{m_{D(1),kr}}{m_n} = \frac{3.3}{2.3} = 1.43 \tag{6}$$

$$K_{D(2)} = \frac{m_{D(2),kr}}{m_n} = \frac{1.64}{2.3} = 0.71 \tag{7}$$

Relative difference of the dynamic coefficients indicates on reduction of the reserve of stability of the damaged structure in relation to the undamaged structure (8):

$$\Delta K_D = \frac{K_{D(2)} - K_{D(1)}}{K_{D(1)}} = \frac{0.71 - 1.43}{1.43} = -0.503 \tag{8}$$

Negative difference of the coefficients ΔK_D shows importance of the role of taking the dynamic influence of one of the angled rods in the area of suspension crane that can be damaged and therefore reduced effectiveness (element E33).

The angled rods E34 and E36 of the correct structure behave almost equally in taking of dynamic forces in the incident. The rods E34 and E36 of the correct structure, in one period of calming after incident, alternately change the sign of stress (tension-pressure).

The rod E35 in the damaged structure (case 2) suffers the largest pressure force - about 400 kN (Table 1).

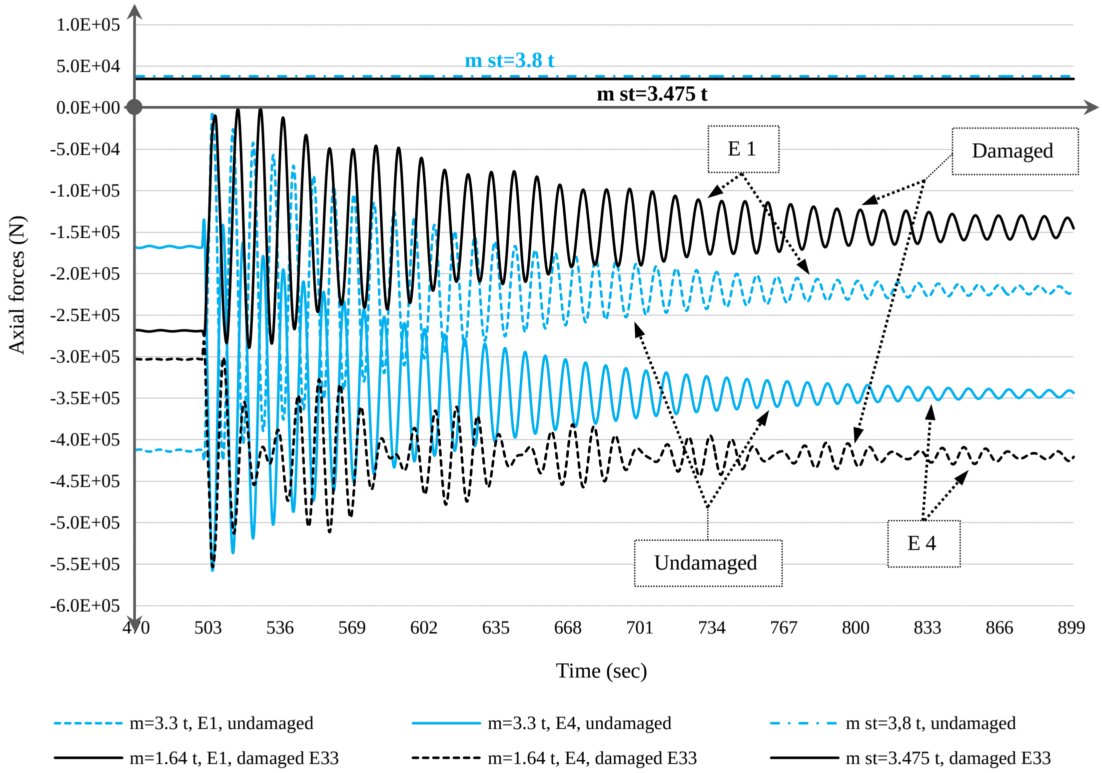

Fig. 4. *Axial forces in two supported elements of the damaged and undamaged structure of the crane*

In the case of damaged structure, load distribution and the sign of axial forces are quite different. In this case, the rod E34 during overall period of calming, takes a part stress on pressure, while the rod E36 continues changing the sign of stress, from time to time strained or pressed.

Amplitudes of forces vary around mean values where the highest mean value is -26 kN (the lowest mean pressure force) and relates to the rod E36 of damaged structure, while the lowest mean value is -284 kN (the highest mean pressure force) and relates to the rod E35 of damaged structure too (Table 1).

Table 1. *Axial forces in angled rods for two cases of correctness*

	Angled rod - element E34		Angled rod - element E35		Angled rod - element E36	
	Undamaged structure	Damaged structure (fault-E33)	Undamaged structure	Damaged structure (fault-E33)	Undamaged structure	Damaged structure (fault-E33)
Max. axial force (N)	≈ E36	-95114	-23730	-155832	98767	115191
Min. axial force (N)	≈ E36	-246590	-431392	-408857	-304037	-166695
Average value (N)	≈ E36	-172838	-226100	-284500	-107100	-25700

The sole form of high structures, with the existence of damage of some of the elements (especially in the area of suspension) and the occurrence of disturbance forces (due to incidents), is a generator of oscillatory movement of large amplitudes, especially of the nodes at the end of elements of the lattice structure (furthest from the center of gravity), in the first place, in the nodes of the boom. The model contains two nodes at the end of the boom (N291, N293). The most attention is dedicated to the movement of nodes in the coordinate z-direction (vertically) when the test load is equal with critical load for dynamical stability of the structure. The difference in the length of displacement, and thus the size of the amplitudes of oscillations of these two nodes is very small during the tests and in three cases of correctness of structure varies to maximum rank of second decimal (0 to 9 cm). Therefore, in further consideration of the problem only one of the nodes is taken into account - the node N293 (Fig. 5).

Maximum absolute displacement of the node at the end of the boom of undamaged structure in vertical direction (state 1) begins in the moment of disruption of link between the hook and the load and takes a few seconds after the fall of load on the ground. Then the node N293 is moved in the z-direction even 7.4 m. For time of calming of the boom, the node oscillates around the value of z=+1.1 m. In the case of damaged element E33 on counter-weight side, law of oscillation is significantly different, and the initial amplitudes in the z-direction are not so pronounced. Oscillating of the node N293 during the calming of structure is around the value of z=+1.6 m. Node N293 of the structure with two damaged elements (E33, E34) oscillates around the value of z=+1.3 m.

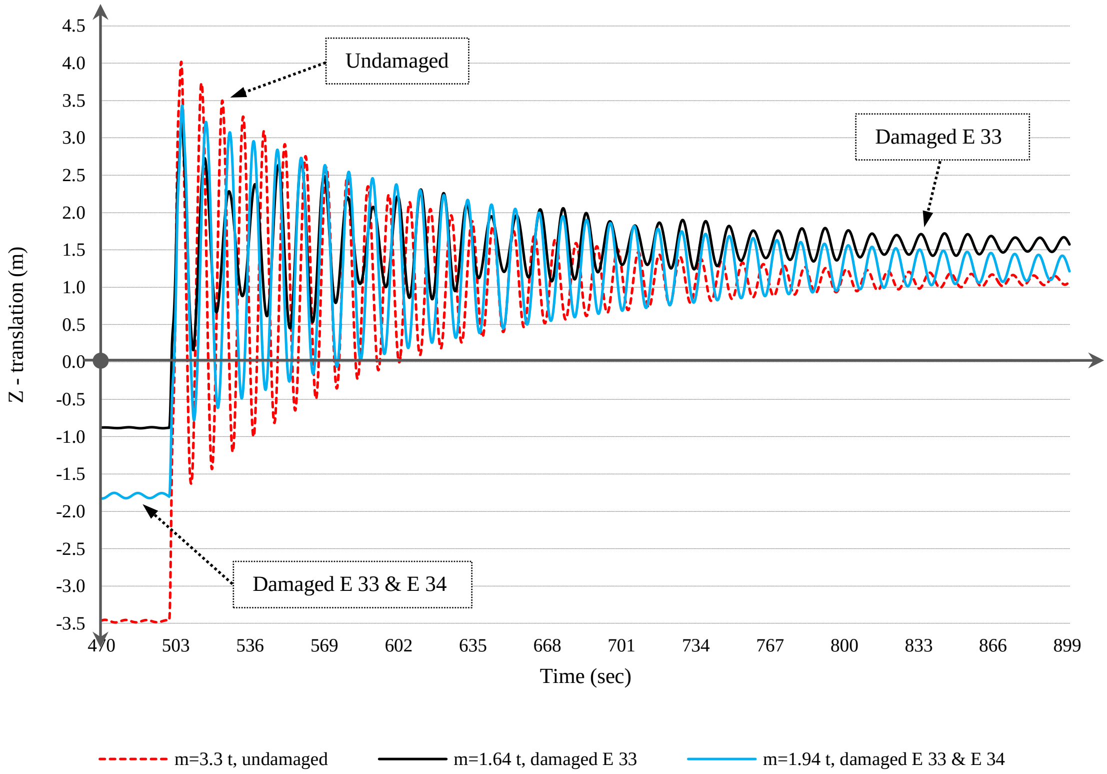

Fig. 5. *Moving the node N 293 in the global z-direction*

Periods of oscillation for different cases of damaged structure are different from those of the correct structure of the crane, and their values are:

- T=9.2 sec (ω=0.1087 Hz) - for correct structure,
- T=10.5 sec (ω=0.095 Hz) - for structure with the damaged element E33,
- T=10.6 sec (ω=0.0943 Hz) - for structure with the damaged elements E33 and E34.

4 CONCLUSION

A better FEM model is obtained by introducing the elements of elasticity and clearance (SPRING and GAP finite elements). Application of these finite elements provides more realistic picture of dynamic behavior of the structure and makes the results of analysis more accurate.

The own frequencies (eigenvalues) of the first hundred modes of oscillation are requested by modal analysis. Selected dominant values of frequencies cause significant displacement of nodes at the end of the boom of crane in the vertical direction, and do not affect on deformation the local structure of the boom. They represent the input frequencies of transient dynamic analysis.

Dynamic responses of the structure are significantly different depending on occurence of damage in structure of elements in the reliance zone under the influence of external disturbance forces. The difference is shown in the coefficient of dynamic stability where the dynamic reserve of the damaged structure is for 50% less than the reserve of the correct structure. Damage in more elements of lattice structure leads to the limit stress states in some of the horizontal rods of the pedestal, which indicates the need to strengthen the structure.

Reserve of dynamic stability of correct structure is positive and gives the possibility to overdraft the nominal load (for 40%). Dynamic reserve in partially correct structure (state 2) has a negative sign and indicates the danger of loss stability during work with loads (m_2), which do not satisfy condition (9):

$$m_2 \le K_{D(2)} \cdot m_n \tag{9}$$

in the case of incidental event.

Lattice structures have a characteristic to download external dynamic effects caused by random events, when some of the elements of structure, due to damage, can't fully perform its function. Apart from angled rods, significant part of dynamic influence overtake vertical rods (tension, pressure) and horizontal rods (bending) of structure in the reliance area of tower crane.

The highest amplitudes of oscillation of the node N293 at the end of the boom in the z-direction appear in the correct structure. In other models with partially correct structure, the oscillations have a more expressed spatial character, and displacement vector of node N293 has components in all three global directions.

Nonlinear problems of complex structures require the formulation of quality dynamic model and use of the finite element method, and then solving with numerical methods in direct transient analysis. From this aspect, software FEMAP and MSC NASTRAN are modern and effective tools for modeling, processing and post-processing and risk assessment of the structures with reduced technical correctness and high lattice structures, due to external disturbance effects.

X REFERENCES

[1] Jovanović, M., *Theory of computer design structures*, Faculty of Mech. Eng., Niš, 1994

[2] Fu, F., "3D Nonlinear Dynamic Progressive Collapse Analysis of Multi-storey Steel Composite Frame Buildings – Parametric Study", Engineering Structures, Vol.32, pp 3974-3980, 2010

[3] Radoičić, G., P. Milić, M. Jovanović, "Dynamic behavior of damaged structure of crane in the next incidental event", The 7th International Conference Research and Development of Mechanical Elements and Systems, Zlatibor, Serbia, 2011

[4] Yow, P., R. Rooth, K. Fry, "Crane accidents 1997-1999: A report of the crane unit of the division of occupational safety and health", Department of Industrial Relations / Division of Occupational Safety and Health, California, USA, 2000

[5] FEMAP, Siemens PLM Software, Plano, TX 75024, USA, http://www.plm.automation.siemens.com

[6] MSC NASTRAN (2004), MSC. Software Corporation, Santa Ana, CA 92707, USA, www.mscsoftware.com

[7] Gašić, M., Savković, M., "Dynamic influence of lifting a load with portal-rotating crane", IMK-14 Research and Development, Vol.(7)1/1998, pp 15-19, ISSN 0354-6829, 1998.

ACKNOWLEDGEMENTS

The dynamic research is realized with the Ministry of Science and Education of Republic Serbia funds within the project 35049 in 2011. The authors would like to thank the sponsor.

HEAVY MACHINERY - HM 2011, 85-88 Paper accepted: 30.05.2011
ISBN 978-86-82631-58-3

Modelling Resistance of Digging of Hydraulic Excavators

Dragoslav Janošević [1*], Nikola Petrović[1], Predrag Milić[1], Vesna Nikolić[1]
[1]University of Niš, Mechanical Engineering Faculty

In paper firstly analyzes the geometric, kinematic and dynamic variables which have influence on the resistance of digging deep buckets of hydraulic excavators. Then are given the developed mathematical models for determination of digging resistance when during the digging only moving bucket and when are at the same time moving arm and bucket manipulator of excavator. Developed mathematical models of digging resistance can be used for dynamic simulation of excavators.

Keywords: hydraulic excavators, digging resistance

1. INTRODUCTION

For optimal development of hydraulic excavators it's need to make a detailed dynamic analysis of all their systems using appropriate mathematical models. The implementation of such complex analysis is achieved by numerical simulation based on the direct process dynamics, where, assign parameters of manipulative task excavators in function of time, by using defined mathematical model of kinematic chain excavators, determined: position, speed and acceleration of each chain member and loading, the necessary energy and power in the joints of the machine chain [1].

In this paper is observed the mathematical model of kinematic chain excavators with configuration which consists: thrust-motional segment L_1 (сл.1), revolving platform L_2, and the deep manipulator with boom L_3, arm L_4 and bucket L_5.
To complete determine the simulation procedure, beside appointed mathematical model of kinematic chain, are defining and models of parameters of machine functions which are related to: a) structure functions, b) trajectory, v) the time and g) technological resistance of manipulative task in the whole working area of excavator.
Work of hydraulic excavators is characteristic by fact that the manipulation tasks are numerous and cyclical but with the same structure of operations which consists: choosing a location digging, digging process, transfer and selection of planes unloading and loading of the affected material. However, in each cycle, the operations have different parameters.
Each operation of manipulative task is defined by its parameters: trajectory of movement, duration and resistance movement.

2. MODELS OF DIGGING RESISTANCE

Resistance movement of segments kinematic chain excavators appear in the form of internal (gravity), inertial (dynamic) and external (technological) loading.
External (technological) loading occur during digging operations in the form of digging resistance force W (Fig. 1) and torque M_w digging resistance. In the simulation adopts are symmetrical continuous loading of digging resistance along the cutting edge bucket, so that the moment of resistance digging $M_w=0$.

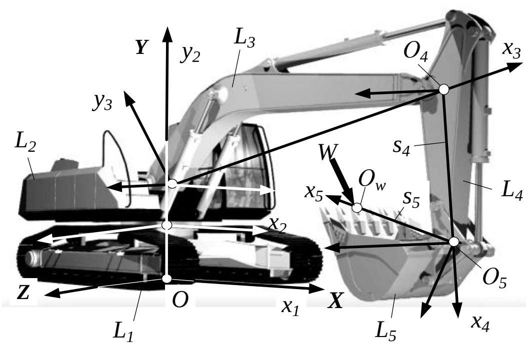

Fig. 1 Mathematical model of hydraulic excavators with deep manipulator

The total resistance of digging W are modeled, depending on the geometry of piece sheared off

*Corr. Author's Address: Mechanical Engineering Faculty, A. Medvedeva 14, 18000 Nis, Serbia, janos@masfak.ni.ac.rs

and physical-mechanical characteristics of the affected land, by the equation [1][2]:

$$W = k_k \cdot b \cdot h \cdot \xi \tag{1}$$

where is: k_k - specific resistance to land digging, b - width of piece sheared off, h - thickness of land piece sheared off, ξ - factor of correction of digging parameters depending on the parameters of management method and working conditions of excavator.

Kinematics of digging is performed, depending on the position of digging, moving bucket or simultaneously moving bucket and arm the manipulator where piece sheared off land has a variable thickness h and constant width, equal to the width of the bucket.

During simulation of excavator, geometry of land piece sheared off, for digging kinematics moving just bucket, defined by the model A (Fig. 2 [2]. For digging kinematics simultaneously moving the bucket and arm is developed a model B (Fig. 2b) [1] for land piece sheared off.

2.1. Thickness of land piece sheared off. - Change the thickness h of land piece sheared off, is determined by the following terms:

$$h = h_o \frac{cos(\varphi_{51} - \frac{\delta_{51}}{2} - \varphi_5) - cos(\frac{\delta_{51}}{2})}{cos(\varphi_{51} - \frac{\delta_{51}}{2} - \varphi_5)\left[1 - cos(\frac{\delta_{51}}{2})\right]}, \forall\ (\varphi_{51} - \delta_{51}) \le \varphi_5 \le \varphi_{51} \tag{2a}$$

б) for digging kinematics of moving a bucket and arm (model B) (Fig. 2b):

$$h = h_o \frac{sin(\varphi_{41} - \varphi_4)}{sin\delta_{41}}, \quad \forall\ (\varphi_{41} - \delta_{41}) \le \varphi_4 \le \varphi_{41}, \tag{2b}$$

where is: h_o - maximum thickness of land piece sheared off during digging operation, $\varphi_{41}, \varphi_{51}, \varphi_4, \varphi_5$ - initial and current angles of hand and bucket position at digging, determined in relation to an absolute coordinate system of excavator, δ_{41}, δ_{51} - angles of range of moving arm and bucket while digging operation.

Max thickness of piece sheared off h_o, is determined by the following terms:

a) for digging kinematics of moving a bucket (model A) (Fig. 2a):

$$h_o = s_5\left[1 - cos(\frac{\delta_{51}}{2})\right]k_{pr}, \ \forall\ \delta_{51} = \delta_{51}(V, b_5, s_5, k_p, k_r), \tag{3a}$$

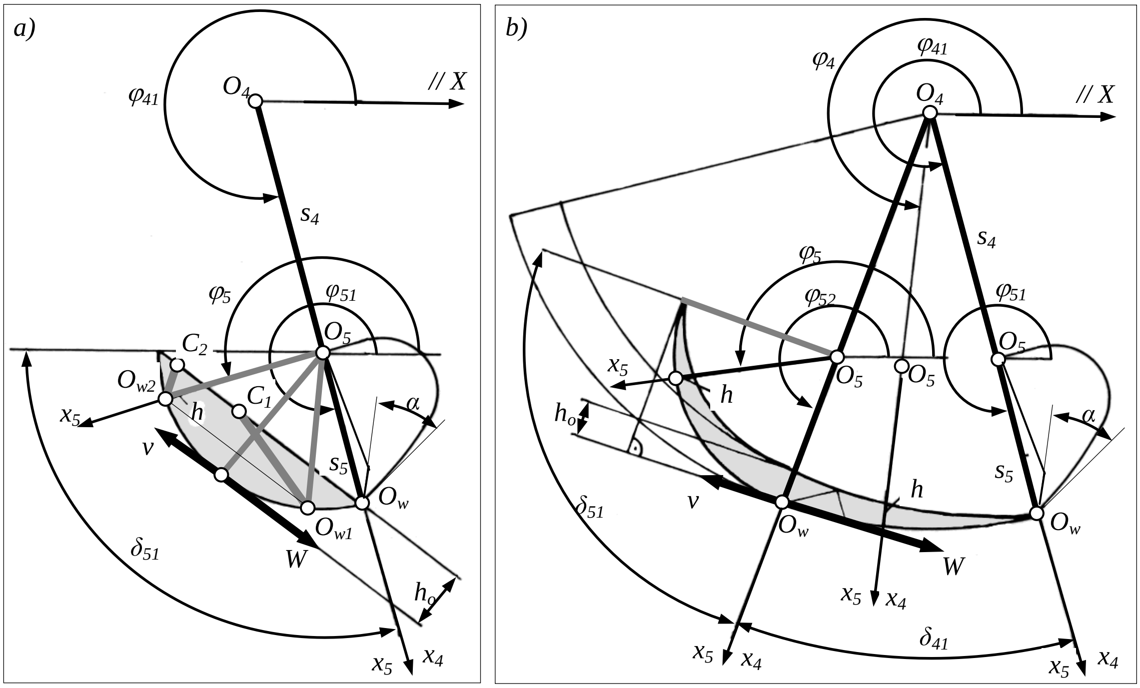

Fig. 2 Models piece sheared off land with bucket hydraulic excavators with depth manipulator: a) moving only bucket - model A, b) simultaneously moving bucket and arm - model B

(model A) (Fig. 2):

arm (model B) (Fig. 2b):

$$h_o = \frac{k_v V}{l_5 s_5} k_{pr},\ \forall\ \delta_{51} = \frac{\pi}{2},\ \delta_{41} = \delta_{41}(V, b_5, s_4, s_5, k_p, k_r, k_v) \tag{3b}$$

where is: k_p - coefficient of charging bucket, k_p - coefficient of loosening land, $k_v=V_5/V$ - factor of digging kinematics moving bucket and arm which represents the ratio of volume part V_5 bucket filled with land while moving only bucket and total volume V of bucket, s_4, s_5 - kinematic length of arm and bucket of excavator manipulators.

2.2. Range of motion. - For geometry of piece sheared off at the digging kinematics of bucket moving, model A, from equality of volumes of piece sheared off and bucket volume, expressed by equation:

$$\frac{l_5 \cdot s_5^2(\delta_{51} - \sin\delta_{51})}{2} k_r = k_p \cdot V \tag{4}$$

gets are equation:

$$\delta_{51} - \sin\delta_{51} - \frac{2k_{pr} \cdot V}{l_5 \cdot s_5^2} = 0 \tag{5}$$

from which are determines the angle δ_{51} range of bucket motion to are bucket full.

For geometry of piece sheared off at the digging kinematics of bucket and arm moving, model B, from equality of part volume of piece sheared off and bucket part of volume bucket that are fill up:

$$\frac{h_o}{\sin\delta_{41}}(s_4 + s_5)(1 - \cos\delta_{41}) l_5 \cdot k_r = k_p(1 - k_v)V \tag{6}$$

Substitution h_o from equation (3b), is find the angle δ_{41} range of motion hand:

$$\delta_{41} = \arccos\frac{(s_4 + s_5)^2 k_{pr}^2 \cdot k_v^2 - s_5^2(1 - k_v)^2}{(s_4 + s_5)^2 k_{pr}^2 \cdot k_v^2 + s_5^2(1 - k_v)^2} \tag{7}$$

where the angle range of bucket motion: $\delta_{51}=\pi/2$.

From the condition: $\delta_{51}= \delta_{41}=\pi/2$ and equality of part volume of piece sheared off which is realized by moving of arm and bucket part of volume bucket that are fill up:

$$h_o(s_4 + s_5) l_5 \cdot k_r = k_p(1 - k_v)V \tag{8}$$

By substitution h_o, from equation (3b), determined the limits of the interval of changing the factor digging kinematics k_v moving bucket and arm:

$$1 \geq k_v \geq \frac{s_5}{s_4 + 2s_5} \tag{9}$$

2.3. Correction factor. - Correction factor ξ of parameters digging include influences at digging conditions and methods of managing on the size of the resistance to digging.

For example, at digging kinematics moving the bucket, model A, as researches [2] showed, for the same thickness of land piece sheared off, appear are different resistance to digging due to the occurrence of different areas (O_{w1}-C_1, O_{w2}-C_2) (Fig. 2a) of slipping land separated from the massif.

For model B of piece sheared off, with correction factor take into consideration the impact of uneven management and working conditions on the insistence of digging.

The value of correction factor parameters of digging for the model is determined by the equations:

a) for digging kinematics of moving a bucket (model A) (Fig. 2a):

$$\xi = \frac{[1 + \cos(\alpha + \varphi)][\cos(\varphi_{51} - \frac{\delta_{51}}{2} - \varphi_5) - \cos(\frac{\delta_{51}}{2})]}{[1 + \cos(\alpha + \varphi - \varphi_{51} + \frac{\delta_{51}}{2} + \varphi_5)]\left[1 - \cos(\frac{\delta_{51}}{2})\right]} \tag{10a}$$

б) for digging kinematics of moving a bucket and arm (model B) (Fig. 2b):

$$\xi = 1 + k_o \sin(\pi\frac{t}{t_1}) \sin(2n_o\pi\frac{t}{t_1}) \tag{10b}$$

where is: α - angle of digging (cutting) (Fig. 2a), φ - friction angle land on the steel edge of the bucket, k_o - coefficient changes the size of digging resistance, n_o - coefficient period change of resistance digging, t, t_1 - current and total operation time of digging.

Values of coefficients change the size and period of digging resistance taken within the limits:

$k_o= 0{,}05\text{-}0{,}15$, $n_o=3\text{-}6$. Are chosen depending on the duration of the operation of digging, working conditions (categories land) and signals transmission systems (management system) of excavator.

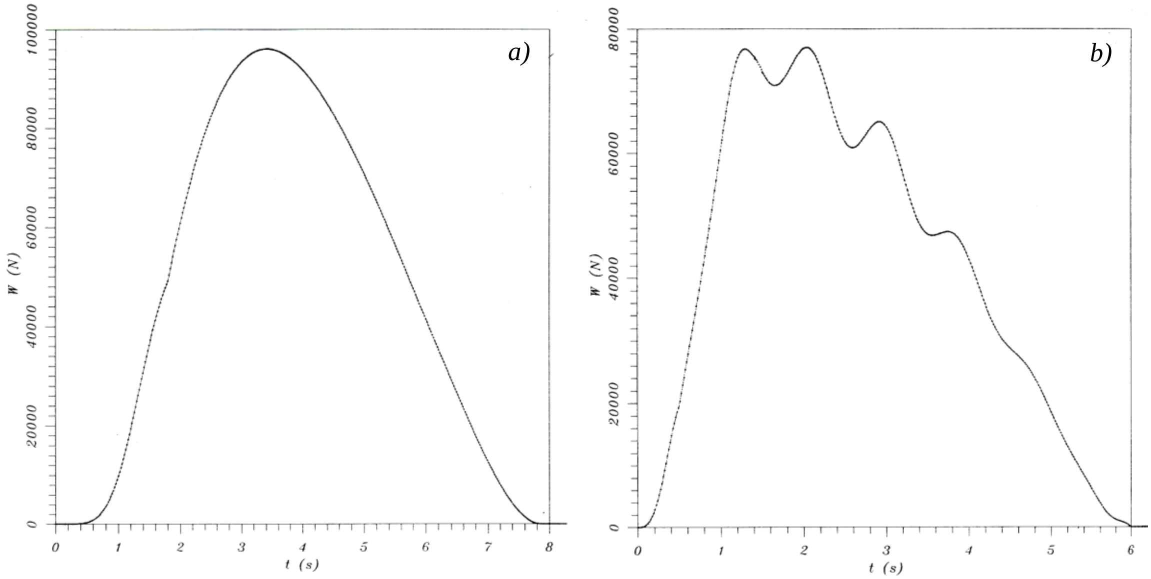

Fig. 3 Changes in resistance digging of hydraulic excavator mass 17000 kg determined for digging kinematics: a) moving only bucket - model A, b) simultaneously moving bucket and arm - model B

Difficult working conditions of excavator corresponding higher values of coefficients to change the size and period of resistance to digging.

For simulation process of digging, it is assumed to resist digging *W* (Fig. 2a,b) has direction of speed *v* of digging: *ort* ***W***=-*ort* ***v***.

Based on defined mathematical models, developed is a program for the determination and analyze resistance to digging by using the computer as a potprogram of the main program for dynamic simulation of the excavator via a computer.

As an example, determined is change resistance to digging of deep bucket excavator, mass 17000 kg for digging technology: moving only bucket (model A) (Fig. 3a) and digging technology of simultaneously moving the bucket and arm (model B)(Fig. 3b).

3. CONCLUSION

Mathematical models of resistance to digging deep bucket excavators, defined in this paper were developed as part of a general mathematical model of excavator which forms the basis of developed program for their dynamic simulation using computers.

The comparative analysis showed that the developed mathematical model of digging resistance for technology digging with simultaneous moving bucket and the arm (model B), in relation to the developed model for the digging kinematics of the moving only bucket (model A), gives results that are closer to those obtained by measuring the resistance of the digging in exploitation conditions excavator [1].

4. REFERENCES

[1] Д Јаношевић: *Оптимална синтеза погонских механизама хидрауличких багера*, докторска дисертација, Универзитет у Нишу, Машински факултет, 1997.

[2] Д.П. Волков, В.Я. Крикун, П.Е. Тотолин, К.С. Гаевская, П.Н. Никулин: *Машины для земляных работ,* Машиностроение, Москва, 1992.

[3] Д. Јаношевић: *Пројектовање мобилних машина*, Универзитет у Нишу, Машински факултет, 2006.

[4] Н.Г Гаркави, В.И Аринченков, В.Б. Карпов,...: *Машины для земланых работ*, Высшая школа, Москва, 1982.

Acknowledgment

This paper is financially supported by the Ministry of Education and Science of Republic of Serbia, Project No. 035049. This support is gratefully acknowledged.

HEAVY MACHINERY - HM 2011, 89-98
ISBN 978-86-82631-58-3
Paper accepted: 23.05.2011

Integrated approach of cutting teeth design in excavator of continual action

Popović, M.,[1,*], Jugović, Z., Slavković, R.[2], Grujović, N.[3], Milićević, I.[1], Borota, J.[4]
[1] University of Kragujevac, Technical Faculty Čačak,
[2] University of Kragujevac,Faculty of Mechanical Engineering Kragujevac,
[2] Center for Information Technology of Faculty of Mechanical Engineering Kragujevac

Considerations shown within this paper are aimed at defining an appropriate methodology of integrated development of the product and its applications in designing the cutting elements for continual excavators. Since this kind of approach places modern computing systems in the foreground, thus in the scope of this paper CAD/CAM/CAE system is represented and its application in the process designing of modular cutting teeth for bucket chain excavator ERS 1000/20.

Key words: design, cutting teeth, CAD/CAM/CAE, bucket wheel excavator, bucket chain excavator

0 INTRODUCTION

The process of digging with the excavator of continual action is performed directly by the shovels with cutting teeth located in the front of the cutting. In order to destroy the excavated material, it is necessary to affect it by certain force. Depending on the type of stone material, different cutting force is necessary for destruction. By application of the cutting teeth the available cutting force is concentrated on a small cutting length and in this way it facilitates the penetration of the complete bucket into the material. This occurs because the cutting teeth reach the confined areas of stone material by the cutting edge and make strains sufficient for the destruction. Consequently, the cutting teeth are subjected to intensive dynamic and shock-load in combination with abrasive wear and tear. Such an effect of load leads to the progressive wear of the teeth material, and in more difficult cases even to the distortion or breakage. The tooth thus cannot perform properly its basic function, directly or indirectly reflecting on the overall excavator's operation. Hence, it is highly important to correctly design, make and assemble the cutting tooth on the excavator.

The existing knowledge and corresponding references do not explain nor give recommendations to a sufficient extent for the mode and methodology of cutting teeth design with the continual excavators, so that the designing process mainly narrows down to practiced information, assumptions and rather approximate conclusions without entering into the essence of the problem. The approach presents the issue in the moment when a step forward wants to be made from the existing form and generate a constructional and technologically better solution of cutting elements, such as is the case with development of the new teeth generation. On the other hand, modifying and adjusting the existing cutting teeth are traditionally performed on the basis of experience of the designers and by experimenting of the "trial and error" type. This kind enables coming to the solution that most frequently deviates from the optimal solution both from the technological and economic aspect.

1 INTEGRATED DESIGNING APPROACH AND ITS APPLICATION IN PRODUCT DEVELOPMENT

The very end of the twentieth century has been marked by a wide application of information technologies in all spheres of productive systems. The information technologies are characterized by the features such as flexibility, quality, agility, promptness of market occurrence, responsibility, team work, simultaneous course of larger number of activities and integrations. One of the key concepts enabled precisely by the development and application of information technologies and aimed at fulfilling the complex requests in the process of product development relates to the integrated approach of the product design. The approach basic characteristic is reflected in simultaneous course of a greater number of activities in the product development and the

*Corr. Author's Address: University of Kragujevac, Technical Faculty, Svetog Save 65, 32000 Čačak, Serbia, marko@tfc.kg.ac.rs

accompanying processes [6]. The purpose of the integrated approach is to shorten the development period, and to additionally improve the product in the phase of designing. The realizations of the advanced vision have been suggested in many systematic approaches which can be narrowed to a simultaneous and virtual concept of the product development [7].

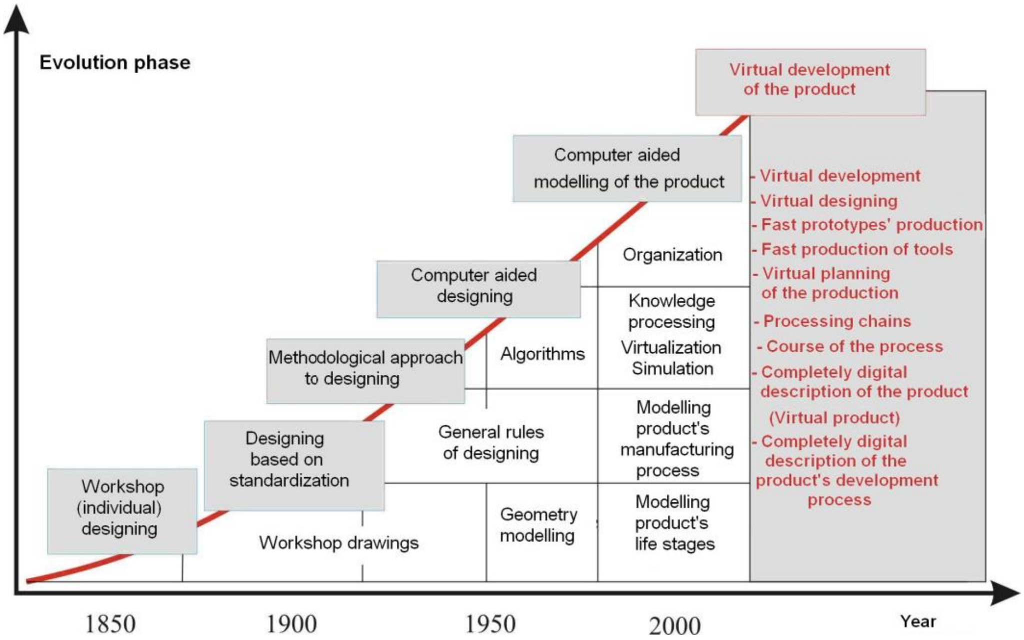

Fig. 1. Evolution of the designing process [1]

The simultaneous concept represents the methodology of work based on parallelization of performing different engineering tasks. In that way in the product development process, various engineering fields such as designing, analysis, industrial technology, etc. are integrated for the purpose of decreasing the time necessary for the emergence of the product on the market. On the other hand, virtual concept is based on joining spatially and temporally the process of product development. Since models, modeling and simulations are the basis of the concept; virtual engineering is actually defined as integration of geometry models and corresponding engineering tools (tools for analysis, simulation, optimization, etc.) into computing generated environment, enabling a multidisciplinary collaborative development of the product.

Generally speaking, regardless of the system applied, the concept of integrated design of the product is directed to join all the processes in the product development which can and have some effect on the product itself. In that way all the elements of the product's life-cycle are included, from the beginning of the idea to the product's recycling. The gravity of the integrated approach practical realization is based on building of appropriate virtual models (prototypes) [9]. The virtual model does not only have the task to visually present the product but to describe and simulate its physical behavior as well. In that way the possibility to examine the functional and technical characteristics in virtual environment on the design are gained and the direct effect of it is a smaller number of physical prototypes that should be produced and tested. In distinction from physical prototypes, the virtual ones use all the advantages of modern computing technique and play a fundamental part in the developing process due to their flexibility and possibility of fast visualization of the process in case of alteration of the prototype's certain characteristics. Besides modeling of the product's individual geometrical characteristics, it is possible to model the complex physical behavior of the product in the virtual environment as well [2] (dynamic behavior, loads distribution, tension status, etc.).

2 PROBLEM OF CUTTING TEETH DESIGN OF CONTINUAL EXCAVATOR

The process of cutting teeth designing in the excavator is distinctive due to the following factors:

a. The designing process' complexity is associated to the high level of correlation of the design's basic properties. In that way, the final appearance, dimensions and production technology is highly sensitive to current modifications during the designing process.
b. Great influence of the users; specific requests and tendency toward unique production. Therefore it is necessary to accomplish great flexibility in the designing and production process.
c. The complexity of defining the external load and adoption of the appropriate suppositions which are the basis for the carrying capacity calculation.
d. The distinctiveness of cutting teeth production technology reflected on existence of a large number of complex technical-technological parameters of casting and their interdependence.
e. The production of physical prototype of the cutting tooth requires significant preparation and realization time. On the other hand, examining the physical prototype under the exploitative conditions is highly complicated and also requires significant temporal and financial expenditures.

a) The cutting teeth, as well as any other machinery, are defined with a set of features.
The features include all physical dimensions, qualities and other characteristics completely defining the cutting teeth. The cutting teeth features can be classified into four groups: function, shape, material and production technology. In that way, the cutting tooth is totally defined if all the previous features are defined. A complete correlation must exist among the features of one group, but also among the groups. It means that one feature cannot be chosen independently from the other. Further, it means that each of the features is determined by the other features already chosen, namely known [5].
b) On today's level, the cutting teeth development should be based on the product realization according to individualized requests, including also the case of unique production wherein the cutting teeth are designed and realized according to the specific requests of a concrete user (the characteristics of the rock material, the bucket design, the excavator distinctiveness, etc.). In this context through introducing a new paradigm of production technologies, the concept of the product's mass personalization is defined, which, by the technological efficacy and by the production costs is equivalent to the concept of mass production [5]. For fast reaction on the new demands of the users, besides the flexibility and manufacturing technology, it is necessary to provide flexibility in all phases of the cutting teeth realization, starting from the early phase of development and the designing process.
c) In general case, a designing process places in the foreground knowledge of working load, namely knowledge on the direction, course and intensity of external forces and moments, but also of their influence on the cross section of the element being designed. When speaking about designing, firstly it is necessary to define the external load to which the cutting teeth are subjected to under the exploiting conditions. The forces generated during the teeth interaction with stone material, during the process of penetration and digging, represent the domineering value of the load. A great problem appearing herein is that the force is an unknown value, both according to the course and direction and according to the intensity as well, with unknown time drift and distribution on different cutting teeth. Obtaining adequate solutions for the external load of the cutting teeth, as the basis in the process of their design, is possible to be performed in many ways, such as by defining the analytical form from theoretical considerations, by generating the simulation environment, namely by application of the computing techniques on the basis of numerical methods and defining the empirical forms, on the basis of exploitation examinations and/or laboratory analyses. On the other hand, the complexity related to solving the problem within the stone material mechanics, imposes the necessity of application of modern numerical methods. With prompt advance of computer engineering, the numeric methods provide a powerful tool for analysis and synthesis of the engineering systems with complex factors, wherein it is not possible or it is highly difficult to perform, to get adequate results only by application of conventional methods, which are usually based on closed forms of the analytical solutions.

d) The cutting teeth are mainly produced by casting, whereat the finishing work is done by cutting, and also applied are various procedures of thermal treatment. The complex conditions of working environment have conditioned a rather complicated operating geometry of modular cutting teeth and with it also the complex volumetric form. For production of the cutting elements the technological process of casting is a lot cheaper and more practical than the other technological procedures (hammering, cutting, etc.), provides rather good quality and under such conditions, casting can be considered an unsurpassable technological process in the production technology of the cutting teeth of the continual excavators [2]. The casting technology is specific because, before performing the process by itself, all production and auxiliary technological parameters have to be adjusted precisely, if the high quality of cast is desired. It is also important because by applying the casting process, the very expenses of starting the production can be highly great. On the other hand, each time when the cutting tooth is not cast properly, the resources invested into energy necessary for melting, workforce and additional mechanical processing are being lost. One should not disregard that if the rejects passes the projected level, there could come to even greater losses due to starting a new series in order to satisfy the contracted quantities. Further, the cutting teeth not correctly cast (inference, the residual voltages, geometry change, etc.), during the operation quickly come to the critical state and are not able to properly perform their basic function, whether because of the breakage, excessive or irregular wear, indirectly having a great influence on the costs and performance of the digging process in itself.

e) An important characteristic of the continual excavators is that they represent the first segment in the continual excavation process and transport of coal in the open-pit mining. Two relevant features these machines are distinguished by are the capacity and the excavation continuity. Since systems such as these are predicted to work so to say constantly, with considering planned stoppages and repairs, each unplanned stoppage generates serious problems in fulfilling the tasked capacity and makes great economic expenses. The critical point in almost all the processes of designing of new or redesigning of the existing structural elements of the continual excavator represents the production and testing of the physical prototype. On the other hand, the prototypes are an unavoidable instance having a vital role in the final confirmation of the design adopted solution. Therefore it is necessary to find an alternative, in which a physical prototype would be fitted on the excavator only when all the possible previous adjustments have been executed and tested and all other possibilities exhausted.

One of the alternatives in solving the previous problems which can be very easily incorporated and applied within the production process of the continual excavators' cutting teeth is adoption and realization of the integrated designing approach. The basis of the approach lies in development and application of appropriate virtual models. The virtual models can be used for obtaining an image on the cutting teeth appearance even in the early phase of development, to simulate and check its features before production of the physical prototype, therewith accomplishing a significant saving or complete elimination of the expenses and time needed for production and modification of the physical prototypes. In this case the virtual model does not only have a task to show the design of the cutting teeth and its environment, but also to describe and simulate its physical behavior, which is highly important for the purpose of correct dimensioning and perceiving the technological procedure of casting. By the integrated approach application, the expensive iterations of the casting tools modifications are being transferred from the production plant to the computer. The earlier precise settings of the casting parameters, through various simulations also have additional advantages such as constant quality of the cast cutting teeth, meeting deadlines and speed of adoption of new design, possibilities of precise planning of the production, etc. In contrast to the physical prototypes, virtual models use all the advantages of modern computer engineering, thus moving the gravity of designing process from physical into virtual environment, which is a huge advantage for solving the problems at the excavators in open-pit mining [2].

3 INTEGRATED CAD/CAM/CAE SYSTEM

The information foundation on which the integrated designing approach is based on is the integrated CAD/CAM/CAE system. The first step in the system's application is generating a virtual model. Obtaining the virtual model can be executed in numerous ways, such as direct 3D software modeling of the new design, alteration of the existing parameter 3D model, translation of the existing 3D documents into 3D solid model, application of reverse engineering, namely by different types of digitalization and so on (Figure 2 shows the digitalized virtual model of wear and tear of a cutting teeth section under the exploiting conditions, used in the process of modular cutting teeth development).

Once the virtual model of the cutting tooth is generated, during the total lifetime, it represents the centre for managing the information on its geometry. The produced virtual model can be used for optimization, analysis by the method of final elements, making of the documents, simulations, animations, production, fast production of the prototypes, etc. Apart from it, the subsequent changes of the design, redesigning and advancements, in case of need, can be conducted fast and all the processes following the product development are consistently at disposal. Regardless whether it is about a variant solution or an adopted design, it is beneficial to examine right after the production of the basic model of the cutting teeth design its behavior at the specified load and ascertain whether the tensions and deformations fall within the allowed limits.

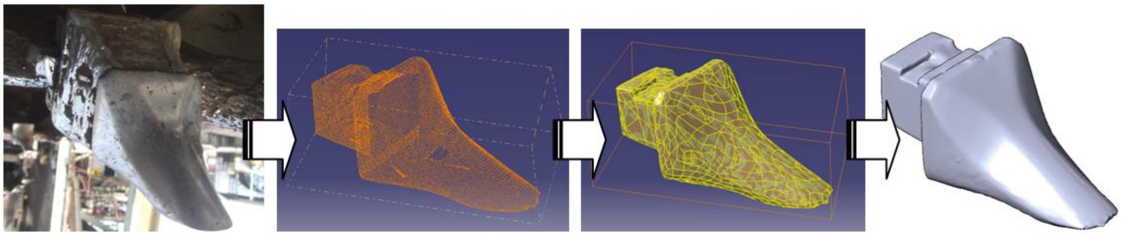

a) b) c) d)

Fig. 2. Application of RE for obtaining the 3D image of the wear model. A) Cutting tooth on the bucket, b) Generating the cloud of dots by means of scanner, c) The creation of surfaces, d) 3D solid model of worn cutting tooth

Afterwards, further analysis should include the simultaneous usage of design optimization tools, casting process simulation, thermal treatment simulation, thorough strain analyses, etc., but also their integration into the overall designing and production cycle. Therewith it is ensured that the conditions of the technological procedure are early integrated into the process of cutting tooth design and that the actual potential of the casting process is completely utilized. At planning the casting technology, significant attention is paid to eliminating the possibilities of occurrence of either perceptible or imperceptible errors in the drip-molding, because they can be the main cause of the cutting teeth breakage in the process of exploitation [4]. On the other hand, adoption of the philosophy of a specific date of the products' delivery (Just-In-Time) during the installation, in order to decrease the warehousing and stock expenses requires from the foundries to deliver the drip-moulds just in time (often precisely on specified date, time and location). The concept of virtual production of the drip-molding enables the foundry a more direct cooperation with the moldings' buyer in the sense of design optimization and the moulds' functionality [3]. Based on the results obtained from earlier analyses, tools and models can be made for the chosen design of the cutting teeth. Figure 3, shows a system of CAD/CAM/CAE integration, used during modular cutting tooth development for bucket excavator ERS 1000/20.

The integrated CAD/CAM/CAE system which represents the basis of the methodology from Figure 6 should enable the analysis and synthesis of all relevant factors in the cutting teeth lifecycle. In that way, by observing the cutting teeth development through application of the integrated designing process concept, performed and/or solved are the following relevant factors:

CAD

1. Generating 3D solid model of a cutting tooth
2. Generating 3D solid model of the environment: buckets, subsystem of digging,

complete excavator, stone massifs, captured material, etc.

3. Excavating kinematics analysis
4. Obtaining the geometrical parameters of excavation such as the characteristic angles (front and rear angle of the cutting tooth, the cutting edge angle, etc), cutting depth, the cut shape, defining the characteristic cross sections of the cut, etc.

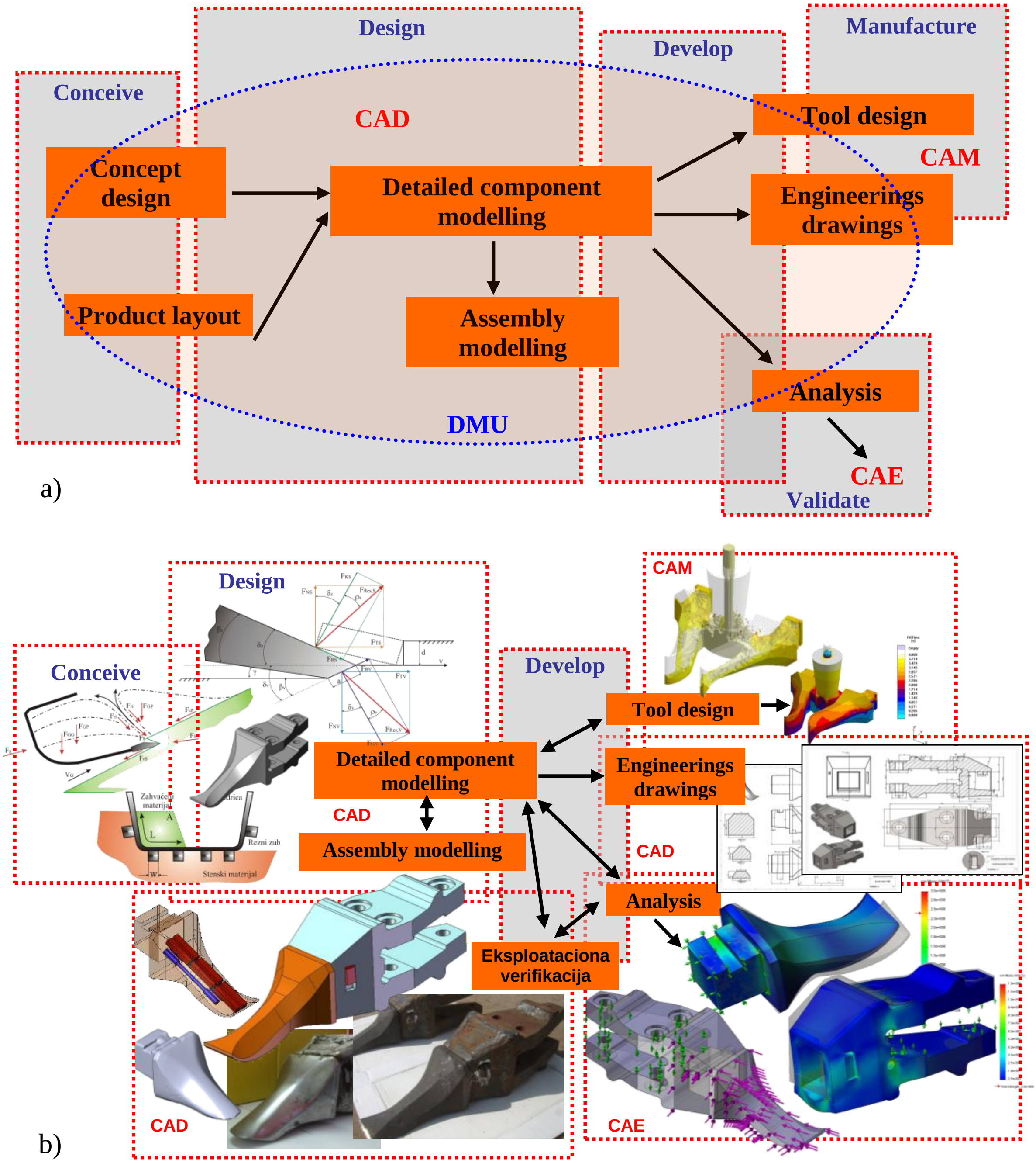

Fig 3. CAD/CAM/CAE integration. a) Theoretical consideration, b) The process applied in the cutting teeth designing process

5. Production of the background (parameterized representative) for the cutting tooth typization and unification.
6. Automatic production of the cutting teeth operating documentation
7. Generating dependant 3D solid model of the cutting tooth casting tools (with or without making the model)
8. Production of the background for the casting tools typization and unification.
9. Automatic production of the casting tools technical documentation.
10. Application of RE (Reverse Engineering) in generation of 3D solid model
11. RE application in the process of control (molding preparation, wear, etc.).

CAE

1. MKE analysis (calculation of the cutting tooth carrying capacity, cutting tooth and bucket assembly, etc.).
2. Simulation of capturing the stone material and determining the diggings' resistance.
3. The cutting tooth shape and dimension optimization
4. Dynamic analysis of the digging subsystem

CAM

1. Simulation and analysis of the cutting tooth casting process
2. Simulation and analysis of the overall process of the cutting tooth production
3. CNC route programming for production of the cutting tooth casting tools
4. Fast production of a pre-model for production of the cutting tooth casting tools
5. Fast production of the cutting tooth prototype and the cutting tooth and bucket assembly

Tensions and changes of tension are the main cause of the fatigue of the cutting teeth structure material, their deformation, occurrence of cracks and breakages. The tensions per the cutting tooth volume are as a rule unbalanced distributed. The degree of unbalance is directly dependent on the value and distribution of the external load, on the shape and manner of attaching the cutting tooth to the bucket, but also on the position and orientation of the cutting tooth at the moment of gripping. The values of the tensions and their distribution are of extraordinary significance for development and analysis of the cutting tooth state and working capacity. By application of the integrated approach, a simultaneous analysis is provided, with the purpose of generating the cutting tooth form and dimensions and it based on the analysis of the obtained results on the tension value and distribution. In that way, on virtual model it is possible to perform adequate changes very quickly and optimize the shape and dimensions, until reaching the optimum distribution both of the tension and deformation. Figure 4 shows one of the analysis conducted for the needs of development of modular cutting tooth for bucket excavator.

The shape of the machinery is technological if it is suitable for production predicted by the technology. The acceptable form is the one that is reached in a technologically simpler and economically more favorable manner. The form's simplicity from this aspect is achieved by adjusting the designing details to the needs of production procedure simplification herewith not endangering the function, solidity or any other condition. In the cutting teeth production the technological procedure of sand casting is used. Casting by this procedure implies making a sandy mould, casting in of the melted material and its cooling, then destroying the sandy mould and cleaning of the drip-molding. For the mould production a model made of wood is used (often also the one made of the alloy of light metal) which by its shape with adequately enlarged dimensions (due to the shrinkage during the metal cooling) completely corresponds to the adopted design of the cutting tooth. At planning the casting technology a significant attention is paid to eliminating the possibilities of occurrence of either perceptible or imperceptible errors in the mould, namely to predicting and solving of potential problems that could arise during the casting process. The final qualities of the drip-mould are possible to be predicted if the following parameters of the casting process are known: the material mass flow, the casting thermal flow, cooling of the casting material, the hardening process, tensions, gases, thermal treatment, deformations, convection, segregation, chemistry and metallurgy. By the application of the cutting teeth designing integrated approach, an adequate selection of previously selected parameters is provided as well as their check through simulations on the virtual models. In that way a precise adjustment of all relevant casting factors are provided and influenced on corrections of possible errors in the cast cutting tooth.

Further, by this approach the simultaneous development of the cutting teeth shape and production technology is provided.

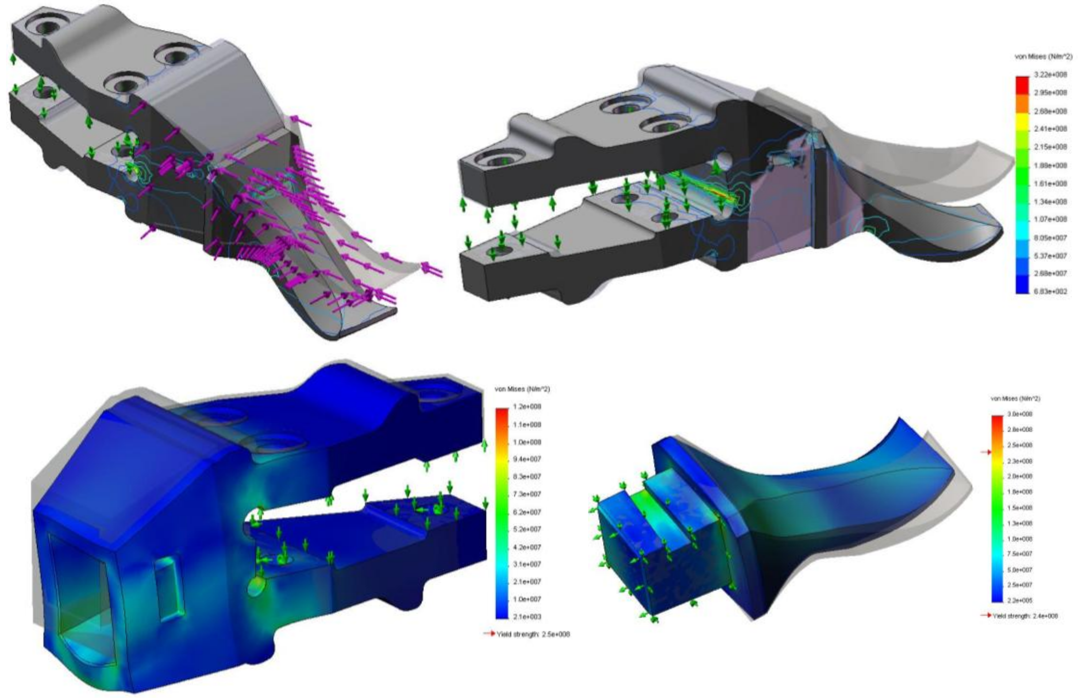

Fig. 4. The adopted model of load and analysis of the tension state of modular cutting tooth TF14038 for bucket excavator ERS 1000/20.

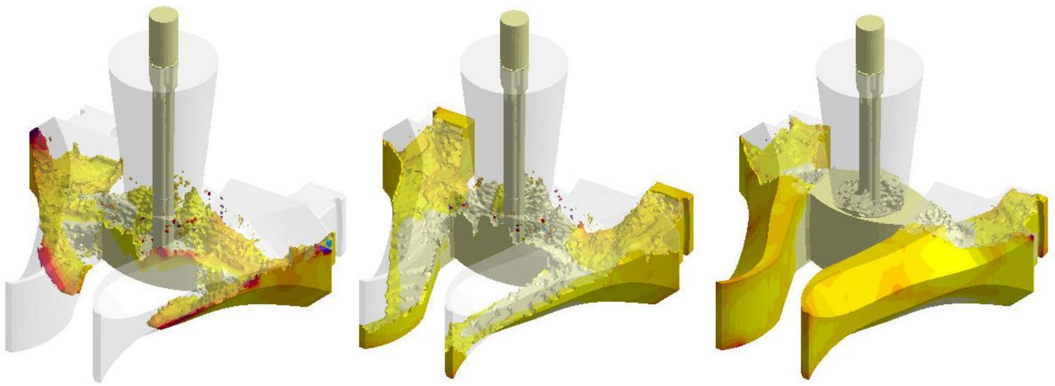

Fig. 5. Simulation of the casting process of the modular tooth cutting part with the temperature field of the mould filling

For every new design of the cutting tooth, a check is performed on the defined technologies of casting (metals), and afterward the quality of the defined technology is checked, the identified errors are changed and the simulation is run again. The approach application is justifiable by obtaining a proper drip-molding in the shortest possible period. In that way, without consumption of the energy for casting, without consumption of the metal and time for trials all the errors are made perceptible. The designer is able to ascertain in any part of the drip-molding whether there is the porosity or cavity, he/she can follow the process of the mould filling, the hardening process, the residual tensions, metallurgy structure of the drip-molding and many more. By application of the integrated approach of designing in the cutting teeth development process and the technology of their casting, the need for the experimental casting is eliminated, the time needed for obtaining of the new or modified design is reduced and there is no incertitude with regards to the drip-molding quality [3]. Figure 5 shows an example of the analysis of the casting in of metal into the mould and its cooling during the cutting parts production of the modular cutting teeth. The even cooling of the casting enables even shrinkage without any residual tensions and deformation. In casting, it is very difficult to fulfill this condition completely, but it is possible to significantly influence on its decrease through optimization of the forms and technological parameters of casting.

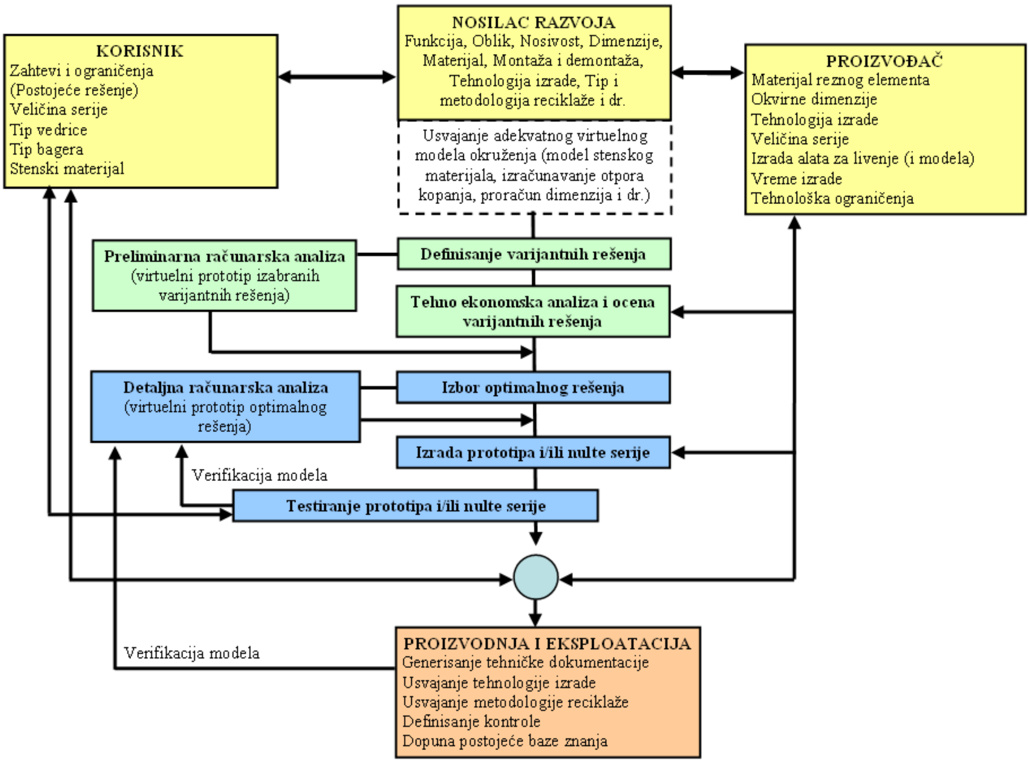

Fig. 6. Methodology of the cutting teeth integrated development for continual excavators

In Figure 6., the schematic diagram shows the methodology and procedure used for development of modular cutting tooth TF14038, for bucket excavator ERS 1000/20. The previous technology has been confirmed in practice both through development and reconstruction of the cutting teeth for rotary excavators. Therewith, the methodology is adopted as general methodology of development of the cutting teeth for continual excavators and it is based on the application of integrated designing approach through CAD/CAM/CAE system.

4 CONCLUSION

In this paper the methodological approach of modular cutting teeth development for continual excavators is given, which is based on the application of integrated designing approach. The aim of this kind of approach is that before the very production of the cutting teeth there is a clear notion on how the product will look like, how and in what way wills the adopted production technology influence on the definite quality, how it will behave under the operating conditions, etc. Since this approach places modern computing CAD/CAM/CAE systems in the foreground, the development of virtual model (prototype) and the appropriate environment for its analysis represents the starting step in the designing. According to the results of computing analysis, and after production of the physical prototype, it is possible to perform the verification of the adopted conceptual solution through laboratory and exploitation testing. Thus, the adopted analysis and obtained results can be used in the subsequent analyses with the defined level of accuracy, decreasing the need for producing the physical prototypes and their exploitation testing.

The suggested methodological approach in the development of the cutting teeth modular design for the continual excavators gravitates towards the following positive effects:

→ Minimizing the risk of failure of the adopted conception and final design of the cutting tooth
→ Reducing the time needed for the prototype development and testing
→ Decreasing the number and better organization of the repetitive steps in the designing and testing
→ Increase of the design process reliability
→ Repeatability of the similar design testing, as well as the possibility of expanding the testing to the excavator's remaining components
→ Generating the optimum solution for initially defined limitations

5 ACKNOWLEDGEMENTS

The project No.TR35037: "Development of new bucket design for continuous excavators due to the installation of modular cutting teeth", is financed and supported by the Ministry of Science of the Republic of Serbia. The authors would like to acknowledge this contribution.

6 REFERENCES

[1] Miltenović, V., Vereš, M., Banić, M., Concept of virtual product development, Proceedings The Sixth International Symposium KOD 2010, pp. 7-12, 29-30 September, Palić, 2010.
[2] Kolarević, M., Brzi razvoj proizvoda (Fast development of the product), Beograd, Zadužbina Andrejević, 2004.
[3] Radiša, R., Marković, S., Pristavec, J., Kvrgić, V., Manasijević, S., Upotreba CAE tehnike za tehnologiju virtuelnog dizajna odlivaka-ušteda u livnicama Srbije (The application of CAE technique for the technology of the mould virtual design-savings in the foundries of Serbia) , Časopis Livarstvo (Magazine Livarstvo), Vol.47, No.1, ISSN 0456-2933, pg.12-24, 2008.
[4] Slavković, R., Milićević, I., Popović, M., Radiša, R., Simulacija procesa livenja kao osnova CAD/CAM projektovanja dinamički opterećenih odlivaka u mašinogradnji (Simulation of the casting process as the basis of CAD/CAM designing of dynamically loaded moulds in machine building industry), 37. Jupiter konferencija (37. Jupiter Conference), Zbornik radova (Proceedings), ISBN 978-86-7083-724-9, pg.2.30-2.35, Belgrade, 2011.
[5] Petrović, P., Danilov, I., Lukić, N., Novi pristupi u projektovanju ekstremno varijantnih proizvoda (New approaches in designing the extremely variant products) 37. Jupiter konferencija, Zbornik radova, (37. Jupiter Conference, Proceedings) ISBN 978-86-7083-724-9, pg.3.26-3.35, Belgrade, 2011.
[6] Devedžić, G., CAD/CAM tehnologije (CAD/CAM technologies), Mašinski fakultet Faculty of Mechanical Engineering), Kragujevac, 2009.
[7] Ognjanović, M., Konstruisanje mašina (Designing machines), Mašinski fakultet (Faculty of Mechanical Engineering), Belgrade, 2003.
[8] Trajanović, M., Grujović, N., Milovanović, J., Milivojević, V., Računarski podržane brze proizvodne tehnologije, Monografija, Mašinski fakultet, Kragujevac, 2008. (Computer aided fast production technologies, Monography, Faculty of Mechanical Engineering, Kragujevac, 2008.)
[9] Popović, M., Jugović, Z., Slavković, R., The concept of Functional Virtual Prototype in the design of excavator cutting teeth, Tribology in Industry, Vol 3-4, 2009.
[10] Popović, M., Jugović, Z., Slavković, R., Primena DEM numeričke metode u analizi problema opterećenja reznih elemenata kod rotornih bagera, Časopis IMK-14, Broj 34, ISSN 0354-6829, 2010. Application of DEM numerical method in the analysis of the cutting elements load problem in rotor excavators) Magazine IMK-14, Number 34, ISSN 0354-6829, 2010.

HEAVY MACHINERY - HM 2011, 99-104
Paper accepted: 30.05.2011
ISBN 978-86-82631-58-3

Applying Finite Element Method for Research Static and Dynamic Properties of Electro-mechanical Two Post Lift

Rade Vasiljević [1,*] - Zoran Petković[2] - Srđan Bošnjak[2]
[1] IRC NIC j-s.c., Užice, Serbia
[2] University of Belgrade, Faculty of Mechanical Engineering, Serbia

The static and dynamic analysis of electro-mechanical two post lift aplining finite element method is considered in this paper. Fields of displacements, stress states, frequencies and oscillation modes of crane construction are given. Research of static and dynamic properties by the finite element method has been resulted with satisfactorily values of static and dynamic properties of crane construction and with small deviations comparing with resuls obtained by the method of direct measurement.
Keywords: FEM, static analysis, dinamic analysis, electro-mechanical two post lift.

0 INTRODUCTION

Nowadays, modern design and construction of mechanical engineering is largely supported by computer [9].

Finite element method (FEM) belongs to the group of modern numerical methods [8]. It can be used for static and dynamic analysis of complex parts and assemblies [1] to [9] and [11].

During studying of static and dynamic behavior of electro-mechanical two post lift, complex interactions of supporting columns and lifting mechanisms present a special problem [11]. Stiffness of driving and following column is equal to the superposition of supporting columns and threaded screws stiffness, whereat columns are console connected to the base of the crane, while threaded screw are beam placed in columns over bearings. Analytical method of determining the influential coefficients is complex and therefore, the first step in static and dynamic analysis of electro-mechanical two post lifts should not be creation of analytical models.

From one side, 3D CAD became a standard. On the other side, making geometry of electro-mechanical two post lift does not take much time and it is payable due to this crane presents the series product. Also, created geometry in 3D CAD software can be used in static and dynamic analysis. This means that the first step in static and dynamic analysis of electro-mechanical two post lift should be making 3D models in specialized software package for 3D modeling, and then determining the static and dynamic parameters in a specialized software package for finite elements.

For making of 3D models of implemented solution for electro-mechanical two post lift, a specialized software package Inventor is selected, while a specialized software package ANSYS is selected for determination of static and dynamic parameters.

1 SOLVING STATIC AND DYNAMIC ANALYSIS IN ANSYS PROGRAM

Mathematical modeling means using mathematical formulas and relations in order to simulate real situations [1] and [2].

Structural diagram of solving static and dynamic analysis of electro-mechanical two post lift in the ANSYS program is represented at Figure 1.

Structural diagram shows that the first step in solving static and dynamic analysis by software ANSYS is import of 3D model from Inventor software. In this phase, a geometric figure of the final model is being created.

The second phase is the selection of elements and material properties (physical, mechanical and technological). Element type is determines, for example, whether the final model will be plane (2D) or spatial (3D). For modeling crane, 3D finite elements have been selected.

The third phase is model shaping. It is a process where finite element model is being built on the base of solid body. It is necessary to select appropriate size and number of specific elements in order to get solutions of static and dynamic analysis as accurate as possible, but in the same time, the calculation should not be too long as a result of large number of elements.

*Corr. Author's Address: IRC NIC j-s.c., Nikole Pašića 38b/IV, Užice, Serbia, rvasiljevic@ptt.rs

The fourth phase is setting of analysis, causing loads, determining boundary conditions and making decisions. Before loading it is necessary to set up the parameters of the analysis, i.e. type of analysis methods of solution (Newton-Raphson) and some other parameters that are required for solving the specific analysis. Solving starts by giving command SOLVE (solved) after determining general boundary conditions.

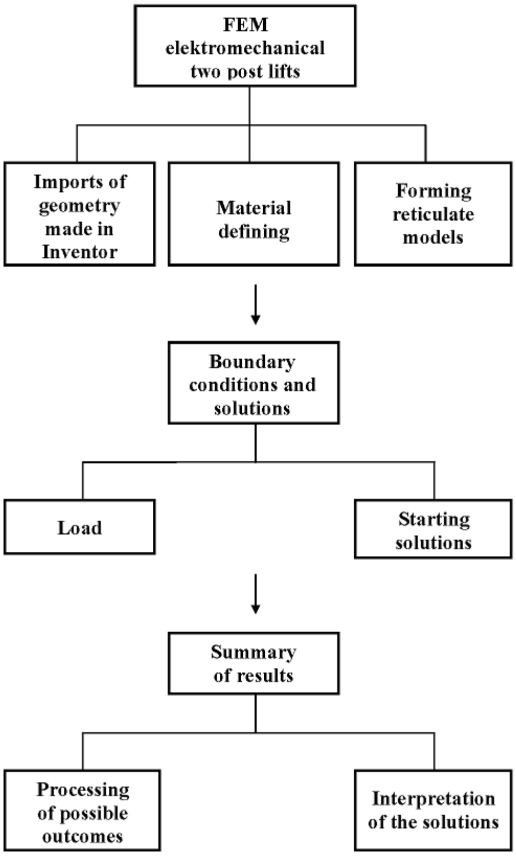

Fig. 1. *Structural diagram of solving static and dynamic analysis, program ANSYS*

Analysis of the results and evaluation is the last phase. By using the module post-processing, we can review results of the solutions. This module consists of two sub modules POST1 and POST26. POST1 is used for analysis of the results in the whole model at certain moment. POST26 gives results only in the certain point of the model depending on the time. Results can be presented in textual or graphical form. Charts offer considerable clarity in the analysis of the results.

3 FORMATION OF FINITE ELEMENT MODELS

Based on the technical data given in [10] and [11] original 3D model of implemented solution for electro-mechanical two post lift, type DB2, by manufacturer "Universal" from Banja Luka, applying specialized software package Autodesk Inventor 10, Figure 2, is made. Technology of making this 3D models is exposed in [12].

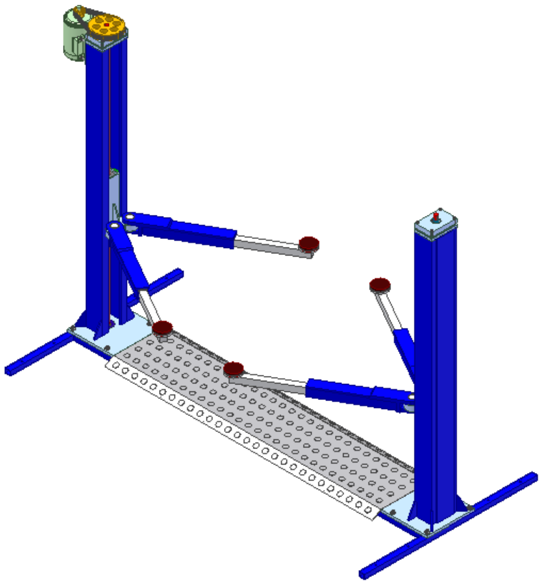

Fig. 2. *3D model of electro-mechanical two post lift, program Autodesk Inventor 10*

For purposes of determining the static and dynamic characteristics, original 3D model, made in Autodesk Inventor, has been imported into specialized software package ANSYS 11, Figure 3.

At the created 3D model, according to the manufacturer recommendation, the base of crane is connected for the concrete plate dimensions 3500x1600x180mm over the anchor bolts.

At this solution regarding 3D model of electro-mechanical two post lift, threaded screws are radial and axial fixed in upper case, while at the lower case they are radial fixed and axial free.

Crane load is represented by homogeneous steel plate, mass $m_Q = 2500$kg.

In accordance to the created geometry of electro-mechanical two post lift, 3D reticulate model is formed in ANSYS program, Figure 4.

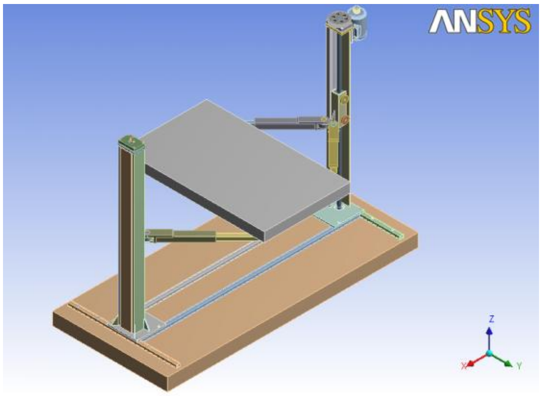

Fig. 3. *3D model of electro-mechanical two post lift, program ANSYS 11*

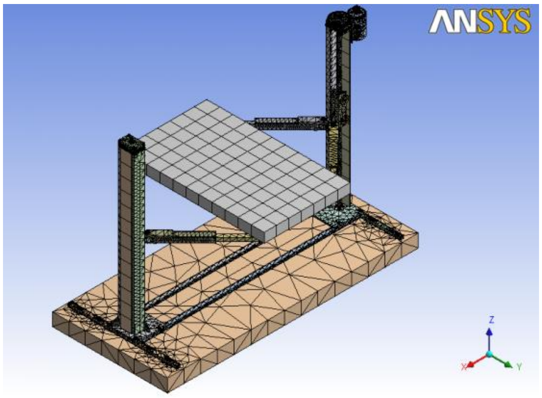

Fig. 4. *Reticulate 3D model of electro-mechanical two post lift, program ANSYS 11*

3 STRUCTURAL ANALYSIS

The static and dynamic analysis has been done at the formed FEM using the software ANSYS 11. Three characteristic positions of mobile consol carriers are analyzed [11]:

- The lower end position of mobile console carriers (position I),
- Middle position of mobile console carriers (position II), and
- Upper end position of mobile console carriers (position III).

3.1 Static Analysis

Supporting structure as well as threaded screw character and maximum values of the following static properties, have been analyzed:

- Static displacement, and
- Static stress.

3.1.1 Static displacements

By comparative analysis of displacements in regard with three characteristic cases, it was found that maximum displacement are at console pedals zone. Displacement of console pedals are slightly larger in the upper end position according to middle position of mobile consol carriers (δ_{II}=5,92mm, δ_{III}=6,04mm). Displacements of the columns tips are the largest in middle position of the mobile console carriers and specially at foolowing columns (δ_{II}=0,78mm). Threaded screws, according to the change of stiffness, have the largest displacement in the middle position of mobile console carrier (δ_{II}=0,295mm).

Comparing the values of displacements for all three positions can be concluded that crane is the most sensitive to static effects when mobile console carriers are located in the middle position (position II). It means that from the aspect of static displacement, middle position of mobile console carriers is critical position.

Deformation of crane when it is loaded with maximum weight of ballast at upper end position are represented at Figures 5 and 6.

3.1.2 Static stresses

Analogically to the analysis of displacement, from the comparative analysis of normal stresses for three characteristic cases, it is noticeable that maximum normal stresses are in the zone of mobile console carrier. Normal stresses in the zone of mobile console carrier are slightly larger in upper end position than in the middle position of mobile console carriers (σ_{II}=508,38Mpa, σ_{III}=540,83Mpa). The threaded screws, according to the change of stiffness and derived stresses distribution, have concentration of larger normal stresses in the middle position of mobile console carrier. Consequently, supporting columns have concentration of larger normal stresses in the middle position of mobile console carriers. Also, based on the distribution of stresses in the interaction zone of leading wheels of the mobile console carriers and supporting columns, local bending is noticeable and it is larger for the middle position of mobile console carriers.

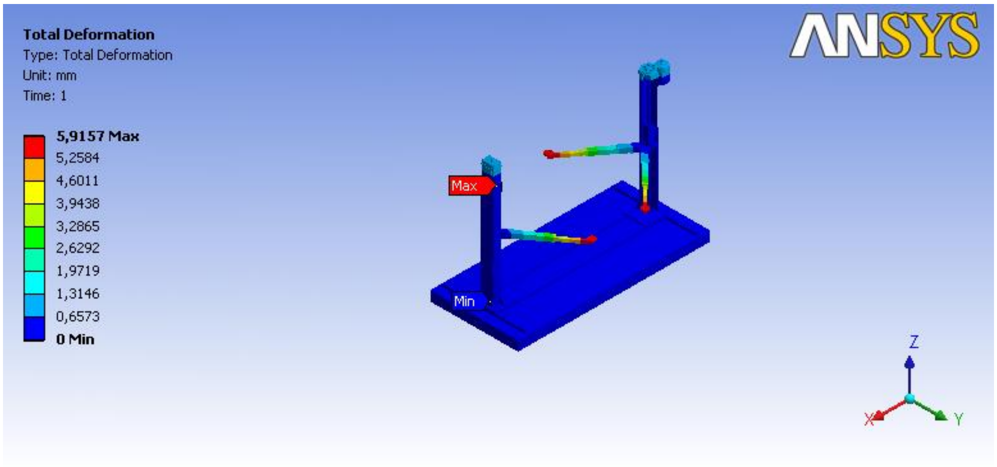

Fig. 5. *Total deformation*

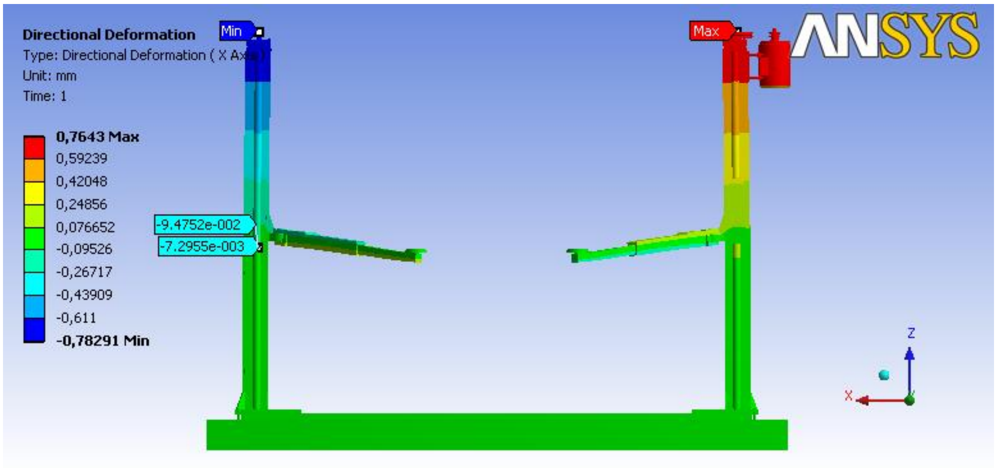

Fig. 6. *Deformation in the direction of X*

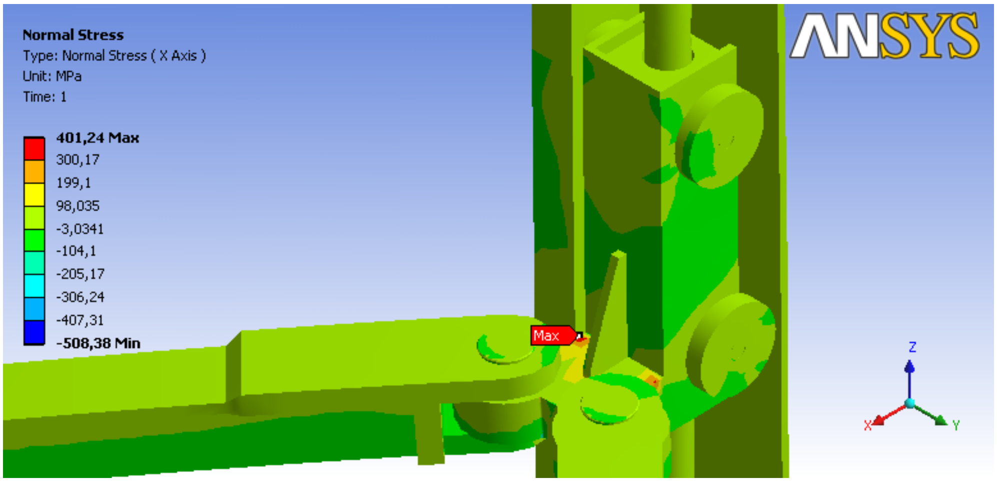

Fig. 7. *Normal stresses on the detail of interaction leading wheels mobile carrier with supporting column*

Distribution of stresses at the crane construction, when it is loaded with maximum weight ballast in the middle position, is represented at Figure 7.

3.2 Dinamic Analysis

Efficient and reliable work of electro-mechanical two post lift is under effects of its own frequencies. Own frequencies are directly depending on the stiffness and mass of the construction. Determination these own frequencies is the first step in implementing of dynamic analysis of electro-mechanical two post lift.

Numerical determination of the following modal parameters:

- Frequencies of oscillation, and
- Forms of oscillation,

is conducted by Finite element method, applying software package ANSYS 11.

3.2.1 Frequencies of oscillation

For all three positions of mobile console carriers, first six oscillation frequencies of 3D model are determinated which is default number in the ANSYS.

Comparing of the frequencies values for all three cases, it can be concluded that crane is the most sensitive dynamic from the aspect of the lowest fundamental frequency in the case when mobile console carriers are in upper end position. But, as fundamental frequency in upper end position is slightly different from fundamental frequency in the middle position, from one side, and as stiffness of threaded screw is the lowest in the middle position and displacement of the crane columns ends is the largest in the middle position, on the other side, so position II is the most proper for further description of dynamic state of the construction.

The first six frequencies, when the crane is loaded with maximum weight of ballast in the middle position, derived by applyning software package ANSYS 11, are represented at Figure 8.

Own circular frequencies are:

ω=(41,14; 51,83; 69,85; 91,42; 92,90; 149,73) s^{-1}

3.2.2 Forms of oscillation

Modal analysis gave first six oscilation forms of electro-mechanical two post lift for the middle position of mobile console carriers, when the crane is loaded with maximum weight of ballast. The first main form of oscillation is represented at Figure 9.

At Figure 9 can be observed that form of oscillation in the direction of lifting and lowering the vehicle (1. mode) corresponds to the elastic line in the vertical plane, apropos to the deformed form due to retention of vehicle on the certain elevation head. Also, there is dominance of console oscillation in the vertical direction, relative to other elements of construction.

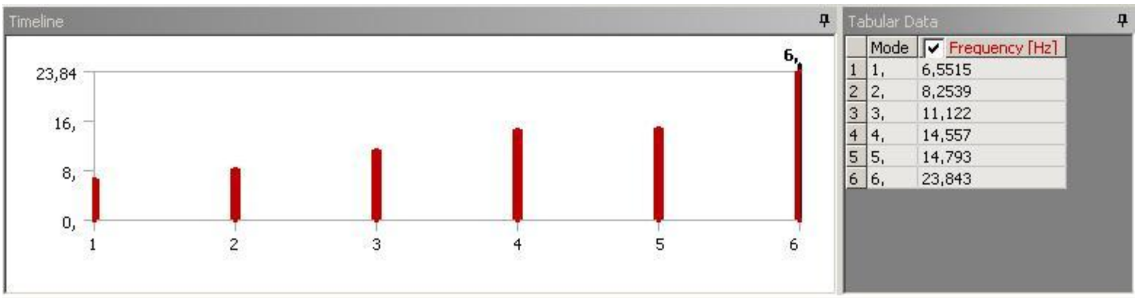

Fig. 8. *Frequencies for position II*

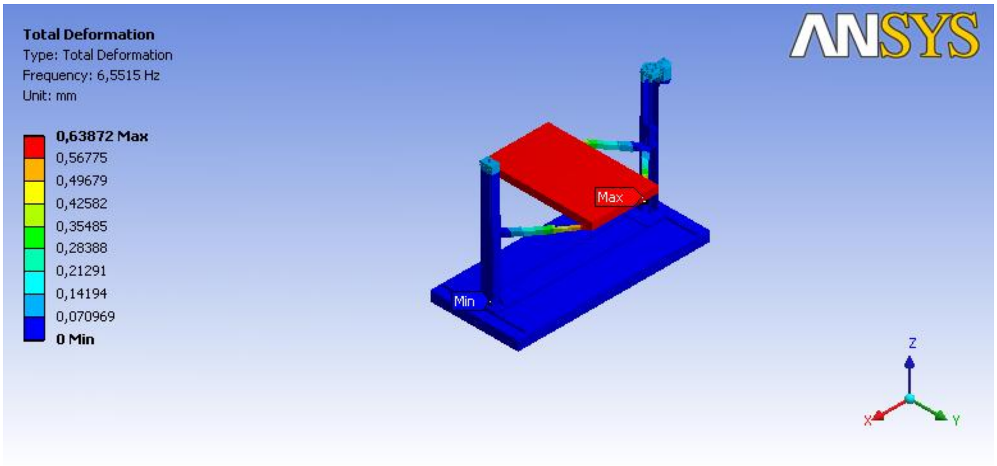

Fig. 9. *1. mode*
$T_1=0,153$ s

4 CONCLUSION

In the first step of this paper, the FE model for concrete example of crane is formed. Good contact conditions are provided, from one side, between parts of the crane and from the other side, between console pedals and the ballast. During simulation there was no appearance of bad elements and conflicts. It is approved that FE model is very important and necessary for the static and dynamic analysis of this kind of crane, due to the existence of a complex interaction of mechanism for lifting and supporting structure.

Presented research of static and dynamic properties of crane construction by FEM resulted with satisfactory values as from static displacements and static stresses in referential zones, as well from frequencies and modes of oscillation. Differences between results from analysis of FEM and experimental results are within the limits of engineering accuracy and in amount of 10% [11]. By comparative analysis of static and dynamic parameters for the three positions of mobile console carriers it was indicated that the middle position is critical.

Derived static and dynamic parameters can be used for further analysis of this crane type. In [11], based on the results of performed dynamic analysis, equivalent dynamic models are formed and solved in unstationary regimes due to the work of lifting mechanism. Further, results of this paper may provide a good basis for analyzing the impact of moving ballast and optimization of supporting structure.

5 REFERENCES

[1] ANSYS Inc, “ANSYS Structural Analysis Guide”, Release 11.0, Cononsburg PA, 2007.
[2] ANSYS Inc, www.ansys.com
[3] Georgijević, M., “Dinamika dizalica - eksperimentalna i modelska analiza” Zadužbina Andrejević, Beograd, 1996.
[4] Letić D., “CAD mašinskiih elemenata i konstrukcija”, Kompjuter biblioteka, Čačak 2004.
[5] Ostrić D., “Dinamika mosnih dizalica”, Mašinski Fakultet, Beograd, 1998.
[6] Ostrić D. i Tošić S., “Dizalice”, Mašinski Fakultet, Beograd, 2005.
[7] Petković Z., “Metalne konstrukcije u mašinogradnji 2”, Mašinski Fakultet, Beograd, 2005.
[8] Sekulović M., “Metod konačnih elemenata”, IRO Građevinska knjiga, Beograd, 1988.
[9] Stoiljković M. i Milosavljević M., “Projektovanje podržano računarom - CAD”, CIM Colelege, Mašinski fakultet, Niš, 1995.
[10] Univerzal, “Uputstvo za rad i održavanje mehaničke autodizalice dvostubne DB2”, Banja Luka, 1989.
[11] Vasiljević R., “Dinamička analiza elektro-mehaničke dvostubne dizalice”- Magistarska teza, Mašinski Fakultet, Beograd, 2009.
[12] Vasiljević R., “Higher Levels Modeling Based on Inventor Software”, *Journal of Applied Engineering Science*, 4(8), 215-221, 2010.

HEAVY MACHINERY - HM 2011, 105-110
ISBN 978-86-82631-58-3
Paper accepted: 30.05.2011

Dynamic loads effects on the characteristics of compressive monocable chairlift towers

Milomir Čupović [1,*] - Milomir Gašić[2] - Mile Savković[2] - Nebojša Zdravković[2] - Desimir Jovanović [3]
[1] State University of Novi Pazar
[2]University of Kragujevac, Faculty of Mechanical Engineering Kraljevo;
[3]Zastava arms

Passage of the grip over chair lift compression battery is followed by a series of tower trembles. On that very moment grip has contact with the wheel, passing under the wheel and then lost the contact. The consequences of this phenomenon on the tower structure are not researched well.

This paper research the behavior of not real, but pre-installed structures in real operational conditions. In laboratory conditions, initiative load represents a combination of several basic types of signals. In the research carried out under real conditions, the initiative load was very complex. The possibilities of modeling complex nature of real initiative with satisfy acceptability, were used. The passage of the chair causes a forced damped vibration, which can have stress implications.

The paper describes complex identification of initiative, analysis of the oscillation types of the tower structure, as well as correlated relations of the initiative excitation and tower stress response.

Keywords: Compression tower, monocable chairlifts, impact, modal analysis, the FE model, validated model, oscillation, frequency range, stress consequence.

0 INTRODUCTION

Many authors have studied the problem of the passage of chair under the compression sheave assembly on monocable chairlifts. In [1] to [3] we have investigated the influence of impact load on the behavior of sheave assembly itself, without response of the tower.

Fig. 1. *The consequences of energy exchange*

Passage of the grip over chairlift compression sheave assembly is characterized by energy transfer. Part of kinetic energy that comes from the movement of the vehicle connected with a rope, is transferred to the sheave assembly. Then, part of the kinetic energy that is transferred to the sheave assembly causes the movement of the its components, rotations and displacements of sheave assembly in a vertical direction. The second part is transformed into energy of deformation of the sheave assembly and tower. The author of this paper was interested on the consequences of such energy exchanges on the tower structure, Fig. 1.

1 PASSAGE OF THE GRIP UNDER COMPRESSION SHEAVE ASSEMBLY

In the case of negative sheave assembly, the grip arrives facing the bottom of the rope. Passing under the sheave assembly top surface of the grip, which has the geometry resulted from the calculation of strength, is *n* times in contact with the wheel and the same number of times the contact is lost (*n* - number of wheels in the sheave assembly). The passage of grip, it is usually followed by a series of tower trembles. Driving on the chairlift the passenger has the feeling of driving on the road full of

*Corr. Author's Address: State University of Novi Pazar, Vuka Karadžića bb., 36300 Novi Pazar, Serbia, mimocupovic@gmail.com

small holes. Details [4].

On the Fig. 2. we clearly recognized contact of two elements the grip and the wheel as a collision of two objects. Grip has multiple weight (reduced mass of passenger and chairs M>> m), and also there is a difference in speed at the point of collision. There is also a difference in materials. The cover of the wheel is made of rubber, and the grip was made of wrought steel. During the impact moment a impact pulse occurs, which by its intensity could be several times bigger than static force on one single wheel. But according to time velocity it is defined as the instantaneous value.

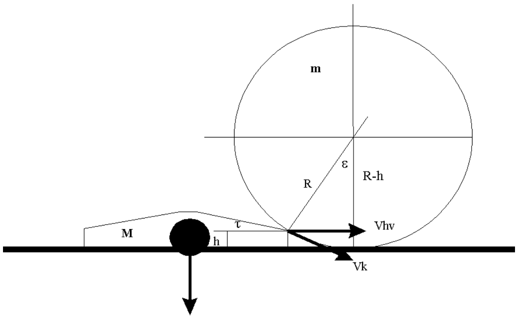

Fig. 2. *Grip and wheel contact*

Load redistribution is the consequence of the appearance of the impact pulse. At the moment of impact, impact pulse is transmitted to the rope through the second wheel, the pair of the hitteed wheel, Fig. 3.

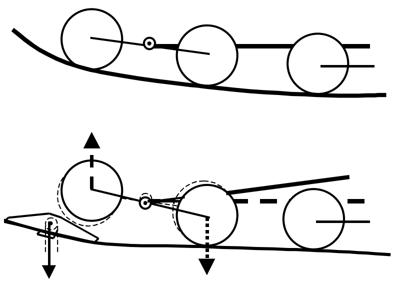

Fig. 3. *The transfer of the impact pulse*

The frequency of this occurrence can be calculated:

$$f = \frac{1}{\frac{l}{v}} \quad [Hz] \tag{1}$$

where: *l – the distance between wheels*
v – line speed of the chairlift

For dimensional relations that are most frequent, for the chairlifts with a fixed grip, it is in the range of f = 4 to 12 Hz. The frequency of occurrence is relatively low and there is danger of their coinciding with its own tower frequency. In the static considerations of the construction, this phenomenon are includes by increasing the vertical force for double velocity of the vehicle mass.

2 METHODOLOGY

We used an experimental modal analysis and validated FE model of the tower to investigate the consequences of this described phenomenon on the dynamic behavior of a tower structure. It is common that modal analysis researches are carry out in the laboratory on prototype models. In that case it is necessary to solve the problem by fastening the structure, in a way that coinsided to real conditions. Depending on the type of structure, this step is the most common source of disagreement with the actual experimental conditions.

This paper examines the behavior of installed structures in real operational conditions. In the researches carried out under real conditions the initiative load is the one which in all its complexity affects the structure. When we research the tower of the chairlift we have to consider their behavior over the influence of stiffness of the rope. This research was done for the established operational regime, were inertia forces have no significance.

2.1 Initiative load

Acceleration sensor is attached to the chair structure, and the figure shows the acceleration signal measured in the vertical direction. The figure clearly shoves arrival moment of a chair on the sheave assembly (650) and moment when the grip losing contact with the sheave assembly (1600). Fig. 4.

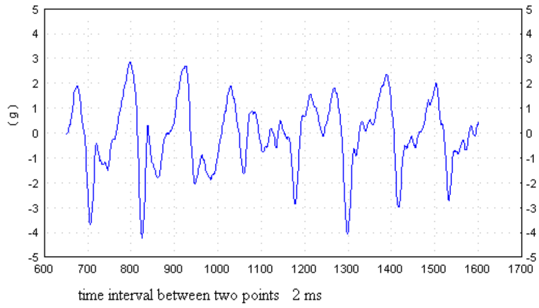

Fig. 4. *The vertical component of chair acceleration on the assembly of 8 wheels*

There is isolated segment, which is used for modeling of dynamic excitation approximating to 12 points. Fig. 5.

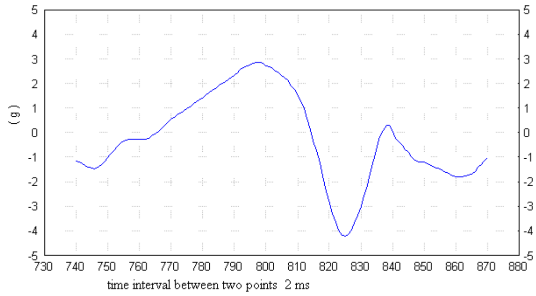

Fig. 5. *Segment acceleration functions used to model load*

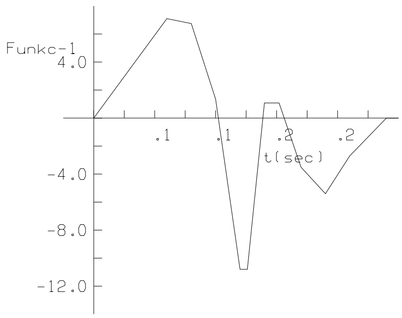

Fig. 6. *Model of the excitation load*

Fig. 6. shows the shape of the excitation load, force [kN] in a function of time [sec]. Thus modeled load included the total time were the grip is in contact with the wheel. If there are *n* wheels on the sheave assembly, this type of load will appear *n* times in calculated model. Performed spectral analysis of real and modeling load, shows a correlation higher than 80%, which justify our assumption of the model with 12 interpolation points.

2.2 Validation of the numerical model

Plate girder model was formed for research purposes. The model is formed with a kinematics freedom of all elements of the sheave assembly. Model validation was performed in a manner that compared the real mode shapes of the structure and mode shapes of a numerical model with a given modeled excitation. Measuring points are shown in Fig. 7, and also they are response points of the model.

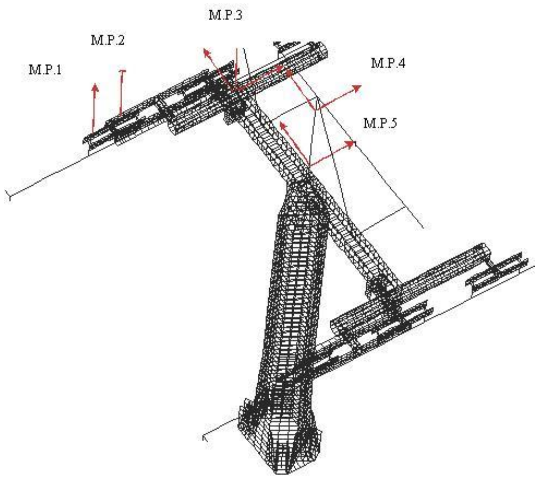

Fig. 7. *Measuring points*

Correlation data degree was estimated higher than 80%. (Example M.P.1 and M.P.5.). For this type of testing in real environment conditions, it can be considered sufficient. Fig. 8.

.

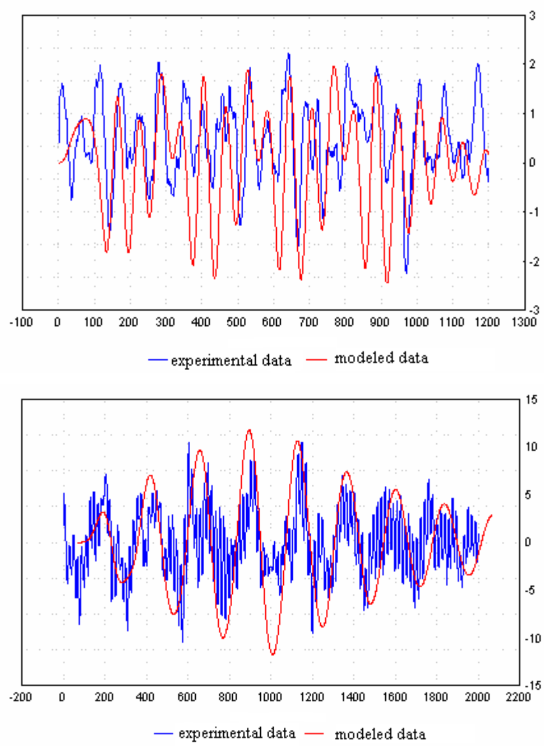

Fig. 8. *An example of correlation of experimental and model data - validation of models*

2.3 Identification of the dynamic behavior of validated model

In the first two modes, on the frequency of ω = 4.25 Hz and ω = 9.6 Hz, the oscillations of the yoke are primary in the longitudinal and lateral direction. The amplitudes of these oscillations are high and at the top of the yoke they move up to 60 mm. In the third mode of oscillation, at frequency of ω = 12.7 Hz, a tower itself and yoke oscillating in the longitudinal plane, with significantly smaller amplitudes of 5.4 mm. The other three modes are oscillations of the sheave assembly, together with the tower itself. Oscillation of the sheave assembly is not a problem because it kinematics allows that, but we can expected that moving of the tower itself has some stress implications.
The proximity of their frequent oscillations in the first three modes of oscillation and the frequent spectrum excitation indicates the possible resonant states.

2.4 Forced damped oscillations in the frequent domain

Anchor structure: studies have shown that the amplitude gain for a given excitation in the vertical direction, measured in the direction of alignment lifts, from 6 - 8 times in the frequency range of 15 - 20 Hz. So, for the last four types of oscillation in which it takes part and tree steps. Significant amplitude enhancement is the still the anchor that is closer to the source of excitation.

The tower itself: if the excitation acts on the return side it show very high values of amplitude states (12-25 times) and the response is monitored at points that are diagonally opposite. Considerably lower but still unacceptably high values are shown if the excitation acts from drafted side. Frequency range of the reported phenomena is from 10 - 20 Hz.

Yoke: The analysis indicates that the yoke oscillates in resonance with the excitation, Fig. 9. The rest of the tower in this process plays the role of the dynamic absorber and this is the main reason that yoke does not separate from cross carrerier. The frequency distribution diagram of the experimental load frequency of 4 - 5 Hz exists with 2 / 3 share in the frequency spectrum.

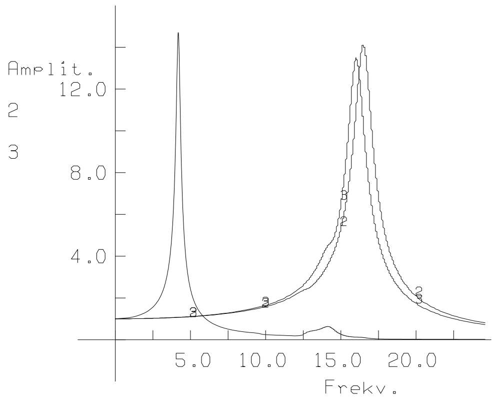

Fig. 9. *Diagram of amplitude intensify of the top of yoke*

2.5 Stress consequences of the passage of seats

Fig. 10. *Measuring poin , strain gauges*

.

Tension changes on the tower itself were monitored for the purposes of experimental verification of research results. Strain gauges, Fig. 10, are placed around a light contours on the tower

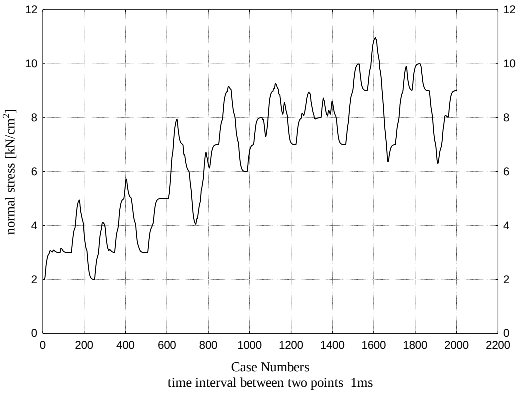

Fig. 11. *Tension signal from the strain gauges*

Passage of the seat is registered by changing of stress and an increase of the stress state, Fig. 11. Comparing the signals in Fig. 4, Fig. 11, it is clear correlative relationship. Stress signal in Fig. 11, represents the relative change in stress. Strain gauges were attached on a tower, which was already loaded with a rope and empty chairs (during maintenance). It is expected that the stress changes are around some constant values. In Fig. 9 it is not that situation, because load distribution along the corresponding suspension bridge and the load on the opposite side, affects the value of stress. For this reason, we can talk about an average increase of stress state caused by the passage of the chair.

For researched structure of the tower average increase in normal stress is 4 kN/cm^2 and tangential 1.2 kN/cm^2, for given measuring point. Alternating stress change nature should be carefully examined

Spectral analysis on Fig. 12, showed grouping of stress states at a frequency of 4 Hz in other words excitation frequency.

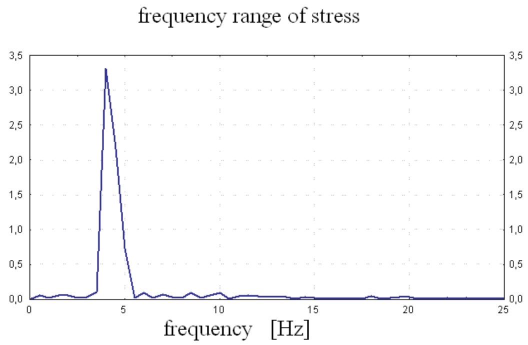

Fig. 12. *Frequency spectrum of tension*

3 OTHER SOURCES OF DYNAMIC EXCITATION

Geometry of the rope were selected depending on the chairlift load. Monocable chairlift ropes are mainly type 6 x (9 +9 +1). Ropes with larger diameter has larger strand diameter, which results in a larger hollow between the strands. Depending of rope step the wheel alternating comes across the top of the strand and then go down of it, Fig. 13. The frequency of this occurrence can be calculated:

$$f_{užeta} = \frac{v}{\frac{\lambda}{n}} \qquad [Hz] \tag{2}$$

where: *v – linear velocity of the rope (chairlift)*
λ – rope step
n – number of strands

For the dimensional ratio that are most frequent for the chairlift with a fixed clip, it is in the range f = 50 - 130 Hz.

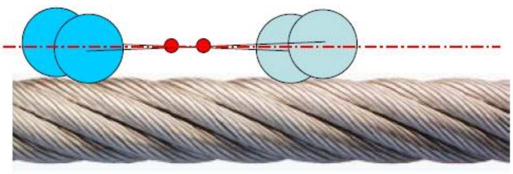

Fig. 13. *Rope as the source of dynamic excitation*

The frequency of this occurrence is high and possibility of resonant states is not a threat. To reduce the consequences to a minimum, it is necessary to take care about the schedule of the wheels within the sheave assemblie.

The next source of excitation may be a line wheel itself and its geometry in terms of oval shape. That shape is a consequence of irregular wear of rubber cover. This phenomenon can be calculated also:

$$f_{toč.} = \frac{v}{2 \cdot \pi \cdot R} \qquad [Hz] \tag{3}$$

where: v – *line speed of the rope (chairlift)*
R – *radius of the line wheel*

For the dimensional relatios that are most frequent R = 450 mm, for chairlifts with a fixed grip, it is in the range f = 2.8 - 4.2 Hz. Frequency of this phenomenon is relatively low, so its match with tower own frequency is possible.

4 CONCLUSION

Compression towers can not be avoided on the chairlift route. The research presented in this paper aimed to highlight the need for serious analysis of the dynamic behavior of compression towers of monocable chairlifts.

Studies have shown that the frequency spectrum of dynamic loads depends mainly on the structural properties of the sheave assembly. Frequency range of that load is low, which may result in a resonant state of the tower structure. Amplitude values of this loads depends mostly of: chairlift line speed, mass of full and empty chairs and grip geometric characteristics.

Part of the dynamic loading may occur as a result of imbalance between rope structure and disposition of the wheel in the sheave assembly. The frequency and amplitude, themselves, could not provoke problems.

Photos from the introduction part were recorded in the first tower, just before the double sit chairlifts operation section. Chairlifts with a fixed connection during the day has more than 50 stops and starts. Further studies will be extended to the measurement and modeling of these.

5 REFERENCES

[1] L. R. Padovese: “Étude des phénomènes dynamiques dans les pylônes compression des téléphériques monocâbles”, *Thèse, Université Joseph Fourier*, Grenoble. 1992.

[2] L. R. Padovese, J. M. Terriez , N.Martin: «Etude des phénomènes dynamiques dans les pylônes compression des téléphériques monocâble », vol 48, n°4,Décembre 1995 .

[3] F.Combet, P.Jaussaud & N. Martin “ Motion estimation and pulse detection in a detachable chairlift station”, *third workshop on Physics in Signal and Image Processing*, Grenoble, France, 2003 Jan. 29-31, pp 49-52

[4] A.Kopanakis: “Schwingungen bei Seilbahnen”, *INTERNATIONALE SEILBAHN-RUNDSCHAU 3/2010*, WIEN

[5] H. Renezeder, A. Steindl, H.Troger:”Three-Dimensional Simulation of a Circulating Monocable Ropeway*”, PAMM · Proc. Appl. Math. Mech. 6*, 327–328 (2006)

[6] M. Čupović:“Relevantni faktori od uticaja na statičko i dinamičko modeliranje jednoužetnih žičara“, *Doktorska disertacija*, Beograd, 2003.

[7] G.Chen: “FE Model validation for structural dynamics”, *Department of Mechanical Engineering Imperial College of Science, Tehnology and Medicine London*, Thesis, 2001.

ACKNOWLEDGMENT

A part of this work is a contribution to the Ministry of Science and Technological Development of Serbia funded Project TR35038

HEAVY MACHINERY - HM 2011, 111-116
ISBN 978-86-82631-58-3
Paper accepted: 30.05.2011

Special Design Of Freight Elevator With Diagonal Guiding And Instantaneous Type Eccentric Safety Gear

Mile Savković[1,]*- Milomir Gašić[1] - Nebojša Zdravković[1] - Goran Marković[1]
[1]University of Kragujevac, Faculty of Mechanical Engineering Kraljevo

The paper presents special design of freight elevator, customized to the particular characteristics of the embedding space and user requirements. Forklift three-sided access during operation is achieved by diagonal guiding concept of the elevator car along channel guides by means of cylindrical and tapered wheels. This guiding concept has imposed special design of car frame, which is made of two X-frames connected by columns. The instantaneous type eccentric safety gear is applied. Self-locking condition is ensured due to the existence of teeth on the eccentric disc.

Keywords: freight elevator, diagonal guiding, eccentric instantaneous safety gear

1 INTRODUCTION

Elevator, as typical example of mechatronic machine (mechanical electronically controlled executive), is inevitable part of modern multistorey buildings and make their exploatation pratictal and economic. Generally, elevators are hoists with periodical action that lift people and/or freight in a car upward and downward in such way that the car moves along rigid parallel guides, with maximum vertical inclination of 15° [1].

For lower lifting heights, hydrocylinders can be used for drive, while for higher lifting heights (few tenths of meters) traction system with the suspension cable and drum or pulley operated by an electric motor is used (Fig. 1).

Fig. 1. The most common elevator drive types
a) pushing up from below by hydrocylinders
b) pulling up from above by electric drive and traction cables

Common concept of an electric drive elevator for higher lifting heights is shown in Fig. 2. During designing new multistorey architectural objects, a separate space for elevator shaft, machine room and pit must be considered. Also, each storey level must have a slot for an elevator entrance. Besides, basic parameters, such as load capacity and rated speed, are to be defined in very early phase of building planning, in order to properly calculate space and support structures. In other words, with these predefined conditions in new objects, elevator design is very much reduced to combination and selection of existing standardized subassemblies and components out of assortment of numerous elevator equipment manufacturers.

On the other hand, within embedding into already built objects, in which no particular space is predefined for elevator operating purposes, it is very often the case that designer is forced to deviate from typical solutions and find a customized solution, usually only possible, according to situation. This kind of situation was handled in the case of customer requirements for designing, manufacturing and installing the freight elevator for overhaul purposes in existing industrial multistorey crushing mill facility Drmno in Kostolac, Serbia. Figure 3 shows the model of the facility building section where freight elevator was intended to be installed.

The building has five storeys, with a slot in each one, framed by steel columns and reinforcement girders. Storey slots cuold not be

*Corr. Author's Adress: Faculty of Mechanical Engineering Kraljevo, Dositejeva 19, Kraljevo, Serbia, savkovic.m@mfkv.kg.ac.rs

cosidered as common elevator shaft with concrete walls, which makes elevator car guiding more difficult. Transportation of overhauled equipment need to be carried out from fourth storey and ground floor and vice versa. Additionally, user required that elevator loading and unloading had to be done by forklifts, through three-sided access, in order to achieve easier manipulation of freight. The lifting height is 16m, and the load capacity is 8 t. Maximum dimensions of the elevator car are limited by embedding space. Figures 4 and 5 are photos of workspace for this freight elevator.

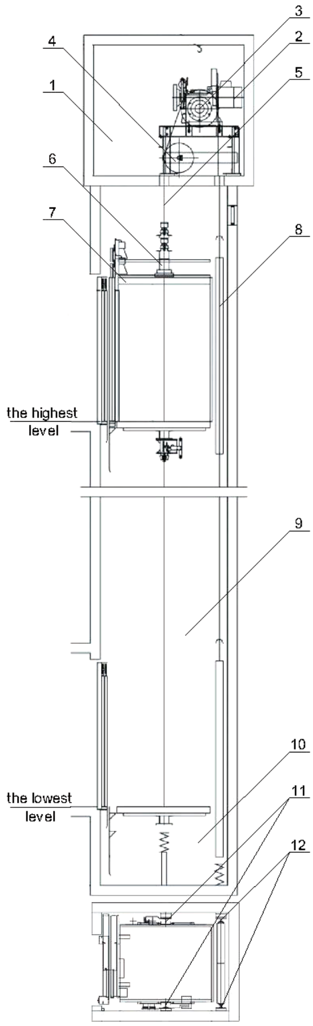

Fig. 2. Common concept of an electrical elevator 1-machine room, 2-electric motor, 3-drive pulley 4-auxiliary pulley, 5-traction cable, 6-suspension assembly, 7-car, 8-counterweight, 9-elevator shaft, 10-pit, 11-car guide rails, 12- counterweight guide rails

The concentration of particles and coal dust is increased in operating ambient air, due to the nature of coal crushing process.

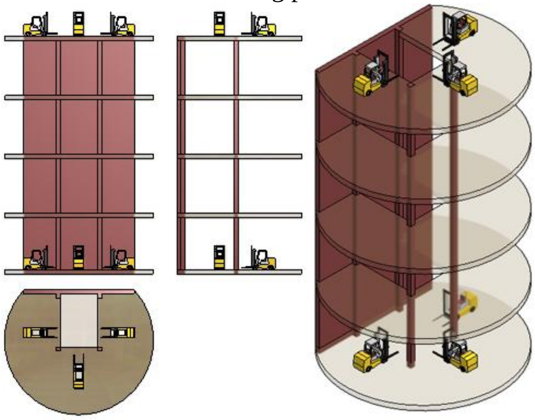

Fig. 3. Model of the facility building section with enforced storey slots

Fig. 4. Elevator embedment space - bottom view

Fig. 5. Elevator embedment space - top view

2 FREIGHT ELEVATOR DESIGN

2.1. Car Guiding

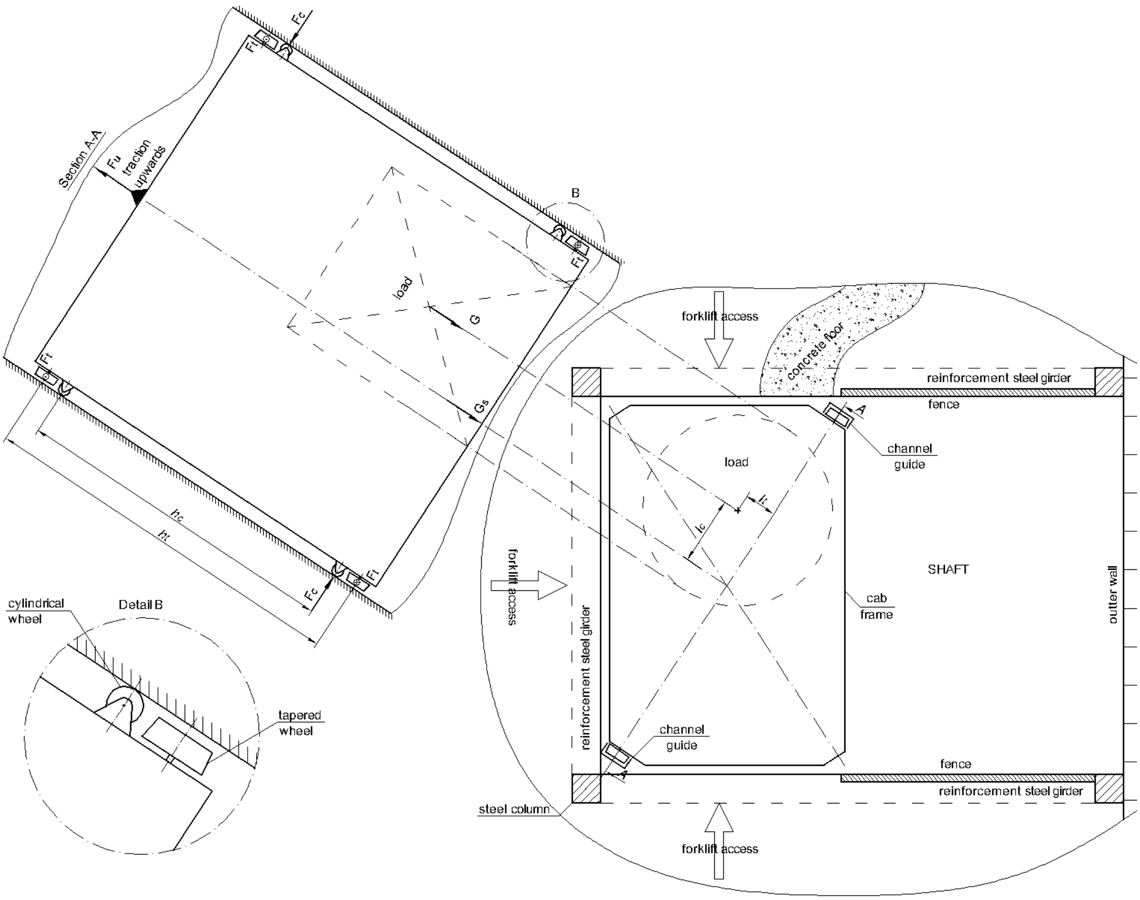

Fig. 6. Car guiding concept

Car guiding concept which meets user requirements and installing conditions is shown in figure 6.

In order to ensure three-sided forklift acces to the elevator car, the elevator car guiding was solved diagonally relative to the car frame by means of two pairs of tapered and two pairs of cylindrical guiding wheels and channel rails as guides. Cylindrical guiding wheels roll on the channel web and tapered ones roll on inner side of flanges. The channel guides are bolted via flange plates to the horizontal steel girders incorparated in concrete storey floors.

According to figure 6, eccentricity of load weight relative to the traction axis makes following forces onto the cylindrical and tapered guide wheels:

$$F_c = G\frac{l_c}{h_c} \quad (1)$$

$$F_t = G\frac{l_t}{2h_t} \quad (2)$$

Figure 7 shows realized design of the freight elevator car frame. The car frame 1 is welded structure made of standard steel shapes and plates. It consists of upper and lower X-frame, connected by columns. Suspension assembly carries the car frame through contact area on bottom side of the upper X-frame. Traction rope and suspension frame are connected by pulley. Both upper zones of car frame are equipped with eccentric safety gears 3.

Subassemblies of cylindrical and tapered guide wheels, 4 and 5, are mounted to the car frame by bolted connection and flange plates.

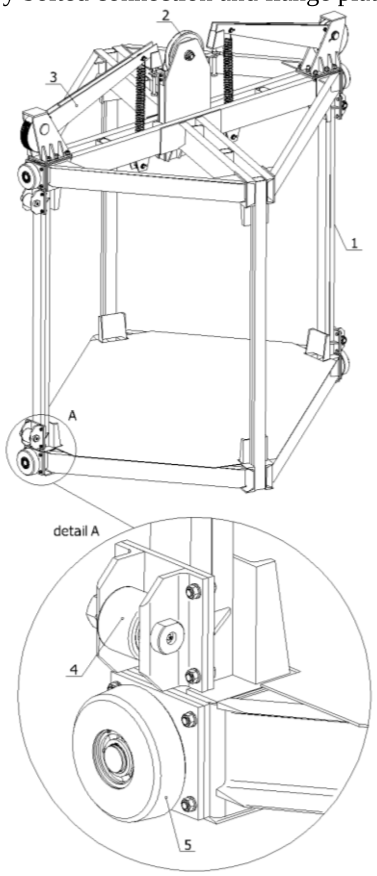

Fig. 7. Car design with guiding wheels detail 1-car frame, 2-suspension assembly, 3-eccentric safety gear, 4- cylindrical guiding wheel, 5-tapered guiding wheel

2.2. Eccentric Safety Gear

Elevator car must be equipped with safety gear, e.g. gripping device for stopping, and maintaining stationary on the guides the elevator car in case of over speeding in the downward direction or breaking of the suspension ropes [2]. In other words, every elevator cab has a clamping device that is activated if downward speed of the cab reaches certain limit [3].

The functions of the guide rails are to [4]:

(a) guide the car and counterweight in their vertical travel by controlling horizontal movement,

(b) prevent tilting of the car under eccentric loads,

(c) stop and restrain the car when safety gear is applied.

In relation to elevator rated speed as well as to the way of acting, there are three types of safety gear: instantaneous type safety gear, instantaneous type with damping effect safety gear and progressive type safety gear. Instantaneous type safety gear is used for rated speeds less or equal to 0,63 m/s and it can be with wedge, balls, rollers or eccentricity [1].

Figure 8 shows applied design solution of an eccentric safety gear, attached on upper side of car frame. Executive part is eccentric disc with small teeth 1, which rotates about pin 2. The pin accomplishes the joint connection between eccentric disc and shoulder frame 3, which is mounted by bolts 4 to the welded structure of car frame. An arm 5 is firmly fixed to the eccentric disc. Tension spring 6 is strained while arm is rotating by tightening the adjusting screw 7.

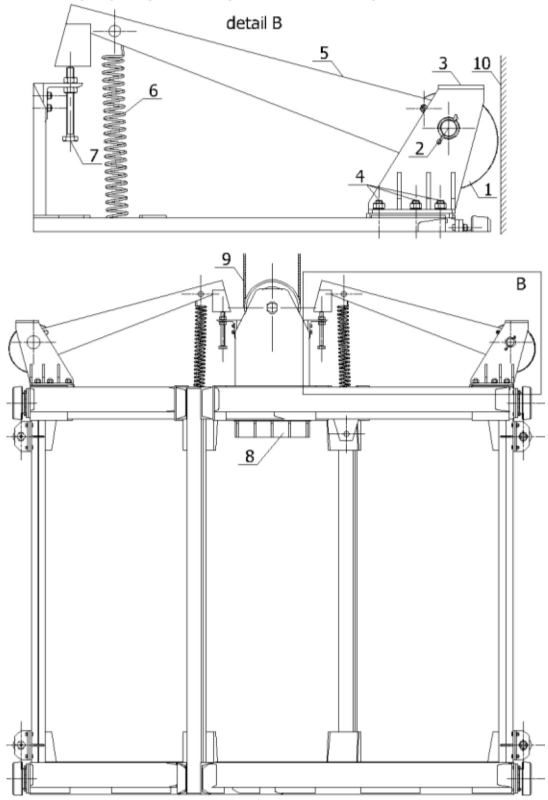

Fig. 8. Special design of eccentric safety gear 1-eccentric disc with teeth, 2-pin, 3-shoulder, 4-bolted connection, 5-arm, 6-tension spring, 7-adjusting screw8-suspension assembly, 9-suspension cable, 10-guide channel

During normal working regime, safety gear is unblocked because of gap existing between eccentric disc teeth 1 and guide channels 10. The arm is rested on the adjusting screw, which is a part of the suspension assembly with pulley 8. Suspension cable 9 is bent around the pulley. In case of suspension ropes breakdown or some other reason for loss of the suspension force, suspension assembly 8 with adjusting screw 7 fall downwards on the top of the car frame. The arm 5 loses its support and, forced by tension spring, rotates altogether with eccentric disc 1 about pin 2. The eccentric disc teeth approach and make contact with guide channels and embed into the channel material and so stop the car moving downwards. Condition for contact realization between eccentric disc and guides is (figure 9):

$$e \cdot \sin\varphi = \Delta \tag{3}$$

where
e - rotation pole eccentricity in relation to center of the disc,
φ - safety gear rotation angle at realized contact,
Δ - starting distance between the disc and the channel guide.

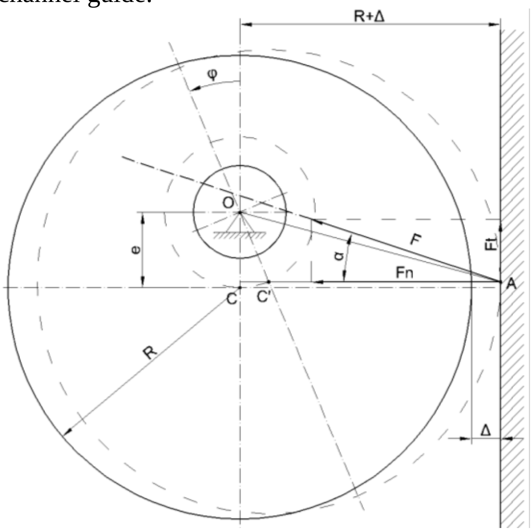

Fig. 9. Conceptual sketch of safety gear eccentric disc

The contact is being established in point A where perpendicular force Fn and tangent force Ft occur:

$$F_t = \mu \cdot F_n \tag{4}$$

where μ stands for friction coefficient.

In order to fulfil self-locking condition, the resultant of Fn and Ft must make such moment in relation to rotation pole O that additionaly pushes eccentric disc towards channel guide. Mathematical formulation of this condition is:

$$tg\alpha > \frac{e \cdot \cos\varphi}{R + e \cdot \sin\varphi} \tag{5}$$

Considering equation (5) and following expression

$$tg\alpha = \frac{Ft}{Fn} = \mu \tag{6}$$

it is obtained

$$\mu > \frac{e \cdot \cos\varphi}{R + \Delta} \tag{7}$$

After trigonometry transformation, final expression for self-locking condition is:

$$\mu > \frac{\sqrt{e^2 - \Delta^2}}{R + \Delta} \tag{8}$$

As elevator stops, direction of resultant F goes through rotation pole O. The values of friction force and perpendicular force are:

$$F_t = \frac{G + G_s}{2} \tag{9}$$

$$F_n = \frac{R + \Delta}{\sqrt{e^2 - \Delta^2}} \cdot \frac{G + G_s}{2} \tag{10}$$

where: G - load weight , G_s - self-weight.

2.3. Freight Elevator Drive

Freight elevator drive is shown in fig. 10.

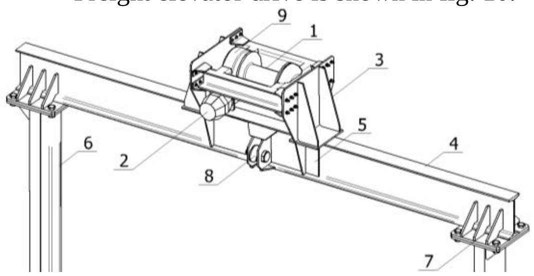

Fig. 10. Freight elevator drive
1-drum, 2-hydromotor, 3-drum frame, 4-top girder, 5-girder reinforcement, 6-guide channels, 7-bolted connection, 8-anchor point, 9-worm gear

The traction of the freight elevator is done by cable reeving on the drive drum 1, which is connected to hydromotor 2 via worm gear 9. Drive drum and hydromotor have own frame 3, which is welded to the girder 4. The girder is I-section beam, reinforced with steel plates 5 in the middle. It is placed at top of the elevator shaft and connected by bolts 7 to the end guide channels 6. Free end of cable is fixed to anchor point 8.

Hydromotor gets power from hydraulic set which is placed beside top girder, on highest storey floor. Hydraulic installation layout is shown in figure 11.

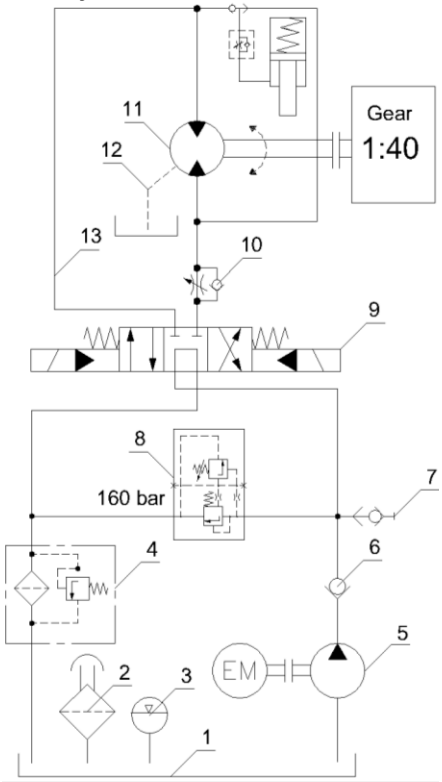

Fig. 11. Hydraulic installation layout
1-oil tank, 2-instil with vent, 3-level indicator, 4-filter, 5-oil gear pump, 6-blocking valve, 7-measuring port, 8-relief valve, 9-slide valve, 10-throttle-blocking valve, 11-hydromotor, 12,13-pipelines

3 CONCLUSION

The features of people and freight vertical transportation as well as the numerous embeddings of freight and passenger elevators in new multistory residential and industrial objects, made this type of hoists design most automated and reduced it to a procedural calculation and selecting standardized subassemblies and parts. Purpose, type, rated load and elevator embedding space which consists of elevator shaft and machine room if existing, are defined in the early phase of construction plan development. Yet, sometimes occures that customer requirements are such that elevator design must have particularities which, more or less, sort it out from common concepts. This paper presents one such freight elevator construction with diagonal guiding concept and eccentric instantaneous safety gear, designed to meet specific exploatation and embedding requirements

4 REFERENCES

[1] Tošić, S. “Liftovi”, Mašinski fakultet, Univerzitet u Beogradu, 2004
[2] Ostrić D. “Dizalice”, Mašinski fakultet, Univerzitet u Beogradu, 2004
[3] Menjić, M., Tošić, S., Bošnjak, S., Vasiljević, N. “Contribution to the solving of problem of noise and vibrations transfer of the personal elevator’s rail and cabin vibrations by using the elastic supports”, XIV International Conference on Material Handling and Warehousing, Faculty of Mechanical Engineering in Belgrade, 1996
[4] Bangash M.Y.H., Bangash T. “Lifts, elevators, escalators and moving walkways/travelators”, Taylor & Francis e-Library, 2007, ISBN 0-203-02076-6
[5] Галиченко, А.Н., Гехт А.Х. “Строителъные подъемники”, Высшая школа, Москва, 1984
[6] Волков, Д.П., Ионов, А.А., Чутчиков, П.И. “Атлас конструкций лифтов”, Машиностроение, Москва, 1984
[7] New Orona TDS, Technical Catalogue
[8] Schindler Freight and Special Elevators, Technical documentation, Schindler lift Ltd.

ACKNOWLEDGMENT

A part of this work is a contribution to the Ministry of Science and Technological Development of Serbia funded Project TR35038

HEAVY MACHINERY - HM 2011, 117-120
ISBN 978-86-82631-58-3
Paper accepted: 30.05.2011

Usage of movable laser and photo electric screen for crane rails measurement

Zoran Petrović M.Sc. ME[1,*] - Prof. Uglješa Bugarić Phd. ME[2], Prof. Dušan Petrović Phd. ME[2]
[1] Tecon Sistem d.o.o. – Demag Cranes AG Agency
[2] University of Belgrade, Faculty of Mechanical Engineering

Installing the new crane is relatively easy task. But installing new, or refurbished crane on old rails can be, and usually is, very complex. Before installing the crane, in order to keep permitted toleranced values, geodetic measurements of rails are necessary. After determining problematic part of rails, some correction must be done and after it new set of measurements is needed. This is, usually, very time and money consuming, since it requires geodetic crew to be present all the time during reconstruction of the rails. Another problem is that it is often very difficult to find good reference point for positioning of the instruments, regarding difficult access to the rails. New approach with laser installed on the trolley, is more accurate and less time consuming technique.

Keywords: crane rail survey, tolerances, measurement, laser, photosensitive, screen, descriptive statistics

0 INTRODUCTION

When speaking about installation of the new cranes on existing rails, problem is in time that is needed for measuring and correcting tolerances of the rails according to standard values. [1]

If the rails are not inside of tolerances, damage to the rails, or crane subassemblies are inevitable consequence.

Typical damage to the crane wheels comes in majority of the cases from the same cause – problems with rails alignment.

Consequence of this problem is skewing of the crane and excessive wear of the crane wheels. This is increasing operational cost of the cranes, since travel wheels have to be replaced prematurely.

Lateral displacements of the rails are causing changing in the travelling speed of the cranes. Problem is emphasized with automated cranes, since problems with speed changing can cause wrong position readings. Lateral displacement of the rails produces damaging of the wheels, but also damaging of the end carriages and sway of the load, which can produce damage on the hoists, but can also endanger complete production process.

Large difference in height between rails can cause lateral displacement of the crane itself. Again, most effected are wheels and rails and the result is severe wear and rear of both and increased repair costs (Fig. 1.).

Inclination of the rails to one another are producing additional lateral forces in the steel superstructure of the crane, which affects both crane design (crane geometry) and increases wheel pressures. Result is faster wear and tear of the material of the wheels, which endangers operational safety and causes expensive repairs.

Fig. 1. Heavy lateral damage of crane rail

For all above reasons, survey of the rails is necessary corrective measure in order to prevent damage of the crane subassemblies and additional cost for replacing of the parts as consequence of excessive wear and tear. (Fig. 2.)

*Corr. Author's Address: Tecon Sistem d.o.o. – Demag Cranes AG Agency, Antifašističke borbe 21 b, Belgrade, Serbia, zoran@tecon.rs

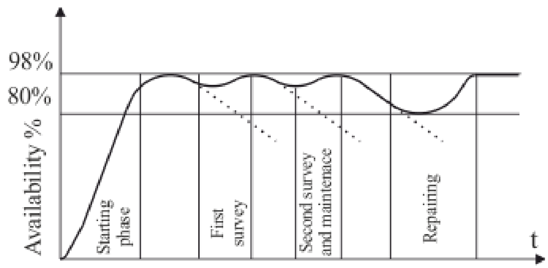

Fig. 2. Service life of material handling system

1 METHODOLOGY OF RESEARCH

Since no valid data about usage of moveable laser measuring systems could be found, small statistical study was performed in order to check validity of results from such procedure. Results were compared to ones from static laser measurement (geodetic measurement).

Main working hypothesis of the research is that there is no statistic significant difference between measurements taken by static laser measurement device and movable Laser Measurement System (LMS).

For the static laser measuring system Leica TCA 2003 infra-red laser measuring system was used. Standard precision of the system is: ±1 mm + 1 ppm/3,0 s.

Measurement with mentioned system is compared with Demag LMS system, which was patented by Demag Cranes & Components.

Technical characteristics of LMS systems are: laser type is He-Ne gas laser, diameter of the beam is 11 mm, laser class A3 [3]. Measuring accuracy depends of the size of the receiver. Two types of receivers were possible to use: 125 x 100 mm (accuracy +-0,5 mm/100 m) and 250 x 200 mm (accuracy +-1,0 mm/100 m). LMS system consists of automated alignment laser, radio controlled self-propelled trolley, laptop computer with radio modem and specially designed software. (Fig. 3.)

Maximum measured distance without additional equipment (special lenses) is 100 m, because of the diffraction of the laser beam. [4]

Self propelled trolleys are moving along the rails with step motors and are equipped with photo sensitive screen. Behind the screen is camera which is measuring exact position of the laser beam in time.

Laptop computer is through radio modem connected to the camera, from which is getting information about relative movement of the laser beam across the screen.

For the static measuring system one measurement was performed as reference value.

Fig. 3. LMS crane rails survey system

For LMS system rails were examined in 4 independent measurements. First measurement was performed while adjusting the equipment so, statistically different results from rest of the measurement were expected.

Measurement was done with first speed which is between 1,5 and 2 m/min. Total of 54 points on the rails were measured and compared.

2 RESULTS

Results of the research are presented below. (Fig. 4.-6.) First test that was performed was examination of each measurement to Normal distribution N(n,σ) according to Kolmogorov-Smirnov test.

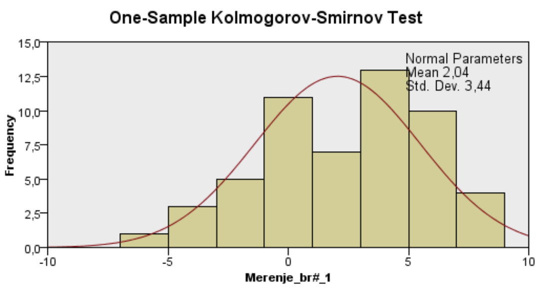

Fig. 4. First measurement analyses

As it can be seen, for the static laser measuring , hypothesis for Normal distribution N(μ,σ) can be assumed. Parameters of normal distribution are N(2.04,3.44).

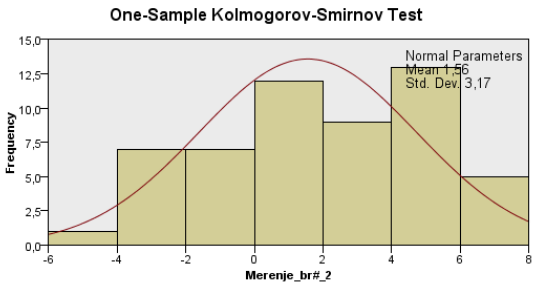

Fig. 5. Second measurement analyses

For the second measurement hypothesis for normal distribution can also be assumed. Parameters of normal distribution are N(1.56,3.17).

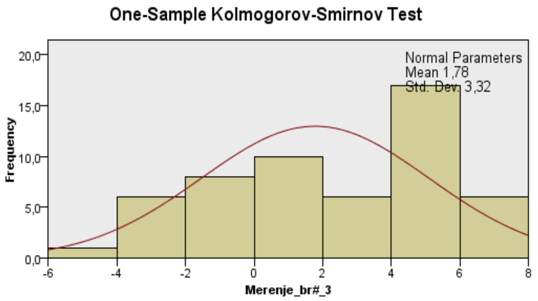

Fig. 6. Third measurement analyses

In the third set of measurement hypothesis for normal distribution can also be assumed. Parameters of normal distribution are N(1.78,3.32).

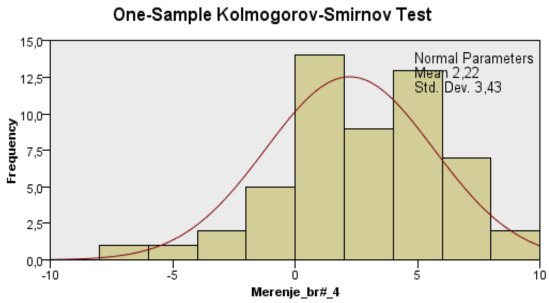

Fig. 7. Fourth measurement analyses

For the fourth measurement, hypothesis for normal distribution can also be assumed. Parameters of normal distribution are N(2.22,3.34).

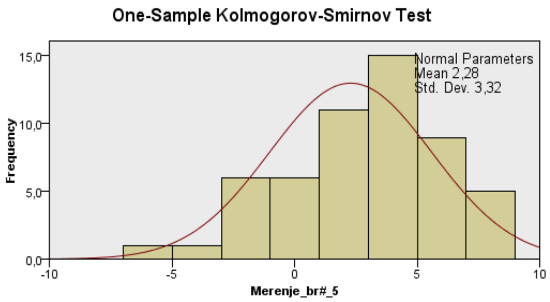

Fig. 8. Fifth measurement analyses

Regarding fifth measurement, hypothesis for normal distribution can also be assumed. Parameters of normal distribution are N(2.28,3.32).

3 EVALUATION OF THE RESULTS

In order to estimate if mean values (μ) are significantly different, Wilks lambda value is used. Wilks lambda value can have value between 0 and 1.

Values of Wilks lambda closer to 1, are showing that mean values of independent measurements are not significantly different, which is the case in taken measures.

Tab. 1 Wilks lambda value

Eff.	Val.	Err. df	Sig.	Part. η^2
l	0,725	50,000	0,003	0,275

Tab. 2 Table of pairwise comparisons

(I) Meas.	(J) Meas.	Sig.
1	2	0,002
	3	0,848
	4	1,000
	5	0,572
2	1	0,002
	3	1,000
	4	0,010
	5	0,002
3	1	0,848
	2	1,000
	4	0,092
	5	0,151
4	1	1,000
	2	0,010
	3	0,092
	5	1,000
5	1	0,572
	2	0,002
	3	0,151
	4	1,000

On the other side, value of partial η^2 is showing that, according to Cohen [5], values above 0,14, are showing big influence between different measures.

In order to estimate in which set of measurements is significant difference pairwise comparisons between groups was made.

Results are showing that there is significant difference between second and first, second and fourth and second and fifth measurement, which is consequence of adjusting the equipment which was done in second measurement (first measurement with LMS system while adjusting).

4 CONCLUSION

According to the given results, there are no significant differences between measuring with static system and LMS system. Further measurements are necessary in order to get more accurate results, if required.

Advantage of LMS system is possibility to run railway survey on hard approaching places (for example with no maintenance platform), on which static systems can’t be positioned.

5 REFERENCES

[1] DIN 4132:1981 Craneways; Steel structures; Principles for calculation, design and construction

[2] Demag surveying service manual, Demag service, 2005

[3] B.Struve, W.Luhs, G.Litfin, Crystal optics and its importance in laser technology, Year book for optics and precision mechanics 1989

[4] W.Luhs, B.Struve, G.Litfin, Tuneable multi lines He-Ne laser, Laser and optoelectronics, 4. 1986, ATFachverlag GmbH Stuttgart

[5] Cohen,J.W. Statistical power analyzes for behavioural studies, Hilsdale NJ: Lawrence Erlbaum Associates

HEAVY MACHINERY - HM 2011, 121-125
ISBN 978-86-82631-58-3
Paper accepted: 30.05.2011

One approach in testing pioneer machines

Snežana Jovanović[1,*] – Aleksandar Đurić[1] – Dragan Repajić[1]
[1] TECHNICAL TEST CENTER

This paper present one approach in pioneer machine (combined backhoe – loader) sample testing. We described product testing in laboratory conditions and some off-road (exploitation) testing.

In conclusion, beside general mark about implementation demanded characteristic of machine, we gave opinion on modern solutions and construction machine perspectivity.

Keywords: Pioneer machine, backhoe – loader, testing.

0 INTRODUCTIONS

Combined backhoe – loader is made for land working, material excavation and its loading in transport vehicles and cargo loading with integrated fork lift. With additional equipment this machine can brake materijals, drill holes in ground with dimeter of 250 – 950 mm, striping layers of asphalt and concrete width 400 mm and depth up to 120 mm, cutting and destruction concrete constructions and several others demands in dependence from addition equipment.

Technical test center is performing testing of machines with aim to mark: implementation demanded technical characteristic and tactical-technical demands; machine usableness in real work conditions in relationship with demands dictated by user; up to date and perspectivity of applied technical-technological solutions and machine in whole.

Measurements are based and defined in standards, domestic and international. Likewise, Technical test center is making standards and methods for testing based on experience and modern achievements in measuremet technics and new standards.

1.TESTING

For every individual machine we make program of testing. All tests are being made according to testing program. In general, machine testing has several parts:

- previous examination;
- laboratory tests;
- exploitations and training ground tests;
- final examination.

Fig. 1. *Machnine figure from right side*

Fig. 2. *Machnine figure from reverse*

1.1 Previous examination

Intention in this part of testing is:

- Identification of all constituting parts, assembly and machine sets according to documentation;
- checking level of working fluids in engine, transmission sets and hidraulic parts;

Corr. Author's Address: TEHNIČKI OPITNI CENTAR, Vojvode Stepe 445, Beograd, Srbija, sneza.jovanovic.toc@gmail.com

- checking engine and engine sets, its functionality and correctness, specifically measurement of minimal and maximal idle engine speed, air suction sistem, fuel sistem, lubricating, exhaust sistem, engine stand, cooling sistem, backhoe dashboard in cabin, heating and ventilating sistem;
- build in transducers for checking engine parameters like oil temperature, cooling fluid temperature…;
- identification in transmission sistem, tyres, tyre presure, checking functionality of transmission sistem and sets in all gearwheels, checking level of working fluids in sets (transmission, breaking sistem, hidraulic parts…);
- identification and checking of break sistem, steering sistem;
- basic checking of hidraulic sistem in backhoe, valves, hidraulic hoses, hidraulic pumps, attachments for small additional tools;
- EMC characteristics checking;
- basic work-testing and simulation of work with different tools.

After all previous tests a trial run (about 20 km long) at asphalt road is necesary, where we can see working of all parts, sets and whole machine.

1.2 Laboratory testing

Laboratory testing is specific for every individual machine. Most often, laboratory testing has several parts and measurements, like:

- Geometric characteristics;
- reverse wheel turning;
- mass characteristics (mass disposition by wheels, total mass, centre of mass);
- phonics characteristics (internal noise level inside cabin, level of external machine noise, horn noise level);
- backhoe characteristics at ultra environment conditions (temperature levels from -30oC to +50^{o}C), checking engine start at low (-12°C) and high environment temperatures (+46°C);
- determinating PMV and PPD index at low external temperature (-16^{o}C) and normal external temperature;
- characteristics of all electro-wirring sistem and electro-equipment, voltage levels, currecurent intensity, insulance, alternator voltage, short protection;
- EMC characteristics.

These are most common characteristics that are being made in laboratory testing. Specific test list we made for every machine itselfe.

1.3 Exploitations and training ground testing

These testing include:

- dinamic characteristics;
- driving;
- reliability and efficacy of working tools.

1.3.1 Dinamic characteristics testing

Within backhoe – loader dinamic characteristics testing following verifying are being made:

- static and dinamic wheel radius,
- lowest and highest velocity in all gears, in both working conditions (manual and automatic)…

Some dinamic-characteristics testing are:

- vehicle resistance testing using coast method;
- Retarder system efficacy (where efficacy of parking break are being made in driving testing);
- testing of ability to overcome longitudinal and lateral inclination.

1.3.2 Intensive driving machine construction testing

This testing includes about 500 km in several different road conditions: about 250 km plain and hill ground road and about 250 km heavy off-road conditions.

While driving, we monitor some basic indicators like:

- total road that has been driven;
- time of driving;
- time of standing (non-work time);
- road conditions, ground and meteorology conditions while driving;
- failures, fracture, and posible crushing parts of machine construction that occur while testing is being done, with

registering number of kilometres by failure happends;
- working on regular maintenance, seting and servicing while testing with registering number of kilometres;
- durability of parts and sets in transport.

1.3.3 Testing operating safety while working with different tools

This testing includes:
- working with digger spoon in time of 25 engine working hour, while excavate, laying-off, and loading land up to category, and
- working with loading spoon in time of 25 engine working time.

The purpose of this testing are to control:
- maximum digging depth;
- reach of digger hand on ground;
- velocity of digging spoon, width of digging spoon, carrying capacity of digging spoon, velocity of loading shovel;
- hidraulic regulator function checking, maximum working presure in hidraulic instalation, conditions of hidraulic hoses, checking for leaking in instalation etc.

Also, while testing are being conducting, we check for engine oil quality, engine fuel consumption, engine working characteristics while working with maximum load and high external temperature etc.

If addition tools are build-in (hidraulic hammer, drill, concrete saw etc), additional test are being made:
- functionality checking in working time of 5 hours, while working in breaking different materials,
- drilling holes in ground up to diameter 950 mm,
- stripping asphalt layers and concrete width 400 mm and 120 mm deep,
- cutting and destruction of concrete constructions,
- snow sweeping etc.

2. ANALISING OF TESTING RESULTS

2.1 Conclusions of previous examinations

At previous examination we concluded that:
- All sets are workin properly, they are fill with working fluids according to maintenance manual;
- machine start is normal, without jerky actions, gear set is working properly in both directions (forword ane reverse) etc;
- backhoe – loader sets are workin properly;
- additional tools are working properly;
- combined backhoe – loader has "powershift" automatic transmission;
- machine hasturn over prevention and prevention from falling objects, accommodate steering veel, ventilation, safety belt, warning sirene etc.

.

2.2 Some results of laboratory testing

Measured dimensions (transport height, width, lengt, spoon width etc.) are meeting the required specification, with neglect deviation.

Angles of turning back weels are from 14° to 17°, and it should be from 21° to 25°. Values of total mass and mass disposition by axles are acceptable.

Noise level in backhoe – loader cabin, with open and close windows is 77 dB (A), and it is abowe declassed 72 dB (A). With open windows noise level is 82 dB (A), what is below 86 dB (A), according to noise Directive.

In low external temperature testing (12 hours at set temperature) engine in vehicle was naked to cooling at -12°C, until equalizing oil, fuel and cooling fluid temperature with external temperature. Valid capacity of bateries was 75% from 125 Ah. Engine started successfully. In high external temperature test (+46°C) in 12 hours engine heating, he started successfully. While working, at external temperature of +45^{o}C, oil temperature reached maximum +95^{o}C, and temperature of cooling fluid was 80°C. For cabin heating sistem efficacy, backhoe was at external temperature of -12°C during 10 hours, with all windows opened. After machine start, all windows were closed, and heating fan turned on. The cabin heating sistem has pleased efficacy criteria, becouse in time of 51 minute (efficient cabin heating sistem must meet the required specifications in maximum 60 minute from the sistem start) comfor parameters. Index PMV was -0,5; demand was:

$$\mathbf{-0.5 \leq PMV \geq +0.5} \tag{1}$$

Index **PPD=10%**; demand was:

$$\mathbf{PPD \leq 10\%} \tag{2}$$

Electroinstalation characteristics were:

- Conductors are protected from mechanical influence;
- alternator enables quality supply of current and maintenance of bateries;
- before driving, measured voltage fall was in boundaris were from ΔU=0,30 V to ΔU=1,27 V, and after 500 km test drive and 50 engine working hours in exploitation (land digging), measured voltage fall was in boundaries of ΔU=0,70 V to ΔU=2,25 V, wich is widely enlarging from the first measurement. Voltage is constant at 14,4 V, with rpm engine from 500 o/min to 3000 o/min at voltage controller in alternator;
- minimum value of insulation resistance was 400 MΏ. Values for narrow-band difficulty at high frequencies are slightly crossing over 400 MHz (maximum crossing permit value is 5 dB).

2.3 Results of exploitations and training ground testing

Dinamic characteristics were:

- Velocity values of combined backhoe – loader are equal, at all gear wheel, no metter it moves forward or reverse, except in 4. gear. Measured velocity of 38,4 km/h in moving reverse was less than forward velocity. Working machine meet the demand for highest velocity at 40 km/h, or in range of 40 km/h to 50 km/h;
- tire rolling radius were satisfied;
- efficacy of machine brakes, type "0" with on and off clutch was good, becouse the maximum brake road is smaller than permit; efficiacy of brakes type " I" was good. Handbrake was holding machine at highest testing slope (30%).

Testing of machine in intensive driving conditions was made an plain ground road (with average velocity of 13 km/h) and heavy off-road conditions (with average velocity of 15.4 km/h), and it was mark as positive.

Functional correcteness and drive safety at exploitation conditions was tested while backhoe – loader was working with backhoe spoon and loading spoon, in 50,6 engine working hours. Backhou spoon was conducting land working with 2. type land. Loader spoon worked with 2. type land too. In this testing temperature of engine fluids was measured. Results were satisfactory.

Within exploitation testing we made measurements of some backhoe characteristics, like:

- Maximum digging depth with backhoe spoon is 5900 mm, wich fulfil the demand of 5800 mm;
- velocity of digging spoon was declassed 0,24 m3;
- lifting forse of digging spoon in full reach with extracted telescope was 1200 kg, and with sucked telescope was 1550 kg, what is declassed;
- velocity of loading spoon was declassed 1,2 m3;
- lifting forse of forks integrated with spoon was 1000 kg;
- Together with exploitation testing checking additional tools was made. We determinate that combined backhoe – loader is working properly with all additional tools;
- measurement of total rate of flow and maximum working presure. Measured data for working presure was 225 bar, and for total rate of flow was 151 l/min.

3. CONCLUSION OF TESTING

Based on comparation with similar solutions all ower wourld, we consider aftre all testing that tested combined backhoe – loader is modern and perspective product concerning predict usage.

Combined backhoe – loader has all-purpose loading hidraulic opening spoon, model 6 in 1, with teeth, teeth protection and add-on fork, Power shift transmission and high level of comfor. Backhoe construction ensure fast fit-in additional equipment (hidraulic hammer, concrete mill, spiral drill).

Disadvantage of construction and manufacture are reverse weeels less turn angle, higher tital mass, higher noise in cabin, enlarging voltage fall at some parts of electric instalation (direct factor of driving and working in exploitation conditions).

4. REFERENCES

[1] Marković, V. "Građevinske mašine za zemljane radove", Naučna knjiga, Beograd, 1975.

[2] ISO 6394, ISO 6396, Earth-moving machinery – Determination of emission sound pressure level at operator's position, 2008.

[3] ISO 13766, Earth-moving machinery – Electromagnetic compatibility, 2006.

[4] SRPS EN 12643 – Mašine za zemljane radove – Mašine sa mehanizmom kretanja na pneumaticima – Zahtevi za upravljanje, 2009.

[5] SORS 0028 - Karakteristike dinamike vojnih vozila. Ispitivanje brzinskih karakteristika, 2003.

[6] SORS 0142 - Metoda ispitivanja. Startne karakteristike motora sa unutrasnjim sagorevanjem na niskoj temparaturi okoline,2002.

[7] SORS 1026 - Karakteristike motora i motorskih uredjaja. Ispitivanje startnih karakteristika motora SUS na visokim temperaturama okoline, 1986.

[8] SORS 5574 - Elektroenergetska instalacija i oprema. Metode ispitivanja električne otpornosti, 2003.

[9] SORS 6711 - Borbena i neborbena vozila i orudja. Elektroenergetska instalacija. Metode ispitivanja padova napona.

[10] SORS 8419 - Ispitivanje toplotne ugodnosti radnih prostora vojnih vozila, 2002.

[11] SORS 9156 - Karakteristike prohodnosti vojnih vozila. Uzdužni i poprečni nagib, 1998.

[12] SORS 9303 - Karakteristike, dinamičke, vojnih vozila. Opšti tehnički propis za završna ispitivanja kočnih sistema, 1998.

C SESSION

AUTOMATIC CONTROL AND FLUID TECHNIQUE
DESIGN AND MECHANICS

HEAVY MACHINERY - HM 2011, 1-6
ISBN 978-86-82631-58-3
Paper accepted: 27.05.2011

Auto-tuning of PID Controller for System Turbine - Condenser in the Thermal Power Plant

Novak N. Nedić[1], Vojislav Ž. Filipović[1], Saša Lj. Prodanović[2,*]

[1] University of Kragujevac, Faculty of Mechanical Engineering Kraljevo, Dositejeva 19, Kraljevo, Serbia,
[2] University of East Sarajevo, Faculty of Mechanical Engineering, Vuka Karadžića 30, East Sarajevo, Bosnia and Herzegovina

This paper contains auto-tuning of PID controller for level in condenser of thermal power plant Gacko. It shows method of compensation static load disturbance during relay feedback test. This auto-tuning is carried out with saturation relay, but disturbance rejection is obtained using automatic bias. In this way, errors in estimating of the ultimate gain and ultimate period are minimized. Simulation of mentioned test is performed on the mathematical model of system turbine-condenser, which are taken as second–order process.

Keywords: PID control, level in condenser, saturation relay, disturbance rejection, automatic bias.

1 INTRODUCTION

The application of PID controllers in industry is subject of many researches. This paper explores their role in controlling of level in condenser in the thermal power plant Gacko. System turbine-condenser in this power plant was taken as object of research.

Adequate tuning of PID controllers enables appropriate static and dynamic system behaviour. Large numbers of auto-tuning methods are derived based on Ziegler and Nichols and later Åström and Hägglund works. Each of them has main idea to tune PID controller with as little as possible information about process response [1]. In this paper, simulation of relay feedback test is carried out at the system turbine-condenser. They are modelled together as second order system in order to improve presenting of object's behaviour. This approach enables and suggests using exact procedure for calculating parameters of PID controller instead of current method of trial and errors in thermal power plant Gacko [2]. Because of comparing, there is presented auto-tuning method using ideal and saturation relay [3]. Very substantial part of paper is simulation and proposing of compensation of eventual static load disturbance. Its negative effects during auto-tuning test were overcome by applying automatic bias [4].

2 DESCRIPTION OF CONTROL SYSTEM OF LEVEL IN THE CONDENSER

In this chapter, condenser of turbine in thermal power plant Gacko will be described taking in account all its connections with other components of control system.

2.1 Object's structure

Level in condenser is determined by the amount of steam which comes from turbine (directly and from heater for regenerative heating), supply of demineralised (DEMI) water, drain of condensate and work of vacuum pumps for obtaining vacuum in condenser, as shown in Fig. 1. Control of level is performing by using two closed-loops. In the first, level control is carried out over valve for condensate drainage from the condenser, while in the second loop mentioned control is carried out using valve for DEMI water supply. Therefore, in both closed-loops within the system, the control part of the object is valve i.e. it is used damping control method [2].

The main goal is to obtain good dynamic behavior of system and keep desired level value in steady state. This set point (reference value of level) is $h_{ž}$ = 1,2 m.

[*] Corr. Author's Address: University of East Sarajevo, Faculty of Mechanical Engineering, Vuka Karadžića 30, East Sarajevo, Bosnia and Herzegovina, elsing123@yahoo.com

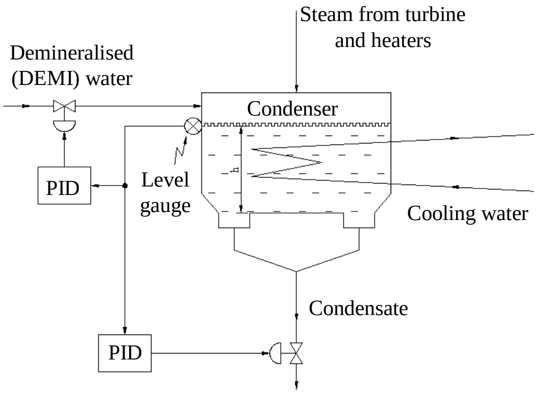

Fig. 1. *Control system of level in condenser in thermal power plant Gacko*

2.2 Mathematical model of system turbine-condenser

Previous investigations of control system of level in condenser in thermal power plant Gacko have used mathematical model of process as first order model [2,3]. This transfer function is given by

$$G_k(s) = \frac{2}{0{,}2784 \cdot s + 1}\,. \tag{1}$$

In order to enhance description of level as function of time, mathematical model of turbine was derived, because of vast influence of inlet steam from turbine into condenser [5]. So, transfer function of turbine follows

$$G_t(s) = \frac{1}{T_1 \cdot s + 1} \tag{2}$$

where T_1 is the time constant of the turbine rotor and its value in this considered system is T_1 = 1800 s = 0,5 h [6], hence

$$G_t(s) = \frac{1}{0{,}5 \cdot s + 1}\,. \tag{3}$$

Serial connecting of those two transfer function gives second order process.

3 AUTO-TUNING OF PID CONTROLLER

Knowing that this process is researched as second order system, the PID (proportional-integral-derivative) controller is tuned for its control. Simulation of relay feedback test was used for that purpose [1]. Like in experiment, simulation gives process response for estimating ultimate gain (a) and ultimate period (T_u). It can be seen in Fig. 2. Therefore, the main step is obtaining sustained oscillation.

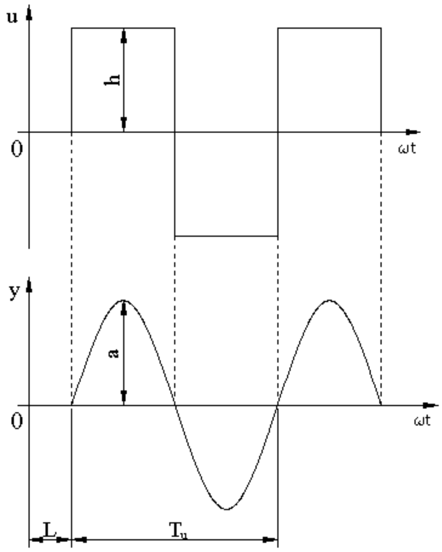

Fig. 2. *Input u(t) and output y(t) response of the process*

3.1 Relay feedback test with ideal relay

Configuration for this test contains two part: nonlinear (relay) and linear (process) as shows Fig. 3 [1,3]. In order to tune PID controller, according to this method, it is necessary to know folowing values: *h*, a, T_u, i.e., height of ideal relay characteristic (for our case *h* = 0,12 m), amplitude of output signal of linear system, ultimate period of the oscillation, respectively.

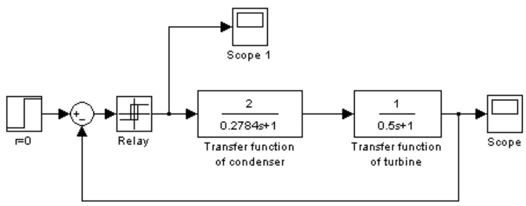

Fig. 3. *Configuration which provides steady oscillations of the process*

Simulation gives graphics in Fig. 4. and 5.

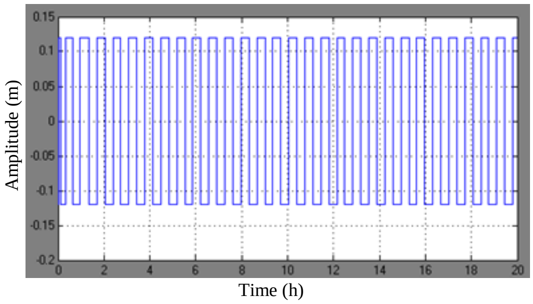

Fig. 4. *Output of ideal relay*

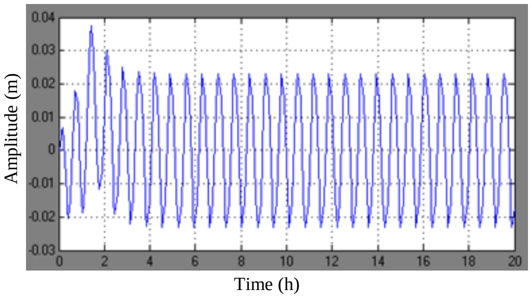

Fig. 5. *Process response with steady oscillations*

Graph in Fig. 5. gives following values: T_u = 0,467 h and a = 0,0099 m. Then the ultimate gain is given by:

$$K_u = 4h/\pi a = 15{,}44 . \qquad (4)$$

Robustness of system is increased using Tyreus-Luyben method for calculating PID parameters. Hence: K_p = 7,02 ; K_i = 6,82 ; K_d = 0,49.

3.2 Relay feedback test with saturation relay

Because of well known disadvantages of ideal relay, auto-tuning of PID controller by applying saturation relay was carried out [1]. Namely, saturation relay is closer to the graph of sine function, which is used in calculating of ultimate gain K_u. Then, configuration witch provides steady oscillations can be seen in Fig. 6.

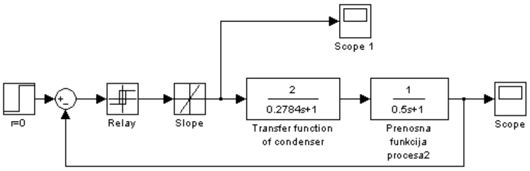

Fig. 6. *Configuration for relay feedback test using saturation relay*

Based on [1], previously completed relay feedback test with ideal relay gives k_{min} = 15,44. Than the slope of saturation curve is

$$k = 1{,}4 k_{\min} = 21{,}62 . \qquad (5)$$

For that values, simulation gives relay output and oscillatory response as it shown Fig. 7. and 8. respectively.

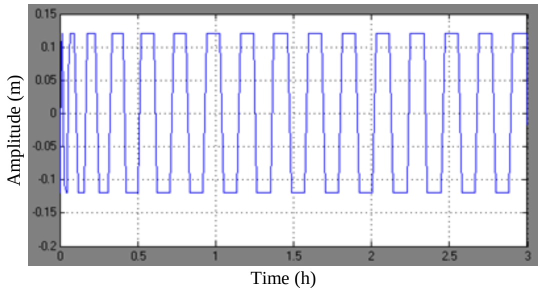

Fig. 7. *Output of saturation relay*

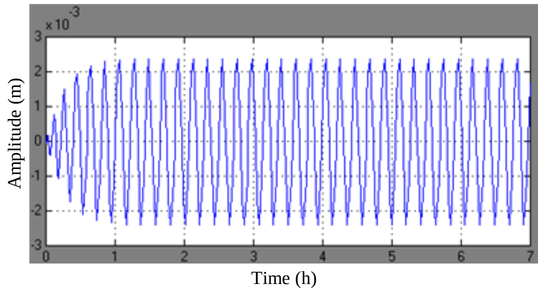

Fig. 8. *Oscillatory process responce in presence of saturation relay*

These responses are purposely shown on shorter interval for improving their view. Now, following values are estimated from graph in Fig. 8: T_u = 0,213 h and a = 0,0024 m. In accordance with

$$k = \frac{h}{h_1} \qquad (6)$$

the slope coordinate is $h_1 = h/k$ = 0,006 m.

Whereas a < h_1 [1], i.e. (0,0024 < 0,006) ultimate gain is K_u = h/h_1 = 21,62. Then parameters of PID controller are calculated according Tyreus-Luyben method: K_p = 9,83 ; K_i = 20,91 ; K_d = 0,29.

Appliance of those parameters in block diagram of current control system of level in condenser in thermal power plant Gacko [2] (Fig. 9) enables object's output with no overshoot and satisfactory speed of system's reaction, which is its appropriate behavior. This is shown in Fig. 10.

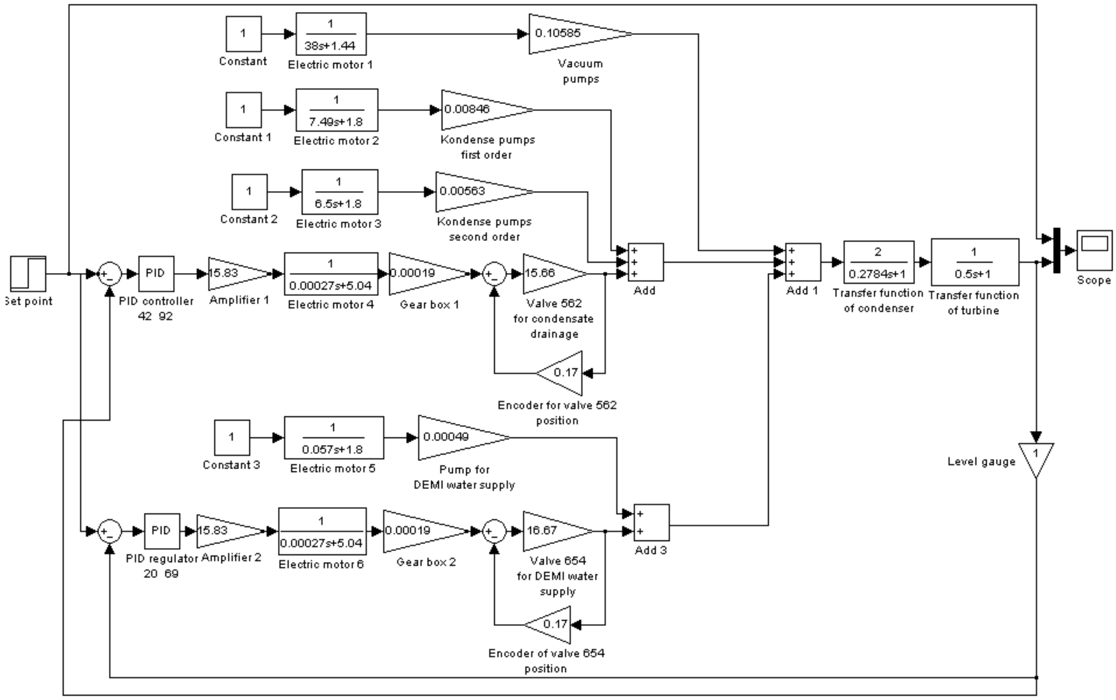

Fig. 9. *Block diagram of control system of level in condenser in thermal power plant Gacko [2]*

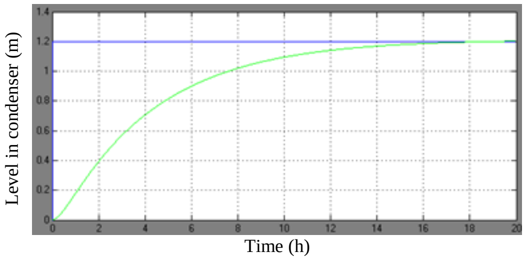

Fig. 10. *Response of control system of level in condenser with controller's parameters obtained using saturation relay*

4 COMPENSATION OF STATIC LOAD DISTURBANCE

Static load disturbance (d) has very negative impact on auto-tuning process, particularly in estimating of ultimate gain (K_u) and ultimate period (T_u). Errors in this parameters cause wrong tuned PID controller. The main idea is to compensate disturbance during relay feedback test instead of its analyzing afterward.

Mentioned disturbance affects on asymmetry appearance in process response as shows Fig. 11. In order to improve efficiency in restoring symmetry and reducing necessary time, exact method for deriving automatic bias is applied [4].

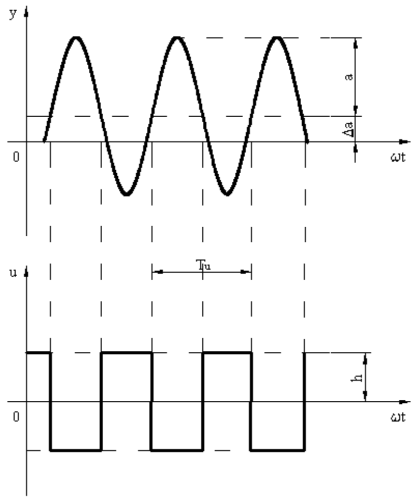

Fig. 11. *Input u(t) and output y(t) of the process in the presence of static load disturbance [4]*

Considering that our process is linear, according [4], linear interpolation can be used for expression correlation between asymmetry in the output response (Δa_0) and bias value (δ_0). Hence

$$\frac{\Delta a_0}{\delta_0} = \frac{a}{h} \tag{7}$$

The solution is to take asymmetry value in (7) as negative value, i.e. $\Delta a_0 = -\Delta a$ because bias have to affect contrary to the load. Now automatic bias can be calculated as follows

$$\delta_0 = -\left(\frac{\Delta a}{a}\right)h \tag{8}$$

The advantage of this method is possibility to determine all necessary values for (8) directly from process response [4].

Configuration which enables simulation of relay feedback test in the presence of static load disturbance (d) is presented in Fig. 12. System turbine-condenser in thermal power plant Gacko is taken as a process (linear part).

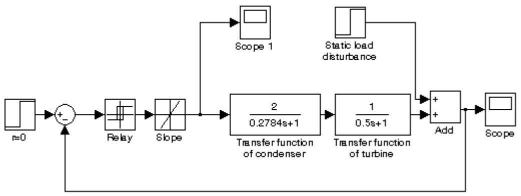

Fig. 12. *Configuration for relay feedback test in the presence of static load disturbance*

For example, in case of $d = 20\% \cdot h = 0{,}2 \cdot 0{,}12 = 0{,}024$ process response is shown in Fig. 13.

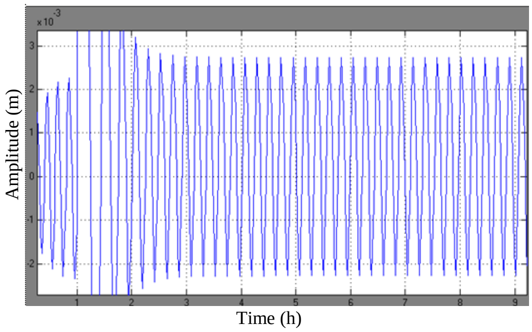

Fig. 13. *Process response with static load disturbance d = 0,024*

Asymmetry calculated from Fig. 13. is $\Delta a = 0{,}0002$ m and amplitude is $a = 0{,}0025$ m.

Now automatic bias can be calculated using (8): $\delta_0 = -0{,}01$. Its appliance into configuration (Fig. 14) restores the symmetry in process response and avoids eventual errors in estimating of ultimate gain and ultimate period, as graph in Fig. 15 shows.

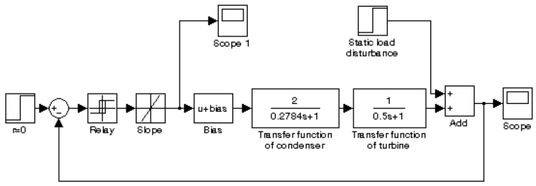

Fig. 14. *Configuration for biased relay feedback test in the presence of static load disturbance*

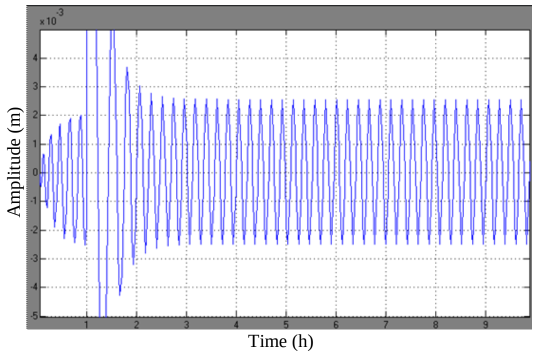

Fig. 15. *Process response for biased ($\delta_0 = -0{,}01$) relay feedback test in the presence of static load disturbance*

5 CONCLUSIONS

Taking in account constant need for properly tuned PID controllers, in this paper, the relay feedback test had been explored for control system of level in condenser in thermal power plant Gacko. Second order model of system turbine-condenser had enabled better description of its dynamic behavior.

Saturation relay was utilized for mentioned test because of its advantages over ideal relay in estimating of ultimate gain and ultimate period. In order to improve system robustness, parameters of PID controller were calculated using Tyreus-Luyben method. Validity of obtained parameters had been proved by their application into this researched control system of level.

Prevention of effects of eventual static load disturbance on accuracy of auto-tuning had been achieved by applying of automatic bias during simulation of relay feedback test.

REFERENCES

[1] Filipović, V. Ž., Nedić, N. N. "PID Controllers", University of Kragujevac, Faculty of Mechanical Engineering, Kraljevo, 2008. (in Serbian).

[2] Prodanović, S. "Analysis and improvement of control system of condensate level in condenser of turbine in thermal power plant Gacko" (master thesis). Kraljevo, Serbia: University of Kragujevac; 2009. (in Serbian).

[3] Prodanović, S. LJ, Nedić N. N., Filipović V. Ž. "Improved Auto-tuning PID Controller of Level in Condenser of Turbine in Thermal Power Plant Using Saturation-relay Feedback" in *Proc. of the X Triennial International SAUM Conference on Systems, Automatic Control and Measurement*, Niš, Serbia, 2010, pp. 68 – 71.

[4] Yu, C. C. "Autotuning of PID Controllers", National Taiwan University, Taipei, Taiwan, Springer, 2006.

[5] Milojković, B. R., Grujić, Lj. T. "Automatic Control" , University of Belgrade, Faculty of Mechanical Engineering, Belgrade, Serbia, 1993. (in Serbian).

[6] Technical documentation of the control system of condensate level in condenser of turbine and of the entire thermal power plant Gacko.

HEAVY MACHINERY - HM 2011, 7-12
ISBN 978-86-82631-58-3 Paper accepted: 30.05.2011.

Switching Predictive Control: Controller Design and Simulations

V. Filipovic[1,*] - V. Stojanovic[1]
[1] University of Kragujevac, Faculty of Mechanical Engineering Kraljevo, Kraljevo, Serbia

Abstract: *In this paper we will consider one class of switching controllers. Such control strategy is a mix of continuous dynamics and discrete events philosophy. Here we consider a finite set of the model predictive controllers (MPC) which are the only advanced control technique to have had a significant and wide spread impact on industrial process control. There are several advantages for wide acceptance of MPC: guaranteed stability, constraints handling and easy extension to multivariable and nonlinear systems. In this paper we add else one important property: significantly increasing of the transient performance using switching control strategy. Also, illustrative example is presented.*
Keywords: *Railway vehicle, independently rotating wheelset, active steering*

1 INTRODUCTION

The model predictive control (MPC) is the only advanced control methodology which has made a significant impact in industrial control engineering. We will mention that the main features of MPC are

(i) The extension to multivariable case is easy

(ii) It handles constraints. The higher performance levels are associated with pushing the limits. That frequently leads to more profitable operation

(iii) In industrial applications control update rate are relatively low and there is enough time for on-line computation.

Several important publications, in the form of survey papers and books, provide introduction to theoretical and practical issues associated with the MPC philosophy [1] and [2].

They noticed that most control laws, for example PID, do not explicitly consider the future implication of the current control actions. MPC, on the other hand, explicitly computes the predicted behavior over some horizon. One can therefore restrict the choice of current proposed input trajectories to those that do not lead to difficulties in the future.

Originally developed to meet the specialized control needs of the power plants and petroleum industry, MPC strategies can now be found in a wide variety of application areas such as discrete-event systems [3], cooperative control [4], digital electronic [5] and financial engineering [6].

For control of complex systems very important is the field of hybrid control. The hybrid systems describe the interaction of software, modeled by finite state systems such as finite state machines, with the physical world, described by differential or difference equations [7]. Specific problems in this field are presented in references [8] and [9]. The paper [10] presents a hybrid MPC. Authors propose frame for modeling and controlling models of the systems described by interacting physical laws, logical rules, and operating constraints.

As pointed out in [1] the consideration of hybrid systems opens up a rich area of research. Interesting application is presented in the field of power electronics (design of DC-DC converters). The application of hybrid model predictive control for step-down DC-DC converter is described in [11].

In this paper we introduce different strategy for switching predictive control in comparison with above mentioned papers. The controller is based on conventional optimal control that is obtained by minimization of some performance criteria. To be more specific, in the paper is considered the switching receding horizon control with the quadratic performance criterion. The performance criterion includes the prescribed degree of stability. The switching rule is based on the selection of the best performance from the finite set of the closed-loop systems. The main ingredient of the switching predictive controllers is the solution of the finite set of Riccati equations. Here is considered control of stable unconstrained systems.

[*] Corr. Author's Address: Faculty of Mechanical Engineering Kraljevo, Dositejeva 19, Kraljevo, Serbia, v.filipovic@open.telekom.rs

2 MULTIPLE MODELS

In this part of paper we consider multiple models description of processes. It will be assumed that the process model is a member of admissible process models

$$F = \underset{p \in P}{U} F_p \tag{1}$$

where P is index set which represents the range of parametric uncertainty so that for each fixed $p \in P$ the subfamily F_p accounts for unmodeled dynamics. Usually, P is compact subset of the finite-dimensional, normed linear vector space [12].

Here we will suppose that system for the large class of structured uncertainty can be described with collection of linear time invariant systems

$$x(k+1) = A_p x(k) + B_p u(k)\,,\ p = 1,2,\ldots,s \tag{2}$$

where $x \in R^n$ and $u \in R^m$ are state and control signal of the system respectively. Relation (2) describes the continuous part of the system. The event driven part can be described in next general form

$$p(k+1) = \phi(k, p(k), x(k), z(k)) \tag{3}$$

where $p(k)$ is discrete event variable, $z(k)$ is external signal produced by other devices and $\phi(\cdot,\cdot,\cdot,\cdot)$ is a function which describes behavior of $p(k)$. In our case the switching signal is given as

$$p(k+1) = f(J_p)\,,\ p = 1,2,\ldots,s \tag{4}$$

where J_p, $p = 1,2,\ldots s$ corresponding performance index for subsystem collection.
The form of a function $f(\cdot)$ will be described later (see relation (19)).

3 THE SWITCHING MODEL PREDICTIVE CONTROL

Generally, no single controller is capable of solving the regulation problem for the entire set of process models (1). Owing that we will use the family of controllers [13]

$$\{C_q : q \in D\} \tag{5}$$

where D is index set. It is supposed that this family is sufficiently rich so that admissible process model can be stabilized by controller C_q for some index $q \in D$. In this paper we will consider the case

$$F = D\,. \tag{6}$$

According with [14], for non-switching stable systems, an orthonormal basis for discrete time system is

$$V_k = \begin{bmatrix} 0 & 0 & .. & 0 & I_{mN_u} & 0 & 0 & ... \end{bmatrix}^T \tag{7}$$

where I_{mN_u} is on the $k-th$ location. Function V_k is complete in the space of square summable inputs. Also N_u - dimensional projection of the input into the basis is

$$u^N = [I_N, 0] \sum_{k=k_0}^{N-1} V_k u(k) \tag{8}$$

where $u(k)$ is the control move at sample time $k, u(k) = 0$ for all $k \geq N_u$ and u^{N_u} is the mN_u vector with the nonzero inputs in the horizon N_u.

The control signal is given by minimization

$$\min_{u^{N_u}} \sum_{k=k_0}^{\infty} \lambda^{-2k} \left[x^T(k) Q x(k) + u^T(k) R u(k) \right] \tag{9}$$

where $\lambda \in (0,1]$.

A receding horizon regulator is based on minimization of the next criterion [14]

$$\begin{aligned} \min_{u^{N_u}} \Bigg\{ & \sum_{k=k_0}^{N_u-1} \lambda^{-2k} \left[x^T(k) Q x(k) + \right. \\ & \left. + u^T(k) R u(k) \right] + \sum_{k=N_u}^{\infty} \lambda^{-2k} x^T(k) Q x(k) \Bigg\} \end{aligned} \tag{10}$$

When the matrices $A_p\ (p = 1,2,\ldots s)$ are stable the last term in the relation (10) can be transformed into a penalty on the terminal state

$$\sum_{k=N_u}^{\infty} \lambda^{-2k} x^T(k) Q x(k) = \lambda^{-2N_u} x^T(N_u) Q_{N_u p} x(N_u)$$

$$p = 1,2,\ldots s\,;\ j = N_u, N_u + 1, \ldots \tag{11}$$

The problem (10) now is

$$\begin{aligned} \min_{u^{N_u}} \Bigg\{ & \sum_{k=k_0}^{N_u-1} \lambda^{-2k} \left[x^T(k) Q x(k) + \right. \\ & \left. + u^T(k) R u(k) \right] + \lambda^{-2N_u} x^T(N_u) Q_{N_u p} x(N_u) \Bigg\} \end{aligned} \tag{12}$$

$$p = 1,2,\ldots s\,;\ j = 0,1\ldots, N_u - 1$$

The terminal state penalty matrices are computed from the next discrete Lyapunov equations

$$Q_{N_u p} = \lambda^{-2} A_p^T Q_{N_u p} A_p + Q\,,\ \ p = 1,2,...s \qquad (13)$$

According to the theory of the finite-time regulator problem [15] it is possible to get the feedback gain of switching predictive controller

$$K_{(N_u-1)p} = \lambda^{-1}\left(R + B_p^T P_{(N_u-1)p} B_p\right)^{-1} B_p^T P_{(N_u-1)p} A_p \quad (14)$$

$p = 1,2,...s$

where Riccati difference equations have a form

$$P_{(j+1)p} = Q +$$
$$\lambda^{-2} A_p^T \left[P_{jp} - P_{jp} B_p \left(B_p^T P_{jp} B_p + R \right)^{-1} B_p^T P_{jp} \right] A_p \quad (15)$$

$$P_{0p} = Q_{N_u p}\ \ , N_u > 1 \qquad (16)$$

$p = 1,2,...s$; $\quad j = 0,1...,N_u - 1$

The control law is

$$u(k) = -K_{(N_u-1)p}\, x(k) \qquad (17)$$

$p = 1,2,...s$, $k = 0,1,2,...$

The basic concept of receding horizon control is as follows. The optimal control, at the current time k, is obtained on a fixed horizon $[k, k+N_u]$. Among the optimal controls on the horizon $[k, k+N_u]$ only the first one is used as the current control law. The procedure is then repeated at the horizon $[k+1, k+1+N_u]$.

Finally we will determine the function $f(\cdot)$ in relation (4). The optimal value of the objective function (13), for fixed p, is given as in [15]

$$-\lambda^{-2k} x^T(k) P_{N_u p} x(k)\,,\ k = 0,1.... \qquad (18)$$

The discrete feedback (function $f(\cdot)$) is

$$p(k+1) = \arg\min\left\{\lambda^{-2k} x^T(k) P_{N_u p} x(k)\right\} \qquad (19)$$

$p = 1,2,...s$, $k = 0,1,2,...$

A last relation is a specific form of supervisor in switching control systems.

Remark 1. The hybrid LQ control in continuous-time domain, based on performance guarded principle, is considered in [16].

Remark 2. The system (2) can be written in the referenced predictive form [2]

$$x(k+j+1/k) = \mathrm{A}_\mathrm{p} x(k+j/k) + B_p u(k+j/k)$$

In that case for MPC it is possible to introduce two performance criterias

A) with free terminal cost

$$J_{FTC} = \sum_{j=0}^{N-1}\Big[x^T(k+j/k)\ Qx(k+j/k) +$$
$$u^T(k+j/k) Ru(k+j/k)\Big] + x^T(k+N/k)\ Qx(k+N/k)$$

B) with terminal equality constraint

$$J_{TEC} = \sum_{j=0}^{N-1}\Big[x^T(k+j/k)\ Qx(k+j/k) +$$
$$u^T(k+j/k) Ru(k+j/k)\Big],\ \ x(k+N/k)\ = 0$$

But proof for stability is different and not presented in literature.

Remark 3. Suppose that the input and state have constraints

$D_\mathrm{p} u(k) \le d_p$, $D_\mathrm{p} \in R^{m_1 xm}$, $d_\mathrm{p} \in R^{m_1}$

$p = 1,2,...s$, $k = 0,1,...,N_u - 1$

and

$H_\mathrm{p} x(k) \le h_p$, $H_\mathrm{p} \in R^{n_1 xn}$, $h_\mathrm{p} \in R^{n_1}$

$p = 1,2,...s$, $\forall k > k_2$

where k_2 is determined in [14].

The solution of receding horizon problem can be found by quadratic programming. The closed-loop system can be expressed as follows [17]

$$x(k+1) = A_p x(k) + B_p \psi(x(k))$$

$p = 1,2,...s$, $k = 0,1,...$

where $\psi(x(k))$ is control input $u(k)$ determined as the solution of quadratic program. Owing the constraints presence $\psi(x(k))$ is nonlinear function of the state $x(k)$. Reference [18] discusses the nonlinearity properties of the solution of the linear model predictive control quadratic program. For the constrained receding horizon regulator the *Theorem 1* is not applicable.

Remark 4. Very new investigations which can be interesting for further development of switching receding horizon control are

a) Robustness of MPC is a very important property of MPC [19], [20]. The robust MPC utilizes a description of the model uncertainty and is aimed at guaranteeing both constraints satisfaction and closed-loop stability. In [20] is proposed a robust output feedback MPC design for a class of open-loop stable systems having non-vanishing output disturbances, hard constraints and linear time invariant model uncertainty.

b) Early implementations of MPC where constrained in the process industry. In such applications the sample periods is long and set-points are constant. But, new techniques and faster sampling rates include the new applications:electromechanical, power electronics and telecommunications problems. In these areas the reference signal is not constant or even piecewise constant. In [21] is described a novel strategy for MPC design which incorporates feedback, reference feed-forward and preview.

c) Stochastic MPC is, also, important field of investigations. In [22] is proposed the MPC strategy which handles probabilistic constraints with acceptable computational load. This is achieved by fixing the cross-sectional shapes of tubes containing predicted states and allowing their centers and scaling to vary with time.

4 ILUSTRATIVE EXAMPLE

Consider the following collection of stable plants

$$A_1 = \begin{bmatrix} 0.2 & 2 \\ 0 & 0.8 \end{bmatrix},\ b_1 = \begin{bmatrix} 1 \\ 1 \end{bmatrix}$$

$$A_2 = \begin{bmatrix} 0.5 & 1 \\ 0 & 0.7 \end{bmatrix},\ b_2 = \begin{bmatrix} 0 \\ 1 \end{bmatrix}$$

$$Q = \begin{bmatrix} 0.9 & 0 \\ 0 & 0.8 \end{bmatrix},\ x(0) = \begin{bmatrix} 1.5 \\ -2 \end{bmatrix}$$

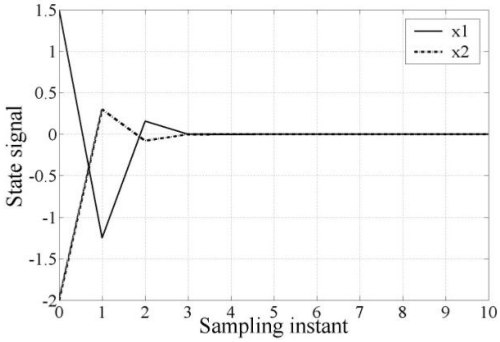

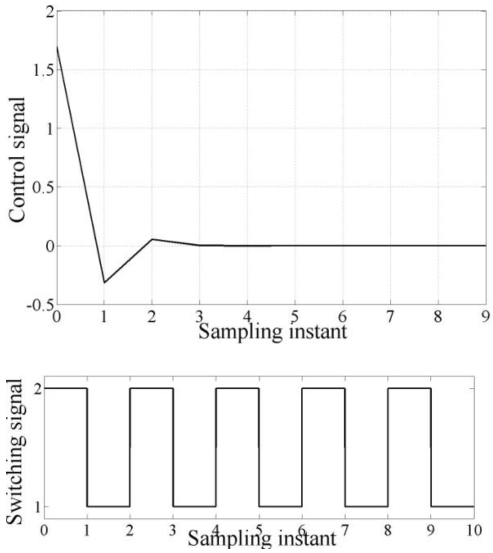

Fig. 1. *States, control signal and switching signal for* $r = 0.05$, $N_u = 4$ *and* $\lambda = 1$

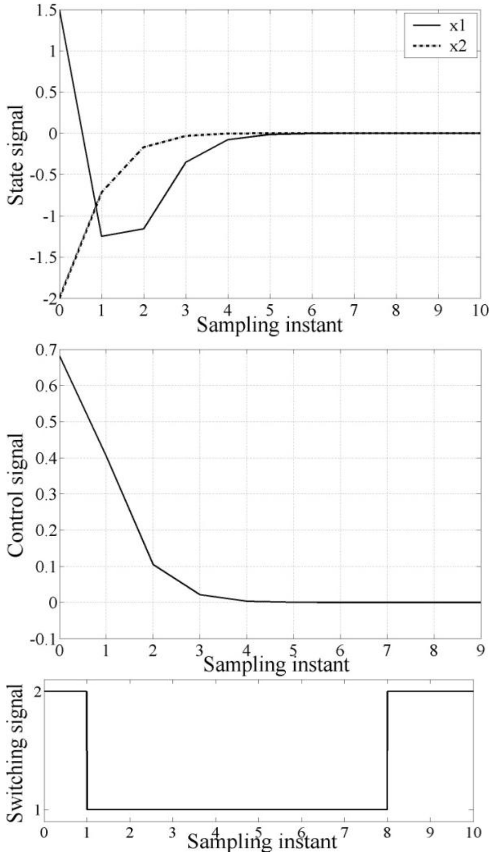

Fig. 2. *States, control signal and switching signal for* $r = 10$, $N_u = 4$ *and* $\lambda = 1$

With tuning parameters R (in quadratic criterion), N_u (control horizon) and λ (degree of the stability). In our case R is scalar and will be denoted with r .

In what follows we consider tuning parameter r (in the Fig.1. and Fig.2).

From above figures we see that if it is more important that the control energy be small, then we should select a large value of r (see Fig. 2). Also, it is possible to notice that exists correlation between choice of r and a form of control signal and switching signal. For small r the control u is a large and switching between subsystems is fast but the state trajectory convergence is, also, faster. (See Fig. 1)

In the next figure we consider the case when control horizon is $N_u = 10$

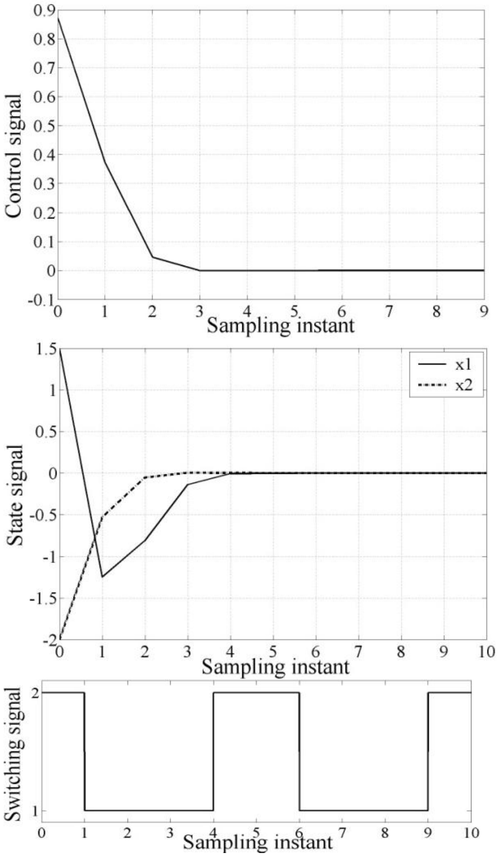

Fig. 3. *States, control signal and switching signal for* $r = 10$, $N_u = 10$ *and* $\lambda = 1$

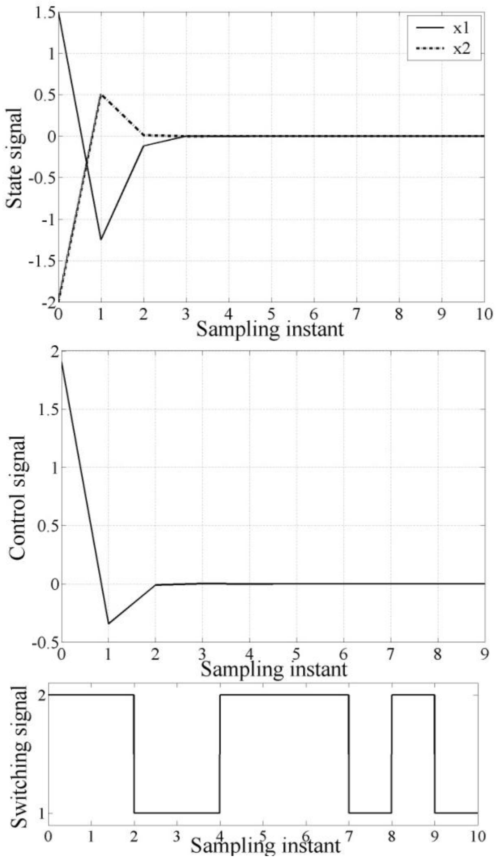

Fig. 4. *States, control signal and switching signal for* $r = 0.5$, $N_u = 4$ *and* $\lambda = 0.8$

From comparison of Fig.2 and Fig.3, it is possible to conclude that for last case the transient behavior is better whereby the control signal is slightly larger.

From Fig. 4 it is follows that closed-loop system has a good behavior (only 3 sampling instants is enough for practical state convergence).

Finally, from intensive simulations the acceptable set of tuning parameters is: $r = 0.5$, $N_u = 4$ and $\lambda = 0.8$.

5 CONCLUSION

In this paper the problem of design of switching model predictive controllers is considered. The main motivation for such type of controllers is performance improvement of feedback system. Also, very important fact is that in practice exist systems which impossible to control using classical control strategy. In this paper is shown that by using index of performance, which is uniformly bounded, it is possible to design MPC switching controllers which guarantee stability of feedback system. Further investigation is oriented toward the unstable plants with constraints.

6 REFERENCES

[1] D. Mayne, L. Rawlings, C. Rao, P. Sockert, Constrained model predictive control: stability and optimality, Automatica 30 (2000) 789-814

[2] W.H. Kwon, S. Han, Receding Horizon Control. Model Predictive Control for State Models, Springer, Berlin, 2005

[3] L. Miao, C. Cassandrass. Receding horizon control for a class of discrete-event systems with real-time constrains. IEEE Transactions on Automatic Control 1993, 38 (8): 1512-1516

[4] Kuwata Y, Richards A, Schouwenaars T, How J. Distributed robust receding horizon control for multivehicle guidance. IEEE Transactions on Control Systems Technology 2007, 15 (4): 627-641

[5] Quevedo D. Goodwin G. Multistep optimal analog - to- digital conversion. IEEE Transaction on Circuits and Systems – I: Regular Papers 2005, 52 (3): 503-515

[6] J. Primbs, LQR and receding horizon approaches to multi-dimensional option hedging under transactions costs, Proceedings of American Control Conference ACC (2010) 6831-6896

[7] P. Tabuada, Verification and Control of Hybrid Systems. A Symbolic Approach, Springer: Berlin, 2009

[8] V. Filipovic, Switching control in the presence of constrains and unmodeled dynamics. In: H. Ascheman (Ed), New Approaches in Automation and Robotics, I Tech, Vienna, 2008, .225-238

[9] V. Filipovic, Exponential stability of stochastic switched systems, Transanctions of the Institute of Mesaurement and Control 31(2009) 205-212

[10] A. Bemporad, M. Morari, Control of systems integrating logic, dynamic and constraints, Automatica 35(1999) 407-428

[11] T. Geyer, G. Papafotion, M. Morari, Hybrid model predictive control of the step-down DC-DC converter, IEEE Transaction on Control Systems Technology 16(2008) 1112-1124

[12] J. Hespanha, D. Liberzon, S. Morse, B. Anderson, T. Brinsmead, T. De Bruyne, Multiple model adaptive control. Part 2: switching, International Journal on Robust and Nonlinear Control 11(2001) 479-496

[13] A.S. Morse, Supervisory control of families of linear set-point controllers. Part 1: exact maching, IEEE Transactions on Automatic Control 41(1996) 1413-1424

[14] J.B. Rawling, K.R. Muske, The stability of constrained receding horizon control, IEE Transactions on Automatic Control 38(1993) 1512-1516

[15] B.D.O. Anderson, J. Moore, Optimal Control and Linear Quadratic Methods, Prentice-Hall, New Jersey, 1989

[16] L.Y. Wang, P. Khargonekar, A. Beydoun, Robust control of hybrid systems. Performance guaded strategies. In: P. Antsaklis, W. Kohn, M. Lemmon, A. Nerode, S. Sastry (Eds), Hybrid Systems V, Springer, Berlin, (1999) 356-389

[17] K. Muske, Linear model predictive control of chemical processes, PhD 1995, The University of Texas at Austin, USA

[18] N. De Oliveira, L. Biegler, Constraint handling and stability properties of model predictive control, AIChE Journal 40(1994) 1138-1155

[19] J. Rawlings, D. Mayne, Model Predictive Control. Theory and Design, Nob Hill Publishing, Wiskonsin, 2009

[20] C. Lovaas, M. Seron, G. Goodwin, Robust output-feedback MPC with integral action, IEEE Transactions on Automatic Control 55(2010) 1531-1545

[21] D. Carrasco, G. Goodwin, Prevew and feedforward in model predictive control. A preliminary robustness analysis, 18th IFAC World Congress, Milan, Italy, 2011

[22] M. Cannon, B. Kouvartiaks, S. Rakovic, Q. Cheng, Stochastic tubes in model predictive control with probabilistic constraints, Proceedings of American Control Conference (2010) 6274-6279

HEAVY MACHINERY - HM 2011, 13-17
ISBN 978-86-82631-58-3
Paper accepted: 30.05.2011

Design of Electromechanical Positioning Systems With Controlled Jerk

Mihajlo J. Stojčić[1,*]
[1]Faculty of Mechanical Engineering, University of Banja Luka

In this paper we consider design of an electromechanical positioning system with controlled jerk. A system that is formed from a load and an actuating device is used as an object. For the proposed linear change of the jerk were found the appropriate changes of the acceleration, velocity and displacement. The algorithm, that ensures the motion of the object with controlled jerk so that the requirements which related to the maximum values of the acceleration, velocity and displacement are satisfied, is also proposed. Appropriate feedforward and feedback controllers are found. The simulation of the proposed system is performed, that confirmed the theoretical considerations.

Keywords: Trajectory planning, positioning system, feedforward design, controlled jerk

1. INTRODUCTION

Positioning systems are often used in industrial electromechanical drive or as the drive of a robot. The task of this system is to achieve adequate movement between point A to point B, where the system in the initial and final points is in the idle state. In this, we assume that the times of the acceleration and deceleration are the same, or equivalently, the trajectory symmetric with respect to the velocity. To design such a system is necessary to solve several problems, such as:

- trajectory planning: the determination allowable trajectory and all parameters of motion (jerk, acceleration,...) for all degrees of freedom and for each actuating device, separately
- controller design: design feedback and/or feedforward controller that ensures realizations of the desired trajectory for each actuating device, even in circumstances when disturbances (internal and/or external) act on the object, and there exists an unmodelled dynamic of the object , and
- other problems, such as: diagnostic, internal checks, communications, etc.

The solutions of the above problems are generally reduced to one actuator unit, that is, on one axis or a degree of freedom.

A motion of the object (plant) between two point typically can be divided into three phases: accelerating, motion with constant speed, and decelerating. Traditionally, mainly used trapezoidal velocity profile. This means that the object (for a time t_a) is accelerated by a constant acceleration until it reaches a maximum velocity, then keeps this constant velocity (for a time t_v), and is decelerated by a constant deceleration (also, for a time t_a), so that the total time τ of the movement is $\tau = 2t_a + t_v$.

One of the main problems with trapezoidal velocity profile is a large changes of the jerk, and consequently a large inertial forces. Further, that can induce a large vibrations of the mechanical parts of the system, which leads to large (often unacceptable) a stationary error and settling time.

To improve the performance there exist several approaches, which can be roughly split as:

1. Trajectory smoothing or shaping: The result can be very good, but it can lead to a significant increase in execution time of the trajectory. This approach is considered in [2,3,7,8].
2. Feedforward control based on plant inversion: This approach gives good results only if the plant model is well known, but with important disadvantage with respect to robustness of the system. Different examples of this approach can be found in the papers [2,3,4].
3. Feedback control optimization: Since the feedback controller is integral part of almost all positional system, then its optimization leads to decrease of the stationary errors and settling time, but at the same time may to increase the overshoot and reduce the stability of the closed system. This approach is considered in [1,8,9].

In this paper we use approach that somehow includes all of this above approaches.

2. TRAJECTORY PLANNING

2.1 Mathematical model of the object

*Corr. Author's Address: Faculty of Mechanical Engineering, University of Banja Luka, stojcicmihajlo@gmail.com

We consider an electromechanical positioning system, Fig. 1, where the mass m includes the masses of the all moving parts (load and actuator). In the initial time, $t_0 = 0$, we assume that the values of the jerk j, acceleration a, velocity v and displacement r are zero, ie. $j(0) = a(0) = v(0) = r(0) = 0$. The force $F(t)$ generated by the actuator must overcome the force of inertia $f_i = ma$ (of the all moving masses) and viscous friction force $f_v = bv$. The other frictions (for example Columb frictions) are neglected

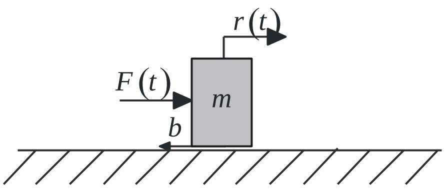

Fig. 1. *Electromechanical positioning system*

and their effect is modeled through disturbance $w(t)$, so that the equation of its behavior is given as:

$$F = m\ddot{r} + b\dot{r} = ma + bv\,. \tag{1}$$

After Laplace transformation, the transfer function $G_o(s)$ of the plant (object) is obtained as

$$F(s) = \left(ms^2 + bs\right)R(s) \Rightarrow G_o(s) = \frac{1}{ms^2+bs} = \frac{R(s)}{F(s)}. \tag{2}$$

2.2 Smoothing the trajectory

In order to get a little changes of the acceleration (trajectory smoothing) we assume that the jerk in the acceleration phase, for the time $t_j = t_a$, changes linearly as:

$$j = \frac{J}{T} \times \begin{cases} t & ,\ t \in [0,T] \\ -(t-2T) & ,\ t \in [T,3T] \\ (t-4T) & ,\ t \in [3T,4T] \end{cases}, \tag{3}$$

where the time T is $T = t_j/4$ and J is the maximum value of the jerk. In the rest phases of motion the jerk has next values: $j = 0$, $t \in [t_a, t_a + t_v]$ and the jerk $= -j, t \in [t_a + t_v, \tau]$, where j is given by Eq. (3), see Fig. 2.

Since the trajectory is symmetric, in the sequel we observe change of the motion parameters (a, v, r) only for the time interval $[0, t_a]$. The acceleration $a(t) = \int jdt + C_a$ is given from Eq. (3), as

$$a = \frac{J}{2T} \times \begin{cases} t & ,t \in [0,T] \\ 2T^2 - (t-2T)^2 & ,t \in [T,3T] \\ (t-4T)^2 & ,t \in [3T,4T] \end{cases}. \tag{4}$$

where the constant C_a is determined from initial conditions for every time interval.

In the similar way we can get the velocity $v = \int adt + C_v$ as

$$v = \frac{J}{6T} \times \begin{cases} t^3 \\ 6T^2(t-T) - (t-2T)^3 \\ 12T^3 + (t-4T)^3 \end{cases}, \tag{5}$$

and the displacement $r = \int vdt + C_r$ as

$$r = \frac{J}{24T} \times \begin{cases} t^4 \\ \left(2T^4 - (t-2T)^4\right) + 12T^2(t-T)^2 \\ (t-4T)^4 + 48T^3 t - 96T^4 \end{cases}, \tag{6}$$

for each time interval ($[0,T]$, $[T,3T]$ and $[3T,4T]$).

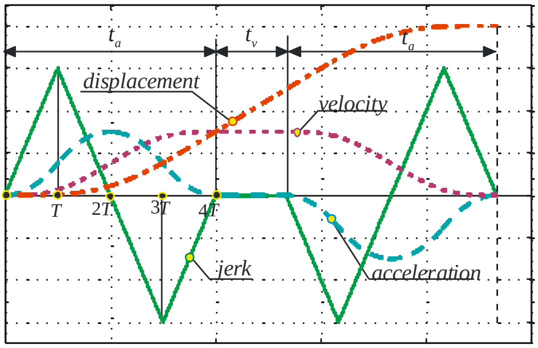

Fig. 2. *Change of the jerk, acceleration, velocity and displacement at time interval* $[0, 2t_a + t_v]$

The changes of the jerk, acceleration, velocity and displacement that are given by Eqs. (3), (4), (5) and (6) are shown in Fig. 2. respectively.
If the jerk is changed by Eq. (3), then from the Eqs. (4,5,6) is easy to determine that the maximum values of the acceleration, velocity and displacement on the interval $[0, t_a]$ are given as:

$$a(2T)=\frac{1}{4}Jt_j, v(4T)=\frac{1}{8}Jt_j^2, r(4T)=\frac{1}{16}Jt_j^3. \qquad (7)$$

2.3 Trajectory planning - algorithm

From the practical viewpoint, and depending on the desired application and possibility of the control system (force or torque of the actuator), at the beginning trajectory planning we give the maximum values of jerk J, acceleration A and velocity V and the total displacement R.

Now is necessary to determine the shortest time $t_j = t_a$ and t_v, so that the limitations that are given through the maximum values of the J, A, V and R are not exceeded. In this sense, we give the following algorithm:

1. The shortest time within which the motion can be performed is calculated from Eq. (7) as

$$R = 2\times r(4T)=\frac{1}{8}Jt_j^3 \Rightarrow t_j = 2\sqrt[3]{\frac{R}{J}}. \qquad (8)$$

2. Now we can test whether the acceleration bound A is exceeded by calculating maximal acceleration using the time t_j from (8) and Eq. (7). We give $\hat{a}=\frac{1}{4}Jt_j$. If $\hat{a}<A$ we continue, but if $\hat{a}>A$ we re-calculate t_j as: $t_j=\frac{4A}{J}$.

3. In the similar way we test whether the velocity bound is satisfied. The maximal velocity is $\hat{v}=\frac{1}{8}Jt_j^2$. Test $\hat{v}<V$. If it is true we continue, but if it is false we re-calculate t_j as $t_j=\sqrt{\frac{8V}{J}}$.

4. And finally, using $\hat{v}$ from item 3. and V we determined the velocity $\bar{v}$ as $\bar{v}=\min(\hat{v},V)$, and calculate the time t_v as

$$t_v=\frac{R-\bar{v}t_j}{\bar{v}}. \qquad (9)$$

3. CONTROLLER DESIGN

The configuration of the overall system as in Fig. 3. is proposed, where r, y and w are denoted

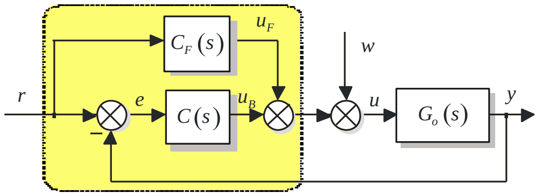

Fig. 3. *System with feedback $C(s)$, feedforward $C_F(s)$ controllers and object $G_o(s)$*

a reference, output and immeasurable disturbance respectively. The controller of the system includes both, the feedback controller $C(s)$ and feed-forward controller $C_F(s)$. The output error $e(s)$ (see Fig. 3.) is obtained as

$$r-(Ce+C_Fr+w)G_o = e \Rightarrow$$
$$e=\frac{1-CC_F}{1+CG_o}r-\frac{G_o}{1+CG_o}w. \qquad (10)$$

3.1 Design of feedforward controller

From Eq. (10) we can see that the output error contains two components, one of the reference r (error e_r) and the other from the disturbance w (error e_w). In order to object asymptotically tracking the reference the condition $e_r=0$ must be satisfied. This leads that the transfer function of feedforward controller $C_F(s)$ is given as

$$C_F(s)=\frac{u_F(s)}{r(s)}=G_o^{-1}(s)=ms^2+bs. \qquad (11)$$

We got a non-proper transfer functions, that can be realized using differentiation , see [2,3], as

$$u_F = C_F(s)r = G_o^{-1}(s)\frac{1}{s^2}\ddot{r}(t)$$
$$=\frac{ms^2+bs}{s^2}\ddot{r}(t)\Rightarrow \qquad (12)$$
$$u_F(t)=ma+bv.$$

This controller is shown in Fig. 4.

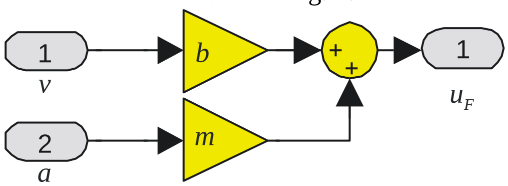

Fig. 4. *Feedforward controller*

3.1 Design of feedback controller

The main task of the feedback controller is compensate some unknown disturbances and unmodelled behavior of the object. We request that the controller $C(s)$ rejects all the step disturbances, so that the output error tends to zero without oscillations. There are several different approaches for its design, [8,9]. In this paper we use a standard PID controller, so now the task becomes determining its parameters, that ensures the desired behavior of the overall system. The transfer function of the feedback controller $C(s)$ is

$$C(s)=k_p+\frac{k_i}{s}+k_d s=\frac{k_d s^2+k_p s+k_i}{s} \qquad (13)$$

This transfer functions together with transfer function of the object (2), and using (10), gives the characteristic polynomial of the closed system as,

$$\Delta(s)=\tfrac{1}{m}\left[s^3+(k_d+b)s^2+k_p s+k_i\right]. \qquad (14)$$

This is the third order polynomial, so it can be written as

$$\Delta(s)=(s+\alpha)\left(s^2+2\xi\omega_n s+\omega_n{}^2\right). \qquad (15)$$

In order to the output error tends to zero without oscillations, must be $\xi\geq 1$ and the pole $s_1=-\alpha$ much further in the left half plane of s-plane than the poles of polynomial $\left(s^2+2\xi\omega_n s+\omega_n{}^2\right)$. We adopt the $\xi=1$, so that the poles of this polynomial are $s_{2,3}=-\omega_n$. Using these values and Eqs. (14) and (15), finally we get the parameters of PID controller as

$$\begin{aligned} k_d &= m(2\omega_n+\alpha)-b \\ k_p &= m\omega_n(2\alpha+\omega_n) \\ k_i &= m\alpha\omega_n{}^2. \end{aligned} \qquad (16)$$

It is easy to prove that the system (see Fig. 3.) with controller (13) and object (2) rejects all step disturbances, $w(s)=\frac{w_o}{s}$. From the Eq. (10) follows,

$$e_w(s)=\frac{G_o}{1+CG_o}w(s)=\frac{s}{\Delta(s)}\frac{w_o}{s}. \qquad (17)$$

where $\Delta(s)$ is given by Eq. (15). From this Eq. we calculate the stationary error $e_w(\infty)$, due to disturbance, as

$$\begin{aligned} e_w(\infty) &= \lim_{t\to\infty} e_w(t)=\lim_{s\to 0} s e_w(s) \\ &= \lim_{s\to 0} s\frac{s}{\Delta(s)}\frac{w_o}{s}=0. \end{aligned} \qquad (18)$$

4. RESULTS OF SIMULATIONS

Simulation of the systems with the controllers (12) and (13) , the object (2) and in configuration as on Fig, 3. are carried out in Fig. 5. As the simulation system we use MATLAB/SIMULINK system that is shown in Fig. 6. As the poles $s_{2,3}$ are used values $s_{2,3}=-\omega_n=-2$, and for value of the pole s_1 is selected value $s_1=-\alpha=10\omega_n=-20$.

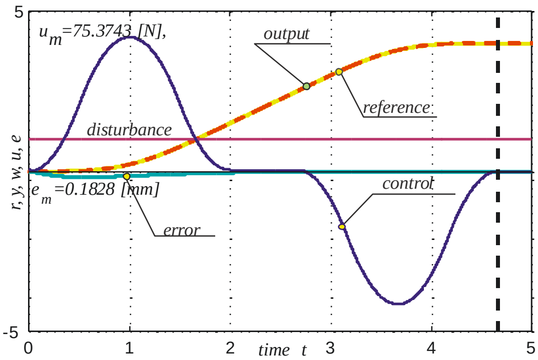

Fig. 5. *Results of simulations for:* $\omega_n=2$, $\alpha=10\omega_n$ *and the parametres from Eq. (16)*

.

4. CONCLUSIONS

In this paper is designed system that asymptotically follows a given reference and rejects all step disturbances. The reference is obtained from the condition that the jerk is changed by pre-defined manner. As the controller are used feedback and feedforward controllers. The feedback is the standard PID controller, and as the feedforward controller is used controller that is obtained by plant inversion. An algorithm of planning trajectory which ensures that all bounds values of the jerk, acceleration, velocity and movement, is given also. The results of simulation confirm the theoretical considerations that are given.

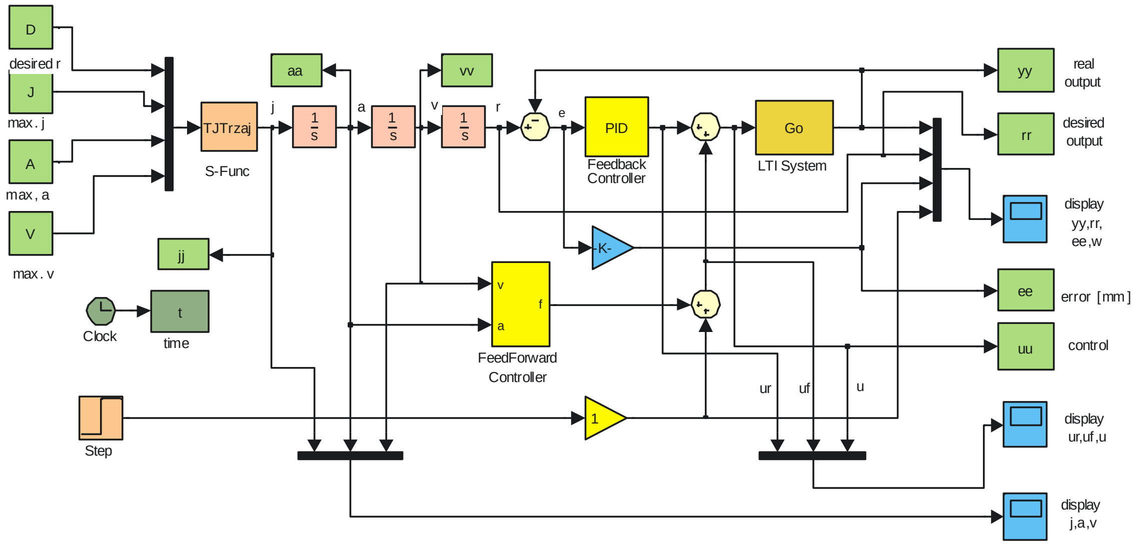

Fig. 6. *The simulation system*

5. REFERENCES

[1] Anton Cervin , Johan Eker, Bo Bernhardsson, Karl-Eric Arzen, "Feedback Feedforward Scheduling of Control Tasks ," *Real Time Systems (Special Issue on Control Theoretical Approaches to Real Time Computing), To appear in 2002*

[2] Paul Lumbrechts, "Trajectory planning and feedforward design for electromechanical motion systems," *Report nr. DCT 2003-08*, University of Technology Eindhoven

[3] Paul Lambrechts, Matthijs Boerlage, Maarten Steinbuch, "Trajectory planning and feedforward design for electromechanical motion systems," *Control Engineering Practice 13 (2005) 145-157*, ScienceDirect

[4] Vito Cerone, Mario Milanese, Diego Regruto, "Robust feedforward design for a two-degrees of freedom controller ," in

[5] H. Z. Li, Z. M. Gong, W. Lin, and T. Lippa, "Motion profile planning for reduced jerk and vibration residuals," *SIMTech technical reports, Volume 8, No 1, 2007, pp 32-37*

[6] Kim Doang Nguyen, Teck-Chew Ng and I-Ming Chen, " On Algorithms for Planning S-curve Motion Profiles," *International Journal of Advanced Robotic Systems*, Vol. 5, No 1 (2008), ISSN 1729-8806, pp. 99-106

[7] G.M. Clayton, , S. Tien, A.J. Fleming, S.O.R. Moheimani, S. Devasia," Inverse feedforward of charge controlled piezopositioners," *Mechatronics 18 (2008) 273–281* , ScienceDirect

[8] Mihajlo J. Stojčić, Bojan Knežević, " The controller design for tracking trajectory with controlled jerk," *DEMI 2011 Proceedings, Banja Luka, (2011), pp. 905-911*

[9] Mihajlo J. Stojčić, Bojan Knežević, „Design of digital controller that ensures robust tracking trajectory with controlled jerk,“ (In Serbian), *JUPITER 37 Proceedings, Belgrade 2011, pp. 4-11-4.16*

HEAVY MACHINERY - HM 2011, 19-26
ISBN 978-86-82631-58-3
Paper accepted: 30.05.2011

Optimization of the parameters of PID controller on the model of inverted pendulum by using algorithm of particle swarm optimization

Vladimir Đorđević[1,*], Dragan Pršić[1] , Radovan Bulatović[1]
[1] University of Kragujevac, Faculty of Mechanical Engineering Kraljevo

In the paper, two models for adjustment of the parameters of PID controller are analyzed. The first one is conventional relay method, which is based on artificially induced oscillations in the system. The second is unconventional, metaheuristics method of particle swarm optimization. Comparative results of the object simulation are managed by a controller, the parameters of which are adjusted by using these two methods. Inverted pendulum is used as controlled plant. The model of the object is determined by applying bond graph methodology. A response of non-linear and linear model for different initial conditions is analyzed.

Keywords: PID controller, inverted pendulum, Bond-graph, parameter optimization, particle swarm optimization.

1. INTRODUCTION

PID controllers represent the most used type of controllers in the industry, but despite that fact, a significant part of controllers does not provide good control because of badly chosen parameters [1]. PID controller is relatively simple, but for its adequate behaviour a lot of experience is necessary. In 1942, Zigler and Nichols suggested experimental method of the adjustment of PID controllers, which gives rather good results. A problem with the Zigler-Nichols method occurs because it is necessary to bring the system to the limit of stability in order to find critical amplification and oscillation period, which are necessary in order to determine the parameters of the PID controller, which can be dangerous in some systems. In 1980s, the relay method appeared and it solved the problem. It implies the introduction of non-linearity (relay) into the main branch that causes system oscillation, and in that way, we can determine amplification and oscillation period.

Over the past few years, numerous metaheuristic optimization methods have appeared. These methods search randomly the solution space, looking for the solution that best satisfies the optimization criteria. The majority of these new algorithms are inspired by biological systems. In this paper, the method of particle swarm optimization is used. It is a relatively new method and it has given good results for different optimization problems. By using this method, parameters of the controller that provide a transitional process of much better quality than the parameters obtained by using the relay method.

2. ALGORITHM OF PARTICLE SWARM OPTIMIZATION

Particle swarm optimization (PSO) represents metaheuristic method of optimization based on agents (particles) population, which was accidentally discovered by James Kennedy and Russell Eberhart in 1995, while studying the simulation of social behavior of bird flocking [2].

Figure 1 represents the algorithm of this method. Just as it is the case with all algorithms based on population, initial particle population is generated first. Position of the particle represents vector of parameters that are optimized: $\mathbf{x} = (x_1, x_2, ..., x_n)$, or a potential solution. Random position in space which is explored, as well as initial velocities, is given to each particle. After that, the value of the objective function of each particle is determined, and that value is added to it as the best value for the particle in question, while the initial position becomes the best position of the particle $\mathbf{p_{best}}$. When all the best values of particles are determined, the

*Corr. Author's AddressFaculty of Mechanical Engineering Kraljevo, 36000 Kraljevo, Dositejeva 19, vladadj@blueisp.rs

particle with the minimum value is searched, and its position becomes the best position for the entire swarm $\mathbf{p}_{\mathbf{gbest}}$. Afterwards, it is checked whether the criteria of optimization are satisfied, and if they are, the obtained results are displayed. If the criteria are not satisfied, new velocities and positions are to be calculated.

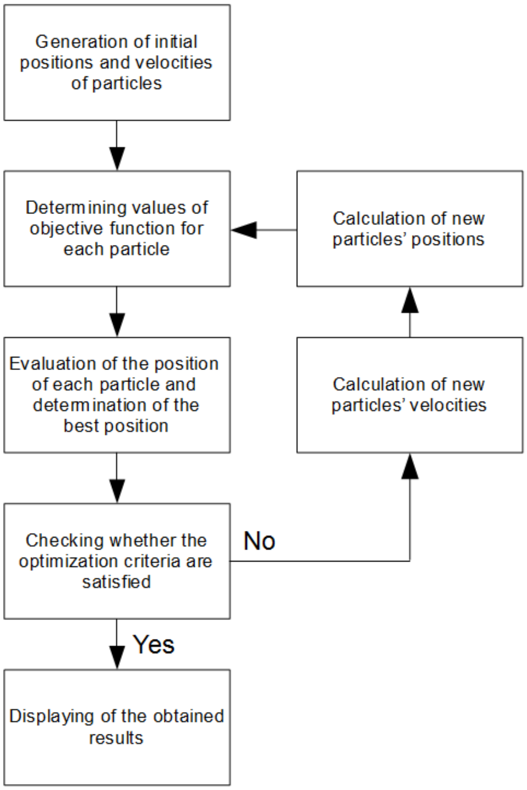

Fig. 1. *Algorithm of the method of particle swarm optimization*

Figure 2 graphically shows how to determine new velocities and positions in two-dimensional space of search.

New velocity of each particle consists of three components:

1. the component which depends on instantaneous particle velocity,
2. the component which is proportional to the distance of instantaneous position of the particle and its best value,
3. the component which is proportional to the distance of instantaneous position of the particle and its best position for the entire swarm.

$$\mathbf{v}_{i+1} = w \cdot \mathbf{v}_i + c_1 \cdot \mathbf{r}_1 \circ \left(\mathbf{p}_{\mathbf{best}i} - \mathbf{x}_i\right) + c_2 \cdot \mathbf{r}_2 \circ \left(\mathbf{p}_{\mathbf{gbest}i} - \mathbf{x}_i\right)$$

Where w represents inertia weight, c_1, c_2 are acceleration coefficients or correction factors, $\mathbf{r}_1, \mathbf{r}_2$ represent two random vectors of the length n within the limits [0,1]. The symbol $\circ$ represents Hadamard product:

$$\left(A \circ B\right)_{i,j} = \left(A\right)_{i,j} \cdot \left(B\right)_{i,j}$$

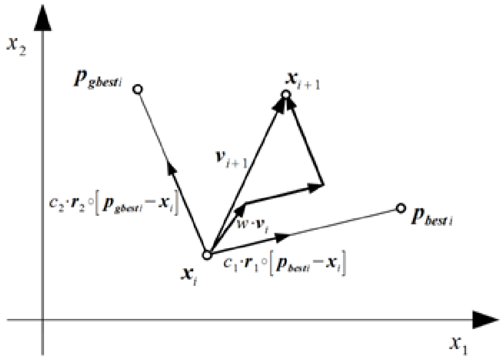

Fig. 2. *Updating of velocity and position of the i-th particle*

Inertia weight w impacts the first component, and for the values in the range of 0,9 – 1,2 [4] it gives the best results, that is, the algorithm has greater chances of finding the global minimum for a reasonable number of iterations. For coefficient values which are smaller than 0,8, if algorithm finds global minimum it will find it fast. Particles in this case move quickly and it can happen that they "fly over" some area, so it can happen that they do not find global minimum. On the other side, if inertia weight has bigger value, then particles search the solution space more thoroughly and the chances of finding global minimum are greater.

New position of the particle is determined by simple adding of the current position $\mathbf{x}_i$ and new particle velocity $\mathbf{v}_{i+1}$.

$$\mathbf{x}_{i+1} = \mathbf{x}_i + \mathbf{v}_{i+1}$$

The values of the objective function for new positions of the particle are determined again, and for each particle new and old values of the objective function are compared. If the new value is smaller, then it becomes new best value and the current position becomes the best position of that particle. The position of the particle with the smaller value becomes new best position for the entire swarm. Again, it needs to be checked whether the optimization criteria are satisfied; if they are, the results are shown, and if not, the entire procedure will be repeated until the criteria are satisfied.

3. PID CONTROLLER OPTIMIZATION

In this paper, parameter optimization of PID controller is performed, parameters of amplification are optimized (K_p, K_i, and K_d). Algorithm of the PSO randomly chooses amplification, and after that, it calculates the system response, and determines the error. The given optimization criterion, which also presents objective function, is applied, and the values of amplification for which the function is minimum are chosen.

Four optimization criteria are used [6]:

1. IAE - integral absolute error ,
2. ISE - integral squared error,
3. ITAE - integral time multiplied absolute error,
4. ITSE - integral time multiplied squared error.

These criteria are defined in the following way:

$$J_1 = \int_0^T \left| e(t) \right| dt \,,$$

$$J_2 = \int_0^T e(t)^2 \, dt \,,$$

$$J_3 = \int_0^T t \left| e(t) \right| dt \,,$$

$$J_4 = \int_0^T t e(t)^2 \, dt \,.$$

Each of these criteria has its advantages and disadvantages. IAE provides good responses with relatively small overshoot, but with longer settling time. ISE decreases error very quickly, but oscillations occur. In order to get better performances and decrease the settling time, criteria ITAE and ITSE are used.

4. MATHEMATICAL MODEL OF INVERTED PENDULUM

Methodology used in modelling of physical systems primarily depends on the purpose of a model. If theoretic-analytical approach is used in studying of a system, mathematical models in form of differential and algebraic equations are usually used. However, optimization of controller parameters, which is used in this paper, is based on the results of simulation. For that reason, in this paper modelling is viewed from the simulation angle, that is, from performing of the "experiment" with the model. The final objective is not a mathematical model, but the model in the form that can be simulated easily on the computer.

For the inverted pendulum modelling we use bond graph (BG) [1, 2]. Bond graph is a graphical, object–oriented language, which is used for describing of energy processes in the system. The system is described as a network of domain-independent energy primitives each of which represents an ideal physical process. At the lowest level, the nodes in BG represent the main energy processes, and the edges among them represent the paths along which energy is exchanged. The main advantage is bigger flexibility of the model with the structure that follows the structure of a real system. Bond graph is translated easily into mathematical model by using the standard procedures [1, 2].

Figure 3 schematically shows inverted pendulum with the parameters. Pendulum is a uniform rigid rod of length $2l$, mass m, and moment of inertia J. The pendulum is coupled to the cart mass M, which moves under the influence of the force $F(t)$ along plane area.

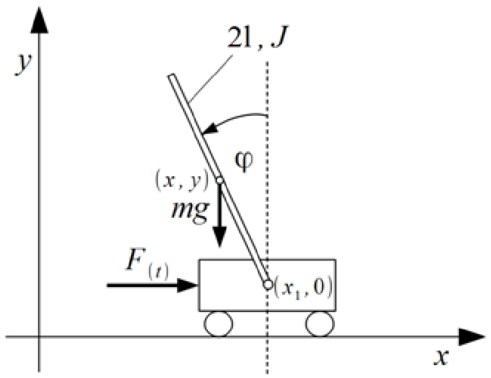

Fig. 3. *Schematic of an inverted pendulum*

In order to get to the model of the entire system, pendulum and cart models will be performed individually, and then they will be linked in a unique system. Figure (3) shows that the following geometrical relations are valid:

$$x(t) = x_1(t) - l\sin\varphi(t) \quad (1a)$$

$$y(t) = l\cos\varphi(t) \quad (1b)$$

Differentiation with respect to time gives:

$$\dot{x}(t) = \dot{x}_1(t) - l\omega(t)\cos\varphi(t) \quad (2a)$$

$$\dot{y}(t) = -l\omega(t)\sin\varphi(t) \quad (2b)$$

The velocity constraints (2) can be represented by the BG of Fig.4.

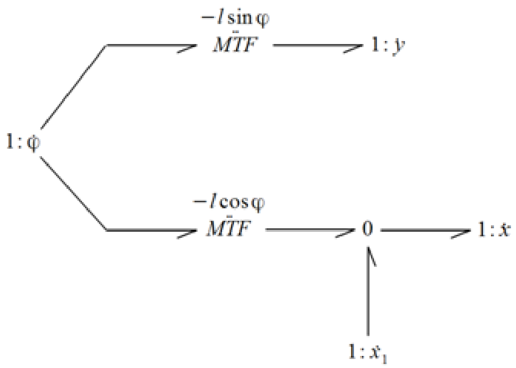

Fig. 4. *Bond graph representation of the velocity constraints (2)*

By adding the BG elements on the structure shown in fig.4, we come to the BG model of pendulum shown in fig 5.

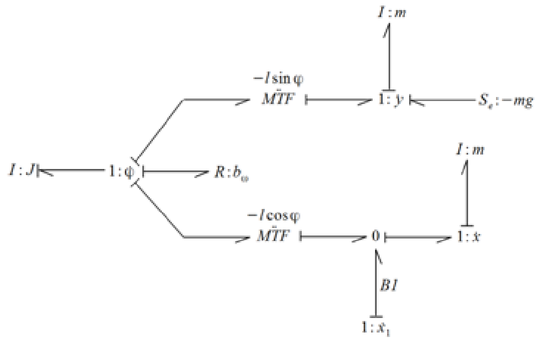

Fig. 5. *Bond graph of the pendulum*

The force of gravity is modeled by the effort source. Kinetic energy of translational and rotational movement is modeled by I storage elements: $I:m$ and $I:J$. Resistor models the moment of viscous friction. For simplicity, a linear friction characteristic is assumed. Bond B1 represents the channel through which the energy from the cart towards the pendulum is transmitted. By using the procedure SCAP [1], causality is assigned to the model, as it is shown in the figure. It can be seen that I elements which correspond to the translator movement have differential causality, that is, the pendulum has one degree of freedom. It can also be seen that the cart dictates the translational movement velocity along the axis x. The pendulum reacts with force, which acts upon the cart along the same direction.

Bond graph of the cart with causality is shown in Fig. 6.

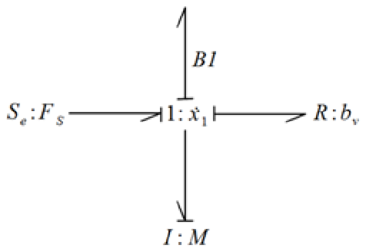

Fig. 6. *Bond graph of the cart*

The energy that comes from the external force is transformed into: kinetic energy of the cart, energy of losses due to viscous friction, and the part that is transmitted towards the pendulum.

All of these transformations have a common cart velocity.

By linking the model from Fig. 5, and the model from Fig. 6 by using bond B1, model of nonlinear bond graph is obtained. Nonlinearity comes from modulated transformers (MTF)

Linear model of the pendulum is obtained by introducing the assumption that rotations around the angle are small. In that case i is valid, and so, two transformers are obtained in the model (one modulated, and the other non-modulated) with coefficients i. Besides, based on the previous assumption, kinetic energy of translational moving along the axis is disregarded. This is how we get to the linearised model of the pendulum, which is shown in Figure 7.

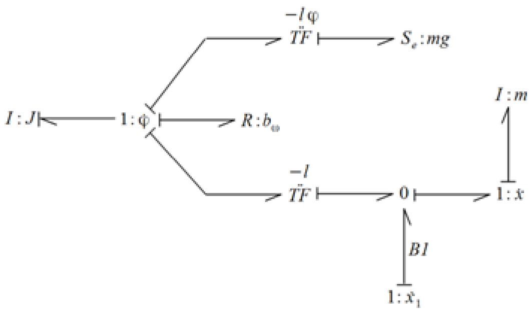

Fig. 7. *Linearised bond graph model of the pendulum*

By using the models shown in figure 5 and figure 6, that is, figure 6 and figure 7, in the continuation, we give the optimization results of parameters of controlling device of the inverted pendulum.

5. RESULTS

During the simulation of linear and non-linear model, the following parameters are used:

M	m	l	b_v	b_ω	g
0,5	0,2	0,3	0,1	0,05	9,81

and the following parameters of the algorithm of particle swarm optimization (algorithm):

Number of particles	30
Number of iterations	20
Inertia weight w	1
Acceleration coefficient c_1	2
Acceleration coefficient c_2	2
Boundaries for K_p	$0-1000$
Boundaries for K_i	$0-1000$
Boundaries for K_d	$0-1000$

The controller parameters obtained by using the relay method for linear model are:

Controller	K_p	K_i	K_d
P	$1{,}8791\cdot10^5$	$-$	$-$
PI	$1{,}5032\cdot10^5$	$2{,}5917\cdot10^5$	$-$
PID	$1{,}5032\cdot10^5$	$1{,}9272\cdot10^7$	137,167

Optimization resulted in the following values for amplification of P controller for linear model of inverted pendulum:

Optimization criterion	K_p
IAE	52,0890
ISE	52,0887
ITAE	98,0892
ITSE	52,0879

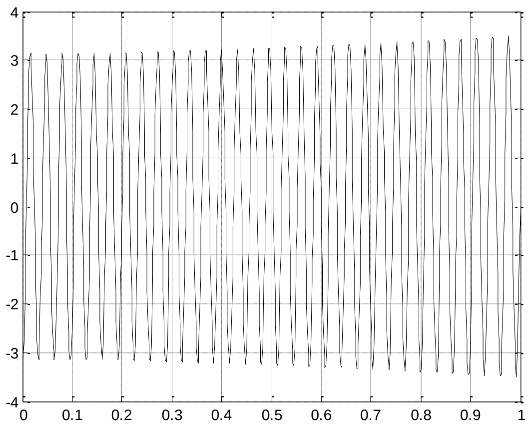

Fig. 8. *System response for the P controller that is adopted by relay method*

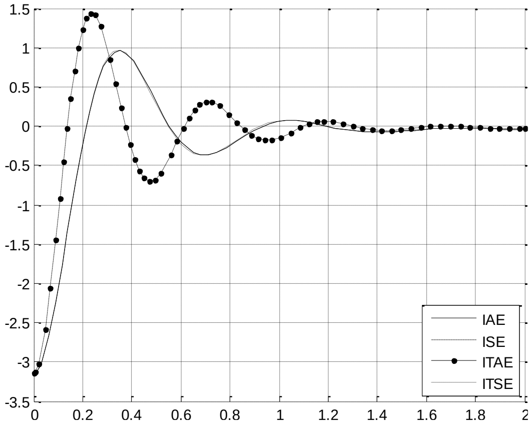

Fig. 9. *System responses with P controllers that are obtained by using PSO optimization*

Optimization resulted in the following values for amplification of PI controller for a linear model of inverted pendulum:

Optimization criterion	K_p	K_i
IAE	36,3938	5,0456
ISE	52,0914	0
ITAE	37,3143	5,4657
ITSE	52,1357	0,9683

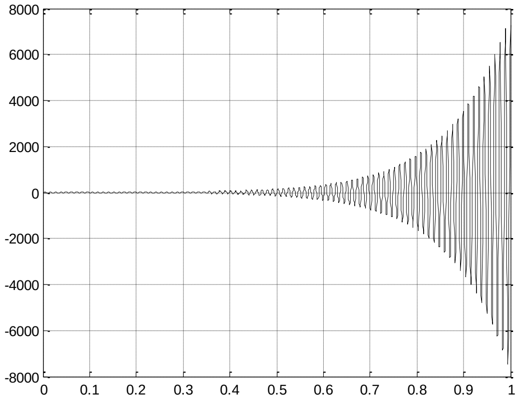

Fig. 10. *System responses with PI controllers that are obtained by using relay method*

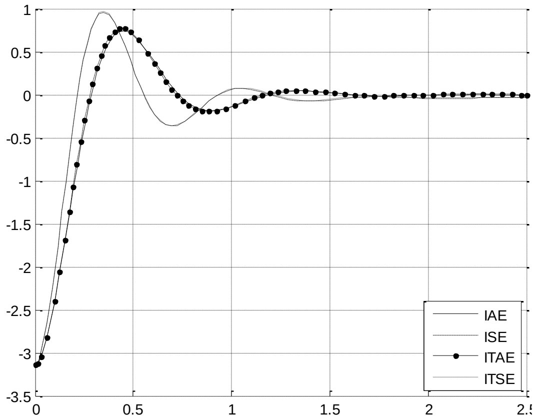

Fig. 11. *Linear system responses with PI controllers that are obtained by using PSO optimization*

Optimization resulted in the following values for amplification of PID controller for a linear model of inverted pendulum:

Optimization criterion	K_p	K_i	K_d
IAE	557,4205	0	12,1933
ISE	665,4343	0	8,4662
ITAE	1000	15,5363	24,7509
ITSE	1000	0	20,3392

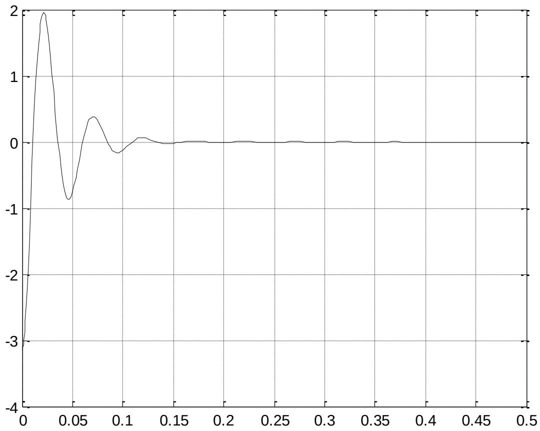

Fig. 12. *System responses with PID controllers which are obtained by using relay method*

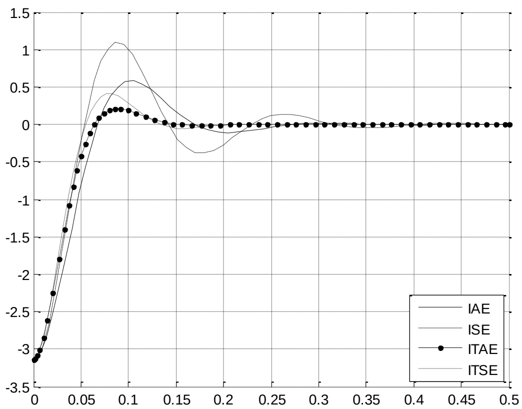

Fig. 13. *System responses with PID controllers that are obtained by using PSO optimization*

Optimization resulted in the following values for amplification of PID controller for a nonlinear model of inverted pendulum:

Kriterijum optimizacije	K_p	K_i	K_d
IAE	1000	25,5908	67,2648
ISE	1000	0	67,0131
ITAE	416,6178	1000	48,2147
ITSE	1000	12,5959	71,6567

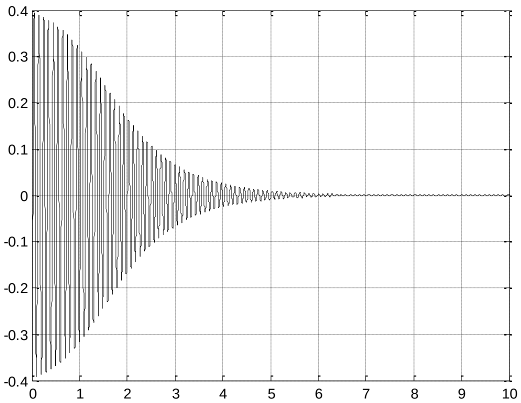

Fig. 13. *Nonlinear system responses with PID controllers that are obtained by using relay method*

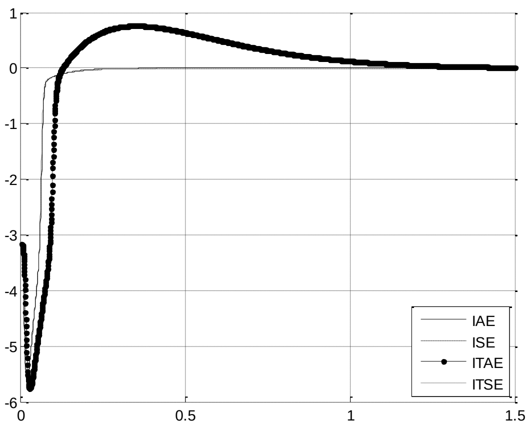

Fig. 14. *Nonlinear system responses with PID controllers that are obtained by using PSO optimization*

6. CONCLUSION

By using the relay method for obtaining controller parameters, we only obtained stable response for the case of PID regulator for linear and nonlinear model, while unstable response is present when P I PI controllers are used on the linear model. Likewise, PID controller at nonlinear model has a narrow region in which it works well, and that is the region around the vertical axis in which nonlinearity is expressed the least.

On the other side, controllers with the parameters obtained by using particle swarm optimization provided stable responses for both linear and nonlinear model of inverted pendulum. Optimized parameters are several times smaller than the parameters obtained by using the relay method. For both linear and nonlinear model, optimized controllers reduced the angle of the rod to zero, with the initial angle of 180°; in other words, the rod was in the lower position at the initial moment.

7. REFERENCES

[1] V. Filipović;N. Novak „PID Regulatori“, Faculty of mechanical engineering Kraljvo, 2008

[2] J. Kennedy;R. Eberhart (1995) “Particle swarm optimization” *Proceedings of IEEE*

International Conference on Neural Networks IV pp. 1942-1948

[3] Shi Y,; Eberhart R. (1998) “A modified particle swarm optimizer” *Proceedings of IEEE International Conference on Evolutionary Computation* pp. 69-73

[4] D.C. Kamopp, D.R. Margolis, R.C. Rosenberg, “System Dynamics: A Unified Approach”, Second Edition, Wiley Interscience, 1990

[5] W. Borutzky, “Bond Graphs: A Methodology for Modelling Multidisciplinary Dynamics Systems” SCS Publishing House, Erlangen, San Diego, 2004

[6] V. Ranković “Inteligentno upravljanje”, Faculty of mechanical engineering Kragujevac 2008

HEAVY MACHINERY - HM 2011, 27-32
ISBN 978-86-82631-58-3 Paper accepted: 30.05.2011

The criteria for selection of control algorithms for electro-hydraulic power actuator

Dragan Nauparac[1,*]
PPT-Engineering Department Belgrade

Generalized approach to selection of the control algorithm for electro hydraulic actuator does not exist. This paper presents a method of systematic approach defining the selection of control algorithm. The initial criterion is defined based on natural frequencies of the previously selected distributor and cylinder that are building the basic configuration of electro hydraulic actuator. This is bringing the question of modeling of load and its influence on selection of the control algorithm. The ideal control algorithm is defined. Finally, simulation results are given for electrical-hydraulic system with variable load, such as electro hydraulic actuator for a flexible nozzle for thrust vector control of rocket engines.
Keywords: electro-hydraulic actuator, control algorithms, mathematical model, flexible nozzle

1. INTRODUCTION

After the selection desired configuration and dimensioning of electro-hydraulic actuators, the next step is to consider the possible control algorithms. It is very important to do proper selection of control algorithms that can be rationally applied in this case. Rationality is reflected in the assumption that the synthesis of control must be done with relative ease, in accordance with criteria defined by the designer of the system and which are very important for the concrete application of electro-hydraulic actuators. When selecting the control algorithm that will be the subject of synthesis, it is necessary to define a set of criteria for the selection of control algorithm, which are, both in theory and practice, verified for use in electro-hydraulic actuated systems. The initial criteria are: the character of the desired value, the expected bandwidth of actuation system, the type of external load, changeability of system parameters and external disturbances. It is assumed that the character of electro-hydraulic actuator system is predefined as having position character, speed character or force control character. In any case, all that is mentioned above represent the basis of how to approach previously known and verified algorithmic solutions. But this also opens the question of whether the ideal control algorithm has been defined and if after the selection of algorithmic solution based on above defined criteria can clearly be understood why and for what reason it deviates from the ideal.

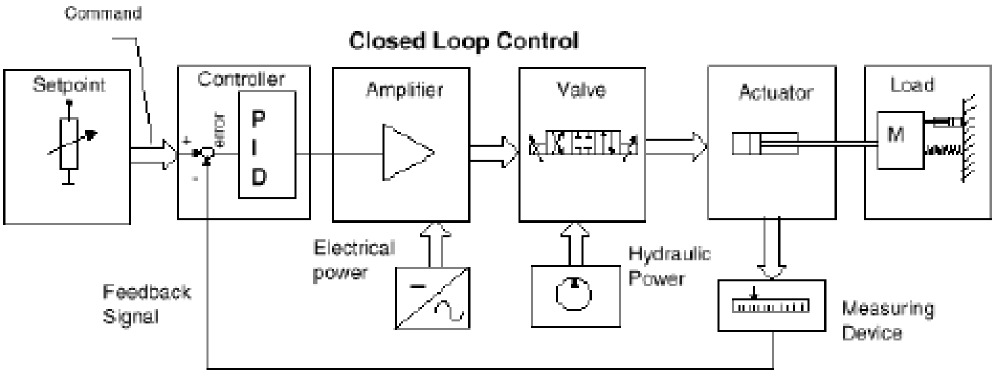

Fig. 1. *Electro-hydraulic actuator with a linear hydro-motor (cylinder)*

*Corr. Author's Address: PPT-Engineering Department Belgrade, Beograd, Serbia, dnauparac@beotel.net

2. THE IDEAL ALGORITHM

In available literature there are very few papers that deal with the problem of an ideal control algorithm and in case that paper exists it is not doing it in a direct way. Intuitively, it is clear that it is very difficult to say what actually is the ideal control algorithm and that it is not easy define it. In the literature [1], the author defined the ideal control algorithm in the following manner: Feed forward compensation loop, good feedback and highly dynamic control element. Feed forward compensation by definition compensates for the "disturbance" that is brought in by change of input value while highly dynamic control element ensures virtually maximum speed of response to the effect of disorder, which in an indirect way to simplifies the dynamic requirements that need to be met by the control algorithm. Consult figure 2: The structure of feed forward control.

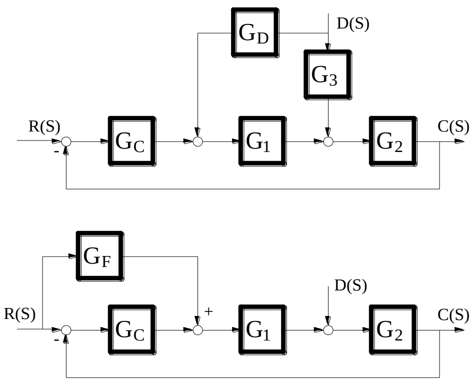

Fig. 2 - *Structure of feed forward control*

Such definition of ideal control algorithm directly gives priority to algorithms that were developed on the basis of the linear mathematical model. This highlights foremost the need for creation of an accurate mathematical model. Even in case of giving preference to algorithms that do not require the knowledge of mathematical model, mathematical model is still needed for simulation testing of the so-called robust control algorithms, for whose definition the knowledge of mathematical models is not necessary, but is required for simulated testing of operation before performing tests on a real model. The conclusion is that the mathematical modeling of actuation system virtually can not be avoided, unless a robust control algorithm is used so that it is set up and tested immediately on a real model, which is extremely rare in practice. Mathematical modeling is a very complex task and the main problem is what would be included in mathematical model, i.e. it is always an open question what is in modeled and what in non-modeled dynamics. This represents the hardest design mission, which solution is very complex meaning that universal approach to solving it does not exist here and is the subject of constant research. In some cases, when possible, certain authors, [2] suggest that the designer relies on the identification of mathematical model, but the implementation of this idea is possible and rational only in certain cases.

3. PRE-SELECTION OF CONTROL ALGORITHMS

The first criterion is the character of change of desired value. If, in mathematical sense, there is no interruption of the first kind, that is, if there is a smooth change in preferences, it is then clear that the primary requirement of accuracy and quality characteristic of stability (exuberance of amplification and exuberance of phase) is not the primary requirement, but that the actual value of the output follows the desired change of input values. The question is then raised of choice of algorithms that provide good tracking characteristics or algorithms that, by definition, provide tracking. If the output values are of such change, that there are large changes in amplitude at the entrance, the question arises whether the control algorithm ensures that the internal system nonlinearities of saturation type, limit by speed and acceleration do not cause saturation of the output signal based on the large changes of the input signal. The second criterion is the analysis of external loads. If there is great friction in the external load, for its compensation in the algorithmic solution the most important is the introduction of feedback by acceleration or feedback by pressure difference in the chambers of the hydraulic cylinder or by direct measurement of force. A size calculation of the cylinder is done before the analysis of possible algorithmic solutions in accordance with criteria of maximum force for the selected nominal operating pressure. Cylinder size dictates the nominal size of the servo distributor, whose nominal size basically limits the bandwidth of the servo distributor by providing that within selection of control algorithms an additional criterion can be defined which is particularly used in practice, and that is in accordance with own frequencies of the cylinder and servo distributor. Other elements of the actuation system, sensors and electronic amplifier of the distributor have, by one order of magnitude, higher own frequency that are not taken into account when analyzing the dynamics of actuation system. In literature (3) is well known the following criterion for selection of basic control algorithms of electro-hydraulic actuator. The name "basic control algorithm" is used, since the basic design idea is to achieve the initial quality of control by using linear control algorithm. Criterion for basic control algorithm is given in Table 1.

Table 1:

Case 1: $\frac{f_{o_{cyl}}}{f_{o_v}} \approx 0.3$ - Best results are achieved with pressure or acceleration feedback

Case 2: $\frac{f_{o_{cyl}}}{f_{o_v}} \approx 1$ - A simple PT_1 controller offers best results

Case 3: $\frac{f_{o_{cyl}}}{f_{o_v}} \approx 3$ - A PD controller will provide best results

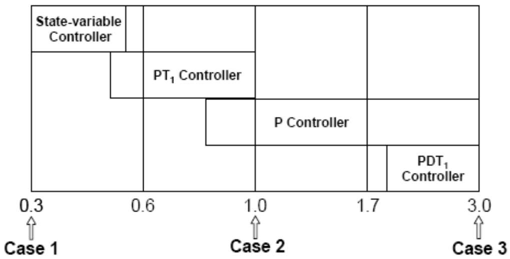

Fig.3-*The initial algorithm selection for the synthesis of control based on the criterion of own (natural) frequencies*

Electro hydraulic actuators have very high nonlinear nature. Very often in the literature it is shown that by choosing the algorithm with nonlinear nature the nonlinear nature of actuating electro-hydraulic system can be compensated. Changeability of parameters of actuating electro-hydraulic system is often present during the operation of electro-hydraulic system. This refers to the parameters that are important for the algorithm, first of all different gain for different operating conditions i.e. value of error between the actual value at the output of the system and desired output value. Aside of this the compressibility in the system, rigidness of connections or the nature of the load can be variable in time.

4. SELECTION OF CONTROL ALGORITHMS FOR ELECTRO HYDRAULIC SYSTEM

The integral nature of electro-hydraulic actuator represents a significant limiting factor for application of certain control algorithms well-known in the theory of automatic control systems. It is simply not possible to determine the nominal position for certain nominal controls. This means that it is not possible to use mathematical model by discrepancies, but only the record of mathematical model in total coordinates is used. In any case, this limitation is most pronounced in application of variable structure algorithms with flexible (sliding) working regime. Natural following control algorithms are also sensitive to the integral nature of electro-hydraulic actuator with hydraulic cylinder. This problem is overcome with introduction of special differentiator that ensures the condition of natural traceability. In defining the electro-hydraulic system as positioning system often a mistake is made because preference is given to control of position even when the inertial load is not free (it is connected to a piston rod and has a further limitation in the form of connection, for example the construction of flexible nozzle). In such cases, priority is given to control by the force and the position of desired point of the inertial load is controlled indirectly. Naturally tracking algorithms have been thoroughly investigated and experimentally verified on the example of electro hydraulic actuator with linear motor, but only in case of small inertial load (consult the references [4], [5], [6]). All mentioned above define that classic path to selection of control algorithm is implemented in the following way: first the PID control algorithm is used and then, if the results are not as expected, the area of state space is encroached and, accordingly, the control algorithm is defined within the state-space. The state-space is opening a wide range of designer solutions that arise as a result of many possible modifications of the basic control algorithm within the state space. Beside the choice of structure of control algorithm, particularly important is its position in the configuration of electro hydraulic systems.

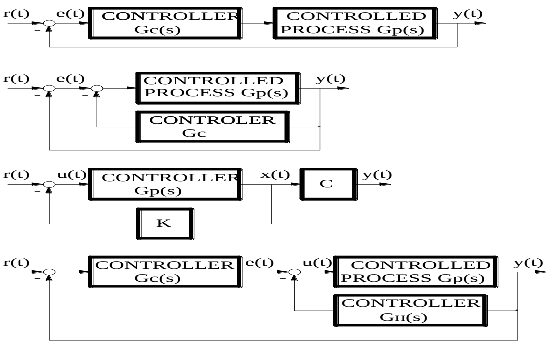

Fig.4. *The different positions of controller within structure of actuator*

In Figure 4, some basic positions of controller and/or correction body to which control algorithm has been implemented. The most common is that the input of controller represents the error between desired and actual values, but as seen in Figure 4 that can also be a real value of output; the desired value of output, in the state-space the control that is formed on the basis of feedback and the desired value of output. One of the basic principles of design practice is to initially choose the simplest controller structure that can fulfill the required demands. Only analysis of the behavior of the system with such choice of controller structure can direct the designer to choose a better and a more optimal solution in accordance with set criterion.

5. PID CONTROL IN THE INPUT-OUTPUT SPACE

Designer practice says that the simplest algorithm from which should be started is PID. In sub-variants it can be seen all that it is capable to:

Table 2:

PD	-Improving damping and reducing maximum overshoot -Reducing rise time and settling time -Improving GM, PM and M_R Increasing BW
PI	-Zero steady state error
PID	PD & PI
Phase-lead	The high pass filter
Phase-lag	The low pass filter

The choice of control algorithm within the option limits of PID algorithms can be viewed as filter issue. Based on previous experience from practice, there are two important conclusions:

- If hydraulic system is presented with mathematical model whose order is greater than 3, the PID control algorithm does not represent optimal solution.
- If the system is discrete with the sampling rate of less than 0.01 s (100Hz) PID control algorithm does not represent adequate solution.

One particularly important and relatively simple modification of PID control algorithm is to achieve its robustness by changing the value of the coefficient of proportional gain. General approach is based on the fact that the value of the gain represents the function of error and that this may be linear or nonlinear function, like, for example, is the square error. If all mentioned above does not give the expected result, we are proceeding to the selection of control algorithms that are related to state-space. This is, in any case, more complex and expensive (all the properties of state-space must be measured) but at the same time, according to definition of size of state-space, we have available all necessary information about the system and thus we provided conditions that by further search for algorithmic solutions in state-space we achieve that chosen control ensures that real output value follows the desired output value and that the system is stable. This means that further selection of control algorithm is based on checking of features of tracking for such algorithmic solutions.

6.0 ALGORITHMIC SOLUTIONS IN STATE-SPACE

Figure 5 shows the structure of electro-hydraulic actuator with linear motor in the state-space.

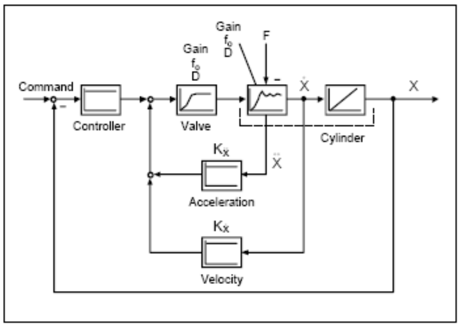

Fig.5. State space

7.0 ROBUST CONTROL ALGORITHM

In general, the control algorithm should provide robustness of the system to the change of parameters and the effects of external disturbances. Theoretically, it can be shown that position feedback in electro-hydraulic system reduces the impact of disturbance and variation of parameters, but this is only true in conditions of large amplifications (gains) that disrupt the operational stability of electro-hydraulic actuator. In addition to the previously mentioned definition of robust control algorithms, in term of not requiring the knowledge of mathematical models, we can show the following by taking into account the aforesaid about feed-forward compensation. Figure 9 gives a response of electro hydraulic system with PID control and with addition to the PID in the form of feed-forward compensation. According to the quality of response it is clear that there is much greater impact of non linearity without feed forward compensation (higher harmonics in response) than in the case of the feed-forward compensation.

8. ELECTRO-HYDRAULIC ACTUATOR - FLEXIBLE NOZZLE OF ROCKET ENGINE

Thrust vector control of rocket engines with liquid or solid rocket fuel represents a special area of application of electro-hydraulic actuators, where they have a special advantage due to the following reasons:

1. Large power density per unit weight of actuation system, over 10 kW / kg.
2. High speed of deflection of flexible nozzle.
3. Large and rapid changes of force

The general design of a flexible nozzle is shown in Figure 6. It can be seen that flexible connection of the chamber of rocket engine and nozzle requires very large forces to be applied in order to deflect the nozzle. Due to sudden changes in ambient temperature and internal temperature as a result of the operation of rocket motor, the force that opposes the deflection of the nozzle has specific character of change.

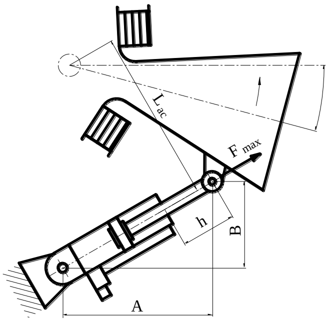

Fig. 6. *The general design of a flexible nozzle*

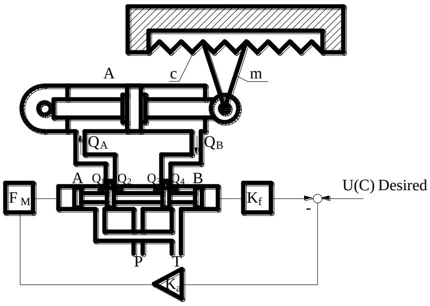

Fig.7. *Schematic description of load of flexible nozzle actuator*

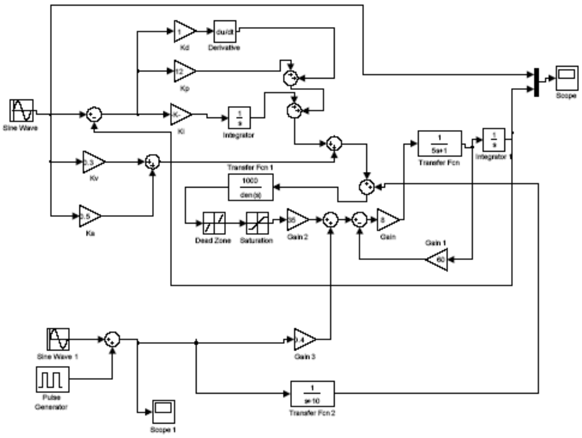

Fig.8. *Block diagram of the mathematical model of actuation system with feed-forward compensation and flexible load modeling*

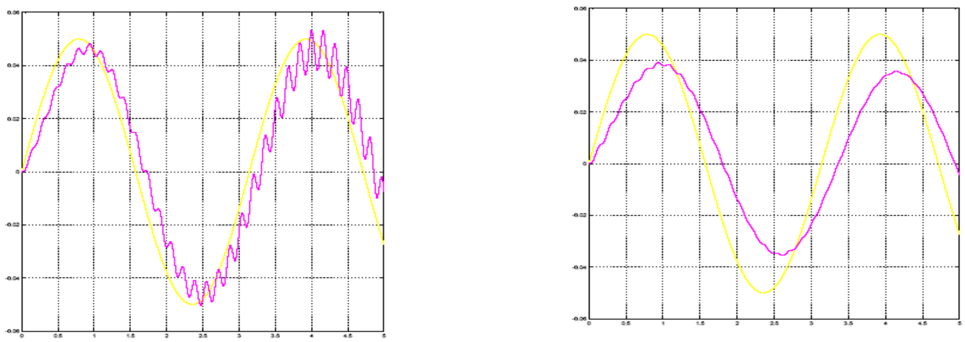

Fig.9 *Response of a system with PID control and PID control with feed-forward compensation*

9. CONCLUSION

This paper presents a systematic way of selecting the optimal control algorithm for electro-hydraulic actuator. It also emphasizes the importance of PID algorithm where control algorithm can be viewed as a problem of filters. In this way the properties of systems are observed that are important in selection of advanced control algorithms. Here it is provided an example of synthesis of feed-forward control as a possible optimal solution when electro-hydraulic actuator is exposed to a load from flexible nozzles that are specifically modeled.

10. REFERENCES

[1] Wane R. Anderson, Controlling Electro hydraulic systems, New York, 1988.
[2] M.Jelali, A.Kroll, Hydraulic Servo-systems, Modeling, Identification and Control, Springer
[3] Rob Decker, Dave Saaski, Design and Control of Proportional and Servo Systems, 2008, Bosch-Rexroth Industrial Hydraulics.
[4] A.Bonchis, P.I.Corke, D.C.Rye, Q.P.Ha, Variable structure methods in hydraulic servo systems control, Automatica 37 (2001), 589-595
[5] G. A.Sohl, J.E.Bobrow, Experiments and Simulations on the Nonlinear Control of a Hydraulic Servosystem
[6] T.O.Andersen, M.R.Hansen, H.C.Pedersen, F.Conrad, Comparison of linear controllers for a hydraulic servo system, 6 th JFPS International Symposium on Fluid Power, TSUKUBA . 7-10 November 2005.

HEAVY MACHINERY - HM 2011, 33-36 Paper accepted: 30.05.2011
ISBN 978-86-82631-58-3

The Method for Extracting Region of Absolute Stability-Loop - Controlled Time Delay Systems

Vesna Brašić[1,*] –Ljubiša Dubonjić[1]
[1] University of Kragujevac, Faculty of Mechanical Engineering Kraljevo

This paper presents D-decomposition method in the area of absolute stability, developed from Neimark [10] in order to extract region of absolute stability in two-parameters plane for special class of time – delay system.. It means that the open loop transfer function has specific expression with linearly connected open loop gain K=1/α,where α is one variable parameter and the second one is time delay constanτ which is connect with is in non-linear function in open loop transfer function.[4].Now we develop the method for synthesis and analysis of controlled-loop system with proportional regulator for circulating reservoir for mixing liquids and presents and investigates the further expansion of last obtained results .With this method it is possible to separate the region in three-dimensional space(frequency ω (Hz), gain K=1/α and time delay constant (τ), sothat adjustable parameters guarantee absolute stability of synthetized automatic control system.

Keywords: loop – controlled time delay system, absolute stability, parametric plane, circulating reservoir for mixing liquids

0. INTRODUCTION

This method which Russian scientist Neimark [9],[10] was first started to develop is the method for testing stability of time-delay systems so-called D-composition method. All works about this method was given in [1]. The method for separation the region in the parameter plane, which enables closed- loop system will have pre-settling timewas also particularly developed and explained in [4] and this paper will continue extend last mentioned results and their application.

1.1Definition the class of loop-controlled time delaysystem-mathematical model of circulating reservoir for mixing liquids

This part has already been presented in[1],[2].The class of closed-loop system with a single delay, when the adjustable parameters are non-linearly related to polynomial coefficients ofquasicharacteristic equation [10] is defined by following open loop transfer function.

$$W_{ok} = \frac{N(s)}{\alpha D(s)} e^{-\tau s} \qquad (1)$$

so that quasicharacteristic equation has the following form:

$$f(s,\ e^{-\tau s}) = \propto D(s) e^{\tau s} + N(s) = 0 \qquad (2)$$

where K = 1/α is proportional regulator gain, so α is a regulator parameter linearly related to polynomial coefficients of quasicharacteristic polynomial. Pure time delay is τ, which in the case of circulating reservoir for mixing liquids [4] introduced into the control parts of the object, through valves and pipes to reservoir, as described in the definition of a mathematical model of this system [4].

1.2 Separation the region of absolute stability

The system will possess an absolute stabil.ity only if all the roots of quasicharacteristic equation are in left part of complex plane.
The method is transforming this part of complex plane to parametric plane τ-α:

1.2.1 Decomposition curve

For ω- Im(s) complex variable s has the form:

$$s = j\omega, \qquad (4)$$

Then N(s) and D(s) become:

*Corr. Author's Address: Faculty of Mechanical Engineering Kraljevo, Dositejeva 19, Kraljevo, Serbia,brasic.v@mfkv.kg

$$N(j\omega) = N_1(\omega) + jN_2(\omega) \qquad (5)$$

$$D(j\omega) = D_1(\omega) + jD_2(\omega)$$

when (5) puts in (2) it gives:

$$N_1(\omega) + \alpha[D_1(\omega)\cos\omega t - D_2(\omega)\sin\omega t] = 0 \qquad (6)$$

$$N_2(\omega) + \alpha[D_1(\omega)\sin\omega t + D_2(\omega)\cos\omega t] = 0 \qquad (7)$$

When α from (6) puts in (7) it gives:

$$tg(\omega t) = \frac{N_2(\omega)D_1(\omega) - N_1(\omega)D_2(\omega)}{N_1(\omega)D_1(\omega) - N_2(\omega)D_2(\omega)} \qquad (8)$$

Conditions for (8) are:

$$N_1(\omega) \neq 0, D_1^2(\omega) + D_2^2(\omega) \neq 0, \qquad (9)$$

From (6) we got

$$\alpha = \frac{-N_1(\omega)}{\cos(\omega t)\left[D_1(\omega) - D_2(\omega)tg(\omega t)\right]} \qquad (10)$$

So we know that:

$$:\cos(\omega t) = \frac{1}{\pm\sqrt{1 + tg(\omega t)}} \qquad (11)$$

and then substituting (8) in (11) next decomposition curves follows:

$$\alpha = \pm\sqrt{\frac{N_1^2(\omega) + N_2^2(\omega)}{D_1^2(\omega) + D_2^2(\omega)}} \qquad (14)$$

$$\tau = \frac{1}{\omega}\left[arctg\frac{N_2(\omega)D_1(\omega) - N_1(\omega)D_2(\omega)}{N_1(\omega)D_1(\omega) + N_2(\omega)D_2(\omega)} + 2k\pi + \frac{\pi}{2} \pm \frac{\pi}{2}\right] \qquad (15)$$

for $k \in Z, \omega \in [-\infty, +\infty)$

Note:The upper sign of (14) correspondents to the upper sign of (15) and the lower sign of (14) correspondents to the lower sign of (15).

1.2.2 Curve shading

Shading of decomposed curves is determined by the sign of Jacobians (as in systems without delays).

$$F(j\omega) = R_F(\omega) + jI_F(\omega) \quad (15)$$

$$R_F = N_1(\omega) + \alpha[D_1(\omega)\cos(\omega\tau) - D_2(\omega)\sin(\omega\tau)]$$

$$I_F = N_2(\omega) + \alpha[D_1(\omega)\sin(\omega\tau) + D_2(\omega)\cos(\omega\tau)]$$

Jacobians of the system as follows:

$$J = \begin{vmatrix} \frac{\partial R_F}{\partial \tau} & \frac{\partial R_F}{\partial \alpha} \\ \frac{\partial I_F}{\partial \tau} & \frac{\partial I_F}{\partial \alpha} \end{vmatrix} = -\alpha \cdot \omega \cdot [D_1^2(\omega) + D_2^2(\omega)] \qquad (16)$$

1.2.3. Singular lines

Singular lines, in the case of extracting area of pre-settling time is defined for boundary cases ω→-∞ and ω→+∞, in (2), (14) and (15):

$$\lim_{s\to\pm\infty}\frac{N(s)}{D(s)} = -\lim_{\omega\pm\infty}\alpha\cdot\left[\cos(\tau\omega) + j\cdot\sin(\tau\cdot\omega)\right] \qquad (17)$$

Because of nature of expresion (17) it is necessary to be sin(τω)=0 i.e. τ=k∏/ω so (17) becomes:

$$\lim_{s\to\pm\infty}\frac{N(s)}{D(s)} = -\lim_{\omega\pm\infty}\alpha\cdot(-1)^k$$

$$\alpha = (-1)^{k+1}\lim_{s\to\pm\infty}\frac{N(s)}{D(s)} \qquad (18)$$

τ=0 and τ ⇨∞ (19)

Expresion (18) and (19) are singular lines

The decomposition curves shows that we are getting for every single values k hatched area area between those curves and singular lines (18) and (19). So lets mark hatched area for some vakue marked k with s_k [4] it is clear that the hatched area adequate to left part of complex plane is defined with following expression:

$$s = \bigcup_k \{s_k\} \qquad (20)$$

Now we can choose in parametric three-dimensional space parameter τ and α from that hatched area s (better view in τ - α projecting plane)

2.1 **Aplication the method – circulating reservoir for mixing liquids**

Application of the methods described here will be illustrated with the example of circulating reservoir for mixing two liquids. A mathematical model is developed for control systems with proportional controller which gain is K = 1 / α and given object [4] for some nominal parameter values, with time delay identical for both liquid flows as τ. The open loop transfer of feedback system is:

$$W_{ok} = \frac{(2{,}31\cdot 10^{-4}s+1{,}34\cdot 10^{-7})\cdot e^{-\tau s}}{\alpha\cdot(s^2+17{,}3\cdot 10^{-4}\cdot s+61{,}5\cdot 10^{-8})} \qquad (21)$$

2.1.1Synthesis of controlled-loop system

According to the methods described in chapter 1 equations (14), (15) and (16) become:

$$\alpha = \pm\sqrt{\frac{5{,}34\cdot 10^{-8}\omega^2+1{,}8\cdot 10^{-14}}{3{,}78\cdot 10^{-13}+1{,}76\cdot 10^{-6}\cdot\omega^2+\omega^4}}$$

$$\tau = \frac{1}{\omega}\begin{bmatrix} -arctg\,\dfrac{9{,}02\cdot 10^{-11}\omega+2{,}31\cdot 10^{-4}\cdot\omega^3}{3{,}78\cdot 10^{-13}+2{,}65\cdot 10^{-7}\cdot\omega^2}+ \\ +2k\pi+\dfrac{\pi}{2}\pm\dfrac{\pi}{2} \end{bmatrix} \qquad (21)$$

$$J = -\alpha\cdot\omega\cdot\left[\omega^4+1{,}76\cdot 10^{-6}\omega^2+3{,}78\cdot 10^{-13}\right]$$

Singular lines are: α=0 τ=0 and and τ ⇨+∞

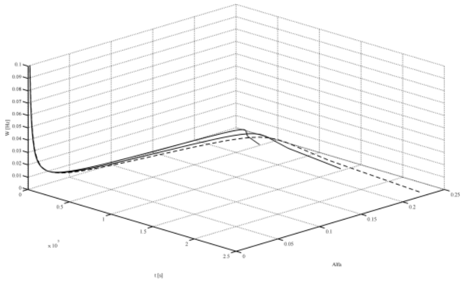

Figure 2. Separation the area of absolute stability

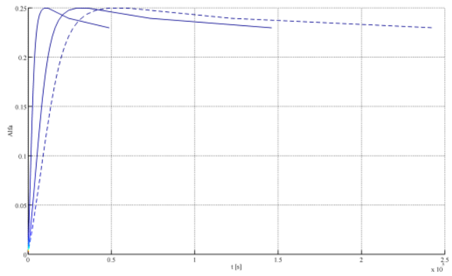

Figure 3.Area of absolute stability in parametric plane
Line - - - - - - for k=0,-1
Line ______ for k=1,-2
Line ______ for k=2,-3

From the union of this areas we can highlight the point α=0,3 and τ=10 000s (22)

Dashed line represents the boundary of region of absolute stability.

B.Dynamic analysis of synthesized system

With chosen parameters from absolute stability region and on the basis of (21) we receive the open loop transfer function of the system. Simulation of the system behavior is done with MATLAB software with step function.Simulation result of step response is shown on Fig 4.

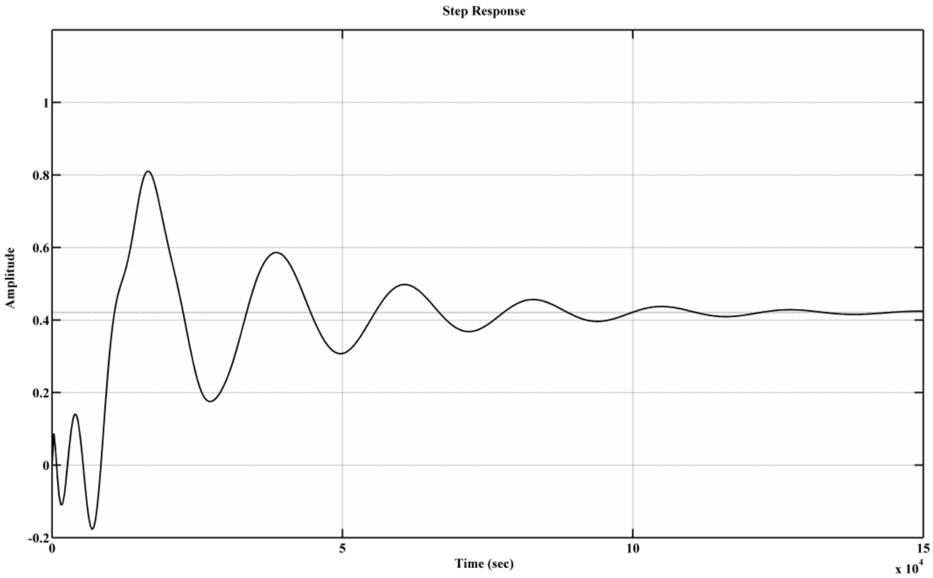

Figure 4. Step response

IV.CONCLUSION

This part could be the same like ones in [1].New software package MATLAB enables to obtain more precocious method for separation the field of absolute stability in the parametric plane of α-τ [4]. The results presenting here overview variation and dependences of parameters in three-dimensional form(α, τ, ω_n) where could be possible to choose from the given space curve the values for parameters which guarantee much better accuracy in methodology than the last obtained results [4].

REFERENCES:

[1]V.S.Brašić, Lj.Dubomjić,N.Nedić „Parametric Methods in Analysis and Synthesis of Controlled Time Delay System– Circulating Reservoir for Mixing Liquids“, SAUM 2010

[2]D.Lj.Debeljković, V.S. Brašić, S.A.Milinković and M.B.Jovanovć ”On relative stability of linear stationary feedback control systems with time delay”, *IMA Journal of Mathematical Control&Information, Oxford University Press,* pp.13-

[3]Milojković B,Grujić Lj. „Automatsko upravljanje“, Mašinski fakult. Beograd, 1977.17, 1996.

[4] V. S. Brašić, ”Analysis and synthesis of feedback control systems with transport lag”, Report, Department of Control Engineering, Faculty of Mech. Eng., Belgrade, June, 1994.

[5] Y. Chu, *Trans.Am.Inst. Elec. Eng*.**71** (2)

[6] L. Eisenberg, “Stability of linear systems with transport lag”*IEEE Trans*AC **11,**247, 1966.

[7]S. Loo, “Stability of linear stationary systems with time delay”*Int.J.Control***9**,103,1969.

[8] O. Mikić, “Some extensions of Mitrovicev’s method in analysis and synthesis of feedback control systems with time delay”, *Proc*.USAUM, Belgrade.Pp.52-67,1982.

[9] Yu. Neimark, “O Opredelenii Značenii Parametrov, prikatorih SAR ustoičiva. Avt.Telem, **3**,190,1949.

[10] Yu. Neimark,“D-razbienie prostransvov kvazipolinomov” *Prikl. Mat.i Meh.13,* 349, 1949.

[11] D. Šiljak, “Generalization of Mitrovicev’s method”,*IEEE Trans.Ind. Appl*.314, September 1964.

[12] D. Šiljak, “Analysis and synthesis of feedback control systems in the parametric plane –Parts I, II, III. *IEEE Trans.Ind.Appl.449, November1964*

[13] D. Šiljak, “Generalization of the parametric plane method”, *IEEE Trans*AC**11**,

HEAVY MACHINERY - HM 2011, 37-40 Paper accepted: 30.05.2011
ISBN 978-86-82631-58-3

Separation of constant settling time area with D-composition method for controlled time delay systems

Ljubiša Dubonjić[1,*] - Vesna Brašić[1]
[1]University of Kragujevac, Faculty of Mechanical Engineering Kraljevo

D-decomposition method in the area of relative stability, developed from Loo [7] in order to separate constant time settling area in parametric space which ensures the system having predefined settling time.[4].This paper develops the methods for synthesis and analysis of controlled-loop system with proportional regulator for circulating reservoir for mixing liquids and presents and investigates the further expansion of last obtained results .

Now it would be possible to separate the region in three-dimensional space(frequency ω (Hz), gain $K=1/\alpha$ and time delay constant (τ), so that adjustable parameters guarantee settling time Ts of controlled system will have a priori defined value .

Useful of this researches is that checking of obtained results can be made with MATLAB software package actually the simulation of dynamic behaviour will be done with this package at the end.

Keywords: loop – controlled time delay system, relative stability, parametric plane, settling time

0. INTRODUCTION

The method for separation the region in the parameter plane, which enables closed- loop system will have pre-settling time was first developed from Loo also particularly developed and explained [4] and this paper will continue extend last mentioned results and their application.

1.1 The class of loop-controlled time delay system -

This method is reserved only for special class of time - delay systems.
The class of closed-loop system with a single delay, when the adjustable parameters α and τ are non-linearly related to polynomial coefficients of quasicharacteristic equation [1],[2],[10] is defined by following open loop transfer function.

$$W_{ok} = \frac{N(s)}{\alpha D(s)} e^{-\tau s} \qquad (1)$$

so that quasicharacteristic equation has the following form:

$$f(s, e^{-\tau s}) = \propto D(s) e^{\tau s} + N(s) = 0 \qquad (2)$$

1.2 Separation the region of pre-settling time

The system will possess an appropriate settling time only if all the roots of quasicharacteristic equation are within this contour C shown on Fig.1

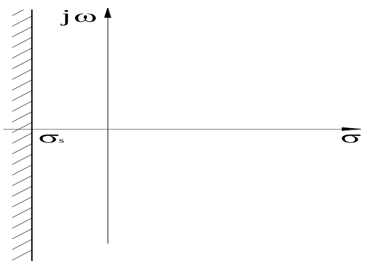

Fig.1**.**The method is transforming this contour C from complex plane to parametric plane τ-α
It was shown in [3] that setting time is defined by the expression

$$T_s = \frac{1}{\sigma_M} \ln \frac{\delta}{\Delta}, \Delta > 0, \delta < \Delta \qquad (3)$$

where amplitude of step response is minor from δ for time t= Ts of transient.

*Corr. Author's Address: Faculty of Mechanical Engineering Kraljevo, Dositejeva 19, Kraljevo, Serbia, dubonjic.lj@mfkv.kg.ac.rs

1.2.1 Decomposition curve

For ω - Im(s) and σ - Re(s), complex variable s has the form:

$$s = \sigma + j\omega, \tag{4}$$

Their deegres are given with:

$$s^k = x^k + jy^k, k = 0,1,2... \tag{5}$$

where is:

$$\begin{bmatrix} x_{k+1} \\ y_{k+1} \end{bmatrix} = \begin{bmatrix} \sigma & -\omega \\ \omega & \sigma \end{bmatrix} \cdot \begin{bmatrix} x_k \\ y_k \end{bmatrix}, k = 0,1,2... \tag{6}$$

$$\begin{bmatrix} x_0 \\ y_0 \end{bmatrix} = \begin{bmatrix} 1 \\ 0 \end{bmatrix} \tag{7}$$

From (6) and (7) it is clear that $x_k$and y_k are the real function of σ and ω. So if (5) put into polynomials D(s) and N(s) we got:

$$D(\sigma,\omega)=R_D(\sigma,\omega)+jI_D((\sigma,\omega) \tag{8}$$
$$N(\sigma,\omega)=R_N(\sigma,\omega)+jI_N((\sigma,\omega) \tag{9}$$

So equation (2) gives a form

$$f(\sigma,\omega)=R_F(\sigma,\omega) + jI_F(\sigma,\omega) \tag{10}$$

If (8) and (9) put in (2) we got following equation:

$$R_F(\sigma,\omega) = \alpha \cdot e^{\tau\sigma}\left[R_D(\sigma,\omega)\cos(\tau\cdot\omega) - I_D(\sigma,\omega)\cdot\sin(\omega\cdot\tau)\right] + R_N(\sigma,\omega) \tag{11}$$
$$I_F(\sigma,\omega) = \alpha \cdot e^{\tau\sigma}\left[R_D(\sigma,\omega)\sin(\tau\cdot\omega) + I_D(\sigma,\omega)\cdot\cos(\omega\cdot\tau)\right] + I_N(\sigma,\omega)$$

In polar coordinates (8) and (9) gives a form:

$$D(\sigma,\omega) = r_D(\sigma,\omega)\cdot e^{j\Phi_D(\sigma,\omega)} \tag{12}$$

$$N(\sigma,\omega) = r_N(\sigma,\omega)\cdot e^{j\Phi_N(\sigma,\omega)} \tag{13}$$

and then substituting (12) and (13) in (2) next decomposition curves follows:

$$\alpha = \pm\frac{r_N(\sigma,\omega)}{r_D(\sigma,\omega)}e^{-\tau\sigma} \tag{14}$$

$$\tau = \frac{1}{\omega}\left[\Phi_N(\sigma,\omega) - \Phi_D(\sigma,\omega) + 2k\pi + \frac{\pi}{2} \pm \frac{\pi}{2}\right] \tag{15}$$

for $k \in Z, \omega \in \left[-\infty, +\infty\right)$

Note:The upper sign of (14) correspondents to the upper sign of (15) and the lower sign of (14) correspondents to the lower sign of (15).

1.2.2 Curve shading

Shading of decomposed curves is determined by the sign of Jacobians (as in systems without delays).
Jacobians of the system as follows:

$$J = \begin{vmatrix} \frac{\partial R_F}{\partial \tau} & \frac{\partial R_F}{\partial \alpha} \\ \frac{\partial I_F}{\partial \tau} & \frac{\partial I_F}{\partial \alpha} \end{vmatrix} = -\alpha\cdot\omega\cdot e^{2\sigma\tau}\cdot r_D^2(\sigma,\omega) \tag{16}$$

1.2.3. Singular lines

Singular lines, in the case of extracting area of pre-settling time is defined for boundary cases ω→-∞ and ω→+∞, in (2), (14) and (15):

$$\lim_{s\to\pm\infty}\frac{N(s)}{D(s)} = -\lim_{\omega\pm\infty}\alpha\cdot e^{\tau\sigma_M}\left[\cos(\tau\omega) + i\cdot\sin(\tau\cdot\omega)\right] \tag{17}$$

Because of nature of expresion (17) it is necessary to be sin(τω)=0 i.e. τ=k∏/ω so (17) becomes:

$$\lim_{s\to\pm\infty}\frac{N(s)}{D(s)} = -\lim_{\omega\pm\infty}\alpha\cdot e^{\frac{k^*\pi}{\omega}\sigma_M}(-1)^{k^*}$$

$$\alpha = (-1)^{k^*+1}\lim_{s\to\pm\infty}\frac{N(s)}{D(s)} \tag{18}$$

τ=0 (19)

Expresion (18) and (19) are singular lines

The procedure of selection periodicity factor k = k * is defined by procedure of selection the area of absolute stability for required automatic control system.[4]. Thus the first of all it is necessary to define area of absolute stability[4],[6],[9] in order to obtain corresponding period k=k*and with that value of k* we are getting (14) and (15) which extract the area of pre-settling time in parametric three-dimensional space.

2.1 **Mathematical model of circulating reservoir for mixing liquids**

Application of the methods described here will be illustrated with the example of circulating reservoir for mixing two liquids. A mathematical model is developed for control systems with proportional controller gain $K = 1/\alpha$ and given object (Fig. 2) for some nominal parameter values, with time delay identical for both liquid flows as τ. The open loop transfer of feedback system is:

$$W_{ok} = \frac{(2{,}31\cdot 10^{-4}s + 1{,}34\cdot 10^{-7})\cdot e^{-\tau s}}{\alpha\cdot(s^2 + 17{,}3\cdot 10^{-4}\cdot s + 61{,}5\cdot 10^{-8})} \qquad (20)$$

2.1.1Synthesis of controlled-loop system

According to the methods described in chapter 1,for $\sigma=\sigma_M$= 1sec equations (14), (15) and (16) becomes:

$$\alpha = \pm\sqrt{\frac{5{,}34\cdot 10^{-8}\omega^2 + 5{,}33\cdot 10^{-8}}{\omega^4 + 2\cdot\omega^2 + 1}}\, e^{\tau}$$

$$\tau = \frac{1}{\omega}\begin{bmatrix} arctg\,\dfrac{5{,}33\cdot 10^{-8} + 5{,}34\cdot 10^{-8}\cdot\omega^2}{\omega^4 + 2\cdot\omega^2 + 1} + \\ +2k^*\pi + \dfrac{\pi}{2} \pm \dfrac{\pi}{2} \end{bmatrix} \qquad (21)$$

$$J = -\alpha\cdot\omega\cdot e^{-2\tau}\cdot\left[\omega^4 + 2\omega^2 + 1\right] \qquad (22)$$

Singular lines are: α=0 and τ=0 and $\tau \Rightarrow \infty$

k^*represents k for absolute stability in previous paper k*=0,-1

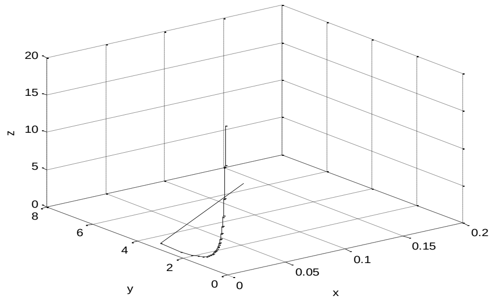

Figure 2. Area for σ_M=1s for α>0

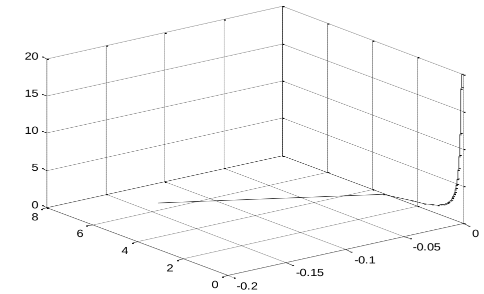

Figure 3.Area for settling time σ_M=1s for α<0

It could be possible to define region for 3D space consisting of parametric plane α-τ (x-y axis) and the axis $\omega_=$z for $\sigma_{M=}$1s from (3) and [3] obtains Ts = 58s, which for σ =0 represents the boundary of region of absolute stability. In that case results obtained with this method are the same like the well- known ones. [9], [10].

B.Dynamic analysis of synthesized system

We highlight the point which determines the controller parameters α = 1/180 and τ = 3s from the region of σ_M=1s which is defined with extracting lines (21) and singular lines α=0 and τ=0, and on the basis of (20) receives the open loop transfer function of the system. Simulation of the system behavior is done with MATLAB software with step function. Simulation result of step response is shown on Fig 4.

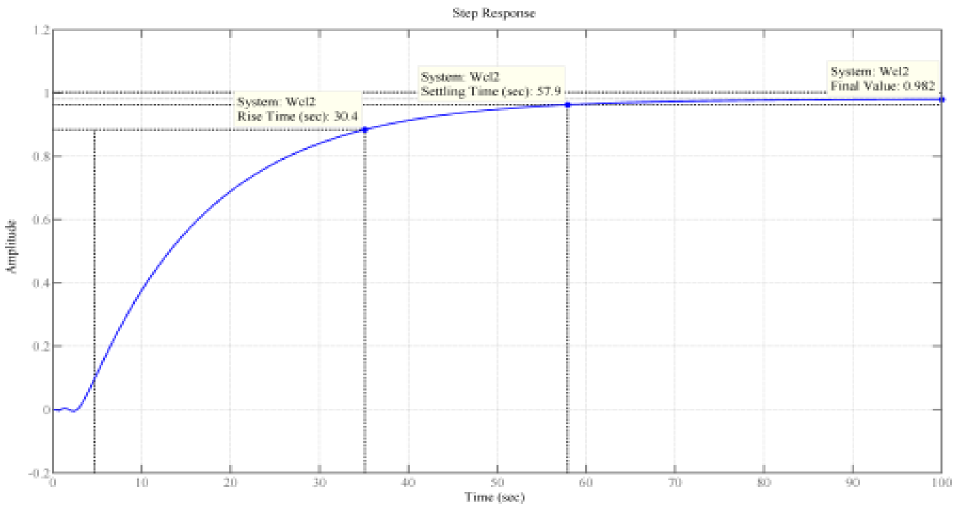

Figure 4. Step response

IV.CONCLUSION

The results obtaining with MATLAB have proven the value of pre-settling time Ts=57,9s of synthetiezed system. This software package enables to us more precisious results and proven of this theory than obtained in [4].

REFERENCES:

[1] V.S.Brašić, Lj.Dubojić,N.Nedić „Parametric Methods in Analysis and Synthesis of Controlled Time Delay System– Circulating Reservoir for Mixing Liquids“, SAUM 2010

[2]D.Lj.Debeljković, V.S. Brašić, S.A.Milinković and M.B.Jovanovć ”On relative stability of linear stationary feedback control systems with time delay”, *IMA Journal of Mathematical Control&Information, Oxford University Press,* pp.13-

[3]Milojković, B,Grujić Lj „Automatsko upravljanje“,
Mašinski fakult. Beograd, 1977. 17, 1996.

[4] V. S. Brašić, ”Analysis and synthesis of feedback control systems with transport lag”, Report, Department of Control Engineering, Faculty of Mech. Eng., Belgrade, June, 1994.

[5] Y. Chu, *Trans.Am.Inst. Elec. Eng*.**71** (2)

[6] L. Eisenberg, “Stability of linear systems with transport lag”*IEEE Trans*AC **11,**247, 1966.

[7]S. Loo, “Stability of linear stationary systems with time delay”*Int.J.Control***9**,103,1969.

[8] O. Mikić, “Some extensions of Mitrovicev’s method in analysis and synthesis of feedback control systems with time delay”, *Proc*.USAUM, Belgrade.Pp.52-67,1982.

[9] Yu. Neimark, “O Opredelenii Značenii Parametrov, prikatorih SAR ustoičiva. Avt.Telem, **3**,190,1949.

[10] Yu. Neimark,“D-razbienie prostransvov kvazipolinomov” *Prikl. Mat.i Meh.13*, 349, 1949.

[11] D. Šiljak, “Generalization of Mitrovicev’s method”,*IEEE Trans.Ind. Appl*.314, September 1964.

[12] D. Šiljak, “Analysis and synthesis of feedback control systems in the parametric plane –Parts I, II, III. *IEEE Trans.Ind.Appl.449, November1964*

[13] D. Šiljak, “Generalization of the parametric plane method”, *IEEE Trans*AC**11**,

HEAVY MACHINERY - HM 2011, 41-46
ISBN 978-86-82631-58-3
Paper accepted: 30.05.2011

Modeling and simulation of Hydraulic Long Transmission Line by Bond Graph

Dragan Pršić[1,*], Novak Nedić[1], Ljubiša Dubonjić[1]
[1]University of Kragujevac, Faculty of Mechanical Engineering Kraljevo, Kraljevo 36 000, Serbia

This paper address the issue of modeling of the hydraulic long transmission line. In its base, such model is nonlinear with distributed parameters. Since general solution in closed-form for such model is not available, certain simplifications have to be introduced. The pipeline in the paper has been divided to a cascaded network of π segments so that a model with lumped parameters could be reached. For segment modeling, a standard library of bond graphs element has been used. On the basis of models with lumped parameters, the effect of the number of segments, pipeline length and effective bulk modulus on the dynamics of long transmission line has been analyzed.

Keywords: Long transmission line, lumped parameters, π segments, bond graph

1. INTRODUCTION

Existence of a long transmission line (LTL) in hydraulic systems makes their dynamics significantly complex. This is especially emphasized with building and mining machines, agricultural machines, transportation machines, machine tools and other devices where connection between the actuators energy source achieved by a long hydraulic line. Physical variables, pressure and volumetric flow featuring the energy transfer along the hydraulic line, besides the time coordinate, depend on spatial coordinate as well. These physical variables' dependency on spatial coordinate conditions spatial distribution cannot be neglected in long hydraulic line modeling. Therefore they are described with models with distributed parameters. Models with distributed parameters are described with partial differential equations and they are of infinitesimally high order. Use of such a model in analysis o dynamic behavior in time domain is not practical because it requires work with transcendent transfer functions and their approximations using Bessel functions.

In this paper we have used the method of description of a long hydraulic pipe with lumped parameters in a way that it was divided to *n* equal segments of *Ls* length. π and *T* model with lumped parameters have been used whose electrical analogies are given in the paper. On the basis of equivalent electric circuits, adequate bond graphs of these circuits were made and connected into a cascade of n segments, which defines the mathematical model of the hydraulic pipe. On the basis of the mathematical model and simulation, we have analyzed the impact of certain parameters on the character of the transfer process and its results are given in the paper.

2. MODELING OF HYDRAULIC LONG TRANSMISSION LINE

One-dimensional flow of compressible, viscous fluid through the LTL is represented by a set of nonlinear partial differential equations [1]. Applying physical principles of mass conservation, Newton's second law and energy conservation leads to:

$$\frac{A}{a^2}\frac{\partial p}{\partial t} = -\rho\frac{\partial Q}{\partial x} \tag{1a}$$

$$\frac{1}{A}\frac{\partial Q}{\partial t} + g\sin\alpha + \frac{\lambda}{2dA^2}Q^2 = -\rho\frac{\partial p}{\partial x} \tag{1b}$$

That is a pair of quasilinear hyperbolic partial differential equations describing pressure change p and volumetric flow rate Q depending on time t and distance x along the pipeline. Generally, there is no closed-form solution for these equations. The problem is particularly expressed in case of turbulent flow which introduces stochastic parameters. Models with distributed parameters are described by differential equations and the model thus obtained is of infinitesimally high order [2-5].

*Corr. Author's Address: Faculty of Mechanical Engineering Kraljevo, Kraljevo 36000, Serbia, prsic.d@mfkv.rs

In order to find analytical or numerical solution, certain simplifications have to be introduced. One approach is based on division of non-homogenous fields ($p(x,t)$, $Q(x,t)$) on segments with homogenous fields ($p(t)$, $Q(t)$) of all physical variables. In other words, instead of models with distributed parameters we move to the model with lumped parameters. Exactly this is the approach used in this study. LTL is observed as a cascaded network of small lumped elements (Fig.1) where dynamics of each of them is described by common differential equations.

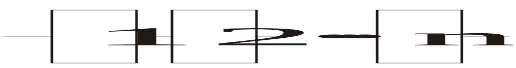

Fig.1. *A cascaded network representing a transmission line*

Each of lumped elements presents spatial abstractions of distributed physical properties. Physical dimensions of each segment are much smaller than the shortest wavelength of interest. Connections between lumped elements represent physical constraints on the physical quantities associated to the elements [6]. Practically, we need to do a model of one segment and then serially connect those models into the system model (LTL).

What we usually find in literature are two single-lump approximations for a short fluid line [7,8]. Those two approximations are known as π and T circuits. Their electrical analogies are given in Fig. 2.

Same elements for modeling of the lumped elements were used in both models. Using capacitor (C element), we model fluid compressibility, using coil (L element) we model fluid inertia, and with resistor (R element) we model losses due to friction. Difference is in the way those elements are connected. In the first case, there are two distinctive pressures: P1 on one end and P2 on the other end of the segment. Same flow rate Qi is adopted along the whole segment length. In the second case, there is one distinctive pressure of Pi segment and two flows Q1 and Q2 on the segment's ends.

Which model is to be used depends on the remaining part of the circuit where the given pipeline is located. Namely, each segment is connected with the surrounding with two energy flows.

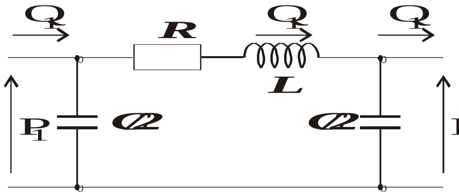

a) π circuit

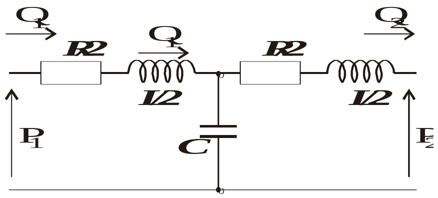

b) T circuit

Fig.2. *Equivalent electrical analogy of short fluid line*

On one end, the energy flow is P_1Q_1, and on the other P_2Q_2. This means that interaction of segments with the environment can be described with four variables. In regard to the segment, two values must be independent, and the other two dependent, provided that the independent values must be on different segment ends. For example, it is not allowed for the values P_1 and Q_1 to be independent. Therefore, it is possible to make four combinations of independent-dependent variables: $Q_1Q_2 \rightarrow P_1P_2$, $Q_1P_2 \rightarrow Q_2P_1$, $P_1Q_2 \rightarrow Q_1P_2$ and $P_1P_2 \rightarrow Q_1Q_2$. Model of the segment, i.e. the whole pipeline depends on the combination appearing in the circuit. It should be noted that when the segment cascade is made, regardless if we use *π* or *T* model, there are blocks inside the model shown in Fig. 3 that periodically repeat.

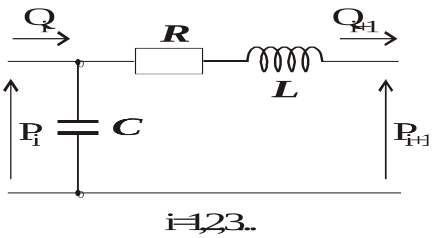

Fig.3. *Block of LTL model repeating periodically*

Difference in models comprising of π and T segments is in the end blocks – interfaces according to the remaining of systems symmetric in regard to internal blocks. Equivalent electrical circuits of end blocks of the cascade with π segments (π interfaces) are shown in Fig. 4 and cascades with T segments (T interfaces) in Fig. 5.

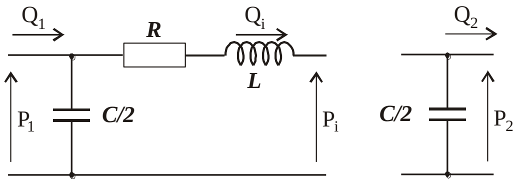

Fig.4. *LTL model interfaces with π segments (π interfaces)*

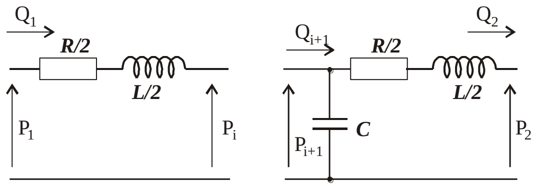

Fig.5. *LTL model interfaces with T segments (T interfaces)*

Suitable bond graphs of the electric circuits in Fig. 3, 4 and 5 are shown in Fig. 6, 7 and 8 in respectively.

On the basis of drawn causality it can be seen that all internal blocks are second rate models. The end blocks for the π cascade have internal causality for one-junction and arbitrary causality for zero-junctions. It is similar with the T cascade where zero-junction has integral causality and one-junctions the arbitrary one. This means that the LTL model can have minimum order of (n-1)*2+1 and maximum (n-1)*2+3. For example, cascade of n=5 segments can be minimally 9 order and maximum 11. Order of the model depends on the hydraulic circuit where the given LTL is found. In order to avoid the differential causality and reduce the numerical problem, recommendation is to use the π cascade if the flow is independent value. If pressure is independent value, differential causality is avoided with use of the T cascade.

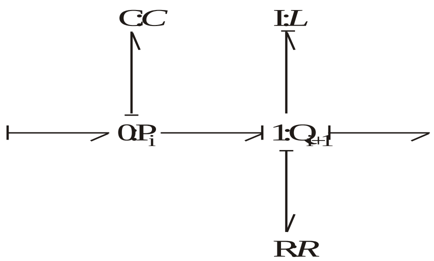

Fig.6. *LTL model bond graph repeating periodically*

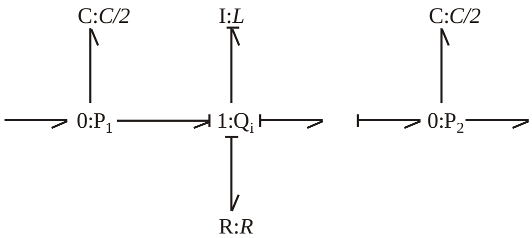

Fig.7. *LTL model interface bond graph with π segments (π interfaces)*

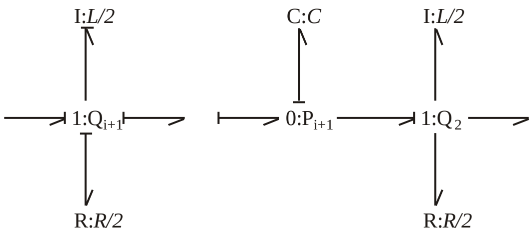

Fig.8. *LTL model interface bond graph with T segments (T interfaces)*

In this study, we observe the response of the system on the independent flow change. Diagram of hydraulic installation is shown in Fig. 9.

As a source of trigger, variable flow rate source is used. LTL is represented as a cascade of n segments. At the end of the circle there is a orifice of constant resistance. Model order is determined with 2n+1.

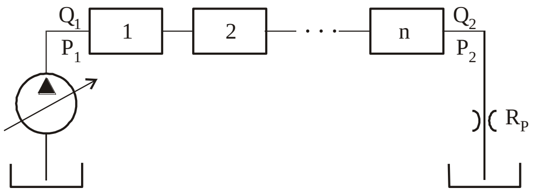

Fig.9. *Schematic of a circuit for LTL simulation*

3. SIMULATION ANALYSIS

On the π model with interface shown in Fig. 4, behavior of LTL in circuit shown in Fig. 9 is simulated. Aim is to analyze the impact of several parameters on the transfer process.

The parameters at which the simulation was performed: $Be = 1.4 \cdot 10^9 Pa$, $Qref = 3.5 \cdot 10^{-4} m^3/s$, $d = 1 \cdot 10^{-2} m$, $\rho = 860 kg/m^3$, $\upsilon = 9.7 \cdot 10^{-5} m^2/s$

Before the beginning of simulation, we need to define initial conditions for each segment's flow and pressure. It is assumed that streaming is in the steady-state regime before the beginning of the transition process.

Results on figures 10, 11 and 12 show the impact of the number of segments in the LTL model. For pipe length *L=16 m* relevant Q_2 flow changes and P_1 and P pressures are shown to a unit step input of flow rate Q_1.

Three cases were observed: *a) n=1, Ls=16 m*; *b) n=4*, *Ls=4 m* and *c) n=16*, *Ls=1m*. Figure 10 shows relevant change of Q_2 flow to step change of Q_1 flow. Figure 11 shows relative pressure change for the same change of Q_1 flow.

With increase in the number of segments, non-linearity in response comes to expression, overshoot is bigger, frequency of higher frequencies appears and delay in response becomes greater.

The following three figures (Fig. 13, 14,15) show impact of the pipeline length on transfer processes in LTL. In all three cases π segments of same length *Ls=2m* are used. Difference is only in the number of segments.

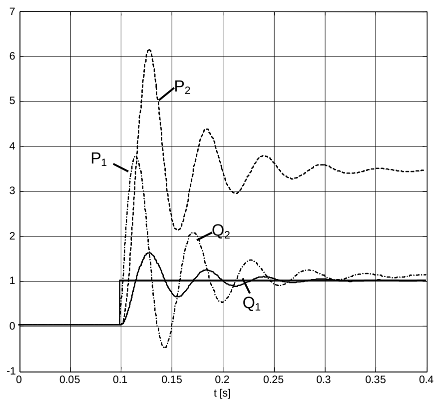

Fig.10. *Transient processes for n=1 and Ls=16 m*

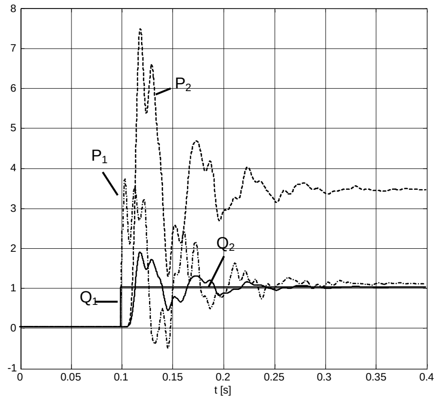

Fig.11. *Transient processes for n=4 and Ls=4 m*

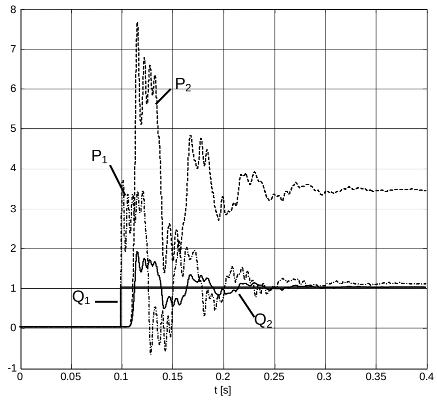

Fig.12. *Transient processes for n=8 and Ls=2 m*

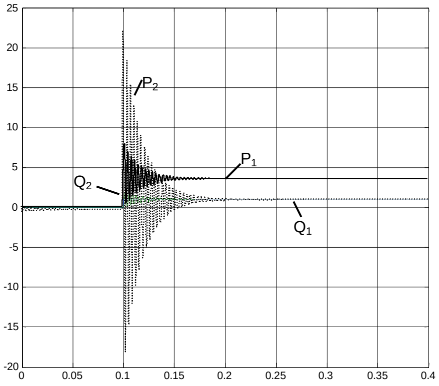

Fig.13. *Transient processes for n=1 and Ls=2 m*

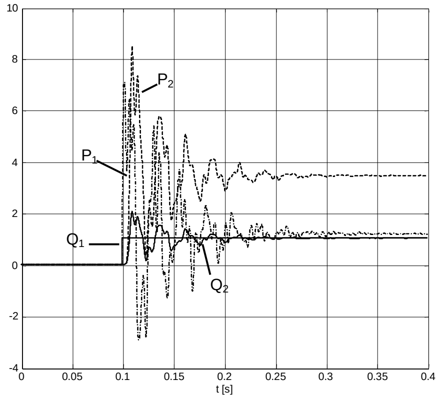

Fig.14. *Transient processes for n=4 and Ls=2 m*

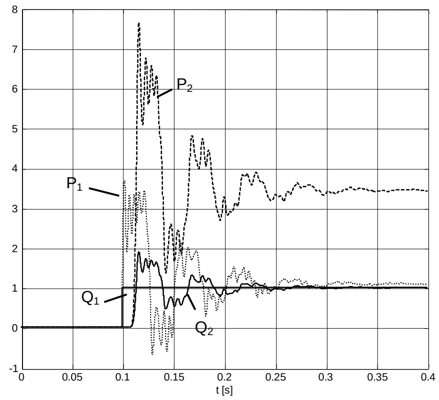

Fig.15. *Transient processes for n=8 and Ls=2 m*

With the increase of pipeline length response velocity reduces, frequency of damped oscillations reduces and response delay increases. Particularly noted is reduction of intensification on pressure P_2.

The last parameter which influence on the transfer process we are analyzing is effective bulk modulus. In previous examples we assumed that the elasticity of hydraulic pipe wall can be neglected. We also assumed that there is no entrapped vapor or gas in the fluid. Effective bulk modulus can be approximately determined using the expression [9]:

$$\frac{1}{B_e} = \frac{1}{B_c} + \frac{1}{B_l} + \frac{V_g}{V_t}\frac{1}{B_g} \tag{2}$$

where:

B_c - bulk modulus of hydraulic pipe, B_l - bulk modulus of liquid, V_g / V_t - portion of vapor or gas in total volume, B_g - bulk modulus of entrapped gas.

If we assume that $B_c = 3.45 \cdot 10^{10}\, Pa$, $B_l = 1.4 \cdot 10^9\, Pa$, $B_g = 2 \cdot 10^5\, Pa$ then transient processes for different gas percentage in the fluid look like in figures 16, 17 and 18 (n=8, Ls=2m).

Simulation results show that presence of air in LTL can have great influence on dynamics. Even with small volume share of air, character of the transfer process changes completely. Instead of oscillations, we have an aperiodic transfer process and significantly slower system reaction.

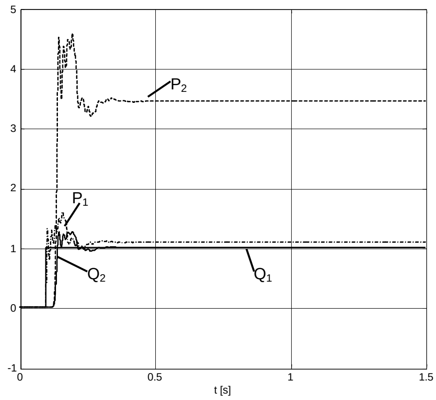

Fig.16. *Transient processes for Vg/Vt=0.001*

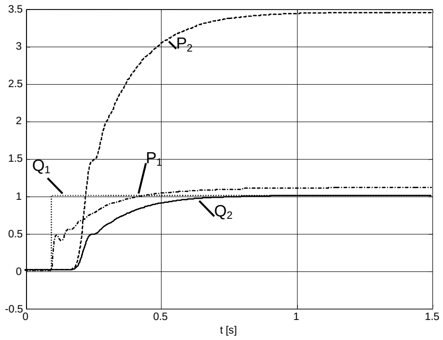

Fig.17. *Transient processes for Vg/Vt=0.01*

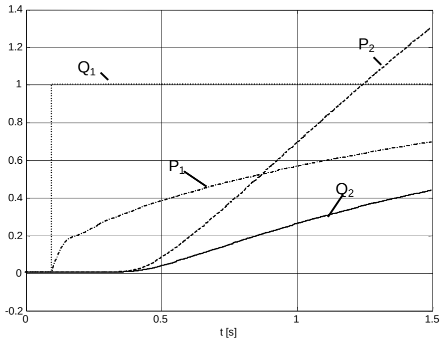

Fig.18. *Transient processes for Vg/Vt=0.1*

4. CONCLUSIONS

Model of long transmission line is derived by using the method of pipeline division on final length segments. Inside each of the segments, spatial change is abstracted and value time change is observed. Friction, inertia and compressibility are included in the model with use of bond graph elements. Simulation shows that accuracy of results depends on the number of segments the pipeline is aproximated. That number depends on the hydraulic circuit where the pipeline is located. Practically, the number o segments should be chosen so that length of one segment is no less than 2 m. This is how the mathematical model of the final order is derived with, which can further be reduces to a lower order and there with correctly describe the transient process. Besides the pipeline length, effective compressibility of fluid also greatly affects the dynamics. Presence of entrapped vapor or gas slows the transfer process and reduces oscillations in the system.

5. REFERENCES

[1] Matko, D., Geiger, G., Gregoritza, W., Pipeline simulation techniques, Mathematics and Computers in simulation, 52 (2000) 211-230.

[2] Stecki, J.S. and Davis, D.C.: Fluid transmission lines – distributed parameter models. Part 1: A review of the state of the art, Proceedings of the Institution of Mechanical Engineers. Part A: Journal of Power and Energy, Vol. 200, No. 4, pp. 215-228, 1986.

[3] Stecki, J.S. and Davis, D.C.: Fluid transmission lines – distributed parameter models. Part 2: Comparison of models, Proceedings of the Institution of Mechanical Engineers. Part A: Journal of Power and Energy, Vol. 200, No. 4, pp. 229-236, 1986.

[4] Hullender, D.A. and Healey, A.J.: Rational polynomial approximations for fluid transmission line models, in: Proceedings of the ASME Winter Annual Meeting – Fluid Transmission Line Dynamics, 15-20.11.1981, Washington, USA, pp. 33-55.

[5] Hullender, D.A., Woods, R.L. and Hsu, C.-H.: Time domain simulation of fluid transmission lines using minimum order state variable models, in: Proceedings of the ASME Winter Annual Meeting – Fluid Transmission Line Dynamics, 13-18.11.1983, Boston, USA, pp. 78-97.

[6] Söderman U. Conceptual Modelling of Physical Systems - a frame of reference Ph.D. Thesis. Linköping, Sweden: Linköping University; 1995.

[7] Watton, J., Fluid power systems: modeling, simulation, analog and microcomputer control, Prentice Hall International, 1989.

[8] Nedić, N., Filipović, V., Dubonjić, Lj., Design of Controllers With Fixed Order for Hydraulic Control System With a Long Transmission Line, FME Transactions (2010) 38, 79-86.

[9] Herbert Merritt, Hydraulic Control Systems, John Wiley & Sons, 1967.

HEAVY MACHINERY - HM 2011, 47-52
ISBN 978-86-82631-58-3
Paper accepted: 30.05.2011

Stochastic Model of a Pneumatic Actuator

Vladimir Stojanovic[1] - Vojislav Filipovic[1,*] - Novak Nedic[1]
[1] University of Kragujevac, Faculty of Mechanical Engineering Kraljevo, Kraljevo, Serbia

Abstract: *Intensive research in the field of mathematical modelling of the pneumatic cylinder has shown that its mathematical model is nonlinear and that a lot of important details cannot be included in the model. Selection of the model and the identification method have been conditioned by the following facts:*

a) The nonlinear model of the system can be approximated by a linear model with time-variant parameters

b) There is the influence of the combination of heat coefficient, unknown discharge coefficient and change of temperature on the pneumatic cylinder model. Therefore it is assumed that the parameters of the pneumatic cylinder are random (stochastic parameters)

c) In practical conditions, observations have a non-Gaussian distribution.

Due to the abovementioned reasons, it is assumed that the pneumatic cylinder model is a linear stochastic model with variable parameters. The Masreliez-Martin filter (robust Kalman filter) was used for identification of parameters of the model. For the purpose of increasing the practical value of the filter, the some heuristic modifications were performed. The behaviour of the new approach to identification of the pneumatic cylinder is illustrated by simulations.

Keywords: *pneumatic actuator, stochastic model, time-variant parameters, non-Gaussian distribution, robust filter*

1 INTRODUCTION

Since pneumatically driven systems have a lot of distinct characteristics of energy-saving, cleanliness, simple structure and operation, and high efficiency and are suitable for working in a harsh environment, they have been extensively used for many years in robot driven systems and industrial automation [1].

However, the problem with complex nonlinear models, such as the pneumatic servo cylinder, is that it is difficult to choose the large number of physical parameters involved in the model. Although a lot of parameter values are known a priori with reasonable accuracy, a large number of parameters are only known within a certain range, and some are even completely unknown. This may be due to manufacturing tolerances, or due to the fact that manufacturers do not provide parameter values because they consider them as proprietary information.

Furthermore, it is extremely difficult to accurately acquire some system parameters (such as component dimensions, internal leakage coefficients, static and dynamic friction forces, etc.) because the mentioned parameters cannot be directly measured or calculated. This causes a great difficulty in system modelling and control.

The consequence of these problems is that the theoretical model is often not useful for quantitative analysis of the pneumatic servo-system behaviour.

The purpose of this paper is to use the theory and findings of system identification to obtain a mathematical model, so that the controller can be designed on the basis of the model.

Östring et al. [2] identified the behaviour of an industrial robot in order to model its mechanical flexibilities, while Johansson et al. [3] used a state-space model to identify the robot manipulator dynamics. Assuming most parameters in pneumatic servo system do not change during operation, Shih and Tseng [4] performed the identification offline and adjusted servo-control before the operation accordingly. Furthermore, they investigated the impact of different parameters (sampling time, order model, different supply pressures, etc.) in the identification process.

The mentioned references consider the linear models of the pneumatic cylinder which are ad hoc adopted, without considering justification

[*] Corr. Author's Address: Faculty of Mechanical Engineering Kraljevo, Dositejeva 19, Kraljevo, Serbia, v.filipovic@open.telekom.rs

of such an approach. It is necessary to notice the following details:

i. The pneumatic cylinder is a nonlinear system (presence of friction force)

ii. There is a significant influence of the combination of the heat coefficient, unknown discharge coefficient and change of temperature on the behaviour of the pneumatic cylinder [5]. The mentioned influences cannot be easily included in the cylinder model and have random character.

On the other hand, recent research has shown that the nonlinear model of the system can be approximated by a linear system with time-variant parameters [6]. In this paper it is assumed that the parameters of the pneumatic cylinder model change randomly. The change of parameters is described by the random walk method, where the corresponding noise is modelled as the Gaussian stochastic process. The output error (OE) method is used as the identification algorithm. It is assumed that the measurement noise is non-Gaussian. Justification of this approach was confirmed in practice [7]. Namely, in measurements there are rare, inconsistent observations with the largest part of population of observations (outliers). Therefore, synthesis of robust algorithms is of primary interest.

The Masreliez-Martin filter is the natural frame for realization of the described algorithm. The model in the state space in which the process noise has a Gaussian distribution, and the measurement noise has a non-Gaussian distribution corresponds to the adopted model for the pneumatic cylinder.

2 MODELLING OF A PNEUMATIC SERVO SYSTEM

The system under consideration consists of an electro-pneumatic position control servo drive and a pneumatic actuator with a load as shown in Fig. 1.

Applying Newton's second law to the forces on the piston, the resulting force equation is

$$A_a P_a - A_b P_b = m\ddot{y} + \beta_e \dot{y} + F_f(\dot{y}) + k_e y + F_{ext} \quad (1)$$

where P_a and P_b denote the pressure of the chamber a and b, respectively, m denotes the total mass of the piston and the load referred to the piston, y is the piston displacement, β_e is the nonlinear viscous friction coefficient, k_e denotes the load spring gradient; and F_{ext} denotes the load force disturbance on the piston. The term F_f in equation (1) describes the summing nonlinear effects of static and Coulomb friction forces of the system.

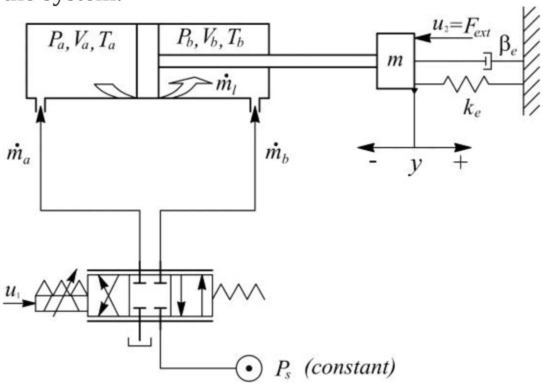

Fig. 1 *Schematic representation of the valve controlled asymmetric piston*

Pressure dynamics in the chambers, for $i = a,b$, is given by [5]:

$$\frac{dP_i}{dt} = -\alpha(t) g_i(P_i, y, \dot{y}) + \beta(t) h_i(t, P_i, y) u_1 \quad (2)$$

in which:

$$g_i(P_i, y, \dot{y}) = \frac{P_i \dot{V}_i(\dot{y})}{V_i(y)} \quad (3)$$

and

$$h_i(t, P_i, y) = \frac{\sqrt{RT_S}}{V_i(y)} W f(P_i)\,\mathrm{sgn}(u_1) \quad (4)$$

where

R is the universal gas constant, W is a spool constant, T_S is ambient absolute temperature.

If the state variables and the input variables are defined as $x_1 = y$, $x_2 = \dot{y}$, $x_3 = P_a$, $x_4 = P_b$, u_1 (valve input) $u_2 = F_{ext}$ (external disturbance) then a completely nonlinear model of the pneumatic servo-system, can be written as:

$$\begin{aligned}
&\dot{x}_1 = x_2 \\
&\dot{x}_2 = \frac{1}{m}\left(A_a x_3 - A_b x_4 - \beta_e x_2 - F_f(x_2) - \right. \\
&\left. -k_e x_1 - u_2 \right) \\
&\dot{x}_3 = -\alpha(t) g(x_1, x_2, x_3) + \beta(t) h(t, x_1, x_3) \\
&\dot{x}_4 = -\alpha(t) g(x_1, x_2, x_4) + \beta(t) h(t, x_1, x_4)
\end{aligned} \tag{5}$$

Uncertain heat coefficient $\alpha(t)$ depends on the actual heat transfer occurring during the process. As it can be seen from [5], $\alpha(t)$ takes values between 1 and 1.3997.

Uncertain bound parameter $\beta(t)$, which takes values between 0.075 and 1.3297 (see [5]), is used to characterize the combination of the heat coefficient $\alpha(t)$, the unknown valve discharge coefficient $C_d(t)$ and the variation of the temperature $\tau(t)$. Thus, $\beta(t)$ is generally expressed by:

$$\beta(t) = \alpha(t) C_d(t) \sqrt{\tau(t)} \tag{6}$$

Since uncertain heat coefficient $\alpha(t)$ and uncertain bound parameter $\beta(t)$, are only known in the certain range, it can be considered that their changes have random character. Since mentioned uncertain coefficients are involved (directly or indirectly) in the state variables, previous analysis has justified the assumption that the system is considered as stochastic.

3 STOCHASTIC MODEL OF THE PNEUMATIC ACTUATOR

The previous section shows that the mathematical model of the pneumatic cylinder in nonlinear and that it is not possible to include a large number of important details in the model. The natural way of solving this problem is to apply the identification theory. In that case the following problems arise:

- Type of the model (linear, nonlinear, deterministic, stochastic)
- Nature of disturbance (uniformly constrained, stochastic)

The following three facts have conditioned the choice of the model:

a) Recent research has shown that the nonlinear model of the system can be correctly approximated by a system with time variant parameters [6]

b) A more detailed analysis of the pneumatic cylinder model described in the previous section shows that the combination of heat coefficient, unknown discharge coefficient and change of temperature influences the model of cylinder [5]. Those influences are random and therefore it is assumed that the parameters of the pneumatic cylinder are random.

c) Practical and theoretical research has shown that in a stochastic model of the system there are some observations that are inconsistent with the largest part of the population (outliers) [7], and that is why the disturbance in the model (measurement noise) is non-Gaussian.

The mentioned reasons lead to the assumption that the model of the pneumatic cylinder is a stochastic linear model with time variant parameters.

Taking into account the physics of the problem, it will be assumed that the change of the parameters has the form of random walk

$$\theta(k+1) = \theta(k) + \omega(k) \tag{7}$$

where the stochastic process $\omega(k)$ is Gaussian with the mean value zero and the covariance matrix $W(k)$.

The output error method based on systems with a reference model will be used as a model which describes the dynamics of the pneumatic cylinder.

The output of the model without disturbance will be denoted as $y_n(k)$. The dynamics of the model in that case is described as

$$\begin{aligned}
&y_n(k) = -a_1(k) y_n(k-1) - \ldots - a_n(k) y_n(k-n) \\
&+b_1(k) u(k-1) + \ldots + b_m(k) u(k-m)
\end{aligned} \tag{8}$$

Let us introduce the following vectors

$$\theta(k)=[a_1(k),\ldots,a_n(k),b_1(k),\ldots,b_m(k)]^T \tag{9}$$

$$\begin{aligned}\varphi_0(k)=[-y_n(k-1),\ldots,-y_n(k-n),\\ u(k-1),\ldots,u(k-m)]^T\end{aligned} \tag{10}$$

In that case the dynamics of the system with disturbance is given by the following relation

$$y(k)=\theta^T(k)\varphi_0(k)+\nu(k) \tag{11}$$

The disturbance $\nu(k)$ is non-Gaussian and includes the presence of outliers.

The problem with the relation (8) is that the values $y_n(k-i)$, $(i=1,2,\ldots,n)$ cannot be measured. Therefore, these values are calculated by using the current estimates of the parameters θ. It results in

$$\begin{aligned}\hat{y}_n(k)=-\hat{a}_1(k)\hat{y}_n(k-1)-\ldots-\hat{a}_n(k)\hat{y}_n(k-n)\\ +\hat{b}_1(k)u(k-1)+\ldots+\hat{b}_m(k)u(k-m)\end{aligned} \tag{12}$$

the following vectors are introduced

$$\hat{\theta}(k)=[\hat{a}_1(k),\ldots,\hat{a}_n(k),\hat{b}_1(k),\ldots,\hat{b}_m(k)]^T \tag{13}$$

$$\begin{aligned}\varphi(k)=[-\hat{y}_n(k-1),\ldots,-\hat{y}_n(k-n),\\ u(k-1),\ldots,u(k-m)]^T\end{aligned} \tag{14}$$

the relation

$$\hat{y}_n(k)=\hat{\theta}^T(k)\varphi(k) \tag{15}$$

is obtained. At the moment k, before the estimate $\hat{\theta}(k)$ is known, the prediction of the model is [8]

$$\hat{y}(k)=\hat{\theta}^T(k-1)\varphi(k) \tag{16}$$

The natural definition of the prediction error is

$$\nu(k)=y(k)-\hat{y}(k) \tag{17}$$

Let us assume that the system in the state space can be described as

$$x(k+1)=F(k)x(k)+w(k) \tag{18}$$

$$y(k)=H(k)x(k)+v(k) \tag{19}$$

where

$x(\cdot)\in R^n$, $F(\cdot)\in R^{n\times n}$, $w(\cdot)\in R^n$

$y(\cdot)\in R^1$, $H(\cdot)\in R^{1\times n}$, $v(\cdot)\in R^1$

The value $x(\cdot)$ is the state vector, $y(\cdot)$ is the system output, and $w(\cdot)$ and $e(\cdot)$ are the process noise and the measurement noise, respectively. It is assumed that the process noise is Gaussian $\mathrm{N}(0,\mathrm{W(k)})$, where $\mathrm{W(k)}$ is the covariance matrix, and $\nu(\cdot)$ is the measurement noise which has non-Gaussian distribution.

In reference [9] Masreliez and Martin proposed the robust Kalman filter for the mentioned situation. This filter has small sensitivity to the presence of outliers in comparison with the standard Kalman filter deduced for the case when the values $w(\cdot)$ and $\nu(\cdot)$ have Gaussian distribution.

The originally proposed robust Kalman filter [9] includes two values which are not easy to determine in practical conditions. They are the scalar transformation $T(k)$ as well as the member in the a posteriori covariance matrix $E_{f_0}\left\{\psi^{'}(\nu(k))\right\}$. The mentioned member represents Fisher information for the least favourable probability density [10]

$$I(p)=\int_{-\infty}^{\infty}\frac{p^{'2}(\zeta)}{p(\zeta)}d\zeta \tag{20}$$

In order to increase the practical values of the robust Kalman filter [9] the following heuristics were performed:

a) For the scalar transformation $T(k)$ it has been adopted that $T(k)=1$
b) The member $E_{P_\varepsilon}\left\{\psi^{'}(\nu(k))\right\}$ was approximated by the realization of $\psi^{'}(\nu(k))$

Intense simulations justified such interventions. Now the proposed robust Kalman filter [9] obtains the following modified form:

$$\begin{aligned}\hat{x}(k|k)=F(k-1)\hat{x}(k-1|k-1)+P(k|k-1)\cdot\\ H^T(k)\cdot\psi[y(k)-H(k)F(k-1)\hat{x}(k-1|k-1)]\end{aligned} \tag{21}$$

$$\begin{aligned}P(k|k-1)=F(k-1)P(k-1|k-1)F^T(k-1)+\\ +W(k-1)\end{aligned} \tag{22}$$

$$P(k|k) = P(k|k-1) - P(k|k-1)H^T(k)H(k)\cdot$$
$$P(k|k-1)\cdot \qquad (23)$$
$$\cdot\psi'\left(y(k) - H(k)F(k-1)\hat{x}(k-1|k-1)\right)$$

It is important to notice that the second heuristic modification increases the rate of convergence (21)-(23) in the initial iterations. Namely, the relations (21)-(23) for the robust Kalman filter gain result in:

$$K(k) = F(k-1)\left[P(k-1|k-2) -\right.$$
$$-P(k-1|k-2)H^T(k)H(k)P(k-1|k-2)\cdot \qquad (24)$$
$$\left.\cdot\psi'\left(\nu(k)\right)\right]F^T(k-1)H^T(k) + W(k-1)H^T(k)$$

If $|\nu(k)| > k_\varepsilon$, the relation (24) becomes

$$K(k) = F(k-1)P(k-1|k-2)F^T(k-1)\cdot$$
$$H^T(k-1) + W(k-1)H^T(k) \qquad (25)$$

It means that the bigger the estimation errors, the higher the filter gain and thus the higher rate of estimation convergence.

By comparing the relations (7) and (11) with the relations (18) and (19) and taking care that the vector $\varphi_0(k)$ should be replaced with $\varphi(k)$ and by substituting for the values

$$F(k) = I\,,\ H(k) = \varphi^T(k)\,,\ \hat{x}(k|k) = \hat{\theta}(k) \qquad (26)$$

a recursive algorithm for estimation of time-variant parameters is obtained in the relation (21)-(23).

4 ILUSTRATIVE EXAMPLE

The model of a pneumatic cylinder whose time varying parameter vector has the expected value:

$$\bar{\theta} = [-0.9131 \quad -0.3523 \quad 0.1118 \quad 0.2318$$
$$-0.0413 \quad 0.0766 \quad 0.0115 \quad 0.0647]^T \qquad (27)$$

is considered for the purpose of demonstrating the performance of the proposed robust procedure for parameters estimation. The process noise $\omega(k)$ is Gaussian with the zero mean value and the covariance matrix

$W(k) = E\left\{\omega(k)\omega(k)^T\right\}$, where

$$\omega(k) = [w_1(k) \quad w_2(k) \quad w_3(k) \quad w_4(k)$$
$$w_5(k) \quad w_6(k) \quad w_7(k) \quad w_8(k)]^T \qquad (28)$$

If the probability density is denoted as $p_N(\cdot) \sim N(m,\sigma_N^2)$ where m is the mean value, and σ_N^2 is the dispersion, then:

$$p_N(w_1) \sim \mathrm{N}(0;2\cdot10^{-6}), \qquad p_N(w_5) \sim \mathrm{N}(0;2\cdot10^{-8}),$$
$$p_N(w_2) \sim \mathrm{N}(0;3\cdot10^{-6}), \qquad p_N(w_6) \sim \mathrm{N}(0;2.2\cdot10^{-8}),$$
$$p_N(w_3) \sim \mathrm{N}(0;2.5\cdot10^{-6}), \qquad p_N(w_7) \sim \mathrm{N}(0;2.5\cdot10^{-8}),$$
$$p_N(w_4) \sim \mathrm{N}(0;2.2\cdot10^{-6}), \qquad p_N(w_8) \sim \mathrm{N}(0;3\cdot10^{-8}).$$

Figures 2 to 5 show the system output, parameter estimates, and mean square error in the case when the contamination $\varepsilon = 0.05$.

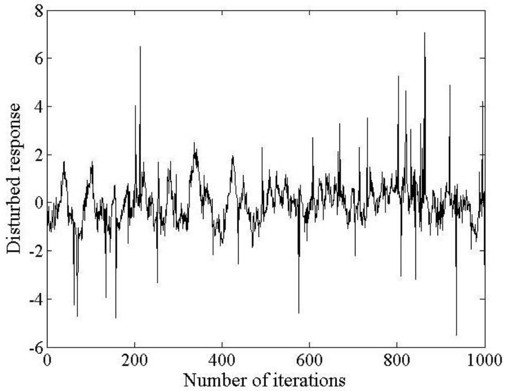

Fig. 2 *Simulation of the measured output signal of the system with the contamination* $\varepsilon = 0.05$

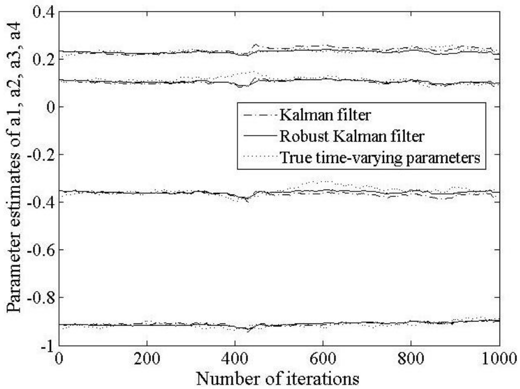

Fig. 3 *Estimates of the parameter* a_i *obtained in a non-Gaussian noise environment with the contamination* $\varepsilon = 0.05$

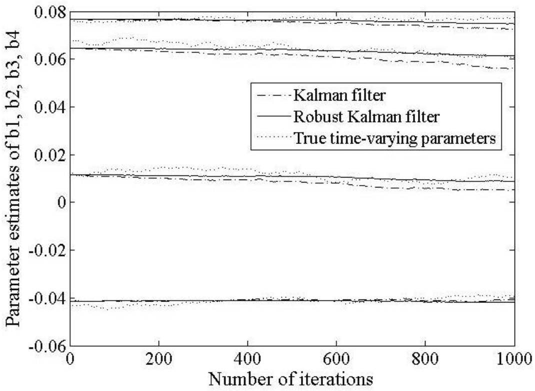

Fig. 4 *Estimates of the parameter* b_i *obtained in a non-Gaussian noise environment with the contamination* $\varepsilon = 0.05$

The simulation results are compared in terms of mean square error (MSE), defined by

$$MSE = \log\left(\left\|\hat{\theta}(k) - \theta(k)\right\|^2\right) \quad (29)$$

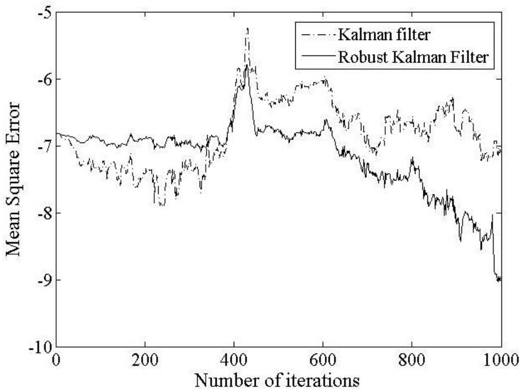

Fig. 5 *Mean square error, obtained in a non-Gaussian noise environment with the contamination* $\varepsilon = 0.05$

***Remark 1*:** The presented results have shown that the classical Kalman filter is very sensitive to the non-Gaussian measurement noise presence, as opposed to the proposed robust Kalman filter.

5 CONCLUSION

The paper considers a new mathematical model of the pneumatic cylinder. Change of parameters of the model is described by random walk. It is assumed that the cylinder is described by means of the output error model, where the measurement noise is non-Gaussian. Since the system is described with a stochastic model with variable parameters, the natural frame for identification is the Masreliez-Martin filter (the robust Kalman filter). Heuristic modifications of the mentioned filter which considerably increase its practical values were performed. The results of this paper can be the starting point for design of an adaptive regulator.

6 REFERENCES

[1] Pu J, Moore PR, Wong CB (2000) Smart components-based servo pneumatic actuation systems. Microprocessors and Microsystems 24: 113–119

[2] Östring M, Gunnarson S, Norrlöf M (2003) Closed-loop identification of an industrial robot containing flexibilities. Control Engineering Practice 11(3): 291-300

[3] Johansson R, Robertsson A, Nilsson K, Verhaegen M (2000) State-space system identification of robot manipulator dynamics. Mechatronics, 10(3): 403-418

[4] Shih MC, Tseng S (1995) Identification and position control of a servo pneumatic cylinder. Control Engineering Practice 3(9): 1285-1290

[5] Khayati K, Bigras P, Dessaint LA (2008) Force control loop affected by bounded uncertainties and unbounded inputs for pneumatic actuator systems. Transactions of the ASME – Journal of Dynamic Systems, Measurement, and Control, 130(1): 1-9

[6] Rodriguez MT, Banks SP (2010) Linear, time-varying approximations to nonlinear dynamical systems: with applications in control and optimization. Springer

[7] Barnett V, Lewis T (1994) Outliers in Statistical Data. 3rd ed. Wiley-Blackwell, New Jork

[8] Landau ID, Lozano R, M'Saad M (1998) Adaptive Control, 1st edn. Springer

[9] Masreliez CJ, Martin RD (1977) Robust Bayesian estimation for the linear model and robustifying the Kalman filter. IEEE Transactions on Automatic Control 22(3): 361–371

[10] Filipovic VZ, Kovacevic BD (1994) On robust AML identification algorithms. Automatica, 30(11): 1775-1778

HEAVY MACHINERY - HM 2011, 53-58
ISBN 978-86-82631-58-3
Paper accepted: 30.05.2011

Determination of the Optimal Strategy For Preventive Maintenance of the Control Block of Special Purpose Vehicle

Stojko LJ. Biočanin[1,*], Dušan D. Golubović[2], Ranko C. Božičković[2], Milan R. Pavlović[1]
[1]Tehnički remontni zavod "Čačak"
[2]Mašnski fakultet Istočno Sarajevo

The application of preventive maintenance contributes significantly to providing the required level of readiness of complex technical systems used in organizations of special purpose. The basic requirement in applying this model of maintenance is to determine the optimal periodicity that should satisfy some, mutually conflicting criteria. This paper presents a methodology for determining the periodicity of preventive maintenance control block on the basis of collecting and processing statistical data about their malfunctions. This problem can be solved if all important requests and limitations are determined. The basis of the presented methodology is the reliability parameters of the analyzed control block, obtained by observing this unit behaviour, from the aspect of occurrence of failure in real service conditions, and also its maintenance costs.

Key words: control block, maintenance, optimization, availability, reliability, costs

1. INTRODUCTION

Having applied the preventive maintenance model, the optimization of maintenance system endeavours to find the answer whether it is useful to apply preventive maintenance as maintenance model, and if so, to determine after how much time, the procedure of preventive maintenance should be applied.

For the given control block and conditions of use and maintenance which enable the preferences to be known in advance, there is just one optimal solution of maintenance strategy. In this case the most favourable values of reliability, readiness, costs of use and maintenance are achieved and total costs of the lifecycle. The task of the optimization of maintenance system of the control block is to find that optimum.

2. DETERMINATION OF THE LAW ON SERVICE TIME DISTRIBUTION TO CONTROL BLOCK BREAKDOWN

Finding the adequate mathematical model which can represent the law on behaviour of the control block, from the aspect of breakdown occurrence, is one of the basic elements for the optimization of its maintenance. This phase of analysis is very important since all further conclusions and decisions regarding the appropriate measures related to the maintenance of the requested level of reliability of control block depend on the determination of the model of reliability distribution. The methodology of determination of the most acceptable model of control block maintenance is presented for the selected special purpose vehicle.

The object of research is a hydraulic control block of the device for control of special purpose vehicle.

The procedure for determination of the law on operation time distribution to breakdown, based on empiric data, is executed in three steps. The first step includes the evaluation of the reliability values and/or determination of the statistic set features and evaluation of values of complete features of random variable. Based on the values obtained in the first step, the second step includes determination of the theoretical model of distribution which may be used for the approximation of the empiric distribution. The third step includes the confirmation of the adopted theoretical model of distribution with empiric distribution [1].

92 breakdowns of special purpose vehicles have been registered. All 92 breakdowns are distributed into two groups: first, which consists of vehicle operation times to control block breakdown, as it is presented in columns 1 to 3 of table 1; and second, which consists of special purpose vehicle operation times to the moment of exclusion from further testing due to vehicle breakdown whose cause is not control block.

Based on data from columns 1 to 3 of table 1, the reliability values are determined – functions

*Corr. Author's Address: Tehnički remontni zavod Čačak., trzca@ptt.rs

of cumulative probability distribution (unreliability function), reliability function, breakdown intensity function and frequency function (density) of breakdown state, by using the small sample method and with exclusion from results on vehicle breakdown whose cause is not control block breakdown [3].

Evaluated values of reliability indexes are given in columns 4 to 11 of table 1

Table 1. *Data on operation time to control block breakdown and evaluated values of reliability indexes*

No. of control block breakdown	Ordinal number of vehicle breakdown	Opera-tion time to breakdown t [mh]	Increase in ordinal number -- P	Actual rank – SR	Median rank -MR [%]	Operation time between breakdowns Δt [mh]	Unreliability function – F	Reliability function – R	Breakdown intensity function h [mh^{-1}]	Density function in state of breakdown – f [mh^{-1}]
1	2	3	4	5	6	7	8	9	10	11
1	5	111	1,0449	1,0449	0,8062	36	0,0081	0,9919	3,03E-04	3,01E-04
2	6	147	1,0449	2,0899	1,9371	96	0,0194	0,9806	1,15E-04	1,13E-04
3	20	243	1,2285	3,3184	3,2667	8	0,0327	0,9673	1,40E-03	1,35E-03
4	22	251	1,2456	4,5640	4,6147	50	0,0461	0,9539	2,27E-04	2,16E-04
5	32	301	1,4264	5,9904	6,1584	29	0,0616	0,9384	3,98E-04	3,73E-04
6	36	330	1,5002	7,4905	7,7820	38	0,0778	0,9222	3,09E-04	2,85E-04
7	45	368	1,7451	9,2356	9,6706	21	0,0967	0,9033	5,71E-04	5,15E-04
8	48	389	1,8210	11,0566	11,6413	86	0,1164	0,8836	1,42E-04	1,26E-04
9	60	475	2,4101	13,4667	14,2497	57	0,1425	0,8575	2,21E-04	1,90E-04
10	68	532	3,0590	16,5257	17,5602	87	0,1756	0,8244	1,51E-04	1,24E-04
11	79	619	5,0983	21,6240	23,0779	80	0,2308	0,7692	1,76E-04	1,35E-04
12	84	699	7,1376	28,7616	30,8026		0,3080	0,6920		

Table 1 shows:

- total number of data (sample size): n= 12,
- minimal operation time to breakdown: t_{min} = 111 mh,
- max. operation time to breakdown: t_{max} = 699 mh.

Statistical measures are calculated based on data from table 1:

- median of operation time to breakdown: t_{sr} = 372,0833 mh,
- standard deviation of operation time to breakdown: SD = 181,2294 mh,
- median operation time to breakdown: median = 349 mh,
- rank (range) of operation time to breakdown: rank = 588 mh.

Based on data from table 1, by the methodology application [1, 2, 3], for approximate theoretical model of reliability of control block, Weibull distribution is adopted with the parameter $\beta = 2{,}0121$ and scale parameter

η = 1.169,7455, thus the expression for reliability function of control block is:

$$R(t) = e^{-\left(\frac{t}{\eta}\right)^{\beta}} = e^{-\left(\frac{t}{1.169{,}7455}\right)^{2{,}0121}}$$

In calculating the reliability function in accordance with the above expression, the variable "t" is expressed in special-purpose vehicle motor hours of operation.

3. DETERMINATION OF PERIODICITY OF CONTROL BLOCK MAINTENANCE

ACCORDING TO CRITERION OF MAXIMUM READINESS

For special purpose vehicles, the most appropriate is the application of the optimization criteria according to the model of maximum readiness.

Value of exploitation readiness may be determined by the expression [4]:

$$G(t) = \frac{t_r + t_{čr}}{t_r + t_{čr} + t_p + \frac{F(t)}{R(t)} \cdot t_k}$$

Where:

- t_r – operation time,
- $t_{čr}$ – time of waiting for operation in good working order,
- t_p – time of preventive maintenance,
- t_k – time of correction maintenance,
- R(t) – reliability function,
- F(t) – unrealiability function.

By varying the periodicity of time between preventive maintenance, functional dependence of readiness on maintenance periodicity is obtained, based on which the periodicity of maintenance may be determined which gives maximum

Table 2. *Results of readiness determination for different periodicities of maintenance of special purpose vehicle control block*

Periodicity of maintenance [mh]	100	200	300	400	500	600	700	800	900	1000
Operation time t_r [mh]	100	200	300	400	500	600	700	800	900	1000
Preventive maintenance time t_p [mh]	0,8	0,8	0,8	0,8	0,8	0,8	0,8	0,8	0,8	0,8
Correction maintenance time t_k [mh]	9,3	9,3	9,3	9,3	9,3	9,3	9,3	9,3	9,3	9,3
Unreliability function F(t)	0,0071	0,0282	0,0627	0,1090	0,1654	0,2297	0,2994	0,3722	0,4457	0,5178
Reliability function R(t)	0,9929	0,9718	0,9373	0,8910	0,8346	0,7703	0,7006	0,6278	0,5543	0,4822
Number of corrective maintenances between two preventive n_k	0,0071	0,0290	0,0668	0,1223	0,1982	0,2982	0,4274	0,5929	0,8042	1,0739
Time of corrective maintenance between two preventive t_{k2p} [mh]	0,0662	0,2700	0,6216	1,1379	1,8435	2,7733	3,9753	5,5144	7,4787	9,9876
time of waiting for operation in good working order $t_{čr}$ [mh]	2.300	4.600	6.900	9.200	11.500	13.800	16.100	18.400	20.700	23.000
Readiness G(t)	0,99964	0,99978	0,99980	0,99980	0,99978	0,99975	0,99972	0,99967	0,99962	0,99955

Table 2 shows that the maximum readiness for t_r in interval from 200 to 500 mh.

Discretization of intervals of periodicity of maintenance (= operation time t_r) from 100 to 1000 with step 1 is used to calculate maximum value of readiness and periodicity of maintenance for maximum readiness.

Image 1 presents graphical representation of dependence of readiness on periodicity of preventive maintenance of control block.

As the result of discretization and based on image 1, it may be concluded that the maximum readiness of control block G_{max} = 0,9998 is obtained for periodicity of maintenance t_r = 325 mh, because for that periodicity of maintenance function $G(t_r)$ reaches its local maximum, thus it may be considered that the optimal periodicity of maintenance of control block for the criterion of maximum readiness.

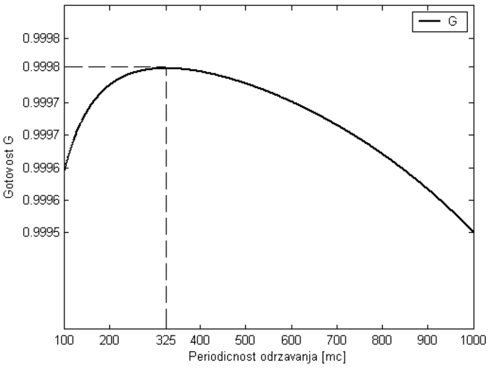

Fig. 1. *Graphical representation of dependence of readiness on periodicity of preventive maintenance of control block*

4. DETERMINATION OF PERIODICITY OF MAINTENANCE OF CONTROL BLOCK ACCORDING TO THE CRITERION OF MINIMAL COSTS

Optimization of maintenance system may be performed based on the model which as the criterion of optimization uses minimal maintenance costs.

Maintenance costs may be expressed in the form [4]:

$$C(t) = \frac{C_k - (C_k - C_p)\cdot R(t)}{\int_0^T R(t)dt}$$

Where:

- C(t) – total specific maintenance costs,
- Ck – corrective maintenance costs,
- Cp – preventive maintenance costs,
- R(t) – reliability function,
- T – operation time of control block to breakdown.

By application of the above mentioned expression for the maintenance costs, for different periods of preventive maintenance of control block, the values of maintenance costs have been obtained, which are presented in table 3.

Table 3. *Results of determination of maintenance costs for different periodicities of control block maintenance*

Maintenance periodicity [mh]	100	200	300	400	500	600	700	800	900	1000
Corrective maintenance costs C_k [nj]	966	966	966	966	966	966	966	966	966	966
Preventive maintenance costs C_p [nj]	350	350	350	350	350	350	350	350	350	350
Reliability function R(t)	0,9929	0,9718	0,9373	0,8910	0,8346	0,7703	0,7006	0,6278	0,5543	0,4822
$\int_0^T R(t)dt$	99,765	198,116	293,679	385,188	471,541	551,840	625,417	691,849	750,947	802,750
Total specific costs C(t) [nj]	3,552	1,854	1,323	1,083	0,958	0,891	0,855	0,837	0,832	0,833

Note: sign "nj" in table 4 means "currency". Table 4 shows that minimal costs of maintenance are achieved for periodicity of maintenance from 800 to 1000 mh.

By discretisation of interval of periodicity of maintenance from 100 to 1500 with step 1, minimal total specific costs and periodicity for minimal total specific costs are calculated.

Image 2 is graphical representation of total specific costs for periodicity of preventive maintenance of control block.

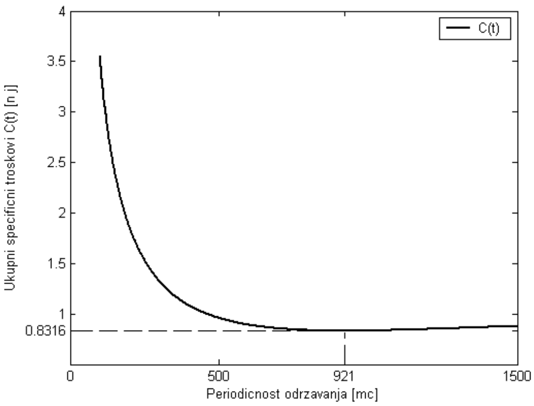

Fig. 2. *Graphical representation of dependence of total specific costs on periodicity of preventive maintenance of control block*

As the result of dicretisation and based on image 2, it may be concluded that the smallest costs, C_{min} = 0,8316 [nj], are obtained for the periodicity of maintenance t_r =921 mh, because for that periodicity of function $C(t_r)$ the local minimum is achieved, thus it may be considered the optimum periodicity of maintenance of control block for the criterion of minimal costs.

5. DETERMINATION OF THE OPTIMUM PERIOD OF PREVENTIVE MAINTENACE OF CONTROL BLOCK BY APPLICATION OF MULTI-CRITERIA OPTIMIZATION

Since the optimum periodicity of implementation of the procedure of preventive maintenance determined according to the criterion of maximum readiness and the one determined according to the criterion of minimum costs of maintenance, differ, it is necessary to apply methods of multi-criteria analysis and determine the value of requested optimum periodicity of implementation of procedures of preventive maintenance, taking into consideration both criteria of optimization. In order to solve this problem, the method of weight coefficients [5].

The set of alternatives is represented by the set of index alternatives. The problem is represented by the matrix: L = [l_{ik}].

l_{ik} is the value of the criterion of optimization **k** for alternative **i**:

- $l_{i1} = G_i$ – value of the criterion of readiness optimization for alternative **i**,
- $l_{i2} = C(t_i)$ value of the criterion of optimization of costs for alternative **i**.

The operation period t_r is considered from 100 to 1000 [mh] in which both criteria achieve local extremes.

In order to determine the optimum period of preventive maintenance, regarding the criterion of maximum readiness (G) and minimum maintenance costs (C(t)), interval from 100 to 1000 [mh] by discretization with step 1.

In general case, the criteria of optimization are different in nature, they have different values and different measurement units. That means that the values of the optimization criterion, for one alternative **i** cannot be compared. Due to this reason it is necessary to carry out the procedure of normalization through which all values l_{ik} are used in interval [0,1].

When using vector normalisation, the problem of decision making can be presented by the matrix: L = [l_{ikn}], where likn – normalised value of the optimization criteria **k** for alternative **i**.

In order to select the best, to each considered alternative is added a certain value:

$$a_i = \frac{\sum_{k=1}^{2} w_k \cdot l_{ikn}}{\sum_{k=1}^{2} w_k}$$

where w_k – weight coefficients [5].

Regarding the purpose of the vehicle, it may be considered that the criterion of the readiness optimization is more important than the criterion of costs optimization and in accordance with this the following shall be adopted $w_1=0{,}7$ *i* $w_2=0{,}3$. The best alternative **i** is the one for which a_i has the biggest value.

Image 3 is the graphical representation of finding the best alternative.

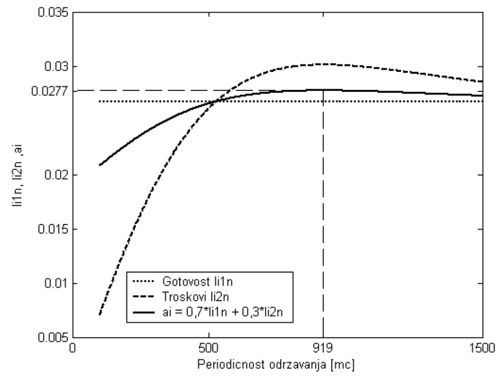

Fig.3 .*Graphical representation of finding the best alternative*

As the result of discretization and based on image 3, it can be concluded that maximum value a_{imax} = 0,0277 is obtained during preventive maintenance (operation time) t_r = 919 mh.

Optimized period of prevention change of control block, with regard to the criterion of maximum readiness (as more important with weight coefficient 0,7) and criterion of minimum maintenance costs (as less important with weight coefficient 0,3) is 919 mh.

6. CONCLUSION

Optimized periodicity of implementation of procedures of prevention maintenance differs whether it is determined according to the criterion of maximum readiness or according to the criterion of minimum costs. Therefore, it is necessary to apply methods of multi-criteria analysis and determine the value of searched optimum periodicity of implementation of procedures of preventive maintenance, taking into consideration both optimization criteria.

The value of optimized periodicity of implementation of procedures of preventive maintenance of control block is determined according to the criteria of maximum readiness as 325 mh, and according to the criterion of minimum maintenance costs is 921 mh. Having applied the method of multi-criteria analysis, we have obtained the value of optimum periodicity of implementation of procedures of preventive maintenance, taking into consideration both criteria of optimization is 919 mh of operation.

The presented methodology of multi-criteria decision making may be applied in order to obtain the values of periodicity of implementation of procedures of preventive maintenance of control block for special purpose vehicles, but also for other integral parts. It is necessary to have the data obtained by monitoring of the set during its exploitation, based on which indexes of its reliability may be determined, as well as system characteristics of its maintenance.

7. REFERENCES

[1] Dr Dobrivoje Ćatić: Razvoj i primena metoda teorije pouzdanosti, Mašinski fakultet, Kragujevac, 2005

[2] Dr Gradimir Ivanović, dr Dragutin Stanivuković: Pouzdanost – analiza i projektovanje, Tehnička uprava SSNO, 1988

[3] Dr Jezdimir Knežević: Upravljanje procesima održavanja i obnavljanja tehničkih sistema na osnovu teorije pouzdanosti, "OMO" Belgrade, 1988

[4] Dr Božidar Krstić: Eksploatacija motornih vozila i motora, Mašinski fakultet, Kragujevac, 1997.

[5] Dr Serafim Opricović: Višekriterijumska optimizacija, Građevinski fakultet Univerziteta u Beogradu, Naučna knjiga, Belgrade, 1986

HEAVY MACHINERY - HM 2011, 59-62
ISBN 978-86-82631-58-3 Paper accepted: 30.05.2011

On Some Energy Losses And Flow Energetic Parametrs of Transitions Regimes of Hydrodinamic Processes of Pumps

Zoran Glavcic[1,*]
[1] University of Kragujevac, Faculty of Mechanical Engineering Kraljevo

The aproach to the problem is original and consists of defining and establishing integral perameters of swirling flow where special attention is paid to the so called energetic parameters. Effects of a local ressitence and causal losses of flow energy on the course of transition process in hydraulics pumps are analysed in the paper.

Keywords: Swirling flow, hydrodinamic pump, energetic parameter, flow energetic los

1. I NTRODUCTION

Complexity of hydrodynamic and dynamic processes in pumps (pump cylinder, intake and discharge space, discharge valve and pipeline of high pressure) demands very studious physical and mathematical analysis the same processes. Based on the experimental research results and the results of the mathematical modeling developing and application of the identification method of unknown parameters of the mathematical modeling of non stationary high dynamic processes and optimization technique.

Intake and discharge space, discharge valve and pipeline can be expressed as local resistence the so/called whirling flow is formed that appears only in case of non/stationary flow of fluids. Figure 1 and Figure 2 expressed local resistence, in case constructions vane and piston/radial pumps.

To form the said whirling flow additional energy is introduced wich remains in the whirl itself for entire process duration. As this energy remains in the whirling flow, it is reactive by its character unlike the active energy that turns later into heat. Energy losses greatly infkuence transition processes advancement, they have to be briefly defined and explained.

Flow at the level of macro/swirl takes place at those thubing spots where there are complex geometric structures.

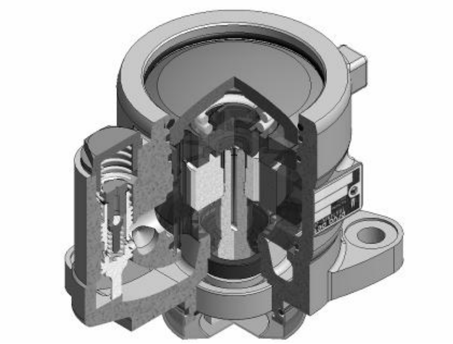

Fig. 1. *Construction and control spaces of a vane pump*

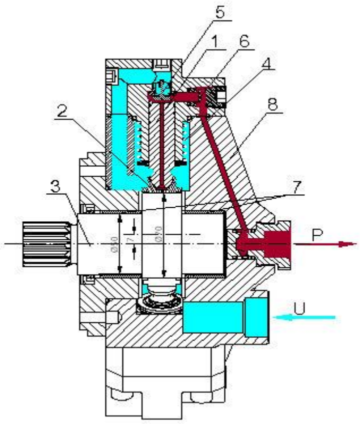

1- piston, 2- shoe, 3-drive shaft, 4-spring, 5-inlet valve, 6- outlet valve, 7-bearing, 8-housing

Fig. 2. *Construction and control spaces of a piston-radial pump*

---

*Corr. Author's Address: Faculty of Mechanical Engineering Kraljevo, Serbia, glavcic.z@mfkv.kg.ac.rs

2. ENERGY LOSS OF WHIRLE FLOW IN CONTROL SPACE OF PUMPS

The papers [2], [3] showed that

$$\frac{\varsigma_v}{\varsigma} = 1 + \frac{k}{\Omega_0^m}, . \qquad (1)$$

where are: ζ - coefficinet of axial energy loss on axial flow, k and m - coeficients of flow and Ω_0 - parameter of swirl flow directly after local resistence. Whirl flow parameter has the following:

$$\Omega = \frac{\dot{V}}{R\Gamma} = \frac{\int_0^R v_x r dr}{R\int_0^R r v_\varphi v_x r dr}, . \qquad (2)$$

where is

$$\Gamma = \frac{4\pi^2}{\dot{V}} = \frac{\int_0^R v_x r dr}{R\int_0^R r v_\varphi v_x r dr}.$$

mean-made unit circulation.

Mathematical model of whirl flow, after local resistence on entire of pump, based on kinetic energy change, is given in the following shape:

$$\begin{aligned} &\zeta_v \rho \frac{v_x^2}{2} + \frac{1}{2} v_x^2 \int_x \frac{\partial \beta_v}{\partial t} dx \ + \\ &+\rho \frac{dv_x}{dt} \int_x \beta_v dx + \lambda_v \frac{\rho v_x^2}{2} = 0, \end{aligned} . \qquad (3)$$

where are: index "v" is whirle flow, "x" index mean stream and β- Businesk's coefficient.

The paper [4] and [5] is defined and Coriolis's coeficient. Upon analysis, we come to:

$$\alpha_v = \frac{1}{Av_x^3}\left[\int_A v_x^3 dA \left(1 + \frac{\int_A v_\varphi^2 v_x dA}{\int_A v_x^3 dA}\right)\right], . \qquad (4)$$

$$\beta_v = \frac{1}{Av_x^2}\left[\int_A v_x^2 dA \left(1 + \frac{\int_A v_\varphi^2 dA}{\int_A v_x^2 dA}\right)\right].. \qquad (5)$$

Based on papers [2] and [3], expressions (4) and (5) are transformed into the following shapes:

$$\alpha_v = \alpha(1+\Theta), . \qquad (6)$$

$$\beta_v = \beta\left(1 + \frac{\int_A v_\varphi^2 dA}{\int_A v_x^2 dA}\right).. \qquad (7)$$

whwre is Θ - magnitude of swirl defined as

$$\Theta = \frac{\int_A v_\varphi^2 v_x dA}{\int_A v_x^3 dA}.. \qquad (8)$$

Defined and swirl flux as

$$S = \frac{\int_A r v_\varphi v_x dA}{\int_A v_x^2 dA}.. \qquad (9)$$

Parameters Ω, Θ and S defining losses energy on intake of pumps. From expression (7) we can define coefficient

$$E_v = \frac{\int\limits_A v_\varphi^2 dA}{\int\limits_A v_x^2 dA},. \qquad (10)$$

which can be called energetic parameter of swirl flow, as it represents the relation between kinetic energy of circumference flow and kinetic energy of axial flow.

3. INFLUENCE OF ENERGETIC PARAMETERS ON OTHER INTEGRAL PARAMETERS IN CONTROL SPACE OF PUMP

By taking equations (4) to (10), it is obtained that

$$\alpha_v = (1+\Theta)\left(\frac{3}{2\Omega S} - 2\right),. \qquad (11)$$

and

$$\beta_v = \frac{(1+E_v)}{3}\left(\frac{3}{2\Omega S} - 4\right) \quad \text{or}$$
$$\beta_v = \frac{(1+E_v)}{3}\left(\frac{\alpha_v}{1+\Theta} - 2\right). \qquad (12)$$

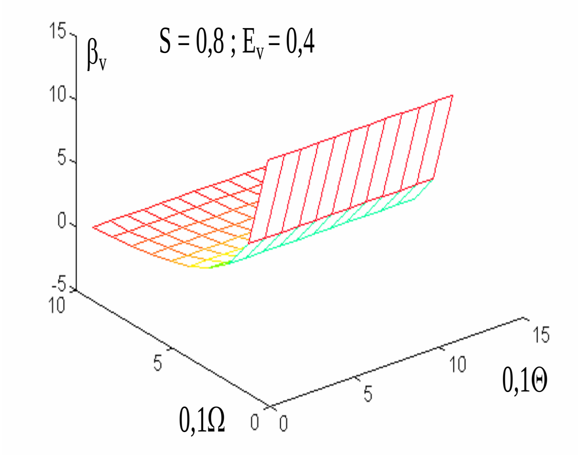

Fig. 3. *Depends of Businesk's coefficient from parameters Θ and Ω*

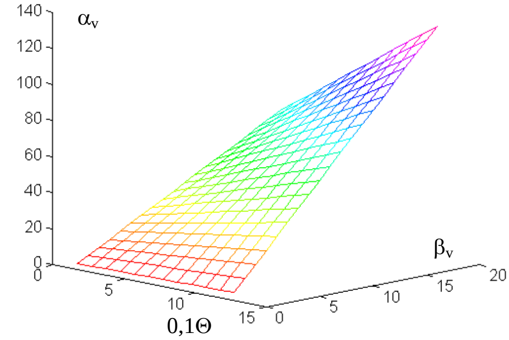

Fig. 4. *Depends of Coriolis's coefficient from parameters Θ and Businesk's coefficient β_v*

Figure 3 and 4 shows some influences parameters swirlig flows on Coriolis's and Businesc's coefficients.

For practical conditions, nedds know minimal values of coefficients α_v and β_v.

Differenting of equation (11), equation transforming

$$\frac{\partial \alpha_v}{\partial \Theta} = \frac{3}{2\Omega S} - 2,$$

from which is

$$\Omega = \frac{3}{4S}.$$

Differenting of equation (12), equation transforming

$$\frac{\partial \beta_v}{\partial \Theta} = \frac{-\alpha_v(1+E_v)}{3(1+\Theta)^2},$$

from which is

$$E_v = -1.$$

Figure 5. shows influence of parameter Θ on Coriolis's coefficient .

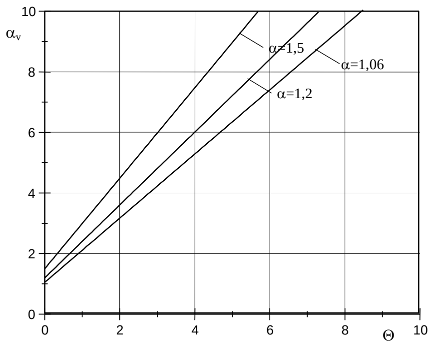

Fig. 5. *Depends of parameter Θ on Coriolis's coefficient*

4. CONCLUSION

Effects of swirl flow on energy losses in control spaces of pumps duurring transition process were considered in the paper.

Conclusion is that parameter of swirl flow Ω, which is significant because expressed over a flow of medium circulation. Swirl intensity, represents the relation of kinetic energy fluxes of circumference flow and kinetic energy of axial flow. Parameter E_v is energetic parameter and represents relation of kinetic energy of circumference and axial flow.

5. REFERENCES

[1] Glavcic Z., Cantrak S., Petrovic R., “Analysis of flow energy losses in transition regimes of flow energetic parameter”, IV Triennial International Conference HEAVY MACHINERY HM 2002 MF Kraljevo, 2002

[2] Benisek M., “Investigation of swirl flow in straight tubes of circular section” Doctorial dissertation, Faculty of Mechanical Engineering Belgrade, Belgrade, 1979.

[3] Glavcic Z., “Physical/mathematical modelling of transition processes in hydro/pneumatic systemsMaster of Science paper, Faculty of Mechanical Engineering, Belgrade, 2000.

[4] Čantrak S., Glavčić Z., Pavlović M., “About an model of transient process in hydraulic system” Procesna tehhnika, page 34-38, Belgrade 2001.

[5] Esudier M., Zehnder N., “Vortex-flow regimes,” Journal Fluid Mechanical, vol. 115, 1992.

[6] Glavčić Z., Petrović R. “Computer program for mathematical modeling and identification of hydrodynamic processes of a radial piston pump,” 6th FPNI *Symp.*,page 191-198 West Lafayette, USA, 2010.

[7] Petrović R., Savković M., Ivanović P., Glavčić Z., “Experimental verification of mathematical modeling of parameters of vane pump with double effectVi International Conference HM 08, page A23-A28, Kraljevo, 2008.

[8] Hoffmann W. "Dynamisches Verhalten hydraulischer systeme Automatischer Modellaufbau und digitale Simulation - Dissertation TH Aachen 1986,

HEAVY MACHINERY - HM 2011, 63-66
ISBN 978-86-82631-58-3
Paper accepted: 25.05.2011

Some linearity characteristics for homogeneous Vekua equation with analytical coefficients

Jelena Vujaković[1,*]- Miloje Rajović[2]
[1] University of Priština, Faculty of Sciences and Mathematics, Lole Ribara 29, 38 200 Kosovska Mitrovica, Serbia
[2] University of Kragujevac, Faculty of Mechanical Engineering, Dositejeva 19, 36 000 Kraljevo, Serbia

There are very little data in literature about Vekua equations with analytical coefficients. That is why they present an interesting area of scientific work. It is known (see [1-6]) that they have been solved by analytical substitution method or by a series-iteration method. Basis for these methods is the principle of fixed point.

In this paper we have presented that homogeneous Vekua equation, with analytical coefficients, is only apparently linear. Actually, it is typically transcendental equation.

Keywords: Conjugate derivate, analytical functions, Vekua equation, a series iteration method.

0 INTRODUCTION

Equation

$$\frac{\partial w}{\partial \bar{z}} = Aw + B\bar{w} \tag{1}$$

where $A = A(z, \bar{z})$ and $B = B(z, \bar{z})$ are analytical functions in certain finite region G, is called homogeneous Vekua equation. Operation $\frac{\partial w}{\partial \bar{z}}$, denoting conjugate derivative,

$$\frac{\partial w}{\partial \bar{z}} = \frac{1}{2}\left[\left(\frac{\partial u}{\partial x} - \frac{\partial v}{\partial y}\right) + i\left(\frac{\partial u}{\partial y} + \frac{\partial v}{\partial x}\right)\right] \tag{2}$$

is linear, so is applicable

$$\frac{\partial}{\partial \bar{z}}(w_1 \pm w_2) = \frac{\partial w_1}{\partial \bar{z}} \pm \frac{\partial w_2}{\partial \bar{z}}$$

$$\frac{\partial}{\partial \bar{z}}(cw_1) = c\frac{\partial w_1}{\partial \bar{z}}, c = const.$$

Conjugate derivative is very similar to ordinary derivative, so the operational rules for product, quotient are easy to perform, as well as the rules for conjugate derivatives of elementary complex or conjugate complex functions.

If in equation (1) coefficient is $B = 0$, then equation (1) is called Theodoresku equation.

With these rules it can be easily transferred to reverse operation to conjugated derivative, that is, integral $\hat{\int}$. In order to more relate this integral to ordinary integral, we are introducing sign

$$\hat{\int} F(z, \bar{z}) = \int F(z, \bar{z}) d\bar{z} + \phi(z),$$

where $\phi(z)$ is arbitrary analytical function in the role of integral constant. This is not line integral, but symbolic record that is necessary to integrate only by one variable $\bar{z}$, considering second variable z as a constant.

Due to these characteristics, derivatives and integrals, solving of equation (1) was reduced to procedures very similar to solving of ordinary differential equations with real argument. Main difference is because the main role of the ordinary constant here is taken over by arbitrary function $\phi(z)$.

In monograph [1] was pointed out the importance of this equation in mathematical physics. Many boundary problems have been solved there. It is interesting that Vekua [1-2], solves equation where coefficients $A = A(z, \bar{z})$ and $B = B(z, \bar{z})$ do not have to be analytical functions, but are some function of the space $L_p(G), p > 2$, where G is finite closed region.

In the lines [2-6] are given new, but abbreviated and more practical formulas for solving of equation (1), providing A and B are analytical functions in finite region.

Among other things, it has been shown that general solution of homogenous Vekua equation (1) with analytical coefficients, $w = w_{A,\phi} + w_{B,\phi} + w_{A,B,\phi}$, contains part which only

*Corr. Author's Address: Faculty of Sciences and Mathematics, Lole Ribara 29, 38 200 Kosovska Mitrovica, Serbia, enav@ptt.rs

depends on A and $\phi(z)$, part which only depends on B and $\phi(z)$, as well as the part which depends on both coefficients and $\phi(z)$. This means that it can be presented in the form of series- iterations

$$w(z,\bar{z}) = \phi(z) + \int A\phi(z)\,d\bar{z} + \\ + \int B\overline{\phi(z)}d\bar{z} + \int A d\bar{z}\int A\phi(z)\,d\bar{z} + \\ + \int A d\bar{z}\int B\overline{\phi(z)}d\bar{z} + \int B d\bar{z}\int \bar{A}\overline{\phi(z)}dz + \\ + \int B d\bar{z}\int \bar{B}\overline{\phi(z)}dz + \int A d\bar{z}\int A d\bar{z}\int A\phi(z)\,d\bar{z} + \cdots$$

From the previous if apparent that homogeneous Vekua equation (1) always has trivial solution. If $\phi(z)=1$, then there is particular solution in the form of series with integral form coefficients with symmetric disposition of elements. On the other hand, if $A = A(z,\bar{z})$ and $B = B(z,\bar{z})$ are complex constants, then solution of equation (1) is nonlinear function of an arbitrary analytical function $\phi(z)$. If A and B are real constants, then results given in the form of series of the first, second, …, nth integral of $\phi(z)$, or its conjunction, and series coefficients are power series by z or by $\bar{z}$.

1 MAIN RESULTS

We shall present now the main results of this paper.

Theorem 1. *If w_1 is solution of Vekua equation (1), then cw_1, where $c \neq 0$ is real constant, also the solution of the same equation.*

Proof. $\triangleleft$ Let w_1 is solution of equation (1). So applies

$$\frac{\partial w_1}{\partial \bar{z}} = Aw_1 + B\overline{w_1}. \tag{3}$$

Substituting cw_1 in (1) we obtain

$$\frac{\partial (cw_1)}{\partial \bar{z}} = Acw_1 + B\overline{cw_1},$$

that is, $c\dfrac{\partial w_1}{\partial \bar{z}} = cAw_1 + cB\overline{w_1}$. Dividing with $c \neq 0$ we obtain (3). With this proof is completed. $\triangleright$

Theorem 2. *If w_1 and w_2 are solutions of Vekua equation (1), then any linear combination $w = c_1w_1 + c_2w_2$, where c_1 and c_2 are real constant, is also the solution of equation (1).*

Proof. $\triangleleft$ Let w_1 and w_2 are by assumption the solution of equation (1). Substituting $w = c_1w_1 + c_2w_2$ in (1) we obtain

$$\frac{\partial}{\partial \bar{z}}(c_1w_1 + c_2w_2) = A(c_1w_1 + c_2w_2) + B\overline{(c_1w_1 + c_2w_2)} = \\ = c_1\left(Aw_1 + B\overline{w_1}\right) + c_2\left(Aw_2 + B\overline{w_2}\right) \\ = c_1\frac{\partial w_1}{\partial \bar{z}} + c_2\frac{\partial w_2}{\partial \bar{z}}.$$

By this we have proven the assertion. $\triangleright$

Theorem 3. *By linear substitution $w = \alpha v$, where $\alpha = \alpha(z,\bar{z}) = \phi(z)\exp\left(\int A d\bar{z}\right) \neq 0$ and $v = v(z,\bar{z})$ is new unknown function, Vekua equation (1) transforms to homogeneous Theodoresku equation.*

Proof. $\triangleleft$ Substituting $w = \alpha v$ in (1) and applying the rule for conjugated derivative of product we obtain

$$\frac{\partial \alpha}{\partial \bar{z}}v + \alpha\frac{\partial v}{\partial \bar{z}} = A\alpha v + B\overline{\alpha v}.$$

When we divide this equation with $\alpha \neq 0$ and calculate $\dfrac{\partial v}{\partial \bar{z}}$, we obtain

$$\frac{\partial v}{\partial \bar{z}} = \left(A - \frac{1}{\alpha}\frac{\partial \alpha}{\partial \bar{z}}\right)v + B\frac{\bar{\alpha}}{\alpha}\bar{v}. \tag{4}$$

We have obtained a new Vekua equation, but according to known $v = v(z,\bar{z})$.

This equation can be transformed into Theodoresku homogeneous equation, if we eliminate element to v. Namely, from $A - \dfrac{1}{\alpha}\dfrac{\partial \alpha}{\partial \bar{z}} = 0$ we have $A = \dfrac{\partial \ln \alpha}{\partial \bar{z}}$.

From here

$$\ln \alpha = \hat{\int} A = \int A d\bar{z} + \ln \phi(z),$$

that is $\alpha = \phi(z)\exp\left(\int A d\bar{z}\right)$. $\triangleright$

It is obvious that coefficient to $v = v\left(z, \bar{z}\right)$, in equation (4) cannot be annulled.
With linear substitution it can only be made equal to one.
Specially applies:

Theorem 4. *With linear substitution* $w = w_1 u$, *where* w_1 *is particular integral of equation (1), and* $u = u\left(z, \bar{z}\right)$ *new unknown function, Vekua equation (1) transforms to Vekua equation with one coefficient.*

Proof. ◁ As w_1 is particular integral, then applies (3). If we look for conjugated derivative from product $w = w_1 u$ and all that substitute in Vekua equation (1), we obtain

$$\frac{\partial w_1}{\partial \bar{z}} u + w_1 \frac{\partial u}{\partial \bar{z}} = A w_1 u + B \overline{w_1} \bar{u} .$$

Here is

$$\frac{\partial u}{\partial \bar{z}} = \left(A - \frac{1}{w_1} \frac{\partial w_1}{\partial \bar{z}} \right) u + B \frac{\overline{w_1}}{w_1} \bar{u} .$$

Since from (3), $A - \frac{1}{w_1} \frac{\partial w_1}{\partial \bar{z}} = -B \frac{\overline{w_1}}{w_1}$, so at the end after arrangement of equation is

$$\frac{\partial u}{\partial \bar{z}} = B \frac{\overline{w_1}}{w_1} \left(\bar{u} - u \right).$$

We have obtained equation which has only one coefficient, and role $A = A\left(z, \bar{z}\right)$ from equation (1) plays particular integral w_1. ▷

Corollary. *With linear substitution* $w = \alpha \bar{v}$, $\alpha = \alpha\left(z, \bar{z}\right) \neq 0$, $v = v\left(z, \bar{z}\right)$, *Vekua equation (1) transforms to its conjugated equation.*

Proof. ◁ Substitution of conjugated derivative from $w = \alpha \bar{v}$ in equation (1) we obtain

$$\frac{\partial \alpha}{\partial \bar{z}} \bar{v} + \alpha \frac{\partial \bar{v}}{\partial \bar{z}} = A \alpha \bar{v} + B \overline{\alpha} v .$$

From here $\alpha \frac{\partial \bar{v}}{\partial \bar{z}} = \left(A\alpha - \frac{\partial \alpha}{\partial \bar{z}} \right) \bar{v} + B \overline{\alpha} v$. Since $\frac{\partial \bar{v}}{\partial \bar{z}} = \overline{\left(\frac{\partial v}{\partial z} \right)}$, then the final equation, after dividing with $\alpha \neq 0$ becomes

$$\overline{\left(\frac{\partial v}{\partial z} \right)} = \left(A - \frac{1}{\alpha} \frac{\partial \alpha}{\partial \bar{z}} \right) \bar{v} + B \frac{\overline{\alpha}}{\alpha} v . \qquad (5)$$

With conjugation (5) at the end we obtain

$$\frac{\partial v}{\partial z} = \left(\bar{A} - \frac{1}{\bar{\alpha}} \overline{\left(\frac{\partial \alpha}{\partial \bar{z}} \right)} \right) v + \bar{B} \frac{\alpha}{\bar{\alpha}} \bar{v} . \quad ▷$$

2 CONCLUSION

According to above elaborated, we are making the following conclusion
1. Vekua equation (1) has linear characteristics only regarding the real constants.
2. Its solutions are not linear functions of arbitrary integration elements. This is important characteristics of linear differential equations.

Therefore, Vekua equation actually is not linear. It is typically transcendental equation. The operation $\bar{w}$, which is transcendental operation, has lead us to this. Namely, from $w = \rho e^{i\theta}$ we have $\bar{w} = \rho e^{-i\theta} = w e^{-2i\theta}$. We can see that $\bar{w}$ is rotation for 2θ in reverse direction. It is known that rotation is not linear function.

In this sense it is necessary to state precisely the linearity definition itself in areolar and partial equations.

REFERENCES

[1] Vekua, I. N., “Generalized of analytic functions”, (in Russian), Nauka, Moskva, 1988

[2] Vekua, I. N., “ System of differential equations of elliptic type and boundary value problems with application of shell theory”, (in Russian), Math. Sbornik, 31 (73), 2 (1952), 217-314

[3] Dimitrovski D., Ilievski B. Mitevska J. and Rajović M., “The Vekua equation with analytical coefficients”, (in Macedonian), Special editions III (24), Skopje, 1995

[4] Rajović M., Dimitrovski D. and Stojiljković R., “The generalization of the I. N. Vecua

equation with analytic coefficients in $z, \bar{z}$", Filomat Niš, 11, (1997), 29-32

[5] Rajović M., Dimitrovski D. and Stojiljković R., "Elementary solution of Vecua equation with analytic coefficients on $z, \bar{z}$", Matematički vesnik Skopje, 49, (1997), 123-128

[6] Vujaković J., Dimitrovski D. and Rajović M.,"On location of zeros of second order complex differential equations", Journal of Computational Technologies, Novosibirsk, Vol. 15, No 4, (2010), 27-30

D SESSION

DESIGN AND MECHANICS

HEAVY MACHINERY - HM 2011, 1-5
ISBN 978-86-82631-58-3
Paper accepted: 20.05.2011

Gearing Line And Gearing Profile Of Precessional Gearing Determined Based On The Fundamental Law Of Gearing

Adrian Bruja[1,*], Marian Dima[1], Catalin Francu[1]
[1] Technical University of Civil Engineering Bucharest

In this paper is presented the way to determine the parametric equations of the line of contact for the precessional gearing based on the fundamental law of gearing and by applying the corresponding transformation relations the profile of the central toothed wheel which is a part of the precessional gearing.

Keywords: **Precessional gearing, gearing law, line of contact**

0 INTRODUCTION

The precessional transmission [1], figure 1,b,c, was obtained from the bevel simple satellite planetary transmission, figure 1,a, by eliminating the central wheel 1, modifying the 2-3 gearing from external to internal gearing and replacing the 1-2 gearing with a universal joint.

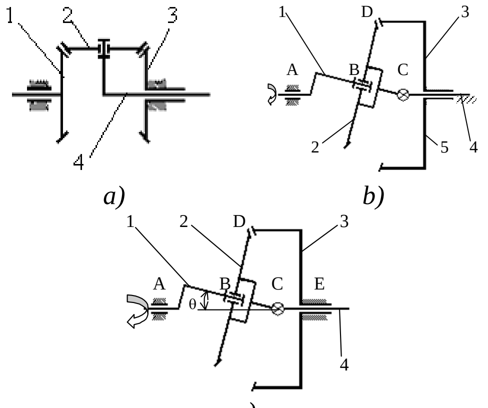

Fig. 1. Precessional transmission with simple satellite

The driving element of this transmission is the driving shaft 1 which rotates around A-E axis driving in spherical motion the bevel satellite 2 which is in contact on its generator with the wheel 3. The satellite has a precession movement due to the inclination of the shaft 1 by the angle θ and an intrinsic rotation around the inclined axis B-C due to the roll on the interior bevel surface of the fixed wheel. The movement resulted from the composition of these 2 movements is transmitted either to the central wheel 3, fig. 1,b, or to the output shaft 4 through the coupling C.

The transmission ratio of this transmission is determined with the equations:

$i_{14}^{3} = \dfrac{z_2}{z_2 - z_3}$, when the central wheel is fixed and $i_{13}^{4} = \dfrac{z_3}{z_3 - z_2}$ when the central wheel is moving.

The interior bevel gear is created using some conical rolls with their axes placed regularly on the lateral surface of the rolling cone, figure 2,a. The rolls apexes coincide with the apex of the rolling cone. The lateral surface of any roll limited by 2 planes perpendicular on the roll's axis, represent the side teeth of the interior bevel gear. The teeth of the central gear are conjugated to the conical rolls on the interior bevel gear, figure 2,b.

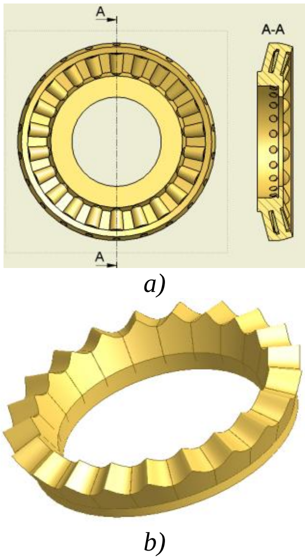

Fig. 2. The gears of the precessional gearing

*Corr. Author's Address: Technical University of Civil Engineering Bucharest, Romania, bruja@utcb.ro

1. THE LINE OF CONTACT [2]

The fundamental law of gearing can be enounced as: (I) In any point of contact of the conjugated side teeth the common geometrical normal must be perpendicular on the respective relative velocity.

This law is expressed through the vector gearing equation

$$\vec{v}_{21} \cdot \vec{n} = 0 \tag{1}$$

For the parallel and concurrent gearings the fundamental law of gearing can be formulated as follows: (II) In any point of contact of the conjugated side teeth the common geometrical normal intersects the instantaneous axis Δ_{21} of the relative rotation movement.

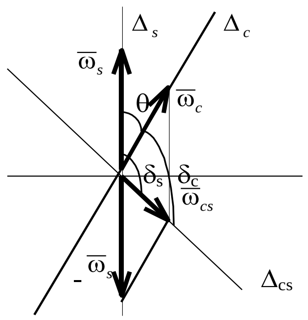

Fig.3 Rotation vectors for the planetary gearings

It is considered the concurrent gearing composed of the gears s (interior gearing) and c (exterior gearing) having axes Δ_s and Δ_c with the angle θ between them, figure 3. The gears have the angular velocities $\vec{\omega}_s$ and $\vec{\omega}_c$ respectively. The angular velocity is determined with the Euler equation

$$\vec{\omega}_{cs} = \vec{\omega}_c - \vec{\omega}_s \tag{2}$$

And has the direction of the rotation axis of the relative movement Δ_{cs}.

Applying the sinus theorem in the triangle formed by the vectors $-\vec{\omega}_s$, $\vec{\omega}_c$ şi $\vec{\omega}_{cs}$ the angles between the gears axes and the axis of the relative movement are obtained:

$$\delta_s = \operatorname{arctg}\left(\frac{\sin\theta}{\cos\theta - i_{sc}}\right) \tag{3}$$

$$\delta_c = \operatorname{arctg}\left(\frac{i_{sc}\cdot\sin\theta}{1 - i_{sc}\cdot\cos\theta}\right)$$

i_{sc} is the transmission ratio. These angles represent the apex half-angles of the rolling cones of the gears and in the case of the planetary gearing these cones are becoming the axoids of the spherical movement, respectively the mobile axoid geometric locus (Δ_s axis) and fixed axoid geometric locus (Δ_c axis). During the movement, the mobile axoid geometric locus is rolling without slipping over the fixed axoid geometric locus, the interior tangency being made along the common generator Δ_{cs}.

The direction of the axis of relative movement, the versor $\vec{u}_{cs}$, is obtained by rotation of the versor $\vec{k}$ Oz axis around Oy axis with the angle δ_s, figure 4,

$$\vec{u}_{cs} = R_y(\delta_s)\cdot\vec{k} \tag{4}$$

where

$$R_y(\delta_s) = \begin{pmatrix} \cos\delta_s 0 - \sin\delta_s \\ 010 \\ \sin\delta_s 0 \cos\delta_s \end{pmatrix}$$

represents the rotation matrix.

After calculating, results

$$\vec{u}_{cs} = \sin\delta_s\vec{i} + \cos\delta_s\vec{k} \tag{5}$$

The gear s has is created using some conical rolls with their axes placed regularly on the lateral surface of the rolling cone Cr with the apex half-angle δ_{sr} ($\delta_{sr} \geq \pi/2$, $\delta_{sr} \neq \delta_s$). The rolls apexes coincide with the apex of the rolling cone C_r. The lateral surface of any roll limited by 2 planes perpendicular on the roll's axis, represent the side teeth of the bevel gear s. The equation of this surface is determined by having the condition that the roll's generator, written under parametric form:

$$x_g = \frac{x_0 + kx}{1+k} \qquad y_g = \frac{y_0 + ky}{1+k}$$
$$z_g = \frac{z_0 + kz}{1+k} \tag{6}$$

Where k is the generator parameter of the right, to be tangent to the sphere

$$(x - x_1)^2 + (y - y_1)^2 + (z - z_1)^2 = \rho^2 \tag{7}$$

having radius ρ and centre in O_1' with coordinates x1, y1, z1. The point O_1' represents the joint of the satellite's roll and it's placed on the generator of the cone C_r to a distance r from the apex.

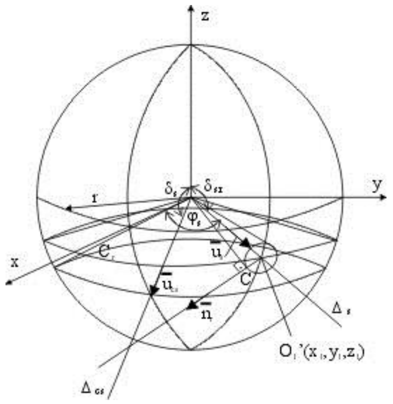

Fig. 4 Determining the gearing surface

By placing the condition that the apex of the roll to be the origin of the reference frame, meaning

$$x_0 = 0;\quad y_0 = 0;\quad z_0 = 0,$$

And replacing the relations (6) in the equation (7) it's obtained the equation of the side teeth of the gear s in implicit form,

$$(xy_1 - yx_1)^2 + (yz_1 - zy_1)^2 + (zx_1 - xz_1)^2 - \rho^2(x^2 + y^2 + z^2) = 0 \tag{8}$$

Solving the equation (6) in relation to z it's obtained the explicit equation of the same surface,

$$z_{1,2} = \frac{-B \pm \sqrt{B^2 - 4AC}}{2A} \tag{9}$$

where:

$$A = x_1^2 + y_1^2 - \rho^2;\quad B = -2z_1(xx_1 - yy_1)$$

$$C = \left(z_1^2 - \rho^2\right)\left(x^2 + y^2\right) + \left(xy_1 - yx_1\right)^2$$

The coordinates x1, y1, z1 of the centre's large base of the roll are obtained from the following relation

$$\begin{pmatrix} x_1 \\ y_1 \\ z_1 \end{pmatrix} = R_z(\varphi_s) \cdot R_y(\delta_{sr}) \cdot \begin{pmatrix} 0 \\ 0 \\ r \end{pmatrix}, \tag{10}$$

where:

$$R_z(\varphi_s) = \begin{pmatrix} \cos\varphi_s - \sin\varphi_s\, 0 \\ \sin\varphi_s\ \cos\varphi_s\, 0 \\ 0\,0\,1 \end{pmatrix}$$

$$\varphi_s = \varphi_0 + p \cdot \frac{2\pi}{Z_s},\quad p = 1,2\ldots Z_s,$$

Z_s - is the number of rolls of gear s.

By doing the calculus we obtain:

$$x_1 = r \cdot \sin\delta_{sr} \cos\varphi_s, \tag{11}$$
$$y_1 = r \cdot \sin\delta_{sr} \sin\varphi_s,$$
$$z_1 = r \cdot \cos\delta_{sr},$$

And the versor of the generator's rolling cone of the satellite, $\vec{u}_s$, is ($\varphi_s \in (0,2\pi)$)

$$\vec{u}_s = \sin\delta_{sr} \cos\varphi_s \vec{i} + \sin\delta_{sr} \sin\varphi_s \vec{j} + \cos\delta_{sr} \vec{k} \tag{12}$$

The plane Π which contains the normal $\vec{n}_r$ to the side teeth (8) is the plane determined by the directions $\vec{u}_{cs}$ (fixed) and $\vec{u}_s$ (variable), concurrent in the origin of the reference frame. The Cartesian equation of this plane is

$$n_x(x - x_0) + n_y(y - y_0) + n_z(z - z_0) = 0, \tag{13}$$

where nx, ny, nz are the parameters of the normal $\vec{n}$ la plan. The normal $\vec{n}$ is obtained from the cross product of the versors $\vec{u}_{cs}$ şi $\vec{u}_s$,

$$\vec{n} = \vec{u}_{cs} \times \vec{u}_s = \begin{vmatrix} \vec{i}\ \ \vec{j}\ \vec{k} \\ \sin\delta_s\ \ 0\ \cos\delta_s \\ \sin\delta_{sr}\cos\varphi_s \sin\delta_{sr}\sin\varphi_s \cos\delta_{sr} \end{vmatrix} =$$

$$= (-\sin\delta_{sr}\sin\varphi_s\cos\delta_s)\vec{i} + (\sin\delta_{sr}\cos\varphi_s\cos\delta_s - \cos\delta_{sr}\sin\delta_s)\vec{j} + (\sin\delta_{sr}\sin\varphi_s\sin\delta_s)\vec{k},$$

which means:

$$n_x = -\sin\delta_{sr}\sin\varphi_s\cos\delta_s,$$
$$n_y = \sin\delta_{sr}\cos\varphi_s\cos\delta_s - \cos\delta_{sr}\sin\delta_s, \tag{14}$$
$$n_z = \sin\delta_{sr}\sin\varphi_s\sin\delta_s$$

The graphic construction based on the second formulation of the fundamental law of gearing made for the studied gearing in this paper is presented in figure 4. According to this figure, the gearing surface is obtained as geometrical locus of all the C points related to the fixed reference frame when $\varphi_s \in (0,2\pi)$ şi $r \in (0,R)$. Analysing the figure, can be seen that the variation of the parameters φ_s and r in previously presented limits, the normal $\vec{n}_r$ is describing the plane Π and the gearing surface can be determined as the intersection between the roller (8) and plane Π, which can be expressed through

$$\begin{cases} xn_x + yn_y + zn_z = 0 \\ (xy_1 - yx_1)^2 + (yz_1 - zy_1)^2 + \\ + (zx_1 - xz_1)^2 - \rho^2 (x^2 + y^2 + z^2) = 0 \end{cases} \quad (15)$$

By fixing the radius r to any value the line of contact is obtained as an intersection between the gearing surface with the sphere of r radius. From the figure 5 can be seen that the normal $\vec{n}_r$ in C to the roll is the same with the normal in C to the sphere with the centre in O_1' and radius $\rho' = \rho / \cos\beta$. Knowing these, the line of contact is determined as an intersection between plane Π, sphere of radius $\rho' = \rho / \cos\beta$ with the centre in in O_1' and sphere of radius r and centre in O

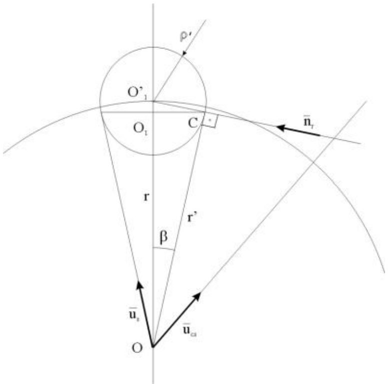

Fig. 5 Determining the line of contact

$$\begin{cases} xn_x + yn_y + zn_z = 0 \\ (x - x_1)^2 + (y - y_1)^2 + (z - z_1)^2 = \rho'^2 \\ x^2 + y^2 + z^2 = r^2 \end{cases} \quad (16)$$

The solution of the system (16) is:

$$z_l = \frac{-b - \sqrt{b^2 - 4ac}}{2a} \quad (17)$$

$$y_l = \frac{2z_l (n_z x_1 - n_x z_1) + n_x (x_1^2 + y_1^2 + z_1^2 + r^2 - \rho'^2)}{2(n_x y_1 - n_y x_1)}$$

$$x_l = -\frac{n_z z_l + n_y y_l}{n_x},$$

$\varphi_s \in (0, 2\pi)$ and $r = ct$.

where:

$$a = 4(n_x^2 + n_y^2)(n_z x_1 - n_x z_1)^2 + \\ + 4(n_x^2 + n_z^2)(n_x y_1 - n_y x_1)^2 + \\ + 8n_y n_z (n_z x_1 - n_x z_1)^2 ,$$

$$b = 4n_x (n_x^2 + n_y^2)(n_z x_1 - n_x z_1) \cdot \\ \cdot (x_1^2 + y_1^2 + z_1^2 + r^2 - \rho'^2) + \\ + 4n_x n_y n_z)(n_x y_1 - n_y x_1) \cdot \\ \cdot (x_1^2 + y_1^2 + z_1^2 + r^2 - \rho'^2) \quad (18)$$

$$c = n_x^2 (n_x^2 + n_y^2)(n_z x_1 - n_x z_1) \cdot \\ \cdot (x_1^2 + y_1^2 + z_1^2 + r^2 - \rho'^2)^2 - \\ - 4r^2 n_x^2 (n_x y_1 - n_y x_1)^2$$

The relations (17) represent the parametric equations of the line of contact, the parameter being the angle φ_s. If in this equation the radius r is modified the line of contact is obtained:

$$z_{sa} = \frac{-b - \sqrt{b^2 - 4ac}}{2a}, \quad (19)$$

$$y_{sa} = \frac{2z_l (n_z x_1 - n_x z_1) + n_x (x_1^2 + y_1^2 + z_1^2 + r^2 - \rho'^2)}{2(n_x y_1 - n_y x_1)}$$

$$x_{sa} = -\frac{n_z z_l + n_y y_l}{n_x},$$

$\varphi_s \in (0, 2\pi)$ and $r \in (0, R)$

2. THE PROFILE OF THE CENTRAL GEAR [2]

The point C belonging to the central gear, means that the relations (19) give the coordinates of the side tooth of this gear related to the fixed reference frame. In order to find the parametric equations of the side tooth of the central gear, these coordinates need to be related to the gear's reference frame coordinates. This is done by doing a rotation of a -θ angle around Oy axis followed by a rotation of a $\varphi_c = -\varphi_s / i_{cs}$ angle around Oz axis. Mathematically this relation is expressed as:

$$\begin{pmatrix} x_c \\ y_c \\ z_c \end{pmatrix} = R_z(\varphi_c) \cdot R_y(-\theta) \cdot \begin{pmatrix} x_{sa} \\ y_{sa} \\ z_{sa} \end{pmatrix} \qquad (20)$$

Based on this method of determining the line of contact and the side toothof the central gear software was created which determines the coordinates of the points on the contact surface and on the side teeth of the satellite's and central; gear. The same software is able to display the teeth and the contact surface and the user can choose the viewing point.

In figure 6 is presented the gearing of a frontal harmonical transmission with rigid element rotated with 30° around Oy axis and in figure 7 is represented the intersection of the same gearing with a sphere projected in yOz plane. Corresponding to this intersection, results the profile of the tooth of the central gear on the sphere and the line of contact in frontal spherical gearing.

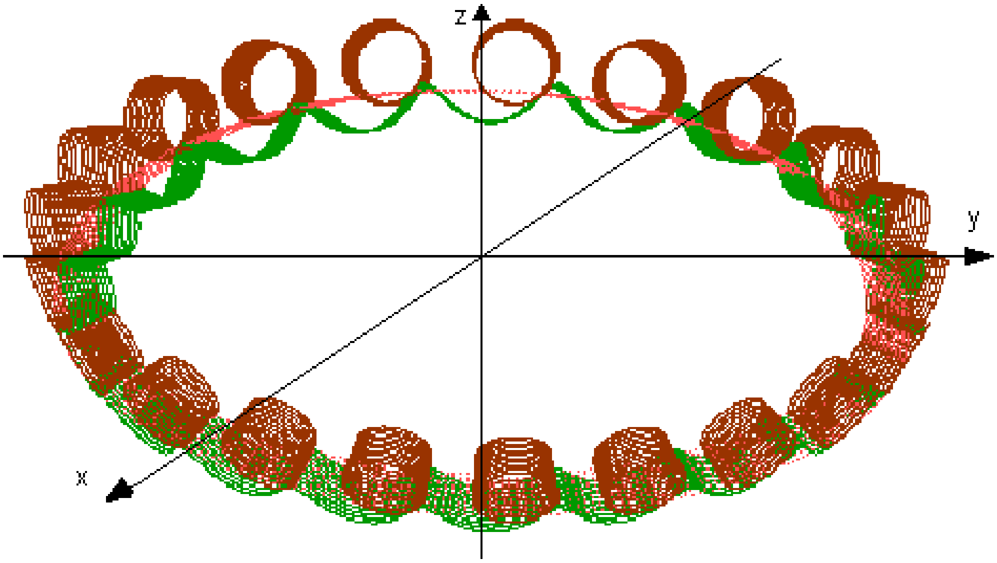

Fig. 6 The gearing of a frontal harmonical transmission with rigid element

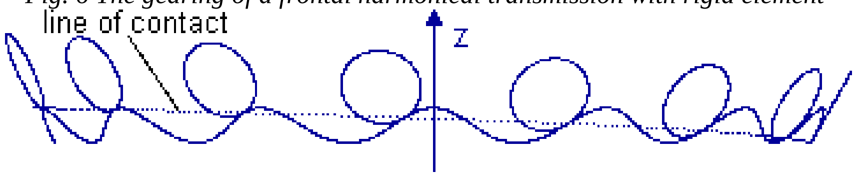

Fig. 7 Section with a sphere of the gearing of a frontal harmonical transmission with rigid element

3 CONCLUSION

Knowing the equations of the surface of contact represents the key to the study of precessional gearing. Starting from the gearing surface, the conjugated profile of the satellite's rolls is determined. Knowing the parametric equations of the profile of the teeth of the central gear, the shape of this profile can be optimized following different criteria and the forces in the gearing can be determined.

4 REFERENCES

[1] Bostan, I.A. - Preţessionnîe peredaci s mnogoparnîm zaţepleniem. Ed. “Ştiinţa” Chişinău, 1991

[2] Dima, M - Contribuţii la studiul transmisiilor armonice cu elemente rigide. Teza de doctorat. Bucureşti, 2002.

HEAVY MACHINERY - HM 2011, 7-12 Paper accepted: 20.05.2011
ISBN 978-86-82631-58-3

Mechano-Mathematical Modeling of Motor-Vehicle Motion With Reading the Stabilizing Moment of the Driving Wheels

Stanimir Karapetkov[1], Ivanka Moneva[1,*], Maria Gramenova[1], Mina Tsoneva[1]
[1] Technical University of Sofia, Faculty of Engineering and Pedagogy in Sliven, Bulgaria

The mechano-mathematical modeling of motor-vehicle motion is exceptionally of present interest, especially with the increase of the necessity of adequate investigation of the road-transport accidents. In this article a model of motor-vehicle motion with reading the complex motion of the driving wheels and the mechanism of friction in the wheels is described, as the motion is influenced by outside interference due to the road pavement roughness.

The stabilizing moment dependences on road reactions and tyre elasticity, and the moment dependence on the resistance in the steering gear that are influencing the driving wheels, are deduced.

The numerical solution of the system of equations is accomplished in Matlab medium, toolbox Simulink.

Keywords: mechano-mathematical modeling, motor-vehicle, stabilizing moment, friction.

INTRODUCTION

The increased number of road-transport accidents, the high technologies in motor industry, and the development of computer engineering imposes a precise modeling of motor-vehicle motion in order to be made an adequate identification of accident mechanism. In the specialized scientific references [1, 7, 8] there are a series of models characterizing the motor-vehicle motion in one or other degree of accuracy. The reading of the complex character of the parametres determines the adequacy of the models with the real motion processes.

The motor-vehicle reaction to outside interferences depends on the motor-vehicle static and dynamic characteristics, which are determined by its constructional parametres, such as kinematics of steering gear, tyre elasticity, elasticity of motor-vehicle suspension, etc.

The goal of this article is the working out of mechano-mathematical model of motor-vehicle motion with reading of the wheels rotation, the changeable character of the normal reactions occurring in them, the complex character of friction process, and the stabilizing moment in the driving wheels.

A Dynamic Model

A model of motor-vehicle with front driving wheels suggested in [3, 4] is shown in Fig. 1.

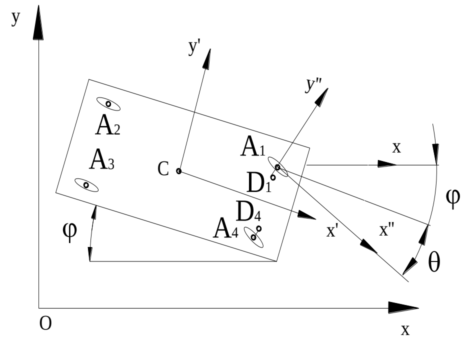

Fig.1 A scheme of motor-vehicle

The motion of motor-vehicle body is accepted to be a quasi-plain motion of perfectly-rigid body. The movable coordinate system $Cx'y'z'$ and the movable coordinate system $Ax''y''z''$ are connected with the centre of mass "C" of the motor-vehicle and the centre of mass "A" of the driving wheel, respectively.

As generalized coordinates of motor-vehicle motion are accepted the coordinates x, y of its centre of mass towards the immovable coordinate system; the angle φ of motor-vehicle turning; the own angle γ of wheels turning, and the average angle θ of driving wheels turning round the axis of steering knuckle.

*Corr. Author's Address: Technical University of Sofia, Faculty of Engineering and Pedagogy in Sliven,Bourgasko Shosse N59, Sliven 8800, Bulgaria, imoneva@abv.bg

The plain motion of motor-vehicle body is described by the system of differential equations:

$$m \cdot \ddot{x} = \sum_{i=1}^{4} F_{ix} + m \cdot g \cdot \sin\alpha$$

$$m \cdot \ddot{y} = \sum_{i=1}^{4} F_{iy} + m \cdot g \cdot \sin\beta \qquad (1)$$

$$I_a \cdot \ddot{\varphi} = \sum_{i=1}^{4} \left\{ \begin{array}{l} F_{iy}\left[\begin{array}{l} x_i' \cdot \cos(\varphi+\theta) - \\ - y_i' \cdot \sin(\varphi+\theta) \end{array}\right] - \\ - F_{ix}\left[\begin{array}{l} x_i' \cdot \sin(\varphi+\theta) + \\ + y_i' \cdot \cos(\varphi+\theta) \end{array}\right] \end{array} \right\}$$

The motion of each wheel is described with the differential equation

$$\begin{aligned} & I_i \cdot \ddot{\gamma}_i = F_{i\tau} \cdot r_i + \\ & + sign(\dot{\gamma}_i)\left[- f_i \cdot N_i + M_{is}\right] \end{aligned} \qquad (2)$$

The normal reactions N_i are determined by the method of dynamic force analysis, and are described with the system of equations of the form

$$\begin{aligned} & b \cdot N_1 + b \cdot N_4 = \\ & = -m \cdot (\ddot{x} \cdot \cos\varphi + \ddot{y} \cdot \sin\varphi) \cdot h_c + \\ & + I_{x'z'} \cdot \dot{\varphi}^2 - G_{z'} \cdot x'_2 - G_{x'} \cdot h_c \\ & - 2 \cdot y'_1 \cdot N_1 - 2 \cdot y'_2 \cdot N_2 = \\ & = m \cdot (-\ddot{x} \cdot \sin\varphi + \ddot{y} \cdot \cos\varphi) \cdot h_c + \\ & + I_{x'z'} \cdot \ddot{\varphi} - G_{z'} \cdot y' - G_{y'} \cdot h_c \\ & N_1 + N_2 + N_3 + N_4 = G_{z'} \\ & \frac{N_1}{c_1} - \frac{N_2}{c_2} + \frac{N_3}{c_3} - \frac{N_4}{c_4} = 0 \end{aligned} \qquad (3)$$

where is put

$$\begin{aligned} & G_{x'} = G_x \cdot \cos\varphi + G_y \cdot \sin\varphi; \\ & G_{y'} = -G_x \cdot \sin\varphi + G_y \cdot \cos\varphi; \\ & G_{z'} = G_z; \\ & G_x = m \cdot g \cdot \sin\alpha; \\ & G_y = m \cdot g \cdot \sin\beta; \\ & G_z = -m \cdot g \cdot \sqrt{1 + \left(tg^2\alpha + tg^2\beta\right)}. \end{aligned}$$

An equation describing the turning of driving wheels round the axis of steering knuckle that is the form

$$I_j \cdot \ddot{\theta} = \sum_{ik=1}^{n} M_{ik} , \qquad (4)$$

is added to the system of differential equations.

The designations in the system (1), (2), (3) and (4) are the following: m is the motor-vehicle mass; g is the acceleration of gravity; α and β are the angles of road slope along the axes x and y, respectively; $F_i\ /i = 1 \div 4/$ are the forces of friction in the wheels; $F_{i\tau}$ is the tangential component of friction forces; h_c is the height of the motor-vehicle centre of mass; $I_{x'z'}$ is the centrifugal moment of inertia; b is the longitudinal base of the motor-vehicle; $c_i\ /i = 1 \div 4/$ are the equivalent vertical elastic constants of suspension and tyres; $\gamma_i\ /i = 1 \div 4/$ are the angles of wheels turning round their own axis; I_a is the moment of inertia of the motor-vehicle towards its central vertical axis; I_i are the equivalent moments of inertia of the wheels towards their axis of rotation; M_{is} is the engine moment equivalent to the driving wheels; N_i are the normal reactions in the wheels; r_i are the dynamic radii of the wheels; I_j is the equivalent moment of inertia of each driving wheel towards the axis of steering knuckle ($j = 1$ and $j = 4$ are for the outside and inside wheel during turning, respectively); M_{ik} are the moments (n in number) applied upon the driving wheels towards the axis of steering knuckle.

The number of degrees of freedom of the system of equations (1), (2), (3) and (4) is changeable in accordance with the number of wheels performing a pure rolling, and for the wheels a kinematic relation is introduced.

The force of friction for each wheel is determined from the expression

$$\vec{F}_i = -\mu_i \cdot N_i \cdot \frac{\vec{V}_{Pi}}{V_{Pi}} , \qquad (5)$$

where μ_i is the coefficient of friction; V_{Pi} is the velocity of point P for each driving wheel (P is the centre of the contact spot between the tyre and road pavement).

Figure 2 represents a front driving wheel turned round the axis of steering knuckle at an angle θ read from the neutral position, and the applied tangential force of friction $\vec{F}_\tau$, the normal force of friction $\vec{F}_n$ and the normal reaction $\vec{N}$. The axis of steering knuckle S concludes an angle β' and an angle α' with the longitudinal vertical plane and with the cross plane of motor-vehicle, respectively.

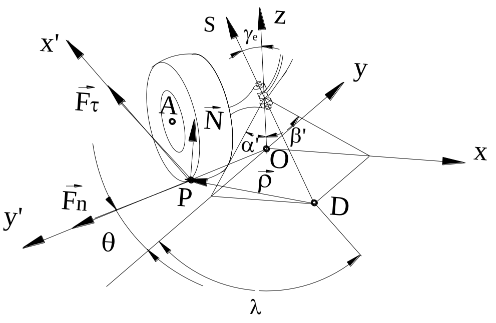

Fig. 2. A scheme of forces applied in the contact plot of the wheel

The velocity of point P is determined according the law of distribution of velocities as the complex motion of the driving wheels is read with the sum angular velocity

$$\vec{\omega} = \vec{\omega}_a + \vec{\omega}_k + \vec{\omega}_{sk},$$

where $\omega_a = \dot{\varphi}$ is the angular velocity of the motor-vehicle; ω_κ is the angular velocity of the wheel round the centre A; ω_{sk} is the angular velocity round the axis of steering knuckle.

The behavior of a motor-vehicle at rectilinear motion after the driving wheels deviate from their equilibrium position due to some outside interference is studied. The speed of wheel return in the equilibrium position depends on the stabilizing moment created by the reactions in the wheels and tyres elasticity. The moment of the force of resistance in the steering gear has also an influence.

During the rectilinear motion of a motor-vehicle after the momentum deviation of the driving wheels, we can assume with a significant accuracy because of the system inertia that the velocity of the contact point P will be of the form

$$\begin{aligned} V_{P_x} &= \dot{x} + r\cdot\dot{\theta}\cdot\cos\gamma_e\cdot tg\beta' - r\cdot\dot{\gamma}\cdot\cos\theta \\ V_{P_y} &= \dot{y} + r\cdot\dot{\theta}\cdot\cos\gamma_e\cdot tg\alpha' + r\cdot\dot{\gamma}\cdot\sin\theta \end{aligned} \tag{6}$$

The stabilizing moment due to the reactions of road pavement ($\vec{F}_i$, $\vec{N}_i$) and due to the tyre elasticity for each driving wheel towards the axis of steering knuckle is determined from the expression

$$\vec{M}_{st_j} = \left\{\left[\vec{\rho}_j \times \left(\vec{F}_i + \vec{N}_i\right)\right] + \left(\vec{\rho}_g \times \vec{R}_{iy}\right)\right\}\cdot\vec{e}, \tag{7}$$

where $\vec{\rho}_j$ is the radius-vector of point P_i towards the pierced point D_j of the axis of steering knuckle with the plane Oxy; $\vec{e}$ is the unit vector of the axis of steering knuckle; α_e, β_e and γ_e are the angles of the unit vector with the coordinate system $Oxyz$; $\vec{\rho}_g$ is the radius-vector of the applied point of the cross reaction $\vec{R}_{iy}$ from the tyre elasticity towards point D_j.

The motion of the motor-vehicle wheel after outside interference is accompanied with the appearance of tyre deformation, as the wheel can roll over without slip under an angle towards the middle wheel plane [2, 5, 6]. The angle between the middle wheel plane and the vector-velocity of wheel centre is the angle of a side entrainment δ. During the rolling of an elastic wheel with side entrainment a moment acts upon the tyre. This moment strives to return the wheel in a neutral position, i.e. this is the stabilizing moment due to the tyre elasticity.

At small magnitudes of the side force the dependence between the cross force and the angle of the side entrainment δ is accepted as

$$P_y = k_y\cdot\delta, \tag{8}$$

where k_y is the coefficient of resistance against side entrainment, and is measured experimentally.

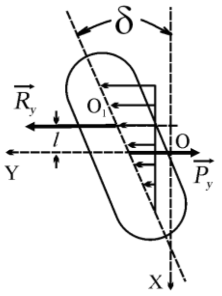

Fig. 3. A scheme of elementary forces in the contact plot

The reading of the angle of the side entrainment changes the dependences of the turning angles, and they get the form

$$\begin{aligned} \theta_1 &= \theta - k\cdot|\theta| + sign(\theta)\cdot\delta \\ \theta_4 &= \theta + k\cdot|\theta| + sign(\theta)\cdot\delta \end{aligned} , \qquad (9)$$

where $k = \dfrac{L}{2B}$ is the relation between the motor-vehicle dimensions.

The character of tyre deformation determines the position of the applied point O_1 of the cross reaction R_{iy} at a distance l from point O.

A total stabilizing moment acts on each driving wheel, and it is determined from the dependence

$$M_{st_j} = M_{ik}^{F_{i\tau}} + M_{ik}^{F_{in}} + M_{ik}^{N_i} + M_{ik}^{R_{iy}} , \qquad (10)$$

where $M_{ik}^{F_{i\tau}}$ is the moment created by the tangential force of friction; $M_{ik}^{F_{in}}$ is the moment created by the normal force of friction; $M_{ik}^{N_i}$ is the moment created by the normal reaction; $M_{ik}^{R_{iy}}$ is the moment created by the tyre elasticity.

The stabilizing moment for each wheel obtained by the vector product has the form

$$M_{st_1} = \begin{bmatrix} \left(\rho_{1x}\cdot F_{1\tau y} - \rho_{1y}\cdot F_{1\tau x}\right) + \\ + \left(\rho_{1x}\cdot F_{1ny} - \rho_{1y}\cdot F_{1nx}\right) + \\ + \left(\rho_{1x}\cdot N_{1y} - \rho_{1y}\cdot N_{1x}\right) + \\ + \rho_g\cdot R_{1y}\cdot\cos\delta \end{bmatrix}\cdot\cos\gamma_e , \qquad (11)$$

$$M_{st_4} = \begin{bmatrix} \left(\rho_{4x}\cdot F_{4\tau y} - \rho_{4y}\cdot F_{4\tau x}\right) + \\ + \left(\rho_{4x}\cdot F_{4ny} - \rho_{4y}\cdot F_{4nx}\right) + \\ + \left(\rho_{4x}\cdot N_{4y} - \rho_{4y}\cdot N_{4x}\right) + \\ + \rho_g\cdot R_{4y}\cdot\cos\delta \end{bmatrix}\cdot\cos\gamma_e \qquad (12)$$

The total moment created by the forces applied to the outside and inside wheel during turning presents the motor-vehicle stabilizing moment.

$$M_{st} = M_{st_1} + M_{st_4} \qquad (13)$$

The moment M_c created by the resistance force in the steering gear is presented by the vector product

$$\vec{M}_c = \vec{\rho}' \times \vec{F}_c \qquad (14)$$

where $\vec{\rho}'$ is the radius-vector of the applied point of the resistance force in the steering gear; $\vec{F}_c$ is the resistance force in the steering gear.

$\vec{F}_c$ is a linear function of the velocity and has the form

$$\vec{F}_c = -\beta\cdot\vec{V} , \qquad (15)$$

where β is the coefficient of resistance of the steering system with and without accelerator; $\vec{V}$ is the velocity of the applied point of the resistance force obtained from the kinematics analysis of a synthesized mechanism according the method of the closed vector loops.

Therefore, for the right side of equation (4) we obtain

$$\sum_{ik=1}^{n} M_{ik} = M_{st} + M_c \qquad (16)$$

A numerical experiment

A numerical experiment in the medium of Matlab, toolbox Simulink is carried out at the following initial data:

$$\theta_0 = \frac{1.5\pi}{180}[rad]; r = 0.3[m]; l_{oc} = 0.26[m];$$
$$I_1 = I_4 = 0.108[kgm^2]; \beta = 1200[\text{kg/s}];$$
$$\text{k}_\text{y} = 1000[N/\deg]; M_{is} = 450[Nm]; f = 0.02$$

The results from the numerical experiment are shown in Fig. 4 - 9.

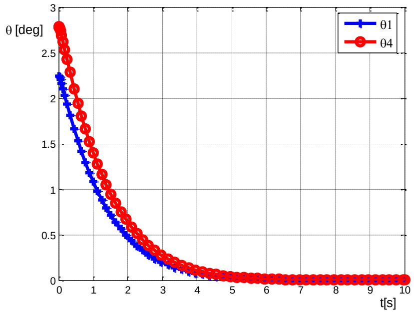

Fig. 4. A change of turning angles of the driving wheels round the axis of steering knuckle.

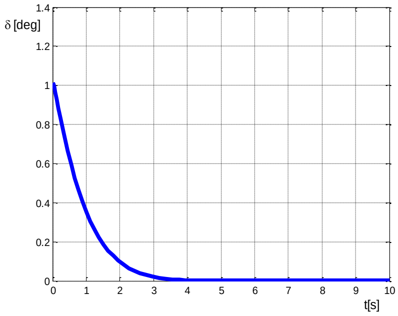

Fig. 5. A time dependence of side entrainment.

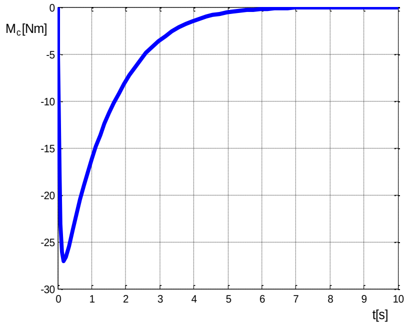

Fig. 6. A time dependence of the moment of resistance.

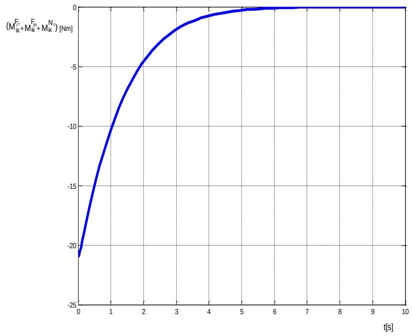

Fig. 7. A time dependence change of the stabilizing moment due to the reactions.

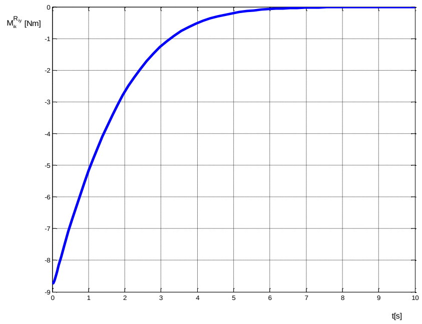

Fig. 8. A time dependence change of the stabilizing moment due to the tyre elasticity.

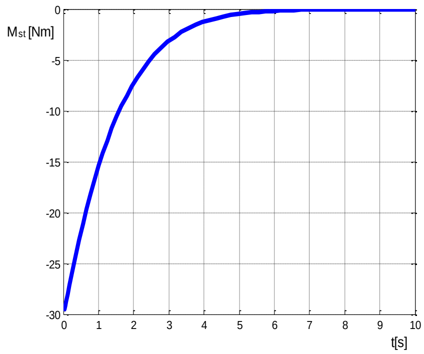

Fig. 9. A time dependence of the total stabilizing moment.

The created mechano-mathematical model gives the opportunity for evaluation of motor-vehicle stability during accidental side interference in the driving wheels. This model in a generalized form is also applied for more precise identification of motor-vehicle motion after the loss of its cross stability in the cases after turn, after rush in another vehicle, after inadequate turning of the steering wheel, etc.

REFERENCES

[1] CarSim Math Models, Version 5, Draft July 2001. MSC /Mechanical Simulation Corporation/ (USA), 2001

[2] Gerdes J. C., Yung-Hsiang J. H. Stabilization of a steerby- wire vehicle at the limits of handling Using feedback linearization, Proceedings of IMECE 2005 ASME International Mechanical Engineering Congress and Exposition, November 5-11, 2005, Orlando, Florida, USA

[3] Karapetkov, St. A computer simulation of motor-vehicle motion after a rush with reading the wheels rotation, Mechanics of Machines, Varna, 2002

[4] Karapetkov, S., Z. Kalitchin, H. Uzunov. Determination of Vehicles' Velocities in CarCrash Using Different Friction Coeffiecients. 4-th International Conference on Tribology, Kayseri, Turkey, 12 - 14 June, 2002, Proceedings, Volume II, p. 455 - 463

[5] Kurtev, N., N. D. Minchev. A stability during turning, Mechanics of Machines, Varna, 2003

[6] Litvinov, A. S. Steering and stability of vehicle, Moscow, 1971

[7] Steffan, H., A. Moser. The Collision and Trajectory Models of PC-CRASH. Graz University of Technology, 1998.

[8] Steffan, H. PC-CRASH, A Simulation Program for Car Accidents. ISATA; 26 th International Symposium on Automotive Technology and Automation, Aachen 1993

HEAVY MACHINERY - HM 2011, 13-18
ISBN 978-86-82631-58-3 Paper accepted: 20.05.2011

The Design and Redesign of Mechanized Slipways

Zoran D. Petković[1] - Srđan M. Bošnjak[1,*] - Nebojša B. Gnjatović[1] - Ivan LJ. Milenović[1]
[1] University in Belgrade - Faculty of Mechanical Engineering

Mechanized slipways are the backbones of the shipyards' transportation systems. Their characteristics, above all the carrying capacity and the maximum vessel length, define the technological possibilities of the shipyard. The first part of the paper presents the original design of the mechanized slipway for side launching used for river, sea and oversea vessels with overall weight up to 2400 t and maximum length of 140 m. The second part contains a brief presentation of the redesign procedure of the mechanized longitudinal slipway for sea vessels up to 300 t.

Keywords: Side slipway, longitudinal slipway, design, redesign

0 INTRODUCTION

Mechanized slipways are the backbones of the shipyards' transportation systems [1] and [2]. Their characteristics, above all the carrying capacity and the maximum vessel length, define the technological possibilities of the shipyard. This paper presents:

- An original concept and design of the mechanized slipway for side launching vessels with an overall weight up to 2400 t and maximum length of 140 m;
- The redesign procedure of the mechanized longitudinal slipway for sea vessels up to 300 t.

1 DESIGN OF THE SIDE SLIPWAY FOR RIVER, SEA AND OVERSEA VESSELS

The newly built slipway of "Shipyard Bomex 4M", Fig. 1, thanks to its performances, makes building river and sea ships possible and, by that, improves export possibilities of Serbia in the area of ship building [3] to [5]. Until now, all contracted production has been aimed at foreign markets.

Fig. 1. *Shipyard Bomex 4M*

Basic functional elements of the slipway mechanization system, Fig. 1, are:

- Carriage of 300 t capacity - "big carriage", Fig. 2;

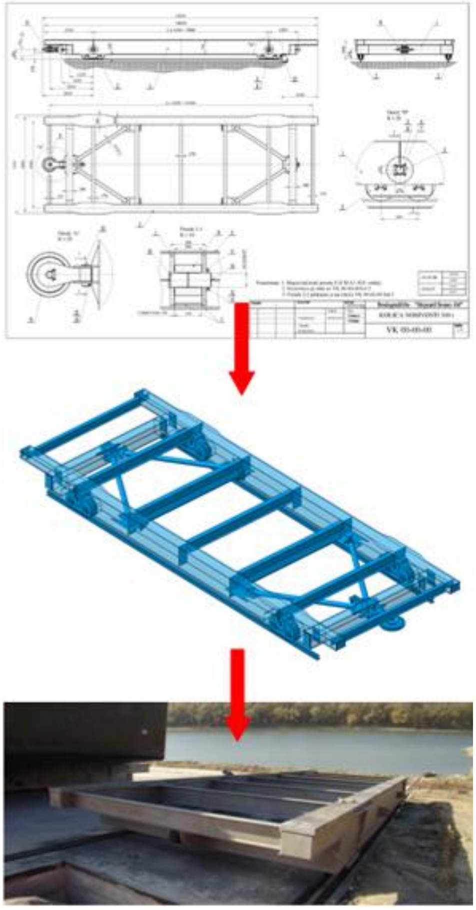

Fig. 2. *Carriage of 300 t capacity*

---

[*]Corr. Author's Address: Faculty of Mechanical Engineering, Kraljice Marije 16, Belgrade, Serbia, sbosnjak@mas.bg.ac.rs

- Carriage of 150 t capacity - “small carriage”; two small carriages are connected by a truss-type structure and form the so-called carriage tandem of 300 t capacity, Fig. 3;

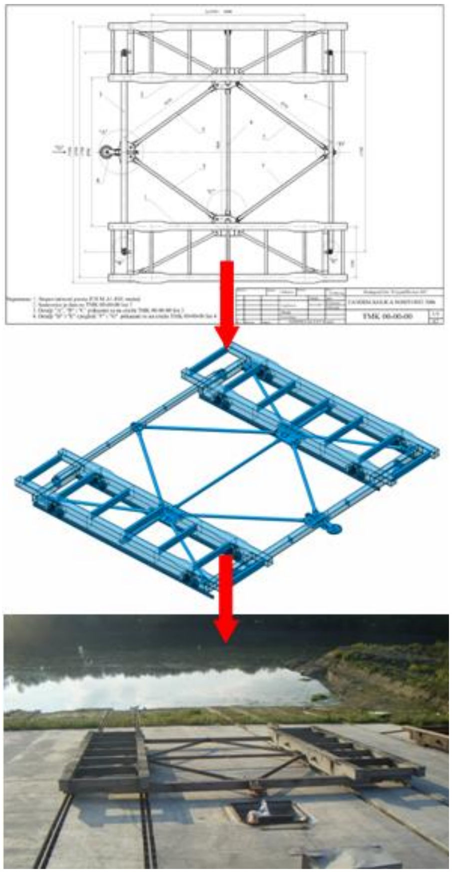

Fig. 3. *Carriage tandem of 2 x 150 t capacity*

- Winch, maximal pulling force of 282 kN - “big winch”, Fig. 4;
- Winch, maximal pulling force of 75.5 kN - “small winch”, Fig. 5;
- Guiding cable rollers, Fig. 6;
- Control system, Fig. 7.

Fig. 4. *Big winch - pulling force of 282 kN*

Fig. 5. *Small winch - pulling force of 75.5 kN*

Fig. 6. *Guiding cable rollers*

Fig. 7. *Control system*

The concept of carriage assembling in tandems, powered by only one winch, represents an original solution. Besides that, the design of the carriage structure and subtle stress – strain analysis of all elements of the system enabled the project to conform to a very important design restriction – the possibility of launching a vessel of maximum weight and length even at river Begej’s lowest water level.

All slipway subsystems and parts are produced in Serbia according to the project documentation made by the University of Belgrade – Faculty of Mechanical Engineering.

Winches, pulling sheaves, guiding cable rollers and two wheel boogies are produced by “GOŠA FOM”. Steel carriage structures are produced by “Shipyard Bomex 4M”.

Validation of the presented slipway mechanization system in the case of extreme load was done by launching a fishing vessel, weight of 1200 t, Fig. 8(a). Because of the relatively small length, approximately 80 m, the total load is distributed on three carriage tandems, Figs. 8(b,c,d).

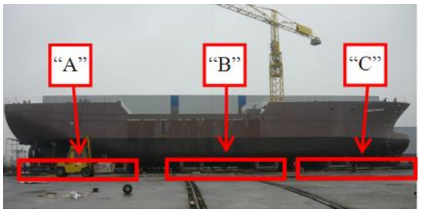

(a) leaning of the vessel

(b) detail A

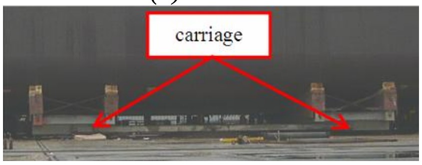

(c) detail B

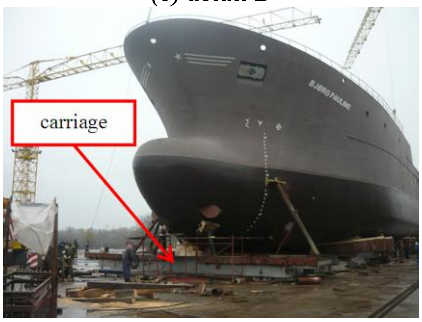

(d) detail C

Fig. 8. *Launching of the 1200 t fishing vessel*

Besides extreme load conditions present during vessel launching shown in Fig. 8, environmental conditions (water-level) were extreme as well, Fig. 9.

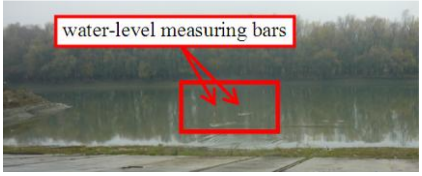

(a)

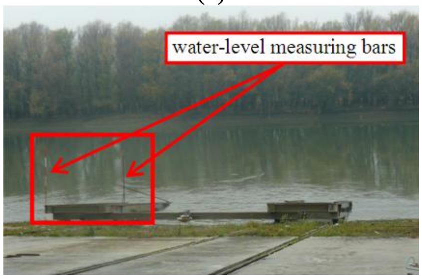

(b)

Fig. 9. *Carriage with water - level bars used in case of extreme shallow waters*

2 REDESIGN OF THE LONGITUDINAL SLIPWAY MECHANIZATION FOR SEA VESSELS

The longitudinal slipway mechanization system consists of the towing subsystem, Fig. 10, and the subsystem of three carriages, capacity of 100 t each, Figs. 11 and 12. Carriage structures are basically the same, differing only in the zones of connections. . The total length of carriage 1 is 10680 mm, while total lengths of carriage 2 and 3 are 10000 mm.

The carriage structures’ basic parts, Figs. 13 to 15, are:

- Main girders right (1);
- Main girders left (2);
- Cross girders (3) and (4).

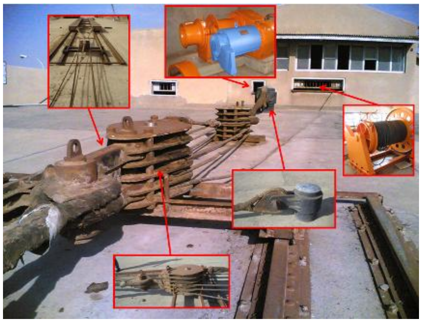

Fig. 10. *Towing subsystem*

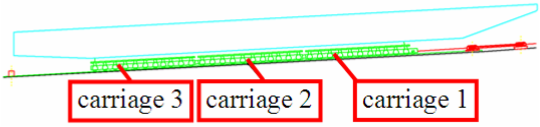

Fig. 11. *Vessel leaning*

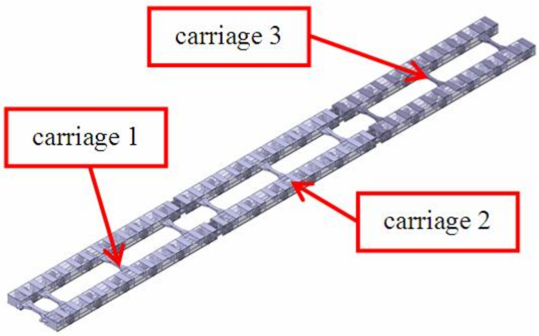

Fig. 12. *Carriage subsystem*

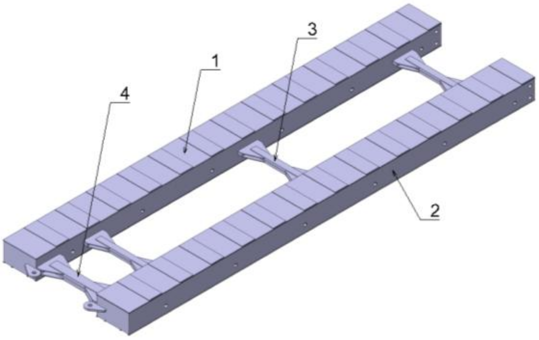

Fig. 13. *Structure of carriage 1*

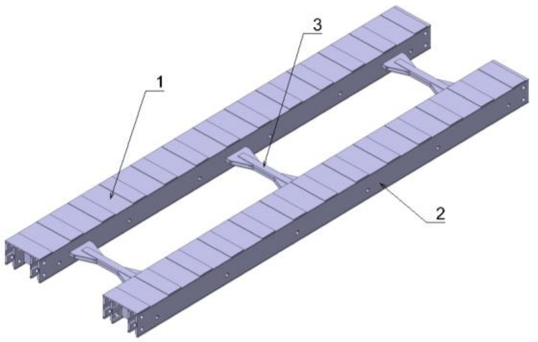

Fig. 14. *Structure of carriage 2*

Perennial exploitation in heavy environmental conditions caused extremely pronounced corrosion of carriage structures, Figs. 16 and 17. In order to achieve functionality and reliability of the slipway mechanization system, repair and revitalizaton of the most jeopardized parts was done as presented in Figs. 18 and 19.

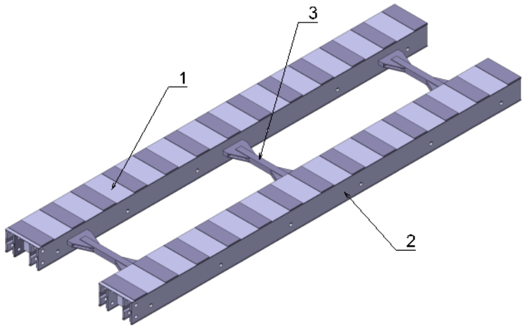

Fig. 15. *Structure of carriage 3*


Fig. 16. *Corrosion of the main vertical panel*


Fig. 17. *Corrosion of the secondary vertical panel*


Fig. 18. *Repair of the main vertical panel*


Fig. 19. *Repair of the secondary vertical panel*

The goals of study [6] were:

- To define the repair and revitalization procedure and the reconstruction design;
- To verify the reconstructed structure by numerical analysis, i.e. by comparing the maximum stresses for the structure with the designed and measured, Fig. 20, thickness of plates.

Fig. 20. *US thickness measuring*

The 3D models of carriage structures, Figs. 13 to 15, were discretized by the parabolic tetrahedron elements, Fig. 21.

Stress – strain identifications were done for the designed carriage structures, Figs. 22 and 23, as well as for structures with minimum measured thickness of the main vertical panels, Table 1.

Fig. 21. *Detail of mesh*

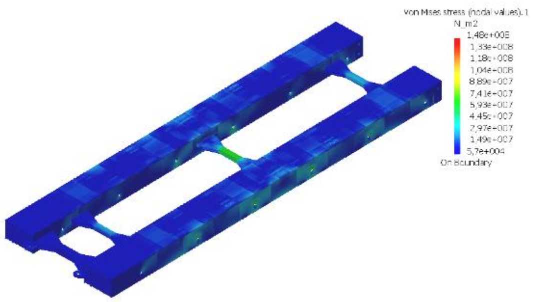

Fig. 22. *Von Misses stress field*

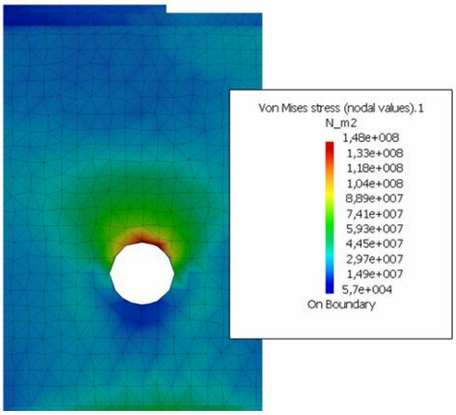

Fig. 23. *Detail of stress field in critical zone*

Table 1. *Maximum Von Misses stresses*

(a) Designed main vertical plate thickness

Carriage	Thickness	Stress $\sigma_{vM,D}$
	mm	kN/cm^2
1	10	14,8
2	10	14,9
3	10	14,7

(b) Measured main vertical plate thickness

Carriage	Minimum thickness	Stress $\sigma_{vM,M}$
	mm	kN/cm^2
1	5,4	18,2
2	5,9	17,4
3	5,3	18,2

(c) Ratio of maximum stress values

Carriage	$\frac{\sigma_{vM,D}-\sigma_{vM,M}}{\sigma_{vM,D}}\times 100$
1	23,0 %
2	16,8 %
3	23,8 %

Maximum stress values were obtained in the zones of axles bearing, Fig. 23. As it can be observed, they are quickly damped. Besides that, the influence of contact stress is dominant in the considered zones. Having in mind that permissible stress values in this case are considerably greater than the calculated stress values, it is conclusive that carriage structures satisfy the strength criterion even in the case of minimum measured thickness of the vertical panels.

3 CONCLUSION

Slipway mechanization systems determine the technological possibilities of a shipyard, and present its very responsible part. Their eventual failure inevitably leads to catastrophic consequences. Exactly because of that, calculation of structures and other parts of the system should be done by taking into account all unfavorable impacts and their possible combinations. Calculations of the presented slipway mechanization systems were done by applying FEM, which enables subtle stress – strain analysis and achievement of high safety and minimum weight of carriage structures as well as other system parts.

4 REFERENCES

[1] Rawson, K. J., Tupper, E. C. “Basic ship theory”, Butterworth-Heinemann, Oxford, 2001.

[2] Šuša, M. “Shipbuilding technology“, University in Belgrade - Faculty of mechanical engineering, Belgrade, 2007. (in Serbian)

[3] Petković, Z., Lepović, M. “Shipyard Bomex 4M – Feasibility study“, University in Belgrade - Faculty of mechanical engineering, Belgrade, 2006. (in Serbian)

[4] Petković, Z., Bošnjak, S., Gnjatović, N., Đorđević, M. “High - Performance Mechanized Side Slipway for River, Sea and Oversea Ships“, Proceedings of the 19th International Conferece on Material Handling, Constructions and Logistics - MHCL’09, University in Belgrade - Faculty of Mechanical Engineering Belgrade, ISBN: 978-86-7083-672-3, pp. 89-94, Belgrade, 2009.

[5] Petković, Z., Bošnjak, S., Gnjatović, N., Đorđević, M. “The Design of High - Performance Mechanized Side Slipway for vessels up to 1800 t“, Investor Bomex 4M, University in Belgrade - Faculty of Mechanical Engineering Belgrade, Belgrade, 2007.

[6] Petković, Z., Bošnjak, S., Gnjatović, N., Đorđević, M. “The Redesign of Morton’s Slipway“, University in Belgrade - Faculty of Mechanical Engineering Belgrade, Belgrade, 2008.

Acknowledgement

This work is a contribution to the Ministry of Science and Technological Development of Serbia funded project TR 35006.

HEAVY MACHINERY - HM 2011, 19-24
ISBN 978-86-82631-58-3
Paper accepted: 30.05.2011

Design of 3-Dof Machine Tool Based On Hybrid Mechanism

Cvijetin Mlađenović[1] – Slobodan Tabaković[1] – Milan Zeljković[1]
[1] Faculty of Technical Sciences, Novi Sad

As a consequence of development of product design, materials, tools and machining processes, there were requirements for the processing operations that are difficult to perform on conventionally built machine tools. Therefore is intensified the development of machine tools with hybrid kinematics, which can meet the new requirements.

This paper, for the given dimensions of working space (x = 500mm, y = 25 mm, z = 80mm), presents a modern approach to designing machine tools based on hybrid mechanisms, using the software system Pro / Engineer and Mathematica. The characteristics of hybrid mechanism relevant to their application to machine tools are described in this paper. Also was performed the kinematics analysis of hybrid mechanism which is applied to the designed machine tools. Using system software Mathematica the workspace of the machine tool has been analyzed and provided the dimensions of the hybrid mechanism and the basic dimensions of machine tools. On a virtual model of the hybrid mechanism, formed in the module SimMechanic within Matlab, was performed an analysis of velocity of certain moving elements (sliders).

Keywords: Machine tools, Parallel mecanism, Pro/Engineer, Mathematica, SimMechanic, simbolic modeling

1. INTRODUCTION

Ever present growth of market demands has caused the continuous development of machine tools that includes the improvement and development of their components. This mean increased productivity of machine tools, with the improvement of exploitation characteristics and improvement in the field of achievable accuracy and surface quality.

During the last fifteen years, an extensive research of machine tools components has caused a development of the machine tool with a larger number of numerically controlled axes, with more main spindle velocity, and with greater feed velocities.

One of the directions for the development of machine tools are machine tools based on the application of parallel mechanisms.

Along with the idea of the application of parallel mechanisms in the development of machine tools, there is also the idea of combining conventional machine tools (serial) and parallel kinematics. In this way were created machine tools based on the hybrid mechanisms.

In this paper is discussed a conception of the parallel and hybrid mechanisms applicable to machine tools. Also, it should be noted that considered hybrid mechanisms have been created on the basis of the parallel. And therefore below will be considered only the basic characteristics of the parallel mechanisms.

2. SPECIFICS AND CHARACTERISTICS OF PARALLEL MECHANISMS

From the first idea until today a great number of different conceptions and constructions of the parallel mechanisms has been developed. The only characteristic possessed by all now known concepts of parallel mechanism is a fact that the complex, spatial, movement of the movable platform is realized by simultaneous action of mutually independent elements.

Figure 1 presents a parallel mechanism *Hexaglide* with its main components.

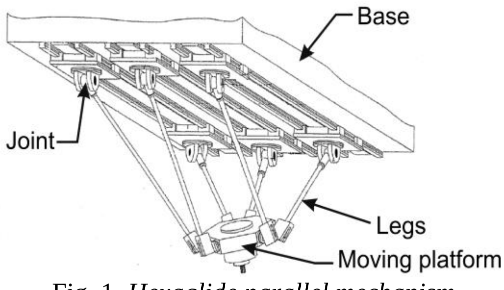

Fig. 1. *Hexaglide parallel mechanism*

*Corr. Author's Address: Faculty of Technical Science, Novi Sad, Serbija, mladja@uns.ac.rs

2.1 The basic components of the parallel mechanisms

Regardless to the type of the mechanism, the components of the parallel mechanisms (Figure 1) can be classified in several groups, including:

- Fixed platform (base),
- Mobile platform,
- Legs or rods, and
- Joints, as elements of connection between the legs and the platforms.

When it comes to machine tools, in addition to previous characteristics it is also necessary to consider the following: the base, control systems, main spindles, drive systems, linear guides, etc.

3. KINEMATIC ANALYSIS OF THE APPLIED HYBRID MECHANISM

Hybrid mechanism applied for the development of the concrete machine tool consists a plane parallel mechanism wich linearly moves along the longitudinal guides. This parallel mechanism is made of two or more constant length rods, that connect the moving platform with sliders, which move along the transversal guides. By moving the slider per transversal guides also is achieved the movement of the movable platform in the *y*-*z* plane. The positioning per *x*-axis is performed by moving the entire parallel mechanism per longitudinal guides.

Figure 2 shows the scheme of machine tools based on this hybrid mechanism.

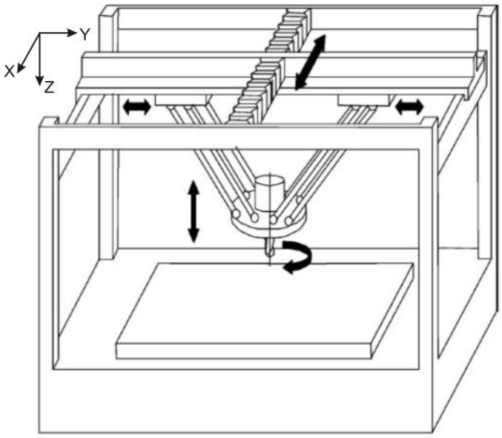

Fig. 2. *Schematic view of the hybrid machine tool*

As the basis of a hybrid mechanism is planar parallel mechanism, kinematic analysis of a hybrid mechanism is performed for two different positions of the parallel mechanism - for the stretched and the crossed position of its rods.

Kinematic analysis of plane parallel mechanism involves studying the movement of its elements in two separate analysis: direct and inverse kinematics analysis.

Direct kinematic analysis of parallel mechanism is a process of determining the position of the movable platform for the known values of transverse sliders position.

Inverse kinematic analysis is the opposite problem, for the known value of the position of the moving platform, mathematically are determined positions of the transverse sliders.

3.1 Kinematic analysis of a hybrid mechanism in streched position

Kinematics analysis of the mechanism in stretched position was performed on the basis of plane scheme are presented in Figure 3.

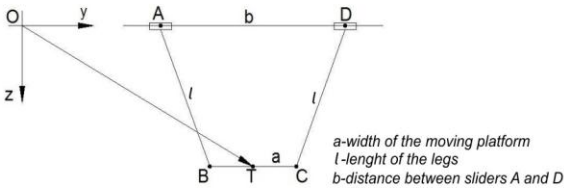

Fig. 3. Scheme of the hybrid mechanism in streched position

The presented scheme shows that the center of gravity of the movable platform (T) is determined by a vector $\overline{OT}$, which can be expressed in two ways:

$$\begin{aligned} \overline{OT} &= \overline{OA} + \overline{AB} + \overline{BT} \\ \overline{OT} &= \overline{OD} + \overline{DC} + \overline{CT} \end{aligned} \quad (1)$$

By projecting these equations on the axis *y* and *z* the following equation are formed:

$$\begin{aligned} y_T &= y_A + y_{AB} + y_{BT} \\ z_T &= 0 + z_{AB} + 0 \\ y_T &= y_D - y_{DC} - y_{CT} \\ z_T &= 0 + z_{DC} + 0 \end{aligned} \quad (2)$$

This system of equations is undefined and therefore need to add the following restriction:

the movable platform should always be horizontal, or:

$$l^2 = y_{AB}^2 + z_{AB}^2$$
$$l^2 = y_{DC}^2 + z_{DC}^2 \qquad (3)$$

Solving these equations by inverse kinematic analysis, for a given position and orientation of the moving platform, it can be determined position of the sliders on the guides and the distance between the rods.

Position of the sliders A and D along the y-axis:

$$y_A = y_T - \left(\frac{a}{2} + \sqrt{l^2 - z^2}\right)$$
$$y_D = y_T + \left(\frac{a}{2} + \sqrt{l^2 - z^2}\right) \qquad (4)$$

Distance between slider A and D:

$$b = a + 2\sqrt{l^2 - z^2} \qquad (5)$$

Solving the previous equation by direct kinematic analysis it is possible, for a given position of the slider, to determine the position and orientation of the moving platform. Position of the movable platform is determined by the position of its center of gravity (T).

Position of platforms center of gravity in the *y* direction:

$$y_T = y_A + \left(\frac{a}{2} + \sqrt{l^2 - z^2}\right) \quad \text{or}$$
$$y_T = y_D - \left(\frac{a}{2} + \sqrt{l^2 - z^2}\right) \qquad (6)$$

Position of platforms center of gravity in the *z* direction:

$$z = \frac{1}{2}\sqrt{4l^2 - (b-a)^2} \qquad (7)$$

3.2. Kinematic analysis of a hybrid mechanism in crossed position

Kinematic analysis of the mechanism in crossed position was performed on the basis of plane scheme presented in Figure 4.

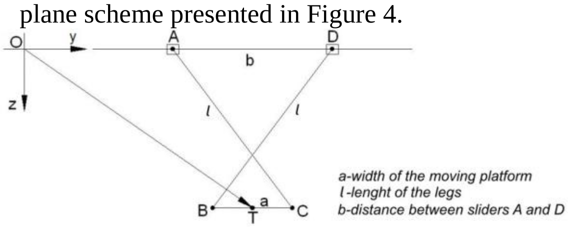

Fig. 4. *Scheme of the hybrid mechanism in crossed position*

The presented scheme shows that the center of gravity of the movable platform (T) is determined by a vector $\overline{OT}$, which can be expressed in two ways:

$$\overline{OT} = \overline{OA} + \overline{AC} + \overline{CT}$$
$$\overline{OT} = \overline{OD} + \overline{DB} + \overline{BT} \qquad (8)$$

By projecting these equations on the axis *y* and *z* the following equation are formed:

$$y_T = y_A + y_{AC} - y_{CT}$$
$$z_T = 0 + z_{AC} + 0$$
$$y_T = y_D - y_{DB} + y_{BT} \qquad (9)$$
$$z_T = 0 + z_{DB} + 0$$

This system of equations is undefined and therefore need to add the following restriction: the movable platform should always be horizontal, or:

$$l^2 = y_{AC}^2 + y_{AC}^2$$
$$l^2 = y_{DB}^2 + y_{DB}^2 \qquad (10)$$

Solving these equations by inverse kinematic analysis, can be determined a position of the sliders on the guides and the distance between the rods.

Position of the sliders A and D along the y-axis:

$$y_A = y_T + \left(\frac{a}{2} - \sqrt{l^2 - z^2}\right)$$
$$y_D = y_T - \left(\frac{a}{2} - \sqrt{l^2 - z^2}\right) \qquad (11)$$

Distance between slider A and D:

$$b = 2\sqrt{l^2 - z^2} - a \qquad (12)$$

Solving the previous equation by direct kinematic analysis it is possible to determine the position and orientation of the moving platform.

Position of platforms center of gravity in the *y* direction:

$$y_T = y_A - \left(\frac{a}{2} - \sqrt{l^2 - z^2}\right) \quad \text{or}$$
$$y_T = y_D + \left(\frac{a}{2} - \sqrt{l^2 - z^2}\right) \qquad (13)$$

Position of platforms center of gravity in the *z* direction:

$$z = \frac{1}{2}\sqrt{4l^2 - (a+b)^2} \qquad (14)$$

4. WORKSPACE ANALYSIS

When designing machine tools, one of the main input data are dimensions of its workspace and the material of the workpiece.

In this case the dimensions of the workspace are: $x = 500\ mm$, $y = 250\ mm$ and $z = 80\ mm$, where the dimensions y and z are achieved by a parallel mechanism, and the dimension x by its movement along the x-axis.

4.1. Determining the length of rods

The length of rods of the parallel mechanisms, necessary to achieve the required dimensions of the workspace, is determined by analyzing the 3D diagram which shows the dependence of the moving platforms position along the z axis from the rods length and position of the platform along the y axis.

The diagram, which is shown in Figure 5, is created in the software system *Mathematica* by entering the equation calculated in direct kinematic analysis and varying the position of the slider A, position of the movable platform center of gravity and the length of the sticks.

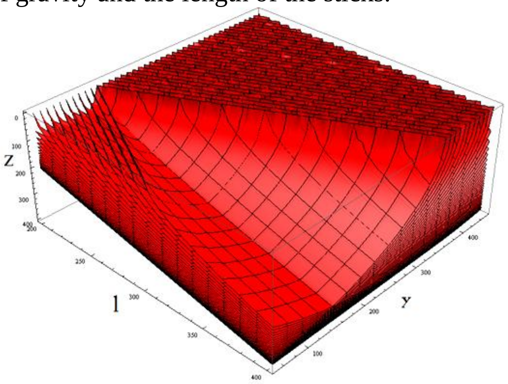

Fig. 5. Change of the movable platform center of gravity position in the direction of z axis according to the length of rods and center of gravity position in the direction of y axis

4.2. Determining the length of the transverse guides

The maximum value for the distance between sliders A and D (b_{max}) occurs when the mechanism is in a maximum crossed position. Figure 6 shows the dependence of the distance between the sliders from the position of moving platform's center of gravity (T).

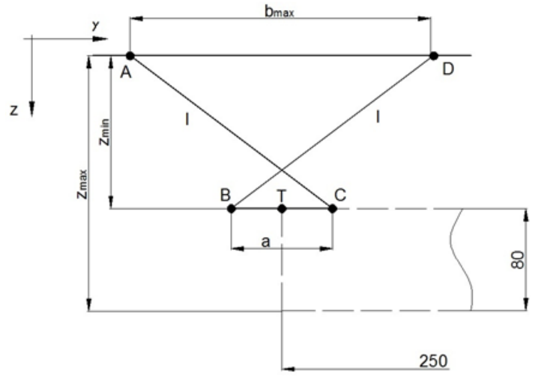

Fig.6. The dependence of the distance between the sliders from the position of moving platform's center of gravity

Maximum distance between sliders A and D:

$$b_{\max} = 2 \cdot \sqrt{2l\Delta z - \Delta z^2} - a \qquad (15)$$
$$b_{\max} = 266{,}6\ \ mm$$

for: $\Delta z = 80mm$, $l = 250mm$, $a = 100mm$

The guides length:

$$l_{guide} = b_{max} + 250$$
$$l_{guide} = 516{,}6\ \ mm \qquad (16)$$
$$l_{guide} = 520\ \ mm$$

Figure 7 shows the theoretical workspace of the designed machine tools, formed on the basis of the previously calculated values.

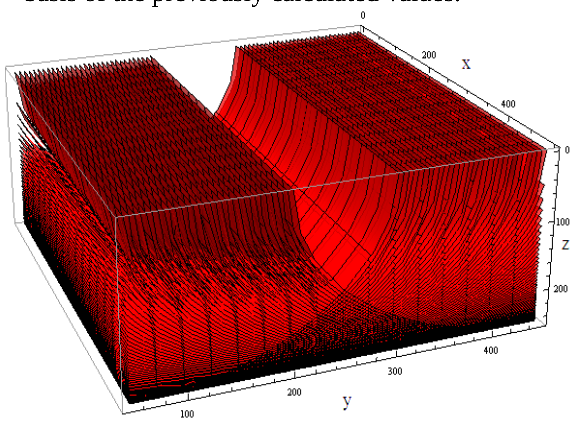

Fig.7. *Theoretical workspace of the designed machine tools*

5. THE MAIN CHARACTERISTICS OF DESIGNED MACHINE TOOLS

The basic input data for the definition of the main characteristics of machine tools are:

- Workpiece material: Aluminum,
- Dimensions of workspace: $500x250x80\ mm$
- Tool material: high-speed cutting steel
- Maximum tool diameter: $D_{max} = 6\ mm$

Calculation of the main characteristics of the designed machine tool was made based on the calculation of the main characteristics of vertical milling machine, according to [2], and the following results were obtained:

- The maximum tool feed velocity:

$$s_{1max} = 0{,}75 \cdot 10^{-3}\ {}^{m}\!/\!{}_{tooth} \qquad (17)$$

- The minimum tool feed velocity:

$$s_{2\,min} = 0{,}25 \cdot 10^{-3}\ {}^{m}\!/\!{}_{tooth} \qquad (18)$$

- The maximum tool revolutions per minute:

$$n_{max} = 250\ {}^{rev}\!/\!{}_{s} = 15000\ {}^{rev}\!/\!{}_{min} \qquad (19)$$

- Power of main spindle driving motor:

$$P_m = 1100\,W \qquad (20)$$

Based on these values are elected the basic elements of machine tools.

6. VIRTUAL MODEL ANALYSIS OF THE DESIGNED HYBRID MACHINE TOOLS

In the module SimMechanic within Matlab, using symbolic modeling was formed the virtual model of the designed machine tools. On this virtual model it is possible to perform a number of analyzes that provide an insight in the behavior of individual elements and the entire machine tool in exploitation.

As the main element of the projected machine tool is a parallel mechanism, in continuation is performed a speed analysis of his sliders. During the analysis, mobile platform is moving in the direction of y axis at the speed of 20 m/min, whereby is defined a friction between the sliders and guides, and the friction in the joints. Figure 8 shows the comparison of sliders velocities at the crossed and at the stretched position of the mechanism.

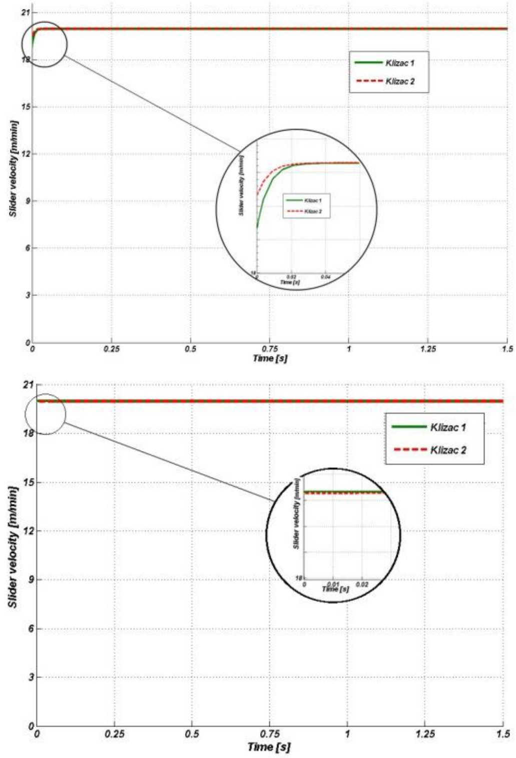

Fig. 8. *Velocity of sliders at the stretched (up) and at the crossed (down) position of the mechanism.*

As it can be seen on the figure, for a constant speed of the moving platform, in both cases are obtained smooth speed of the sliders, which is from the point of machine tools controlling very convenient.

7. CONCLUSION

This paper presents the modern approach in the development of machine tools based on the hybrid mechanisms. A special accent is put on the kinematic analysis of the applied parallel mechanism, which represents the basis of designed machine tools, and on the analysis of the machine workspace. Workspace analysis was performed in software system Mathematica. Also was performed the calculation of the main characteristics of machine tools in order to select its basic components.

Based on these components it was formed a virtual model of the machine tool on which is performed an analysis of the sliders velocities of the parallel mechanism.

Reviewing the results of this analysis, it can be concluded that the idea of the possibility of sliders crossing could be in future used for the development of new machine tools which would be based on the parallel mechanisms.

REFERENCIS

[1] Altintas, Y., Brecher, C., Weck, M., Witt, S.: Virtual Machine Tool, CIRP Annals - Manufacturing Technology, Vol 54, Issue 2, pp. 115-138, 2005

[2] Gatalo, R., Borojev, Lj., Zeljković, M.: Proračun glavnih karakteristika mašina alatki za obradu rezanjem, udžbenik, Fakultet tehničkih nauka, Novi Sad, 1992.

[3] Mlađenović, C., Zeljković M., Tabaković S.: Razvoj troosne mašine alatke sa paralelnom kinematikom, Zbornik radova Fakulteta tehničkih nauka, Vol.13/2010, Novi Sad, str. 2625-2628, ISSN 0350-428X.

[4] Rehsteiner, F., Neugebauer, R., Spiewak, S., Wieland, F.: Putting Parallel Kinematics Machines (PKM) to Productive Work, Annals of the CIRP, Vol 48, No. 1, pp.; 345-350, 1999., ISSN 1726-0604

[5] Tabaković, S., Zeljković, M., Gatalo, R.: Methodology of workspace analysis of machinetools based on parallel mechanisms, Facta Universitatis Series:Mechanical Engineering Vol. 7, No 1, pp. 61 - 72, 2009.

[6] Tabaković, S.: Razvoj programskog sistema za automatizovano projektovanje mašina alatki na bazi paralelnih mehanizama i optimalni izbor njihovih komponenti, doktorska disertacija, Fakultet tehničkih nauka, Novi Sad, 2008.

[7] Tabaković, S.: Razvoj programskog sistema za automatizovano projektovanje mašina alatki na baziparalelnih mehanizama i optimalni izbor njihovih komponenti, doktorska disertacija, Fakultet tehničkih nauka, Novi Sad, 2008.

[8] Zou, P.: Kinematic analysis of a biglide parallel grinder, Jurnal of Materials Processing Technology, Vol.138, pp.461-463, Elsevier, 2003., ISSN: 0924-0136

ACKNOWLEDGEMENTS

In this paper are presented some results of the project: *"Contemporary approaches to the development of special solutions related to bearing supports in mechanical engineering and medical prosthetics"* – TR 35025. The project is supported by Ministry of education and science of the Republic of Serbia.

HEAVY MACHINERY - HM 2011, 25-29 Paper accepted: 20.05.2011
ISBN 978-86-82631-58-3

Determination Of The Meshing Forces Of Gearing Teeth With Precession Movement

Marian Dima[1,*], Adrian Bruja[1], Catalin Francu[1]
[1] Technical University of Civil Engineering Bucharest

Starting from the central wheel teeth profile for the case of precession-moving reducer with satellite's teeth as tapered rolls, are determined the analytical equations of the common normal of the two profiles and thus the direction of force at different points on the gearing line (determined by the authors in another paper). Further, magnitudes of the forces are determined at the same points of contact

Keywords: Precessional gearing, gearing law, line of contact, forces

0 INTRODUCTION

Having the advantages enabled by these transmissions: - High and very high gear ratios, very good efficiency, reduced dimensions and mass, can remove backlash in reversing direction, reliability, etc. - can be used on machines that require a very large gear ratios (hoists, machinery, production lines, etc.) as well as in robotics.

The paper continues a series of research by the authors in this field such as kinematics and kinetics of the equivalent bar mechanism of this type of transmission, gearing kinematics, tooth profile etc, whose results were published in several publications in the country and abroad. Based on this work, we developed a new method of calculation and design for such transmissions.

1. DETERMINING THE DIRECTION OF MESHING FORCES

The kinematic scheme of the precession-moving reducer with simple satellite is shown in Figure 1. Determination of meshing forces starts from Figure 2. As this figure shows the intersection with a sphere of radius R and center O consists of a precession gearing composed of the satellite gear with rolls 2 and the central wheel 3, the two wheels having fixed axes.

The contact between tooth flanks is on the gearing line [1] C_p, p = 1, 2…m, m - number of pairs of teeth that are engaging. These points are located at a distance r_p related to the wheel axis, measured in a plane perpendicular to the central wheel axis and z_p distance related to point O of axes intersection.

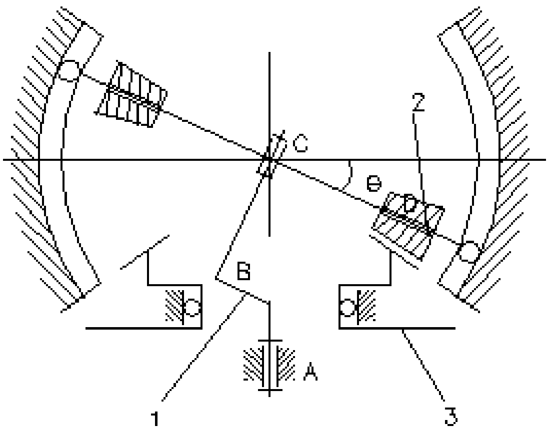

Fig. 1 Precession motion reducer
1- input shaft, 2- satellite gear with rolls;
3- central wheel

The action of twisting moment $\overline{M}_c$ at the central wheel shaft, at the points of contact, forces $\overline{F}_p$ located on common normal of the side teeth at points of contact. The direction of forces $\overline{F}_p$ is given by the moment $\overline{M}_c$. Effect of forces $\overline{F}_p$ is the deformation of side teeth in the contact area and the central wheel rotation angle $d\varphi$. Let the deformation measured in a plane perpendicular to the central wheel axis with δ_p.

Between r_p, δ_p and $d\varphi$ we have the equation.

$$\delta_p = r_p d\varphi \tag{1}$$

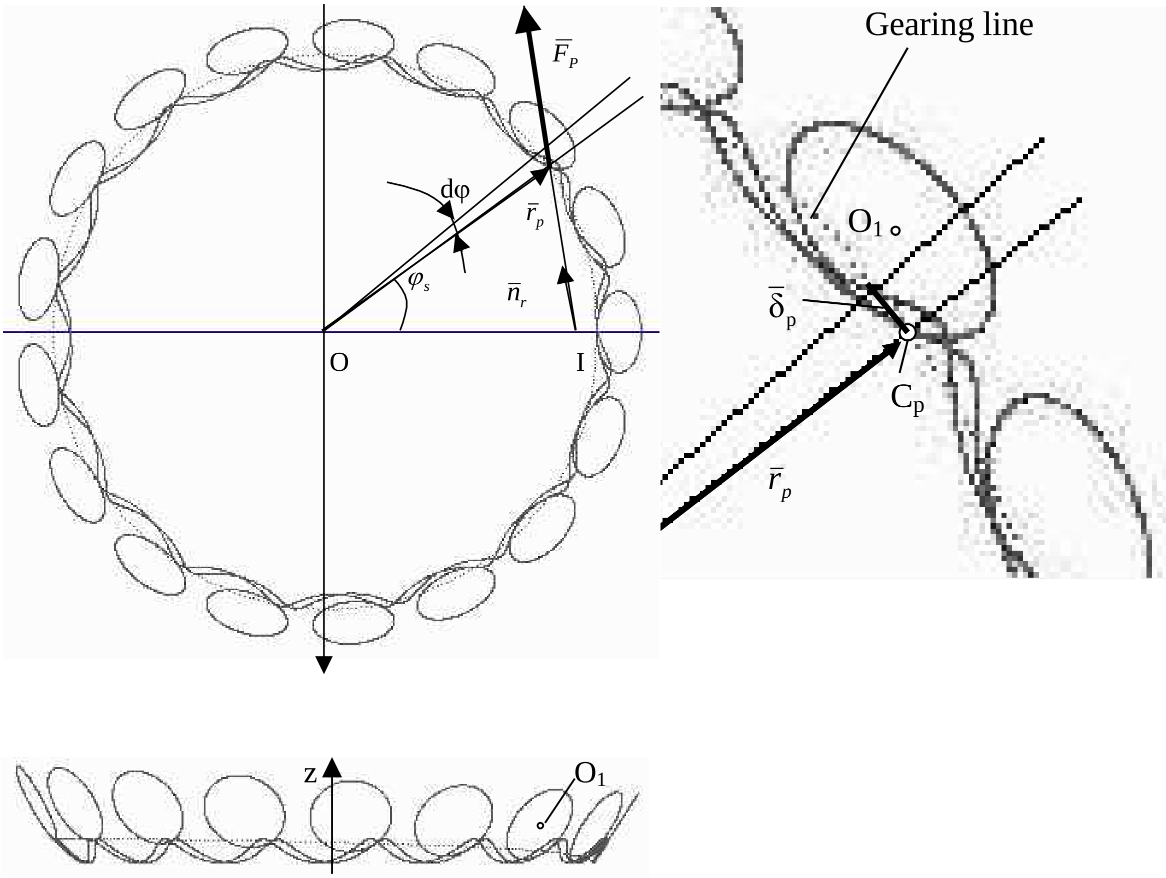

Fig. 2 Schema de calcul pentru forţele din angrenare

Position vectors of the contact points C_p related to the origin of the reference frame have the analytical expression

$$\bar{r}_{lp} = x_l \bar{i} + y_l \bar{j} + z_l \bar{k} \tag{2}$$

where the projections x_l, y_l, z_l are given by the gearing line expression, determined for the values of the angles φ_s according to the rolls positions. These values are determined by the expression

$$\varphi_s = \varphi_0 + p\frac{2\pi}{Z_s}; \text{ p = 1, 2 …m,} \tag{3}$$

where φ_0 - the angle between the roll's axis and the reference frame axis

Z_s – number of rolls of the satellite wheel.

The direction of the normal force $\bar{F}_p$ in the point of contact C_p is given by the common normal versor $\bar{n}_r$ of the side teeth in contact, figure 3.

$$\begin{aligned} \bar{n}_r &= \frac{\overline{CO_1'}}{CO_1'} = \frac{1}{\rho'}(x_l - x_{O_1'})\bar{i} + \\ &+ (y_l - y_{O_1'})\bar{j} + (z_l - z_{O_1'})\bar{k} = \\ &= n_{rx}\bar{i} + n_{ry}\bar{j} + n_{rz}\bar{k} \end{aligned} \tag{4}$$

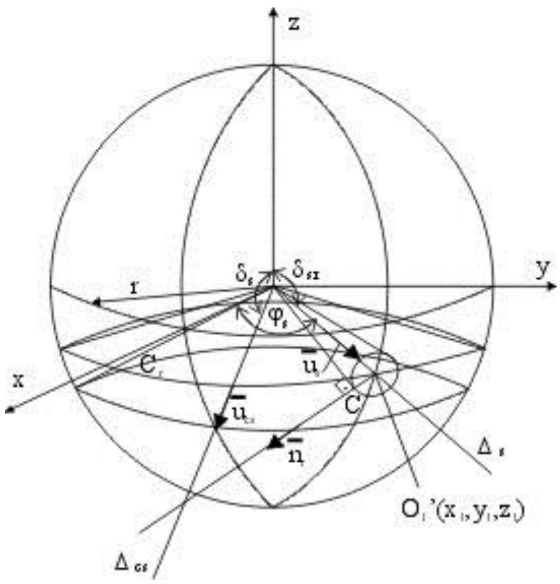

Fig. 3 The common normal $\bar{n}_r$ with side teeth in contact

2. DETERMINING THE FORCES MAGNITUDE

Side teeth gap δ_{pF} (deflection of side teeth in contact by the normal force direction) depends of the magnitude of force $\bar{F}_p$. This dependency for steel bodies is,

$$\delta_{pF} = 1{,}504 \cdot 10^{-10} \frac{F_p^{0,9}}{l^{0,8}} \tag{5}$$

according with [3]
or,

$$\delta_{pF} = 0{,}579 \frac{q}{E}\left(\ln \frac{4R_1R_2}{b^2} + 0{,}814\right) \tag{6}$$

according with [4]
where:
l – length of contact;
q - distributed force along the contact line;
E – the equivalent elasticity module;
b – width of the contact area;
R1, *R2* – curvature radius in the point of contact.

In order to determine the gearing forces the expression (5) it is used for its simplicity.

Using the expression (5), the magnitude of the normal force can be written

$$F_p = K \cdot \delta_{pF}^n \tag{7}$$

where: n = 10/9, $K = 1{,}504^{-n} \cdot l^{8/9}$ and thus obtaining the analytical expression of the force.

$$\bar{F}_p = F_p \cdot \bar{n}_r = K\delta_{pF}^n (n_{rx}\bar{i} + n_{ry}\bar{j} + n_{rz}\bar{k}) \tag{8}$$

The moment $\bar{M}_p$ of this force related to the frame origin is determined with the following determinant:

$$\bar{M}_p = \bar{r}_{lp} \times \bar{F}_p = K\delta_{pF}^n \begin{vmatrix} \vec{i} & \vec{j} & \bar{k} \\ x_l & y_l & z_l \\ n_{rx} & n_{ry} & n_{rz} \end{vmatrix} = \tag{9}$$

$$K\delta_{pF}^n[(y_l n_{rz} - z_l n_{ry})\vec{i} + \\ + (z_l n_{rx} - x_l n_{rz})\vec{j} + \\ + (x_l n_{ry} - y_l n_{rx})\vec{k}]$$

And its components are as follows

$$\begin{aligned} M_{xp} &= K\delta_{pF}^n (y_l n_{rz} - z_l n_{ry}) \\ M_{yp} &= K\delta_{pF}^n (z_l n_{rx} - x_l n_{rz}) \\ M_{zp} &= K\delta_{pF}^n (x_l n_{ry} - y_l n_{rx}) \end{aligned} \tag{10}$$

Due to static equilibrium, the twisting moment $\vec{M}_c$ is the sum of projections on z axis of the moment $\bar{M}_p$,

$$\begin{aligned} M_c &= \sum_{p=1}^{m} M_{zp} = \\ &= K \cdot \sum_{p=1}^{m} \delta_{pF}^n (x_l n_{ry} - y_l n_{rx})_p \end{aligned} \tag{11}$$

Side teeth gap δ_{pF} represents the displacement projection δ_p on the direction of normal force. This projection is determined through approximation of the arc $\delta_p = r_p d\varphi$ with the chord $\bar{\delta}_p$ corresponding to this arc. Vector expression is written:

$$\delta_{pF} = \bar{n}_r \cdot \bar{\delta}_p \tag{12}$$

The vector $\bar{\delta}_p$ has the magnitude δ_p and direction perpendicular to $\bar{r}_p$. The vector $\bar{r}_p$ is the component of the position vector $\bar{r}_{lp}$ in the plane xOy,

$$\bar{r}_p = x_l \vec{i} + y_l \bar{j} \qquad (13)$$

The direction $\bar{u}_p$ of the vector $\bar{\delta}_p$ is obtained by versor rotation with π/2 around z axis,

$$\bar{u}_{rp} = \frac{\bar{r}_p}{|\bar{r}_p|} = \frac{x_l}{\sqrt{x_l^2 + y_l^2}}\vec{i} + \frac{y_l}{\sqrt{x_l^2 + y_l^2}}\bar{j} = = u_{rpx}\bar{i} + u_{rpy}\bar{j} \qquad (14)$$

$$\bar{u}_p = R_z(\pi/2)\cdot \bar{u}_{rp} \qquad (15)$$

which means

$$\begin{pmatrix} u_{px} \\ u_{py} \\ u_{pz} \end{pmatrix} = \begin{pmatrix} \cos\frac{\pi}{2} & -\sin\frac{\pi}{2} & 0 \\ \sin\frac{\pi}{2} & \cos\frac{\pi}{2} & 0 \\ 0 & 0 & 1 \end{pmatrix} \begin{pmatrix} u_{rpx} \\ u_{rpy} \\ 0 \end{pmatrix} = \begin{pmatrix} -u_{rpy} \\ u_{rpy} \\ 0 \end{pmatrix}$$

or

$$\bar{u}_p = -u_{rpy}\bar{i} + u_{rpx}\bar{j} = = -\frac{y_l}{\sqrt{x_l^2 + y_l^2}}\vec{i} + \frac{x_l}{\sqrt{x_l^2 + y_l^2}}\bar{j} \qquad (16)$$

Having this versor, the vector $\bar{\delta}_p$ can be written

$$\bar{\delta}_p = \delta_p \bar{u}_p = r_p d\varphi\left(-\frac{y_l}{r_p}\vec{i} + \frac{x_l}{r_p}\bar{j}\right) = = \left(-y_l\vec{i} + x_l\bar{j}\right)d\varphi \qquad (17)$$

By replacing the expressions (4) and (17) in the expression (12) is obtained the side teeth gap in the point of contact C_p

$$\delta_{pF} = \left(n_{rx}\vec{i} + n_{ry}\bar{j} + n_{rz}\bar{k}\right)\cdot \cdot\left(-y_l\vec{i} + x_l\bar{j}\right)d\varphi = = \left(x_l n_{ry} - y_l n_{rx}\right)d\varphi \qquad (18)$$

If the value of the side teeth gap from (18) is replaced in the equilibrium expression (11) is determined the value of rotation $d\varphi$,

$$M_c = K\cdot(d\varphi)^n \cdot \sum_{p=1}^{m}\left(x_l n_{ry} - y_l n_{rx}\right)_p^{n+1}$$

$$d\varphi = \sqrt[n]{\frac{M_c}{K\cdot\sum_{p=1}^{m}\left(x_l n_{ry} - y_l n_{rx}\right)_p^{n+1}}} \qquad (19)$$

Replacing the equation (19) in expression (18) results

$$\delta_{pF} = \left(x_l n_{ry} - y_l n_{rx}\right)_p \cdot \cdot\sqrt[n]{\frac{M_c}{K\cdot\sum_{p=1}^{m}\left(x_l n_{ry} - y_l n_{rx}\right)_p^{n+1}}} \qquad (20)$$

And further, in expression (7) is determined the magnitude of the force normal to the side teeth in the point of contact C_p

$$F_p = \frac{M_c\cdot\left(x_l n_{ry} - y_l n_{rx}\right)_p^n}{\sum_{p=1}^{m}\left(x_l n_{ry} - y_l n_{rx}\right)_p^{n+1}} \qquad (21)$$

The number m of gearing pairs of teeth transmitting the motion is determined provided that the displacement's $\bar{\delta}_p$ projection in the direction of normal force $\bar{F}_p$ is positive, ie

$$\bar{n}_r \cdot \bar{\delta}_p > 0 \qquad (22)$$

which by using the expressions (4) and (17), means

$$x_l n_{ry} - y_l n_{rx} > 0 \qquad (23)$$

3 REFERENCES

[1] Bruja, A., Dima, M. “La détermination de la ligne d’action pour l’engrenage avec mouvement de précesion”, The Annals of “Dunărea de Jos” University os Galaţi, Fascicle XIV- Mechanical Engineering, 1999

[2] Dima, M. “Dinamica şi regimul de solicitare a transmisiilor armonice frontale cu element rigid”, Referat pentru doctorat, UTCB, 1999

[3] Gafitanu, M.,s.a. “Organe de masini”,Vol. II. Ed. tehnica, Bucuresti, 1983

[4] Ponomariov, S.D., s.a. Calculul de rezistenta în constructia de masini. Vol. II. Ed. tehnica, Bucuresti, 1963.

HEAVY MACHINERY - HM 2011, 31-36
ISBN 978-86-82631-58-3
Paper accepted: 20.05.2011

Planetary Gear Transmissions Optimization in the Case of the Particular Criteria Preferences

Jelena Stefanović-Marinović[1,*] - Miloš Milovančević[1] - Boban Anđelković[1]
[1] University of Niš, Faculty of Mechanical Engineering

The aim of this paper is the application of multicriteria optimization to planetary gear transmissions. A model of planetary gear multicriteria optimization based on an original algorithm is appointed. Optimization task is defined by the variables, objective functions and conditions. The following criteria are selected in mathematical model presented in this paper: volume, mass, efficiency and production costs. For optimization variables are adopted: teeth numbers, number of planetary gears, gear module and gear width. Conditions required for the proper system functioning, conditions in the scope of geometry and strength are expressed by the functional constrains. Determination of the Pareto optimal solutions set is a first step in optimal solution finding. Next step is optimal solution choice from Pareto solutions. In this paper optimal solution finding is considered in the case of preferences of particular criteria. Since that, weighted coefficients method, lexicographic method and the ε constraints method are applicated for choosing optimal solution from Pareto solutions.

Keywords: multicriteria optimization, mathematical model, methods for optimal solution choice

0 INTRODUCTION

Multicriteria optimization problems are common in many scientific and technical problems. In this type of optimization it is not possible to express the solution quality by one criterion, but several unharmonized criteria must be discussed. The functions which express these criteria cannot all have optimal values at the same time. Such problems are called non-trivial *multicriteria* (or *multiple objective, multiple criteria*) optimization problems.

Optimization tasks for gear transmissions as concrete mechanical systems are compound processes of abundant theoretical researches which integrate knowledge of mechanical systems design in general, uniqueness of concrete mechanical system and methods of mathematical optimization.

Planetary gear trains are important kind of gear transmissions, and they can be subject of multicriteria optimization application, too. Since it is impossible all types of planetary gear transmissions include in the same paper, the basic type of planetary gear is considered in this paper.

1 MATHEMATICAL MODEL FOR PLANETARY GEAR OPTIMIZATION

The basic type of planetary gear train (Fig.1), i.e a design which has a central sun gear (external gearing - 1), central ring gear (toothed rim, internal, annulus gear - 3), and planetary gears (satellites - 2), is the subject of the paper, limited to geared pairs. Satellites are simultaneously in contact with sun and internal gear.

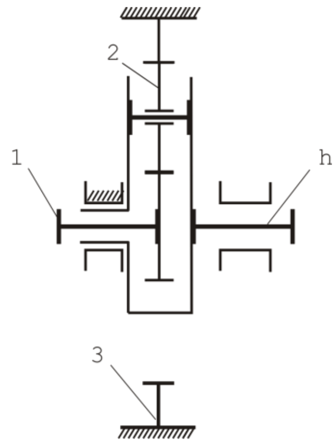

Fig.1. *Basic type of planetary gear transmission*

This type of planetary gear transmission is often used as a single stage transmission and thus as a building block for higher compound planetary gear trains.

Optimization procedure begins by mathematical model determination. An optimization task is defined by the variables,

*Corr. Author's Address: Faculty of Mechanical Engineering, Aleksandra Medvedeva 14, Niš, Serbia, jelenas@masfak.ni.ac.rs objective functions and conditions required for the proper functioning of a system determent by the functional constraints.

1.1 Variables

In the scope of the mathematical model definition, it is necessary to determine the variables since each objective function is the function of several parameters.

In this paper, the following variables are considered: teeth number of central sun gear z_1, teeth number of planetary gears (satellites) z_2, teeth number of ring gear z_3, number of planetary gears n_w, gear module m_n and gear width b.

The optimization variables are of mixed type: numbers of gear teeth (z_1, z_2, z_3) are integers, positive and negative, number of planetary gears (n_w) is a discrete value, module (m_n) is a discrete standard value (acc. to DIN 780), while gear width (b) is a continual variable. Numbers of gear teeth and number of planetary gears are non-dimensional values, while module and gear width are given in millimeters.

1.2 Objective functions

In this model, the following characteristics are chosen for objective functions of a planetary gear train: volume, mass, efficiency and production cost of gear pairs.

The approximation of gear volume by cylinder volume with diameter equal to pitch diameter and height equal to gear width is used. The fact that satellites are inside the ring gear makes it possible for the gear volume to be expressed by:

$$V = \frac{\pi}{4} \cdot b \cdot \left(\frac{m_n \cdot z_3}{\cos\beta} \cdot \frac{\cos\alpha_t}{\cos\alpha_{wt23}} \right)^2 \tag{1}$$

where α_t is the pressure angle at pitch cycle, α_{wt23} is the working transverse pressure angle for the pair 2-3 and β is the helix angle at the pitch diameter.

Mass is determined as sum of all gear masses in transmission. Since the mass of a particular gear is determined as gear volume multiplied by the density of gear material, $m_z = \rho \cdot V_z$, this criterion receives the form $m = \rho \cdot V_1 + n_w \cdot \rho \cdot V_2 + \rho \cdot V_3$

The final expression of this function is:

$$m = 0.25 \cdot \pi \cdot b \cdot \rho \cdot \frac{m_n^2}{\cos^2\beta} \cdot [k_1 \cdot z_1^2 \cdot \frac{\cos^2\alpha_t}{\cos^2\alpha_{wt12}} + n_w \cdot k_2 \cdot z_2^2 \cdot \frac{\cos^2\alpha_t}{\cos^2\alpha_{wt12}} + k_3 \cdot z_3^2 \cdot \frac{\cos^2\alpha_t}{\cos^2\alpha_{wt23}}] \tag{2}$$

To determine the gear mass, the factor of deviation of real gear shape from cylinder (k) has to be taken into account also. For purposes of optimization, i.e. the comparison of gears with different parameters, this factor does not have a great significance. Since that, it is given in advance due to the hub of gear wheel shape and it is a constant in the process of optimization.

Power losses in planetary transmissions consist of losses in gears contact, losses in bearings and losses due to oil mixing and spraying. The calculation of gear transmissions efficiency is generally confined to losses depending on friction on tooth sides, i.e. on calculation of contact power losses. According to previous efficiency remarks, we consider the following expression for efficiency [1, 7]:

$$\eta = 1 - \frac{z_3}{z_3 - z_1} \left[\frac{0.15}{z_1} + \frac{0.35}{z_2} + \frac{0.20}{z_3} \right] \tag{3}$$

Economic demands must also be taken into consideration in techno-economic optimization. First, these demands are related to *production costs*. These costs consist of costs for production material and costs of the production process itself. The time needed for the production of gears is taken as a measure of production costs and as an economic factor. This function is then determint as a sum of times needed for the production of central sun gear (T_1), satellites (T_2) and ring gear (T_3), i.e.

$$F_T = T_1 + n_w \cdot T_2 + T_3 \tag{4}$$

Production times are determined according to the technologies of Fette [8], Lorenc [9] and Höfler [10].

1.3 Functional constraints

Planetary gears represent a specific group of gear transmissions. Therefore, there are numerous exceptions that need to be taken into account for these transmissions to function correctly compared with classical gear transmissions. The exceptions considered in this model are related to mounting conditions, geometrical conditions and strength conditions.

The mounting conditions comprise the condition of coaxiality, the condition of adjacency and the condition of conjunction [3,4].

Geometrical conditions relate to undercutting and profile interference, ratio of pressure angle to working transverse pressure angle, tooth thickness and space width, transverse contact ratio value, sliding speeds, ratio of gear facewidth to reference diameter of the driving gear, etc. These conditions are ensured in accordance with the actual standards (ISO TC 60 list of standards 090915) [4].

As strength conditions, safety factors for bending strength and surface durability of each gear are provided [4,11].

2 OPTIMIZATION PROCEDURE

The mathematical model of nonlinear multicriteria problem can be formulated as follows:

$$\begin{aligned}&\max \{ f_1(x), f_2(x),..., f_k(x)\}\\ &\text{subject to } x \in S\end{aligned} \quad . \tag{5}$$

Functions $f_1(x),\ldots, f_k(x)$ are *objective functions* and $x = (x_1,\ldots, x_n)$ is vector of *variables*. These variables must satisfy given constraints which are expressed as inclusion $x \in S$ where S is the set of *feasible solutions* (or *feasible set*). The notation "max" means the simultaneous maximization of all the objective functions. If some objective function needs to be minimized a simple fact that minimization of the function $f_i(x)$ is equivalent to the maximization of the function $-f_i(x)$ can be used. Every point $x \in S$ is mapped to the point $(f_1(x), f_2(x),..., f_k(x))$ in k- dimensional objective space. Therefore it can be introduced the objective set:

$$F = \{(f_1(x), f_2(x),..., f_k(x)) \mid x \in S\}. \tag{6}$$

In this optimization task, six variables exist, corresponding to the basic design parameters, thus vector of decision variables receives the form:

$$x = (x_1, x_2, x_3, x_4, x_5, x_6) = (z_1, z_2, z_3, n_w, m_n, b) \tag{7}$$

This vector is a solution of optimization task.

The objective functions equal to the *volume* $V(x)$, *mass* $m(x)$, *efficiency* $\eta(x)$ and *production costs* $T(x)$ are defined by equations (1) to (4). Since mass, volume and production costs should be minimized, and efficiency should be maximized, the following has to be denoted in formulated mathematical model (5):

$$\begin{aligned}&f_1(x) = -V(x),\ f_2(x) = -m(x),\\ &f_3(x) = \eta_p(x),\ \ f_4(x) = -T(x)\end{aligned} \tag{8}$$

According to the structure of the set S, there exist *discrete* and *continuous* multicriteria optimization problems, depending on whether the set S is finite or continuous [2]. In the formulated optimization task, the discrete multicriteria optimization problem is obtained.

It is often useful to know the best possible values for each objective function. These values form a so-called *ideal point* $f^* = (f_1^*,\ldots, f_k^*)$ in the objective space. Its components are computed as:

$$f_i^* = \max_{x\in S} f_i(x), \ \text{ for all } \ i = 1,\ldots,k.. \tag{9}$$

As it can be seen from the definition, multicriteria optimization problems are mathematically ill-defined. This means that they have a set of mathematically "equally good" optimal solutions in the objective space. The most important criterion for selecting these "equally good" solutions is *Pareto optimality concept*:

Solution $x \in S$ is Pareto optimal if there is no solution $y \in S$ such that holds $f_i(x) \le f_i(y)$ for all $i = 1,\ldots, n$ and for at least one index i holds strict inequality, i.e. $f_i(x) < f_i(y)$.

Thus, some additional information is needed in order to be able to select one of them as a final solution. This final decision is usually made either by decision maker (human expert) or by the corresponding *scalarized problem*. In the latter case, one or more single criterion optimization scalarized problems have to be constructed and solved.

Since the subject of the paper is optimization task in the case of preferences of particular criteria, next methods are suitable for application: weighted coefficients method, lexicographic method and the ε - constraints method [2]. All of them reduce the problem to one criterion optimization problem.

The shortened algorithm for the complete optimization procedure is shown in Fig. 2

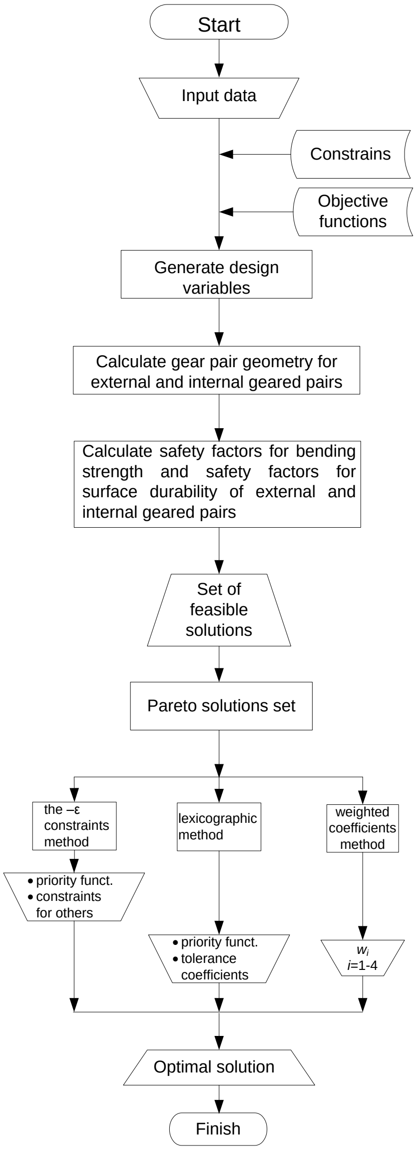

Fig.2. *Shortened algorithm for optimization procedure*

2.1 Weighted coefficients method

In this method the following scalarized problem is constructed:

$$\max\ f^M(x) = w_1 f_1^0(x) + \ldots + w_m f_m^0(x) \qquad (10)$$
$$\text{s.t. } x \in S$$

Here, weighted coefficients (or weights) w_i are positive real numbers and $f_i^0(x) = (f_i^0)^{-1} f_i(x)$ are normalized objective functions where f_i^0 are normalizing coefficients. In this approach, the components of ideal point $f^* = (f_1^*, f_2^*, f_3^*, f_4^*)$ are used as normalizing coefficients, i.e. $f_i^0 = f_i^*$ for $i = 1, 2, \ldots .m$. Therefore, absolute values of all objective functions are between 0 and 1, which simplifies the choice of the weighted coefficients. All solutions obtained by this method are Pareto optimal [4].

2.2 Lexicographic method

In the application of lexicographic method objective functions need to be sorted by the given priorities. It can be said that $f_{k_1}(x)$ has maximum priority, then $f_{k_2}(x)$, etc. and $f_{k_m}(x)$ has the least priority. The following list of scalarized problems for $i = 1, \ldots, m$ can be solved:

$$f_{k_i}^{opt} = \max f_{k_i}(x)$$
$$\text{s.t. } x \in S \qquad (11)$$
$$f_{k_j}(x) = f_{k_j}^{opt}, \text{ for } j = 1, \ldots, i-1$$

In other words, objective functions are maximized sequentially, but in each iteration the feasible set is reduced to the set of optimal solutions in previous iteration. A solution given by this method is also Pareto optimal [4].

2.3 The ε constraints method

In the ε constraints method, one objective function $f_q(x)$ which has to be maximized under the starting and additional conditions is chosen. These additional conditions are of the form

$f_i(x) \geq \varepsilon_i$, where ε_i, $i \neq q$ are given thresholds. Therefore, the following scalarized problem is solved:

$$\max f_q(x)$$
$$\text{s.t. } x \in S \qquad (12)$$
$$f_i(x) \geq \varepsilon_i, \text{ for } i = 1, \ldots, n, \ i \neq q$$

In this case, a systematic variation of ε_i yields a set of Pareto optimal solutions. This method is commonly used because it is possible to exactly control the values of all objectives, which is also very important in practical applications [4].

3 NUMERICAL EXAMPLES

The complete optimization procedure is implemented in the newly developed *Plan Gears Optimization* software. Numerical examples obtained using this software are presented in this section.

The input data are:

$i = 6.353$, $n_{in} = 3000$ min^{-1}, $T_{in} = 39.787$ Nm,
$T = 3000$ h, $K_A = 1.1$, $IT6$ for all gears,
$S_{H\min} = 1.2$, $S_{F\min} = 1.4$,
material z_1/material z_2/material z_3 =18CrNi8/18 CrNi8/34CrNiMo6, $\Delta i = 3\%$, $z_1 = 15 \div 36$

These input data are in accordance with a realized planetary transmission, manufactured by MIN-FITIP-Niš (Serbia).

Set of feasible solutions consists of 33 elements. The number of Pareto solutions is 6.

Function f_1 is adopted as a priority function.

Weighted coefficients method demands application of weighted coefficients values first, which has significant influence on optimal solution selection. Thus, much bigger weighted coefficient is given to the first function, i.e. $w_1 = 0.7$, $w_2 = w_3 = w_4 = 0.1$. The obtained solution is given in Table 4, with the set of objective functions in Table 5. Other variations of weighted coefficients with $w_1 >> w_2 > w_3 > w_4$, for example $w_1 = 0.8$, $w_2 = 0.1$, $w_3 = w_4 = 0.05$, etc., also direct on the same solution.

Table 4. *Solution obtained by weighted coefficients method*

Variable values					
z_1	z_2	z_3	n_w	m_n	b
15	30	-78	3	2	16

Table 5. *Objective functions for solution shown in table 4*

f_1 in mm^3	f_2 in *kg*	f_3	f_4 in *min*
293205.63	1.417	0.984	82.967

The application of Lexicographic method is on the same example with priority of functions 1,2,3,4. Mentioned solution given in table 4 is also obtained.

The ε- constraints method demands choosing the priority function and others are translated into constraints by giving the lower or upper bounds. In this example, priority is given to the first function. The following values are taken for the ε- constraints: 1.7 for second function, 0.98 for the third and 100 for the fourth. These values are generally taken arbitrary. Values for ε constraints are in this case chosen according to the ideal values of functions, by increasing or decreasing of these values for approximately 20%. Moreover, this method also points to the same solution, table 4.

Based on the solution in this example if the first function has priority, we choose the solution shown in table 4. Reason for this is in fact that all the methods point to this solution. Also, values for first, second and fourth function of this solution are values of ideal solution components, while difference between the third function components is 0.3%.

It can be concluded that, in the case of priority functions existence, it is suitable to give precedence to the weighted coefficients method due to very clear physical meaning and experience in application on technical systems optimization [4].

The coordination between the weighted coefficients method and the lexicographic method can be easily observed. These two methods, although starting from different prepositions and having different mathematical bases, lead to harmonized results, which provide a physical meaning.

The ε-constraints method can be important if significant constraints are known. This method is especially applicable in situations when one function has the most importance (i.e. mass due to building in some objects or volume due to overall dimensions etc.), while others must be in the range of some allowed limits. Setting the limits for functions has significant influence on the result. Reassigning the limits, more or less, influence the problem solution.

4 CONCLUSION

In this paper, an original model for multicriteria techno-economic optimization of planetary gear transmissions is presented. Furthermore, this approach indicates a possibility for mathematical methods application in planetary gear transmission optimization. The mathematical model consists of objective functions, variables and functional constraints.

Besides the determination of the set of Pareto optimal solutions, the presented original approach includes methods which select an optimal solution from the Pareto solutions set: weighted coefficients method, lexicographic method and the ε - constraints method.

According mentioned example it can be concluded that these methods although start from different prepositions and have different mathematical basis have very strong correlation and they lead to the same result in numerical example, which provides them a physical meaning. It is shown that the established optimization model gives good results and can be used for this type of planetary gear transmission.

Procedure applied here would be the same for other types of planetary gear transmissions, only mathematical expressions would be different.

X REFERENCES

[1] Del Castillo, J.M., "The Analytical Expression of the Efficiency of Planetary Gear Trains", Mechanism and Machine Theory 37, 2002, pp 197-214.

[2] Miettinen, K., Kirilov, L. "Interactive reference direction approach using implicit parametrization for nonlinear multiobjective optimization", MCDM 2004, Whistler, Canada

[3] Niemann, G., Winter, H. MASCHINENELEMENTE, Band II, Springer-Verlag Berlin, 1989.

[4] Stefanović-Marinović, J. "Višekriterijumska optimizacija zupčastih parova planetarnih prenosnika", doktorska disertacija, Mašinski fakultet Univerziteta u Nišu, Niš, 2008.

[5] Stefanović-Marinović J., Milovančević M., "Weighted coefficients method application in planetary gear transmissions optimization", The 6th International Symposium about Forming and Design in Nechanical Engineering, KOD, Proceedings, pp151-154, Novi Sad, Serbia; 2010.

[6] Stefanović-Marinović J., Milovančević M., "An application of multicriteria optimization to planetary gear transmissions", The International Conference Mechanical Engineering in XXI Century, Proceedings, pp 133-136; Niš, Serbia, 2010.

[7] Volmer, J., GETRIEBETECHNIK, UMLAUFRÄDERGETRIEBE, Verlag Technik, Berlin, 1990.

[8] FETTE-Technologie-Ihr Profit, *Die Schnittbedingungen beim Wälzfräsen*, WILHELM FETTE, GMB

[9] Verzahnwerkzeuge, Ein Handbuch für Konstruktion und Betrieb 3 (1977). Auflage, LORENZ GmbH&Co Ettlingen

[10] BHS HÖFLER operating instructions, 630-1000/2./125÷630-1000/2./166, 630-1000/4./01÷630-1000/2./67

[11] ISO 6336 (1996) Calculation of load capacity of spur and helical gears: ISO 6336-1, ISO 6336-2, ISO 6336-3.

HEAVY MACHINERY - HM 2011, 37-42
ISBN 978-86-82631-58-3
Paper accepted: 30.05.2011

Characterization of the properties of expolision processed materials for the construction of mining parts exposed to abrasion

Radovan Ćirić[1,*], Biljana Savić[1], Zvonimir Jugović[2], Radomir Slavković[2], Nedeljko Dučić[2]
[1] Technical College Cacak, Sv. Save 65, Cacak, Serbia
[2] University of Kragujevac, Technical Faculty, Sv. Save 65, Cacak, Serbia

The results of comparative studies of the properties of wear-resistant steels for the development of parts exposed to abrasion are presented in this paper. Experiment has included the analysis of the properties of explosion hardened steel 120Mn12, as well as the skills of bimetal (50Mn7 + S355). The results show that explosion processing in case of both variants of material lead to the improved resistance of the hammer to abrasive wear.

Keywords: wear resistant steel, abrasion, explosion hardening, explosion welding, mechanical properties, microstructure.

0 INTRODUCTION

Production processes in all industrial branches are accompanied by material wear and use of energy, workforce and means of production (production equipment, tools and supplies). The use of energy and means of production are to a great degree caused by friction in contact zones, i.e. wear due to friction. That is why research whose purpose is the reduction of tribological loss is very inportant. Tha selected material has a great influence on life of a machine element or part,so special attention is paid to this activity.

Mechanical systems in mining (elements of working and walking part of the excavator, mills and other systems that are in contact with tailings and ore) are exposed to abrasive wear. As a rule, mechanical parts of these systems are subjected to shock loads, so in acse of the same, in addition to high resistance of surfaces to wear, also requires the tough core [1]. For that reason, these mechanical parts are often made of high- and low alloyed Mn-steels resistant to wear. The example of some of the vital elements of mining technological equipment exposed to intensive wear are given in Figure 1.

a)

b)

c)

*Corr. Author's Address: Technical College Cacak, Sv. Save 65, Cacak, Serbia, radovan.ciric@vstss.com

d)

Fig. 1. *Examples of the parts of mining industries exposed to intensive wear: a) excavator's tooth, b) pod of the segment, c) pin and d) sliding rails*

Systematization of main groups of ternary alloys Fe-Mn-C, based on microconstituents in the structure, gives Guillet's diagram, Figure 2. [2].

According to the same, manganese steels are divided into: pearlitic, martensitic and austenitic, where only ferrite-pearlitic (up to 2% Mn) and austenitic steels with more than 10% Mn have technical significance.

Mn partially enters the solid solution, and partially it forms complex carbides of $(Fe,Mn)_3C$ type and it is included in the elements that move the point A_3 towards lower temperatures, so with sufficiently high concentration of manganese $\gamma\rightarrow\alpha$, the transformation is completely suppressed.

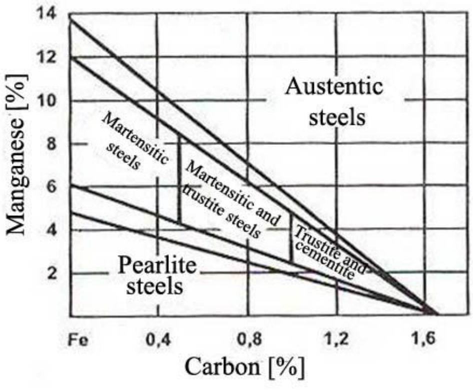

Fig. 2. *Guillet's diagram*

Austenitic manganese steels have high resistance to shock abrasive wear and very tough core. Toughness of this steel is achieved with subsequent sudden cooling in water (quenching). The aim of this procedure is to achieve the dissolution of carbid phase in solid solution of austenite. Resistant of these steels to wear is achieved with the increase of hardness, which is achieved by the procedure of plastic deformation of surface layers, where martensitic structure appears [3, 4, 5].

In accordance with vertical cross-section of the diagram of the state of Fe-Mn-C system, fig. 3., steel with 1,2-1,3% C and 13% Mn in cast condition at temperatures above 940°C has stable austenitic structure. Below that temperature field, the particles of complex carbide $(FeMn)_3$ are extracted from solid dissoultion, while at temperatures below 600°C there is also ferrie phase. Below 400°C, the structure consists of ferrite and carbides $(FeMn)_3$ [6].

[1] The mechanism of hardening of these steels under the influence of cold plastic deformation has not yet been fully explored. There are views according to which that mechanism is not much different than the mechanism of conventional deformation. According to [7], it is considered that the deformation takes place according to the doubling mechanism, but there are also the views [8] that the mechanism of hardening of this steels with fine grain is based on the interaction of doubling and dislocation changes. According to [9], the presence of ε-martensite i α-martensite was determined with these explosion expossed steels.

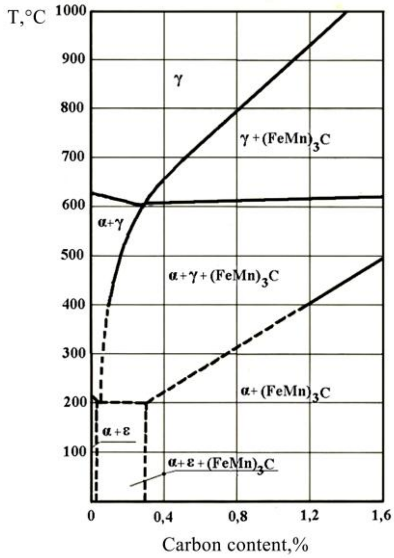

Fig. 3. *Vertical cross-section of the diagram of the system Fe-Mn-C for steel with 13% Mn [6]*

Low alloy medium carbon manganese steels resisant to wear achieve the best combination of mechanical properties after quenching and high release of initial martensitic structure. However, in case of the parts exposed to abrasive wear, it is common practice to apply medium and, in some cases, low release. This group of manganese steels is susceptible to overheating since mix carbides $(Fe, Mn)_3$ C are more rapidly dissolved in austenite than the carbides Fe_3C. Also, they are susceptible to brittleness after the release, increase of transition temperature and formation of band structure (anisotropy of properties).

Methods of explosion welding and explosion hardening of surface layer of high alloy manganese steels are relatively more recent technological processes [4]. The basic parameters of the regime are the type and quantity of explosives. As a result of explosion, shock load of the size order of the tens of GPa affects the surface layer of the metal. The process takes place with extremely high speeds of deformation. Effects of the change of properties can be quantified by examining mechanical properties and microstructure of materials.

The aim of this paper is the anaysis of the properties of steels resistant to wear processed by shoch effect of explosion wave.

I DATA ABOUT MATERIAL AND EXPERIMENT

Experimental hardening is performed on the hammer of the mill for grinding coal in slaked condition, figure 4.

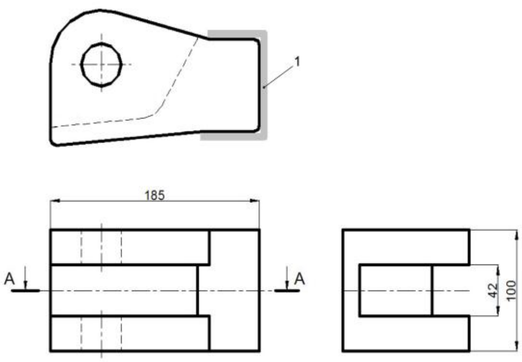

Fig. 4. *Hammer of the mill made of ČL 3160 1-explosion layer*

Hammer of the mill for ore grinding works in the conditions that can lead to catastrophic fracture. It requires high resistance of the working part on shock abrasion and high resistance of the core to brittle fracture. The usual solutions are to make it of high alloy Mn-steel or low alloy steel with improved core and high hardness of the working part. In literature, there are also the data about making a steel of bimetal materials.

Panels, figure 5, are working in conditions of abrasive wear with significantly lower level of shock loads. In the procedures of explosion welding, the entire surface of the sheet-iron (on one side) is covered with explosives.

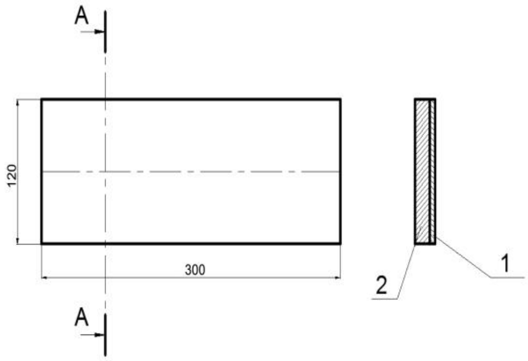

Fig. 5. *Panel, 1- Č3134, ≠5 mm, 2- Č0361, ≠15mm*

As means for causing the explosion, plastic high explosive with filled weight from 0,5 – 0,7 g/cm^3. Detonation velocity of the explosive is from 7000 – 8000 m/s, where the loads of the size order of the tens of Gpa are acquired.

After explosion hardening (welding), the testing of mechanical properties was done, as well as metallographic analysis and non-destructive testing.

II RESULTS AND DISCUSSION

2.1 Properties of ČL 3160 after explosion hardening

Hardness of the hammer of the mill made of Č3160, after explosion hardening, is measured in the cross-section A-A (plane of axial symmetry of the hammer) I – VII, fig. 6.

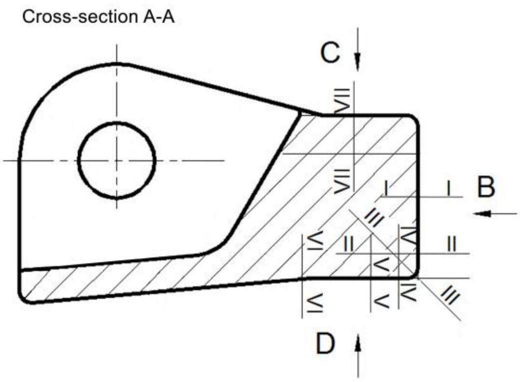

Fig. 6. *Scheme of the place of hardness measurement (directions from I-I to VII-VII)*

Results of hardness measurement, according to Vickers method, in measuring directions according to Figure 6, are given in Figure 7.

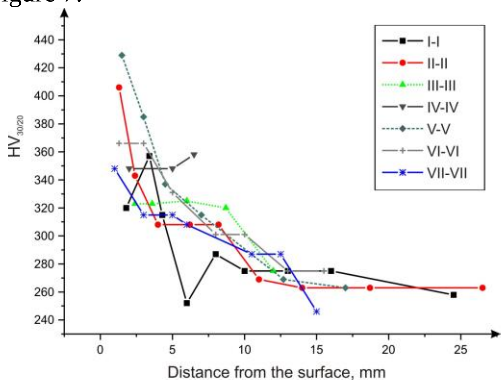

Fig. 7. *Hardness of the explosion hardened surface layer of the hammer made of steel Č 3160*

Based on the results, it was determined that the biggest hardness is achieved in the place that is immediately next to frontal surface B (406 HV). The depth of hardened layer with hardness higher than 300 HV in the direction I-I is 4,3 mm, and in direction II-II - 8,2 mm.

The highest hardness measured on lateral surface C (VII-VII) is 348 HV, while the depth of the layer with hardness above 300 HV – 6 mm.
On the lateral surface D, directions IV-IV, V-V i VI-VI, the hardness up to 366 HV is achieved. Depth of the hardened layer with the hardness higher than 300 HV is more than 6,5 mm (IV-IV), more than 7 mm (V-V) and about 10 mm (VI-VI).

In general, the highest hardnesses on working surfaces B, C and D are achieved in zones close to the angles.

Results of measuring micro-hardness in cross-section VII, fig. 8., show that micro-hardness of surface layer is significantly higher than the hardness determined by the method HV_{30}.

According to Figure 7, maximal measured hardness is 593 $MHV_{0,2}$, while the hardness higher than 400 $MHV_{0,2}$ is achieved to the depth of 0,15 mm minimum.

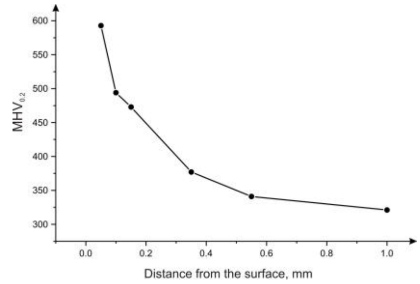

Fig. 8. *Micro-hardness Č 3160 after explosion hardening in the function of distancing from the surface*

Micro-structure of surface layer where it has come to explosion hardening is given in Figure 9. Main micro-constituent in the structure is martensite (dark needles). In micro-structure there is also significant share of retained austenite (fields with martensite needles) and carbides. Dark zones in Figure 8 represent gas pores or non-metallic inclusions.

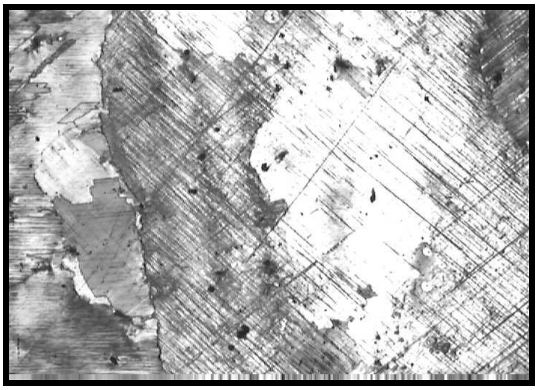

Fig. 9. *Micro-structure of the ČL 3160 hammer in the explosion hardened area*

2.2 Properties of bimetal 50Mn7 + S355

Properties of explosion welded bimetal are tested in the condition after the completion of heat treatment (annealing + quenching – release).

Results of testing the properties of bimetals on bending, tension, shear and toughness, performed in a way that is shown in Fig. 10-13, are given in Table 1.

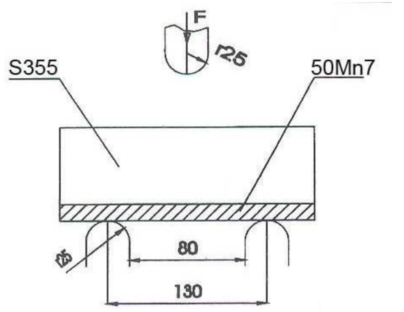

Fig. 10. *Sheme of the bending investigations of a bimetal test specimens, dimensions 14x12x145mm*

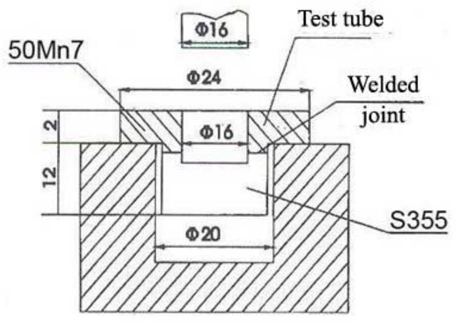

Fig. 11. *Scheme of tension testing*

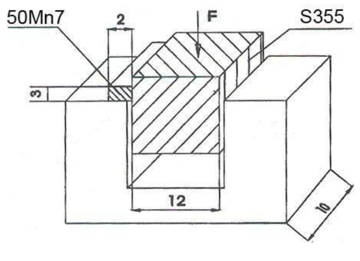

Fig. 12. *Scheme of shear testing*

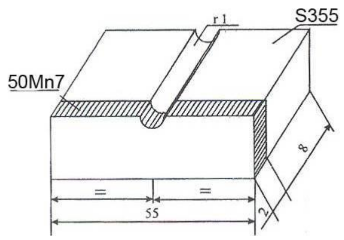

Fig. 13. Test tube for examining the toughness

Table 1. *Results of mechanical and technological examination*

State	Method				
	Tension	Shear	Bending		Toughness
	F (kN)	F (kN)	F (kN)	Bending angle (°)	(J)
Welded	93	15,2	18,3	14	24,6
Soft anelaed	119	12,0	20,0	90° without the formation of cracks	78,0
Hardened at 800°C in oil, annealed 180°	133	16,8	17,5	16	43,2

Based on the distribution of hardness at the cross-section of bimetals, it is observed that bz choosing a regime of final heat treatment can significantly influence the properties of wear parts of the steel panel 50Mn7, fig.14.

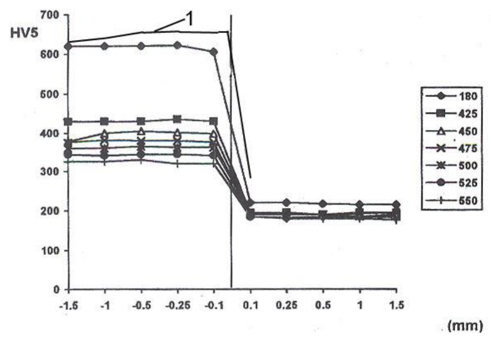

Fig. 14. *The hardness distribution in the zone of explosion welded joint bimetals steels 50Mn7 and S355 after quenching at 800°C (curve 1) and quenching at 800° and annealed (other curves)*

The microstructure in welded joint in the HAZ corresponds to thermodeformation conditions applied during explosion welding welded joint is wavelike, with waves bent in the explosion and interaction of both metals followed by a high degree of plastic deformation.

III CONCLUSION

Explosion hardening procedure leads to great changes of mechanical properties and micro-structure of surface layer. Basic effects that lead to the increase of hardness are cold plastic deformation and emergence of martensitic structure. Because of the shape of the hammer, and in addition to the same thickness of the explosive used, the hardening effects are significantly different in different zones.

Measured depths of hardened layer are, depending on measurment zone, within the limits from 4,3 – 10 mm. The highest micro-hardness of 593 HV_{02} is measured in surface layer of the sample. Microhardness above 400 HV_{02} is achieved up to the depth of 0,15 mm minimum.

Applied procedure of explosion welding provides a reliable quality of products for a great number of parts exposed to abrasion. The properties of the wear layer of the parts can be significantly influenced by the selection of the regime of interphase and final heat treatment.

IV REFERENCES

[1] Jugović, Z., Ćirić, R., Katana, R. „An investigation of double layer metallic materials used for elements that wear“, Science of Sintering, 28 spec. Issue, pp.197-202, 1996.

[2] Šuman H., Metalografija (translation from German) Zavod za udžbenike, Belgrade, 1965.

[3] Efstathiou, C., Sehitoglu, H., „Strain hardening and heterogeneous deformation during twinning in Hadfield steel“, Acta Materialia 58, pp 1479–1488, 2010.

[4] Zhang, F., Lv, B., Wang, T., Zheng, C., Zhang, M., Luo, H. And Liu, H., “Microstructure and Properties of Purity High Mn Steel Crossing Explosion Hardened”, ISIJ International, Vol. 48, No. 12, pp. 1766–1770, 2008.

[5] Kopač, J. „Težavnost obdelave obrabno odpornih avstenitnih jekel – 12 Mn“, Zbornik radova XVI Savetovanja proizvodnog mašinstva Jugoslavije, Mostar, pp. 67-70, 1982.

[6] Bolanowski, K., „Wear of hadfield cast steel machine parts due to impact and abrasion in service environment“, Kielce University of Technology, Poland, УДК 621.891.

[7] Roberts, W. N., *TMS-AIME*, 23, pp. 372, 1964.

[8] Champion, A. R., Rohde, R. W., *J. Appl. Phy.*, 41, pp. 2213, 1970.

[9] Верезинај, В. Н. и др. (1981) Физика и химија обработки материалов, 1, с. 60.

[10] Kowaleskij, V. et.al., Anwendungsmoglich-keiten des Exprosionsschweissens fur die Herstellung von Verbundmaterialen, Zeitschriff fur Metallkunde 70 (1979), 2.

[11] A. A. DORIBAS, Fizika uprochneniya i svarki vzrivom, Nauka Novosibirsk, 1980.

V ACKNOWLEDGEMENTS

This paper is a result of the project with the serial number 35037, faunded by the Ministry of Science and Technological Development.

HEAVY MACHINERY - HM 2011, 43-48
ISBN 978-86-82631-58-3
Paper accepted: 30.05.2011

Structure of centrifuge flight simulation

Zorana Dančuo[1,*], Vladimir Kvrgić[1], Radisav Milićević[1] ,Vladimir Zeljković[1]
[1] LOLA institute, Belgrade

In this paper, some aspects of centrifuge construction are presented. In real flight, the pilot is subject to different nonstationary effects (high G motion, control, visualisation, comunucation,etc). The centrifuge flight simulation contributes to pilot training and adaptation to real flight conditions. The centrifuge is a very complex system (structure, power, control, visualization, data recording, safety, etc). The initial structural plane is presented in this paper. Also, the requirement for the onset acceleration rate of 9g/s was considered, and the effect on the main electric motor characteristic and selection.

Keywords: Motion simulator, Centrifuge, Flight Dynamics, Control.

0 INTRODUCTION

The aircraft flight simulation is widely used in the aircraft design and operation. It should be pointed out, that modern aircraft are designed as 'agility' concepts [1], opening the flight envelope by post-stall flight, jet engine thrust-vectoring, FBW control system, with new technology (data links, calculation, sensors, ..). The agility concept requires simulation and testing during the development phase, to optimize, test and verify the aircraft flight and maneuverability. The other aspect is pilot preparation for such missions. Economical, psychological, technical factors, as well as pilot training and many other reasons lead to the development of flight simulator.

Different simulation concepts and realization are developed such as : Six Degrees of Freedom Motion Systems, 5 degrees of freedom motion simulators, Human Centrifuges (3 and 4 degrees of freedom) [2]. Whitin the pilot training, there is the application of different objectives, such as high G tolerance, rapid onset rate profile up to 9 G forces, aerial combat maneuvers, enhanced training [3,4].

Aircraft flight is a six degrees of freedom motion, while the simulator may be a 3, 4, 5 degrees of freedom system. Many researches are investigating the centrifuge control system in order to simulate, as much as possible, the real flight environment [5, 6].

A centrifuge with 3 degrees of freedom of motion is presented in this paper. The part of the control system for the main arm requirement is pointed out.

1 AIRCRAFT FLIGHT DYNAMICS

An aircraft is a dynamic system with six degrees of freedom of motion. As flight dynamics studies the impact of forces on the movement of rigid bodies, forces acting on the aircraft during the flight will be briefly presented in this section In reality, an aircraft is not a rigid, but an elastic body. For simplicity it will be aproximated and held as a rigid, symetric body. It is necessary to define a coordinate system, in order to define forces acting on the aircraft during the flight. The coordinate system, which is related to the aircraft is Cartesian, with right orientation, and its x-axis is oriented-along the fuselage towards the nose of the aircraft, the y-axis on the right side and z-axis downwards.

There are several possibilities to place the origin of the coordinate system: in the cross-section of the wing leading edge and airfoil chord at the root, then the wing aerodynamic center or on the tip of the nose of the aircraft. With the majority of aircrafts, the x-z plane is the plane of symmetry.

Forces acting on an aircraft in flight come from four sources: aerodynamic forces, propulsive forces, the force of gravity and inertia and other forces (eg, landing gear, flaps, airbrakes). Precise determination of aerodynamic forces is very complex. Forces and moments acting on an aircraft are complex functions of air flow and other diverse factors.

Before motion equations are introduced, the term of supermaneuverabilty will be described. The term implies the ability of aircraft to be controllable and safe for flight, beyond the standard flight envelope.

Supermaneuverable flight is characterized by high angle of attack $\alpha,\ \alpha > \alpha_{kr}$, high load

*Corr. Author's Address: Zorana Dančuo, LOLA institute, Kneza Viseslava 70a, Beolgrade, Serbia, zorana.dancuo@li.rs

factor onset rate, so that the aircraft stays controlable. Variables of state define the state of the aircraft at a given moment. Basic state variables are the position of the center of gravity of the aircraft (wich changes during flight)- x_c, y_c, z_c in the earthbound coordinate system, then Euler angles Φ, Θ, Ψ and four quarternions e_0, e_1, e_2, e_3, which determine the aircraft position relative to the local coordinate system attached to the axis. There are many state variables, and depend on the type and purpose of the aircraft.

According to the Newton's Second Law, $\vec{F} = m\,\vec{a}$, aircraft equations of motion are derived. Equations will be only presented, but not derived in this paper. Equations of motion for a symetrical aircraft are:

$$\dot{u} = rv - qw + X/m$$
$$\dot{v} = pw - ru + Y/m$$
$$\dot{w} = qu - pv + Z/m$$
$$\dot{p} = \frac{I_{xy}L' + I_{xx}N'}{I_{xx}I_{zz} - I_{xz}^2}$$
$$\dot{q} = \frac{M - (I_{xx} - I_{zz})rp + I_{xz}(p^2 - r^2)}{I_{yy}}$$
$$\dot{r} = \frac{I_{zz}L' + I_{xz}N'}{I_{xx}I_{zz} - I_{xz}^2} \qquad (1)$$

L' and N' are given by

$$L' = L - (I_{zz} - I_{yy})qr - I_{xz}pq$$
$$N' = N - (I_{yy} - I_{xx})pq - I_{xz}qr \qquad (2)$$

X,Y,Z,L,M,N .are forces and moments.

Kinematic equations for Euler angles are:

$$\dot{\Phi} = p + q\sin\Phi\tan\Theta + r\cos\Phi\tan\Theta$$
$$\dot{\theta} = q\cos\Phi - r\sin\Phi$$
$$\dot{\psi} = q\sin\Phi\sec\Theta + r\cos\Phi\sec\Theta \qquad (3)$$

2 SIMULATOR – CENTRIFUGE MOTION

The centrifuge has the main objective to familiarize pilots with the aircraft flight motion and forces. Moderne aircraft (agility concept) are designed to perform variable high G maneuvers, post stall flight, vectored thrust, or some aspects in aerodynamics, airframe, engine, systems. To prepare pilots for real flight mission, the centrifuge may contribute in several aspects:

- Pilot tolerance to high G forces (open loop system),
- Pilot training to G protective measures,
- Pilot in the loop dynamics
- Dynamic flight simulation

The centrifuge may be used for research purposes, investigating human factors effects on pilots. The material testing may be performed.
The Human Training Centrifuge is a very complex system with different subsystems (structure, power, control, visualization, data acquisition and monitoring (recording), safety …).

2.1. Structure of the centrifuge

The centrifuge is a 3 degree of freedom system (main arm rotation, roll and pitch). The centrifuge arm carries at its end a gimbaled gondola, capable of rotating in two axes (roll, pitch), Fig.1, Fig. 1a.
The centrifuge design parameters are listed in table 1.

Table 1. *The centrifuge design parameters*

Centrifuge parameter	Value
Max G - Research Mode - Training Mode 9g	 15g 9 g
G onset value	9 g/s
Arm	8 m
Mass (approximated)	90.000 kg
The gondola equipment	• adjustable pilot seat • audio, video and intercom equipment • G-protection equipment • medical monitoring equipment
Medical monitoring system	32 channel

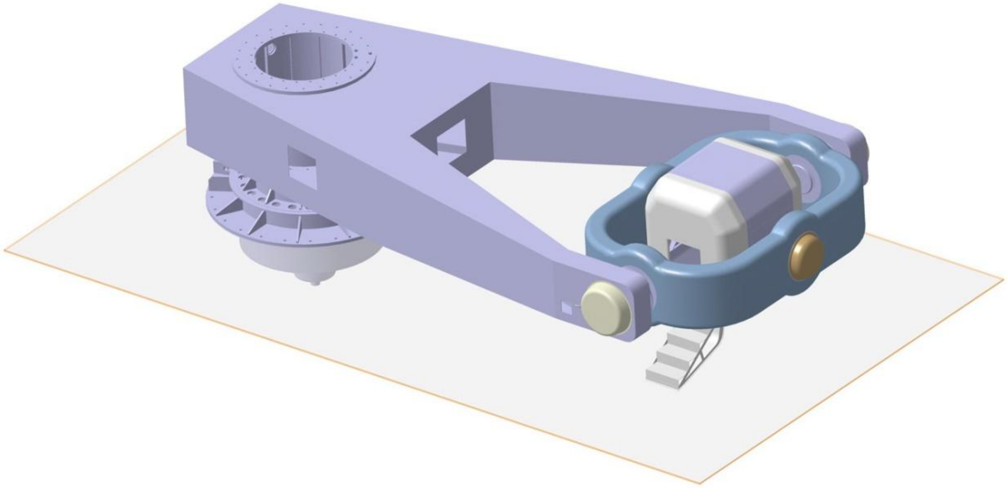

Fig. 1 *The centrifuge 3 degree of freedom system*

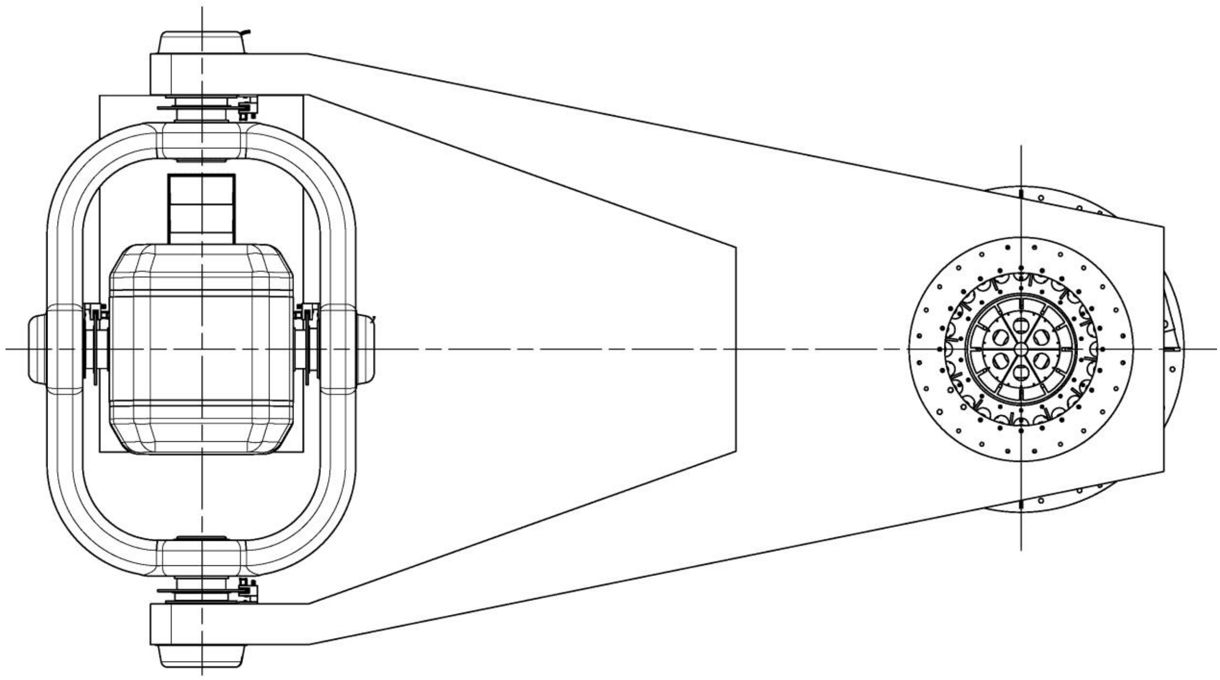

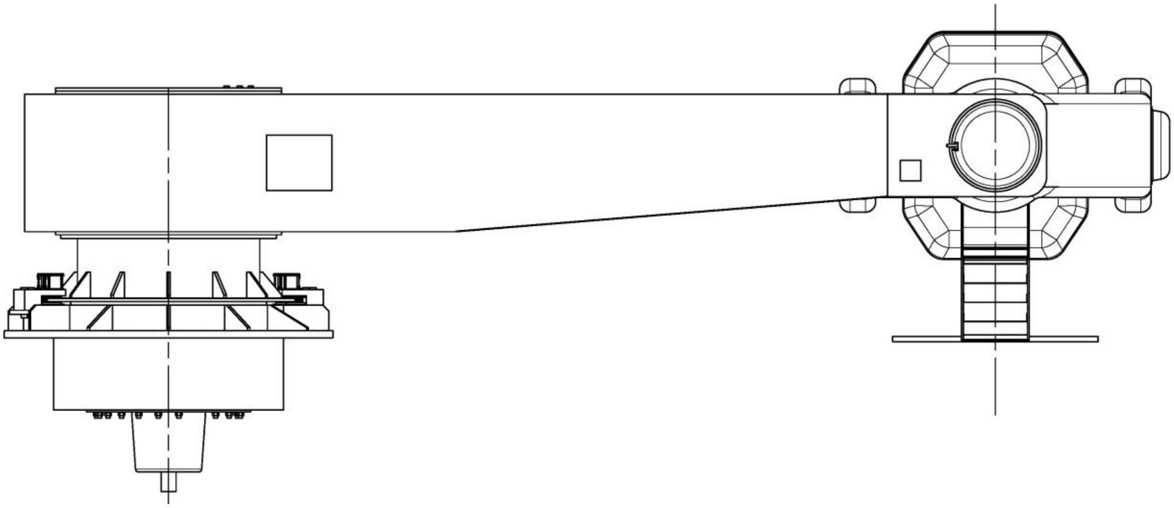

Fig. 1a. *The centrifuge- view*

2.2. Main arm control

One of the tasks for the control system was to reach the required time history of the main arm rotation. The requirement for onset acceleration rate was 9g/s, from the starting position to stationary 15g acceleration. This requirement is given by equation (4).

$$\frac{da_n}{dt} = \frac{d}{dt}(r\,\omega_z^2) = = r\frac{d}{dt}\omega_z^2 = 2\,r\,\omega_z\,\dot{\omega}_z = \frac{9\,g}{s} \qquad (4)$$

The solution of the equation gives the arm motion values and parameters for electric motor selection (arm r=8m, inertia Jz=350.000 kgm^2), table 2.

Table 2. The arm motion values and parameters for electric motor selection

t [s]	ω_z - Eq. (4)	$a_n = \omega_z^2\, r$	n_z [min^{-1}]	$\dot{\omega}_z$ -	φ_z [rad]	φ_z [°]	$v = \omega_z\, r$ [km/h]	$M_z = J_z\,\dot{\omega}_z$	$P = M_z\,\omega_z$
0,0	1,3100243	1,4 g	12,510		0	0			
0,1	1,6791104	2,3 g	16,034	3,2852165	0,28607	16,390	37,729	1.149.826	1.930.684
0,2	1,9805706	3,2 g	18,913	2,7851775	0,46946	26,898	48,358	974.812	1.930.684
0,3	2,2418537	4,1 g	21,410	2,4605713	0,68086	39,010	57,040	861.200	1.930.684
0,4	2,4757133	5,0 g	23,641	2,2281420	0,91693	52,536	64,565	779.850	1.930.684
0,5	2,6893130	5,9 g	25,681	2,0511709	1,17533	67,341	77,452	717.909	1.930.684
0,6	2,8871530	6,8 g	27,570	1,9106160	1,45427	83,323	83,150	668.715	1.930.684
0,7	3,0722794	7,7 g	29,338	1,7958796	1,75234	100,401	88,482	628.421	1.930.684
0,8	3,2466887	8,6 g	31,005	1,6989423	2,06837	118,509	93,505	594.630	1.930.684
0,9	3,4125352	9,5 g	32,587	1,6164641	2,40141	137,591	98,281	565.762	1.930.684
1,0	3,5705245	10,4 g	34,096	1,5449385	2,75062	157,599	102,831	540.728	1.930.684
1,1	3,7218131	11,3 g	35,407	1,4821380	3,11529	178,493	107,188	518.748	1.930.684
1,2	3,8671888	12,2 g	36,929	1,4264217	3,49479	200,237	111,375	499.248	1.930.684
1,3	4,0072920	13,1 g	38,267	1,3765507	3,88856	222,798	115,410	481.792	1.930.684
1,4	4,1426607	14,0 g	39,559	1,3315695	4,29609	246,148	119,309	466.049	1.930.684
1,5	4,2737437	14,9 g	40,811	1,2907280	4,71695	270,261	123,083	451.755	1.930.684
1,51112	4,2880610	15,0 g	40,948	1,2864180	4,76455	272,989	123,496	450.246	1.930.684
1,6	4,4009242	15,8 g	42,026	1,2524278	5,15071	295,114	126,747	438.700	1.930.684

The data from table 2 show the constant acceleration increment and variable angular rotation, figure 3a,b.

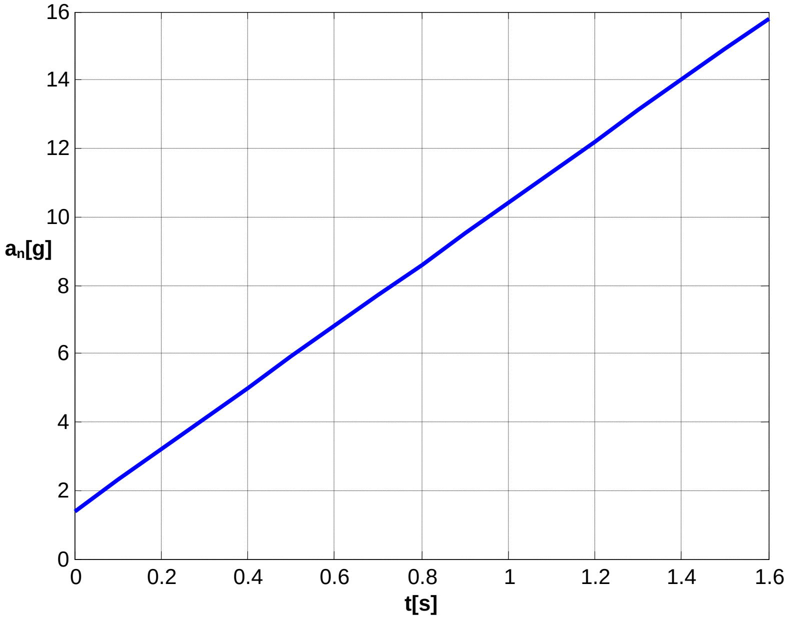

Fig. 3a. *Acceleration a_n as a function of time t*

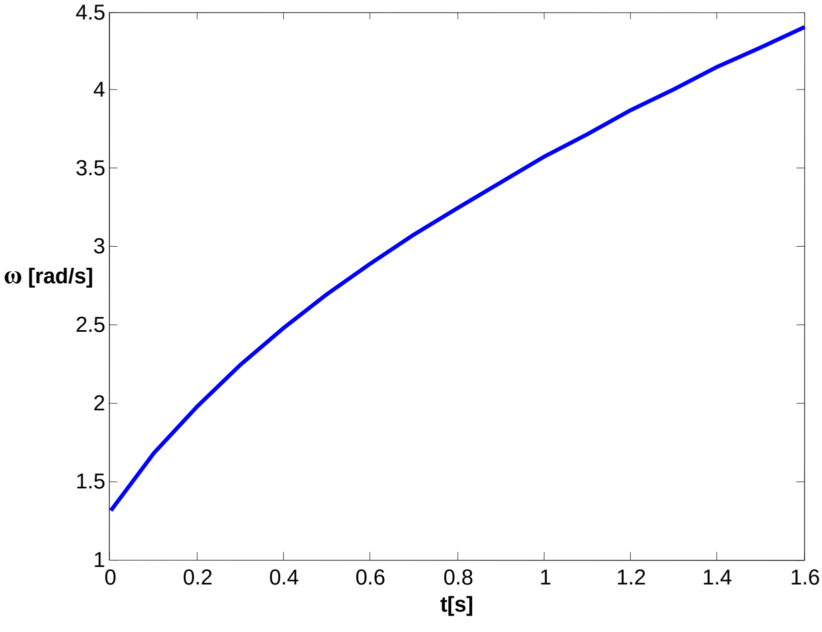

Fig. 3b. *Angular velocity ω as a function of time t*

Table 2 gives the data for motor selection. The required values for electric engine (torque and power) are very high, table 2

CONCLUSION

The Human Training Centrifuge shall provide a safe and reliable environment for G-awareness training (high-G and high-G onset training) of modern aircraft pilots. It shall be used for pilot evaluation of individual G-tolerance, refresher training and training of G-protection measures. The centrifuge may be also used for physiological research and material testing.

The Human Training Centrifuge is very complex system with different subsystems (structure, power, control, visualization, data acquisition and monitoring (recording), safety …). The main task of control system is drive the gondola in similar way as the real flight motion.

In this paper, a part of the research of the control system is presented. Particularly, the requirement for onset acceleration rate 9g/s was considered and effect to the main electric motor characteristic and selection.

X REFERENCES

[1] Patrick Le Blaye: 3. AGILITY: DEFINITIONS, BASIC CONCEPT, AND HISTORY, ONERA Systems Control and Flight Dynamics (DCSD), France

[2] W. Albery: 8. SIMULATION, Air Force Research Laboratory AFRL/HEPA, USA

[3] B. Levin, D. Keifer: Dynamic Flight Simulation for Enhanced Pilot Training, SAFE Europe, March 2002

[4] High G Centrifuge, Department of Acceleration Physiology , India, Ind J Aerospace Med 50 (1), 2006, Pp 1-7

[5] Y. C. Chen, D. W. Repperger: A STUDY OF THE KINEMATICS< DYNAMICS AND CONTROL ALGORITHMS FOR A CENTRIFUGE MOTION SIMULATOR, Mechanics, Vol. 6, No. 7, Pp. 829-852, 1996

[6] Crosbie; Richard J.: Dynamic flight simulator control system, United States Patent4,751,662, http://www.patents.com/us-4751662.html

[7] Banks, C .“A DISCUSSION OF METHODS OF REAL-TIME AIRPLANE FLIGHT SIMULATION, The Pennsylvania State University Graduate School College of Engineering

Acknowledgement: This paper is part of research whitin the projekt TP 35023, Ministry of Education and Scienses, Republic of Serbia

HEAVY MACHINERY - HM 2011, 49-54
ISBN 978-86-82631-58-3
Paper accepted: 30.05.2011

Turbine Shaft Failure Cause Analysis

Miodrag Arsić[1,*] - Brane Vistać[1], Z. Savić[1] , Z. Odanović[1], M. Mladenović[1]
[1] Institute for Materials Testing, Belgrade

After approximately 20 years of service horizontal bulb turbine Kaplan, 28 MW of nominal output power, stopped because of shaft failure due to the occurrence of the through crack. Turbine shaft has been designed as a welded structure which consists of a cylindrical body of the hollow shaft and a flange (estimated service lifetime of the shaft is 40 years).

Through experimental tests and calculations (analytical and numerical) it has been determined that values of bending stresses of the turbine, which occur due to the action of fatigue and corrosion, as well as stress concentration, are bigger than 25 MPa for flanges exposed to water, and in other case bigger than 40 Mpa for flanges exposed to `corrosive water` and can cause the occurrence of surface cracks on the transition radius between the cylindrical part of the shaft and the flange. It has been determined that stress values in the zone under the influence of bending stresses were bigger than allowable values, which led to the occurrence of many cracks due to fatigue corrosion. One of those cracks caused the failure of the shaft and of the whole turbine.

Keywords: turbine shaft, bending stress, stress concentration, fatigue, crack.

INTRODUCTION

Turbine and hydro-mechanical equipment loads originate during the production of components and equipment assembling (residual stresses), during the process of performing functional requirements in exploitation (stationary and dynamic loads) and during the disturbed process of exploitation (non-stationary dynamic loads). It`s clear that component and equipment loads can`t be expressed by a simple mathematical function knowing that unpredictable influence of corrosion, erosion and cavitation during exploitation should be taken into account. That`s the reason why extensive researches, tests and inspections of hydropower plant equipment have been undertaken. Researches carried out in Serbia have been very modest. A few of them which, among others, have been used in the preparation of this paper are listed among the references, from [1] to [7].

At HPP„ĐERDAP II“, in the period from 1984 to 1987, 8 hydro-electric generating sets PL-15/826-G-750 produced by LMZ, USSR were put into operation with the following parameters: maximum head 12.75 m, nominal head 7.45 m, minimum head 5 m, turbine power at nominal head 28 MW, runner diameter 7500 mm, number of revolutions 62,5 min-1, number of runner blades 4. Turbine shaft is presented in fig. 1 /7/. In the period from 1998 to 2000, two more hydro-electric generating sets of the same type, produced by UCM Resita, were put into operation.

Turbine shaft was assembled by welding the cylindrical body of the hollow shaft (outer diameter 1200 mm, internal diameter 600 mm) to the flange, made of 20GSL steel, fig. 1 [7]. During welding heat-affected zone has been created, which overlapped the transition diameter. Residual stresses were accumulated at the external surface of the transition area from the shaft to the flange. Anti-corrosive protection in the shaft flange area has been exposed to water.

In January 2007, after 163.411 hours of exploitation, a huge loss of oil from the regulating system of the A6 hydroelectric generating set was noticed. After the exclusion of the hydroelectric generating set from the service and visual inspection of all suspicious locations a crack, 2.100 mm long, was detected, through which the turbine oil from the servo motor leaked, on the transition radius R80 from the cylindrical part of the shaft toward the runner hub, fig. 2 [7].

1.1 Analytical Calculation of the Critical Cross-Section Strength of the Turbine Shaft Transition Radius

Turbine shaft is subjected to tensile stress due to the effect of the hydraulic force on turbine runner.

*Corr. Author's Address: Institute for Materials Testings, Bulevar vojvode Mišića 43, Belgrade, Serbia, miodrag.arsic@institutims.rs

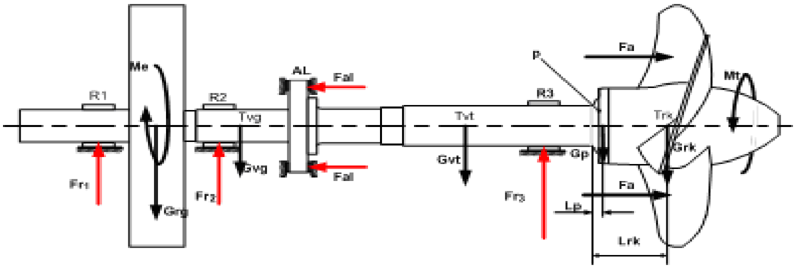

Fig. 1. Turbine shaft with hydro-electric generating set loads

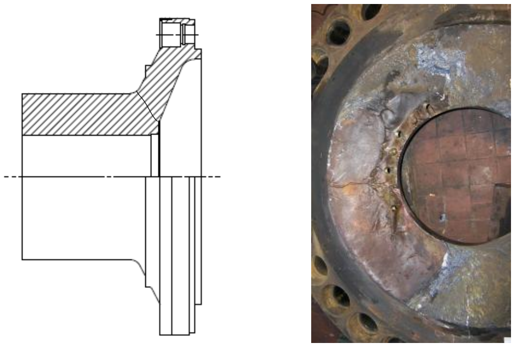

Fig. 2 Through crack location and fractured area of the shaft

Pressure of oil in the servo motor of the runner in the closing stroke and axial hydraulic force load subject the flange to bending. The weight of the runner and of the shaft itself subject the shaft to cyclic bending. Due to the transfer of the force the shaft is subjected to torsion as well.

Cyclic loads, to which the turbine shaft is subjected, in combination with the corrosive environment (leakage of water through the seal, poor execution and non-renewal of the corrosion protection) led to the occurence of the corrosion fatigue on the transition radius (location where value of the stress concentration factor is 3). Corrosion fatigue damages, as far as stress concentration is concerned, act like cracks (stress concentration value is ranging from 3 to 6) [7].

1.1.1 Analysis of the Fracture Cross-Section of the Turbine Shaft

During the exploitation under high-cycle fatigue conditions in a corrosive environment the initiation of cracks occured, and their joining led to the formation of 20 - 30 mm long cracks, which was confirmed by the existance of corrosion products on the smooth fracture surface. When the load bearing area of the turbine shaft, under low-cycle fatigue conditions, fell under the critical value in the crack growth area the fracture occured. That segment of the area is embossed and deprived of corrosion products.

1.1.2 Load Analysis of the Critical Cross-Section of the Shaft

Calculation regarding the critical cross-section of the shaft has been carried out through the use of the Theory of Elasticity and data provided by the manufacturer (LMZ, Saint Petersburg, Russia). Critical cross-section area is Ak, and cross-sectional area of the fracture is Ap. Taking into account the fact that the fracture is irregularly shaped, it has been adopted that the critical cross-section is positioned at the end of the cylindrical part of the shaft, fig. 3.

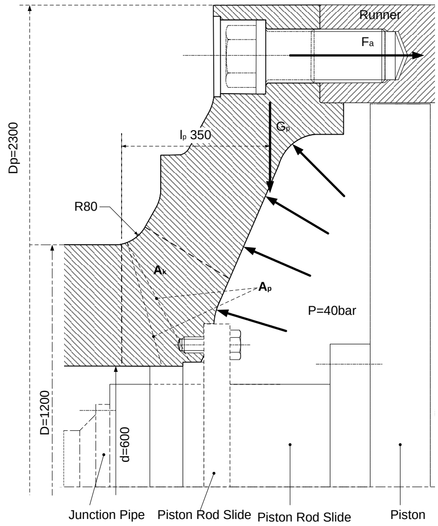

Fig. 3 Critical cross-section of the shaft

Critical cross-section of the turbine shaft is subjected to [8]:

- Axial hydraulic force $F_a = 5{,}5426 \cdot 10^6$ N, according to the data provided by the turbine manufacturer,
- Moment of torsion Mt:

$$M_t = \frac{P}{2\pi n} = 4{,}278 \cdot 10^6\, Nm \tag{1}$$

where: P = 28000 kW - turbine power, n = 1,04166 s^{-1} (62,5 min^{-1}) - turbine shaft number of revolutions.

- Bending moment that occurs due to the action of the axial hydraulic force and force that occurs due to the oil pressure in the cylinder of the servo motor of the runner Mo = 337768 Nm, according to the data provided by the turbine manufacturer,
- Bending moment that occurs due to the weight of the runner and weight of the part of the flange as far as the critical cross-section:

$$M_s = G_{rk} \cdot l_{rk} + G_p \cdot l_p = 1964943\, Nm \tag{2}$$

where: G_{rk} = 941760 N - weight of the runner, l_{rk} = 2050 mm - distance from the center of gravity of the runner to the critical cross-section, G_p = 98100 N - weight of the flange with bolts as far as the critical cross-section, l_p = 350mm - distance from the center of gravity of the flange to the critical cross-section.

1.1.3 Static Stresses at the Critical Cross-Section

- Tensile stress due to the action of the axial hydraulic force:

$$\sigma_z = \alpha_z \frac{F_a}{A_k} = 14{,}3\, MPa \tag{3}$$

where: α_z = 2,19 - stress concentration factor during tension for

$$\frac{D_p}{D} = \frac{2300}{1200} = 1{,}916 \quad \frac{R}{D} = \frac{80}{1200} = 0{,}066 \tag{4}$$

$$A_k = \frac{\pi}{4}\left(D^2 - d^2\right) = 0{,}8482\, m^2 \tag{5}$$

where: A_k critical cross - section area.

- Bending stress due to the action of the axial force and force that occurs due to the pressure in the servo motor of the runner

$$\sigma_o = \frac{M_o}{W_o} = \frac{M_o}{h^2/6} = 22{,}52 MPa \tag{6}$$

where: W_o - moment of resistance per length unit of the critical cross-section.

- Torsional stress:

$$\tau = \alpha_t \frac{M_t}{W_t} = \alpha_t \frac{M_t}{\frac{\pi \cdot D^3}{16}\left[1 - \left(\frac{D}{d}\right)^4\right]} = 20{,}85 MPa \tag{7}$$

where: W_t - polar moment of resistance per length unit of the critical cross-section, α_t = 1,55 - stress concentration factor during torsion for

$$\frac{D_p}{D} = \frac{2300}{1200} = 1{,}916 \quad \frac{R}{D} = \frac{80}{1200} = 0{,}066 \tag{8}$$

- Equivalent static stress at the critical cross-section:

$$\sigma_m = \sqrt{(\sigma_z + \sigma_o) + 4\tau^2} = \sqrt{(14{,}3 + 22{,}52)^2 + 4 \cdot 20{,}85^2} = 55{,}6 MPa \tag{9}$$

1.1.4 Cyclic Stress at the Critical Cross-Section

Cyclic stress at the critical cross-section occurs due to the bending moment caused by weights of the runner and of the part of the flange as far as the critical cross-section

$$\sigma_a = \alpha_s \frac{M_s}{W_s} = \alpha_s \frac{M_s}{\frac{\pi \cdot D^3}{32}\left[1 - \left(\frac{D}{d}\right)^4\right]} = 24{,}46 MPa \tag{10}$$

where: W_s - moment of resistance per length unit of the critical cross-section, α_s = 1,98 - stress concentration factor during bending for

$$\frac{D_p}{D} = \frac{2300}{1200} = 1{,}916 \quad \frac{R}{D} = \frac{80}{1200} = 0{,}066 \tag{11}$$

1.1.5 Factor of Safety in Relation to Corrosion Fatigue

Factor of safety of the turbine shaft, in relation to corrosion fatigue and in conditions of cyclic loading of amplitude σ_a=24,4 Mpa and corrosion is obtained through the use of the following equation:

$$S_\sigma = \frac{\sigma_{-1} - \psi_\sigma \cdot (\sigma_m + \sigma_{MO})}{\sigma_a} \tag{12}$$

where: σ_{-1} = 26,5 MPa - permanent corrosion fatigue strength of steel 20GSL during the action of the alternating changeable load in the corrosive environment, ψ_σ - coefficient that takes into account the asymmetry of the cycle and is equal to the ratio of the corrosion fatigue strength σ_{-1} and tensile strength R_m.

$$\psi_\sigma = \frac{\sigma_{-1}}{R_m} = \frac{26,5}{480} = 0,0552 \tag{13}$$

σ_m – maximum value of static exploitation stresses at the calculated cross-section, eq. (9).
σ_a – amplitude of cyclic stresses, eq. (10).
σ_{MO} – residual stresses present after casting and heat treatment have not been taken into account (σ_{MO} = 0 MPa) because there were no exact values available.

Permanent corrosion fatigue strength is being determined experimentally by inspecting the samples in the water and correcting the obtained results through the use of dimensional factors. For this analysis experimental results regarding the testing of 20GSL material during the calculation process for the cover of the runner for HPP „ĐERDAP I“ [9] have been used. Obtained equation contains the correction factors:

$$\begin{aligned}\log\sigma_{-1} &= A - B\cdot\log N\\ \log\sigma_{-1} &= 2.787 - 0,155\cdot\log N\end{aligned} \tag{14}$$

where: N – true number of loading cycles.

$$\begin{aligned}N &= n\cdot T = 62,5\cdot 60\cdot 163411\\ N &= 0,63\cdot 109\ \text{cycles}\end{aligned} \tag{15}$$

where: n = 62,5min^{-1} - number of revolutions per minute of the shaft, T = 163411 h - service lifetime of the hydro-electric generating set until the breakdown.

After placing appropriate values into the equation the following is obtained:

$$\begin{aligned}\log\sigma_{-1} &= 2.787 - 0,155\cdot\log\left(0,63\cdot 10^9\right)\\ \log\sigma_{-1} &= 1,423\\ \sigma_{-1} &= 26,5MPa\end{aligned} \tag{16}$$

Factor of safety in relation to corrosion fatigue:

$$S_\sigma = \frac{\sigma_{-1} - \psi_\sigma\cdot(\sigma_m + \sigma_{MO})}{\sigma_a} = 0,96 \tag{17}$$

Factor of safety is less than S_σ = 1,5, the value predicted by the manufacturer's designation.

1.1.6 Effect of Stress Concentration and Corrosion on Fatigue Strength

At locations of sudden changes of shape of loaded structural components local increase of stress (stress concentration) occurs. Level of stress increase is defined by the ratio of the maximum local (σ_{max}) and nominal (σ_{nom}) stress, which is being called the theoretical stress concentration factor:

$$K_t = \frac{\sigma_{max}}{\sigma_{nom}} \tag{18}$$

Values of the theoretical stress concentration factor for various shapes of components and various loading type are presented in Peterson's paper [10].

Fatigue strength due to the action of the corrosive environment is defined by the following factor:

$$k_{kor} = \frac{\sigma_{\max(-1)kor}}{\sigma_{\max(-1)}} \tag{19}$$

where: $\sigma_{max(-1)kor}$, $\sigma_{max(-1)}$) - fatigue strengths of smooth specimens in the corrosive environment and in the air atmosphere, respectively.

Fatigue strength in the corrosive environment depends on the number of cycles, but also on the length of exposure period of elements to the corrosive environment. Thus the effect of stress change frequency is significant. In relation to that, Wöhler corrosion fatigue curve is a constantly descending line, therefore permanent fatigue strength practically does not exist [7].

The joint effect of corrosion and stress concentration can be expressed by the following coefficient:

$$K_{fkor} = K_f + \frac{1}{k_{kor}} - 1 \tag{20}$$

where: K_f =1,98 - effective stress concentration factor for testing in the air atmosphere, k_{kor} = 0,5 (for R_m = 480 MPa) - coefficient of the effect of corrosion for smooth specimens. As far as the turbine shaft is concerned, value of stress concentration coefficient, including the effect of corrosion, is K_{fkor} = 2,98.

Through the analysis of the corrosion fatigue during the asymmetric cycle it has been determined that mean tensile stress unfavorably affects, or in other words significantly decreases the dynamic durability amplitude. Mean pressure stresses favorably affect the resistance to corrosion fatigue. This effect is commonly used for the method of surface strengthening of elements that operate in the corrosive environment.

Decrease of fatigue strength of an element with respect to fatigue strength of the smooth specimen is calculated through the use of the overall fatigue strength reducion factor:

$$K_D = \left(\frac{K_f}{k_3} + \frac{1}{k_{kor}} - 1 \right) \frac{1}{k_{po} k_A} \qquad (21)$$

Coefficients included in the expression for the calculation of K_D take into account the following effects on fatigue strength: K_f = 1,98 - stress concentration coefficient, k_3 = 0,6 - cross-section coefficient, k_{po} = 1 - coefficient that takes into account technological methods of surface strengthening, k_A = 1 - coefficient of anisotropy for steel castings, k_{kor} = 0,5 - corrosion coefficient. By putting values of influential coefficients into equation (21) we get K_D = 4,28 for the turbine shaft. Factor K_D determined in such a fashion can be used in formulas for determination of the factor of safety.

1.2 Numerical Calculation of the Stress State in the Critical Cross-Section of the Transition Radius of the Shaft

Calculation of the stress state of the turbine shaft with the transition radius R80 between the cylindrical and flange area of the shaft has been carried out by the turbine manufacturer LMZ (Russia), UCM Resita (Romania), Institute for Materials Testing and LOLA Institute (Serbia). All calculations showed that the values of bending stresses, which occur due to the action of the load and corrosion fatigue, including stress concentration factors, are higher than 25 MPa for flanges subjected to "corrosive water" and can cause the occurence of surface cracks on the transition radius between the cylindrical and flange area of the shaft.

1.3 Analysis of Fracture Mechanics Parameters

Behavior of the material subjected to alternating load in the presence of a crack is defined by the following parameters which are being determined through fatigue crack growth analysis: fatigue crack growth rate (da/dN) and minimum critical stress intensity factor that causes no crack growth or fatigue threshold (ΔK_{th}), fig. 4. Analysis of stress state and deformations on the tip of a fatigue crack by the use of linear-elastic fracture mechanics for stable crack growth is being formulated by Paris - Erdogan equation, which is applicable for all metals and alloys (eq. 22). Results of tests performed in order to determine crack growth rate in relation to stress intensity factor (ΔK) are presented in Table 1.

$$\frac{da}{dN} = C \cdot (\Delta K)^m \qquad (22)$$

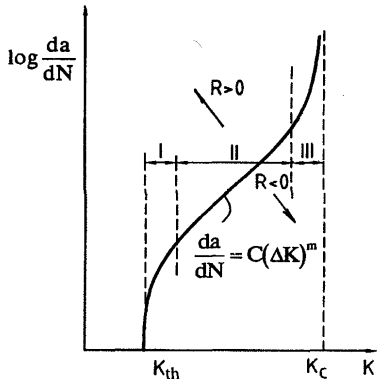

Fig. 4 Typical fatigue crack growth rate curve

Obtained results for fatigue threshold ΔK_{th} indicate that the casting of the flange area of the turbine shaft in the longitudinal direction (crack is transversely oriented) is more resistant to the propagation of the existing crack, which confirms the conclusions reached through the analysis of the fracture area of the turbine shaft. Effect of notch orientation on fatigue crack growth rate da/dN is directly related to parameters in the Paris equation, coefficient C and exponent m. For the analysis the stress intensity factor range ΔK=10 MPa $\cdot$ $m^{1/2}$ has been taken, because that value resides in the area of stable crack growth in da/dN versus ΔK graphs for which the Paris law [11] is applicable.

Table 1. *Fracture mechanics parameters for specimens taken longitudinally and transversally from the casting*

Specimen	Fatigue threshold ΔK_{th}, MPa $m^{1/2}$	Coefficient C	Coefficient m	da/dN, m/cycle at ΔK=10 MPa $m^{1/2}$
Longitudinal	8,7	$3.0 \cdot 10^{-11}$	3.14	$5.62 \cdot 10^{-08}$
Transversal	7,4	$3.2 \cdot 10^{-11}$	3.1	$6.36 \cdot 10^{-08}$

CONCLUSION

On the basis of theoretical considerations, testing results regarding the fatigue strength, fracture mechanics parameters and effect of the stress concentration in the corrosive operating environment it can be concluded that cracks and fracture of the turbine shaft of the hydro-electric generating set nr. 6 before its predicted service lifetime passed occured due to the inadequate construction solution regarding the production of the shaft, referring to the following:

- high stress concentration on the transition radius of the flange area of the turbine shaft and operation in a corrosive environment, which caused the occurence of initial cracks in that area,
- insufficient moment of resistance in the critical cross-section of the transition radius and shaft operation in the corrosive environment, as well as exposure to the leaking water, which caused the bending stress and other components of stress to grow beyond acceptable values,
- inadequate construction solution regarding the seal caused the exposure of the flange area of the shaft to the corrosive environment (leaking water),
- corrosion protection was poorly executed and not renewed,
- absence of periodic inspections by non-destructive testing methods.

ACKNOWLEDGEMENT

We thank the Ministry of Science and Technological Development of the Republic of Serbia for financing the work on the following theme within the EVB project: 35002-TR.

REFERENCES

[1] Angehrn, R., Eckert R., “Service Life of Horizontal Shafts in Low Head Turbines under Corrosion Fatigue”, IAHR 15th Symposiym, Belgrade, 1990.

[2] Ohashi. H., “Vibration and Oscillation of Hydraulic Machinery”, Avebury Technical, 1991.

[3] Vladislavlev. L. A., “Machine Vibration of Hydroelectric Plant”, (in Russian), Moskva, 1972.

[4] The Guide to Hydropower Mechanical Design, ASME “Hydro Power Technical Committee”, HCI Publications, New edition planned, 2009.

[5] Pejovic S., “Profit Management and Control of Hydropower and Pump Plants”, Proceeding of the International Joint Power Generation Conference, Denver, Colorado, 1997, pp. 539 - 545.

[6] Pejovic S., “Profit On Line Management and Control of Hydroplants”, IAHR Work Group on the Behaviour of Hydraulic Machinery under Steady Oscillatory Conditions, Chatou, France, 1997, Paper G2, pp. 10.

[7] Arsić M., Vistać B., “Study on Materials Testing and A6 Turbine Shaft Fracture Analysis HPP „ĐERDAP II”, Section: A6 Turbine Shaft Fracture Analysis, HPP „ĐERDAP II”, Belgrade, 2008.

[8] “Рекомендации по оценке прочности крупногабаритиых конструкций с примеменениjем характеристики механики разрушения”, Центральий научно-иследовательский институт технологии машиностроених Москва, 1977.

[9] Пиљев М., “Анализ прочности измененной по эскизу Э-18070 конструкциии крышки рабочего колеса гидротурбины ГЭС Джердап-1”, Отчет но. 3033, 2008.

[10] Peterson R.E., “Stress concentration factors”, John Wiley&Sons, New York, 1974.

[11] Hertzberg R., “Deformation and fracture mechanics of engineering materials”, New York: John Wiley & Sons, Inc., 1995.

HEAVY MACHINERY - HM 2011, 55-60 Paper accepted: 30.05.2011
ISBN 978-86-82631-58-3

Stress Concentration at Welded Joins of Bucket-wheel Excavator

Andreja Ilić [1,*] - Lozica Ivanović [1] - Danica Josifović [1] - Zvonimir Jugović [2]
[1] University of Kragujevac, Faculty of Mechanical Engineering
[2] University of Kragujevac, Technical Faculty Čačak, Department of Mechanical Engineering

Stress and strain distribution in welded joints zone is major influential factor to exploitation properties, safety and reliability of bucket-wheel excavators. Stress and strain distribution in zones of welded joints of bucket-wheel excavator is determined by stress concentration forced by geometrical discontinuities and heterogeneous of material. This paper deals with experimental determination of stress concentration influence to mechanical properties of welded joints models. The experimental procedure was done on welded joints models in static load conditions on samples made of commonly used steel strip profile. The experimental procedure involved determination of material properties and determination of strength parameters of butt joint welded samples with different configuration of stress concentrators. The aim of this paper is to highlight the importance of welded joint properties to the resistance of bucket-wheel excavator' welded structure. Stress concentration was analyzed by experimental approach objected to include as much influential factors as it is possible. This paper pointed out the necessity of analyzing the bucket-wheel excavator' welded structure on different dimension levels. Further investigations in this area have to be continued trough development of precise numerical model of the bucket-wheel excavator' welded structure which will, in involvement with adequate software simulation, complete the obtained results.

Keywords: Bucket-wheel excavator, welded joint, stress concentration, mechanical properties.

1 INTRODUCTION

Bucket-wheel excavators are heavy-duty engineering vehicles with primary function of earth-moving in mining. The bucket wheel, as one of the integrated components is a large, round wheel with a configuration of scoops which is fixed to a boom with rotation capability. Material is picked up by the cutting wheel and transferred back along the boom. Material is then through the discharge boom received and carries away to an external conveyor system. The main function of counterweight boom is to balance the cutting boom and is cantilevered on the support structure. The support structure laid on the movement systems. The support structure of bucket-wheel excavators is capable of rotating about a vertical axis. The cutting boom can be positioned by rotation up and down. The object of observation in the study presented in the paper is bucket-wheel excavator by FAM at Kolubara, Serbia (Fig.1). The origin equipment consisted of five SRs 1200.24/4 VR FAM-Buckau bucket-wheel excavators, dated in the 1960s. The support structure was ruined in accident in 1995. The massive rebuild was done and the steelwork and support structure were upgraded. The tower and ballast boom from the Type SRs 1300 were fitted which gave better transmission of force for rope guidance and the wheel boom hoisting gear. A new lightweight bucket-wheel drive was used and drive power was increased from 400 kW to 630 kW, capacity was increased from 3450-4000 m^3/h while improving the specific digging force to 1,000 N/cm and belt speed was increased by 15%.

Fig. 1. *Bucket-wheel excavator by FAM at Kolubara, Serbia*

*Corr. Author's Address: Faculty of Mechanical Engineering, gilic9@sbb.rs

The support structure of the observed bucket-wheel excavator is typically complex welded steel structure. It is estimated that 70-80 % of the total weight of bucket-wheel excavator consists of steel plates and steel castings with welding as the main joining method. The assessment of properties of the welded joints is in focus of the paper due to facts that the welds are the determining factor of expected life of bucket-wheel excavator. Accordingly, the zones of welded joints are the regions of weakness in a structure and must be fully understood.

During exploitation this welded structure are subjected to severe static and dynamic loading which can result in fatigue damage in the zones of the welds. Due to significance of safety and reliability, design against fatigue failure and developments for improving the fatigue strength of welded structures must be done. Material fatigue is local phenomenon and involves a gradual decline in mechanical properties within exploitation. Failure occurs in local zones of the structure that are subject to high stresses and where weld defects are significant [1, 2, 3, 4 and 5].

2 STRESS CONCENTRATION IN ZONES OF WELDED JOINTS

Changes in shape or discontinues cause the redistribution of stresses within the loaded element and represent the stress concentrators due to the diversion and densification of stress lines. Stress concentration is, also, caused by, inhomogeneity of material, and with other structural discontinuities. The welded joint itself, by its nature, is a source of stress concentration as consequence of applied welding technology. Element joints zones in welded constructions are the areas of multiple stress concentration. The properties of those zones determine the behavior and stability of the entire constructions. Errors in the joints, cracks and sharp cuts, which most often exist in these zones of stress concentration with a high level of load, are dangerous spots that cause the loss of structural integrity. Welded joints are zones with high residual stress level as a consequence of applied welding technology. Residual stresses have great influence on the properties, quality and exploitation characteristics of mechanical structures made by process of welding. Furthermore, zones of welded joints determined the safety and reliability of whole welded constructions [6, 7, 8, 9 and 10].

The stresses in the welded joints zones are of highly unpredictable character. Efficient and reliable methods for stress state analysis conditioned by stress concentrations represent the basis for the assessment of structural integrity of support structure of bucket-wheel excavator as welded construction.

3 MODEL TESTING

Due to importance of welded joints' properties model testing of typical joints of bucket-wheel excavator with common configuration of stress concentrators was done. The models for testing were prepared with required geometrical similarity to welded joints of real bucket-wheel excavator construction. Tests were carried out on specimens made of a strip profiles of material Č0361, chemical composition 0.17% C, 0.05% S, 0.05% P, 0.007% N, which is used for responsible welded structures without risk of brittle fracture. For model preparation, specimens are welded in protective atmosphere of CO_2 with flow rate 9 l / min, welding device VARMIG 400 D 42 and wire electrode ESAB AUTROD 12:51, d = 1 mm, the specification EN 440, from ESAB producers, Sweden. Welding parameters were: welding current I = 105 A, welding voltage U = 21 V and welding speed v_z = 28 m/h. The machine is equipped with a device for registering force dependence on elongation (Fig.2). Force increase speed was adequate for static tests. Experimental testing was performed at the Laboratory for welding and Laboratory for machining materials at Faculty of Mechanical Engineering in Kragujevac.

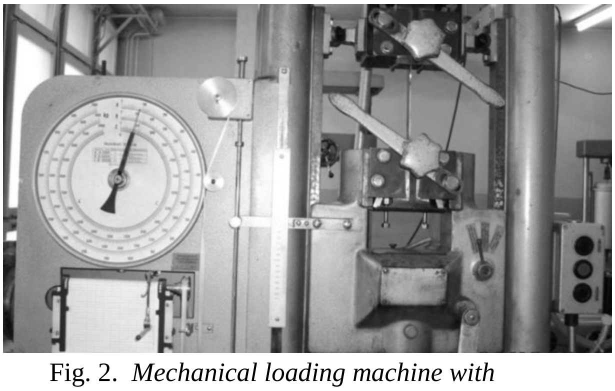

Fig. 2. *Mechanical loading machine with measuring device*

4 PROCEDURES OF EXPERIMENTAL TESTING

For experimental testing of stress concentration influence on mechanical properties of the joints models, specimens were used. Firstly, testing was done on samples with flat sides, with and without welded joints. Then, samples with welded joints and the circular holes in the axis ware tested. At the end, in order to examine the influence of stress concentration due to shapes of welded joints' zones testing were conducted on specimens with concave sides and welded joints and holes in the axis. Shape and dimensions of specimens used for testing are shown in Fig.3. Testing was conducted according to defined procedure on a series of five specimens for each configuration of stress concentrator.

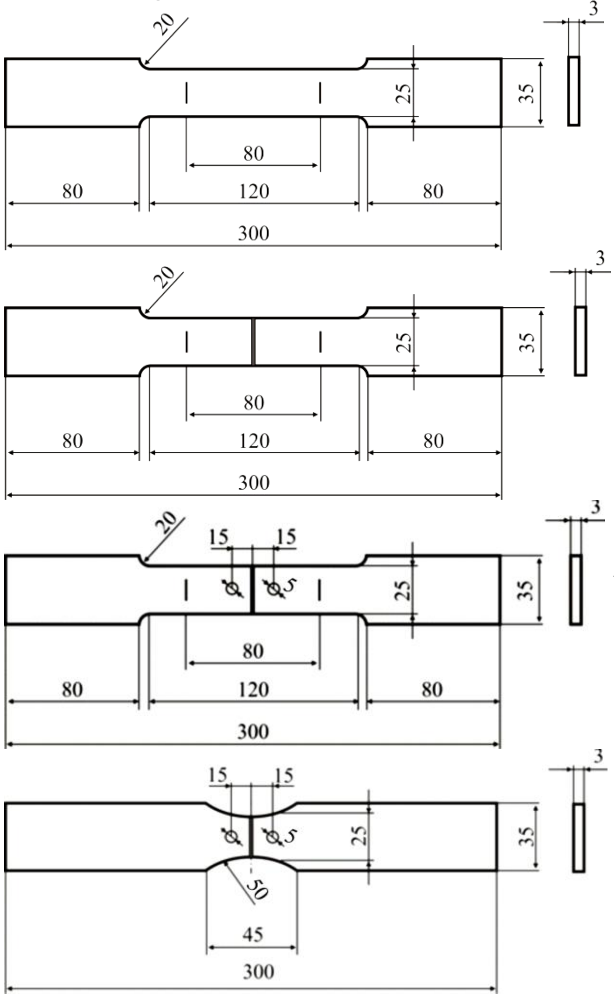

Fig. 3. *Shapes and dimensions of tested specimens*

Force on the yield limit and tensile strength ware measured. Elongation to the limit of breaking was determined. The obtained results show very small relative variations and can be taken as relevant for further analysis. The force dependence on elongation for specimens with parallel sides and welded joint is presented at Fig.4. For specimens with parallel sides, welded joint and holes, force dependence on elongation is presented at Fig.5. Fig. 6. presented force dependence on elongation for specimens with concave sides, welded joint and holes in axis.

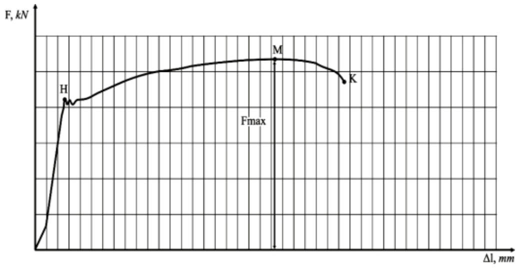

Fig. 4. *Force dependence on elongation for specimens with parallel sides and welded joint*

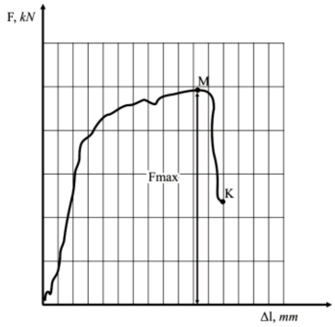

Fig. 5. *Force dependence on elongation for specimens with parallel sides, welded joint and holes in axis.*

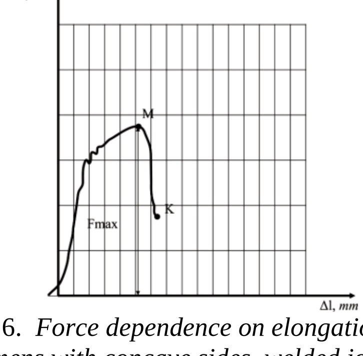

Fig. 6. *Force dependence on elongation for specimens with concave sides, welded joint and holes in axis.*

The presented diagrams showed different material behavior due to different multiple stress concentration within samples. Mechanical properties comparisons of specimens are shown in Fig.7, 8 and 9.

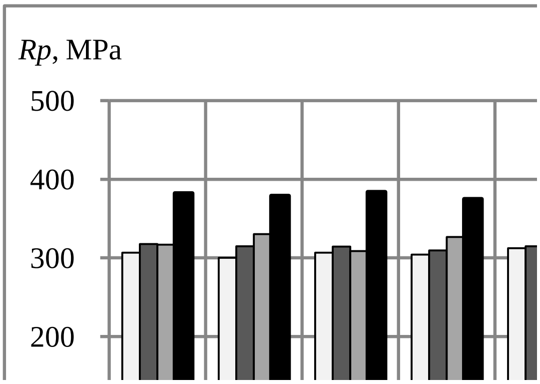

Fig. 7. *Yield limit for tested specimens*

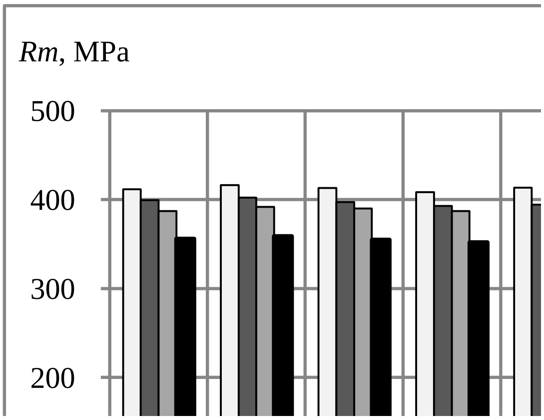

Fig. 8. *Tensile strength for tested specimens*

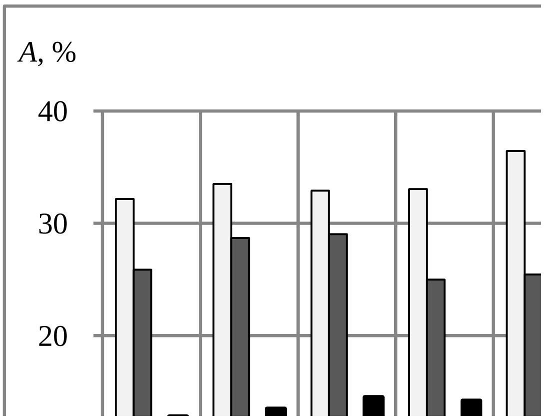

Fig. 9. *Elongation for tested specimens*

Due to very small relative variations obtained results, can be taken as relevant for further analysis.

5 OBTAINED RESULTS EVALUATIONS

The used material for testing is structural steel of commercial quality that fully meets the required mechanical properties, both in terms of mechanical strength and plasticity, which was experimentally confirmed. Mechanical properties of samples with welded joint remain within the limits of base material. By that, it can be concluded that good utilization of the mechanical characteristics of the used base material can be achieved by appropriate welding process. In Fig.10, the appearance of specimen with flat sides, welded joint and the circular holes in the axis after testing is shown.

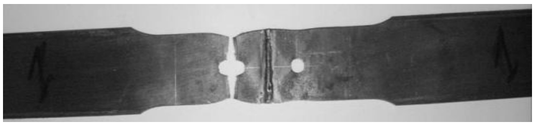

Fig. 10. *Appearance of specimen after testing with flat sides [6]*

The plasticity of welded joints is lower than the plasticity of the base material which is confirmed experimentally (Fig.10), and it is in accordance with current literature sources related to this area [11 and 12]. By testing the specimens with parallel sides, welded joint and circular holes in the axis, the reached tensile strength values show the tendency of decline of mechanical properties due to multiple stress concentration. The highest concentration of stresses occurred in the area of holes for specimens with welded joints and holes in the axis. The position of breaking zone pointed out this fact (Fig.10). Specimens with welded joints and holes in the axis shoved highest stress level on the yield limit and the highest plasticity. These concentration sources affect the increase of deformations that occur until the final breaking of specimen (Fig.10). The self obtained results are in agreement with literature sources that analyze the stress concentration and stress-strain state of metallic materials [13, 14, 15 and 16]. Achieved stresses on yield limit and tensile strength of specimen with concave sides, weldment and holes in axis show the trend of decline, so that the stress concentration caused by the shape of tested specimen can't be ignored. At Fig.11. appearance of specimen with concave sides, welded joint and the circular holes in the axis after the testing is shown.

Fig. 11. *Appearance of the specimen with concave sides after testing[6]*

The position of the breaking zone shows that dominant stress concentration is caused by circular holes (Fig.11). The experimentally obtained results are in accordance with the results shown in the literature [12, 14 and 17].

6 CONCLUSIONS

Present state of the earthmovers, especially bucket-wheel excavator as continuous excavation machines, which is dominant component in mining system, is characterized by progressive growth in dimensions, increase of capacity and permanently improving performances all together with decrease of exploitation costs. This must be followed by proper calculation methods in which zones of welded joints have to be adequately treated. Bucket-wheel excavators belong to the group of complex welded mechanical structures, and for its proper design, construction and use, a number of influencing factors should be analyzed. Welded construction of support system of bucket-wheel excavator is a complex system of heterogeneous elements by dimensions and shapes, structures, mechanical characteristic with complex interactions between those elements. Heterogeneity of welded construction elements provoked its different answers to load. Inhomogeneity of microstructure at zones of welded joints causes additional complexion of stress state. Stress concentration caused by characteristic shape of construction elements completely changed the stress state distribution, position of maximal stresses, and by that the position of danger cross section zone which act as safety risk for damage and integrity of the construction. Distribution of the stress state in welded construction is changeable due to load characteristic. The essence of determining the stress state in welded joints zones is to form its' more accurate analytical model, which will provide data and information for the constructural analysis, elaboration and detailed calculations of bucket-wheel excavator. All that facts are the consequence of the influence of welding join methods and its parameters to the stability and performance of construction itself. Mechanical resistance and stability of support structures of bucket-wheel excavators as welded constructions are analyzed and proven by calculation of capacity of welded structure for the anticipated loads and exploitative conditions. In analytical models used for these analyses and calculations, the stress concentration is one of the major factors in determining the correct stress state. Further researches in this area should be continued by developing and obtaining the precise numerical model of welded joints of bucket-wheel excavator which would complete the calculation and verify the experimental model testing.

Safety and reliability requirements for this kind of heavy equipment are very strict. On the other side, maintenance costs of bucket-wheel excavator are very high. Failure costs increase with increased excavation capacity. All the pointed facts impose the necessity or adequate design optimization of bucket-wheel excavator. The design process must be done on adequate capacity calculations and must be verified through numerical simulation and experimental model testing. The whole construction must be treated on different dimension levels in order to enclosed the influence of welded joint zons.

REFERENCES

[1] Bošnjak, S., Zrnić, N., Petković, Z. “Bucket wheel excavators and trenchers – computer aided calculations of loads caused by resistance-to-excavation”, Machine design (monograph), pp. 121 – 128, 2008, Novi Sad.

[2] Bošnjak, S., Petković, Z., Zrnić, N., Simić, G., Simonović, A. “Cracks, repair and reconstruction of bucket wheel excavator slewing platform”, Engineering Failure Analysis, Vol. 16, pp. 1631–1642, 2009.

[3] Bošnjak, S., Arsić, M., Zrnić, N., Rakin, M., Pantelić, M. “Bucket wheel excavator: Integrity assessment of the bucket wheel boom tie-rod welded joint”, Engineering Failure Analysis, Vol. 18, pp. 212-222, 2011.

[4] Bošnjak, S., Zrnić, N., Simonović, A. Momčilović, D. "Failure analysis of the end eye connection of the bucket wheel excavator portal tie-rod support", Engineering Failure Analysis, Vol. 16, pp. 740-750, 2009.

[5] Bošnjak, S., Simonović, A., Petković, Z., Zrnić, N. "Comparative analysis of strength for variant structural solutions of lower structure for bucket wheel excavator KRUPP C-700S", Research and designing for industry, Vol. 4, pp. 19-28, 2006.

[6] Jovanović, M., Adamović, D., Lazić, V. "Welding technology", Faculty of Mechanical Engineering, Kragujevac, 1996 (in Serbian).

[7] Josifović, D. "Examinations of mechanical construction I", Faculty of Mechanical Engineering in Kragujevac, 2000 (in Serbian).

[8] Ilić, A., Josifović, D., Lazić, V. "Experimental determination of the construction form influence on stress concentration in welded joints", 8th YSESM, Proceedings of extended abstracts, pp. 6 – 7, 2009, Hungary.

[9] Ilić, A. "Stress concentration and welded construction form influence on its durability", PhD entrance thesis, Faculty of Mechanical Engineering, Kragujevac, 2010 (in Serbian).

[10] Ilić, A., Josifović, D., Lazić, V., Ivanović, L. "Experimental determination of stress concentration influence on welded constructions stability", IRMES 2011, Proceedings, pp. 219 – 224, Zlatibor, Serbia, 2011

[11] Dally, J. W., Riley, W. F. "Experimental Stress Analysis", McGraw-Hill Book Company, 2008, USA.

[12] James, F. D. "Modern Experimental Stress Analysis", John Wiley & Sons Ltd, 2004, England.

[13] Radaj, D., Helmers, K. "Bewertung von Schweißverbindungen hinsichtlich Schwingfestigkeit nach dem Kerbspannungskonzept", Konstruktion Vol. 49, pp. 21-27, 1997, Germany (in German).

[14] Davies, C. "The Science and Practice of Welding", Vol. 2, Cambridge University Press, 2003, England.

[15] ENV 1993-1-1. Eurocode 3: Design of steel structures - Part 1-1. CEN 1992.

[16] Ludwig, M. J. "Design of Welded Connections", American Welding Society, 2000, USA.

[17] David, S. A., Debroy, T., Dupont, J., Koseki, T., Smartt, H. "Trends in Welding Research", Proceedings of the 7th International Conference, American Welding Society, 2008, USA.

ACKNOWLEDGMENT

This work is a contribution to the Ministry of Science and Technological Development of Republic Serbia funded Project TR 35037.

HEAVY MACHINERY - HM 2011, 61-67
ISBN 978-86-82631-58-3
Paper accepted: 30.05.2011

Effect of Design Parameters to Modal Behaviour of Gear Unit Housings

Snežana Ćirić Kostić[1,*] – Milosav Ognjanović[2] – Aleksandar Vranić1
[1]Faculty of Mechanical Engineering Kraljevo, University of Kragujevac, Serbia
[2]Faculty of Mechanical Engineering, University of Belgrade, Serbia

The spectra of the emitted noise of gear units are in direct correlation with the modal response of their housings, which is consequence of excitation by the internal disturbances. The process of excitation of modal response of the gearbox housing is a deterministic process. Excitation of certain modal shapes (modes) depends on frequencies of the disturbances and the elastic deformations they cause. Modal damping of the modal vibrations, as a result of complex processes of the wave motion in the walls of the housing, is also a key parameter of the modal behavior. In addition, modal behaviour, as characteristic structure property, is determined by the material properties (mass, stiffness and damping) and boundary conditions of the structure. Change of any of those characteristics leads to changes of modal behaviour. The aim of the paper is elaboration of the mechanism of excitation of natural vibrations of a gearbox housing including both the effects of excitation disturbances (direction and place of action, frequency, damping) and parameters (shape, dimensions, material) of the structure. Numerical and experimental methods were applied and their results allowed for analytical clarification of processes in elastic structure of system.

Keywords: vibrations, modal analysis, excitation, modes, gear unit

0. INTRODUCTION

A sound wave that is the gear unit noise is emitted from the housing walls into the surrounding. The housing surface also emits the sound which penetrates from the inner space through the walls, as well as the sound generated by the housing with its natural oscillation. From this aspect, the housing walls have a double role: to be an obstacle to penetration of sound waves from the inside, i.e. to be the insulator of inner (internal) sound sources and the generator of tertiary sound waves due to natural oscillation. Insulation properties sound of acoustic partitions, i.e. the housing walls are also in direct relation with modal properties (natural frequencies and shapes of oscillation). Therefore, it is very important to find an answer to the question what are possible modal shapes of oscillation of the housing walls and under which conditions each of them can be excited. The way and conditions of excitation of natural oscillation are, in this sense, of special interest. They are important, before all, because they will offer answers to many questions relating to penetration of sound waves trough the housing walls. On the other hand, the "mechanism" of excitation of natural oscillation represents an unexplored field, which is the main aim of this paper. Phenomena and processes in elastic structure, which cause accoustic emission, are not adequately investigated. In the papers, which explore the basic processes, simplified models are used. In the other hand, the housings with real and complex geometry are investigated in the papers aimed at the direct application of the results. Varying schedule of ribs and determining their influences on acoustic emission of a gearbox are treated in [4, 5]. Tanaka et al. have developed a method for predicting gear noise. For calculating of sound radiation of a two-stage gearbox with helical cylindrical gears, they used the results of FEM and commercial software. The authors in [5] work on the optimization noise of of two-stage gearbox by varying the position of the ribs and wall thickness at the position where are situated the bearings. **I**n both articles, the whole gearbox is modeled. For the worm gear, Hubner et al. [2] have analyzed the influences: the size of the input torque, changes of direction, change of producer of shafts, and the natural vibrations of the housing, on the general level of sound power. Planetary gearbox is treated in

[*]Corr. Author's Address: Faculty of Mechanical Engineering -Kraljevo, Dositejeva 19, 36000 Kraljevo, cirickostic.s@mfkv.kg.ac.rs

[3]. Authors determine the dynamic response and noise of the selected gearbox, using commercial software I-Deas to apply FEM. Inoue with colegues [6] has developed a methodology for the application of FEM (using elements of the plate) and the BKE in order to calculate the sound power which is radiated by a housing which have shape of rectangular parallelepiped. He also proposes a program to determining the optimal thickness of the walls of the same model of housing [7, 8]. In [1], Inoue uses FEM and BKE to reduce vibration, and works on the optimization of simple forms of housing, by considering the influence of radius curves of the upper part of housing. Finally, with Yamanaka and Kihara [9] he discusses the best position of ribs on the housing with thin walls, for purpose reducing vibration and noise.

For the purpose of elaboration of procedure and conditions of excitement, i.e. for the purpose of defining rules of excitation, we have used the results of modal analysis by applying FEM, by using the method of direct integration within FEM and results of modal testing.

1. EXCITATION OF CERTAIN MODAL SHAPES OF THE GEAR UNIT HOUSING

1.1. Modal analysis

The mention research is realized on the example of a housing shown in Figure 1. It is a cast housing of a two-degree gearbox, reinforced with ribs and rings for increasing stiffness. In relation to the overall dimensions of (760x500x260 mm) the walls have relatively large thickness (15 and 20 mm). A complex shape was thus obtained having small sensitivity to excitation. As such, it offers a possibility for detection of all-important details in clarification of excitation mechanisms and nature of natural oscillation of each structure.

Modified models of the housing were developed, with purpose to determine the influence of correction of structure on its modal response. By varying the thickness of the wall, placing the ribs or the their elimination, by changing the dimensions, materials and other properties is carried out variations of modal structures. Figure 1 shows the developed geometric models of gearbox housings, with thick and thin walls, with and without ribs, on which are studied conditions under which there is a modal excitation.

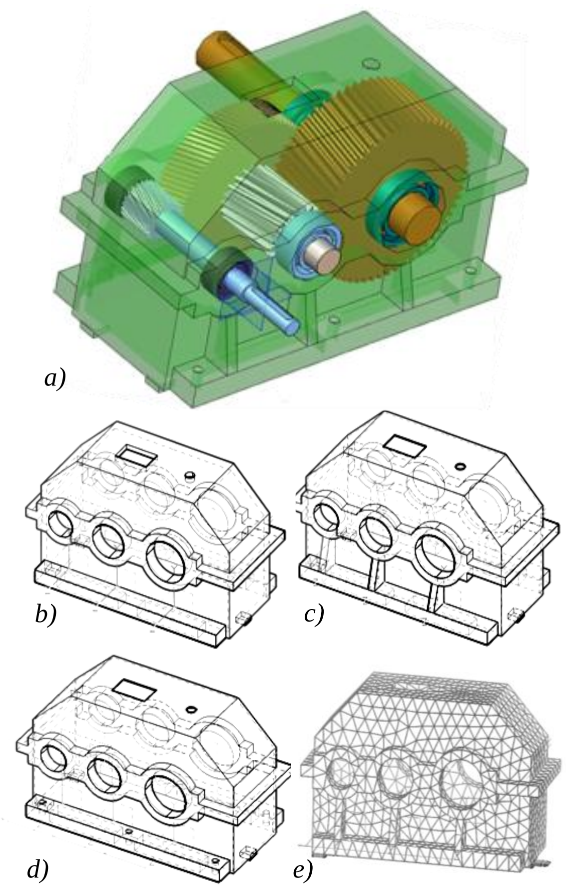

Fig. 1. *The chosen models of gearbox housing: a) basic, b) basic model without ribs, c) thin walls model, d) thin walls model without ribs, e) FE model*

Modal analysis of the given housing was performed by applying the finite elements method. The linear 3D-brick finite element with 12 degrees of freedom (three translations per each node) was used. For the basic model of housing, the finite elements mesh contains a total of 6385 finite elements, 12950 nodes with 38850 degrees of freedom. For the frequency range of 0-3000Hz, 88 natural frequencies and modal shapes of oscillations is calculated. Some of them are presented in Fig 2.

With increase in natural frequency, the shape of oscillation, i.e. deformations during oscillation become more complex. The structure is divided into a certain number of zones, which oscillate separately from one another with the same frequency. Waves propagate from the middle of every modal zone and get into "collision" at points, which represent "partitions" between these zones and zones by itself represent together stationary (standing) wave (Fig. 2).

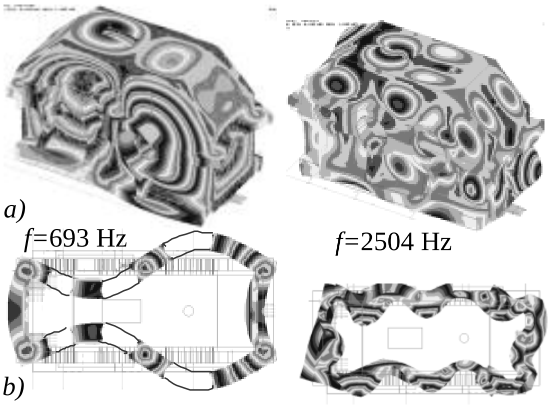

Fig. 2. *Distribution of deformations in modal shape of oscillation with frequencies f=693 Hz and 2504 Hz: a) axonometric presentation, b) chosen section*

Sources of those waves are at the points of greatest displacements (middle of zone), and they, at points of nodal partitions (nodes) displacements, are close to zero. The stresses of these waves are also calculated and the values of stresses are opposite to displacement. Stresses are greatest at the points of nodal partitions that act as clamping (constraining), and they are smallest at the points of wave sources, where displacements are greatest.

With purpose of determination of influences of shapes, thickness of walls, stiffness, mass of structures, on modal behaviour, the same procedure was applied on the other models. (Fig. 1b,c,d). Calculated frequency (which is shown in Tabele.1), indicating a trend increase in the number of possible modal shape, with a reduction in stiffness, wall thickness and mass.

Reducing the thickness of the wall leads to an increase in number of modal zones on the walls that are deformed the during modal oscillations (Fig.3.a). In places where at certain frequencies is expected formation of nodes, add the ribs on the structure increases the number of modal zones and reduces the maximum amplitudes of the oscillation (Fig. 3b).

Tab.1. *Details about discretized models of housing*

	Model Fig.1b	**Model Fig.1c**	**Model Fig.1d**
Length of FE	42 mm		
Final elements	6 383	6 694	6 566
Nodes	12 999	13 559	13 369
Degrees of freedom of discretized model	38 997	40 667	40107
Freq. range	0-3000 Hz		
Calculated natural frequencies	95	131	135

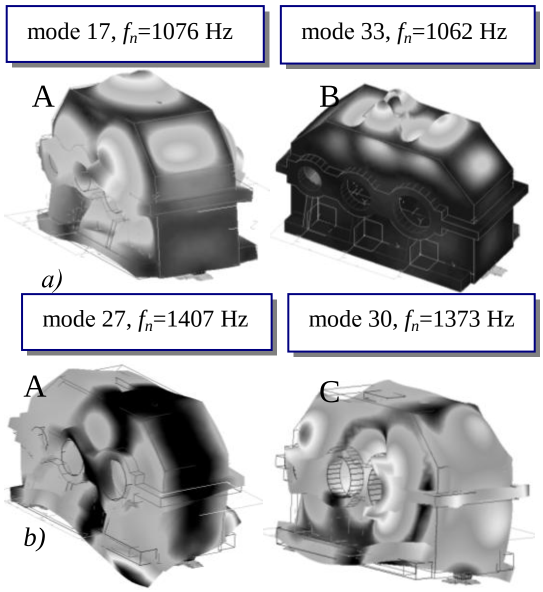

Fig. 3. *a) Influence of wall thickness in modal response of the housing, b) Influence of ribs on the modal response of the housing; A- basic model (thickness of walls is 15 mm), B-thickness of walls is three times smaller (5 mm), C-basic model without ribs*

During the natural vibration of housing walls with frequencies 1407 Hz and 1373 Hz, the front and rear vertical walls are deformed with creating three nodes, on model with ribs, while on model without ribs smaller modal zones are created with reduced modal amplitudes of vibrations relative to the second model (C).

1.2. Conditions for certain modal shape excitations

The modal analysis allowed establishing certain (modal) shapes of oscillation and their modal characteristics. They are possible shapes of oscillation which can be excited under certain conditions. If those conditions are not fulfilled, natural oscillation by the corresponding mode will not be realized. In real conditions, only a small number of modes out of a large number of them (theoretically infinite) are active. The other modes are not excited because there are no appropriate conditions for excitation.

Excitation of a certain modal shape can be realized if the following conditions are satisfied:

- If the excitation elastic deformations (direction and place of action) completely or partly coincide with the elastic deformations arising during oscillation by a certain modal shape;
- If the excitation frequency is close or equal to the frequency of the modal shape which should be excited;
- If modal attenuation is of sufficiently small value so that it could not result in partial or complete attenuation of this oscillation.

These conditions were checked by the numerical integration method and modal testing. The discretized (by FEM elements) model of housing was excited by the impulse force of 1000 N with duration of 0.02 seconds in the area of maximal modal displacement (Fig. 4b). This force excites the corresponding modal shape together with similar shapes and frequencies. One of these results is presented in Fig. 4. By the force in the direction *z*, in the area of the middle hole, natural frequencies 155 Hz and 359 Hz are excited (the red line in Fig. 4a) because the force direction is the same as the direction of maximal displacement for these modal shapes (Fig. 4b and 4c). By force in *x* and *y* directions, the modal shape with 359 Hz is not excited because these directions are not the same as the corresponding displacement. The force in the *y*-direction succeeds in exciting only the modal shape with 155 Hz because the force direction corresponds to the displacement direction for this frequency.

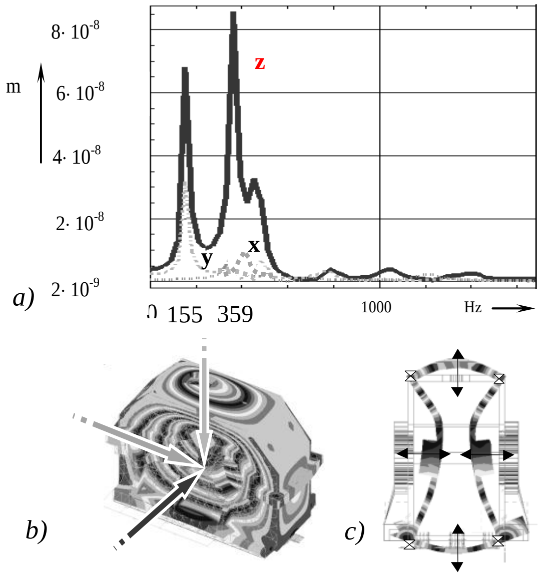

Fig. 4. *The example of using the results of numerical modal excitation by impulse force: a) numerical integration results, b) exciting force directions, c) modal shape displacement in chosen sections (359 Hz)*

It is possible to excite the corresponding modal shape by disturbance with the same frequency. The maximal effect can be obtained with the excitation force which acts in the place and direction of maximal displacement and fluctuates with the corresponding frequency of modal shape.

Random excitation produced by the impact of a modal hammer or by a shaker with random frequencies is used for practical applications (experimental) excitation.

Figure 5 presents the frequency responses measured at point 0 with excitation by a modal hammer at points 6 (in the middle of the lateral side of the housing) and 7 (at the front vertical wall, right above point 0). The modal response obtained experimentally is similar to the response obtained numerically. Differences in the calculated and measured values of frequencies range from 0.7 to 9 % with the tendency to reduce the difference with the increase of frequency.

The procedure of investigation and elaboration of conditions under which there is excitation of a certain modal shape is presented in [10] in a detailed way

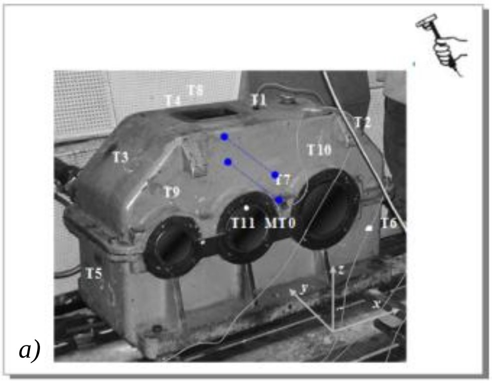

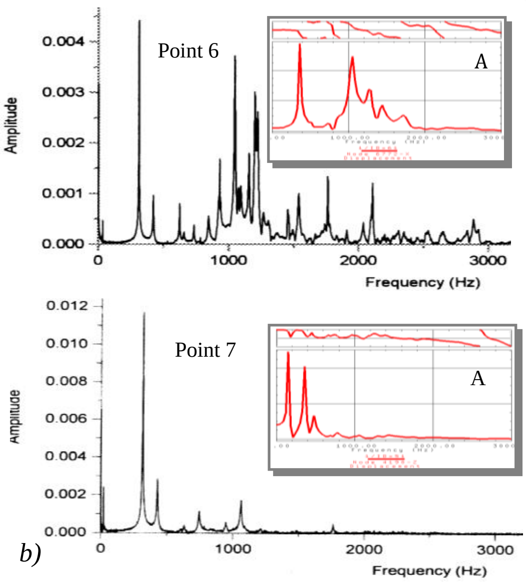

Fig. 5. *a) Modal testing, b) Amplitude-frequency diagrams obtained by modal testing and numerically (A)*

2. INFLUENCE OF THE DESIGN PARAMETERS ON MODAL BEHAVIOUR OF STRUCTURE

Modes are the properties of the structure. Characteristics of material (mass, stiffness and damping) and boundary conditions of structure determine properties of modes. Change any of these properties leads to changes in activity mode. Adding mass Δm to the existing mass of the structure, natural frequency will be reduced to values

$$\omega_n = \sqrt{\frac{c}{m+\Delta m}}$$

under the condition that other parameters remain unchanged. This change leads also to a reduction in damping. Therefore, removing of mass from the existing model will result in higher frequencies with smaller amplitudes of response, provided that the stiffness does not change. However, mass change leads to changes in stiffness.

Correction of stiffness is usually performed by adding ribs on the structure of the zones of increased levels of vibration. Higher natural frequencies with higher modal damping ie. small amplitudes of oscillation are the result of the increased stiffness of the structure (Fig.6) (Fig.6).

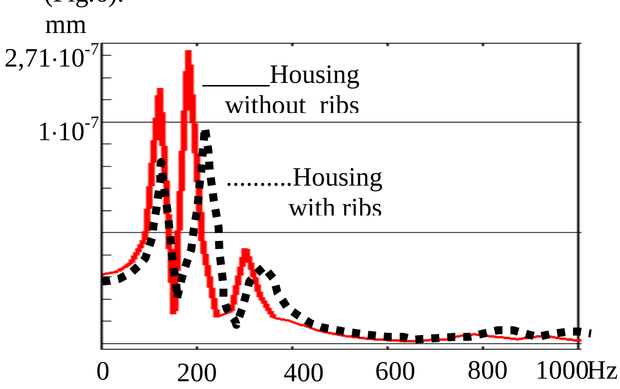

Fig. 6. *Influence of adding ribs on the frequency response of housing*

It should also be noted that each of these corrections can also be an indirect cause of changes in the remaining parameters. Increasing of stiffness, depending on how it the achieved, may have influence on increasing of mass of structure. In the final dynamic responce should be consider influences of both corrections (direct and indirect). It can even happen to overcome the influence of indirect (consequential) correction and to achieve the opposite effect.

For example, change of mass can be implemented simply by adding of mass, and than the response depends on the place where you add mass. Also, one mass part may be transferred from one place to another and it can also be distributed evenly on the structure or it can be removed. All these details and their mutual connections, depending on the shape and complexity of the structures, affect on the change in its frequency response.

According our preliminary analysis, if wall thickness reduce three times, resulting in the reduction of the total mass of the housing, at first moment might be expected that there will be increasing of the active frequencies. However, according to the diagrams in Figure 7, we can see the opposite. New natural frequencies are shifted towards lower values with increasing levels of vibration (from $1{,}18\cdot10^{-8}$ mm, which corresponds to the maximum amplitude at the point 6 of the basic model, to the amplitude of $4{,}21\cdot10^{-8}$ mm for the same point on the model with less mass). Reduction of wall thickness directly affects the decrease of frequencies and increasing of amplitude of oscillation. In this case, changes in wall thickness, at the same time, causes changing of mass and a significant reduction in stiffness of housing of the structure.

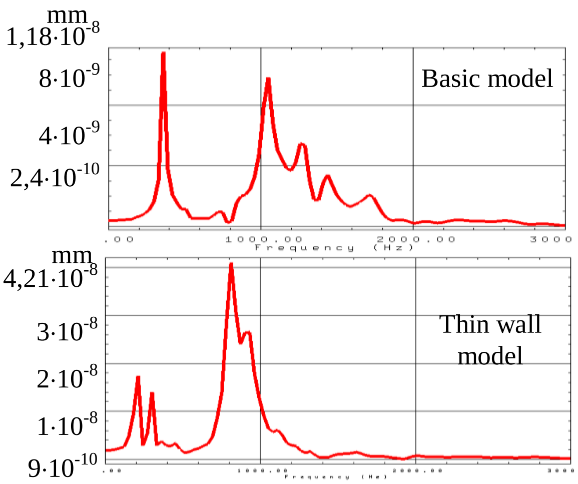

Fig. 7. *Influence of wall thickness on frequency response: a) basic model with a wall thickness of housing 15... 20 mm, b) modified the model of housing with a reduced wall thickness to 5 mm*

Changing of material that has different structural damping *b* (instead of cast steel housing, for example) could be reflected on a change in the amplitude of oscillation as shown in Figure 8. Stainless steel housing with a lower damping in the material will oscillate with higher level of vibration, while the larger damping will effect on higher amplitude of the vibration while maintaining the same natural frequency. This reduction in amplitude of oscillation is especially pronounced at higher frequencies due to increased damping.

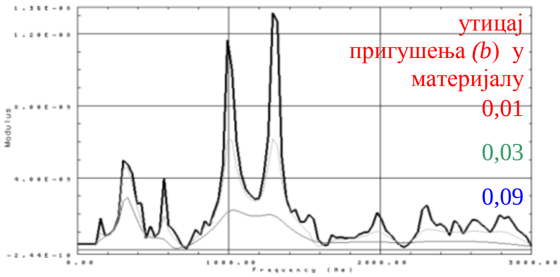

Fig. 8. *Influence of changes in materials (with different factor of damping), b) the frequency response - the basic model without ribs*

3. CONCLUSION

The mechanism of excitation of modal oscillation of some structure which gives answers to many questions that could be classified in the following groups is elaborated.

1. By modal analysis (by applying the FEM) it is can be obtain only possible modal shapes. In reality, conditions for this shapes excitation cannot be fulfilled. Only several out of an extremely large number of modes are usually active.
2. Excitation of the chosen modal shape consists selection of point and direction of force action, selection of frequency of excitation and selection of damping. This mechanism of certain modal shape excitation are elaborated.
3. Changing some of design parameters change the modal responses of the structure. Reducing the thickness of the wall leads to an increase in number of modal oscillations at lower frequencies. This contributes to the generation of tertiary sound waves in low-frequency excitation. Removing of the ribs is reflected in the increase of amplitude of oscillation. In this case frequency is decreased but modal form keep the same form. This increases the sound intensity, which is produced by natural oscillations of housing (sound waves tertiary).

4. ACKNOWLEDGMENT

This work is a contribution to the Ministry of Science and Technological Development of Serbia funded projects TR 035006.

5 REFERENCES

[1] Inoue, K.: *Shape Optimization of Gerabox Housing for Low Vibration*, Proceeding of the International Conference on Power Transmission, Paris, pp. 2053-2064, 1999.

[2] Hubner, C., Predki, W., Jarchow, F.: *Noise Emission of Worm Gears*, Proceedings of the International Conference on Gears- VDI-Berichte N^o 1665, pp. 811-837, 2002.

[3] Liu, W., Lin, T.J., Li, R.F., Du, X.S: *Finite Element Analysis of Dynamic Response and Structure Borne Noise of Gearbox*, Journal of Chongqwing University-English Edition, Vol. 6, N^o 2, pp. 119-124, 2007.

[4] Tanaka, E., Houjoh, H., Mutoh, D., Motoshiromizu, H., Ohno, K., Tanaka, N.: *Vibration and Sound-radiation Analysis for Designing a Low-Noise Gearbox with a Multi-stage Helical Gear System*, JSME International Journal, Series C, Vol. 46, N^o 3, pp. 1178-1185, 2003.

[5] Zhang, T., Kohler, H.K.: *Noise Optimisation of a Double Helical Parallel Shaft Gearbox*, Proceedings of the International Gearing Conference, London, pp. 93-97, 1994.

[6] Kato, M., Inoue, K., Shibata, K.: *Evaluation of Sound Power Radiated by a Gearbox*, Proceedings of the International Gearing Conference, London, pp. 69-74, 1994.

[7] Inoue, K., Townsend, D. P., Coy, J. J.: *Optimum Design of a Gearbox for Low Vibration*, Transaction of the ASME/Journal of Mechanical Design, Vol. 115, pp. 1002-1007, 1993.

[8] Inoue, K., Krantz, T. L.: *Minimization of the Vibration Energy of Thin-Plate Structures and the Application to the Reduction of Gearbox Vibration*, Army Research Laboratory Technical Report ARL-TR-722, 1995.

[9] Inoue, K., Yamanaka, M., Kihara, M.: *Optimum Stiffener Layout for the Reduction of Vibration and noise of Gearbox Housing*, Transaction of the ASME/Journal of Mechanical Design, Vol. 124, pp. 518-523, 2002.

[10] Ćirić Kostić, S., Ognjanović, M.: Excitation of Modal Vibration in Gear Housing Walls, FME Transactions, Vol. 34, No.1, pp. 21-28, 2006.

HEAVY MACHINERY - HM 2011, 69-74
ISBN 978-86-82631-58-3
Paper accepted: 30.05.2011

Optimization of Kinematic Characteristics of Geneva Mechanism

A. Nikolic[1*] - R. Bulatovic[1]
[1]University of Kragujevac, Faculty of Mechanical Engineering Kraljevo, Kraljevo, Serbia

In this paper, the possibility of introducing variable angular velocity of a driving wheel is considered, with the purpose of optimization of kinematical characteristics of Geneva mechanism. The purpose is to reduce the rise that occurs at angular acceleration of Geneva wheel during engagement and disengagement, while angular velocity of the driving wheel remains limited. Kinematical analysis of this mechanism is performed. Expressions for angular velocity and angular acceleration of Geneva wheel are obtained. Optimization of the polynomial parameters of the law of the rotation angle of the driving wheel is performed.

Keywords: Geneva mechanism, optimization, driving wheel, acceleration, kinematical analysis.

0 INTRODUCTION

In designing various machines and devices, the need for implementation of motion with intermittent motion often occurs, where the relation between operating time and time of inaction is a given size. This kind of motion can be implemented by using Geneva mechanism. The basic division of these mechanisms is into mechanisms with external and internal coupling, even though they can also be spherical, where axes of inlet and outlet shaft are passing by perpendicularly**.** Without the loss of generality, we will consider kinematical characteristics of Geneva mechanism with external coupling, which is most frequently considered in scientific papers.

This mechanism is not appropriate for use when angular velocities of the driving wheel are high because then the rise of angular acceleration of Geneva wheel occurs during engagement and disengagement from a coupling with the driving wheel.

Many papers are dedicated to solving this problem. Fenton [2] presented a method based on graphs for calculating the forces and torques acting on various parts of the mechanism. Fenton and Wu [3] calculated the dynamic, static forces and deformations of the Geneva wheel using the finite element method. Fenton et al. [4] transformed the slots of a Geneva wheel to a curved shape and eliminated the non-zero initial and final accelerations. Takanashi [5, 6] analyzed the error of the output motion induced by the manufacturing tolerances and clearances. Cheng C., Yui L., [7] suggested that nonlinear elastic element is introduced between the pin on a driving wheel and slot wall of Geneva wheel, in order to reduce the rise of acceleration that occurs. Sujan ad Meggiolaro [8] modified driving wheel of this mechanism, that is, four-bar linkage was introduced instead, in order to provide an appropriate variable entry by choosing the lengths of the wheels of this mechanism. Lee and Cho used optimal control method to improve kinematic characteristics of Geneva wheel [9]. Heidari et all [1] used the idea of variable input velocity of the mechanism in order to obtain the desired kinematical characteristics of the mechanism. They assumed that the law of rotation angle of the driving wheel could be written in the form of the 7th degree polynomial, so by using genetic algorithm they conducted the optimization of parameters of this polynomial in order to obtain the reduction of the maximum of angular acceleration of Geneva wheel, as well as a jerk that occurs then. However, as far as angular velocity of the driving wheel is concerned, the authors did not introduce limitations.

In this paper, optimization will be conducted, with the purpose of reducing the angular acceleration of Geneva wheel, and the attention will be paid that angular acceleration of the driving wheel is within the corresponding boundaries. The achieved results will be compared to the results obtained in the paper [1].

[*]Corr. Author's Address: Faculty of Mechanical Engineering Kraljevo, Dositejeva 19, Kraljevo, Serbia, aco_nikolic@yahoo.com

1. KINEMATICAL ANALYSIS

Basic elements of Geneva mechanism are driving wheel 1 with pin 2, and slotted wheel 3 which contains z equally spaced radial slots.

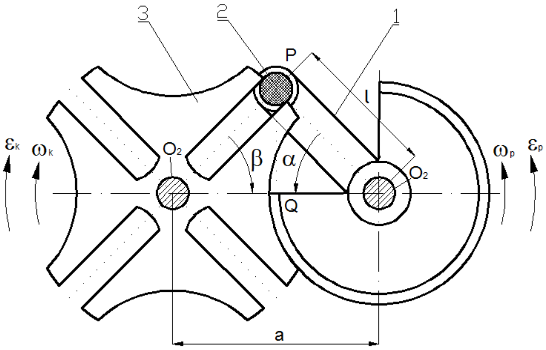

Fig. 1 *Geneva mechanism with four slots*

The number of slots z can be from 3 to 15, but mechanisms with more than 9 slots are seldom used. It is because the length of the driving wheel needs to be small, and a very large torque is required to drive the wheel. Without loss of generality, we are to consider kinematical characteristics of the 4- slot mechanism.

Fig. 1 shows basic geometrical sizes of this mechanism. It can be observed:

$$tg\beta = \frac{\overline{PQ}}{\overline{O_2Q}} = \frac{l\sin\alpha}{a - l\cos\alpha}, \tag{1}$$

that is,

$$\beta = arctg\frac{l\sin\alpha}{a - l\cos\alpha}, \tag{2}$$

Angular velocity of Geneva wheel is:

$$\omega_k = \frac{d\beta}{dt} = \lambda\dot{\alpha}\frac{\cos\alpha - \lambda}{1 + \lambda^2 - 2\lambda\cos\alpha}, \tag{3}$$

where λ is obtained on the basis of condition that at the beginning of coupling a shock does not occur, that is, $\overline{O_1P} \perp \overline{O_2P}$, that is:

$$\lambda = \frac{l}{a} = \frac{l}{l\sqrt{2}} = \frac{\sqrt{2}}{2}, \tag{4}$$

By differentiation of expression (3) according to time, expression for angular acceleration of Geneva wheel is obtained:

$$\varepsilon_k = \ddot{\beta} = \lambda\ddot{\alpha}\frac{\cos\alpha - \lambda}{1 + \lambda^2 - 2\lambda\cos\alpha} - \lambda\dot{\alpha}^2\sin\alpha\frac{1 - \lambda^2}{\left(1 + \lambda^2 - 2\lambda\cos\alpha\right)^2}, \tag{5}$$

Let's define following dimensionless parameters:

$$T = \frac{t}{\tau}, \tag{6}$$

$$A = \frac{\alpha}{\pi/2}, \tag{7}$$

According to the relations (6) and (7), the following applies:

$$\alpha(t) = \frac{\pi}{2}A(T), \tag{8}$$

$$\dot{\alpha}(t) = \frac{\pi}{2\tau}\dot{A}(T), \tag{9}$$

$$\ddot{\alpha}(t) = \frac{\pi}{2\tau^2}\ddot{A}(T), \tag{10}$$

where,

$$\dot{\alpha}(t) = \frac{d\alpha}{dt}, \dot{A}(T) = \frac{dA}{dT},\ t \in [0,\tau],\ \alpha \in [0,\frac{\pi}{2}].$$

Therefore, T vary between 0,1 and *A(T)* between -0,5 and 0,5.

By including relations (8), (9), (10) into expressions (3) and (5), the following is obtained:

$$\Omega_k = \frac{\lambda\pi}{2\tau}\dot{A}\frac{\cos\left(\frac{\pi}{2}A\right) - \lambda}{1 + \lambda^2 - 2\lambda\cos\left(\frac{\pi}{2}A\right)}, \tag{11}$$

$$\mathrm{E}_k = \frac{\lambda\pi}{2\tau^2}\ddot{A}\frac{\cos\left(\frac{\pi}{2}A\right) - \lambda}{1 + \lambda^2 - 2\lambda\cos\left(\frac{\pi}{2}A\right)} - \lambda\left(\frac{\pi}{2\tau}\dot{A}\right)^2\sin\left(\frac{\pi}{2}A\right)\frac{1 - \lambda^2}{\left(1 + \lambda^2 - 2\lambda\cos\left(\frac{\pi}{2}A\right)\right)^2}, \tag{12}$$

From previous expressions it is obvious that angular velocity and angular acceleration of Geneva wheel Ω_k, and E_k, respectively, are hypersensitive to the variation of angular rotation $A(T)$. It can guide us to use input angular displacement to control output characteristics.

.

1.1 Variable angular velocity of the driving wheel

It turned out that introducing of variable angular velocity of the driving wheel is efficient method for improvement of kinematical characteristics of the mechanism. We are to assume that the law of rotation angle of the driving wheel can be written in the form of 7th degree polynomial:

$$A(T) = \sum_{i=0}^{7} a_i T^i , \tag{13}$$

Figure 2 shows angular acceleration and angular speed of Geneva wheel, where $\dot{A} = 1$.

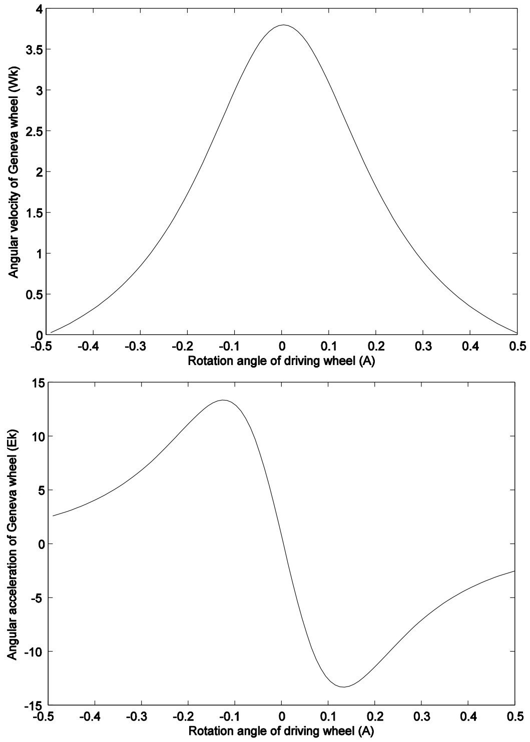

Fig.2 *Angular acceleration and angular velocity of Geneva wheel*

It is obvious that angular acceleration at the beginning and at the end of coupling is not equal to zero, so therefore, the occurrence of the shock is not possible. For that reason, angular acceleration of Geneva wheel needs to be obtained at the beginning of coupling and as low as possible. Aside from that, the equation (13) needs to satisfy the following boundary conditions.

$$A(0) = -0.5, \tag{14}$$

$$A(1) = 0.5, \tag{15}$$

$$\dot{A}(0) = 0, \tag{16}$$

$$\dot{A}(1) = 0, \tag{17}$$

2 OPTIMIZATION

In paper [1], the optimization of engagement polynomial parameter is conducted with the purpose of reducing the chosen acceleration of Geneva wheel. The law of angular change of the driving wheel is obtained in the following form:

$$A(T) = 0.65735T^7 - 1.33785T^6 + 0.19029T^5 + 1.63741T^4 - 0.2992T^3 - 1.4501T^2 + 1.6T - 0.5, \tag{18}$$

The obtained results are presented in the figure 3. The authors obtained reduction of maximum value of angular velocity for 40.5% and angular acceleration for 32.5%.

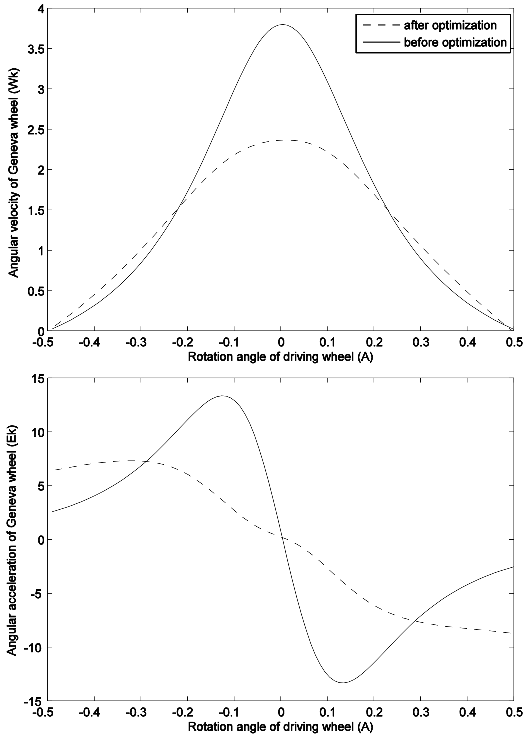

Fig. 3 *Kinematical characteristics of Geneva wheel before and after optimization*

The obtained results are satisfying. The figure 4 shows kinematical characteristics of the driving wheel accomplished after the optimization. It is observed that the driving wheel acceleration reaches the values $E_p(1) = 6.2\,[\,s^{-2}\,]$.

We are to conduct the new optimization procedure with the purpose of accomplishing reduction of angular acceleration $E_k(T)$ with the condition that inlet angular acceleration is $E_p(T) < 5\,[\,s^{-2}\,]$.

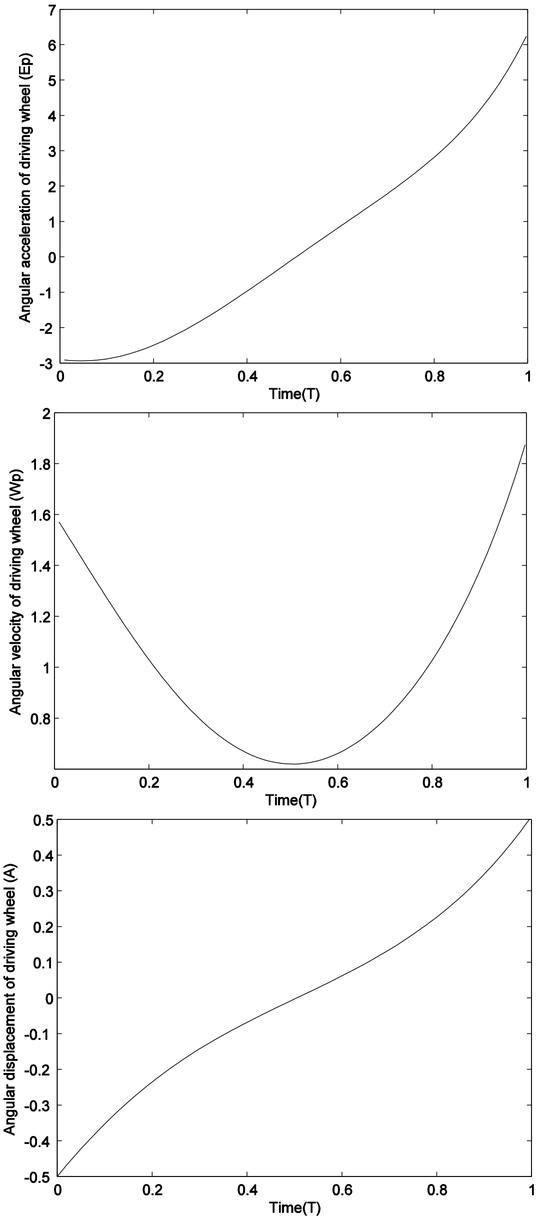

Fig. 4 *Kinematical characteristics of the driving wheel after the optimization*

2.1 Multicriteria optimization

In this paper, optimization is considered by setting up two criterial functions, one representing angular acceleration of Geneva wheel, and the other angular acceleration of the driving wheel. Values of these objective functions should be minimum in order to achieve better kinematical characteristics. Firstly, we are going to determine minimum values of each objective function, and after that, we are to form the final objective function in the form:

$$f = f_1(E_k - E_k^*) + f_2(E_p - E_p^{\,*}), \qquad (19)$$

whereby E_k^* and $E_p^{\,*}$ are desired values of angular acceleration of Geneva wheel and driving wheel, and E_k and E_p are the functions of projective variables that ensue from the equation (13). Constraints are represented in the form of the equations (14), (15), (16) and (17).

In this paper the algorithm of Differential evolution (DE) [11, 12], which gives very efficient solution to the problem, is used during the optimization. Optimization parameters are polynomial coefficients that are used for defining the law of rotation angle of the driving wheel**.** Initial values of upper and lower variable boundaries are represented in Table 1. Likewise,parameters of algorithm are: NP=70 (population size),CR=0.9 (intersection constant), F= 0.6 (mutation constant) and D=7 (the number of projective variables).

i	1	2	3	4	5	6	7
$a_{i\,\min}$	-2	-2	-2	-2	-2	-2	-2
$a_{i\,\max}$	2	2	2	2	2	2	2

Table 1. *Boundary values of polynomial parameters*

After conducted optimization procedure, we are to obtain the law of rotation angle of the driving wheel in the following form:

$$\begin{aligned} A(T) &= 0.733520T^7 - 0.781195T^6 - \\ &0.971799T^5 + 1.875107T^4 - 1.077826T^3 + \\ &0.442468T^2 + 0.699640T - 0.5, \end{aligned} \qquad (20)$$

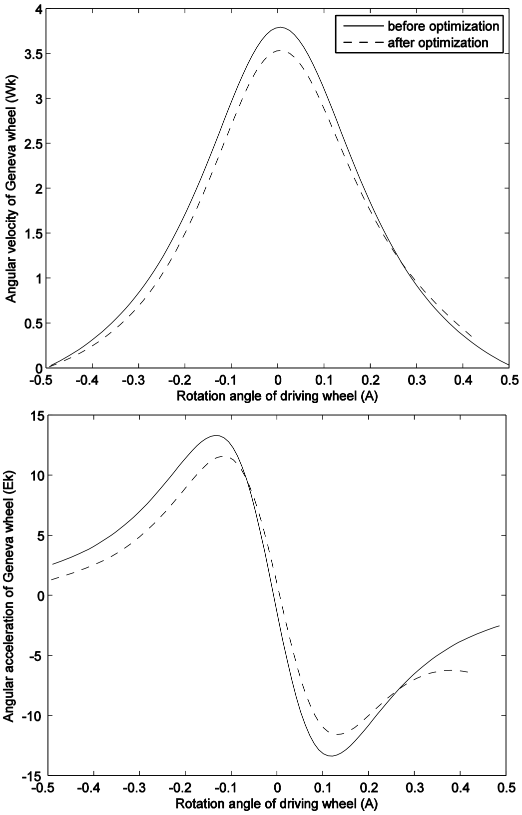

Fig. 5 *Kinematical characteristics of Geneva wheel before and after the optimization*

Fig. 5 represents kinematical characteristics of Geneva wheel, before and after conducted optimization. Maximum value of angular velocity is decreased from $3.8\,[s^{-1}]$ to $3.4\,[s^{-1}]$, that is, for 10.52 %, while maximum value of angular acceleration is decreased from the original $13.25\,[s^{-2}]$ to $11.4\,[s^{-2}]$ for 14%. Besides that, maximum value of angular acceleration of the driving wheel is decreased from previous $6.2\,[s^{-2}]$ to $4.8\,[s^{-2}]$ that is, for 22.6 %.

Fig. 6 represents comparative view of optimization results that are conducted in the paper [1] and in this paper. It is clear that by optimization in the paper [1] lower extreme values of angular velocity and angular acceleration of Geneva wheel are obtained, but the intensity of angular acceleration at the beginning of coupling is three times lower in the case of the second optimization. This fact is very significant, because the shocks at the beginning of coupling are significantly avoided by that. Besides, by using optimization in this paper it is achieved that maximum value of angular acceleration of the driving wheel is lower for $1.4\,[s^{-2}]$, that is ,for 22.6 %.

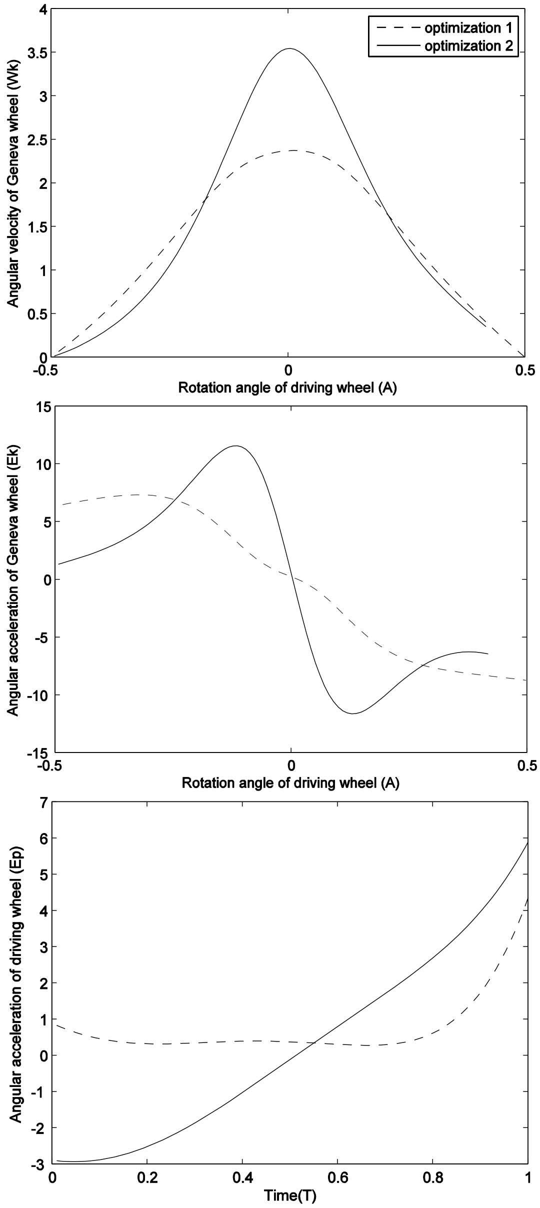

Fig. 6 *The comparison of the optimization results*

3. CONCLUSION

Based on the conducted optimization procedure we can observe that relatively small demands for reduction of maximum value of inlet acceleration (22.6%) maximum values of angular velocity (48%) of Geneva wheel increase when compared to the conducted procedure of optimization in the paper 1. However, given that the initial angular acceleration of Geneva wheel is considerably lower, as well as that we can influence the reduction of maximal values of angular acceleration of the driving wheel, these results are significant when for some reason angular acceleration of the driving wheel needs to be reduced.

4. REFERENCES

[1] M. Heidari, M. Zahiri, and H. Zohoor, "Optimization of Kinematic Characteristic of Geneva Mechanism by Genetic Algorithm", World Academy of Science, Engineering and Technology 44 2008, pp. 387-395.

[2] R. G. Fenton, Machine Design, 37, 177-182 (1965).

[3] R. G. Fenton and Z. Wu, Trans. of CSME 12, 115-118 (1988).

[4] R. G. Fenton, Y. Zhang and "J. Xu, J. Mech. Design 113, 40-45 (1991)

[5] A. Takanashi, B. JSME 16, 1401-1409 (1973).

[6] A. Takanashi, B. JSME 16, 1755-1766 (1973).

[7] Cheng, C.-Y. Lin," Improving dynamic performance of the Geneva mechanism using non-linear spring elements" Mech. Mach. Theory, vol. 30, no. 1, pp. 119-129, 1995.

[8] Vivek A., Marco A., "Dynamic Optimization of Geneva Mechanisms", MA 02139, http://www.scribd.com/doc/54433408/C021-UK00-Dynamic-Optimization-of-Geneva.

[9] J. J. Lee; C. C. Cho, Improving kinematic and structural performance of Geneva mechanism using the optimal control method, Proceedings of the Institution of Mechanical Engineers; 2002; 216, 7; ProQuest Science Journals pg. 761.

[10] R.L. Norton, Design of machinery (An introduction to the synthesis of the mechanism and machines), McGRAW-HILL, third edition, Worcester Polytechnic Institute Worcesete, Massachusetts, 2004.

[11] Storn, K. Price, Differential evolution – a simple and efficient heuristic for global optimization over continuous spaces, Journal of Global Optimization 11 (4) , 341-359, (1997).

[12] K. V. Price, R. M. Storn, J. A. Lampinen, Differential Evolution – A Practical Approach to Global Optimization, Springer-Verlag Berlin Heidelberg, 2005.

HEAVY MACHINERY - HM 2011, 75-80
ISBN 978-86-82631-58-3
Paper accepted: 30.05.2011

Determination of working regime during experimental investigations of rotational machines

Zlatan Šoškić[1] - Snežana Ćirić Kostić[1], Nebojša Bogojević[1] and Asti Radovani[2]
[1] University of Kragujevac, Faculty of Mechanical Engineering Kraljevo, Kraljevo, Serbia
[2] DIEM department of University of Bologna, viale Risorgimento 2, 40126 Bologna, Italia

During many experimental runs rotational machines undergo changes of working regimes, usually passing through sequence of acceleration, stationary run and deceleration. On the other hand, theoretical and numerical models of rotational machines frequently consider rotation speed as constant, so that experimental data can be compared to such models only in stationary regimes. For various reasons, the experimental data contain noise which makes correct identification of working regime a demanding task from the point of view of data processing.

This paper presents a method for determination of working regime of rotational machines based on quantization of experimental data and further algorithm for detection of start and end of certain regime of the machine

Keywords: Data processing, rotational machines, working regime.

1. INTRODUCTION

Research work oriented to analysis of data acquired during experimental runs of rotation machinery is continuous, and is driven by the need for real-time monitoring and detection of faults of machines with rotation motion. An overview of data processing of vibration analysis is shown in [1,2], while standard approach to the problems of diagnostics of rotational machinery with extensive list of references is shown in [3].

Contemporary treatment of the problem is characterized by two approaches to the analysis of vibrations induced by rotation motion of the rotational machinery: the first is characterized with application of the wavelets as modern tool for data processing of non-stationary regimes and cyclostationary regimes [4-9], while the other approach includes application of artificial intelligence methods and neural networks for recognition of working regimes and irregularities arising during the work of rotational machinery [10-13].

Both approaches are characterized by application of mathematical apparatus and software tools that are seldom known to engineers and researchers who are not specialists in the respective fields of data processing and mathematical modelling. This paper presents a simple algorithm that may be used in wide class of practical problems which require application of spectral analysis to vibrations of rotational machines during stationary regime. This class of problems contains testing of machines for purposes of verification of machine design, re-design and maintenance, but also detection of faults arising in stationary regime of the machines.

One of frequent tasks in analysis of stationary regimes of rotational machinery is separation of experimental data that correspond to stationary regime; rotational machines usually have transition regime of acceleration followed by stationary regime, which is ended by transition regime of deceleration, leading to halting of the machine. Being that spectral contents of signals in transition and stationary regimes are different, proper recognition of starting and ending moment of stationary regime is necessary for the intended evaluations of machine characteristics in stationary regime. While average values of measured quantities and their time derivatives are different in stationary and non-stationary regime, which may serve as the initial point for separation of working regimes, the considered task is additionally made difficult by the presence of electronic noise and disturbances caused by electromagnetic induction.

The paper presents an algorithm for recognition of stationary regime on the basis of recorded vibrations. The algorithm is based on analysis of data which are obtained by quantization in time and amplitude of the recorded signal, so that it does not require complex mathematical procedures, and is, therefore, simple and quick for implementation through computer programs. The algorithm is

*Corr. Author's Address: Faculty of Mech. Eng Kraljevo, Dositejeva 19, Kraljevo, Serbia, soskic.z@mfkv.rs

applied to the case of analysis of work of a packing machine, and the results of the algorithm are analyzed.

2. METHODOLOGY

The problem of determination of stationary regime from experimental data is separated into two tasks, and both are solved by application of quantization of the recorded signal.

2.1 Detection of running and halted state

The first task is separation of data recorded in running and halted state of the machine.

Initial idea for separation of running and halted state is to analyze the first derivative of the signal, with the assumption that the first derivative is to be zero without excitation of the system. However, this basic idea has to be corrected for two reasons, both of which are the consequence of presence of electrical noise, even in the cases, when it is relatively small:

- as the first, numerical calculation of derivative is unstable operation with the result that heavily depends on presence of small changes of the signal for which the derivative is calculated; when the real values of the calculated first derivative are small (and in the considered problem they are ideally equal to zero), then the derivative of the recorded signal is practically the derivative of recorded electrical noise, which can have large values; therefore, even the presence of small electrical noise may lead to completely incorrect calculation of the first derivative of the recorded signal;
- as the second, the concept of zero in numerical analysis and data processing is very sensitive; in numerical analysis and data processing, all values below a certain threshold are to be considered as zero; determination of the thresholds depends on the considered system and the analyzed quantities.

Besides the described problems, which are of practical nature, application of the zero values of the first derivative of the signal for determination of zero level has also one conceptual drawback that has to be overcame in any algorithm: the signal may have also numerous points where the first derivative is equal to zero also during the work of the machine; in fact each maximum or minimum of the function is characterized by zero value of the first derivative, and the developed algorithm is to make distinction between zero values of the first derivative during the run of the investigated machine and zero values of the first derivative of the signal recorded while the machine is in rest.

The solution to the problem of the small values of the first derivative of the signal in comparison to the first derivative of the electric noise can be found in quantization of the signal in time and calculation of finite differences instead of differentials, and calculation of a slope instead of the first derivative, by application of the formula:

$$d\left(t\right)=\frac{y\left(t+\tau\right)-y\left(t\right)}{\tau}. \tag{1}$$

where d denotes the calculated slope, y value of the recorded signal, t stands for time, and τ is time interval between the points used for calculation of the slope, further referred as derivation time-step. The value of τ must be carefully chosen to avoid aliasing, which may lead to small or zero values of the first derivative of the signal recorded during the period of run of the machine. To that purpose, τ has to satisfy Nyquist condition $\tau < 1/2f_{max}$, where f_{max} represents the highest frequency existing in the spectra of the vibrations' signal recorded during the work of the machine. The condition puts upper theoretical limit to the selected value of τ, but in practice it can be adopted that

$$\tau=\frac{1}{10\,f_{max}}, \tag{2}$$

where f_{max} can be estimated as the highest frequency of the forced vibration of the system.

Running and halted state of the machine may be distinguished by the difference in overall behavior of the first derivative of the recorded signal during those regimes: during the running regime the measured quantities change, and have generally higher values of the first derivative, while in halted state, those quantities (and the respective signal) remain constant, having low values of the first derivative. In order to emphasize the difference between the working regimes, and to avoid problem of erroneous recognition of the existing zero value derivatives during work of the machine, a moving average of the absolute values of derivatives may be calculated, according to the formula:

$$D(t)=\frac{1}{T}\int_{t-T/2}^{t+T/2}\left|d(\theta)\right|d\theta\,, \tag{3}$$

with T being the duration of the averaging interval. Averaging of the absolute values of the first derivative, instead of the first derivative itself, has the aim to avoid cancellation of positive and negative values of the first derivative, being that the large value of either sign indicates running regime of the machine. The effect of the moving average is basically digital filtering, and while it emphasizes the difference between the first derivatives of signal in running and halted state of the machine, it also blurs the difference in the transition regimes. Generally, the longer the averaging time is, mean values of derivatives in running and halted state differ more, but the transition is softer. Therefore, the averaging duration T has also to be carefully selected to provide distinct and sharp transition. To that goal, T should be smaller than used derivation time-step τ, and value

$$T = \frac{\tau}{2} = \frac{1}{20 f_{max}}, \tag{4}$$

showed good results in research described in this paper.

The dataset $D(t)$, obtained by the described procedure, has emphasized difference between intervals corresponding to running ad halted state, but the transition between those states is still gradual and, due to the presence of electronic noise, not easy to identify. While values of $D(t)$ in running state are generally higher than the values in halted state, they still vary both in the halted and the running state. The distinction between the running and the halted state may be further emphasized by quantization of the amplitude of the averaged derivatives $D(t)$ so that variations within running and halted state are removed. In the process of quantization, a signal is transformed to a series of impulses with discrete amplitudes, similar to what is achieved in process of analog-to-digital conversion. The simplest way to determine discrete amplitude levels is to determine discretization step Δ by division of maximal value of $D(t)$ with selected number of amplitude levels n, and then to calculate equidistant amplitude levels D_m:

$$D_m = m\Delta, \quad \Delta_D = \frac{D_{\max}}{n} \tag{5}$$

Quantization is then performed by assigning to quantized signal the ordinal number m of the largest level D_m that is smaller than the value of $D(t)$, which has mathematical equivalent of integral division of the value of the averaged derivative $D(t)$ by the quantization step Δ_D.

$$q_D(t) = \left\lfloor \frac{D(t)}{\Delta_D} \right\rfloor. \tag{6}$$

Quantization step should be determined to be larger than the variation of derivative in running and halted state, but smaller than the difference between average values of $D(t)$ in those states. Unfortunately, this condition cannot be always fulfilled because of strong electric glitches that sometimes arise during halted state, and it is usually enough to have 4-6 separate levels for quantization of the signal.

Ideally, quantized signal $q_D(t)$ should have a plateau of maximal value, indicating running state, with large plateaus of minimal value on both sides, indicating halted state, and transitional zones of medium values between them. Therefore, recognition of working regimes according to the valued of the quantized signals should be easy and straightforward. However, electric noise causes the appearance of high values of quantized signal during halted state and oscillatory behavior of quantized signal in transitional zones, so that the procedure for recognition of working regimes should be refined, and the following rule is recommended here:

- the starting point of running state of machine is the last moment when quantized signal of averaged absolute derivative changes the value from zero to one before it reaches maximal value;
- the ending point of running state of machine is the last moment when quantized signal of averaged absolute derivative starts continually decreasing the value from maximum, before reaching zero value.

2.2 Detection of transitional and stationary regimes

The second task that should be performed in course of proper detection of stationary regime is separation of transitional and stationary regime from the data describing running state. The idea that is presented here is applicable to rather wide class of cases when centrifugal force affects signal. In such cases, mean value of the measured quantities is proportional to centrifugal force, and is hence constant during stationary regime and changes during transitional regime.

The task is made difficult by the fact that both during transitional and stationary state exists vibrations and fluctuations of the measured quantities that affect the recorded signal, and hence separation of the contribution of centrifugal force cannot be assessed without data processing. The idea of separation of the contribution of centrifugal force is based on the fact that all other influences to the recorded signal also have constant mean values during stationary regime, according to the definition of stationary regime. Therefore, determination of moving average of the recorded signal is the first step towards separation of stationary and transitional regimes. The moving average is calculated according to the formula

$$Y(t)=\frac{1}{T}\int_{t-T/2}^{t+T/2} y(\theta)\,d\theta\,, \tag{7}$$

where averaging time T should be determined to remove the effects of vibrations and fluctuations, but to preserve character of transitional regime. On the basis of the fact that rotation of the machine is the source of recorded vibrations and fluctuations, it can be adopted that averaging time T is equal to period of rotation of the machine.

The averaged data should have shape of a wide plateau, corresponding to the stationary regime, with slopes corresponding to the transitional regimes on both sides of the plateau. In order to make recognition of the shape easier, the averaged signal $Y(t)$ should be quantized in a manner similar to the quantization described in the algorithm for separation of halted state, creating quantized averaged signal:

$$q_Y(t)=\left[\frac{Y(t)}{\Delta_y}\right]. \tag{6}$$

Quantization removes variation within averaged signal and makes plateau easily detectable. However, successful distinction between stationary and transitional regime by quantization of amplitude is possible only if mean values of the signal are considerably different in transitional and stationary regime, which is usually caused by action of centrifugal force in rotating machinery.

Even if the signal has proper shape, with the described plateau, variations of the signal within stationary regime and the presence of electric noise cause oscillatory behavior of quantized signal, both in stationary and transitional regime. Therefore, the starting and ending moment of stationary regime are to be carefully selected, and the following rule is recommended here:

- the starting moment of stationary regime is the first moment when quantized averaged signal reaches maximal value;
- the ending moment of stationary regime is the last moment when quantized averaged signal has maximal value.

3. EXPERIMENT

The research presented in this paper was motivated by investigations carried out by University of Bologna in order to reduce vibrations of a packing machine. The machine has a coil with the wrapping foil mounted on a horizontal ring that performs rotation in horizontal plane. The ring is supported by horizontal frame to which it is connected by six wheels that enable the rotation of the ring. In exploitation conditions, customers observed vibrations of the frame around a horizontal axis.

Among other experimental and numerical studies, measurements of strains arising in selected points of the rotating ring and the supporting frame were performed. Ten experimental pointes were selected, five of them at the ring and five at the frame. Four of the points at the ring were placed at bottom horizontal surface (referred as points A1 to A4), and the remaining point (referred as B1) was at inner surface of the ring. Points at the frame are referred as C1-C5. Locations of the points are presented in Fig.1.

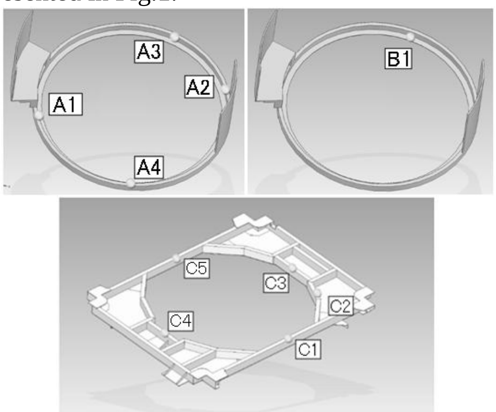

Fig.1: Location of measurement points at the rotating ring and the supporting frame

The measurements were performed by strain gauges sealed at the selected points of the structure and powered by two commercial devices that contained voltage supply, amplifier, D/A converter and wireless transmission unit as main parts. The transmitted data were acquired by a remote receiver connected to a personal computer that was used for data recording. Data acquisition frequency was 100 Hz, and the machine was tested in working regimes when the rotation of the ring had speed of 40, 64, 72 and 80 rpm, corresponding to the 50%, 80%, 90% and 100% of nominal working speed. In total, fifty experimental runs were carried out in different exploitation conditions that included variation of rotation speed, mass of the wrapping coil and pre-stretching force acting upon wrapping foil.

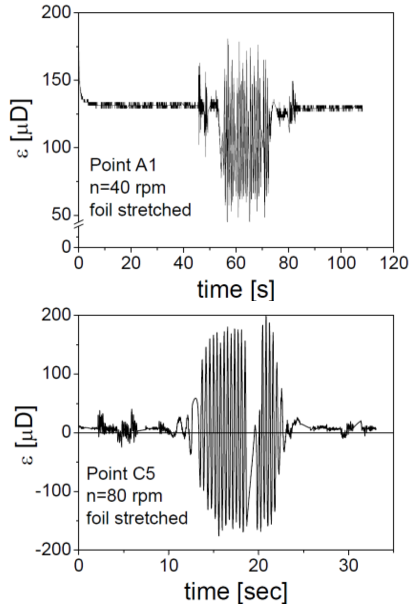

Fig.2: Diagrams of measured strains in points at the rotating ring and the supporting frame

In order to perform spectral analysis of the recorded strains, it was necessary to separate the data describing stationary regime. The procedure [14] and results [15] of the spectral analysis are described elsewhere, and here will be presented just the results of application of the described algorithm for detection of stationary regime. According to the previously described measurement points, it follows that strains in points A and B, located at rotating ring, are sensitive to centrifugal forces and suitable for detection of stationary regime, while strains in points C are not suitable for such detection, because the centrifugal forces resulting from the rotation of the ring are not transferred to the frame in points C. Besides, it can be expected that with increase of rotation speed, detection of stationary regime by the proposed algorithm becomes easier.

A typical diagrams of the strains measured in points A and C are shown in Fig.2. While both diagrams show intensive difference between running and halted state, a noticeable difference between changes of mean values in running and halted state may be observed: mean value of strain in point A decreases around 50 μD after start of the rotation, while mean value of the strain in point C5 does not differ at all in running and halted state. It is interesting to see how the proposed algorithm recognizes the shapes of the diagrams.

4. ANALYSIS

The application of the proposed algorithm detected the running state in all of 50 experimental runs. Manual check confirmed the obtained results also in all the cases. Due to the fact that in all runs were measured two strains simultaneously, it was possible to check the estimations of running and halted state obtained by analysis of the both strains in each of experimental runs. Application of the algorithm for detection of running regime to statistically relevant set of 24 simultaneous measurements of strains showed that the maximal difference between durations of detected running regimes was 2,8%, but mean values of the difference was just 0,87% with standard deviation of 0,77% and estimation error of 0,16%. The analysis shows that the proposed algorithm for detection of running and halted state on the basis of quantization of derivative of the signal is, in spite of its simplicity, highly reliable.

On the other hand, the algorithm for detection of stationary state of the machine was applicable only to 22 experimental runs, and for the sake of the fact that one of the strain measurements was always performed on the frame, there was no possibility for comparison of reliability of detection of stationary regime. However, the analysis of the obtained results showed that the proposed algorithm detected stationary regime only in the case of the highest rotation speed of 80 rpm. On the other hand, it was also not possible to clearly visually detect the stationary regime in detected data. Therefore, application of other techniques for the purpose of the recognition of stationary regime is recommended.

5. CONCLUSION

The paper presents algorithms for detection of halted and running state, and separation of transitional and stationary regime during work of rotational machines. The algorithms are based on quantization of averaged derivative of the signal and averaged signal, respectively, so they have common simple principle in their background.

However, the results of analysis of their application to the case of analysis of vibrations of a packing machine are strikingly different. The algorithm for detection of halted and running state has wide applicability and is highly reliable. The algorithm for separation of transitional and stationary regime, on the other hand, is applicable only to the case of strong centrifugal forces, and is, therefore, very limited in practice.

6. ACKNOWLEDGEMENT

The authors wish to express their gratitude to Serbian Ministry of Science and Technology for support through project TR37020 and Laboratory of DIEM department of University of Bologna for provision of the experimental data.

7. REFERENCES

[1] V. Wowk, "Machinery Vibration: Measurement and Analysis", McGraw-Hill (1991)

[2] M.Norton and D.Karczub, "Fundamentals of Noise and Vibration Analysis", Cambridge University Press (2003)

[3] S. Edwards, A.W. Lees and M.I. Friswell, "Fault Diagnosis of Rotational machinery", The Shock and Vibration Digest, 30, 4-13, (1998)

[4] S.K . Goumas, M.E. Zervakis, G.S. Stavrakakis, "Classification of washing machines vibration signals using discrete wavelet analysis for feature extraction", IEEE Transactions on Instrumentation and Measurement, 51, 497 – 508 (2002)

[5] Gary Brent McHale, Jr. “Fast, real-time monitoring of rotational machines”, MSc thesis, Texas Tech University, 2003

[6] J. Antoni, F. Bonnardotb, A. Raada and M. El Badaouib, "Cyclostationary modelling of rotational machine vibration signals", Mechanical Systems and Signal Processing, 18, 1285-1314 (2004)

[7] Benjamin B. Wagner, “Rotating Equipment Defect Detection Using the Algorithm of Mode Isolation”, PhD thesis, Georgia Institute of Technology, 2007

[8] Q. Hua, Z. Hea, Z. Zhanga and Y. Zia, "Fault diagnosis of rotational machinery based on improved wavelet package transform and SVMs ensemble", Mechanical Systems and Signal Processing, 21, 688-705 (2007)

[9] Gianluca D'Elia, "Fault detection in rotational machines by vibration signal processing techniques", PhD thesis, DIEM department of University of Bologna, academic year 2007/2008

[10] Y. Zhan, V. Makis and A.K.S. Jardine, "Adaptive model for vibration monitoring of rotational machinery subject to random deterioration", Journal of Quality in Maintenance Engineering, 9, 351-375 (2003)

[11] C. Chen and C. Mob, "A method for intelligent fault diagnosis of rotational machinery", Digital Signal Processing, 14, 203-217 (2004)

[12] Y. Leia, Z. Hea, and Y. Zia, "A new approach to intelligent fault diagnosis of rotational machinery", Expert Systems with Applications, 35, 1593-1600 (2008)

[13] C. He, C. Liu, Y. Li and J. Yuan, "Intelligent fault diagnosis of rotational machinery based on multiple relevance vector machines with variance radial basis function kernel", Proceedings of the Institution of Mechanical Engineers, Part C: Journal of Mechanical Engineering Science, 225, DOI: 10.1177/0954406211400526 (2011)

[14] Zlatan Šoškić, Zoran Petrović, Branko Radičević and Snežana Ćirić Kostić, "Spectral Analysis of Machine Vibrations in Conditions of Heavy Data Transmission Losses", Proceedings of XI Symposium "Acoustics and Vibration of Mechanical Structures AMVS 2011", 26th May 2011, Timisoara (Romania) p.55-62

[15] Giangiacomo Minak, Zlatan Šoškić, Snežana Ćirić Kostić, Cristiano Fragassa, "Analysis of an Automatic Wrapping Machine: Numerical Models and Experimental Results", Proceedings of The 7th International Scientific Conference "Research and Development of Mechanical Elements and Systems", 27th&28th of April 2011, Zlatibor, (Serbia) p.69-76

HEAVY MACHINERY - HM 2011, 81-84
ISBN 978-86-82631-58-3
Paper accepted: 20.05.2011

Distribution of Bending Moments on the Plates of Carrier with Trapezoidal Cross Section

Mirko Đelošević[1,*] - Vladeta Gajić[2], Dragan Petrović[1], Milan Bižić[1]
[1] Faculty of Mechanical Engineering Kraljevo, University of Kragujevac
[2] Faculty of Technical Sciences Novi Sad, University of Novi Sad

This paper presents analysis of carrying capacity of the elements of cross-section (plates) with trapezoidal shape in carriers of box type. According to the model of linear character, some exact equations are formed. These equations are used for determination of moments that are transferred by flanges and webs of box carrier of trapezoidal cross-section. The criteria for application of the simplified expressions depending on the slenderness of the plate and the required accuracy of calculation are defined. This identification enabled the exact definition of plane compressive forces in order to analyze the buckling of plate carriers. Application of the results of this paper is a contribution to the process of optimal design of supporting structures, especially those that are used for construction of transport equipment, where the effect of reducing the weight affects on the efficiency of transport in supply chains.

Keywords: bending moment, plate, carrier, trapezoidal cross section

0 INTRODUCTION

Design of supporting structures is carried out through several phases, including a special procedure that is used to define the shape and dimensions based on the analysis of stress state, for whose definition it is necessary to identify the value of attack load. Carriers of steel structures are usually designed as thin-walled open profiles or box profiles (Fig.1,2) which are formed of plate elements and they are predominantly exposed to bending moments. In this paper, the analysis is limited to the linear distribution of normal stresses and bending moments (Fig. 3). The aim of this paper is primarily to correct expressions for the distribution of moments of attack (M_{P1}, M_{P2}, M_r) at the plate carrier of complex cross section (such as a trapezoidal), and then to point to the expediency of application of simplified expression, in certain cases.

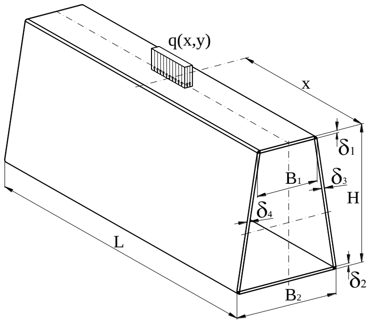

Fig. 1. *Nosač trapeznog poprečnog preseka*

Recent studies have paid special attention to the importance of box girder with a trapezoidal cross-section [1-3]. Researchers [1] have pinpointed that trapezoidal cross section has much more favourable stress state for the same requirements of global capacity and slender vertical plate, in comparison to the traditional rectangular shape (Fig. 2). Research [2] refers to the optimization of trapezoidal cross section in terms of global capacity indicating the usefulness of practical application. Trapezoidal shapes for carriers are particularly important to reduce the effect of local stress [1, 3].

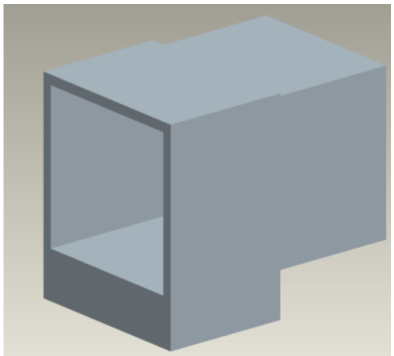

Fig. 2. *Segment carrier of boom track crane*

1 PROBLEM ANALYSIS

The total carrying capacity of any box beam corresponds to the sum capacity of its segments

*Corr. Author's Address: Faculty of Mechanical Engineering Kraljevo, Dositejeva 19, Kraljevo,Serbia, djelosevic.m@mfkv.kg.ac.rs

or plates (flanges and ribs). Under the influence of external loads, each segment of the cross section is subjected to the appropriate load according to their rigidity and resistance to deformation.

In order to make equations for attack sizes, it is necessary to know the following sizes:

$$\frac{N_r(y=H_{C1})}{H_{C1}}=\frac{N_r(y)}{y}\text{ , for } y>0 \tag{1}$$

$$N_r(y)=\frac{N_r(y=H_{C1})}{H_{C1}}\cdot y \tag{2}$$

That is:

$$\frac{N_r(y=H_{C2})}{H_{C2}}=\frac{N_r(y)}{y}\text{ , for } y<0 \tag{3}$$

$$N_r(y)=\frac{N_r(y=H_{C2})}{H_{C2}}\cdot y \tag{4}$$

Taking this into consideration:

$$\frac{N_r(y=H_{C1})}{H_{C1}}=-\frac{N_r(y=H_{C2})}{H_{C2}} \tag{5}$$

We get:

$$N_r(y=H_{C2})=-\frac{H_{C2}}{H_{C1}}\cdot N_r(y=H_{C1}) \tag{6}$$

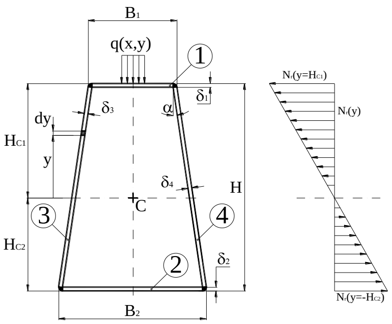

Fig. 3. *Distribution of force $N_r(y)$*

$N_r(y)$ - force per unit area, the function of "y"

H_{C1} - Distance between the centre of gravity C and the flange "1"

H_{C2} - Distance between the centre of gravity C and the flange "1

q(x,y) - arbitrary continuous load

2 MATHEMATICAL FORMULATIONS

The mathematical model is related to the bending moments of linear distribution. Areas of materials away from the neutral axis convey intense moments. Maximum acceptance of moments is achieved through flanges, while the remaining difference from the total moment is taken by web beams.

Moment of flange "1" (M_{p1}) is:

$$\begin{aligned}M_{p1}&=\int_{H_{C1}-\delta_1}^{H_{C1}}N_r(y)\cdot(B_1dy)\cdot y=\int_{H_{C1}-\delta_1}^{H_{C1}}\frac{N_r(y=H_{C1})}{H_{C1}}\cdot B_1\cdot y^2\cdot dy\\ M_{p1}&=\frac{N_r(y=H_{C1})}{H_{C1}}\cdot B_1H_{C1}^2\delta_1\cdot\left(1-\frac{\delta_1}{H_{C1}}+\frac{\delta_1^2}{3H_{C1}^2}\right)\end{aligned} \tag{7}$$

where:

B_1 - flange width "1"

δ_1 - flange thickness "1"

Moment of flange "2" (M_{p2}) is:

$$\begin{aligned}M_{p2}&=\int_{-(H_{C2}-\delta_2)}^{-H_{C2}}N_r(y)\cdot(B_2dy)\cdot y=\int_{-(H_{C1}-\delta_1)}^{-H_{C1}}\frac{N_r(y=-H_{C2})}{H_{C2}}\cdot B_2\cdot y^2\cdot dy\\ M_{p2}&=\frac{N_r(y=H_{C1})}{H_{C1}}\cdot B_2H_{C2}^2\delta_2\cdot\left(1-\frac{\delta_2}{H_{C2}}+\frac{\delta_2^2}{3H_{C2}^2}\right)\end{aligned} \tag{8}$$

where:

B_2 - flange width "2"

δ_2 - flange thickness "2"

Resulting flange moment (M_p) is:

$$M_p = M_{p1} + M_{p2} \tag{9}$$

By replacing (7) and (8) into (9), we get:

$$M_p=\frac{N_r(y=H_{C1})}{H_{C1}}\cdot\left[\begin{aligned}&B_1H_{C1}^2\delta_1\cdot\left(1-\frac{\delta_1}{H_{C1}}+\frac{\delta_1^2}{3H_{C1}^2}\right)+\\ &+B_2H_{C2}^2\delta_2\cdot\left(1-\frac{\delta_2}{H_{C2}}+\frac{\delta_2^2}{3H_{C2}^2}\right)\end{aligned}\right] \tag{10}$$

Web moment above the heavy axis (M_{r1}) is:

$$\begin{aligned}M_{r1}&=2\int_0^{H_{C1}-\delta_1}N_r(y)\cdot\left(\frac{\delta_3}{\cos\alpha}dy\right)\cdot y=2\int_0^{H_{C1}-\delta_1}\frac{N_r(y=H_{C1})}{H_{C1}}\cdot\frac{\delta_3}{\cos\alpha}\cdot y^2\cdot dy\\ M_{r1}&=\frac{2}{3}\cdot\frac{N_r(y=H_{C1})}{H_{C1}}\cdot\frac{\delta_3}{\cos\alpha}\cdot H_{C1}^3\cdot\left(1-3\frac{\delta_1}{H_{C1}}+3\frac{\delta_1^2}{H_{C1}^2}-\frac{\delta_1^3}{H_{C1}^3}\right)\end{aligned} \tag{11}$$

where:

δ_3 - web thickness "3"

α - web slope angle "3" and "4" to the vertical axis

Moment of web under the heavy axis (M_{r2}) is:

$$\begin{aligned}M_{r2}&=2\int_0^{-(H_{C2}-\delta_2)}N_r(y)\cdot\left(\frac{\delta_4}{\cos\alpha}dy\right)\cdot y=2\int_0^{-(H_{C2}-\delta_2)}\frac{N_r(y=-H_{C2})}{H_{C2}}\cdot\frac{\delta_4}{\cos\alpha}\cdot y^2\cdot dy\\ M_{r2}&=\frac{2}{3}\cdot\frac{N_r(y=H_{C1})}{H_{C1}}\cdot\frac{\delta_4}{\cos\alpha}\cdot H_{C2}^3\cdot\left(1-3\frac{\delta_2}{H_{C2}}+3\frac{\delta_2^2}{H_{C2}^2}-\frac{\delta_2^3}{H_{C2}^3}\right)\end{aligned} \tag{12}$$

where:

δ_4 - web thickness "4"

Resulting moment of web (M_r) is:

$$M_r = M_{r1} + M_{r2} \tag{13}$$

$$M_r=\frac{2}{3}\cdot\frac{N_r(y=H_{C1})}{H_{C1}}\cdot\left[\frac{\delta_3}{\cos\alpha}H_{C1}^3\left(1-3\frac{\delta_1}{H_{C1}}+3\frac{\delta_1^2}{H_{C1}^2}-\frac{\delta_1^3}{H_{C1}^3}\right)+\frac{\delta_4}{\cos\alpha}H_{C2}^3\left(1-3\frac{\delta_2}{H_{C2}}+3\frac{\delta_2^2}{H_{C2}^2}-\frac{\delta_2^3}{H_{C2}^3}\right)\right] \quad (14)$$

The resulting moment (M_{uk}), which carries the observed carrier under the influence of the external moment (M) is:

$$M_{uk} = M_p + M_r \quad (15)$$

Resulting internal load corresponds to the external load, so:

$$M_{uk} = M \quad (16)$$

From the previous expression the force per unit area is defined (N_r) for $y = H_{C1}$.

$$N_r(y=H_{C1})=\frac{H_{C1}}{B_1H_{C1}^2\delta_1\left(1-\frac{\delta_1}{H_{C1}}+\frac{\delta_1^2}{3H_{C1}^2}\right)+B_2H_{C2}^2\delta_2\left(1-\frac{\delta_2}{H_{C2}}+\frac{\delta_2^2}{3H_{C2}^2}\right)+\frac{2}{3}\left[\frac{\delta_3}{\cos\alpha}H_{C1}^3\left(1-3\frac{\delta_1}{H_{C1}}+3\frac{\delta_1^2}{H_{C1}^2}-\frac{\delta_1^3}{H_{C1}^3}\right)+\frac{\delta_4}{\cos\alpha}H_{C2}^3\left(1-3\frac{\delta_2}{H_{C2}}+3\frac{\delta_2^2}{H_{C2}^2}-\frac{\delta_2^3}{H_{C2}^3}\right)\right]}\cdot M \quad (17)$$

The moment of upper flange (M_{p1}) is defined according to the equation:

$$M_{p1}=\frac{B_1H_{C1}^2\delta_1\cdot\left(1-\frac{\delta_1}{H_{C1}}+\frac{\delta_1^2}{3H_{C1}^2}\right)}{B_1H_{C1}^2\delta_1\cdot\left(1-\frac{\delta_1}{H_{C1}}+\frac{\delta_1^2}{3H_{C1}^2}\right)+B_2H_{C2}^2\delta_2\cdot\left(1-\frac{\delta_2}{H_{C2}}+\frac{\delta_2^2}{3H_{C2}^2}\right)+\frac{2}{3}\cdot\left[\frac{\delta_3}{\cos\alpha}H_{C1}^3\left(1-3\frac{\delta_1}{H_{C1}}+3\frac{\delta_1^2}{H_{C1}^2}-\frac{\delta_1^3}{H_{C1}^3}\right)+\frac{\delta_4}{\cos\alpha}H_{C2}^3\left(1-3\frac{\delta_2}{H_{C2}}+3\frac{\delta_2^2}{H_{C2}^2}-\frac{\delta_2^3}{H_{C2}^3}\right)\right]}\cdot M \quad (18)$$

The moment of upper flange (M_{p2}) is defined according to the equation:

$$M_{p2}=\frac{B_2H_{C2}^2\delta_2\cdot\left(1-\frac{\delta_2}{H_{C2}}+\frac{\delta_2^2}{3H_{C2}^2}\right)}{B_1H_{C1}^2\delta_1\cdot\left(1-\frac{\delta_1}{H_{C1}}+\frac{\delta_1^2}{3H_{C1}^2}\right)+B_2H_{C2}^2\delta_2\cdot\left(1-\frac{\delta_2}{H_{C2}}+\frac{\delta_2^2}{3H_{C2}^2}\right)+\frac{2}{3}\cdot\left[\frac{\delta_3}{\cos\alpha}H_{C1}^3\left(1-3\frac{\delta_1}{H_{C1}}+3\frac{\delta_1^2}{H_{C1}^2}-\frac{\delta_1^3}{H_{C1}^3}\right)+\frac{\delta_4}{\cos\alpha}H_{C2}^3\left(1-3\frac{\delta_2}{H_{C2}}+3\frac{\delta_2^2}{H_{C2}^2}-\frac{\delta_2^3}{H_{C2}^3}\right)\right]}\cdot M \quad (19)$$

Web moment (M_r) is defined according to the equation:

$$M_r=\frac{\frac{2}{3}\cdot\left[\frac{\delta_3}{\cos\alpha}H_{C1}^3\left(1-3\frac{\delta_1}{H_{C1}}+3\frac{\delta_1^2}{H_{C1}^2}-\frac{\delta_1^3}{H_{C1}^3}\right)+\frac{\delta_4}{\cos\alpha}H_{C2}^3\left(1-3\frac{\delta_2}{H_{C2}}+3\frac{\delta_2^2}{H_{C2}^2}-\frac{\delta_2^3}{H_{C2}^3}\right)\right]}{B_1H_{C1}^2\delta_1\cdot\left(1-\frac{\delta_1}{H_{C1}}+\frac{\delta_1^2}{3H_{C1}^2}\right)+B_2H_{C2}^2\delta_2\cdot\left(1-\frac{\delta_2}{H_{C2}}+\frac{\delta_2^2}{3H_{C2}^2}\right)+\frac{2}{3}\cdot\left[\frac{\delta_3}{\cos\alpha}H_{C1}^3\left(1-3\frac{\delta_1}{H_{C1}}+3\frac{\delta_1^2}{H_{C1}^2}-\frac{\delta_1^3}{H_{C1}^3}\right)+\frac{\delta_4}{\cos\alpha}H_{C2}^3\left(1-3\frac{\delta_2}{H_{C2}}+3\frac{\delta_2^2}{H_{C2}^2}-\frac{\delta_2^3}{H_{C2}^3}\right)\right]}\cdot M \quad (20)$$

Distributions of moments of attack for monotonous load (M=1) are given on the following diagrams ($x=\delta_1/H_{C1}$; $y=\delta_2/H_{C2}$):

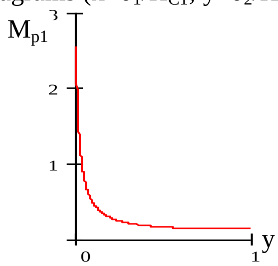

Fig.4. Diagram of flange moment distribution *(M_{p1})*

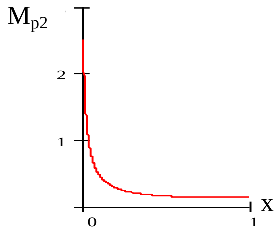

Fig.5. Diagram of flange moment distribution *(M_{p2})*

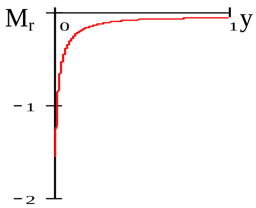

Fig.6. Diagram of web moment distribution *(M_r)*

Diagrams on the fig.2, fig.3 and fig. 4 show that the increase of relation δ_1/H_{C1} and δ_2/H_{C2} results in decrease of moment that is transferred by the flanges, whereas the difference is taken over by the webs of the carrier.

Expressions (17-20) can be simplified if the values $x=(\delta_1/H_{C1})$ and $y=(\delta_2/H_{C2})$ are small sizes in relation to other members in the abovementioned equations. Then these expressions get more simplified form that is suitable for practical application, so we have:

Force per unit areas (N_r) for $y = H_{C1}$.

$$N_r(y=H_{C1})\approx\frac{H_{C1}}{B_1H_{C1}^2\delta_1+B_2H_{C2}^2\delta_2+\frac{2}{3}\cdot\left[\frac{\delta_3}{\cos\alpha}H_{C1}^3+\frac{\delta_4}{\cos\alpha}H_{C2}^3\right]}\cdot M \quad (21)$$

Moment of upper flange (M_{p1}) is determined according to the equation:

$$M_{p1} \approx \frac{B_1 H_{C1}^2 \delta_1}{B_1 H_{C1}^2 \delta_1 + B_2 H_{C2}^2 \delta_2 + \frac{2}{3} \cdot \left[\frac{\delta_3}{\cos\alpha} H_{C1}^3 + \frac{\delta_4}{\cos\alpha} H_{C2}^3 \right]} \cdot M \qquad (22)$$

Moment of the lover flange (M_{p2}) is determined according to the equation:

$$M_{p2} \approx \frac{B_2 H_{C2}^2 \delta_2}{B_1 H_{C1}^2 \delta_1 + B_2 H_{C2}^2 \delta_2 + \frac{2}{3} \cdot \left[\frac{\delta_3}{\cos\alpha} H_{C1}^3 + \frac{\delta_4}{\cos\alpha} H_{C2}^3 \right]} \cdot M \qquad (23)$$

Web moment (M_r) is determined according to the equation:

$$M_r \approx \frac{\frac{2}{3} \cdot \left[\frac{\delta_3}{\cos\alpha} H_{C1}^3 + \frac{\delta_4}{\cos\alpha} H_{C2}^3 \right]}{B_1 H_{C1}^2 \delta_1 + B_2 H_{C2}^2 \delta_2 + \frac{2}{3} \cdot \left[\frac{\delta_3}{\cos\alpha} H_{C1}^3 + \frac{\delta_4}{\cos\alpha} H_{C2}^3 \right]} \cdot M \qquad (24)$$

In some special cases, when we have the box carries with rectangular cross section, we get:

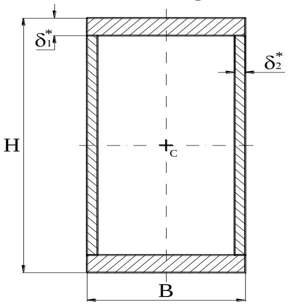

$H_{C1} = H_{C2} = H/2$
$B_1 = B_2 = B$
$\delta_1 = \delta_2 = \delta_1^*$
$\delta_3 = \delta_4 = \delta_2^*$
$\alpha_3 = \alpha_4 = 0$

Fig. 7. Rectangular cross section of carrier

Force per unit area N_r for y=H/2 is:

$$N_r(y = \frac{H}{2}) = \frac{1}{B_1 H \delta_1^* + \frac{1}{3} H^2 \delta_2^*} \cdot M \qquad (25)$$

Web moment (M_r) is:

$$M_r = \frac{2 \cdot \frac{\delta_2^* H^3}{12}}{\frac{B H^2 \delta_1^*}{2} + 2 \cdot \frac{\delta_2^* H^3}{12}} \cdot M = \frac{I_r}{I_p + I_r} \cdot M \qquad (26)$$

where:

I_r - axial moment of inertia of the web
I_p - axial moment of flange
I - axial moment of inertia of the whole carrier

$I = I_r + I_p$ (27)

Moment of carrying flanges:

$M_p = M – M_r$ (28)

3 CONCLUDING REMARKS

The criterion for the application of equations (17-20) depends on the required accuracy of calculation and it is in the function of the cross sectional geometry, i.e. Of the sizes δ_1/H_{C1} or δ_2/H_{C2}. For the classical calculation, tolerated error in the moment of attack must be less than 10%, which corresponds to the size δ_1/H_{C1} (δ_2/H_{C2}) < 0,05. Analysis of the distribution of bending moments based on the linear distribution can be used for materials with approximately linear characteristic in the domain of elastic behaviour. Conducted on the basis of identification, we are able to carry deformational stress calculations, the global and local stability of the carrier [4], complex structures, using the attack load (moment) of the exact values that correspond to the real ones. Analysis of an exact determination of moments of attack on the carrying elements is particularly important in structures subjected to high loads (bridges, truck crane, etc.) with a very strong effect of buckling plate. A further aspect of the application of this analysis is reflected in the rationalization of weight of carrying elements of the transport equipment, applied especially to serve in distribution supply chains. Given the fact that in warehouse centers a working process is characterized with a large number of cycles, reduction of mass of the transport equipment without reduction of carrying capacity, significantly effect on the reduction of energy costs, and therefore on the total costs of the distribution process.

4 REFERENCES

[1] M. Đelošević, M. Gašić, M.Savković, D. Petrović, M. Bižić (2011): *Analysis of the Influence of Local Stress on the Carrying Capacity of Box Beams*, 7th International conference research and development of mechanical elements and systems, 26-28.04.2011, Zlatibor, pp. 279-284.

[2] Savković, M., Gašić, M. (2001): *Optimization of geometry of trapezoidal cross section of boom of truck crane*, IMK-14 Research and development, vol.7, No.1-2, pp 7-11 (In Serbian).

[3] Savković, M. Gašič, M., Petrović, R., Čupović, M. (2007): *Stress analysis of interactive contact between the telescopic boom segments in auto cranes*, IMK-14 Research and development, vol.13, No. 1-2, pp 17-22 (In Serbian).

[4] Savković, M. (2003): *Contribution to modelling of boom truck crane*, IMK-14 Research and development, vol.9, No. 1-2, pp 123-128 (In Serbian).

HEAVY MACHINERY - HM 2011, 85-89
ISBN 978-86-82631-58-3
Paper accepted: 30.05.2011

Modeling of flexible planar structures by a system of rigid bodies

Slaviša Šalinić[1,*]
[1] University of Kragujevac, Faculty of Mechanical Engineering Kraljevo

In this paper a uniform Euler-Bernoulli beam is approximated by a system of rigid bodies. The rigid bodies are connected by passive revolute and prismatic joints with corresponding springs in them. Elastic properties of the beam are modeled by the springs introduced. The modeling process is illustrated on the example of a flexible cantilever beam.

Keywords: flexible beam, Ding-Holzer method, lumped-mass model, rigid multibody system

1 INTRODUCTION

Among various methods for analysis of elastic bodies, the ones that especially single out are those methods that are based on the idea to replace the elastic bodies with a suitable system of rigid bodies. In such a way, application of well developed methods and formalisms of dynamics of rigid bodies is achieved in the analysis of dynamics of elastic bodies.

Therefore, modeling of planar elastic beams with use of rigid-elastic superelements has been done in [1]. A rigid-elastic superelement consists of three rigid bodies connected by two revolute joints. Bodies within the rigid-elastic superelements are also interconnected by suitable springs. The rigid-elastic superelements are rigidly connected to one another. The applications of this methodology to the problems of robotics and flexible wind turbine were given in [2] and [3], respectively. In [4] the spatial flexible bodies in wind turbine structures was considered. The flexible bodies (rotor blades, tower, shafts etc.) are modeled by cardanic joint beam elements. The cardanic joint beam element represents a system of four rigid spatial bodies connected by two cardanic joints and one cylindrical joint. In [5] the finite segment method for modeling of flexible beams was developed. This method consists in that a flexible beam divides into the finite number of rigid segments connected with springs of adequate stiffness.

In this paper planar flexible beams are considered. On the basis of the ideas from the reference [6], a method for approximate analysis of dynamics of these beams with the system of rigid bodies has been proposed. In the first phase of modeling, with use of the Ding-Holzer lumped-mass method [7,8], the flexible beam is replaced with concentrated masses connected by massless flexible beams. In the second phase, using the technique of modeling body motion with fictitious rigid bodies [9], each flexible massless beam is modeled with the system of three bodies connected with prismatic and revolute joints. The joints contain springs of adequate stiffness which model elastic features of massless flexible beams. In this manner a system of rigid bodies in the form of open kinematic chain without branching is achieved, what enables application of methods of multibody dynamics in studying motion of elastic beams.

2 MODELING OF A FLEXIBLE BEAM

2.1 Potential energy of a cantilever flexible beam

Consider a uniform flexible beam having clamped end A and free end B shown in Fig.1. Under a static load $(F, M)^T$ at the B end, where F is the force and M is the torque of a couple, the deflection u and slope θ are determined by the following relation of the linear elastostatics theory (see for example [1])

$$\begin{bmatrix} F \\ M \end{bmatrix} = \frac{E\,I_z}{L^3}\begin{bmatrix} 12 & -6L \\ -6L & 4L^2 \end{bmatrix}\begin{Bmatrix} u \\ \theta \end{Bmatrix} \equiv \left[C\right]\begin{Bmatrix} u \\ \theta \end{Bmatrix} \qquad (1)$$

where $\left[C\right]$ is the stiffness matrix of the beam calculated for the end B, L is the length of the beam, E is the Young's modulus of elasticity,

*Corr. Author's Address: Faculty of Mechanical Engineering, Dositejeva 19, 36000 Kraljevo, Serbia, salinic.s@mfkv.kg.ac.rs

and I_z is the axial moments of inertia for the principal axis z of the cross section of the beam. Due to small elastic deformations of the beam, the quantities u and θ are small. Introduce the following vectors:

$$\vec{u} = u\,\vec{j}, \quad \vec{\theta} = \theta\,\vec{k}\,. \tag{2}$$

Now imagine that a rigid planar massless whole is rigidly connected to the free end of the beam. Denote by P the point of the rigid whole which coincides with the middle of the undeformed beam. Since the quantities u and θ are small, the following kinematical relations hold (see for example [10])

$$\vec{u}_P = \vec{u} + \vec{\theta} \times \vec{\rho}, \quad \vec{\theta}_P = \vec{\theta} \tag{3}$$

where $\vec{\rho} = \overrightarrow{BP} = -L/2\,\vec{i}$, or in the matrix form

$$\begin{Bmatrix} u_{Px} \\ u_{Py} \\ 0 \end{Bmatrix} = \begin{Bmatrix} 0 \\ u \\ 0 \end{Bmatrix} + \begin{bmatrix} 0 & 0 & 0 \\ 0 & 0 & -L/2 \\ 0 & L/2 & 0 \end{bmatrix} \begin{Bmatrix} 0 \\ 0 \\ \theta \end{Bmatrix}. \tag{4}$$

From Eq.(4) it follows that

$$u_{Px} = 0, \quad u_{Py} = u - \theta L/2 \tag{5}$$

as well as

$$\begin{Bmatrix} u \\ \theta \end{Bmatrix} = \begin{bmatrix} 1 & L/2 \\ 0 & 1 \end{bmatrix} \begin{Bmatrix} u_P \\ \theta \end{Bmatrix} \tag{6}$$

where $u_P = |\vec{u}_P|$. Based on (1), the potential energy of the considered elastically deformed beam is

$$\Pi = \frac{1}{2}(u,\theta)[C]\begin{Bmatrix} u \\ \theta \end{Bmatrix}. \tag{7}$$

Putting Eq.(6) into (7) yields

$$\Pi = \frac{1}{2}(u_P,\theta)\begin{bmatrix} 1 & 0 \\ L/2 & 1 \end{bmatrix}[C]\begin{bmatrix} 1 & L/2 \\ 0 & 1 \end{bmatrix}\begin{Bmatrix} u_P \\ \theta \end{Bmatrix} =$$

$$= \frac{1}{2}(u_P,\theta)[C_P]\begin{Bmatrix} u_P \\ \theta \end{Bmatrix}. \tag{8}$$

where $[C_P] = diag(12EI_z/L^3,\ EI_z/L)$ is the stiffness matrix corresponding to the point P. Equation (8) in a developed form reads

$$\Pi = \frac{1}{2}\left(\frac{12EI_z}{L^3}u_P^2 + \frac{EI_z}{L}\theta^2\right). \tag{9}$$

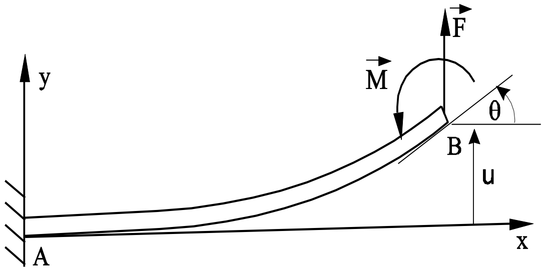

Fig.1. *A cantilever flexible beam with static load*

2.2 Discretization of the flexible beam

Let us make now the discretization of the beam shown in Fig.1 using the Ding-Holzer lumped mass method [7,8]. In accordance with this method, the elastic beam is replaced by the system composed of three particles connected with flexible massless beams (V_1^*) and (V_2^*) as in Fig.2a. Further, using the technique of modeling body motion with fictive bodies [9] (a fictive body means a body whose mass is equal to zero, whose dimensions are arbitrary and whose fictive center of mass can be arbitrarily chosen), each of beams (V_1^*) and (V_2^*) is represented by a system of three rigid beams. Connections between the beams as well as places of rigid connection of particles to the corresponding beams are shown in Fig.2b.

The relative joint displacements $q_i (i = 1,\ldots,4)$ are determined by the following relation

$$\mathbf{q} \equiv (q_1, q_2, q_3, q_4)^T = (u_{P_1}, \theta_1, u_{P_2}, \theta_2)^T \tag{10}$$

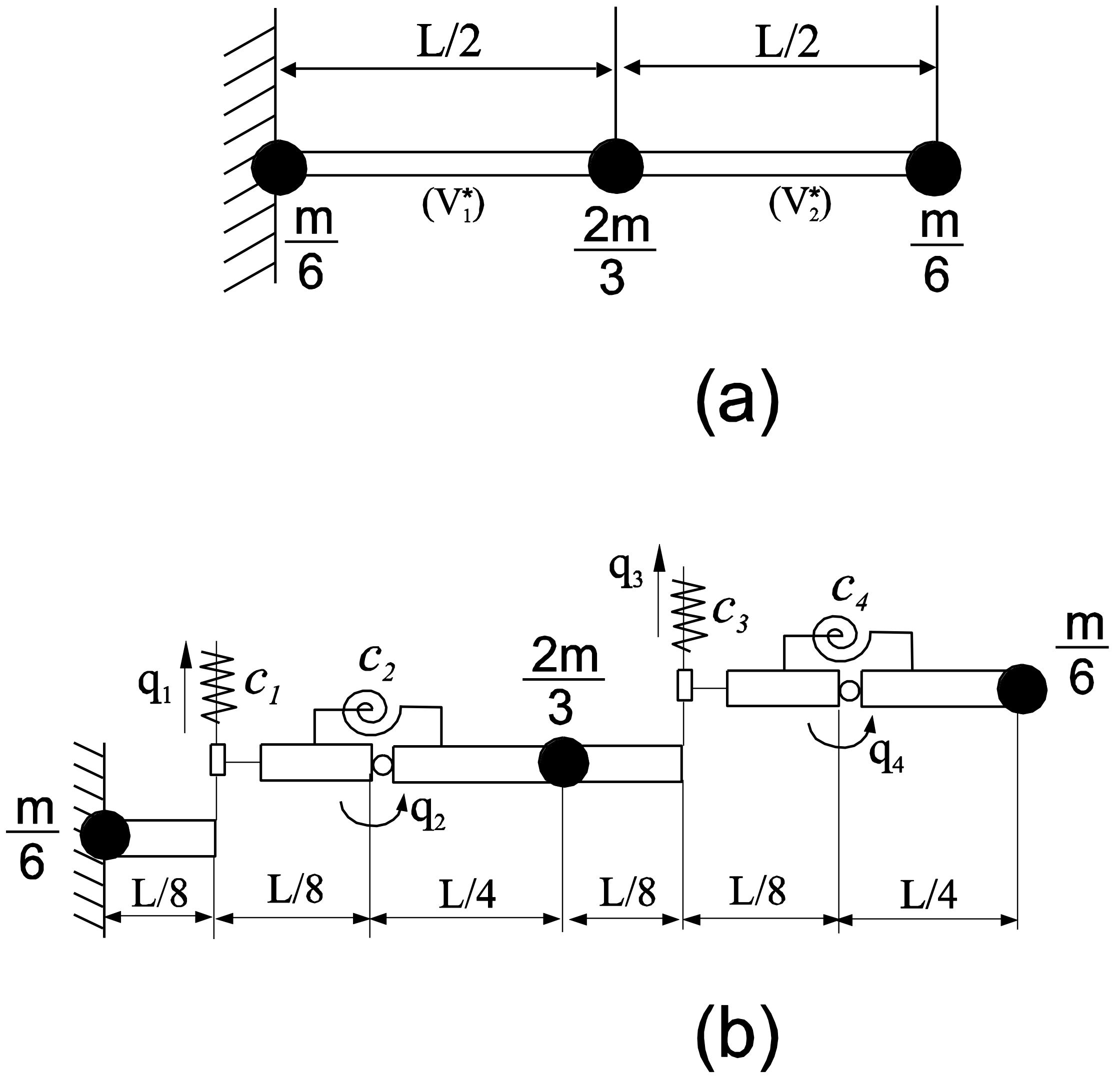

Fig. 2. *The rigid multibody model of a cantilever flexible beam*

where the quantities u_{P_1} and θ_1 correspond to the body (V_1^*) and the quantities u_{P_2} and θ_2 correspond to the body (V_2^*). Appropriate springs are placed in the joints depending on the type of joint (cylindrical for the prismatic joint, and spiral for the revolute one). Stiffnesses of the introduced springs are such that the potential energy of this system of springs is equal to the potential energy of the both flexible beams (V_1^*) and (V_2^*). In accordance to this, the stiffnesses of the springs in the joints in Fig.2b, on the basis of (9) and the fact that the lengths of the beams (V_1^*) and (V_2^*) are equal to $L/2$, are

$$c_1 = c_3 = \frac{96E\,I_z}{L^3}\,,\ \ c_2 = c_4 = \frac{2E\,I_z}{L}\,. \tag{11}$$

In this way, a model of an elastic beam has been formed in the form of rigid multibody system by which the motion of the flexible beam can be approximatively analyzed.

3 NUMERICAL EXAMPLE AND DISCUSSION

In this part, the previously formed discretized flexible beam model will be used for determining frequency of small transversal vibrations of the cantilever beam depicted in Fig.1 where the B end is unloaded. Gravity is not considered in this example. For the purpose of later comparison of results let the beam, as in [3], has the following characteristics:

$$L = 50\,m,\ \ E = 21\times 10^{10}\ N/m^2,\ \ A = \pi\, m^2$$

$$I_z = \frac{\pi}{4} m^4,\ \ m = 392500\pi\ kg.$$

Let the beam performs small transversal vibrations around the equilibrium position (undeformed state of the beam). Let us represent the beam by a system of rigid bodies as in Fig.2b. The equilibrium position of the beam corresponds to the equilibrium configuration of the multibody system in which $q_1 = \ldots = q_4 = 0$, that is, $\mathbf{q} = \mathbf{0}$, $\mathbf{0} = (0,0,0,0)^T$. For small vibrations the kinetic energy T of the considered multibody system is approximated by (see e.g. [11])

$$T \approx T(\mathbf{q} = \mathbf{0}) = \frac{1}{2}\dot{\mathbf{q}}^T [A]\, \dot{\mathbf{q}} \tag{12}$$

where $\dot{\mathbf{q}} = (\dot{q}_1, \dot{q}_2, \dot{q}_3, \dot{q}_4)^T$, and $[A] \in \Re^{4\times 4}$ is the mass matrix determined by:

$$[A] = \begin{bmatrix} \frac{981250\pi}{3} & \frac{17171875\pi}{3} & \frac{196250\pi}{3} & \frac{2453125\pi}{3} \\ \frac{17171875\pi}{3} & \frac{797265625\pi}{6} & 2453125\pi & \frac{61328125\pi}{2} \\ \frac{196250\pi}{3} & 2453125\pi & \frac{196250\pi}{3} & \frac{2453125\pi}{3} \\ \frac{2453125\pi}{3} & \frac{61328125\pi}{2} & \frac{2453125\pi}{3} & \frac{61328125\pi}{6} \end{bmatrix} \tag{13}$$

According to (11), the stiffness matrix reads

$$[C] = diag\left(4032\,\pi\times 10^4,\ 21\pi\times 10^8,\ 4032\,\pi\times 10^4,\ 21\pi\times 10^8\right). \tag{14}$$

Hence, for the considered case, the differential equations of motion of the multibody system are

$$[A]\ddot{\mathbf{q}} + [C]\mathbf{q} = \mathbf{0} \tag{15}$$

where $\ddot{\mathbf{q}} = (\ddot{q}_1, \ddot{q}_2, \ddot{q}_3, \ddot{q}_4)^T$. Since the multibody system contains massless beams, the mass matrix $[A]$ is singular ($rank[A] = 2 < 4$). In regard to this, using approach from [12] the linearized differential equations of motion (15) may be reduced to a system of two differential and two algebraic equations. Taking this into account, the frequency equation

$$\det\left([C] - \omega^2 [A]\right) = 0 \tag{16}$$

is reduced to the equation

$$1056825875\omega^4 - 279163584\times 10^3\omega^2 + 3584673792\times 10^3 = 0\,, \tag{17}$$

which has the solutions

$$\omega_1^2 = 13.5342\,\mathrm{s}^{-2},\ \ \omega_2^2 = 250.619\,\mathrm{s}^{-2} \tag{18}$$

so that the natural frequencies of the system are

$$\omega_1 = 3.67889\ \mathrm{s}^{-1},\ \ \omega_2 = 15.8309\ \mathrm{s}^{-1}. \tag{19}$$

The first two exact natural frequencies of the considered Euler-Bernoulli beam (see [3]) are

$$\omega_1 = 3.6371\,\mathrm{s}^{-1},\ \ \omega_2 = 22.7933\,\mathrm{s}^{-1}. \tag{20}$$

Comparing these exact values with the values (19) it is found that the relative numerical error in determination of first frequency amounts to $1.15\ \%$, and in the case of second frequency it is $-30.55\ \%$. For comparison only, in [3], using the approximation based on one superelement, it is obtained that

$$\omega_1 = 3.599\ \mathrm{s}^{-1},\ \ \omega_2 = 36.86\ \mathrm{s}^{-1}, \tag{21}$$

with relative numerical errors in determination of these frequencies $-1.048\ \%$ and $61.71\ \%$, respectively. In comparison to the approache in

[1,2,3], the method in this study uses prismatic joints besides the rotational ones.
Furthermore, the springs, used for modeling the elastic features of a flexible beam, are placed in joints only, while springs in superelements [1,2,3] are also connected between the nonadjacent bodies within superelements. The method presented can be used as an alternative for the existing methods for approximative analysis of vibrations of flexible beams.

REFERENCES

[1] Schiehlen W.O., J. Rauh, "Modeling of flexible multibeam systems by rigid-elastic superelements", *Revista Brasiliera de Ciencias Mecanicas* 8(2), (1986), pp. 151-163.

[2] Rauh J., W.O. Schiehlen, "Various approaches for the modelling of flexible robot", in *Proceedings of the Euromech-Colloquium 219 on Refined Dynamical Theories of Beams, Plates, and Shells and their Applications*, Kasel, (1986) Springer-Verlag, Berlin Heidelberg, pp. 420-429.

[3] Molenaar, D.P., S. Dijkstra, "Modeling the structural dynamics of the Lagerwey LW-50/750 wind turbine", *Wind Engineering* 22(6), (1998), pp.253-264.

[4] Zhao X., P. Maisser, and J. Wu, "A new multibody modelling methodology for wind turbine structures using a cardanic joint beam element", *Renewable Energy* 32, (2007), pp. 532-546.

[5] Wang, Y., R.L. Huston, "A lumped parameter method in the nonlinear analysis of flexible multibody systems", *Computers and Structures* 50(3), (1994), pp.421-432.

[6] Šalinić, S., "Modelling of a light elastic beam by a system of rigid bodies", *Theoretical and Applied Mechanics* 31(3-4), (2004), pp.395-410.

[7] Ding, X., J.M. Selig, and Q. Zhan, "Study on dynamic modeling of compliant manipulators", in *Proceedings of the 4th World Congress on Intelligent Control and Automation*, Shanghai, P.R.China, (2002), pp. 1347-1353.

[8] Ding, X., J.M. Selig, "Lumped parameter dynamic modelling for the flexible manipulator", in *Proceedings of the 5th World Congress on Intelligent Control and Automation*, Hangzhou, P.R.China, (2004), pp. 280-284.

[9] Medvedev, V.S., A.G. Leskov, and A.S. Yuschenko, "The systems of control of manipulation robots", Nauka, Moscow, (1978).

[10] Chernousko, F.L., N.N. Bolotnik, and V.G. Gradetsky, "MANIPULATION ROBOTS: Dynamics, control, optimization", Nauka, Moscow, (1989).

[11] Meirovitch, L., "Fundamentals of vibrations", McGraw-Hill Higher Education, (2001).

[12] Belonozhko, P.A., M.M. Zhechev, S.V. Tarasov, "Mathematical modeling of the dynamics of a system of two bodies coupled by an elastic multiple-element chain", *International Applied Mechanics* 22(7), (1986), pp. 683-688.

HEAVY MACHINERY - HM 2011, 91-94 Paper accepted: 30.05.2011
ISBN 978-86-82631-58-3

Vehicle Dynamics In Overtaking

Lalovic Ljubica [1,*] - Lalovic Dragomir [2] –Knezevic-Miljanovic Julka [3]
[1]Faculty of Mechanical Engineering Kraljevo, University of Kragujevac
[2]PhD candidate of Mechanical Engineering Kragujevac
[3]Faculty of Mathematics Belgrade

The paper considers the dynamics of the vehicle when overtaking. Giving an analysis of relevant parameters for monitoring the vehicle stability and handling. The plane vehicle model with the characteristics of sprung mass (mass, moment of inertia and gravity position), wheelbase, tire lateral characteristics and impact steering system (steering transmission ratio and angles of rotation of the wheels) is observed. This results in lateral and longitudinal displacement and rotation of the sprung mass speed of rotation around a vertical axis and in the speed and direction of the sprung mass velocity, turning angles of all wheels and the current center of rotation. Based on these parameters the vehicle handling and stability at the given mode of motion can be determined.In this paper, an example of overtaking vehicles with the input dimensions and results of relevant parameters.

Keywords: vehicle dynamics, vehicle overtaking

INTRODUCTION

Under the term vehicle overtaking we mean avoiding another vehicle, moving to the parallel track and moving back to the original track having completed the avoiding. During such movement of vehicles lateral force, longitudinal braking and acceleration force, velocity and acceleration in the longitudinal and transverse direction as well as the angular velocity around a vertical axis are present. However, the driver that changes the size and nature of external forces acting on the vehicle has a large impact.The Driver via certain commands affects the size of the traction force and braking force, and through steering wheel he/she affects the size of lateral force.
The paper views the plane passenger car middle-class classical structure model in which the following parameters are monitored on the basis of which the car's behavior is defined depending on the force generated by overtaking vehicles. Two coordinate systems are introduced here: stationary coordinate system OXYZ and the mobile one related to the location of the vehicle oxyz where:
x-axis longitudinal axis of centre of gravity
y-axis perpendicular axis of centre of gravity
z-axis vertical axis of centre of gravity

1.1 Mathematical model

Bearing in mind the objective of this work a complex vehicle model has been made that allows the analysis of the following parameters:
x- body moving along the x axis
y- body moving along the y axis
ψ - swimming, oscillations about the z axis
a, b - distance between the center of gravity and the front and rear axles
h - height the center of gravity
2s - rut
In Figure 1, the horizontal dynamics of the vehicle with an analysis of forces and displacements is given.
Define horizontal angles relevant to the dynamics shown in figure 1

$$\beta = (\beta_1 + \beta_2)/2 \quad (1)$$

$$\alpha_1 = \beta_1 - (y' + a \cdot \psi')/(x' - d_1 \cdot \psi') \quad (2)$$

$$\alpha_2 = \beta_2 - (y' + a \cdot \psi')/(x' + d_2 \cdot \psi') \quad (3)$$

$$\alpha_3 = -(y' - b \cdot \psi')/(x' + d_3 \cdot \psi') \quad (4)$$

$$\alpha_4 = -(y' - b \cdot \psi')/(x' - d_4 \cdot \psi') \quad (5)$$

$$\alpha_p = \beta_p - (y' + a \cdot \psi')/x' \quad (6)$$

$$\alpha_z = -(y' - b \cdot \psi')/x' \quad (7)$$

$$\alpha = y'/x' \quad (8)$$

Differential equations of motion of vehicles have the following form:

*Corr. Author's Adress: Faculty of Mechanical Engineering Kraljevo, Dositejeva 19, Kraljevo, ljubicakg@yahoo.com

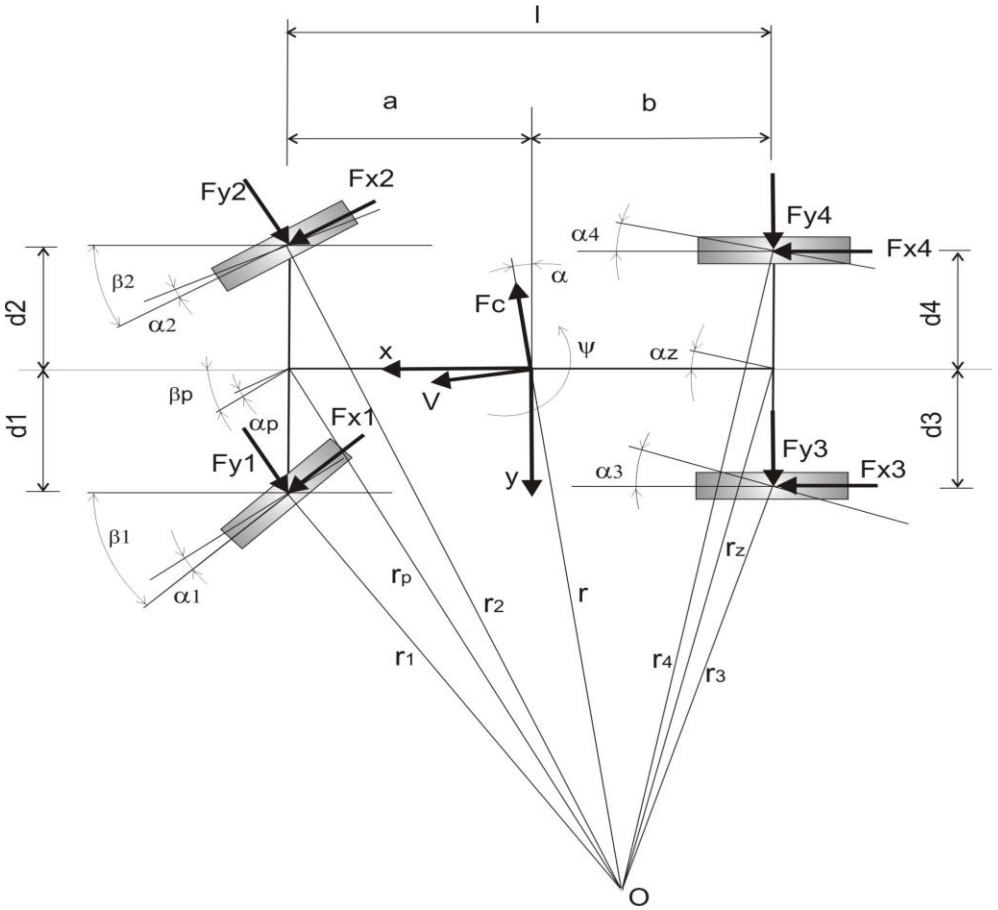

Fig. 1. *Horizontal dynamics of the vehicle*

$$
\begin{aligned}
m\cdot x'' &= F_{1x}\cdot\cos\beta_1 + F_{2x}\cdot\cos\beta_2 - c_{y1}\cdot\left(\beta_1 - \frac{y'+a\cdot\psi'}{x'-d_1\cdot\psi'}\right)\cdot\sin\beta_1 - c_{y2}\cdot\left(\beta_2 - \frac{y'+a\cdot\psi'}{x'+d_2\cdot\psi'}\right)\sin\beta_2 + \\
&\quad + F_{3x} + F_{4x} + F_c\cdot\sin\left(\frac{y'}{x'}\right) \\
m\cdot y'' &= F_{1x}\cdot\sin\beta_1 + F_{2x}\cdot\sin\beta_2 + c_{y1}\cdot\left(\beta_1 - \frac{y'+a\cdot\psi'}{x'-d_1\cdot\psi'}\right)\cos\beta_1 + c_{y2}\cdot\left(\beta_2 - \frac{y'+a\cdot\psi'}{x'+d_2\cdot\psi'}\right)\cdot\cos\beta_2 + \\
&\quad + c_{y3}\cdot\alpha_3 + c_{y4}\cdot\alpha_4 - F_c\cdot\cos\left(\frac{y'}{x'}\right) \\
J_z\cdot\psi'' &= \left(F_{1x}\cdot\sin\beta_1 + F_{2x}\cdot\sin\beta_2 + c_{y1}\cdot\left(\beta_1 - \frac{y'+a\cdot\psi'}{x'-d_1\cdot\psi'}\right)\cos\beta_1 + c_{y2}\cdot\left(\beta_2 - \frac{y'+a\cdot\psi'}{x'+d_2\cdot\psi'}\right)\cdot\cos\beta_2\right)\cdot a - \\
&\quad - \left(c_{y3}\cdot\alpha_3 + c_{y4}\cdot\alpha_4\right)\cdot b - F_{1x}\cdot\cos\beta_1\cdot d_1 + F_{2x}\cdot\cos\beta_2\cdot d_2 + F_{3x}\cdot d_3 - F_{4x}\cdot d_4 + \\
&\quad + c_{y1}\cdot\left(\beta_1 - \frac{y'+a\cdot\psi'}{x'-d_1\cdot\psi'}\right)\cdot\sin\beta_1\cdot d_1 - c_{y2}\cdot\left(\beta_2 - \frac{y'+a\cdot\psi'}{x'+d_2\cdot\psi'}\right)\cdot\sin\beta_2\cdot d_2
\end{aligned}
\tag{9}
$$

Where is

$F_c = mv^2 / r$ centrifugal force

$\alpha = y' / x'$ angle of rotation of the center of mass supported

c_{yi} $i = 1, 4$ lateral stiffness of the tire

Lateral force:

$F_{1y} = c_{y1} \cdot \alpha_1$

$F_{2y} = c_{y2} \cdot \alpha_2$

$F_{3y} = c_{y3} \cdot \alpha_3$

$F_{4y} = c_{y4} \cdot \alpha_4$

Longitudinal braking force can be or pulling. It can be shown through axle ratio, which can be positive or negative sign.

F_p - front axle,

F_z - rear axle,

F_x - total longitudinal force.

$$F_p = K_o \cdot F_x \qquad (10)$$

$$F_z = (1 - K_o) \cdot F_x \quad \text{where} \qquad (11)$$

$K_o = 0$ $\quad F_{px} = 0;\ F_{zx} = F_x$

$0 < K_o < 1$ $\quad F_{px} = K_o \cdot F_x;\ F_{zx} = (1 - K_o) \cdot F_x$

$K_o = 1$ $\quad F_{px} = F_x;\ F_{zx} = 0$

Distribution of the front wheels

$0 \le K_{tp} \le 1$

$F_{1x} = K_{tp} \cdot F_{px}$

$F_{2x} = (1 - K_o) \cdot F_{px}$

Distribution of the rear wheels

$0 \le K_{tz} \le 1$

$F_{3x} = K_{tz} \cdot F_{zx}$

$F_{4x} = (1 - K_{tz}) \cdot F_{zx}$

1.2 Calculation results

An example was done in case of overtaking vehicles

Input

a=1.2; b=1.3; s=0.7; d1=s; d2=s;d3=s;d4=s; l=2.5; h=0.6;

Iz=2000; m=1000 kg;

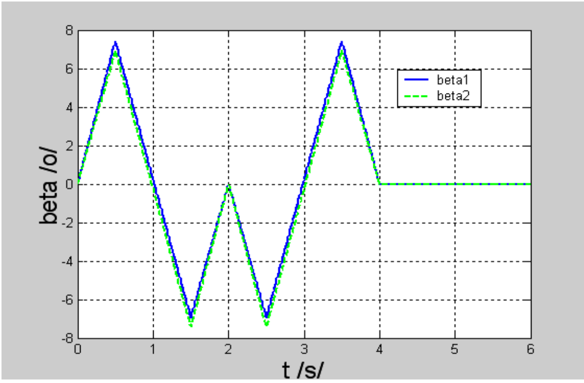

Fig. 2. *The corners of the front wheels turning*

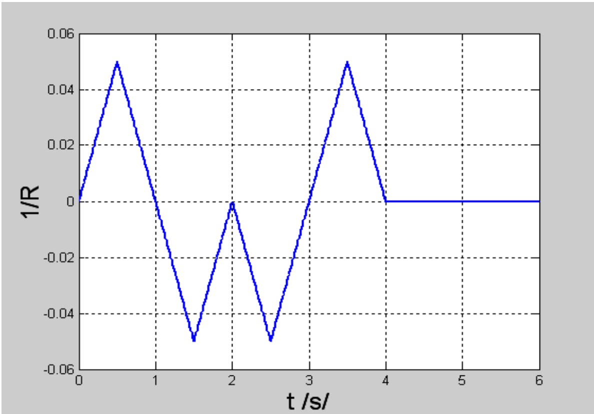

Fig. 3. *Reciprocal radius of rotation*

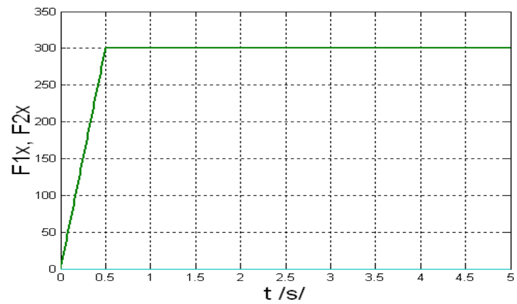

Fig. 4. *Traction forces at the front*

Based on the given inputs (diagrams 2 to 4) you receive the results displayed in the following diagrams (dijagrams 5 to 10).

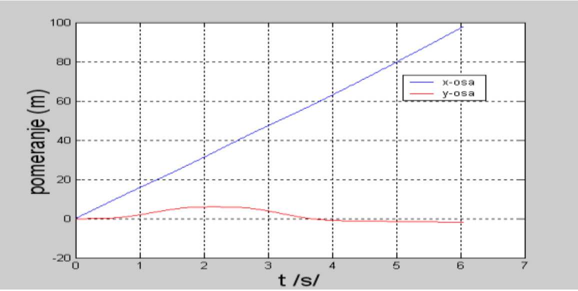

Fig. 5. *Moving the center of gravity in x and y direction*

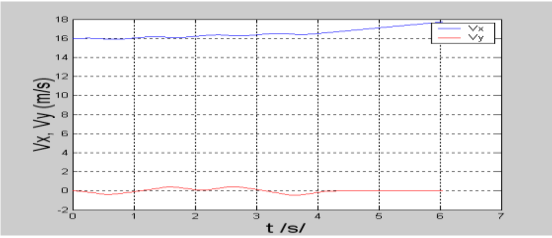

Fig. 6. *Speed of gravity in the x and y direction*

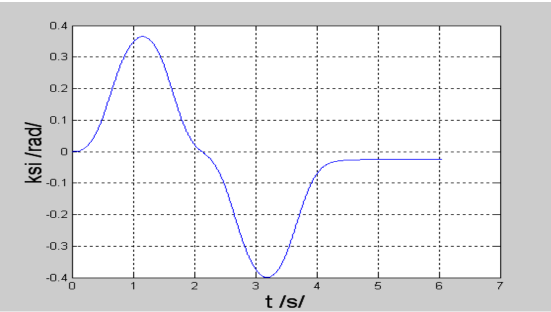

Fig. 7. *Rotation supported mass around the axis z*

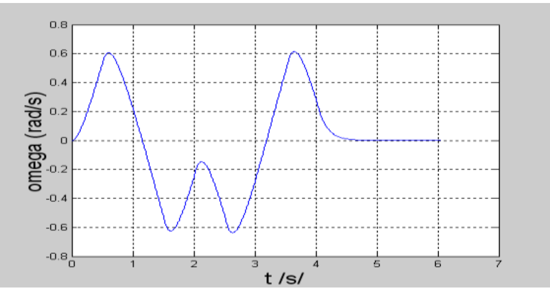

Fig. 8. *Angular velocity of rotation around the z axis*

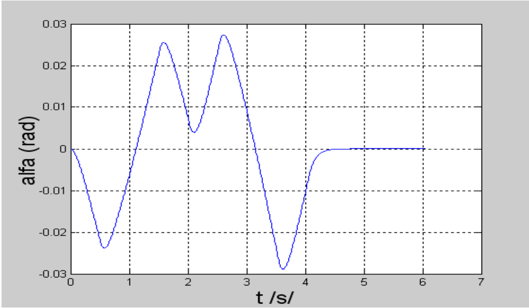

Fig. 9. *The angle of movement of mass center of gravity resting*

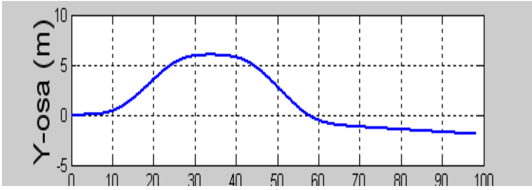

Fig. 10. *The path of movement of vehicles center of gravity*

Conclusion

The paper represents a theoretical analysis vehicle overtaking , which examines the impact of relevant parameters important for the stability of the vehicle.
It can also be observed when handling vehicle overtaking with the presence of a braking force and an accelerating force
This analysis is especially important in the design stage of vehicles in order to optimize parameters of the suspension system and vehicle steering.
In further research experimental measurements will be done and compared with the calculation results.

REFERENCES

[1] N. Cucuz, L. Rusov, Dynamics motor vehicle, Privredni pregled, Belgrade,1973.
[2] Matschinsky W.: Die Radfuhrungen der Strabenfahrzeuge, Werlag ,Rheinland,1987.
[3] Ellis J.R.: Vehicle dynamics, Business Books, 1969.
[4] Remling J.: Brakes, John Wiley @ Sons, New York, 1978.
[5] Reimpell J.: Fahrwerktechnik 1, Woge Werlage, 1971.
[6] Reimpell J.: Fahrwerktechnik 2, Woge Werlage, 1973.

HEAVY MACHINERY - HM 2011, 95-100
ISBN 978-86-82631-58-3
Paper accepted: 30.05.2011

Setting up car hood to improve pedestrian protection - tests and measurements with the optical 3D metrology

Roman Potočnik - Džemal Kovačević, Martin Zadnik, Blaž Japelj[1],
Nenad Drvar and Tomislav Hercigonja[2]
[1] CIMOS d.d.
[2] TOPOMATIKA d. o. o.

Changes in the direction of improving the safety of passengers in passenger cars as well as the other road users engaged Cimos in 2002 into a global development of hinge hood systems concept of active and passive pedestrian safety. From the initial conceptual phase, some projects in cooperation with our customers developed up to a level of industrialization and mass production. Desiring to enhance the competitiveness of the company we constantly seek the ways to offer the we offer the market the best design solutions in terms of strength, price and implementation times. To achieve these objectives, we use the results of the FEM numerical analysis and physical measurements of bonnet motion kinematics and strength requirements of the product. For physical testing of our pedestrian safety system we use GOM measuring equipment and DSD testing machine for simulations of pedestrian head impact in the hood. In this paper testing procedures of hinge and bonnet displacement measurements will be presented, together with impact test simulation of pedestrian head model with activated bonnet. The concept of active safety system will also be presented, for which Cimos developed kinematics and design of hinges and the lock brackets (hood holding system - lock). Experiments and measurements Cimos conducted in cooperation with Topomatika, distributor of the optical measurement system GOM PONTOS HS.

Keywords: Ptical measurements, Deformation measurement, Pedestrian protection

1 INTRODUCTION

According to the data for traffic safety provided by the EU Commission, the number of fatalities on European roads in 2009 was a total of 34 500 people. 20% of victims were pedestrians *(Figures 1 and 2).*

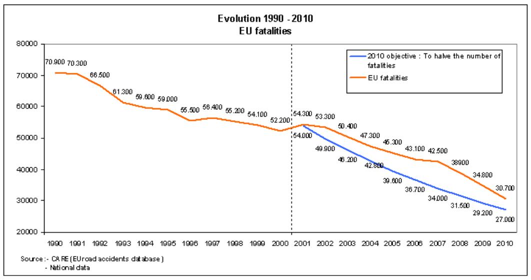

Fig. 1: Number of victims on the European roads 1990 - 2010. [1]

Based on a statistical analysis of the data in the alst decade it can be concluded that number of victimes in the road traffic is not declining as fast as the EU Commission anticipated *(figure 1).* The aim of the Commision for the next decade is to reduce number of victimes by half, in order to increase overall road safety.

In order to reach the goal of road victime reduction UN accepted GTR 9 directive, which created a framework for a globaly applicable pedestrian safety law. Car manufacturers are due to legal changes, but also by increased rating requirements as EuroNCAP, forced to introduce new systems to improve safety of road users.

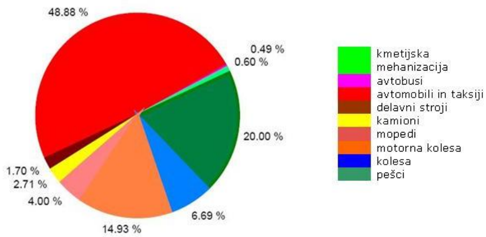

Fig. 2: Distribution of traffic victimes in 2009 [2]

Pedestrian safety is one of the requirements on the basis Cimos has in 2002 turned in into the global development of pedestrian protection systems and in the development and production of the active hood hinges. Purpose of active safety systems is to protect the pedestrian from

*Corr. Author's Address: Ilica 231, 10000 Zagreb, Croatia, n.drvar@topomatika.hr the serious injuries. Activation of the safety system should increase hood deformation area thus reducing the injury. It consists of the car hood, special hood hinges with activators, acceleration sensors and the control unit. When car hits the pedestrian sensors transmit this information to the control unit, which activates pyrotechnical activators which by the help of hinge kinematics lift the car hood approximately 50mm in the area closest to the driver *(figure 3)*.

Fig. 3: Pedestrian safety–active safety system. [3]

2 EQUIPMENT AND TESTS

List of testing equipment *(figure 4 and 5).*

- DSD HyperG Actuator
- Head model
- Trigger Interface
- PULSE by Bruel&Kjaer.
- Trigger Box by Messer HuDe
- High speed camera
- Optical measurement system GOM Pontos HS

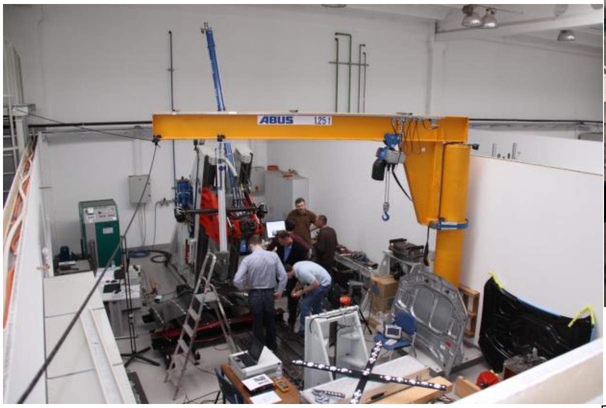

Fig. 4: Testing area

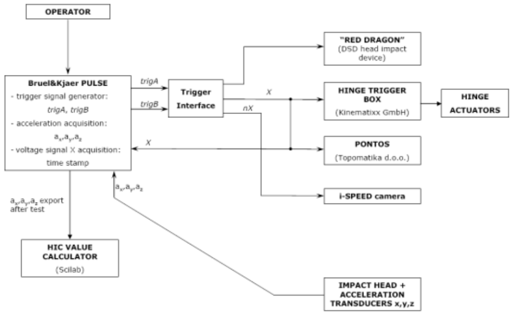

Fig. 5: Schematics of the equipment setup.

2.1.1 List of active safety system elements

Each tested hood sample consisted of:

- car hood 1pcs
- front hood holder 2pcs
- hood lock 2pcs
- hinges 2pcs
- gas shock absorber 2pcs
- activator 2pcs
- test bench 1pcs

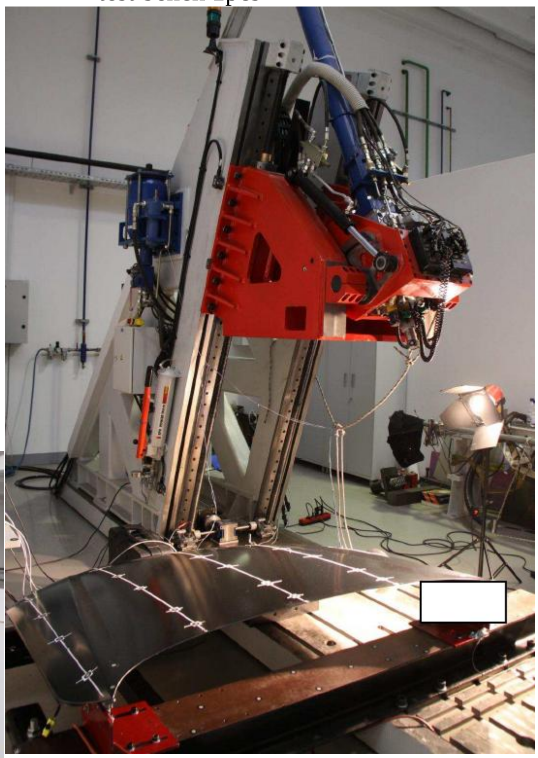

Fig. 6: Test bench with jig and the DSD system for performing the head impact tests

Testing bench was placed directly in front of DSD machine *(figure 6 and 7)*. Active hinges and hood locks were attached to the testing bench. Car hood bonnet was attached to the movable arm of the hinges. Gas shock absorbers and the pyrotechnic activators were attached between the hinge movable elements.

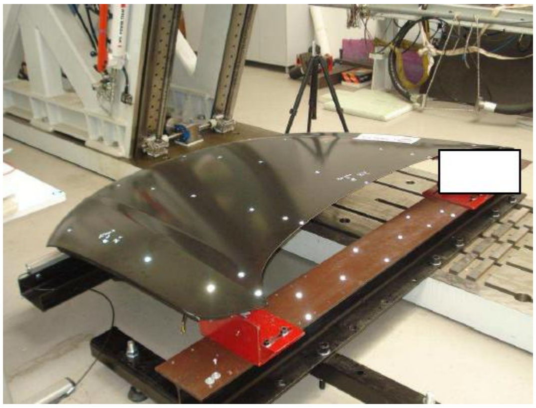

Fig. 7: Test bench with mounted hood

2.2 Deployment test workflow

Controlling device was used to send triggering signal over the Messer HuDe Trigger Box to the activators, which lifted the hood for the approx 50mm. *(figure 5).* At the same time this signal was used to start GOM Pontos HS measurements and the high-speed camera recordings.

2.3 Head impact test workflow

After the activation process ended, head model was deployed onto the partly opened car hood *(figure 8 and 9)* aimed at the predefined location.

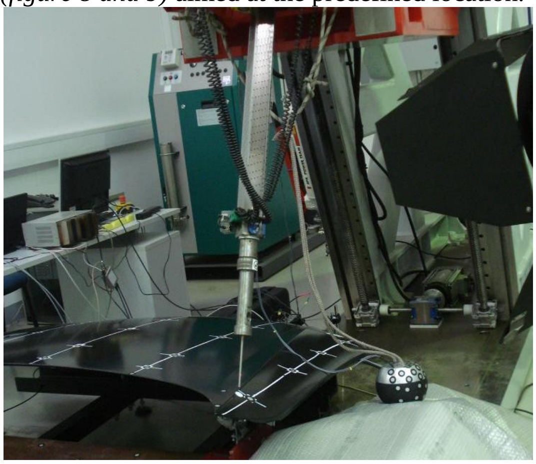

Fig. 8: Point of impact location testing before the head model deployment

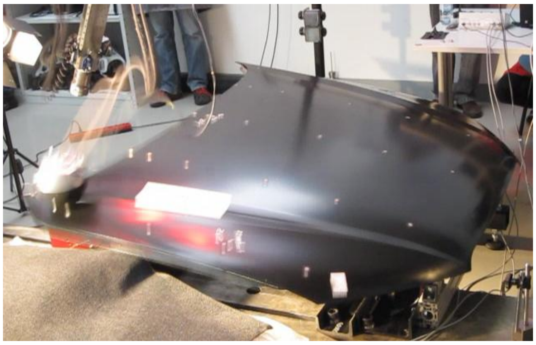

Fig. 9: Visualization of the head model impact

Tests were controlled by the PULSE device producet by Bruel&Kjaer. It was used to submit two signals, *trigA* and *trigB*, which were used by the specially developed trigger interface to deploy the following devices in the controlled time frames:
- DSD HyperG Actuator – device for head model deployment
- GOM Pontos HS optical dynamical displacement and deformation measurement system
- i-Speed high-speed camera recordings

During the flight and impact of the head model, data from the three accelerometers inside the head (perpendiculary placed) was also recorded. Resultant of the three values is used to additionaly calculate the HIC value (Head Injury Criterion), which has to fall in a predefined range.

HIC value calculation formula:

$$HIC = \left\{ \left[\frac{1}{t_2 - t_1} \int_{t_1}^{t_2} a(t)dt \right]^{2.5} (t_2 - t_1) \right\}_{max}$$
(1)

Head Injury Criterion (HIC) is a value which describes probabilty of head injury. Large accelerations can only be allowed for a short time frame. Tests conducted in Cimos observed the worst case scenario, in a point directly over the hinge where the largest HIC value can be expected. That location was chosen because it has the smallest deformation degree. Measured HIC values *(figures 10 and 11)* were well within the range required by law. [3]

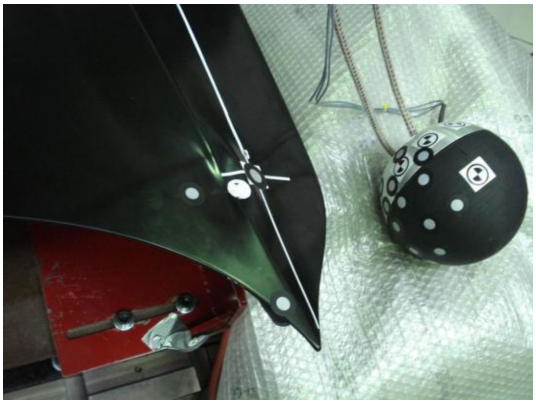

Fig. 10: Point-of-impact visualization

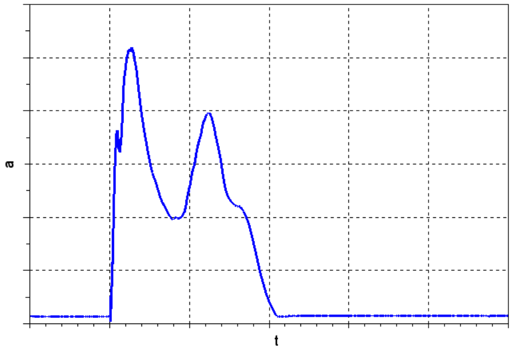

Fig. 11: Head model acceleration vs time.

Fig. 12: Optical measuring equipment used for the conducted tests.

2.4 Measurements of the kinematic effectiveness of the pedestrian active safety system with the optical measurement system GOM PONTOS HS

Measurements in Cimos were conducted with the measurement system PONTOS HS, which measures displacements without direct contact with the measuring object. It consists of the two high-speed cameras with triggered LED flashes. System measures shape, position displacement, velocity acceleration and deformations in discrete measuring points. Cameras enable recordings of image pairs with the frequency of 500Hz with the full resolution of 1,3 Mpx. By the reduction of image size it is possible to increase recording frequency. In order to triangulate locations of the measuring points in space measurement system PONTOS HS was photogrammetrically calibrated before the measurements took place. System enables high speed measurements that are controlled by a sensor controller which transmits signals for the recordings of the measurement images of the points attached to the bonnet.

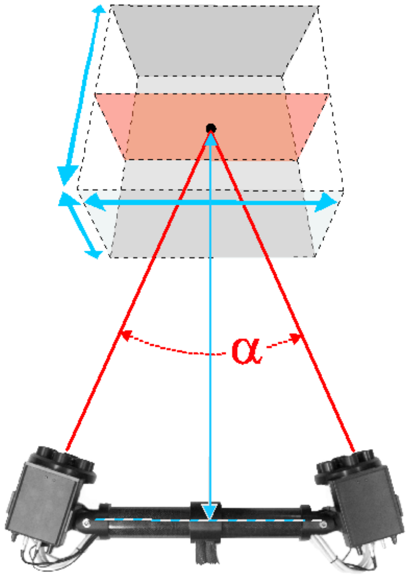

Fig. 13: Visualization of measurement volume

Cameras were attached to the 1,2m carbon fiber frame and fixed approximately 2,5m above the bonnet. In order to determine positions of measurement points, which are simultaneously recorded by two fixed cameras, their position, orientation and lens type has to be determined by system calibration. In order to reduce image distortions we used two identical cameras and camera lenses that were set to observe area of approximately 1,5x1,5m^2. On the measured car bonnet we attached retro reflective adhesive markers, which serve as the measurement points for the conduction of dynamic measurements *(figure 14).* Orientation of the measurement cameras was determined by the calibration cross with 1,7m bar length. Calibration cross was used to calibrate measurement volume at the exact distance from the system as the measured car bonnet. It consists of the adhesive coded and uncoded white markers that were used for the camera calibration. Displacement analysis was conducted relative to the original bonnet state, which was recorded during the activation of the car bonnet. Recording frequency of cameras was set to 500Hz, images were recorded in a system frame grabber. After the image recording, images were transferred onto the computer hard drive and analyzed. Results of X and Z displacements are presented in reports in the global car coordinate system.

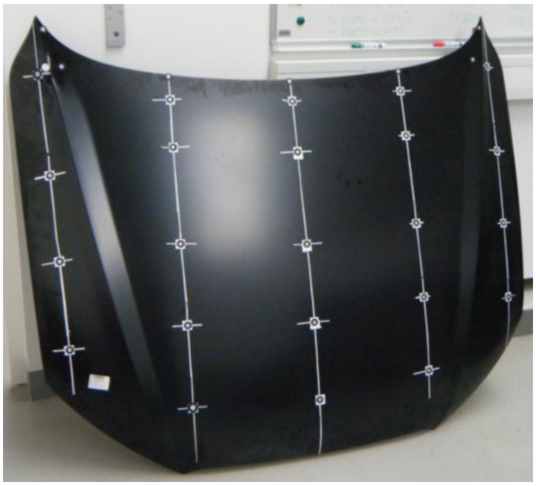

Fig. 14: Bonnet with the applied adhesive markers.

3 RESULTS

Measurement results can be presented as a graphical video 3D visualization (figure 16 shows a single frame during the maximum displacement) or as graphs shown by figures 17, 18 and 19. Measured results can be exported as ASCII and analyzed elsewhere. Displacements can be visualized as 3D vectors which change in time. Together with the accompanying diagrams the analysis and result presentation is possible in a clear and visually attractive manner.

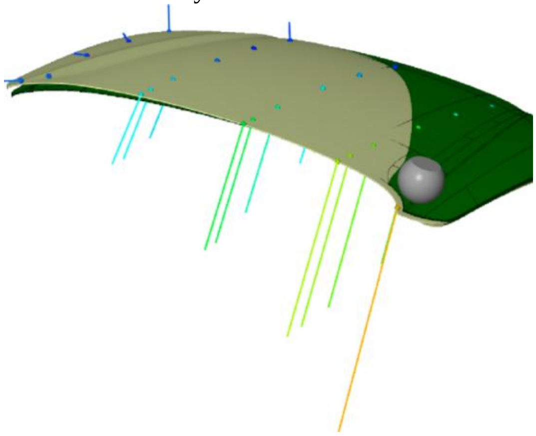

Fig. 16: Visualization of displacement vectors in the moment of head contact

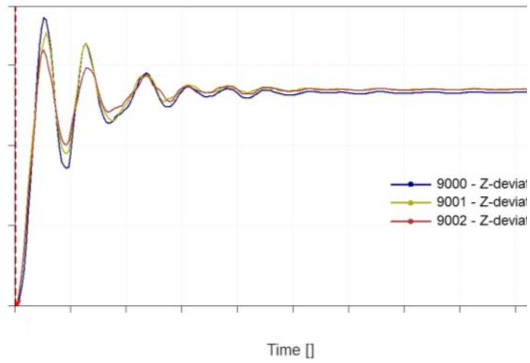

Fig. 17: Bonnet displacement measurement as a result of the pedestrian safety system activation

4 CONCLUSIONS

Tests were conducted in order to inspect how system developed and produced by Cimos in cooperation with customer works in practice. Our inten was to test how the existing equipment works together with the additional Pontos HS measurement system. Results achieved were withing the customer requirements regarding the bonnet displacement as well as for the HIC value (Head Injury Criterion). The conducted tests confirmed that the active pedestrian saferty system works as requested by customer and the 78/2009EC directive. The experiment has also shown that the equipment and professionalism of the staff of the Cimos test laboratory are appropriate and will enable us to competently continue the test of the pedestrian safety systems.

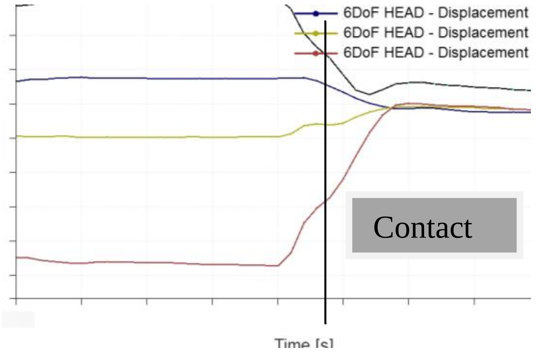

Fig. 18: Change of the head velocity because of the impact

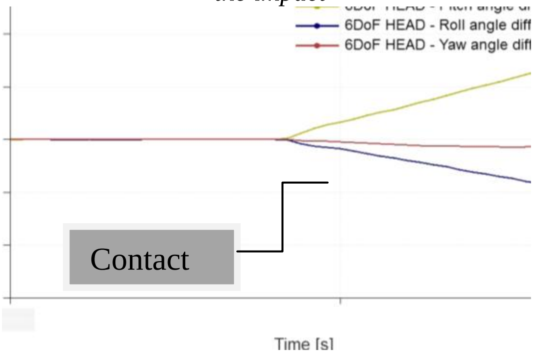

Fig. 19: Head rotation angles after the impact

5 REFERENCES

[1] European Commission Road Safety : Statistics trends http://ec.europa.eu/transport/road_safety/specialist/statistics/trends/index_en.htm

[2] European Commission Road Safety : 2009 transport mode graph, http://ec.europa.eu/transport/road_safety/pdf/statistics/2009_transport_mode_graph.pdf

[3] Automotive Technology : Pedestrian protection http://rb-kwin.bosch.com/br/en/safety_comfort/occupant_protection/pedestrianprotection.html

[4] McHenry G.B.: ATB *User´sGroup 2004* .

E SESSION

PRODUCTION TECHNOLOGIES

HEAVY MACHINERY - HM 2011, 1-6
ISBN 978-86-82631-58-3
Paper accepted: 30.05.2011

A methodology for forming the regression model of ternary system

Milan Kolarević[1,*], Miomir Vukićević[1], Branko Radičević[1], Mišo Bjelić[1], Vladan Grković[1]
[1]University of Kragujevac, Faculty of Mechanical Engineering Kraljevo, Serbia

SUMMARY. *This paper presents a methodology of multiple regression analysis of three-component systems. There are several stages: 1) calculation of the parameters of regression models, 2) checking the adequacy of mathematical models, 3) selection of regression model, 4) assessment of the significance of model parameters, 5) calculation of confidence limits of regression coefficients and 6) graphical representation of a mathematical model with the triangular surface plots or contour plots.*
Keywords: Multiple regression, Triangular Coordinates, Contour plot, Surface plot

1. INTRODUCTION

Three-component systems can be graphically displayed in two-dimensional space using triangular plots. The basic conditions for application of the triangular plots are:

$$0 \le X_i \le 1; \qquad \sum_{i=1}^{3} X_i = 1 \qquad (1)$$

X_i – the relative weight of the components in the mixture.
From the above presented condition, it is evident that the contribution of each component in the mixture depends on the share of the remaining two components.

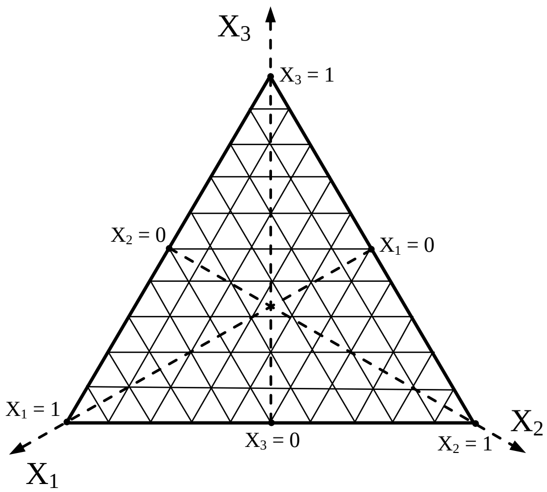

Fig. 1. *Display of vertical sections and direction increase of share of individual component in a triangular diagram*

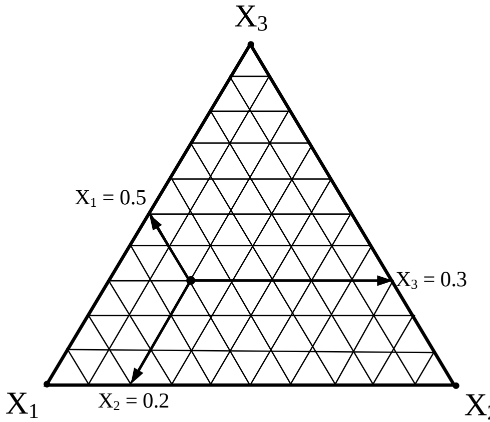

Fig. 2. *Determining the composition of alloys in the ternary system*

Each point within the triangle represents an appropriate composition of a three-component system. The vertices of the triangle represent a pure substance, while points on the sides of the triangle represent two-component systems. For a point inside the triangle, the content of each component is determined by drawing lines parallel to the sides of the triangle, and reading the value that corresponds to intersections between the lines and the sides of the triangle.

2. REGRESSION ANALYSIS

For three-component system, regression models can be generally set in the form of polynomials of lower degree (usually the first, second and third) which are usually defined by the following canonical forms [1] [2]:

*Corr. Author's Adress: University of Kragujevac, Faculty of Mechanical Engineering Kraljevo, Dositejeva 19, 36 000 Kraljevo, Serbia, kolarevic.m@mfkv.kg.ac.rs

- Linear regression model

$$y = b_1X_1 + b_2X_2 + b_3X_3 \tag{2}$$

- Square regression model

$$y = b_1X_1 + b_2X_2 + b_3X_3 + b_{12}X_1X_2 + b_{13}X_1X_3 + b_{23}X_2X_3 \tag{3}$$

- Incomplete cube regression model

$$y = b_1X_1 + b_2X_2 + b_3X_3 + b_{12}X_1X_2 + b_{13}X_1X_3 + b_{23}X_2X_3 + b_{123}X_1X_2X_3 \tag{4}$$

- Complete cube regression model

$$\begin{aligned} y &= b_1X_1 + b_2X_2 + b_3X_3 + b_{12}X_1X_2 \\ &+ b_{13}X_1X_3 + b_{23}X_2X_3 + b_{123}X_1X_2X_3 \\ &+ \delta_{12}X_1X_2(X_1 - X_2) + \delta_{13}X_1X_3(X_1 - X_3) \\ &+ \delta_{23}X_2X_3(X_2 - X_3) \end{aligned} \tag{5}$$

Selection of the regression model for ternary system depends primarily on available number of experimental points (Table 1). However, when a sufficient number of experimental points exist, it still does not mean that the model of the highest level will be the best.

Table 1. *The required number of experimental points for the formation of the regression model at ternary system*

Regression model	*Response subscripts*	*Numberof regression coefficients*	*Σ*
Linear	*i*	3	3
Second degree	*i* *ij*	3 3	6
Incomplete third degree	*i* *ij* *ijk*	3 3 1	7
Complete third degree	*i* *iij* *ijk*	3 6 1	10

In order to undergo the procedure of regression analysis of the ternary system and to select an appropriate regression model is necessary to implement the following steps:

- Selection of possible canonical forms of regression models
- Calculation of regression coefficients
- Checking the adequacy of the mathematical model
- Selection of regression model
- Assessment of significance of regression coefficients of the selected model
- Calculation the confidence limits of regression coefficients at the selected model
- Graphical interpretation of the mathematical model.

Procedure for implementation of regression analysis is shown in the example of measuring the electrical conductivity of ternary alloys *Ga-Sb-Zn* (Table 2). Mole fractions of component values are indicated by *X1, X2* and *X3* and the mean value of electrical conductivity (*MS /m*) with *Y*.

Table 2. *Experimental values of electrical conductivity of ternary alloys Ga-Sb-Zn*

	Ga	*Sb*	*Zn*	*EP [MS/m]*
	X1	*X2*	*X3*	*Y*
1	0	0,5	0,5	0,198
2	0,4	0,3	0,3	0,352
3	1	0	0	6,780
4	0,5	0	0,5	2,324
5	0,3	0,4	0,3	0,743
6	0	1	0	2,880
7	0,5	0,5	0	0,224
8	0,3	0,3	0,4	0,604
9	0	0	1	16,600

3. CALCULATION OF MODEL PARAMETERS

Modern software tools enable selection of all possible regression models depending on the number of available experimental points. Based on data from Table 1 it is possible to perform regression analysis for linear, quadratic and incomplete cubic regression model. Equations (2) - (4) can be written in matrix form:

$$\boldsymbol{Y = X\, b} \tag{6}$$

where:

$$Y = \begin{bmatrix} y_1 \\ y_2 \\ . \\ . \\ . \\ y_k \end{bmatrix}, \; X = \begin{bmatrix} x_{11} & x_{12} & . & . & . & x_{1k} \\ x_{21} & x_{22} & . & . & . & x_{2k} \\ . & . & & & & . \\ . & . & & & & . \\ . & . & & & & . \\ x_{n1} & x_{n2} & . & . & . & x_{nk} \end{bmatrix}, \; b = \begin{bmatrix} b_1 \\ b_2 \\ . \\ . \\ . \\ b_k \end{bmatrix}$$

Unknown coefficients of multiple regression b_i, b_{ij} and b_{ijk} are determined by the method of least squares [3], [4], [7] i.e. from the condition that the sum of squared deviations:

$$S = \sum_{i=1}^{N} \varepsilon_i^2 = \sum_{i=1}^{N} (Y_i - \hat{Y}_i)^2 \tag{7}$$

becomes minimal.

The function $S = S(b_i, b_{ij}, b_{ijk})$ will have a minimum only for those values of the variables b_i, b_{ij},i b_{ijk} which are its partial derivatives equal to zero:

$$\frac{\partial S}{\partial b_i} = 0, \quad \frac{\partial S}{\partial b_{ij}} = 0, \quad \frac{\partial S}{\partial b_{ijk}} = 0, \qquad (8)$$

which leads to systems of 3, 6 and 7 equations with 3, 6 and 7 unknown parameters. This system of equations can be reduced to a system of seven normal homogeneous linear equations with seven unknowns. Regression coefficients are calculated from the equation:

$$B = (X'X)^{-1} XY \qquad (9)$$

From data in table 2 matrix X and vector Y are:

$$X = \begin{bmatrix} 0.0 & 0.5 & 0.5 & 0.00 & 0.00 & 0.25 & 0.000 \\ 0.4 & 0.3 & 0.3 & 0.12 & 0.12 & 0.09 & 0.036 \\ 1.0 & 0.0 & 0.0 & 0.00 & 0.00 & 0.00 & 0.000 \\ 0.5 & 0.0 & 0.5 & 0.00 & 0.25 & 0.00 & 0.000 \\ 0.3 & 0.4 & 0.3 & 0.12 & 0.09 & 0.12 & 0.036 \\ 0.0 & 1.0 & 0.0 & 0.00 & 0.00 & 0.00 & 0.000 \\ 0.5 & 0.5 & 0.0 & 0.25 & 0.00 & 0.00 & 0.000 \\ 0.3 & 0.3 & 0.4 & 0.09 & 0.12 & 0.12 & 0.036 \\ 0.0 & 0.0 & 1.0 & 0.00 & 0.00 & 0.00 & 0.000 \end{bmatrix}, Y = \begin{bmatrix} 0.198 \\ 0.352 \\ 6.780 \\ 2.324 \\ 0.743 \\ 2.880 \\ 0.224 \\ 0.604 \\ 16.600 \end{bmatrix}$$

Matrix X′X is:

$$X'X = \begin{bmatrix} 1.840 & 0.580 & 0.580 & 0.236 & 0.236 & 0.108 & 0.036 \\ 0.580 & 1.840 & 0.580 & 0.236 & 0.108 & 0.236 & 0.036 \\ 0.580 & 0.580 & 1.840 & 0.108 & 0.236 & 0.236 & 0.036 \\ 0.236 & 0.236 & 0.108 & 0.099 & 0.036 & 0.036 & 0.0119 \\ 0.236 & 0.108 & 0.236 & 0.036 & 0.099 & 0.036 & 0.0119 \\ 0.108 & 0.236 & 0.236 & 0.036 & 0.036 & 0.099 & 0.0119 \\ 0.036 & 0.036 & 0.036 & 0.012 & 0.0119 & 0.0119 & 0.0039 \end{bmatrix}$$

Vektor X′Y is:

$$X'Y = \begin{bmatrix} 0.00 & 0.40 & . & . & . & . & 0.0 \\ 0.50 & 0.30 & . & . & . & . & 0.0 \\ 0.50 & 0.30 & . & . & . & . & 1.0 \\ 0.00 & 0.12 & . & . & . & . & 0.0 \\ 0.00 & 0.12 & . & . & . & . & 0.0 \\ 0.25 & 0.09 & . & . & . & . & 0.0 \\ 0.00 & 0.036 & . & . & . & . & 0.0 \end{bmatrix} \begin{bmatrix} 0.198 \\ 0.352 \\ 6.780 \\ 2.324 \\ 0.743 \\ 2.880 \\ 0.224 \\ 0.604 \\ 16.600 \end{bmatrix} = \begin{bmatrix} 8.599 \\ 3.675 \\ 18.431 \\ 0.241 \\ 0.763 \\ 0.243 \\ 0.061 \end{bmatrix}$$

Values of inverse matrix $(X'X)^{-1}$ are:

$$(X'X)^{-1} = \begin{bmatrix} 0.640 & -0.153 & -0.153 \\ -0.153 & 0.640 & -0.153 \\ -0.153 & -0.153 & 0.640 \end{bmatrix}$$

$$(X'X)^{-1} = \begin{bmatrix} 0.987 & -0.0115 & -0.0115 & -1.7593 & -1.7593 & 0.2565 \\ -0.0115 & 0.987 & -0.0115 & -1.7593 & 0.2565 & -1.7593 \\ -0.0115 & -0.0115 & 0.987 & 0.2565 & -1.7593 & -1.7593 \\ -1.7593 & -1.7593 & 0.2565 & 18.853 & -0.989 & -0.989 \\ -1.7593 & 0.2565 & -1.7593 & -0.989 & 18.853 & -0.989 \\ 0.2565 & -1.7593 & -1.7593 & -0.989 & -0.989 & 18.853 \end{bmatrix}$$

$$(X'X)^{-1} = \begin{bmatrix} 0.9989 & 0.0005 & 0.0005 & -2.0053 & -2.0053 & 0.0105 & 2.963 \\ 0.0005 & 0.9989 & 0.0005 & -2.0053 & 0.0105 & -2.0053 & 2.963 \\ 0.0005 & 0.0005 & 0.9989 & 0.0105 & -2.0053 & -2.0053 & 2.963 \\ -2.005 & -2.005 & 0.0105 & 23.895 & 4.0525 & 4.0525 & -60.741 \\ -2.005 & 0.0105 & -2.005 & 4.0525 & 23.895 & 4.0525 & -60.741 \\ 0.0105 & -2.005 & -2.005 & 4.0525 & 4.0525 & 23.895 & -60.741 \\ 2.963 & 2.963 & 2.963 & -60.741 & -60.741 & -60.741 & 731.687 \end{bmatrix}$$

Based on the method of least squares from equation (9) values of regression coefficients are:

a) for a linear model

$$B_{lin} = \begin{bmatrix} b_1 \\ b_2 \\ b_3 \end{bmatrix} = \begin{bmatrix} 2.1131 \\ -1.7946 \\ 9.9165 \end{bmatrix}$$

b) for a quadratic model

$$B_{kv} = \begin{bmatrix} b_1 \\ b_2 \\ b_3 \\ b_{12} \\ b_{13} \\ b_{23} \end{bmatrix} = \begin{bmatrix} 6.5284 \\ 2.6600 \\ 16.3430 \\ -13.3042 \\ -32.7144 \\ -33.1010 \end{bmatrix}$$

c) for incomlete cubic model

$$B_{sk} = \begin{bmatrix} b_1 \\ b_2 \\ b_3 \\ b_{12} \\ b_{13} \\ b_{23} \\ b_{123} \end{bmatrix} = \begin{bmatrix} 6.7713 \\ 2.9029 \\ 16.5859 \\ -18.2825 \\ -37.6928 \\ -38.0794 \\ 59.9695 \end{bmatrix}$$

4. CHECKING ADEQUACY OF MODEL

After determining the numerical values of model parameters (regression coefficients), it is needed in the next phase to check the adequacy of selected models. Checks are conducted using **F**-test. The test relies on the following hypotheses:

$$H_0 \ldots b_1 = b_2 = \ldots = b_k = 0; \; H_1 \ldots \exists b_i \neq 0, i = 1, 2, \ldots, k.$$

The claim contains a null hypothesis that neither variable in the regression model was not significant, i.e. that all the parameters of the regression variables are equal to zero. An alternative hypothesis *H1* states that out of the *k* regression variables, there is at least one that is significant in explaining the variability of the dependent variable, i.e. that there is at least one parameter different of zero. For testing is used F-ratio:

$$F = \frac{\frac{SS_R}{\nu_1}}{\frac{SS_E}{\nu_2}} = \frac{\sum_{i=1}^{n}(\hat{y}_i - \bar{y})^2 / k}{\sum_{i=1}^{n}(y_i - \hat{y}_i)^2 / n-k} \qquad (10)$$

where: n – total number of experimental points
k – number of regression coefficients
SS_R – regression sum of squares
SS_E – error sum of squares
ν_1, ν_2 – degrees of freedom

Sums of squares can be calculated using the matrix:

$$SS_R = (\hat{Y} - \bar{Y})'(\hat{Y} - \bar{Y})$$
$$SS_E = (Y - \hat{Y})'(Y - \hat{Y}) \qquad (11)$$

The decision on the adequacy of the model is made based on comparison of empirical values of the size of F and theoretical values of F-distribution. Area of accepting the null hypothesis is $F < F_{\alpha,\nu_1,\nu_2}$. Area of rejection of the null hypothesis is $F > F_{\alpha,\nu_1,\nu_2}$.

Table 3. *Checking the adequacy of the model*

	Model		
	Linear	*Quadratic*	*Inc.cubic*
SS_R	149,452	286,036	290,951
$\nu_1=k$	3	6	7
SS_E	142,0065	5,4230	0,5078
$\nu_1=n-k$	6	3	2
F	2,105	26,373	163,696
$F_{\alpha,\nu 1,\nu 2}$	4,757	8,941	19,353
Adequacy	Model is not adequate	The model is adequate	The model is adequate
$\hat{\sigma}^2$	23,6678	1,8077	0,2539

By accepting the null hypothesis, it is also accepted the assumption that the regression variables in the model are not significant. Otherwise, it is considered that there is at least one of the k regression variables that significantly contributes to explaining of the variability of the dependent variable Y. After calculations with the data from the example for a significance level of α = 0.05, we can conclude that only the linear model is not significant (Table 3).

5. SELECTION OF REGRESSION MODEL

For quality evaluation of the model and a comparison of regression models are available the following statistical and analytical indicators [7]:

- coefficient of determination R^2
- corrected coefficient of determination $\bar{R}^2$
- variance of regression $\hat{\sigma}^2$
- Mallows indicator C_p
- Prediction Sum of Squares Statistic - *PRESS*
- Akaike′s Information Criterion - *AIC*
- Schwartz′s Bayesian Criterion - *SBC*
- Bayes′ Information Criterion - *BIC*
- Amemiya′s Prediction Criterion - *PC*

For the purpose of this study, it was slected criterion is the minimum value of variance regression model, which is calculated as the ratio of residual sum of squares (sum of squared errors SS_E) and the associated number of degrees of freedom $\nu_1=n-k$, ie.

$$\hat{\sigma}^2 = \frac{\sum_{i=1}^{n}(y_i - \hat{y}_i)^2}{n-k} \qquad (12)$$

Statistical representativeness of the model increases with decrease of value of variance regression model and it is logical that between the available models, whose adequacy has been confirmed, the one with the lowest estimate of the variance regression is selected. In the example (Table 3), are adequate quadratic and incomplete cubic model. Incomplete cubic model is better, because it has a smaller value of variance.

Finally, we can write the expression for the selected regression model:

$$\begin{aligned} \hat{y} &= 6.7713X_1 + 2.9029X_2 + 16.5859X_3 \\ &-18.2825X_1X_2 - 37.6928X_1X_3 \\ &-38.0794X_2X_3 + 59.9695X_1X_2X_3 \end{aligned} \qquad (13)$$

6. EVALUATION OF THE SIGNIFICANCE OF MODEL PARAMETERS

Assessment of the significance of the parameter model is reduced to testing of the hypotheses about the significance of the parameter b_j (regression variable X_j). The claim contains a null hypothesis that the parameter b_j is zero, i.e. that the variable X_j in the model is redundant. An alternative hypothesis claims the opposite. For evaluation of significance are available **t**-test or **F**-test because there is a their correlation at the shape $F(1;\nu) = t^2(\nu)$. Hypothesis and decision-making by **t**-test is given in Table 4. Test indicator is an empirical t-ratio

$$t = \frac{\hat{b}_j}{\sigma_{\hat{b}_j}} \quad (14)$$

which is distributed by the Student distribution with $\nu = nk$ degrees of freedom.

Table 4. *Evaluation of significance of parameters by t-test*

Null hypotesis	$H_0 ... b_j = 0$
Alternative hypotesis	$H_1 ... b_j \neq 0$
Acceptance area H_0	$\lvert t \rvert < t_{\alpha/2}$
Rejection area H_0	$\lvert t \rvert > t_{\alpha/2}$

It can also be applied to ***F***-test with a test indicator empirical F-ratio

$$F = \left[\frac{\hat{b}_j}{\sigma_{\hat{b}_j}}\right]^2$$

which has F distribution with $\nu_1=1$ and $\nu_2=n\text{-}k$ degrees of freedom. The decision is made by comparing the empirical values with the theoretical value of F distribution in the familiar way.

Table 5. *Evaluation of the significance of parameters*

$\hat{\sigma}$	C_{jj}	$\sigma_{\hat{b}_j}$	*t*	t_α
0,5039	0,999	0,50363	13,4448	4,303
	0,999	0,50363	5,7638	
	0,999	0,50363	32,9324	
	23,895	2,46317	-7,4223	
	23,895	2,46317	-15,3025	
	23,895	2,46317	-15,4594	
	731,687	13,63026	4,3997	

Standard error of regression coefficient is:

$$\sigma_{\hat{b}_j} = \hat{\sigma}\sqrt{C_{jj}} \quad (15)$$

where: $\hat{\sigma}$ - estimates the standard deviation

C_{jj} – diagonal element of matrix $(X'X)^{-1}$

The group parameters of the model which are insignificant can be excluded from the model without correcting of the values of other parameters that remain significant in the model. Evaluation of the significance of parameters in the selected regression model is shown in Table 5. The value of t_α=4,303 is taken for α=0.05 and $\nu=n\text{-}k=9\text{-}7=2$. It may be noted that all parameters are eligible ($\lvert t \rvert > t_{\alpha/2}$).

7. CONFIDENCE INTERVAL OF PARAMETERS OF MODEL

For information about the precision of parameters of model it is not enough just to make estimation of parameters, but is necessary to determine and limits of confidence interval. These are the limits defined by the general expression:

$$P\left(\hat{b}_j - t_{\alpha,n-k}\sigma_{\hat{b}_j} < b_j < \hat{b}_j + t_{\alpha,n-k}\sigma_{\hat{b}_j}\right) = (1-\alpha) \quad (16)$$

where the following notation is adopted:

$\hat{b}_j$ - estimate the parameters b_j with number

$t_{\alpha,n-k}$ - value ***t*** -distribution for the probability of α and *n-k* degrees of freedom

(1-α) – reliability of evaluation

$\sigma_{\hat{b}_j}$ - standard error of regression coefficient

The values of the interval of evaluation of regression coefficients in the regression model is adopted for the significance level of α=0,05 are shown in Table 6.

Table 6. *Confidence interval of the regression coefficients*

	$\hat{b}_j - t_{\alpha,n-k}\sigma_{\hat{b}_j}$	$\hat{b}_j$	$\hat{b}_j + t_{\alpha,n-k}\sigma_{\hat{b}_j}$
b_1=	4,6043	6,7713	8,9382
b_2=	0,7359	2,9029	5,0698
b_3=	14,4189	16,5859	18,7528
b_{12}=	-28,8807	-18,2825	-7,6843
b_{13}=	-48,2910	-37,6928	-27,0946
b_{23}=	-48,6776	-38,0794	-27,4812
b_{123}=	1,3232	59,9695	118,6158

8. GRAPHIC INTERPRETATION OF MATHEMATICAL MODEL

There is a lot of software for drawing diagrams in a ternary system. However, for our own research needs arising from the cooperation of Mechanical Engineering in Kraljevo and the Technical Faculty in Kosovska Mitrovica, the regression analysis for the three-component system and procedure for obtaining triangular surface plot and respective 2D contour plot of triangular system were developed using MATLAB 2008b software package.

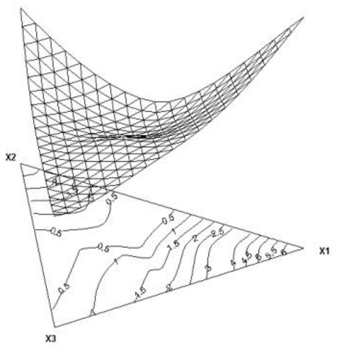

Fig. 3. *3D triangular graph of dependence of the electrical conductivity of the mole fraction of Ga-Sb-Zn*

The mathematical model of the dependence electrical conductivity (in MS/m) of the mole fraction of Ga-Sb-Zn, i.e. from selected parameters X1, X2 and X3 defined by equation (13) is graphically represented with surface triangular graph and its corresponding 2D contour graph in Fig. 3 and Fig. 4.

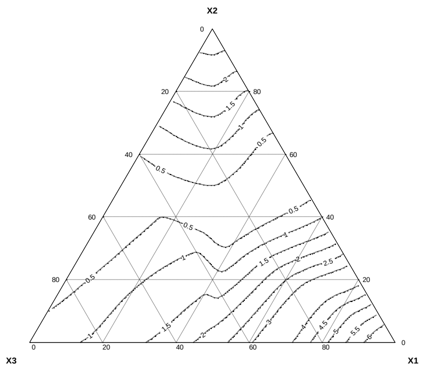

Fig. 4. *2D contour graph of dependence of the electrical conductivity of the mole fraction of Ga-Sb-Zn*

The possibility of obtaining such a graphic display allows easy interpretation of the observed features of the dependence of the dependent variables in the ternary system.

9. CONCLUSION

In the process of exploring of electrical and mechanical properties of alloys, three-component systems play an important role. Regression analysis provides an opportunity to obtain theoretical dependence of the size of the mole fraction of individual components of the mixture. To obtain an adequate regression model, it is necessary to implement the presented methodology.

Application of computers provides the ability to analyze several possible regression models and select one that is the best for description of a given phenomenon. Being that this is a multi-dimensional problem, it is of great importance to visualy display the results with graphic diagrams.

The advantage of a triangular diagram (Ternary graph) is that it can be visualize five dimension problems with the categorized Ternary graph.

10. ACKNOWLEDGEMENTS

The authors wish to express appreciation to the Ministry of Education and Science Republic of Serbia for supporting this research through project TR37020.

REFERENCES

[1.] Conell, *Experiments with Mixtures,*2nd ed., John Wiley&Sons, Inc, New York, 1990.

[2.] Lazić Ž. *Design of Experiments in Chemical Engineering*, Wilez-VCH Verlag GmbH&Co.KGaA, Weiheim, 2004.

[3.] Nenadović M. *Matematička obrada podataka dobijenih merenjem*, Srpska akademija nauka i umetnosti, Beograd, 1988.

[4.] Kolarević M, Rajović.M, Bjelić M. *Ternary graph i njegova primena u regresionoj analizi,* IMK-14 Istraživanje i razvoj, časopis instituta IMK "14 OKTOBAR" - Kruševac, Godina XI, broj (22-23) 3-4, Kruševac 2005, str. 113-122.

[5.] Kolarević M. *Brzi razvoj proizvoda*, Zadužbina Andrejević, Beograd, 2004.

[6.] Minic D, Aljilji A, Kolarević M, Manasijević D, Živković D. *Mechanical and Electrical Properties of Alloys and Isothermal Section of Ternary Cu-In-Sb System at 673 K* High Temperature Materials and Processes. Volume 11(2011), Issue 1-2, Pages 131–138;

[7.] Šošić I. *Primijenjena statistika*, Školska knjiga, Zagreb, 2004.

HEAVY MACHINERY - HM 2011, 7-12
ISBN 978-86-82631-58-3
Paper accepted: 30.05.2011

Comparison of conventional and robotic workplace based on economic and production indicators

Miomir Vukićević[1,*] - Mišo Bjelić[1]- Milan Kolarević[1]- Aleksandra Petrović[1]
[1]University of Kragujevac, Faculty of Mechanical Engineering, Kraljevo

Semi-automatic GMAW process can ensure high quality of welded seams. However, the problem of finding enough qualified welders hit a large number of companies in our industry. A large number of certified welders in recent years were retired or is very close to retirement. On the other hand, a very demanding training for acquiring certificates and the general climate in the country related to mechanical engineering and mechanical engineering industries, have made that fewer and fewer young people opt for this job. The development of robotics in recent years made the welding robots with highly improved performance at significantly lower prices. The same welding process – GMAW process applies at robotic workplace. Advanced software features, ease of programming and improved reliability have made the robotic welding cells represent a solution that is imposed by itself.

Keywords: welding, GMAW process, the robot, costs, productivity

1. INTRODUCTION

Welding is dominant technology that is the used in the production of boilers for central heating of one domestic manufacturer. Preparing of parts is performed on the equipment that provides high-accuracy of measures and shapes, trained welders are engaged, modern semiautomatic GMAW equipment and gas mixtures are used and welding technology is designed by certified engineers.

The interest of the company is to ensure consistency of its product quality, higher productivity and efficiency, higher profits and sales of products to the European market. It is expected that these goals will be achieved in case that finalization of the production would be done by robot.

The structure of costs in the process of welding according to the Lincoln Electric Company, Fig. 1, shows that 80% belong to labor costs and material costs account for 20%. Reducing of these costs, even to a small extent, leading to significant savings and increased profits. Participation of component in the total cost implicitly suggests two possible conclusions:

- materials have very low rates (and additional supplies), or
- very high cost of labor.

The aim of this study is to determine this relationship in our environment and whether it is justified to apply robots, i.e. to assess conditions in which their use is justified.

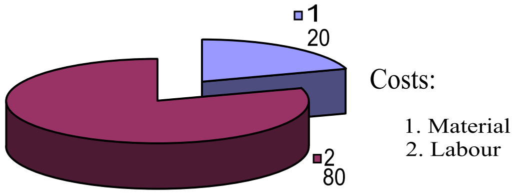

Fig. 1. Structure of welding costs [1]

2. COST ANALYSIS

Operating expenses are monitored by constant reviewing of the costs level in the following segments:

- training of welders,
- overtime work,
- shielding gases,
- filler material (NJ / kg),
- workspace (NJ/m^2)
- safety equipment,
- ventilation,
- control of welded joints,
- scrap and finishing of parts,
- other costs.

It is desirable to constantly monitor level and transormation of costs and to bilance it for each business year (calendar), because it creates the basis for determining the strategy for the future. Of course, the current changes are used for prompt actions. Still, important decisions need knowledge of the state of costs for longer period of time. Decision to install a robot can not be made based on consideration of the current level

[*]Corr. Author's Adress: Faculty of Mechanical Engineering, Dositejeva 19, Kraljevo, Serbia, vukicevic.m@mfkv.kg.ac.rs

of costs. The shortest period is one year, but it is not reliable if the management does not follow the trends over a longer period of time and if not realize the prediction of changes in the near or distant future.

Table 1 shows the reduced cost structure in terms of application of welding equipment for semi-automatic GMAW. Shown structure does not explicitly take into account all the cost elements listed in the previous chapter, because it starts from the fact that they do not change significantly.

Table 1. Costs structure for GMAW welding.

No.	Label	Equation		Value	Note/Description
1.	ℓ			34 m	Length of all boiler's weld seams
2.	m			250 kg	Mass of one boiler
3.	m_{dm}	$0.05 \cdot m$	$0.05 \cdot 250$	8 kg	Mass of filler material for one boiler
4.	m_{dm1}	m_{dm}/ℓ	8/34	0.235 kg/m	Mass of filler material per 1m of weld seam
5.	C_{dm}			75 NJ/kg	Price of filler material
6.	T_{dm1}	$m_{dm1} \cdot C_{dm}$	$0.235 \cdot 75$	17.63 NJ/m	Costs of filler material per 1m of weld seam
7.	V_{gm}	$k \cdot V_b$	$1.8 \cdot 40$	72 ℓ	Consumption of gas mixture, V_b=40 ℓ volume of gas tank
8.	C_b			2650 NJ	Price of full tank of gas mixture
9.	C_{b1}	C_b/V_b	2650/40	66.25 NJ/ℓ	Price of 1 ℓ of gas mixture
10.	T_{gm}	$V_{gm}/\ell \cdot C_{b1}$	$72/34 \cdot 66.25$	140.29 NJ/m	Costs of gas mixture per 1m of weld seam
11.	NS			190.25 NJ/h	Costs of welder per one hour of work
12.	Pr			20 m/smena	Productivity of welder per shift
13.	Pr_1	Pr/8	20/8	2.5 m/h	Productivity of welder
14.	T_{r1}	NS/P_{r1}	190.25/2.5	76.1 NJ/m	Costs of welder per 1m of weld seam
15.	T_1	$T_{dm1}+T_{gm}+T_{r1}$	17.63+140.29+76.1	234.02 NJ/m	Unit costs of weld seams per 1m
16.	T_{pa}	$T_1 \cdot \ell$	$234.02 \cdot 34$	7956.68 NJ	Production costs for all seams

The typical cost elements are:

- T_{dm1} = 17.63NJ/m - Cost of filler material per 1 m of weld seam (7.53%),
- T_{gm} = 140.29 NJ/m - Cost of gas mixture per 1 m of weld seam (59.95%)
- T_{r1} = 76.1 NJ/m - Labour costs per employee per 1 m of weld seam (32.52%)
- T_1 = 234.02 NJ/m - unit costs for a weld seam made by semi-automatic process (100%).

Figure 2. which is made based on these data, shows that the cost of materials (filler and consumables) constitute 40.05% of the total cost, which is twice the value of one wich is shown in bilance on Figure 1. The reasons for these differences are in a lower cost of human labor in our conditions. On the other hand, costs of filler materila are four times lower than the cost of protective atmosphere.

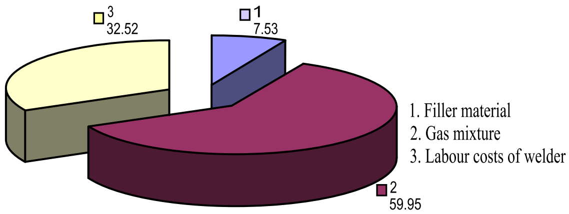

Fig. 2. Structure and participation of costs for production of all weld seams made by GMAW

Half of length of the boiler seams can be made by robot. The costs of such variants of the boiler production are shown in Table 2. Since the length of seams that are made in this way, it is normal that the same would happen with the cost of semiautomatic GMAW(implemented by welders). Unit costs of filler materials and gas mixtures are not significantly changed since the implementation of the robot does not change amount of deposit and gas mixture which are consumed per unit of seam length. Although the robot can achieve greater welding speed, practically it is not feasible considering the technological capabilities (speed of dissolution of materials, metallurgical reasons).

Integrated cost T_{IT} = 9513.37 NJ, column 17 in Table 2, are calculated by superposition of costs that belong to the conditions of manual and robotic technology implementation, when one half of seam lengtheach is carried out by each of them. There is an obvious increase in the absolute amount of costs compared to those that are typical for a human workplace (T_{PA} = 7956.68 NJ, column 16, Table 1). This increase is not negligible (16.36%) and it is particularly pronounced when it is determined for the entire one-year series.

Table 2. Welding costs for classic and robotic GMAW

No.	Label	Equation		Value	Note/Description
1.	T_1				Costs of GMAW per 1m of weld seam
2.	ℓ			17 m	Length of seams made by semiautomatic GMAW
3.	T_{pa}	$T_1 \cdot \ell$	234.02·17	3978.34 NJ	Costs of seams made by semiautomatic GMAW
4.	ℓ_R			17 m	Length of seams made by robot
5.	m_{dm}			4 kg	Mass of filler material for robor
6.	m_{dm1}		4/17	0.235 kg/m	Mass of filler material per 1m of weld seam
7.	T_{dm1}	$m_{dm1} \cdot C_{dm}$	0.235·75	17.63 NJ/m	Costs of filler material per 1m of weld seam
8.	V_{gm}	$k \cdot V_b$	0.9·40	36 ℓ	Consumption of gas mixture, V_b=40 ℓ volume of gas tank
9.	C_b			2650 NJ	Price of full tank of gas mixture
0.	C_{b1}	C_b/V_b	2650/40	66.25 NJ/ℓ	Price of 1 ℓgas mixture
1.	T_{gm}	$V_{gm}/\ell_R \cdot C_{b1}$	36/17·66.25	140.29 NJ/m	Costs of gas mixture per 1m of weld seam
2.	NS_R			6400 NJ/h	Costs of robot per one hour of work
3.	ν_R	0.5m/min		30 m/h	Robot welding speed
4.	T_{R1}	NS_R/ν_R	6400/30	213.33 NJ/m	Costs of robot per 1m of weld seam
5.	$T_{\{1}$	$T_{dm1}+T_{gm}+T_{R1}$	17.63+140.29+213.33	371.25 NJ/m	Unit costs of weld seam made by robot
6.	T_R	$T_{R1} \cdot \ell_R$	371.25·17	6311.25 NJ	Costs of weld seams made by robot
7.	T_{IT}	$T_R + T_{pa}$	6311.25+3978.34	10289.59 NJ	Costs of weld seams production using integrated technologies (semiautomatic+robot) per boiler

Typical elements of cost for robotic workplace:

T_{dm1} = 17.63 NJ / m – Costs of filler materials per 1m of seam length (4.75%, a), or 2.9%, b))

T_{gm} = 140.29 NJ / m - Costs of gas mixture per 1m of seam length (37.79%, a), or 23.18%, b))

T_{R1} = 213.33NJ / m - Costs of robot per 1m of seam length (57.46%, a), or 35.24%, b))

T_{S1} = 371.25 NJ / m - Unit costs achieved by applying robots per 1m of seam length (100%, a))

T_{r1} = 234.02 NJ / m - Labour costs per employee per 1m of seam length (38.66%, b))

T_{IT} = 10289.59/17 605.27 = NJ / m - Cost of integrated technology of boiler production (100%, b))

Fig 3a. clearly shows increase of the material costs share in total costs compared to those shown at Fig 1 (filler and consumables material). Robot costs in relative comparation (57.46%) are less than the cost of human labor (59.95, Figure 2). However, the absolute amounts of human labor unit costs are lower for almost three times (76.1 NJ / m, Table 1) compared to the absolute amount of unit work costs of robot (213.33 NJ / m, Table 2). Production of all seams in terms of combinations of human and robotic work, Figure 3b shows that the share of materials is still larger than those which is shown in Figure 1 (26.8% vs. 20%), and that, for the same amount of work, labor costs of welder (35.24%) lower than the work costs of robots (38.66%).

Fig 3. Structure and participation of costs at boiler seams production at robotic workplace (a) and at both workplaces (b)

3. ANALYSIS OF PRODUCTIVITY

In essence, productivity is defined as the number of processed workpieces per unit time, [1]. Following analysis is conducted in accordance with this definition. Table 3 shows systematized indicators of productivity in case when all seams are made by GMAW procedure implemented on conventional workplace (welder). Table 4 contains data on productivity in two cases. When the robot is applied for production of half the length of boiler seams (A) and when applied for production of all seams (B), i.e. in case when welders are completely excluded from the production.

If, however, unchanged number of welders would be involved in the production of half the total length of seams on the boiler, then in one year they could twice as much boilers or N_{z2} = 13,920 units / year. In this case, the second half of seams would be made at robotic workplace, table 4A. For one year it could weld total amaounts of boilers N_R = 13,875. It is obvious that in analyzed company similar studies has led to employed number of welders. They can work in one shift or multiple shifts, but can not produce more units than what is calculated. Working in over shifts provides less investment costs in the company.

Table 3. Elements of productivity for classic workplace

No.	Label	Equation		Value	Note/Description
1.	n			40	Number of engaged welders
2.	L_z			20 m/smena	Length of weld seams made by welder per shift
3.	ℓ_R			34 m	Length of weld seams made by robot per boiler
4.	ν_z	L_z/t	20/8	2.55 m/h	Welding speed (welder)

No.	Label	Equation		Value	Note/Description
5.	n_{kz}	$\nu_z \cdot n/\ell$	2.55·40/34	3 kom/h	Number of boilers which cam be made by 40 welders for an hour
6.	N_{kz1}	$n_{kz} \cdot 8$	3·8	24 kom/dan	Number of boilers per day
7.	t_z			290 dana	Number of working days for welder
8.	N_z	$N_{kz1} \cdot t_z$	24·290	6 960 kom/god	Annual production of boilers

Table 4. Elements of productivity for robotic workplace

No.	Label	Equation			Value		Note/Description
			A	B	A	B	
1.	n_R				1	1	Number of robots
2.	ℓ_R				17 m	34 m	Length of weld seams made by robot per boiler
3.	ν_R	0.5 m/min			30 m/h	30 m/h	Welding speed
4.	η_R				90%	90%	Robot efficiency (annual)
5.	t_R	$\eta_R \cdot 24$	0.9·24	0.9·24	21.6 h	21.6 h	Effective working time of robot per day
6.	n_{kR}	ν_R/ℓ_R	30/17	30/34	1.76 kom/h	0.88 kom/h	Number of boilers made by robot per hour
7.	N_{kR1}	$n_{kR} \cdot t_R$	1.76·21.6	0.88·21.6	38.016 kom/dan	19.0588 kom/dan	Number of boilers made by robot per day
8.	t_{Rg}				365 dana	365 dana	Number of working days per year
9.	N_R	$N_{kR1} \cdot t_{Rg}$	38.016·365	19.0588·365	13 875 kom/god	6956 kom/god	Number of boilers made by robot per year

4. EPILOGUE

These data suggest the following conclusions.

1. At the total bilance of the welding cost, European / American relations of work and material, there is not significant differences than at us. - pictures 1 and 2

2. Use of robots is not profitable, i.e. substitution of human labor in conditions of relatively low salaries of workers (comparison of absolute amounts of the costs in Tables 1 and 2).

3. Even less profitable is complete substitution of human labor by two robots that are based on data obtained from column 16, Table 2 (TR = 2 · 6311.25 = 12622.5 NJ). The cost of one boiler would be 36.96% higher than the price of the boiler-made by semi-automatic GMAW.

4. The integrated operation of robots, which produces NR = 13,875 pcs / year boilers, and semi-automatic GMAW (40 welders working and producing N = 2 · 2 · Nz = 6960 = 13,920 pcs / year) achieved twice as much productivity compared to those when only welders works.

5. Substitution of all welders with two robots (production without people), would gain to productivity of $N = 2 \cdot 2 \cdot N_R = 13{,}875 = 27{,}750$ units / year, which is almost four times higher than if all seams are produced only by welders.

ACKNOWLEDGMENTS

Authors wish to acknowledge their gratitude to Ministry of Education and Science of Republic of Serbia for the support to the research through project grant TR37020.

5. REFERENCES

[1] Lincoln Electric
[2] Radojević, Z.: "Organizacija i ekonomika zavarivačkih radova", Zavod za zavarivanje, Beograd
[3] Nesti}, D.: "2. Bilješka o proizvodnosti– definicija, mjerenje i povezanost s politikom plaća", Privredna kretanja i ekonomska politika 101, str. 55 do 74, 2004
[4] Jovanović, M., Adamović, D., Lazić, V., N. Ratković: "Gasno zavarivanje–priručnik", Mašinski fakultet, Kragujevac, 2006
[5] Lukić, B.: "Tehnologija zavarivanja u praksi", Izdavački centar PP "IR–MIR", Užice, 200

HEAVY MACHINERY - HM 2011, 13-16
ISBN 978-86-82631-58-3
Paper accepted: 30.05.2011

Numerical simulation of welding parameters influence on temperature field during GMAW welding.

Mišo Bjelić[1,*] - Miomir Vukićević[1] – Milan Kolarević[1]– Aleksandra Petrović[1]
[1] University of Kragujevac, Faculty of Mechanical Engineering, Dositejeva 19, 36000 Kraljevo

Welding is the dominant method for joining materials by indissoluble bond in most industrial applications. The trend of automation and robotisation of welding processes is exponential, so the continued development requires understanding and modeling of welding parameters influence on the distribution of power in the electric arc, heat and mass transfer in the welding area and the geometry and structure of the weld. In this article, the results of temperature field simulations are interpreted for different values of input parameters. The influence of heat input, welding speed, thickness of welded plates, the coefficient of efficiency of electric arc and type of base material on the temperature field i.e. geometry of molten pool and HAZ during welding is shown.
Keywords: welding, simulation, temperature field, GMAW process

1.INTRODUCTION

Simulation modeling and analysis are the processes of creating and experimenting with mathematical models of physical processes adapted for computer use. System in this sense can be understood as a set of interrelated elements which give proper output based on input data. Systems that can be simulated are very different and thus may include simulation modeling of manufacturing systems, transportation systems, services, etc. Modeling of welding process is very complex and difficult considering nonlinearity and complexity of welding processes, and requires knowledge of several areas of science.
Development of simulation models on the macroscopic level is a thermo mechanical problem that involves temperature distributions, displacements, stresses and strains. At the microscopic level there are problems of phase transformation and microstructure of materials. Interaction of essential factors for the development of simulation models in welding is shown in Fig. 1.
Influence of microstructure and mechanical strain on the process of heat transfer during welding is not great but the reverse effect of the heat exchange process at the micro-structure of the welded joint and the stress-strain conditions is very important. In order to simplify the model, model shown in Fig. 1 does not include the impact of flow of molten metal on the process of heat transfer, microstructure and stress and

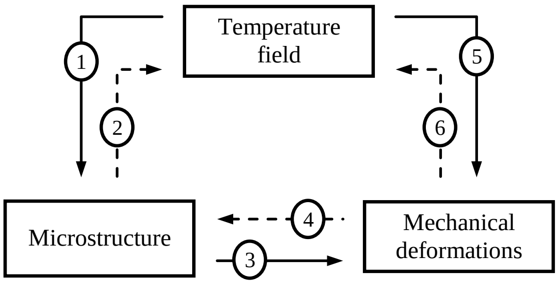

Fig 1. Interaction of factors [10]

strain states during the welding process. Velocity of transformations (development of microstructure of welds and heat affected zone) depends on the thermal welding cycle:

1. latent heat,
2. phase transformation,
3. velocity transformation,
4. thermal expansion,
5. plastic deformation.

In the field of welding process modeling there are three basic approaches:

1. Analytical models
2. Numerical models
3. Experimental models

2. MODEL OF HEAT TRANSFER

This article shows a numerical model that was developed based on partial differential equations of heat transfer. Finite difference and finite element method can be used to obtain solutions which include complex geometry of welded parts, more complex initial conditions, the de-

*Corr. Author's Adress: Faculty of Mechanical Engineering, Dositejeva 19, 36000 Kraljevo, Serbia, bjelic.m@mfkv.kg.ac.rs

pendence of physical properties of materials on the temperature, the effect of latent heat of melting, etc...

Process of heat transfer during welding is a very complex problem. Its solution is associated with a number of difficulties related to the dependence of physical properties of welded materials on the temperature, the complexity of boundary conditions, the selected arc model, etc... Obtaining analytical solutions is conditioned by a number of simplifications of the model which results in less accurate solution. To obtain more reliable solutions it is necessary to use numerical methods. Partial differential equation of heat transfer during welding of thin sheets [5] is given below:

$$\frac{\partial T}{\partial \tau} = \frac{\lambda}{c \cdot \gamma}\left(\frac{\partial^2 T}{\partial x^2} + \frac{\partial^2 T}{\partial y^2}\right) + \frac{q_l}{c \cdot \gamma \cdot t} - \frac{h_{uekv}}{c \cdot \gamma \cdot t}\left(T - T_a\right)$$

c – Specific heat capacity, J/kgK
γ - Material density, kg/m^3
λ - Thermal conductivity, W/mK
q_l – heat effect of arc, W/m^2
T_a – ambient temperature, K

Using finite differences, equation (1) becomes:

$$T_{i,j} = A\left(T_{i-1,j} + T_{i+1,j} + T_{i,j-1} + T_{i,j+1}\right) + \\ + B\left(T_{i+1,j} - T_{i-1,j}\right) + Cq_l + D$$

where coefficients A, B, C, D are equal to:

$$A = \frac{2\alpha}{8\alpha + 2b\delta^2} \qquad B = \left(\frac{v\delta}{8\alpha + 2b\delta^2}\right)$$

$$C = \frac{2a\delta^2}{8\alpha + 2b\delta^2} \qquad D = \frac{2b\delta^2}{8\alpha + 2b\delta^2}T_a$$

3.NUMERICAL SIMULATION

The shape and size of the molten pool influence on the mechanics and kinetics of crystallization and therefore structure and properties of the weld. Together with the shape and size of the heat affected zone, they affects at the formation and size of residual stress and strain. Understanding the impact of heat transfer and distribution of temperatures on the size and format of such zones has a crucial impact on the understanding, prediction and control characteristics of the weld. The shape and size of the molten pool depends on material properties, welding speed and heat input and can be measured from isotherms obtained by simulation. In order to show the influence of certain parameters on the formation of temperature fields during welding i.e. influence on geometric characteristics and properties of the weld, comparative results of simulations for different values of individual parameters are shown at Figures 2. to 9. The influence of five different parameters: welding speed, thickness of welded plates, efficiency of electric arc and type of welded materials Characteristic isotherms are especially prominent for easy visual comparison. isotherms for 100, 300, 500, 800 ° C are shown.

Figures 2. and 3. shows influence of welding speed on temperature distribution at top surfaces of welded steel sheets. In both cases the simulation was done for the power source q = 3 kW while the welding speed in the case shown in Figure 2. is v = 4 mm / s, and in the case shown in Figure 3. is v = 8 mm / s. It can be seen that increasing of welding speed leads to a narrowing of the characteristic isotherm and consequently it can be concluded that the width of the weld and heat affected zone compared to the speed of welding are in inverse relationship. This phenomenon is due to the fact that increasing of welding speed while keeping other parameters constant leads to reduction in line energy of the heat source. In the area in front of the heat source, there is a compression of isotherms as a result of the increase of welding speed. This actually means that the temperature gradient in the zone in front of the heat source increases with increasing of source speed. This increase in gradient may be explained by the fact that the welding speed exceeds the speed of heat transfer from the zone of welding.

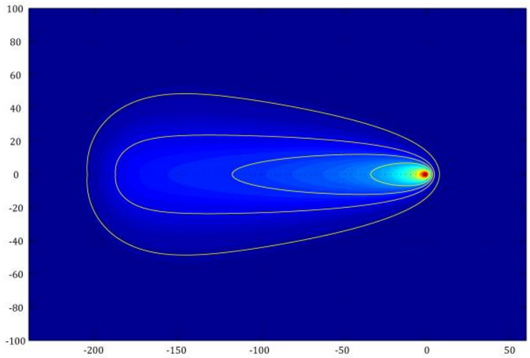

Fig. 2. Influence of welding speed, v=4mm/s

HEAVY MACHINERY - HM 2011, 13-16
ISBN 978-86-82631-58-3

Paper accepted: 30.05.2011

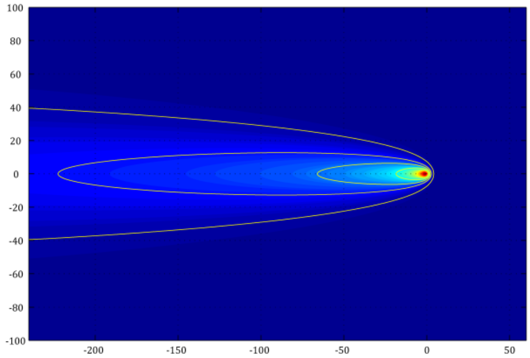

Fig. 3. Influence of welding speed, v=8mm/s

Figures 4. and 5. show the influence of sheet thickness on the temperature field. In both cases the simulation was done for the power source q = 3 kW and welding speed v = 8 mm / s. Thickness of the sheets in the simulation shown in Figure 4. is 3 mm, while in the simulation shown in Figure 5. is 6 mm. From the pictures can be seen that increasing of the thickness leads to a narrowing and shortening of the characteristic isotherms.

This phenomenon occurs because of increased volume of material. Due to the increased mass, at the same power and same welding speed, the amount of heat that can be given to unit of mass decreases. Likewise, the temperature gradient in the zone behind the heat source is higher in case of welding of thicker sheets. Results of simulation lead to conclusion that the smaller thickness of welded sheets under the same conditions results in higher weld seam width and greater width of the HAZ.

Figures 6. and 7. show the effect of arc efficiency coefficient η. The simulation was done for the power source q = 3 kW and welding speed v = 8 mm / s while η was varied between 0.65 and 0.85. Itmay be noted that due to the increase of the coefficient of arc efficiency leads to stretching and enlargement of typical isotherms, and that the temperature gradient behind the heat source is higher in case of smaller value of η. These changes come from the fact that increasing the arc efficiency coefficient leads to increase in the effective amount of heat generated by arc.

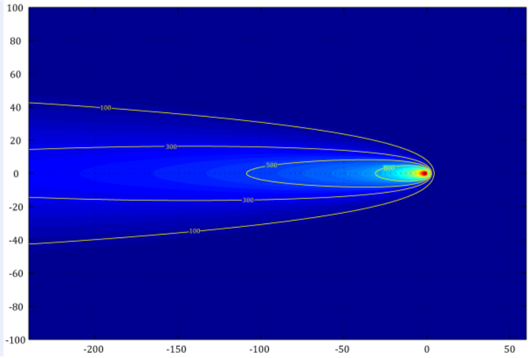

Fig. 4. Influence of sheet thickness, δ=3 mm

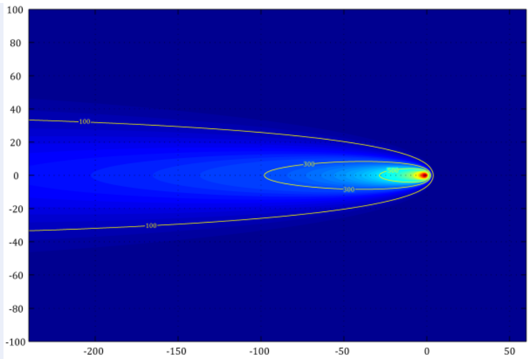

Fig. 5. Influence of sheet thickness, δ=6 mm

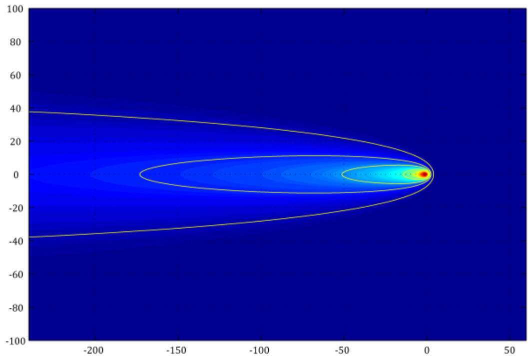

Fig. 6. Influence of arc efficiency, η=0.65

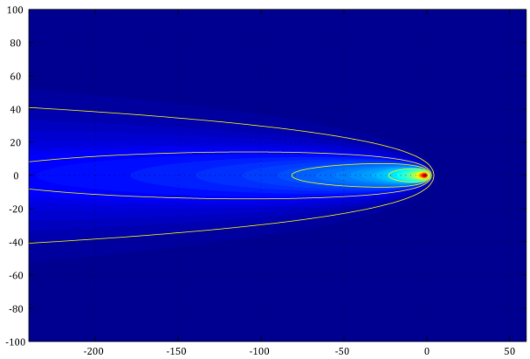

Fig. 7. Influence of arc efficiency, η=0.85

*Corr. Author's Adress: Faculty of Mechanical Engineering, Dositejeva 19, 36000 Kraljevo, Serbia, bjelic.m@mfkv.kg.ac.rs

Performed simulations indicate that the width of the weld seam and HAZ increase with increasing portof arc efficiency.

Figures 8. and 9. show the influence of the type of welded material for power source q = 3 kW and welding speed v = 8 mm / s. Materials used in the simulations are aluminum and low carbon steel. Simulation for aluminum welding shows that isotherms are much shorter and wider, and its shape is more elliptical than circular as in welding of low-carbon steel. In the area in front of the heat source, temperature gradient is lower during welding of aluminum sheets, while in the area behind the heat source temperature gradient is higher. These phenomena are due to the large difference in thermal conductivity of these two materials, ie, a consequence of the much larger thermal conductivity of aluminum compared to the low carbon steel. The weld seam and the HAZ during welding at the same conditions are wider at aluminum welding, i.e. they are proportional to the thermal conductivity of the material that is being welded.

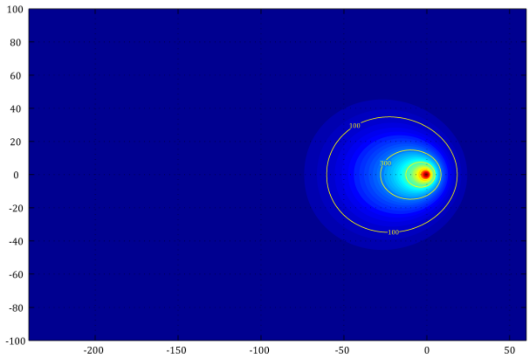

Fig. 8. Influence of welded material, Aluminum

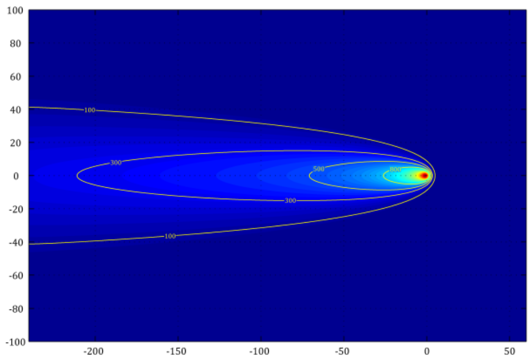

Fig. 8. Influence of welded material, Steel

4.CONCLUSIONS

Simulation models together with the corresponding experimental procedures are the basis for better understanding of the impact of welding parameters on the geometry of the weld and HAZ's. Based on the simulation results we can conclude that each of these parameters during arc welding of thin sheet metal have a significant impact on the temperature field in welded sheets and the geometry of the weld and HAZ's. Combination of simulation models and methods of artificial inteligence represents a solid base for formation of appropriate control systems.

ACKNOWLEDGMENTS

Authors wish to acknowledge their gratitude to Ministry of Education and Science of Republic of Serbia for the support to the research through project grant TR37020.

5. REFERENCE

[1] Goldak A. J., Akhlaghi M., Computational welding mechanics, Springer, New York, 2005.

[2] Lindgren E. L., Numerical modelling of welding, Computer methods in applied me¬c¬hanics and engineering (195) 6710–6736, Elsevier Applied Science, 2006.

[3] Özişik Necati M., Heat Conduction, Wiley-IEEE, 1993.

[4] Schäfer M., Computational Engineering – Introduction to Numerical Methods, Sprin¬ger, New York, 2006.

[5] Bjelić M., Simulacija temperaturskog poqa pri zavarivanju tankih limova MAG postupkom, Magistarska teza, Mašinski fakultet, Kraljevo, 2009

HEAVY MACHINERY - HM 2011, 17-23
ISBN 978-86-82631-58-3
Paper accepted: 30.05.2011

Calculation of failure criticality in Reliability - Centred Maintenance

Branko Radičević [1,*] - Zoran Petrović[1]– Slobodan Ivanović[1] - Margarita Georgieva[2]
[1] University of Kragujevac, Faculty of Mech. Engineering Kraljevo
[4] VTU „Todor Kableshkov“ Sofia

The paper presents methodology for calculation of criticality of failure of components of technical systems in reliability-centred maintenance. Criticality of failure is complex function that depends on the adopted criteria: safety, standstill duration, quality of system functions during the malfunction, total costs and frequency of failures. Depending on characteristics of the analyzed system, the criteria for calculation of criticality may be extended or reduced, and the degree of their influence may be increased or decreased. The proposed methodology is applied to the case of pump station for water supply.

Keywords: Criticality, RCM, FMECA, Risk Priority Number, Pump station

0 INTRODUCTION

The majority of modern maintenance strategies contain RCM (Reliability Centred Maintenance) analysis. Many authors classify RCM into maintenance strategies.

The leading theorist of RCM (Reliability Centred Maintenance) methodology, John Moubray, defined RCM as a process that is essentially the same as FMECA (Failure Modes, Effects and Criticality Analysis). The difference is that in it the manufacturer sums up its knowledge about potential failures and RCM summarizes several years of experience of operators and those who maintain the equipment.

The analysis of mode and effects of failures (FMCA) is the procedure for the estimation of reliability of the device in all phases of its operating circle, which is based on observing all potential failures of items and their effects on the device. FMEA is a systematical technique and formal help in thinking which enables the weak places in technical system known from the experience, the potential failures, consequences and risks, to be seen on time, and to be brought into the process of decision making together with measures of corrective maintenance

By identifying characteristics of technical systems and quantitative assessment of factors of occurrence, the consequences and nondetection of the cause of failure, with the risk priority index - R (Risk Priority Number - RPN), the identification of the weak and the risky places in the system is enabled. Risk priority index for all causes of potential failure modes is obtained by multiplying the partial values of risk factors. In this way calculated values of risk factor R are compared with critical values of RPN, which is determined by common consent of FMEA team.

1. RCM ANALYSIS

Before commencing a comprehensive RCM analysis and defining of requirements, it is necessary to establish a detailed catalog of technological systems that are the subject of maintenance, as well as conducting detailed familiarization with the production process. After implementation of these two necessary steps, for each of the defined technological systems it is necessary to ask the seven basic questions / requests of RCM conception and provide detailed answers for each one of them.

These seven questions are:

1. Which functions of equipment are essential in the current exploitation?
2. Which equipment failures can occur?
3. What are the causes of failure?
4. What happens when there is a failure?
5. How important is each failure?
6. What can be done to prevent a failure?
7. What to do, if you can not find a suitable preventive action?

1.1 Effects of failure modes in RCM

After making the list of failure modes for each of the components of the system and finding a functional dependence between all failure

[*]Corr. Author's Adress: Faculty of Mech. Engineering Kraljevo, Dositejeva 19, Kraljevo, Serbia, radicevic.b@mfkv.rs

modes of components and functional failures, it is necessary to determine the impact of each failure mode at the local level, system level and the level of the plant. Such decisions are not at all simple, so that is why logic tree of decisions shown in Figure 1 is used.

In this way classified failure modes can be placed in one of the three branches of the logic tree (algorithm, figure 1): EVIDENT, SAFETY andOUTAGE. Classification of the effects of failure modes according the logic tree of decisions classifies each failure mode to one of four groups:

A - safety problem
B - problem of outage
C - minor (insignificant) economic problem
D - hidden failure

From this analysis, given the huge number of combinations that can occur when the failure modes and their causes are concerned, once again the necessity for forming a database of failures is confirmed.

2. FMEA AND FMECA ANALYSIS

FMEA is a basic process for qualitative assessment of the reliability of technical systems. Logical continuance of FMEA is quantifying of appropriate values relating the failure of the elements of technical systems and review of criticality. Upgrading of FMEA, related to the assessment of the degree of criticality of components to the system or mission of the system is called criticality analysis (Criticality Analysis CA) [4,5]. By the term criticality it is usually meant a relative measure of consequences of failure modes, and frequency of its occurrence. The joint analysis of FMEA and CA is called the analysis of failure modes, effects and criticality (Failure Modes, Effects and Criticality Analysis - FMECA). All general considerations regarding FMEA, also apply to FMECA, because this method is the continuation of the previous one.

By systematic monitoring of the failure of elements and forming of a database, a basis for the application of the FMECA process is created. In this way one can reach the necessary conclusions for the enactment of corrective measures to remedy the detected deficiencies. Existing standards relating to the FMEA method are different from each other. The differences are, depending of the standards, more or less expressed. Frequently it comes to the form for documenting of FMEA, terminology, labeling of certain values and so on.

3. RISK PRIORITY NUMBER

In accordance with the above mentioned all potential failure modes should be quantified against the possibility of failure, significance of the consequences and appropriated measures for verification of the potential causes of failure. The evaluation is done through the factors of the risk of failure R_1, consequences of failure R_2, and nondetection of the cause of failure R_3, based on expert assessments of people from the FMEA team.

The values of the risk factors are usually ranked by number in the interval of 1. At the risk factor of failure R1, and severity of consequence R2, smaller numbers indicate a lesser and larger numbers greater probability of failure, i.e. severity of consequences of failure. With factor of nondetection of the cause of failure R_3, smaller numbers correspond to larger and larger numbers to smaller possibility to detect the failure. If the description of the established situation is between two values on the scale, as a choice of risk factor it is recommended to adopt higher value. The probability of failure (Probability of Failure - PF) in the exploitation of technical systems is the probability that the suitable potential cause of failure will result in a failure of components or the system. Existence of a failure cause by itself does not mean the automatic occurrence of the failure.

The probability of failure is measured by factor of the occurrence of failure R_1, based on the adopted qualitative and quantitative criteria. Depending on the frequency of failure in the literature there are recommendations for the values of risk factor R_1, [4].

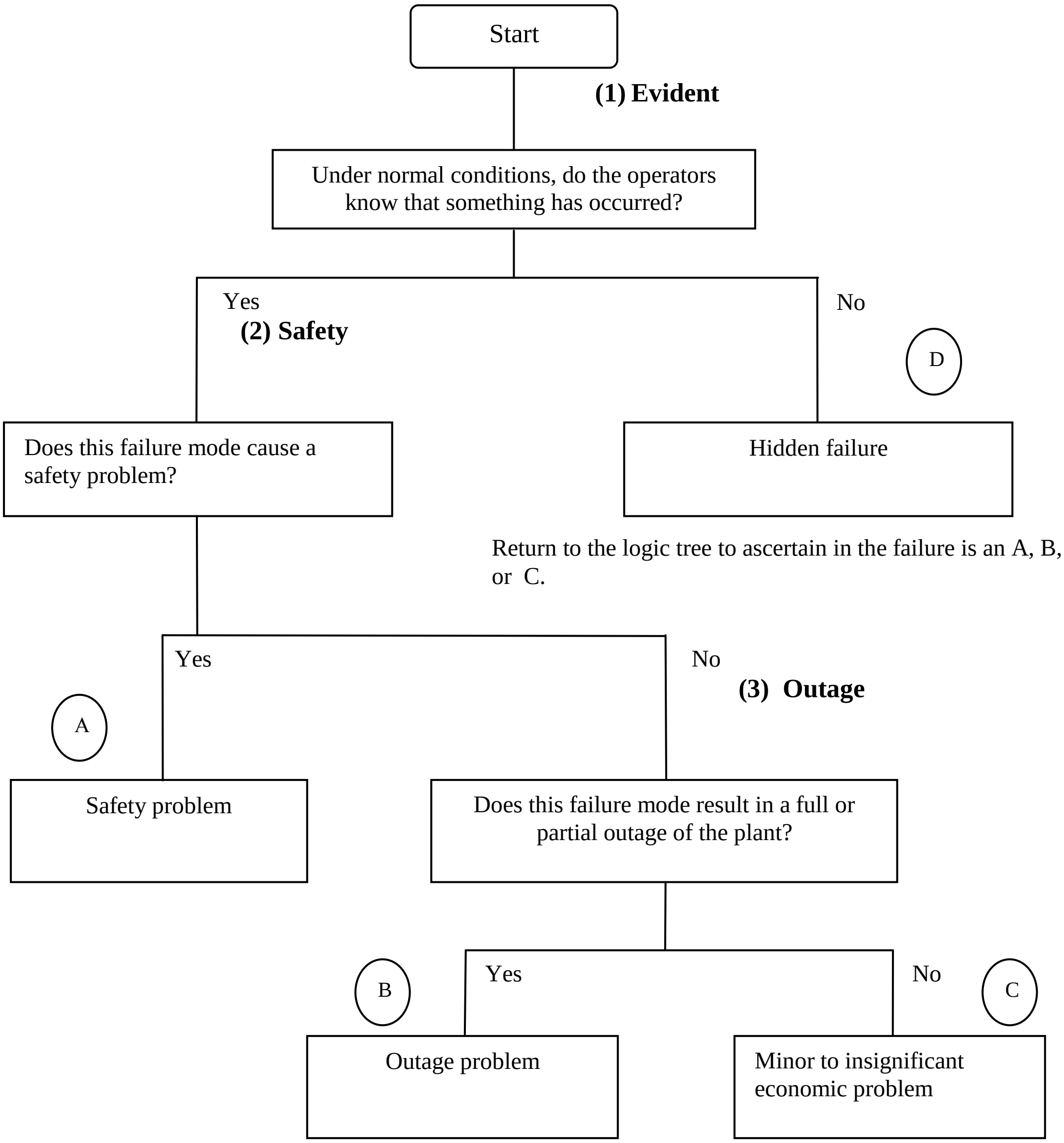

Fifure 1. Logic tree analysis structure

Severity of the consequences of failure (Failure Demerit Value - FDV) is a measure of the impact of potential failure modes of components of the considered system on the working capacity of the system, the user and/or surroundings . While considering the significance of the results of failure, the violation of binding legislation must be taken into consideration. The consequences of failure are usually described by the effects on the user of the technical system. Risk factor values of consequences occurrence R2, are obtained through the analysis of a number of works in this field, by taking the specificity relating to the maintenance-oriented approach for reliability. For each technical system in which FMEA analysis is conducted it is necessary to establish its own criteria, by adhering some general principles [4].

The probability of discovering the causes of failure (Probability of Failure Remedy - PFR) is an estimate of the ability to check the technical systems, detection of the potential disadvantages before the system is put into operation (risk factor R_3).

By identifying characteristics of technical systems and quantitative assessment of factor occurrence, the consequences and nondetection of the failure cause, with the risk priority number - R (Risk Priority Number - RPN), the identification of the weak and risky places of the system is enabled. Risk priority number for all causes of potential failure modes is obtained by multiplying the value of the risk of failure factor R_1, occurrence of the failure consequences R_2, and nondetected failure causes R_3. Value of R, defined in this way, shows the relative priority of importance of individual causes of failure. Based on the above, the risk priority number of *k* cause of *j* failure mode of *i* element of each pair of the causes of failure – failure, is calculated using the equation:

$$R(i,j,k)= R_1(i,j) \cdot R_2(i,j) \cdot R_3(i,j,k) \qquad (1)$$

where:

R1(i,j) – value of the risk of occurrence

R2(i,j) – value of risk factor of failure consequences

R3(i,j,k) – value of the risk factor for nondetection of causes of failure mode of element

In this way, the calculated R values of risk factors are compared with critical values of R_{krit}, determined in common consent by the FMEA team by using table 1 [4].

Table 2 Overall risk rating

S.No.	Mark	Total risk R
1.	Low	1÷50
2.	Medium	50÷100
3.	High	100÷200
4.	Critical	200÷1000

If the individual values of all the causes of failure modes of components are $R < R_{krit}$, the discussed solution is rated satisfactory. Otherwise, for all potential causes of failure modes, whose values are $R > R_{krit}$, it is necessary to propose and implement appropriate preventive and corrective measures to reduce the value of some or all of the risk factors R_1, R_2, and R_3. In defining and implementing these measures, priority should be given to component failure modes and their causes with the highest value of R.

3.1 Risk Priority Number in RCM

The methodology for determining the risk priority index which is given in the Section 3, relates primarily to FMECA in the phase of designing and production of technical systems. Since RCM is actually FMECA in operation of technical systems, the same methodology as in the FMECA can be adopted for determining the risk priority number in RCM analysis. Since it is a phase of exploitation of technical means, the value of the risk factors of nondetection of causes of failure modes of element R_3 is much smaller than in the stages of designing and production. Therefore, a risk factor R3 in the equation (1) can be neglected. [1]

$$R(i,j,k)= R_1(i,j) \cdot R_2(i,j) \qquad (2)$$

where:

R_1(i,j) – value of the risk of failure (failure rate)

R_2(i,j) – value of risk factor of consequence occurrence

Given the above, the criticality of any failure mode in RCM analysis can be written as:

$$K = F \cdot(B + Z + Q + T) \qquad (3)$$

Where:

K – Criticality of failure mode; F - Frequency of failure mode; B – Safety; Z – Standstill; Q – Quality; T - Total costs

Table 2 Assessment of frequency

Frequency	F
Daily	10
Weekly	9
Monthly	8
At intervals of 1 to 12 months	7
Yearly	6
At intervals of 1 to 5 years	5
At intervals of 5 to 10 years	4
Rarely, for example, 1 x in 10 years	1

Table 3 Values of risk factors of consequence occurrence

Consequences	Risk factor

Safety (B)	
Casualties	20
Disability	18
Severe injuries	14
Minor injuries	6
No injuries	0
Standstill (Z)	
Standstill $\geq$ 7 days	10
Standstill 3 to 7 days	9
Standstill 1 to 3 days	8
Standstill 1 day	7
25% of capacity	6
50% of capacity	4
75% of capacity	2
Without influence	0
Quality (Q)	
Completely unacceptable	10
Acceptable - improvement needed	5
Without influence	0
Total Costs (T)	
Costs $\geq$ 5000 EUR	10
Costs 1250÷5000 EUR	8
Costs 500÷1250 EUR	6
Costs 250÷500 EUR	4
Costs 100÷250 EUR	2
Costs < 100 EUR	1

Factor of frequency of failure mode F, is among the risk factors R1, and other factors (B, Z, Q, T) belong to the group of factors of occurrence of failure consequence risk R_2.

4. DETERMINING THE CRITICALITY OF FAILURE ON THE EXAMPLE OF PUMP STATION

Water from the well is pumped using two centrifugal pumps that are installed on a pedestal and connected for parallel operation on a common pressure and suction line.

As a drive pumps use the standard three-phase asynchronous motors. With the pump with controlled flow, control work is performed by microprocessor of frequent controller.

Chlorination system is designed to ensure that the chlorinated installation is under vacuum, i.e. that the lower part of the installation is under gage pressure.

Notice for failure m ode according to Equation(3) can be determined by RPN. Critical component is defined as the sum of all RPN failure related to the component.

Table 4 shows the ranking of states according to the cancellation RPN.

Table 4

Failure mode #	**Failure Mode**	**Component**	**Category of the FM**	**RPN**
1.34.01	chlorine leak at the entrance to the vacuum regulator	Vacuum regulator	A	195
1.35.01	chlorine leak on the chlorine valve	Valve for chlorine	A	195
1.33.02	partially interrupted flow of chlorine	Vacuum hose	B	192
1.39.02	dirty or clogged filter	Free chlorine analyer	C	168
1.07.08	distorted pump shaft	Centrifugal pump	B	135
…	…	…	…	…

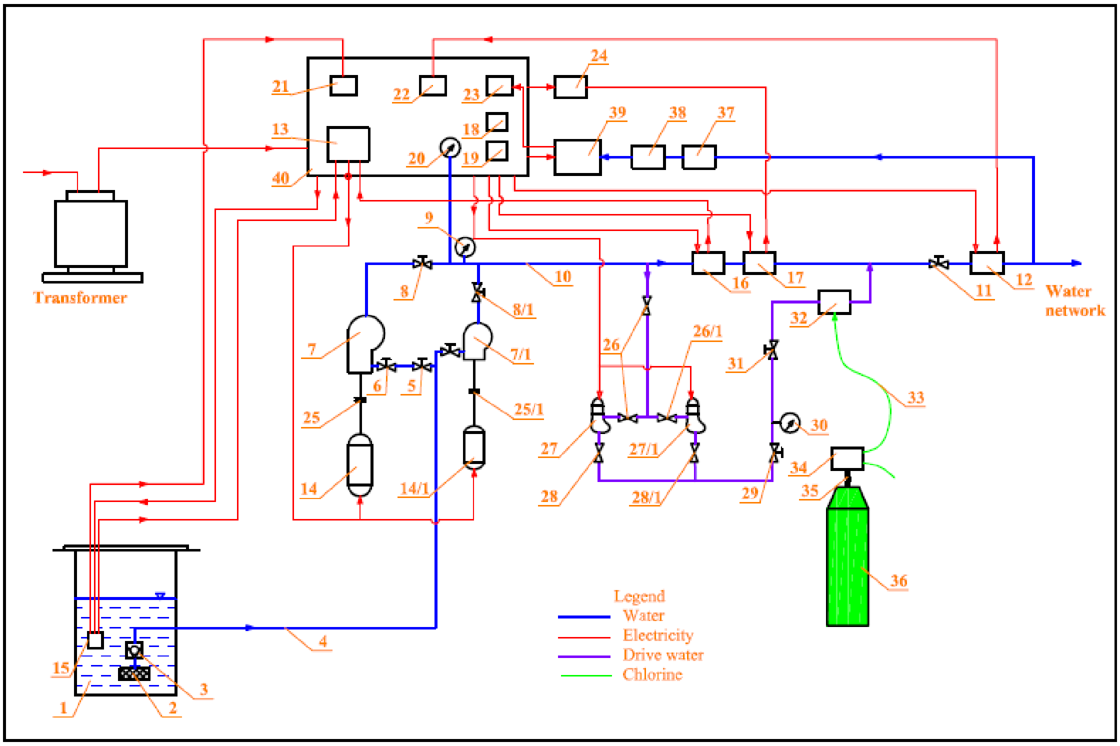

Fig. 2. *Pump station for water supply*

Pumping station consists of the following basic components(Figure2):
1 - well, 2 – suction chamber, 3 - irreversible valve, 4 - suction pipeline, 5 - valve on the suction branch, 6-tap of the pipeline for filling; 7-centrifugal pump, 8-valve on the pressure pipeline, 9-pressure gauge, 10 pressure pipeline, 11-valve V2, 12-flow meter, 13-frequent regulator, 14-motor, 15-hydrostatic level sensor, 16-pressure transducer, 17-flow transducer, 18-switch with indicator of centrifugal pump; 19 - switch with indicator for booster pump operation, 20-sensor for pressure in the pressure pipeline, 21-sensor for water level in the well; 22-sensor of flow in the pressure pipeline, 23- sensor of chloral level 24- flow indicator; 25-connector, 26-gate valve ; 27-booster pump, 28-valve Z3, 29-valve on the pressure branch of the water flow, 30-gauge of water flow, 31 - valve V3, 32-injector, 33-vacuum hose, 34-vacuum regulator, 35-valve for chlorine ; 36-bottles for chlorine; 37-flow regulator of chlorine analyzer; 38 - pressure regulator of chlorine analyzer; 39-analyzer of free chlorine, 40-distribution cabinet.

Critical components of the pumping station is given in Table 5.

Table 5

Component #	**Component**	**Criticality K**
1.14	Electromotor	1404
1.34	Vacuum regulator	970
1.07	Centrifugal pump	967
1.39	Free chlorine analyer	497
1.32	Injector	486
…	…	…

The number of components to the overall risk assessment is shown in Table 6.

Table 6.

S.No.	Mark	Number of components
1.	Low	10
2.	Medium	10
3.	High	9
4.	Critical	11

5. CONCLUSION

By identifying characteristics of technical systems and quantitative assessment of factors of occurrence, the consequences and nondetection of the cause of failure, with the risk priority index - R (Risk Priority Number - RPN), the identification of the weak and the risky places in the system is enabled.

Criticality rating islogical continuation of the RCM analysis. The proposed modified method for determining the critical components of technical systems is easy to apply in the RCM methodology.

Acknowledgement

"Two of the authors (B.R.) and (Z.P) wishes to acknowledge his gratitude to <Ministry of Education and Science of Republic of Serbia> for the support to the research through project grant TR37020."

6. REFERENCES

[1] Radičević B., Master thesis „Računarska podrška održavanju orijentisanom ka pouzdanosti“, The Faculty of Mechanical Engineering Kraljevo, Kraljevo, 2009

[2] Radičević B., Petrović Z., Kolarević M., Dinić M. “The analysis of mode, consequences and criticality at potential failure of gear pump”, VI Triennial International Conference HEAVY MACHINERY HM 2008 MF Kraljevo, 2008

[3] Petrović Z., Radičević B., Vukićević M., Bjelić M., „Klasifikacija aktivnosti održavanja na bazi RCM-a na primeru pumpnog postrojenja“, IMK “14 OCTOBER“, Year XV, Issue (30-31) 1-2/2009, Krusevac, 2009

[4] Ćatić D., „Metode pouzdanosti mašinskih sistema“, The Faculty of Mechanical Engineering Kragujevac, , 2009

[5] Petrović Z., Radičević B., „Održavanje i dijagnostika – zbirka zadataka“, The Faculty of Mechanical Engineering Kraljevo, Kraljevo, 2009

HEAVY MACHINERY - HM 2011, 25-30
ISBN 978-86-82631-58-3

Paper accepted: 30.05.2011

Module for update of technological parameters in postprocessor generator of NC programs in flexible manufacturing system

Slobodan Ivanović*, Ljubomir Lukić[1]
[1] University of Kragujevac, Faculty of Mechanical Engineering Kraljevo

In accordance with changes of input parameters, functional and procedural machining conditions in flexible manufacturing system and there are large problems in completing of technological demands during production process. Changes of machining regimes and/or tools in NC programs are leading up to changes of machining times and production costs, therefore it is necessary to execute an optimization of production process before NC program executing.

NC programs are generated for working pieces spectrum, afterwards alternative tools are defined for each operation and all of alternative machining regimes are defined for each alternative tool according to technological database or knowledge base.

Keywords: Flexible manufacturing system, Database, NC program.

0 INTRODUCTION

Change of technological demands during production process brings to change of total production time that leads up to change of machining regimes and/or cutting edges on all of machining centres in flexible manufacturing system. This change is founded on knowledgebase that contains limits of machining regimes for tools and materials from technological database. For every place in magazine tool of machining centre is assigned one or more tools that results with an array of combinations of alternative tools for use in NC programs for machining of assortment of working pieces on one machining centre. According to alternative tools for each place in magazine tool called from NC program here are created all of combinations of alternative tools in machining centre magazine tools and all of combinations of alternative machining regimes for those tools. For each of those combinations are computed machining regimes and criterions for estimating of technological demands completion. If technological demands are completed, changes are updating in NC programs, but if technological demands are not completed, procedure is repeating from assigning of technological demands. Postprocesor generator of NC programs has task to update generated NC programs. Update refers to changes of values of cutting feed and spindle speed widh keeping all of rest kinematic and techonological parameters.

I FUNCTIONAL MODEL OF POSTPROCESSOR GENERATOR OF NC PROGRAMS IN FLEXIBLE MANUFACTURING SYSTEM

According to pallet contents, system configuration and technological database (materials, tools, machining regimes) CAM system generates NC programs (Fig.1.). Parameters from initial NC programs are transforming into NC tables (into technological database tables). In accordance to alternative tools for each place in magazine tool called from NC program, all of combinations of alternative tools and of alternative machining regimes for those tools are creating. Machining regimes and criterions for estimating of technological demands completion are computing for each of those combinations. If technological demands are completed, changes are updating in NC programs and NC programs are ready for executing. If technological demands are not completed, procedure is repeating from assigning of technological demands until meeting of technological demands.

CAD and CAM modules are required in system only during generating of initial NC programs. In all of next repetitions of generating of NC programs, procedure is repeating from computing of machining regimes and criterions, also in case of change of number of machining centres or number of pallet contents.

*Corr. Author's Address: Faculty of Mechanical Engineering Kraljevo, Dositejeva 19., Kraljevo, Srbija, bboby@sbb.rs

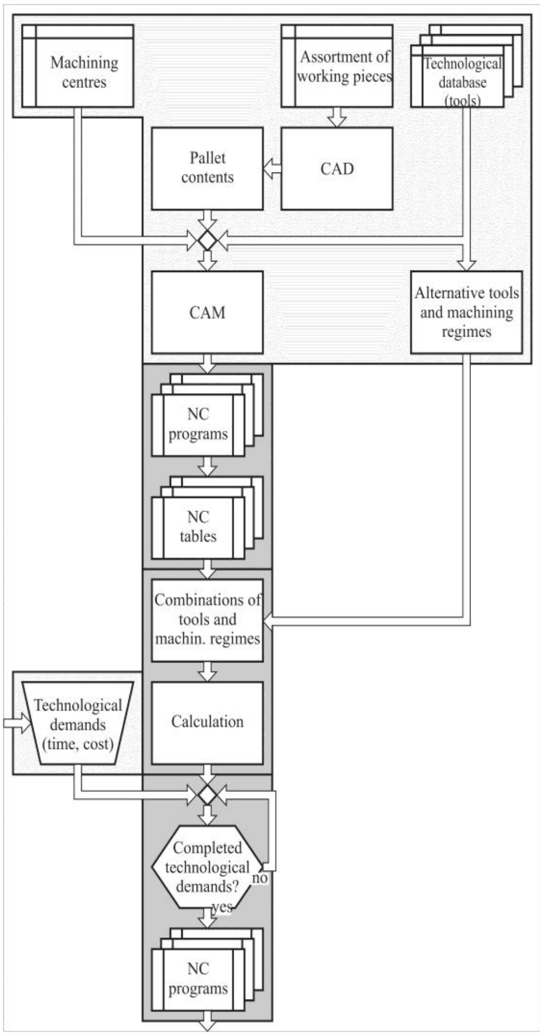

Fig.1. Designed flow of NC programs generating

Assigning of technological demands is executing when database is completed and prepared for browsing and searching. Whereas, NC programs are input and output from postprocessor generator NC programs (Fig.2.) and in constantly processing.

System configuration, pallet contents, technological database and assigned technological demands are parts of control module. Reading data from NC programs and their transformation to NC tables, and writing changed data into NC programs are execiting in input-output module. Creating of combinations of alternative tools and allowed machining regimes, and calculation are part of variant module.

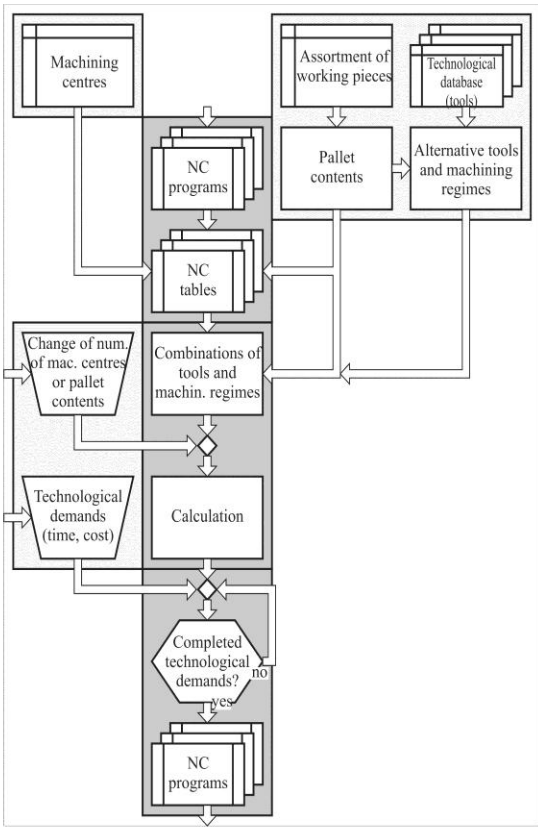

Fig.2. Modules of postprocessor generator NC programs u flexible manufacturing system

Therefore, input-output module is module for update of technological parameters in postprocessor generator of NC programs in flexible manufacturing system.

II UPDATE PARAMETERS IN NC PROGRAMS

Update of technological parameters in NC programs is, in fact, change values of machining regimes in program words with values of machining regimes from selected configurations. Selected configuration of tools in accordion to assigned criterions

$$K_{j,h}^{a} = \{b_{j,1,h} \quad b_{j,2,h} \quad \cdots \quad b_{j,i,h} \quad \cdots \quad b_{j,m_j,h}\}$$

$$K_{j,h,d}^{o} = \{K_{j,1,h,d}^{o} \quad K_{j,2,h,d}^{o} \quad \cdots \quad K_{j,i,h,d}^{o} \quad \cdots \quad K_{j,m_j,h,d}^{o}\}$$

,

$$\kappa^{o}_{j,i,h,d} = \begin{Bmatrix} \varpi_{j,i,1,h,d} \\ \varpi_{j,i,2,h,d} \\ \vdots \\ \varpi_{j,i,l,h,d} \\ \vdots \\ \varpi_{j,i,r_{j,i},h,d} \end{Bmatrix}$$

$$h,d: \quad t^{z}_{j,h,d} = t^{z}_{j} \ \wedge \ C^{z}_{j,h} = C^{z}_{j} \ \wedge \ \varphi^{pa}_{j,h,d} = \varphi^{u}_{j}$$

are assigning to tools in magazine tools with arrays

$$\tau_j = \{t_{j,1} \quad t_{j,2} \quad \cdots \quad t_{j,i} \quad \cdots \quad t_{j,m_j}\}$$

that are using for machining in operations

$$\omega_{j,1} = \begin{Bmatrix} o_{j,1,1} \\ o_{j,1,2} \\ \vdots \\ o_{j,1,l} \\ \vdots \\ o_{j,1,r_{j,1}} \end{Bmatrix}, \qquad \omega_{j,2} = \begin{Bmatrix} o_{j,2,1} \\ o_{j,2,2} \\ \vdots \\ o_{j,2,l} \\ \vdots \\ o_{j,2,r_{j,2}} \end{Bmatrix}, \ldots$$

$$\ldots \ \omega_{j,i} = \begin{Bmatrix} o_{j,i,1} \\ o_{j,i,2} \\ \vdots \\ o_{j,i,l} \\ \vdots \\ o_{j,i,r_{j,i}} \end{Bmatrix}, \quad \ldots \ \omega_{j,m_j} = \begin{Bmatrix} o_{j,m_j,1} \\ o_{j,m_j,2} \\ \vdots \\ o_{j,m_j,l} \\ \vdots \\ o_{j,m_j,r_{j,m_j}} \end{Bmatrix}$$

Arrays for tool places in NC tables remains unchanged, and machining regimes

$$\varpi_{j,i,l,h,d} = \left(s_{j,i,l,h,d}, n_{j,i,l,h,d}\right) = \left(s_{obr}, n_{obr}\right)$$

are assigning to corresponding NC program blocks that contain program word begins with S, or word begins with F:

$$b^{NC}_{i} = n_{obr} \rightarrow f('S'), 'S' \exists \, b^{NC}_{i}$$
$$b^{NC}_{i} = s_{obr} \rightarrow f('F'), 'F \exists \, b^{NC}_{i}$$

where:

$f('S')$ - is evaluation of spindle speed

$f('F')$ - is evaluation of cutting feed

b^{NC}_{i} - is i^{th} program block

Only values of spindle speed and cutting feed are updating in NC programs, and all of other parameters are remaining unchanged because of structures of initial NC programs are staying unchanged

III SOFTWARE MODULE FOR UPDATE PARAMETERS IN NC PROGRAMS

This program module is a part of input-output module of postprocessor generator of NC programs in flexible manufacturing system. Selected configurations of tools are using for update machining regimes in NC programs located in ASCII files and update is executing in this module.

First, in accordion to machining centre, configuration of tools and variation of machining regimes in database (Fig.3.) software is searching for corresponding values of generated machining regimes for each tool and operation (Fig.4.). Afterwards, in accordion to marks of NC programs and tools in magazine tools of machining centres and corresponding operations in initial NC tables (Fig.5.), software is changing values of spindle speed and cutting feed with new values (Fig.6.).

Finally, in accordion to number of program rows (blocks), that values are placing into corresponding program words, respectively into words are beginning with letters „F“ or „S“ (Fig.7.).

IV CONCLUSIONS

The choice of optimal parameters of manufacturing process represents the choice of optimal configurations of tools (sets of tools and variation of machining regimes) in accordion to three criterions: total time required for machining of assigned assortment of working pieces, total tools costs for machining of assigned assortment of working pieces and blunting coefficient of magazine tools. One of these three criterions represents primary, and rest are secondary criterions. The choice can be executed on interactive way, from group of tools configurations meeting assigned technological demands, or automaticaly, the best marked tools configuration by postprocessor, for each machining centre.

Updated NC programs are downloading from host computer to control units of machining centres with new values of machining regimes.

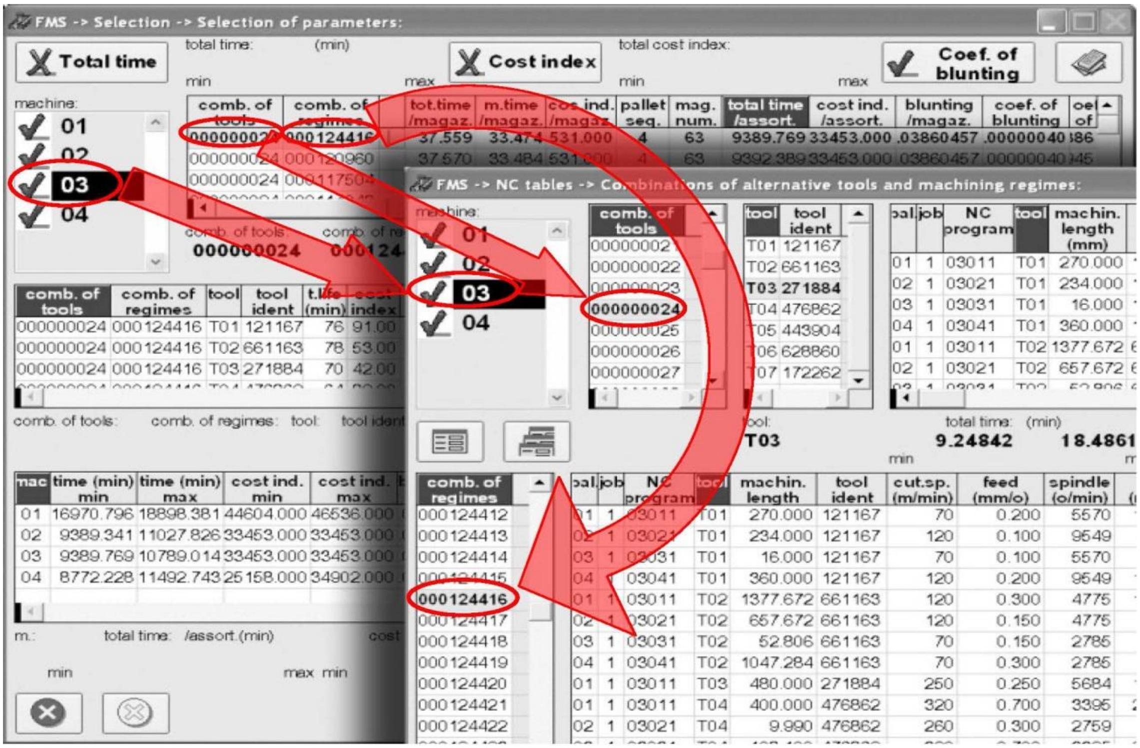

Fig.3. Browse of generated tools configuration

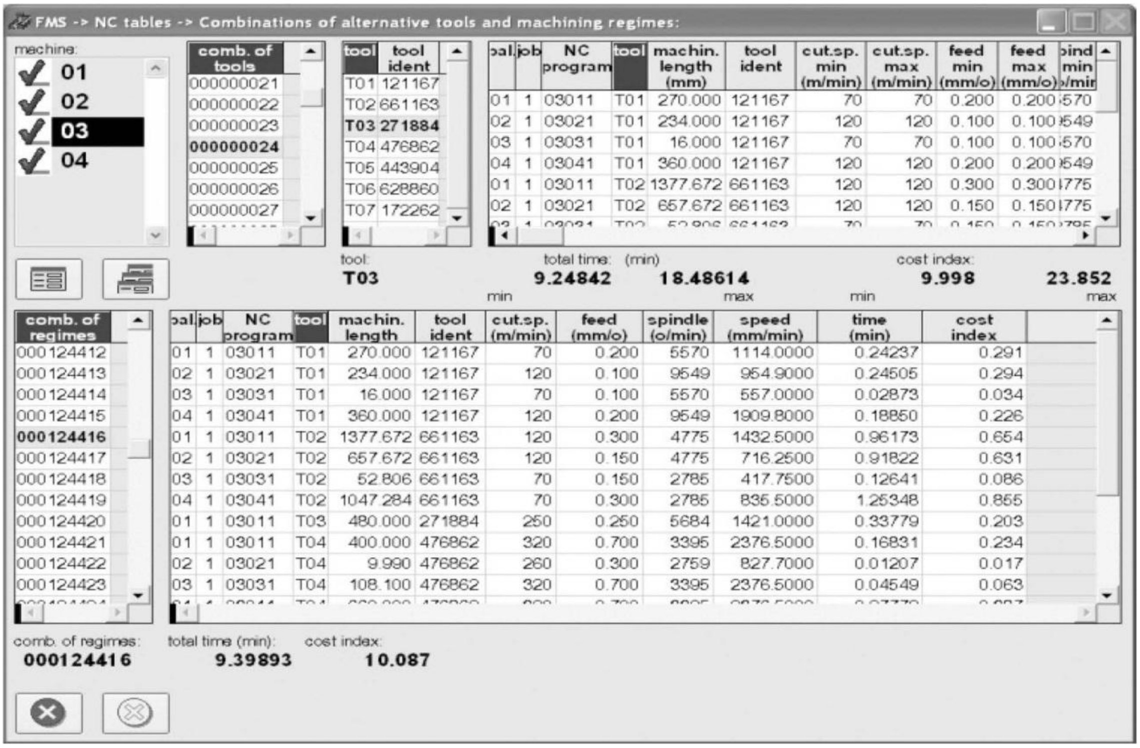

Fig.4. Generated tools configuration

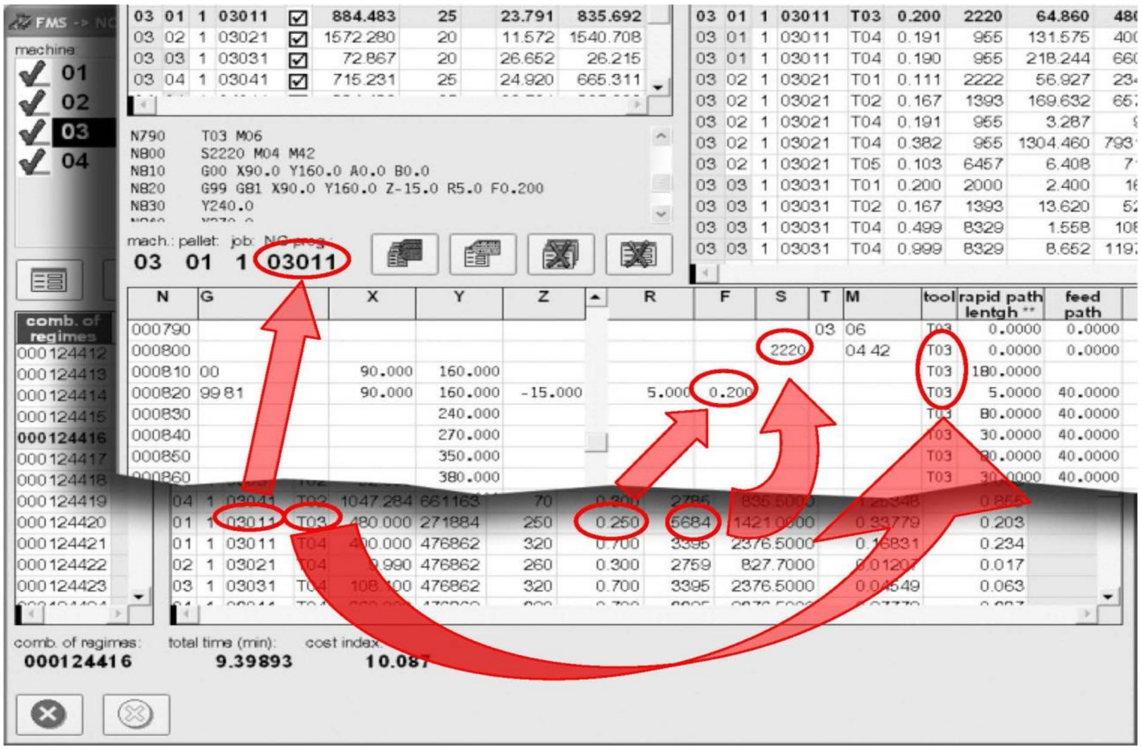

Fig.5. Update of NC tables

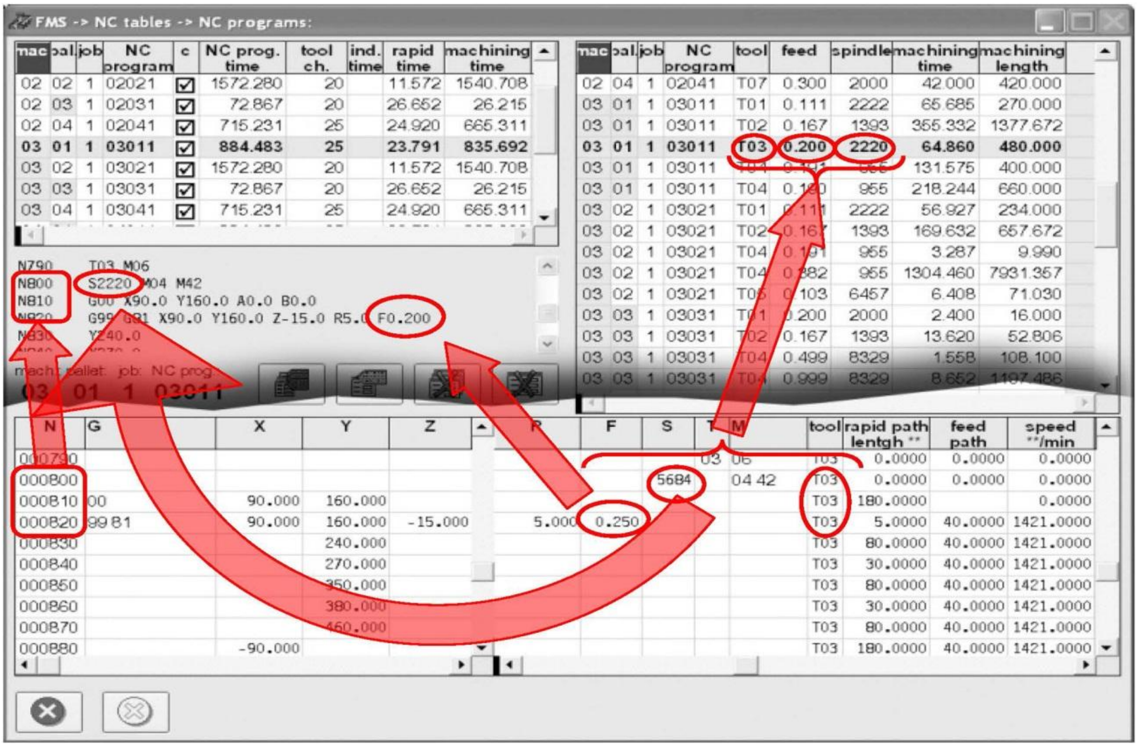

Fig.6. Update of NC programs

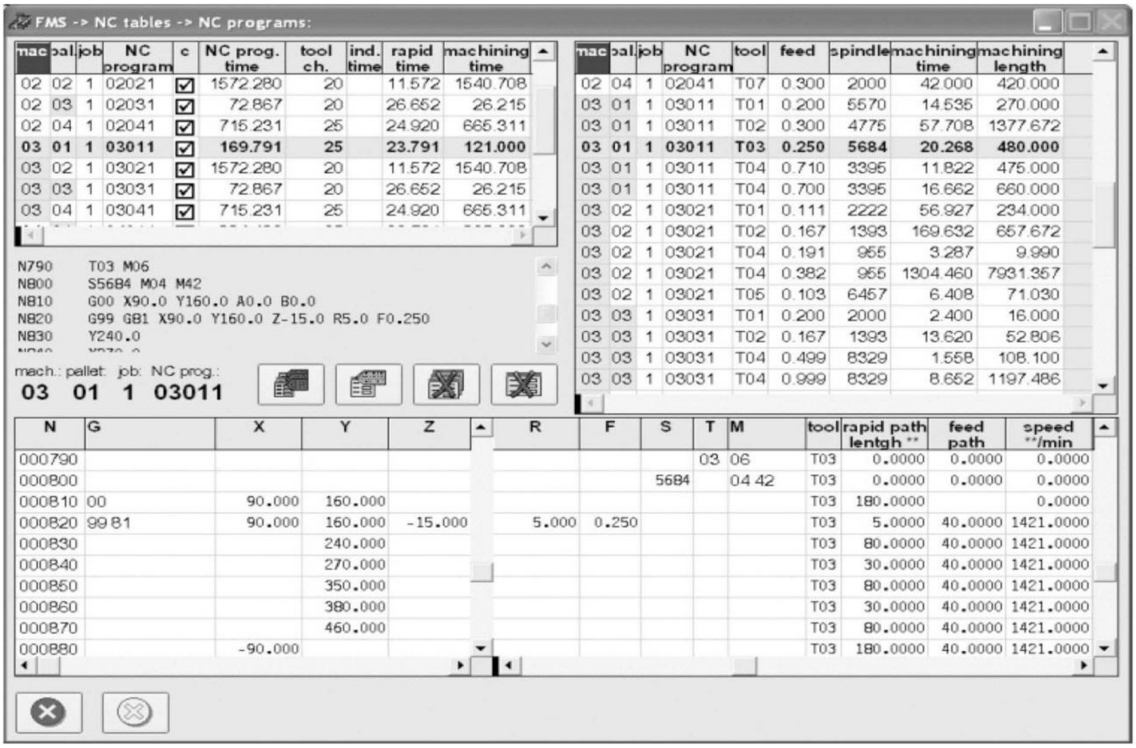

Fig.7. Updated NC programs and NC tables

V REFERENCES

[1] Lukić Lj., Ivanović S. - Postprocessor generator of CNC programs in the flexible technologies - 8th International Conference on Flexible Technologies MMA 2003, Novi Sad, June 2003.

[2] Ivanović S., Lukić Lj. - Database design from techonological and kinematic parameters of NC program for production in flexible manufacturing system - The Sixth Triennial International Conference HM 2008, Mataruška Banja, 26.-29.06.2008.

[3] Ivanović S., Lukić Lj., Petrović Z. - Database reconfiguring in flexible manufacturing system according to parameters of NC program - IMK-14 Research and Development - Journal of Institute IMK "14. Oktobar" Kruševac, No (28-29) 1-2/2008, October 2008.

[4] Ivanović S., Petrović Z., Đapić M., Lukić Lj. - Functional model of postprocessor generator of NC programs in flexible manufacturing system - IMK-14 Research and Development - Journal of Institute IMK "14. Oktobar" Kruševac, No (30-31) 1-2/2009.

[5] Ivanović S., Petrović Z., Lukić Lj., Đorđević Lj. - Tool system of postprocessor generator of NC programs in flexible manufacturing system - IMK-14 Research and Development - Journal of Institute IMK "14. Oktobar" Kruševac, No (30-31) 1-2/2009.

HEAVY MACHINERY - HM 2011, 31-36
ISBN 978-86-82631-58-3

Paper accepted: 30.05.2011

Foodstuffs Machine Harmonization with EU Regulations

Vladimir Zeljkovic[1,*] - Milos Veselinovic[2] - Mirko Djapic[3] - Ljubomir Lukic[3]
[1] LOLA Institute, Belgrade
[2] NTIM TEHNOLOGY, Belgrade
[3] University of Kragujevac, Faculty of Mechanical Engineering, Kraljevo

Some aspects of foodstuffs machinery harmonization with EU regulation and Directive are presented in this paper. Machinery Directive 2006/42/EC, Annex I define tow parts as: part 1. General essential health and safety requirement applicable to all machinery and part 2.1. The supplementary essential health and safety requirement for foodstuffs machinery. Also, harmonized standards gives more details about design, concept, hygiene requirements, verification. As an example we present some of results in the harmonization "SOLARIS 1" which is intended for drying fruits, vegetable, medical herbs, spices and mushrooms.

Keywords: EU Directives, Foodstuffs Machinery, Conformity Assessment, Food Quality.

0 INTRODUCTION

The requirements for products that could be ready and could satisfy European Union market requirements depend on whether products are included in the technical legislation of the New Approach or not. If the products are in frame of the technical legislation than the product conformity assessment is defined in eight modules due to Council Decision of European Union for product conformity assessment. These products pass through the so called "mandatory" procedures of conformity assessment. As a verification of successful implementation of the procedure the manufacturer is liable to put a CE mark on his product, and that means an acknowledgement of conformity with essential safety requirements defined in adequate Directives.

If the product is not implied in technical legislation of the New Approach than it belongs to the so called "voluntary" verification. Hence, in other words, it means that the manufacturer is open to choose or not to certify a product. The manufacturers used to do the certification in aim to get customers and as an objective to create a market advantage over competition. The size of different systems of certifications could be large. ISO book (ISO 1992) gives eight different systems of third party certification for products.

On the other side, EU put requirement for food safety which are representative through Directives, Regulations and Standards. This documents pose strict requirements for food product in regards of quality, hygiene requirements, content of different substances, controls, verification, etc. Important part of this requirement are safeties of foodstuff processing. Machinery Directive 2006/42/EC, Annex I define general essential health and safety requirement applicable to all machinery In its part 2.1 there are supplementary essential health and safety requirement for foodstuffs machinery.

In this paper we present approach to general food safety, some of requirement for foodstuffs machinery and as an example some of the results from conformation dryer machine "SOLARIS 1" in regards to EU requirements. This machine is intended for drying fruits, vegetable, medical herbs, spices and mushrooms.

1 EU APPROACH TO PRODUCT CONFORMITY ASSESSMENT

There are different ways for placing products on the European Union market. The manufacturers and suppliers use diverse techniques, which very often involve engaging an independent body, third party, for conformity assessment of the product. The figure 1 gives an overview concerning the main routes for mandatory or voluntary routes for product conformity assessment.

Required first answer to the question: is the products in frame of the technical legislation of the New Approach or not.

If the product pertains to technical legislation, namely it is enclosed by directives of the New Approach, the procedures of conformity assessment are defined in Council Decision of

*Corr. Author's Address: LOLA Institute, Kneza Viseslava 70a, 11030 Belgrade, Serbia, vladazz@yahoo.com

European Union as introduction of conformity assessment modules.

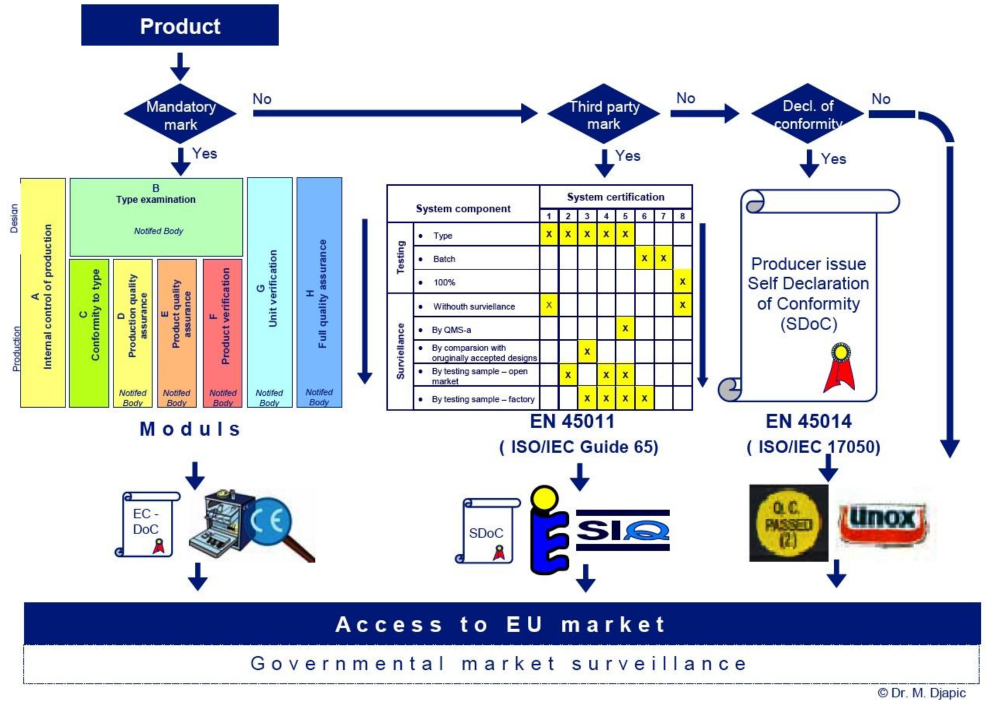

Fig. 1. *EU Approach to Conformity Assessment [13]*

Procedures of conformity assessment included in directives are based on modules for conformity assessment (Fig. 1). Variety of modules require from producer to include an independent third party in the procedure of conformity assessment, notified bodies respectively. Engagements of these bodies are principally required in procedures of conformity assessment, which are related to high risk products hazardous to human health and environment.

2 EU REQUIREMENTS FOT FOODSTUFFS MACHINERY

Foodstuffs have to fulfill two groups of regulations:

- Regulations for foods
- Technical regulations for product/machine which are included in the processes of production foods

International and European regulation {Regulation (EC) No 178/2002, Food law etc.[1]} and standards (HACCP, ISO 22000 for food safety management system) for food safety is intended to provide security by ensuring that there are no week links in the food supply chain. By ensuring integrity of food supply chain it helps to minimize the failures in food supply which can be dangerous and cost plenty. Food and feed imported to the EU shall comply with the relevant requirements of food law or conditions recognized by the Community to be at least equivalent with requirements contained therein.

The key objectives of this regulation are:

- To produce safety food product every time
- To demonstrate that the process is safety
- In the unfortunate event of persecution it can provide evidence of diligence and
- To provide and promote confidence in the food product.

Technical regulations for machine which are included in the processes of production foods also have to fulfill requirement of EU Technical legalization (EU Directives). Machinery Directive (MD) 2006/42/EC [2], is one of them. In its Annex I there are supplementary essential health and safety requirements for "Foodstuffs machinery". Point 2.1 of the Annex I define supplementary requirements for the machinery design for food processing. Some of the requirements are:

(a) *materials in contact with, or intended to come into contact with, foodstuffs ..must satisfy the condition ... cleaned before each use ... disposable.*

(b) *all surfaces in contact with foodstuffs must be: smooth, designed to reduce the projections, easily cleaned and disinfected, ...*

(c) *it must be possible for liquids, ... deriving from foodstuffs, ...cleaning, ...*

(d) *machinery must be designed and constructed in such a way as to prevent any substances or living creatures, in particular insects, from entering, or any organic matter from accumulating in, areas that cannot be cleaned,*

(e) *machinery must be designed and constructed in such a way that no ancillary substances hazardous to health, including lubricants used, can come into contact with foodstuffs, ...*

In the point 2.1.2 state that instruction for foodstuffs must indicate recommended products and methods for cleaning, disinfection etc.

Also, EU standardization body (CEN) published standard EN 1672-2:2005+A1 *Food processing machinery – Basic concepts – Part 2: Hygiene requirements* to cover the MD requirements and to give guides to risk assessments and verification foodstuffs machinery[8].

3 "SOLARIS 1" DRYER

SOLARIS 1 is intended for drying fruits, vegetable, medical herbs, spices and mushrooms. It is fully automated and capable of performing all drying processes according to programmed parameters, giving possibilities of on-site control or over internet and GSM module, allowing to control the drying processes from any place in the world. This means that, with this innovative technology, the buyer of dried products gets a guaranteed quality and an insight into a full drying process, as well as the possibility to review all drying processes during the last couple of years, unlike other standard types of dryers.

This advanced dryer, powered by solar energy, is a product unique in the world. It is patented in Serbia and as well by international patents P-2007/0441 and WO/2009/061229 [9,10]. It is important to mention that in "SOLARIS 1" (Fig. 2) have been implemented nine new designs solution and completely new technical solutions. The dryer is mobile, with installed wheels, and can be handled according to the client's needs.

Fig. 2. *Solar Electric Energy Dryers "NTIM TEHNOLOGI"*

The process in the dryer is controlled by a microprocessor including 50 different programs and allows an automatic transfer from solar to electric energy and vice versa. Microprocessor chooses the source of energy itself, which means that it uses daylight (sun) as source of energy until it is possible, otherwise it uses electric energy.

The control system gives the possibility of setting parameters for 50 different drying modes. The parts of the plant which contain material to be dried, as well as the components for air distribution, are made entirely of stainless steel conforming to HACCP and ISO food industry production standards (HACCP, ISO 22000; Regulation (EC) No 178/2002, Food law etc.).

This SMART DRYER uses daylight, absorbed by a solar panel, as primary source of energy, and electric energy is used as secondary source of energy.

4 RISK ASSESSMENT AND TESTING IN THE CONFORMITY ASSESSEMNT "SOLARIS 1" DRYER

In this point we present some of the opinion in regard to quality of the "SOLARIS 1" dryer food processing [12], and parts of experimental results witch show effect of drying process by quality of dried fruits, Fig. 3 [11].

We also present results of the risk assessment procedure (Table 1.) from the harmonized standards EN ISO 14121 and EN ISO 12100

According to the Standard EN 1672-2:2005+A1, the Supplementary essential health and safety requirements (MD 2006/42/EC , Annex I, 2.) "Foodstuffs machinery" (MD 2006/42/EC, Annex I, 2.1), are listed in Table 2.

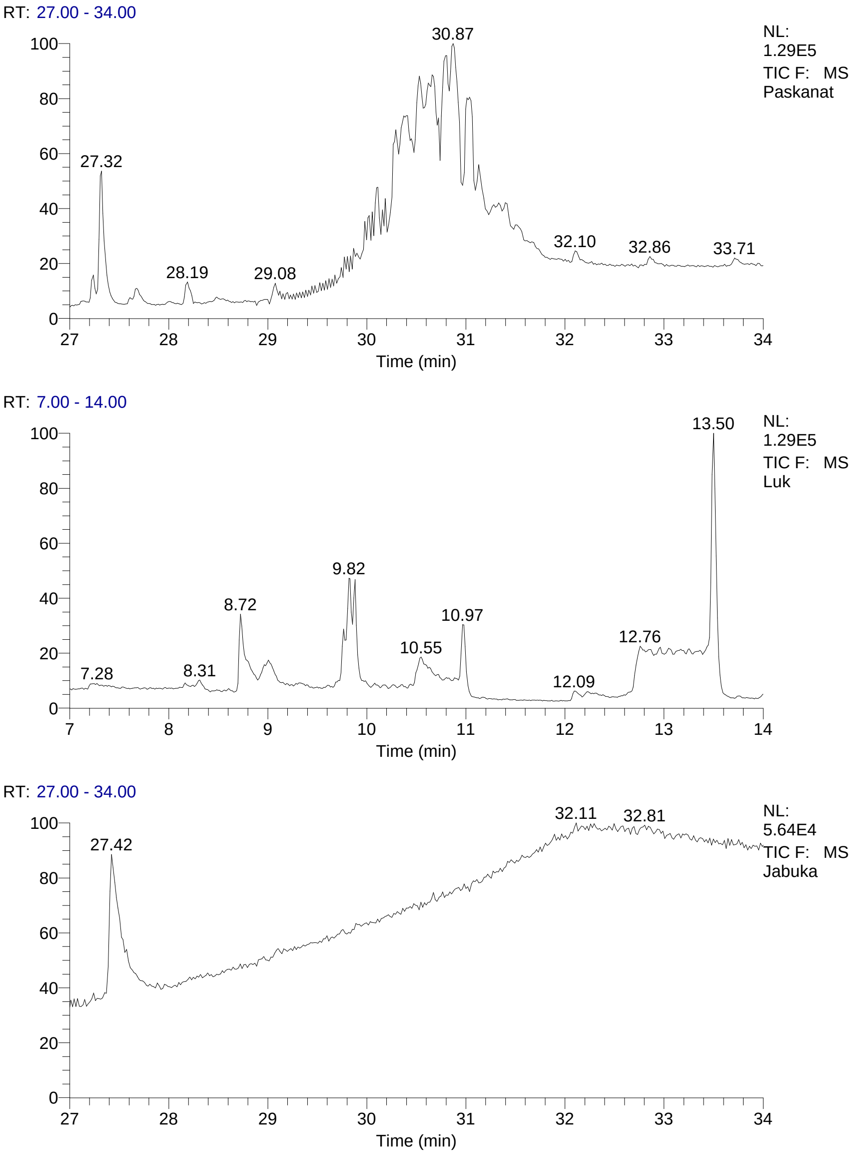

Fig. 3. *Testing result of dried parsley, onion and apple contents*

Tabel 1. *Risk assessment*

No.	Type or group	Hazards	Analysis/ Standard(s)	Verification	Note
1	Mechanical hazards	Kinetic energy, ..., Stability, Sharp edges			
2	Electrical hazards	Arc, Live parts, Short-circuit, ...			
3	Thermal hazards	Objective or materials with a high or low temperature, ...	√	Instruction manual	
8	Ergonomic hazards	Access, ...			
9	Hazards associated with environment in which the machine is used	Dust and fog, EMC, Lighting, Pollution, Temperature, Water, ...			
10	Combination of hazards				

Table 2. *Risk assessment, hazards grouped, measure, verification*

Reference subclasses	Requirement	Verification	Status
5.1	Hygiene risk assessment	Documentary evidence	
5.2.1	Durable	Material specification (food, process and cleaning) and/or practical or functional test	
5.3.1.1 5.3.2	Cleanable and/or capable of being disinfected	Visual inspection (of technical drawing and/or machinery) and/or practical test, micro biological test or functional test	√
5.2.2 5.3.3	Corrosion resistant	Material specification (food, process and cleaning) and/or practical or functional test	
5.2.2	Non toxic	Material specification or practical test for materials intended to come into contact with food	
5.3.1.1	Surface design	Visual inspection (of technical drawing and/or machinery)	
5.3.1.1 5.3.2	Surface finish	Measuring e.g. according to EN ISO 4288	
5.3.1.2.1	Permanent joints	Visual inspection	
5.3.1.2.2	Dismountable joints	Visual inspection	
5.3.1.6	Dead spaces	Visual inspection	
5.3.3	Non-food area	Compliance with Reference subclasses	

5. CONCLUSION

European Directives defines the requirement for the machinery intended to use in food processing. Machinery Directive 2006/42/EC, Annex I define general essential health and safety requirement applicable to all machinery (part 1), and the supplementary essential health and safety requirement for foodstuffs machinery (part 2.1).

This requirements has to be fulfilled before the machine is placed on European market.

In this paper, the requirements for the machinery intended to use in food processing are presented. Also we present some of the results in the process of conformity assessment "SOLARIS 1" which is intended for drying fruits, vegetable, medical herbs, spices and mushrooms processing.

6. REFERENCES

[1] REGULATION (EC) No 178/2002 general principles and requirements of food law, Official Journal of European Communities L 31/1, 1.2.2002.
[2] Directive 2006/42/EC of the European Parliament and Council of 17 May 2006 on machinery, L 157/24 Official Journal of the European Union, 9.6.2006.
[3] Low Voltage Directive 2006/95/EC.
[4] EMC Directive 2004/108/EC.
[5] Pravilnik o bezbednosti mašina "Службени гласник РС" Број 13/10.
[6] EN 12100-1-2 Safety of machinery – Basic concept, general principles for design – Part 1 Basic terminology, methodology, Part 2 – Technical principles.
[7] EN 14121 -1 Safety of machinery – Risk assesment - Part 1 – Priciples.
[8] EN 1672-2:2005+A1 Food processing machinery – Basic concepts – Part 2: Hygiene requirements, March 2009.
[9] Veselinović N., Veselinović M., Patent WO/2009/061229, http://www.wipo.int/patentscope/search/en/detail.jsf?docId=WO2009061229&recNum=1&docAn=RS2008000034&queryString=FP:(WO/2009/061229)&maxRec=1.
[10] Veselinović N., Veselinović M., Patent US Patent Application 20100223807 – Solar And Electric Energy Dryers, http://www.patentstorm.us/applications/20100223807/claims.html.
[11] Simić M., Simić B., Izveštaj o analizi kondenzata dobijenih pri sušenju jabuke, paškanata i crnog luka, University of Belgrade, Institute of General and Physical Chemistry, Belgrade, 2001-03-25.
[12] Zlatković B., Mišljenje o radu sušare SOLARIS 1, Izveštaj 22/123, University of Belgrade, Faculty of Agriculture, 9.2.2011.
[13] Djapic, M., Zeljković, V., *European Approuch to Product Conformity Asssessment*, The Fifth International Conference ”Heavy Machinery - HM 2005”, Kraljevo, 28. June – 03 July, 2005., pp (IIC.13 – IIC.17).

The results presented in this work are a result of project TR 35031, which is funded by the Ministry of Education and Science of the Republic of Serbia.

HEAVY MACHINERY - HM 2011, 37-42
ISBN 978-86-82631-58-3
Paper accepted: 30.05.2011

Structural Health Management of Complex Engineering Structures

Dragoljub Vujić[1,*]
[1]Military Technical Institute, Belgrade, Serbia

This paper deals with methods for structural health monitoring. Two methods are presented in detail. The first one is based on changes on frequency response, which occurs as result of the mass and rigidity changes due to the structural damages. The second one is based on changes on wave propagation. It has shown that the structural health monitoring will have a strong impact on conventional design and maintenance philosophies and processes. Damage will be put on a mechanically more realistic basis.

Key words: **Structural health monitoring, engineering structures, damage tolerance concept, maintenance actions**

INTRODUCTION

As it is known, large and complex engineering structures are mainly made to last for a long period. This is specifically important for civil engineering buildings but also for heavy machinery, trains, ships or aircraft. Any of these items are used intensively. Long endurance combined with intensive usage leads to deterioration.

Of course, an engineering structure is designed to withstand deterioration for a certain foreseeable lifetime. However, the longer this lifetime becomes, the more difficult it is to predict. Such a structure may therefore have to be designed for maintainability. As we know, this has often not too much been done in the past and possibly not even today. The reason is that most of the limited life items are considered for an extended lifetime, once their initial design life has been achieved.

1. STRUCTURAL HEALTH MONITORING

Structural Health Monitoring (SHM) aims to give, at every moment during the life of a structure, a diagnosis of the „state" of the constituent materials, of the different parts, and of the full assembly of these parts constituting the structure as a whole. The state of the structure must remain in the domain specified in the design, although this can be altered by normal aging due to usage, by the action of the environment, and by accidental events. Thanks to the time-dimension of monitoring, which makes it possible to consider the full history database of the structure, and with the help of usage monitoring, it can also provide a prognosis (evolution of damage, residual life, etc.).

If we consider only the first function, the diagnosis, we could estimate that Structural Health Monitoring is a new and improved way to make a Non-Destructive Evaluation. This is partially true, but SHM is much more. It involves the integration of sensors, possibly smart materials, data transmission, computational power, and processing ability inside the structures. It makes it possible to reconsider the design of the structure and the full management of the structure itself and of the structure considered as a part of wider systems. This is schematically presented in Figure 1.

In Figure 1 the organization of a typical SHM system is given in detail. The first part of the system, which corresponds to the structural integrity monitoring function, can be defined by: 1) the type of physical phenomenon, closely related to the damage, which is monitored by the sensor, 2) the type of physical phenomenon that is used by the sensor to produce a signal (generally electric) sent to the acquisition and storage sub-system. Several sensors of the same type, constituting a network, can be multiplexed and their data merged with those from other types of sensors. Possibly, other sensors, monitoring the environmental conditions, make it possible to perform the usage monitoring function. The

*Corr. Author's Address: Military Technical Institute, Belgrade, Serbia, vujicd@eunet.rs

signal delivered by the integrity monitoring sub-system, in parallel with the previously registered data, is used by the controller to create a diagnostic. Mixing the information of the integrity monitoring sub-system with that of the usage monitoring sub-system and with the knowledge based on damage mechanics and behaviour laws makes it possible to determine the prognosis (residual life) and the health management of the structure (organization of maintenance, repair operations, etc.). Finally, similar structure management systems related to other structures which constitute a type of super system (a fleet of aircraft, a group of power stations, etc.) make possible the health management of the super system. Of course, workable systems can be set up even if they are not as comprehensive as described here.

1.1 Structural health monitoring concept

With the development of structural health monitoring (SHM) methods and techniques, systems allowing usage monitoring, inspection of structural components, damage detection and analysis will be integrated in the structural components. All mentioned actions are automatically executed and particularly the prognostic and diagnosis of the structures health could be continuously performed, dramatically reducing the time period necessary for the inspections. From the application of the SHM concept will result: increase on structure safety and reliability, reduction of preventive and corrective maintenance actions, increase in the structures operation readiness and reduction of the operational costs. On the other hand, by applying these active safety improvement methods, passive measures can be decreased, resulting in a decrease on the overall weight, as the increase on weight due to the use of new integrated systems will be largely compensated by the decrease due to reduction of safety factors and redundancy. Again, a reduction on the operational costs will result.

A clear indicator for the increased importance of SHM is the number of hits (publications, patents, etc.) related to structural health monitoring obtained with academic search engines. The data in Fig. 2 clearly show that the number of published topics is exponentially growing since more than 15 years.

Moreover, structural health monitoring is a well-established technology already operational in a number of appropriate civil structures, such as bridges and chemical installations.

In contrast to the above mentioned structures, SHM for civil aviation is nowadays still in an experimental phase. The concepts followed are partially based on a number of different well-established nondestructive evaluation methods, such as ultrasonic inspection or eddy current methods.

1.2 Structural Health Monitoring Methods

Structural health monitoring methods emerged from the field of smart structures, integrating several disciplines such as: microelectronics, sensors and actuators, signal acquisition and processing, structural dynamics, materials and structures, fatigue and fracture, nondestructive evaluation methods. Here, we are going to present two methods. The first one is based on changes on frequency response, which occurs as results of the mass and rigidity changes due to the structural damages. The second one is based on changes on wave propagation.

1.2.1 Frequency Response Based Methods

This method is based on the natural frequencies that every single structure possesses. Generally, these frequencies depend on the mass and on the rigidity of the structure. A damaged structure can be seen as one that has its mass and rigidity altered, hence with different natural frequencies. This conclusion can also be applied for free frequency response, i.e., differences will emerge when responses from the same structure, with and without damage, to the same external excitation are compared. Consecutively, 2D computational models were developed on NASTRAN (and ANSYS, to compare) to study this theory. Both isotropic and orthotropic materials were tested. Those models consisted of rectangular shaped plates, with one clamped edge and the remaining free, as seen on Figures 3 and 4.

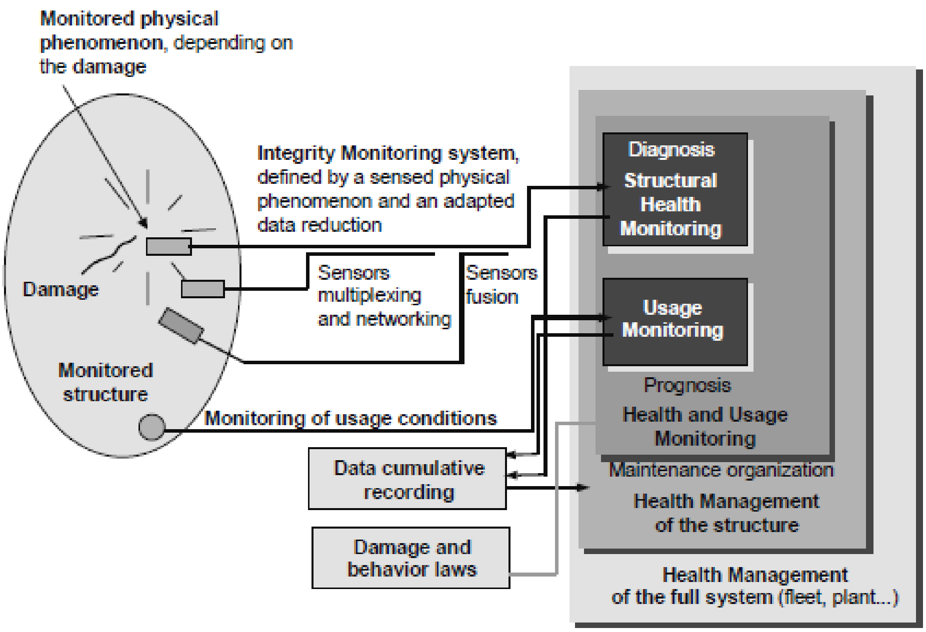

Fig. 1. *Principle and organization of a SHM system*

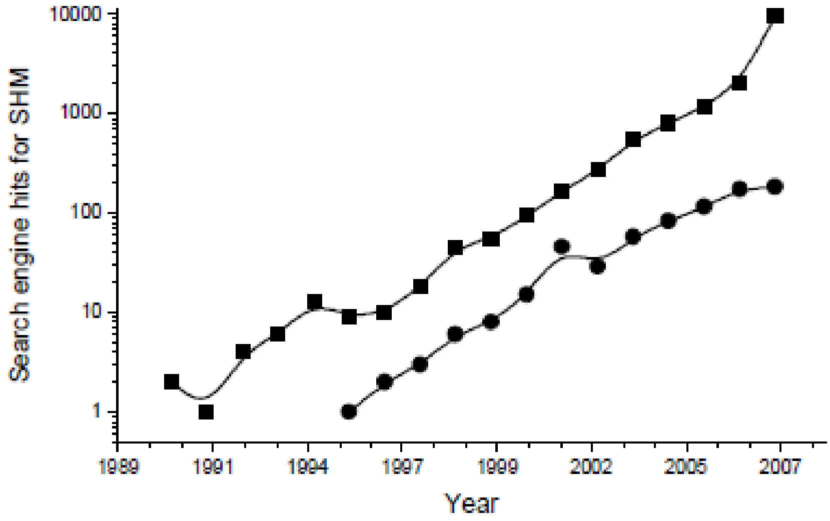

Fig. 2. *The number of the published topics during the last two decades*

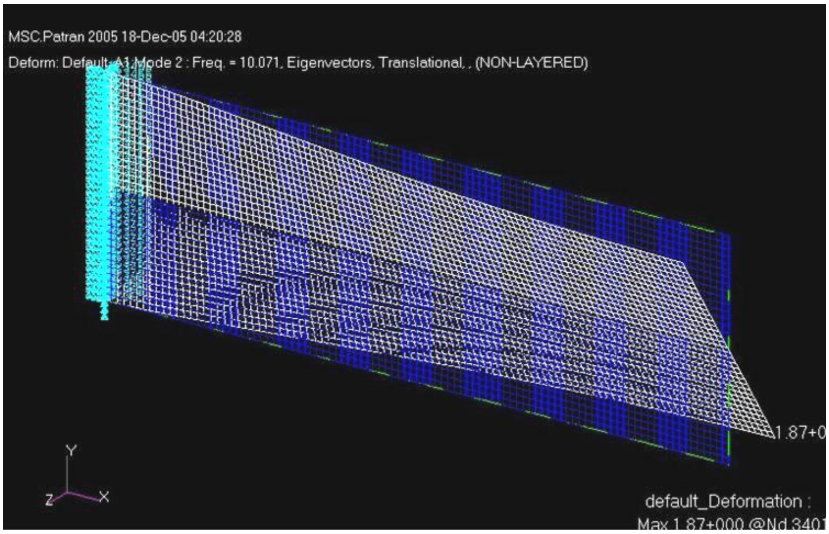

Fig.3. *Computational analysis of an aluminum plate*

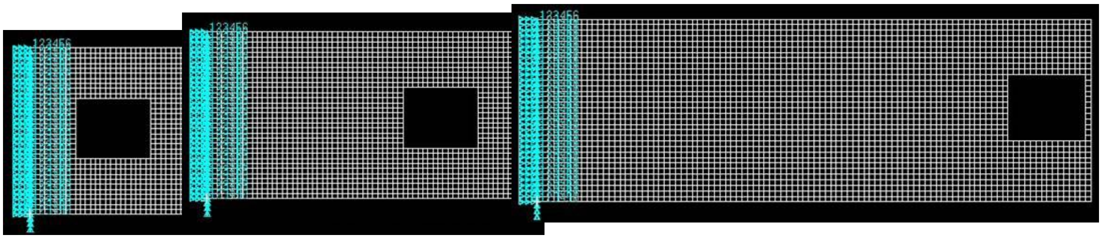

Fig.4. *Imposed damages to the plates*

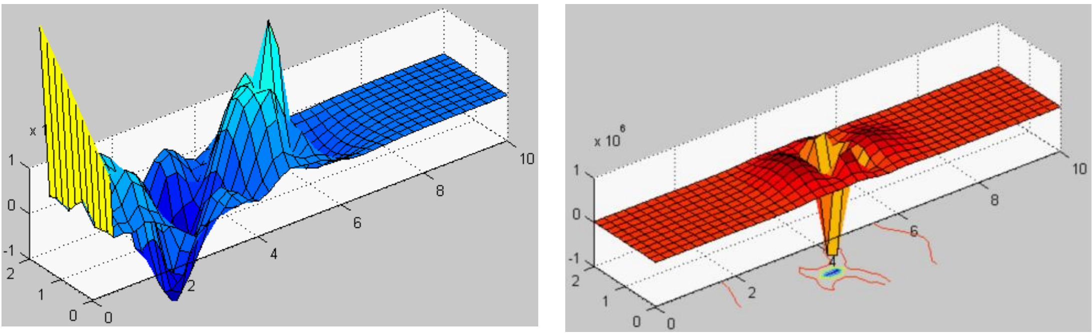

Fig. 5. *Elastic deformation – Lamb waves propagation*

Several tests were running, starting from an undamaged structure and then placing damages on different locations to access the (changes) on natural frequencies and modes of vibration. Damages were simulated using mass/rigidity reduction, by removing certain finite elements. Preliminary tests revealed that 10% differences, in 1st natural frequency, can be observed starting from 5% of elements/mass/area reduction. Damages near the clamped edge induce mainly a decrease in the rigidity, resulting in a decrease of the first natural frequency of 12.75%. While damages far from this edge, have as preponderant effect the decrease of mass, resulting in an increase of the first natural frequency of 9.25%. The damage in the middle of the plate produced only a slight variation of 2.7%.

From this study, a limitation of this method can be retained: significant frequency variation occurs only for high values of mass/area reduction, which corresponds to large structural defects. This method can be applied using low frequencies, what represents an advantage. Also, damages far or near clamped boundaries are better detected.

1.2.2 Wave Propagation Based Methods

Ultrasonic testing is one method used in nondestructive evaluation methods. Current ultrasonic inspection of thin wall structures is a time consuming operation. One method to increase the efficiency is to use guided waves, like Lamb waves, instead of the conventional pressure waves. Guided waves propagate along the mid-surface of thin-wall plates and shallow shells. They can travel at relatively large distances with very little amplitude loss and offer the advantage of large area coverage with a minimum of installed sensors. Guided Lamb waves have opened new opportunities for cost-effective detection of damage in aircraft structures.

Initially, 1D analytical model were tested, based on multiple spring/mass systems. This study permitted to fully understand the behavior of 1D elastic medium and the influence of boundary conditions. As a starting point, this type of solution can be used for application frequency response SHM methods, since it allows calculating modes and response of the system to external excitation, with and without damage. Damage can be modeled by local mass or/and spring rigidity increase/decrease.

Considering the dynamic response of each mass, their respective displacement amplitude at a certain time and the elapsed time between two consecutive masses reaching their maximum displacement, strain wave propagation can be modeled. Considering the differences between that propagation (and boundary reflections), with or without damage, and resulting damage reflections, damage can be assessed (wave propagation method).

Furthermore, 2D analytical models were developed from this 1D system. 2D computational models based on rectangular shaped isotropic plates, with different sets of boundary conditions, were developed on NASTRAN, ANSYS and MATLAB to study this theory. Several tests were running, starting from an undamaged structure and then placing damages on different positions. Structural response/wave propagation to different strain impulses and step excitations in one or more nodes of the structure was tested. Some results are shown on Figure 5, including the response from an undamaged plate, the same plate with a central damage and the difference between both cases.

On left, wave longitudinal propagation in an undamaged plate is easily to seen, as the lateral boundaries reflections/interference. On right are shown differences for a plate with a central damage. The strain concentration in the damage location and its consequent propagation are also seen.

2. CONCLUSIONS

This paper presents a contribution to the development of methods for structural health monitoring. This system was used to validate and demonstrate some developed methods, namely by the ability to apply wave propagation SHM methods to detect damages in an aluminum plate similar to a wing skin panel of the aircraft.

Structural health monitoring allows for integration latest technology into structures. The market for such systems is possibly much larger than we can still anticipate today and sequentially it becomes more and more relevant with regard to worldwide limited resources.

Structural health monitoring will also have a strong impact on conventional design and maintenance philosophies and processes. For example, in the aeronautics, time such as flight hours will possibly not be the key parameter anymore to describe damage. Damage will be put on a mechanically more realistic basis. This will not only allow to make maintenance more specific to usage but also to make prognostics with regard to any maintenance actions to be taken.

Maintenance procedures are then planned and applied, involving the diagnosis of the structures health by inspection of structural components, in order to detect and evaluate existing flaws, using nondestructive evaluation methods. These maintenance and inspection actions are expensive and require long periods of immobilization.

Structural health monitoring is a multidisciplinary approach. It is not limited to structural design and strength only but also has to include the various aspects of sensor technology, non-destructive testing and advanced signal processing. In excess it also has to include a more profound knowledge about structural design and the resulting impacts on the structure coming from usage. This includes all the maintenance actions as well as the related issues to economics.

3. REFERENCES

[1] Vujic D., Health monitoring and prognostic sensors applied in mechanical and elecronic systems, 11th International Conference DEPENDABILITY AND QUALITY

[2] Vujic D., Aviation engine health conditions on the oil debris monitoring, The fifth international scientific conference HEAVY MACHINERY, Faculty of Mechanical Engineering, June 29-July 03, 2005, pp.6

[3] Vujic D., Modern on-condition maintenance concept of aircraft engines (in Serbian), Comulative scientific technical information, ISSN 1820-3418, Vol. XVII, No.2, Military Tecnical Unstitute, Belgrade, 2008.

[4] Helge Pfeiffer, Martine Wevers, Aircraft Integrated Structural Health Assessment – Structural Health Monitoring and its implementation within the European project AISHA, Leuven, Belgium, June 2007.

[5] Reis L, Fonseca A, de Freitas M. Methodology for Fatigue Life Assessment of the Structural Integrity of Fighter Aircraft, Fatigue&Fracture Engineering Materials&Structures, Vol. 27, Issue 9, pp 873-877, 2004.

HEAVY MACHINERY - HM 2011, 43-48
ISBN 978-86-82631-58-3
Paper accepted: 30.05.2011

Harmony search and genetic algorithms for engineering optimization: theory and practice

Danijel Markovic[1,*], Milos Madic[1], Zoran Marinkovic[1], Vojislav Tomic[1], Goran Petrovic[1]
[1] University of Nis, Mechanical Engineering Faculty of Nis, Department of Transport Technique and Logistics

Various optimization problems in various fields of engineering have been solved using diverse optimization algorithms. Traditional optimization techniques such as linear programming (LP), non-linear programming (NLP), dynamic programming (DP), Taguchi method (TM) etc. have had major roles in solving these problems. However, these algorithms have certain drawbacks, and the more recent approach to solving optimization problems includes application of meta-heuristic algorithms (simulated annealing, tabu search and evolutionary algorithms). In this paper, two meta-heuristics algorithms for solving optimization problems in engineering, namely genetic algorithm and harmony search, were presented. These algorithms are widely used in the optimization in engineering. The paper presents a theoretical approach and practical application of these two algorithms and their comparison.
Keywords: Optimization, Genetic Algorithm, Harmony Search

1 INTRODUCTION

Over the last four decades, a large number of algorithms have been developed to solve various engineering optimization problems. Traditional optimization techniques, such as linear programming (LP), non-linear programming (NLP), and dynamic programming (DP) have had major roles in solving these problems. Among these, experimental techniques that include statistical design of experiment, such as response surface method (RSM) and Taguchi method (TM) have been often applied. These techniques can guarantee global optima in simple and ideal models. However real-world engineering optimization problems are very complex in nature and quite difficult to solve using these algorithms. If there is more than one local optimum in the problem, the result may depend on the selection of an initial point, and the obtained optimal solution may not necessarily be the global optimum. When solving problems with high dimensional search space and many local optima, metaheuristic algorithms are preferable allthough they provide near optimal solutions.

Since the 1970s, many meta-heuristic algorithms that combine rules and randomness imitating natural phenomena have been devised to overcome the computational drawbacks of existing numerical algorithms when solving difficult and complex optimization problems [1]. Meta-heuristic algorithms imitate natural phenomena, i.e., physical annealing in simulated annealing, animal behavior in tabu search, and evolution in evolutionary algorithms. There are many meta-heuristic algorithms such that are often applied as: Simulated annealing [2], Tabu search [3], Genetic algorithm [4], Ant Colony Optimization [5], Shuffled Frog Leaping [6], Harmony Search [1], Bees Algorithm [7].

One of the recent meta-heuristic algorithms is Harmony Search (HS) algorithm [1]. Some of the real optimization problems that were solved using the HS algorithm include: vehicle routing problem [8], reliability [9] and many other difficult and complex engineering optimization problems.

Application of HS algorithm is a new field of optimization. In this paper a theoretical description and practical application of HS algorithm was presented. Results were compared with results obtained using GA.

2 META-HEURISTIC HARMONY SEAR CH ALGORITHM

A new meta-heuristic algorithm Harmony Search (HS) was conceptualized using the musical process of searching for a perfect state of harmony. HS algorithm was developed by Geem et al. in 2001 [1]. Musical performances seek to find pleasing harmony (a perfect state) as determined by an aesthetic standard, just as the optimization process seeks to find a global

*Corr. Author's Address: University of Niš, Mechanical Engineering Faculty of Niš, Serbia, danijel@masfak.ni.ac.rs

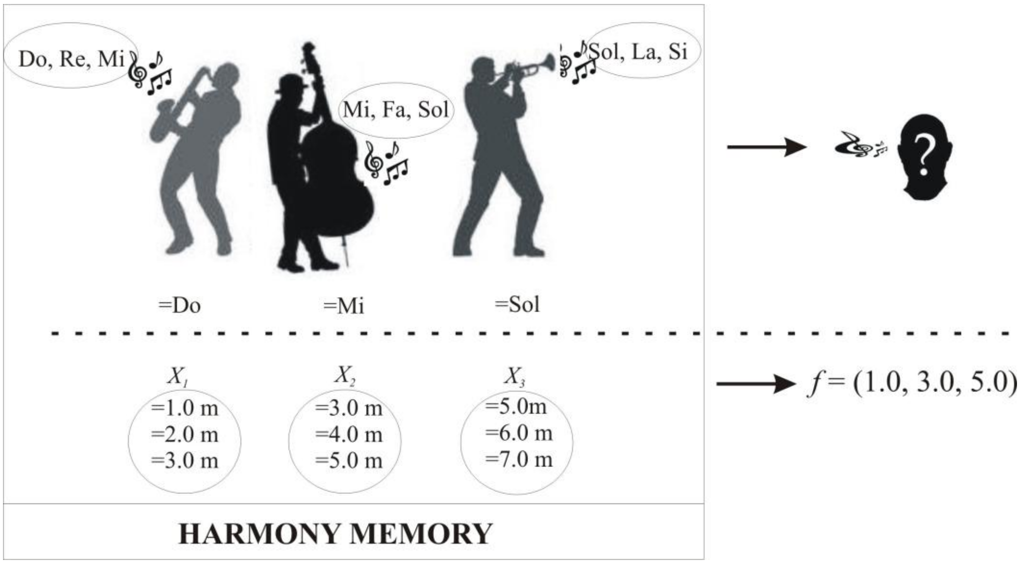

Fig. 1. Structure HM and analogy between music improvisation and optimization function

solution (a perfect state) as determined by an objective function. The pitch of each musical instrument determines the aesthetic quality, just as the objective function value is determined by the set of values assigned to each decision variable. The new HS meta-heuristic algorithm was derived based on natural musical performance processes that occur when a musician searches for a better state of harmony. Structure of the harmony memory (HM) and analogy between music improvisation and optimization function shown in the fig 1.

Consider a jazz trio composed of saxophone, double bass, and trumpet. There exists certain amount of preferable pitches in each musician's memory: saxophonist = {Do, Re, Mi}; double bass = {Mi, Fa, Sol}; and trumpet = {Sol, La, Si}. If saxophonist randomly plays {Do} out of its memory {Do, Re, Mi}, double bassist {Mi} out of {Mi, Fa, Sol}, and guitarist {Sol} out of {Sol, La, Si}, that harmony (Do, Mi, Sol) makes another harmony. If new harmony is better than existing worst harmony in the HM, the new harmony is included in the HM and the worst harmony is excluded from the HM. This procedure is repeated until fantastic harmony is found.

In real optimization, each musician (saxophonist, double bassist and trumpet) can be replaced with each decision variable (x_1, x_2 and x_3), and its preferred sound pitches can be replaced with each variable's preferred values. If first variable chooses {1.0m} out of {1.0m, 2.0m, 3.0m}, second {3.0m} out of {3.0m, 4.0m, 5.0m}, and third {5.0m} out of {5.0m, 6.0m, 7.0m}, those values (1.0m, 3.0m, 5.0m) make another solution vector. If this new vector is better than existing worst vector in the HM, the new vector is included in the HM and the worst vector is excluded from the HM. This procedure is repeated until certain termination criterion is satisfied.

Optimizations procedure of the HS algorithm includes five steps [1, 8]: (1) initialize the parameters optimization; (2) initialize the harmony memory; (3) improvise a new harmony from the HM; (4) update the HM; (5) repeat steps 3 and 4 until the termination criterion is satisfied.

(1) *Step 1. Parameters initialization*. In this step, the optimization problem is specified as follows:

$$Minimize/Maximize\ f(x) \qquad (1)$$

subject to: $x_i \in X_i$, $i = 1, 2, \ldots, N$.

where *f(x)* is the objective function is *x* the set of each design variable (x_i); X_i is the set of the possible range of values for each design variable, that is X_i = {$x_i(1)$, $x_i(2)$,…, x_i(K); *N* is the number of design variables (= number of music instruments) and *K* is the number of candidate values for the discrete decision variables (=

number of pitches for each instrument). The HS algorithm parameters are also specified in this step: Harmony memory size (number of simultaneous solution vectors in harmony memory, HMS), harmony memory considering rate (HMCR), pitch adjusting rate (PAR), and number of improvisations (maximal number of searches). These algorithm parameters are explained in the following steps.

(2) *Step 2. Initialize the harmony memory (HM).* In Step 2, the ‘‘harmony memory’’ (HM) matrix, as shown in Equation (2), is filled with randomly generated solution vectors and sorted by the values of the objective function *f(x).*

$$HM = \begin{bmatrix} x_1^1 & x_2^1 & \cdots & x_N^1 \\ x_1^2 & x_2^2 & \cdots & x_N^2 \\ \vdots & \vdots & & \vdots \\ x_1^{HMS} & x_2^{HMS} & \cdots & x_N^{HMS} \end{bmatrix} \quad (2)$$

(3) *Step 3. Improvise a new harmony from the HM*. In this step, a new harmony vector, $x' = x_1', x_2', \ldots, x_N'$ is improvised by following three rules: HM consideration, pitch adjustment and random selection. As a musician plays any pitch out of the preferred pitches in his/her memory the value of decision variable is chosen from any pitches stored in HM ({ $x_i^1, x_i^2, \ldots, x_i^{HMS}$ }) with a probability of HMCR ($0 \le$ HMCR ≤ 1) while it is randomly chosen with a probability of (1-HMCR) in random selection process as previously described.

$$x_i' \leftarrow \begin{Bmatrix} x_i' \in \{x_i^1, x_i^2, \ldots, x_i^{HMS}\} & w.p.\ HMCR \\ x_i' \in X_i & wp.\ (1-HMCR) \end{Bmatrix} \quad (3)$$

The Pitch adjusting process is one pitch is obtained in HM consideration, a musician can further adjust the pitch to neighboring pitches with a probability of HMCR x PAR ($0 \le$ PAR ≤ 1) while the original pitch obtained in HM consideration is just kept with a probability of HMCR x (1-PAR).

$$x_i' \leftarrow \begin{Bmatrix} x_i(k+m) & w.p.\ HMCR \times PAR \\ x_i' & w.p.\ HMCR \times (1-PAR) \end{Bmatrix} \quad (4)$$

where x_i' obtained in HM consideration and x_i (k) (the k^{th} element in $\boldsymbol{X}_i$) are identical; m ($m \in \{..., -2, -1, 1, 2, ...\}$) is a neighboring index used for discrete decision variables (m has normally +1 or - 1).
Random selection is when a musician plays any pitch within the instrument range, the value of decision variable x_i' is randomly chosen within the value range X_i.

(4) *Step 4. Update the HM*. In Step 4, if the new harmony vector $x' = x_1', x_2', \ldots, x_N'$ is better than the worst harmony in the HM in terms of the objective function value, the new harmony is included in the HM and the existing worst harmony is excluded from the HM. The HM is then sorted by the objective function value.

(5) *Step 5. Repeat Steps* 3 and 4 until the termination criterion is satisfied. In Step 5, the computations are terminated when the termination criterion is satisfied. If not, steps 3 and 4 are repeated.

Pseudo code of the HS algorithm is provided in Figure 2.

Define objective function f(x), $x=(x_1, x_2, \ldots, x_N)^T$
Define harmony Memory considering rate (HMCR)
Define Pitch adjusting rate (PAR) and other parameters
Generate Harmony Memory with random harmonies
While (t<max number of iterations)
While (i <=number of variables)
If (rand<HMCR),
Choose a value from HM for the variable i
If (rand<PAR),
Adjust the value by adding certain amount
end if
else
Choose a random value
end if
end while
Accept the New Harmony (solution) if better
end while
Find the current best solution
end

Fig. 2. Pseudo code of the Harmony Search algorithm

3 GENETIC ALGORITHMS

Evolutionary algorithms (EAs) are search methods that take their inspiration from natural selection and survival of the fittest in the biological world. Genetic algorithms (GAs) are a particular class of evolutionary algorithms that use techniques inspired by evolutionary biology. GA is usually used as a search method in big and complex search space. It belongs into local search method, therefore it is an incomplete search. Basic concepts from biology taken by GA are individual, population, reproduction (crossover, recombination), selection, inheritance, mutation and fitness.

Pseudo-code of the genetic algorithm is provided in Figure 3:

Initialize the population
Evaluate initial population
Repeat
  Perform competitive selection
  Apply genetic operators to generate new solutions
  Evaluate solutions in the population
Until some convergence criteria is satisfied

Fig. 2. Pseudo code of the Genetic algorithm

A detailed description of the implementation of GAs for engineering optimization can be seen in [4, 10, 11, 12].

4 SIMULATION EXAMPLES

The HS algorithms described above have been implemented in MATLAB computer simulation program that can be applied to engineering optimization problems with continuous design variables. In this paper, various benchmark engineering optimization examples including function minimization problems from the literature will be presented to demonstrate the efficiency of the proposed HS meta-heuristic algorithm. Examples include two unconstrained function minimization problems.

For both examples presented in this paper, the HS algorithm parameters that were suggested Yang [13] were applied: harmony memory size (HMS) = 20, harmony memory consideration rate (HMCR) = 0.7-0.95, and pitch adjusting rate (PAR) = 0.1-0.5. Many other authors have recommended the same parameters for HS algorithm.

4.1. Unconstrained function minimization examples

The function *f(x)* is the objective function. This is the function you wish to minimize. The inequality x_1 and x_2 is a constraint. Constraints limit the set of *x* over which you may search for a minimum. You can have any number of constraints, which are inequalities or equations.

4.1.1. Rosenbrock's function

Rosenbrock's function is a standard test function in optimization. It has a unique minimum value of 0 attained at the point (1, 1). Finding the minimum is a challenge for some algorithms since it has a shallow minimum inside a deeply curved valley. Rosenbrock's function is defined as:

$$f(x) = 100(x_2 - x_1^2)^2 + (1 - x_1)^2 \tag{5}$$

The HS algorithm was applied to the Rosenbrock function problem using bounds between -10.0 and 10.0 for the two design variables, x_1 and x_2, given Eq. (5).

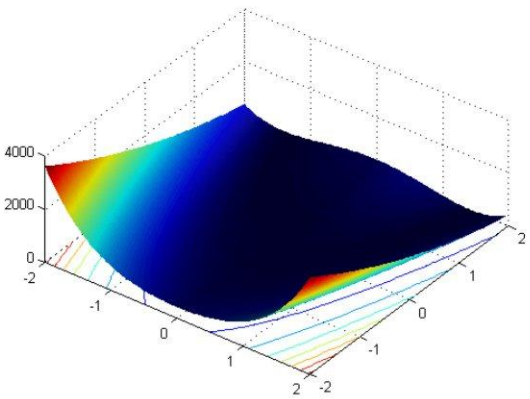

Fig.2. Rosenbrock function

Optimal results of Rosenbrock's function using the HS algorithm and GA algorithm shown in table 1.

4.1.2. Rastrigin's function

Rastrigin's function is also used as a test function in optimization, because its many local minima make it difficult for standard, gradient-based methods to find the global minimum. For two independent variables, Rastrigin's function is defined as:

$$f(x) = 20 + x_1^2 + x_2^2 - 10 \cdot (\cos 2\pi x_1 + \cos 2\pi x_2) \qquad (6)$$

Rastrigin's function has many local minimum. However, the function has just one global minimum, which occurs at the point [0 0] in the x-y plane, as indicated by the vertical line, where the value of the function is 0 (fig. 3). At any local minimum other than [0 0], the value of Rastrigin's function is greater than 0. The farther the local minimum is from the origin, the larger the value of the function is at that point.

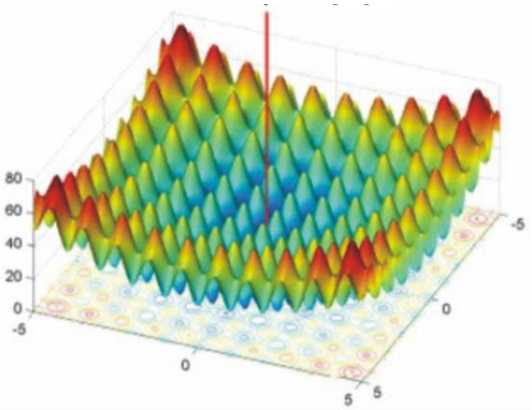

Fig. 3 Rastrigin function

The HS algorithm was applied to the Rastrigin's function problem using bounds between -10.0 and 10.0 for the two design variables, x_1 and x_2, given Eq. (6).

Optimal results of Rosenbrock's function using the HS algorithm and GA algorithm shown in table 2.

Table 1: *Optimal results of the unconstrained function minimization examples obtained using the HS and Ga algorithm*

Function name	Interval	Best so far		Population size	Variables (optimization) value	
		Genetic algorithm	Harmony search		*HS*	*GA*
					x_1 , x_2	x_1 , x_2
Rosebrock	[-10 10]	0.005302	**0.00408419**	40	[1.0047, 1.0031]	[1.0047, 1.0031]
Rosebrock	[-1 1]	4.00577e-004	**2.06311e-010**	20	[0.9999, 0.9997]	[0.98, 096]
Rastrigin	[-10 10]	0.99495e-002	**8.20678e-005**	100	[-0.0003, 0.0005]	[0.995 0]
Rastrigin	[-1 1]	8.43766e-008	**1.93658e-011**	30	[0.00001 -0.000006]	[0 0.995]

6 CONCLUSION

The recently developed HS meta-heuristic optimization algorithm was conceptualized using the musical process of searching for a perfect state of harmony. Compared to gradient-based mathematical optimization algorithms, the HS algorithm imposes fewer mathematical requirements and does not require initial value settings of the decision variables. As the HS algorithm uses stochastic random searches, derivative information is also unnecessary. Furthermore, the HS algorithm generates a new vector, after considering all of the existing vectors based on the harmony memory considering rate (HMCR) and the pitch adjusting rate (PAR), whereas the GA only consider the two parent vectors. These features increase the flexibility of the HS algorithm and hence it provides better solutions.

This paper described the new meta-heuristic HS algorithm-based approach for engineering optimization problems. It should be noted that the HS algorithm is a new method for optimization here. Various engineering optimization problem including two unconstrained function, were presented to demonstrate the effectiveness of the new algorithm compared to genetic algorithm. These examples revealed that the new HS algorithm can be easily applied to various engineering optimization problems. The results obtained using the HS algorithm may yield better solutions than those obtained using GA-based approaches. Our paper suggests that the new HS algorithm is potentially a powerful search and optimization technique for solving engineering optimization problems.

6 REFERENCES

[1] Geem, Z.W. Kim, J.-H. Loganathan, G.V. *A new heuristic optimization algorithm: harmony search, Simulation* 76 (2), pp 60–68. 2001.

[2] Koulamas, C., Antony, S., Jaen, R. *A survey of simulated annealing applications to operations research problems*. Omega 22 (1), pp 41–56, 1994.

[3] Glover, F. Laguna, F. *Tabu search*, Kluwer Academic Publishers, Norwell, MA, USA 1997.

[4] Konak, A. Coit DW, Smith, AE. *Multi-objective optimization using genetic algorithms: a tutorial*, Reliability Engineering and system safety, 91, pp 992-1007, 2006.

[5] Dorigo, M. and Stutzle, T. *Ant colony optimization*, MIT Press, Cambridge, 2004.

[6] Eusuff, M. Lansey, K. Pasha, F. *Shuffled frog leaping algorithm: A memetic meta-heuristic for discrete optimization*, Enginee-ring Optimisation, 38(2), 129-154, 2006.

[7] Baykosoglu, A.,. Ozbakir, L Tapkan, P. *Artificial bee colony algorithm and its application to generalized assignment problem.* In Swarm Intelligence: Focus on Ant and Particle Swarm Optimization, pp 532- 564 Austria, 2007.

[8] Geem, ZW., Kang, SL., Youigjin, P. *Application of Harmony Search to Vehicle Routing*, American Journal of Applied Sciences 2 (12): pp 1552-1557, 2005.

[9] Zou, DX. Gao, LG., Wu JH., Li, S., Li, YA. *Novel global Harmony Search Algorithm for reliability problems*, Computers & Industrial Engineering, 58, 2010, 307–316.

[10] Petrovic, G., Cojbašic, Ž., Marinkovic, Z., *Optimal preventive maintenance using the theory of Markov processes and genetic algorithms*, The 7th international conference research and development of mechanical elements and systems, IRMES 2011, Proceedings, University of Niš, Mechanical Engineering Faculty, Zlatibor, Serbia, pp. 431 – 436, 2011.

[11] Petrovic G., Cojbašic Ž., Marinkovic D., Marinkovic Z., Markovic D., *Multi-objective optimization of maintenance process using advanced evolutionary methods*, The fourth symposium with international participation - transport and logistics TIL 2011, University of Niš, Mechanical Engineering Faculty, Niš, Serbia, pp 74 – 77, 2011.

[12] Raghuwanshi MM, Kakde OG. *Survey on multiobjective evolutionary and real coded genetic algorithms.* The 8th Asia Pacific Symposium on Intelligent and Evolutionary Systems, Cairns, Australia: pp 150-161, 2004.

[13] Yang, XS, *Nature-inspired metaheuristic algorithm*, Luniver Press, UK, 2008.

HEAVY MACHINERY - HM 2011, 49-54
ISBN 978-86-82631-58-3
Paper accepted: 30.05.2011

Application Possibilities Of Artificial Intelligence Methods In Design For Assembly

Aleksandra Petrović [1,*] - Miodrag Manić [2] - Branko Radičević[1] – Zlatan Šoškić[1]
[1] University of Kragujevac, Faculty of Mechanical Engineering Kraljevo
[2] Mechanical Engineering Faculty University of Nis

The recent research activity in design for assembly (DFA) has been directed towards the development of architectures and ontologies to apply artificial intelligence, in order to assist the design activity and to apply automation to the more complex, conceptual and decision-making tasks. The present paper surveys the application of artificial inteligence (AI) techniques in engineering design. Within this context, fuzzy logic (FL), genetic algorithms (GA) and artificial neural networks (ANN), as well as their fusion are reviewed in order to examine the capability of this methods and techniques to efectively address various assembly design tasks and issues. Representative approaches with high relation to the assembly planning are presented.

Keywords: fuzzy logic, genetic algorithms, artificial neural networks, engineering design, design for assembly, assembly planning

1. ENGINEERING DESIGN

The scientific community has extensively studied design during the last decades for the establishment of general purpose and domain-independent scientific rules and methodologies. Besides summarizing and reviewing the developed design models and methodologies, the researchers investigated the nature and the characteristics of the design process, classified the design models into categories and located possible research opportunities.

Three general design models are identified: the descriptive, the prescriptive and the computerbased model. The descriptive models for design tend to capture the processes, strategies and methods that designers use in order to address certain design problems. The prescriptive models are well addressed in preliminary design stages and are extensively used by the designers since they provide an intuitive sense to the design process. The computer-based models enhance features from the both aforementioned categories and are capable of performing many different design activities. On the basis of these three general design models, several design methods have been proposed with the characterization 'design-for-X', each of them viewing a different aspect of design. The applicability of a design model or a design methodology highly depends on the type of the problem under consideration. Through the review of the existing literature, the following issues regarding the design process become distinguishable: (a) the design knowledge representation (modeling), (b) the search for optimal solutions, (c) the retrieval of pre-existing design knowledge and the learning of new knowledge [1].

2. INTELLIGENCE (AI) METHODOLOGIES IN ENGINEERING

Soft Computing (SC) is an evolving collection of artificial intelligence methodologies aiming to exploit the tolerance for imprecision and uncertainty that is inherent in human thinking and in real life problems, to deliver robust, efficient and optimal solutions and to further explore and capture the available design knowledge [1]. Some authors suggest term SCAD (Soft Computing-Aided Design) for describing the research domain where engineering design meets fuzzy logic (FL), artificial neural networks (ANN) and genetic algorithms (GAs), which are the core methodologies of soft computing.

Artificial Neural Networks mimic biological information processing mechanisms. They are typically designed to perform a nonlinear mapping from a set of inputs to a set of outputs. They are non-programmed adaptive information processing systems that can autonomously develop operational capabilities in response to an information environment. ANNs learn from experience and generalize from

*Corr. Author's Address:Faculty of Mechanical Engineering Kraljevo, Dositejeva 19, Kraljevo, Serbia, petrovic.a@mfkv.rs

previous examples. They modify their behavior in response to the environment, and are ideal in cases where the required mapping algorithm is not known and tolerance to faulty input information is required [2]. Artificial neural networks are being applied to a wide variety of automation problems including adaptive control, optimization, decision making, as well as information and signal processing.

The transition from the Aristotelian logic (between two competing states one and only one is true) to the fuzzy logic (multiple competing states may be true at the same time, each one at a different degree of truth) was accepted by the scientific community with hesitation. The ability, however, of modeling the uncertainty through fuzzy logic attracted many researchers that contributed to the foundation of various fuzzy logic concepts relative to engineering design. During the last decades, researchers have been using fuzzy logic as a representation framework in design problems characterized by inherent uncertainty during decision-making [1]. Fuzzy logic has also been applied to design activities where there are needs other than knowledge representation, e.g. for cognitive support in reverse engineering and for decision making in demanding domains, such as conceptual design.

The genetic algorithms are members of a collection of methodologies known as evolutionary computation (EC). These techniques are based on the selection and evolution processes that are met in nature and imitate these principles in many scientific domains. Like biological individuals whose characteristics are encoded in their genetic material, GAs encode the contents of each candidate solution for a mathematical optimization problem into the genome of a hypothetical individual. Individuals compete for survival by gaining a higher probability of reproduction which depends upon their fitness score (the objective score of the candidate solution they represent). Mating mechanisms based on crossover and mutation manipulate the genomes of the parents to produce offspring that then form a new generation of solutions. Over several generations the genetic characteristics of the population improve until optimal solutions arise. GAs are not influenced by the search start point, or by the continuity of the search space, or assumptions about convexity. Since they are highly parallel, they are well suited to combinatorial problems. [1].

Saridakis and Dentsoras [1] identified strong and weak points of SCAD techniques using a simple arithmetic methodology in order to determine potential areas of improvement and possibilities for further application of these techniques. The authors determined dependency strengths (arithmetic values from zero to three) between the three design tasks and the eight design issues (see table 1, legend). For each area of soft computing technique they identified how efficiently each approach of the specific area addresses the design tasks (table 1, first colmun). Then, an average evaluation metric for all approaches in the specific field is extracted ranging from one to three. This evaluation metric is then multiplied by the strength of their dependency with the design issues, thus providing an evaluation denoted with a percentage about how well the design issues are addressed by the referenced (table 1, second colmun). The results of this arithmetic evaluation process are depicted in the diagrams shown in Table 1.

Very low percentages reveal a large efficiency gap and significant opportunity for further research. It is evident that the fusion of SC techniques provides more robust design frameworks, which address the set of the identified design issues more efficiently. Finally, the combination of SC techniques with case-based design approaches provides even more efficient results.

This research shows that soft computing techniques are mainly utilized to perform specific design tasks (e.g. representation, optimization, etc.) and the approaches that deploy soft computing methods in an integrated manner are rare. The expansion of SCAD systems in industrial activities render the deployment of supportive technologies such as agent-based, web-based and AI systems imperative in order to address the identified design issues [1] .

3. ASSEMBLY DESIGN

Assembly has traditionally been one of the most important stages for product development which generally accounts for 50% or more of manufacturing costs, and also affects the product quality. To reduce manufacturing costs, it would be prudent to carry out assembly oriented and related research and development. Design for assembly is now an accepted technique and used widely throughout many large industries [5].

Table 1. Evaluation diagrams per research area [1]

Design Tasks	**Design Issues**
Fuzzy logic in Engineering design	
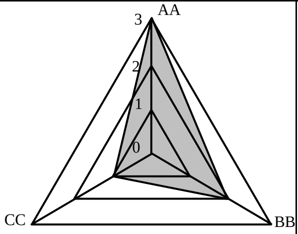	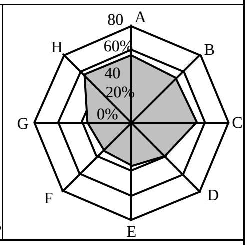
Genetic Algorithms in Engineering design	
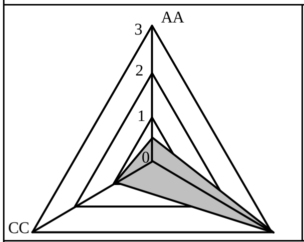	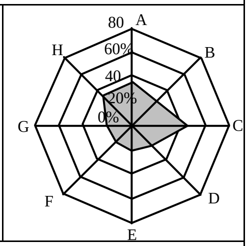
Neural Networks in Engineering design	
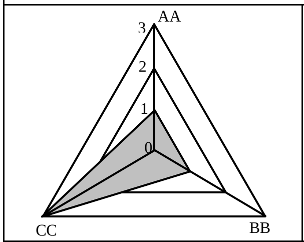	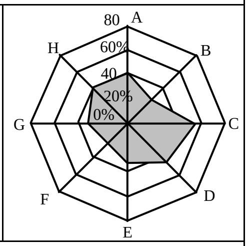
Fusion of SC techniques in Engineering design	
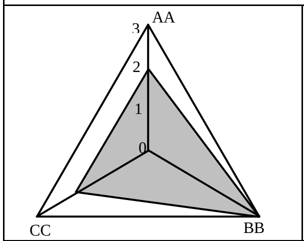	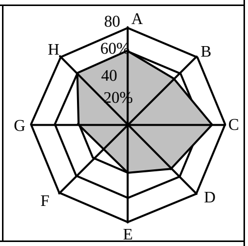
Case-Based Design and SC	
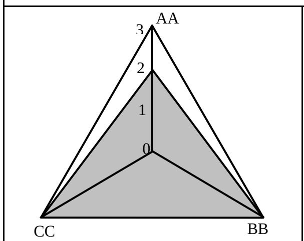	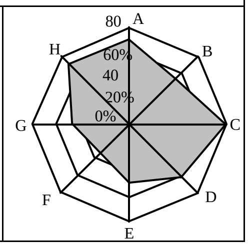

Legend:	
AA: Design knowledge representation, BB: Search for optimal solutions, CC: Retrieval and learning of design knowledge. Dependency strengths: 3 = strong, 2 = medium, 1 = light, 0 = none.	A: Uncertainty management and conceptual design, B: Collaboration, communication and coordination, C: Solution extraction under lacking knowledge/ uncertainty, D: Management and reuse of existing design knowledge, E: Generality and domain-independence, F: Extensibility and connectivity to other tools, G: Balance between automation and human activities, H: Simplicity.

DFA was first systematized in the 1960s by Geoffrey Boothroyd and his colleagues Alan Redford and Ken Swift at the University of Salford, England. Research first focused on methods of feeding parts by means of vibratory and other mechanical. Attention turned in the 1970s to classifying parts and assembly tasks in an effort to provide a simple way for engineers to judge the assembleability of their designs. Hitachi developed a set of assembleability evaluation methods at this time as well. [6].

Assembly involves the integration of components and parts to create a product or system. Assembly planning is a crucial design step for generating a feasible assembly sequence. Good assembly sequence planning has been recognized as a practical way to reduce operation difficulty, the number of tools and working time. The implementation of design for assembly (DFA) and design for manufacturing (DFM) resulted in enormous benefits, including the simplification of products, reduction of assembly product costs, improvement of quality, and shrinkage of time to market. Generally, assembly sequence planning (or assembly planning) can be classified into two major aspects: assembly modeling dedicated to CAD models and its capability, and assembly sequence generation. The common approach for assembly modeling is graph-based shown as parts mating graph and topological relation between components of a design [3].

Assembly planning includes generation, representation and selection of assembly part sequences. It is a very important issue in the design of assembly as different part sequences can drastically affect the eficiency of the assembly process [5]. The main purposes of assembly analysis and evaluation are concerned with minimizing the cost of assembly within the constraints imposed by the requirements to meet the functionalities of the product being assembled. Assemblability and assembly sequence evaluation play a crucial role in assembly oriented design. In the conceptual design of an assembly, it is important to consider the assemblability, disassemblability and control flexibility. An assembly sequence is the most important part of an assembly plan and it affects other aspects of the assembly process: resources, assembly line layout, efficiency and cost as well as various details in the product design. Automating the generation of assembly sequences and their optimisation can ensure the competitivity of manufactured goods and increase profit margins.

4. AI METHODOLOGIES IN ASSEMBLY DESIGN

Due to complexity of assembly and product design, there is an increasing need to integrate artificial intelligence with the designer intelligence for maximum benefits and expediting advanced design process. As such, it is necessary to apply knowledge-based systems techniques to the assembly oriented product design processes [6]. Automatic identification of assembly attributes from a CAD description of a component have been investigated and resulted with developed intelligent CAD system by encoding the Boothroyd design for assembly knowledge with feature-based representation. Such a system provides users with suggestions in order to improve a design and also to help obtain better design ideas. Another famous knowledge-based design for assembly system was developed by LUCAS Engineering. This system runs through a length phase of questioning the designer for product data needed for the analysis. The output gives specific advice on which product or component would benefit from a change to its design.

Numerous researchers employed artificial intelligence tree search, or graph search methodology to generate an assembly sequence. Unfortunately, the search space increases explosively when the number of components in a design grows. For relieving this combinational complexity, heuristic rules and genetic algorithms (GAs) have been used in the searching process. Other studies used the Hopfield and back propagation neural network (BPNN) as the means to generate optimum or sub-optimum assembly sequences [3].

Chen [3] proposes a three-stage integrated approach with some heuristic working rules to assist the planner to obtain an optimal assembly plan. In the first stage, Above Graph and transforming rules are used to create a correct explosion graph of the assembly model. In the second stage, a threelevel relational model is developed to generate a complete relational model graph and the incidence matrix. The relational model graph can be advanced transformed into an assembly precedence diagram (APD), which is used to describe the assembly precedent relations of the parts. Based on these graphs, the designer can easily find the feasible sequences and evaluate the difficulty of assembly. In the third stage, a case study is utilized to evaluate the feasibility of the proposed model in terms of the differences of underlying assembly characteristics and to generate a near-optimal assembly sequence according to the defined performance criteria.

The experimental results for the case study verify the feasibility of the proposed approach which facilitates the DFA in potential applications of 3D component models to assist manual or automatic assembly in a virtual environment, and allows the designer to recognize the relative position, geometry constraints and relationships of the 3D components using graph-oriented methods: Above Graph, APD and relational model graph.

An approach proposed by Zha [6], [7], [8], [10], can be used to generate all feasible assembly sequences of the product by reasoning and decomposing the leveled feasible sub-assemblies, and representing them through Petri-net graph and assembly tree. A new unified class of object-oriented knowledge based Petri nets, incorporating knowledge based expert systems and fuzzy logic into ordinary place–transition

Petri nets, is defined and used for the representation and modeling of the distributed design processes. In this work, a fuzzy comprehensive approach to assemblability and assembly sequence evaluation is used. Model for assemblability evaluation is based on the additive aggregation of the degree of dificulty of assembly operations. The proposed intelligent approach and framework focus on the knowledge-based integration of product design, assemblability analysis and evaluation, and design for assembly with economical analysis.

Senin in his work [12] investigates the application of GA-based search techniques to concurrent assembly planning, where product design and assembly process planning are performed in parallel, and the evaluation of a design configuration is influenced by the performance of its related assembly process. Feasible decompositions of product are recombinated into assembly plans and encoded into genomes. Each individual represents a plan, with its fitness score representing the plan performance evaluation score, which is defined as a simplified evaluation of plan execution time.

Marian et al. used GA with a classical structure for the optimisation of assembly sequences [13], but modified genetic operators, to avoid the combinatorial explosion. Proposed GA works only with feasible assembly sequences and has the ability to search the entire solution space.

Dini et al. [14] also deploy genetic algorithms to generate optimal assembly plans. The genetic algorithm produces near-optimal assembly plans starting from a randomly initialised population of assembly sequences in the context of minimizing both the orientation changes of the product and the gripper replacements, while grouping technologically similar assembly operations. The quality of the generated assembly sequences is assessed by a space-state search algorithm that adopts a best-first search algorithm and seeks the path that corresponds to a feasible sequence with the lowest total cost.

Another approach for the assembly line planning problem is proposed by Chen et al. [15]. In this study, a hybrid genetic algorithm addresses assembly planning with various objectives, including minimizing cycle time, maximizing workload smoothness, minimizing the frequency of tool change, minimizing the number of tools and machines used and minimizing the complexity of assembly sequences. Moreover, a self-tuning method was developed to enhance the effective schema of chromosomes during the deployment of the proposed genetic operators.

Although genetic assembly planners find improved assembly plans with some success, they also tend to converge prematurely at local-optimal solutions. Smith [16], [17] presents an assembly planner, based upon an enhanced genetic algorithm, that demonstrates improved searching characteristics over an assembly planner based upon a traditional genetic algorithm. The author introduces two new genetic operators to help reduce premature convergence in genetic assembly planners.

Zha [9] studies the assemblability and the assembly sequence evaluation in the engineering design through a neuro-fuzzy approach. According to this approach, the fuzziness is a property of the degree of difficulty assigned to the operation which can be represented by a fuzzy number between 0 and 1. The assembly operations have been evaluated based on various criteria, such as time and equipment required, although the analysis focuses on the difficulty of operation. Moreover, a neural network automatically tunes the membership functions of assemblability factors, so as to adjust the assembly difficulty score. Using the neuro-fuzzy approach, the relationships between product definition data, assembly factor, and assemblability can be formulated followed by sensitivity analysis that could predict how a design parameter change will affect the assemblability.

Zha [11] also presented a neuro-fuzzy approach to intelligent design and planning of manual assembly workstation. Simulated assembly tasks were carried out on a multi-adjustable workstation, and the posture and motion data of operators were recorded and analyzed. The trained neural network is capable of memorizing and predicting the angles of human joint motions associated with a range of workstation configurations. The developed algorithms can generate the design/layout results more quickly and accurately than other existing heuristic or analytic algorithms.

5. CONCLUSION

Numerous researchers employed successfully artificial intelligence methodologies to generate an optimal or near optimal assembly sequence. Complete AI-based integrated assembly oriented design process is still complicated by the complex interactions and domain knowledge between the technical and economical aspects of design process of assembly. Therefore, the development of a truly intelligent methodology and system for the concurrent integration of design for assembly process is stil in progress.

Acknowledgement
Authors A.Petrović and B. Radičević wish to acknowledge their gratitude to „Ministry of Education and Science of Republic of Serbia“ for the support to the research through project grant TR37020.

REFERENCES

[1] K.M. Saridakis, A.J. Dentsoras; Soft computing in engineering design – A review; Advanced Engineering Informatics 22 (2008) 202–221
[2] L.C. Jain; N.M. Martin; Fusion of Neural Networks, Fuzzy Systems and Genetic Algorithms: Industrial Applications; CRC Press 1998
[3] W.C. Chen, P.H. Tai, W.J. Deng , L.F. Hsieh; A three-stage integrated approach for assembly sequence planning using neural networks; Expert Systems with Applications 34 (2008) 1777–1786
[4] W.C. Chen, Y.Y. Hsu, L.F. Hsieh, P.H. Tai; A systematic optimization approach for assembly sequence planning using Taguchi method, DOE, and BPNN; Expert Systems with Applications 37 (2010) 716–726
[5] D. E. Whitney; Mechanical Assemblies; New York Oxford, Oxford University Press 2004
[6] X.F.Zha, H.J.Du, J.H.Qiu; Knowledge-based approach and system for assembly oriented design, Part I: the approach; Engineering Applications of Artificial Intelligence 14 (2001) 61-75
[7] X.F.Zha, H.J.Du, J.H.Qiu; Knowledge-based approach and system for assembly oriented design, Part II: the system implementation; Engineering Applications of Artificial Intelligence 14 (2001) 239–254
[8] X.F. Zha; An object-oriented knowledge based Petri net approach to intelligent integration of design and assembly planning; Artificial Intelligence in Engineering 14 (2000) 83–112
[9] X.F. Zha, Neuro-fuzzy comprehensive assemblability and assembly sequence evaluation, Artificial Intelligence for Engineering Design, Analysis and Manufacturing 15 (2001) 367–384.
[10] X.F. Zha; A knowledge intensive multi-agent framework for cooperative/collaborative design modeling and decision support of Assemblies; Knowledge-Based Systems 15 (2002) 493–506
[11] X.F. Zha, S.Y.E. Lim; Intelligent design and planning of manual assembly workstations: A neuro-fuzzy approach; Computers & Industrial Engineering 44 (2003) 611–632
[12] Nicola Senin, Roberto Groppetti, David R. Wallace; Concurrent assembly planning with genetic algorithms; Robotics and Computer Integrated Manufacturing 16 (2000) 65}72
[13] Romeo M. Marian, Lee H.S. Luong, Kazem Abhary; A genetic algorithm for the optimisation of assembly sequences; Computers & Industrial Engineering 50 (2006) 503–527
[14] G. Dini, F. Faillil, Lazzerini, F. Marcelloni; Generation of Optimized Assembly Sequences Using Genetic Algorithms; CIRP Annals - Manufacturing Technology; 48 (1999), 17-20
[15] Ruey-Shun Chen, Kun-Yung Lu, Shien-Chiang Yu; A hybrid genetic algorithm approach on multi-objective of assembly planning problem; Engineering Applications of Artificial Intelligence 15 (2002) 447–457
[16] Greg C. Smith, Shana S.-F. Smith; An enhanced genetic algorithm for automated assembly planning; Robotics and Computer Integrated Manufacturing 18 (2002) 355–364
[17] Shana Shiang-Fong Smith; Using multiple genetic operators to reduce premature convergence in genetic assembly planning; Computers in Industry 54 (2004) 35–49

HEAVY MACHINERY - HM 2011, 55-60
ISBN 978-86-82631-58-3

Paper accepted: 20.05.2011

Time localization of abrupt changes in cutting process using Hilbert Huang Transform

Zivana Jakovljevic[1]
[1] University of Belgrade, Faculty of Mechanical Engineering

Cutting process is extremely dynamical process influenced by different phenomena such as chip formation, dynamical responses and condition of machining system elements. Different phenomena in cutting zone have signatures in different frequency bands in signal acquired during process monitoring. The localization of signal's frequency content in time is extremely important in machining operations studying and monitoring. An emerging technique for simultaneous analysis of the signal in the time and frequency domain that can be used for time localization of certain frequencies is Hilbert Huang Transform (HHT). It is based on empirical mode decomposition (EMD) of the signal into intrinsic mode functions (IMFs) as simple oscillatory modes. IMFs can be processed using Hilbert Transform and instantaneous frequency of the signal can be computed.

This paper gives a methodology for time localization of cutting process stop during intermittent turning. Cutting process stop leads to abrupt changes in acquired signal correlated to certain frequency band. This frequency band is localized in time using HHT. To address the problem of low-frequency pseudo components an improvement to HHT is introduced in this paper. The proposed methodology is experimentally verified. The potentials and limitations of HHT application in machining process monitoring are shown.

Keywords: Cutting process monitoring, Hilber-Huang Transform, time localization of signal

0 INTRODUCTION

Sensor based monitoring of cutting process gives valuable information that can be used for process and quality control. In situ monitoring systems are usually based on measurements of cutting force, acceleration, acoustic emission or audible sound close to the cutting zone. All these methods are suitable for practical online application. A comparison of frequency contents of the signal that can be obtained using different sensors is given in Fig. 1.

Cutting process is extremely dynamical process. Besides phenomena related to the chip formation itself, cutting process dynamics is influenced by the dynamical responses and condition of machining system elements (machine, tool, workpiece). Different stages of material removal process: shearing, ploughing, plastic deformation are correlated to the different frequency contents of the signal [1]. As shown in the Fig. 1, interaction of the tool tip with the workpiece microstructural features: voids, inclusions, grain boundaries also leads to different spectral components [2, 3]. Besides, tool condition (wear or breakage) can be identified in signal. Using signal processing techniques, different frequencies carrying information on various phenomena can be extracted from signal.

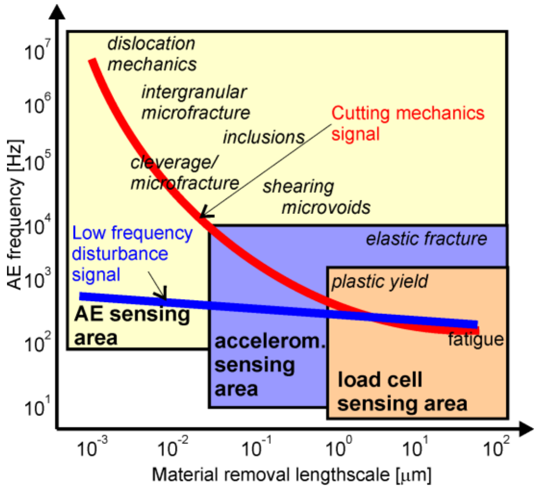

Fig. 1. *Sources of AE in material removal [1]*

The information from sensory system is useful for process and quality control only if it is available in due time. In order to detect tool condition or to detect or link the surface finish or material microstructure to the chip formation mechanism e.g., it is not enough to identify the presence of corresponding frequency in signal. The frequency should be localized in time/space.

*Corr. Author's Address: University of Belgrade, Faculty of Mechanical Engineering, Kraljice Marije 16, 11000 Belgrade, Serbia, zjakovljevic@mas.bg.ac.rs

In machining operations monitoring different signal processing methods can be used for simultaneous analysis in time and frequency domain [4]. Short time Fourier Transform (STFT) and specially Wavelet transform (WT) have obtained significant attention. WT was extensively applied in methods for tool condition monitoring [4], or in studying of phenomena related to the chip formation [3] e.g. Nevertheless, in STFT the time and the frequency resolutions are fixed in the whole spectrum. The shortcoming of WT is the poor frequency resolution at high frequency range.

An emerging technique for simultaneous analysis of the signal in time and frequency that gives good resolution in both domains is Hilbert Huang Transform (HHT) [5]. There have been some applications of HHT in general machine health monitoring [6]. Tool condition monitoring methods based on HHT were also researched. In [7] an approach to flute breakage detection in end milling based on HHT is proposed. A tool wear correlation to HHT during end-milling is explored in [8], were the marginal Hilbert spectrum was considered and the changes were not localized in time.

The most dramatic phenomena in cutting process are perceived as abrupt changes during short time interval in acquired signal. Two characteristic conflict situations that lead to abrupt changes are catastrophic tool failure and collision of tool with workpiece, fixture or machine. The third class of phenomena inherently containing abrupt changes is intermittent cutting, while turning splined shaft e.g. This situation does not have conflict contents, it is regular, but delicate state of cutting process. The detection of cutting process start and stop in intermittent cutting is especially important in micromachining. Generally, the exact time localization of abrupt changes in signal is of the most importance.

This paper gives a methodology for time localization of cutting process stop during intermittent turning. Cutting process stop leads to abrupt changes in acquired signal correlated to certain frequency band. The frequency band related to abrupt changes is localized in time using HHT. This approach is different from approach given in [7] since only the energy in frequency band of interest is considered rather than the energy of the whole spectrum.

1 HILBERT HUANG TRANSFORM

In the traditional Fourier analysis the notion of frequency is connected to the sine and cosine functions' wavelength. In order to determine certain frequency using Fourier Transform (FT), one needs data for at least full wave. FT is created for linear, stationary data. Nevertheless, the most of the natural systems are nonlinear and data are usually non-stationary, but for the lack of alternatives, FT is still applied. The typical example is cutting process. In non-stationary data, frequency is changed in each instant, and time localization of frequency is very important. For definition of instantaneous frequency of the signal, Hilbert Transform (HT) can be used. For time series $x(t)$, it is defined by:

$$y(t)=\frac{1}{\pi}\int_{-\infty}^{\infty}\frac{x(\tau)}{t-\tau}d\tau\,. \tag{1}$$

where $x(t)$ and $y(t)$ represent complex conjugate pair and define an analytic signal $z(t)$:

$$z(t)=x(t)+jy(t). \tag{2}$$

which can be represented in polar coordinate system as:

$$z(t)=a(t)e^{j\theta(t)}. \tag{3}$$

with

$$\begin{aligned} a(t)&=\sqrt{x(t)^2+y(t)^2}\\ \theta(t)&=arctg\big(y(t)/x(t)\big) \end{aligned}. \tag{4}$$

where $a(t)$ and $\theta(t)$ represent instantaneous amplitude and phase of the analytic signal. They give the best local fit of an amplitude and phase varying trigonometric function to $x(t)$. From instantaneous phase, an instantaneous frequency can be derived as:

$$\omega(t)=\frac{d\theta(t)}{dt}=\frac{\dot{y}(t)x(t)-y(t)\dot{x}(t)}{x^2(t)+y^2(t)}\,. \tag{5}$$

As shown in [5] the instantaneous frequency $\omega(t)$ will have the physical meaning only if $\theta(t)$ is monocomponent function. Since θ(t) is derived from $x(t)$, $x(t)$ should be monocomponent signal. This means that $x(t)$ has to wave around, that is to be symmetrical with respect to the zero mean level, without riding waves (purely oscillatory function).

The most of the real world data and specially nonlinear and non-stationary data do not meet given prerequisites. In order to prepare this kind of signals for Hilbert Transform, Empirical Mode Decomposition (EMD) method is introduced [5]. EMD starts from assumption that each signal represents a superposition of simple purely oscillatory functions. These functions are called Intrinsic Mode Functions (IMFs) and represent the counterpart of harmonic functions in FT. IMFs should satisfy the following conditions: 1) the number of extrema and number of zero crossings in the whole data set must be either equal, or differ at most by one, 2) the mean value of the envelopes defined by local maxima and local minima at any point should equal to zero.

EMD decomposes signal into IMFs using sifting process as follows. First, the local maxima and minima are identified and upper and lower envelop are created by connecting local maxima and minima, respectively using cubic splines. The mean of envelopes m_1 is subtracted from signal $x(t)$ and the first component h_1 is obtained:

$$h_1 = x(t) - m_1 . \qquad (3)$$

Ideally, h_1 is IMF, but usually this is not fulfilled. In order to create IMF sifting process is repeated more times. In sifting process, h_1 is treated as data and then:

$$h_{11} = h_1 - m_{11} \qquad (6)$$

and procedure is repeated k times:

$$h_{1k} = h_{1(k-1)} - m_{1k} \qquad (7)$$

until IMF is obtained.

A criterion for sifting process stop is given by setting the standard deviation between two consecutive sifting results:

$$SD = \sum_{t=0}^{T} \left[\frac{\left(h_{1(k-1)}(t) - h_{1k}(t)\right)^2}{h_{1(k-1)}^2(t)} \right]. \qquad (8)$$

to 0.2-0.3. The first IMF component is defined as:

$$c_1 = h_{1k} . \qquad (9)$$

c_1 is then separated from the rest of the signal by:

$$x(t) - c_1 = r_1 . \qquad (10)$$

The residue r_1 still contains information about lower frequency components, and it is treated as a new signal and the same sifting process is applied to it, c_2 is obtained, etc:

$$r_2 - c_1 = r_1, \ldots, r_{n-1} - c_n = r_n . \qquad (11)$$

The procedure is repeated n times, until one of the following criteria is fulfilled: 1) c_n or r_n have very small values, 2) r_n is monotonic function.

Sifting process eliminates the riding waves and makes the wave profiles more symmetric. The signal is represented by:

$$x(t) = \sum_{i=1}^{n} c_i + r_n . \qquad (12)$$

After IMFs are obtained, Hilbert Transform is applied to each IMF and instantaneous frequencies are computed using eq. (5). Since the starting signal $x(t)$ is multicomponent, it has more than one instantaneous frequency. Applying given procedure signal is represented as:

$$x(t) = \mathrm{Re}\left(\sum_{i=1}^{n} a_i(t) \exp\left(j \int \omega_i(t) dt \right) \right). \qquad (13)$$

with time dependant amplitude and frequency.

The signal representation given by (13) represents its HHT. FT representation of the same signal is given by:

$$x(t) = \mathrm{Re}\left(\sum_{i=1}^{\infty} a_i(t) \exp\left(j \omega_i t \right) \right). \qquad (14)$$

with a_i and ω_i constant.

Equation (13) enables the representation of the signal in time-frequency-amplitude (energy) 3D space. This representation (in which the amplitude axis can be in the form of colour e.g.) is called the Hilbert spectrum. In Hilbert spectrum the existence of energy at certain frequency means that there is high likelihood that such a wave has appeared locally at that time instant.

As an example, IMFs and Hilbert spectrum in parallel with Fourier spectrum of a synthetized signal are given in Figure 2. A time localization of frequences (20, 30 and 15 Hz) and amplitudes (10, 5 and 7) can be percieved.

One of the shortcomings of EMD is that it generates undesirable IMFs at low frequencies. This is ilustrated in HHT presented in Fig. 2 where the frequencies near 0 Hz which do not exist in the signal are detected. This can lead to missinterpretation of the results.

The low frequencies in HHT come from the low frequency IMFs that do not represent the real components of the signal [9]. In order to addres given problem, the cross corelation of the IMFi with the original signal - μ_i should be checked. Only those IMFs whose cross corelation μ_i crosses predefined treshold λ, should be considered as real IMFs. The IMFs whose μ_i does not cross λ should be treated as pseudo-components and added to the residue.

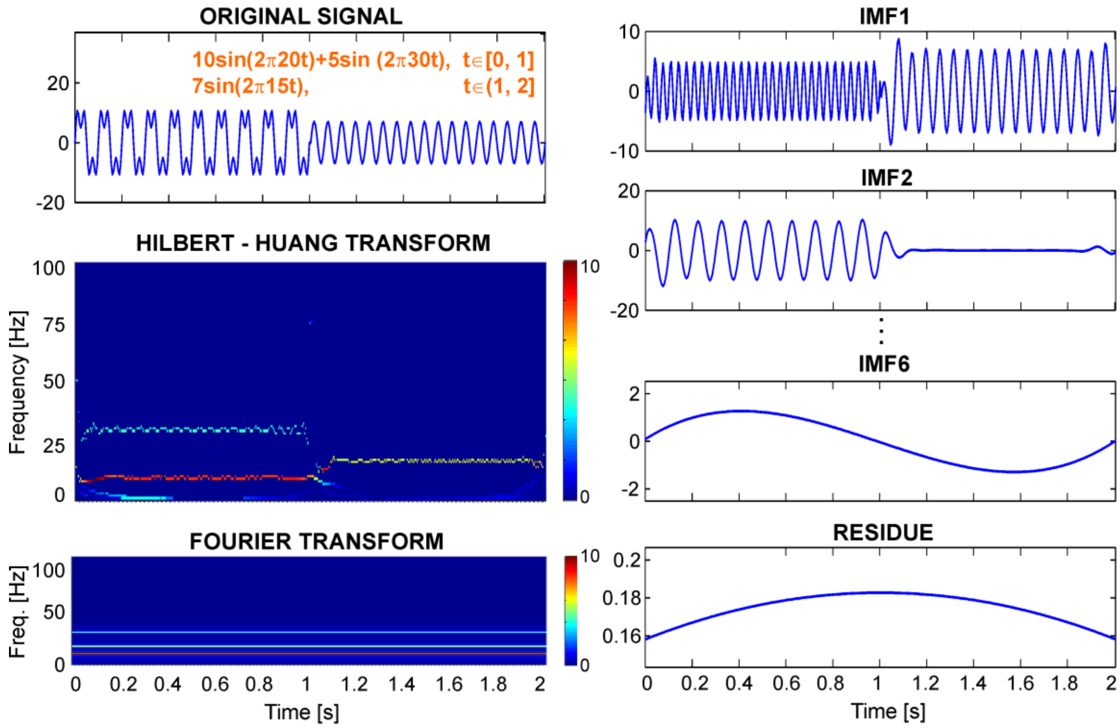

Fig. 2. *Synthesized signal: a.)signal, b) Hilbert spectrum of the signal, c) Fourier transform of the signal, d) IMF components obtained using original EMD*

2 TIME LOCALIZATION OF ABRUPT CHANGES IN CUTTING PROCESS

HHT with introduced improvement is exploited for detection of cutting process stop during intermittent turning.

The kind of intermittent turning applied in this study was chosen because it can be used for simulation of tool breakage [10]. Experiments have shown [11] that tangential force (as well as induced vibrations) at tool breakage increases suddenly when a broken tool part jams between the tool and workpiece and then drops to zero when gap is formed. When tool approaches the workpiece again, forces increase beyond their original value.

Although it seams that the cutting process stop can be clearly recognized, it is not so straightforward. It is covered by free vibrations of entire machining system. The interruption of cutting process is strong energy impulse and it is followed by dynamical response of mechanical system. After the stop, the transients with huge vibrations occur. Besides, there are some other phenomena, like cutting process start, or chip breakage that lead to the similar change in signal.

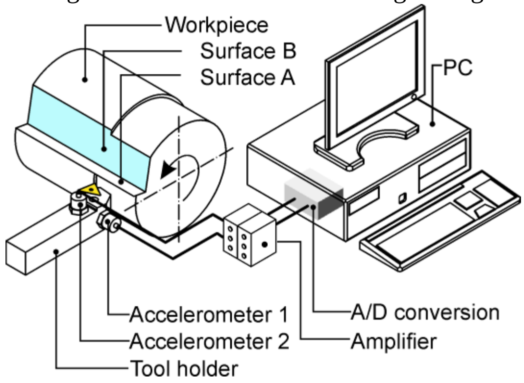

Fig. 3. *Experimental setup*

The experimental setup is shown in Fig. 3. Workpiece is grooved and has two mutually perpendicular flat surfaces of interest. In this way intermittent turning is performed. Surface A provides an extremely sharp decrease (step excitation), while surface B is inclined, thus providing relatively gradual increase of cutting force (ramp excitation). The vibrations caused by cutting process are measured. Experimental setup is shown in Fig. 4. Experiments are carried out on Hasse & Wrede lathe. During experiments speed (118–950 rpm) and feed (0.05–0.2 mm/r) were varied. Two types of P25 tool inserts (TNMM 220408 and TNMM 220424) were used. For measurement purposes, a pair of accelerometers (Kistler 8002) was fixed on tool holder at two perpendicular axes. Signal is acquired using 10 kHz sampling rate.

A signal from one accelerometer acquired during an experiment (n=475rpm, s=0.05mm/r, tool insert TNMM 220408-4025) is shown in Fig. 4. EMD of given signal revealed a total of 13 IMFs. The cross correlation of the first 8 IMFs with original signal was greater than 0.05. These IMFs (Fig. 4) are taken as real IMFs. The remaining 5 IMFs are added to the residue.

The 2d and 3d views of Hilbert spectrum of the signal are given in Fig. 4. Thorough analysis of given spectrum shows that cutting process stop is correlated to high energy in the spectrum at frequencies from 1.8 to 2.3 kHz. The marginal spectrum for this frequency band is shown in Fig. 4. At these frequencies cutting process stop is clearly extracted from all other phenomena with similar signature in signal (transients after process stop, cutting process start, chip breakage, etc.).

The proposed procedure gave the same results for all the experiments.

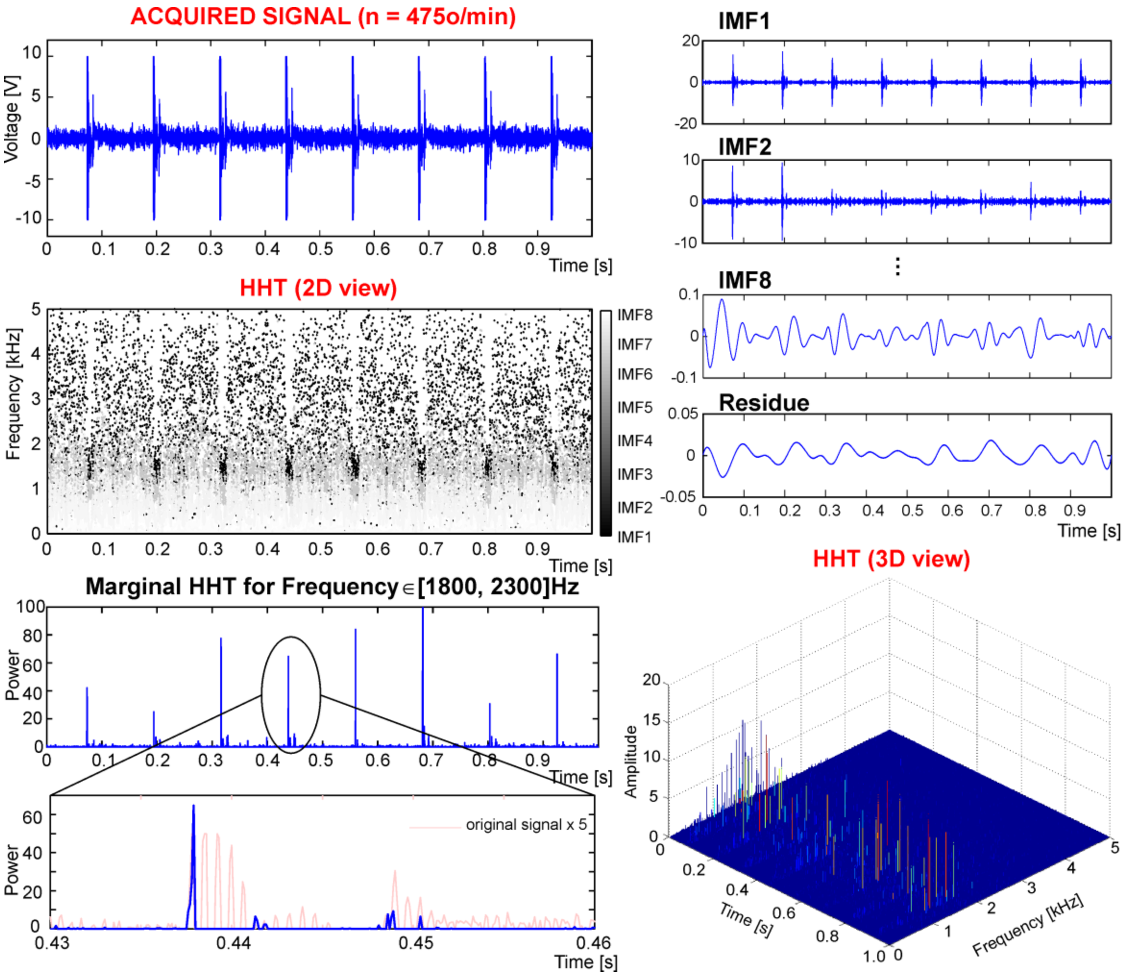

Fig. 4. *Experimentally obtained signal: a.) acquired signal, b) Hilbert spectrum of the signal – 2D presentation, c) Marginal Hilbert spectrum for the frequencies 1800-2300Hz, d) IMF components obtained using improved EMD, e) 3d view of Hilbert spectrum*

3 CONCLUSION

In the monitoring, as well as in the studying of machining operations, time localization of certain frequency bands represents an important issue. The time-frequency analysis technique used in this paper, HHT, gives much sharper resolution in frequency and a more precise location in time when compared to STFT and WT. In HHT the resolutions in both domains can be as high as sampling rate allows. HHT is intuitive, direct, a posteriori and adaptive. The decomposition into IMFs is obtained from the data, while harmonic functions and wavelets are chosen a priori. IMFs represent complete, adaptive and almost orthogonal representation of the analyzed signal.

Nevertheless, HHT has some shortcomings: 1) EMD generates undesirable IMFs at the low frequency region that may cause misinterpretation of the result; 2) In order to make instantaneous frequency physically meaningful, IMFS should be in narrow frequency band; depending on the analysed signal, the first IMF may cover too wide frequency range, so that the property of monocomponent can not be achieved; 3) the EMD can not separate signals that contain low-energy components.

The first shortcoming was addressed in this paper. The pseudo IMFs are excluded from decomposition using cross correlation with original signal as a criterion. In this way the number of IMFs that should be computed online is reduced, and real-time applicability of the method is improved.

The cutting process stop in intermittent turning studied in this paper is correlated to the certain frequency band in Hilbert spectrum. It is shown that the HHT can be used as a powerful tool for exact time localization of cutting process stop.

4 REFERENCES

[1] Liu, X., DeVor, R., E., Kapoor, S., G., Ehmann, K., F., The Mechanics of Machining at the Microscale: Assesment of the Current State of the Science, Trans of the ASME, Vol. 126, pp 666-678, 2004

[2] Lee, D., E., Hwang, I. Valente, C.,M.,O., Oliveira, J.,F.,G., Dornfeld, D.A. Precision manufacturing process monitoring with acoustic emission, Int J of Machine Tools and Manufacture, Vol.46, pp 176–188, 2006

[3] Mian, A., J., Driver, N., Mativenga, P., T., Chip formation in microscale milling and correlation with acoustic emission signal, Int J of Adv Manuf Techn, Available online, DOI 10.1007/s00170-011-3185-x, 2011

[4] Teti, R., Jemielniak, K., O'Donnell, G., Dornfeld, D., Advanced monitoring of machining operations, CIRP Annals - Manuf Technology Vol. 59, pp 717–739, 2010

[5] Huang, N., E., Shen, Z., Long, S., R., Wu, C., M., Shih, H., H., Zheng, Q., Yen, N., C., Tung, C., C., Liu, H., H., The empirical mode decomposition and the Hilbert spectrum for nonlinear and non-stationary time series analysis, Proceedings of Royal Society London, Vol. 454, pp 903-995, 1998

[6] Yan, R., Gao, R., X., Hilbert-Huang transform based vibration signal analysis for machine health monitoring, IEEE Trans on Instr and Meas, Vol. 55, pp 2320-2329, 2006

[7] Bassiuny, A., M., Li, X., Flute breakage detection during end milling usin Hilbert-Huang transform and smoothed nonlinear energy operator, International Journal of Machine Tools and Manufacture, Vol.47, pp 1011-1020, 2007

[8] Kalvoda, T., Hwang, Y., R., A cutter tool monitoring in machining process using Hilbert–Huang transform, International Journal of Machine Tools & Manufacture, Vol. 50, pp 495–501, 2010

[9] Peng, Z., K., Tse, P, W., Chu, F., L., An improved Hilbert Huang transform and its application in vibration signal analysis, Journal of Sound and Vibration, Vol. 286, pp 187-205, 2005

[10] Petrovic, P., B., Jakovljevic, Z., Milacic, V., R., Context sensitive recognition of abrupt changes in cutting process, Expert Systems with Applications, Vol. 37, pp 3721-3729, 2010

[11] Haili, W., Hua, S., Ming, C., & Dejin, H. On-line tool breakage monitoring in turning. Journal of Materials Processing Technology, 139, 237–242. 2003

Acknowledgment: The author would like to express the gratitude to Ministry of Education and Science of Republic of Serbia for providing financial support that made this work possible under the grants TR35007 and TR35020

HEAVY MACHINERY - HM 2011, 61-65
ISBN 978-86-82631-58-3
Paper accepted: 30.05.2011

DfX approaches and CAX tools in integrated development of products and processes

Aranđel Babić [1,*] – Nemanja Ilić [1] – Vladimir Jakovljević [1]
[1] University of Kragujevac, Faculty of Mechanical engineering Kraljevo

Integrated development of product and process IDPP evolved in industry as an outgrowth of efforts such as Concurrent Engineering to improve customer satisfaction and competitiveness in a global economy. It is a management technique that integrates all acquisition activities starting with requirements definition through production, fielding/deployment and operational support in order to optimize the design, manufacturing, business and supportability processes. IDPP uses design tools such as modeling and simulation, teams, and best commercial practices to develop products and their related processes concurrently. It is based on using of DfX approaches and CAX tools as support for DfX.

Key words: Integrated development of product and processes, DfX, CAX, integration

INTRODUCTION

Integrated product development is defined as a systematic approach for product development and, with it, related processes, in order to fully meet the expectations of users. To be successful, companies must develop, produce and deliver products which fulfil a multitude of different requirements.The challenge for the companies product development engineers is to deliver products that not only meet the customers requirements, but also respond to constraints imposed on the design process.The structure of integrated development of product and processes is shown in Figure 1.

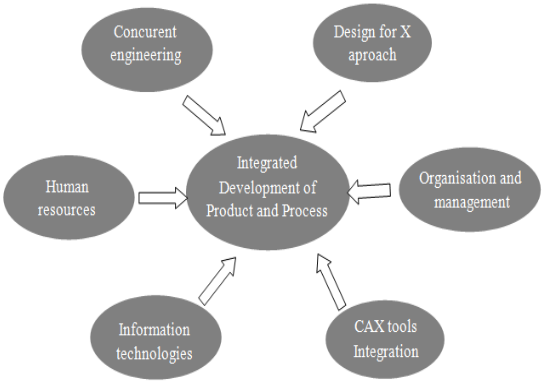

Fig.1. *The structure of integrated development of product and processes*

Important aspects of integrated product development are:

1. systems approach to product development - the application of principles, processes and tools of system engineering, and is engaging in product development from the point of all phases of product lifecycle,
2. navigation to the user - means satisfying customer demands and means that producers are required to manufacture excellent, attractive, and products that exceed customer requirements,
3. DfX method application - a promising approach to identify efficient ways to manage the optimization of resources at different stages of product development, and shall be dealt with in subsequent chapters,
4. organization and management - which involves the substitution of traditional sequential approach to product development organization with a parallel approach,
5. application of information and communication technologies,
6. application and integration of automated engineering tools - CAD/CAPP/CAM integration.

1. DESIGN FOR X

Design for X (DfX) has emerged as a promising approach to identify an efficient way to manage resource optimization throughout all the different stages of the product development process. DfX offers strategies for supporting fundamental decisions at the planning stage of the developmental process and can also provide guidance during the later stages. In addition, DfX can assist the broader goal of distributing limited people, time, energy, material and environmental

*Corr. Author's Address: Faculty of Mechanical Engineering Kraljevo, Dositejeva 19, Kraljevo, Serbia, babic.a@mfkv.kg.ac.rs

resources in an optimal way in response to market pressures.

DfX means that the designer has to follow many guidelines during the whole product development process, starting from the conceptual stage up to the embodiment and detail design, these guidelines and rules are constraints on his or her path to the optimal design solution. In the literature there is no useful structure for classifying DfX criteria.

A structure for different DfX criteria has been developed by Bauer, 2003. The criteria are classified and hierarchical dependencies are defined, based on the fundamental aims of a company, namely: design for profit, design for resources and design for staff (Figure 2.)

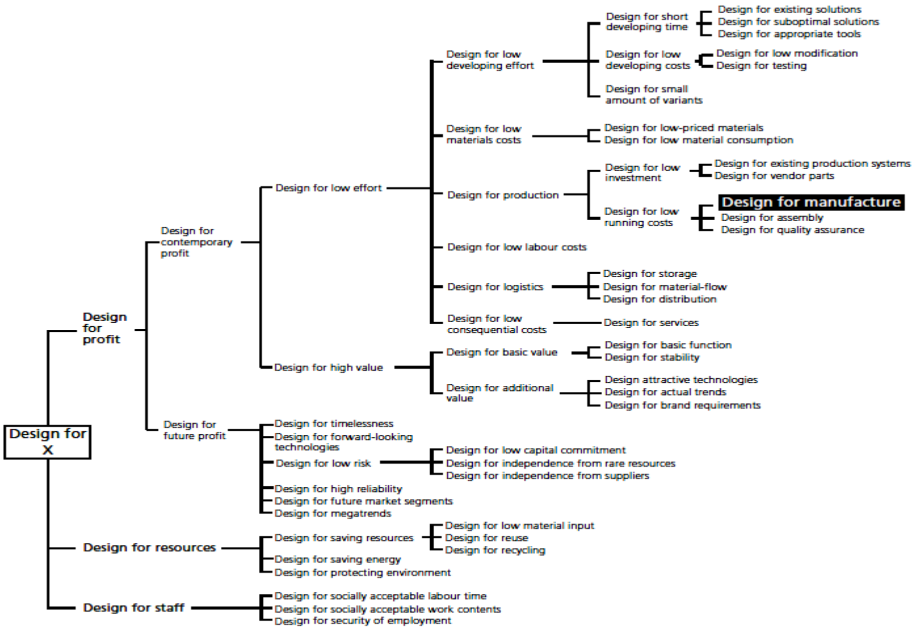

Fig. 3. *An approach for structuring DfX criteria (Bauer, 2003)*

Each DfX method can be divided into sub-criteria. For example, the design for manufacturing DFM can be broken down into its sub-criteria (Figure 3.). This particular example shows both the variety of DfX and the fact that different criteria are spread over a wide range of hierarchy levels.

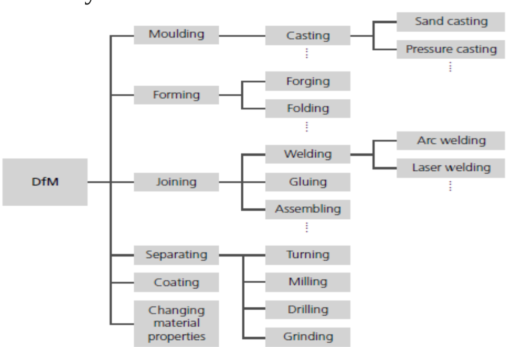

Fig.3. *DFM sub-criteria*

2. CONCURRENT ENGINEERING

Concurrent engineering CE refers to the simultaneous development of the deliverable product and all of the processes necessary to make the product and to make that product work. These processes can significantly influence both the acquisition and life-cycle cost of the product. Process examples include the manufacturing processes needed to fabricate the product, the logistics support processes needed to support the product, or, for a data collection system, the process to collect and disseminate the information gathered. Emphasizing the design of these processes at the same time the product is being designed ensures that the product design does not drive an unnecessarily costly, complicated, or unworkable supporting process when the product is actually produced and fielded.

CE is considered to be an ideal environment for the DfX approach to product development.The objective of CE is to reduce the system or product development cycle time through better integration of activities and processes. CE provides an integrated, parallel approach to design. The connection between DfX and CE is shown on Figure 4.

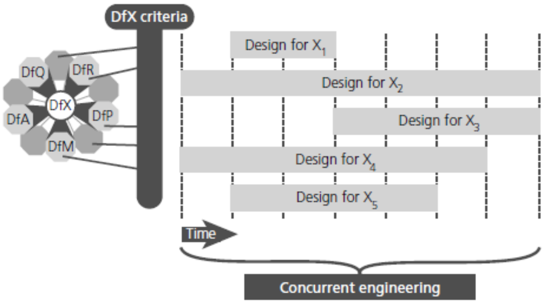

Fig. 4. *Connection between design for X and concurent engineering*

3. CAX TOOLS AS DFX SUPPORT

These software tools deal with different, independent aspects of the design for X approach called CAX tools. Some of these tools are based on the application of the finite element method (FEM), focusing on stress and deformation analysis of mechanical properties of the product. Other tools focus on testing products technologicality, for example. simulation of injection moldings, based on CAD models of products. In this case, the 3D product model is simulated in one of CAD software packages carry information that is imported through special interfaces in the program used for simulation. Using CAX tools, can be simulated casting process (for example, filling the mold and/or behavior in the cooling process) to determine the real casting process conditions (for example, the speed of pouring).

The next group of tools supports the CAX cost calculation. With these tools, each component is divided into primitives that define the preparation time, processing time and extra time which defines the total cost of production. Links between manufacturing primitives and production costs must be stored in the knowledge base for the calculation of costs. To calculate the cost of materials, the relationship between geometry/materials and intermediate products from which it receives, must also be defined.

For product design CAD tools are used (for example, Solid Edge Part module), CAPP tools for technology design, for the design of assembly structures CAA tools (for example, Solid Edge Assembly module), and the manufacturing design, as support to the DFM approach, CAM tools are being used, as EdgeCAM.

4. CAD/CAPP/CAM/CNC INTEGRATION

Technologies concerning using of computer-aided: design-CAD, process planning-CAPP, manufacturing-CAM and computer numerical control-CNC can be used independent from each other. The term “islands of automation” has been used to describe these disconnected groups of systems with no integration between them. As the engineering businesses are increasingly being run in a more globalized fashion, these islands of automation need to be connected.

In order to achieve CAD/CAPP/CAM/CNC integration, there have been two types of traditional models in use, centralized model (Model A) and collaborative model (Model B).

In a centralized model, manufacturing activities occur within a single manufacturer or a few manufacturers that have similar information infrastructure.

In a collaborative model, a middle tier is added using for example a neutral data exchange format. As such, collaborative activities in the manufacturing environment become easier. Figure 5. illustrates the data flows in these two models.

In Model A, both CAD and CAM systems use the same proprietary data format. Over the years, CAD/CAM system vendors have been successful in developing different proprietary data formats to support their systems throughout design and manufacturing processes. CAD and CAM systems are using the same data format so that data incompatibilities between them are eliminated. Furthermore, since there is no data-transferring barrier, system vendors have more freedom to model information. In addition to pure geometry, integrated CAD/CAM systems can support activities ranging from design to NC programming.

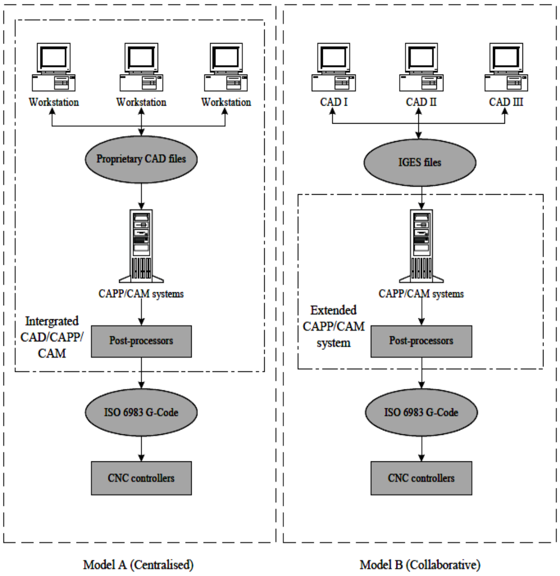

Fig 5. *Data flows in model A and B*

5. MILLING HEAD PARTS MODELLING IN A CAD/CAM SYSTEM

The product in this study is a milling head. First, all components are designed in CAD system, in case of milling heads it is Solid Edge. Each component is designed variantly and parametricly. On next Fig. 6. is shown CAD model of milling boom modelled in Solid Edge.

Fig. 6. *CAD model of milling boom*

To allow for correct placement and adjustment, pattern of two holes are design on milling boom, to ensure proper placing of tool holders. Using these geometry, on tool holders are designed two pins, which help easier assembly process (Figure 7.). The case study starts from part design to all the down-stream activities related to manufacture of the part.

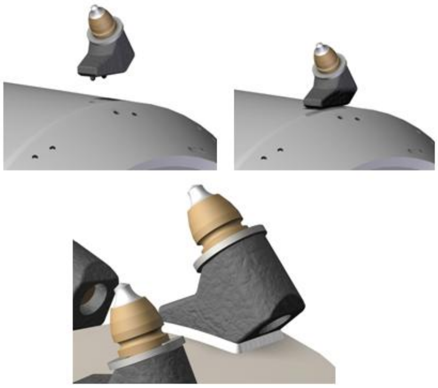

Fig. 7. *Easy of tool holder placement*

This milling head is designed using a Solid Edge system. Some of the components are machined on a CNC milling machine. Process planning and NC code generation are carried out within EdgeCAM.

In this case a typical example is a milling head drum with positioning holes of tool holder arranged in the shape of a helicoid. The functional demand of cutting holes depends on the drum diameter, number of tools and helicoid feet. Case is modelled variantly and parametricly in SolidEdge, and it is then imported in the programme package for technology design, EdgeCAM (Figure 7.) whose exit is NC code for drilling holes which is then postprocessed for appropriate CNC machine tool.

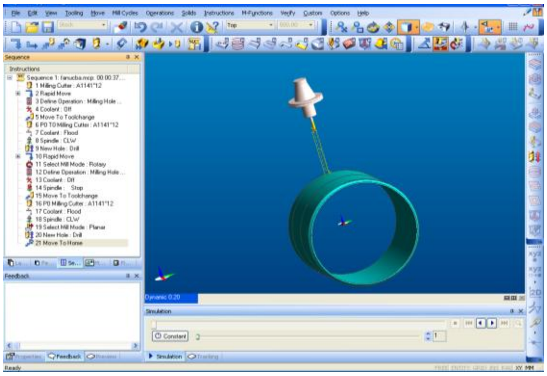

Fig 7. *A window in programme EdgeCAM*

The condition is that an NU machine tool should be able to position workpiece on axis C and to have tool movement along axis Y (numerically managed lathe with Y/C management). Machine tool compound from fund standard modules, able to support this kind of process, is shown on next fig. 8. In EdgeCAM NC program need to be postprocessed for this machine according to available movements, spindle speeds, working space, and etc.

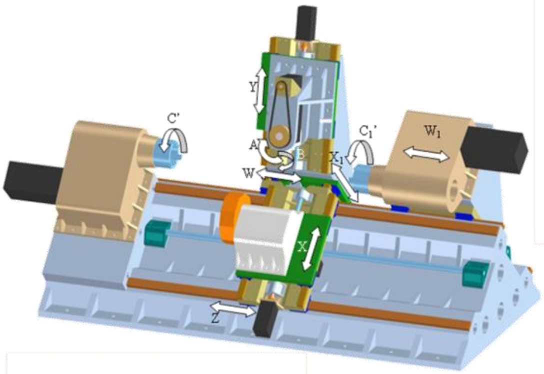

Fig 8. *Lathe witn Y/C management*

6. CONCLUSION

Product design in this integrated environment is one of the key conditions that influence the cost savings generated in the process of engineering design during the product life cycle.

Integration of product design and process planning can achieve a better design of a product. This integration, application of DfX approaches, using CAX, and integration of CAX is one of the key conditions for concurent product development.

One of the best ways to integrate all processes is using of features within the context of the STEP standard. Next work should be based on application of features, and STEP standard in integration of CAD/CAPP, CAPP/CAM, and CAM/CNC. Additional implementation methods should be defined to describe all STEP instances for building product exchange models.

7. REFERENCES

[1] FORTIN, É., CHATELAIN, J-F., & RIVEST, L. (2004). An innovative software architecture to improve information flow from CAM to CNC. Computers & Industrial Engineering, 46(4), 655-667.

[2] DoD, Integrated Product and Process Development Handbook, OFFICE OF THE UNDER SECRETARY OF DEFENSE (ACQUISITION AND TECHNOLOGY) WASHINGTON, DC 20301-3000.

[3] Lee, K. (1999). Principles of CAD/CAM/CAE systems. Rolland, USA: Addison Wesley Longman, Inc.

[4] BABIĆ, A., PETROVIĆ, A., ILIĆ, N., PRŠIĆ, D., Integracija CAD/CAM u projektovanju putnih glodačkih glava, SPMS08, 501-504, Novi Sad, FTN, Novi Sad, Septembar 2008.

[5] Nemanja ILIĆ, Marina PLJAKIĆ, Aranđel BABIĆ, „Inteligent CAD design and assembly plan of milling heads“, The 7th International Scientific Conference, Research And Development Of Mechanical Elements And Systems, IRMES 2011 April 27th to 28th, 2011 in Zlatibor, Republic of Serbia, p 109.-112., ISBN

[6] SINGH, N.. Systems Approach to Computer-Integrated Design and manufacturing. New York, USA: John Wiley & Sons, Inc. (1996)

[6] SMILJKOVIC, I., Conceptual modelling of machine tools according to criteria of chosen cutting process, Diploma work, Faculty of Mechanical engineering Kraljevo, 2005.

HEAVY MACHINERY - HM 2011, 67-72
ISBN 978-86-82631-58-3
Paper accepted: 30.05.2011

Computer Integrated Production Technologies

Nenad Nikolić[1,*] - Ljubomir Lukić[1] - Mirko Djapić[1] - Goran Stojanović[1] – Zvonko Petrović[1]
[1] University of Kragujevac, Faculty of Mechanical Engineering Kraljevo, Sebia

Contemporary products of complex geometric forms are the achievements of modern technology and solve problems posed by the continuous industrial development, others, however, occurred much earlier in its basic, unchanged forms have long been represented in all spheres of human life. But they share the complexity of construction, the complexity of geometric forms and computer-integrated production technologies. For this reason, the design of technologies for the space of complex surfaces is aided by computers and largely relies on the development of both hardware systems and software solutions that support engineering activities in product design and technology. Computer integrated production technologies make it possible to connect virtually all phases of production processes that consist of a variety of technical, technological and organizational activities. Highly sophisticated software and hardware can now minimize the cost price, increase quality, increase productivity, reduce development time, in order to create competitive products.

This paper presents a characteristic example of the manufacturing practices which is modeled by a product, a tool designed for its production, designed and simulated by the technological process, generated NC code for making the working area of tools and tool path simulated in the production process, thus effectively demonstrated the effect of computer integrated technology in engineering practice.

Keywords: CAD/CAE/CAM, plastic injection, integrated production technologies

0 INTRODUCTION

Computer-aided design (***CAD Computer Aided Design***) makes it easier and faster design and construction of products starting from conception, various illustrations, models and prototypes. It can quickly and fully perform the analysis of various structures, starting from, say, a simple prop, to very complex structures, such as aircraft wing. With the help of computer aided engineering (***CAE Computer Aided Engineering***) it is possible for a structure to simulate, analyze and effectively test the static and dynamic behavior, thermal behavior, and others. Finally, it is possible to optimize the structure in accordance with the objectives and set criteria. Computer aided production planning (***CAPP Computer Aided Process Planning***) can improve productivity by optimizing the planning process, the planned cost reductions and improved manufacturing quality. Time of individual operations and estimation can be incorporated into the system. An important feature of ***CAD / CAM*** systems relates to their integration, which results in the interaction process of product design and technology or other engineering activities that exist between the two.

During the course of each stage of design can be achieved by feedback. This provides that if it encounters an error or defect in the implementation of some of the previous phase, it can be reversed and corrected. Computer systems are important in all areas of plastics processing industry, starting from the product design, through manufacturing, then marketing and sales, through to recycling. The application of advanced software tools has drastically shortened the time of introducing new products to market, making the replacement of expensive prototypes much faster and less expensive prototypes simulated on a computer. One technique that has brought a revolution in plastics processing in the last decades of the computer simulation and analysis of the empty plastic cooling process. Unlike the traditional method of making a row of very expensive prototypes and debugging, it has become possible, with a high degree of certainty, predict that a new product to get right the first time, and thereby meet the required quality. The plastics processing industry, especially in the field of plastic injection molding, computers allow the use of a very useful method in the phase of product design (CAD) and in the stage of simulation and analysis (CAE) and design phase

[*]Corr. Author's Address: Faculty of Mechanical Engineering Kraljevo, Dositejeva 19, Kraljevo, Serbia, lukic.lj@mfkv.kg.ac.rs

of technology (CAM), allowing the design of technology Spatial processing of complex surfaces into a routine process. The application of ***CAD / CAE / CAM*** technology for plastic injection molding so reduces tooling costs by 10% to 40%, reduce time to market product launches from 10% to 50%, reduction of material used from 5% to 30% and reducing the production time 50% to 80%.

1 MODELING OF PARTS

Computer-aided design (***CAD*** *Computer Aided Design*) is the process of product design by computer and includes activities that take place between the electronic drawing and work on software systems that support automatic product design. *CAD* can be defined as the use of computers and graphic software to support engineering activities in the development or improvement of product design from conception to documentation. The basic advantages of *CAD* systems are:

1. *Increase productivity (speed)* - automation of routine tasks to increase creativity, the input of standard parts from the database and rapid prototyping.
2. *Support changes in the structure* - no need for re-drawing of all parts after each change, the designers kept the previous iteration.
3. *Communication* - with other teams / engineers (manufacturers, suppliers), with other applications (CAD, CAM, CAE), the marketing (a realistic view of the structure), tidiness (high-quality pictures).

Modeling, body extractors, we used the program *SolidWorks*. Over Sketch command created a sketch which is required for the design of the workpiece.

After forming the initial sketches, using *Revolve* command performs the rotation about a fixed axis profile (Fig. 1). With the previous two pictures can be seen to be a very easy and simple way, the basic shape of objects. In this case it is the body of citrus fruit (Fig. 2).

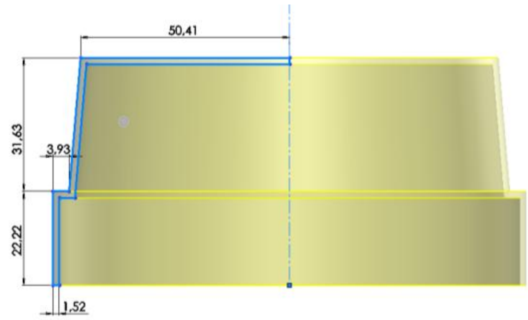

Fig.1. *Turning the basic profile around the axis*

Fig. 2. *The appearance of the finished model*

3 TECHNOLOGY PLASTIC INJECTION AND SIMULATION OF TECHNOLOGICAL PROCESS

Injection molding cycle is the most important procedure for processing of polymers, and depending on their technological level and most modern. This procedure is one of the primary processing of polymers, because the shape of molded part obtained from starting material that has no definite shape (pressings, chips, etc.).. Injection molding to shape all polymers: thermosetting plastics, elastomers, thermoplastic, and is particularly widespread plastomenih processing of materials, better known under the old name of injection molding. Injection molding can be defined as the processing of thermoplastics injection quick tempered thermoplastic melt in the mold cavity and simultaneously curing the desired product form, pressings. The biggest advantage of this procedure is the possibility that the dimensions of the pallet can be determined in advance, the application of certain laws that apply to obtaining the finished molded parts injection molding. Injection molding is performed on special machines (Figure 3), which consists of the injection unit drive sisitema, the unit for closing the mold, the mold device to temper and control units. The process of designing the injection takes place in several phases of which the basic are:

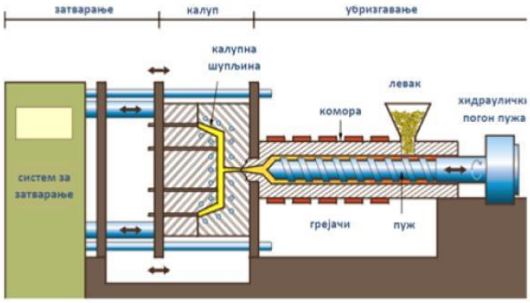

Fig.3. *Scheme of machines tools for injectione*

1. The first stage is heating plastic to the melting point and closing the mold.
2. In the second phase, axial moving snail, melted material is injected through pouring channels in the mold cavity. It is off the rotation snail, and its displacement is realized axial hydraulic cylinder.
3. In the third phase the workpiece is cooled with intensive circulation of coolant through the cooling system tools. In addition, the snail acts on the melted material subsequent pressure to make up for lack of material shrinkage pressings. After completion of cooling the pressings, at the end of the subsequent phases of operation pressure, the snail is backwards, rotates and retracts the new amount of granules, melt it and powder coating.
4. The final stage is to open the mold and eject blank. Injection unit returns to the back, and the nozzle is closed by a valve. Mold opening provided by the system for opening the given drive can be mechanical or hydraulic. Workpiece is ejected from the mold by ejector, and the extraction of surplus material from pouring shells made extractor.

In the design phase, plastic molding tools, especially tools for injection molding large parts of the complex, valuable assistance provided by specialized software packages for process simulation. One of the most popular software packages used for this purpose is *Moldflow Plastic Adviser 2010 (**MPA**)* which is produced by *Moldflow*. The program is used to analyze the process of injection molding. The input data necessary for analysis are:

- CAD 3D model,
- types of materials and
- technological process parameters (temperature of the molten polymer, mold temperature, injection pressure...).

As a result of the simulation is obtained by simulation of flow (Fig. 4), and mold filling, cooling time, the distribution of pressure and temperature along the element and forecast quality of workpiece. Linking *CAD* and *CAE* systems, in this case *SolidWorks* and *Moldflow Plastic Adviser*, may be a very complicated process, because it is necessary to transfer the geometric and nongeometrical information between the two systems.

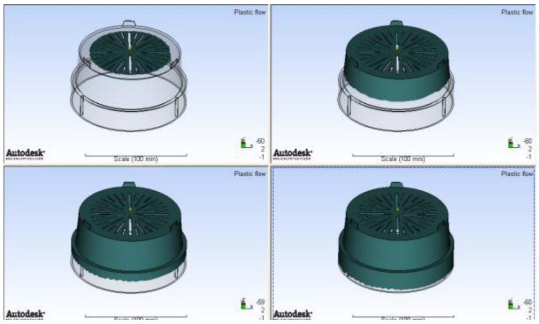

Fig. 4. *Simulation of plastic flow when filling the test section*

Manufacturers of *CAD* systems in addition to recording data in the format used allows the use of standard formats for transferring data, the most significant *IGES* and *STEP*. In recent years, the manufacturer software package the tendency of direct downloading of data from other software packages. *Moldflow* and offers full integration with the following software packages: *SolidWorks***,** *Solid Edge***,** *Pro / ENGINEER***,** *Autodesk Inventor***,** *CATIA* and other.

4 DESIGN TOOLS FOR INJECTION

The tool is an essential element of working system for injection molded parts that directly shape and typically is used to produce a single product. The main tasks of the mold are: acceptance of molten thermoplastics and its cooling to achieve the shape molded part, the suppression of the pressings from the mold cavity and cycle injection molding operation of the system. To mold could execute the tasks must have the following elements:

- pouring system,
- mold,
- The system for ejecting the part
- The system for managing mold
- Housing and
- Elements of the cooling of the mold.

In addition to these elements of the mold may have some other elements that are used only in special die design. What will be the type of mold that needs to be constructed depends on the shape and size of pallet capacity injection machines, and thus the number of mold cavities, type of polymer. In constructing the tools should seek to mold the work is automated, so they could be more shortened injection cycle. Design and construction of modern products, which typically occur plastic products, it is almost unthinkable without the use of modern *CAD* software packages. Special significance implementation of appropriate and specialized software programs for design tools and other elemnata machining systems for plastic molding. *Solid Edge Mold Tooling*, software company Siemens *PLM* Software is an integrated module software package, *Solid Edge*, which provides a simple integrated process of designing and manufacturing molds for injection. He gives us a great decrease in the time of designing the mold, provides high accuracy in construction of mold cavities and the automatic generation of standard components of molds first step in construction of tools is to create an opening in the working part of the mold (Figure 5), consisting of core, cavity and the plane separation.

After the formation of holes in the test section follows the mold defining the housing or the tool (Figure 6). The software allows automatic generation of standard elements of the mold. Define them according to size of *LKM* mold base catalog. These are the pole guides, screws, cooling system, transportation system, pouring system, ejectors, connectors and other elements.

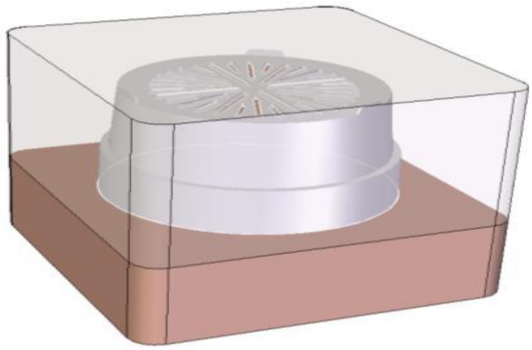

Fig.5. *Create a plane separation and the mold cavity*

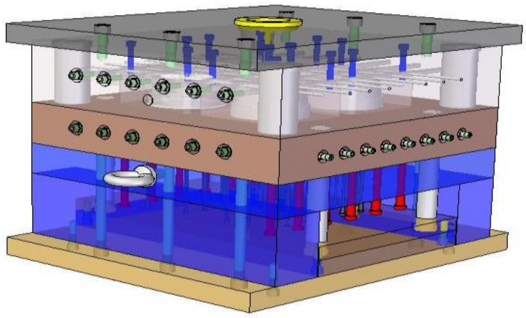

Fig.6. *Create a standard mold elements*

5 *NC CODE* GENERATION FOR THE JOB OF TOOLS

The logical continuation of the implementation information technology in the design and construction tools for plastics is to use *CAM*, and appropriate software that allows the forming of complex parts of the tool, especially mold with the highest level of accuracy of machined surface quality and scope of the *CNC* machine tools for metal cutting.

Relative motion of the blade tool along the contour of the workpiece in the machining process, carried out the execution of *NC* program by the *CNC* control system. *NC* program contains all the instructions for the process of cutting and the holder of the technological expertise of the designer of technology.

CAM systems allow automatic generation of *NC* code and have several advantages compared to manual *NC* programming or *NC* programming using one of the symbolic programming language (Figure 7). The most important advantages are:

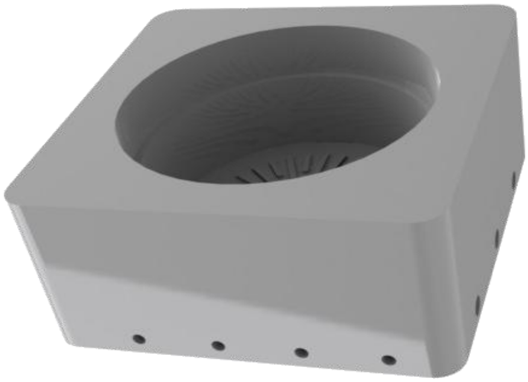

Fig.7 **.** *Workpiece – core of plastic injection molds*

- Programming without knowledge of the standards (eg DIN 66025),
- programmed processing full workpiece contour defining pripremka and final processed workpiece geometry, not the tool path,
- Built-in - Technology application with the plan of treatment - technology,
- The sophistication and complexity of the workpiece does not affect the complexity of the NC programming,
- Good graphics support during the *NC* programming.

SolidCAM can import various *CAD* formats for the exchange, and in this instance the *CAD* model can be directly imported from *SolidWorks*. When importing part of one of the first tasks is to define beginning part and set in a coordinate start the machine.

Output and objective of all activities in the *CAM* software packages is the automatic generation of *NC* code that contains all the instructions for the process of cutting. *NC* code is created based on information about the sequence of operation of unit operations using the application *Code Generator*. Thus the data on the tool path, defined in the *SolidCAM'**s*** order of procedure of unit operations, converted the files with *NC* in the format for the *CNC* turning center control system. Postprocessor generator for the formation of *NC* code is defined by the control unit. Code generator creates a file containing the *NC* code for machining order, whose introduction in the Editor can make all changes directly in the code, if necessary. *NC* program can be directly loaded into the *CNC* machine control system using the CD-ROM, floppy disks, magnetic tape, transferred electronically to the computer network of CAD / CAM workstation, or DNC communication between the "cell" and the CNC controller system.

6 SIMULATION TOOL PATH

Simulation is a realistic view of machining process, showing the movement of the tool and the process of removing material. Simulation makes it possible to identify any errors or collisions tool paths, tool holders, or in contact with the workpiece. Eg. simulator will give an error if the cutting geometry is not adequate, so the tool touches the workpiece, not only cutting edge, but the handle. Also, it is often the case that the short handle tools, and tool holder in contact with the workpiece. The program allows you to easily make changes, if irregularities are detected, as the tools, strategies and cutting conditions. Then, re-process simulation is repeated until you get the desired processing sequence. The command that runs the simulator Simulate Machining (Fig. 8). There is a possibility of simulation processing in real time, and rapidly, which is especially suitable when machining complex parts, whose processing can take up to several hours.

7 CONCLUSION

The plastics processing industry, especially in the field of plastic injection molding, computer integrated systems allow the implementation of modern methods of design, both at the stage of product design ***CAD***, and downstream, simulation and analysis in the design phase ***CAE/CAM*** technology, ensuring that the design of technologies for processing spatial complex area into a simple engineering process. The design of modern products, which certainly include plastic products, is greatly facilitated by using ***CAD*** software packages, some of which are commonly used ***Solid Works***.

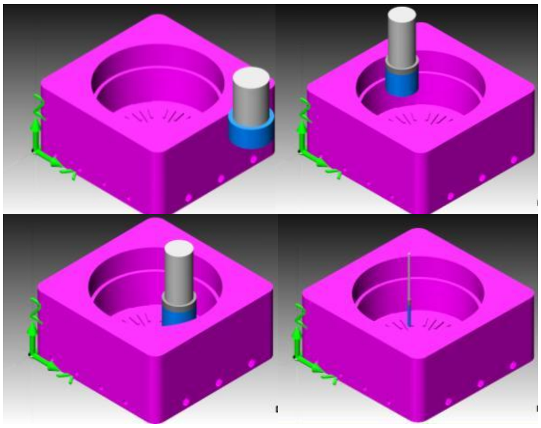

Fig.8. *Simulation of movement of the tool when processing workshops nest*

As shown in this paper, it is crucial preparation, and uses the definition of the geometry of ***3D*** models, allowing very rapid correction of the model, where there is a need arise in the later stages of design. As input into the process of computer-integrated design tools for plastic takes up a model that was previously analyzed in ***Moldflow*** software package on the basis of which was carried out simulations of flow and cooling of plastic and injection mold filling, and forecast the quality of the workpiece obtained. Thus, the obtained significant cost savings and eliminated the process of repeated testing, which, as corrections made after them, are very expensive.

The biggest advantage of using modules for integrated design of tools for plastic injection ***Mold Tooling***, software package, ***Solid Edge***, are reflected in the use of standard parts of the tool. Due to various catalogs of standard housing, pouring system, the system discharge, and all other elements of standard tools, significantly shortens the time of design tools during the supply of standard elements, and therefore the time product release.

The last step in the design and construction tools for plastics is to use ***CAM***, which allows the forming of complex parts of the tool, especially mold with the highest level of accuracy and surface quality of the ***CNC*** machines. ***CAM*** systems, as output, enables automatic generation of ***NC*** code. ***NC*** code is generated in the paper processing business area consists of core many number of ***NC*** blocks (rows). Practically is difficult to create such a long code manual ***NC*** programming, ***NC*** programming or using any of symbolic programming languages. The real strength of the ***CAM*** system is reflected in the fact that the complexity and the complexity of the geometric shapes of the workpiece does not affect the complexity of creating ***NC*** programs. Graphical simulation shows complete processing, with automatic display of any errors occurring in the process of defining the processing parameters, thereby eliminating these errors in advance, before the fabrication process, and without prior testing of workpieces.

8 REFERENCES

[1] Nikolić,N.: Design of CNC Technology and automatic generation of NC programs for the treatment of working tools for the production of plastic parts, *Master's thesis*, Faculty of Mechanical Engineering Kraljevo (2011).

[2] Polajnar,D., Polajnar,J., Lukić,Lj., Djapić,M.: Complexity Challenges in CAPP Systems and Promises of Multi-Agent Technology, Proceedings The Sixth Triennial International Conference "Heavy Machinery HM 2008", Kraljevo, 24-29 June 2008, pp.F.19-P.24.

[3] Djapić,M., Lukić,Lj., Arsovski, S.: Integrated Management Systems – Requirement of Contemporary Business Practices, Proceedings The Sixth Triennial International Conference "Heavy Machinery HM 2008", Kraljevo, 24-29 June 2008, pp.G.1-G.6.

[4] Ivanovic,S., Lukić,Lj.: Database Design from Technological and Kinematic Parameters of NC Program for Production in Flexible Manufacturing Systems, Proceedings The Sixth Triennial International Conference "Heavy Machinery HM 2008", Kraljevo, 24-29 June 2008, pp. G.7-G.12.

The results presented in this work are a result of project TR 37020, realized by the Faculty of Mechanical Engineering in Kraljevo, University in Kragujevac and funded by the Ministry of Education and Science of the Republic of Serbia.

HEAVY MACHINERY - HM 2011, 73-78
ISBN 978-86-82631-58-3
Paper accepted: 30.05.2011

Optimization of the Parameters of Broaching Machining Mode by Using the Method of Particle Swarm Optimization (PSO)

Zvonko Petrović[1,*], Ljubomir Lukić[1], Radovan Bulatović[1], Vladimir Đorđević[1], Nenad Nikolić[1]
[1] University of Kragujevac, Faculty of Mechanical Engineering Kraljevo, Kraljevo, Serbia

Optimally chosen parameters of the processing mode directly influence total costs of production of a single product and therefore the profit of the company as well. In this paper, the choice of optimum parameters of the broaching processing mode by using the method of particle swarm optimization (PSO) is shown. The goal of optimization is represented through the goal function (optimization function or optimization criterion) and by using the method of optimization PSO, minimum costs of machining process are obtained. Optimization function is also represented graphically for the purpose of clearer analysis on the technological area in which the values of machining mode that give minimum costs of machining process are presented.

Keywords: Broaching, Cutting parameters, Particle Swarm Optimization

1. INTRODUCTION

Optimization of parameters of the machining mode is the method of knowledge implementation in designing of machining process with the purpose of their analysis, improvement, and reaching a higher techno-economic analysis. A basic assumption is that the costs of machining process will be optimum if costs of machining process in all technological operations of production process are optimum as well. Mathematical model of the goal function is designed by Stanić [1] and that model of function was applied by Mečanin [2] on optimization of costs of machining process by scraping of the pin. Mathematical model of function can be applied to all elementary operations with appropriate limitations, which are different for different procedures. Goal and limitation functions should contain enough influencing factors in order to accomplish objective impact on the model of machining process.

2. MATHEMATICAL MODEL OF FUNCTION OF PROCEDURE COSTS DEPENDING ON BROACHING PROCESSING MODE

Function of costs, by which, depending on the entrance into the machining system and state (condition) of the machining system, direct procedure costs are described mathematically, represents in a trihedral OSVTz the area located in the first octane, and it is always concave because parameters of the machining mode must have values bigger than zero. Its form is:

$$T_Z = A_{1i} + A_{2i} \cdot V_i^{-1} \cdot S_i^{-1} + A_{3i} \cdot V_i^{\frac{1}{q_1}-1} \cdot S_i^{\frac{q_2}{q_1}-1} \tag{1}$$

where $i = 1, 2, \ldots, n$ is a number of operations that is optimized. Geometric position of points of conditional maxima at the area of function of costs comprises in the coordinate plane OSV a hyperbole, whose arms, depending on the state(condition) of entrance into the system, asymptotically approach the coordinate axis at faster or slower rate. A set of points is used for identifying the line of optimum costs at which machining process should be managed in order to achieve maximum effects regarding the costs of machining.

Optimal levels of costs are located in the region $\{S_{max}, V_{min}\}$, that is, the highest levels of machining are achieved when the values of steps are maximum and when cutting speed values are minimum. Inversely, the region $\{S_{min}, V_{max}\}$ is characterized by relatively high level of machining costs. There are special cases $q_2 = 1$ и $q_2 > 1$. For $q_2 = 1$ the same level of costs is obtained for the entire mode area $\{S, V\}$, while in case of $q_2 > 1$ maximum effects of machining which are located in the region $\{S_{min}, V_{max}\}$, and minimum in the mode points $\{S_{max}, V_{min}\}$.

Machining beyond the curve of optimum costs, unjustifiably frequent in production practice, conditions relatively great efficiency

*Corr. Author's Address: Universitu of Kragujevac, Faculty of Mechanical Engineering Kraljevo, 36000 Kraljevo, Dositejeva 19, zvonko@bluenet.rs

losses, especially in mode areas $\{S_{max}, V_{min}\}$ and $\{S_{min}, V_{max}\}$, because it is under such circumstances that high costs of reproduction occur in machining process [1].

Coefficient **(parameter**) A $_1$, is always constant since it represents basic costs in a company, which do not depend on machining parameters, but influence total price of production of products. Coefficients (**parameters)** A_{2i} i A_{3i} depend on machining mode, influence total costs of production and thus define position of minimum which cannot be smaller than value A_{1i} .

3. ALGORITHM PSO

Particle swarm optimization PSO (Figure 1) represents metaheuristic method of optimization based on agents (particles) population, which was accidentally discovered by James Kennedy and Russell Eberhart in 1995, while studying the simulation of social behaviour of bird flocking [3]. Just as it is the case with all algorithms based on population, initial particle population is generated first. Position of the particle represents vector of parameters which are optimized:

$$\mathbf{x} = \left(x_1, x_2, \dots, x_n\right) \tag{2}$$

or potential solution. Random position in space which is explored, as well as inital velocities, is given to each particle. After that, the value of goal function of each particle is determined, and that value is added to it as the best value for the particle in question, and the initial position becomes the best position of the particle $\mathbf{p_{best}}$. When all the best values of particles are determined, the particle with the minimum value is searched, and its position becomes the best position for the entire swarm $\mathbf{p_{gbest}}$. Afterwards, it needs to be checked whether the criteria of optimization are satisfied, and if they are, the obtained results are shown. If the criteria are not satisfied, new velocities and positions need to be calculated.

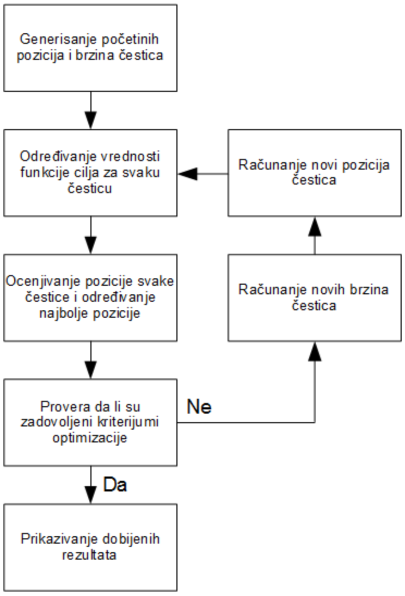

Fig.1 *Algorithm of the method of particle swarm optimization.*

Figure 2 graphically shows how to determine new velocities and positions in two-dimensional space of search.

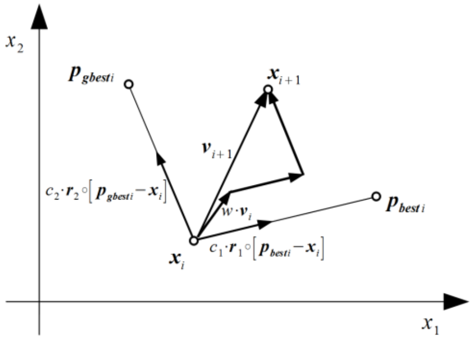

Fig.2 *Updating of velocity and position of the I particle.*

New velocity of each particle consists of three components:

1. the component which depends on instantaneous particle velocity,
2. the component which is proportional to the distance of instantaneous position of the particle and its best value,
3. the component which is proportional to the distance of instantaneous position of the particle and its best position for the entire swarm.

$$\mathbf{v}_{i+1} = w \cdot \mathbf{v}_i + c_1 \cdot \mathbf{r}_1 \circ \left(\mathbf{p}_{\mathbf{best}i} - \mathbf{x}_i\right) + c_2 \cdot \mathbf{r}_2 \circ \circ \left(\mathbf{p}_{\mathbf{gbest}i} - \mathbf{x}_i\right) \quad (3)$$

where w represents inertia weight, c_1, c_2 are acceleration coefficients or correction factors, $\mathbf{r}_1, \mathbf{r}_2$ represent two random vectors of the length n within the limits $[0,1]$. The symbol $\circ$ represents Hadamard product:

$$\left(A \circ B\right)_{i,j} = \left(A\right)_{i,j} \cdot \left(B\right)_{i,j} \quad (4)$$

Inertia weight w impacts the first component, and for the values in the range of 0,9 – 1,2 [4] it gives the best results, that is, the algorithm has greater chances of finding the global minimum for a reasonable number of iterations. For coefficient values which are smaller than 0,8, if algorithm finds global minimum it will find it fast. Particles in this case move quickly and it can happen that they “fly over” some area, so it can happen that they do not find global minimum. On the other side, if inertia weight has bigger value, then particles search the solution space more thoroughly and the chances of finding global minimum are greater.

Acceleration coefficients c_1 and c_2, when multiplied by random vectors $\mathbf{r}_1$ and $\mathbf{r}_2$, stochaistically manage the impact of the two other velocity components. Usually, their assumed value is approximately 2, in order for the middle value of the product of acceleration coefficient and random vector to be approximately 1. New position of the particle is determined by simple adding of the current position $\mathbf{x}_i$ and new particle velocity $\mathbf{v}_{i+1}$.

$$\mathbf{x}_{i+1} = \mathbf{x}_i + \mathbf{v}_{i+1} \quad (5)$$

The values of the goal function for new positions of the particle are determined again, and for each particle new and old values of the goal function are compared. If the new value is smaller, then it becomes new best value and the current position becomes the best position of that particle. The position of the particle with the smaller value becomes new best position for the entire swarm. Again, it needs to be checked whether the optimization criteria are satisfied; if they are, the results are shown, and if not, the entire procedure will be repeated until the criteria are satisfied.

This is the simplest version of the algorithm of particle swarm optimization. Other versions do not have constant values for the parameters *w*, c_1 and c_2, but they alter by specific rules during the implementation of the algorithm. In addition, other PSO algorithms also include different swarm topologies, that is, the way in which particles in the swarm communicate.

4. GOAL AND LIMITATION FUNCTION

In this paper, 25 broaching operations are optimized and in them, machining mode parameters are step $S\left[\text{mm/o}\right]$ and technological cutting speed:

$$V = \frac{\pi \cdot D \cdot n}{1000} \left[\text{m/min}\right] \quad (6)$$

in which the number of rotations $n\left[\text{o/min}\right]$ is. They are directly related to the main processing time, so for optimum values of these parameters we have optimum time of duration of each operation, and therefore, the optimum processing time of machine part. Machine mode parameters that give minimum costs of machining process must be found within given limitations because there is a limitation by characteristics of tools and machine. Figure 3 shows 3D model of valve casing and section where the greatest number of different openings are located.

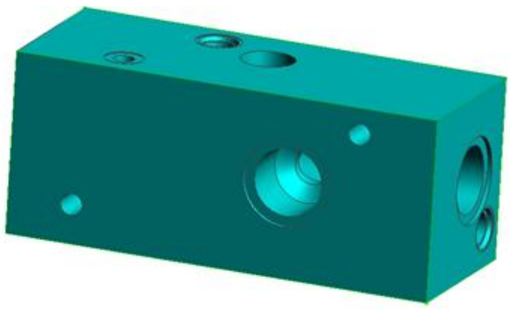

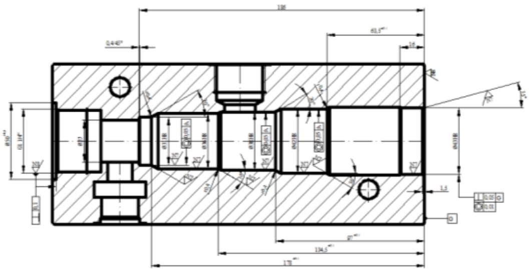

Fig.3. *Valve casing – a machine part whose broaching operations are optimized.*

Goal function which is optimized has the following form:

$$f\left(S_i,V_i\right)=\sum_{i=1}^{25}T_i = \sum_{i=1}^{25} A_{1i} + A_{2i}\cdot V_i^{-1}\cdot S_i^{-1} + A_{3i}\cdot V_i^{\frac{1}{q_1}-1}\cdot S_i^{\frac{q_2}{q_1}-1} \qquad (7)$$

Values of coefficients A_1, A_2, A_3, for each of 25 goal functions, are given in table 1 :

Table 1. Coefficient values A_1, A_2, A_3, a_i .

i	A_{1i} $[\min]$	A_{2i} $\left[\frac{\text{din}}{\min}\cdot \text{m}^2\right]$	A_{3i} $\left[\frac{\text{din}\cdot\min}{\text{m}^2}\right]$	a_i $[\text{mm}]$
1	1707,801	0,340	0,295	0,2
2	1707,801	0,378	0,547	0,2
3	1707,801	0,301	0,614	0,2
4	1707,801	0,240	0,578	0,2
5	1707,801	0,161	0,471	0,2
6	1707,801	0,123	0,421	0,2
7	1707,801	0,340	2,062	0,05
8	1707,801	0,378	2,188	0,05
9	1707,801	0,302	1,840	0,05
10	1707,801	0,161	0,942	0,05
11	1707,801	0,123	0,771	0,05
12	1707,801	0,007	0,227	0,2
13	1707,801	0,007	0,246	0,05
14	1707,801	0,003	0,063	0,2
15	1707,801	0,003	0,067	0,05
16	1707,801	0,040	1,244	0,2
17	1707,801	0,041	1,321	0,05
18	1707,801	0,020	0,278	0,05
19	1707,801	0,020	0,295	0,05
20	1707,801	0,005	0,115	0,2
21	1707,801	0,005	0,121	0,05
22	1707,801	0,001	0,015	0,05
23	1707,801	0,001	0,017	0,05
24	1707,801	0,003	0,106	0,2
25	1707,801	0,003	0,110	0,05

where coefficients A_1, A_2, A_3 have the following form:

$$A_{1i}=C_{LD2}\cdot t_{reg}+C_{M7}\cdot t_{ph}+C_{LD1}\cdot\frac{t_{pz}}{n_s\cdot z}+ +\left(C_{LD1}+\sum_{i=1}^{5}C_{Mi}\right)\cdot\left(t_p+t_m+\sum t_i\right) \qquad (8)$$

$$A_{1i}=3\,\frac{\text{din}}{\min}\cdot 480\ \min+1\,\frac{\text{din}}{\min}\cdot 1{,}4\ \min+ +3\frac{\text{din}}{\min}\cdot\frac{3\ \min}{300\cdot 25}+\left(3\,\frac{\text{din}}{\min}+11{,}8\,\frac{\text{din}}{\min}\right)\cdot \cdot\left(18\ \min\right)=1707{,}801\left[\text{din}\right]$$

$$A_{11}=A_{12}=\ldots=A_{125}=1707{,}801\left[\text{din}\right]$$

$$A_{2i}=\psi_i\cdot\left(C_{LD1}+\sum_{i=1}^{6}C_{Mi}\right)=\psi_i\cdot 15{,}8\left[\frac{\text{din}}{\min}\cdot\text{m}^2\right]$$

$$\psi_i=10^{-6}\cdot\pi\cdot D_i\cdot i\cdot L_{0i}\left[\text{m}^2\right] \qquad (9)$$

$$A_{3i}=\psi_i\cdot\left(K_3\cdot t_s+K_4\right)\cdot C_i^{-\frac{1}{q_1}}\left[\frac{\text{din}\cdot\min}{\text{m}^2}\right] \qquad (10)$$

$$K_3=\left(C_{LD1}+\sum_{i=1}^{5}C_{Mi}\right)=14{,}8\left[\frac{\text{din}}{\min}\right] \qquad (11)$$

$$K_4=1400\left[\frac{\text{din}}{\min}\right];\ C=Q\cdot D^{q_3}\cdot a^{-q_4}k_V \qquad (12)$$

Size Q =300 is the size of the series which is machined, kv=1,1 is the factor of the state of the machine, $q_1=0,75$; $q_2=1$ are the parameters of the machinability, $t_s=0{,}15$ min is the time of the change of the tools. Values D_i, L_{0i}, ψ_i, C_i are given in the table 2 and 3.

Table 2. Values of sizes D_i, L_{0i}, ψ_i, C_i

i	D_i $[\text{mm}]$	L_{0i} $[\text{mm}]$	ψ_i $\left[\text{mm}^2\right]$	C_i $\left[\text{mm}^2\right]$
1	30,95	186	18,076	186
2	35,95	178	20,093	178
3	37,95	134,5	16,027	134,5
4	42	97	12,792	97
5	42,95	63,5	8,564	63,5

6	43,95	47,5	6,555	47,5
7	31	186	18,105	186
8	36	178	20,121	178
9	38	134,5	16,049	134,5
10	43	63,5	8,574	63,5
11	44	47,5	6,563	47,5
12	12,65	10	0,397	10
13	12,7	10	0,399	10
14	20,55	2,6	0,168	2,6
15	20,6	2,6	0,168	2,6
16	15,95	43	2,154	43
17	16	43	2,160	43
18	34	9,95	1,062	9,95
19	34	10	1,068	10
20	25,95	3,5	0,285	3,5
21	26	3,5	0,286	3,5
22	40	0,45	0,057	0,45
23	40	0,5	0,063	0,5
24	21,75	2,6	0,178	2,6
25	21,8	2,6	0,178	2,6

A part made of steel S0545, is machined on five-axis machining center **Pinnacle LV85** (CONTROL SYSTEM: FANUC 0i-MC / 18i-MB) which has motive power of 15 Kw. Based on this fact we form the limitation which follows this goal function and refers to motive power machine , wich is 15kW , and material of the part.

$$0{,}345 \cdot S_i^{0{,}8} \cdot V_i < 15000 \left(i = 1, 2, ..., 25\right) \qquad (13)$$

In addition to the limitation of the value of steps, technological cutting speeds must be found within boundaries given in the table 3.Values of steps must be bigger than zero and smaller than maximum reccomended values for the tool which is used in performance of broaching operation. Values of technological cutting speed must also be bigger than zero and smaller than maximum velocity, which a machine is able to achieve for the appropriate diameter, that is, for the maximum number of rotations of the machine $n_M = 10000\,[\text{o/min}]$ is:

$$V_i < \frac{\pi \cdot D_i \cdot n_M}{1000}\,[\text{m/min}] \qquad (14)$$

Table 3.*Upper and lower boundary values of steps and velocity :*

i	S_i [mm/o]		V_i [m/min]	
	Lower boundary	Upper boundary	Lower boundary	Upper boundary
1	0	0,08	0	971,83
2	0	0,08	0	1128,83
3	0	0,08	0	1191,63
4	0	0,08	0	1318,8
5	0	0,08	0	1348,63
6	0	0,08	0	1380,03
7	0	0,08	0	973,4
8	0	0,08	0	1130,4
9	0	0,08	0	1193,2
10	0	0,08	0	1350,2
11	0	0,08	0	1381,6
12	0	0,08	0	397,21
13	0	0,08	0	398,78
14	0	0,08	0	645,27
15	0	0,08	0	646,84
16	0	0,08	0	500,83
17	0	0,08	0	502,4
18	0	0,08	0	1067,6
19	0	0,08	0	1067,6
20	0	0,08	0	814,83
21	0	0,08	0	816,4
22	0	0,08	0	1256
23	0	0,08	0	1256
24	0	0,08	0	682,95
25	0	0,08	0	684,52

5. OPTIMIZATION RESULTS

50 parameters are obtained as the results of this optimization process which represent optimum values of technological cutting speed and steps for 25 broaching operations , and so the costs of these procedures have minimum value.

Optimum values of the steps ,velocity and cost price of all operations individually and collectively are given in table 4:

Table 4. *Optimum values of the steps, velocity and cost price of all operations individually.*

i	S_i [mm/o]	V_i [m/min]	T_i [din]

1	0,006	546,8	1708,35
2	0,778	19,3	1708,68
3	0,159	79,5	1708,70
4	0,002	415,7	1708,66
5	0,444	46,8	1708,48
6	0,009	109,2	1708,34
7	0,012	66,8	1710,14
8	0,001	1034	1710,29
9	0,001	402,8	1709,86
10	0,002	352	1708,86
11	0,026	23,9	1708,66
12	0,002	125,6	1707,97
13	0,021	8,1	1707,98
14	0,012	251,4	1707,89
15	0,057	11,7	1707,86
16	0,033	500	1708,73
17	0,044	501,19	1708,78
18	0,039	7,5	1708,05
19	0,066	72,2	1708,07
20	0,043	810,5	1707,90
21	0,037	645,4	1708,15
22	0,059	250	1707,84
23	0,085	193,3	1707,82
24	0,015	23,1	1707,89
0,015	307,04	0,178	1708,00
		$\sum_{i=1}^{25} T_i$	42711,96

Number of iterations : 143

Graph of one of the 25 function costs :

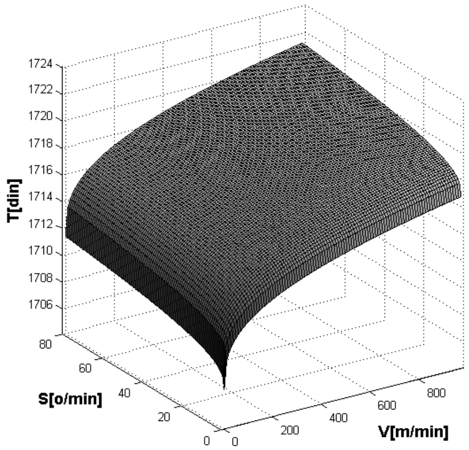

Fig.4 *Area of the function costs of the first procedure.*

According to figure we can see that the value of costs for the first operation is very close to the value 1707,8 din which represents constant cost, which means that we have reached the minimum cost , and so for the entire 25 operations, and the sum of all this costs gives us the total production price of this machine part, which is going to be minimum.

6. CONCLUSION

In this paper, the optimization of the costs of technological process of a part of a complex structure is performed by using the method PSO. For instance, in optimization of the flexible technology when real processing time is less than given, optimization of machining parameters is implemented in order to decrease costs of production. In this case, we can choose cheaper tools of lower level of cutting characteristics [5], and by using the method PSO, in a very short time, we can obtain results on which procedure allows decreasing of the machine mode and which does not, all of which can be presented in the space as in figure, for the purpose of checking of the obtained results.

7. REFERENCES

[1] Stanic, J. “Uvod u teoriju tehnoekonomske optimizacije procesa”, Mašinski fakultet univerziteta u Beogradu , Beograd, 1983.

[2] Mecanin, V. “Optimizacija obradnih procesa u masinogradnji”, Mašinski fakultet Kraljevo, Kraljevo, 1996.

[3] J. Kenedy and R. Eberhart, “Particle swarm optimization”. In IEEE International Conference on Neural Networks, 1995, pp. 1942-1948.

[4] Shi, Y.; Eberhart R. (1998). „A modified particle swarm optimizer“ Proceedings of IEEE International Conference on Evolutionary Computation. pp. 69-73.

[5] Lukić, Lj. “Fleksibilni tehnološki sistemi”, Mašinski fakultet Kraljevo , Kraljevo, 2008.

HEAVY MACHINERY - HM 2011, 79-84
ISBN 978-86-82631-58-3
Paper accepted: 30.05.2011

Application of AI techniques in Design for Manufacturing

Nemanja Ilić [1,*]- Miodrag Manić[2] - Aranđel Babić[1]
[1] University of Kragujevac, Faculty of Mechanical engineering Kraljevo
[2] University of Nis, Faculty of Mechanical engineering Niš

Concurent engineering is one of the key solutions for companies to respond to world competition. It requires the integration of all aspects of product life cycle (design, manufacturing, assembly, distribution, service, disposal). Design and manufacturing are very important fases in product life cycle, and as their integration link serve process planing. So, in the concurent engineering, process planing is one of the most important fases, in translation process from raw material into final product.

It is important to notice that process planning provides the instructions necessary to manufacturing parts, and creates a bridge between design and manufacturing. Process planning requires knowledge of processes and machine capabilities.

Work of new process planning systems is based on the application of certain artificial inteligence methods. Those are usually expert systems, genetic algorithms and neural networks. Their support are knowledge based engineering technologies, that are used for process of acceptance of knowledge and its implementation in a knowledge base.

This paper is part of the exam: Artificial inteligence in modelling of products and processes, on Ph.D. studies on Faculty of mechanical engineering in Kraljevo.

Key words: Manufacturing Processes, CAPP, Artificial Inteligence, Knowledge, Features

INTRODUCTION

Products are designed to perform functions according to functional demands that come from market. Design specifications ensure the functionality aspects, so the manufacturing need to produce the components that meet the design specifications. The components can be then assembled into the final products. Computers are used as support to the process planning and manufacturing. The related technologies are computer-aided process planning CAPP and computer-aided manufacturing CAM. They can not be strictly separated and need to be discussed in tandem.

Process planning should not be only taken into consideration for metal-cutting processes. We need process planning for many other manufacturing processes such as casting, forging, sheet metal forming, composites and ceramic fabrication. There are two process planning approaches – manual, experience-based method and computer-aided process planning method. The focus is on two computer-aided process planning methods, the variant approach, and generative approach.

1. OVERVIEW OF MANUFACTURING PROCESSES

Manufacturing can be thought of as a system (Fig. 1) in which product design is the input, and the delivery of finished products to the market is the output.

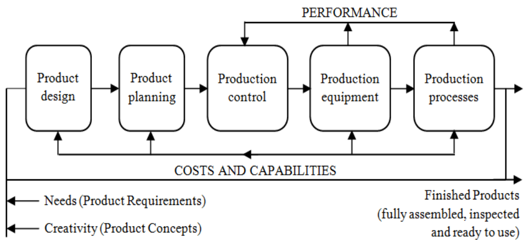

Fig.1. *The system of manufacturing*

Since the field of manufacturing integrates many disciplines in engineering and management, it is useful to divide it in such a way so as to facilitate the identification of issues and to allow a scientific approach to the problems encountered. Manufacturing can be subdivided into the areas of:

- manufacturing processes, which alter the form, shape and/or physical properties of a given material,
- manufacturing equipment, used to perform manufacturing processes,

*Corr. Author's Address: Faculty of Mechanical Engineering Kraljevo, Dositejeva 19, Kraljevo, Serbia, ilic.n@mfkv.kg.ac.rs

- and manufacturing systems, which are the combinations of manufacturing equipment and humans.

The machines that perform manufacturing processes are the embodiment of these processes. There is a close relationship between machines and processes, since the capabilities and limitations of a process often depend on the design and operation of the machine that performs it. A manufacturing process is defined as the use of one or more physical mechanisms to transform the shape of a material's shape and/or form and/or properties. Manufacturing processes can be classified into five categories:

1. Forming or primary forming processes - processes in which an original shape is created from a molten or gaseous state, or from solid particles of an undefined shape.
2. Deforming processes - processes that convert the original shape of a solid to another shape. without changing its mass or material composition. These processes are performed with machines such as: screw and excenter presses, belt operated drops, drop air hammers, hydraulic presses, wire-drawing machines, extrusion machines, bending machines, rolling machines, rotary rolling machines, and etc.
3. Removing processes - processes during which material removal occurs. Machines related to these processes are: broaching machines, lathes, drilling machines, milling machines, grinding machines, honing and lapping machines, lasers, and etc.
4. Joining processes - processes that unite individual workpieces to make subassemblies or final products, like welding, athesion, sintering.
5. Material properties modification processes - processes that purposely change the material properties of a workpiece in order to achieve desirable characteristics without changing its shape.

These categories are applied to a variety of engineering materials, which can be classified into metals, ceramics, polymers and composites. Table 1. indicates the application of different processes to different materials.

Table 1. *Overview of materials and processes*

		PROCESSES				
		Forming	Deforming	Removing	Joining	Modifying
MATERIALS	Metals	XX	XX	XX	XX	XX
	Ceramics	XX	--	X	--	--
	Polymers	XX	X	X	X	--
	Composites	XX	--	X	X	--

XX : Widely used
X : Seldom used
-- : Not used

The selection as to which process should apply to a particular material, is influenced by a number of factors, which affect cost, production rate, flexibility and part quality.

2. PROCESS PLANNING

When the design of a mechanical component is completed, it is usually documented in a drawing or a CAD file, which specifies its geometric features, dimensions, tolerances, etc. In order for the design to be manufactured, a set of instructions is needed regarding the processes, equipment, and/or people to be involved in the manufacturing process. Process planning logic determines the kind of processes to be used for the different geometric features of the component by matching process capabilities with design specifications.

The essential activities in generating a process plan, and that need to be taken into consideration, are:

- Analysis of part requirements.
- Selection of raw workpiece/material.
- Determination of manufacturing operations and their sequences.
- Selection of machine tools.
- Selection of tools, work-holding devices and inspection equipment.

The manual experience-based process planning method is still widely used. The basic steps involved are essentially the same as described above. The biggest problem with this approach is that it is time-consuming and the plans developed over a period of time may not be consistent.

The primary purpose of process planning is to translate the design requirements into manufacturing process details. This suggests a feed forward system in which design information is processed by the process planning system to generate manufacturing process details. Unfortunately, this is not what is expected in a concurrent engineering environment, whose goal is to optimise the system performance in a global context. Therefore, there is a necessity of integrating the process planning system into the inter-organisational flow. For example, if changes are made to a design, one must be able to fall back on a module of CAPP to quickly re-generate the cost estimates for these design changes. Similarly, if there is a breakdown of a machine(s) on the shop-floor, the process planning system must be able to generate alternative process plans so that the most economical solution for the situation can be adopted.

3. VARIANT AND GENERATIVE PROCESS PLANNING

Computer-aided process planning (CAPP) can be categorized in two major areas: *variant process planning*, where library retrieval procedures are applied to find standard plans for similar components, and *generative process planning*, where plans are generated automatically for new components without reference to existing plans.

In the variant process planning approach, a process plan for a new part is created by recalling, identifying and retrieving an existing plan for a similar part and making necessary modifications for the new part (Fig. 2.). Quite often, process plans are developed for families of parts. Such parts are called master parts. The similarities in design attributesand manufacturing methods are exploited for the purpose of formation of part families. A number of methods have been developed for part family formation. Among them, GT (Group Technology) is the most commonly used.

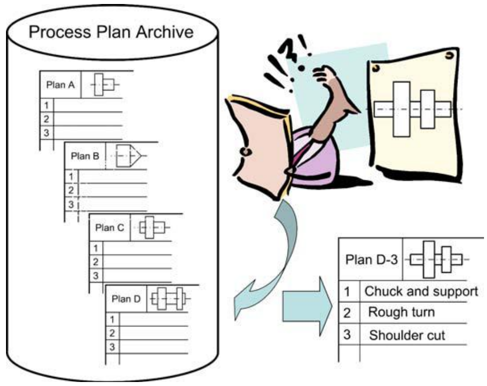

Fig 2. *The variant CAPP approach*

In the generative approach, process plans are generated by means of decision logic, formulas, technology algorithms and geometry-based data to uniquely perform processing decisions. The knowledge-based CAPP system is most commonly used. It refers to a computer program that can store knowledge of a particular domain and use that knowledge to solve problems in an intelligent way. In such a system, computers are used to simulate the decision process of a human expert.

There are two major problems to be solved: knowledge representation and inference mechanism.

The knowledge representation is a scheme by which a real-world problem can be represented in such a way that the computer can manipulate the information.

The inference mechanism is the way in which the computer finds a solution. One approach is based on IF-THEN structured knowledge.

2. EXPERT SYSTEMS

The most important processes and functions making up human intelligence are learning and using knowledge, ability to generalize, perception and cognitive abilities, e.g.

ability to recognize a given object in any context. The so-called man-made intelligent machines may be programmed to imitate only in a very limited scope, a few of above listed elements making up human intelligence. Artificial intelligence techniques such as formal logic, for describing components, and expert systems, for codifying human processing knowledge, are also applicable to process planning problems. An expert system can be defined as a tool which has the capability of understanding problem-specific knowledge and of using the domain knowledge intelligently to suggest alternative paths of action. The expert system applies knowledge and reasoning (inference) procedures in order to solve problems which require human experience (expert). The idea of expert systems consists in transposing the expert knowledge of a given domain to a knowledge base. The basic elements of an expert system are:

1. a knowledge base,
2. an inference machine and
3. a user's interface.

The knowledge base is made of a set of facts and rules. The rules are logical sentences which define some implications and lead to creation of new facts, which as a result allow to solve a given problem. The inference machine is a module which uses the knowledge base. This module may use different inference methods to solve the problem.

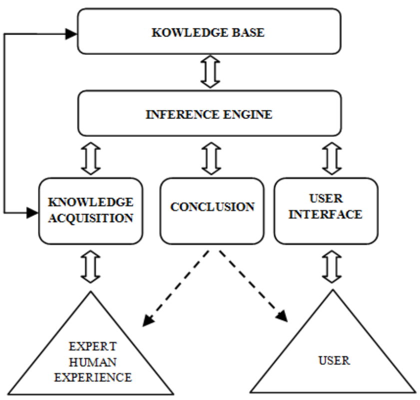

Fig. 3. *Expert system structure*

These are computer programs with a designed inference machine and an empty knowledge base. These programs are all equipped with special editor programs allowing to enter rules concerning a given problem the user wishes to solve. The issues of constructing expert systems are part of the so-called knowledge engineering. The scope of interest of specialists operating in the domain of knowledge engineering covers such issues as knowledge acquisition, its structuralization and processing as well as designing and selection of appropriate inference methods (inference machine) and designing appropriate interfaces between the computer and its user. Knowledge base is consisted of:

1. procedural knowledge, it is knowledge about procedures used in the performance of some task, and
2. declarative knowledge, it is knowledge about problem observation, about objects, states and conections.

ES development includes the construction of knowledge base - entering knowledge to the system. Knowledge acquisition, ES development process, is shown on figure 4.

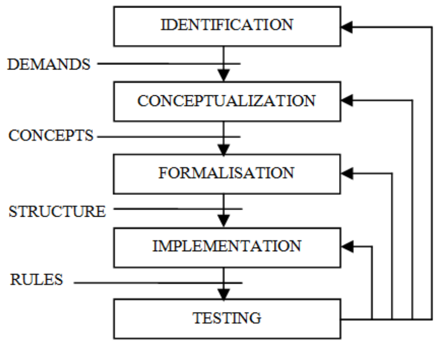

Fig. 4. *Knowledge acquisition-ES development*

It consists of next five phases: identification phase - identifying the task, studing of existing knowledge; conceptualization phase - the knowledge engineer sets the concept of access, which define the facts and hypotheses on which the task is based; formalization stage - knowledge is brought into a form suitable for presentation (in the program and Expert shell); implementation Phase - formed structures are transferred to the computer and its product is a knowledge base; testing phase - expert sees semantic irregularities and a knowledge engineer irregularities in the implementation procedures.

5. FEATURES IN CAPP

Features can be used in reasoning about the design, performance or manufacture of the part or assemblies that they constitute. Feature technology is also expected to be able to provide for a better approach to integrate design and applications such as engineering analysis, process planning, machining, and inspection.

As it is mentioned, CAPP systems are link between CAD and CAM. It is only a partial link, because most of CAD systems do not provide part feature information, which is essential information for CAPP. They don´t recognize geometrical informations in their engineering meaning related to manufacturing and assembly. It is most common problem and it is well known as feature recognition problem.

Feature recognition converts a general CAD model into an specific feature model. Feature recognition system should be able to:

- Extract design information from CAD model
- Identify all surfaces of the model
- Recognize, reason about, and/or interpret these surfaces in terms of part features

All the functions shoul be performed automatically, without human intervention. After feature recognition, CAPP systems are able to automatically develop the process plans for the part.

6. FEATURE RECOGNITION APPROACHES

Many feature recognition approaches have been developed, for prismatic and rotational parts:

- Syntactic pattern recognition
- Geometry decomposition
- Expert system rule logic
- Graph based approach
- Set theoretic

For recognition of rotational parts offten are used feature recognition systems based on syntactic pattern recognition and/or expert logic approach.

For prismatic pars, because there is no rotational property, and difficulty of feature recognition increases extensively.

Methods for extraction of geometric features from CAD model of a part can be divided in external and internal ones. Internal approaches comprehend use of API (application protocol interface) of the software by which the part was designed, in order to access topological and geometrical information relating to the part. In external approaches CAD model of the part is exported from software by which it was designed in a neutral data format (STEP, IGES, ACIS, etc.) ASCII file. That file is then translated (using interface program - written in Prolog, C++, or some other program language) in a part representation suitable for form feature extraction.

5.1 Methods for automated feature recognition with rule-based pattern recognition

The methods for automated feature recognition with rulebased pattern recognition apply a common basic principle: the structures identified in a part representation, formed using one of the methods given in Table 1, are matched with some pattern in the knowledge base, using if–then rules. It is essential that these rules provide uniqueness of form feature definition: there must not exist two forms with a unique definition or one form with more than one definition in the knowledge base. If set up correctly, these systems provide accurate and thorough form feature identification. The major disadvantage of these systems is the lack of knowledge acquisition mechanisms, which becomes a serious problem when form feature is extracted that cannot be matched with any pattern in the knowledge base.

There are numerous systems, developed using logic approach for manufacturing pattern recognition, that differ one from another in a model of part representation in which a form feature identification is to be carried out:

1. syntactic pattern recognition;
2. state transition diagrams and automata;
3. logic (if–then) rules and expert systems;
4. graph-based approach;
5. convex hull volumetric decomposition;
6. cellbased volumetric decomposition;

7. hint-based approach; and
8. hybrid approach.

6. CONCLUSION

In the design for manufacturing, it is very important to notice that manufacturing require making decisions as early as in the phase of product design. Successful solutions of these problems are reached by using features during product design and analysis, and that they can be technologically recognized and analyzed. All decisions should be based on technological knowledge incorporated into the system. The presented methodology enables the realization of simultaneous design and development of a product within integrated CAD/CAPP/CAM systems.

Process planning as a link between design and manufacturing is very important activity to translate the design of products into manufactured products. There are a number of key steps in the development of a process plan. It is important to note that these activities are inter-connected. Therefore, iterations are common activities in process planning. Of the two types of CAPP approaches, the variant approach continues to be used by some manufacturing companies. The trend though is to strive for a generative approach.

Expert systems are useful in process planning and allows the capturing of knowledge from experts, and is able to simulate the problem solving skill of a human expert in a particular field. The benefits of expert systems are the accurate decision, time gains, improved quality and more efficient use of resources.

7. LITERATURE

[1] SINGH, N.. Systems Approach to Computer-Integrated Design and manufacturing. New York, USA: John Wiley & Sons, Inc. (1996)
[2] Alting, L., & Zhang, H. (1989). Computer aided process planning: The state-of-the-art survey. International Journal of Production Research, 27(4), 553-585.
[3] Cay, F., & Chassapis, C. (1997). An IT view on perspectives of computer aided process planning research. Computers in Industry, 34(3), 307-337.
[4] Manic Miodrag, Miltenovic Vojislav, Stojkovic Milos, Banic Milan (2010): Feature Models in Virtual Product Development, STROJNISKI VESTNIK-JOURNAL OF MECHANICAL ENGINEERING, vol. 56 br. 3, str. 169-178
[5] Lee, K. (1999). Principles of CAD/CAM/CAE systems. Rolland, USA: Addison Wesley Longman, Inc.
[6] Babić, A.: Projektovanje tehnoloških procesa, udžbenik, Mašinski fakultet Kraljevo, 2005.

HEAVY MACHINERY - HM 2011, 85-90
ISBN 978-86-82631-58-3
Paper accepted: 30.05.2011

Basic principles of artificial intelligence in modeling assembly operations in CAM

Marina Pljakić[1,*] - Aranđel Babić[1]
[1] University of Kragujevac, Faculty of Mechanical Engineering Kraljevo

Abstract: *Virtual product design represents a technological key for reduction of costs arising from the errors generated in the processes of engineering design during product life cycle. It is important to establish a connection between CAD design of products and complex limitations of assembly operations in CAM so that the design process is provided with the conditions for development and modification in a virtual environment before the beginning of production. The advantage of this linking in design processes is in overcoming creation of expensive physical production systems so that all variant research could be carried out on a virtual model. This integration can be seen on the example of tank waggons.* *Artificial intelligence is designed to collect, represent, organize, and use computer knowledge, and in the possession of properties, has a significant effect in establishing intelligent production.*

This paper is realized as part of exam on Ph.D. studies: Integrated design of prefabricated structures and processes, Faculty of Mechanical Engineering in Kraljevo.

Keywords: CAD, CAM, assembly, artificial intelligence.

1. INTRODUCTION

Assembly processes during the product life cycle represent a considerably higher level than composing parts into a whole, be it design of products or design of manufacturing technology at the component level. It is a milestone in the technological cycle, the point at which the product begins its lifetime and for the first time has the possibility of functioning. Hence, the most visible aspect of the product quality is reflected in the designed assembly process.

Traditionally, Design for Assembly DFA is based on studying Design for Disassembly DFDA, most frequently on the assumption that "if a part can be disassembled, it can also be assembled and vice versa". In a real environment, this can be quite different from the inverse process of joining. It is known that the number of feasible assembly structures for a given product increases exponentially in accordance with the number of components. The analysis of conceptual solutions provides a conclusion that a designed optimum process of disassembly does not have to represent the best conceptual solution for assembly. Design for Assembly is an engineering process which integrates a large number of DFX approaches within simultaneous design of products and processes.

The complexity of assembly processes and technological processes for manufacturing components for the designed product has a huge influence on costs, profit and possibility of recycling. The engineering model of product integrates a large number of DFX approaches, where only after a detailed consideration can it be estimated and adjusted before it is launched into production (the milestone in product development). According to some authors, product design makes 6% of the costs intended for product development, where more than 70% of production costs refer to the phases of conceptual design. It means that good preliminary design decisions can be made only after detailed analyses of the complexity of production and product life cycle. *[1]*.

*Corr. Author's Address: Faculty of Mechanical Engineering Kraljevo, Dositejeva 19, Kraljevo, Serbia, pljakic.m@mfkv.kg.ac.rs

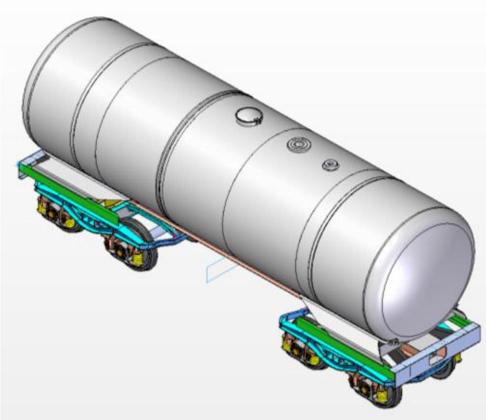

Fig. 1. *A model of a tank wagon*

2. ARTIFICIAL INTELLIGENCE AND DESIGN FOR ASSEMBLY

In addition to a half-century of intensive development, artificial intelligence is still the area that is difficult to define. One can say that it is part of computer science that deals with systems that connect the features normally associated with intelligence in human behavior. Intelligent human behavior including perception, reasoning, problem solving, understanding language, learning, communication and action in complex systems. Artificial Intelligence deals with intelligent behavior of artificial systems, with its main goal the simulation of human behavior on a computer, where the knowledge and use of the key features.

Research activities in the world is focusing on different aspects of design and planning for assembly process. Various approaches have been undertaken to develop specific aspects of the design and planning process, including product and process design methodologies, CAD and manufacturing (CAD/CAM), design for manufacture and assembly (DFMA), a detailed analysis of production and assembly operations, an automated sequence planning, layout and equipment selection, computer simulation of the assembly process, integrated systems and intelligent assembly and disassembly of the system.

Due to the complexity of assembly and product design, there is an increasing need to integrate artificial intelligence (AI) such as knowledge-based expert systems, and neural network, for maximum benefits and for expediting advanced design processes.

Introducing artificial intelligence to DFAD and implementing it effectively can yield several advantages. First, increase the design quality. Designers may need less training and expertise for utilizing CAD tools. Designers can obtain on-line advice on how to improve their work. Better quality designs with fewer errors can be expected. Secondly, artificial intelligence can reduce the cycle time of the design procedure. Besides saving the time of training, it can also save time for designers to obtain specific knowledge and problem solutions, thus, the overall design time is reduced, resulting in reduced cost. These advantages are important for wider application of DFAD practices in industry.

There are several ways to introduce artificial intelligence into DFAD, which are summarized as follows:

• *Rule-based knowledge (expert) systems* are programmed in LISP, PROLOG or expert system shells, and have been applied in industry (O'Grady and Oh, 1991)).

• *KBS for interface with assembly CAD*. Design for Assembly Consultation (DACON) was developed by Swift (1987) and provides a CAD interface for drawing assembly components after they are designed with expert analysis; Hernani and Scarr (1987) developed an expert system interfaced with CAD to recommend assembly design rules.

• *KBS for interface with facility design*. Facility Design Expert System (FADES) (Fisher and Nof, 1987) provides economic analysis and selection of assembly technology.

• *KBS for assembly and manufacturing design*. or Assisted Design for Assembly and Manufacture (ADAM) (Sackett and Holbrook, 1988)), generates advice on reducing the number of components, rationalizing the assembly and insertion guidelines. Chen and Pao (1993) combine neural network and rule-based systems for the design and planning of mechanical assemblies.

• *Constraint net knowledge systems*. In this approach, design knowledge is represented not as a collection of rules, but as a collection of interconnected assembly constraint objects. An efficient search can be performed over these networks to evaluate the propagation of design changes (Oh et al., 1995)). *[2][3][4][5]*.

3. ASSEMBLY OPERATIONS

Complex assembly operations considerably increase the costs of production of complex products. Also, the products whose dismantling requires complex operations increase the maintenance and recycling costs. Costs for assemblying and disassemblying significantly influence the costs in product lifetime, which requires the application of design solutions that provide efficient assemblying.

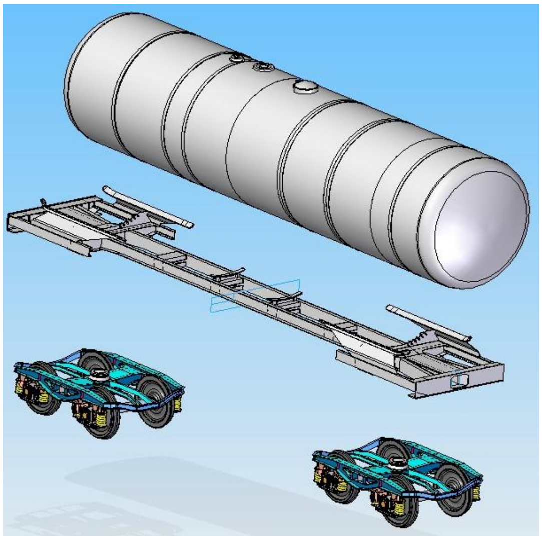

Fig. 2. *The main elements of the assembly of a tank waggon*

The complexity of assemblying can be defined as the complexity of restriction of mutual motion of the parts which are assembled. In order to prevent problematic assembly operations in the CAM environment, it is necessary to foresee the complexity of mutual assemblying of components during product design in the CAD environment by applying virtual tools for assemblying. The virtual system which connects design solutions from the CAD environment with the complexity of assembly operations in the CAM environment virtually evaluates and validates the design of product and assembly structure. The modelling and assembly technology can be used for manufacturing a tank waggon, whose main elements are the underframe, the bogie and the tank *[1]*.

3.1 Structural connections at the component level

In the design of assembly processes, a much better effect of assembly rationalization is accomplished by simultaneous analysis of the product structure and the analysis of connections at the component level. It is very important to design components in such a way that their problems in assembly could be solved at the same time. It means that the application of assembly criteria results, from the aspect of defined shapes, in well designed parts. The solution of the appropriate assembly process depends on the correct description of these characteristics of the part. From the aspect of assembly, the shape and assembly surfaces have a big influence.

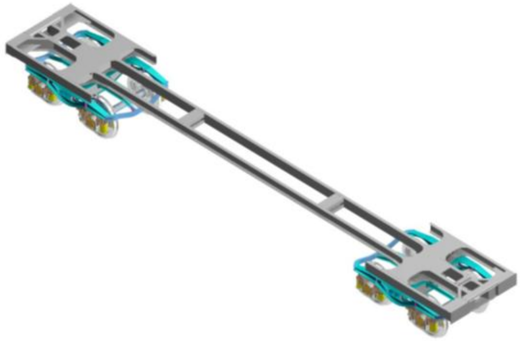

Fig. 3. *The assembly of the underframe and the bogie*

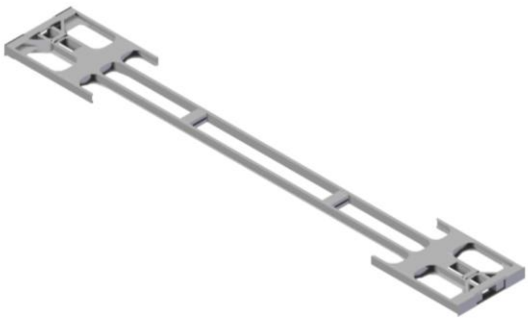

Fig. 4. A model of the underframe

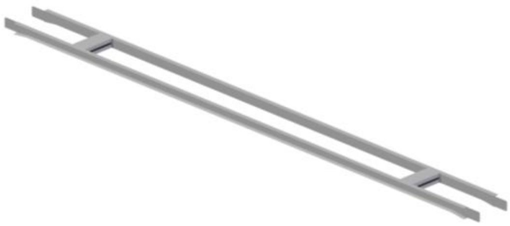

Fig. 5. *The central/medium girder*

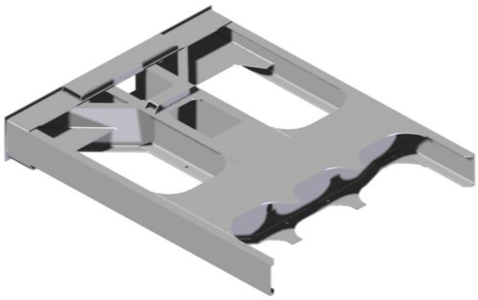

Fig. 6. *A model of subassembly of the cross bearer, headstock and sidemembers*

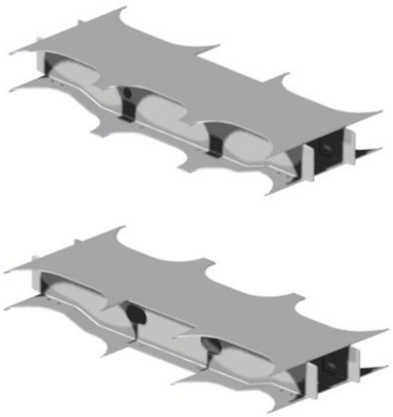

Fig. 7. *A model of the cross bearer*

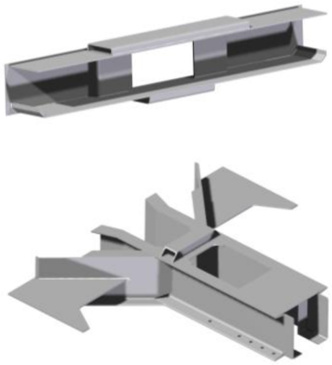

Fig. 8. *A model of the headstock with the beam*

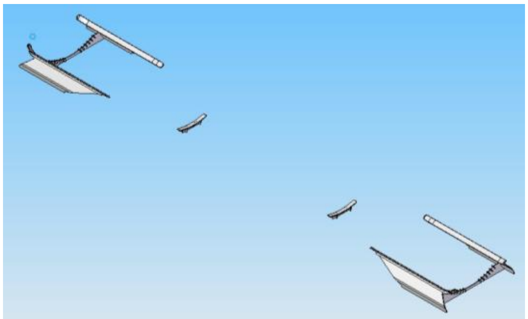

Fig. 9. Connecting elements between the tank and the underframe of a tank waggon

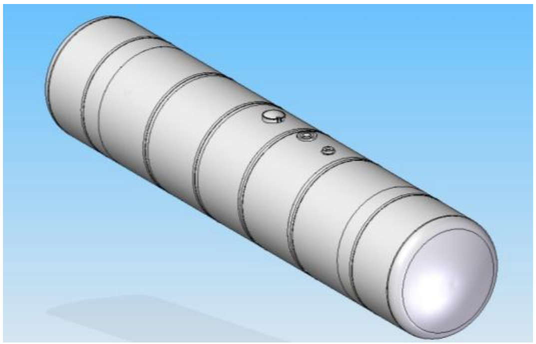

Fig. 10. *A model of the tank*

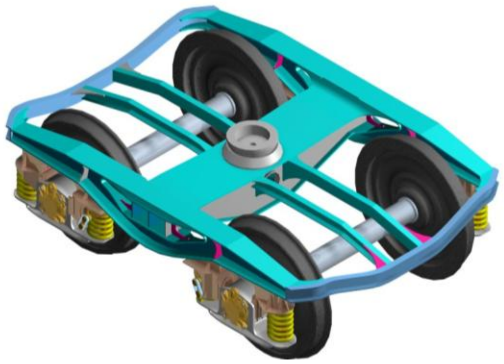

Fig. 11. *A model of the bogie*

4. A SYSTEM FOR CODING ASSEMBLY STRUCTURES

Most assembly operations can be divided into several elementary operations of joining parts which cover fitting a part into another one. Each part has a primitive vector (F) which shows the orientation of the part and the vector of the main axis which shows the part symmetry. A basic system for coding assembly structures was developed by studying geometrical similarities between different pairs of parts. The code actually contains the information equivalent to CAM operations.

In design of assembly processes, a much better effect of assembly rationalization is accomplished by simultaneous analysis of the product structure and the analysis of connections at the component level. It is very important to design components in such a way that their problems in assembly could be solved at the same time. It means that the application of assembly criteria results, from the aspect of defined shapes, in well designed parts. The solution of the appropriate assembly process depends on the correct description of these characteristics of the part. From the aspect of assembly, the shape and assembly surfaces have a big influence.

4.1. The generator of sequence of assembly operations

In order to determine the sequence of assembly operations, it is necessary first to recognize all pairs of parts that can be mutually assembled. The geometrical information provided through STEP can give information on maximum and minimum limits of each part in all three directions. A simple algorithm is used for examining whether there is a mutual intersection of these limits of parts, i.e. the possibility of their joining. Examination of each part results in a list of all parts with which it is intersected and with which it can be joined. Modelling of tank wagons at the level of assembly structure is very important because kinematic requirements are fulfilled by definition of assembly relations. Solid Edge possesses a module for modelling products at the assembly level, the so-called *assembly* module. The assembly structure is established on the basis of assembly relations defined, in this software package, through fitting of surfaces, alignment of elements, parallelism, perpendicularity, etc.

5. ASSEMBLY PROCESSES

5.1 Assembly at the local and global levels

It covers all assembly steps and actions, including descriptions of the part surfaces that are called joining surfaces. Also, it covers all motions and paths that are included in any part of the assembly process. At the global level, the design of assembly structure of tank waggons was performed by using the “Bottom-up“ approach, where the components were joined for the purpose of obtaining an assembly structure as the highest level of hierarchical structure. The parts were joined through joining primitives, by establishing corresponding relations among the surfaces.

Tank waggons represent products with a complex assembly structure, where certain components are manufactured by a lot of small and medium enterprises using the principle of distributed production. Definition of manufacturers/suppliers of certain assembly components by the principle of distributed production requires analysis and coding of complex structures of products for the purpose of generation, and then adding of components to the assembly structure. The wish is to form, on the basis of general assembly principles, a system for coding the sequence of CAM operations in assembly structures, which should be the basis for introduction of distributed production of tank waggons.

6. CONCLUSION

The development of complex products such as tank waggons is based Computer Aided Design (CAD), then the sequence of assembly operations in CAM for the purpose of generating distributed support to the production of components. Artificial intelligence is one of the most significant impact on improving the CAD/CAM technology and will continue to be an effective tool in their development. Namely, how many parameters the planning process based on long experience in manufacturing, they can not be mathematically modeled. It is expected that great ability of artificial neural networks are extensively applied in the development of intelligent CAD/CAM systems.

REFERENCES

[1] Babić, A., Pljakić, M., Ilić, N., Petrović, A., Linking the Product Design Process in CAD with Assembly Operations in CAM on the Example of Milling Heads, 33rd Conference on Production Engineering, Faculty of Mechanical Engineering Belgrade, Belgrade, pp. 147-150, 2009,

[2] Pljakić, M., Ilić, N., Babić, A., ARTIFICIAL INTELIGENCE IN CAM MODELING OF ASSEMBLY OPERATIONS OF TANK WAGONS, THE 7TH INTERNATIONAL CONFERENCE RESEARCH AND DEVELOPMENT OF MECHANICAL ELEMENTS AND SYSTEMS, Faculty of Mechanical Engineering Niš, Zlatibor, pp. 109-112, 2011,

[3] Hernani, J. T. and Scarr, A. J.: 1987, An expert system approach to the choice of design rules for automated assembly, in: M. M. Adreasen (ed.), *Assembly Automation*, IFS Publications, London, pp. 129–136,

[4] S. Y. NOF and J. CHEN, Assembly and Disassembly: An Overview and Framework for Cooperation Requirement Planning with Conflict Resolution, Journal of Intelligent and Robotic Systems 37: 307–320, 2003,

[5] Chen, C. L. and Pao, Y. H.: 1993, Integration of neural network and rule-based systems for design and planning of mechanical assemblies, *IEEE Trans. Systems Man Cybernet.* **23**(5), 1359–1371,

[6] Fisher, E. L. and Nof, S. Y.: 1987, Knowledge-based economic analysis of manufacturing systems, *J. Manufacturing Systems* **6**(2), 138–150.

HEAVY MACHINERY - HM 2011, 91-93 Paper accepted: 30.05.2011
ISBN 978-86-82631-58-3

Assembly plan design in integrated development of milling heads

Nemanja Ilić[1,*] – Aranđel Babić[1]
[1] University of Kragujevac, Faculty of Mechanical engineering Kraljevo

Integrated product development is a process with many procedures, which needs many aspects of knowledge and experience, as well as lot of people or teams need to work together. An integrated intelligent engineering environment should be developed to provide information for rapid and intelligent decision-making throughout the entire design and process planning.

AI techniques such as knowledge-based DFA expert systems, fuzzy logic, neural networks, genetic algorithms, case-based reasoning, and their hybrids should be a tool for creating a system which will be able to provide users with suggestions in order to improve a design and also to help obtain better design ideas.

This paper is part of the exam: Integrated design of assembly structures and processes, on Ph.D. studies on Faculty of mechanical engineering in Kraljevo.

Key words: Artificial intelligence, Assembly planning, Expert systems

INTRODUCTION

In recent period CAD/CAM integration has been research focus of many researchers in advancing design and manufacturing automation. Till now many CAD softwares still adopts the traditional product-process design method with various design activities being carried out sequentially but without the integration of the design activities. This sequential approach does not help in optimizing the product-process design. In order to obtain better design solutions for a product, the product design, process planning, assembly planning, economic and ergonomic analysis and evaluation should be carried out concurrently.

In industrial manufacturing, process planning for assembly is very important fase in product development. In case of variant design of complex products, planning of assembly, and also disassembly or maintenance, is still very complex. Computer aided assembly planning is one of a solution to reduce the effort necessary to produce assembly plans while improving their quality and production cost.

Therefore, in recent years more and more attention is paid for creating an optimal assembly plan with computer support. Assembly plan consists of three phases:

1. determination of all posible ways,
2. choosing the most suitable assembly plan,
3. distribution of assembly operations.

Bigest problem is combining of possible ways. Number of feasible assembly plans is very large. Ideal product is one that has no assembly restriction. In most cases of assembly plan designing is nesesary to take into acount all feasible plans. In some metods for reduction of numbers of possible assembly plans are introduced restrictions based on geometry or on element stability in assembly structure. However, introducing too many restrictions and the possible rejection of most of the plan assembly, can lead to the rejection of solutions that can later turn out to be interesting.

The choice of the sequence in which components or subassemblies are put together in the mechanical assembly of a product can drastically affect the efficiency of the assembly process. For example, one feasible and reasonable sequence may require less fixturing, less changing of tools, and include simpler and more reliable operations than others. Therefore, assembly sequence planning plays an important role in designing and planning the product assembly process.

1. ARTIFICIAL INTELIGENCE IN PROCESS OF ASSEMBLY PLANNING

Integration of product development processes and assembly plan generation is based on application of artificial intelligence methods. There are large number of AI methods that can be used in the design and planning of products

*Corr. Author's Address: Faculty of Mechanical Engineering Kraljevo, Dositejeva 19, Kraljevo, Serbia, ilic.n@mfkv.kg.ac.rs

and assemblies, such as: expert systems, fuzzy logic, neural networks, genetic algorithms, case-based reasoning. A complete AI based integration of product design and assembly process planning is still complicated by the complex interactions and domain knowledge between the technical, economical and ergonomic aspects of design and planning. Main aspects are technical and economical and they need to be integrated. Figure 1. show scheme of this integration. To ensure this integration next steps must be taken into the consideration:

1. Assembly design (conceptual design, preliminary design, detailed design, assemblability analysis and evaluation).
2. Assembly process planning.
3. Assembly system layout and design.
4. Assembly simulation.
5. Econo-technical and ergonomic analysis and evaluation.

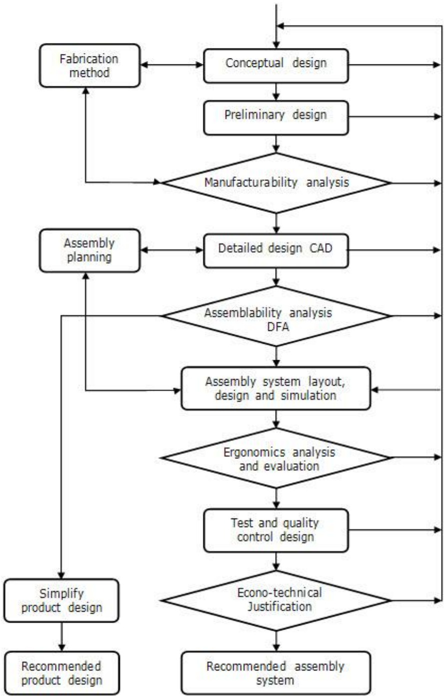

Fig.1. *Integration of assembly design and planning*

Figure 2. describes how the current assembly model has been supported by computer software and knowledge-based approaches. It starts with assembly methodology as a core part of the overall assembly procedures, which consist of assembly system/process selection, DFA and assembly planning. The left and right sides of the core assembly methodology show how the methodologies have been supported by software and knowledge-based or AI tools respectively. The large arrows shown in outline indicate the existence of support links at each core level of the assembly methodology.

DFA is the activity in product design which is employed to simplify a product structure. Therefore, computer support software, such as B&D DFA Method, TeamSet (Lucas), Hitachi (AEM), PDM, etc has been established to enhance DFA activity.

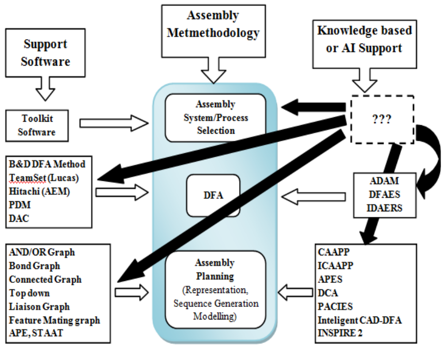

Figure 2. *Assembly metodology support*

Assembly planning is another important area in assembly methodology that has a strong, influence on assembly system and product design, and the cost of assembly either directly or indirectly. The selection of an efficient set of assembly representations, sequences or models is important in assembly planning. Therefore, much research work has focused on the various aspects of assembly planning. Various approaches and tools such as AND/OR Graph, Bond Graph, Contact Graph, Top Down, Liaison Graph, Feature Mating Graph, Simulated Annealing etc have been developed to implement it. Substantial research work has also been involved in the use of knowledge-based or AI approaches in assembly planning. Some of the approaches are CAAPP, ICAAPP, ADAM, DCA, PACIES and Intelligent CADDFA.

However, there seems to exist a gap in knowledge-based or AI support for assembly process or system selection. This is highlighted in figure 1, where the opportunity for intelligent software support in assembly process selection to bridge the gapis shown as an empty box.

2. EXPERT SYSTEMS

One of AI techniques which can be used for assembly planning support are expert systems. The expert system is an intelligent computer program that applies knowledge and reasoning (inference) procedures in order to solve problems which require human experience (expert). The idea of expert systems consists in transposing the expert knowledge of a given domain to a knowledge base. The basic elements of an expert system are:

1. a knowledge base,
2. an inference machine and
3. a user's interface.

The knowledge base is made of a set of facts and rules. The rules are logical sentences which define some implications and lead to creation of new facts, which as a result allow to solve a given problem. The inference machine is a module which uses the knowledge base. This module may use different inference methods to solve the problem.

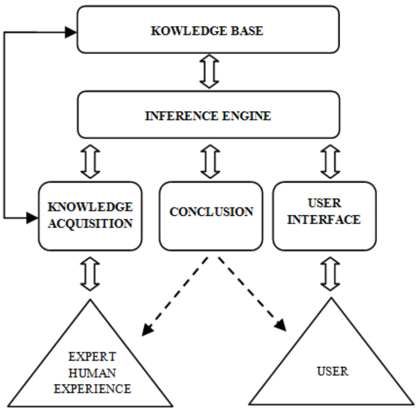

Fig. 3. *Expert system structure*

These are computer programs with a designed inference machine and an empty knowledge base. These programs are all equipped with special editor programs allowing to enter rules concerning a given problem the user wishes to solve. The issues of constructing expert systems are part of the so-called knowledge engineering. The scope of interest of specialists operating in the domain of knowledge engineering covers such issues as knowledge acquisition, its structuralization and processing as well as designing and selection of appropriate inference methods (inference machine) and designing appropriate interfaces between the computer and its user. Knowledge base is consisted of:

1. procedural knowledge, it is knowledge about procedures used in the performance of some task, and
2. declarative knowledge, it is knowledge about problem observation, about objects, states and conections.

ES development includes the construction of knowledge base - entering knowledge to the system. Knowledge acquisition, ES development process, is shown on figure 4.

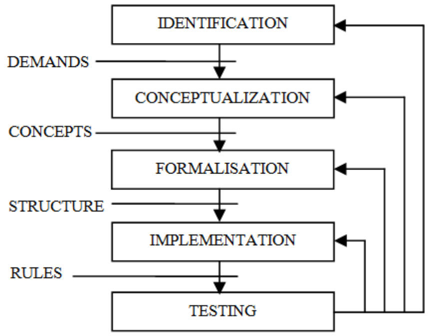

Fig. 4. *Knowledge acquisition-ES development*

It consists of next phases: *identification* phase - identifying the task, studing of existing knowledge; *conceptualization* phase - the knowledge engineer sets the concept of access, which define the facts and hypotheses on which the task is based; *formalization* stage - knowledge is brought into a form suitable for presentation (in the program and Expert shell); *implementation* Phase - formed structures are transferred to the computer and its product is a knowledge base; *testing* phase - expert sees semantic irregularities and a knowledge engineer irregularities in the implementation procedures.

3. ASSEMBLY CONSTRAINS

An operation is said to be feasible if it respects the assembly constraints coming from product, assembly process or assembly facility.

Assembly constraints take into account the assembly operation (for example geometrical feasibility or stability of subassemblies) or the process of optimal plan selection (for example minimizing time or maximizing the number of subassemblies). The nature and weight affected to a specific criterion are sensitive as they can lead directly to eliminating entire groups of assembly solutions.

3.1. Constrains on the level of assembly operations

These are fundamental constrains. Most common of them are:

- geometrical feasibility: is the strongest constrain, there must be possibility for mating components,
- assembly tool access: requires that sufficient space be available for the tool used to assemble.
- minimizing dificult assembly operations: avoid ackward operations,
- stability: mean that all subassemblies must be in stabile state.

3.2. Constrains on the level of assembly plan

This type of constrains is used during selection of best assembly plan. Some of them are:

- minimizing the time needed for assembly process,
- minimizing assembly process costs,
- minimizing numbers of inserting directions in assembly process,
- maximizing number of operations performed in parallel directions,
- minimizing number of different tools for performing assembly operations.

Theese constrains are used as a filter during process of assembly plan generation. If these constrains are failed to comply, the user can take into account all the "families" of the possible plans.

4. ASSEMBLY PLAN OF MILLING HEAD SYSTEMS

Milling head systems are systems consisted of several subassemblies, shown on figure 5. Each subassembly can be further divided into next level of subassemblies. For example, milling head subassembly, is consisted of cutting tool subassembly and drum construction.

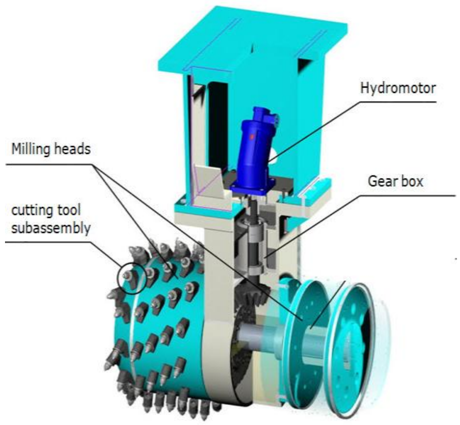

Fig.5.*Milling head system subassemblies*

Milling head subassembly is shown on figure 6., where can be seen all elements included in hierarchical structure. Bill of material is shown in table1.

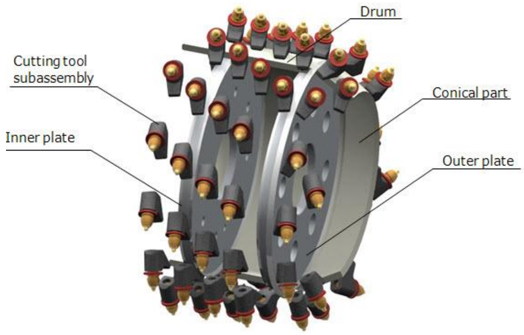

Fig.6. *Milling head components*

Table 1: Bill of Material of milling head subassembly

art. No	Part name	Part code	Quantity
1.	Toolholder	Mh01-1	64
2.	Tool	Mh01-2	64
3.	Drum	Mh01-3	1
4.	Conical part	Mh01-4	1
5.	Inner plate	Mh01-5	1
6.	Outer plate	Mh01-6	1

Hierarchical structure of milling head is shown on next figure 7.

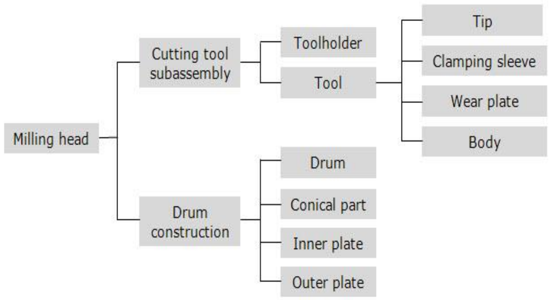

Fig.7.*Milling head hierarchical structure*

Depending on milling head system type, different number of these cutting tools can be used (42,54, 66 or even more) on a single milling head. Cutting tools are considered as assembled because they can be bought as a spare part.

Assembly plan, shown in Table 2., of milling head consider no technological constraints, while the other, shown in Table 3. does.

Table 2. *Assembly plan that consider no technological constrains*

Operation No.	Description
Step 1.	Positioning part 3.
Step 2.	Positioning part 5.
Step 3.	Positioning part 6.
Step 4.	Positioning part 4.
Step 6.	Performing welding operation according to information W1
Step 7.	Performing welding operation according to information W2
Step 8.	Performing welding operation according to information W3
Step 9.	Positioning part 1
. . .	. . .
Step 73.	Positioning part 1.
Step 74.	Performing welding operation according to information W4
. . .	. . .
Step 138.	Performing welding operation according to information W4
Step 139.	Positioning part 2.
Step 140.	Performing axial force to push part 2 into part 1
. . .	. . .
Step 268.	Positioning part 2.
Step 269.	Performing axial force to push part 2 into part 1

First assembly plan consider no technological constrains. In this case, first all components need to be positioned (drum, inner plate, outer plate, conical part). Then welding operation need to be performed.

Also there haven't been taken into consideration assembly tool access (requires that sufficient space be available for the tool used to assemble). Welding gun can't access in zone where inner and outer plate need to be welded, shown on next figure.

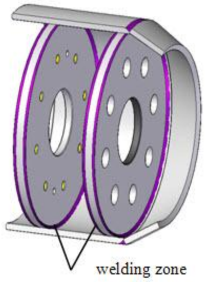

Fig.8.*Welding zone where welding gun can't access*

After these operations, all tool holders need to be positioned and then to be wellded. Also, there haven't been taken into consideration constrains about stability (mean that all subassemblies must be in stabile state). All tool holders can not be in the stabile state, in the same time, figure 9., without performing welding operations.

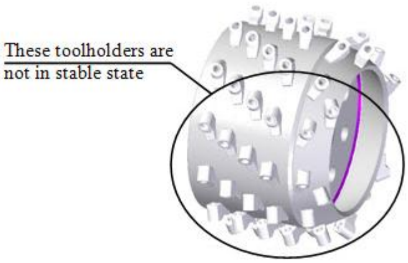

Fig.9.*Toolholder which are not in stable state*

The second assembly plan take into consideration all the constrains that haven't been taken in previous assembly plan. After milling drum construction parts positioning and welding operations, tool holders are positioned and welded one by one, and all tools are positioned (pushed) in tool holders using a force.

Table 3. *Assembly plan that consider technological constrains*

Operation No.	Description
Step 1.	Positioning part 3.
Step 2.	Positioning part 5.
Step 3.	Performing welding operation according to information W1
Step 4.	Positioning part 6.
Step 5.	Performing welding operation according to information W2
Step 6.	Positioning part 4.
Step 7.	Performing welding operation according to information W3
Step 8.	Positioning part 1.
Step 9.	Performing welding operation according to information W4
Step 10.	Positioning part 2.
Step 11.	Performing axial force to push part 2 into part 1
.	.
.	.
.	.
.	
Step 132.	Positioning part 2.
Step 133.	Performing welding operation according to information W4
Step 134.	Positioning part 2.
Step 135.	Performing axial force to push part 2 into part 1

On the next fig. 10., is shown milling head at the end of assembly process.

Fig.10. *Milling head*

2. CONCLUSION

It is a big issue to construct a knowledge base of assembly process planning, which enables the accumulation, sharing and maintenance of knowledge and experience of process engineers. An intelligent decision support system could impact on many areas of the assembly process planning.

Product design and assembly planning can be carried out simultaneously and intelligently in an entirely computer-aided concurrent design system. The design of manufacturable, cost-effective, usable products can therefore be achieved more rapidly and flexibly. Integration of product design and assembly process planning can achieve a better design of a product. Product design in CAD/CAA environment is one of the key conditions that influence the cost savings generated in the process of engineering design during the product life cycle.

5. REFERENCES

[1] Michel MARTINEZ • Viet HUNG PHAM • Joël FAVREL, Optimal assembly plan generation: a simplifying approach: Université de Lyon, Bât Nautibus 8, Boulevard Niels Bohr, Villeurbanne Cedex 69622, France

[2] X. F. ZHA, S. Y. E. LIM and S. C. FOK, Development of Expert System for Concurrent Product Design and Planning for Assembly: School of Mechanical and Production Engineering, Nanyang Technological University, Singapore; and School of Mechanical Engineering, Nanjing University of Aeronautics and astronautics, Nanjing, China

[3] Nemanja ILIĆ, Marina PLJAKIĆ, Aranđel BABIĆ, „Inteligent CAD design and assembly plan of milling heads“, The 7th International Scientific Conference, Research And Development Of Mechanical Elements And Systems, IRMES 2011 April 27th to 28th, 2011 in Zlatibor, Republic of Serbia, p 109.-112., ISBN

[4] T. A. ABDULLAH, K. POPPLEWELL and C. J. PAGE, A review of the support tools for the process of assembly method selection and assembly planning, int. j. prod. res., 2003, vol. 41, no. 11, 2391–2410

[5] BABIĆ, A.: Tehnologija montaže, udžbenik, Mašinski fakultet Kraljevo, 2005.

HEAVY MACHINERY - HM 2011, 97-102
ISBN 978-86-82631-58-3
Paper accepted: 30.05.2011

The integral development of products using the DfX approaches and CAx tools

Marina Pljakić[1,*] – Vladimir Jakovljević[1]
[1] University of Kragujevac, Faculty of Mechanical Engineering Kraljevo

Abstract: *Approach of integrated design represents the bridge that connects individual stages of the product designing and the technology and has a significant role in the reduction of the overall design time, as well as the production costs. That means that the technological processes design should be connected with production planning as well,, that is the choice of tools, equipment, pressing devices and machine tool. Design for eXcellence is a philosophy that promotes rapid and successful products by encouraging communication and cooperation between the functional departments that are responsible for the design and manufacture of a product. Implementation of a successful DfX programme will decrease product development time, product cost and manufacturing cycle time while increasing product quality, reliability and ultimately, customer satisfaction.*

This paper is realized as part of exam on Ph.D. studies: Integral development of products and processes, on Faculty of Mechanical Engineering in Kraljevo.

Keywords: DfX, CAx, CAD/CAM integration, technological process.

INTRODUCTION

Integrated product and processes design is basically intended to form a competitive product. In the cycle of conceptual design variant and variable product solutions and adopted technologies have a dominant influence on the choice of machine tools for the support in the realization of the adopted technology.

To create a competitive product is an important approach to integrated product design and technology. This approach represents a bridge that connects the individual stages of product design and technology and have a significant influence in reducing overall design time and production costs. Of course, total time and costs can be reduced through the chosen approach in the management of production. This means that the design of technological processes should be linked with production planning, ie. range of tools, accessories, devices for clamping and machine tools [1].

1. DESIGN FOR 'X'

Design for 'X' suggests that the X is used as a variable term that can be substituted with, for example, **A**ssembly, **C**ost, **E**nvironment, **F**abrication, **M**anufacture, **O**bsolescence, **P**rocurement, **R**eliability, **S**erviceability or **T**est.

1.1 DfX and Concurrent Engineering

Figure 1 and Figure 2 show the traditional sequential process of product development and the equivalent concurrent process. The savings in time and money are due to the reduction or elimination of product respins due to changes and corrections to the design from the manufacturing functions upstream. The term 'respins' refers to the reworking of a design appears to derive from the record industry and is quite common within the ASIC community.

Concurrent engineering can be viewed as the simultaneous development of the whole design, its components and its assembly process and tooling requirements.

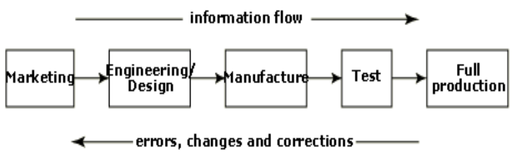

Fig. 1. *Traditional sequential product development*

---

[*]Corr. Author's Address: Faculty of Mechanical Engineering Kraljevo, Dositejeva 19, Kraljevo, Serbia, pljakic.m@mfkv.kg.ac.rs

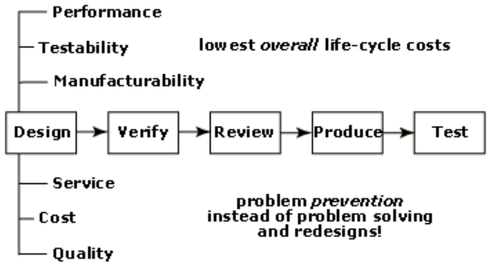

Fig. 2. *Concurrent product development*

DfX is a methodology that involves various groups with knowledge of different parts of the whole lifecycle of a product advising the Design Engineering functions during the design phase. This knowledge can take the form of guidelines that the designer will follow during design, or design review meetings with the field experts [2].

2. CAx-TOOLS

Tasks in the design process were supported by CAx-tools during the last 30 years. Starting with drafting and surfacing also classical mechanical design was replaced by 3D wire frame, solid modeling and parametric and feature based design. Today the complete product creation process, including production preparation, is completely running with CAx-techniques. According to the various application fields different CAx-systems were developed, named by different CAx-methods: Computer Aided Styling (CAS), Computer Aided Aesthetic Design (CAAD), Computer Aided Conceptual Design (CACD). All these technologies are covered by the expression Computer Aided Design (CAD). Two very important CA-fields were historically developed almost independently: Computer Aided Manufacturing (CAM) and Computer Aided Engineering (CAE). The last is mainly used in a limited sense for simulation and Finite Element Analysis.

With the growing integration of these CAx-tools the data and information management became more and more important. Nowadays the complex network of CAx-systems and their various data cannot be handled without Product Data Management Systems (PDMS). They are regarded as the backbone of modern product development and now extended to support the whole product lifecycle. This overall information management leads to the concept of Product Lifecycle Management (PLM).

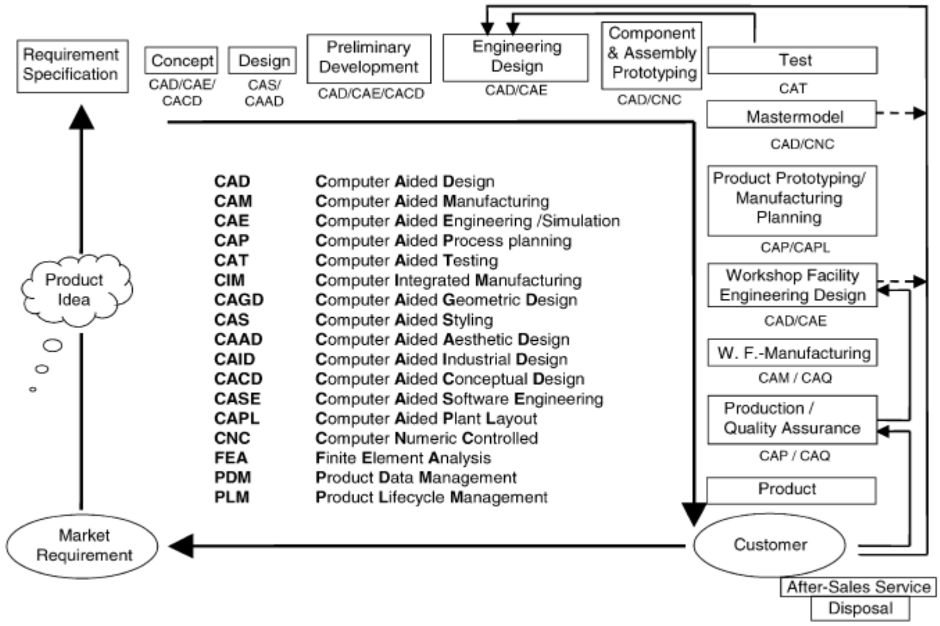

Fig. 3 *General process chain of product development*

In an exemplary simplified process chain (Fig. 3) it is shown that CAD is only a part of the product development process. This process begins with an idea, requirements and specifications for the product and ends with the serial production, customer after sales service, recycling, scrapping and disposal. CAD is embedded in the development process together with many other CAx technologies. In order to avoid unnecessary loops the engineer has to have knowledge of the surrounding process steps as well as the kind and quality of data, respectively information, they produce or require. The knowledge about the previous process steps is to maintain the design intend, the knowledge about the following process steps is to guarantee their feasibility. In addition to this economical aspect the quality of the product describing information has to be taken into account [3].

3. CAD/CAPP/CAM INTEGRATION

CAD / CAPP / CAM integration is aimed at improving the process of product design and technology significantly reduce production costs, and provide conditions for easy and economical technology of processing and assembly. Since installation costs are a significant part (25-65%) production cost, design for assembly DFA (Design for Assembly) along with the technological design of assembly processes CAAPP (Computer Aided Assembly Process Planning), close interaction in the process of product design, processing technology and assembly.

In relation to the modeling of the component domain, makes more complex the problem is significant in research approaches and ways of modeling the assembly structure and executive functions and processes, in this case to model assembly structures of machine tools. Defining the prefabricated structure of machine tools based on the principles of design for assembly DFA as the main strategy of simultaneous projects, and is considered the key to successful design in a competitive environment.

Taking into consideration criteria of product design and technology, the goal is to make technological advancement, reduction of production time, reducing the preparatory and the operational time, reliable technical support and increase production efficiency.

3.1 Basic features of CAD/CAM system

Computer-aided design (CAD - Computer Aided Design) is the process of product design by computer and includes activities that take place between the electronic drawing and work on software systems that support automatic product design. CAD can be defined as the use of computers and graphics software to assist in the development or improvement of product design from conception to documentation.

CAD is a series of methods and tools to assist the design process in creating a geometric presentation of what is constructed, dimensioning and tolerances, changes in construction management, archiving (saving), exchange of information on parts and assemblies, with the help of computers. CAD model of the input for the next step in the design manufacturing (CAM), and analysis (CAE).

The application of CAD / CAM system provides many benefits to users, so it is now practically no question whether they should be used but that the optimal solution for a specific product or a development company. The basic advantages of CAD system are:

- Increase productivity (speed)
- Support changes in the structure
- Communication
- Some basic analysis

3.2 Development of products in CAD systems

The rapid development of information technology products has led to revolutionary changes in the planning, execution and control of engineering and business processes, and integrated logistics support process in which the role integration just take information technology. It can be said that the transition to digital technology, as holders of the integration process in modern business, the condition of surviving and growing company in a competitive environment. In this sense, considering integration processes in product design and technology, CAD/CAM to the concept of concurrent engineering as a framework for the globalization of business companies, detailed consideration are the basic approaches in the process of engineering design.

Cycles in engineering proces planing represent the backbone of the analysis process where the design as a thinking process associated with the

two characteristics of the human mind: originality and skill.
Another characteristic of the adopted design process is the objectification of computer aided design products and technologies. Uncertain consideration are elements of the design process based on knowledge. Then presents the main factors of formation of knowledge in engineering design as a condition for entering the field of expertise [2], [4].

4. SOME EXAMPLES OF INEGRATION

This work shows the process of the design on the example of hydro engine back lid on the hydraulic motor. Within the process of forming a competative product, special attention is paid to the elements, that is the parameters of the technological process which significantly reduce production costs, e.g. choice of tools and the way of tightening and positioning of the part. By the technological analysis of the object it has been established that the tightening device of the working pieces presents a predominant factor in the production realization. For that reason special attention was paid to the modelling of the machine tool with the special tightening device which in this case represents an additional fourth control axis [5].

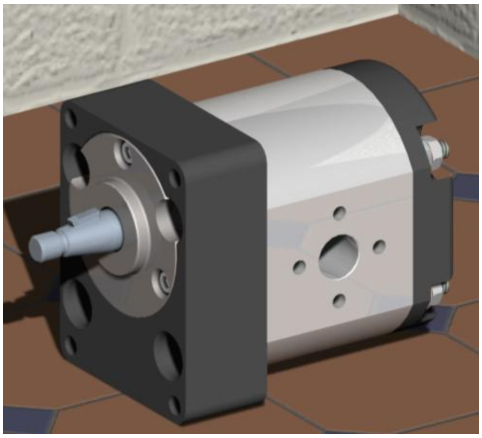

Fig. 4. *Hydro engine*

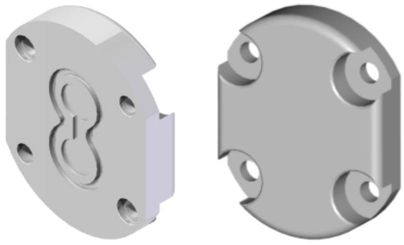

Fig. 4. *Prepared and finished part*

The processing of a mechanically correct part requires qualitative prepared part, its correct pressing and location definition (of the position and orientation) in the space. As an addition to the definition of spesific surface positioning, it is necessary to design the way of firmly holding the part in the given position under the influence of outer forces like gravitation force, cutting force, vibrations, centrifugal forces, etc. It must not influence the previously determined function of positioning, but it has the function of providing stability of the part. The pressing devices must have the appropriate pressing force so as not to damage the part in the points of contact with its excessive pressure.

4.1 Types of pressing in cases of miling and drilling

Pressing tools design and devices for pressing the working part on the machine design are realized by the application of contemporary CAD/CAM programme packages. The position of pressing, previously described, has to follow the rules of the precision of the production and respect the relation between the segments of the part. It also has to ensure that the part doesn’t move during the processing, that the parts of the pressing equipment don’t interrupt the movements of the tools or cause increase in the tool operation and that it is easy to remove filing [7].

4.2 Modelling of the installation structure of the machine tool

The concept of the machine tool in the narrower sense is defined to support the adopted production process. In order to perform the necessary operations while processing the back lid of the hydro engine, machine variants have to have the appropriate movements which provide independent wholes – modules. For every movement, whether main or additional, there has to be the right module that provides such a movement. In order to press the processing part it is necessary to design a pressing device. Thus modular analysis is done based on which the pressing device design is done with certain modifications in relation to the already existing vices, and in particular pressing prism. From the available modules CIRPP those that meet the given demands are chosen.

4.2.1Vice module

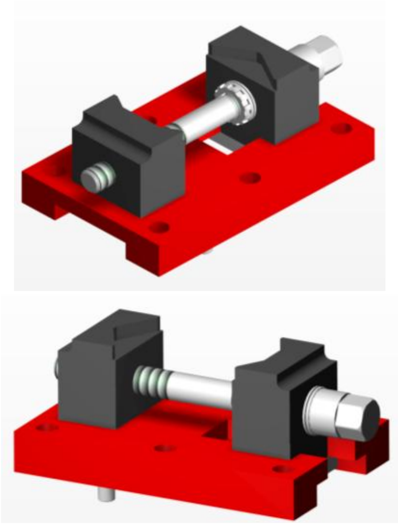

Fig. 5. *Vice module*

Vice module assembled with the holder, bearing and rotation desk represents an additional axis on the tool machines. For the processing of the back lid of the hydro engine, three-axis verticall drill/miling machine and three-axis horizontal drill/miling machine are chosen, so that the assembly of the vice represents the fourth additional axis. This additional axis increases the productivity, in one pressing, 16 back lids and housing of hydroengine are processed. The number of simultaneously processed lids is conditioned by maximum tool stability, so that the tool can process all 16 lids, without changing the tool in the meantime. After the processing, the changing of tools and working objects is done. The vice is modelled parametrically and variantly so that it can be used for pressing of the hydro engine's back lid of different dimensions and for the appropriate number of parts that can be accepted [6].

4.2.2Realization of the adopted technological process on variantly chosen machine tools

The prepared part for the production of the back lid of the hydroengine is an extradited aluminium pole and it's shown in fig. 4. Based on the technology that represents a way out of the matrix of following, the process of the hydroengine's back lid production is done in two pressing moves. In the first pressing move the prepared parts are put into the vice, one by one, and the look of the prepared parts [2].

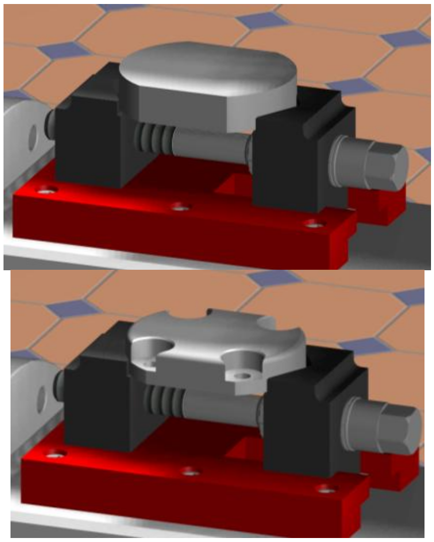

Fig. 6. *Vice module*

Tightening device, together with the girder, sinking and rotary table presents an additional axis on machine tools. In this and the next variant triaxial horizontal driller/cutter, and the triaxial vertical driller/cutter are chosen, so that the structure of the tightening device presents the fourth additional axis. By this additional axis productivity is increased, within one tightening 16 hydraulic motor back lids are processed. The number of the back lids that are processed at the same time is conditioned by the maximum stability of the tools, so that tools can process all 16 back lids, without having to change the tools in the meantime. The process having been done, the tools and working objects are changed. In the next picture we can see what the tightening device looks like, this one is modelled parametrically and variantly so that it can be used for tightening of the hydraulic motor back lids of different dimensions and for the right number of pieces that are acceptable [6].

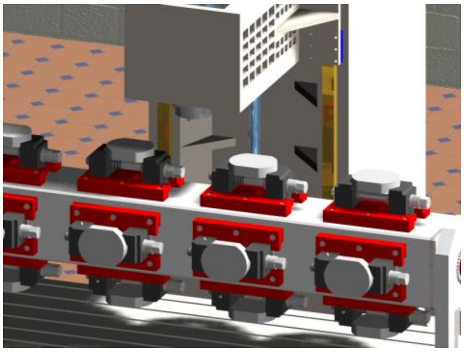

Fig. 7. *Hydro engine*

One variant machine tool used to process hydraulic motor housings and back lids is a vertical drilling/cutter fig.8. This machine tool has two translations and one rotation of the working object, one translatory and one rotary movement of the tools. On this machine 4 axis- X’,Y’,Z, and A’ are numerically controlled [6].

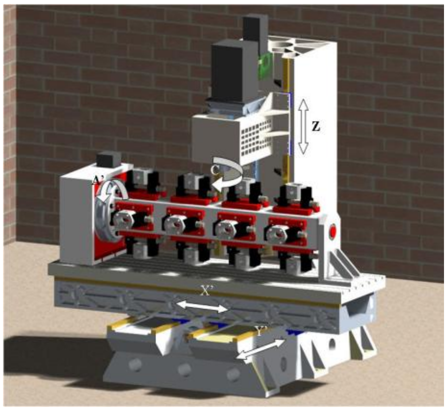

Fig. 8. *Vertical driller/cutter*

5. CONCLUSION

Achieved results in this work are reflections of the research of variant option in the technological production process of the hydro engine back lid using already existing tool machines.

The results of the research come from a very large theoretical analysis of the individual parametres which directly influence generating of technological process.

REFERENCES

[1] Halevi G., Weill R., Principles of Process Planning, Alogical approach, Chapman&Hall, London, 1995.

[2] Babić, A., Projektovanje tehnoloških procesa, Mašinski fakultet Kraljevo, 2005.,

[3] C. Werner Dankwort, Roland Weidlich, Birgit Guenther, Joerg E. Blaurock, Engineer’s CAx education – it’s not only CAD, University of Kaiserslautern, Research Group for Computer Application and Enginnering Design, Kaiserlautern Germany www.elsewier.com

[4] Babić, A., Tehnologija montaže, Mašinski fakultet Kraljevo, 2005.

[5] Diplomski rad, Marina Pljakić, 2007.,

[6] M. Pljakić, A. Babić, N. Ilić, Modelling of the additional axis of the machine tool in order to improve technological process of the production of the, HEAVY MACHINERY - HM 2008, Faculty of Mechanical Engineering Kraljevo, Kraljevo, Jun 2008., pp. G.37-G.42,

[7] Babić A., Pljakić M., Ilić N., Modelling of processes and machines for the support to hydroengine components production, 10th International Scientific Conference, mma2009, Novi Sad, Oktobar 2009, pp.183-185.

F SESSION

URBAN ENGINEERING

HEAVY MACHINERY - HM 2011, 1-6
ISBN 978-86-82631-58-3
Paper accepted: 30.05.2011

Acoustical Arrangement of the Road Superstructure

Vasile Bacria[1,*] Nicolae Herişanu[1]
[1] Politehnica University of Timişoara

The road transportation means generate noise and vibrations which are highly detrimental for human being's life and activity. An important contribution to the noise generated by the road transportation means in the environment has the noise produced by the contact between the wheel and the rolling surface.

This noise can be reduced and through acoustical arrangement of the superstructure of the road. In this paper we present an investigation on the effects of the acoustical arrangement of the road superstructure on decreasing the noise produced by the contact between the wheel and the rolling surface in the road traffic.

In order to characterize the noise we have accomplished some measurements. The results of the measurements were processed, analysed, interpreted and compared.

Keywords: noise, acoustical arrangement

0 INTRODUCTION

Every day on the streets of the towns it is developing an intense traffic. The road transportation means generate noise and vibrations which are highly detrimental for human being’s life and activity. The noise generated by the road transportation means depends on the traffic intensity and composition, as well as on the speed of vehicles and it is mainly generated by three sources: the engine, the transmission system and the contact between the wheels and the rolling surface. The noise generated by the contact between wheels and the road represents around 75% of the total noise generated by vehicles. This depends on the nature and the state of the rolling surface. The noise generated by the contact between the tire and the road is due to the vibrations caused by the interaction between the rolling surface of the tire and the asperities of the road clothes and in the case of smooth surfaces it is generated by the expansion of the air contained between the profiles of the tire and the road. The noise is significant at speeds which exceed 50 km/h.

In order to decrease the noise generated by the contact between the wheel and the road one can perform acoustical arrangements for the road superstructure by using rubberized asphalt. In this paper we present an investigation of the effects of acoustical arrangement of the road superstructure on decreasing the noise generated by the contact between the wheel and the rolling surface in the road traffic.

1 PROPAGATION AND NOXIOUS EFFECTS OF THE NOISE

The noise generated by the road transportation means propagates in the environment by spherical or cylindrical waves, as well as by plane waves at long distance from the sources [1]. The noise is extremely injurious for human being’s system generating psycho-physiological and blood circulation modifications, as well as sleep disturbances. The visual function and the endocrine gland are adversely affected as well. Moreover, the noise generates auditory tiredness and sonorous trauma, it reduce the working productivity and speech intelligibility [2], [3].

In order to reduce the effects of the noise, limit values which cannot be exceeded are established. These limits are characterized by the equivalent noise levels and the noise curves (C_z). The equivalent noise level is defined by the expression

$$L_{Aeq,T} = 10\lg\left[\frac{1}{t_2 - t_1}\int_{t_1}^{t_2}\frac{p_A^2(t)}{p_0^2}\,dt\right] \qquad (1)$$

where $L_{Aeq,T}$ is the continuous equivalent level of the acoustic pressure A-weighted, measured in dB, determined in a time interval which starts at t_1 and ends at t_2, p_0 is the refereed acoustic pressure (20 μPa) and $p_A(t)$ is the weighted instantaneous pressure of the acoustic signal.

The noise curves C_z define the relation between the characteristic frequency of a sound

*Politehnica University of Timişoara, Bd.M.Viteazu, nr.1, Timişoara, Romania, bacria@mec.upt.ro

and the proper acoustic pressure level in the conditions of a subjective equivalent sensitivity.

In this respect, the Romanian standard STAS 10009-88 “Urban acoustics” established the admissible limits of the noise level in urban environment, differentiated on zones and functional endorsements or technical category of streets established on the base of the technical settlements. For the noise levels generated by on the streets, these values are presented in table 1.

Table 1. *Admissible limits*

Street types (according to STAS 10144-80	L_{eq} [dB]	C_z [dB]	L_{10} [dB]
I – main	75-85	70-80	85-95
II – linking	70	65	70
III – collecting	65	60	75
IV – local serving	60	55	70

In the same time the disposition of buildings on the streets of different technical types and also the road traffic organization must be made so that be assured the admissible limits for the street exterior noise level established in accordance with STAS 10009-88 to 50 dB, measured at 2 m distance from the building, respectively the C_z45 curve.

Taking into consideration that the tire/road contact is an important source of noise in the road traffic and the generated acoustic field is extremely complex, its study is recommended to be experimentally performed.

2 MEASUREMENTS AND ANALYSIS OF THE RESULTS

In order to estimate the noise generated during the displacement of vehicles on the road thoroughfare by the contact between the wheel and the rolling surface, it is necessary to measure its characteristic parameters.

For this purpose, one can use the methods indicated by the Romanian standard STAS 6161/3-82 “Acoustics in constructions. Determination of the noise level in urban localities. Determination method”.

In this way, one must determine the equivalent acoustic level, the spectral distribution in frequency bands of 1/1 octave, as well as the statistical distribution of the noise levels. These measurements were performed using two Hand-held analyzers type Bruel & Kjaer 2250. The location of the measurements was chosen on the straight section of a thoroughfare depicted in fig.1, where l_g represents the wheelbase of the considered vehicle, l_m is the length of the path between the start end the end of the measurement, A-A is the starting line, B-B is the arrival line, C-C is the circulation axis, D-D is the line of microphones mounted at 1.3 meters high from the ground.

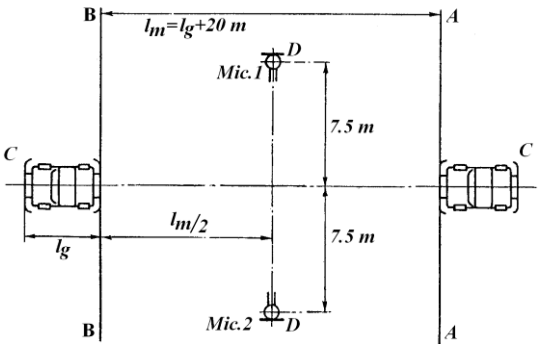

Fig. 1. *Sketch of the measurements place*

Tests were performed with an empty vehicle. The recordings started when the front line of the vehicle overtaken the starting line and they were finished when the back line of the vehicle overtaken the arrival line. During recordings, the vehicle has been driven on the test route with constant speed.

Two Hand-held analyzers B&K 2250 were used simultaneously in order to record the characteristic parameters of the noise, the time-history of the noise level, as well as the spectral and statistical distributions of the noise.

In order to characterize the noise generated during vehicles their displacements by the contact between the wheel and the rolling surface, some distinct test were performed in similar environmental conditions for two types of asphalt: rubberized asphalt and concrete asphalt. These types of carriageway surfacing were applied on a dual road where measurements were performed.

Tests were carried out for displacements with and without the functioning of the vehicle’s engine, at 30, 40, 50, 60 and 70 km/h, respectively.

Three different models of vehicles were employed: a Peogeot 307 equipped with summer tyres, a Golf 4D Diesel equipped with Pirelli all-seasons tyres and a BMW 520D equipped with winter Yokohama B902 tyres.

An initial test was performed before the rehabilitation of the road, when the surface was characterized by a certain wear and some portions were partially repaired. The results of these test performed with the Peugeot 307 are presented in Table 2.

Table 2. *Results before rehabilitation*

Speed [km/h]	Leq – position 1 [dB]	Leq – position 2 [dB]	Average value [dB]
30	62	67	64.5
40	63.3	66.3	64.8
50	65	65.3	65.15

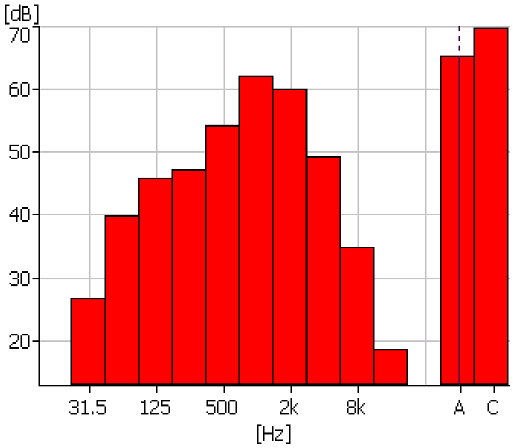

Fig. 2. *Spectral distribution of the noise for the initial test*

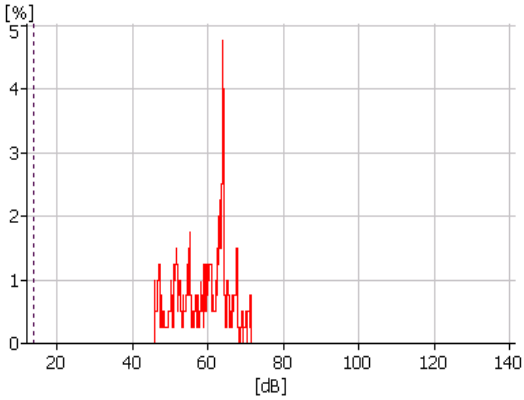

Fig. 3. Statistical distribution of the noise for the initial test

Figures 2 and 3 show the diagrams of the spectral distribution of the noise in frequency bands of 1/1 octave (fig.2) and statistical distribution (fig.3) at the speed of 50 km/h.

After rehabilitation of the dual road with a band coated with rubberized asphalt (R.A.) and another parallel band coated with regular concrete asphalt (C.A.16), tests were repeated. The most eloquent test was performed with the vehicle Golf 4T Diesel without the functioning of the engine at successive displacements with 30, 40, 50, 60 and 70 km/h, respectively. The results of these tests were presented in Table 3.

Table 3.*Results without engine functioning*

Nature of the road coating	Speed [km/h]	Leq [dB]
R.A.	30	63.0
C.A.16	30	64.3
R.A.	40	62.7
C.A.16	40	64.7
R.A.	50	64.8
C.A.16	50	66.2
R.A.	60	65.1
C.A.16	60	68.6
R.A.	70	66.9
C.A.16	70	73.0

Fig. 1 depicts the variation of the equivalent noise level generated by the contact between the tire and the rolling surface in two cases: for R.A. (dashed line) and CA16 (solid line).

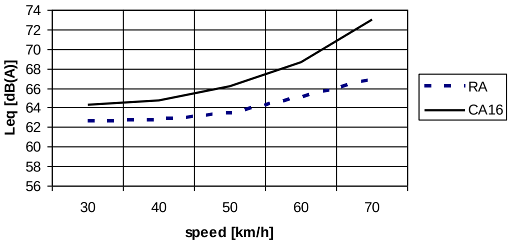

Fig. 4. *Comparison between the noise levels obtained for regular and rubberized asphalt*

In figures 5 and 6 we present the diagrams of spectral distribution (fig.5) and statistical distribution (fig.6) of the noise levels for displacement on the road coated with concrete asphalt CA16 for the speed of 70 km/h while in figs. 7 and 8 we present similar diagrams recorded for displacements on the road coated with rubberized asphalt at the same speed.

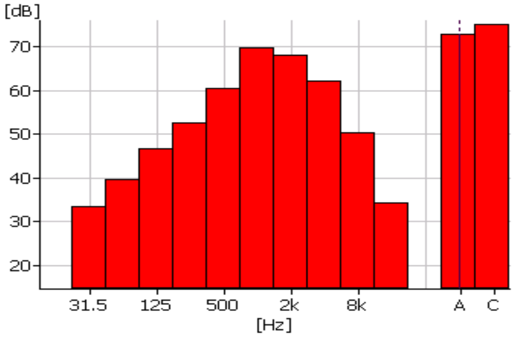

Fig. 5. *Spectral distribution of the noise on CA16 at 70 km/h*

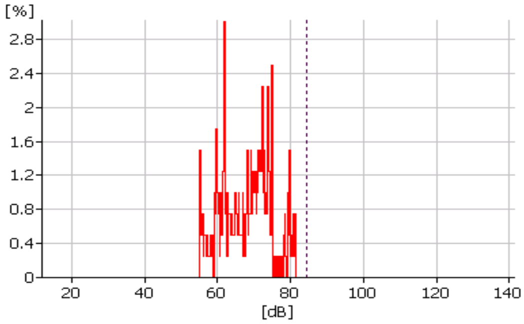

Fig. 6. Statistical distribution of the noise on CA16 at 70 km/h

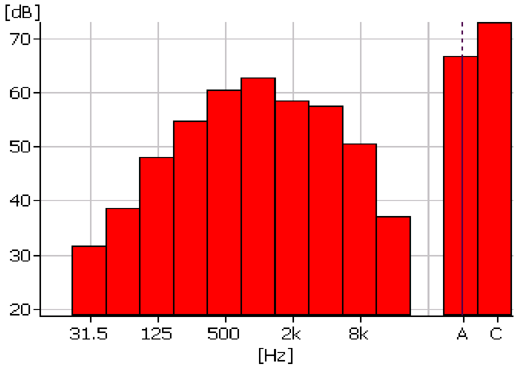

Fig. 7. Spectral distribution of the noise on RA at 70 km/h

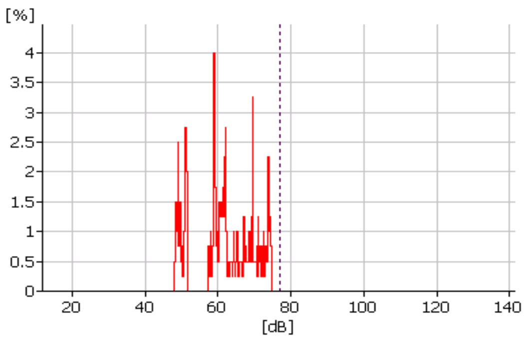

Fig. 8. Statistical distribution of the noise on RA at 70 km/h

It must be mentioned that the levels recorded in the circumstances described above are influenced by the configuration of the place where measurements were taken, since the location is a canyon-type street, and therefore a correction of -5 dB should be applied to obtain real values, according to ISO 1996-2.

The tests performed in the conditions depicted in fig.1 to determinate the total noise levels on R.A. and CA16, including the noise generated by the engine lead to the results presented in table 4, for different speed of displacement. Two vehicles were employed: (1) – the Golf 4T Diesel with all-seasons tyres Pirelli 195/65 R16 and (2) – BMW 520 D with winter tyres Yokohama B902.

Table 4. *Values of the total noise*

Nature of the road	Vehicle	Speed [km/h]	Leq-1 [dB]	Leq-2 [dB]	Av. [dB]
R.A.	(1)	30	59.8	57.5	58.65
CA16	(1)	30	58.7	60.0	59.35
R.A.	(1)	40	61.7	61.1	61.4
CA16	(1)	40	62.2	62.1	62.15
R.A.	(1)	50	63.4	63.1	63.25
CA16	(1)	50	64.7	64.1	64.4
R.A.	(1)	60	65.9	65.8	65.85
CA16	(1)	60	66.8	67.7	67.25
R.A.	(1)	70	69.9	69.6	69.75
CA16	(1)	70	71.2	71.4	71.3
R.A.	(2)	30	58.5	58.6	58.55
CA16	(2)	30	59.6	59.5	59.55
R.A.	(2)	40	60.9	58.1	59.5
CA16	(2)	40	61.4	59.6	60.5
R.A.	(2)	50	60.9	60.7	60.8
CA16	(2)	50	61.9	61.6	61.75
R.A.	(2)	60	64.4	60.8	62.6
CA16	(2)	60	65.2	63.9	64.55
R.A.	(2)	70	63.7	63.8	63.75
CA16	(2)	70	65.4	65.1	65.25

In figs. 9 and 10 it is represented the dependence of the total noise on the speed during displacements two of the vehicles on the road coated with R.A. (dashed line) and CA16 (solid line). Fig.9 shows the results for the Golf 4T Diesel equipped with tyres of type Pirelli 195/65 R16, while fig.10 show the results for the BMW 520 D equipped with tyres of type Yokohama B902. We mention that also the noise generated by the engine is included in these levels.

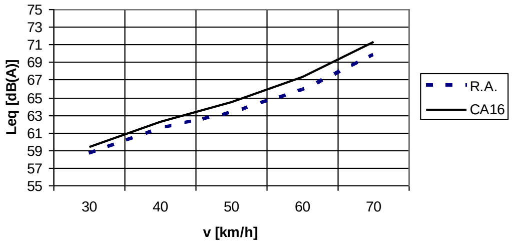

Fig. 9. *Comparison between the total noise levels obtained for the Golf 4T*

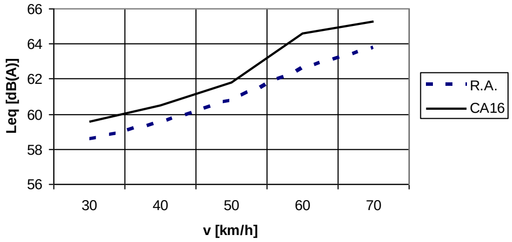

Fig. 10. Comparison between the total noise levels obtained for the BMW 520D

In figs. 11 and 12 we present the diagrams of spectral distribution (fig.11) and statistical distribution (fig.12) of the total noise levels obtained in case of displacements of the BMW 520D on the route coated with CA16 at the speed of 60 km/h. Figs. 13 and 14 shows similar diagrams recorded in case of displacements on rubberized asphalt for the same speed. We underline again that these levels of noise include the noise generated by the engine.

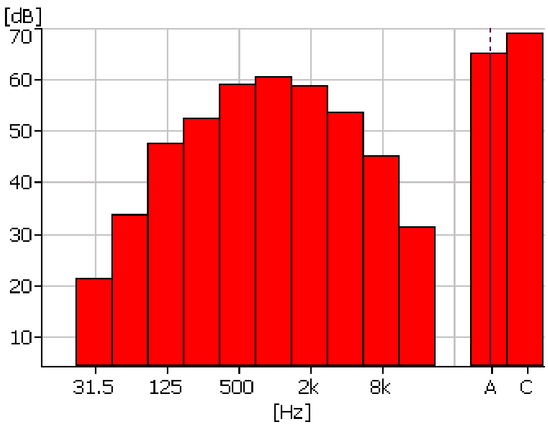

Fig. 11. *Spectral distribution of the total noise on CA16 at 60 km/h*

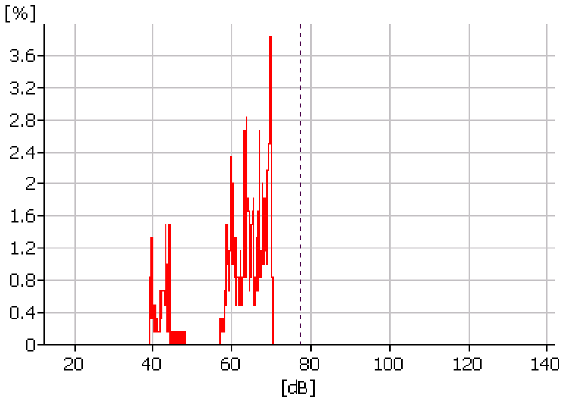

Fig. 12. Statistical distribution of the total noise on CA16 at 60 km/h

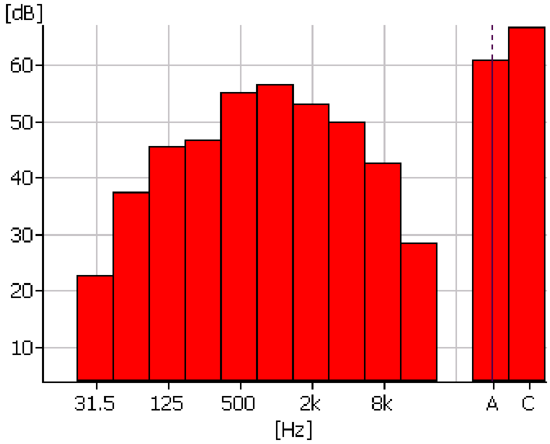

Fig. 13. Spectral distribution of the total noise on RA at 60 km/h

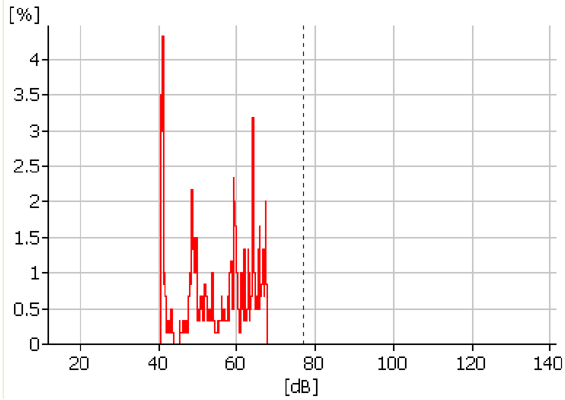

Fig. 14. Statistical distribution of the total noise on RA at 60 km/h

From the values presented in table 2 and in diagrams from figs.2 and 3, we observe that the noise due to rolling contact slowly increases along with increasing the speed. Analysing the values from table 3 and the diagrams from fig.4, we observe in the case of the vehicle Golf 4T Diesel that the rubberized asphalt ensure a mitigation of the rolling noise between 1.3 and 6.1 dB, depending on the speed of displacement. This mitigation is growing once with the increasing of the speed. These conclusions recommend the use of the rubberized asphalt for acoustical arrangement of the road superstructure, which is very efficient especially for high speeds.

From figures 5 and 7 we observe the mitigation of the noise level for every frequency band, but the most significant mitigation of the noise level is remarked for the frequency bands corresponding to 1 kHz and 2 kHz. Also, analysing the statistical distribution of the noise presented in figs. 6 and 8, it can be emphasized the same mitigation.

From the values presented in table 4 and the diagrams from figs.9 and 10, we observe that the rubberized asphalt ensure a mitigation of the total noise between 0.7 and 1.55 dB for the vehicle Golf 4T Diesel, while the mitigation for the vehicle BMW 520D ranged between 1 and 1.95 dB. It is observed that these mitigations are growing once with increasing the speed.

Analysing the diagrams of the spectral distribution from figs. 11 and 13 it can be observed and evident mitigation of the noise levels in frequency bands. A similar conclusion concerning the mitigation can be drawn analysing the statistical distribution presented in figs. 12 and 14.

3 CONCLUSIONS

A mitigation of the noise generated by the contact between the tire and the rolling surface can be achieved by the arrangement of the road superstructure. This acoustical arrangement can be performed by coating the road with rubberized asphalt.

Because the noise generated by the contact between the contact between the tire and the rolling surface represents about 75% from the total noise generated by the vehicle, it means that the acoustical arrangement of the road superstructure contributes significantly to the mitigation of the noise generated by the road traffic in the urban environment, especially for high speeds.

4 REFERENCES

[1] Enescu N, Magheţi I., Sârbu M.A., Acustica tehnică, Ed. ICPE, Bucureşti, 1998

[2] Grumăzescu M., et al., Combaterea zgomotului şi vibraţiilor în tehnică, Ed. Tehnică, Bucureşti, 1964

[3] Iudin E.Ia, Izolarea împotriva zgomotelor, Ed. Tehnică, bucureşti, 1962

[4] Stan A., et al., Consideraţii asupra nivelului intensităţii zgomotului de trafic în exteriorul clădirilor din zona centrală şi semicentrală a municipiului Bucureşti, Construcţii, nr.10, 1973

[5] Bacria V., Herişanu N., Investigation of the effects of rubberized aspalt on decreasing the noise, Proceedings of the 3rd Symposium "Durability and Reliability of Mechanical Systems, C. Brâncuşi Univ. of Târgu Jiu, 20-21 May 2010., pp.5-10

[6] Herişanu N., Bacria V., Toader M., Popa Radovan S., Investigation of the noise pollution in an urban area, WSEAS Transaction of Systems, 7(5), 2006, pp.1642

[7] *** Lärmbekamfung in Wien, Enwichlung Stand Tendenzen, Magistratabteilung 22 Umweltschutz

[8] *** Städtebauliche Lärmfibel, Hinweise fur die Bauleitplanung, Baden Würterberg Innenministerium, 1991

HEAVY MACHINERY - HM 2011, 7-14
ISBN 978-86-82631-58-3
Paper accepted: 30.05.2011

Organization of Distribution Centers, the Case of "Idea" Niš

Vojislav Tomić[1,*], Zoran Marinković[1], Danijel Marković [1], Goran Marković[2]
[1.] University of Niš, Faculty of Mechanical Engineering, Serbia
[2.] University of Kragujevac, Faculty of Mechanical Engineering, Serbia

The choice of warehousing, organization, and material flow management technology in distribution centers represents a complex process which demands special attention. One of the ways of solving such problems is the application of warehouse system planning, modeling, simulation, and analysis methods. The subject of the research in this paper are distribution centers, their working systems and optimization. The first part of the paper is on the role of distribution centers within logistic chains and on the systems present in those centers. Further, an actual example is provided concerning the distribution center of Idea Niš which represents one of the largest distribution centers in Southern Serbia. A detailed analysis of the warehouse space within this center was performed using mathematical models and a 3D system simulation was created upon which certain improvements were proposed. The aim of the research is presented using a structural, parametric, and functional analysis, while possible improvements are also given.

Keywords: Distribution Centers, Warehousing, Analysis, Improvements

1. INTRODUCTION

Cargo industry has had an impressive increment in recent years and this trend is still present in the distribution of goods. The distribution of goods is supported by a significantly sustainable presence of global integrated logistic networks [1] and rapid progress of e-trade [2], while distribution centers represent a link in the distribution process between macro and micro distribution. The main formation goal of these centers is the optimization of transport and distribution of material goods, with all of the following activities and subsystems, through application of modern transport technologies based on logistic principles.

Distribution center (DC), represents a node in logistic activities, and has the function of temporally ensuring the availability of goods in relation to customers. DC handling the distribution of goods according to customer demands. Realization of DC functions is performed using various warehousing systems which are constructed within them.

Distribution centers represent a node of logistic activities and production capacity of a company on the one hand, while they can also be nodes of supply chains on the other [3].

The subject of the research in this paper are DC, their working systems and optimization.

The first part of the paper is on the DC and the systems present in those centers, with a short historical review of the development of DC.

Further, an actual example of the DC of Idea Niš is provided, within which a detailed analysis of the system, and later optimization, was performed using appropriate mathematical models.

The aim of the research is presented using a structural, parametric, and functional analysis of the working system, while possible improvements are also given. In this part of the paper, the following topics concerning this center are presented: a short review of the company Idea is provided, the warehousing system of DC Idea in Niš is described, the DC organization model is presented and illustrated, a detailed analysis of the warehousing system is performed, bottlenecks and shortcomings of the warehousing system are observed and finally we give suggestions for the improvement of the system.

2. DISTRIBUTION CENTERS

Warehouse facilities first appeared in the distant past, practically at the moment when human beings reached that level of development which allowed them to produce and collect enough food during the summer to ensure normal nourishment in the winter period. Today, warehouses are defined as facilities or organized spaces, where resources (equipment,

[*]Corr. Author's Address: University of Niš, Mechanical Engineering Faculty of Niš, Serbia, Vojislav@masfak.ni.ac.rs

staff) and other technologically compatible and organized system elements used for preservation and organization of goods are present [4].

The greatest shift in the construction of warehouses and warehousing technology, without any tendency to diminish the significance of prior periods in the development of humanity, was made during the Industrial Revolution. The increasing intensity of ship transport and the beginnings of industrial production, which implied the supply of assembly lines, led to new requirements both in the construction of warehouses and warehousing technology [5]. During the 20th century, the development of goods management and transport technologies became more apparent, and new constructions of industrial buildings and warehouses were formed alongside the development of civil engineering, where steel or concrete support structures were applied, while there were numerous examples of warehouse acting as the support construction of the building.

Today, DCs are modern buildings, which are often architectural marvels, and whose trend is based on ecology. Modern DCs are a consequence of contemporary supply chains which are a present application phase of logistic concepts. Supply chain model represents a logistic flow with transport from production, including external production from cooperation to retail and/or wholesale distribution, where DCs are the nodes of this supply chain.

A DC as a node in logistic activities has the function of temporally ensuring the availability of goods in relation to customers, that is, handling the distribution of goods according to customer demands. Realization of DC functions is performed using various warehousing systems which are constructed within them, and the basic components of a modern DC are: facility – building, resources (machines-devices and staff), input-output processes, and information systems [6].

3. DC IDEA NIŠ ORGANIZATION MODEL

Goods and transport flows are the basic component of a DC. All of the terminal activities and subsystems are in the function of goods and transport flows. The connection of structures and characteristics of flows which pass through the DC is necessary for all planning, managing, and control activities, as well as system and process analysis in the terminal.

When creating management in a DC it is necessary to analyze the structure of flows, their characteristics, and their requirements in the view of activities of different terminal systems. Managing the work of the terminal, predicting business activities, and controlling flows is impossible without a system that would enable flow monitoring.

On the basis of the aforementioned, the model of DC Idea in Niš flows is analyzed in this paper (Fig. 1). DC Idea allows for goods to be received or delivered exclusively using road transport. Aiying and Martin apply a similar approach in [7] where they position loading/unloading docks for air transport in place of the input road side, thus creating the concept of a cargo terminal.

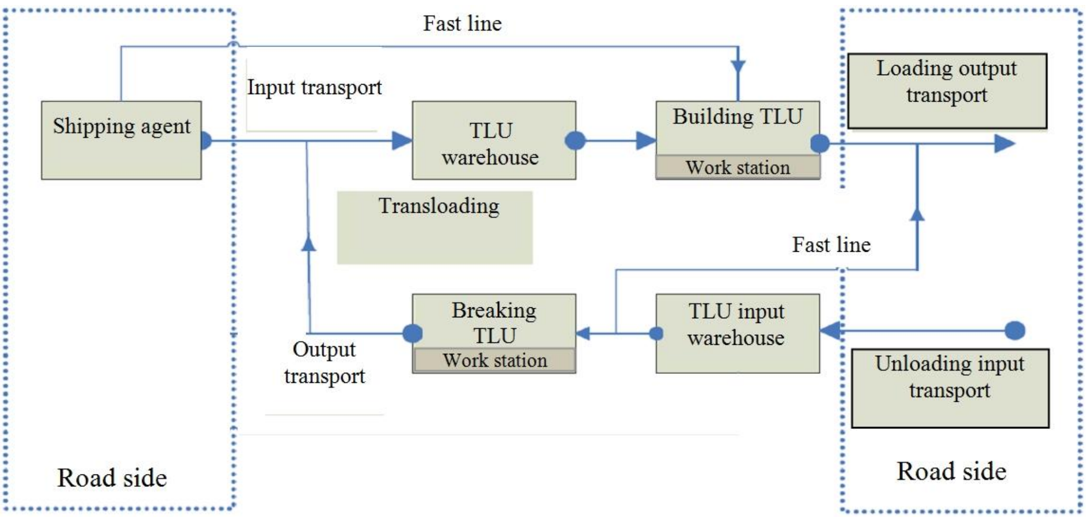

Fig. 1. Model of DC Idea Niš Flows

According to the presented model of DC Idea in Niš flows, the load is delivered to the DC by a shipping agent in transport logistic units (TLU). The load is delivered using both road sides of the terminal, where one is assigned for domestic manufacturers and the other for import goods. The load arriving in TLU can be directly transformed into the final output TLU using the fast line. The goods that arrive in inadequate TLU, or which are not for any other reason ready to be shipped directly, are sent to the section where TLU are built or broken. Such a great amount of load is consolidated into TLU in the construction section using workforce at work stations. After building of an adequate TLU, the goods are directly stored or shipped using the fast line to the output transport.

If the input transport is in inadequate transport logistic units, it is necessary to break it at work stations. At these stations, load is separated, sorted, scanned, and wrapped in thermal shrinking foil, building a compact warehouse TLU. Such new TLU is then stored, and the goods await for the commissioner to remove them.

When the commissioner receives an order for removing a certain quantity of goods, TLU are sent to the TLU construction zone, where new TLU are built in accordance with the picking list. As mentioned above, certain TLU do not need to be sent to the construction section, but they are directly moved to the storing zone for shipment preparation. In the same way, certain transloaded transports can be moved directly to the next connection transport over the fast line without the need to break and build TLU again. This happens only in the case when the connection route is compatible with the previous one, that is, when it requires the same TLU containing the exact same goods.

The possible goods at the work stations in this model are: output goods that need to be built, input goods that need to be broken, and transloaded goods that need both to be broken and built. The executor of building and breaking activities is a person employed at the work stations, and only a limited number of workers can work at the same time at each of the work stations.

The layout given in Fig. 2 corresponds to the adapted general model of DC Idea flows.

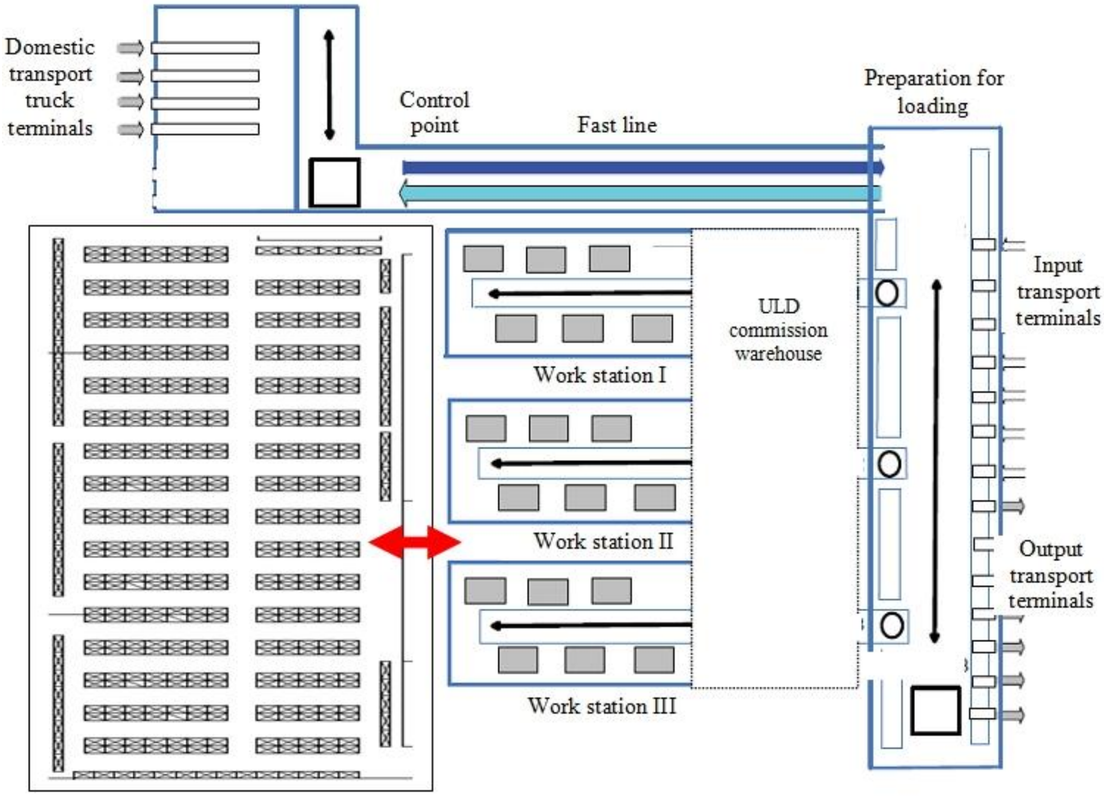

Fig. 2. Layout of DC Idea Niš

4. SYSTEM EFFICIENCY ANALYSIS

This paper defines a mathematical model which supports an efficient usage of workforce and operations that are necessary for breaking the existing and building new TLU. This model is applied in DC Idea in Niš. The problem of work plan and number of workers can be divided into dealing with two problems. The first problem is to determine the necessary workforce requirements. Workforce requirements must satisfy the delivery demands, time of departure and arrival of the shipping agent, supporting documentation, etc. The second problem lies in creating an efficient day plan which would satisfy previously mentioned workforce requirements.

One of the main tasks of this paper is to determine the necessary workforce for proper functioning of the DC warehouse system. On the basis of the obtained results it is possible to evaluate the efficiency of the warehouse system.

The evaluation comprises the following parts:

1. calculation of forklift and commission routes,
2. calculation of forklift and commissioner time needed to store and remove goods,
3. calculation of pellet turnover on the annual level,
4. calculation of time for storing/removing spent by forklift and commissioner on the annual level,
5. analysis of calculation results and comparison with the current situation,
6. assessment of warehouse systems efficiency in DC Idea in Niš.

5. MATHEMATICAL PROBLEM DESCRIPTION

In order to successfully solve the problems, mathematical restrictions are presented in the paper in the form of functions. Diagram in Fig. 3 illustrates the incoming function of output TLU [8]. Such a function is always increasing, making its distribution cumulative.

Load expected to be loaded into an output truck at the end of time interval t begins to arrive at time t - τ (τ > 0) (for the sake of simplicity, it is assumed that the expected time of transport is equal to the means of transport arrival time, excluding the time needed for loading goods into the truck).

Here L(j) represents the percentage of the arrival of load until time t-j (j = 0,...,τ, which yields L(0) = 100% and L(τ) = 0%), having in mind that all of the transport demands for output transport end at time t.

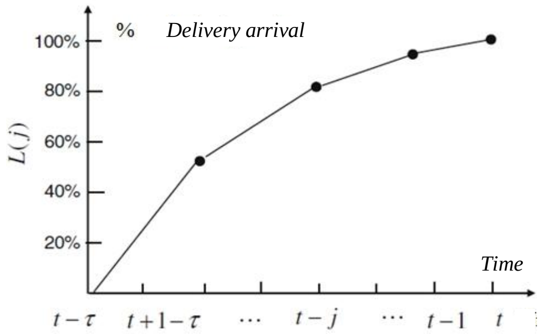

Fig. 3. Arrival of leaving TLJ

This means that transport is built in the range of the start of period τ until period t + 1 – τ, ending with time t (period t is the time between times t-1 and t).

The mathematical description of the problem:

The target function which needs to be minimized:

$$\min \sum_{s\in S}^{n} \sum_{q\in Q}^{n} \left(C_{s,q}^{break} g_{s,q}^{break} + C_{s,q}^{build} g_{s,q}^{build} \right) \qquad (1)$$

Where: S – the total number of shifts during the planned time, s – one shift; q – type of worker (workers who build or break a pellet), Q∈ {p, f}– workers do part-time or full-time shifts, respectively; $C_{s,q}^{break}$ - shift costs s for type q, workers who break TLU; $C_{s,q}^{build}$ - shift costs s for type q, workers who build TLU; $g_{s,q}^{break}$ - number of type q workers for breaking TLU per shift s; $g_{s,q}^{build}$ - number of type q workers for building TLU per shift s.

Using the balance method illustrated by expression (2) and flow diagram in Fig. 4, it is possible to calculate average routes which forklift or commissioner travel when storing or removing goods [9]:

$$\frac{\sum S_p \cdot n_{ps}}{\sum n_{ps}} = S_{sr}, \qquad (2)$$

where: S_p – partial routes per section, n_{ps} – number of pellets per section.

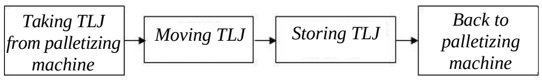

Fig. 4. Movement of forklift or commissioner when storing pellets

After the calculation of forklift routes (2), it is possible to calculate the time needed to store or remove TLU (t) using expression (3).

$$t = t_{up} + S \cdot t_{pv} + t_s + S \cdot t_e \ , \qquad (3)$$

where: t_{up}, t_{pv}, t_s and t_e - average time for picking up, moving, and storing pellets, and returning the forklift, respectively.

These times are taken from the catalogue of the manufacturer of a certain type of forklift. In this case, DC Idea uses "Linde" forklifts, while standard average times needed to perform the same operations are taken for the commissioner.

The time needed to store all pellets T_{uk} at the annual level is obtained as the product of time needed to store and remove one TLU (t) and the annual turnover of the number of pellets (G_{obrt}) in the DC (4):

$$T_{uk} = \sum_{i=1}^{n} G_i \cdot t_i \cong G_{obrt} \cdot t \qquad (4)$$

Where:

G_i – maximum number of pellets in each of the warehouse sections, t_i – time needed by forklift or commissioner to store a pellet for each section.

Finally, the necessary number of forklifts can be obtained using expression (5), where T_g – total number of working hours in a year.

$$N = T_{uk} / T_g \qquad (5)$$

On the basis of previous formulations, the goal of function (1) is the evaluation of the warehouse system efficiency upon which it is possible to obtain the potential minimization of workforce and costs during the planning time horizon. The planning time horizon is one month, where the number of work days is 21, and the number of working hours ranges from t=1h to 168h, i.e. t=1,..,T.

Since it is necessary to satisfy this function, 10 restrictions should be imposed:

First restriction:

Restriction (6) ensures that the cumulative formation of the amount of load for previous τ periods up to t period, should satisfy the demand for goods until the end of period t.

$$\sum_{q\in Q}^{\tau-1} X_{t-j,t} = d_t \quad \mathrm{t}=1,..,\mathrm{T} \quad , \qquad (6)$$

where $X_{t-j,t}$ - the built amount of TLU in kg in period t-j ready for output transport that arrives at the end of time t (j=0...τ-1), d_t - demands for goods (in kg) for output transport at the end of time t.

Second restriction:

Restriction (7) connects the cumulative building of TLU amounts before time t on the basis of the diagram of output transport arrivals. These restrictions guarantee that the load is available before the TLU building operation.

$$\sum_{j=k}^{\tau-1} X_{t-j,t} \le L(k) d_t \quad \mathrm{t}=1,..,\mathrm{T} \quad \mathrm{k}=1...0-1 \ , \qquad (7)$$

here $L(j)$ is the percentage of TLU arrivals until time t-j which is calculated for transport requirements of all departing trucks at the end of time t, where j = 0, . . . ,τ (Fig. 3).

Third restriction:

Restriction (8) shows the total built amounts of transport in period t and it is represented using the following relation:

$$\sum_{j=k}^{\tau-1} X_{t,t+1} = y_t \quad \mathrm{t}=1,..,\mathrm{T} \quad , \qquad (8)$$

where y_t is the total amount of built transport in kg during time t.

Fourth restriction:

Restriction (9) checks that input transport is broken up to the amount of period ω.

$$\sum_{j=k}^{\tau-1} u_{t+1,t} = e_t \quad \mathrm{t}=1,..,\mathrm{T} \quad , \qquad (9)$$

where $u_{t+1,t}$ is the amount of broken TLU in kg for period t+j, arriving from input transport at the end of time t (j=1,...ω), e_t - demands (in kg) for input transport at the end of time t.

Fifth restriction:

Restriction (10) shows the total amount of broken goods for period t.

$$\sum_{j=k}^{\tau-1} u_{t,t-1} = v_t \quad \mathrm{t}=1,..,\mathrm{T} \quad , \qquad (10)$$

where v_t is the total amount of goods units for breaking in kg for time t.

Six and seventh restriction:

The left side of restrictions (11) and (12) determines demands for workforce needed to build or break TLU in each of the periods, respectively. The right side of restrictions (11) and (12) determines the number of workforce which deals with TLU building (11) and the total number of workers which deal with both building and breaking of TLU (12) in each period.

$$\alpha y_t \le \sum_{q\in Q}\sum_{s\in E_{qt}} g^{build}_{s,q} \quad t=1,..,T \quad , \tag{11}$$

where α is the number of people needed to build 1kg of load.

$g^{build}_{s,q}$ is the number of type q workers needed to break TLJ per shift s.

$E_{q,t}$ is the sum of all shifts for type q workers, for period t, e.g. if a worker works full 8h shifts $E_{f,1}$ = {162, 163, 164, 165, 166, 167, 168, 1}, or part-time 4h shifts $E_{q,1}$ = {166, 167, 168, 1}.

$$\alpha y_t + b v_t \le \sum_{q\in Q}\sum_{s\in E_{qt}} g^{build}_{s,q} + g^{break}_{s,q} \quad t=1,..,T \quad , \tag{12}$$

where b is the number of people needed to break 1kg of load, $g^{break}_{s,q}$ is the number of type q workers for breaking per shift s.

Restrictions (11) and (12) especially mark the hierarchy between workers who deal with building of TLU and workers who deal with breaking of TLU, where TLU building operations are exclusively performed by workers in charge of building (11) while TLU breaking operations are performed by both workers who are in charge of breaking and workers who are in charge of building TLU (12).

Eight restriction:

Restriction (13) determines that only a limited number of workers can work in synchronization at work stations.

$$\sum_{q\in Q}\sum_{s\in E_{qt}} g^{build}_{s,q} + g^{break}_{s,q} \le N \quad t=1,\ldots,T \quad , \tag{13}$$

where N is the capacity of workforce for each work station.

Ninth and tenth restriction:

Functions (14) and (15) enforce availability restrictions for various types of workers in charge of building TLU and workers in charge of breaking TLU during the planning time horizon, respectively.

$$\sum_{s\in S} g^{breack}_{s,q} \le N^{break}_q \quad q\in Q \quad , \tag{14}$$

where N^{break}_q is the maximum number of workforce, type q workers for breaking TLU, per shift during the planning time horizon.

$$\sum_{s\in S} g^{build}_{s,q} \le N^{build}_q \quad \mathrm{q}\in \mathrm{Q} \quad , \tag{15}$$

where is the maximum number of workforce, type q workers for building TLU, per shift during the planning time horizon.

6. ANALYSIS RESULTS

On the basis of the presented mathematical model and its application on the illustrated warehouse model of DC Idea in Niš, the following results were obtained:

The necessary number of forklifts per shift for proper functioning of this DC was obtained by calculation and it equaled 3, which was in accordance with the current situation at this DC. The analysis was further verified using simulation in the 3D software package Flexsim 5.0. The model simulation where real system parameters were used (Fig. 5) (5748 pellet spaces, 38 shelving racks with actual warehouse dimensions, etc.) confirmed the necessary number of forklifts obtained in the previous calculation.

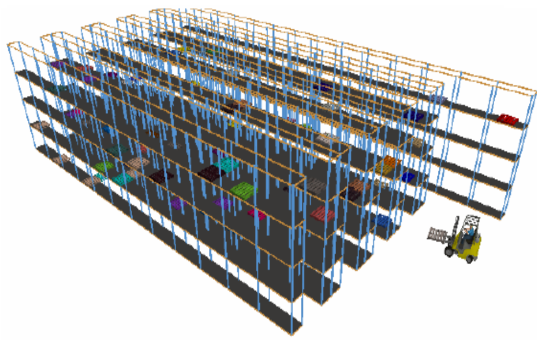

Fig. 5. 3D simulation of DC Idea Niš warehousing model

Since the commissioning costs were highest in the DC on average, the activity of the commissioner was analyzed. By applying previous expressions with given restrictions, 3 commissioners were followed and their working performance was measured for 3 randomly selected days, and the results are shown in diagrams in Fig. 6, 7, 8.

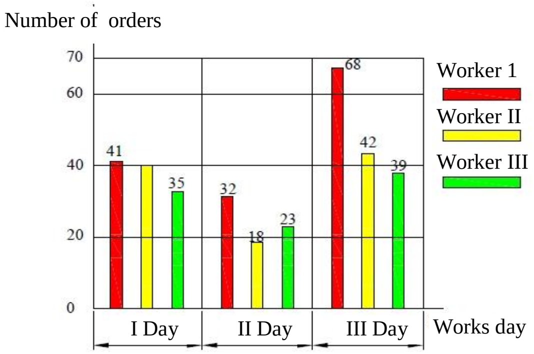

Fig. 6. Number of orders per day for each individual worker

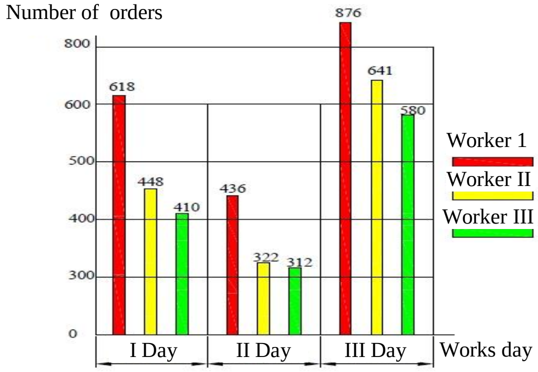

Fig. 7. Number of articles processed by the commissioner

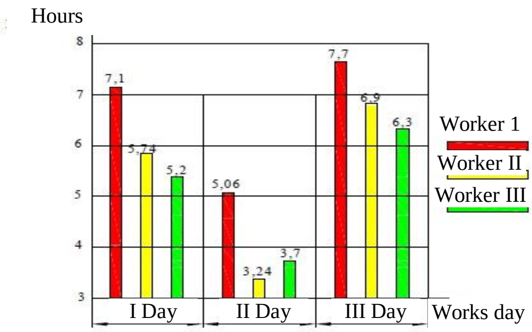

Fig. 8. Number of hours needed for the commissioner to carry out tasks

On the basis of the performed analysis, the uneven employment of the workers can easily be observed. Thus, worker number 3 is least employed, while worker number 1 has the greatest performance. On the other hand, on the basis of these measurements, the diagram in Fig. 9 illustrates how much the commissioning worker is exploited on average. From the obtained data, one can determine the average time needed to process the average number of orders. Thus, according to the obtained results, the average number of orders per day would be 37.5, for which 5.6 hours of effective work in total would be needed, which points to the fact that the commissioner is fully exploited for the given working conditions since 70.75% of the effective 8 working hours are used.

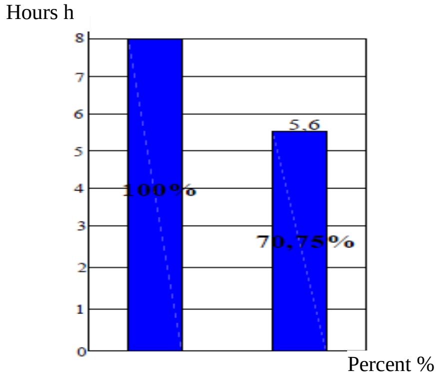

Fig 9. Average effective working hours of the commissioner

On the basis of everything presented here, it can be concluded that the system being currently used in DC Idea is satisfactory, but not optimal in the current situation. Analysis results show that DC Idea uses its workforce effectively in the warehouse, however, these results are the outcome of research based on the applied technical and information warehousing system which is currently being used by Idea Niš in its warehouse, and which is not at the highest level.

7. CONCLUSION

The mathematical method applied within the analysis provides the foundation for evaluating the warehousing system efficiency of DC Idea in Niš. It can be said that the functioning of the system concerning the number of workers and their exploitation is satisfactory in relation to currently used technical and information technologies. If the warehousing system is innovated using certain improvements primarily of information and technical character, the existing warehouse can become even more efficient. These are some of the improvement examples that could be applied in DC Idea Niš:

1) Implementation of informatics technology (IT):
Introducing new IT solutions for improvement of internal processes in logistics is becoming a necessity for survival of big distribution companies. For example, automatic identification (AI) of products would substantially improve the current product warehousing system in Idea Niš. AI is a term used to describe the automated input of goods label data into a computer system, programmable logic controller (PLC), or some other microprocessor control device. This way, using compatible scanners, the flow of goods would be controlled much more easily, and the number of commissioning workers would be reduced at the same.

2) Improving the technical system in DC:
The manner of warehousing without the use of loading ramps and pelletizers is almost unimaginable in modern DCs. The exploitation of a larger number of workforce for this purpose is not justifiable, and DC Idea does not have such resources, which makes their implementation into such a system necessary.

3) Certain restrictions for sending goods:
DC Idea enables customers and users to order unit goods which implies, as explained earlier, the need to break and build TLU again, that requires a great number of employed commissioners. In order to reduce the commissioning costs, it is possible to pose restrictions on ordering goods, e.g. minimum amount would be ½ pellet per product.

4) Yet another way to improve the system would be to introduce the season warehouse. It could be a floor warehouse, small in dimensions, near the loading zone. Seasonal and discount goods which has a great turnover in certain parts of the year would be stored there.

5) Application of high shelving racks:
A warehouse with high shelving racks would be constructed using 15-level shelving racks that would cause the warehouse to reach 35 meters in height. If this way of warehousing is applied, ten high shelving racks would be used to store the same number of pellets. This would lead to the increase in both the area and volume usage of the warehouse, and allow for a greater number of pellet units to be stored. One shelving rack would ensure 576 pellet spaces, while the area of the warehouse would be 4 times smaller than the current one. Such a warehousing system requires huge investments, thus it is necessary to analyze its justifiability in more detail.

By establishing given measurements of a system improvement, the warehousing system of Idea in Nis would be more effective. Delivery responses would be faster and workers who work in working stations would be more flexible. Mathematical and simulation model have been fully implemented in such a system and it facilitates qualitative analysis flaws in DC.

8. LITERATURE

[1] Zhang, A. *„Analysis of an international air cargo hub: the case of Hong Kong”*. Journal of Air Transport Management 9 (2), 123–138., 2003.

[2] Zhang, A., Zhang, Y. *„Issue on liberation of air cargo services in international aviation”* Journal of Air Transport Management 8 (5), 275–287., 2002.

[3] Europlatforms, FV-2000. Feight Village 2000: *„Increasing the attractiveness of intermodular transport“*, Bruxelles/ Bologna 1999.

[4] Marinković. Z: “*Container transport*”, Faculty of Mechanical Engineering, Niš 2009.

[5] Zečević S.: “*Goods terminals and transporting centers*“, Faculty of transportation networks, Belgrad 2006.

[6] J.Berg., W.Zijm.. *„Models for warehouse management”,* International Journal of production Economics 59, 519-528., 1999.

[7] Aiying, R., Martin, G. *„Shift designs for freight handling personnel at air cargo terminals“*, Journal of transportation research, 725–739., 2009.

[8] Nobert, Y., Roy, J. „*Freight handling personnel scheduling at air cargo terminals*“. Transportation Science 32, 295–301., 1998.

[9] Barac N, Milovanović G.: *Strategijski menadžment logistike*, Ekonomski fakultet Univerziteta u Nišu, Niš 2006.

HEAVY MACHINERY - HM 2011, 15-24
ISBN 978-86-82631-58-3
Paper accepted: 30.05.2011

A Review of Multi-Stage Allothermal Gasifiers

Vladan Karamarković[1,*] - Rade Karamarković[1] , Miljan Marašević[1]
[1] University of Kragujevac, Mechanical engineering in Kraljevo

A review of the present development of multi-stage allothermal gasifiers is given. These reactors obtain part or all heat necessary for endothermic gasification reactions outside of the reactor space, and are usually only a segment in complex systems for cogeneration and production of other biofuels and chemicals. Their purpose is to produce as clean as possible product gas with the composition adapted to the final use of the gas. In this way designed gasifiers, substantially improve the efficiency of biomass conversion and the economics of the systems since they require less expensive gas cleaning equipment downstream of the reactor. Different types of gasifiers that obtain heat for endothermic gasification reactions by the use of: preheated medium, chemically active or not hot bed material, high heat fluxes over the solid reactor surfaces, electrical and solar energy are presented. They have significant potential for the combine use of biomass energy together with solar energy, excess electricity and high temperature waste heat.

Keywords: biomass gasification, allothermal gasification, gasifier, multi-stage gasifiers.

0. INTRODUCTION

Taking into consideration current developments in the construction of biomass gasifiers, the future belongs to allothermal reactors, i.e. the reactors that obtain all or part of the heat necessary for endothermic gasification reactions outside of the reactor. These gasifiers should enable the combine use of the energy of biomass and different forms of energy: thermal energy of the product gas, solar energy, recuperated high temperature industrial waste heat, excess electric power etc. By employing these methods it is possible to produce a product gas with medium or high heating values

The contemporary multi-stage gasifiers have arisen from the need to produce the gas with required composition, heating value, free from tar and other impurities, and to optimize the reactor in accordance to the characteristics of the used biomass. The development of the reactors is of a high importance to the complex systems that use the product gas for cogeneration and production of other biofuels. In these systems the gasifiers are the least efficient devices and present bottleneck for wider application of these technologies [1], [2]. E.g. it is of great importance for the Fischer-Tropsch synthesis of liquid biofuels to produce so called synthesis gas free from methane and with the desired ratio of $H_2/CO \approx 2$. Auto-thermal reactors that are self-sufficient in heat, obtain heat for the endothermic reactions: Boudouard reaction,

$$C + CO_2 = 2\ CO + 172\ MJ/kmol \qquad (1)$$

heterogeneous water-gas reaction,

$$C + H_2O = CO + H + 131\ MJ/kmol \qquad (2)$$

and homogeneous methane reforming reaction

$$CH_4 + H_2O = CO + 3H_2 + 206\ MJ/kmol, \qquad (3)$$

by simultaneous exothermic oxidation reactions. In allothermal gasifiers, the heat required for the endothermic gasification reactions is obtained in numerous ways (3) by:

- ✓ preheating gasifying medium (air, oxygen, water vapor or their mixtures). In this way only part of the heat necessary for conducting the endothermic reactions is obtained. When steam is used as the gasifying medium the rest of the heat for the completion of the endothermic reactions is obtained by one of other methods given in this classification.
- ✓ supplying a hot solid material (usually sand or mixture of sand, a catalyst and biomass ash), which is heated by an exothermic reaction in the second reactor and circulates between the endothermic gasification reactor and an exothermic reactor. These are usually fluidized bed reactors.
- ✓ addition of heat into an allotehermal reactor over a solid surface. This way has become common in allothermal gasifiers. Usually the sensible heat of the product gas is used to

[*]Corr. Author's Address: Faculty of Mechanical Engineering Kraljevo, Dositejeva 19., Kraljevo, Serbia, karamarkovic.v@mfkv.rs

drive pyrolysis reactions in the first stage by the use of recuperative heat exchangers or by the use of liquid metal heatpipes.

- ✓ addition of electric power, like in plasma gasification.
- ✓ introduction of concentrated solar radiation.

Various ‘multi-stage’ processes are currently under development or already in operation. The high volatile amount of biomass, which is released rapidly as gaseous substances during pyrolysis, is taken into account in numerous reactor concepts by spatial subdivision of the fuel conversion steps (4). This makes it possible to influence and optimize the operating parameters in each conversion step. These concepts can be categorized as ‘single-line’ or ‘double-line’ processes (4). ‘Single-line’ processes use only one main stream of mass through a number of reactors which are arranged in series. ‘Double-line’ processes divide the mass stream into at least two partial streams which pass through parallel-arranged reactors (4).

In Fig. 1(a) a two-stage ‘single-line’ gasification process according to Ref. (5) is shown. This, so called Viking gasification concept will be explained in the following section of the paper.

Another gasification approach is to divide the mass stream into at least two partial streams which are processed in several parallel-arranged reactors (4). The heat needed for gasification can be produced separately by using air for combustion without affecting the gas quality of the gasification reactor, see Fig. 1(b) Combustion and gasification reactors are kept separate and are only interconnected by heat transfer. In principle, a pyrolysis stage is necessary to split the fuel into gas and char. To provide the heat necessary for autothermal operation, the char or part of the pyrolysis gas must be oxidized outside the pyrolysis reactor (6), as cited in (4).In the remainder of this paper three processes of this kind are presented.

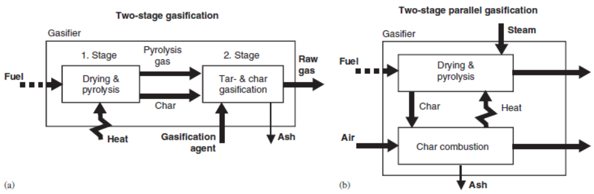

Fig. 1. Two-stage single-line and two-stage double-line gasification concept (4).

1. VIKING GASIFICATION CONCEPT

This gasification concept was developed at the Denmark Technical University. The motive for its development was the solving of tar problems in the product gas (5). Tar is a great obstacle for wider use of gasification, because it damages internal combustion engines, blades of gas turbines and other equipment downstream from the gasifier. Gasification processes producing only very low amounts of tars will have great potential as tar treatments can be avoided (7). This happens because the production of tar-free gas eliminates the expensive equipment for its elimination downstream of a gasifier.

The gasifier called ‘Viking’ (see Fig. 1 and Fig. 2) is a traditional two-stage gasifier which means that the pyrolysis and char gasification takes place in separate reactors.

Between the pyrolysis and the gasification, the pyrolysis products are partially oxidised by means of air addition. Thus the tar content in the volatiles is reduced by a factor of 100 and thermal energy for the endothermic char gasification is produced.

When the partially oxidised pyrolysis products pass through the char bed in the char gasification reactor, the tar content is further reduced by a factor of 100 (5).

The resulting tar content in the produced gas is less than 15 mg per Nm^3 (5).

This gasification concept was developed earlier as McKendry (8) cited Warren (9) who had proposed operating a two-stage, two-reactor process. Pyrolysis of the biomass would take place in the first stage using external heating at 600 ^{0}C. The gases formed in the first stage would then react with steam to crack the tars. In the second stage the gases react with the char from the first stage to produce the final product gas.

The experimental cogeneration system, shown in Fig. 2 had been worked for 2000 hours until 2006. The two-stage reactor had thermal capacity of 75kW (5).

The exhaust gas from the connected gas engine is used for external heating of the pyrolysis reactor. A screw conveyer transports the biomass through the pyrolysis reactor. In the first part of the pyrolysis reactor, the biomass is dried. In the second part, the pyrolysis takes place. Pyrolysis demands higher temperatures than drying, and to satisfy this, the exhaust gas is split into two streams (see Fig. 2). One stream is heated further by heat exchanging with the hot producer gas, and the other is led directly to the pyrolysis unit where it joint the other stream (5).

The efficiency of the system for the production of electricity from wood chips was around 25% (5). The temperature of the pyrolysis products was around 600^0C. The highest temperature was in the oxidation zone at the top of the reactor, and was in the range from 1100 to 1200^0C, while the product gas was leaving the reactor with the temperature in the range from 725 to 800^0C (5). Cited Gobel et al. (10), Gassner and Marechal (1) gave the average composition of the product gas for the gasification of wood chips with 30 wt% of moisture, which is shown in Table 1.

Table 1. The volume composition of the product gas produced in the Viking gasifer for the gasification of wood chips with 30 wt% moisture (1).

Component	vol.%
CO	18.3
CO_2	14.2
CH_4	1.2
H_2	30.4
H_2O	3.2
N_2	32.7

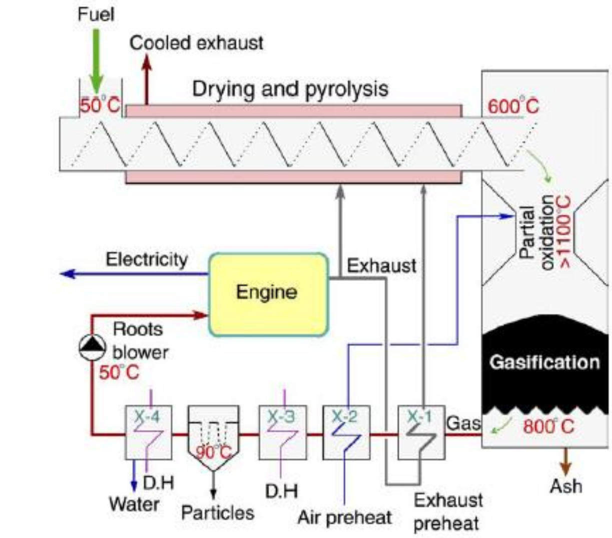

Fig. 2. The Viking gasifier (5).

2. BATTELLE (SYLVAGAS) PROCESS

This two-stage atmospheric biomass gasification process was developed by Battelle, and the first commercial demonstration unit with a feed capacity of 200 t/d was built in Burlington, Vermont (11).

The system is composed of two fluid-bed reactors, as it is shown in Fig. 3. In one, an endothermic process takes place for the gasification of biomass. The necessary heat for the reaction is supplied by a hot solid (sand, catalyst, or coke), which is heated by an exothermic reaction in the second reactor. As in all biomass gasification processes, a feed preparation stage is necessary in which the biomass is reduced to 30–70 mm-length chips and oversize or foreign material such as metals are removed. The biomass is fed to the gasifier where it is mixed with hot sand (at about 980°C) and steam (11). During the ensuing endothermic cracking reaction, light gaseous hydrocarbons are formed together with hydrogen and carbon monoxide. After separating the heat carrier and the gas in cyclones, the relatively cold heat carrier and residual unreacted char are discharged to the combustor or regenerator. The sand is reheated in the combustor by burning the char with air. The reheated sand is removed from the flue gas by a cyclone separator and returned to the gasifier.

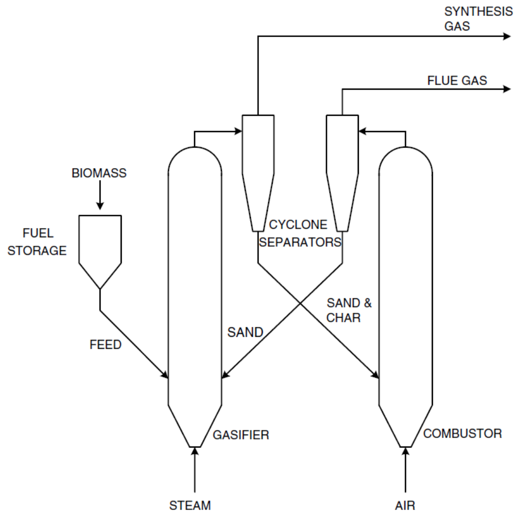

Fig. 3. The schematic diagram of the Battelle biomass gasification concept (11).

The flue gas is a valuable source of heat. Using it for pre-drying of the biomass feed helps increase the efficiency of the process, but alternative uses such as steam production may be applied if site-specific conditions favor this (11). The composition of the product gas produced in the Battelle reactor is given in Table 2.

Table 2. The composition of the product gas produced by the Battelle process ((12) cited by (11)).

CO vol%	44.4
CO_2 vol%	12.2
H_2 vol%	22.0
CH_4 vol%	15.6
C_2H_4 vol%%	5.1
C_2H_6 vol%	0.7
Higher heating value, MJ/m_N^3	17.3

3. FAST INTERNALLY CIRCULATING FLUIDIZED BED (FICFB) REACTOR

This reactor concept was developed at Technical University in Vienna. It is well documented concept (11), (13), (14), (15), and is nowadays still innovated and improved. The basic idea on which this principle is based is the same as for the previously presented Battelle process, and is shown in Fig. 1(b).

Fig. 4 shows the principle of the dual fluidized bed steam gasification processes. The fundamental idea of this gasification system is to physically separate the gasification reaction and the combustion reaction in order to gain a largely nitrogen-free product gas. Biomass entering the stationary fluidized bed gasification reactor is heated up, dried, devolatilized and converted to CO, CO_2, CH_4, H_2, H_2O_g as well as char. Simultaneously the strongly endothermic gasification reactions (reactions with water vapor) take place (1, 2). The heterogeneous char gasification reactions take place at bed temperatures of about 850 ◦C (16). A chute connects the gasification with the combustion section, operating as a circulating fluidized bed. Bed material together with any non-gasified carbon is transported through this chute into the combustion section, where the remaining carbon is fully combusted. The heated bed material is separated by a cyclone and fed back into the gasification section. The heat required for the gasification reactions is produced by burning carbon brought into the combustion section along with the bed material. Additionally, the temperature in the combustion section is controlled by supplementary fuel, like recirculated product gas or wood. The combustion zone is operated at about 920 ˚C (16). The gasification section is fluidized with steam, the combustion section with air, resulting in two different gas streams, a nearly nitrogen-free product gas with a calorific value of 12 MJ/Nm^3 (dry) and a flue gas from the combustion section (13).

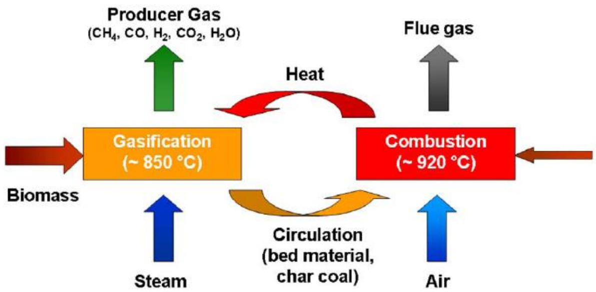

Fig. 4. The principle of two-stage FICFB gasifier (16).

The schematic diagram of the FICFB gasifier that operates in a cogeneration plant in the town of Güssing is shown in Fig. 5. Having undergone optimization and operation adjustment, the gasifier has been operated reliably. Characteristics of the product gas produced in this gasifier together with the cogeneration plant in Güssing operating data are given in Table 3.

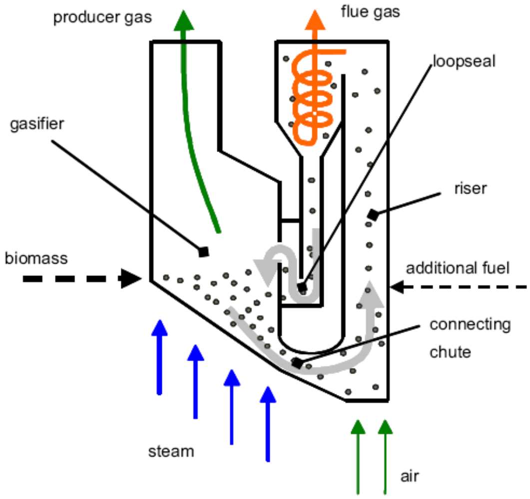

Fig. 5. The schematic diagram of FICFB gasifier (16).

Table 3. The characteristics of the dry product gas produced in the FICFB gasifier together with the cogeneration plant in Güssing operating data (13).

Characteristics of dry product gas		The plant operating data	
CO	20-30 vol%	Fuel Power	8000 kW
CO_2	15-25 vol%	Electrical output	1800 kW
H_2	35-45 vol%	Thermal output	4500 kW
CH_4	8-12 vol%	Electrical efficiency	25.0%
C_2H_4	2-2.5 vol%	Thermal efficiency	56.3%
N_2	3-5 vol%	Electrical/thermal output	0.44

The same team that developed FICFB reactor tries to improve its work by implementing selective transport of CO_2 from gasification to combustion zone. The principle of this innovation is shown in Fig. 6. The aim is to produce the product gas without carbon dioxide and tar (16), (17), (18), and (19).

Modifications are based on the implementation of the limestone, which is chemically active bed material. It has twofold role in the bed circulation material: to bring with its heat capacity from the combustion reactor, the heat required for the endothermic gasification reactions in the endothermic reactor, and to absorb CO_2 in the gasification reactor. The use of $CaO/CaCO_3$ as the bed material allows selective transport of CO_2 from the gasification reactor to the combustion reactor by repeated carbonation and calcination. The reactive bed material (limestone) used in the dual fluidized bed system realizes the continuous CO2 removal by cyclic carbonation of CaO and calcination of CaCO3.

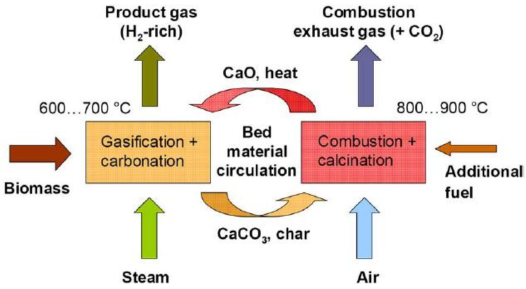

Fig. 6. Steam gasification with selective transport of CO_2 (16).

The overall reaction in the bed material is:

$$CaO_{(s)} + CO_2 = CaCO_{3\,(s)} – 181 MJ/kmol. \quad (4)$$

The necessary driving force for the carbonation and calcination is the difference between the CO_2 partial pressure in the reactor and the CO_2 equilibrium partial pressure.

The steam gasification of solid biomass by means of the absorption enhanced reforming process yields a high quality product gas with increased hydrogen content. The experimental investigation that took place at the cogeneration plant in Güssing with calcium carbonate as the active bed material showed stable production of the product gas with more than 50 vol% H_2 (19). The additional advantage of calcium carbonate as the bed material is that the carbonation reaction takes place in the endothermic reactor, where the heat necessary for the endothermic gasification reactions is required. The calcination reaction takes place in the combustion reactor.

The requirements on the CO_2 sorbent material are:

– high mechanical stability in the dual fluidized bed system to avoid dust problems in the plant,
– sufficient CO_2 capacity and reaction rate of carbonation and calcination under specified process conditions and
– catalytic activity towards tar removal and CO shift reaction.

Carbonates, especially limestone, meet these requirements in principle. They are non-toxic and widely available at low costs, essential for industrial scale applications. Used bed material exits the gasification process as dust together with biomass ash and can be used as fertiliser in forestry and agriculture to be recycled into nature (19).

4. HERHOF-IPV-VERFAHREN GASIFIER

This process was developed at the University of Siegen in Germany for the gasification of residual domestic waste that is upgraded to waste-derived fuel by means of biological drying and mechanical separation of inerts and metals (4). The principle of the reactor is given in Fig. 1(b) and the schematic diagram of the reactor is shown in Fig. 7.

This process is characterized by the parallel arrangement of a fixed bed and a bubbling fluidized bed reactor (see Fig. 7) (4). The fuel is fed directly into the fixed bed reactor filled with hot bed material. Through its contact with the hot bed material, rapid drying and pyrolysis of the fuel occurs. The volatiles released, including tars, pass through the hot ash layer above the fuel feed and leave the reactor at the top. Adding steam in the upper part of the bed enhances tar conversion by catalytic and/or thermal cracking in the presence of the hot ash particle surface. The remaining char and the bed material move towards the bottom of the gasification reactor and are transported by a screw conveyor into the fluidized bed combustor. The char combustion leads to a heat-up of the fluidized bed material which is then discharged towards the gasification reactor by a fluidized loop seal. The energy required for pyrolysis and gasification in autothermal plant operation is generated by char combustion. The combustion and gasification reactors are connected by circulating solid material, ensuring separation of gasifier raw gas and combustor flue gas. Thus a dilution of the product gas by nitrogen from the ambient air required for combustion can be avoided. Downstream of the gasification reactor, the remaining tars and other impurities are separated from the product gas by a gas scrubber and an electrostatic precipitator. The water/tar/dust mixture generated in the gas cleaning can be burnt directly in the fluidized bed combustor to ensure economic operation of the plant (4). Nitrogen free the dry product gas obtained by this process has higher heating value of 13.3 MJ/m_N^3 (4).

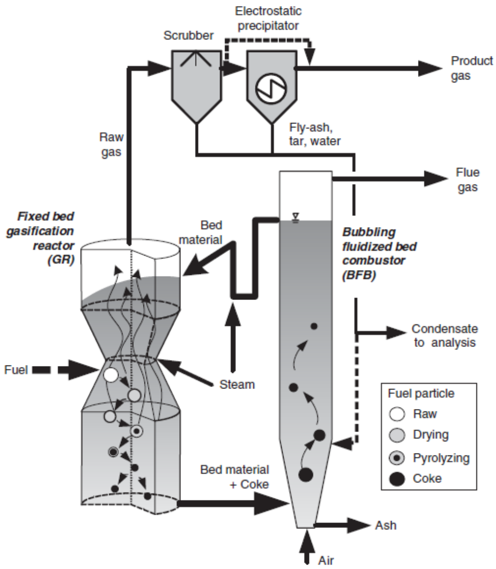

Fig. 7. The two-stage parallel-arranged gasifier designed for the processing of waste-derived fuels (4).

5. BIOMASS HEATPIPE REFORMER (BIOHPR)

BioHPR reactor, developed at the Technical University in Munchen, works at the principle shown in Fig. 1(b). The difference between this and three previously presented reactors is the absence of the circulation bed. This BioHPR utilises liquid metal heatpipes in order to create high heat fluxes from a combustion chamber to the gasifier, where the endothermic gasification reactions take place (20). High temperature heatpipes are metal pipes containing an alkali metal (Na, K, etc.). Heat is transferred into the heatpipe at the evaporation zone. This heat is released at the condensation zone from the heatpipe to its environment as shown in Fig. 8.

The reactor consists of three main parts as shown in Fig. 9. The first part is a bubbling fluidized bed gasifier. Biomass is fed into upper part of this reactor through a specially designed lock hopper system. The gasification can take place either in atmospheric pressure or under pressures of up to 5 bar. The product gas from the endothermic reactor is first driven to the sand filter, which is the second part of the BioHPR. This integrated sand filter separates dust and coke particles from the product gas. After its way through a cyclone and a ceramic or metallic filter, the product gas can be analyzed and used in a gas turbine or a fuel cell. The third part of the BioHPR is the fluidized bed combustion chamber. The dust and coke particles, which are filtered in the integrated filter, enter the combustion chamber with the help of a siphon system, which separates the gasifier and the filter from the combustor. Liquid metal heatpipes filled with sodium transfer the heat from the combustion to the gasification chamber (20).

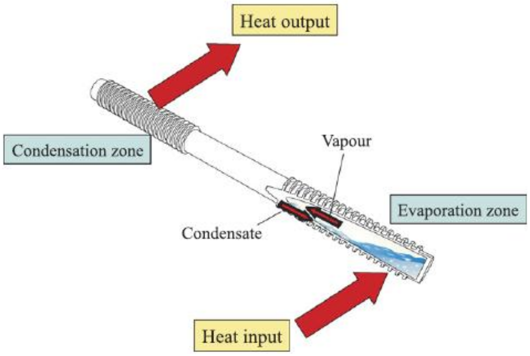

Fig. 8. Functionality of a heatpipe (20).

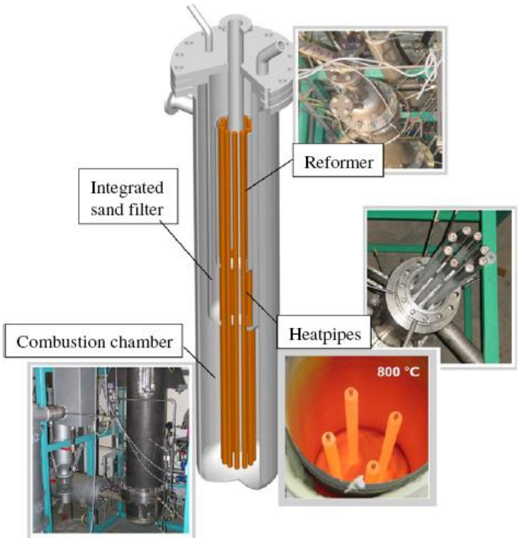

Fig. 9. Biomass Heatpipe Reformer (20).

6. PLASMA GASIFICATION

According to Mountouris et al. (21) this is one of the most effective and environmentally friendly methods for solid waste treatment and energy utilization.

This gasification concept differs in its structure from the concepts shown in Fig. 1. In principle, plasma gasification is a partly allotheramal process since a part of the energy required for the endothermic gasification reactions is obtained by the introduction of electrical energy into the reactor.

The block diagram for a plasma waste treatment plant is shown in Fig. *10*. The pretreatment implies drying and shredding of the feedstock for size reduction prior to entering the plasma furnace.

The plasma furnace is the central component of the system where gasification/vitrification are taking place. Two graphite electrodes, as a part of two transferred arc torches, extend in plasma furnace (21). An electric current is passed through the electrodes, and an electric arc is generated between the tip of the electrodes and the conducting receiver, i.e. the slag in the furnace bottom. The most often air is introduced between the electrode and the slag, although oxygen, helium or some other can be introduced. Prior to its final use for the production of electricity, heat or other biofuels the produced gas must be cleaned as in all other gasification systems.

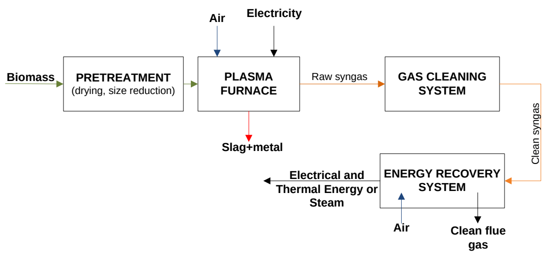

Fig. 10. Block diagram of waste plasma gasification process (21).

7. SOLAR GASIFICATION

This branch of gasification technology is in a close relation with the development in research for the use of solar energy. The aim of this field is storage, transport, and continual use of solar energy. The biggest obstacle for its use are very serious drawbacks: solar radiation reaching the earth is very dilute (only about 1 kW per square meter), intermittent (available only during day-time), and unequally distributed over the surface of the earth (mostly between 30° north and 30° south latitude).

Fig. 11 illustrates the basic idea for solar energy harvesting (22). If the diluted sunlight is concentrated over a small area with the help of parabolic mirrors and then that radiative energy captured with the help of suitable receivers, heat at high temperatures for driving a chemical transformation and producing a storable and transportable fuel would be obtained. Regardless of the nature of the fuel, the theoretical maximum efficiency of such an energy-conversion process is limited by the Carnot efficiency of an equivalent heat engine. With the sun's surface as a 5800 K thermal reservoir and the earth as the thermal sink, 95% of the solar energy could, in principle, be converted into the chemical energy of fuels (22).

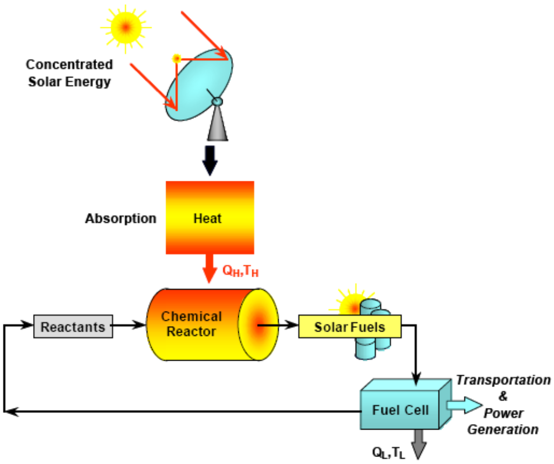

Fig. 11. Schematic of solar energy conversion into solar fuels. Concentrated solar radiation is used as the energy source for high temperature process heat to drive chemical reactions towards the production of storable and transportable fuels (22).

Schematic of the three main optical configurations for large-scale collection and concentration of solar energy is shown in Fig. 12. The capability of these collection systems to concentrate solar energy is often expressed in terms of their mean flux concentration ratio $\tilde{C}$ over a targeted area A at the focal plane, normalized with respect to the incident normal beam insolation I as follows:

$$\tilde{C} = \frac{Q_{solar}}{IA}$$

where Qsolar is the solar power input into the target. $\tilde{C}$ is often expressed in units of ''suns'' when normalized to 1 kW/m^2. The solar flux concentration ratio typically obtained at the focal plane varies between 30 and 100 suns for trough systems, between 500 and 5,000 suns for tower systems, and between 1,000 and 10,000 suns for dish systems (23).

Biomass and fossil fuels can be transformed by different thermochemical process into char, liquid biofuels and synthesis gas (24), (25), (26). Solar gasification of biomass with steam uses concentrated solar energy to transform solid biomass in a high quality synthesis gas, composed mainly of H_2 и CO that can be used for electricity production by combine cycle or by fuel cells or for Fischer-Tropsch synthesis of liquid biofuels ((24) cited in (25)). By the use of solar gasification, the heating value of the biomass is upgraded for the value equal to the enthalpy of the endothermic gasification reactions that take place in a solar gasifier. The gas produced by this process is almost free from carbon dioxide. This type of gasification is a way to store intermittent solar energy in the form of chemical energy that can be transported (25).

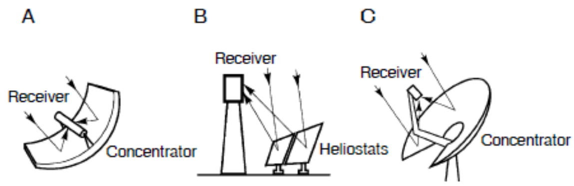

Fig. 12 Schematic of the three main optical configurations for large-scale collection and concentration of solar energy: (A) the trough system, (B) the tower system, and (C) the dish system (23).

8. CONCLUSIONS

The technology of multi-stage allothermal gasifiers is an emerging technology that should pave its way to the market. The current development is in a demonstration or laboratory phase with a few commercial examples that mainly use internally circulated hot bed material. There is a huge potential for the use of the chemical energy stored in biomass by the presented technology for the cogeneration, and production of different biofuels and chemicals. In addition, there is a potential for combining the energy of biomass with solar energy, excess electricity and high temperature waste heat. The gasifiers presented in this paper supply external heat to drive endothermic gasification reactions by the use of: preheated medium, chemically active or not hot bed material, high heat fluxes over the solid reactor surfaces, electrical and solar energy have been presented.

The purpose of these reactors is to produce as clean as possible product gas with the composition adapted to the final use of the product gas. In this way designed gasifiers, substantially improve the efficiency of biomass conversion and the economics of the systems, because they require less expensive gas cleaning equipment downstream of the reactor.

From this paper it can be concluded that the near future of gasification technology lies in: chemically active bed materials, combine use of the energy of biomass and solar energy, solution of tar problems in the reactor, and in greater use of this technology in cogeneration plants that use combine cycles.

9. REFERENCES

[1] *Thermodynamic comparison of the FICFB and Viking gasification concepts.* Gassner, Martin / Marechal, Francois. s.l. : Elsevier, 2009., Energy.

[2] *Exergeti evaluation of 5 biowastes-to-biofuels routes via gasification.* Sues, Anna, Jurascik, Martin and Ptasinski, Krzysztof. s.l. : Elsevier, 2009.

[3] *Energy and exergy analysis of biomass gasification at different temperatures.* Karamarković, Rade / Karamarković, Vladan. 2, Amsterdam : Elsevier, February 2010., Energy, T. 35, pp. 537-549.

[4] *Autothermal two-stage gasification of low-density fuels.* Hamel, S, Hasselbach, H, Weil, S / W, Krumm. 1, s.l. : Elsevier, 2007., Energy, T. 32, pp. 95-107.

[5] *The designe, construction and operation of a 75 kW two-stage gasifier.* Henriksen, U et al. 10, Amsterdam : Elsevier, 2006., Energy, T. 32, pp. 1542-1553.

[6] Uil, den and H.:, CASST. A new and advanced process for biomass gasification. [book auth.] AV Bridgwater. [ed.] AV Bridgwater. *Progress in biomass thermochemical conversion.* 2001, pp. 287–97.

[7] *A review of the primary measures for tar elimination in biomass gasification processes.* Devi, L, Ptasinski, KJ / Janssen, FJJG. s.l. : Elsevier, 2003., Biomass Bioenergy, T. 24, pp. 125-40.

[8] *Energy production from biomass (part 3): gasification technologies.* McKendry, Peter. s.l. : Elsevier, 2001., Bioresource technologies, Vol. 83, pp. 55-63.

[9] *Converting biomass to electricity on a farm-sized scale using downdraft gasification and a spark-ignition engine.* Warren, T, Poulter, R / Parfitt, R. 1995., Bioresource Technology, T. 52.

[10] *Status - 2000 hours of operation with the Viking gasifier.* Gobel, B, и други. Rome : s.n., 2004. . Proceeding of the 2nd world conference and technology exhibition on biomass for energy and industry.

[11] Higman, Chris / van der Burgt, Maarten. *Gasification.* Amsterdam : Elsevier, 2003. T. I.

[12] *Verification of the Performance of Future Energy Resources SilverGas Biomass Gasifier Operating Experience in the Vermont Gasifier.* Paisley, M. A. / Overend, R. P. Pittsburgh : s.n., 2002. 19th International Pittsburgh Coal Conference.

[13] *Gasification demonstration plants in Austria.* Nordenkampf, MB / Hofbauer, H. Bratislava : s.n., 2004. Slovak biomass forum. pp. 227-230.

[14] *Thermodynamic comparison of the FICFB and Viking gasification concepts.* Gassner, M / Marechal, F. Amsterdam : Elsevier, 2009., Energy, T. 34.

[15] Institute of Chemical Engineering TUV. Introduction. *Fast Internal Circulating Fluidized Bed Reactor.* [На мжрежи] Technical University in Vienna, 2004. [Cited by : 11 January 2010.] http://www.ficfb.at.

[16] *Comparison of dual fluidized bed steam gasification of biomass with and without selective transport of CO2.* Pfeifer, C., Puchner, B. / Hofbauer, H. Vienna : Elsevier, 2009., Chemical Engineering Science, T. 64, pp. 5073-5083.

[17] *Model development and validation: Co-combustion of residual char, gases and volatile fuels in the fast fluidized combustion chamber of a dual fluidized bed biomass gasifier.* Kaushal, Priyanka, Pröll, Tobias / Hofbauer, Hermann. Vienna : Elsevier, 2007., Fuel, T. 86, pp. 2687-2695.

[18] *Development of catalytic tar decomposition downstream from a dual fluidized bed biomass steam gasifier.* Pfeifer, Christoph /

Hofbauer, Hermann. Vienna : Elsevier, 2008., Powder Technology, T. 180, pp. 9-16.

[19] *H2 rich product gas by steam gasification of biomass with in situ CO2 absorption in a dual fluidized bed system of 8 MW fuel input.* Koppatz, Stefan, et al. Vienna : Elsevier, 2009., Fuel Processing Technology, T. 90, pp. 914-921.

[20] *An innovative biomass gasification process and its coupling with microturbine and fuel cell systems.* Karellas, S, Karl, J and Kakaras, E. 3, Amsterdam : Elsevier, 2008., Energy, Vol. 33, pp. 284-291.

[21] *Solid waste plasma gasification: Equilibrium model development and exergy analysis.* Mountouris, A, Voutsas, E / Tassios, D. 6, s.l. : Elsevier, 2006., Energy Conversion and Management, T. 47.

[22] Steinfeld, A / Palumbo, R. Solar thermochemical process technology. [аут. књиге] RA Meyers. [ур.] RA Meyers. *Encyclopedia of Physical Science and Technology*. Zurich : Elsevier, 2001., T. 15, pp. 237-256.

[23] Steinfeld, Aldo / Meier, Anton. Solar Fuels and Materials. *Encyclopedia of Energy.* s.l. : Elsevier, 2004., T. 5.

[24] *Solar thermochemical conversion of biomass.* Lédé, J. s.l. : Elsevier, 1999., Solar Energy, T. 65, pp. 3-13.

[25] *Solar-driven biochar gasification in a particle-flow reactor.* Melchior, Tom, et al. s.l. : Elsevier, 2009., Chemical Engineering and Processing: Process Intensification, T. 48.

[26] *Hydrogen production by steam-gasification of carbonaceous materials using concentrated solar energy - IV. Reactor experimentation with vaccum residue.* Z'Graggen, A, et al. Zurich : Elsevier, 2008., International Journal of Hydrogen Energy, T. 33, pp. 679-684.

HEAVY MACHINERY - HM 2011, 25-30
ISBN 978-86-82631-58-3
Paper accepted: 30.05.2011

Modern systems of identification and production logistics management in machine building

Aleksandar Cupic [1,*] Goran Markovic [2] Milan Bukumirovic [1]
[1] Faculty of Transport and Traffic Engineering, Belgrade
[2] Faculty of Mechanical Engineering, Kraljevo

Production management in modern machine building is based on use of automatic identification and identification systems on the base of information technologies bar code and RFID systems. These identification systems are base for managing workflow and products in production logistics.
Keywords: Identification, RFID, goods flow.

1 AUTOMATIC IDENTIFICATION USE

Logistics processes in the industry, storage, commodity and transportaion centres, and distribution have recently been characterised by new principles, new technologies and strategies out of which the most important are:

1. Constant, reliable, fast and well supply of production and other customers along with production improvement and improving the quality of services.

2. Constant supplying of commodity and transport centres storages and application of standarized logistics units.

3. Use of different sizes (dimensions), product volume and unit load (shipments, pack units, packiging units) in all links of transport and/or logistics chain.

Introduction of new technologies is impossible without application of automatic identification and bar code as the symbol for labeling packages and pack unit, with the help of which all relevant data are precisely and unequivocally introduced into the computer system.

1.1 Qualitative reasons for the use of bar code in production and transport

Bar code is mechanically readible by optical laser reader (scanner), passing beam of light trough the lines (scanning bar code). Reading is based on the difference in the reflection of light and dark lines of the symbol, which evoke certain signals in reader sensors, and these are, in digital form, conveyed into the computer, by which the automatic input of certain data contained in the bar code is done.

Bar code contribute to the increase of the productivity and economy thanks to the following features.

1. Speed: For the use of manual scanner for reading bar code on small objects it does not take longer than two seconds. Reading is possible in the state of sleep but at the high speed of transport as well.

2. Accuracy: it allows enough length during the reading. Manual insertion of the data over keyboard could be inaccurate. Bar code has a number for checking, it could be possible to find only one mistake in billion of signs.

3. Reliability, technology easy to use: it is reliable even after multiple use. Operater could be trained for scanner handling in a few minutes time.

4. Integration: automatic information gathering, for example in the industry, is enabled by use of laser scanners and camera systems. Information inside it is fixed programmed. Information is visible through clearly written line below line code.

5. Price: comparing to the present systems of identification which can be found on the market, the price of the medium and the equipment is good. Data carrier production cost is good (bar code).

1.2 Radio frequent identification (RFID)

The most modern system for commodity identification is the system for identification with electronic data carrier, so-called RFID technology.

RFID (radio frequncy identification), automatic registration system and data identification with contactless communications on the basis of radio frequency technology. RFID is

[*] Faculty of Transport and Traffic Engineering, Vojvode Stepe 305, Belgrade, Serbia, a.cupic@sf.bg.ac.rs

the technology which use radio waves for automatic identification of the single products (it has great advantage comparing to bar code as the data carrier can be programmed).

Identiication system with the electronic data carrier (see the picture) consists of:

- More information carrier- RFID transponder
- One or more (programmed) units for reading- RFID reader
- Units for (calculation) data readings processing- central computer

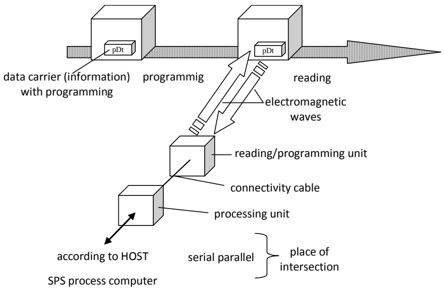

Fig. 1. *Components of identification system with electrical carrier (RFID- Systems) [1,2,4]*

The purpose of RFID technology is to enable automatic information gathering about some product which is marked, as well as about time and location of selling, and all of that without staff active physical participation.

Integrated information chain for monitoring of goods, from location of goods, through monitoring of stock and production status, to the final buyer delivery- RFID technology characteristic.

2 IDENTIFICATION SYSTEMS

In modern company management, connectivity between material and information flow (picture 2) represents very signigicant factor. In order information to be mechanically created and read, transmission goods (packages, raw materials, parts etc) and transmission assets (pellets, reservoirs and similar) are marked with codes which can be mechanically read. Such assets can be individually identified through appropriate systems for recognition.

Material flow in one company, DC has to be connected with all segments of his. While, on the one hand, information from various segments in the production, purchase and delivery are exchanged, on the other hand, on the base on these information, movement of phisical, transport and storaging units from entry to the delivery of the goods is managed.

Automatic reading process enables efficient application of data gathering without papers. This ability enables interconnection of systems and represents, from the material flow point of view, important aspect of automatization for system. Managing in material flow has a task to coordinate product and propulsion with target information in order to lead and follow the process. Some information system elements of automated process of flow, material, subject, transfer of goods, apart from internal communication in information process, have to communicate with the elements of phisical flow of material, goods, production transport assets as well. It means that physical flow elements- products on machines, material/goods in packaging, pallets, loaded transport assets (with material, goods) have to establish a connection- contact (constantly or at certain time intervals) on operational level with information system sensors.

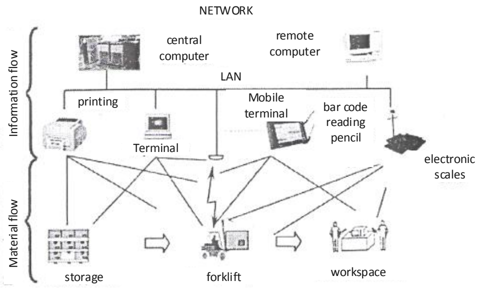

Fig. 2. *Material and informational flow*

3 INFORMATION TECHNOLOGIES USE (BAR CODE AND RFID) IN CAR INDUSTRY LOGISTICS PROCESSES

Use of the strategy just in time in production supplying, especially in large-scale and mass production, for example car industry, conditions introduction of modern control system and systems for identification of material and products flow, in the production process as well as in the distribution. Identification systems, structured according to standard recommendations (technical organizations), represent important element for managing and the main area for improving of individual logistics processes (transport, packaging, storage, commissioning, delivery) as well as for lowering total logistics costs in car industry. Identification systems integrate bar code and RFID technology.

Systems for logistics processes management in any area consists of data identification systems connected to commodity, subject as well as of the data giving systems, carrier data systems and processing data systems. Area of logistics processes management as well as production logistics starts actually from the initial functions of an enterprise: from ordering, production, selling, through storaging and material flow of goods and flow of information on relation supplier- forwarder- buyer. In that way managing the logistics processes integrate material and information flows as well as many activities and services.

We can see circling identification model in the function of integrated informational and physical managing functions in the area of logistics in picture 3.

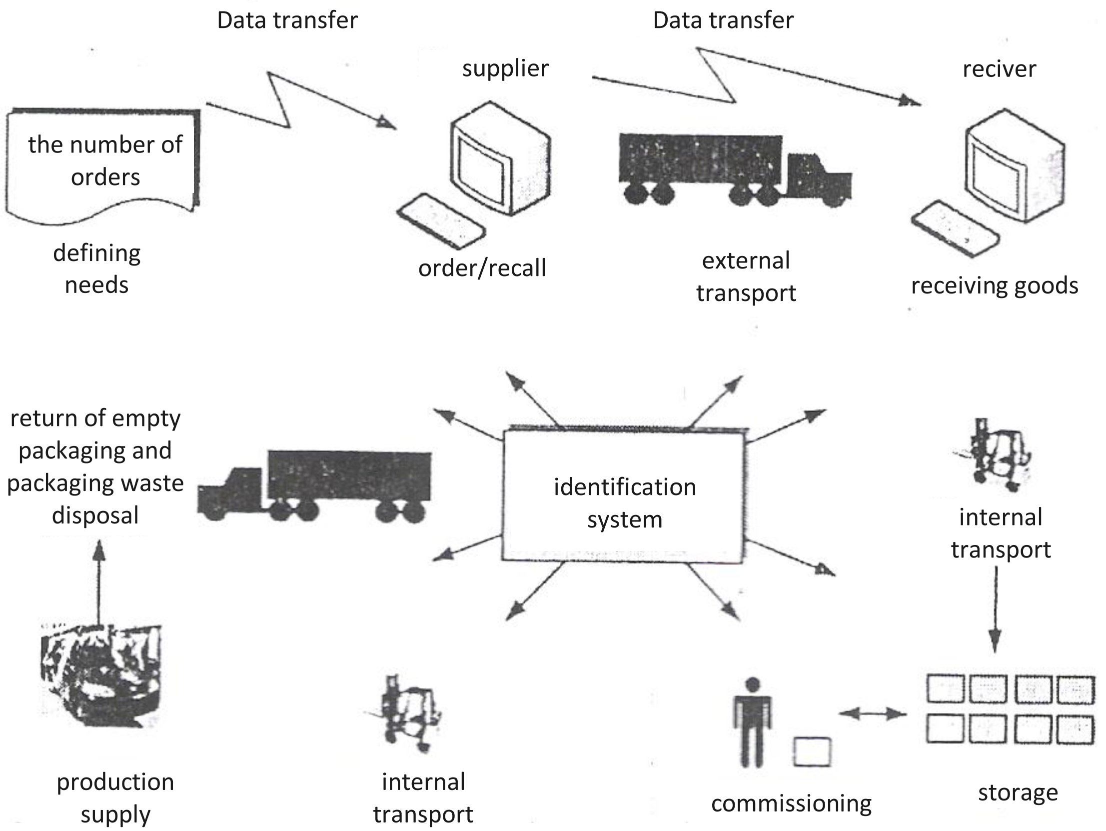

Fig. 3. *Identification systems ODETTE in chains of material flow in the area of logistics*

4 IDENTIFICATION SYSTEMS DURING THE WORK PROCESSES IN PRODUCTION

While choosing the information system for the specific application, the following issues should be analyzed:

- Space and time position of the information source and target
- Sort and range of data group necessary for information providing
- Media for information transfer and transfer distance

• Data access frequency and suggested waiting periods

• Actuality and redundancy in data keeping

• Influence from and on the environment

• Compatibility of the existing systems (in goods and material flows and in information exchange)

• Availability and expanding possibility

• Users' confirmation

• Planning costs, hardware, installation, software, education, work, maintenance

Since identification systems are a priori conceptualized for the flow of information that follow products, goods or movable objects, the question has been raised how much information is necessary for physical goods-material flow tracing and with a presumption that all of that has sense. In that case one of the following options can be chosen:

• Object, as a piece of information, is assigned with a so called identification numeration which requires centralized management of products, goods flow and central data maintenance

• Object is assigned with all information necessary for the process maintaining. That allows decentralized products and goods flow maintenance and requires decentralized data keeping

• Mixture of the both previous possibilities defines hybrid management of the products and goods flow and data keeping

4.1 Centralized management of products flow

Picture 4 represents the way of data management and keeping. All information, necessary for the process is in the central main computer which should be supplied with all the information arising during the production process. Information sensors of the automotive managing process are the information systems within the processor itself.

Usually, an identification number, which is physically connected to the products and is also connected to the information via the scanning place and, through the local area network (LAN), is reported to the central computer, is being shown. That is where the identification number is connected with the current information regarding products management process and is again recorded via the network of the process management. Data changing in the central computer is possible only via the defined transactions.

Identification systems with optically readable data carrier are especially suitable for this management concept, especially those with so called bar codes. In special cases identification systems with firmly coded electronic data carriers are applied. The decision is significantly influenced by environment conditions and data carriers costs.

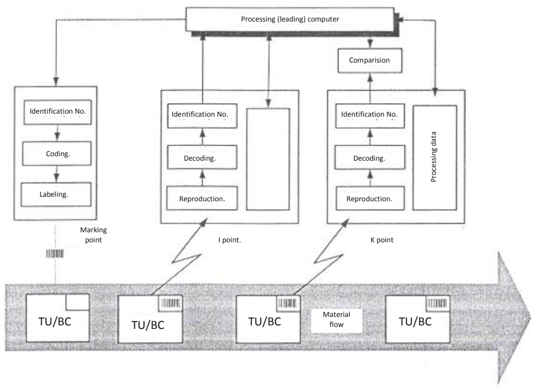

Fig. 4. *Material flow central management (TU – transport unit; LC – bulk carrier)*

Drawbacks of the central management are the disturbance causing and small expansion flexibility. If one component of the network fails, there will be consequences for the entire system. Disturbance in the area of logistics process management will lead to the complete failure of the entire system. System expanding is difficult and limited.

4.2 Decentralized management of products flow

Picture 5 represents this management and data keeping system: all necessary information for the process management is kept nearby the processor, which means that it is memorized at the very stationary unit of the material flow system or at the very object in motion.

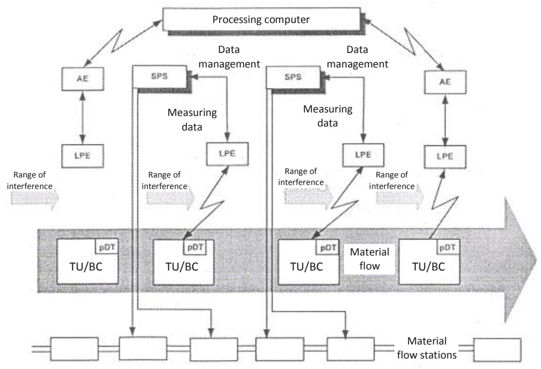

Fig. 5. *Decentralized management of the material flow (AE – transparency, TU – transport unit, pDt – programmed data transporter, LPE – programmed reading unit, BC – bulk carrier)*

But for the beginning of the process, all pieces of information have to be available (for instance, production machines management, inner transport for goods commissioning in CD) as well as memorizing. Also, information generated in the logistics process, and which may be necessary later on, can be simply autonomously memorized.

4.3 Hybrid (mixed) management of products flow

Hybrid management (hybrid information system) is a mixture of centralized and decentralized management system (and data memorizing).

This sort of memorizing is suitable for both target management of goods flow and for tracing of an object within the goods flow in a logistics chain.

While effecting the information tracing an object over the standard bar code, the data (from numerous bar codes) on the goods producer, on consumers, products, number of requests directed towards the warehouse or distribution center for delivery, level of the stock etc are obtained. After identification of the goods at the entrance into a system (for example, a CD) different calculations and managing of the goods flow are possible. The same is applicable for the material flow in production.

5 SYSTEMS FOR IDENTIFICATION AND MANAGEMENT OF PRODUCTS AND GOODS FLOW IN THE PROCESSES OF THE GOODS TRACEABILITY

Systems for identification and management of products and goods flow are necessary and they practically enable function and traceability processes. Namely, participants in the logistics chain of supply have to be able to identify any of the participants, side, object, goods user. Thus, systems and procedures that enable all necessary information as per a (competent) request to be collected, kept (memorized) and provided are applied for these participants in all phases from the product – goods appearance to the delivery to the customer. That is how the origin of the product and the production process are traced. In accordance to this, systems and procedures for unique identification have to be stated for all the participants in the chain and for their availability. That means that, beside other participants, the goods on the market should be properly marked in order to assure its identification and traceability.

The basic use of the tracing mechanisms is identification and location of material, work objects, semi products, products – goods, transport.

6 CONCLUSION

Application of automatic products – goods identification on the basis of a bar code and RFID technology is a base of identification systems and management of products flow in production. The management itself can be achieved through centralized, decentralized or mixed (hybrid) management. Which of the systems will be applied, depends on the product complexity and on the information requirement during the tracing of the physical flow of products and goods.

VII REFERENCES

[1] 1. Arnold, D. “Material flows”, Project Tempus, Faculty of Mechanical Engineering in Nis, Nis, 2004

[2] 2. Bukumirovic, M. “Urban logistics” Faculty of mechanical engineering in Kraljevo, Kraljevo, 2004

[3] 3. Bukumirovic, M. “Work process automatization”. Faculty of Transport and Traffic Engineering, Belgrade, 1999

[4] 4. Cupic, A., Bukumirovic, M., Markovic, D. “Technologies for identification and traceability of goods and technical means in processes” XV symposium of information and experimental systems for hygiene, pharmaceutical and food industry – IES 2004, Belgrade 2004

HEAVY MACHINERY - HM 2011, 31-34
ISBN 978-86-82631-58-3
Paper accepted: 25.05.2011

Zoning in the Order Picking Systems

Živanić Dragan,[1,*] Vladić Jovan,[1] Đokić Radomir,[1] Gajić Anto[2]
[1] University of Novi Sad, Faculty of Technical Sciences, Novi Sad
[2]Mine and Thermal Power Plant Ugljevik, Republic of Srpska,

In recent ten years picking activity has achieved a significant role in the context of the supply chain, both from the production system point of view and from the point of view of the distribution system. In fact this activity is characterized by high intensity of manual work, which deeply impacts both upon overall logistic costs and upon the level of the service provided to the customer. Zoning is the problem of dividing the whole picking area into a number of smaller areas and assigning order pickers to pick requested items within the zone. The zoning is classified into synchronized zoning, where all zone pickers work on the same orders (single or batch) at the same time, and progressive zoning, where each orders (single or batch) is processed at zone at a time. Progressive zoning, also called pick and pass or sequential order picking systems. In this paper, each order picking zoning solution will be briefly described.

Keywords: order picking, zoning, pickers

0 INTRODUCTION

One key component in a supply chain is a distribution center, which plays the vital role of obtaining materials from different suppliers, performing value added activities, and assembling (or sorting) them to fulfil customer orders.

The activities within a distribution center include the receipt of items and customer orders, storing items, order picking, shipping, customer service and reclamation, and control. Through distribution centers are designed to deliver some level of service to the manufacturers and customers, they do so by providing material handling and storage capabilities, which come at a cost. Therefore, the efficient design of a distribution center is necessary to provide a better flow of material and to reduce these facility logistics costs.

In a distribution center, the major logistics activity is order picking, which refers to the operation of retrieving articles from storage locations to fulfil customer orders.

1 ORDER PICKING SYSTEMS

In recent years picking activity has achieved more and more a crucial role in the context of the supply chain, both from the production system point of view of and from the point of view of the distribution activities. In fact this activity is characterized by high intensity of manual work, which deeply impacts both upon overall logistic costs and upon the level of the service provided to the customer.

Recent trends show that customer orders changed from few and large orders to many and small ones, which arrive late at distribution centers but still need to be picked and distributed in short time. These changes require efficient and flexible order picking systems in distribution centers for companies to remain competitive.

Many different order picking system types (methods and technologies) can be found in distribution centers. Sometimes a combination of picking methods is needed to handle diverse product and other order characteristics.

There are four most frequently applied technologies in the order picking systems: paper picking, pick by light, pick to voice and radio frequency identification. Finding the correct solution or combination of technologies is the most important factor in creating an efficient picking system. [4]

There are many different methods for order picking: single order picking, batch picking, wave, put system, bulk, automated picking,...

Using the data collected earlier will help you select the approach that meets goals in the most cost effective manner.

A given order may be split across zones for picking. This order picking concept is called zone picking

The focus of this paper is on zone order picking systems.

*Corr. Author's Address: Faculty of Technical Sciences, Trg Dositeja Obradovica 6, Novi Sad, Serbia, zivanic@uns.ac.rs

2 ZONE PICKING

Zone picking is a flexible and highly structured order picking concept. Zoning is the problem of dividing the whole picking area into a number of smaller areas (zones) and assigning order pickers to pick requested articles within the zone. Order pickers are assigned a specific zone, and only pick articles within that zone. Zone picking is the order picking version of the assembly line. Orders are moved from one zone to the next as the picking from the previous zone is completed. Usually, conveyor systems are used to move orders from zone to zone.

Zone picking can be used for a wide range of applications and is highly efficient, especially when pickers can pick directly into shipping cartons or totes.

The picking process across zones may occur in one of two basic ways:

- progressive zoning and
- synchronized zoning.

Each solution will be briefly described on the basis of the main equipment components, highlighting the impact on the resources (labour, space, capital) and on the service level (above all order picking accuracy and response time).

In progressive zoning, each batch of orders (or single orders) is processed at zone at a time. In progressive zoning, the batch of orders is passed from one zone to the next. This systems are also called pick and pass (or sequential) systems. The pick and pass zone picking strategies are illustrated in Figs. 1.

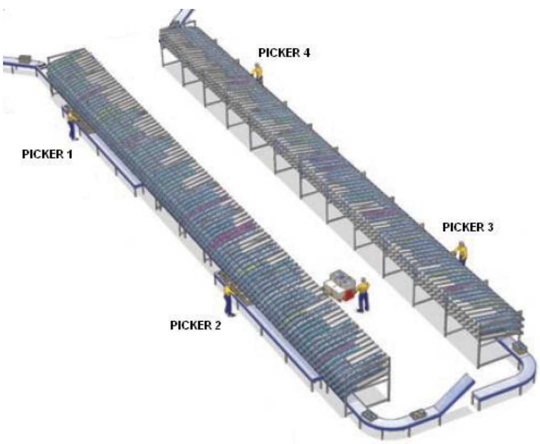

Fig. 1. *Pick and pass zone picking system*

Because only one order is handled at a time, pick and pass zone picking reduces the pick rate of pickers, but eliminates the requirement of a sorters system.

Pick and pass order picking systems are widely used in practice.

In contrast, in synchronized zoning all zone pickers work on the same batch of orders (or single orders) at the same time. In synchronized zoning all articles corresponding to batched orders are picked simultaneously from all the zones, and then orders are consolidated through a sorters system. Therefore, synchronized zone picking increases the pick rate of pickers as the entire batch is picked at a time, but requires a sorters system.

Computer's models (Flexsim) of synchronized zone picking strategies are illustrated in Figs.2.

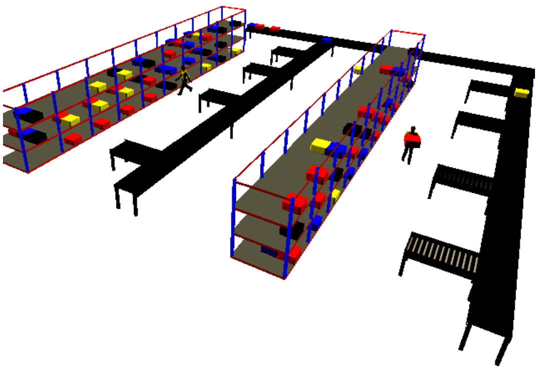

Fig. 2. *Computer's model of the synchronized zone pick method*

For a fixed picking area size and fixed number of order pickers, larger pick zones with more order pickers per zone and hence a smaller number of zones increase service time per zone due to longer travel time in zones. They also tend to increase the picker utilization in pick zones due to higher arrival rates, therefore leading to an increase of mean order throughput time. But on the other hand, more pickers per zone will decrease the utilization of pickers and fewer zones lead to less zone visits of an order or a batch of orders hence less order setup time, which implies a decrease of the mean order throughput time.

The zoning problem in order picking system is to find the right trade off between these problems and hence to find the optimal number of zones minimizing the mean order throughput time.

In zone picking it is important to equilibrium the number of picks from zone to zone to maintain a consistent flow. Zones are usually sized to accommodate enough picks for one or two order pickers.

Creating fast pick areas close to the conveyor is essential in achieving high productivity in zone picking. Zone picking is most effective in large operations with high total numbers of articles, high total numbers of orders, and low to moderate picks per order. Separate zones also provide for specialization of different picking techniques. [6] Application of pick to light technology in pick and pass systems are illustrated in Figs. 3.

Fig. 3. *Pick and pass with combination pick to light technology*

Workload imbalance occurs when the workload assigned between pickers is not equal.

An analysis must be done for all the orders that will be picked. This is necessary to determine the design of the picking area. Order quantities must be broken down by week, by day, and hourly. Order quantities should be charted by averages, minimums, and maximums in those specific time period. Some operations may have unusual peaks of activity on specific days of the week or during particular hours of the day depending on the business they are in. [5]

In general the following two factors affect the process of generating a balanced workload for pickers: item to zone assignment and order batching. Considering item to zone assignment, if the items are inappropriately assigned to zones, then it implies that a few zones are assigned a larger pool of frequently requested items than other zones. As a result, when the orders are batched, the pickers in these few zones may be required to pick a larger number of items than the pickers in other zones. Considering order batching, if the orders are inappropriately batched, then more workload may be assigned to some pickers than others. This may be because of an inappropriate policy used for batching orders. This results in workload-imbalance.

If using zone picking strategy, different pick zones can have different pick methods or technologies, for example possible to do wave pick in case zone and cluster pick in slow moving unit pick zone. [1]

Application of pick to voice technology in pick and pass systems are illustrated in Figs. 4.

Fig. 4. *Pick to voice technology in pick and pass systems*

3 VARIATIONS OF ZONE PICKING

There are a several variations of zone picking.

Zone batch

In zone batch version of zone picking, picker is assigned a zone and picks a part of one or more orders, depending on what articles are stored in the zone. This is fundamental version of zone picking.

Zone wave

In zone wave, picker is assigned a zone and picks all articles for orders group stocked in the zone during a specific time period.

Zone batch wave

In zone batch wave picker is assigned a zone and picks for all orders stocked in the zone, picking for more than one order at a time and for multiple scheduling periods during a shift.

Zone picking with aggregation on the shipping dock

In this version of zone picking, from each zone, picker sends a transport units (tote, case, carton) to shipping for each order, and the completed transport units from each zone are palletized together on the shipping dock.

Zone picking with aggregation at packing

In zone picking with aggregation at packing, from each zone picker sends a transport units (tote, case, carton) to packing with its portion of the order. At packing, all transport units for an order are consolidated, and the outbound cartons are packed.

Zone picking without aggregation

In zone picking without aggregation, from each zone picker fills its transport units (tote, case, carton) for the one order, and these are sent directly to the shipping trailer.

Unit sortation

Pickers drag a transport units batches of articles from their zones that are then sorted to the order by a sorter (tilt tray or cross belt).

CONCLUSION

Designing an order picking system for a distribution center is a very complex task. A designer is required to make several decisions related to throughput and storage considerations.

The order picking operation represents the highest cost element in a typical distribution center. Although modern distribution center are automated in a large extent, it is in most cases impossible to replace the human with the machine. Order picking systems can be very simple systems in small operations or become very complex systems using a little quantity of different articles.

Zone picking is a flexible and highly structured order picking concept. Every worker achieves optimal performance through a continuous supply of articles for picking and by eliminating or reduction unnecessary movements, waiting for articles and walking.

In zone picking systems it is important that the pickers are assigned a workload that is nearly the same for all pickers within and across all waves. A balanced workload will ensure that all pickers finish their picking activity at the end of the wave. The advantage of doing so, in addition to minimizing the labour cost, is the efficient scheduling of sorting and shipping operations.

ACKNOWLEDGEMENT

This paper has been supported by the Ministry of Science and Technological Development, Republic of Serbia, (Project No. 036024: „Transport system integration models“).

X REFERENCES

[1] Tompkins, J.A., White, J.A., Bozer, Y.A., Tanchoco, J.M.A., “A literature survey on planning and control of warehousing systems” Facilities Planning, 3rd ed. John Wiley & Sons, New York, IIE Transactions 31 (8), pp. 751-762, 2003.,

[2] Vladić, J., Živanić, D., “Optimum Choice of Picking to Order Technologies within the Systems for Transportation and Storage”, III Serbian Conference Transport and Logistics TIL2008, Niš, May 30, pp 21.1-21.8, 2008.,

[3] Živanić, D., Vladić, J., Đokić, R., Gajić, A., ”Picking Technologies in Distribution Centers”, 31. Conference HIPNEF 2008, Vrnjačka Banja, 15.-17. October 2008, Paper No 517-522, 2008.,

[4] Živanić, D., Gajić, A., Bogdanović, V. “Design of Modern Order Picking Systems”, The 6th International Symposium about Forming and Design in Mechanical Engineering KOD 2010., Palic, 29-30 September, pp. 261-264, 2010,

[5] Koster, R., Le-Duc, T., Roodbergen, K. “Design and Control of Warehouse Order Picking: A literature review”, European Journal of Operational Research 182, pp. 481–501, 2007,

[6] Manzini, R., Gamberi, M., Regattieri, A., “Design and Control of a Flexible Order-picking System (FOPS)”, Journal of Manufacturing Technology Management, Vol. 16 No. 1, pp. 18-35, 2005.

HEAVY MACHINERY - HM 2011, 35-38
ISBN 978-86-82631-58-3
Paper accepted: 20.05.2011

NAISS model validation based on measured data of noise monitoring

Momir Praščević[1,*] - Dragan Cvetković[1] - Darko Mihajlov[1]
[1] University of Niš, Faculty of Occupational Safety of Niš

Starting from the measurement results collected by systematic traffic noise monitoring in urban areas of Nis city, mathematical model for prediction of traffic noise called NAISS model has been formed by extracting function relation among the equivalent noise level and the traffic parameters. In the optimization process of the models, the model constants were obtained by experimental data fitting by Nelder - Mead method using computer program.

The used experimental data in optimization process were collected near the main city traffic arteries with typical properties of commercial, residential, industrial and hospital areas. All measurements were taken on working days of the week during 1995, excluding all atypical conditions. Each of the measurement points was to be determined from an acoustic point of view by the equivalent noise level. In addition, data relative to the urban circumstances of each point were taken, as well as measurement of traffic density, according to the number of each type per hour.

In order to examine validity of formed model, data collected by traffic noise monitoring in urban areas of Nis city in 2008-2010 has been analyzed and compared with the values predicted by NAISS model based on collected traffic parameters. Scatter plot for model validation will be shown in this paper as well as the results of statistical analysis of measured and calculated data differences.

Keywords: traffic noise, noise prediction, noise monitoring, model validation

0 INTRODUCTION

Noise is one of the environmental pollutants that are encountered in daily life. Noise pollution has become a major concern of communities living in urban areas. In view of the rapid development it is essential to study environmental noise with respect to various causative factors.

With urbanization and corresponding increase in number of vehicles in cities, the pollution is increasing at an alarming rate. Main areas of concern are related to air and noise pollution. More than 70% of total noise in our environment is due to vehicular noise. Noise levels are showing an alarming rise and infact level exceeds the prescribed levels in most of the areas. Investigations in several countries in the past decades have shown that noise has adverse effect on human health, living in urban areas near traffic lane, [1] - [5].

Therefore, the control of traffic noise has become a matter of major concern for communities trying to maintain a satisfactory environment in which to live and work.

The level of traffic noise depends mainly on the following factors:

- Volume of the traffic,
- Speed of the traffic,
- Number of the heavy vehicles in the flow of traffic.

To create a healthy and noise pollution free environment a noise prediction model is needed so that the noise level can be predicted and investigated in advance during the planning and design process.

In order to modeling traffic noise and selecting corresponding noise control measures it is necessary to know functional relationships between noise emission and certain numbers of traffic parameters.

The classical functional relationships available in literature have been stated based on data measured through semi-empirical models, typically regression analysis.

Of all the mathematical models available in literature, the ones which present this feature are those proposed by Burgess [6], Josse [7], Fagoti [8], CEE [8]. These functional relationships are essentially based on statistical analysis (i.e. regression techniques).

Although these correlations are nonlinear they do not provide very accurate approximation of the trend followed by sound pressure level

*Corr. Author's Address: Faculty of Occupational Safety of Niš, Čarnojevića 10a, 18000 Niš, Serbia, momir.prascevic@znrfak.ni.ac.rs

according to a certain number of physical parameters because any models itself includes the flow and composition of the road traffic which may be different than examined urban areas. Because of that, the prediction model of motor vehicle noise which to be valid for the flow and composition of the road traffic of Nis city is formed by Laboratory of Noise and Vibration, [9] - [11].

In order to examine validity of formed model, data collected by traffic noise monitoring in urban areas of Nis city in 2008-2010 has been analyzed and compared with the values predicted by NAISS model based on collected traffic parameters.

1 MATHEMATICAL BACKGROUND OF NAISS MODEL

Starting from the measurement results collected by systematic traffic noise monitoring in urban areas of Nis city, mathematical model for prediction of traffic noise of motor vehicle is formed by extracting function relation among the equivalent noise level and the traffic parameters, [9] - [11]. The model was named as NAISS model.

Traffic noise on observed measurement points are mainly caused by the motor vehicle. In order to make it easier to appreciate the variability of three components of urban traffic, the total number of motor vehicles was decomposed into the number of light vehicles N_c, the number of heavy vehicles N_{hv} and the number of buses N_b. The scheme of NAISS model is shown in Figure1.

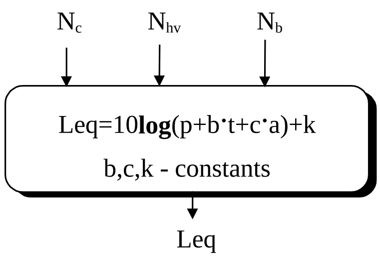

Fig. 1. *The scheme of NAISS model*

In the optimization process of the models, the model constants were obtained by experimental data fitting by Nelder - Mead method using computer program. Three variants of model are formed.

The experimental data collected near the main city traffic arteries with typical properties of commercial, residential, industrial and hospital areas on working days of the week during 1995, excluding all atypical conditions, are used in the optimization process.

Based on the analysis of different variants of traffic noise prediction model the authors were noted that prediction traffic noise of motor vehicles in urban areas of Nis city by separate equations for two ranges of noise level, listed below,

$$Leq = 10\log(N_c + 3.7N_{hv} + 1.9N_b) + 38.2 \quad 55dB(A) < Leq < 65dB(A) \tag{1}$$

$$Leq = 10\log(N_c + 11.7N_{hv} + 3.1N_b) + 44.3 \quad 65dB(A) < Leq < 75dB(A) \tag{2}$$

is rather correctly with satisfactory precision, [9] to [11]. In addition, selected variant of model is very easy for use regard to its simplicity based on only two equations for describing traffic noise in urban areas of Nis city.

2 COMPARATIVE ANALYSIS WITH OTHER MODELS

In order to give as satisfying and complete results as possible, it is necessary to confine the comparison to classical prediction methods available in literature, which show the greatest possible number of analogies with the hypotheses underlying the proposed method. These analogies essentially consist of the number of parameters on which the equivalent noise level is made to depend.

The comparison between NAISS model and selected prediction model available in literature (Burgess [6], Josse [7], Fagoti [8], CEE [8]) was made based on measured data collected by systematic traffic noise monitoring in urban areas of Nis city during 1995. Therefore, the comparison was made on the basis of measured data used to form NAISS model.

In order to compare different models, statistical analysis of differences of measured noise levels referring to urban areas of Nis city and calculated noise levels according to the model equations and the flow and composition of the road traffic in urban areas of Nis city was carried out. The average values of absolute differences of noise levels and standard deviations of differences (σ) have been calculated. The parameters of comparative analysis of different models are given in the Table 1.

Table 1. *The results of comparative analysis of models*

model	measured data group			
	55 ÷ 65 dB(A)		65 ÷ 75 dB(A)	
	$\overline{\Delta L}$	σ	$\overline{\Delta L}$	σ
Burgess	7.94	2.10	2.46	1.63
Josse	3.53	1.23	1.61	1.29
Fagoti	6.04	2.52	3.18	1.31
CEE	4.36	2.52	4.60	3.13
NAISS	1.07	0.75	1.29	0.92

The results of comparative analysis clearly show that the NAISS model based on equations (1) and (2) allows better prediction of noise pollution of motor vehicles in urban areas of Nis city than any other empirical relationship.

The success of the NAISS model can without doubt be attributed to performance of model formed on the basis of measured data used in the comparative analysis of different models.

Therefore it was necessary to validate the NAISS model based on measurement data different from those used for forming models.

3 NAISS MODEL VALIDATION

For the validity of NAISS model for road traffic noise prediction in urban areas given by equations (1) and (2), the equivalent noise levels calculated by equations (1) and (2) are compared with measured values of the equivalent noise levels obtained by systematic traffic noise monitoring in urban areas of Nis city during year 2008-2010.

The measured data were collected near the main city traffic arteries with typical properties of commercial, residential, industrial and hospital areas, five times during daytime period for all locations. All measurements were taken on working days of the week during year 2008-2010, excluding all atypical conditions. Each of the measurement points was to be determined from an acoustic point of view by the equivalent noise level. In addition, data relative to the urbanistic circumstances of each point were taken, as well as measurement of traffic density, according to the number of each type per hour. The standard apparatus based on the statistical noise level analyzer was used to determine the equivalent noise level.

For model validation scatter plots of measured and calculated values are shown in figure 2 to figure 4 for year 2008, 2009 and 2010, respectively. In the same figures the regresion line of 45° slope is shown.

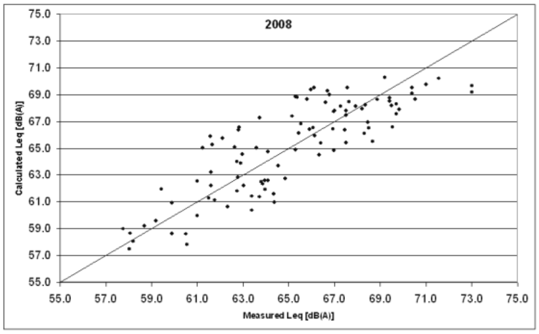

Fig. 2. *Measured L_{eq} against calculated L_{eq} by NAISS model for year 2008*

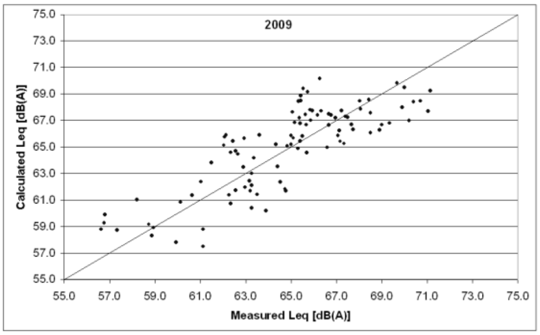

Fig. 3. *Measured L_{eq} against calculated L_{eq} by NAISS model for year 2009*

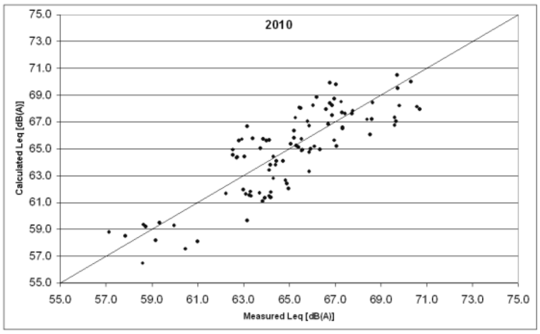

Fig. 4. *Measured L_{eq} against calculated L_{eq} by NAISS model for year 2010*

In order to examine validity of NAISS model, statistical analysis of differences of measured and calculated equivalent noise levels according to the model equations, the flow and composition of the road traffic was carried out.

The average values of absolute differences of calculated and measured equivalent noise levels $\overline{\Delta L}$ and standard deviations of differences (σ) have been calculated. The parameters of statitistival analysis are given in the Table 2, where N is number of measured data.

Table 2. *The results of statistical analysis of differences of calculated and measured data*

	2008	2009	2010
$\overline{\Delta L}$ [dB(A)]	1.63	1.66	1.52
σ [dB(A)]	1.08	1.10	0.95
N	110	97	98

4 CONCLUSION

The NAISS model described in the present paper can be used for traffic noise prediction for the urban areas of Nis city based on the flow and composition of the road traffic.

The results of comparative analysis clearly show that the NAISS model allows better prediction of traffic noise pollution of motor vehicles in urban areas of Nis city than any other empirical relationship.

The good results obtained in the comparasion with classical prediction methods available in literature have been confirmed in the validation process of NAISS model. The measured values during 2008 to 2010 year are compared with the calculated values by NAISS model.

The obtained values of average values of absolute differences of calculated and measured equivalent noise levels and standard deviations of differences show the validity and enforceability of the NAISS model for traffic noise prediction in urban areas of Nis city.

5 REFERENCES

[1] Ohrstrom, E. and R. Rylander "Sleep disturbance by road traffic noise - A laboratory study on number of noise events", *Journal of Sound and Vibration*, 143 (1), pp. 93-101, 1990

[2] Babisch, W., H. Fromme, A. Beyer and H. Ising, "Increased catecholamine levels in urine in subjects exposed to road traffic noise: The role of stress hormones in noise research". *Environment International*, 26 (7-8), pp. 475-481, 2001

[3] Ljungberg, J. K., and G. Neely. "Stress, subjective experience and cognitive performance during exposure to noise and vibration", *Journal of Environmental Psychology*, 27 (1), pp. 44-54, 2007

[4] Rylander, R., "Physiological aspects of noise-induced stress and annoyance", *Journal of Sound and Vibration*, 277 (3), pp. 471-478, 2004

[5] Pirreera, S., E. D. Valck and R. Cluydts. "Nocturnal road traffic noise: A review on its assessment and consequences on sleep and health", *Environment International*, 36 (5), pp. 492-498, 2010

[6] Burgess, M. A., "Noise Prediction for Urban Traffic Conditions - Related to Measurements in the Sydney Metropolitan Area", *Appllied Acoustics*, Vol. 10, pp. 1-7, 1977

[7] Josse, R., "Notions d'acoustique Paris", *France: Ed. Eyrolles*, 1972

[8] Fagotti, C., and A. Poggi, "Traffic Noise Abatment Strategies. The Analysis of Real Case not Really Effective", in *Proceedings of 18th International Congress for Noise Abatment*, Bologna, Italy, pp. 223-233, 1995

[9] Prascevic, M., D. Cvetkovic and V. Stojanovic, "Mathematical Models for Describing Road Traffic Noise", in *Proceedings of the 1997 International Congress on Noise Control Engineering*, Budapest, Hungary, Vol. II, pp. 895-899, 1997

[10] Prascevic, M., D. Cvetkovic, A. Deljanin and V. Stojanovic, "Modeling of Urban Traffic Noise", in *Proceedings of the Fifth International Congress on Sound and Vibration*, Adelaide, South Australia, 1997

[11] Cvetkovic D., M. Prascevic and V. Stojanovic, "NAISS model for traffic noise prediction", *Facta Universitatis Series: Working and living environment protection*, Vol. 1, No. 2, pp. 73-81, 1997

6 ACKNOWLEDGEMENT

This research is part of the project "Development of methodology and means for noise protection from urban areas" (No. TR-037020) and "Improvement of the monitoring system and the assessment of a long-term population exposure to pollutant substances in the environment using neural networks" (No. III-43014). The authors gratefully acknowledge the financial support of the Serbian Ministry for Education and Science for this work.

HEAVY MACHINERY - HM 2011, 39-44
ISBN 978-86-82631-58-3
Paper accepted: 20.05.2011

Estimation of uncertainty in environmental noise measurement

Dragan Cvetković[1,*] - Momir Praščević [1] - Darko Mihajlov[1]
[1] University of Niš, Faculty of Occupational Safety of Niš

It is well known that environmental noise levels can vary over a wide range as a result of the diversity of site conditions and activities occurring during field measurements. Environmental noise very often occurs in the form of randomly fluctuating sound signals. To quantitatively describe this phenomenon, noise index such as equivalent pressure level Leq is widely used. The measured value of Leq based on the sound pressure level measurements by sound level meter will probably differ from the true one due to the effects of the errors throughout the experiment chain and in the physical phenomenon under study.

SRPS EN ISO 1996-2 (2010) contains guidelines on assessing the uncertainties of the determined sound pressure levels. This depends on the sound source, measurement time interval, weather conditions, distance from the source, measurement method and instrumentation.

Guidelines on estimating the measurement uncertainty in compliance with the ISO Guide to Uncertainty in Measurements (GUM) will be given in this paper. Five main sources of uncertainty (measurement chain, operating conditions, meteorological conditions, receiver location and residual noise) are combined to determine the overall uncertainty.

Keywords: environmental noise, measurement, uncertainty

0 INTRODUCTION

Noise can be define as an unwanted or undesired sound whereas environmental noise is any unwanted or harmful outdoor sound created by human activities that is detrimental to the quality of life of individuals.

Worldwide, 130 million of people are exposed to environemtal noise levels above 65 dB(A), while another 300 million live in uncomfortable environmental noise levels (55 dB(A)-65 dB(A)) [1].

Although by listening we detect noise with a great sensitivity, we have often difficulties to describe it and we certainly cannot define it in technical terms - we usually know when noise is excessive, but we cannot predict the required noise reduction and, more important, we cannot determine how to effectively reduce the excessive noise.

The proper environemtnal noise pollution assessment and design of effective noise control measures require noise measurement.

Noise measurement is an important diagnostic tool in noise control technology and noise pollution assessment. The objective of noise measurement is to make accurate measurement which gives us a purposeful act of comparing noises under different conditions for assessment of adverse impacts of noise and adopting suitable control techniques for noise reduction.

It is well known that environmental noise levels can vary over a wide range as a result of the diversity of site conditions and activities occurring during field measurements. Environmental noise very often occurs in the form of randomly fluctuating sound signals. To quantitatively describe this phenomenon, noise index such as equivalent pressure level L_{eq} is widely used. The measured value of L_{eq} based on the sound pressure level measurements by sound level meter will probably differ from the true one due to the effects of the errors throughout the experiment chain and in the physical phenomenon under study. In most physical experiments there will be a random component affecting to environmental noise measurement uncertainty.

A number of authors have already made significant contributions in the field of environmental noise measurement uncertainty determination [2,3].

Guidelines on estimating the measurement uncertainty in compliance with the ISO Guide to Uncertainty in Measurements (GUM) explained in a series of JCGM (“Joint Committee for

*Corr. Author's Address: Faculty of Occupational Safety of Niš, Čarnojevića 10a, 18000 Niš, Serbia, dragan.cvetkovic@znrfak.ni.ac.rs

Guides in Metrology") documents [4-6] and SRPS ISO 1996-2 [7] will be given in this paper.

In this method the separate uncertainties associated with each of the variables affecting the measured noise level are added together to derive a combined overall uncertainty. Because of limited time and resources, each component of the overall uncertainty must normally be estimated based on scientific judgment or practical experience rather than be determined from the results of a large set of repeated measurements.

2 MEASUREMENT UNCERTAINTY CLASIFFICATION

The word "uncertainty" means doubt, and therefore in its broadest sense "uncertainty of a measurement" means a "doubt about the validity of the result of that measurement". The concept of "uncertainty" as a quantifiable attribute is relatively new in the history of measurement.

GUM classifies uncertainties into three categories: standard Uncertainty, Combined Uncertainty, and Expanded Uncertainty.

The standard uncertainty with the symbol "u" is represented by an estimated standard deviation and equals to the positive square root of the estimated variance. The standard uncertainty of the result of a measurement consists of several components, which can be grouped into two types [4]. They are:

- Type A - Uncertainty components obtained using a method based on statistical analysis of a series of measurement.
- Type B - Uncertainty component obtained by means other than repeated observations. Prior experience and professional judgments are part of type B uncertainties.

Combined standard uncertainty of the result of a measurement is obtained from the uncertainties of a number of other quantities. The combined uncertainty is computed via the law of propagation of uncertainty. The result is different if the quantities are correlated or uncorrelated (independent).

Mathematically, expanded uncertainty is calculated as the combined uncertainty multiplied by a coverage factor, *k*. The coverage factor, *k*, includes an interval about the result of a measurement that may be expected to encompass a large fraction of the distribution of values that could reasonably be attributed to the measurand.

Thus, the numerical value for the coverage factor *k* should be chosen so that it would provide an interval $Y = y \pm U$ corresponding to a particular level of confidence.

3 ESTIMATION OF ENVIRONMENTAL NOISE MEASUREMENT UNCERTAINTY

SRPS ISO 1996-2 [7] contains guidelines on assessing and reporting the uncertainties of the determined sound pressure levels. This depends on the sound source and the measurement time interval, the meteorological conditions, the distance from the source and the measurement method and instrumentation. Some guidelines on how to estimate the measurement uncertainty are given, with focus on A-weighted equivalent-continuous sound pressure levels only. Five main sources of uncertainty (measurement chain, operating conditions, meteorological conditions, receiver location and residual sound) are used and combined to determine the overall uncertainty.

The measurement uncertainty shall be determined in compliance with the ISO Guide to Uncertainty in Measurements (GUM).

According to GUM each significant source of error has to be identified and corrected for. If the quantity to be measured is $L_{Aeq,\mathrm{m}}$, which is a function of the quantities x_j the equation becomes:

$$L_{Aeq,m} = f(x_j) \tag{1}$$

If each quantity has the standard uncertainty u_j the combined uncertainty u is given by

$$u(L_{Aeq,m}) = \sqrt{\sum_{j=1}^{n} (c_j u_j)^2} \tag{2}$$

where the sensitivity coefficient c_j is given by

$$c_j = \frac{\partial f}{\partial x_j} \tag{3}$$

The measurement uncertainty is the combined measurement uncertainty associated with a chosen coverage probability. By convention, a coverage probability of 95% is usually chosen, with an associated coverage factor of 2. This means that the true value during the specified conditions $L_{Aeq,true}$ is:

$$L_{Aeq,true} = L_{Aeq,m} \pm 2u \quad (4)$$

Other levels of confidence may be set. A coverage factor of 1.3 will, e.g., provide a level of confidence of 80 % and one of 2 a level of confidence of 95 %.

For environmental noise measurements $f(x_j)$ is extremely complicated and it is hardly feasible to put up exact equations for the function f. Following the principles given in ISO 3745 [8] and ISO 1996-2, some important sources of error can be identified and wrote as

$$L_{Aeq,true} = L_{Aeq,m} + \delta_{slm} + \delta_{sou} + \delta_{met} + \\ + \delta_{loc} + \delta_{res} \quad (5)$$

where δ_{slm} is the error due to the measurement chain (sound level meter in the simplest case), δ_{sou} is the error due to deviations from the ideal operating conditions of the source, δ_{met} is the error due to meteorological conditions and ground conditions deviating from the ideal conditions, δ_{loc} is the error due to the selection of receiver position and δ_{res} is the error due to residual noise. Often δ_{sou} + δ_{met} is determined directly from measurements.

Equation (5) is very simplified and each source of error is a function of several other sources of error. In principle equation (5) could be applied on any measurement lasting from seconds to years. The measurements are divided into long and short term measurements respectively in SRPS ISO 1996-1 [9]. A short term measurement may typically range between 10 minutes and a few hours whereas a typical long term measurement may range between a month and a year.

In according to equation (5) and identified sources of error equation (2) can be rewritten as:

$$u^2(L_{Aeq,m}) = (c_{slm}u_{slm})^2 + (c_{sou}u_{sou})^2 + \\ + (c_{met}u_{met})^2 + (c_{loc}u_{loc})^2 + (c_{res}u_{res})^2 \quad (6)$$

All the sensitive coefficients have been estimated to 1.0 except for the residual noise.

Table 1 of SRPS ISO 1996-2 [7] contains overview of the measurement uncertainty for the A-equivalent noise level. Higher uncertainties are to be expected on maximum levels, frequency band levels and levels of tonal components in noise.

3.1 Uncertainty due to measurement chain

The uncertainty due to measurement chain has been estimated to 1.0 dB. This value concerns the use of Class 1 instrumentation. However, the standard permits the use of instrumentation systems, including the microphone, cable and recorders if any, that conform to the requirements for a class 1 or class 2 instruments laid down in IEC 61672-1 [10]. If class 2 sound level meters or directional microphones are used the value will be larger. Studies carried out at Brüel & Kjær [11] have shown these to be double those of Class 1 instrumentation.

The values of measurement uncertainty include influence of the following factors:

- Directional response
- Frequency weighting
- Level linearity
- Tone burst response
- Power supply voltage
- Static pressure
- Air temperature
- Humidity
- Calibrator
- Windscreen

3.2 Uncertainty due to operating condition

Uncertainty due to operating conditions is determined from at least 3, and preferably 5, measurements under repeatability conditions (the same measurement procedure, the same instruments, the same operator, the same place) and at a position where variations in meteorological conditions have little influence on the results.

3.2.1 Road traffic

When measuring the equivalent noise level the number of vehicle pass-bys shall be counted during the measurement time interval. If the measurement result shall be converted to other traffic conditions distinction shall be made between at least the three categories of vehicles ‘passenger cars’ and ‘medium heavy (2 axles)’ and ‘heavy (> 3 axles)’. To determine if the traffic conditions are representative, the average traffic speed shall be measured and the type of road surface noted.

For the road traffic noise the uncertainty can be calculated by

$$u_{sou} \cong \frac{C}{\sqrt{n}} \tag{7}$$

where n is the number of pass-bys. For mixed traffic C=10, for heavy vehicles only C= 5 and for passenger cars only C = 2.5.

3.2.2 Rail traffic

When measuring the equivalent noise level the number of train pass-bys, the speeds and the train lengths shall be determined during the measurement time interval. If the measurement result shall be converted to other traffic conditions distinction shall be made between at least the following categories: High speed trains, inter-city trains, regional trains and freight trains.

For the rail traffic noise the uncertainty can be also calculated by means equation (7) where C=10 if the sampling was made regardless of the operating conditions and C=5 if the sampling takes into account the relative occurrence of the different train classes (freight, passenger, etc).

3.2.3 Industrial sources

The source operating conditions shall be divided into classes: For each class the time variation of the sound emission from the source shall be reasonably stationary in a stochastical sense. The variation shall be less than the variation in transmission path attenuation due to varying weather conditions. If 5 minute to 10 minute L_{eq}-values measured at a distance long enough to include noise contributions from all major sources and short enough to minimize meteorological effects during a certain operating condition, a new categorization of the operating conditions shall be made.

In order to be able to estimate the uncertainty of the operating conditions for industrial sources it is necessary to repeat the measurements at a distance sufficiently close to the source to make the sound pressure level variations independent of the meteorological conditions. The equation for this is

$$u_{sou} = \sqrt{\sum_{i=1}^{n} \frac{(L_{Aeq,m,i} - \overline{L}_{Aeq,m})^2}{n-1}} \tag{8}$$

$L_{Aeq,m,i}$ is the measured value representing a typical cycle of operation, $\overline{L}_{Aeq,m}$ is the arithmetic average of all $L_{Aeq,m,i}$ and n is the total number of all independent measurements.

In order two measurements to be independent the requirements of table 1 have to be met. “Sou” in table 1 indicates that the minimum time is influenced by the operating conditions of the source.

Table 1. *Minimum time between two measurements to be independent*

distance	<100 m		100÷300 m		>300 m	
	day	night	day	night	day	night
Road	24		48	48	72	72
Rail	24	24/sou	24	48	72	72
Industry	sou	sou	48	48	72	72
Aircraft	sou	sou	sou	sou	sou	sou

The equivalent noise level shall be measured during each class of operating condition and the resulting the equivalent noise level shall be calculated taking the frequency and duration of each class of operating condition into account in according to equation:

$$L_{Aeq,m} = 10 \log \sum_{i=1}^{n} p_i \cdot 10^{0.1 \cdot L_{Aeq,m,i}} \tag{9}$$

where $L_{Aeq,m}$ is the total equivalent noise level for the whole time interval and $L_{Aeq,m,i}$ is equivalent noise level for class of operating condition i, which lasts for p_i of the total time.

The total measured equivalent noise level is a function of equivalent noise level for each class of operating condition and duration of each class of operating condition, so that the sensitivity coefficient can be given by

$$c_{L_{Aeq,m,i}} = \frac{\partial L_{Aeq,m}}{\partial L_{Aeq,m,i}} = \frac{p_i \cdot 10^{0.1 \cdot L_{Aeq,m,i}}}{\sum_{i=1}^{n} p_i \cdot 10^{0.1 \cdot L_{Aeq,m,i}}} \tag{10}$$

$$c_{L_{Aeq,m,i}} = \frac{\partial L_{Aeq,m}}{\partial p_i} = \frac{10^{0.1 \cdot L_{Aeq,m,i}}}{\sum_{i=1}^{n} p_i \cdot 10^{0.1 \cdot L_{Aeq,m,i}}} \tag{11}$$

If $L_{Aeq,m,i}$ is determined with the uncertainty u_{Li} and p_i with the standard uncertainty u_{pi}, then the uncertainty of $L_{Aeq,m}$ is then given by

$$u_{sou} = \sqrt{\sum_{i=1}^{n} c_{p_i}^2 \cdot u_{p_i}^2 + \sum_{i=1}^{n} c_{L_{Aeq,m,i}}^2 \cdot u_{L_i}^2} \tag{12}$$

3.3 Uncertainty due to meteorogical conditions

The variability of noise levels during measurements is influenced by the meteorological conditions. The noise levels must be measured during favourable propagation conditions.

If only one or a few short term measurements are carried out they should be taken during favourable conditions. For the soft ground favourable conditions are assumed to be valid for downward propagation if

$$\frac{h_s + h_r}{d} \geq 0.1 \tag{13}$$

where h_s is source height, h_r is receiver height and d is distance between the source and receiver.

If the ground is hard larger distances may be acceptable.

The favourable sound propagation conditions can be determined based on the radius of curvature, R, which depends on the gradient of wind speed and temperature. Positive values of R correspond to downward sound ray curvature (e.g. during downwind or temperature inversion). Such sound propagation conditions are often referred to as “favourable”, that is the sound pressure levels are high. $1/R = 0$ corresponds to straight-line sound propagation (homogeneous atmosphere, ‘no-wind’); negative values of R correspond to upward sound propagation (e.g. during upwind or on a calm summer day).

The radius of curvature can be calculated from measured meteorological parameters according to Annex A of SRPS ISO 1996-2 [7].

In the case of measurements during favourable conditions the uncertainty is

$$u_{met} = 2 \tag{14}$$

In other conditions the uncertainty can be determined from Figure A.1 [7].

3.4 Uncertainty due to selection of reciever position

The location of receiver position is critical in obtaining accurate and useful sound data. The selection of receiver position should be carefully considered early in the development of a measurement plan, once the objectives for the measurement system have been clearly identified. In order to analyze to what extent a proposed receiver location influences the uncertainty of the results at that site, it is necessary to examine carefully the relation between the residual sound and the sound pressure levels to be measured. For accurate measurements, the level difference should exceed 15 dB.

For the most common cases default values for the standard uncertainties using different receiver positions are given in table 2 for traffic noise. For industrial noise and other positions the uncertainties have to be determined for each individual case based on the repeated measurements and equation (8).

Table 2. *Uncertainty of different reciver location*

Reciver location	u_{oc}
Traffic noise incident from all angles	
Microphone in free field	0.5
Microphone directly on the surface	0.4
Microphone near reflecting surface	0.4
Traffic noise with predominantly grazing incidence	
Microphone directly on the surface	2.0
Microphone near reflecting surface	1.0

2.4 Uncertainty due to residual noise

The uncertainty due to residual sound is dependent on the following primary factors:

- the parameter measured
- the difference between measured total values and the residual sound
- the uncertainty of the assessments of the total values and the residual sound.

The uncertainty due to residual sound varies depending on the difference between measured total values and the residual sound (including self-generating noise in the instrumentation). It is well-known how the residual sound level influences measurement of the specific sound level. At 10dB below, the influence has traditionally been accepted to be insignificant.

In order to determine the uncertainty for the specific sound level, the actual measured overall level, the residual noise level during the measurement and the residual noise used for correction are combined.

The specific noise level is then the overall noise level (the specific noise level $L_{ss,m}$ and the residual noise level during the measurement $L_{res,m}$) corrected for the residual sound level $L_{res,c}$ measured with specific noise source off:

$$L_{ss,m} = 10\log((10^{0.1 \cdot L_{ss,m}} + 10^{0.1 \cdot L_{res,m}}) - \\ - 10^{0.1 \cdot L_{res,c}}) \tag{15}$$

The sensitivity coefficients are

$$c_{res,m} = \frac{\partial L_{ss,m}}{\partial L_{res,m}} \approx 10^{0.1\cdot(L_{res,m} - L_{ss,m})} \tag{16}$$

$$c_{res,c} = \frac{\partial L_{ss,m}}{\partial L_{res,c}} \approx -10^{0.1\cdot(L_{res,c} - L_{ss,m})} \tag{17}$$

The total uncertainty is given by

$$\begin{aligned} u_{ss} &= \sqrt{(c_{res,m} \cdot u_{res,m})^2 + (c_{res,c} \cdot u_{res,c})^2} \\ &\approx \sqrt{2} c_{res} \cdot u_{res} = \sqrt{2} \cdot 10^{0.1\cdot(L_{res,m} - L_{ss,m})} \cdot u_{res} \end{aligned} \tag{18}$$

In equations (16) to (18) it is assumed that there is little difference between the residual noise during the measurement and the residual noise used for correction. If the residual noise level is much smaller than the noise level from the source to be measured the sensitivity coefficient for residual coefficient is:

$$c_{res} \approx 10^{0.1\cdot(L_{res} - L_m)} \tag{19}$$

The uncertainty associated with the residual noise u_{res} is determined in according equation (6) except the last term.

4 CONCLUSION

It is well known that environmental noise levels can vary over a wide range as a result of the diversity of site conditions and activities occurring during field measurements. Environmental noise very often occurs in the form of randomly fluctuating sound signals.

The uncertainty estimation in environmental noise measurement is not an easy procedure, since it is difficult to identify all sources of uncertainty related to the equivalent noise level and determine its contributions to the combined measurement uncertainty. Also, there is not a completely established procedure used on a broad scale to estimate the uncertainty in environmental noise measurement.

This paper is an attempt to provide guidelines on estimating the measurement uncertainty in compliance with the ISO Guide to Uncertainty in Measurements (GUM) and SRPS ISO 1996-2. Five main sources of uncertainty (measurement chain, operating conditions, meteorological conditions, receiver location and residual noise) are combined to determine the overall uncertainty.

5 REFERENCES

[1] Berblund, B., T. Lindvall and D. H. Schwela, “Guidelines for Community Noise”, Geneva: World Health Organisation; 1999

[2] Farrelly, F. A. and G. Brambilla, “Determination of uncertainty in environmental noise measurements by bootstrap method”, *Journal of Sound and Vibration,* Vol. 268, pp. 167–175, 2003

[3] Alberola, J. I. H. Flindell and A. J. Bullmore, “Variability in road traffic noise levels”. *Applied Acoustics,* Vol. 66, pp. 1180–1195, 2005

[4] JCGM 100 “Evaluation of measurement data – Guide to the expression of uncertainty in measurement”, 2008

[5] JCGM 101 “Evaluation of measurement data – Supplement 1 to the Guide to the expression of uncertainty in measurement – Propagation of distribution using a Monte Carlo Method”, 2008

[6] JCGM 101 “Evaluation of measurement data – An introduction to the Guide to the expression of uncertainty in measurement and related documents, 2009

[7] SRPS ISO 1996-2 “Acoustics – Description, assessment and measurement of environmental noise – Part 2: Determination of environmental noise levels”, 2010

[8] ISO 3745 “Acoustics – Determination of sound power levels of noise sources using sound pressure – Precision methods for anechoic and hemi-anechoic rooms”, 2003

[9] SRPS ISO 1996-1 “Acoustics – Description, assessment and measurement of environmental noise – Part 1: Basic quantities and assessment procedures”, 2010

[10] IEC 61672-1 “Electroacoustics – Sound level meters – Part 1: Specifications”, 2002

[11] Douglas M., and A. Erik, “Uncertainties in Environmental Noise Assessments - ISO 1996, Effects of Instrument Class and Residual Sound”, Forum Acousticum, Budapest, 2005

6 ACKNOWLEDGEMENT

This research is part of the project “Development of methodology and means for noise protection from urban areas” (No. TR-37020) and “Improvement of the monitoring system and the assessment of a long-term population exposure to pollutant substances in the environment using neural networks“ (No. III-43014). The authors gratefully acknowledge the financial support of the Serbian Ministry for Education and Science for this work.

HEAVY MACHINERY - HM 2011, 45-50
ISBN 978-86-82631-58-3
Paper accepted: 30.05.2011

Container Yard Performance Evaluation in Port

Maja Škurić[1], Branislav Dragović[1] and Romeo Meštrović[1]
[1] Maritime Faculty, Maritime Transport and Traffic Division, University of Montenegro, Dobrota 36, 85330 Kotor, Montenegro

This paper aims the significance of queuing theory in developing the container performance at terminals (container yard - CY) using analytical expressions. This model presents different models of queuing system. The arrival and service process of containers at CY must give the input data in shape of some statistical distribution. However, it is well known that containers arrive at CY in batches. Considering that, this model discusses the total queuing system costs of containers at CY.

Here, we propose different models of queuing theory in relation to old and new very well known explicit formulae from previous investigations. Some of this results have not been applied in port modeling and planning operations. Comparing these various models with arrival of containers will give the optimal value of queue discipline. For validity reason we use queuing models which confirm analytical results in optimization processes.

At the end, a given comparative analysis between these models and analytical approach will improve the best solution for container performances at CY, container flow, calculating the efficiency of storage capacities and total container costs. Computational experiments are reported to evaluate the efficiency of all considered models for PECT container terminal in Busan port, Republic of Korea.
Keywords: Container yard, Handling equipment, Queuing theory, Container flow

0 INTRODUCTION

A port container yard can be considered as a queuing system defined by basic parameters: the container arrival rate and the container service rate in an observed period of time. It is evident that the optimal number and capacity of servers must be of the greater importance in real system. The total cost of the system can be also determined with the specific number of servers. In ship-berth link, quay cranes are servers and on the other hand, servers at container yard are specific types of yard cranes. Therefore, the costs of yard cranes make important point for obtaining total costs of containers at terminal.

Here the main goal is to simplify the problems at container yard using analytical models of queuing theory. In this paper we illustrate the different results for the queuing models. The objective is to describe these models for defining the strategies at yard and calculate the total cost of system. It is obvious that the arrival and service processes of containers at container yard must give the input data in shape of some statistical distribution.

The efficient operation of a port container terminal is achieved through coordination of particular subsystem capacities and this can be facilitated through modeling a port container terminal using the queuing theory. In determining the optimal capacity of a container yard, a maximum attention should be paid to the yard system with cranes.

The reason for this is that the accommodative capacity of the yard, expressed in number of yard cranes, determines the required capacity of the servers and, hence, the container yard capacity as a whole. It is obvious that containers will represent customers and yard cranes will take place of servers at container terminal.

Here we propose two different models of queuing theory with queuing discipline: $M/E_k/c$ and $M/D/c$ where c reprsents the number of servers (yard cranes (YC)).

This paper is organized as follows. Literature review is given in Section 1, while in Section 2 is shown waiting time of containers at yard. Analytical expressions for total system costs are derived in Section 3. Related numerical examples for PECT (Pusan East Container Terminal that changed the name in 2009 as Korean Busan Express Container Terminal-KBCT) with results are shown in Section 4. Suitable conclusions are given in Section 5.

*Corr. Author's Address: Maritime Faculty, University of Montenegro, Dobrota 36, 85330 Kotor, Montenegro; mskuric@ac.me

1 LITERATURE REVIEW

However, it is well known that containers arrive at yard in batches and its behavior must fit some statistical distribution. Considering that, it is noted that for valid analysis some studies used batch arrival queuing model and batch arrival multi-server queuing system. On the other hand, in this paper are shown two queuing disciplines for single arrival of containers but represent the good step for further investigations. Several authors have investigated this system using different techniques. Gaver [4] used Markov chain method for defining the arrival in batches to a single channel with arbitrary service time distribution. Also, using renewal theorem of batch arrival, Burke [1] solved a single-server queuing system. All these authors have carried out their own theory about queuing systems, specifying the best approach for modeling container terminals in port. Speaking of batch arrival of customers, Kozan [7] made a comparison of analytical and simulation planning models of container terminals and shows the advantages of simulation because it is able to capture all details and the complexity of a real system. He also pointed out the importance of better approach to modeling the container port system by batch arrivals of containers as opposed to ships. He considered the ships as a batch of containers.

The analysis of a queue with batch arrivals and batch-dedicated servers is explained by Gullu [6]. In this paper, it is considered a $M/G/\infty$ queuing system with batch arrivals whose jobs belong to a batch have to be processed by the same server. Here, customer arrivals follow a homogeneous Poisson process. Each arrival brings a positive number of jobs to be processed. The number of jobs arriving in batch size is a random variable, identically distributed with the batch size associated with another job.

In Radmilović [9], it is developed an analytical methodology of bulk queuing system. This methodology determines the optimum number and capacity of berths within seaports and river ports. In this paper, bulk arrivals are presented by pushed and pulled convoys of barges. The queuing system describes system in which the number of barges in convoy has a constant or geometric probability distribution. The obtained results are restrictive because the assumptions about inter-arrival and service time distributions, as well as the convoy size probability distribution must be verified before application in port systems. In Radmilović et al. [10], the authors deal with the port storage locations as queuing systems with bulk arrivals and a single service. These bulk arrivals are represented by groups and storage operations are developed using the mean service position of cargo unit within the arrival group in the queue. Finally, in Radmilović et al. [11] it is determined the optimal number of servers in queuing system with bulk arrivals by minimizing the total costs of system. The optimum number of servers, their utilization, capacity and costs could be used in different analysis of queuing system. On the other hand, Zrnić et al. [12] and Dragović et al. [2] discussed the anchorage-ship-berth link at the river port utilizing queuing theory with bulk arrivals. The developed process is described by the non-stationary multi-channel queuing system. All these assumptions are done for optimizing capacity in the sense of minimum capital costs. In the same manner, Laxmi and Gupta [8] analyzed a multi-server queue with bulk arrivals and finite-buffer space. Their model obtains the partial and total batch rejections and the distributions of the numbers of customers in the system. They proposed the $GI^X/M/c/N$ queue through a combination of the supplementary variable and the embedded Markov chain techniques.

2 CONTAINER FLOW AT YARD

First of all, it is necessary to define basic parameters for a presented queuing system at container yard. On the basis of these parameters, appropriate indices of yard operations can be computed and used for total queuing costs. The basic parameters are: λ - average arrival rate for containers (containers/defined period of time); μ - average service rate of containers (containers/defined period of time); c - number of servers (yard cranes - YC) and ρ - utilization factor or server occupancy which is in single queuing system defined as $\rho = \lambda/(c\mu)$.

Since the yard cranes capacity determines the required capacity of container terminal and the entire accommodation of container terminal, the question of how to determine optimal number of yard cranes. Also, with determination of optimal number of cranes, it should be defined the model for calculating total annual cost. Numerical results and computational experiments evaluate the efficiency of the models. Here we determine the basic parameters for the two queuing models. In a yard queuing system that does not serve each container immediately upon arrival, a container will attempt to arrive at a time that will minimize the expected queue length.

The probability density function of the Erlang distribution is

$$f(x;k,\lambda)=\frac{\lambda^k x^{k-1} e^{-\lambda x}}{(k-1)!} \tag{1}$$

for $x>0$ and $f(x;k,\lambda)=0$ for $x\le 0$. The parameter k is called the shape parameter and the parameter λ is called the rate parameter. If we denote that $P_{ij}(t)$ is a probability that there is i client in moment t, therefore, noone client will be present in moment $t+D$ because it is $M/D/c$ model. Considering that, the probability that i client will be present in interval $(t,t+D]$ is [3]

$$P_i(t+D)=\sum_{j=0}^{s} P_j(t)\frac{(\lambda D)^i}{i!}e^{-\lambda D}+\sum_{j=s+1}^{i+s} P_j(t)\frac{(\lambda D)^{i+s-j}}{(i+s-j)!}e^{-\lambda D} \tag{2}$$

for $t\in R, i\in N_0$.

The containers arrive at the yard according to a time homogeneous Poisson process with mean arrival rate λ. The yard area has c yard cranes for the service. Then these cranes have independent, exponentially distributed service times. For this analysis, we give average waiting time for two models. This parameter is very important for further calculations. For model ($M/E_k/c$), average waiting time equals [2]

$$W_c=\frac{\lambda^c}{\mu^{c-1}(c-1)!(c-\lambda)^2\left(\sum_{n_c=0}^{c-1}\frac{1}{n_c!}\left(\frac{\lambda}{\mu}\right)^{n_c}\right)+\lambda^c(c-\lambda)}\times$$
$$\times\left[\frac{1}{2}\left(\frac{1}{k}+1\right)+\left(1-\frac{1}{k}\right)(c\mu-\lambda)(c-1)\frac{(4+5c)^{1/2}-2}{32c\lambda}\right] \tag{3}$$

where n_c is average number of containers in queue. For second model ($M/D/c$), average waiting time equals [3]

$$W_c(M/D/c)=\frac{1}{2}\{1+f(c)\cdot g(\rho)\}\cdot W_c(M/M/c) \tag{4}$$

where

$$f(c)=\frac{(c-1)(\sqrt{4+5c}-2)}{16c} \tag{5}$$

and

$$g(\rho)=\frac{1-\rho}{\rho} \tag{6}$$

and

$$W_{c(M/M/c)}=\frac{(c\rho)^c}{c!c\mu(1-\rho)^2}\cdot\left[\sum_{n_c=0}^{c-1}\frac{(\rho c)^{n_c}}{n_c!}+\frac{(c\rho)^c}{c!(1-\rho)}\right]^{-1} \tag{7}$$

In first model, service time correspond to Erlang distribution, while in second model service time of containers has queuing discipline first come first served (FCFS).

3 TOTAL QUEUING SYSTEM COSTS

The total annual cost for queuing systems with c yard cranes can be obtained as the sum of the annual operating cost of yard cranes as servers at yard and the annual container cost at the yard as customers in the service system [5]. That implies

$$C_{qs}=OT_{cy}+UT_c \tag{8}$$

where
C_{qs} - total annual cost for queuing system with c yard cranes;
OT_{cy} - total annual operating cost of yard cranes at the container yard;
UT_c - total annual container cost at the yard.

The total annual operating cost of yard crane is equal to the daily cost of yard crane, OT_{yc}, multiplied by the number of yard cranes c and defined period of year (365 days), T_e. Therefore, OT_{cy} can be expressed as follows:

$$OT_{cy}=OT_{yc}\cdot T_e\cdot c \tag{9}$$

Similarly, the total annual container cost at the container yard is equal to the daily cost of containers, OT_c, multiplied by the average number of containers that are present in a queuing system, n_c and by the defined period of year (365 days), T_e. Then UT_c can be expressed as follows:

$$UT_c = OT_c \cdot T_e \cdot n_c \tag{10}$$

Substituting equations (9) and (10) into equation (8), the following total annual cost for queuing system is obtained ([2], [5])

$$C_{qs} = OT_{yc} \cdot T_e \cdot c + OT_c \cdot T_e \cdot n_c \,. \tag{11}$$

4 NUMERICAL EXAMPLE

In this section, numerical examples are presented and obtained for the PECT container terminal in Busan port. Container terminal consists of five berths with 65 yard cranes and 64 transport means (Fig. 1). Maximum throughput has been realized in 2006 with 2341763 TEU. In past few years, this terminal is one of the most important container terminal in the world with constant throughput over 2.5 million TEU per year.

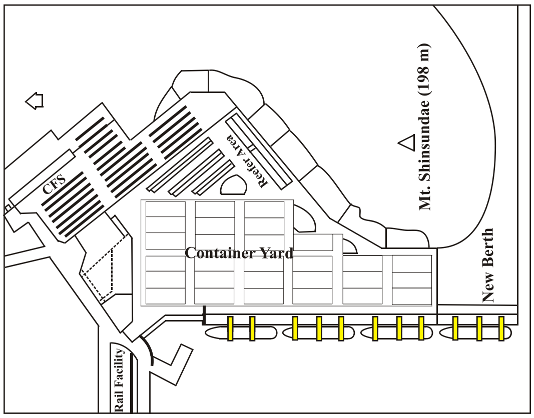

Fig. 1. *Container yard layout of PECT*

An important part of the model implementation is the correct choice of the values of the analytical parameters. The input data for the analytical models are based on the actual ship arrivals at the container terminal of PECT terminal for the one year time period. The total number of ships that arrived during 2006 is 1443 with 567629 import, 645004 export and 1129130 transshipment containers. We give the arrival and service time analysis only for import and export containers. The results are shown and are obtained in MATLAB. All input data are fit in EasyFit 5.5 program and their validity affirms Kolmogorov-Smirnov test at a 5% significance level.

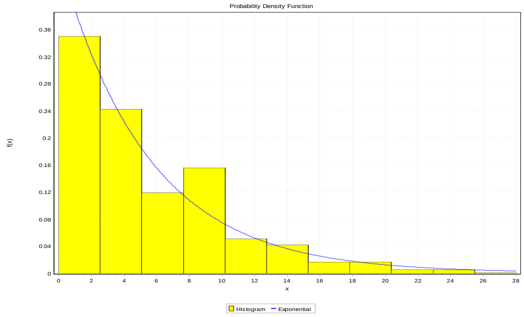

Fig. 2. *Probability density function of inter-arrival time for import and export containers*

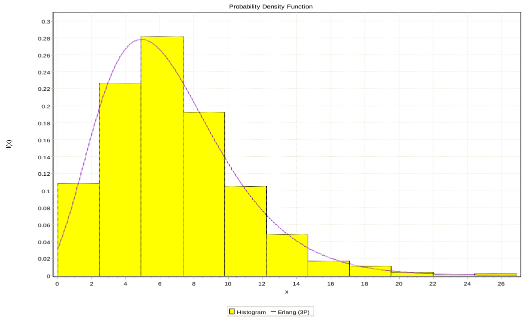

Fig. 3. *Probability density function of service time for import containers*

In Fig. 2 is shown probability density function of inter-arrival time for import and export containers and correspond to exponential distribution while in Figs. 3 and 4 are shown probability density function of service time for import and export containers, respectively. Service time of containers correspond to three-parametric Erlang distribution with $k = 5$ different phases.

As it can be obvious, the arrival time of containers is very dinamic while the service time is very stable. To calculate the total daily costs of containers, the basic parameters are given: working hours per day is 15; arrival and service time of containers is given in hours and minutes; server occupancy is 0.5; number of YC is 5 and service time of containers has 5 phases of Erlang distribution; labor costs are 35.75$/h; operating costs are 35$/YC.

Here, we compare the total daily costs for models $M/E_5/c$ (Model I) and $M/D/c$ (Model II) for five and seven YC at container yard (Figs. 5 and 6).

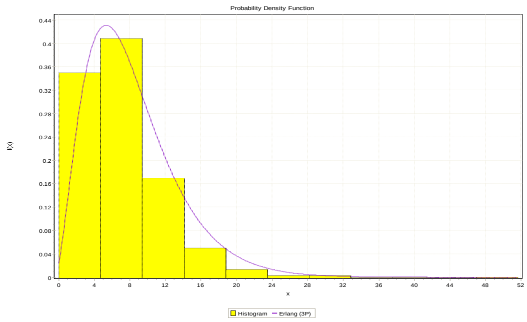

Fig. 4. *Probability density function of service time for export containers*

The results obtained in figures shown that the total daily costs are sharply decrease if there is a bigger number of YC at container blocks. It is obvious that average waiting time of containers is less with bigger number of YC.

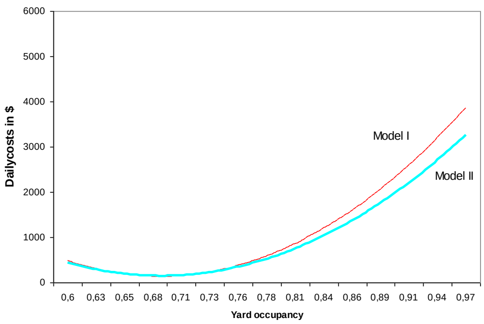

Fig. 5. *Total daily costs of containers with five YC*

The influence of total system costs with bigger number of YC and less waiting time of containers at yard, leads to drastically reduction of the total costs of containers, even for 74%. Therefore, total costs decreased from 18032.15$/day to 4162.85$/day for Model I, and from 15431.03$/day to 4087.55$/day for Model II. It is very important to affirm that increased number of YC leads to decreased total costs of containers.

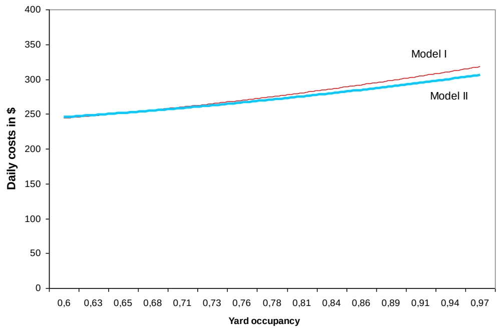

Fig. 6. *Total daily costs of containers with seven YC*

5 CONCLUSION

Unlike previous studies, this paper is based on real container port systems where it is presented a significant improvement in the operational performance as a result of the $M/E_k/c$ and $M/D/c$ queue. Although the costs of queuing system are formulated, but we pay our attention on number of YC in queuing system and on related specific costs. These numerical results in Figures 5 and 6 are partially restricted because of the defined input data and probability distributions of inter-arrival and service times. We conclude that comparing these models, the Model II shows better performances.

It is obvious that this methodology is very convenient and applicable for different analyses, planning and development of service systems. Also, it is illustrative for further computational experiments, yard crane utilization, traffic intensity and associated costs of queuing system in real systems.

6 REFERENCES

[1] Burke, P. J. “Delays in single-server queues with batch input”, *Operations Research*, 23(4): 830-833, 1975.

[2] Dragović, B., Zrnić, Dj. and Radmilović, Z. “Ports & Container Terminals Modeling”, *Faculty of Transport and Traffic Engineering*, University of Belgrade, 2006.

[3] Franx, G.J., “A Simple Solution for the M/D/c Waiting Time Distribution”, Universiteit van Amsterdam, 1998.

[4] Gaver, D. P. "Imbedded Markov chain analysis of a waiting line process in continuous time", *Ann. Math. Statistics*, 30(3): 698-720, 1959.

[5] Guan, C. and Liu, R. "Container terminal gate appointment system optimization", *Maritime Economics* & *Logistics*, 11(4): 378–398, 2009.

[6] Gullu, R. "Analysis of an $M/G/\infty$ queue with batch arrivals and batch-dedicated servers", *Operations Research Letters*, 32: 431-438, 2004.

[7] Kozan, E. "Comparison of analytical and simulation planning models of seaport container terminals", *Transportation Planning and Technology*, 20(3): 235-248, 1997.

[8] Laxmi, P. V. and Gupta, U. C. "Analysis of finite-buffer multi-server queues with group arrivals: $GI^X/M/c/N$", *Queueing Systems*, 36: 125-140, 2000.

[9] Radmilović, Z. "Ship-berth link as bulk queuing system in ports", *Journal of Waterway, Port, Coastal and Ocean Engineering*, ASCE, 118(5): 1-30, 1992.

[10] Radmilović, Z., Čolić, V. and Hrle, Z. "Some aspects of storage and bulk queueing systems in transport operations", *Transportation Planning and Technology*, 20: 67-81, 1996.

[11] Radmilović, Z., Dragović, B. and Meštrović, R. "Optimal number and capacity of servers in $M^{X=\bar{a}}/M/c(\infty)$ queuing systems", *International Journal of Information and Management Sciences*, 16(3): 1-22, 2005.

[12] Zrnić, Dj., Dragović, B. and Radmilović, Z. "Anchorage-ship-berth link as multiple server queuing system", *Journal of Waterway, Port, Coastal and Ocean Engineering*, ASCE, 125(5): 1-27, 1999.

HEAVY MACHINERY - HM 2011, 51-56 Paper accepted: 30.05.2011
ISBN 978-86-82631-58-3

Advanced Systems for Container Terminals Handling Equipment

Branislav Dragović[1], Nenad DJ. Zrnić[2], Maja Škurić[1,*]

[1] Maritime Faculty, University of Montenegro, Dobrota 36, 85330 Kotor, Montenegro

[2] University of Belgrade, Faculty of Mechanical Engineering, Department for Material Handling, Constructions and Logistics, 11000 Belgrade, Kraljice Marije 16, Serbia

This paper deals with new and old systems of planning and operation at container terminals. These systems are focused on the reduction and eventual absence of labor role at terminals. Here, we propose some elementary technologies related to terminal automation. Considering that, many container terminals adopt intelligent planning and operation systems.

For terminal operators, it is very important to reduce the total costs of handling equipment and to follow new standards in technology. These standards are defined in field of automation including berth allocation, ship planning and yard planning. The latest configuration of quay cranes (QCs) and yard cranes show the high utilization and optimization systems are so advanced that many container terminals dispose unmanned monitoring and container allocation.

The main points for determining handling equipment are viewed in terms of cost, productivity, flexibility and reliability. Due to inherent system characteristics, some aspects are more favorable for automated handling systems, whereas others favor conventional systems.

Keywords: Advanced systems, Container terminals, Automation processes

0 INTRODUCTION

It is met worldwide with installed handling capacities for servicing container ships and continental transporters, i.e. container terminals. Concerning the great technological elements capacities of modern handling technologies, not only arranged operation surfaces but handling equipment structures as well, the need has arisen for detailed investment planning and providing for an effective and rational exploitation of these technological entireties. In order to realize that project, it is necessary, of course, to get to know and define past developing trends in order to determine future ones, concerning these modern port segments.

The port container terminals represent the touching points of sea and inland transporters. And, besides, they are fundamental joining parts of intermodal transport corridors. On one side are containerships and on the other inland transporters and they both intensively urge upon terminals in quantitative, operational and temporal sense. Terminals are flexibly adapting to their daily needs concerning space, structure and assortment and they are trying to satisfy all the users of the sea-transport services with their infrastructural and equipment compositions.

Container terminal is a complex, serviceable, dynamic and material system defined with its basic performances: goals, functions, components and links. The goals can be reached by the handling results which are made in a certain period. The basic function of a terminal are the flexibility and effectiveness of container handling, storing, the unit packing and unpacking of containers, the forming and controlling of break-bulk cargoes, as well as linking the internal and correspondence transport system or intermodal transport. The fundamental components of a terminal are: labor, object of work, devices, working conditions and methods, users' needs, monetary units, the scientific development and the protection of environment. The link makes the communication and correspondence between terminal subsystems or the port ones possible as well as with the surrounding.

Noticing some evolution laws to which the technological processes and their derivations in

[*] Corr. Author's Address: Maritime Faculty, University of Montenegro, Dobrota 36, 85330 Kotor, Montenegro; mskuric@ac.me

port container terminals are liable, are based on a detailed analysis of relevant indicators, elements and factors pointing to some advantages of a more intensive and total investing in new terminal complex. Thus, the preliminary projection of container terminal includes at least five linked factors and their consideration which are shown in the block scheme in Fig. 1.

Each one of the presented factors, Fig. 1, has a direct influence on the generalized structure form of container terminal. The joining elements of this factor analysis in combination with its subsystems predetermine the dimensions, size, type and handling capacity of the terminal on the whole

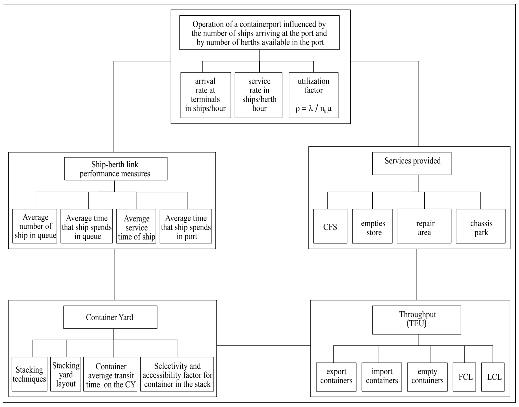

Fig. 1. *The block scheme of basic factors determining terminal activities*

This paper is organized as follows. Section 1 gives a brief description of container terminal operations. Section 2 presents various types of container handling equipment. Section 3 evaluates and compares various cases of relationship between ship and quay crane (QC) in port. Section 4 provides QC productivity and automation. The final Section 5 gives concluding remarks.

1 CONTAINER TERMINAL OPERATIONS

A container terminal can be considered as a network consisting of serial and (or) parallel links and knot points. A terminal link is a micro technological element representing some terminal operations or activities between the past knot point. A knot point is an area of temporal stay of container or break-bulk cargo on the terminal. Fig. 2 shows the structure of container flows and means of transportation of the sea and inland transporters. This is a general structure dependent on real conditions under which certain container terminal functions [1].

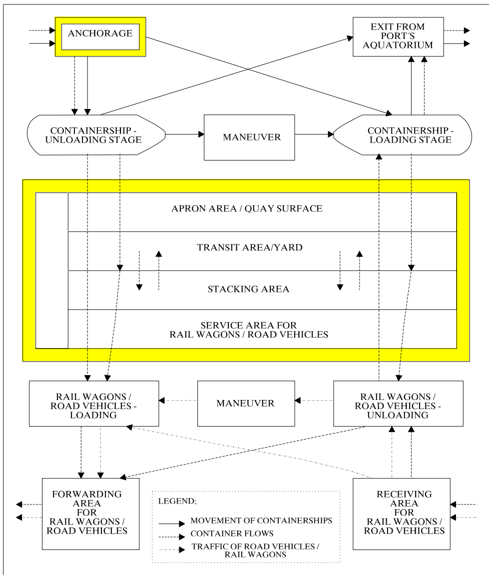

Fig. 2. *Structure of container flows and means of transportation on terminal*

Globally viewed, the realizing process of handling services on container terminals represents the moving process of a container with sea and land transporters, as well as with container terminal equipment structure, including the processes of packing and unpacking of containers and stacking containers. This is the essence of the terminal functioning process in primary form of the realization of handling operations.

A container terminal consists of the storage and sorting area, which is situated between two demands, one associated with the arrival of the containerships, the other associated with the arrival of land rail wagons / road vehicles and Fig. 3 shows the essential features from this viewpoint. Therefore, six basic handling operations on container terminals, Fig. 3, are realized by container equipment, such as:

- 1 - 2 handling on ship - apron area link (quay crane),
- 2 - 1 handling on apron area - ship link,
- 2 - 3 handling on apron area - container stacking area link (flexible equipment),

3 - 2 handling on container stacking area - apron area link,
3 - 4 handling on container stacking area - service area for rail wagons/road vehicles link (flexible equipment),
4 - 3 handling on service area for rail wagons/ road vehicles - container stacking area link.

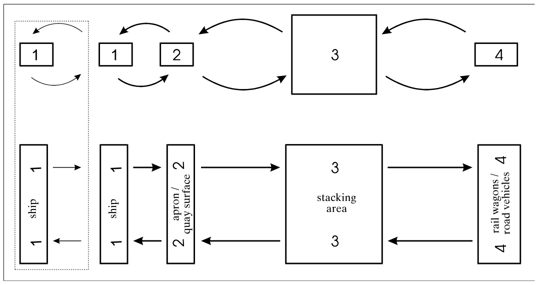

Figure 3. *Basic handling operations on container terminals*

2 CONTAINER HANDLING EQUIPMENT

The evolution process of various container yard equipment systems has left four basic survivors: namely, tractor-trailer systems (chassis systems) = TT or multi tractor-trailer systems = MTT (long train and short train) or seadlifter trailer = SLT, automated guided vehicles = AGV, automated lifting vehicles = ALV, straddle carriers = SC, rubber tyred gantry crane = RTG or rail mounted gantry crane = RMG, automated stacking crane = ASC and various systems forklift trucks (frontlifters = FL, side loader = SL and reach stacker = RS).

Generally, the container yard equipment (CYE) can be used in the following operations: land vehicles to yard; yard to ship shore gantry crane; ship shore gantry crane to yard; yard to land vehicles (terminal transports); handling in the container stack – stacking operations; re-handling in the container stack and container freight station activities.

The investment required for container yard handling equipment increases constantly. It is likely that this ratio will increase, according to the following statements [1]:

- There is tendency to increase utilization of the container stacking area. Such utilization will increase the number of machines used, and hence the increase of equipment investment costs concerning civil engineering work.
- The dialogue between users and traditional manufacturers will result in production of more reliable equipment. This will be demonstrated by increases in purchase price.
- The equipment design to meet demands of high productivity and reduction of driver fatigue will result in an increased cost.

It is likely that the increased capital cost for container yard equipment will be off-set by increased operating hours (less time for breakdown one). Thus, the final result should be in reduced cost per container handled.

Various types of container yard equipment used in container port terminals may be categorized as it is shown in Fig. 4. A wide variety of container yard equipment is utilized in container port terminals worldwide, depending on factors associated with annual throughput, facilities available and local conditions in port processes.

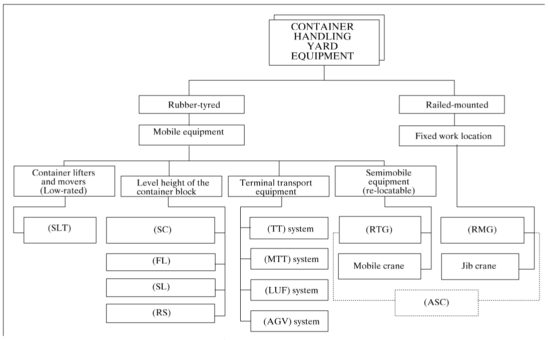

Sources: Block scheme modified and adopted in relation to new trends

Fig 4. *Container yard handling equipment – mobility aspect*

The optimal planning of the CY is the most important terminal performance indicator because it is a synthetic parameter which enables the evaluation of the entire relationship between technical engineers, terminal operators, planers and designers activities (see Fig. 5) [1] .

The harmonization of the handling demand concerning the size and dimension of CY and the handling capacity of the specialized yard equipment to handle container in the short time, shows the efficiency of the containerports and terminals.

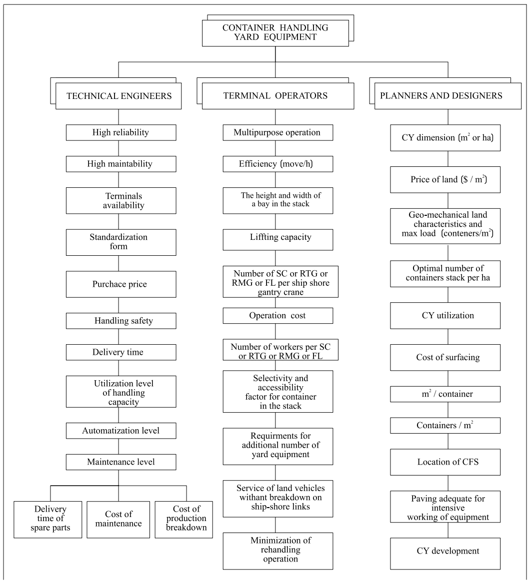

Fig 5. *Block scheme: relationship between technical engineers, terminal operators, planners and designers*

Total container handling time, regarding yard equipment, consists of times shown in Fig. 6. This focuses on how to optimally select the yard equipment systems in order to minimize the total handling time. This problem is formulated as a mixture integral time. The objective function of the formulation in block scheme (see Fig. 6) is to minimize the total handling time of various handling yard equipment systems [1].

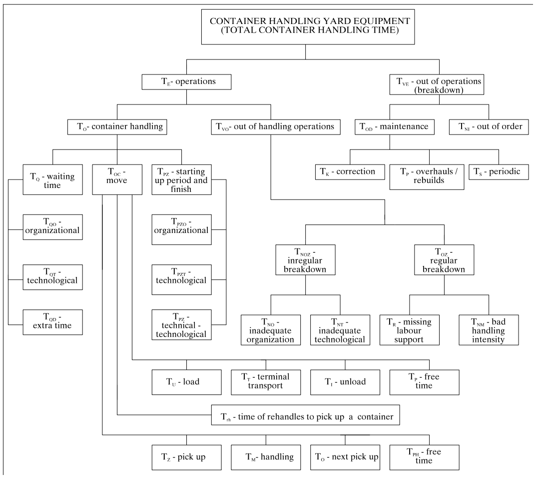

Fig. 6. *Block scheme: container yard equipment – total container handling time*

3 QUAY CRANE DEVELOPMENT

Figure 7 gives a visual impact of what has happened to quay cranes (QCs) and container ships and in 50 years. Structural engineers have had the task of keeping up with size, weight reduction, fatigue life, etc. The civil engineers keep driving more piles to support what the structural engineers develop. This figure is a base reference here for illustration and comparison. It shows two basic subsystems: QCs and container ships. A way has been found to calibrate the combined effect of container ships development, ship service time on the main container port link for main generation of ship and QC evolution, by making certain assumptions which are described in Figure 7 [2, 3 and 4].

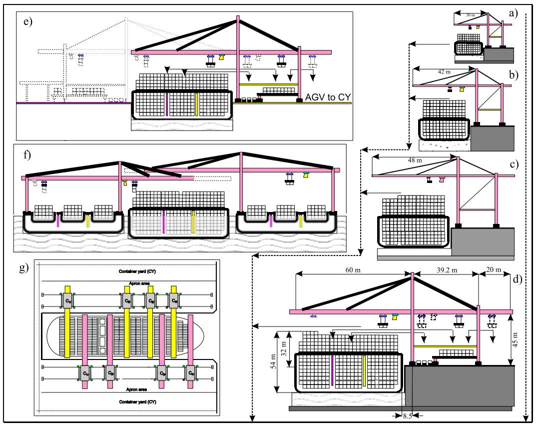

Fig. 7. *The relationship between ship size and QCs*

The new concept port layout regarding efficiency handling system can be explained in two variants (see Figs. 7-e and 7-g). QCs can be either renovated or developed as new concept that are different from existing methods in order to facilitate improved productivity in berth (Figures 7-e – 7-g).

In accordance with above mentioned, there is a question of cargo handling efficiency (loading/unloading speed) in the port links ship to shore and ship to ship. An increase of the efficiency of those systems can be achieved by further reduction of terminal operating costs on the one hand, and to ensure sufficiently short lay times for the ships in port on the other. One of the possible solutions is focused on higher efficiency of container crane and optimal number of cranes allocated per mega ships (see Figure 7).

Figures 7-e – 7-g present the new concepts employed in transfer containers form ship to quay (ship-to-shore) and from ship to ship or barge (ship-to-ship) and vice versa. Figure 7f shows a floating transshipment terminal with two – sided handling. The floating terminal system inverts the notion of a port. Instead of ships coming to port, the port is “coming to ship”. Another radical change allowed by the pontoon – base ship to ship transfer is the handling of multi – box units. This way of serving could enhance productivity and reduce the number of cranes per ship, although the size of cranes needs to increase [2, 3 and 4].

4 PRODUCTIVITY AND AUTOMATION OF QUAY CRANE

QC productivity has always been one of the critical components of terminal productivity. But the crane is only one of the terminal elements that control production. Within the next decade crane productivity may become the limiting component of the terminal production. Increasing productivity is always desirable, but for large ships is necessary. Ship service time in port depends on: ship and crane parameters, operating parameters and container yard performances. It will take nearly four days to service a 12000 TEU ship exchanging 75% of its containers, using 6 assigned QCs producing 30 lifts an hour. Increasing productivity to 55 lifts an hour cuts the turnaround time to a little less than two days. In Figure 8 are presented some typical turnaround times for various vessels and crane lifts per hour. Some improvements increase production incrementally, by 5-20 %, and other improvements make a quantum jump, by 25-40 %. This paper deals merely with the increasing of port terminal productivity, as a part of logistics network, due to automation of QC [4 and 5].

The productivity is usually discussed in terms of lifts per hour, i.e. frequency "*f*". To better evaluate productivity, it should be given the inverse relationship, i.e. hours per lift, or seconds per lift. This value is reciprocal to the frequency, and presents the period, $T = 1/f$. Although, this calculation is very simple, Figure 9 presents the illustration of the difficulty in attempting to decrease period as the period decreases. Considering that dwell times, starting and stopping motions, finding spots on the vessel and quay, and checking clearances, whether automatically or manually, takes about 30 seconds, it can be seen that to achieve e.g. 40-second, only 10 seconds is available to actually move the load. Even a 48-second period leaves only 18 seconds to move the load. However, it should be noticed, this is nearly twice long as for the 40-second case.

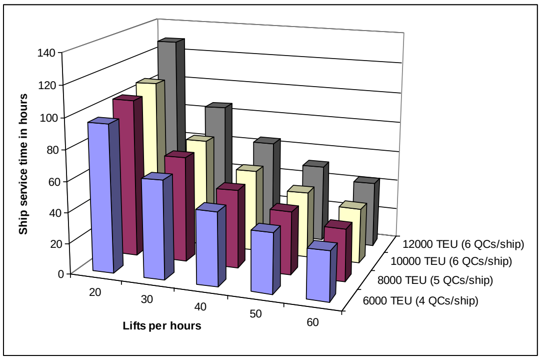

Fig 8. *Ship service time in hours vs. lifts per hour*

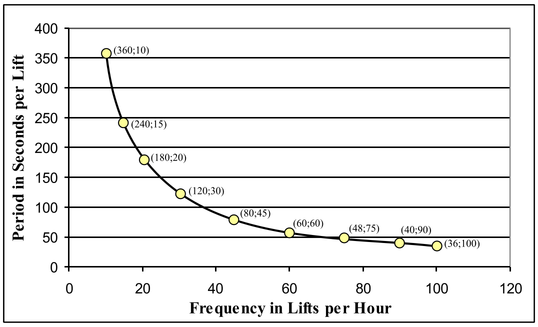

Fig. 9. *Frequency versus period*

The development of efficient, automated, high-technology loading/unloading equipment has the potential of considerably improving the performance of terminal operations. The construction industry is relatively still slow in implementing advanced technology to improve safety. Current practice requires that control of the QCs dynamic behavior is the responsibility of a skilled operator. The operator applies corrective measures based on experience when any undesirable swaying is detected. The absence of automated sensing and control not only leave room for accidents arising because of human error and/or delayed response of the operator, but also can greatly reduced the productivity of the crane's operation, also as the productivity of a whole port terminal. rminal operations once properly implemented.

The assignment of QCs was assumed random with probabilities equal to the number of QCs and percentages of the number of QCs that were allocated for ship servicing. The results of QC assignment and analyzed frequencies are given in Fig. 10 (real case from Korea Express Busan Container Terminal (KBCT)).

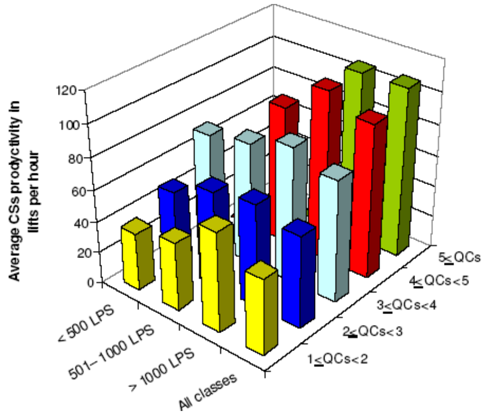

Fig. 10. *Average QCs productivity in lifts per hour*

The average service time of berthed ship can be calculated by dividing the total LPS (lifts per ship) by the product of average number of QCs working of the ship and the average QC rate (the average number of containers handled by a QC in an hour). Fig. 11 represent relationship between average QCs assigned per ship and average LPS per hour (real case from KBCT).

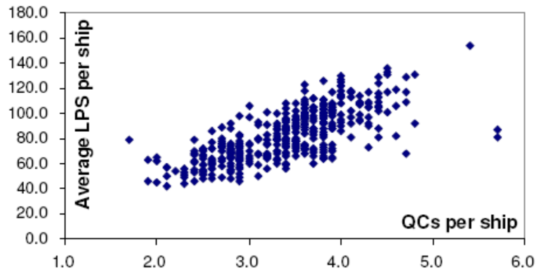

Fig.11. *Relationship between average QCs assigned per ship and average LPS per hour*

5 CONCLUSIONS

Improving port operations and attaining handling processes excellence to gain competitive advantage has attracted a lot of attention in the last few years. Many port operations and many of the technological advances in port and container terminal systems like DSS (Decision Support Systems), AGVs (Automated Guided Vehicles), ALVs (Automated Lifting Vehicles), ASCs (Automated Stacking Cranes), RFID (Radio Frequency Identification), RTLS (Real-time Location System), IT (Information Technologies), QC (quay crane) double cycling, indented container berth, dual-hoist tandem QC and dual-hoist triple tandem QC, automated container terminal and robotized container terminal systems admit modeling via various models.

6 REFERENCES

[1] Dragović, B., Zrnić, Dj. and Radmilović, Z., "Ports & Container Terminals Modeling", *Faculty of Transport and Traffic Engineering*, University of Belgrade, 2006.

[2] Dragović, B. and Ryoo, D.K., "Container ship and port development: A review of state-of-the-art", *Proceedings of the Ninth International Conference on Fast Sea Transportation*, FAST 2007, Shanghai, China, pp. 31-39, 2007.

[3] Dragović, B., Zrnić Dj.N., Ryoo, D.K., "An verview of relationship between container ships and quay cranes in port," *Proceeding of Annual Conference – The International Association of Maritime Economists*, IAME 2010, Lisbon, Portugal, Conference Proceedings on CD, pp. 1-21, 2010.

[4] Dragović, B., Zrnić, Dj. N., Park, N.K., "Container Terminal Performance Evaluation", Research Monograph, University of Belgrade, *Faculty of Mechanical Engineering*, 2011.

[5] Zrnić, N., Hoffmann, K., "Ship-to-Shore container cranes: from the beginning up to now (1959 – 2009)", *Österreichische Ingenieur- und Architekten-Zeitschrift* (ÖIAZ), 154. Jg., Heft 7-12/2009, pp. 267-276, 2009.

HEAVY MACHINERY - HM 2011, 57-61
ISBN 978-86-82631-58-3
Paper accepted: 30.05.2011

The World of Work and the new Sociology of Work or Sophitronics of Work?

Savo Trifunović[1,*]
[1] University of Kragujevac, Faculty of Mechanical Engineering Kraljevo

In this paper our objective is to suggest that the development of the sociology of work actually also implies the necessity to redefine the conceptual approach to exploring and contemplating the new man's position in the world of work and society created by the dizzying development and application of nuclear, biological, electronic and microelectronic technologies (the so-called floating i. e. adventurous technologies).
Microelectronics and the terms of automatisation, robotisation, innovation, quality, computerisation ("chipisation") and miniaturisation are also being used increasingly in our everyday speech. They, essentially, have a collective connotative meaning of change, growth, development. In axiological terms, they can also refer to welfare and danger, the better and the worse; the good and the evil. This paper is one small a plea for the Sophitronics of Work and better understanding new position of the men in the world of the work.
Key words : Sociology of Work, Sophitronics of Work, World of Work, System.

1. INTRODUCTION

We are living in the age of intensive (mild is the term) development of modern sciences – physics, biology, chemistry, genetics ...“ I genuinely believe that we are living through the greatest intellectual moment in history. Bar none. Some may protest that the human being is more than his genes. I do not deny it. There is much, much more to each of us than a genetic code. But until now human genes were an almost complete mystery. We will be the first generation to penetrate that mystery. We stand on the brink of great new answers but, even more, of great new questions.” [1]

Also, we are living in the age of critical megatransition from industrial to information society. “The crisis of mankind” is also the crisis of work. The technology based on, for example, microelectronics is not just a new socio-technological phenomenon or something which is expected to emerge in the nearer or farther future any more - it has also become our reality, an integral part of contemporary life. The outlines of a new society can already be discerned, but no clear picture of the “new” society, its realities and realities of “its” work can be created, yet. Because work is the fundamental process and essence of every society, but also the fundamental principle and standard of each individual.

When we perceive certain processes and phenomena as referring to a relative severing of ties with the past, as something unusual, created outside established clichés and paradigms, we are inclined to call them new or post-. Here likewise. Thus we do not report anything on the causes, nor on the purpose. We only underline subsequence. However, we also consider this approach to designating phenomena, processes, creations and institutions as reflectively and morally consistent, as a transitional stage to clearer crystallisation occurring mainly after practical (that is to say, reflective) differentiation of scientific researches and serious contemplations and with the passage of time.

2. NECESSITY REDEFINING

Our objective is to suggest that the development of the sociology of work actually also implies the necessity to redefine the conceptual approach to exploring and contemplating the new man's position in the world of work and society created by the dizzying development and application of nuclear, biological, electronic and microelectronic technologies (the so-called floating i. e. adventurous technologies). The new conceptual approach and the so-called “wider scope” are not matters of our good will or, perhaps, evil intention, nor of solely our own determinations and perception of (sustainable) development any more. They are seen more and more as a social and scientific need i.e. interest. Therefore, the

*Corr. Author's Address: Faculty of Mechanical Engineering, Kraljevo; Serbia trifunovic.s@mfkv.kg.ac.rs

sophitronics of work must stand not only for a "new" system of sociological and philosophical thoughts in exploring and contemplating the effect of adventurous technologies on man and society – and vice versa, but also for a new view (from a contemporary viewpoint) not only of the previous development of the sociological and work-oriented approach to researching social phenomena, processes, creations and their specific relations, but also of the structure of the relative diversity of subject matter in a broader context of the sociological (and sociological/work-oriented) approach.

3. SOPHITRONICS OF WORK

Specifically, the Sophitronics of Work is a term designating a new quality subliming the terms of: Sociology + Philosophy + Electronics + Work. The subject matter of the sophitronics of work is to explore and research specific relations between and sublimations of sociological, philosophical and electronic cognition and methods in the man (society) – work framework.

The sophitronics of work is a science and thought exploring and contemplating the effect of adventurous technologies, particularly electronics and electronic technologies, on the work process, society, man and the wisdom of life. It is also a system of different forms of thinking and contemplation on a new image of man in the context of the information society. Insofar as the industrial society is "transformed" into the information society, the sophitronics of work will, actually, become a new sociology of work of that and such modern society. The sophitronics of work will be (should already be) an expression of the processual continuity of the development of the scientific approach and philosophical contemplation on (adaptation to) a new social reality and man's position in the work process. The sophitronics of work is also a new research field of the contemporary sociology of work which will (should) not only use and perfect the attained level of sociological/work-related cognition, but will (should) also contemplate it more deeply, in a sense – transcending it, primarily through the totality of scientific, reflective-logical and perceptual approaches. In the broadest context, we also demand the sociology of work be reclaimed by philosophy which was also divested of general sociology by the positivist concept and pragmatistic idolatrous enthusiasm for traditional industrial technologies.

4. SYSTEMATIZATION

The investigation of the social aspects of the work process in a peasant society is the primary subject matter of rural sociology, i. e. the sociology of rurality, among other sciences, as a specific sociological discipline comprising individual sociological disciplines the most important thereof, for the purpose of the present consideration and conceptualisation, being the sociology of peasant work. We can justifiably suggest the following: just as a peasant society is being dealt with by rural sociology, so is an industrial society being dealt with by the sociology of work as a separate sociological discipline and bordering individual sociological disciplines, such as the sociology of work in industry, the sociology of work in agriculture, the sociology of work in administration, etc. Still keeping "within the framework" of the sociology of work, the exploration of work processes and work-related problems in the information society is, naturally, the subject matter of the sociology of work, but a priori in the context of "its" individual science – the sophitronics of work. The term "individual science" used in this context is utterly conditional because the sophitronics of work implies comprehensiveness, consistency, transcendence and refocusing (see Fig. 1).

peasant society	sociology	rural sociology (sociology of rurality)	sociology of peasant work
industrial society	sociology	sociology of work	sociology of work in industry sociology of work in agriculture sociology of work in administration
information society	sociology	sociology of work (sophitronics of work)	sophitronics of work

Fig. 1

At the same time, the sophitronics of work implies the desirable sophitronic basis of the sophitronics of: management, safe work, the environment, work morality, rurbanity, leisure ... (see Fig. 2).

the sophitronics of work	the sophitronics of management the sophitronics of safe work the sophitronics of the environment the sophitronics of work morality the sophitronics of rurbanity the sophitronics of leisure ...

Fig. 2

In the context of the rational and appropriate (and, in practical terms, utterly conditional) sociological division of the machine system development into four stages (the universal machine stage, the specialized machine stage, the automated machine stage and the so-called electronic "machine" stage) and the division of risks to the (otherwise indivisible) integrity of man in the working environment into physical, mental and moral integrity, the sophitronics of work, within its subject matter, focuses particularly on the effects of the components of the automated and electronic work environments on man and social processes, i. e. on man's (and) moral integrity (see Fig. 3).

sociology of work	universal machine stage	physical integrity	sociology of work
	specialised machine stage	mental integrity	sociology of work
	automated machine stage	moral integrity	sociology of work (sophitronics of work)
	electronic "machine" stage	moral integrity	sophitronics of work

Fig. 3

5. SOME PHRASES (SINTAGMAS)

In everyday life, we come across an increasing number of expressions and terms which we sometimes (do not) understand, but which are, in a broader sense, an expression of rapid and complete changes, of a new society, a new technology, new emerging consciousness. The terms and expressions are the following: the technotronic era; by-sphere; control of consciousness; mental breakdown and risk reduction (increase); risks and trends of the future; sensitivity training and bioethics; fields and networks; ecology of the spirit; holistic methodology; creation and the One; images of man varying through his thinking, social conduct, conformities and perspectives. And also: "a chipped society"; "the chipisation of society"; "the chipisolation of society"; "workless society"; workless man; homo studiosus instead of homo faber; "steel workers", manless work; "silicon workers"; titration technology; webs and spiders; "lame duck"; adventurous technologies (electronics, robotics, biotechnology, human engineering, etc.); miniaturisation (of chips – the smaller, the more powerful; of morality, dresses, the brain); maximalisation (of profit, unemployment, lies and manipulation, apathy, social pathology); (not to) know how to stop, ...

Microelectronics and the terms of automatisation, robotisation, innovation, quality, computerisation ("chipisation") and miniaturisation are also being used increasingly in our everyday speech. They, essentially, have a collective connotative meaning of change, growth, development. In axiological terms, they can also refer to welfare and danger, the better and the worse; the good and the evil.

Great are challenges and potentials of microelectronics and biology, but great are also the pitfalls and dangers. Shall we know how to use the advantages and potentials of modern science for the welfare of man and society (for human and sustainable development) or a wave of scientific/technological changes will drown and dehumanise us? This is primarily a social, political, real sophitronic question, a matter of social planning of development and general usefulness, and not just a clear scientific/technological question. Importantly, though, let us underline at this very point that the thoroughly attained reality and future of the information society lie within the sphere of vision developed by people with strong mental powers and distinctive character.

The information society is just one factor (the last one, though, but only for the time being) in a development sequence: primitive community, peasant society, industrial society, information society. The last factor of the development sequence is not the ultimate one – since this would suggest the discontinuance of the historical course of the development of things, institutions and thought. We have, however, already conceived the next factor in the development sequence (although we do not dare presently discuss it), being a post-information society, with new technologies ("new robots" and "new microprocessors", perhaps) determining production, services and our needs on their own without man's intervention. The information society has not "come out of the blue" as something completely new, devoid of the old, lacking tradition and the common consciousness of preceding generations. In a word, the information society has developed within an industrial society; the industrial society developed within a peasant society; ...Deductive thinking is always helpful in understanding the development sequence. Deduction cannot, however, go without its counterpart - induction. An inductive-deductive approach helps understand the development sequence, the picture thereof, however, without other methodological approaches, being nothing but partial. As changes in society never occur without leaving something behind, the information society is also always considered both new and old, i. e. old and new. Only theoretically, at the highest levels of abstraction, will it be able to attain the so-called pure forms and shapes.

6. SOPHITRONICS OF WORK WILL NEED TO

It needs to be emphasised, at this early point, that the subject matter of the sophitronics of work shall define the character of work more as man's relationship towards his own work activity in terms of compulsion or creativity, than as the substance of work referring to all particular activities carried out by a worker employing his physical and intellectual potentials at his workplace in the working environment, because this shall result in a new character of work focused more on purposes (than on goals) which cannot be assessed by quantitative indicators. [2]

The sophitronics of work shall re-evaluate technology as a technical/technological science and accentuate social, human-related, moral and environmental dimensions of technology in terms of ultimate purposes.

The subject matter of the sophitronics of work shall be less oriented towards material production and more towards services, i.e. tertiary, quarterly activities – meaning that the subject matter shall also determine the willingness of society to thoroughly restructure and (or) create new institutions – new relationships and links, a new balance of powers.

Material production in the industrial sector of today, as well as in mechanised, chemicalised, hybridised agriculture has been increasingly "taken over" by machines and robots. Eventually, sooner or later, the sophitronics of work will have to reassess Aristotle's assertion that if Dedalus's creations (the "automata" of the antiquity) worked on their own, there would be no servants or masters. It will also have to meticulously discuss the convictions and projections of R. T. De George, [3] J. Naisbitt, C. Marx and other important thinkers and "futurologists". Richard T. De George, as a matter of fact, refers to the vision of new society as a "proper society" apostrophising its ethical characteristics. John Naisbitt believes that we shall become increasingly more humane in such society and that "we will stress more and more mutual differences, particularly the language difference... The Swedish will become more Swedish, the Chinese even more Chinese." [4] In his philosophema, Carl Marx presumed that it would be a society based on highly developed production forces which would conduct themselves according to ethical standards.

The subject matter of the sophitronics of work shall include the spirit of time, creation, the ecology of the mind and variable images of man and society.

The sociology of work has in a relatively satisfying manner explored the history of human work, relying on both research results and the level of cognition attained by other sciences directly or indirectly dealing with the process of work. Well explored is also the attained level of cognition (particularly after the works of G. Friedman, P. Navil, F. Taylor, E. Maio...) of the first two stages in the development of industrial work environment – the stage of universal machines and the stage of specialised machines. The stages of automated machines and electronic "machines" are insufficiently explored. This is exactly the research field we would like the sophitronics of work to engage in.

Although the sophitronics of work deals with only one segment of the subject matter of the sociology of work, it must ultimately surpass the "medium range" of theoretical outcomes of the sociology of work. In a word, it must pursue a more general range within the subject orientation.

It must pursue the One, [5] that is the another return to the One. At best, it must lie at the confluence of rivers flowing into one river, one science. Because it was, is and will be only one science. All our contemporary knowledges and the knowledge of the sophitronics of work as well, have been only anticipations of this One science. It must be transferred from the sphere of vision into reality. The time for this is not yet, because adequate understanding of the problems and consistently educated personnel are missing. [6] Within the framework of today's deep division among sciences and (still) pronounced tendency of "splitting" them into as high number of individual sciences as possible, with occasional interdisciplinarity and multidisciplinarity, this is (will be) even harder. But, it is not and must not be impossible. On the contrary. It is in this context that our endeavour and "courage" to put out to the high seas of the as yet insufficiently grounded and explored should be looked upon.

REFERENCES

[1] Matt Ridley: Genome: The Autobiography of Species in 23 Chapters, Plato, Belgrade, 2001, p. 12 (in Serbian)
[2] For more detail on the substance and character of work see S. Trifunovic: (2003) An Introduction into the Sociology of Work, (second edition), Faculty of Mechanical Engineering, Kraljevo, Kraljevo, pp. 190-194. (in Serbian)
[3] Richard T. Di George : Business Ethics, Filip Višnjić, Beograd, 2003 (in Serbian)
[4] John Naisbitt: Megatrends, Ten New Directions Transforming Our Lives, Globus, Zagreb, Croatia, 1985, pp. 83-84 (in Serbian)
[5] Savo Trifunović : From One to One , Introduction in Continuum of Cognition , „Faculty ofMechanical Engineering", Kraljevo, 2007. (in Serbian)
[6] Vladimir R. Milacic : Knowledge Industry, new magistrala of sustainable development, „Faculty of Technical Sciences", Novi Sad, 2006. (in Serbian)

HEAVY MACHINERY - HM 2011, 63-70
ISBN978-86-82631-58-3
Paper accepted: 30.05.2011

Location of regional logistic center:multiple criteria decision making and implementation of algorithms under fuzzy environment

Marković Goran[1] - Marinković Zoran[2] -Vojislav Tomić[2] -Aleksandar Čupić[3]
[1] University of Kragujevac, Faculty of Mechanical Engineering Kraljevo
[2] University of Niš, Faculty of Mechanical Engineering Niš
[3] University of Belgrade, Faculty of Transport and Traffic engineering Belgrade

New solution concept in the regional logistics needs to be a driving force of change in solving the problems of distribution and transportation of goods in the given region and the creation of the control and management of goods flows. Research methodology (algorithm) to define the profile of regional logistics should be directed to the analysis of logistic flows in the region and to define potential location which would also constitute a basis for the development of new alternative solutions and their further evaluation.This paper gives the theoretical basis and methodology of selection and ranking of different optimal locations using a hybrid method of multiple criteria decision making using the theory of fuzzy sets.

Key words:logistic centre, location, multiple criteria decision making, fuzzy.

0. INTRODUCTION

In the development of regional logistics and transportation system can be said that the logistic concept is a process of development multivaried model for process optimization of the total regional logistics which primarily affects the development of commercial, transit and supplying function of agglomeration, with the aim of achieving greater economic, spatial and technical technological and environmental effects. The analysis of logistic flows is a complex and complicated process, especially in this area where there is no database and the willingness of subjects to track goods flows [1].

For further analysis, and in accordance with the plans of construction, pre-draft of the general urban plan and strategies of development should be at the very beginning to suggest potential variants of the regional center location. Managerial task of such a choice location, or select one of the alternatives that are assessed by several criteria, is a complex problem whose solution usually possible to use multiple criteria analysis.

Thus, the chosen location is the closest to creating an ideal condition for the realization of the logistic center, which has adequate transportation, technology and information and communication links to the international, national and local level. The transport requirements in supply chains, ecologic requirement and the need for living quality in stated towns in the regions particularly point out the significance of location selection of logistic centers as well as the manner and time for their supply.

1. PREREQUISITE FOR DEVELOPMENT OF CONCEPTUAL LOGISTIC SOLUTIONS

1.1 Factors of choice and the importance of logistics center location

Creating a basis for designing a new logistics concept solution that contains a plan connecting business, transit and supplying functions mentioned regions essentially matching, and connected to the process of development of logistic centers (LC), including concentration, coordination and rationalization of the flow of goods. Founders, function, structure and objectives of logistics centers have historically received different forms and different names and functions, both in terminology and in technological terms. Goods flows are the cause-effect factor to increase the spatial, chronological and quantitative transformation in continuous replaceability of packaging, loading, transportation, storage, re-loading, transport, unloading, storage, delivery, etc. Major industrial regions, industrial areas and large urban areas have always been centers of sources and sinks of important of goods flows and their transformation

*Corr. Author's Address: Faculty of Mech.Engineering, Dositejeva 19, 36000 Kraljevo, markovic.g@mfkv.kg.ac.rs

from macro to micro distribution and reverse. In the places confrontation flows macro and micro distribution of today are demands for a coherent logistics service.These requirements are most appropriate form of goods and transportation center as the most complex form of the logistic center. Development of a network of logistic centers at the national and international level is a prerequisite for optimization of transport and logistics chains.

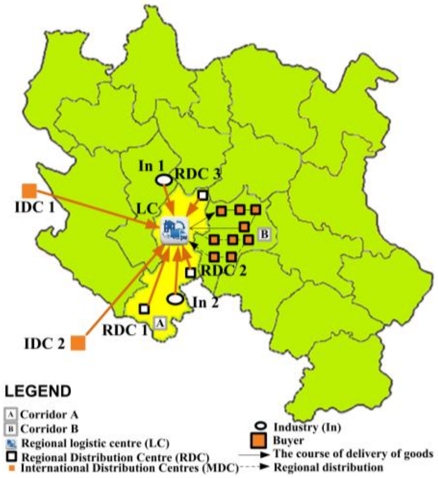

Fig.1 Location of regional logistic centre [1].

The structure and characteristics of flows primarily define the concept of goods and transportation center, and therefore significantly influence the choice of location. Level of location planning depends on the particular role of macro and micro level of distribution flows which deflects in goods transportation center. Any goods and transportation center in the final solution is a variant of micro location problem. In goods and transportation centers that are connected to the macro trends of distribution and location problems have a macro component, and in these cases appear macro-micro-location problems (Fig. 2).

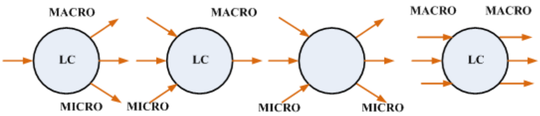

Fig. 2. The flows structure and characteristics as a factor of location selection of goods and transportation centre

Rating of development and construction of logistic centers in large agglomerations, means that holders of decision making and potential investors have a defined system aims. The goals are an integral part of the model of strategic and operational decision-making on the basis of which criteria to develop and establish the relevant estimates for and against the development of the logistics center. The objectives of the development of logistics centers are usually classified according to the area of socio-economic interests, interest groups (decision makers), macro, meta and micro aspects of observation system of goods and transportation center, and various aspects of monitoring and allocation of development goals allow their different structure. In some cases there is overlapping and aims from different groups (Fig.3) [2].

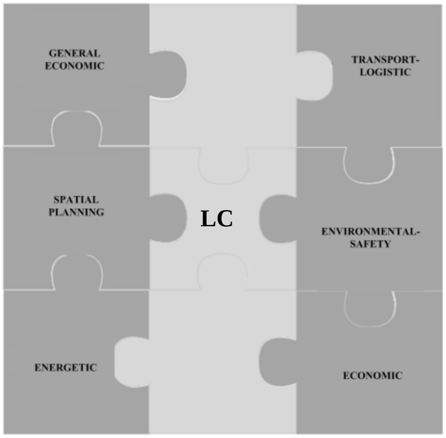

Fig.3. The objectives of the development of logistics centers

1.2 Location problems and the theory of multiple criteria decision making

The modern approach to decision making, normally significant human activity, helps decision maker to link all the data and relations in a rational whole. In other words, regardless of the approach, rational decision-making means to select one from the set of available alternatives. There are many problems deciding which information is spatial (geographic). Such decisions are known as location. The choice of location was part of operations research and management aimed at placing at least one of existing facility to optimize at least one function (such as costs, profits, income, distance, etc.).

There are many methodologies and models which are devoted to this subject. The criterion is the component that is present in almost all cases site selection of logistics centers, regardless of the applied methodology and model. As already mentioned, the process of location selection of logistics center (macro and micro levels of observation) requires defining a set of criteria that are partially or completely be different and match. Based on the structure of problems and criteria of access to choice and implementation methodology and model optimization and validation of location solutions. The procedure of selection criteria for defining the location of terminals may vary from expert assessment to the hierarchical generation of criteria by interest groups, some participants - policy makers, their interests and goals.

Criteria can be generated and classified according to different aspects of observing systems and decision maker. Selection criteria can have a touch of subjectivity of the decision maker. For the choice of location logistic center, the criteria can be grouped in three ways [2]:

- According to the interest groups that have the ability to make decisions and may influence the development concept of the terminal. These include users of terminals and services, owners and investors, operators, and the society, in consideration of the social-control institutions and associations, to individuals, population, etc.
- According to the type of criteria and his membership in one of the following areas: technological, economic, organizational, technical, legal-regulatory, etc.
- According to the level of observation, the criteria for determining the macro location of the micro location of the terminal.

The degree of development of infrastructure, the presence of subsystems that provide synergistic effects, the possibility of extension, legislation and the possibility ofof efficient activation site without ownership and other legal restrictions are very important criteria that take into account the investors, the owners of the terminal .

Quality links to other logistics centers and the possibility of involvement in national and international logistics networks are also important criteria for decision making. Very important for the terminal's position relative to the main transport axes, corridors and roads in urban areas. Society and the state wants to terminal faster the development of all activities, to be in function of the whole system, to protect and preserve natural resources. It is desirable and necessary that the terminal fits into the environment, to be consistent with the spatial and urban plans at the respective location, to fit into the development plans at all levels, from municipal or regional to national or international level planning.

Only with knowledge of the essence of the problem that is solved we can define a set of relevant information needed for comprehensive and objective decision-making. The goal is that, while respecting certain rules and recommendations to decision-making, make the correct decision (in this case, the decision on the optimal location of logistics center). Complexity and multiple layers of decision-making process generally requires a multicriteria model for evaluating alternative solutions, in order to effect a mutual comparison of different alternatives for each of the adopted criteria of, and in order to obtain the final ranking of the total benefits. If the evaluation is done with respect to some criterion of the procedure is considered as one criterion optimization (solution (alternative) that extremes target function).

On the other side of the complex and far more serious problem is the existence of two or more criteria and when to find the best solutions rather than optimal. Its accuracy and analysis is directly related with an attempt to complete scalarization (incorporating multiple criteria in one). Instead of this procedure, mostly level scalarization objective functions controlled by the decision maker (DM). Establishment of relevant criteria and determining their relative importance - weight in the decision making form the matrix of alternatives and criteria to be analyzed and processed, which as a result gives difficulty rating based on which alternative is ultimately the same rank.

Table 1. *Matrix of decision*

Alternative	Criterion C_1 w_1 max /min	C_2 w_1	… …	C_n w_n	Score	Rank
A_1	x_{11}	x_{12}	…	x_{1n}		
A_2	x_{21}	x_{22}	…	x_{2n}		
	…	…	…	…		
A_m	x_{m1}	x_{m2}	…	x_{mn}		

$A_1, A_2, \dots, A_m$ is the set of available alternatives, $C_1, C_2, \dots, C_n$ is a set of criteria, $w_1, w_2, \dots, w_n$ is importance - the weight of criteria and a x_{ij} performance *i*-th alternatives to the *j*-th criterion.

Such an approach to decision making, the choice between possible alternative in recent years takes a lot of space in scientific research worldwide. Procedure for solving many practical tasks of choice and ranking of different decision-alternatives with multicriteria methods of analysis would consist of the following stages:

- the identification and formulation of a problem,
- establishing a model of decision making,
- the application of multiple criteria methods and
- selection of the most acceptable alternative.

2. APPLICATION OF FUZZY SETS THEORY IN MULTICRITERIA DECISION MAKING

Reality and vitality of the problems of multicriteria analysis indicated the rapid development of methods in this field, so that today has a powerful set of methods that are able to most of the real problems and successfully solved. A detailed review of previous efforts and developed the method when it comes to location problems is given in the literature [3]. The reference discusses the use of different methods of multiple criteria, some of which stand out the following: ANP (Analytic Network Process), AHP (Analytic Hierarchical Process), VIKOR (Serbian name VišeKriterijumska Optimizacija I Kompromisno rešenje, means multi-criteria optimization and compromise solution), TOPSIS (Technique for Order Preference by Similarity to Ideal Solution).

Contrary to the traditional approach to the optimization in recent years appears to a wide range of methods and algorithms that significantly eliminates restrictions on the heterogeneity of criteria, subjectivity of decision-makers and so on. That is a large number of authors used the so-called hybrid methods are the integration of one or more methods and for better utilization of their benefits. This paper presents the possibility of applying TOPSIS method extended the theory of fuzzy sets [5] in the multicriteria optimization selection potential sites of regional logistics center. TOPSIS method has the best characteristics to consider multicriteria task is not overly complex, gives the rank of alternatives and alternative by all criteria. The essence of this method is that each alternative is treated as a point in k-dimensional space (k is the number of criteria) and determines the Euclidean distance of each alternative from the ideal and anti-ideal point in this space. TOPSIS (Hwang and Yoon (1981)) method is based on the intuitive notion of the chosen alternative should have the shortest distance from the ideal and the longest by far from anti-ideal alternative in the shape of. For each alternative in relation to the criteria of each account the distance from the ideal and negative ideal solutions. Weight-importance of each alternative are determined by the relative proximity of alternative ideal solution. The procedure of TOPSIS method can be presented through the steps [7,8] :

Step 1: The formation of normalized decision matrix. The normalized value $\left(n_{ij}\right)$ is calculated as

$$n_{ij} = \frac{x_{ij}}{\sqrt{\sum_{i=1}^{m} x_{ij}^2}}, i = 1,2,...,m; j = 1,2,...,n \qquad (1)$$

where x_{ij} is value of alternative i with respect to attribute j.

Step 2: Calculate the weighted normalized decision matrix.The weighted normalized value *i*-th alternative with the respect to *j*-th criterion $\left(v_{ij}\right)$ is calculated

$$v_{ij} = w_j n_{ij}, i = 1,2,...,m; j = 1,2,...,n \qquad (2)$$

where w_j weight - importance *i*-th criterion, and $\sum_{j=1}^{n} w_j = 1$.

Step 3: Determine the pozitive ideal A^+ and negative ideal solution A^-

$$\begin{aligned} A^+ &= \left\{v_1^+, v_2^+, ..., v_n^+\right\} \\ A^+ &= \left\{\left(\max_j v_{ij} \middle| i \in I\right); \left(\min_j v_{ij} \middle| i \in J\right)\right\} \end{aligned} \qquad (3)$$

$$A^- = \{v_1^-, v_2^-, ..., v_n^-\}$$
$$A^- = \left\{\left(\min_j v_{ij} \middle| i \in I\right); \left(\max_j v_{ij} \middle| i \in J\right)\right\} \quad (4)$$

In the ideal point of the highest value is taken by all criteria or the criteria of "the larger the better" takes the maximum value, whereas if the rule is "less is better" takes the minimum value. When searching for anti-ideal point is treated in the reverse logic. Where I is associated with benefit criteria and J is associated with cost criteria.

Step 4: Calculate the separation of each alternative from the pozitive and negative ideal solution. Separation is given as

$$d_i^+ = \sqrt{\sum_{j=1}^{n}\left(v_{ij} - v_i^+\right)^2}, i = 1, 2, ..., m \quad (5)$$

$$d_i^- = \sqrt{\sum_{j=1}^{n}\left(v_{ij} - v_j^-\right)^2}, i = 1, 2, ..., m \quad (6)$$

Step 5: Calculate the relative closeness to the ideal solution is defined as

$$R_i = \frac{d_i^-}{d_i^+ + d_i^-}, i = 1, 2, ..., m \quad (7)$$

Step 6: Rank the preference order.

Multicriteria decision making applies to situations in which the present existence of a number of usually conflicting criteria. This fact is in one important step toward reality model that describes the problem and the other models become more complex in mathematical terms so that there developed a general method with wide applications. Naturally, we must know that in some cases that the value of alternative with respect to some attribute are not given quantitatively, but through corresponding linguistic terms [10].This means, that during ranking of alternatives of regional logistic centre location, some attributes will be expressed through numerical values (investment costs,labour costs, etc.) while the others will be given linguistic variable (high, low, medium, very high ,etc).

According to evrything mentioned, it foolows that some values with respect to some attribute are “good transportation infrastructure of region ” or “low development posibilities of the region ” , etc.In that case, some attributes could not be expressed quantitatively while the others are expressed by fuzzy numbers because of inability to provide the numerical data precision.

2.1 Extension of the TOPSIS methods with fuzzy data

Fuzzy sets theory is a convenient mathematical tool for modeling various processes dominated by uncertainty, ambiguity, subjectivity, uncertainty. The first paper deals with fuzzy sets released in 1965. professor Lotfi Zadeh [11]. The theory of fuzzy sets allows the treatment of those who are insufficiently precise, accurate, complete phenomenon that can not be modeled only possibility theory and interval mathematics. If the uncertainty comes from inaccuracies in the communication between the people of this uncertainty is modeled by the theory of fuzzy sets.

Suppose that we have m alternatives A_1, $A_2, \ldots, A_m$, among which decision makers have to choose, also n criteria C_1, $C_2, \ldots, C_n$, are identified, and $\tilde{x}_{ij}$ is rating of alternative i with respect to criterion j and is a fuzzy number.

In the case of multicriteria optimization problem with fuzzy numbers can be expressed in matrix form - fuzzy decision matrix. Also, we could expressed $\tilde{W} = [\tilde{w}_1, \tilde{w}_2, ..., \tilde{w}_n]$, where $\tilde{w}_j$ is the weight of criterion C_j and is a normalized fuzzy number.

In the following few lines, in order to apply the proposed method, are given some terms related to the theory of fuzzy sets [5].

Unlike classical set theory, which very accurately define the boundary that separates the elements belonging to a given set of elements that do not belong to , the theory of fuzzy sets under well-defined border separating. A fuzzy set is defined as a set of ordered pairs $\{X, \mu_A(x)\}$, where is: X- is a classical set of elements x, $\mu_A(x)$ - membership functions (degree of membership of x in A). Affiliation elements x in A in the theory of fuzzy sets describing the membership function $\mu_A(x)$ as follows:

$$\mu_A(x) = \begin{cases} 1 \text{ if and only if } x \in A \\ 0 \quad \text{otherwise} \end{cases}$$

The function can take any value from the interval $[0,1]$. If $\mu_A(x)$ is a greater, the more there is more truth in the assertion that x belongs to A.

If $\tilde{A}$ be a fuzzy set

$$\tilde{A}=\{(x,\mu_{\tilde{A}}(x))|x\in X\} \quad (8)$$

then *α-cut* of a fuzzy set is a crisp subset of X and is denoted by

$$[\tilde{A}]_\alpha=\{x|\mu_{\tilde{A}}(x)\geq\alpha\},\alpha\in[0,1] \quad (9)$$

The lower and upper points of any *α-cut*, are represented respectively

$$[\tilde{A}]^L_\alpha=\inf[\tilde{A}]_\alpha,\ [\tilde{A}]^U_\alpha=\sup[\tilde{A}]_\alpha \quad (10)$$

A fuzzy number is a convex normalized fuzzy set with continuous membership function that caracterized *confidence interval* [*m, n*] and *level of security α* ($\alpha\in[0,1]$).The triangular fuzzy number can be denoted as $\tilde{A}=(a,m,n)$, where m – left spread, a – central value i n– right spread (Fig.4).

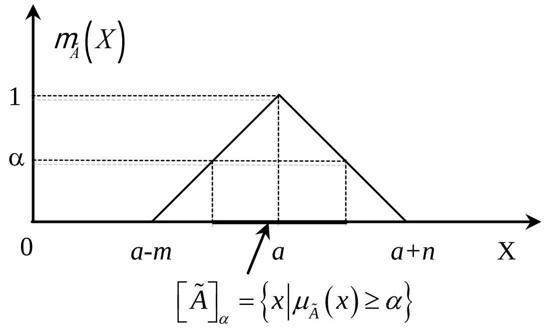

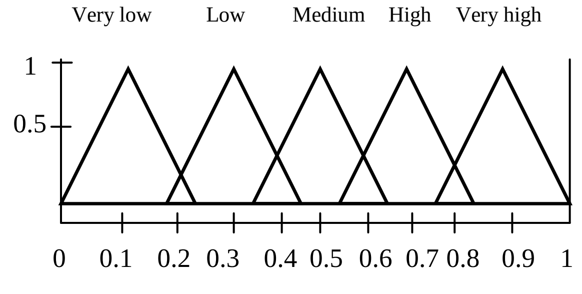

Fig. 4 The triangular fuzzy number and scale of the conversion of linguistic terms in fuzzy numbers

In references [4] the authors foresaw eight scales for conversion of linguistic terms.

With conversion scales it is easy to convert linguistic terms to fuzzy number, for example, linguistic term “low“ for a scale of 6 linguistic terms correspond to triangle fuzzy number (0.1,0.2,0.3).

The approach to extend TOPSIS method to the theory of fuzzy sets starts as the original method, with the identification of criteria, generating alternatives, evaluating alternatives in terms of criteria calculate and identifying the weight of criteria.

Methods can be represented by the following steps [5]:

Step 5:Construct the fuzzy decision matrix, where $\tilde{x}_{ij}$ is triangular fuzzy number $\tilde{x}_{ij}=(x_{ij},\alpha_{ij},\beta_{ij})$.

Step 6:Calculate the normalized fuzzy decision matrix. Therefore, each fuzzy is transform to an interval with *α-cut* concept as follows:

$$\tilde{x}_{ij}=\left[[\tilde{x}_{ij}]^L_\alpha,[\tilde{x}_{ij}]^U_\alpha\right],\alpha\in[0,1] \quad (11)$$

Now, we can transform this interval $\left[[\tilde{x}_{ij}]^L_\alpha,[\tilde{x}_{ij}]^U_\alpha\right]$ in to normalized interval as follows:

$$[\tilde{n}_{ij}]^L_\alpha=[\tilde{x}_{ij}]^L_\alpha\Big/\sqrt{\sum_{i=1}^{m}\left(\left([\tilde{x}_{ij}]^L_\alpha\right)^2+\left([\tilde{x}_{ij}]^U_\alpha\right)^2\right)}, \quad (12)$$

$$[\tilde{n}_{ij}]^U_\alpha=[\tilde{x}_{ij}]^U_\alpha\Big/\sqrt{\sum_{i=1}^{m}\left(\left([\tilde{x}_{ij}]^L_\alpha\right)^2+\left([\tilde{x}_{ij}]^U_\alpha\right)^2\right)}, \quad (13)$$

We can transform this normalized interval in to a fuzzy number $\tilde{N}_{ij}=(n_{ij},a_{ij},b_{ij})$ such that, n_{ij} is obtained when $\alpha=1$ tj. $\tilde{n}_{ij}=[\tilde{n}_{ij}]^L_{\alpha=1}=[\tilde{n}_{ij}]^U_{\alpha=1}$, also when $\alpha=0$ we have $[\tilde{n}_{ij}]^L_{\alpha=0}=n_{ij}-a_{ij}$ i $[\tilde{n}_{ij}]^U_{\alpha=0}=n_{ij}+b_{ij}$, then $a_{ij}=n_{ij}-[\tilde{n}_{ij}]^L_{\alpha=0}$ i $b_{ij}=[\tilde{n}_{ij}]^U_{\alpha=0}-n_{ij}$.

Step 7: $\tilde{N}_{ij}=(n_{ij},a_{ij},b_{ij})$ is normalized positive triangular fuzzy number, we can construct the weighted normalized fuzzy decision matrix as

$$\tilde{v}_{ij}=\tilde{w}_j\tilde{N}_{ij} \quad (14)$$

where $\tilde{w}_j$ is weight *j*-th attribute or criterion.

Step 8 Now, each $\tilde{v}_{ij}$ is normalized fuzzy number and their ranges is belong to $\left[0,1\right]$.

So, we can identify fuzzy positive ideal and fuzzy negative ideal solution as

$$\tilde{A}^{+}=\left\{\tilde{v}_1^{+},\tilde{v}_2^{+},...,\tilde{v}_n^{+}\right\} \tag{15}$$

$$\tilde{A}^{-}=\left\{\tilde{v}_1^{-},\tilde{v}_2^{-},...,\tilde{v}_n^{-}\right\} \tag{16}$$

where $\tilde{v}_i^{+}=\left\{1,0,0\right\}$ i $\tilde{v}_i^{-}=\left\{0,0,0\right\}$, $i= 1,...,n$ for each criteria.

Step 9:The separation of each alternative from the fuzzy positive and negative ideal solution is calculated by

$$\tilde{d}_i^{+}=\sum_{j=1}^{n} d\left(\tilde{v}_{ij},\tilde{v}_{ij}^{+}\right), i=1,2,...,m \tag{17}$$

$$\tilde{d}_i^{-}=\sum_{j=1}^{n} d\left(\tilde{v}_{ij},\tilde{v}_{ij}^{-}\right), i=1,2,...,m \tag{18}$$

Step 10:The realtive closeness coefficient is defined as

$$\tilde{R}_i=\frac{\tilde{d}_i^{-}}{\tilde{d}_i^{+}+\tilde{d}_i^{-}}, i=1,2,...,m \tag{19}$$

The coefficient is defined to determine the ranking order of all alternatives. Obviously, an alternative A_i is closer $\tilde{A}_i^{+}$ and farther from $\tilde{A}_i^{-}$ as $\tilde{R}_i$ approaches 1.

3. NUMERICAL EXAMPLE

Denote the possible potential locations of the regional logistics center in the following way A_1, A_2 *and* A_3. The attributes,which are critical for the selection of optimal location, are the folowing:

C_1- Investment costs
C_2- Labour costs
C_3- Traffic infrastructure
C_4- Region development possibilities
C_5- Climatic condition of region
C_6- Accessibility of labour

Fig.5 shows decision matrix of 3 alternatives under 6 attributes and their corresponding (and standardised) fuzzy numbers. Using defined methodologies, determine the distance of fuzzy positive ideal and negative ideal solutions as well as the relative closeness $\tilde{R}_i$ of which is used for final ranking (Fig.6).

		X_1	X_2	X_3
A_1		**55**	**54**	**75**
min				
A_2	Expert opinions	**Aproximately equal to 6.6**	**Aproximately equal to 7.2**	**Aproximately equal to 11.4**
min	Corresponding fuzzy numbers	(6.4,6.6,6.8)	(7.0,7.2,7.4)	(11.2,11.4,11.6)
	Standardised fuzzy numbers	(0.53,0.55,0.57)	(0.58,0.6,0.62)	(0.93,0.95,0.97)
A_3	Expert opinions	**Very high**	**Very high**	**Very high**
max	Corresponding fuzzy numbers	(0.8,0.9,1)	(0.8,0.9,1)	(0.8,0.9,1,1)
	Standardised fuzzy numbers	(0.8,0.9,1)	(0.8,0.9,1)	(0.8,0.9,1,1)
A_4	Expert opinions	**Low**	**medium**	**Very low**
max	Corresponding fuzzy numbers	(0.1,0.25,0.4)	(0.3,0.5,0.7)	(0,0,0.2)
	Standardised fuzzy numbers	(0.1,0.25,0.4)	(0.3,0.5,0.7)	(0,0,0.2)
A_5	Expert opinions	**High**	**High**	**High**
max	Corresponding fuzzy numbers	(0.6,0.75,0.9)	(0.6,0.75,0.9)	(0.6,0.75,0.9)
	Standardised fuzzy numbers	(0.6,0.75,0.9)	(0.6,0.75,0.9)	(0.6,0.75,0.9)
A_6	Expert opinions	**Very low**	**Very low**	**Very low**
max	Corresponding fuzzy numbers	(0,0,0.2)	(0,0,0.2)	(0,0,0.2)
	Standardised fuzzy numbers	(0,0,0.2)	(0,0,0.2)	(0,0,0.2)

Fig.5 Fuzzy matrix of decision [8]

The best alternative is one that is closest to the fuzzy positive ideal solution and farthest from the fuzzy negative ideal solution.

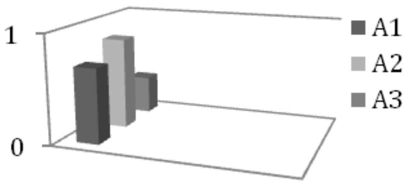

Fig. 6. *The coefficient of closeness and the ranking of alternativies by decision maker*

4. CONCLUSION

The idea of this paper is to give theoretical grounds, the methodology of selecting and ranking the different optimal locations using the hybrid method of multiple criteria. A special part of the analysis belongs to the extended TOPSIS method, reviews the theoretical basis and methods of application itself demonstrated. Multicriteria decision making can occupy a significant part of the selection process of potential location, where the process is based on data whose type is sometimes unclear, resulting in an increasing need for combining existing models and algorithms to the theory of fuzzy sets. Increase the objectivity of decision making in choosing the optimal location of the regional logistic center is possible by applying a mathematical model of fuzzy logic or a combination of several methods for determining the weights.Of course, the methodology presented as a relatively simple and present a solution can be applied to solve other real problem to many areas of management decision,especially in the process of defining a new profile of regional logistics.

5. REFERENCES

[1] Marković G., Gašić M., Marinković Z., i dr.“Suština i značaj formiranja regionalnog logističkog koncepta-strateški pravci razvoja”,Četvrti simpozijum sa međunarodnim učešćem Transport i logistika 2011, Niš.

[2] Marković G.,Gašić, M., Marinković Z.“Teorijski pristup regionalnom razvoju-metodologija istraživanja logističkih tokova”,IMK-14 istraživanje i razvoj, Godina XVI, broj 4/2010, str.25-30, 2010.

[3] Farahani R. Z., SteadieSeifi M., Asgari N.: Hosseinzadeh L., Izadikhah M.: “Multiple criteria facility location problems: a survey”,Applied Mathematical Modelling 34, 2010.

[4] Chen S.J.,Hwang C.L.“Fuzzy Multiple Attribute Decision-Making:Methods and Applications”,Springer-Verlag,New York, 1992

[5] Jahanshahloo G.R., Hosseinzadeh L., Izadikhah M.“Extension of the TOPSIS method for decision-making problems with fuzzy data”, Applied Mathematics and Computation 181,2006.

[6] Olcer A.I.,Odabasi A.Y.“A new fuzzy multiple attributive group decision making methodology and its application to propulsion/manoeuvring system selection problem”,Europian Journal of Operation Research 116,2005.

[7] Lai Y.J.,Liu T.Y.,Hwang C.L.“TOPSIS for MODM”, European Journal of Operational Research 76 (3),1994.

[8] Marković G., Bukumirović M., Čupić A:“The Decision Methodology Of Optimal Location Of Regional Logistic Centre”,VI International conference HM2008, Mataruška Banja,2008.

[9] Slavoljub M.“ Metodologija izbora glavnih poštanskih centara i lokacije poštanskih centara”, PosTel 2007,25 simpozijum,Beograd,2007

[10] Bukumirović M.,Čupić A.“Primena višekriterijumske analize u izboru opreme za sortiranje paketa”,PosTel 2007,25 simpozijum,Beograd,2007.

[11] Zadeh L.A.“Fuzzy sets”, Informations and Control 8, 1965.

[12] Teodorović D.“Fuzzy set theory applications in traffic and transportation”, Europian Journal of Operation Research 74/3,1994,

[13] Yu P. L.“Multiple-Criteria Decision making, Concepts, Techniques and Extensionss”,Plenum Press, New York, 1985.

[14] Bukumirović M., Gašić M., Savković M., Marković G.“Regional city logistics and supply chains in machinery”,V International conference HM2005, Mataruška Banja, 2005.

HEAVY MACHINERY - HM 2011, 71-80
ISBN 978-86-82631-58-3
Paper accepted: 30.05.2011

Railway Vehicles As The Source of the Noise in the Urban Areas

Bojan Tatić[1,*] – Nebojša Bogojević[1] - Zlatan Šoškić[1] - Zoran Petrović[1]
[1]University of Kragujevac, Faculty of Mechanical Engineering Kraljevo

One of dominant sources of noise and vibrations in urban areas is road and rail vehicles traffic. Rail transport is generally considered as one of the most environmentally friendly transport modes. However, the contribution of rail transport to noise pollution can be substantial. The main sources of the noise and vibration from various types of the rail vehicles are: rolling noise, curve squeal, bridge noise, aerodynamic noise and ground vibrations. Factors which significantly influence the level of noise generated by rail vehicles are vehicle speed, vehicle weight, number of wheelsets, type of breaks, curve radii. In order to reduce the noise levels, European Commission has started harmonizing the norms from different European countries into one directive. Until 2014 the new directive should be mandatory for all rail vehicles in Europe in order to achieve sufficiently low level of the noise emission.

Keywords: Noise, traffic noise, railway vehicles.

1 INTRODUCTION

Noise is an unpleasant sound, which negatively affects the physical condition of people. Characteristics and type of noise are determined by physical characteristics of sound-wave phenomena. The appearance of noise is related to working and living environment. When it comes to work environment, there are various measures to protect employees from noise generated in the workspace. In this regard, the noise of the environment isn't a complete protection against noise generated around the area where people live. The obligation of local authorities in the settlement of its activities is to protect its citizens from the source of the noise in the living environment. For this purpose it is necessary to create noise maps settlement, which would define level of noise in regions of origin and determine the source of the noise. In that case appropriate protection from noise is designed according to the noise maps.

A characteristic of modern urban areas is rapidly expanding as a result of that migration from rural areas into suburban and urban area, and migration among cities that arise as a result of uneven economic development. One of the primary sources of noise in urban areas is transport. Urban and suburban areas by their geographical position and role destined to be the intersection of land transport. As a result, road and rail transport are very present in urban areas, linking the spread of the land transport routes that extend outside the urban areas, as is clearly seen in the example of town Kraljevo, as it is shown in Figure 1.

Fig.1. *Transportation network of the urban area of Kraljevo*

Rail transport is the cheapest form of land transport, especially when we talk about to transport large amounts of goods. Urban development has contributed to the railway junction in these cells become very important in the regional transport of goods. As a result of the expansion of cities, the main railway stations are located in the central parts of cities, and railway lines pass through densely populated urban areas, making noise of rail

*Corr. Author's Address: Fac. Mech. Eng. Kraljevo,Dositejeva 19, 36000 Kraljevo, Serbia, tatic.b@mfkv.rs

transport as one of the elements of noise in urban areas. In order to protect the population in proper way from the noise of railway vehicles impact it is necessary to analyze the sources of noise that occur during the passage of trains along the track.

2 THE CHARACTERISTICS OF NOISE

Noise is described by physical sizes that are normally characterized by sound. The volume, pitch and timbre are three basic characteristics of sound and they are certain objective characteristics of sound wave that we describe, the intensity of the frequency, spectrum and harmonic waves.

The strength (intensity) of sound can be subjective and objective size. Objective volume is displayed as the energy emitted sound signal through the unit normal area per unit time and measured in units W/m^2. The subjective strength of the human ear is the ability to sense the volume, which is the logarithm of the intensity of the observed relationship of sound and intensity to detect the weakest of men's ear, and measured in units bell [B].

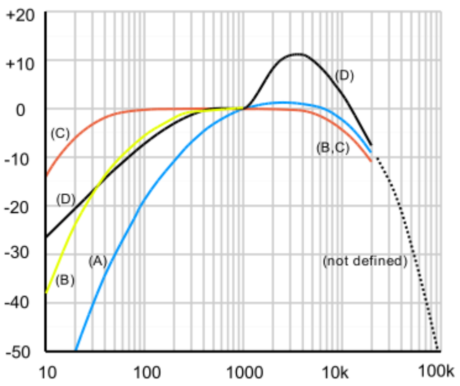

Fig.2. *Acoustic weighting curves:A-weighting(blue), B(yellow), C(red) and D-weighting(black)*

The subjective sense of strength volume is assessed by several weight functions, as it is illustrated by Figure 2. The most methods for determining the volume of the subjective application of weight functions A and C. A-weighting ($L_{A,eq}$) is the most used weighting curve that represents numeric value the sound pressure level over frequency-weight in accordance with a reference wavelength that simulates human hearing response at low sound. C-weighting ($L_{C,eq}$) shows the numeric value the sound pressure level over frequency-weight in accordance with a reference wavelength that simulates human hearing response to sound high-level.

R.M.S. of sound represents statistical size of the root mean square value of pressure during a certain interval [3]:

$$p_{rms} = \left(\frac{1}{T}\int_{t_1}^{t_1+T} p^2\,(t)dt\right)^{1/2} \qquad (1)$$

where:

$p(t)$ - the sound pressure at time t,

T –time averaging.

The equivalent continuous sound pressure level ($L_{eq,T}$) is the sound level corresponding to the middle noise values of sound power during the time period, calculated on the basis of sound pressure and the formula used is [11]:

$$L_{eq,T} = 10\,log\,\frac{1}{T}\int_0^T \left[\frac{p(t)}{p_0}\right]^2 dt \qquad (2)$$

where:

T – the measurement period,

p_0 – reference sound pressure of 20 μN/m^2.

3 THE SOURCES RAILWAY VEHICLES NOISE

When the movement of trains along the track creates sound waves that result from:

- interaction between wheel and rail,
- interaction of the surfaces in contact in circuits of wagon,
- interaction of the outer surface of locomotives and wagons with air in motion,
- interaction between the track and the substrate on which is placed,
- interaction between wheel and brake,
- operation of basic and additional equipment in locomotives and wagons.

It is common that in the circumstances under which it accrues, railway vehicles noise is classified in the following categories::

- rolling noise,
- wheel squeal,
- curve squeal,
- aerodynamic noise,
- bridge noise,
- ground noise and vibration,

- internal noise and vibration,
- other source of railway noise.

Based on the frequency spectrum, the sources of railway vehicles noise are classified according to the following Table 1:

Table 1. *Frequency range for different types of railway noise [7]*

Noise type	Frequency range [Hz]
Rolling	30 - 5000
Flat spots	50 - 250 (as a function of speed)
Ground borne vibrations	4 - 80
Structure borne noise	30 - 200
Top of rail squeal	1000 - 5000
Flanging noise	5000 - 10000

Individual impact of the sources of noise on the overall noise level of trains in motion depends on many factors such:

- weighing railway vehicles,
- radius of curve,
- speed,
- number of axles per vehicle,
- number of vehicles in the train composition,
- type of rail,
- type of brakes and brake-block material,
- there is no contact lubrication,
- method of modification friction.

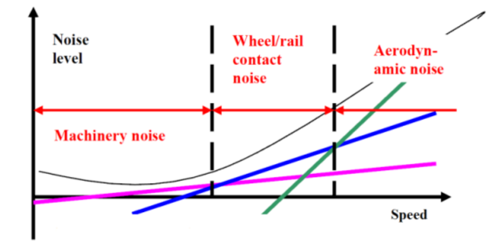

Fig.3. *The noise level comprises contribution from the machinery, the wheel/rail contact and from aerodynamic flow*

Some of these factors are primary factor for the occurrence of certain types of noise, while on other less common sources of noise. So, for example, the onset of squeal (regardless of whether the wheel or curve), radius of curve has a dominant influence. Speed of movement is the primary factor in many sources of noise, and it was sometimes the main factor determining the source of noise that will be dominant, as can be seen from Figure 3.

Form that calculates the noise during acceleration of the train, in function of the speed the train is [11]:

$L_{A,max} = 10\ log(10^6 \cdot K + 447 \cdot V^3)\,[dB]$ (3)

where:

$L_{A,max}$ – maximum A-weighted sound pressure level recorded by a sound level meter set to the standard “Fast” response over the time for the train to pass the microphone,

K – traction noise factor in accordance with Table 2 below,

V – train speed in km/h.

Table 2. *Noise factor K for traction power ratings [11]*

Vehicle Power Range [MW]	Diesel traction	Electric traction
Above 1.0	3160 (95)	1000 (90)
0.3 to 1.0	1260 (91)	400 (86)
Below 0.3	500 (87)	160 (82)

The noise emitted from a train when running at is maximum normal operating speed, with traction equipment idling gets the form [11]:

$L_{A,eq} = 40 + 20\,log\,V + 10\,log\,N \cdot 10\,log\,t\,[dB]$ (4)

where:

N – number of axels in train,

t – time for train to pass microphone [s].

Otherwise, these values of noise levels and noise levels of the value of static (immovable) of the train, obtained by measuring the vertical range of the microphones on the side of the train, the horizontal distance of 7.5m from track centerline at heights of 1.5m to 3.5 above the top of the rails. If we look at the value of C-weighted sound pressure level , the values obtained must not be higher for more than 7 dB compared to those obtained via the A-weighted sound pressure level.

3.1 Rolling noise

Rolling noise is the result of vibration wheel and vibration tracks that appear in direct contact with the wheel/rail due to roughness (asperity) on the surfaces in contact, as it is illustrated by Figure 4 and as it is modeled by Figure 5. It is dominant noise source at speeds of conventional trains.

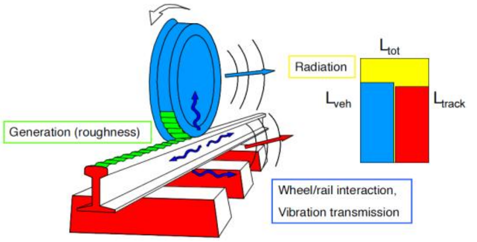

Fig.4. *Illustration of the mechanism of generation of the rolling noise*

Rail roughness occurs due to prolonged use and the passage of large number of train compositions, influenced by weather conditions, especially in winter due to freezing of water in micro cracks, due to the rail wheel skid etc. Roughness point increase in long-term use of wheel traffic, but also depends on the type of brakes that are fitted on the wagons, the entire state assembly wheel set or bogie.

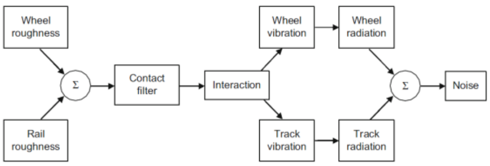

Fig.5. *Model for rolling noise generation*

It is difficult to accurately determine whether the noise comes from the wheel or the infrastructure, although it is known that a high level of noise comes by irregularity of wheels. Irregularities on wheel form waves on the surface of wheel the wavelength values of 5-500mm. If the λ [m] denote the wavelengths and the v [m/s] speed, we can calculate the frequency of the waves through the following relationship [1]:

$$f = \frac{v}{\lambda}\ [Hz] \qquad (5)$$

When contact the wheel/rail, contact isn't in the spot, but when contact the surface of irregular shape, the effects of roughness in the contact zone are small. They come to the fore the occurrence of wave frequencies from 1 to 1.5 Hz and at speeds exceeding 160 km/h or at lower frequency waves at lower speeds.

Therefore, the A-weighted sound pressure level is usually calculated as proportional to the logarithm of speed [1]:

$$L_p = L_{p0} + N \cdot log_{10}\left(\frac{V}{V_0}\right) \qquad (6)$$

where:

L_{p0} – the sound level at a reference speed V_0 ,

$\boldsymbol{N}$ – values of the speed "exponent", determined from measurements on the basis of linear regression, are usually found to be between about 25 and 35, with a typical value of 30.

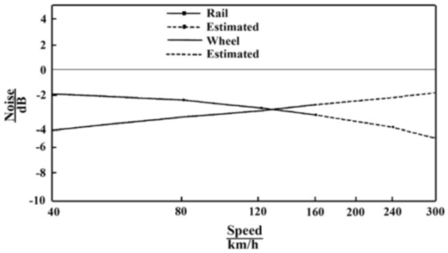

Fig.6. Estimated components of wheel and rail noise relative to A-weighted level as a function of train speed

These considerations suggest that doubling the speed corresponding increase A-weighted level of 8 to 10 dB. Speed affects the dynamics behavior of the wheel and the dynamics behavior of the rail, but also on their interaction and must be taken into account when considering the problem as in Figure 6.

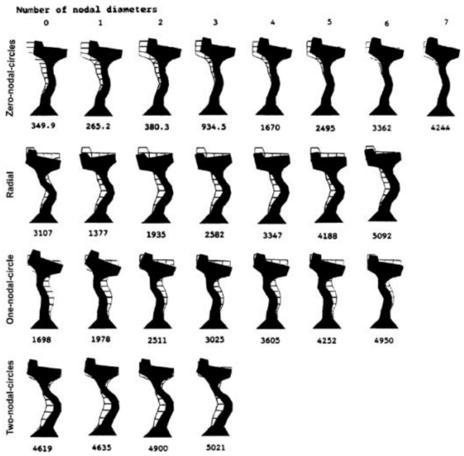

Fig.7. Modes of vibration of a UIC 920mm standard freight wheel shown in cross-section and natural frequencies in Hz

Dynamics behavior of the wheel is seen through the analysis of vibration modes and natural frequencies. Railway wheel design is slightly damped resonant structure. Due to the movement and interaction with the rail, the wheel acts like any other element that vibrate own and natural oscillations. The wheel is like new axle-symmetrical and when is new has no impact places (noodle place diameters) while in use to a greater or lesser extent they appear. Because of this phenomenon comes to the valuation of such oscillations is shown in Figure 7 for a wheel diameter of 920-mm for freight wagons in cross-section.

Especially for mid to wheel and rail is one mechanical system, due to mutual contact wheel oscillates near the rails or track. Rail is connected to a rigid threshold which can be wood or concrete, that all relies on a set of clay and partly covered with ballast. If we accept that link of the rail with the threshold is absolute rigid and the threshold motionless, there was a rail oscillations due to vertical forces that occur in contact with the wheel/rail. Mostly it comes to frequency of the order of 500-1000 Hz.

3.2 Wheel squeal

The main cause of wheel squeal is curving noise. It consists of two kinds of squeal and:

- squeal of flange of wheel,
- squeal in contact the wheel/rail due to the appearance longitudinal stick-slip and lateral slip.

Longitudinal stick-slip phenomenon is the noise of high frequency noise due to the different speeds of the wheels of wheel set on inner and outer rails. The radius of curve, the model (geometry) of wheel and the profile of rail, as well as speed, are the main factors affecting the level of noise that occurs in these cases. The radii of curve up to 600m can reduce this noise compensation speed, while for smaller radii can reduce noise by grinding rails.

Lateral slip is the noise that occurs due to lateral slip surface of wheel on the upper surface of rail, and that is the main cause of this type of noise. This type of noise is most evident when entering the curve with a cant deficiency of rail, as illustrated in Figure 8.

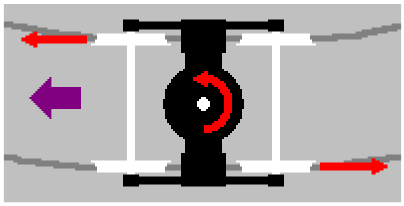

Fig.8. *Schematic of a Rail bogie in a curve*

On that occasion, it creates noise wreath wheel while touching the inside of the rails. By the effect of centrifugal force of the internal crown ,wheel moves away from the inner (or lower) rails, while the crown wheel on the outside (or higher) rail contacts the inner edge of the son as in Figure 9. Profile of wheel should be allowed to touch the surfaces in such cases less due to increased wear. Reduction of friction lubricants are often used. Frequency band noise resulting from wheel squeal is in the range 1400-1600 Hz, depending on the geometry of wheel and rail.

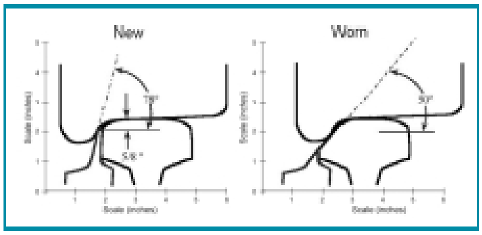

Fig.9. *Actual Wheel & Rail Profiles*

Frequency range of noise known as wheel squeal is around 3000-4000Hz, and these sounds are very high pitched and unpleasant for a person's hearing. Wheel squeal occurs in freight wagons because of the high pressure shaft, which causes an increase in wheel and rail surfaces in contact. There are several solutions to reduce these types of noise such as the Japanese railways employ a method of partial lubrication oil spray special rails that are on the front of the locomotives near the top of rails, dropping oil only when entering a corner to reduce wheel squeal. Australian railways uses specially designed blockers that mounted the suspension to reduce wheel slip by rail.

3.3 Aerodynamic noise

Due to the passage of solid bodies through the air creates a laminar flow of air around the body. However, if speed is high, close to the solid state is coming to the emergence under pressure which causes turbulent air movements, which created sound waves, as on Figure 10.

The level of aerodynamic noise can be expressed as a function of train speed and strength of the external surface of the wagon. Increasing speed increases the influence of aerodynamic noise in the overall level of noise in movement and composition is typically in the range of *(60-80)*$log_{10}V$. This type of noise is very pronounced in high-speed train and a negative impact on the environment, but also on the acoustic comfort of travel.

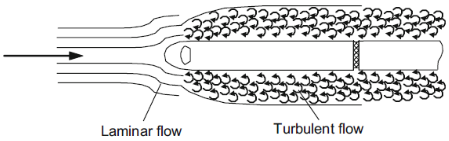

Fig.10. *Aerodynamic moving*

The aerodynamic noise generated on the front of the locomotive, in the spaces between the wagons, carriages on the sides if the sides are made of elastic material, the burden is not compressed during transport open types of freight wagons on the sides due to gust, the pantograph, etc… The values of aerodynamic noise in some places are different, and approximates the sound energy is expressed that occurs [1]:

$$W_{rad} \propto \frac{\rho_0 \cdot U^8 \cdot l^2}{c_0^5} \qquad (7)$$

where:

l – the width of the flow,

U - flow velocity,

c_0 – the speed of sound,

ρ_0 – the fluid density.

Measurement of aerodynamic noise carries out a number of microphones arranged in height and length in the "stellar" form, or in concentric circles, as in Figure 11.

The measurement was shown that the size of the aerodynamic noise at high-speed train TGV (when the velocity of 200 km/h) ranges from 92dB on the frontal glass and the rear locomotive pantograph up to 79dB on the bogie. At high-speed train ICE these values are similar values. Acoustic noise, caused by the movement of railway vehicles, a low-frequency sound waves with noise levels of 60 dB for a speed 100 km/h to 110 dB at speeds of nearly 500km/h.

Reduction of aerodynamics noise is done by defining the appropriate aerodynamic shape of locomotives and trains, but mounting the protector of the basic elements of aerodynamic pantograph. Spaces between the wagons to shut special elastic materials that prevent the occurrence of turbulence in the spaces between the wagons, and again the composition do not violate the security of enrolling in a corner. It also made the side "cover" bogie which prevents air streamlines that pass through a bogie. An interesting choice of engineers high-speed train Eurostar's to get the budget to open diameter of 75mm and a depth of 0.5m makes reduction of frequencies over 300Hz to about 10dB.

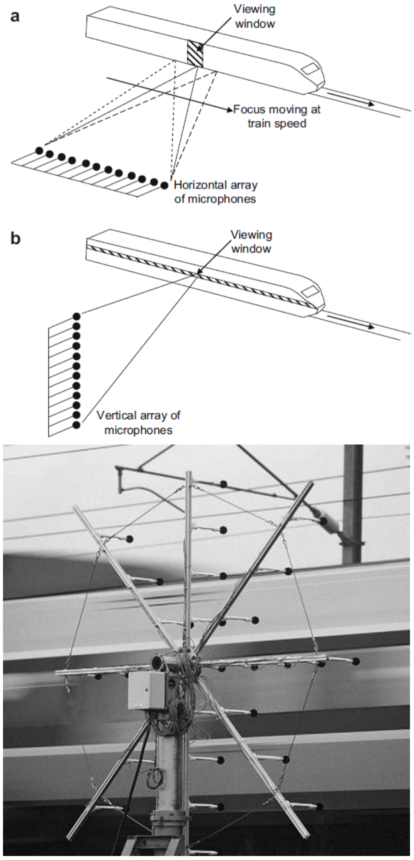

Fig.11. Principles of microphone array:(a) horizontal array with swept focus, (b) vertical array and (c) example of star-shaped microphone array consisting of 29 microphones

3.4 Ground noise and vibration

Besides the noise, it is expressed due to the passage of vibration phenomena of the composition. Specifically, the passage of the train movement can be seen as a rigid body on elastic base. Elastic properties of the substrate condition are creating waves in the environment that we feel as low-frequency vibrations of the ground. This phenomenon is most evident when cargo composition moves with a large number of wagons.

The movement of waves through the surface is expressed in all directions:
- along the direction of movement,
- sideways movement and direction and
- perpendicular to the direction of movement.

There are two methods of calculating the level of vibration when going composition [1]:

1. **Vibration dose values (VDV)** – defined to quantify intermittent vibration. The VDV for a single event is:

$$VDV = \left[\int_0^T a^4(t)dt\right]^{0.25} \left[{}^{m}/_{s^{1.75}}\right] \quad (8)$$

where:
T – the duration of the event,
$a(t)$ – the frequency weighted (filtered) acceleration as a function of time.

The total values of train are:

$$VDV_T = [VDV_1^4 + VDV_2^4 + VDV_3^4 + \cdots]^{0.25} \quad (9)$$

2. **KB value** – uses a running root-mean-square vibration velocity measurement (based on a 0.125 second time constant).

$$KB_{FTr} = \sqrt{\frac{1}{T_r}\sum_j T_{e,j} \cdot KB_{FTm,j}^2} \quad (10)$$

where:
T_r – the evaluation period,
$T_{e,j}$ – the exposure period of each event j,
$KB_{FTm,j}^2$ – the average of the maximum filtered r.m.s. signal values during each 30 sec interval of the whole event.

If there is the substrate steel construction of the bridge, then we talk about the bridge noise. It is specific due to increased enforcement and self-oscillation. The uniqueness of the bridge noise is seen in the fact that there is partial ability to reduce the noise and the use of the fastener stiffness, rail damping, and ballast mats, damping of bridge structure, plate thickness, barriers and enclosures etc.

4 METHODS OF NOISE REDUCTION OF RAILWAY VEHICLES

Noise control can be applied during design of new or redesign of existing vehicles and it has to be retained during maintenance of vehicles and tracks.

For **rolling noise** the following applies:
- smooth wheels and smooth tracks ensure minimal **noise generation**; this implies
    - the use of braking systems that maintain smooth wheel running surface such as disc or drum brakes or composite-block brakes for block-braked vehicles, and
    - appropriate maintenance of the tracks and the wheels;
- compact, massive design incorporating vibration isolation and high damping ensures a minimum of **structure-borne noise transmission** in the track and the wheels. Examples are:
    - smaller wheels and/or wheel dampers, optimized wheel geometry;
    - fewer wheels;
    - wheel-mounted disc brakes;
    - optimized track design, or rail damping devices in combination with railpad selection;
- shielding (secondary measures) can reduce radiated sound, by applying
    - wheel-mounted, bogie-mounted or vehicle-mounted shrouds;
    - low noise barriers close to the rail.

For **traction** noise the following applies:
- for diesel driven locomotives, a low noise design should be ensured for new vehicles, although retrofit may be possible. Noise control measures are:
    - appropriate exhaust and intake design (high insertion loss);

- effective engine enclosure and vibration isolation;
- selection of quieter components such as turbocharger, compressors and fans.

A fundamental issue is that noise specifications are often set for unloaded pass-by, whereas in many operational conditions, locomotives pull a heavy load, producing high noise levels.

- For **electric** locomotives and high speed trains, especially the noise from the cooling equipment can be a problem. This is best tackled in the design stage, although sometimes retrofit may be possible. This might include:
  - elimination or smoothening of obstacles in ducts, intake and outlet;
  - quieter fan design;
  - increase in fan efficiency by selecting the best working point.
- For lower speeds, gear noise can be a problem. This must be dealt with in the design phase. One reduction technique is to create sufficient overall contact ratio in the gear mesh.
-

For **aerodynamic** noise the following applies:

- for high-speed trains the aerodynamic noise can be a predominant noise source at speeds above 250 km/h, with contributions from various heights. Noise barriers lower than 4 m have insufficient effect on sources located at the top of the vehicle such as the pantographs and their recesses. Aerodynamic noise can be reduced by:
  - streamlined covers for the bogies;
  - avoiding extruding parts or cavities along the train;
  - streamlining and covering of the pantograph and its recess area;
  - streamlined front of the vehicle.

At present, the following technology is available for the various noise sources:

- **traction noise**: in principle, all of the above mentioned noise control measures are available to minimize traction noise at the design stage. The remaining issues are then the cost and maintainability. Retrofitting only for the purpose of noise reduction is generally not economically feasible;
- **rolling noise**: the most effective means of control is that of wheel and rail roughness. Here the technology is available (K-blocks/disc brakes, rail grinding systems) but also depends on the cost. Add-on systems such as rail and wheel dampers are available but have limited effect; in particular the effect is not always measured properly, if wheel and track contributions are not separated. The same is true for wheel and bogie shielding. New design of wheels and tracks provides the next best option after roughness control; vehicles with smaller and less wheels, and quieter track design are longer term, but beneficial investments. Local application of low noise track has got the potential to reduce noise at low and medium speeds. This can even be applied for cast iron brake blocked vehicles, thereby adding to the effects of long term retrofit programs before all retrofitting is complete;
- **aerodynamic noise**: recent generations of high speed trains have illustrated the improvements in this field; the streamline design of new trains often benefits both noise and energy consumption. Further streamlining is possible, in particularly the covering of the bogie areas; this however has cost and maintenance consequences.
-

Noise barriers are the most commonly applied noise abatement measure applied in the propagation path. They are applied on a wide scale both on existing and new lines. Typical noise reductions are up to 10 dB depending on the barrier height, distance to source and receiver, and barrier absorption. In many cases barrier performance is severely limited by the track layout (e.g. multiple tracks), the height of the sources and by the height of adjacent multi-story residential buildings. Barrier performance is best if the barrier is close to the source or to the receiver. Noise barriers are generally less cost effective than noise control measures at the source. Barriers also have got other disadvantages such as visual intrusion and high cost. Another way of reducing sound propagation near railways is the construction of non-noise sensitive buildings between the railway and other residential buildings.

5 CONCLUSION

The dominant noise sources in individual urban regions must be detected ,well planned and well executed by measuring the noise level. Based on these measurements, it is necessary to create noise maps and discern the dominant sources of noise coming from the railway traffic. Depending on the level exceeding the noise levels higher than allowed or acceptable values, it is necessary to choose an adequate principle of noise reduction. This reduction can be made by active methods (reducing the impact of noise in the noise source) or passive methods (preventing the spread and impact already made noise in the noise source). Economic opportunities dictate the quality of the works intended for noise reduction. The local governments, owners of rolling stock, the company that designs and maintains railway infrastructure and rail vehicles and manufacturers as well are interested in decreasing the level of noise.

6 REFERENCES

[1] Thompson, D., “Railway noise and vibration – Mechanisms, modeling and means of control”, Elsevier Ltd, UK, 2009.

[2] Iwnicki, S., “Handbook of railway vehicle dynamics”, CRC Press Taylor & Francis Group, Boca Raton, USA, 2006.

[3] Zlatković, A., “Analiza upravljanja bukom kod železničkih vozila”, Diplomski rad, University in Belgrade, Saobraćajni fakultet, Belgrade, 2010.

[4] Torija, A.J. et al., “Relationship between road and railway noise annoyance and overall indoor sound exposure”, in Transportation Research Part D 16 (2011) 15-22, Elsevier Ltd, UK, 2010.

[5] Oertli, J., Hübner, P., “Railway noise in Europe – A 2010 report in the state of theart” UIC, Paris, France, 2010.

[6] Bühler, S., “Rolling noise in railway vehicle type testing”, Recent Developments, in Forum Acusticum, Switzerland, 2005.

[7] Eadie, D.T., Santoro, M., Kalousek, J., “Railway noise and the effect of top of rail liquid friction modifiers: changes in sound and vibration spectral distributions in curvies”, in Wear 258 (2005) 1148-1155, Elsevier Ltd, UK, 2005.

[8] Watson, R., Sohail, M., “Reducing railway noise level - the impact of forthcoming European legislation”, Department of Civil and Building Engineering Loughborough University, Loughborough, UK, 2008.

[9] Tickell, C.E., Downing, P., Jacobsen, C.J., “Rail wheel squeal – Some causes and a case study of freight-car wheel squeal reduction”, in Acoustics 2004, Gold Coast, Australia, 2004.

[10] Dirks, B., Wiersma, P.K., “Asymmetric rail profile to prevent railway squeal noise”, in INTER-NOISE 2007 Istanbul, Turkey, 2007.

[11] Boocock, D., “Design code of practice: Noise and pollution from new railway vehicles”, Safety&Standards, Directorate Rail Track PLC, London, UK,1996.

[12] Jansen, H.W., ”Noise and vibration measurements of freight wagons with LL and K brake blocks for TSI compliance testing”, TNO report MON-RPT-033-DTS-2007-03512, Utrecht, The Netherlands, 2007.

[13] Department of Environment Climate Change NSW, “Interim Guideline for the Assessment of Noise from Rail Infrastructure Projects”, Sydney, 2007.

[14] Dittrich, M.G., “IMAGINE railway noise source model, default source data and measurement protocol”, Technical Report Project: Improved Methods for the Assessment of the Generic Impact of Noise in the Environment - IMAGINE”, WP6, EU, 2005.

[15] Jones, R.R.K., “Measured railway noise source data in the public domain or via the IMAGINE projects”, Technical Report Project: Improved Methods for the Assessment of the Generic Impact of Noise in the Environment - IMAGINE”, WP6, EU, 2005.

[16] Tomičić-Torlaković, M., Stefanović, S., “Railway noise and vibration – current European legislation and research and measurements on Serbian railway”, Facta Universitatis, series: Architecture and Civil Engineering vol. 8 Nº2 pp. 145-153, Belgrade, Serbia, 2010.

[17] WG Railway Noise of the European Commission, Position Paper on the European strategies and priorities for railway noise abatement, ISBN: 92-894-6055-5, Luxembourg, 20

HEAVY MACHINERY - HM 2011, 81-86
ISBN 978-86-82631-58-3
Paper accepted: 30.05.2011

Noise Protected Buildings

Zoran Petrović[1,*] - Branko Radičević[1] - Zlatan Šoškić - Momir Praščević[2]
[1] University of Kragujevac, Faculty of Mech. Engineering Kraljevo
[2] University of Nis, Faculty of Occupational Safety Nis

This paper presents the example of activities to protect occupants from the noise. The analysis was made in case when the boiler for heating of the building and the surrounding colony is settled in the basement of the building. As has often been the case earlier in the design of new settlements heating boilers were housed in the annex building or basement area. As the colony grow, the changes were made in the technology of heating and to increase of heating capacity. Accordingly , there came deterioration of conditions in terms of noise in apartments. In our example, we analyzed primary and secondary sources of noise and their impact on the occupants in the building. On the basis of the analysis of noise levels and insulating capabilities of the walls and ceilings the measures for noise reduction are proposed. Combined methods of active and passive noise abatement measures have been applied in phases in order to achieve a satisfactory level of noise in the most affected dwellings. The paper also presents some results, achieved improvements, derived measures of protection against noise.

Keywords: noise reduction, boilers, fan noise control

0. INTRODUCTION
1.

The solutions of eliminating high levels of noise in these cases are particularly interesting and challenging because the space is limited and there is a greater number of devices and machines that are sources of noise. In this case the engine-room is equipped with two boilers from the 4000 kW, two radial fan for a flue gas 5.5kW and 7.5kW power, the heating pump motor power 18.5kW and pressure maintenance pump motor power 0.55kW. In addition, there are also secondary sources of noise during operation. For example, due to the flow of smoke in the chimney flue pipe noise occurs, also, the noise occurs due to attenuation and air supply to the burner so that the exploitation regimes at lower noise levels appear higher.

The poor quality of mechanical structures, loosening of ties, wear elements also cause a secondary noise. Particularly important is regular and proper maintenance.

1 ANALYSIS OF NOISE SOURCES

Boiler room equipment is housed in the basement of the residential building with five floors and is used for heating not only the building it self but the entire surrounding part of t he town. All equipment is allocated in three rooms. In the first-central room are located two boilers and flue gas fans, which are the main sources of noise. In the second (left to the entrance) room there are circulation pumps for heating and in the third room is fuel (fuel oil).

The disadvantage of this layout is that the loudest devices are just below the apartments. The chimney is physically located in the center of the building so that the sound generated from the oil burning in furnance and the operating fan transfers into the building as airborne sound and the second part as structural sound. Figure1. shows the layout of equipment and position of the nearest apartment.

Because the equipment operates together and there is an increased level of noise, intensity is measured individually for each sound source, bouth in the boiler room and upstairs in the hallway outside the apartments. The results of measurements are shown in Table1.

Table 1 View the noise level in the boiler room and the floor in dB

Noise Sources	Level in boiler room	Level in the build.
Circul.pump	83	44
Boiler 1	90	43
Boiler 2	89	43
Boiler 2 + Fan2	92	49
Fan 2	89	47
Burner Nozzle	104	is set aside

* Corr. Author's Adress: Faculty of Mech. Engineering Kraljevo, Dositejeva 19, Kraljevo, Serbia, petrovic.z@mfkv.rs

The results can be concluded about the impact in each of the individual sources.

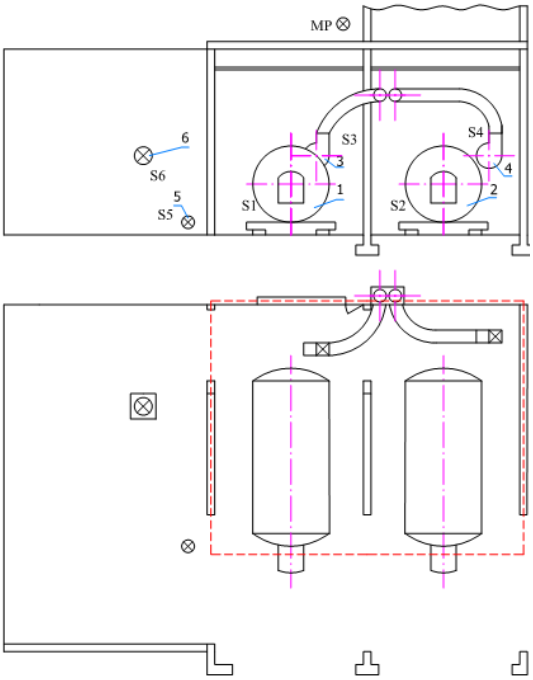

Fig.1. Layout of boiler room

1- boiler No. 1; 2 – boiler No. 2; 3 – flue gas fan (No.1); 4 - flue gas fan (No.2); 5 – pump to maintain pressure; 6 – circulation pump

Circulation pump item.6 located in room 2.(Left to the boilers room) has relatively the same effect on noise in the hallway as boilers, because it is structurally connected to the ceiling and the insolation between the room and hall is much weaker. In this case there is a transfer of airborne and structural noise. Structural noise is transmitted through the pipe and support structure.

Boilers and fans according to Table1. have a single noise level around 90dB. In case when operating both, the boiler and flue gas fan, the noise level increases from 3 to 4dB.

As the fan 2 can be switched on without activating the boiler the measured intensity noise in the boiler room is 89dB and 47dB in hallway of the building. So on the basis of Table 1. it is shown that the highest noise level was transmitted from the Fan2. to the hallway, because sum of the noise level of the boiler 2. and the fan 2 is two decibels higher than the fan2. itself. It is clear deth a fan2 is dominant noise source.

Equation (1) shows that the influence of the boiler to the level of noise in the hallway is:

$$L = 10 \bullet \log\left(10^{L_t/10} - 10^{L_f/10}\right) = 45 \text{ dBA} \qquad (1)$$

where: L_t = 49 dBA- total level of noise
L_f = 47 dBA-fan noise

The importance of eliminating noise from the fan thus becomes the most important.

Measurements in an apartment above the boiler room which were obtained by an equivalent noise level values are presented in Tab.2. It occurs when boilers operate individually and together. In both cases the circulation pump was turned on.

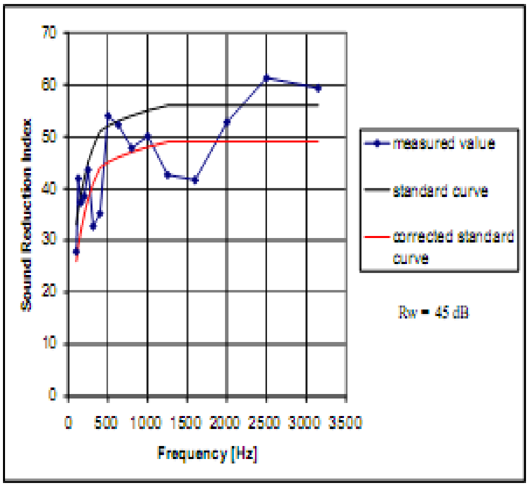

Fig. 2 Assessment of sound insolation

Table 2 Levels of noise in the apartment

Noise Sources	Living Room	Bedroom
Boiler 1	46	47
Boiler 2	41	47
Both the boiler	47	48

As can be seen from Table2. the noise levels at day and night conditions exceed the permissible limits and they are 13 dBA at daytime and 18 dBA at night.

After the measurements of equivalent noise pressure level of each individual noise sources and their third octave analysis, the following conclusions about the characteristics of noisecan be defined:

- Noise is of continuous type
- Transmitted both through air and through the structure of the building
- Structural noise is transmitted through fixed connections of existing equipment and walls and floors
- Chimneys transmit noise emitted by furnance in the building .
- All sound sources have a similar intensity of noise, so it is necessary to show noise reduction of each of them .

2 REDUCING THE NOISE PROGRAM

Since success in solving the problem of noise emited from the equipment in the boiler room depends on many parameters, so can not explicitly find the optimal solution which satisfies legal regulations without being too expensive, cannot be explicitly found. The solution is that the program performs a partial reduction of noise, activity by activity, or in this case in two phases. After each activity is done or achieved control test must be done.

The first phase would be based on the following activities:

- Eliminate all fixed connections of equipment towards the walls, ceiling and floor.
- Mechanical links are necessary to perform over the elastic washer (silencer) or rubber.
- All openings in the ceiling and walls are t o close with the flexible insulating material so as to eliminate contact with the pipeline and walls.
- The ceiling set is to set for ceiling i nsulation against airborne sound.
- Repair or replace all mechanical components that emit high noise levels due to defects or wear and tear, such as: pumps, fans, bearings in terms of reducing noise emissions.
- Regulate fan speed with the required capacity of air.
- Install sound silencers on air intakes at the burner.

The second phase would have continuation with results achieved by the reduction of noise from the first phase and would consist of the following activities:

- Design and installation of flue silencer pipes.
- Vibration insolation of boilers.
- Additional insulation of the supporting walls and barriers.
- Design and construction of low-frequency absorbers (resonant)
- Allocation of existing equipment (transfer to the less critical area)
- Scheduling of different modes of heating.

3. PROGRAM IMPLEMENTATION

3.1. Construction Works

First steps in implementation of this program have been made to repair the building in the construction meaning. As the ceiling is covered with panels are wwcb boards that fell off are cracked in some places, measures have been taken to remove the demaged panels, and replace them with new ones. Also, all openings (eg, the passage of pipes) that were parts of the neighboring buildings are to be sealed with elastic sealing materials such as raw rubber, polyurethane foam, etc..

After seting up sound insolation area the access to the sealing must be implemented in order to reduce the impact of airborne sound influence on ceiling which is also under the nearest dwelling. Suspended ceiling is made in combination of wwcb board and layer of mineral wool in the distances given by Fig.3

3.2 Works on Mechanical Structure

Equipment like boilers, fans, engines, pipes and pums were fixed on walls and ceiling. This fixing method enables directing the sound and vibration transmission through the construction of the building structure which is far less favorable to tenants in respect of air sound. Therefore, wherever possible it is necessery to physically separate the supporting mechanical structure of these devices from the walls and ceiling. Our supporting structure is fixed to the floor by elastic stands. In cases where it is not possible, rigid connection is to be replaced by an elastic one. In Figures 4,5,6 the examples of such interventions aqre given.

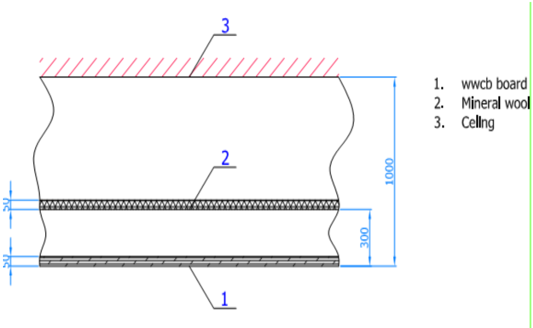

Fig.3 Suspended ceiling

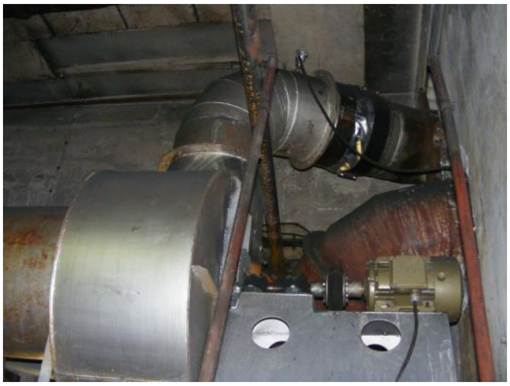

Fig 4. An example of flexible conection

The pump to maintain pressure in the pipes for heating, which works constantly for 24 hours has been replaced by a new one. The reason for replacing the pump is the high level of emitted sound power , which in this case is reduced from 75 dBA to 50dBA. In this way the sound source that disturbes residents in the period when the boilers do not function is eliminated.

In addition, the activities were carried out in mechanical maintenance on equipment in boilers room. Roller bearings where replaced and all position that emite noise where grease . The balancing of the fan rotor was made in aim to reduce vibration and noise.

Circulation pumps and their motors located in room 2. were isolated by the designed enclousures, filled with absorbent material and ventilation directed to the floor. Thus the noise emision was prevented directly towards the ceiling and apartments in the building (see Fig.4).

Fig.5 Place for enclousure

Fig. 6. changes in the way of fixing

3.3 Fan Speed Alignment

Circulation pumps and their motors are located in room 2. were isolated by the designed enclousures, filled with absorbent material and ventilation directed to the floor. Thus prevented the noise emission directly toward the ceiling and apartments in the building (see Fig.4).

Noise emitted from the fan and flue gas is of great importance to the overall noise level in the apartments. Fan noise is emitted as airborne and stuctural noise through the walls and ceiling expands into the building. Also we have, the noise and vibration transmitted through the flue pipe and the structure of the building to the pipe and the chimney himself.

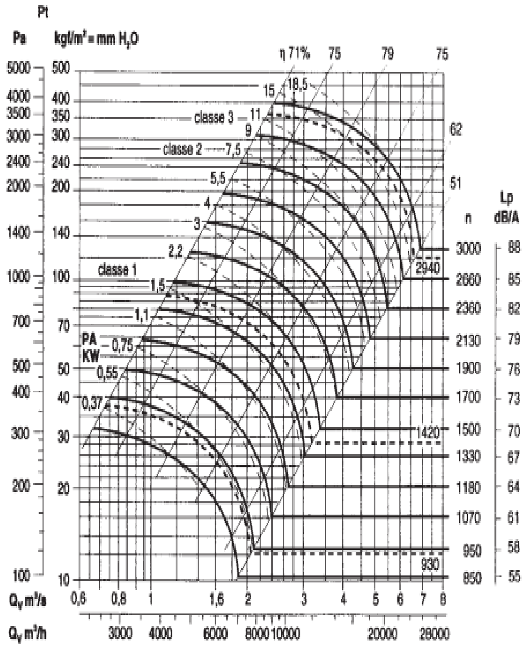

Fig.7 Fan working diagrams

The level of noise issued by fan depends on several components, primarily by the technical characteristics of design and on the other side and the maintenance and adjustment, the system itself.

According to the literature the noise associated with fans is composed of:

1. discrete tones at the fundamental blade passing frequency and integer-ordered harmonics of it: and
2. broad random aerodynamic noise due to vortex shedding from the blades.

When considering the parameters through which one can define the optimal mode of the fan, then these are: type of ventilators, installed capacity, speed, pressure, strain, number of blades, correction and form of adapter on duct. It is clear that the basic requirement to satisfy capacity and pressure. Manufacturers provide the fan working diagrams Fig.6.showing that the reduction of speed is a manner to get the optimal capacity. As is common to the design capacity of the fan system is oversized, it is clear that the reduction in speed can make quieter operation noise of fan. It can be achieved in real terms and up to 15dB.

4. EXPECTATIONS AND CONCLUSION

After the completion of construction and mechanical work, measuring of the reduction of noise levels has been done. It is shown in Fig.7. The measuring was done in 1 / 3 octave band frequency domain and it is evident that there is a significant reduction in noise levels.

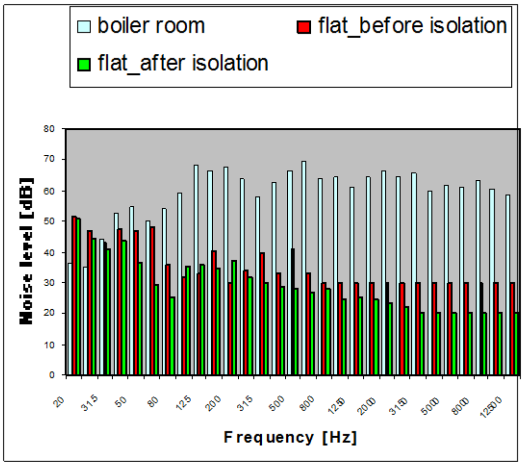

Fig.8 1/3octave band frequency diagram

Total reduction of noise level for the first two activities is at the level of 6dBA. As the measurement was carried out in the hallway between the apartments it is realistic to expect that effective reduction is 10dBA because there is an additional insulation in the apartment such as flooring and carpets.

Expected results of the first phase of protection against noise are given in Table 3.

It is unlikely that the activities of the second stage noise abatement will be necessary when the first stage is comleted.

Table.3 Inspected results of the first phase

Activiti	Noise reduction
Works on Mechanical Structure	2dB
Construction Works	5dB
Fan Speed Alignment	5dB
Burner sound silencer	2dB
Sum	15 dB

Acknowledgement

"Authors wish to acknowledge their gratitude to Ministry of Education and Science of Republic of Serbia for the support to the research through project grant TR37020."

REFERENCES

[1] Petrović Z., Radičević B., Bijelić M.,-Designing main fan noise protection system in mine »Jarando« Baljevac-, Undergraund Mining Engineering 15 (2006), 133-138,2006

[2] Petrović Z., Radičević B., Šoškić Z.,Bjelić M.,-Zaštita od buke industrijskih postrojenja-, XXI Konferencija Buka i vibracije, Tara, str.34., 2008..

[3] Marshall Long, Arhitectural Acoustics, Elseveir Academic Press, 2006

[4] Malcolm J. Crocker, Handbook of Noise and Vibration Control, 2007 John Wiley & Sons, Inc.

[5] Praščević M.,Cvetkovic D., Buka u životnoj sredini, Fakultet zaštite na radu, Niš,2005

G SESSION

STRUCTURES AND MATERIALS IN CIVIL ENGINEERING

HEAVY MACHINERY - HM 2011, 1-5
ISBN 978-86-82631-58-3
Paper accepted: 20.05.2011

Methods of Friction Optimization by Addition of Nano-Particle Composition to Lubricants

Lyubchenko Elena[1], Aksyonova Svetlana[2]
[1]National Technical University “Kharkov Polytechnical Institute”, Kharkov, Ukraine,

The structural changes of friction surfaces and assosiated changes of main tribological characteristics (coefficuient of friction, weight wear) taking place as a result of introduction of additive into the lubricating oil were investigated. It is shown that the mechanism of additive action is based on its specific composition and dispersity. The positive effect of the additive is demonstrated by structural examinations with the help of scanning electron microscopy (SEM), profile recording and microhardness measurements as well as by tribological tests conducted using the pair of “cast iron - chromium” (typical friction pair of the cylinder-piston assembly in the most modern engines).

Keywords: coefficient of friction, wear, additive, lubricating oil, surface structure, scanning electron microscopy, profile recording, microhardness.

INTRODUCTION

Friction and wear-out of mechanisms present important and immediate problems in the modern technological world. One of the most promising ways of mediation of such problems is use of lubricating oils with specialized and highly advanced additives [1]. The use of such additives promotes the optimization of friction processes, reduces wear and friction coefficient, prevents the seizure of mechanisms, provides good running-in ability and, consequently, increases the service life of friction pairs, reduces fuel consumption and improves environmental impact.

Recently, oil additives derived from natural minerals have been widely accepted in different applications [2]. Their positive influence on a friction process is attained by both their structure and chemical composition. The mechanism of these additives acting on a friction surface is based on the formation of “servovite” (*Latin*: “servo” – conserve, “vita” – life, i.e., “life supporting”) ceramic-metal films on the friction surfaces. However, there is no supporting data about the experimental verification of such films presence as well as there is no good understanding about formation mechanism and their influence on friction processes.

In this paper we present the results of the study of additives effect on the changes in friction surface structure, and, as a result, on tribological characteristics of the friction pair “ cast iron - chromium” (typical friction pair of the cylinder-piston assembly in the most modern engines). Specifically, the main interest of the investigation was about the friction coefficient and weight change due to wear out of such friction pair under the nano-particle additives influence.

1. RESULTS

1.1 Additive composition and manufacturing process

The additives which action mechanism was investigated in this work were made by complicated manufacturing process.

The original composition of additive [3] includes the environmentally safe components each one playing the specific roles in realization of required qualities of the additive operation. The additive consists of a powder made by special processing of mineral natural raw materials having in their composition Aluminium, Silicon, Magnesium, etc., that capable to form ceramic-metal servovite films on the rubbing surfaces under the conditions taking place in friction zone. The additive composition also includes chlorides and silicates of Tin and Magnesium that additionally serve as a material for ceramic-metal film creation and carry out plating action, smoothing of working surfaces and protecting the juvenile surfaces of contacting parts.

*Corr. Author's Address: National Technical University «Kharkov Polytechnical Institute», Frunze, 21, Kharkov, Ukraine, e_lyubchenko@ukr.net

The original multistage method [4] of raw materials processing includes milling, annealing, mechanical activation, fine grinding and provides required properties of the additive at all stages of a friction process.

Investigated additive is the mixture of solid nano-particles of different types and compositions placed in viscous carrier (thickened mineral oil). Before introducing into friction zone, additive is admixed with lubricating oil (usually in concentration 1:1000).

1.2. Samples and test methods

To reveal the influence of additive on the coefficient of friction and wear we carried out the test using friction machines 2070 CMT-1 and СМЦ-2. Our testing method was similar to ASTM G77, Ranking Resistance of Materials to Sliding Wear, Modified.

The tribological tests were carried out using the friction pair "cast iron (moving disc) - chrome (chromium-plated fixed disc or block)". This friction pair was chosen for test due to its wide usage in the friction nods, particularly, in the cylinder-piston groups of modern internal combustion engines.

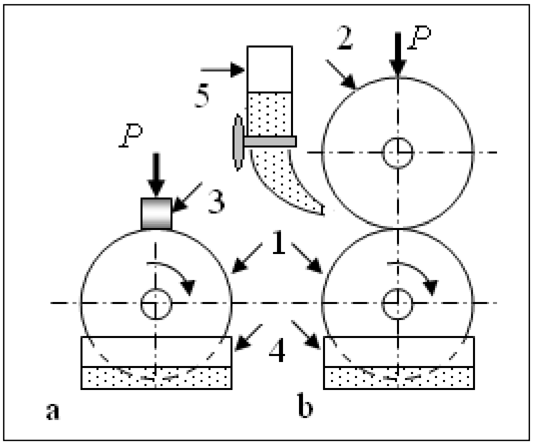

Fig. 1. *Test scheme: 1 – moving disc, 2 – fixed disc, 3 - fixed block, 4, 5 – containers for lubricating oil*

Mobile specimens (discs) were made of the alloy grey cast iron castings. Microstructure was the pearlite with lamellar graphite and phosphide eutectic; hardness – HRB 100 - 105 (240 - 245 HB). To relieve stresses due to the mechanical processing the discs were tempered according to the following scheme: charging into a furnace at 300^{o}C, heating at the rate 100^{o}/hour to 600^{o}C, soaking during 3 hours; cooling to 300^{o}C at the rate 100^{o}/hour, and further air cooling. This treatment regime is corresponded to the treatment regime for the cylinder sleeves of diesel locomotive engines.

Immobile sample (blocks or disks) were of two types – either the segments of piston rings (3 in Fig.1, a) or cast iron discs (2 in Fig.1, b). They were made of the high-strength inoculated magnesium cast iron with spheroidal graphite (hardness HB 105 – 108). Their working surfaces were covered by chromium of the thickness 200-220 µm by means of electrolytic technique. Microhardness of chromium coating was HV_5 790-850 (7-7.5 GPa), $H_{\mu\square 100}$880-1000.

The working surface of the cast iron discs in the initial state was of the 8th surface finishing class (the average height of the roughness R_y was ~0.6-0,8 µm).

Lubricating was made by two methods: either by oil drops from upper container (5 in Fig.1, b) or by dipping of moving disc into container with oil (4 in Fig. 1).

The speed of moving disc (Ø 50 mm) was 1.3 mps. Frictional sliding was 25%.

The testing procedures were following:

- for coefficient of friction measurements: 15 min of run-in at the load of 0.2 kN, then 4 steps of loading (the step was 0.2 kN up to the load of 1 kN; 2 min on each step), off-loading and 15 min at 0.2 kN, and recycling;
- for wear measurements: tests during 1, 5 or 10 hours at the permanent loading of 0.5 kN.

For the friction torque registration the inductive data unit of friction machine СМЦ-2 was used. The coefficient of friction f was calculated according to the formula:

$$f = 2M/(d \cdot P),$$

where M is the friction torque, d is the diameter of mobile specimen, P is the loading magnitude.

The beginning of fretting was determined as the fast growth of the torque magnitude and the appearance of the scores on the working surfaces. The errors in torque and coefficient of friction determination were from 9% at P = 0.2 kN to 2% at P = 1.0 kN.

The wear magnitude was found by weighting on high-accuracy weighing machine before and after the tests with the accuracy ± 0.1 mg.

The investigation of the working surfaces was carried out by means of binocular microscope МБС-9 using the magnifications x8…50 and by means of scanning electron microscope (SEM) РЭММА 101-А in magnification range x30…1000.

Microhardness of the material was determined in initial state and on the friction surfaces by means ПМТ-3 device at the loading 50 g.

The surface topography analysis was performed on all tested specimens including the specimen not subjected to any friction, using TR200 profile recorder. The following measurements were taken: R_y – sum of the height of the highest peak and the depth of the biggest trench relating to the median in the base length limits; R_p – height of the highest peak relating to the median; R_m – depth of the deepest trench of the profile relating to the median.

1.3. Results of tribological tests

The typical dependences of coefficient of friction on the load during step loading for friction pair "cast iron – chrome" are shown in Figure. 2 and 3. Tests were carried out using mineral oil Shell Helix 15 W-40 (MO), synthetic oil Shell Helix Plus 5W-40 (SO) and these oils with additive in concentration (1000:1).

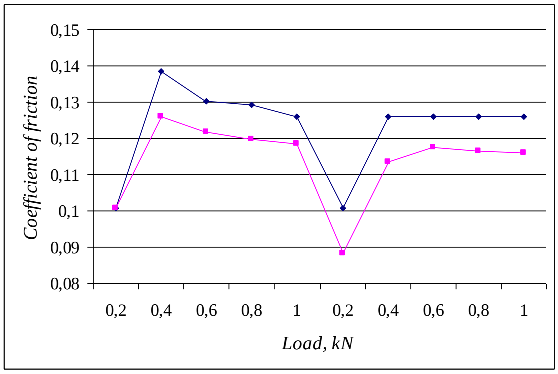

Fig. 2. *Coefficient of friction vs. load for step loading at friction in mineral oil with and without additive (lower and upper lines, respectively).*

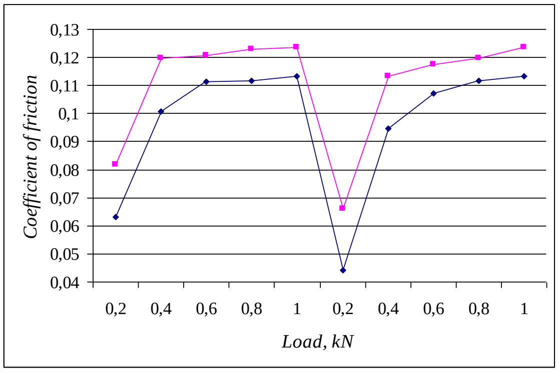

Fig. 3. *Coefficient of friction vs. load for step loading at friction in synthetic oil with and without additive (lower and upper lines, respectively).*

The average improvement of coefficient of friction due to additive introduction was about 8-11% depending on load level and oil type.

The additive introduction into lubricating oil helps to reduce the weight wear both of the discs and blocks. The most clearly this effect was manifested at the analysis of total wear of friction pairs (Fig. 4), i.e. the sum of weight losses of disc and block.

The obtained test results make the positive effect of additive introduction into lubricating oil obvious.

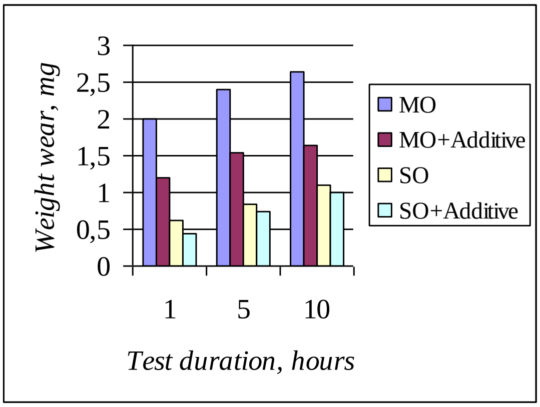

Fig. 4. *Total wear of friction pairs tested in mineral (MO) and synthetic (SO) oils with and without additive.*

1.4. Changes of the surface structure and composition

To explain the reasons of friction characteristics improvement at additive introduction into lubricant the investigations of the friction surfaces and subsurface layers have been conducted.

The carried out SEM investigations showed that there are three types of surfaces: initial (untreated) surfaces and surfaces after friction in oil without and with additive (fig. 5). The surface of the initial untreated metal specimen is characterized by striation due to machining tool motion at machining work. There are two systems of striations: with small and big spacings (~300 and 5-20 μm, respectively). They can be seen on Fig. 5, a. Friction in oil (Fig. 5, b) shows the depletion of the surface topography, its smoothing out. However, the main features of relief formed by mechanical treatment, particularly, the systems of striations with different spacings are still present but they are less clearly defined. Interstriation spacings show significant dispersion. Use of lubricating oil with additive brings on an intensive smoothening of the surface (Fig. 5, c). The relief of mechanical treatment can only be traced. Mainly the striations with large spacing are present. Large areas demonstrate the absence of contrast related to orientated ledges, and, what is more important, to trenches. The structure of these areas is similar to samples manufactured by powder metallurgy, i.e. by sintering of ultra-dispersive powders. We believe that this surface secondary structure was formed also by sintering of nano-particles of additive.

The results of profile recording are demonstrated by bar graph (Fig.6). It was observed that additive utilization helps to reduce the roughness of the surfaces. Smoothing of the surface at additive use is realized not only for the mechanical cutting of the surface peaks but due to the filling of cavities by additive ingredients.

Measurements showed that microhardness of discs and blocks was increased after friction processes due to the mechanical hardening of rubbing surfaces (Table 1). The most significant increase of microhardness was revealed for tests in the lubricating oil with additive. We suppose that this fact reflects the contribution into the surface hardening process of the metal-ceramic film formed due to the additive action.

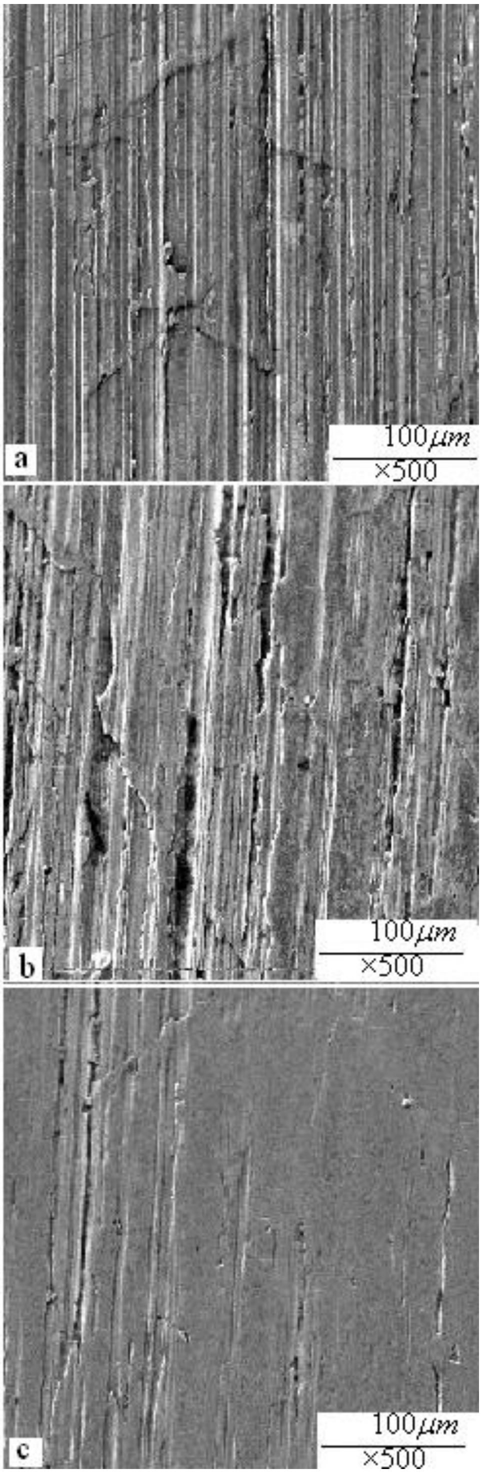

Fig. 5. *SEM images of initial surface (a) and surfaces after friction in oil (b) and in oil with additive (c)*

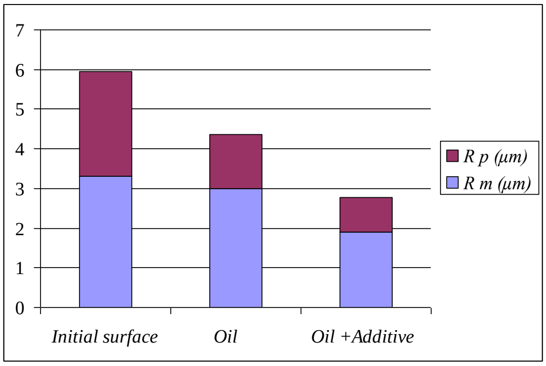

Fig. 6. *The relief measurements in tested specimens (blue – values for R_m, purple – values for R_p, bar height is the R_y value)*

Table 1. *Results of microhardness measurements*

Lubricant	Microhardness, GPa			
	Disc		Block	
	before	after	before	after
MO	3.45	4.3	7.0	10.1
MO+Additive	3.50	6.8	7.2	15.2
SO	3.55	4.5	7.5	11.3
SO+Additive	3.4	7.1	7.3	16.8

1.5. Additive action mechanism

Conducted investigations found out that used additive consisted of at least two types of nano-particles: the particles of ingredient with the layered crystallographic structure and the particles of metals and non-metals salts and oxides. Each type of particles at getting into the friction zone plays the specific role. The particles with layered structure at the initial stages of rubbing act similar to classical layered modifiers of friction, for example, the graphite, facilitating the friction due to slickensides creation.

Another mechanism of additive action based on the process of surface modification due to baking (sintering) of the additive particles under the action of the high temperatures and pressures in the friction zone and, as a result, the formation of the servovite ceramic- metal film

The optimal complex of the secondary structure properties is stipulated by the composition and dispersity of additive particles. Ultra-dispersive state of the additive ensures easy flowing of the sintering process when the particles of oxides are baking at the temperatures and pressures that are realized occasionally in the sites of rubbing surfaces contact. Thin servovite ceramic-metal film (thickness about 0,10…0,15 μm) is in a dynamic state, i.e., it is intermittently formed and destroyed on the rubbing surfaces.

2. CONCLUSION

As the result of this research, it can be concluded that the mechanism of the investigated additive influence on the friction pairs is based on a newly formed thin ceramic-metal layer in the friction zone. Such servovite thin film optimizes the friction process, decreases friction coefficient and reduces wear out.

3. REFERENCES

[1] Lubricant Additives: Chemistry and Applications, Editor Leslie R. Rudnick, 2nd edition, Chemical Industries/124, CRC Press, Taylor &Francis Croup, NY, 2009.

[2] В.Н.Кузьмин, Л.И.Погодаев: Смазочные материалы с добавками, Трение, износ, смазка, Т.11, №38, 2009

[3] Tananko D., Lyubchenko E., Aksyonova S., etc. Nano-particle metal treatment composition for creating a ceramic-metal layer. US Patent 7,304,020, 2007.

[4] Tananko D., Lyubchenko E., Aksyonova S., etc. Method for composing a nano-particle metal treatment composition for creating a ceramic-metal layer. US Patent 7,867,330, 2011.

ISBN 978-86-82631-58-3

Analysis And Testing of Nodal Elements On Prefabricated Industrial Objects

Jovan Vladić[1,*] - Radomir Đokić[1], Dragan Živanić[1]
[1] Faculty of Technical Sciences Novi Sad

By using prefabricated industrial objects of various ranges, there appear significant strains in the supporting, as well as in the nodal elements of outer and inner bars. The cause of those strains are loads caused by wind (transverse and longitudinal considering the axis of the object) and snow, depending on the position and altitude where the object is. Besides strains which are a consequence of the before mentioned outer loads, significant strains appear during the assembly of the bars and their binding to the supports.

The problem emerging during the analysis of nodal elements is that the influence of forces which are transferred from the nodal elements is very difficult to define. That is why in the previous steps it is necessary to consider the prefabricated industrial object as a line structure which transfers all the wind and snow loads to the ground.

This paper will show static analysis of the most endangered nodal elements which are set in the inner bar for cases such as outer loads of the object and loads as a consequence of wrong choice of assembly. After that, there will be presented the results of experimental research of one of nodal elements in the inner bar, in laboratory conditions.

Keywords: Prefabricated industrial objects, nodal elements, static analysis.

0 INTRODUCTION

A contemporary method of industrial objects structure in the world contribute to breaking and adoption of different systems and types of prefabricated industrial buildings. Expanded demands of reliability, efficacy and protection of environment contribute to development and production of objects [6]:

- increased resistance to corrosion,
- importantly larger strength, than with classic construction,
- which significally lower the inside temperature unlike other objects of similar purpose, which is very important from the energy saving point of veiw used for ventilation systems,
- increased resistance to fire,
- increased resistance to atmospheric influences
- have interior which can be easily built up,
- the interior is well used for there are no additional supporting pillars and elements,
- there is no competative price on the market in relation to other ways of constructing buildings.

Another very important adventage of these objects is that they can be easily buit in using "do it yourself"' system, which is very important because it is not necessary to hire highly qualified work force.

With these metal constructions characteristics of calculations, designing and making of supporting structure and designs of extreemely large spectrum of use are calculated. This refers to both civil and mechanical engineering. This process reached its greatest development in the second part of the twenty first century, when informational techology enabled the use of powerful methods of structural analyses, production technology, creation and development of new materials.

Contemporary calculations are done with computers using the program packages, which enable the calculation results to be as closer to the real state of loaded construction as possible.

Prefabricated industrial objects represent a good solution for permanent or occasional needs. Their main advantages are: a good price, quick assembly and a possibility of moving to another location, and there are a few more of the advantages [7]:

- Energy saving – a good heat isolation is a feature of poliurethan sandwich panels, and therefore it decreases the expenses of heating and cooling by 25-50% per season.

*Corr. Author's Adress: Faculty of Technical Sciences, Trg Dositeja obradovića 6, Novi Sad, Serbia, vladic@uns.ac.rs

- Short building period – all prefabricated elements are being cut and made in a factory in suitable dimensions, which helps save time, so their assembly on the site is much more economical, faster and simpler.
- Easy construction – prefabricated industrial objects are easier than objects made of brick, concrete and blocks, so it enables assembly even on surfaces of a low support level. As such, the projected object is more resistant to earthquakes than ordinary houses.
- Better space exploitation – the walls in prefabricated industrial objects are thinner than the ordinary ones, which increases the space exploitation, and provides an option of changing the room settings as well as their size by simple movement of partition panes.

1 ANALYSIS OF NODAL ELEMENTS AND DEFINING THE LOAD

In the analysis and defininig the way of assemblying the prefabricated industrial halls of different ranges, and especially in the system of prefabricated modular building, one of the most significant segments is the behaviour of the most endangered nodal elements in the inner bar of the hall. From the point of view of load and maximum stress, and in the supporting elements of a bar (sigma, C and L profiles), as well as in the nodal elements (various types of panels, fig.1), consideration of the assembly based on “do it yourself“ system, or prefabricated modular building, points out the changing of the bar(inner or outer) from a horizontal position to a vertical one, and its connection to the anchor panels in a concrete basis.

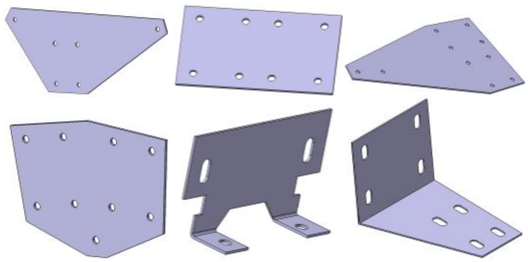

Fig. 1. *Some nodal elements of a hall with the range of 10m*

Besides some significant strains in the hall elements which occur during an assembly and lifting certain bars, even more important strains can appear while using the objects under the effects of wind and snow. In the two familiar cases of load due to wind effect (according to standards which define the loads of buliding constructions due to wind), the values of the load on line beams can be of significance, table 1.

Table 1. *Loads due to wind effect in N/m in the case of the hall discussed(range of 10m), [3]*

1. Load case			2. Load case		
	kN/m^2	N/m		kN/m^2	N/m
Roof-front side	1,18	-805	Roof-front side	-1,18	-805
Roof-front side	-0,77	-630	Roof-front side	-0,77	-630
Roof- back side	-0,77	-525,26	Roof- back side	-0,59	-402,45
Roof- back side	-0,53	433,28	Roof- back side	-0,41	-335,21
Frontal sidewall	0,89	777,42	Calcaneal wall - front	0,44	561,15
Frontal sidewall	0,59	654,31	Calcaneal wall - front	0,68	468
Back sidewall	-0,71	-620,23	Calcaneal wall - back	-0,47	324
Back sidewall	-0,47	-521,21	Calcaneal wall - back	-0,32	408,11

The first case of load shows the wind effect transverse on the hall axis, Fig. 2a, and the other case of load takes wind effect in the direction of longitudinal axis, Fig. 2b.

Table 1 shows load values under the wind effect with the Fig. 2. The shown surfaces are under the influence of a load shown in kN/m^2 , which is connected to the line load in N/m set on the supporting profiles of the created structure model. For example, on the front side of the roof there are two load values: load W_{p1}= -1,18 kN/m^2 which influences the surface that is 6 m from the hall edge (y=6,0 in Fig. 2), and line load W_{l1}= -805 N/m is suitable for it, and there is also W_{p2}= -

0,77 kN/m^2 load which affects the surface in the middle of the roof, and a line load of W_{12}= -630 N/m is suitable for it.

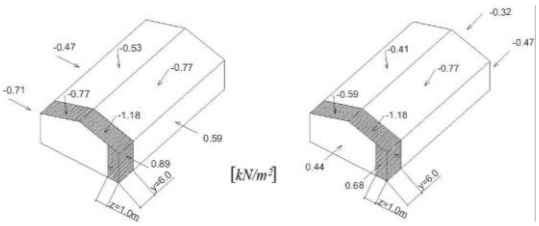

a) *b)*

Fig. 2. *Wind load on the hall transverse and in the direction of longitudinal axis in kN/m^2, [5]*

Static analysis was performed on a nodal element shown in Fig. 3a, by using the method of definite elements through a program package CATIA V5, [4].

a) *b)*

Fig. 3. *Geometrical model of the analysed nodal element*

In discussing the model of nodal element (separated from the model of complete hall, Fig. 4a), the starting point was the theory that outer loads, which affect it, are the forces and moments which occur in the ending nodes of some supporters in the calculation model gained in programme KRASTA, Fig. 4b. The thing is that outer loads are actually inner forces in the ending nodes of beams.

The following text presents a process of a static analysis of a nodal element shown in Fig. 3 which is used in a hall construction to connect the longitudinal beams (sigma profile) to the inner and outer roof bars. Its function is to transfer the wind and snow load, which has an effect in the direction of longitudinal axis and in the transverse direction of the hall. Fig. 3b shows the connection point of this nodal element to the sigma profiles of longitudinal beams and cornea. However, the figure does not show connecting elements (bolts) which are placed in the presented openings.

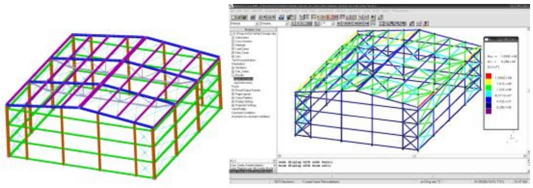

a) *b)*

Fig. 4. *Geometrical and calculation model of the whole hall, [3]*

It should be mentioned that there also was an experimental research of this nodal element in laboratory conditions. Also, the measuring and research was performed on nodal and supporting elements which are exploited, and it is not presented in this paper.

The loads significant for a static analysis of a nodal element have been taken from the considering and results obtained in the KRASTA program. The inner forces and moments occurring at the ends of longitudinal beams in the hall roof are observed as outer loads in a nodal element at the connecting sites with bolts. At the other end of a nodal element, the place of its connection to the cornea, boundary conditions have been set. Calculation model of that nodal element is shown in Fig. 6. Boundary conditions in the calculation are determined by fictive showing of connecting elements, and their connection to the nodal element is presented through “contacts” in a CATIA program package. The fictive elements limit the three degrees of freedom of movement, e.g. a three way translation. In this way we tried to model the boundary conditions occurring in the real objects.

Fig. 5 shows a table with the values of forces and moments (outer loads of a nodal element) gained from a calculation model analysed in the KRASTA program.

The marks in Fig. 5 represent: N_x - a force in the x-axis direction of a sigma profile, S_y - a force in y-axis direction of a sigma profile, S_z - a force in the direction of z-axis of a sigma profile, T_x - moment of torsion around the x-axis of a beam, M_y - moment of torsion around the y-axis of the beam, M_z - moment of torsion around the z-axis of the beam.

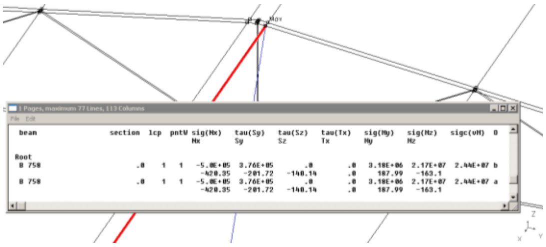

Fig. 5. *Values of forces and moments in a longitudinal hall roof beam*

The values of the forces and moments are in the model in Fig. 6. Method of definite elements provided the results (shown in graphics in Fig. 6b, which is a graphic representation of deformation and stress state). In this calculation, maximum stress in a nodal element is about 560 N/mm^2.

This stress quite exceeds the values allowed, so that is why a nodal element modification was performed, Fig. 7 (welded reinforcement), which is used in objects.

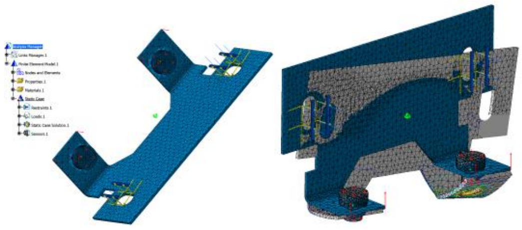

a) *b)*

Fig. 6. *Calculation model of a nodal element*

Fig. 7. *Modified (strengthened) model of a nodal element*

2 EXPERIMENTAL RESEARCH OF A NODAL ELEMENT

The experimental research of a nodal element, Fig. 3a, was performed in the Laboratory of Department for Machine Constructions, Transport Logistics in the Faculty of Technical Science.

Static analysis of a nodal element with the previously described method of definite elements, provided the critical points, i.e. points of maximum stress. Strains, or dilatations, were measured in the points. Diletations are measured with a system of strain gauges. The position of strain gauges and their protection is given in Fig.8.

Two nodal elements out of four in one nodal point on a hall roof, are considered because of a probable dissymetry in transferring the load during its placement in laboratory conditions. Fig.8 shows nodal elements with glued strain gauges. The data transfer (digital inscription) from the strain gauges to a computer was done by a measuring amplifier Spyder 8, Fig. 9a.

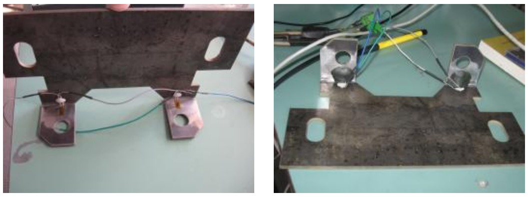

Fig. 8. *Point of placing the strain gauges and their protection*

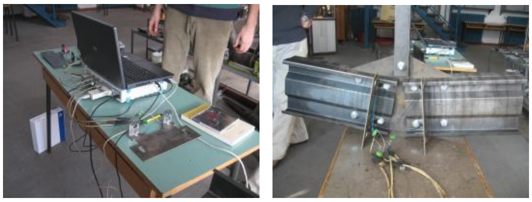

a) *b)*

Fig. 9. *Connecting the strain gauges to the measuring amplifier and assemblying the nodal point*

After preparing the surfaces, setting the strain gauges and a protection for them, it is time to assembly the nodal point through connecting elements (bolts). In that way, the assemblied experimental modal was ready for static research, Fig. 10a.

The research was done by fastening in the direction of longitudinal beams in the hall roof. The fastening force was accomplished through lifting drive of a laboratory overhead travelling crane. In order to controll the process while loading the model, as a connection in series between a crane hook and a model, a force provider is used (1t capacity), which shows force value needed to fasten one side of longitudinal beams at each moment.

Fig. 10b shows the loaded model of a nodal bridge, where longitudinal and calcane beams of a hall roof are confronted.

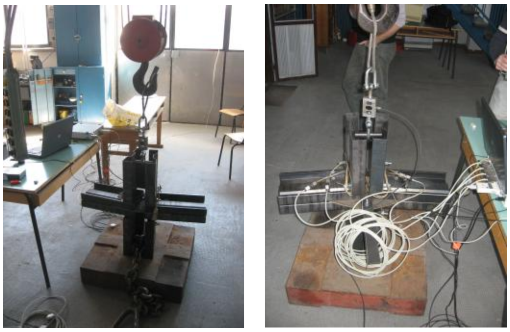

a) *b)*

Fig. 10. Experimental model

If needed, direct and consequtive transfer of diletation values (μm/mm) into stress (N/mm^2) was done in the software for monitoring the measuring results. The stress values measured in measuring points shown in Fig. 9, are presented in the diagram in Fig. 11, in the time function during which loading was performed.

Oscilatory character of inscription which can be seen in the pictures, is a consequence of system elasticity and oscilations of overhead travelling crane elements (main bridge, supporting ropes etc.). Stress values deviations in measuring point no. 4, in comparison to the other three points, is explained by the before mentioned dissymetry of the experimental model, and, which is even more realistic, the incorrectnes and a probable mistake during the placement of strain gauges in that measuring point.

One can see from the diagram that the median stress value is around 130 N/mm^2, and the value obtained from the static analysis on a computer model was a lot bigger. This probably happens because it is impossible to simulate the wind effect in the laboratory conditions, as well as the moments occuring in the longitudinal beams of the hall roof due to wind effects.

This is one more reason why discussion and analysis also included building and assemblying the modifed nodal elements, shown in Fig. 7.

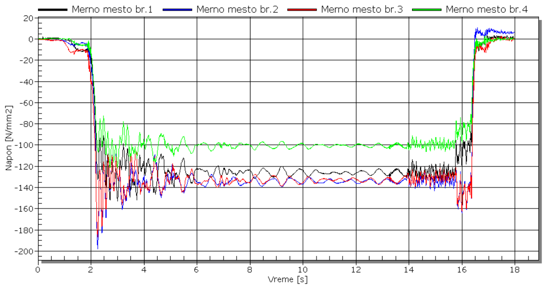

Fig. 11. *Stress time dependence in measuring points of two nodal elements*

The diagram in Fig. 12 shows a change of force during its placement on an experimental model, and it is measured by a force provider. Fig. 13 shows a change of stress in one measurig point during the loading of the model.

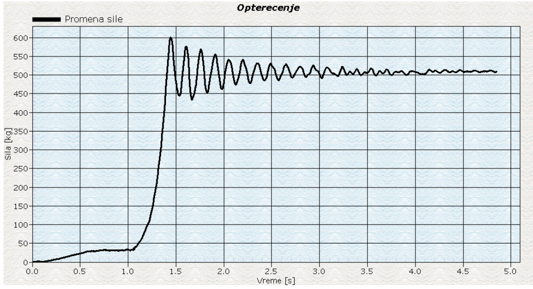

Fig. 12. *Force time dependence*

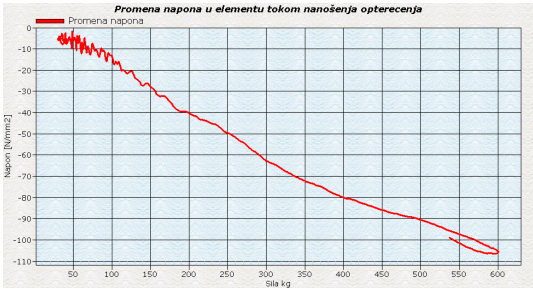

Fig. 13. *Stress dependence on loading*

3 CONCLUSION

Quick changes in production program, readjustments to new demands, fierce competition and less time of keeping the products in the market, all those have conditioned the sudden development of methods for projection and modification of new and existing systems and their elements. This development would not have been possible without the application of modern items such as computers and program packages. Modern software solutions are especially useful and they justify the investments when observed in very complicated systems in machinery. Their usage enables hands-on calculations of all types in engineering, and therefore the prefabricated industrial objects, too. That decreases the time needed for classical changes and increases the accuracy of obtained results.

By using the CATIA and KRASTA program packages, the possiblity of checking the stress state and calculations of values of inner forces in the beam elements is shown, as well as stress state of the nodal elements.

The experiments in laboratory conditions show that outer loads can be simulated in a relatively simple way. Also, experimental node points models make the process of checking the strain in nodal cheaper, and connecting elements, compared to tracking the state of the construction as a whole.

Further research in this area would enable the increase in stability of the supporting constructions, quality improvement, and it would minimize the possible mistakes in the process of object exploitation. In projecting and analysis of prefabricated industrial objects special attention is to be paid to the choice of supporting and nodal elements of the nodal construction. The right choice of elements causes weight decrease, and therefore the load caused by its own weight.

4 REFERENCES

[1] Babin, N., Brkljač, N., Šostakov, R., “Metal structures“, Faculty of Technical Sciences, Novi Sad, 2006.,

[2] Petković, Z., Ostrić, D., “Metal structures I“, Faculty of Mechanical Engineering, Belgrade, 1996.,

[3] Project of the Chair for mechanical construction, transporting systems and logistics, from the program of technologic development „Development, design and optimization of systems and constructive elements of supporting structures prefabricated industrial halls“,

[4] Sekulović, M., “Finite element method“, Faculty of Civil Engineering, Belgrade, 1984.,

[5] Standards of Civil and Mechanical Engineering fields,

[6] Vladić, J., Živanić, D., Đokić, R., “Contemporary Processes to Steel Construction Analisys of Prefabricated Industrial Objects“, Proceedings of the IX International Conference DEMI 2009, 28-29.05. 2009., Banja Luka, pp. 127-134,

[7] Vladić, J., Živanić, D., Đokić, R., Gajić, A., “Analysis and Choice of Prefabricated Industrial Halls Elements“; XIX International Conference on MATERIAL HANDLING, CONSTRUCTIONS AND LOGISTICS, MHCL '09, 15-16 October 2009, Belgrade, Serbia, pp. 257-260,

[8] Vladić, J., Šostakov, R., Đokić, R., Živanić, D., “Automation of prefabricated removable structures designing procedures”, MACHINE DESIGN 2010, pp. 35-38.

HEAVY MACHINERY - HM 2011, 13-16
ISBN 978-86-82631-58-3
Paper accepted: 30.05.2011

Calculation of The Free End Deflection of A Truss Beam with Variable Cross-section

Milan Dedic[1,*] - Milica Todorovic[2]
[1]Faculty of Mechanical Engineering Kraljevo, Kraljevo, Serbia
[2]High Technical Mechanical School, Trstenik, Serbia

Truss beams with repeated cells are widely used load carrying structures in mechanical and civil engineering. They are simple to manufacture, and have low manufacturing costs. Particularly important is their high load-to-weight ratio capacity. Their carrying capacity can be further improved in the case of trusses strained dominantly in bending if instead of repeating cells with the same bars along the whole length a truss with strengthened bars in the more strained part is made. The intention of this paper is to present how a procedure of calculating deflection by means of continuum modelling developed by the same authors can be applied to the cantilever trusses with two different cross-sections. It is shown that using equivalent bending and shearing rigidity concepts lead to the formulas similar to ones used in the strength of materials.

Keywords: trusses, continuum modeling, equivalent stiffness, deformations.

INTRODUCTION

Truss beams are widely used load carrying structures in mechanical and civil engineering because of their high strength to weight ratio, and because of a number of other good characteristics regarding, such as low manufacturing costs and simple technological demands. They are the most commonly calculated by means of finite element method due to high number of bars they are made of.

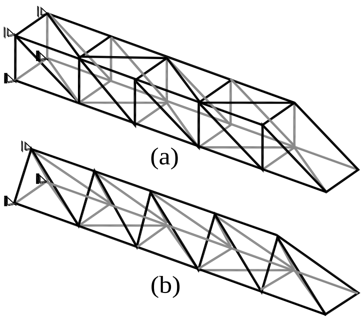

Fig. 1. *Truss beams with repeating cells*

An alternative approach to analyse the truss beams with repeated cells, as those in Fig.1, i.e. the ones that have a constant apparent cross-section along it's length, is to replace a real structure of a truss beam with a continuum body, and treat it as a beam with bulky cross-section. The general idea of that method can be found in [1] and [2]. Theory of continuum modelling (TCM) supplies for the equivalent strength characteristics for that purpose, for example, equivalent bending and shearing rigidity needed to calculate deflections and slopes. Although continuum modelling lacks the generality of the finite element method, it yields simple and useful formulas in many cases. It's useful feature is a possibility to inspect and analyse influence of different design quantities and parameters to the overall quality of the structure. One of the TCM methods is a direct energy approach, elaborated in [3], [4] and [5]. The calculation procedure in this paper is based on the method developed by the same authors and presented in [6] to [11].

1. Calculation of the free end deflection of a planar truss loaded by a transverse force

Let us observe a statically determinate planar cantilever truss made of pin jointed bars with constant cross-section, Fig.2. We restrict our argument here to the planar truss for the sake of simplicity. However, as it has been shown in [11], the results presented can be easily generalized to the spatial trusses with only minor modifications of formulas.

The bars are bound in repeated cells with constant length L, height h and filling angle β.

[*]Corr.Author's Address: Faculty of Mechanical Engineering Kraljevo, Dositejeva 19, 36000 Kraljevo, Serbia, dedic.m@mfkv.kg.ac.rs

Bottom longitudinal bars are denoted with subscript "b", top bars with "t", vertical bars with "v" and diagonal bars with "d". The truss is loaded by a transverse force F at the free end.

This type of truss is the most commonly manufactured with the same cells throughout it's length. However, for the sake of structural strength and making good use of material it is convenient to have the truss with two spans, so that the span near supports, the one in higher bending moment, is made of bars with greater cross-section areas. This can make the structure lighter and closer to an optimum design.

We shall observe in this paper a truss that consists of two spans with the same L, h and β. The first span, span index $s = 1$, has length l_1 and number of cells n_1, so that $l_1 = n_1 L$. Similarly in the second span, with index $s = 2$, we have l_2, n_2 so that $l_2 = n_2 L$. Cell ordinal numbers $k_1 = 1, 2, 3 \ldots n_1$ and $k_2 = 1, 2, 3 \ldots n_2$ are counted from right to left, Fig.2.

Vertical bars are assumed to belong to the *right hand* adjoining cell. Consequently the vertical bar connecting the two spans belongs to the first span. The rightmost top and vertical bars are unstrained, but they have been kept here for the purpose of structural continuity. Bars in the first span have the cross-section areas A_{b1}, A_{t1}, A_{v1} and A_{d1}, and bars in the second span A_{b2}, A_{t2}, A_{v2} and A_{d2}, and they all have the modulus of elasticity E.

With the assumptions listed in the beginning of this chapter, all the bars are strained in pure extension or compression, and from the equilibrium conditions we can calculate forces in the bars for the first span, subscript $s = 1$:

$$N_{b1}(k_1) = k_1 \frac{F}{tg\beta}$$

$$N_{t1}(k_1) = (k_1 - 1)\frac{F}{tg\beta}$$

$$N_{v1}(k_1) = F \qquad N_{d1}(k_1) = \frac{F}{\sin\beta}$$

and for the second span, subscript $s = 2$:

$$N_{b2}(k_2) = \left(n_1 + k_2\right)\frac{F}{tg\beta}$$

$$N_{t2}(k_2) = (n_1 + k_2 - 1)\frac{F}{tg\beta}$$

$$N_{v2}(k_2) = F \qquad N_{d2}(k_2) = \frac{F}{\sin\beta}$$

If the bars are axially strained, the deformation energy in the planar case will be the sum of energies of the first span:

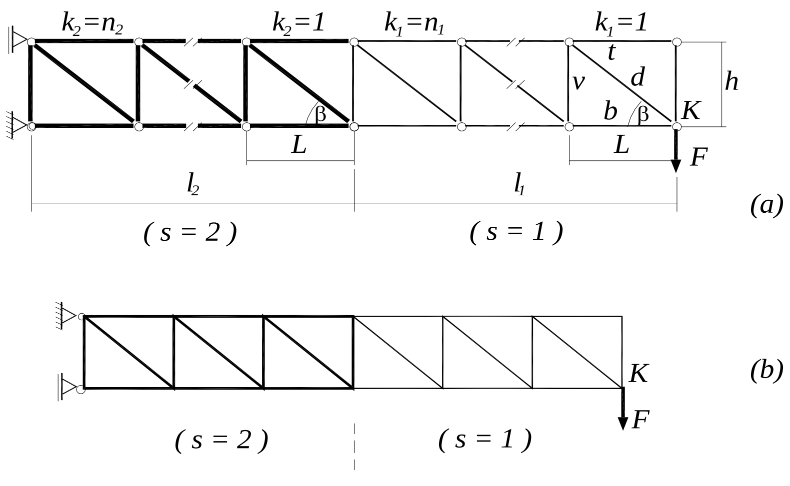

Fig.2 Geometry and load of a two span cantilever truss

$$A_{d1} = \frac{1}{2}\sum_{k1=1}^{n1}\left[\frac{N_{b1}^2(k_1)L}{EA_{b1}} + \frac{N_{t1}^2(k_1)L}{EA_{t1}} \dots \right.$$
$$\left. \dots + \frac{N_{v1}^2(k_1)L}{EA_{v1}} + \frac{N_{d1}^2(k_1)L}{EA_{d1}}\right]$$

and of the second span:

$$A_{d2} = \frac{1}{2}\sum_{k2=1}^{n2}\left[\frac{N_{b2}^2(k_2)L}{EA_{b2}} + \frac{N_{t2}^2(k_2)L}{EA_{t2}} \dots \right.$$
$$\left. \dots + \frac{N_{v2}^2(k_2)L}{EA_{v2}} + \frac{N_{d2}^2(k_2)L}{EA_{d2}}\right]$$

The total deformation energy of both spans will thereby be:

$$A_d = A_{d1} + A_{d2}$$

Applying the Castigliano's theorem to A_d we obtain for the end deflection f_K, the transverse displacement of the point K:

$$f_K = \left[\frac{F\, l_1^3}{3E\, I_{xe1}(n_1)} + \frac{F(l_1 + l_2)^3}{3E\, I_{xe2}(n_1+n_2)} + \right.$$
$$\left. - \frac{F\, l_1^3}{3E\, I_{xe2}(n_1)}\right] + \left[\frac{F\, l_1}{S_{e1}} + \frac{F\, l_2}{S_{e2}}\right] \tag{1}$$

In the above formula quantities $I_{xe(s)}(n)$ are functions of n and the span index s in the form:

$$I_{xe(s)}(n) = \left[\frac{1}{h^2 A_{b(s)}}\left(1 + \frac{3}{2n} + \frac{1}{2n^2}\right) + \right.$$
$$\left. + \frac{1}{h^2 A_{t(s)}}\left(1 - \frac{3}{2n} + \frac{1}{2n^2}\right)\right]^{-1} \tag{2}$$

It is shown in the [7] that this quantity is a result of deformation in which the longitudinal bars "b" and "t" remain parallel, but compressed and elongated respectively, so that this deformation mode can be ascribed to the bending mode of a truss as a whole. Since the bars are not bent, we can understand this as the *structural bending* of a truss. We call $I_{xe(s)}(n)$ the equivalent moment of inertia of the truss cross-section, and consequently the product $EI_{xe(s)}(n)$ the equivalent bending stiffness. Thus the sum in the first square brackets in (1) represent the bending component of the total end deflection f_K.

The quantities $S_{e(s)}$ in (1) have the form:

$$S_{e(s)} = E\left[\frac{tg\beta}{A_{v(s)}} + \frac{1}{sin^2\beta \cos\beta\, A_{d(s)}}\right]^{-1} \tag{3}$$

and can be associated with deformations of solely "v" and "d" bars, while "b" and "t" bars remain parallel. This can be understood as the *structural shearing mode* of the truss. Consequently, fractions F/S_{e1} and F/S_{e2} in (1) represent the components of the first and second span slopes to the horizontal direction. The sum in the second square brackets in (1) is the shearing component of the total end deflection f_K.

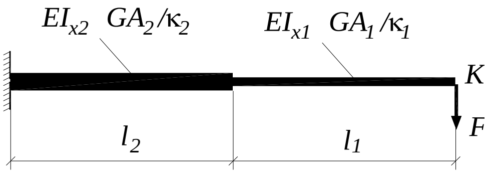

Fig. 3. *A continuum beam with two spans in bending by a transverse force*

2. An analogy with a two span continuum cantilever beam loaded by a transverse force

Let us observe now a continuum cantilever beam loaded by a transverse force at it's free end, Fig.3. Let both spans have constant strength characteristics along their lengths, as indicated in the figure. $I_{x(s)}$, $A_{(s)}$, $\kappa_{(s)}$, E and G denote axial moment of inertia, area and shear number of the cross-section area and the moduli of elasticity and shearing respectively. Conventional method give for the free end deflection of a beam in Fig.3:

$$f_K = \left[\frac{Fl_1^3}{3EI_{x1}} + \frac{F(l_1+l_2)^3}{3EI_{x2}} + \right.$$
$$\left. - \frac{Fl_1^3}{3EI_{x2}}\right] + \left[k_1\frac{Fl_1}{GA_1} + k_2\frac{Fl_2}{GA_2}\right]$$

Comparing term by term the above expression with (1) we can see full analogy. There are, however, a couple of minor differences. One is in that the continuum beam employs G, since it undergoes shearing in material, while a truss does not undergo it, hence in both (2) and (3) modulus of elasticity is employed. We see that equivalent shearing rigidities S_{e1} and S_{e2} in the truss stand for GA_1/κ_1 and GA_2/κ_2 in a continuum beam. Second difference is in that the moments of inertia for the continuum beam depend only on the cross-section geometry. However, the equivalent moments of inertia introduced by the exp. (2) depend on the number of cells n (n_1 and n_2), and therefore on the relative length of the truss. A detailed analysis in [11] has shown that the influence of n decreases when n grows.

3. Conclusion

In this paper a formula for calculating the free end deflection of a two span cantilever truss beam with repeated cells is derived using continuum modelling method developed by the same authors. It is shown that the concepts of the equivalent bending and shearing rigidity established in their earlier papers for single span trusses can be extended to two spanned trusses as well. The method yields the formulas suitable for analysis of how defferent geometric design factors may influence the overall deformation behavior of this type of load carrying structures. The full analogy of formulas for the truss and continuum beam has been identifyed.

REFERENCES

[1] Noor, A. K., Mikulas, M. M. Continuum Modeling of Large Lattice Structures, *Status and Projections*, NASA Technical Paper 2767, 1988.

[2] Dow, J. O., Su, Z. W., Feng, C. C., Bodley, C. Equivalent Continuum Representation of Structures Composed of Repeated Elements, *AIAA Journal*, 1985, Vol.23, No.10, pp.1564-1569.

[3] Kenner, W. S. Lattice Truss Structural Response Using Energy Methods**,** North Carolina A&T State University, A Thesis Submitted to the Faculty of Old Dominion University in Partial Fulfillment of the Requirement for the Degree of Master of Sciences, 1987, 129 pages, NASA-TM-112361.

[4] Burgardt, B., Cartraud, P. Continuum Modelling of Beamlike Lattice Trusses, *Advances in Computational Techniques for Structural Engineering*, Budapest, Hungary, 21.-23. August 1996, pp51-59.

[5] Teughels, A., De Roeck, G. Continuum Models for Beam- and Platelike Lattice Structures, *IASS-IACM 2000 Fourth International Colloquium of Computations of Shell & Spatial Structures*, Channia Crete, Greece, 5.-7. June 2000., pp.1-20.

[6] Dedic, M.; Todorovic, M.: An Analysis of The Equivalent Stiffness of Beam-like Trusses with Constant Cross-section, *Congress of Theoretical and Applied Mechanics*, pp 347-352, April 10-13, Kopaonik, 2007.

[7] Todorovic, M.; Dedic M.: An Analysis of The Deformation of a Beam-like Truss Structure Using Method of Equivalent Continuum Beam, *7th International Conference "Research and Development in Mechanical Industry" RaDMI 2007*, 16 - 20. September 2007, Belgrade, Serbia, pp. 670-674, 2007.

[8] Dedic, M.; Todorovic, M.: Calculation of the Free End Deflection and Slope of a Cantilever Truss in distributed load, *The Sixth Triennial International Conference Heavy Machinery, HM 2008*, E.1, 24-29 June 2008, Kraljevo.

[9] Todorovic, M., Dedic, M.: Calculation of Cantilever Truss Beam Deformations Using Continuum Modeling, *Journal of Modelling and Optimization in the Machines Building Field (MOCM)*, MOCM -15, Vol. 2 (2009). pp 87-98, 2009.

[10] Todorovic, M., Dedic, M., Cajetinac, S., Jevremovic, V.: Influence of Cross-section Areas of Bars to Deformations of a Truss Beam, 9th International Conference *"Research and Development in Mechanical Industry"* RaDMI 2009, pp. 395-400, 16 - 19. September 2009, Vrnjačka Banja, Serbia, ISBN 978-86-6075-007-7, 2009.

[11] Todorovic, M.; Calculation of deformations in the plane of a load carrying truss beam with the constant cross-section by method of equivalent continuum beam, Ph.D. Thesis, 2010., Faculty of Mechanical Engineering in Kraljevo, University of Kragujevac.

HEAVY MACHINERY - HM 2011, 17-21 Paper accepted: 30.05.2011
ISBN 978-86-82631-58-3

Influence of Hole's Shape on the Stress Concentration at A Stress Plate Bending And Tension

Nada Bojić[1*], Zvonimir Jugović[2], Marko Popović[2], Radomir Slavković[2]
[1] *Fabrika sita i ležaja- FASIL A.D- Arilje*
[2]*Univerzitet u Kragujevcu – Tehnički fakultet Čačak*

Stress analysis plate with holes of various shapes is the main problem of this paper.Stress and deformation of complex structures, complex geometrical shapes and complicated boundary conditions that describe the differential equations, often can not be solved by analitical means. In these cases, search approximate particular solutions using numerical methods. To obtain the results of stress distribution in a plane isotropic field weakened holes, was used (finite element method).

Keywords: condition stress, stress concentration, finite element metod, numerical methods.

INTRODUCTION

During the design process of machine parts, one of the most important tasks that the designer has to solve is the determination of stress and stress conditions. The proper approach and solution to this problem depends largely on the quality and reliability of the structure. Mechanical parts of composite forms are often used in construction of mining and construction machinery, which exploitation conditions are extremely difficult. Calculation analyzes of these components is relevant for the construction of metal structures such equipment. The appearance of variation in a local stress increase in the points where cross sections of machine elements varies is called the stress concentration. Sources of stress concentration are critical elements of the machine.

In these so-called. dangerous places, increasing the stress at the straining effect to dynamic endurance decreasing, there are cracks due to fatigue and fracture of elements made of fragile materials, due to static loads. Rating concentrations of the stress concentration factor is over-stress, which is the ratio between the maximum stress in the zone of concentration and the nominal stress.

$$\alpha_k = \frac{\sigma_{\max}}{\sigma_n} \quad , \quad \alpha_{ks} = \frac{\tau_{\max}}{\tau_n} \qquad (1)$$

where σ_n and τ_n are nominal stress.

Stress concentration degree depends on weakened of critical cross-section, and occurrence of stress concentration itself can be explained by the stress flow curves in the zone pad if planes contain the hole, as in the above examples, then the stress intensity increases in the area of the opening. This is because the stress lines for sailing around the opening deviates and intends and to go the shortest route so they focus themselves near the hole. Considerable research on this topic were carried out by $\left[5,6,8,9\right]$.

1 BASIC EQUATIONS OF THE PLANE PROBLEM OF LINEAR THEORIES OF ELASTICITY

Plane stress state and plane strain are two physically different problems involving plane problems of linear elasticity theory of isotropic bodies. To solve the problem in the present investigation is the process of flat stress state. Considered the mechanical part of the plate shape in which one dimension, much smaller in dimension than the other two dimensions.The plate is of thickness loaded by uniformly distibuted surface forces which are attacking line parallel basis. At any point of elastic body, stress state is determined by these problems, the stress components in the absence of volume forces satisfy the equilibrium equation

$$\frac{\partial \sigma_x}{\partial x} + \frac{\partial \tau_{xy}}{\partial y} = 0, \qquad (2)$$

*Corr. Author's Adress: Fabrika sita i ležaja- FASIL A.D- Arilje

$$\frac{\partial \tau_{xy}}{\partial x}+\frac{\partial \sigma_y}{\partial y}=0, \qquad (2)$$

and conditions for compatibility:

$$\left(\frac{\partial^2}{\partial x^2}+\frac{\partial^2}{\partial y^2}\right)\left(\sigma_x+\sigma_y\right)=0. \qquad (3)$$

The whole problem can be simplified if equations (2) and (3) are set under integral formula, if only certain boundary conditions are satisfied. Depending on what is given on the contours of the observed field, two main groups of tasks can be distinguished, as follows: When on contours of the observed area are given external forces X_n and Y_n, boundary conditions can be written in the form:

$$\begin{aligned}\sigma_x \cos(n,x)+\tau_{xy}\cos(n,y)&=X_n\\ \tau_{xy}\cos(n,x)+\sigma_y\cos(n,y)&=Y_n\end{aligned} \qquad (4)$$

where n - external normal to the contour L.

When on contour L given the observed area are given displacements then boundary conditions will have the following form:

$$u=g_1(s), \quad \upsilon=g_2(s), \qquad (5)$$

$g_1(s)$ i $g_2(s)$ - are given displacements of the points on the outline *L*. $[7]$

2 FINITE ELEMENTS METHOD

It should be noted that the analytical solving of certain problems such as stress state, the state of deformation of complex structures and complicated boundary conditions can be difficult because of cumbersome mathematical procedures and deadlines that are set in solving problems. For a more detailed calculation of stress in order to take account of all influencing factors in the field plate, which has weakened the sources of stress concentration, for research in this paper will use the numerical methods that are based on finite element methods that are suitable for the analysis of sources of stress. One of the basic features of numerical methods consists in the fact that the fundamental equations of the theory of elasticity, including the approximate boundary conditions solved numerically.The solutions is approximate, but may be still close to the solution as much as it wants in the given situation. In the finite element method, where the final result obtained by solving systems of algebraic equations, and discretization is performed in the physical model.
In this paper, the finite element mesh generation and calculation, we used licensed software package NASTRAN $[2,3,5,6,8]$.

KE vector fields, can be written in the form of functione:

$$\mathbf{s}=\mathbf{A}\,\mathbf{c}, \qquad (6)$$

Where is:

s- vector displacement in the elements,
A- field finite element matrix,
c- is a vector column
Boundary conditions may generally write:

$$\mathbf{s^k}=\mathbf{S}=\mathbf{s_k};\ \mathbf{A_k}\,\mathbf{c}=\mathbf{s}_\mathrm{k}=\mathbf{S} \qquad (7)$$

$\boldsymbol{A_k}$ – matrix field thresholds. The basic equations can be written in the form of:

$$\mathbf{F^e}=\mathbf{K^e}\ \mathbf{S}+\mathbf{F^t} \qquad (8)$$

Neglecting the influense of temperature stress, the basic equation, we obtain the form:

$$\mathbf{F^e}=\mathbf{K^e}\ \mathbf{S} \qquad (9)$$

$\boldsymbol{K^e}$ –finite element stiffness matrix..

And design equation has the form:

$$\overline{\mathbf{F}}=\overline{\mathbf{K}}\ \overline{\mathbf{S}} \qquad (10)$$

3 RESULTS

In the following example of plate dimensions are the same and they are: *4m x 6m x 0,1m.* Are stressed in bending (picture left)) and stress (picture right) weakened the (triangular, rectangular and circular hole).

Plate is made of steel with modulus of elasticity $E = 2{,}1x10^5\,MPa$ i Poissons ratio $\mu = 0{,}33$.

Example1. In this example, are considered the plates weakened the triangular hole.

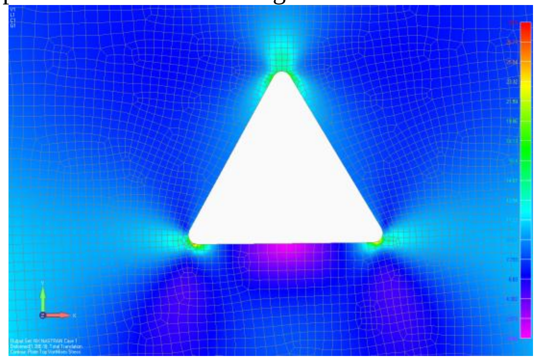

Fig. 1. Stresses in a bending plate weakened the triangular hole

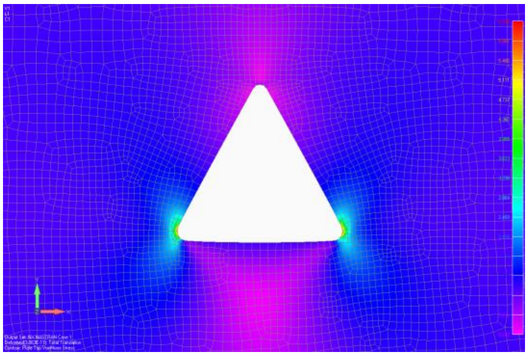

Fig. 2. Stresses at uniaxial tension at weakned plate with a hole in a form of triangular α=0°

The maximum stress value with Figures 1. $\sigma_{\max}$ =28.5 N/m² is obtained numerically.

The maximum stress value with Figures 2. $\sigma_{\max}$ = 6.235 N/m² is obtained numerically.

Example 2. In this example, are considered the plates weakened the rectangular

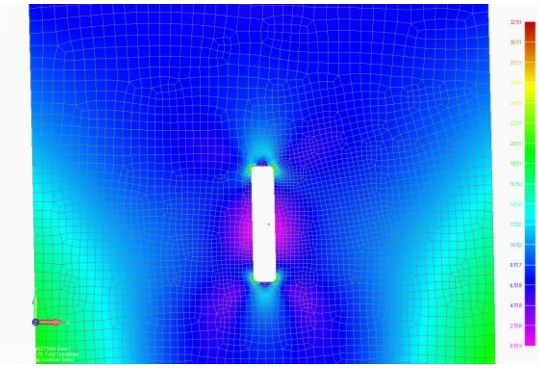

Fig. 3. Stresses in a bending plate weakened the rectangular hole

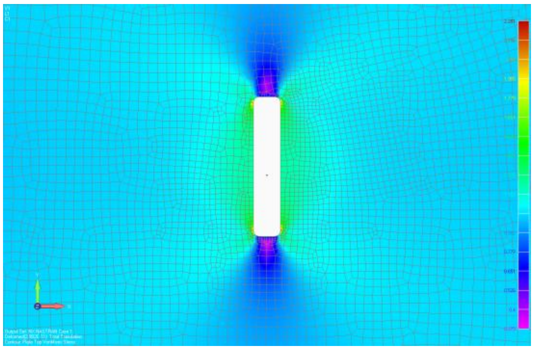

Fig. 4. Stresses at uniaxial tension at weakned plate with a hole in a form of rectangular α =90°

The maximum stress value with Figures 3. $\sigma_{\max}$ = 32,51N/m² is obtained numerically.

The maximum stress value with Figures 4. $\sigma_{\max}$ =2,281 N/m² is obtained numerically.

Primer 3 In this example, are considered the plates weakened the circular hole.

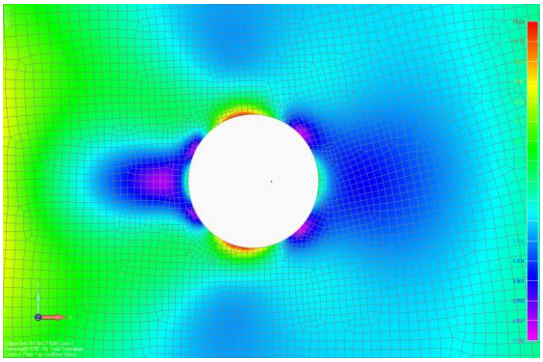

Fig. 5. Stresses in a bending plate weakened the circular hole

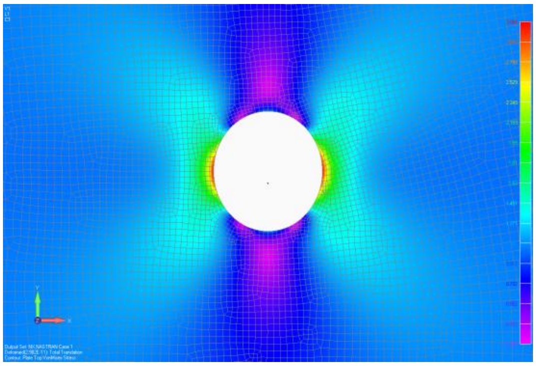

Fig. 6. Stresses at uniaxial tension at weakned plate with a hole in a form of circular

The maximum stress value with Figures 5. σ_{max} = 15,63N/m^2 is obtained numerically.

The maximum stress value with Figures 6. σ_{max} = 3,08N/m^2 is obtained numerically.

Exsample 4 In this example, are considered the plates weakened the ellipse hole.

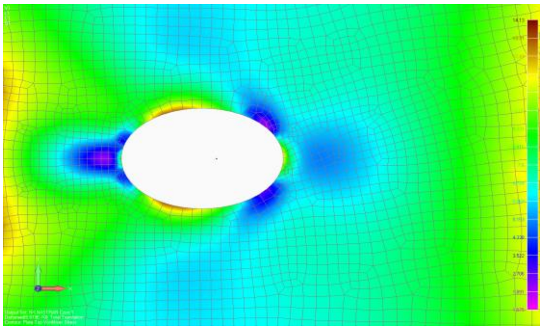

Fig. 7.. Stresses in a bending plate weakened the ellipse hole

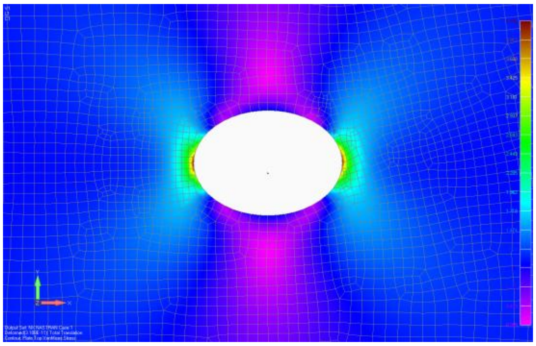

Fig. 8. Stresses at uniaxial tension at weakned plate with a hole in a form of ellipse $\alpha = 0^o$

The maximum stress value with Figures7. σ_{max} = 14,13N/m^2 is obtained numerically.

The maximum stress value with Figures 8. σ_{max} = 4,156N/m^2 is obtained numerically.

Table 1. Values of geometric stress concentration factor for the case of bending

triangular	*rectangular*	*circle*	*ellipse*
$\alpha_{к}$= 2.42	$\alpha_{к}$= 2.43	$\alpha_{к}$= 1.48	$\alpha_{к}$= 1.55

Table 2.Values of geometric stress concentration factor for the case uniaxial tension

triangular	*rectangular*	*circle*	*ellipse*
$\alpha_{к}$= 4.83	$\alpha_{к}$= 5.08	$\alpha_{к}$= 2.62	$\alpha_{к}$= 3.84

4 CONCLUSION

This study is an attempt to create a mathematical model and develop methodology in order to get to the resalts of stress distribution in a plane isotroplic field which is weakned by holes. Depending on the physical and geometrical sizes are reduced to establishing connections between the stresses and external load has been described by differential equations. The results in this paper obtained the finite element method, compared to the results from the literature obtained by analytic and showed the same agreement. The main parameter in all these examples was the relation between plate’s wide and hole’s dimensions. Setting the correlation between this relation and the stress itself it might be concluded that if hole’s dimension is increased the section became weakened, while at the same time, the stress is increased and opposite. Based on obtained results for plates disposed to the extensile stress and bending stress it might be seen that position and the shape of the hole are the parameters that the most impact to the stress concentration. And the concentration itself increases the real stress compared to nominal ones. The most suitable shape is the circle, ellipse, then triangular, and the worst shape rectangular and for case of bending and of case uniaxial tension.

5 REFERENCES

[1] Nada Bojić, Zvonimir Jugović, Marko Popović.:UTICAJ OBLIKA OTVORA NAPONSKO STANJE KOD DELOVA MAŠINSKIH KONSTRUKCIJA PRI JEDNOOSNOM ZATEZANJU PLOČA , IMK 14 oktobar, ISSN 0345-6829, br 35 2/2010, 17-22.

[2] Nada Bojić, Zvonimir Jugović.: ANALYSIS OF STRESS IN PLATES WITH HOLES, RaDMI br 1,189-198, 2010 Donji Milanovac

[3] Nada Bojić, Zvonimir Jugović.: STRESS CONCETRATION IN PLATES WITH ONE HOLE KOD 2010 , 73-77 Palić.

[4] СавинН.Г.:Распределениенапреженииоколо отверстии, Наукова думка, Киев1968.

[5] Bojić Nada.: Magistarski rad.: Naponsko deformaciono stanje u zonama izvora koncentracije napona kod elemenata mašinskih konstrukcija, Kragujevac 2009 godine.

[6] Kojić M., Slavković R., Živković M., Grujović N.: Metod konačnih elemenata I, Linearnaanaliza, Kragujevac, 1998.

[7] Rašković D.: Teorija elastičnosti, Naučna knjiga, Beograd, 1985 godine

[8] Emanuele Maiorana, Carlo Pellegrino , Claudio Modena.: Non-linear analysis operforated stee plates subjected to localized symmetrical load, Journal Constructional Steel Research 65 (2009)959-964.

5 ACKNOWLEDGEMENTS

The project No.TR35037: “Development of new bucket design for continuous excavators due to the installation of modular cutting teeth”, is financed and supported by the Ministry of Science of the Republic of Serbia. The authors would like to acknowledge this contribution.

HEAVY MACHINERY - HM 2011, 23-28
ISBN 978-86-82631-58-3
Paper accepted: 30.05.2011

Alloy characterization and liquidus surface definition of ternary Bi–Cu–In system

Duško Minić[1]*, Zvonko Petrović [2], Milena Premović[1] and Miljana Marković[1]
[1] University in Priština, Faculty of technical science, Kos. Mitrovica, Srbija
[2] University of Kragujevac, Faculty of Mechanical Engineering Kraljevo, Serbia

SUMMARY. *Lead-free solders with copper represent possible substitution for standard lead-tin solders. For the complete definition of the properties of the ternary Bi–Cu–In system, there were performed the investigation of micro structures, hardness by Brinel, and electric conductivity of the alloys. In the range of this ternary system, some ten alloys were tested. The micro structures of the alloys at room temperatures were investigated by application of Scanning Electron Microscopy (SEM) with Energy Dispersive Spectrometer (EDS) and optic microscopy. By application of CALPHAD method there were calculated the isothermal cross section at 25^{0}C and liquidus surfaces. There were also determined the invariant reactions inside the presented system.*

Key words: Bi–Cu–In system, microstructure, hardness, electric conductivity, liquidus

1. INTRODUCTION

The investigations of the low temperature ternary systems in order to substitute the low temperature lead based solders, were performed around the world for a long time now. In recent years these investigations were expanded to the high temperature ternary systems with copper. The great interest for these systems is a consequence of the wide application of these alloys in various industries

The calculated isothermal section at 25^{0}C liquidus surface for ternary Bi–Cu–In system were done by applying (CALPHAD) method [1], using optimized thermodynamic parameters for constitutive binary systems which were included in database COST531 [2].

Binary Bi–Cu system is a simple eutectic system. Thermodynamic parameters for this system were included in reference [2], *Teppo* et al. [3] determined phase diagram and optimization of thermodynamic data. Phase diagram of Bi–In binary system with thermodynamic data was determined by *Boa and Ansara* [4]. The thermodynamic data and phase diagram of constitutive Cu–In binary system were taken from the references [5, 6].

The ternary Bi-Cu-In system was studied by *Itabashi* et al. [7], and they determined the activities of indium in the presented system. *Aljilji* et al. [8] defined several quasi binary sections for the system, comparing the experimental values obtained by using Differential Thermal Analysis and calculated values.

2. EXPERIMENT

The alloy samples were prepared from high-purity (99,999%) indium, bismuth and copper produced by Alfa Aesar (Germany). The samples mass weight of 4 g were prepared in inductive furnace in Argon atmosphere and cooled on air. The samples used for optic microscopy, electric conductivity measurements and hardness tests were prepared by classic metallographic procedure without penetration. The samples of alloy investigated on SEM-EDS were not sealed.

Electron microscopy was done on Scanning Electron Microscopy instrument from JEOL (JSM6460), with Energy Dispersive Spectrometer, EDS by Oxford Instruments.

Optic microscopy was done using Optic microscope OLYMPUS GX41, hardness was measured by Duroscope method using HL-400DL instrument. Electrical conductivity measurements were carried out with SIGMATEST 2.069.

3. RESULTS AND DISCUSSION

Phase names used in this paper with phase names included in thermodynamic data base COST531

*Corr. Author's Adress: Faculty of Technical Sciences, Knjaza Milosa 7, 38220, Kosovska Mitrovica, Serbia, dminic65@open.telekom.rs

[2] with their Pearson's symbols are listed in Table 1.

3.1. Microstructure analysis

In order to determine microstructure of the alloys of the ternary Bi–Cu–In system, the microstructures for numerous alloys were determined, ten to be precise, and the compositions of the considered alloys were given with Isothermal cestion in ternary Bi–Cu–In systema at 25 ^{0}C on Fig. 1. The obtained microstructures were presented on Fig. 2.

Table 1. Considered phases, phase's name in the thermodynamic data base and Pearson's symbols [9].

Phase name	Phase name in thermodynamic data base	Pearson's symbols
L	LIQUID	-
(Cu)	FCC_A1	*cF*4
(Bi)	RHOMBO_A1	*hR*2
BiIn	BIIN	*tP*4
Bi_3In_5	BI3IN5	*tI*32
$BiIn_2$	BIIN_BRASS	*hP*6
(In)	TETRAG_A6	*tI*2
ε	TET_ALPHA1	*tI*2
β	BCC_A2	*cI*2
γ	CUIN_GAMMA	*cP*52
э	CUIN_ETA	*hP*4
δ	CUIN_DELTA	*aP*40
η	CUIN_ETAP	*hP*6
$Cu_{11}In_9$	CUIN_THETA	*mC*20

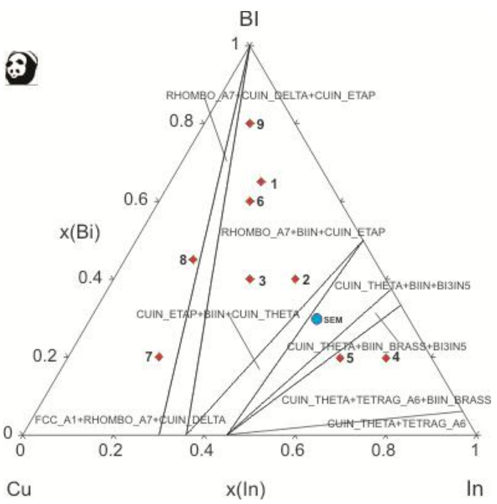

Fig. 1. Isothermal cestion in ternary Bi–Cu–In systema at 25^{0}C

The existence of eight areas, three of them larger and five smaller were showed on Fig. 1. One smaller field were two- phase ($Cu_{11}In_9$+(In)) and all other areas were three phases areas. By observing microstructures showed on Fig. 2, the presence of all three phases in microstructures can be confirmed. For example, microstructure number nine has three phases, the darkest phase is basic, and than there is lighter large grain phase and the lightest small grained and the least phase. If that alloy is observed on Fig. 2, it can be seen that it is situated in the three phase ((Cu) +(Bi) + δ) region. It can be stated that the basic of the microstructure is phase which is the darkest phase rich with copper (Cu), large grained lighter phase is rich with bismuth (Bi) and third phase is the least present in the microstructure, and it is intermetallic copper-indium compound (CUIN_DELTA). In the next part, the alloy with molar ratio x(Bi)=0,3, x(Cu)=0,2 and with 0,5 indium was analyzed on Scanning Electron Microscope (SEM) with EDS, and obtained microstructure was presented on Fig. 3. There were three phases on the microstructure, and there were analyzed three compositions for each phase. Based on the obtained results the phases on the microstructure were marked. The obtained values correspond to phase (BiIn + $Cu_{11}In_9$ + η) in the region from Fig. 1.

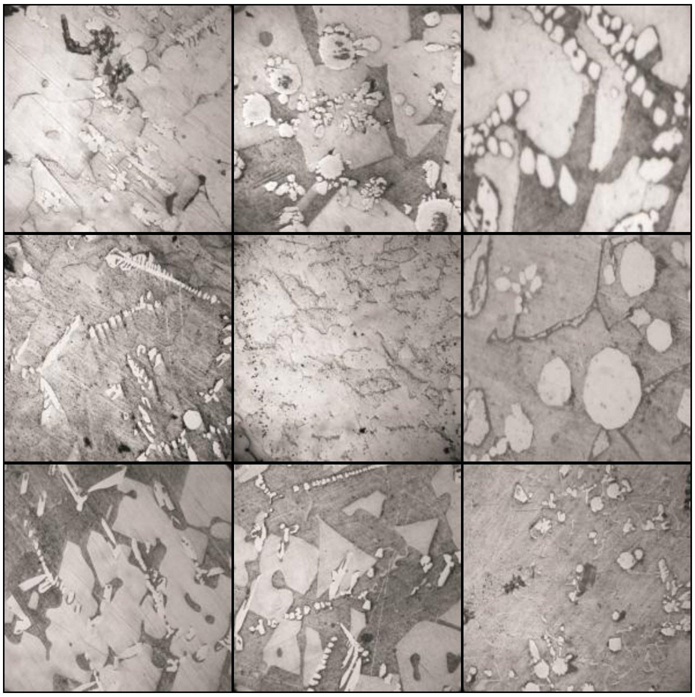

Fig. 2. Microstructures of alloys, 800X.

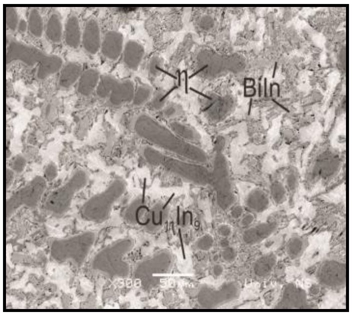

Fig. 3. SEM microstructure.

3.2. Electric conductivity of alloys

As the alloy's properties in the ternary Bi–Cu–In system were not studied properly until now, the electric conductivity was investigated here. The electric conductivity for three quasi binary sections BiCu–In, InBi–Cu and InCu–Bi was investigated. Based on experimentally determined electric conductivities of alloys for three quasi binary sections, the electric conductivity for all ternary Bi-Cu-In system was determined by application of regression model [10]. Theoretic regression model can be presented in a for of multiplied quasi linear regression:

$$\hat{Y} = b_1X_1 + b_2X_2 + b_3X_3 + b_{12}X_1X_2 + b_{13}X_1X_3 + b_{23}X_2X_3 \qquad (1)$$

Unknown values of the coefficients of multiplied regression were determined by the least square method, i.e. from the condition that sum of the quadrates of errors:

$$S = S(b_1, b_2, b_3, b_{12}, b_{13}, b_{23}) = \sum_{i=1}^{N} \varepsilon_i^2 = \sum_{i=1}^{N} (Y_i - \hat{Y}_i)^2 \qquad (2)$$

$$S = \sum_{i=1}^{N} \varepsilon_i^2 = \sum_{i=1}^{N} \begin{bmatrix} Y_i - (b_1X_1 + b_2X_2 + b_3X_3 + b_{12} \\ X_1X_2 + b_{13}X_1X_3 + b_{23}X_2X_3)_i \end{bmatrix}^2 \qquad (3)$$

is minimum. The coefficients of regression were determined, and mathematic model, presented by the equation (1) could be written as:

σ = 11, 449x(In) + 1,89x(Bi) + 56,808x(Cu)-2,166x(In)x(Bi)–106,164x(In)x(Cu)-101,337 x(Bi)x(Cu) (4)

The mathematic model defined by equation (4) is presented as a graph on Fig. 4.

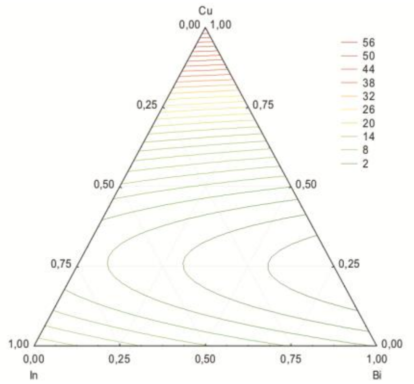

Fig. 4. Iso-lines of electric conductivity for the ternary Bi–Cu–In system.

For quasi-linear model of multiplied regression given by equation (1) the quadrates of discrepancies of empiric values from regression equation and sum of quadrates of discrepancies was obtained SK=110,3626. As the absolute value of the greatest discrepancies was ε_{max}=5.867 and less than 3*E= 6.7192, so based on the three σ rule, the assumed functional dependence was considered accurate.

3.3. Mechanical properties

The hardness of alloys was determined by Brinel. The hardness of alloys in three quasi binary sections of ternary Bi–Cu–In system: BiCu–In, InBi–Cu and InCu–Bi were investigated. The mathematic model presented by equation (1) for alloy's hardness by Brinel in the ternary Bi–Cu–In system could be written:

HB = 140,0377(In) + 118,9386x(Bi) – 4,2773

x(Cu)-113,3939x(In)x(Bi)+88,048x(In)x(Cu)

+539,2145-x(Bi)x(Cu) (5)

Mathematic model defined by equation (5) was presented as graph on Fig. 5.

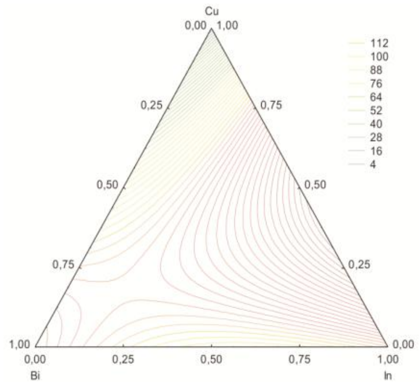

Fig. 5. Iso-lines of hardness by Brinel for ternary Bi–Cu–In system.

For quasi-linear model of multiplied regression, given by equation (1), the quadrates of discrepancies of empiric points from regression equation were calculated, and the sum of discrepancies quadrates was SK=32045,88605. As absolute value of the largest discrepancy was ε_{max}=67,13922 less than 3*E= 114,4975138 so based on three sigma rule, the assumed functional dependence was considered good.

3.4. Liquidus surface

Based on literature thermodynamic data for constitutive binary systems by CALPHAD method with usage of software package Pandat 8.1 the liquidus surface of the ternary Bi–Cu–In system was calculated. The liquidus surface is showed on Fig. 6.

Three large surfaces of primary crystallization were observed on Fig. 6. (FCC_A1, CUIN_DELTA i CUIN_ETA), as well as nine smaller fields (RHOMBO_A7, BIIN, CUIN_ETAP, TET_ALPHA1, TETRAG_A6, CUIN_THETA, CUIN_GAMMA, BCC_A2 i CUIN_DELTA) and field constituted in the miscibility gap in liquid state (LIQUID).

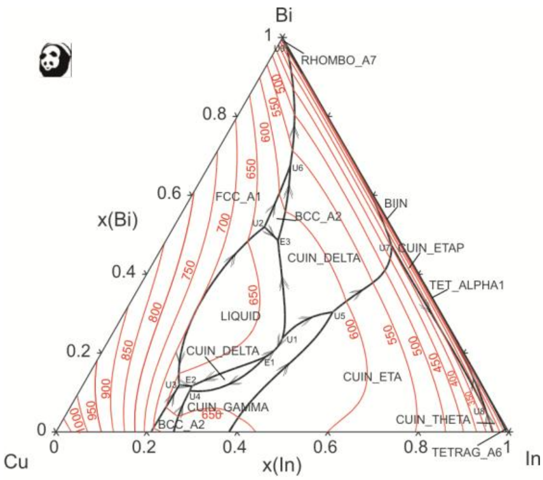

Fig. 6. Liquidus surface of the ternary Bi–Cu–In systema.

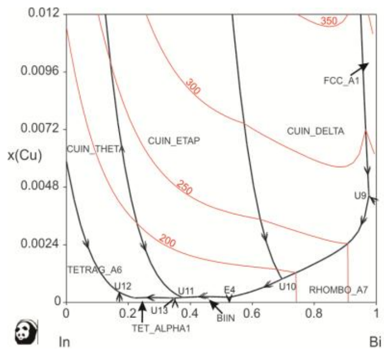

Fig. 7. Magnified view of liquidus surface on the side of In–Bi binary system.

Ternary Bi–Cu–In system forms some very small fields of crystallization on the side of the constitutive binary In–Bi system as showed on Fig. 6, which can not be seen clearly on the liquidus surface for whole ternary system. The magnified view of this part of liquidus surface is given on Fig. 7.

It can be seen on Fig. 6. that ternary Bi–Cu–In system is one complex system, and it can be also concluded on the calculated invariant reactions in ternary Bi–Cu–In system, presented in Table 2.

In the railway industry, one of the significant developments is the use of active controls for railway. There are nineteen invariant reaction going on in the ternary Bi–Cu–In system, six of them are monotectic (E-type of reaction) and other thirteen are transition reaction (U-type of reaction).

Table 2. Invariant reactions in ternary Bi–Cu–In system.

T /^{0}C	Reactions	Type
627,8	CUIN_DELTA -> LIQUID + LIQUID + CUIN_GAMMA	E1
627,8	LIQUID + CUIN_DELTA -> LIQUID + CUIN_GAMMA	U1
624,03	LIQUID + FCC_A1 -> BCC_A2 + LIQUID	U2
624,03	FCC_A1 + LIQUID -> LIQUID + BCC_A2	U3
616,34	LIQUID + CUIN_GAMMA -> CUIN_DELTA + BCC_A2	U4
613,57	LIQUID -> BCC_A2 + LIQUID + CUIN_DELTA	E2
613,57	LIQUID -> LIQUID + BCC_A2 + CUIN_DELTA	E3
612,67	LIQUID + CUIN_GAMMA -> CUIN_ETA + CUIN_DELTA	U5
565,15	LIQUID + BCC_A2 -> CUIN_DELTA + FCC_A1	U6
390,16	LIQUID + CUIN_ETA + CUIN_DELTA -> CUIN_ETAP	U7
294,9	LIQUID + CUIN_ETA -> CUIN_ETAP + CUIN_THETA	U8
266,23	LIQUID + FCC_A1 -> CUIN_DELTA + RHOMBO_A7	U9
183,74	LIQUID + CUIN_DELTA -> CUIN_ETAP + RHOMBO_A7	U10
109,17	LIQUID -> CUIN_ETAP + RHOMBO_A7 + BIIN	E4
95,49	LIQUID + CUIN_ETAP -> BIIN + CUIN_THETA	U11
90,62	LIQUID + TETRAG_A6 -> CUIN_THETA + TET_ALPHA1	U12
88,67	LIQUID + BIIN -> CUIN_THETA + BI3IN5	U13
87,72	LIQUID -> CUIN_THETA + BI3IN5 + BIIN_BRASS	E5
71,73	LIQUID -> CUIN_THETA + BIIN_BRASS + TET_ALPHA1	E6

4. CONCLUSION

The microstructures of the alloys of ternary Bi–Cu–In system are presented in this paper. Phases in microstructures show good agreement with calculated phases at 25^0C. That was confirmed by SEM – microstructure, for which there was analysis done in single point for all existing phases. Based on experimentally determined electric conductivity and hardness by Brinel for many alloys from three quasi binary sections by using regression analysis the mathematic model for electric conductivity and hardness for entire ternary system was established. By using that mathematic model the graphic presentations of he electric conductivity and hardness for ternary Bi–Cu–In system were made.

Acknowledgements
This work was supported by Ministry of Science of the Republic of Serbia (OI172037).

REFERENCES

[1] N. Saunders, A.P. Miodownik, *CALPHAD* (A Comprehensive Guide), Elsevier, London, 1998.
[2] A.T. Dinsdale, A. Kroupa, J. Vízdal, J. Vrestal, A. Watson, A. Zemanova, *COST531 Database for Lead-free Solders*, Ver. 3.0, 2008, Unpublished Research.
[3] O. Teppo, J. Niemela, P. Taskinen, *Report TKK-V-B50*, Helsinki University ofTechnology, 1989.
[4] D. Boa, I. Ansara, *Thermochim. Acta* 314 (1) (1998) 79–86.
[5] X.J. Liu, H.S. Liu, I. Ohnuma, R. Kainuma, K. Ishida, S. Itabashi, K. Kameda, K.Yamaguchi, *J. Electron. Mater*. 30 (9) (2001) 1093–1103.
[6] H.S. Liu, X.J. Liu, Y. Cui, C.P. Wang, I. Ohnuma, R. Kainuma, J.P. Jin, K. Ishida, *J. Phase Equilibr*. 23 (5) (2002) 409–415.
[7] S. Itabashi, K. Kameda,K.Yamaguchi, K. Toshiko, *J. Jpn. Inst. Met*. 63 (7) (1999)817–821.

HEAVY MACHINERY - HM 2011, 29-32
ISBN 978-86-82631-58-3
Paper accepted: 30.05.2011

Design and optimization for truss constructions using the software package Autodesk Inventor 2011®

Mladenovic Goran, dipl.ing,[1,*] Mr Popovic Mihajlo[1]

[1] Faculty of Mechanical Engineering, Department for Production Engineering, Belgrade University, Kraljice Marije 16, 11120 Belgrade 35, Serbia

The use of truss constructions is frequent in mechanical engineering. This paper describes the procedures of construction and optimization for truss constructions at the example of roof structure of the Hall. Frame Analysis is used to understand the structural integrity for given frame with respect to deformations and stresses, when subjected to various loading and constraints. Once when the criteria are defined, it is possible to run the simulation and view the behavior relative to the conditions which are defined. Simulations help to identify performance issues and find better design alternatives. The paper doesn't gives the analysis of load, but structure optimization is performed for defined load. In the process were used two approaches, change of beam geometry without changing the profile and change the profile without changing beam geometry.

Keywords: Truss constructions, Autodesk inventor 2011®, Frame Analysis, Optimization

1. INTRODUCTION

The truss welded structures are commonly used in mechanical engineering. The frameworks used to support the roofs of buildings are perhaps the most common truss constructions. Modeling of these structures is different from software to software. Sometimes it is necessary to draw a sketch of the cross section, and then the sketch extrude through a trajectory. Software Package Autodesk Inventor 2011® has the possibility to select standard profiles from database; it is only necessary to define the frame - skeleton of the structure. The advantage of this type of modeling is because with the starting the Frame Analysis environment and start a new analysis, the Frame Generator assembly is automatically converted into simplified model of beams and nodes. Because of the volume, in this paper we do not address the load problem, but we only perform the structure optimization for predefined concentric load of 15KN. In the process we have used two approaches, the change in beam geometry without changing the profile and the change in the profile without changing the beam geometry.

2. MODELING STRUCTURES

For modeling the structure it is necessary to first sketch the skeleton. It is enough to do sketch within a one sketch, as shown on Fig. 1. In the same figure is shown places where loads are acting.

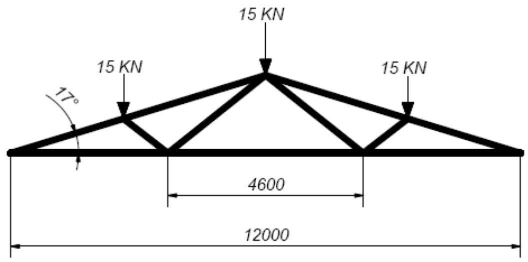

Fig. 1. The skeleton structure with defined loads

After defining the skeleton it is used the command Frame Generator. The above mentioned command requires the selection of standard profiles, materials, and a choice of line from the skeleton on which will be find the selected profile. Length of the selected profiles match the length of lines in the sketch and it is necessary subsequent to repair ends of the profiles using the commands Trim, Extend, Notch, and Miter. Using commands Change it is easy and quick to change a profile on construction which is of great importance for optimization process. After the implemented commands selected 3D model of the structure look like shown on the Fig. 2.

*Corr. Author's Address: FME, Belgrade University, Kraljice Marije 16, 11120 Belgrade 35, Serbia, gmladenovic@mas.bg.ac.rs

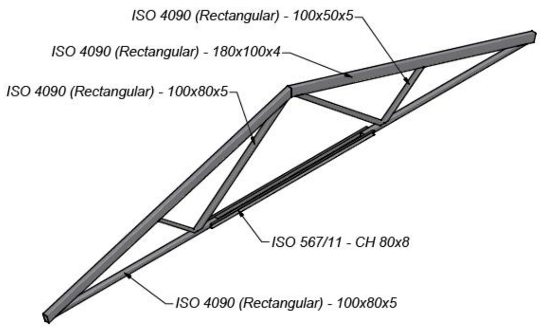

Fig. 2. 3D model of the roof structure

3. STRUCTURAL ANALYSIS

Frame Analysis is used to understand the structural integrity of a given frame with respect to deformations and stresses, when subjected to various loading and constraints. Once when the criteria are defined, it is possible to run the simulation and view the behavior relative to the conditions which are defined. Simulations help to identify performance issues and find better design alternatives. Beam elements are linear. Frame analysis does not support curved beams.

When the Frame Analysis environment is opened and starts a new analysis, the Frame Generator assembly is automatically converted into simplified model of beams and nodes.

From a high-level perspective, a typical frame analysis workflow looks like the following:

1. **Set expectations**: Estimate physical behavior using a conceptual model.
2. **Pre-processing**: Enter physics into the model and define analyses to perform.
3. **Solving**: Solve the mathematical model.
4. **Post-processing**: Display and evaluate the results.
5. **Review expectations**: Compare the results with the initial expectations.
6. **Conclusion** (Improve Inputs).

Next step is to create a simulation, and when the simulation is created it contains:

- Simulation Type
- Materials
- Sections
- Loads
- Constraints
- Releases
- Rigid Links

It should be noted that the software included the weight of the structure as a particularly stressful load.

After all this defined and simulation is finished it is possible to view results of simulation. That result includes:

- Forces
- Moments
- Stresses

On the Fig. 3 and Fig. 4 is shown the calculation results, only for displacements and the maximum normal stresses. It is possible to output results in HTML, MHTML, or RTF format. Reports contain text and PNG images that represent a static snapshot of the analysis results. For the observed structure and loads, the maximum displacement was 4.363 mm, and maximum Normal Stress was 70.7 MPa, the construction weight is 468.391 kg.

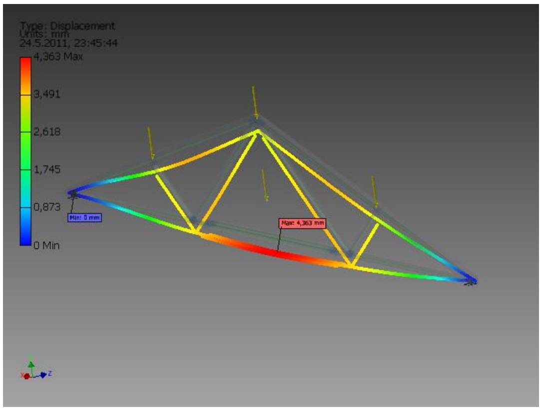

Fig. 3. Displacement

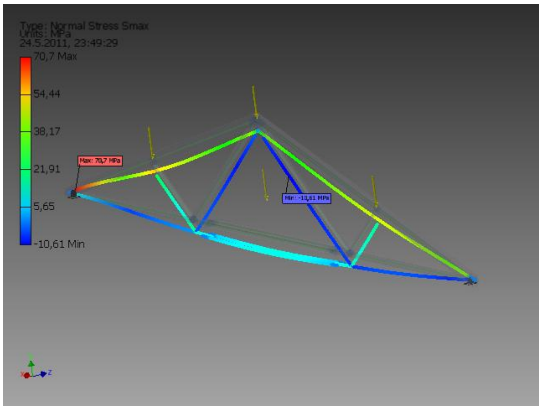

Fig. 4. Normal Stress (S_{MAX})

4. STRUCTURAL OPTIMIZATION

For better visibility beams are numbered with numbers 1 – 5 as shown in Fig. 5.

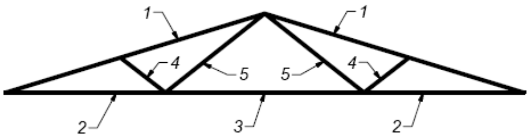

Fig. 5. Numbered beams

The results of optimization are presented in the table 1. Optimization goal is to obtain a uniform stress distribution, and obtain the structure which has a lower weight. In this case the design approach was to vary the profile and restart the simulation with the same load. Based on the table below, it can be concluded that the most appropriate beams form is under number 4, because it gets a smaller displacement in vertical direction and uniform stress distribution than in the first case. The design weight was not significantly different from case to case.

***Table 1**. Results of optimization*

Number	Characteristics of the beam		Mass [kg]	Maximum displacement [mm]	Normal Stress (S_{MAX}) [MPa]
	Beam	Standard profile			
1	1	ISO 4090 (Rectangular) - 200x100x4	477.687	4.158	68.99
	2	ISO 4090 (Rectangular) - 100x80x5			
	3	ISO 567/11 CH 80x8			
	4	ISO 4090 (Rectangular) - 100x60x5			
	5	ISO 4090 (Rectangular) - 100x60x5			
2	1	ISO 4090 (Rectangular) - 180x100x4	464.942	4.235	72.1
	2	ISO 4090 (Rectangular) - 120x60x4			
	3	ISO 567/11 CH 120x12			
	4	ISO 4090 (Rectangular) - 80x60x5			
	5	ISO 4090 (Rectangular) - 80x60x5			
3	1	ISO 4090 (Rectangular) - 160x80x6	508.901	3.77	56.49
	2	ISO 4090 (Rectangular) - 120x60x4			
	3	ISO 567/11 CH 120x12			
	4	ISO 4090 (Rectangular) - 80x60x5			
	5	ISO 4090 (Rectangular) - 80x40x5			
4	1	ISO 4090 (Rectangular) - 160x80x6	471.309	3.843	57.52
	2	ISO 4090 (Rectangular) - 100x80x3			
	3	ISO 567/11 CH 100x10			
	4	ISO 4090 (Rectangular) - 80x60x5			
	5	ISO 4090 (Rectangular) - 80x40x5			

It was considered another case of the structure solution. The profiles are the same as for variant solutions under number 4, with inserted another vertical profile with dimensions 80x40x3. By inserting this profile, the maximum displacement was reduced to 3.13 mm and it was received a uniform stress distribution (maximum stress was 57.14 MPa) what is shown on Fig. 6. It should be noted that the weight of the structure is not significantly increased and in this case it was 480.65 kg.

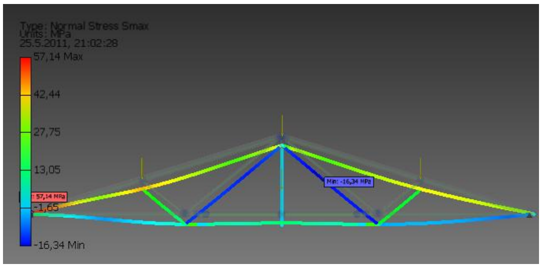

Fig. 6. Stress distribution for the case of added profile

5. CONCLUSION

This paper describes the procedures of construction and optimization of a truss construction at the example of roof structure of the Hall with the range of 12m. It was demonstrated the procedure using the command Frame Generator of the Software Package Autodesk Inventor 2011®, which use reduces the total time of time modeling the structure. Also was shown the process of analysis and design that was executed by command Frame Analysis. Structural analysis led to the optimum design which has the smallest displacement and the most uniform stress distribution for the same load, all in order to reduce the total weight of the construction. The paper doesn't gives the analysis of loads, but structure optimization is performed for defined load which acting in the three points as shown in Fig. 1.

6. REFERENCES

[1] Kalajdžić M., “Metod konačnih elemenata, osnovi statike, statika nosećih struktura, dinamika nosećih struktura, primene”, IAMA, Beograd, 1978

[2] Sekulović, M., “Metod konačnih elemenata”, Građevinska knjiga, Beograd, 1988

[3] Rašković, D., “Otpornost materijala”, Građevinska knjiga, Beograd, 1985

[4] Spyrakos, C. C., “Finite Element Modeling in Engineering Practice”, West Virginia University Press, Morgantown, WV

[5] Mattheck, C., “Design in der Natur”, der Baum als Lehrmeister, Rombach, Freiburg, 1997

[6] Autodesk Inventor 2011® Profesional - Help

[7] http://usa.autodesk.com/

HEAVY MACHINERY - HM 2011, 33-38
ISBN 978-86-82631-45-3
Paper accepted: 30.05.2011

An Analysis of Equivalent Rigidities of A Truss Beam

Milica Todorovic[1,*] - Milan Dedic[2]

[1]High Technical Mechanical School, Trstenik, Serbia
[2]Faculty of Mechanical Engineering Kraljevo, Kraljevo, Serbia

This paper presents how a method of continuum modeling can be applied in deformation analysis of truss structures. The method is based on changing a truss beam in continuum beam with bulk cross-section. By means of this method the expressions for an equivalent bending and an equivalent shearing rigidity of cantilever truss beams are derived in this paper. Different load types have been taken into consideration. The equivalent rigidities obtained were used to calculate the free end deflection and the free end slope of a cantilever truss beam. The paper brings discussion on how values of the equivalent rigidities depend on load type and properties of bars in the truss.

Keywords: trusses, continuum modeling, equivalent stiffness, deformations.

1. Introduction

In this paper we consider deformation properties of load-carrying trusses in the shape of cantilever beams. They are regularly designed with parallel longitudinal bars of equal cross-sections and repeating filling bars to supply for unification and simplicity. Deformation analysis of these trusses can be made by finite element method and by a number of approximate methods [1]. However a complex structure of a truss beam can also be treated as a continuum beam, if we now how to calculate it's equivalent strength characteristics. This method is referred to as continuum modeling. It has been discussed in details, for example, in [2], [3], [4].

The continuum modeling method is based on establishing relation between geometric and material characteristics of a truss beam and an equivalent continuum beam (a beam with bulk cross-section). However, the continuum model does not yield general formulas. It is rather developed depending on type of load, geometric characteristics and type of filling. The method of continuum modeling enables in many cases using simple formulas similar to the engineering formulas in strength of materials for calculating deformations in characteristic points – deflections and slopes. It also enables estimating the influence of design parameters to deformation behavior of the truss structure.

The theoretical foundation of the analysis in this paper has been developed by the same authors in [5], [6], [7], [8], [9], [10]. The focus of this paper is on the analysis of the equivalent bending and equivalent shearing rigidity of the laod carrying truss beams in question.

2. Calculation of deflection and slope of a planar truss beams

As a basic model for our analysis we take a statically determinate cantilever truss beam with unidirectional diagonal filling bars, with n repeating cells. It's geometry and dimensions are shown in Fig.1. Cross-section areas of the lower "*b*" and upper longitudinal "*t*" bars are denoted respectively as A_b and A_t, and of the vertical and diagonal bars as A_v and A_d.

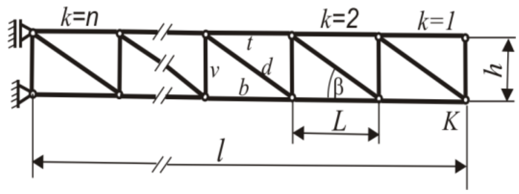

Fig.1. *Geometry and dimensions of a truss beam*

All the bars are of the same material with modulus of elasticity E. They are pin jointed, so that they are strained in pure tension or compression. We shall proceed with discussion for an in-plane truss beam, loaded in its plane, and point out that the same procedure with similar results can be readily derived for plansymmetric truss beams loaded in their plane of symmetry. This was extensively elaborated in [8].

As it was shown in [5], [8], [10], axial bar forces for the load case of transverse force at the truss free end, Fig.2a, can be calculated from the force equilibrium conditions in joints. After that deformation energy of the whole truss can be calculated.

*Corr. Author's Address: High Technical Mechanical School, Trstenik, Serbia, mtodorovic_vtms@yahoo.com

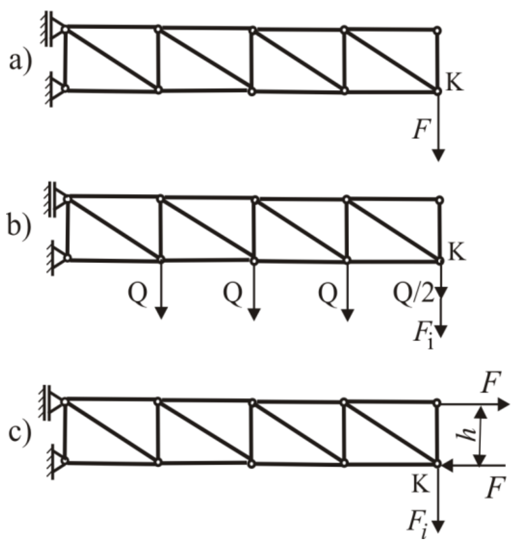

Fig.2. *Calculation of the free end deflection*

At the end we use the Castigliano's theorem to calculate the free end transverse deflection f_K. Introducing quantities $I_{xe}^{fF}(n)$ and S_e, we come to:

$$f_K = \frac{Fl^3}{3EI_{xe}^{fF}(n)} + \frac{F\,l}{S_e} \tag{1}$$

The first term in the above expression represents the bending component f_B and the second term represents the shearing component f_S of the total displacement f_K. Since the bars are axially strained, we can say that these two components are consequences of *structural bending* and *structural shearing* respectively. In the afore mentioned papers of the same authors it has been shown that $I_{xe}^{fF}(n)$ can be understood as *the equivalent axial moment of inertia*:

$$I_{xe}^{fF}(n) = \left[\frac{1}{h^2 A_b}\left(1+\frac{3}{2n}+\frac{1}{2n^2}\right)+\ldots \right. \\ \left. \ldots+\frac{1}{h^2 A_t}\left(1-\frac{3}{2n}+\frac{1}{2n^2}\right)\right]^{-1} \tag{2}$$

and product $EI_{xe}^{fF}(n)$ as the *equivalent bending rigidity*. In the same sense S_e represents the *equivalent shearing rigidity* of the truss beam:

$$S_e = E\left[\frac{tg\beta}{A_v}+\frac{1}{sin^2\beta\cos\beta\cdot A_d}\right]^{-1} \tag{3}$$

We see that the equivalent moment of inertia, as we have defined it in (2), depends on the cell numeber n. It also depends on the load type and deformation it is used for, hence the superscripts "*f*" and "*F*". Accordingly to [8] expression (2) can be put in the general form:

$$I_{xe}^{do}(n) = \left[\frac{K_b^{do}}{h^2 A_b}+\frac{K_t^{do}}{h^2 A_t}\right]^{-1} \tag{4}$$

$K_b^{do}(n)$ and $K_t^{do}(n)$ are rigidity coefficients, which depend on the type of deformation - superscript "*d*" and can be "*f*" (deflection) or "γ" (slope), on type of load, superscript "o" - that can be "*F*" (force) or "*q*" (distributed load), and "*M*" (moment). Expressions for rigidity coefficients used in (2) are given in Table 1.

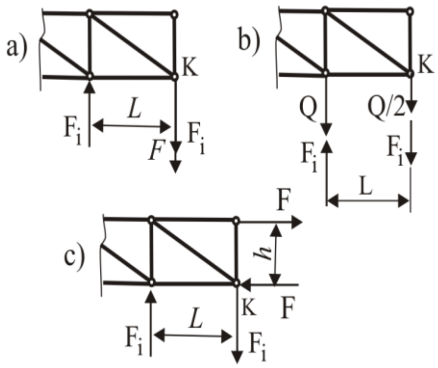

Fig.3 *Calculation of the free end slope*

However, axial moment of inertia of a cross-section of an infinitely long truss beam, if only cross-section areas of longitudinal bars are taken into account, can be obtained in the form:

$$I_{xeLB} = \left[\frac{1}{h^2 A_b}+\frac{1}{h^2 A_t}\right]^{-1} = \frac{h^2 A_b A_t}{A_b + A_t} \tag{5}$$

The same procedure is performed for the case of distributed load q [N/m], save that it is replaced by concentrated joint forces $Q = ql/n$, Fig.2b. To calculate displacements of moment M we introduce couple of forces $F = M/h$, Fig.2c. That way we come to the following expressions:

$$f_K = \frac{q\,l^4}{8EI_{xe}^{fq}(n)} + \frac{q\,l^2}{2S_e} \tag{6}$$

$$f_K = \frac{M\,l^2}{2EI_{xe}^{fM}(n)} \tag{7}$$

In the above formulas $I_{xe}^{fq}(n)$ and $I_{xe}^{fM}(n)$ are the equivalent moments of inertia for these two loas types. The corresponding rigidity coefficients are given in Table 1, uper half.

Table 1: *Rigidity coefficients*	
Load	*for free end deflection* f_K
F	$K_{b,t}^{fF} = 1 \pm \frac{3}{2n} + \frac{1}{2n^2}$
q	$K_{b,t}^{fq} = \left(1 \pm \frac{1}{n}\right)^2$
M	$K_{b,t}^{fM} = 1 \pm \frac{1}{n}$
Load	*for free end slope* γ_K
F	$K_{b,t}^{\gamma F} = 1 \pm \frac{1}{n}$
q	$K_{b,t}^{\gamma q} = 1 \pm \frac{3}{2n} + \frac{1}{2n^2}$
M	$K_b^{\gamma M} = 1 \qquad K_t^{\gamma M} = 1 - \frac{1}{n}$

In calculating the free end slope the previous procedure is repeated, so that the bar forces are obtained accordingly to the load type (F, q or M) and to the dummy moment $M_i = F_i L$, Fig.3a,b,c. That way we obtain:

$$\gamma_K = \frac{Fl^2}{2EI_{xe}^{\gamma F}(n)} + \frac{F}{S_e} \tag{8}$$

$$\gamma_K = \frac{q\,l^3}{6EI_{xe}^{\gamma q}(n)} + \frac{q\,l}{2S_e}\frac{1}{n} \tag{9}$$

$$\gamma_K = \frac{M\,l}{EI_{xe}^{\gamma M}(n)} \tag{10}$$

Again we see the dependence among quantities similar to those in expressions (1), (6) and (7).

3. A comparison of the equivalent moments of inertia for different load types

We shall make a comparison of the equivalent moments of inertia of a cantilever truss beam as the one in Fig.1 with the following data: cell length L = 150cm, angle of diagonals $\beta = 30^0$, cross-section of bars A_b = 3,6cm, $A_t = A_v = A_d$ = = 1,98cm, E = 21000kN/cm^2.

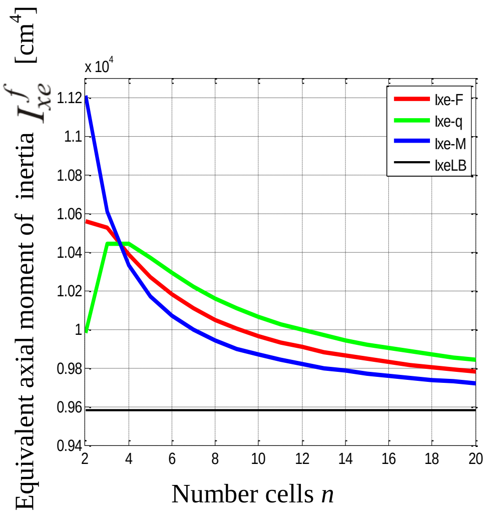

Fig.4. *Variation in the equivalent moment of inertia* $I_{xe}^{f}(n)$ *with the number of cells n due to different load types*

Using MATLAB program and expressions in the upper part of Table 1 curves $I_{xe}^{f}(n)$ in Fig.4 are obtained, and with the expressions in the lower part of Table 1 curves $I_{xe}^{\gamma}(n)$ in Fig.5 are obtained.

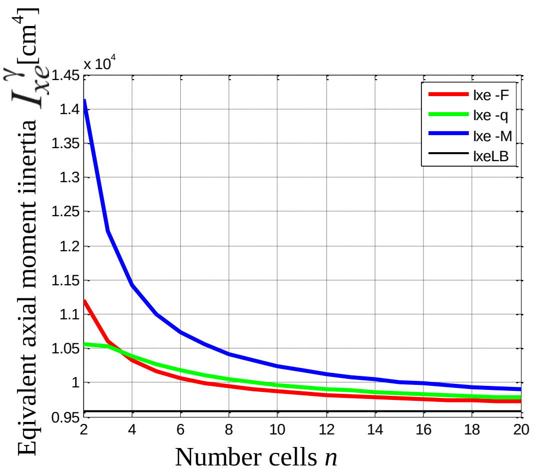

Fig.5. *Variation of the equivalent moment of inertia* $I_{xe}^{\gamma}(n)$ *with number of cells n and different load types*

The first diagram shows that for small number of cells, ($n \leq 4$), curves $I_{xe}^{f}(n)$ differ significantly. We come to the same conclusion regarding the second diagram with curves $I_{xe}^{\gamma}(n)$. However the with increasing n all the curves converge to the values of I_{xeLB} that does not depend on number n. Moreover values of $I_{xe}^{\gamma}(n)$ for F and q are similar. We see also that the maximum $I_{xe}^{f}(n)$ appears for q and the maximum of $I_{xe}^{\gamma}(n)$ appears for M.

4. Influence of variation of cross-section area to the equivalent moments of inertia

In the expressions (2) and (3) for the equivalent bending and shearing rigidity, among others, cross section areas are influencing quantities. In the following text we shall show how the variation of cross-section area of bars influences the equivalent rigidities.

Fig. 6 gives the relation of I_{xe}^{fF} to the number of cells n, and the variation in the cross-section area of the lower longitudinal bars. In the same diagram the change in I_{xeLB} (see expr. (5)) of an infinitely long truss beam is shown. As we

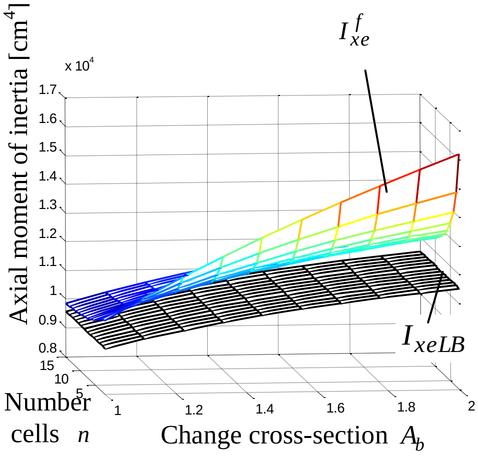

A_b

Fig.6. *Variation of* I_{xe}^{fF} and I_{xeLB} *with number of cells n and the change of cross-section area* A_b

have already mentioned the latter quantity does not depend on n.

With the increase in n values of I_{xe}^{fF} converge to I_{xeLB}, as we can see comparing expressions (2) and (5). With strengthening of the lower longitudinal bars, i.e. with the increase of their cross-section area A_b, value of I_{xe}^{fF} also increases, as expected. However, the increase of A_b in the trusses with smaller n yealds greater effect to encreasing the equivalent moment of inertia (or higher slope in the superficial diagram).

The equivalent shearing rigidity S_e does not depend on the number of cells n, it depends on the diagonal angle β and cross-sections of the vertical and diagonal bars A_v and A_d. Relation between S_e and angle β and the cross-section areas of filling bars is shown in Fig.7. The equivalent shearing rigidity attains it's maximum for β equals 45^o. The same figure also indicates an expected increase in the equivalent shearing rigidity with the increase in the cross-section areas of vertical and diagonal bars. The increase in S_e is uniform, for any angle β between 30 and 60 degrees.

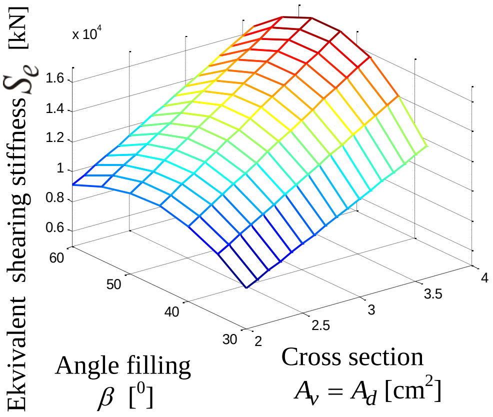

Fig.7 *Variation of the equivalent shearing rigidity with the filling angle β and the cross-section areas* $A_v = A_d$

Fig.7 is a result of an analysis in which the cross-section areas of the vertical and diagonal bars are equal. Fig.8 presents the change of the equivalent shearing rigidity as a function of the diagonal angle β and the variation in the cross-section areas of the filling bars. Naturally, the increase in the diagonal bar's cross-section area significantly enlarges the equivalent shearing rigidity for all angles β. The influence of of the increase of cross-section area of vertical bars is substantially smaller, if not negligible, at diagonal angle β smaller than 40 degrees.

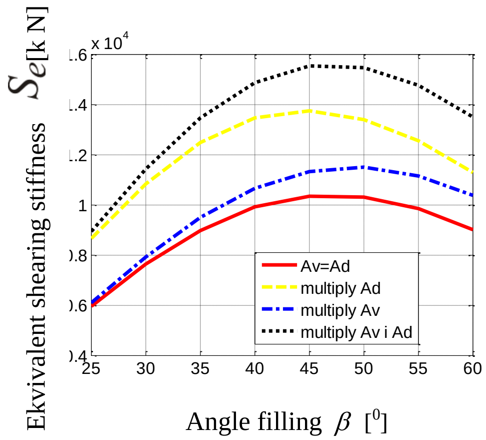

Fig. 8 Variation in $S_e(\beta)$ with the variation of the cross-section areas of vertical and diagonal bars

5. Conclusion

In this paper the expressions for the equivalent bending and shearing rigidity of a cantilever truss beam have been derived. They have been derived for the three most common load types acting on the free end: force F, moment M - represented by a couple of forces and the distributed load q which was assigned to the lower joints. The values of the rigidities obtained were compared for the load types mentioned, and the influence of the variation of the bar cross-sections to the equivalent rigidities was analysed. The results of the analysis were presented in the form of diagrams.

It can be concluded that the equivalent moment of inertia always converge to the value of an infinitely long truss beam regardless of the load type. The increase in the cross-section area of the lower longitudinal bars in shorter trusses yields a significant increase in the equivalent moment of inertia, and thus the rigidity of the truss. Enlarging of the cross-section area of the diagonal bars significantly increases the equivalent shearing rigidity.

REFERENCES

[1] Gasic, M.; Savkovic M.; Markovic G.; Zdravkovic N.: The Approximation of The Equation for Bending Stiffness of Truss Construction, *V International Scientific Conference Heavy Machinery – HM'05*, pp. A.55 – 59, 28 June – 3 July, Kraljevo, 2005.

[2] Kenner, W., S.: Lattice Truss Structural Response Using Energy Methods, North Carolina A&T State University, *A Thesis Submitted to the Faculty of Old Dominion University in Partial Fulfillment of the Requirement for the Degree of Master of Sciences*, 129 pages, NASA-TM-112361, 1987.

[3] Burgardt, B.; Cartraud, P.: Continuum Modelling of Beamlike Lattice Trusses, *Advances in Computational Techniques for Structural Engineering*, pp. 51-59, August 21-23, Budapest, Hungary, 1996.

[4] Teughels A.; De Roeck G.: Continuum Models for Beam- and Platelike Lattice Structures, *IASS-IACM 2000 Fourth International Colloquium of Computations of Shell & Spatial Structures*, pp.1-20, June 5-7, Channia Crete, Greece, 2000.

[5] Dedic, M.; Todorovic, M.: An Analysis of The Equivalent Stiffness of Beam-like Trusses with Constant Cross-section, *Congress of Theoretical and Applied Mechanics*, pp 347-352, April 10-13, Kopaonik, 2007.

[6] Todorovic, M.; Dedic, M.: An Analysis of The Deformation of a Beam-like Truss Structure Using Method of Equivalent Continuum Beam, *7th International Conference "Research and Development in Mechanical Industry" RaDMI 2007*, 16 - 20. September 2007, Belgrade, Serbia, pp. 670-674, 2007.

[7] Dedic, M.; Todorovic, M.: Calculation of the Free End Deflection and Slope of a Cantilever Truss in distributed load, *The Sixth Triennial International Conference Heavy Machinery, HM 2008*, E.1, 24-29 June 2008, Kraljevo.

[8] Todorovic, M.; Dedic, M.: Calculation of Cantilever Truss Beam Deformations Using Continuum Modeling, *Journal of Modelling and Optimization in the Machines Building Field* (MOCM), MOCM -15, Vol. 2 (2009). pp 87-98, 2009.

[9] Todorovic, M.; Dedic, M.; Cajetinac, S.; Jevremovic, V.: Influence of Cross-section Areas of Bars to Deformations of a Truss Beam, *9th International Conference "Research and Development in Mechanical Industry"* RaDMI 2009, pp. 395-400, 16 - 19. September 2009, Vrnjačka Banja, Serbia, ISBN 978-86-6075-007-7, 2009.

[10] Todorovic, M.; Calculation of deformations in the plane of a load carrying truss beam with the constant cross-section by method of equivalent continuum beam, *Ph.D. Thesis*, 2010., Faculty of Mechanical Engineering in Kraljevo, University of Kragujevac

HEAVY MACHINERY - HM 2011, 39-41
ISBN 978-86-82631-58-3
Paper accepted: 30.05.2011

The Analysis of Cross-Sections And Stability of Columns Centricaly Loaded By Axial Compressive Load

Miljan Veljovic[1,*]
Faculty of Mechanical Engineering in Kraljevo

This paper analyzes cross sections and stability of columns centricaly loaded by axial compressive load by using the ω-procedure and standard procedure JUS U.E7.081. In this analysis an example of column with the different cross-sections is presented. By comparison between complex cross-section and ordinary cross-section and comparation between the calculated normal and allowable stresses it can be see that the standard procedure is better because it is more on the safety side.

Keywords: elastic stability, multi-part cross-section, load – carrying capacity, buckling stress

1 INTRODUCTION

The first research in the elastic stability had been done by Euler and the critical force for an ideal bar is:

$$F_{kr} = \frac{\pi^2 E I_{\min}}{l_r^2}$$

and critical buckling stress: $\sigma_{kr} = \dfrac{\pi^2 E}{\lambda_r^2}$

where is I_{min} – minimal moment of inertia
l_r – effective length of the bar
λ_r – effective slendernees ratio is quotient of effective length of the bar l_r and minimal radius of qyration i_{min}

$$\lambda_r = \frac{l_r}{i_{\min}}$$

Load - carrying capacity of axial loaded columns by ω-procedure is:

$$\sigma_\omega = \frac{N}{A}\omega \le \sigma_{dop}$$

where is: N-calculated normal force,
A- the cross-sectional area,
coefficient ω depends on steel and effective slendernees ratio λ.

Relative slendernees ratio is: $\bar{\lambda} = \dfrac{\lambda_r}{\lambda_T}$

λ_T –slendernees ratio at yield strength

Load - carrying capacity of axial loaded columns, with single-part cross section by using the standard procedure JUS U.E7.081, is written as:

$$\sigma_N = \frac{N}{A} \le \sigma_{i,dop} = \chi \sigma_{dop}$$

$\sigma_{i,dop}$ - allowable buckling stress
σ_{dop} - allowable normal stress
χ- dimensionalees buckling coefficient which depends on relative slenderness, shape of cross-section and degree of equivalent geometric imperfectios.

$$\chi = \frac{2}{\beta + \sqrt{\beta^2 - 4\bar{\lambda}^2}}$$

$$\beta = 1 + \alpha(\bar{\lambda} - 0{,}2) + \bar{\lambda}^2$$

Coefficient α depends on competent buckling curve and it is tabelar valeu.

There are many geometrical and structural imperfections at the real bars, and we have several buckling curves ($A_{o,}$ A, B, C, D) which depends on cross-section and degree of equivalent geometric imperfectios.

2.1 The cross-sections of design column

The buckling of column depends on cross-section, and it is illustrated on an example of a column with double U standard JUS profile.
Firstly, it is cross-section of double welded U10 standard profile which is shown in Fig.1,

[*]Corr. Author's Adress: Faculty of Mechanical Engineering Kraljevo, Dositejeva 19, Kraljevo, Republic of Serbia, veljovic.m@mfkv.kg.ac.rs

The column height is *h=3m*, and axial compressive force is *F=100kN*, the material is Č.0461

Selected U10 has following data:

h = 10cm, b = 5cm, e_y = 1,55cm, A_1 = 13,5 cm^2,

I_{x1}= 206 cm^4, I_{y1} = 29,3 cm^4, i_{v1} = 1,47 cm

For this cross-section is:

$$A = 2A_1 = 27cm^2 \qquad I_x = 2I_{x_1} = 412cm^4$$

$$I_y = 2\left[I_{y_1} + (b - e_y)^2 \cdot A_1\right] = 151{,}8cm^4$$

$$i_x = \sqrt{I_x / A} = 3{,}91cm \qquad i_y = \sqrt{I_y / A} = 2{,}37cm$$

$$\lambda_r = \frac{h}{i_{\min}} = \frac{300}{2{,}37} = 127 \quad \rightarrow \quad \omega = 3{,}35$$

Buckling stress is determined by ω-procedure:

$$\sigma_\omega = \frac{100}{27} \cdot 3{,}35 = 12{,}4 \frac{kN}{cm^2} < \sigma_{dop} = 16 \frac{kN}{cm^2}$$

Now, buckling stress is determined by using the standard procedure JUS U.E7.081:

Calculated normal stress is:

$$\sigma_N = \frac{100}{27} = 3{,}70 \frac{kN}{cm^2}$$

Allowable buckling stess is:

$$\sigma_{i,dop} = 0{,}353 \cdot 16 = 5{,}67 \frac{kN}{cm^2}$$

$$\sigma_N \le \sigma_{i,dop}$$

where is: $\lambda_T = \pi \sqrt{\dfrac{E}{\sigma_T}} = \pi \sqrt{\dfrac{21000}{25}} = 91$

$$\bar{\lambda} = \frac{\lambda_r}{\lambda_T} = \frac{127}{91} = 1{,}39$$

$$\alpha = 0{,}489 \ \textit{for C curve}$$

$$\beta = 1 + \alpha(\bar{\lambda} - 0{,}2) + \bar{\lambda}^2 = 3{,}51$$

$$\chi = \frac{2}{\beta + \sqrt{\beta^2 - 4\bar{\lambda}^2}} = 0{,}354$$

2.2 The cross-section of the multi-part columns

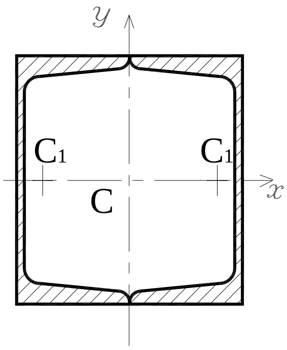

Fig. 1. *Cross-section of a column*

The cross-section of the multi-part columns is characterized by the material and non-material axes. The material axis crosses all parts of the cross-section, while the other does not. The lace sheets and truss bars are positioned perpendicular to the non-material axis.

At this type of multi-part cross-sectons we must check elastic stability around both axis. Firstly, for material x-axis:

$$\lambda_x = \frac{h}{i_x} = \frac{300}{3{,}91} = 76{,}7 \quad \rightarrow \quad \omega = 1{,}49$$

Buckling stress is determined by ω-procedure:

$$\sigma_\omega = \frac{100}{27} \cdot 1{,}49 = 5{,}52 \frac{kN}{cm^2} < \sigma_{dop}$$

Now, for non-material y-axis we calculated:

$$I_y = 2 \cdot \left[I_{y_1} + (\frac{e - 2e_y}{2})^2 \cdot A_1 \right] = 1015cm^4$$

$$i_y = \sqrt{I_y / A} = 6{,}13cm$$

$$\lambda_y = \frac{h}{i_y} = \frac{300}{6{,}13} = 48{,}9$$

$$\lambda_1 = \frac{a}{i_1} = \frac{100}{1{,}47} = 68$$

a =100cm – distance between two lacing bars

m =2 – number of parts in cross-section

$$\lambda_{y_i} = \sqrt{\lambda_y^2 + \frac{m}{2}\lambda_1^2} = \sqrt{48{,}9^2 + 68^2} = 83{,}8 \rightarrow$$

$$\rightarrow \omega_{y_i} = 1{,}62$$

$$\sigma_{\omega y} = \frac{100}{27} \cdot 1{,}62 = 6\frac{kN}{cm^2} < \sigma_{dop}$$

Control of distance between two lacing bars:

$$\lambda_1 = \frac{a}{i_1} = 68 \le 50 \cdot (4 - 3\frac{\sigma_\omega}{\sigma_{dop}}) = 50 \cdot (4 - 3\frac{6}{16}) = 144$$

Now, buckling stress around x-axis is calculated by using the standard procedure JUS U.E7.081:

$$\lambda_x = \frac{h}{i_x} = \frac{300}{3{,}91} = 76{,}8$$

$$\bar{\lambda}_x = \frac{\lambda_x}{\lambda_T} = \frac{76{,}8}{91} = 0{,}844$$

$$\alpha = 0{,}489 \text{ for } C \text{ curve}$$

$$\beta = 2{,}458$$

$$\chi = 0{,}61$$

$$\sigma_{i,dop} = 0{,}61 \cdot 16 = 9{,}76\frac{kN}{cm^2}$$

$$\sigma_N = \frac{100}{27} = 3{,}70\frac{kN}{cm^2}$$

$$\sigma_N < \sigma_{i,dop}$$

And finally we repeate same calculation for non-material y-axis:

$$\bar{\lambda}_y = \frac{\lambda_{yi}}{\lambda_T} = \frac{83{,}8}{91} = 0{,}92 \rightarrow \chi = 0{,}58 \ (curve\ C)$$

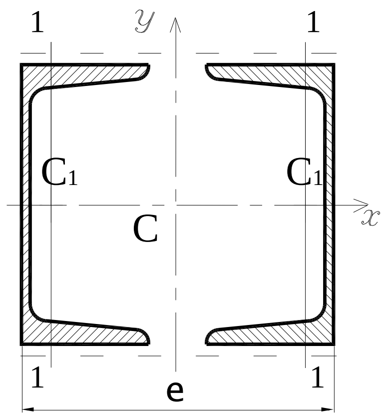

Fig. 2. *Multi-part* cross-*section of a column*

$$\sigma_{i,dop} = 0{,}58 \cdot 16 = 8{,}32\frac{kN}{cm^2}$$

$$\sigma_N \le \sigma_{i,dop}$$

3 CONCLUSION

This paper analyses two different positions of same cross-sectors standard profile. The aim of the analyses was to find out what position is more suitable regarding elastic stability. By comparing the calculated normal stress to allowable stress according to the ω-procedure and the standard procedure we can see that the stresses obtained by lattter procedure smaller than stresses by ω-procedure. The standard procedure is better because it is more on the safety side.

4 REFERENCES

[1] Petković, Z., D. Ostrić, “Metal constructions in Engineering Mechanics I”, Faculty of Mechanical Engineering, Belgrade,1996.

[2] Ostrić, D., “Metal constructions”, Faculty of Mechanical Engineering, Belgrade,1977.

[3] Reference book - Strength of materials, Faculty of Mechanical Engineering, Belgrade, 1991.

[4] Čukić, R., D. Ružić, “Strength of materials”, Faculty of Mechanical Engineering, Belgrade,1992.

HEAVY MACHINERY - HM 2011, 43-47
ISBN 978-86-82631-58-3
Paper accepted: 30.05.2011

Thermodynamic calculation of the Bi-In-Sb phase diagram

Duško Minić[1*], Milan Kolarević[2], Milena Premović[1] and Miljana Marković[1]
1 - University in Priština, Faculty of technical science, Kos. Mitrovica, Serbia
2 -University in Kragujevac, Machinery faculty, Kraljevo, Serbia

Abstract: *Phase equilibria of ternary Bi-In-Sb system was investigated by applying CALPHAD method and using literature thermodynamic data for constitutive binary systems. The liquidus surface and isothermal section at 400^{0}C were calculated. Calculated results were verified experimentally on the alloys samples with the compositions corresponding to the characteristic vertical sections: InSb (1:1)-Bi; BiSb(1:1)-In and BiIn(1:1)-Sb. Phase transitions temperatures were determined by Differential Thermal Analysis (DTA) and Differential Scanning Calorimetry (DSC). Microstructure and phase composition investigation were investigated by using Scanning Electronic Microscopy (SEM) with Energy Dispersive Spectrometry (EDS). The experimental and analytical results showed good agreement, concerning the temperatures of phase transitions and phase compositions of alloys concerned.*

Key words: Bi-In-Sb, phase diagrams, thermal analysis, thermodynamic prediction.

1. INTRODUCTION

InSb and GaSb are two examples of so-called narrow band gap semiconductors with high electron mobility. They have gained increasing interest within the last decade.[1-2], because of their high potential for a number of electronic and optoelectronic applications. In the study of Minića et. al. [3] the comparative view of isothermal section at 300^{0}C is determined by analytical and experimental method. The results were in a good agreement. One of the most powerful methods which can be applied to study thermodynamic properties and phase equilibra of practical alloy systems is the CALPHAD method [4-7]. For metallic solutions, sublattice models developed by Hillert and co-workers have been widely used[8-9]. For the thermodynamic functions of the pure elements in their stable and metastable states, the latest phase stability equations compiled by SGTE [10] were used. The thermodynamic data for the boundary binary systems, used for the calculation of phase equilibria of the ternary Bi-In-Sb systems, were based on the literature data from Boa and Ansara [11] in the case of Bi-In system, Ohtani and Ishida [12] in the case of Bi-Sb system, and Ansara *et al.*[13] in the case of In-Sb system. This thermodynamic data, with some modified and additional thermodynamic parameters, are included in the COST531 database [14] which was used for the calculations in this work. In this paper, the temperatures of phase transition for three vertical sections of ternary Bi-In-Sb system, determined by DSC and DTA method, were presented. The microstructures and the compositions of equilibria phases were obtained by SEM-EDS. The experimentally determined values of the phase transition temperatures were compared to the calculated ones based on optimized thermodynamic data for constitutive binary systems[11-13], by using software package PANDAT 8.1. The results obtained in this work represent a step forward to the complete definition of phase diagram of ternary Bi-In-Sb system, that was incompletely investigated, and have a potential for wide technology application.

2. EXPERIMENT

The alloy samples were prepared from high-purity (99,999%) Bi, In and Sb produced by Alfa Aesar (Germany). Selected samples with compositions from three vertical sections so the molar ratio of two components of 1:1, and molar ratio of the third component was in a range of 0 to 1, with portion of 0,1, are produced by smelting. The samples were prepared as following: the mixtures (~2 g) of the metals were well grained and sealed in quartz tubes under a vacuum and placed in a resistance furnace. The sealed tubes containing the mixed elements were gradually heated to the melting point of Sb (630,7^{0}C)**.** The samples were well stirred and then held at that temperature for 30 minutes. The quartz tubes were taken out of furnace and left for

[*]Corr. Author's Adress: Faculty of Technical Sciences, Knjaza Milosa 7, 38220, Kosovska Mitrovica, Serbia, dminic65@open.telekom.rs

cooling in the air to the room temperature. After that, the sealed quartz tubes with the samples which were planned for SEM-EDS analysis were heated in electric resistance furnace until the annealing temperature of 400^{0}C was reached. At this temperature the samples were annealed over a period of 200 h, and than immediately quenched in icy water. The phase transformation temperatures were determined by DTA and DSC methods. The DTA measurements were carried out on Derivatograph “MOM Budapest” under following conditions: flowing argon atmosphere, sample masses about 1 g, alumina as the reference material, heating rate of 5 ^{0}C /min. The DSC measurements were performed on a SDT Q600 (TA Instruments), under flowing argon atmosphere, with sample masses 50 mg, and heating rate of 5 ^{0}C /min. For microstructure investigation and for phase composition determination was used scanning electron microscopy, SEM (JEOL JSM 6460) with energy dispersive spectrometry, EDS (Oxford Instruments).

3. RESULTS AND DISCUSSION

Based on the values of the thermodynamic parameters the liquidus surface of the Bi-In-Sb ternary system is calculated and plotted in Fig. 1.

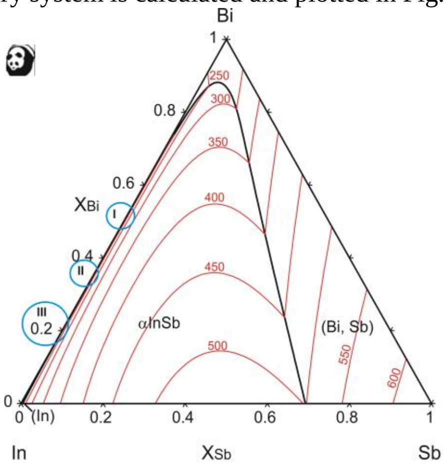

Fig. 1. Calculated liquidus surface of the ternary Bi-In-Sb system

Magnified views of the liquidus surface projection in a vicinity of invariant points are presented on Fig.2. (I)-(III).

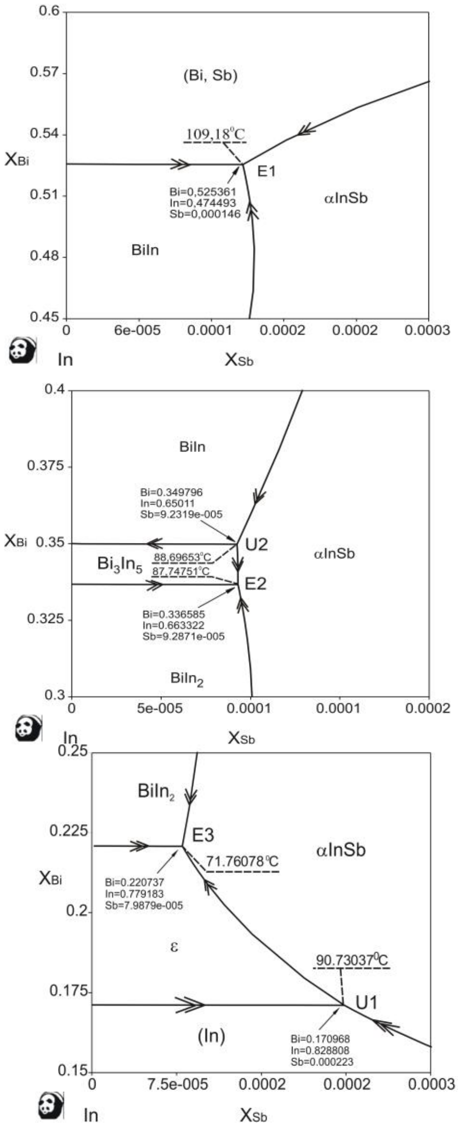

Fig. 2. Magnified views of the liquidus surface projection of Bi-In-Sb ternary system in a vicinity of : I) E1 eutectic point; II) E2 eutectic point; III) E3 eutectic point

The invariant reactions in ternary Bi-In-Sb system are listed in Table 1, as well as the reaction temperatures and the types of those invariant reactions. It can be seen that in ternary Bi-In-Sb system there are five invariant reactions: three eutectic (marked in Table 1 as type E) and two quasi-peritectic (marked as U), and seven regions.

Table 1. Predicted invariant reaction of ternary Bi-In-Sb system

T / ^{0}C	Reaction	Type
109.18	L --> αInSb + (Bi,Sb) + BiIn	E1
90.73	L + (In) --> αInSb + ε	U1
88.69	L + BiIn --> αInSb + Bi_3In_5	U2
87.74	L --> αInSb + Bi_3In_5 + $BiIn_2$	E2
71.76	L --> αInSb + $BiIn_2$ + ε	E3

of primary crystallization (Bi,Sb), αInSb, BiIn, Bi_3In_5, $BiIn_2$, ε and (In), two large regions ((Bi,Sb), αInSb) and five very small regions located on the side of constitutive In-Bi binary system (BiIn, Bi_3In_5, $BiIn_2$, ε, (In)).Three characteristic vertical sections of ternary Bi-In-Sb system were calculated, based on the literature data. The vertical sections were taken from all three corners, Bi, In and Sb with molar ratio equal to In:Sb = 1, Bi:Sb =1 and Bi:In=1, respectively. Calculated phase diagrams for the three vertical sections together with experimentally determined phase transition temperatures by DTA and DSC methods, are presented in Fig. 3.

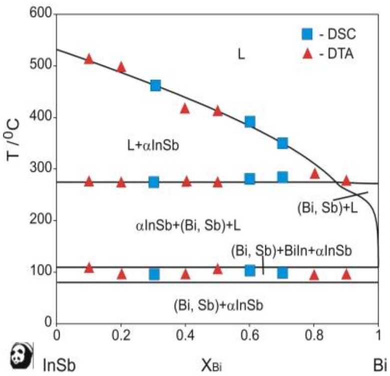

a)

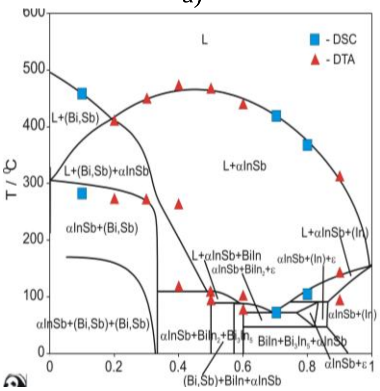

b)

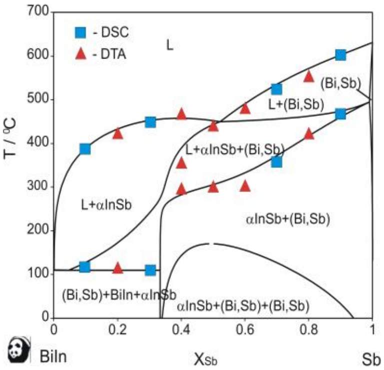

c)

Fig. 3. Calculated phase diagrams for three vertical sections: a)InSb-Bi, b)BiSb-In and, c) BiIn-Sb.

Two samples were investigated using SEM-EDS method and their compositions were presented in Table 2, as well as calculated and experimentally determined (SEM-EDS) equilibrium compositions at 400^{0}C.

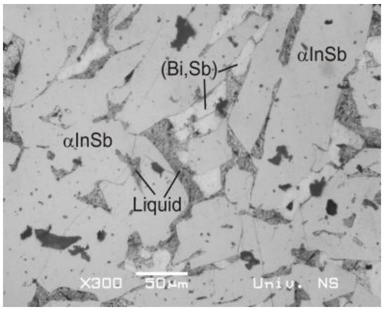

1)

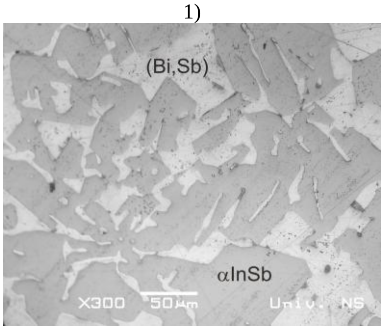

2)

Fig. 4. SEM micrograph of the sample 1 and 2

Table 2. Calculated and experimentally determined phase compositions in the ternary Bi-In-Sb system at 400^0C

	Overall exp. compo.	Theoretically predicted phases	Exp. determined phases	Phase composition					
				Bi / % at.		In / % at		Sb / % at.	
				exp.	calc.	exp.	calc.	exp.	calc.
1.	25 Bi 25 In 50 Sb	αInSb liquid (Bi,Sb)	αInSb liquid (Bi,Sb)	0.012 44.68 16.02	- 46.34 15.49	48.35 18.04 1.76	50 17.42 0.19	50.45 37.28 82.22	50 36.24 84.32
2.	10 Bi 10 In 80 Sb	(Bi,Sb) αInSb	(Bi,Sb) αInSb	11.89 0.56	12.11 -	0.96 47.94	0.18 50	87.15 51.5	87.61 50

The microstructure of the sample 1 and 2 are shown in Fig. 4. On the microphotograph 1 it can be clearly seen the presence of Liquid , αInSb i (Bi, Sb), and on the microphotograph 2 it can be seen the presence of (Bi,Sb) and αInSb.

The calculated isothermal section of the ternary Bi-In-Sb system at 400^0C together with the experimentally determined phase composition for samples 1 and 2 are presented in Fig. 5. It could be seen the existence of the following crystallization fields: single phase field (Liquid); three two-phase fields (Liquid+αInSb; Liquid+(Bi,Sb) and, (αInSb+(Bi,Sb)) and, one three-phase fields (Liquid+αInSb+(Bi, Sb)).

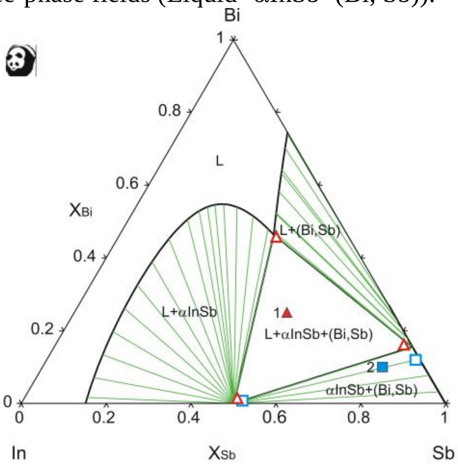

Fig. 5. Isothermal section of the ternary Bi-In-Sb system at 400^0C and experimental values of the

The calculated isothermal section of the ternary Bi-In-Sb system at 400^0C together with the experimentally determined phase compositions for the samples 1 and 2 (full symbols are referred on the overall composition and empty on the compositions of single phase). It could be

4. CONCLUSION

Phase diagram of the ternary Bi-In-Sb system was calculated using optimized literature data for thermodynamic parameters of the constitutive binary systems by CALPHAD method. It can be concluded that system has five invariant reactions. By experimental verification by determined phase transformation temperatures it can be concluded that the phase diagram is well calculated. There were also obtained good agreements of calculated and experimentally determined phase compositions on two investigated samples, whose compositions were in a region of vertical section at 400^0C.

Acknowledgements
This work was supported by Ministry of Science of the Republic of Serbia (OI172037).

REFERENCES

[1]. P. S. Dutta, H. L. Bhat, J. Appl. Phys. 81 (1997) 5821
[2]. T. C. McGill, D. A. Collins, Semicond. Sci. Technol. 8 (1993) 1
[3]. D. Minić, D. Manasijević, D. Živković, Ž. Živković, J. Serb. Chem. Soc., 71 (7) (2006) 843
[4]. www.calphad.org
[5]. M. Hillert, Phase equilibria, phase diagrams and phase transformations: their thermodynamic basis, University Press, Cambridge, 1998
[6]. N. Saunders, A. P. Miodownik, CALPHAD (A Comprehensive Guide), Elsevier,London, 1998
[7]. SGTE (Scientific Group Thermodata Europe), www.sgte.org
[8]. M. Hillert, L. I. Staffansson, Acta Chem. Scand., 24 (1970) 3618

[9]. B. Sundman, J. Agren, J. Phys. Chem. Solids, 42 (1981) 297

[10]. SGTE Unary database, Version 4.4 (Teddington, U. K.: Scientific Group Thermodata Europe, 2001)

[11]. D. Boa, I. Ansara, Thermochimica Acta, 314 (1998) 79

[12]. H. Ohtani, K. Ishida, J. Electron. Mater., 23 (1994) 747

[13]. I. Ansara, C. Chatillon, H. L. Lukas, T. Nishizawa, H. Ohtani, K. Ishida, M. Hillert, B. Sundman, B. B. Argent, A. Watson, T. G. Chart, T. Anderson: CALPHAD 18 (1994) 177

[14]. A.T. Dinsdale, A. Kroupa, J. Vízdal, J. Vrestal, A. Watson, A. Zemanova: COST531 Database for Lead-free Solders, Ver. 2.0, (2006), unpublished research

[15]. P. Villars, Pearson's Handbook, Desk Edition, Materials Park, OH, 1997.

[16]. M. Hillert, L.I. Staffansson, Acta Chem. Scand., 24 (1970) 3618

[17]. B. Sundman, J. Agren, J. Phys. Chem. Solids, 42 (1981) 297.

HEAVY MACHINERY - HM 2011, 49-54
ISBN 978-86-82631-58-3
Paper accepted: 30.05.2011

Analytical and Numerical Investigation of Local and Distortion Stability Loss of Thin Wall Profile with Open Cross-section

Nebojša Radić [1], Spasoje Trifković [1], Miroslav Milutinović [1]

[1] University of East Sarajevo, Faculty of Mechanical Engineering, Vuka Karadžića 30, East Sarajevo, Bosnia and Herzegovina

In this paper, determination of critical stress values of thin wall C profile is carried out by using the analytical methods, finite strip method *and finite element method. Special attention is given to ratio of the local critical stress and critical stress distortion. It is shown that the value of critical stress distortion can be less than the local critical stress and distortional form may be dominant in the post-critical phase. The value of local and distortion critical stress can be very close to each other, so that in the post-critical phase occurs the interaction, which leads to the reduction in carrying capacity.*
Keywords: thin wall profile, finite strip method, finite element method, critical stress.

1. INTRODUCTION

Thin wall profiles with open cross-section are widely applied in various engineering structures because of low weight. One of the biggest problems that arise in their application is their high sensitivity to loss of stability in the elastic range. Nevertheless, the loss of stability occurs at low values of critical stress, an additional complication in the analysis is a occurrence of three different characteristic buckling modes.

These modes are: local, distortional and Euler (global). These three modes differ in the form of the cross section and length of the half wave after the loss of stability. Local mode occurs at half wavelength that is less than the largest characteristic dimension of cross section. Local buckling involves only rotation at connecting points of the individual panels that make up the cross section. At the same time there are no translations of the connecting points. Local buckling involves distortion of the whole cross section. That means, all parts of the profile are bent in both planes.

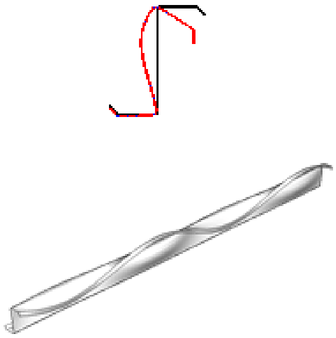

Fig. 1. *Local buckling*

Distortional form of stability loss is complicated than local and global. In contrast to than local forms of stability loss, by distortion, for example C profile, flange and lip rotate around the connecting point of the web and flange, and at the same time they move linearly. The entire cross-section moves in the direction perpendicular to the web. The half wave length of distortion is an average of 5 to 6 times higher than the local forms. A typical distortional form of stability loss of C profile is shown in Fig. 2.

*Corr. Author's Address: University of East Sarajevo, Faculty of Mechanical Engineering, Vuka Karadžića 30, East Sarajevo, Bosnia and Herzegovina, nesor67@yahoo.com

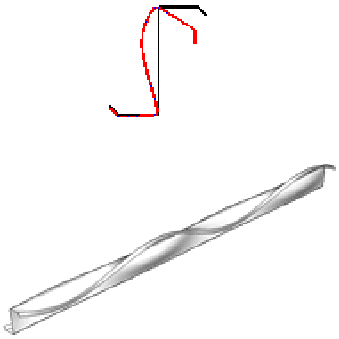

Fig. 1. *Distortional buckling*

Global form of stability loss occurs as the bending, torsion or bent-torsion and unlike the other two, the whole cross-section moves as a solid body without distortion of the cross section. The half wavelength is much higher than in the other two forms and depends on the size of the cross section. The methods for calculating the value of critical stress can be divided into analytic al and numerical.The analytical methods have been developed for all three typical forms, so that there are analytical formulas for determining the value of critical stress and critical length. In the development of suitable analytical formulas a special problem is the distortional form of stability loss, because it is complicated than local and global forms. There are two analytical methods for obtaining the value of critical stress of distortion and critical length, for C and RACK profiles. The first was carried out by Lau and Hancock (1987), and the second by Schafer and Pekoza (1999). The main drawback of these methods is that the formulas for determining the value of critical stress are very complicated, and they are result of a number of simplifications that reduce their accuracy. The numerical methods, such as finite strip method and finite element method(FEM), are very efficient methods for determining the value of critical stress for all three characteristic forms of stability loss. Finite strip method is a specialized FEM and it is the most suitable and efficient method for determining the value of critical stress and its accompanying forms of stability loss. The drawback of this method is that it's applicable only to columns that are simply supported at their ends and for columns that are length enough so that it can appear more half waves on the length of the column.

2. LOCAL LOSS OF STABILITY

2.1 Analytical method

There are two analytical methods for determining the value of local critical stress. These methods are: element method and interactive method. The main deficiency of the element method is that it takes into account the interaction between the elements that make up the cross section and that the relationship between the elements is not joint. The value of critical stress is obtained for each element separately and applies only to it and not for the whole cross-section, such as the case for the value of critical stress which is obtained using the software CUFSM. The second method, which is given by equations 4-7, takes into account interactions between two adjacent elements, so this method is named interactive method. Interaction exists between all elements but it between two adjacent element has the greatest impact.

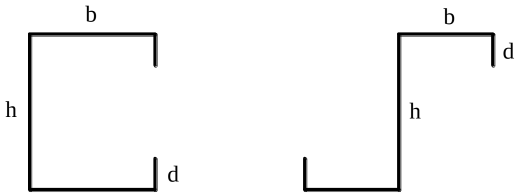

Fig. 3 *C i Z profile*

1. h = 200mm, b = 50 mm, d = 10mm, t = 1mm

Element method: each element was treated separately

a) web k_{web} = 4

$$\left(\sigma_{crl}\right)_{web} = k\frac{\pi^2 E}{12\left(1-\upsilon^2\right)}\left(\frac{t}{h}\right)^2 \qquad (1)$$

$$\left(\sigma_{crl}\right)_{web} = 1.898 \text{ kN/cm}^2$$

b) zone k_{flange}= 4

$$\left(\sigma_{crl}\right)_{flange} = k\frac{\pi^2 E}{12\left(1-\upsilon^2\right)}\left(\frac{t}{b}\right)^2 \qquad (2)$$

$$\left(\sigma_{crl}\right)_{flange} = 30.368 \text{ kN/cm}^2$$

c) lip k_{lip} = 0.43

$$(\sigma_{crl})_{lip} = k\frac{\pi^2 E}{12(1-\upsilon^2)}\left(\frac{t}{d}\right)^2 \quad (3)$$

$$(\sigma_{crl})_{lip} = 81.614 \text{ kN/cm}^2$$

Interactive method: it takes into account the interaction between two adjacent element

a) flange/lip

$$k_{flange/lip} = -11.07\left(\frac{d}{b}\right)^2 + 3.95\left(\frac{d}{b}\right) + 4 \quad (4)$$

$$k_{flange/lip} = 4.347$$

$$(\sigma_{crl})_{flange/lip} = k_{flange/lip}\frac{\pi^2 E}{12(1-\upsilon^2)}\left(\frac{t}{b}\right)^2 \quad (5)$$

$$(\sigma_{crl})_{flange/lip} = 33.002 \text{ kN/cm}^2$$

b) flange/web

$$k_{flange/web} = 4\left(\frac{b}{h}\right)^2\left[2-\left(\frac{b}{h}\right)^{0.4}\right] \quad (6)$$

$$k_{flange/web} = 0.3564$$

$$(\sigma_{crl})_{flange/web} = k_{flange/web}\frac{\pi^2 E}{12(1-\upsilon^2)}\left(\frac{t}{b}\right)^2 \quad (7)$$

$$(\sigma_{crl})_{flange/web} = 2.71 \text{ kN/cm}^2$$

Table 1 - *The value of the local elastic critical stress for C profiles using analytical and numerical methods*

h-b-d-t	$(\sigma_{crl})_{web}$ kN/cm^2	$(\sigma_{crl})_{flange}$ kN/cm^2	$(\sigma_{crl})_{lip}$ kN/cm^2	$(\sigma_{crl})_{flange/lip}$ kN/cm^2	$(\sigma_{crl})_{flange/web}$ kN/cm^2	$(\sigma_{crl})_{CUFSM}$ kN/cm^2
200-50-10-1	1.90	30.37	81.61	33.00	2.71	2.76
200-100-10-1	1.90	7.59	81.61	8.12	2.36	2.52
200-150-10-1	1.90	3.37	81.61	3.33	2.10	2.32
200-200-10-1	1.90	1.90	81.61	1.98	1.90	1.85

2.2 Numerical method: using the software CUFSM

$$(\sigma_{crl})_{CUFSM} = 2.76 \text{ kN/cm}^2$$

It should be noted that the value of the critical local stress obtained using the software CUFSM applies to the entire cross-section, while the values obtained using element method related only to one element of cross section. It can be concluded that the value of critical stress obtained by interactive method, related to the interaction flange and the web, very well agrees with the value of critical stress obtained using software CUFSM.

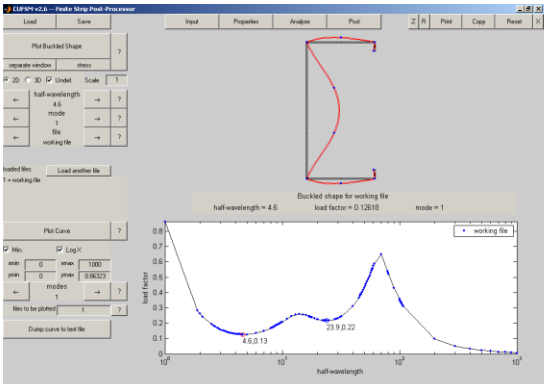

Fig. 4 *Graphical presentation of software CUFSM with the results*

The calculation results for several C profile, in which the changed flange width b, are given in table 1. Based on the results shown in table 1, it can be concluded that element method gives good results only when the dimensions of the webs and flange are the same or nearly the same. However interactive method, which takes into account the interaction between flange and the web, gives results that are very close to those obtained using numerical method and it can be used with acceptable accuracy in the calculation of capacity of thin wall columns.

The last column presents the results obtained using software CUFSM. It can be noted, that with increasing values of the flange width, value of the critical stress decreases. This happens because with increasing the flange width reduces the value of critical stress which refers only to flange and it is closer to the value of critical stress related to the web.

3. DISTORTIONAL LOSS OF STABILITY

For the purpose of constructing, in the existing national specifications, are commonly used analytical solutions that give value of elastic compression force and bending moment. The main characteristic of distortion form of stability loss is the rotation of flange around flange and web connecting line. Besides, the connecting line, which is seen in cross section as a point, has translational movements.

The value of distortion critical force F_{crd} is given in equation (8).

$$F_{crd} = \frac{E}{2}\left\{(\alpha_1+\alpha_2) \pm \sqrt{\left[(\alpha_1+\alpha_2)^2 - 4\alpha_3\right]}\right\} \quad (8)$$

where are:

$$\alpha_1 = \frac{\eta}{\beta_1}\left(\beta_2 + 0,039 I_t L_{crd}{}^2\right) + \frac{k_\phi}{\beta_1 \eta E} \quad (9)$$

$$\alpha_2 = \eta\left(I_{yp} - 2y_0\frac{\beta_3}{\beta_1}\right) \quad (10)$$

$$\alpha_3 = \eta\left(\alpha_1 I_{yp} - \frac{\eta}{\beta_1}\beta_3{}^2\right) \quad (11)$$

$$\beta_1 = h_x{}^2 + \frac{I_{xp}+I_{yp}}{A_d} \quad (12)$$

$$\beta_2 = C_w + I_{xp}(x_0 - h_x)^2 \quad (13)$$

$$\beta_3 = I_{xyp}(x_0 - h_x) \quad (14)$$

h-b-d-t	Hancock	Schafer	CUFSM
100-30-10-2	58.3	54.1	48.26
100-30-15-2	70.7	68.9	56.53
100-50-10-2	41.1	40.4	39.9
100-50-15-2	52.3	53.5	50.64
100-50-20-2	58.4	63.0	56.84
100-100-15-2	20.5	23.2	20.53
100-100-20-2	25.4	29.6	26.10
100-100-30-2	32.5	40.2	34.61

$$\beta_4 = \beta_2 + (y_0 - h_y)\left[I_{yp}(y_0 - h_y) - 2\beta_3\right] \quad (15)$$

$$L_{crd} = 4.80\left(\frac{\beta_4 h}{t^3}\right)^{0.25} \quad (17)$$

$$\eta = \left(\frac{\pi}{L_{crd}}\right)^2 \quad (18)$$

while the distortion critical stress

$$\sigma_{crd} = \frac{E}{2A_d}\left\{(\alpha_1+\alpha_2) \pm \sqrt{\left[(\alpha_1+\alpha_2)^2 - 4\alpha_3\right]}\right\} \quad (16)$$

In the equations (8) to (18) is given a methodology for determining the value of critical stress distortions carried out by Lau and Hancock (1987), which is valid only for centric loaded columns on the pressure. The calculation process is an iterative because of inclusion σ_{crd} in the k_ϕ but it comes to only one iteration, so this method is accepted as relevant for calculating the value of critical distortion stresses on the Australian standard AS / NZS 4600th. The main drawback of this method is that in the case of very wide web, when it buckles at very low load values, can get a negative value for the rotational stiffness k_ϕ .

Therefore, Davis and Jiang (1998) propose the improvement of this method when is obtained a negative value of rotational stiffness. In this case the value of critical stress σ_{crd} is obtained from equation (18), where it is considered that the rotational stiffness is zero. The critical stress for the plate webs is obtained from the formula that derived by Timoshenko and Gere (1961).

$$\sigma_{cr\_web} = \frac{\pi^2 D}{th^4}\left(\frac{h^2 + L_{crd}{}^2}{L_{crd}}\right)^2 \quad (19)$$

Finally, the value of critical distortion stresses is calculated approximately as the mean value of critical stress webs and flanges.

$$f_{crd} = \frac{2\sigma_{crd}A_p + \sigma_{cr\_rebra}th}{A} \quad (20)$$

Where is A_p the surface of band, and A is the surface of the entire cross section

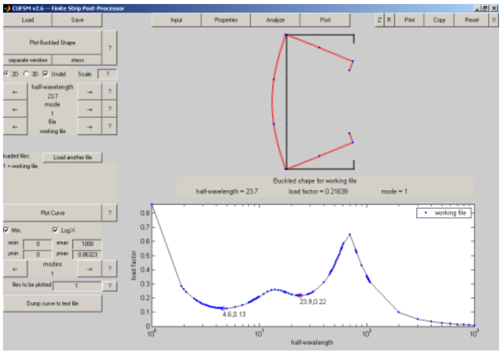

Fig. 5. *Graphical display of software CUFSM in which the shown results of the analysis (distortion minimum)*

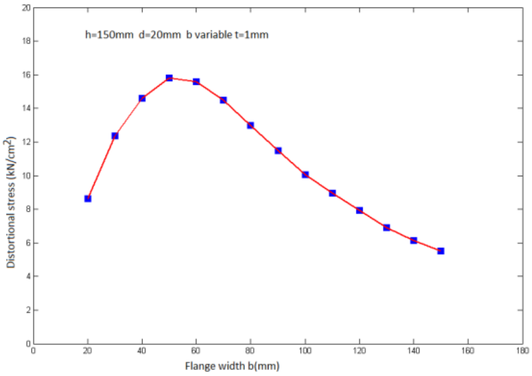

Fig. 6 *The critical distortion stress for h = 150 mm, depending on the flange width (the case of pressure)*

4. LOCAL AND DISTORTNIONAL STABILITY LOSS OF THIN WALL PROFILE IN THE POST-CRITICAL PHASE

Fig. 7 *The collapse of the column (the local form of bending) (Schafer, Yu, 2005.)*

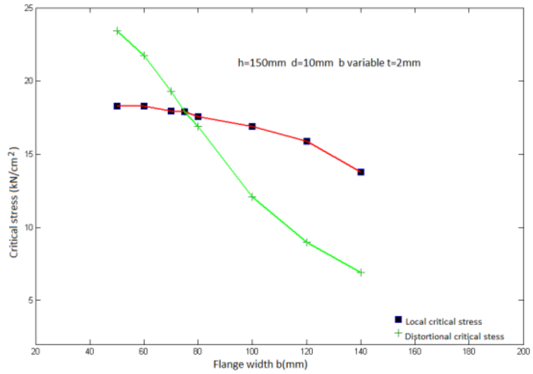

Fig. 8. *Comparison of critical distortion stresses and local critical stresses for C profile web width h = 150 mm and thickness t = 2 mm.*

From figure 3 it is obvious, that in the case of centric pressure, value of the critical distortion stresses can be equal to or less than the value of local critical stresses. In thin wall columns occurs loss of stability at relatively low load values, due to small thickness of the wall, so that the stress value is in the elastic range at all points of column. The value of the load can be further increased, so that the phase at which further increases the load after the primary loss of stability is called post critical phase. There are two methods for determination of capacity of thin wall columns in the post-critical phase: The Effective Width Method and Direct Strength Method. In some cases is the value of the load, in which occurs collapse of the columnss, three times higher than the value of critical load in which there is loss of stability in the elastic range. In cases where are the values of local critical stress and critical distortion stress close to each other in the post-critical phase, it comes to their interactions. In other words, a form of stability loss occurs on the deformed configuration correspond in to the second form of stability loss. This appearance may significantly affect the reduction capacity in post-critical phase as shown in Figure 10. The interaction between local and global (Euler) form is short denoted with L + E, and interaction between local and distortion form with L +D. The interaction of L+R is completely ignored in the calculations, and can be dominant in the mechanism of collapse, especially in the short length columns, when is the Euler stress high. In (1) was carried out four methods for determination of strength in the post critical phase at interaction L + D. In Figure 9 is shown comparison of method 3 and experimental investigation.

a pure distortion-D

$$F_{n3}^{D}=\left(1-0,25\left(\frac{F_{crd}}{F_y}\right)^{0,6}\right)\left(\frac{F_{crd}}{F_y}\right)^{0,6}F_y \qquad (21)$$

L+D

$$F_{n3}^{L+D}=\left(1-0,15\left(\frac{F_{crl}}{F_{nd}}\right)^{0,4}\right)\left(\frac{F_{crl}}{F_{nd}}\right)^{0,4}F_{nd} \qquad (22)$$

CHARACTERISTICS OF CARRIER**:**
C profile (h = 127 mm, b = 63 mm, d = 26 mm, t = 0,81 mm, L = 1295 mm) F_{eksp}=20,7 kN,
σ_y =24,2 kN/cm^2 (R_e),
Loughlan (1979), Pekoz (1987)

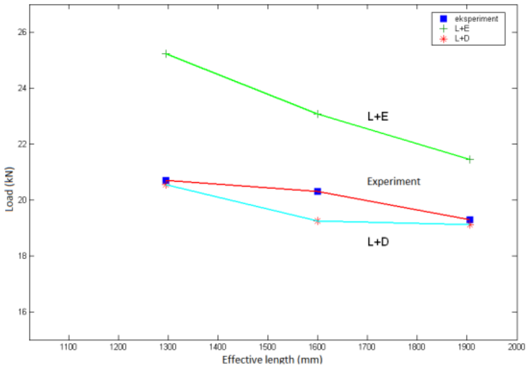

Fig.9. Comparison of method 3 and experiment Loughlan (1979), Pekoz (1987)

5. CONCLUSIONS

Capacity determination of thin wall columns can be a very complex process. The main reason for this is that thin wall columns have three different forms of stability loss in the elastic range, which can occur at very close values of critical load. Therefore, in the post critical phase comes to a significant reduction in capacity (up to 50%), due to the occurrence of different forms of coupling. In relatively short length columns (up to 1500 mm) may be the interactions between the local and distortional forms of stability loss, cause of capacity decrease (L + D). This should be taken into account by forming and designing of thin wall structures. It must be used completely different design model depending, on the length of the columns.

6. REFERENCES

[1] Radić N., Lokalni, distorzioni, globalni i spregnuti oblik gubitka stabilnosti hladnooblikovanih tankozidih profila otvorenog poprečnog presjeka, Doktorska disertacija, 2008.
[2] Brush D.O. and Almroth B.O., Buckling of Bars, Plates and Shells, McGraw-Hill Book Company,1975.
[3] Yu, W.W., Cold-Formed Steel Design, Wiley, New York,2000
[4] Ben Schafer, Finite Strip Analysis of Thin-walled Members .In:CUFSM: Cornell University, 2001

HEAVY MACHINERY - HM 2011, 55-60
ISBN 978-86-82631-58-3
Paper accepted: 30.05.2011

Optimization of the plane truss by using the Method of Particle Swarm Optimization (PSO)

Miljan Veljovic, [1,*] Radovan Bulatović[1], Vladimir Đorđević[1]
[1] University of Kragujevac, Faculty of Mechanical Engineering in Kraljevo

This paper analyses optimization of the tubular plane truss with two case of loads. The aim of the analyses was to find out minimal weight of plane truss using PSO. This optimum design also has to satisfy the stress and the displacement constraints, and the elastic stability too.

Keywords: Particle Swarm Optimization, structural optimization, truss

0 INTRODUCTION

Determining the optimal construction dimensions is one of the major demands in the process of construction.
Their determination importantly influences the reduction of construction overall mass and costs too. According this fact, the construction solution becomes competitive. In the analysis of the metal construction cost, Farkas deduce that the price is primarily influenced by the price of the material (30–73)%, while the other costs are lower: manufacture (16–22)%, assembling (5–20)%, transportation (3–7)%, design (2–3)% [2]. By this data, reducing of material, i.e., weigth, is major tasks in optimization process.
Numerous researchers have dealt with the construction optimization using different methods of optimization[5], [6]. Olsen and Vanderplaats, and Jalkanen too, have treated the problem of ten-bar tubular plane truss [9].
Kennedy and Eberhart[7], studing social behavior of bird flocking, developed one new heuristic optimization method.
Ostrić and Petković [1] have treated the problem of steel truss construction.

In this paper we analyze eigth-bar steel plane truss example. Yet, ten-bars aluminium plane truss is benchmark in the research papers and it can be seen that two additional diagonal bars are needless too, because the kinematical stability is satisfied without its.

1 PARTICLE SWARM OPTIMIZATION ALGORITHM

Particle swarm optimization (PSO) is a population based metaheuristic optimization technique developed by Eberhart and Kennedy in 1995, inspired by social behavior of bird flocking or fish schooling. It is based on the evolutionary cultural model of Boyd and Richerson which states that in social environments individuals have two learning sources: individual learning and cultural transmission. PSO and evolutionary algorithms (EA) such as Genetic Algorithms (GA) and Simulated Annealing (SA) have many similarities, however, some literature suggests they should be treated separately. These methods use a stochastic search process. PSO does not use the concept of survival of the fittest. In the PSO unfit individuals do not die. The system is initialized with a population of random solutions and searches for optima by updating generations. In PSO, the potential solutions, called particles, fly through the problem space by following the current optimum particles. It is demonstrated that PSO gets better results in a faster, cheaper way compared with other methods. Another reason that PSO is attractive is that there are few parameters to adjust. One version, with slight variations, works well in a wide variety of applications. If one sees a desirable path to go (e.g., for food, protection, etc.) the rest of the swarm will be able to follow quickly even if they are on the opposite side of the swarm. This is performed by particles in multidimensional space that have a position and a velocity. These particles are flying through hyperspace (i.e., _n) and have two essential reasoning capabilities: their memory of their own best position and knowledge of the swarm's best („best“ - the position with the smallest objective value). Consider Swarm of particles is flying through the parameter space and searching for optimum. Each particle is characterized by,

* Corr. Author's Adress: Faculty of Mechanical Engineering in Kraljevo, Dositejeva 19, 36000 Kraljevo, University in Kragujevac, Republic of Serbia, veljovic.m@mfkv.kg.ac.rs

Position vector . . . . . $\mathbf{x}_i$ (t)
Velocity vector . . . . . $\mathbf{v}_i$ (t)
as shown in Fig. 1.

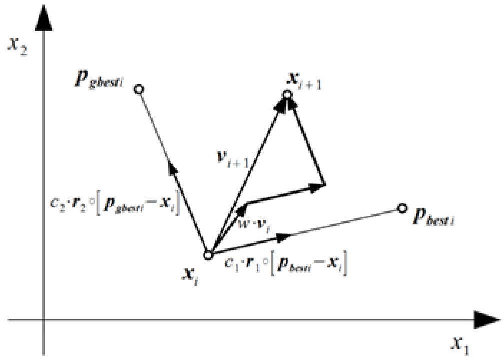

Fig. 1. Updating of position of the i-th particle

During the process, each particle will have its individual knowledge *pbest* and its own best-so-far in the position and social knowledge *gbest.*
Performing the velocity update, using the formula (1) given below,

$$v_i(t+1) = \omega\, v_i + c_1 \times rand \times pbest((t)-x_i(t)) + c_2 \times rand \times gbest((t)-x_i(t)) \quad \ldots (1)$$

where ω is the inertia weight that controls the exploration and exploitation of the search space. Inertia weight w impacts the first component, and for the values in the range of 0,9 – 1,2 it gives the best results, that is, the algorithm has greater chances of finding the global minimum for a reasonable number of iterations. For coefficient values which are smaller than 0,8, if algorithm finds global minimum it will find it fast. Particles in this case move quickly and it can happen that they “fly over” some area, so it can happen that they do not find global minimum. On the other side, if inertia weight is bigger value, then particles search the solution space more thoroughly and the chances of finding global minimum are greater.
Coefficients c_1 and c_2, the cognition and social components respectively are the acceleration constants which changes the velocity of a particle towards the *pbest* and *gbest*, *rand* is a random number between 0 and 1. Usually c_1 and c_2 values are set to 2.
The particle swarm optimization concept consists of, at each time step, changing the velocity of (accelerating) each particle toward its p*best* and *lbest* locations (local version of PSO). Acceleration is weighted by a random term, with separate random numbers being generated for acceleration toward *pbest* and *lbest* locations.
Now, performing the position update(as shown in Fig. 1.),

$$Xi(t+1) = Xi(t) + Vi(t+1) \quad \ldots (2)$$

This process is repeated for each and every particle considered in the solution space and the best optimal solution is obtained.

Basic Flow of Particle Swarm Optimization

The basic operation of PSO is given by,
Step1: Initialize the *swarm* from the solution space
Step 2: Evaluate *fitness* of individual particles
Step 3: Modify *gbest*, *pbest* and *velocity*
Step 4: Move each *particle* to a new *position*
Step 5: Go to step 2, and repeat until convergence or stopping condition is satisfied.

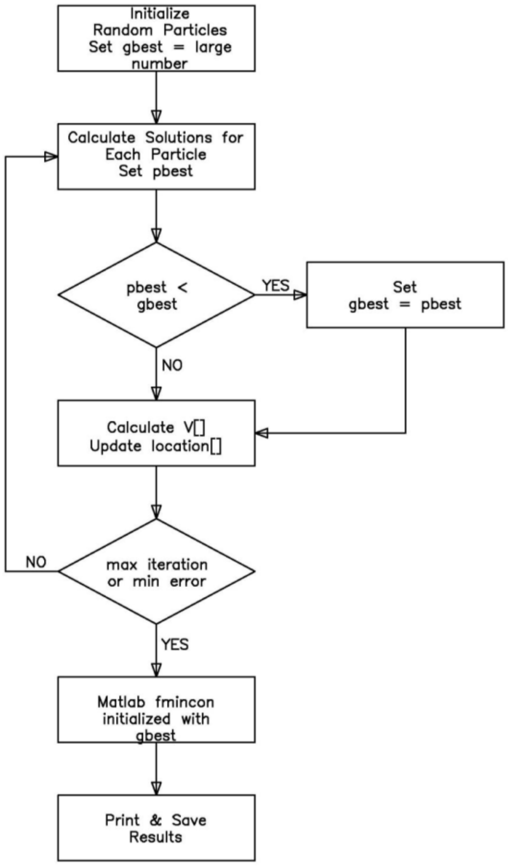

Fig. 2. Particle swarm optimizer flowchart

While maximum iterations or minimum error criteria is not attained Particles' velocities on each dimension are clamped to a maximum velocity Vmax. If the sum of accelerations would cause the velocity on that dimension to exceed Vmax, which is a parameter specified by the user, then the velocity on that dimension is limited to Vmax.

In recent years the concept of PSO has been applied to various engineering problems. Specifically, it has been applied to structural design optimization problems. Ant colony optimization (ACO), a type of PSO, was tested on steel frame optimization problems with discrete variables by Camp et al. The PSO method found better results on these test problems than any of the other optimization algorithms used in previous research.

2 STRUCTUAL OPTIMIZATION

The term *optimal structure* is very vague because a structure can be optimal in different aspects. These different aspects are called objectives, and may for instance be the weight, stiffness or cost of the structure. A numerical evaluation of a certain objective is possible through an *objective function, f,* which determines the goodness of the structure in terms of weight, stiffness or cost [4]. To be well defined solution, the optimization has to be done within some constraints. Firstly, there are *design constraints*, like a limited geometrical extension or limited availability of different structural parts. Secondly, there are *behavioral constraints* on the structure that denotes the structural response under a certain load condition, for instance, limits on displacements, stresses, forces and dynamic response. Finally, there is *kinematical stability* that is valid for all structures, otherwise they are mechanisms. This can be seen as a behavioral constraint. Structures that lie within the constraints are called *feasible* solutions to the optimization problem.

A general expression for structural optimization is given for instance by Christensen &Klarbring [4]:

$$SO \begin{cases} \text{minimize } f(x, y) \text{ with respect to } x \text{ and } y \\ \text{subject to } \begin{cases} \text{design constrains on } x \\ \text{behavioral constrains on } y \\ \text{stability constraint} \end{cases} \end{cases}$$

where *f* is the objective function;

x is a function or vector representing the design variables, and;

y is a function or vector representing the state variables, i.e. the response of the structure.

Multi-objective optimization (also called multi-criterion or vector optimization) can be done with respect to two or more different objective functions.

When it applies to trusses, the optimization can be divided into sizing, shape and topology optimization.

Sizing optimization refers to finding the optimal cross section area of each member of the structure; *shape optimization* means optimizing the outer shape of the structure; and *topology optimization* describes the search for the best inner connectivity of the members.

One way of optimizing these three parameters is to take them into consideration one at a time, starting with the topology optimization, a so called multi-level optimization technique (also called layered optimization). One of the strengths and advantages of a genetic algorithm is that a simultaneous optimization of all three parameters can be done.

Structural optimization, especially discrete structural optimization of practical problems, requires low computational cost and accuracy for all of the processes. By far the most computationally costly process is the FEA. The FEA for large-scale three-dimensional problems and eigenfrequency problems becomes difficult to optimize practically.

2.1 Trusses

As long as the load is applied in some of the nodes, the bars will only be subjected to compressive or tensile normal forces. This is one part of the explanation to why trusses are so light compared to their load capacity; bar effect is more efficient than beam effect. The other part is that the triangle is the simplest *stable* structure that extends in two dimensions. Due to their efficiency, trusses are desirable in long span structures with high demands in stiffness and strength.

There are benefits of weight optimized structures in many engineering fields. In engineering it can for instance be associated with cheaper structural parts and easier transportation. In this paper a

PSO algorithm for weight minimization of steel trusses has been developed in MATLAB.

The objective is to minimize the weight of the plane truss. This optimum design also has to satisfy the stress and the displacement constraints, and the elastic stability too.

2.2 Eight-bar truss

The first numerical example problem deals with the discrete optimization of a eight-bar steel tubular plane truss presented in Fig. 3.

L = 9,1 m, F = 444,8 kN, E=210000Mpa,

ρ = 7800kg/m^3, σ_d = 160Mpa, f_d^{max} = 5cm

Mass of the truss should be minimized so that the normal stress is less than σ_d in all the bars and the maximum deflection in nodes 3, 4, 5 and 6 is less than the maximum allowed value f_d^{max}. The cross section areas Ai are the design variables and their values should be chosen from a set which includes 50 evenly distributed values. The cross section of bars is pipe-shape and its area is:

$$A_i = \frac{\pi d_i^2}{4} - \frac{\pi (d_i - 2t)^2}{4}$$

If the thickness t is constant and it is assumed that t = d/10, then: $A_i = 0{,}09 \pi d_i^2$

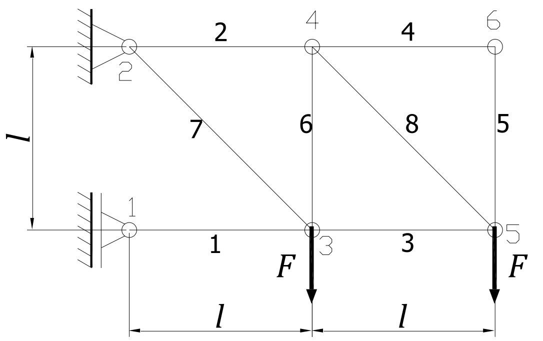

Fig. 3. The eight-bar steel plane truss

The set of discrete variables (diametars) is:

$x \in \{x_1, x_2, ..., x_8\}$

Therefore, the problem can be stated as:

The objective function is:

min $m(\mathbf{x}) = \sum \rho \, L A_i$ (i =1,2,...,8)

Design constraint functions:

$\sigma(\{x\}) - \sigma_d \le 0$, $f(\{x\}) - f\,max \le 0$

Variable regions:

$1 \le d \le 60$,

where the maximum allowable stress (σ_d) is 160 MPa and the only displacement constraint is the maximum (f max) limited to 5 cm.

The structural analysis is done using analitic method. Normal force is the only internal force in bars and results of analyzis are presented in Table1:

N_i	N_1	N_2	N_3	N_4	N_5	N_6	N_7	N_8
$N_{i(1)}$	-2F	F	-F	0	0	-F	√2F	√2F
$N_{i(2)}$	-F	0	0	0	0	0	√2F	0
l_i	l	l	l	l	l	l	$\sqrt{2}l$	$\sqrt{2}l$

In this paper we analyze eigth-bar plane truss example. Although, ten-bars plane truss is benchmark in the research papers and we can see that two additional diagonal bars are needless too, because the kinematical stability is satisfied without its. Furthermore, due to analysis of normal forces, it is obvious that bars 4 and 5 (Fig. 3) are needless and it can be reduced till only the necessary elements are remaining. This shape of 8-bar plane truss example is more practical and very often in constructions.

The deflection analysis is done using method of deformation energy and maximal displacement for load case 1 - force F at the end (node 5) of the truss is calculated as:

$$f_5 = \frac{Fl}{E}\left[\frac{4}{A_1} + \frac{1}{A_2} + \frac{1}{A_3} + \frac{1}{A_6} + \frac{2\sqrt{2}}{A_7} + \frac{2\sqrt{2}}{A_8}\right]$$

Vertical displacement of node 3 for load case 1 is calculated as:

$$f_3^{(1)} = \frac{2Fl}{E}\left[\frac{1}{A_1} + \frac{\sqrt{2}}{A_7}\right]$$

Maximal displacement for load case 2 - force F at the node 3 of the truss is calculated as:

$$f_5^{(2)} = \frac{2Fl}{E}\left[\frac{1}{A_1} + \frac{\sqrt{2}}{A_7}\right]$$

Vertical displacement of node 3 for load case 2 is calculated as:

$$f_3^{(2)} = \frac{Fl}{E}\left[\frac{1}{A_1} + \frac{2\sqrt{2}}{A_7}\right]$$

Analyzing elastic stability of the truss, we have to test only compressed bars which marked 1, 3 and 6.

Firstly, we calculate effective slendernees ratio:

$$\lambda_r = \frac{l_r}{i_{\min}}$$

where is:

minimal radius of qyration i_{min} is calculate as:

$$i_{\min} = \sqrt{\frac{I_{\min}}{A_i}} = 0{,}0597 d_i$$

I_{min} – minimal moment of inertia of tubular cross-section and it is:

$$I^i_{\min} = 0{,}00537\pi d_i^2$$

l_r – effective length of the bar

λ_r – effective slendernees ratio is quotient of effective length of the bar l_r and minimal radius of qyration i_{min}

Now, we compare effective slendernees ratio λ_r with λ_P = 108 (Č.0361).

If the effective slendernees ratio λ_r has bigger valeu than slendernees at proportional limit λ_P Eulers' critical force for a bar is calculated as:

$$F_{kr} = \frac{\pi^2 E I_{\min}}{l_r^2} = \frac{0{,}0537\pi^3 E \cdot d^2}{l^2}$$

$$N_d = \frac{F_{kr}}{\nu} = \frac{0{,}0537\pi^3 E \cdot d^2}{\nu \cdot l^2}$$

where υ=1,5 – coefficient of safety

On the contrary, critical buckling force is:

$$F^i_{kr} = (289 - 0{,}82\lambda_r)\cdot A_i =$$
$$= (289 - 0{,}82\lambda_r)\cdot 0{,}09\pi d^2$$

3 OPTIMIZATION RESULTS

Following parameters of the algorithm of particle swarm optimization (algorithm):

Number of particles	30
Number of iterations	10000
Inertia weight w	1
Acceleration coefficient c_1	2
Acceleration coefficient c_2	2
Boundaries for d	1-60

The truss has to be analyzed ten thousands times during the optimization. The obtained results for the both load cases is represented in table:

d_i (cm)	d_1	d_2	d_3	d_4	d_5	d_6	d_7	d_8
$d_{(1)case}$	25	13	20	1	1	20	16	16
$d_{(2)case}$	20	1	1	1	1	1	12	1

The objective function, i.e., overall mass of the truss is:

-load case 1: m = 3645kg

-load case 2: m = 1038kg

By comparing this results with the other researches, Jalkanen has obtained for total weigth of ten-bar plane truss m = 2303kg, and we can see similarities, but this eigth-bar truss is made of *steel.*

4 CONCLUSION

This paper analyses optimization of the tubular plane truss with two case of loads. The aim of the analyses was to find out minimal weight of plane truss using PSO.

According to results we can see that the value of totalmass for the first load case is very close to the overall value 3645 kg, and the sum of mass all bars for the second load case is 1038 kg, which is expeced due to the position of forces. By comparing this results with the other researches, for example Jalkanen has obtained for total weigth of ten-bar *aluminium* plane truss m = 2303kg, we can see that, regardless three times bigger steel density, this eigth-bar *steel* truss is more practical in engineering problems. The method of PSO is suitable for this type of constructions.

5 REFERENCES

[1] Petković, Z., D. Ostrić, "Metal constructions in Engineering Mechanics I" Institut of Mechanization, Faculty of Mechanical Engineering, Belgrade,1996.

[2] Farkas, J., "Optimum design of metal structures", Akademiai KIADO, Budapest, 1984.

[3] Reference book - Strength of materials, Faculty of Mechanical Engineering, Belgrade, 2003.
[4] Christensen, Peter W. Klarbring, Anders. "*An Introduction to Structural Optimization*" Springer Netherlands, 2008.
[5] Sivanandam, S.N., S.N. Deepa,"Introduction to Genetic Algorithms", Springer Berlin, 2008.
[6] Rao, S.S., "Engineering Optimization", John Wiley & Sons, Inc., Hoboken, New Jersey, 2009.
[7] Kennedy, J., R. C. Eberhart, "Particle swarm optimization", In Proceedings of the IEEE International Conference on Neural Networks, 1995.
[8] Mijailović, R., "Optimum design of lattice-columns for buckling", Structural and Multidisciplinary Optimization, Volume 42 Issue 6, December 2010 .
[9] Jalkanen, J., "Tubular truss optimization using heuristic algorithms", Tampere 2007.